

SUMMARY TECHNICAL REPORT
OF THE
NATIONAL DEFENSE RESEARCH COMMITTEE

This document contains information affecting the national defense of the United States within the meaning of the Espionage Act, 50 U. S. C., 31 and 32, as amended. Its transmission or the revelation of its contents in any manner to an unauthorized person is prohibited by law.

This volume is classified CONFIDENTIAL in accordance with security regulations of the War and Navy Departments because certain chapters contain material which was CONFIDENTIAL at the date of printing. Other chapters may have had a lower classification or none. The reader is advised to consult the War and Navy agencies listed on the reverse of this page for the current classification of any material.

CONFIDENTIAL

Manuscript and illustrations for this volume were prepared for publication by the Summary Reports Groups of the Columbia University Division of War Research under contract OEMsr-1131 with the Office of Scientific Research and Development. This volume was printed and bound by the Columbia University Press.

Distribution of the Summary Technical Report of NDRC has been made by the War and Navy Departments. Inquiries concerning the availability and distribution of the Summary Technical Report volumes and microfilmed and other reference material should be addressed to the War Department Library, Room 1A-522, The Pentagon, Washington 25, D. C., or to the Office of Naval Research, Navy Department, Attention: Reports and Documents Section, Washington 25, D. C.

Copy No.

147

This volume, like the seventy others of the Summary Technical Report of NDRC, has been written, edited, and printed under great pressure. Inevitably there are errors which have slipped past Division readers and proofreaders. There may be errors of fact not known at time of printing. The author has not been able to follow through his writing to the final page proof.

Please report errors to:

JOINT RESEARCH AND DEVELOPMENT BOARD
PROGRAMS DIVISION (STR ERRATA)
WASHINGTON 25, D. C.

A master errata sheet will be compiled from these reports and sent to recipients of the volume. Your help will make this book more useful to other readers and will be of great value in preparing any revisions.

CONFIDENTIAL

SUMMARY TECHNICAL REPORT OF DIVISION 6, NDRC

VOLUME 13

THE DESIGN AND CONSTRUCTION OF MAGNETOSTRICTION TRANSDUCERS

OFFICE OF SCIENTIFIC RESEARCH AND DEVELOPMENT
VANNEVAR BUSH, DIRECTOR

NATIONAL DEFENSE RESEARCH COMMITTEE
JAMES B. CONANT, CHAIRMAN

DIVISION 6
JOHN T. TATE, CHIEF

WASHINGTON, D. C., 1946

CONFIDENTIAL

NATIONAL DEFENSE RESEARCH COMMITTEE

James B. Conant, *Chairman*

Richard C. Tolman, *Vice Chairman*

Roger Adams Army Representative ¹

Frank B. Jewett Navy Representative ²

Karl T. Compton Commissioner of Patents ³

Irvin Stewart, *Executive Secretary*

¹*Army representatives in order of service:*

Maj. Gen. G. V. Strong	Col. L. A. Denson
Maj. Gen. R. C. Moore	Col. P. R. Faymonville
Maj. Gen. C. C. Williams	Brig. Gen. E. A. Regnier
Brig. Gen. W. A. Wood, Jr.	Col. M. M. Irvine
Col. E. A. Routreau	

²*Navy representatives in order of service:*

Rear Adm. H. G. Bowen	Rear Adm. J. A. Furer
Capt. Lybrand P. Smith	Rear Adm. A. H. Van Keuren
Commodore H. A. Schade	

³*Commissioners of Patents in order of service:*

Conway P. Coe	Casper W. Ooms
---------------	----------------

NOTES ON THE ORGANIZATION OF NDRC

The duties of the National Defense Research Committee were (1) to recommend to the Director of OSRD suitable projects and research programs on the instrumentalities of warfare, together with contract facilities for carrying out these projects and programs, and (2) to administer the technical and scientific work of the contracts. More specifically, NDRC functioned by initiating research projects on requests from the Army or the Navy, or on requests from an allied government transmitted through the Liaison Office of OSRD, or on its own considered initiative as a result of the experience of its members. Proposals prepared by the Division, Panel, or Committee for research contracts for performance of the work involved in such projects were first reviewed by NDRC, and if approved, recommended to the Director of OSRD. Upon approval of a proposal by the Director, a contract permitting maximum flexibility of scientific effort was arranged. The business aspects of the contract, including such matters as materials, clearances, vouchers, patents, priorities, legal matters, and administration of patent matters were handled by the Executive Secretary of OSRD.

Originally NDRC administered its work through five divisions, each headed by one of the NDRC members. These were:

- Division A — Armor and Ordnance
- Division B — Bombs, Fuels, Gases, & Problems
- Division C — Communication and Transportation
- Division D — Detection, Controls, and Instruments
- Division E — Patents and Inventions

In a reorganization in the fall of 1942, twenty-three administrative divisions, panels, or committees were created, each with a chief selected on the basis of his outstanding work in the particular field. The NDRC members then became a reviewing and advisory group to the Director of OSRD. The final organization was as follows:

- Division 1 — Ballistic Research
- Division 2 — Effects of Impact and Explosion
- Division 3 — Rocket Ordnance
- Division 4 — Ordnance Accessories
- Division 5 — New Missiles
- Division 6 — Sub-Surface Warfare
- Division 7 — Fire Control
- Division 8 — Explosives
- Division 9 — Chemistry
- Division 10 — Absorbents and Aerosols
- Division 11 — Chemical Engineering
- Division 12 — Transportation
- Division 13 — Electrical Communication
- Division 14 — Radar
- Division 15 — Radio Coordination
- Division 16 — Optics and Camouflage
- Division 17 — Physics
- Division 18 — War Metallurgy
- Division 19 — Miscellaneous
- Applied Mathematics Panel
- Applied Psychology Panel
- Committee on Propagation
- Tropical Deterioration Administrative Committee



NDRC FOREWORD

AS EVENTS of the years preceding 1940 revealed more and more clearly the seriousness of the world situation, many scientists in this country came to realize the need of organizing scientific research for service in a national emergency. Recommendations which they made to the White House were given careful and sympathetic attention, and as a result the National Defense Research Committee [NDRC] was formed by Executive Order of the President in the summer of 1940. The members of NDRC, appointed by the President, were instructed to supplement the work of the Army and the Navy in the development of the instrumentalities of war. A year later, upon the establishment of the Office of Scientific Research and Development [OSRD], NDRC became one of its units.

The Summary Technical Report of NDRC is a conscientious effort on the part of NDRC to summarize and evaluate its work and to present it in a useful and permanent form. It comprises some seventy volumes broken into groups corresponding to the NDRC Divisions, Panels, and Committees.

The Summary Technical Report of each Division, Panel, or Committee is an integral survey of the work of that group. The first volume of each group's report contains a summary of the report, stating the problems presented and the philosophy of attacking them and summarizing the results of the research, development, and training activities undertaken. Some volumes may be "state of the art" treatises covering subjects to which various research groups have contributed information. Others may contain descriptions of devices developed in the laboratories. A master index of all these divisional, panel, and committee reports which together constitute the Summary Technical Report of NDRC is contained in a separate volume, which also includes the index of a microfilm record of pertinent technical laboratory reports and reference material.

Some of the NDRC-sponsored researches which had been declassified by the end of 1945 were of sufficient popular interest that it was found desirable to report them in the form of monographs, such as the series on radar by Division 14 and the monograph on sampling inspection by the Applied Mathematics Panel. Since the material treated in them is not dupli-

cated in the Summary Technical Report of NDRC, the monographs are an important part of the story of these aspects of NDRC research.

In contrast to the information on radar, which is of widespread interest and much of which is released to the public, the research on subsurface warfare is largely classified and is of general interest to a more restricted group. As a consequence, the report of Division 6 is found almost entirely in its Summary Technical Report, which runs to over twenty volumes. The extent of the work of a Division cannot therefore be judged solely by the number of volumes devoted to it in the Summary Technical Report of NDRC: account must be taken of the monographs and available reports published elsewhere.

Any great cooperative endeavor must stand or fall with the will and integrity of the men engaged in it. This fact held true for NDRC from its inception, and for Division 6 under the leadership of Dr. John T. Tate. To Dr. Tate and the men who worked with him — some as members of Division 6, some as representatives of the Division's contractors — belongs the sincere gratitude of the Nation for a difficult and often dangerous job well done. Their efforts contributed significantly to the outcome of our naval operations during the war and richly deserved the warm response they received from the Navy. In addition, their contributions to the knowledge of the ocean and to the art of oceanographic research will assuredly speed peacetime investigations in this field and bring rich benefits to all mankind.

The Summary Technical Report of Division 6, prepared under the direction of the Division Chief and authorized by him for publication, not only presents the methods and results of widely varied research and development programs but is essentially a record of the unstinted loyal cooperation of able men linked in a common effort to contribute to the defense of their Nation. To them all we extend our deep appreciation.

VANNEVAR BUSH, Director
Office of Scientific Research and Development

J. B. CONANT, Chairman
National Defense Research Committee

CONFIDENTIAL

FOREWORD

AS PART OF the broad Division 6 program of research and development in underwater sound, a fundamental investigation of the properties and behavior of "hydroacoustic generators and receivers," more commonly called transducers, was undertaken. It seemed desirable that the West Coast laboratory should pretty largely concern itself with devices based upon piezo-electric effect of certain crystals, while the Harvard laboratory should concern itself with devices employing the magnetostriction effect, most markedly shown by nickel, iron, and their alloys.

The research and development work performed at the West Coast Laboratory at San Diego under a contract with the University of California Division of War Research, including some reference to work by other agencies, is described in Volume 12 of this series. This present report, prepared in large part by Paul E. Sabine of the staff of the Harvard Underwater Sound Laboratory, presents not only the work of the Harvard Laboratory, but also to some extent the work in this same field of other research organizations. While it is not possible accurately to forecast the future requirements of the military, it is very certain that the subject here presented will continue to be of most substantial interest, and it is hoped this material will be helpful primarily to those who may

be concerned with further research and development relating to structures for generating or detecting underwater sounds.

The Division owes its thanks to Sabine, F. P. Bundy, and others of the Harvard staff for their willingness to undertake preparation of this volume. The Division also acknowledges its indebtedness to E. M. Wise and the International Nickel Company. Wise, acting as consultant to Division 6, was ever ready to furnish information to the contractors of the Division and to assist in every way in the obtaining of materials for test. As to Navy liaison the portion of this research and development activity performed by Division 6 was not set up as a formal Navy-NDRC project, and consequently no formal appointment of Navy liaison was made. However, because this work was basic to other formal Navy-NDRC projects, certain Navy officers assigned to these projects were kept fully informed as to progress and plans. Among these were Captain Rawson Bennett, Jr. and Commander J. C. Myers of the Bureau of Ships, who recognized the importance of the subject and gave it their most cordial support.

JOHN T. TATE
Chief, Division 6

PREFACE

THE WORK on magnetostriction transducers at Harvard Underwater Sound Laboratory[HUSL] grew out of the necessity of providing adequate electro-acoustic devices designed to meet the specific requirements of the various projects on which other groups in the laboratory were engaged. Initially, designing and building the requisite transducer for any project was a part of the job of the special group to which the project was assigned. It soon became apparent that this arrangement involved duplication of effort and was not adding materially to the fund of general knowledge on the subject of transducer design and performance.

In August 1942 a special transducer and measurement group was set up, the functions of which were (1) to carry on fundamental studies on magnetostrictive properties of materials, (2) to develop general types of transducers, (3) to design and build special transducers required by other groups, (4) to develop and improve equipment for making electrical and acoustical measurements on transducers, and (5) to assume the responsibility for all such measurements required by the different groups in the laboratory.

Attention at HUSL naturally centered almost exclusively on magnetostriction devices, since it was at Harvard that the pioneer work in this field by G. W. Pierce and his co-workers was done. Very early in the program Pierce generously turned over to this laboratory his original research notes on supersonic magnetostrictive vibrators. Material in these notes furnished the basic ideas on which many of the earlier experimental forms were constructed.

At the outset, very little theoretical material on the dynamics of magnetostrictive vibrators was available. A paper by Butterworth and Smith, published in 1931, and a comprehensive report by Smith to the British Admiralty comprised about all the published matter that had immediate bearing on the specific problem.

The work of the Theory Group at HUSL has been throughout closely coordinated with the experimental work of the Transducer Group. In June 1943, a report from the Theory Group was circulated under the title *Magnetostrictive Transducers*. A year earlier, a report titled *Directivity Patterns* had issued from the same source. The subject matter of these two reports, expanded and revised, constitutes a substantial portion of the present text.

The results of work by other laboratories in this field have been included. Grateful acknowledgment is made to the staffs of the Naval Research Laboratory at Anacostia, of the Columbia University Division of War Research at the U. S. Navy Underwater Sound Laboratory at New London, and of the Bell Telephone Laboratories, for material which they have supplied. Thanks also are due to the Submarine Signal Company for detailed information on QC projectors of their manufacture.

The correct appraisal of transducer performance can only be based on the results of acoustical and electrical measurements. The recognition of the need for improved measuring equipment and technique over the crude methods originally employed has led to an appreciable increase in the precision of both acoustical and electrical measurements. In view of the esoteric nature of the field, it has seemed worthwhile to give a fairly detailed account of the equipment and methods that have been developed at the two open-water stations of the Harvard Laboratory. The same reason is given as warrant for the inclusion of the account of impedance and admittance bridge measurements. These measurements have proved an extremely useful means both of studying transducers in the developmental stage, and of properly assembling multielement units for optimum performance.

The material presented herein has been prepared with a twofold purpose in mind: first, to give a coherent account of the efforts of a fairly large group of workers in an untried field, and second, at the same time to provide a source of information for the guidance of those who hereafter may be called on to carry forward a far-from-completed task. In carrying out the latter, it seemed useful to report some of our mistakes. Space limitations preclude the recording of all of them. The work of preparation is the joint effort of a number of writers, who, for the most part, have worked under the handicap of time limits and the pressure of other duties. The lack of uniformity in style and treatment will be all too evident. While it has been the editorial aim to sandpaper the joints and to eliminate repetition, it has been impossible to do this completely without an amount of rewriting which would exceed the time allotted to the job.

Thought has been given to the order of presentation of the various subjects. The three purely theoretical chapters as well as a chapter on fundamental

research on the magnetic and magnetostrictive properties of materials may seem a somewhat formidable barrier to the reader concerned with the immediate job of building a successful magnetostriction transducer. However, the frequent references in the later text to the theoretically derived relations, and the use of these relations in practical design problems, made the inclusion of this material in the early portion of the report seem necessary even if not inviting.

Possibly a disproportionate amount of space has been devoted to the minutiae of transducer manufacture. However, many of these details had to be

learned the hard way and experience has emphasized the fact that the difference between success and failure in achieving a desired type of vibration in a complicated structure may be a matter of many small and unforeseen factors. We have tried to err on the side of too much rather than too little detail.

We cherish no illusion of having covered our subject completely. We hope only that this record of our efforts will give future workers in the field the benefits of our successes and spare them the embarrassment of repeating our failures.

PAUL E. SABINE

CONTENTS

CHAPTER	PAGE
1 Introduction	1
2 Transducers as Multiterminal Networks	22
3 Magnetostrictive Vibrators and Equivalent Circuits . .	35
4 Magnetic and Magnetostrictive Properties of Materials .	62
5 Directivity Patterns	105
6 Radially Vibrating Transducers	139
7 Longitudinally Vibrating Laminated Stacks	176
8 Tube-and-Plate Transducers	223
9 Measurement of Electrical Characteristics	237
10 Open-Water Measurement at HUSL	288
11 High Power Driving of Magnetostrictive Transducers . .	323
12 Future Developments	356
13 Theory and Design of Magnetostriction Scanning Sonar Transducers	365
14 Construction and Testing of Scanning Transducers . . .	423
Glossary	451
Bibliography	455
Contract Numbers	477
Index	479

Chapter 1

INTRODUCTION

Among the many devices that have been proposed and used for producing and detecting acoustic waves in water, two types have proved to be most effective. The first type employs the piezoelectric properties of crystals for electroacoustic transformation of energy. The second operates by virtue of the magnetostrictive properties of ferromagnetic materials. The magnetization of a specimen of such material involves certain changes in its internal structure which set up stresses in the specimen and minute changes in its physical dimensions. The phenomena associated with these changes are known under the general term *magnetostriction*. According to generally accepted theory, a ferromagnetic material is made up of elementary "domains," regions throughout which the inherent magnetization is unidirectional. In the unmagnetized state, the magnetization of the domains is oriented in random fashion with reference to each other, so that their resultant magnetic moment is nil. Under the action of an imposed magnetic field there is an alignment of the magnetization of the domains in the direction of the applied field, with resultant internal stresses and strains. The effect, in any particular case, is associated with the molecular, crystalline, and grain structure of the metal in question, and the magnetostrictive forces developed in a body under restraint are accordingly very great.

Although a detailed theoretical treatment of the phenomenon is outside the immediate purpose of this book, an elementary account of the mechanics of magnetostrictive action and the relation of magnetostrictive properties to the other magnetic properties of metals and alloys may serve as a useful background for a more detailed presentation later.

1.1 FUNDAMENTAL MAGNETIC RELATIONS — STEADY STATE

The concept of the magnetic field of force is fundamental in electromagnetic theory. Such a field exists in the neighborhood of permanent magnets and of conductors carrying electric currents. It is represented by a space vector whose magnitude and di-

rection at any point correspond to those of the force on an idealized unit North magnetic pole at that point.

For the purpose of illustration and definition of terms, the familiar laboratory experiment is used of measuring by the ballistic method the magnetization of a sample of ferromagnetic material, such as nickel. For simplicity, the magnetizing field is assumed to be set up inside a long solenoid by a direct current i flowing through the windings, and the solenoid and the nickel core are taken to be long enough so that the effect of the free poles induced at the two ends is negligible. Without the core, the uniform field in oersteds within the solenoid is given by the familiar equation

$$H = 4\pi in, \quad (1)$$

where n is the number of turns of the windings per unit length and i the current in abamperes.

Suppose that without the core a thin secondary or search coil of n_s turns enclosing an area of A_s sq cm be placed at the midpoint of the solenoid, and that the terminals of the coil be connected to a ballistic galvanometer. The total magnetic flux Φ (maxwells) through the search coil is $A_s B = A_s(\mu H)$. B is the flux density (gauss), sometimes called the "magnetic induction," and μ is the magnetic *permeability* of the core material. For air, μ is a constant and approximately equal to unity. For ferromagnetic materials μ is a function of H , and for any assigned value of H , the value of μ will depend upon the temperature and the previous history of the sample.

By Faraday's law, the emf in abvolts generated in the search coil by varying the normal component of the magnetic flux through it is given by the equation

$$\epsilon_s = -n_s \frac{\partial \Phi}{\partial t} = -n_s A_s \frac{\partial B}{\partial t} = -n_s A_s \frac{\partial(\mu H)}{\partial t}. \quad (2)$$

Equation (2) will serve to define Φ , B , and μ .

The search coil and the ballistic galvanometer constitute a flux meter, since by an easy analysis it can be shown that the throw Θ of the galvanometer, produced by a sudden change $\Delta\Phi$ in the magnetic

flux through the search coil, is proportional to that change. Hence

$$\Theta = \alpha \Delta B = \alpha \Delta(\mu H), \quad (3)$$

where α is a proportionality constant involving the area, the number of turns of the search coil, and the total resistance of the search-coil circuit.

If a step-by-step increase is made in the current in the primary windings of the solenoid with an air core, then, since μ for air is a constant, the cumulative throws of the ballistic galvanometer will increase linearly with the current. With a ferromagnetic nickel core, however, the results are quite different. Under the action of the magnetizing field, there will be a reorientation of the magnetic fields of the

is zero, I is zero — that is, if the specimen is initially unmagnetized — then for any value of H ,

$$B = H + 4\pi I = \mu H,$$

$$\mu = 1 + 4\pi \frac{I}{H} = 1 + 4\pi \kappa,$$

and κ is called the *susceptibility* of the ferromagnetic material.

In Figure 1 the solid line is the magnetization curve for commercial A-nickel annealed at a temperature of 1000 C in air. Initially the specimen was in the demagnetized state. The magnetizing field was increased from zero in definite steps, with a number of reversals of the field at each step. Each plotted

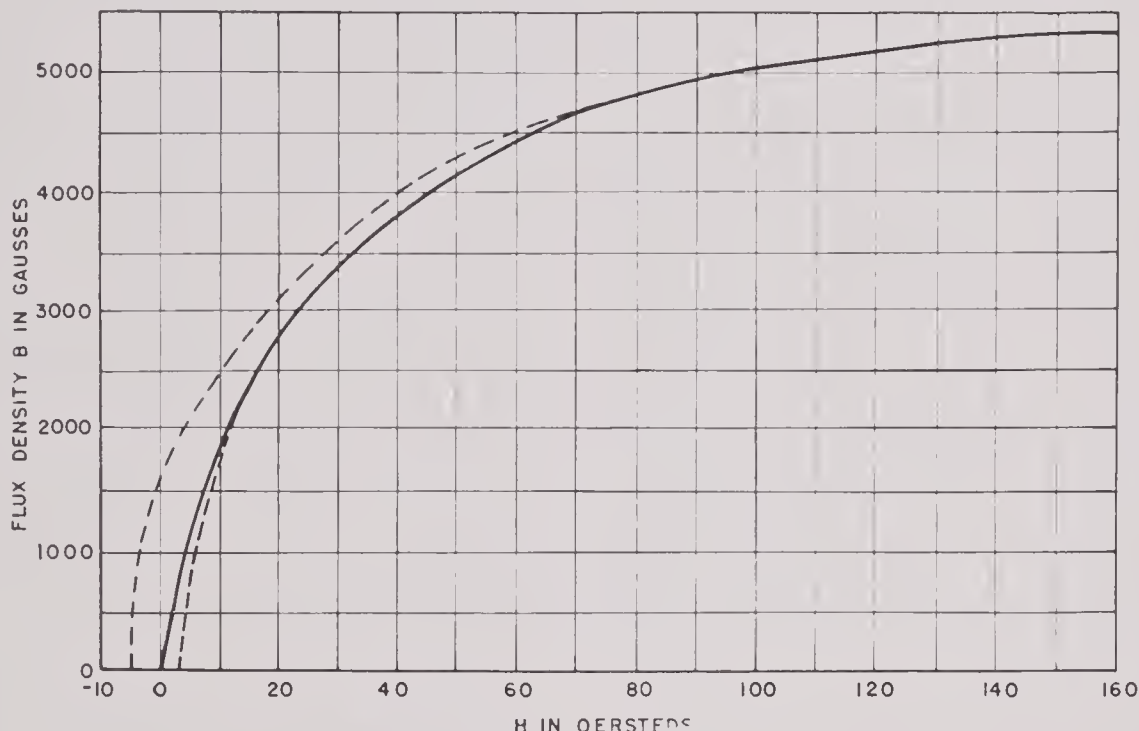


FIGURE 1. Magnetization and hysteresis of annealed A-nickel.

domains, with a resultant increase in the magnetic moment of the core. Assume that the search coil occupies the same position as formerly but lies in a narrow transverse slot cut in the core. Then the increment in the flux through the coil resulting from an increase in H will include also a term due to the increase in the induced magnetization. If it is assumed that the sample is uniformly magnetized and if the magnetic moment per unit volume is denoted by I , then the contribution of the induced magnetization to the flux density through the search coil is $4\pi I$. Hence, for an increment ΔH in the magnetizing field, the increment in B is given by the equation $\Delta B = \Delta(H + 4\pi I) = \Delta(\mu H)$. If when H

point represents the final constant value of B , attained after a series of reversals. Such a curve is referred to as the "normal magnetization curve."

To clarify further the meaning of our terms, suppose a very narrow slot is cut *across* a sample of ferromagnetic material in a magnetic field (Figure 2). There will be in the slot a flux density H due to field. Free poles of strength I per unit area will be induced on the free faces of the slot. The flux density across the slot due to these poles will be $4\pi I$. The total flux density is then $H + 4\pi I$. If, instead of the transverse slot, a long needle-like slot is parallel to the field, then the contribution of the induced magnetization to the flux density at the measuring point

within this slot will be negligible, and the measured flux density will be H alone. It is to be noted that B , H , and $4\pi I$ are all quantities of the same kind and are expressible in the same units. But it is convenient — particularly in the case of the magnetic

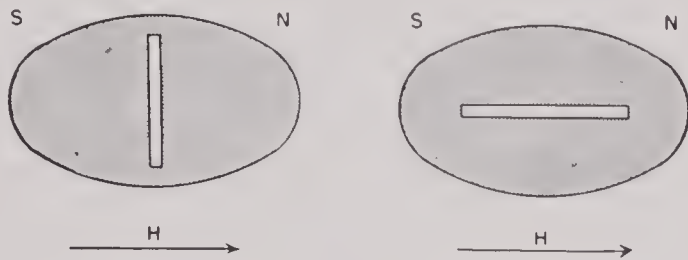


FIGURE 2. The relation $B = H + 4\pi I$.

circuit — to think of the flux as analogous to current and the field as a magnetomotive force corresponding to emf in the electric circuit. Hence H and B are quantities of the same kind, but for convenience are expressed in different units, the first in oersteds, the second in gauss.

In the preceding paragraphs, the various relations have been based on the fundamental laws of electromagnetism. The equations given hold only when the quantities involved are in absolute electromagnetic units. Table 1 gives the numerical relation between the practical and the electromagnetic units.

TABLE 1

Quantity	Symbol	Practical unit	Value in emu
Electric charge	q	coulomb	10^{-1}
Electromotive force (and electric potential)	e	volt	10^8
Capacity	C	farad	10^{-9}
Current	i	ampere	10^{-1}
Resistance	R	ohm	10^9
Inductance	L	henry	10^9
Magnetic pole strength	m		1
Magnetic field strength	H	oersted	1
Intensity of magnetization	I		1
Magnetic induction	B	gauss	1
Flux density			
Magnetic flux	Φ	maxwell	1

Various systems of units are employed in practice, but unless otherwise indicated the practical units as defined above will be used hereafter. Thus, if induced emf is expressed in volts and Φ in maxwells,

$$e \text{ (volts)} = -n_s \frac{\partial \Phi}{\partial t} \times 10^{-8}, \quad (4)$$

The value of H in oersteds in the solenoid, when the current i is expressed in amperes, is

$$H = \frac{4\pi in}{10}. \quad (5)$$

1.2 HYSTERESIS, REMANENCE, COERCIVE FORCE

In Figure 3 are shown the results of measurements made on a sample of hard-drawn unannealed nickel tubing. Starting with the sample in the unmagnetized state, the values of B for increasing values of H are shown by the solid curve. The measured values of B , when H is decreased step by step from its maximum value, are shown on the broken curve. For any given value of H the value of B is greater when the magnetizing field is decreasing than when it is increasing. The phenomenon is known as *hysteresis*. When the field is reduced to zero, the flux density still has a value B_r . The value of the flux density which remains in a magnetic material after the magnetizing field is removed is called the *remanence*. The magnitude of B_r will depend upon the maximum value of B which was initially attained. The value of B at which an increment in H produces no more than an equal increment in B is called the saturation value. *Retentivity* is the remanent flux density after a magnetizing field sufficient to produce saturation has been removed.

If an alternating field is applied, the values of the flux density will describe a closed hysteresis loop, the upper half of which is shown in Figure 3. In such a process the material is said to be cyclically magnetized and the hysteresis loop is symmetrical about the origin. The value H_c for which B is zero is called the *coercive force*. If the initial magnetization has been carried to saturation, then the coercive force is designated as the *coercivity*.

In Figure 3 the solid curve is the “normal magnetization” curve for the sample. Obviously the value of μ as previously defined will depend upon the previous history of the sample. Thus, for any value of H , three different values of B are shown, and hence we have three different values of μ . One of these, the *static permeability*, is considered to be the value of B/H as given by the normal magnetization curve. In Figure 4, the values of μ and κ (susceptibility) for the sample of hard nickel shown in Figure 3 are plotted against H . The magnetic properties of materials under the action of alternating fields will be discussed in Chapter 4.

1.3 STATIC MAGNETOSTRICTION — HISTORICAL

As already noted, the magnetization of ferromagnetic material sets up internal stresses and resultant

strains. Conversely, externally applied stresses generally produce changes in the magnetic state. In 1847, Joule¹⁴ reported "The Effects of Magnetism upon the Dimensions of Iron and Steel Bars." In

the strain in an annealed sample of nickel is plotted against the applied magnetic field. In Figure 6 the linear relation between the logarithm of the strain and the $\log (B - H)^2$ is shown.²³

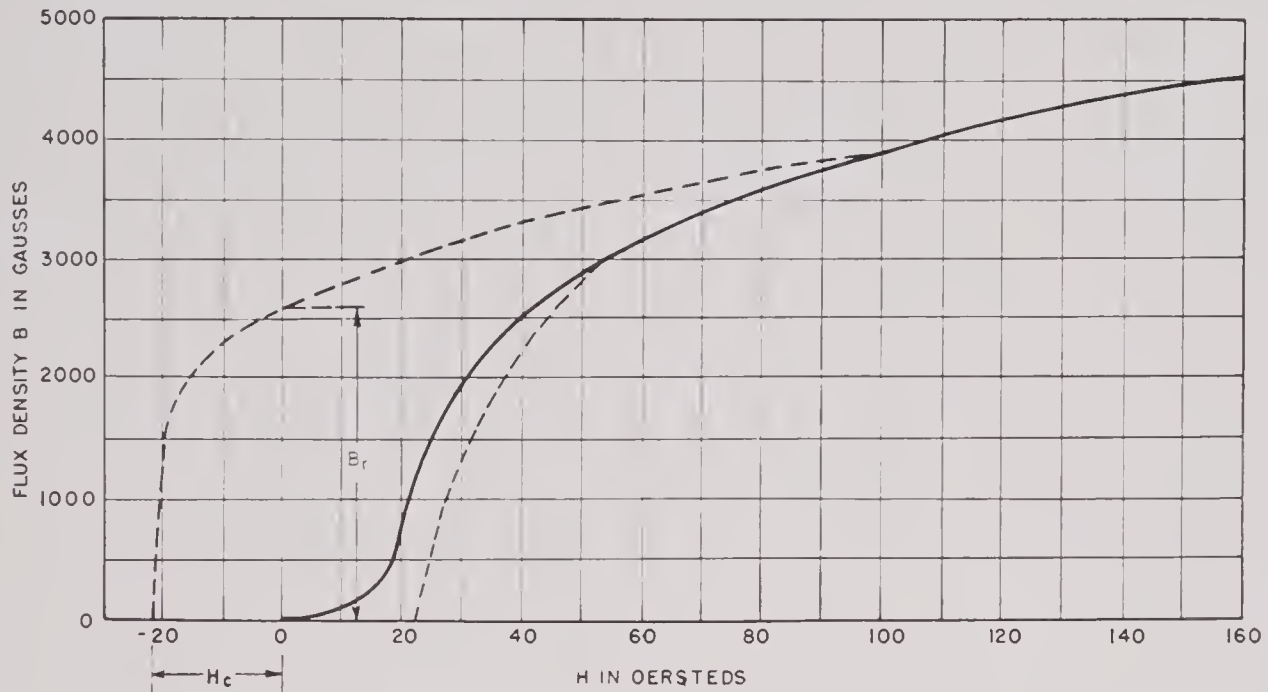


FIGURE 3. Remanence and coercive force of hard-drawn nickel.

his experiments the test specimen, a bar of iron or steel fixed at one end, was mounted in a magnetizing solenoid. The change in length under constant stress was amplified by a system of levers and measured with a micrometer microscope. What he called the "magnetic intensity" was measured by balancing the pull exerted by the induced magnetic pole on one end of a suspended magnet by weights applied to the opposite end. As the results of numerous experiments, he found that the elongation in a given

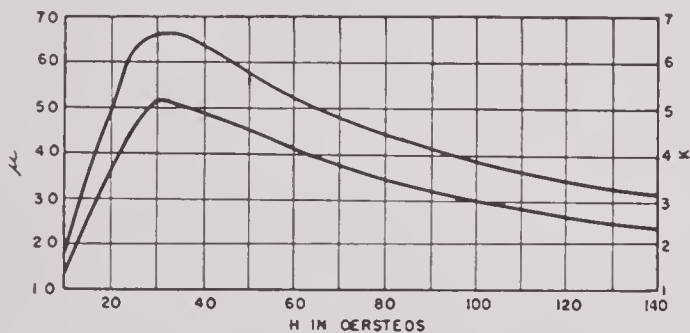


FIGURE 4. Permeability and susceptibility of hard-drawn nickel.

bar is proportional to the square of the magnetic intensity and that the elongation is greater in an annealed than in an unannealed bar. In Figure 5

In 1868, E. Villari¹⁵ reported the reverse magnetostrictive effect, namely, that varying the stress in a magnetized body will produce changes in the induced magnetization or a change in the susceptibility. In his experimental apparatus, the magnetostrictive sample was mounted along the axis of a solenoid. A secondary winding around the sample was connected to a ballistic galvanometer. The galvanometer throw produced by longitudinally stressing the magnetized bar at a constant value of H gave a measure of the change in the induced magnetization. By using bars of iron and steel he arrived at the conclusion that the change of magnetization resulting from a constant stress increases with the magnetizing field up to a certain value of the field. Beyond this value, the change in magnetization for a given incremental stress decreases with increasing field. In Figure 7 the change in magnetization of nickel is plotted for different values of the magnetizing field against the tension which produces it.

Later studies made on ferromagnetic materials of the two magnetostrictive effects (the change in volume with magnetization — the Joule effect — and the change of susceptibility under mechanical

stress) have confirmed the fundamental discoveries of Joule and Villari. They have shown, however, that the relations involved are far from simple and differ widely from material to material and with heat treatment and history for the same material.^a

1.4 HYSTERESIS AND MAGNETOSTRICTION

As in the case of the induced magnetization, the magnetostrictive effect does not follow the same course for a rising as for a falling magnetizing field.

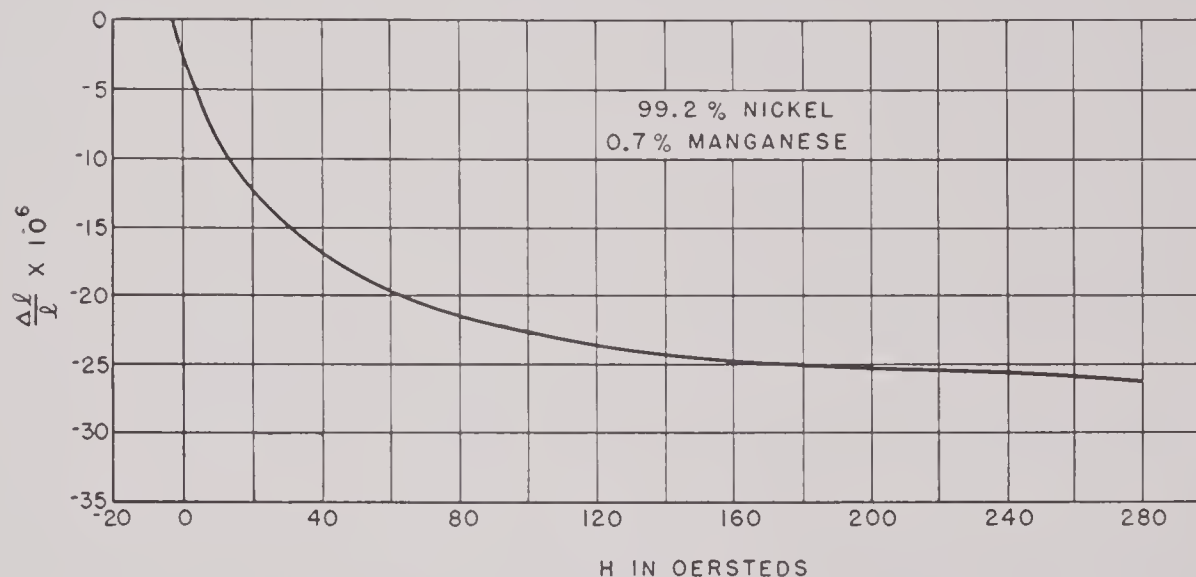


FIGURE 5. Magnetostrictive strain as a function of field for annealed nickel.

This is shown in Figure 8 for a sample of annealed nickel wire.²⁸ Note the low value of $\delta l/l$ when the field is reduced to zero, corresponding to the magnetostriction under remanent magnetization; also note the similarity in shape to the shape of the magnetization curve. However, since the magnetostrictive contraction is not dependent upon the direction of the applied field, the curve does not fall below the horizontal axis for negative fields as does the magnetization curve. Obviously the response frequency of a magnetostrictively driven device without biasing polarization will be double the driving frequency.

Further, the nonlinearity between the exciting field and the strain indicates that distortion is to be expected in magnetostrictive transducers. This effect is mitigated by the fact that such transducers are

usually designed to operate at the resonant frequency of vibrating systems in which the mechanical resonance is comparatively high, thus enhancing the response at the driving frequency relative to the harmonic components of the distorted vibration.

The data for Figure 8 were obtained from static measurements and show a much greater range in the value H than can be attained in actual practice with a-c fields. The somewhat complicated problem of the relation between electric excitation and acoustic response will be considered in detail in later chapters.

1.5 MAGNETOSTRICTIVE CONSTANT AND YOUNG'S MODULUS

Joule concluded from his experiments that the change in length of a rod in a magnetic field is proportional to the square of the induced magnetization. Later work has shown that for moderate flux densities in most ferromagnetic materials the strain is approximately proportional to the square of the flux density. We may therefore write

$$s = cB^2,$$

where c is simply a proportionality factor, which is positive for a material that expands with increasing magnetization and negative for one that contracts. Permalloy expands when magnetized and c is positive. In the case of nickel the reverse is true and c is negative. Following the usual convention, tension and expansion are treated as positive stress and strain respectively, whereas pressure and contraction are considered negative.

^a For an account of this work with reference to original papers, see references 16, 25, and 27. For a résumé of the data on iron and nickel alloys, see reference 31.

If the flux density in a sample of magnetostrictive material is changed from B_0 to $B_0 + \delta B$ without change of stress, then the strain changes by an amount

$$\delta s = \frac{\partial}{\partial B}(cB^2)\delta B = 2cB_0\delta B, \quad (6)$$

or
$$\left[\frac{\partial s}{\partial B}\right]_P = 2cB_0.$$

Conversely, if the length of the magnetostrictive sample is kept constant ($\delta s = 0$) while the flux density changes from B_0 to $B_0 + \delta B$, the stress changes by an incremental amount,

$$\delta P_{(\text{constant } s)} = -\lambda\delta B. \quad (7)$$

The magnetostriction constant λ is defined by the equation

$$\lambda = -\left(\frac{\partial P}{\partial B}\right)_s.$$

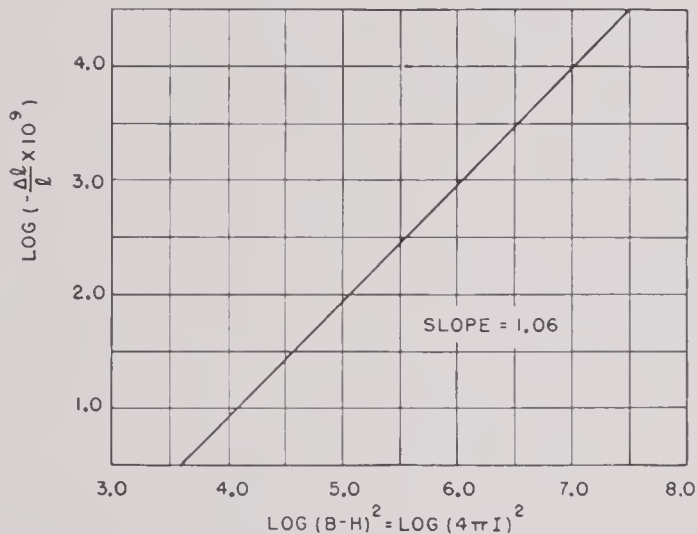


FIGURE 6. Logarithm of strain vs $\log (B-H)$ for annealed nickel.

The negative sign here may perhaps be questioned, but it follows our convention of signs for stresses and strains. If, for example, in a given material under constant stress, an increase in B produces an increase in length (positive strain), then in order to keep the length (strain) constant when B increases, a pressure (negative) stress must be applied. Nickel contracts with increasing B , or $[\partial s/\partial B]_P$ is negative. Hence a tension (positive stress) must be applied to keep the length constant under increasing magnetization, so that λ for nickel is intrinsically negative.

If a magnetostrictive rod is simultaneously subjected to a change of magnetization δB and an in-

cremental strain δs , both acting along its length, then δP , the total stress, is given by the equation

$$\delta P = E\delta s + \left[\frac{\partial P}{\partial B}\right]_s \delta B = E\delta s - \lambda\delta B, \quad (8)$$

where $E = [\partial P/\delta s]_B$ is the Young's modulus at constant flux density.

It will be shown in a later chapter that a change δB in B in a magnetostrictive material arises from two causes—a change δH in the external magnetizing field and a second change produced by the

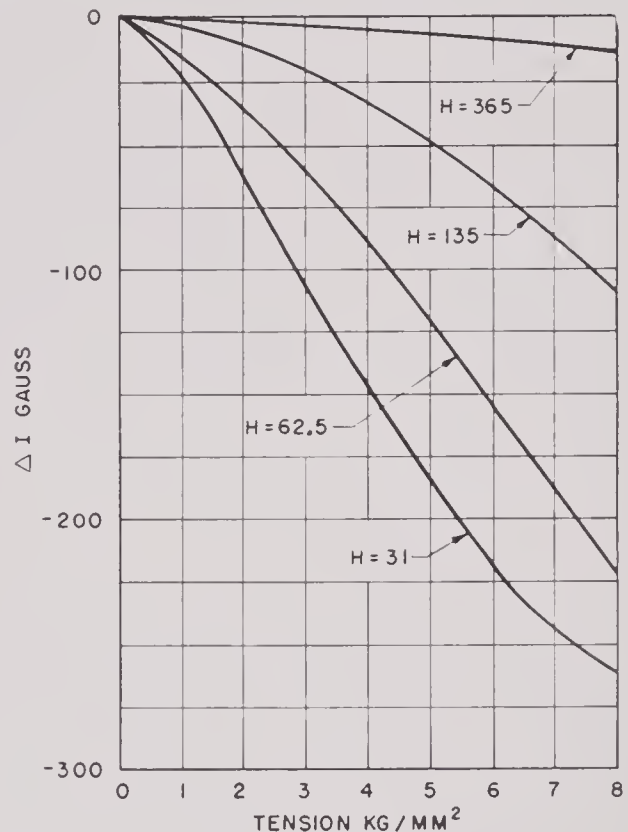


FIGURE 7. Incremental magnetization as function of applied stress in nickel.

incremental strain δs . The total increment in B then is given by the relation

$$\delta B = \mu_r(\delta H + 4\pi\lambda\delta s), \quad (9)$$

where μ_r is the *reversible permeability* (defined in the next section) of the material at the particular value of B_0 from which the change occurs. From equations (8) and (9),

$$\begin{aligned} \delta P &= E\delta s - \lambda\mu_r(\delta H + 4\pi\lambda\delta s) \\ &= -\lambda\mu_r\delta H + (E - 4\pi\lambda^2\mu_r)\delta s. \end{aligned} \quad (10)$$

Suppose that B equals B_0 , H is held constant ($\delta H = 0$) and an incremental stress δP is applied. Then from equation (10),

$$\left[\frac{\partial P}{\partial s}\right]_H = (E - 4\pi\lambda^2\mu_r) = E'. \quad (11)$$

Here E' is the effective Young's modulus of the magnetostrictive material at a given value of H and a corresponding value of B , and it is this modulus that determines the resonant frequency of a magnetostrictive transducer. E' may be written in the form

$$E' = E \left(1 - \frac{4\pi\lambda^2\mu_r}{E} \right) = E(1 - k^2), \quad (12)$$

where $k = \left(\frac{4\pi\lambda^2\mu_r}{E} \right)^{\frac{1}{2}},$

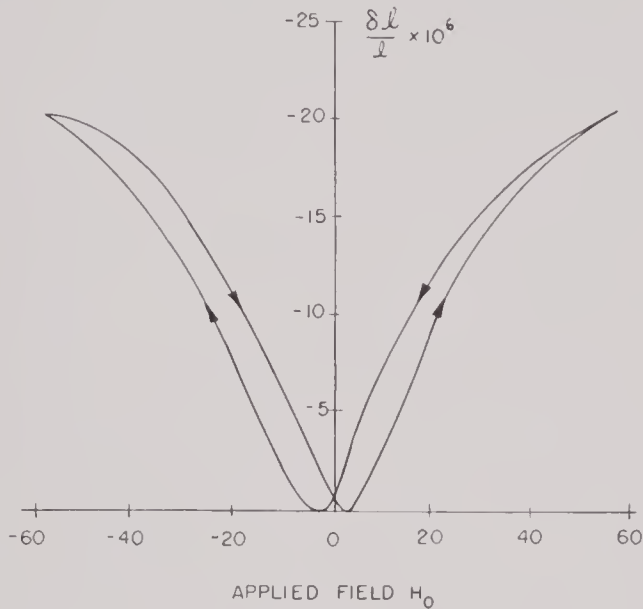


FIGURE 8. Hysteresis in magnetostrictive strain.

and is called the *coefficient of electromechanical coupling*. It is a measure of the degree of coupling that can be obtained between the electrical and mechanical sides of a transducer. Both the efficiency and the breadth of the frequency response will be shown to depend upon the value of k . Since both μ_r and λ are functions of B , it is obvious that the maximum value of k corresponds to the value of B , for which $\lambda^2\mu_r$ is a maximum. Hence the magnetostrictive elements of a transducer should be polarized to give this value of B if the transducer is to operate at maximum efficiency.

Table 2 shows the effect of lamination thickness and polarizing flux density on magnetostrictive quantities. Table 3 gives the several properties of magnetostrictive materials.

1.6 REVERSIBLE PERMEABILITY

Reference has been made in the foregoing treatment to "reversible permeability." If H varies periodically about a constant biasing field H_0 , then B will

describe a minor hysteresis loop. If $H = H_0 \pm \delta H/2$ (Figure 9), then the total swing in H will be δH , from which will result a cyclical change in the flux density. The reversible permeability μ_r is defined as the limiting value of $\delta B/\delta H$ as δH approaches zero. If

TABLE 2. Effect of thickness and polarizing flux density on magnetostrictive quantities.*

Material	Thickness (inch)	B_0	$\lambda \times 10^{-4}$	Max eff
A-nickel (1 hr at 1000 C in H_2)	0.002	4,000	1.25	0.78
	0.002	5,000	1.99	0.83
	0.002	5,500	2.10	0.83
45-Permalloy	0.001	12,000	0.39	0.82
	0.002	12,000	0.32	0.70
	0.002	13,000	0.48	0.75
	0.002	14,000	0.62	0.80
	0.004	12,000	0.35	0.60
	0.006	12,000	0.27	0.25
	0.014	12,000	0.36	0.15
2V-Permendur (annealed 1 hr at 550 C in H_2)	0.002	16,300R†	1.07	0.85-0.93
		to	to	
	0.002	19,400R†	1.25	
	0.004	14,300R†	0.92	0.82
	0.006	18,360R	1.04	0.77
	0.012	10,200R	0.69	0.17

* *Magnetic Materials for Magnetostriction Microphones and Projectors*, Williams, Nesbitt, and Goertz, Bell Telephone Laboratories, Inc., March 22, 1944.

† Remanent flux density.

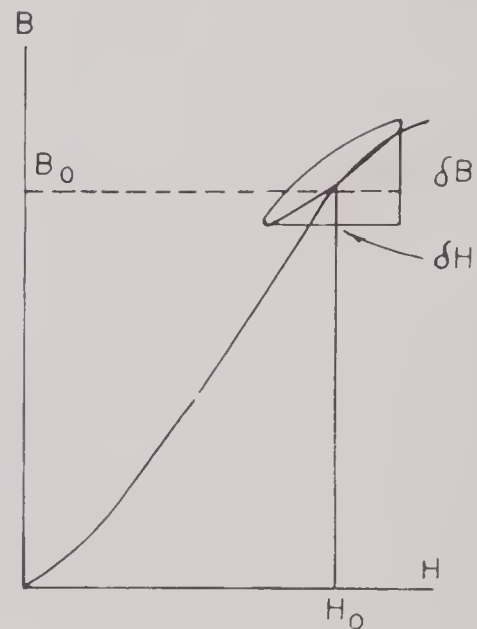


FIGURE 9. Reversible permeability.

in static measurements δH is from 10 to 20 per cent of H_0 , the measured value μ_δ will approach very nearly the true reversible permeability. In Figure 10 are shown measured values of μ_δ plotted against $I = (B - H)/4\pi$ for two samples of commercial nickel

annealed in air at 1000 C. Here is an illustration of what seems to be generally true, that is, for magnetically soft materials, the reversible permeabilities

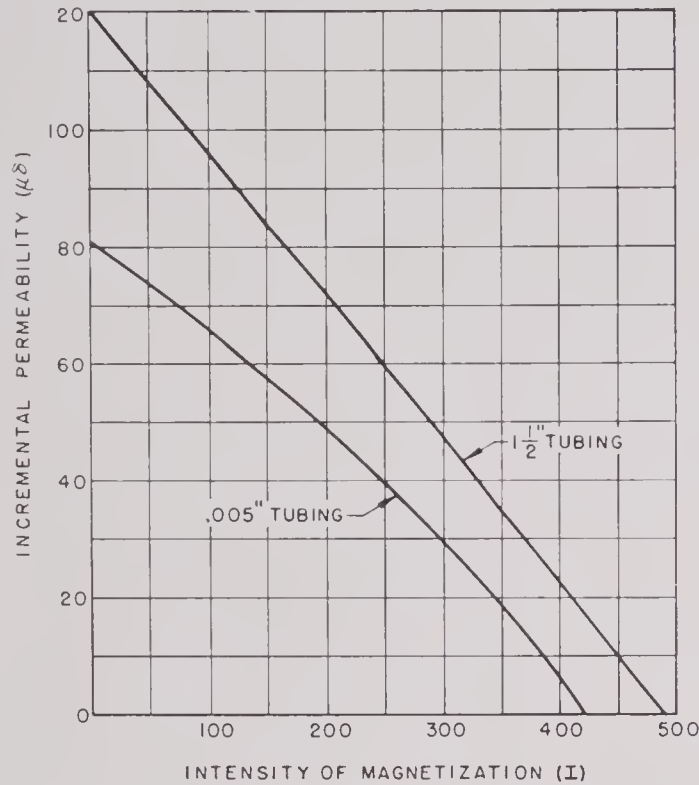


FIGURE 10. Reversible permeability of nickel as a function of $(B - H)$.

so plotted fall on a straight line. More accurate measurements of μ_r can be made by alternating-current methods, which will be considered in detail

in Chapter 4. Hereafter, unless otherwise stated, it will be the reversible permeability with which we are concerned here, designated simply as μ or μ' (see Chapter 4) without the subscript.

1.7 **MAGNITUDE OF MAGNETO-
STRICTIVE FORCES**

Some simple calculations based on the data presented above will serve to give an idea of the order of magnitude of magnetostrictive forces.

For most design purposes the following numerical values for nickel are adequate:

- Young's modulus $E = 2.10 \times 10^{12}$ dynes per sq cm.
- Density $\rho_n = 8.9$ gm per cu cm.
- Velocity of sound $c_n = 4.9 \times 10^5$ cm per sec.

As a numerical illustration, consider a nickel rod whose fundamental longitudinal resonance frequency f_r is 20 kc. The length of the rod having this resonance frequency

$$l = \frac{c_n}{2f_r} = \frac{4.9 \times 10^5}{2 \times 2 \times 10^4} = 12.3 \text{ cm.}$$

For a magnetizing field of 125 oersteds, we have from Figure 5 $\delta l/l = -25 \times 10^{-6}$, and the contraction of the rod would be $25 \times 10^{-6} \times 12.3 = 3.1 \times 10^{-4}$ cm. If by some mechanical restraint the length of the rod is kept constant, the resultant stress equals $25 \times 10^{-6} \times 2.10 \times 10^{12} = 5.5 \times 10^7$ dynes per sq cm = 800 lb per sq in.

TABLE 3. Properties of magnetostrictive materials.*

H_c = Coercive force (oersteds)
 μ = Reversible permeability
 B_0 = Polarizing flux density

k = Coupling coef. = $\left(\frac{4\pi\lambda^2\mu}{E}\right)^{\frac{1}{2}}$
 λ = Magnetostrictive constant
 ρ_e = Resistivity ohms-cm.

Maximum efficiency for an assumed $Q = 4$
All tests made on samples 0.002" thick.

Material	Heat treatment	$\rho_e \times 10^6$	H_c	μ	B_0	$\lambda \times 10^{-4}$	k	Max eff
A-nickel	Unannealed	8.0	19.	13	3,200R†	1.02	0.09	0.61
	600 C	8.0	14.3	30	3,640R†	1.10	0.15	0.79
	1000 C	8.0	0.76	166	2,128R†	0.44	0.14	0.39
	1000 C in H ₂	8.0	78	4,000	1.25	0.27	0.78
	1000 C in H ₂	8.0	41	5,000	1.99	0.32	0.83
45-Permalloy	Unannealed	45	7.60	53	8,600R†	0.31	0.054	0.64
	1000 C in H ₂	45	0.26	1,768	5,840R†	0.05	0.008	0.045
	1000 C in H ₂	45	372	12,000	0.32	0.16	0.70
2V-Permendur	1000 C	25	1.90	42	9,920R†	0.40	0.06	0.76
	800 C	25	91	20,000	1.37	0.32	0.90
	650 C	25	9.1	126	13,950R†	0.85	0.21	0.92
	600 C	25	18.4	59	17,500R†	1.23	0.24	0.92

* *Magnetic Materials for Magnetostriction Microphones and Projectors*, Williams, Nesbitt, and Goertz, Bell Telephone Laboratories, Inc., March 22, 1944.
† Remanent flux density.

The maximum alternating stress that can usefully be produced by the magnetostriction of nickel has been calculated to be between 2.5×10^7 and 10×10^7 dynes per sq cm. For the 20-ke half-wave rod this would correspond to a contraction of 1.47×10^{-4} cm. These values are for the stress within the nickel in the region of maximum strain — that is, at a motion node. The pressure that could be exerted upon water in any actual case would depend on a number of factors, for example, the sharpness of the mechanical resonance of the vibrator and the ratio of the cross section of the surface in contact with the water to the cross section in the region of maximum strain

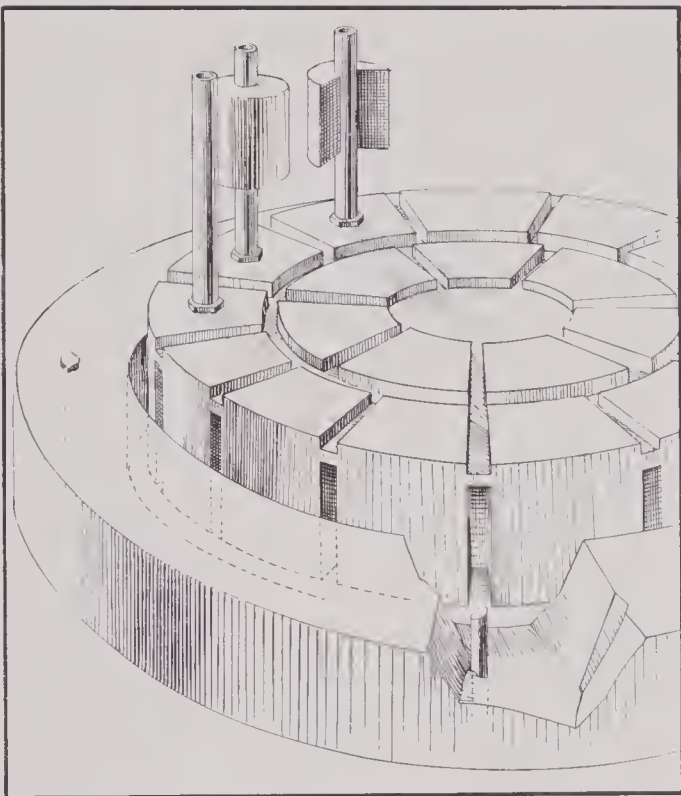


FIGURE 11. Early form of tube-and-plate transducer.

in the nickel. In some experiments on the maximum obtainable output of laminated nickel stacks made at the Harvard Underwater Sound Laboratory [HUSL], acoustic pressures as great as 8×10^6 dynes per sq cm (approximately eight atmospheres) were produced in an oil-filled pressure chamber by a stack of nickel laminations driven by magnetostriction. This is roughly 12,000 times the pressure in an atmospheric sound wave that is at the threshold of pain for the human ear. There is an obvious advantage in applying magnetostrictive vibrations of small amplitude and large force to the generation of acoustic waves in a highly incompressible medium like water.

1.3 MAGNETOSTRICTIVE VIBRATIONS

It is difficult to assign a date or allocate the credit for the first application of magnetostriction to the generation of acoustic waves in water, but it can be said that recognition of the possibility of such an application stems from the researches of G. W. Pierce and co-workers at Harvard in the period beginning about 1925. The original notes of Pierce's experiments, which he placed at the disposal of the HUSL group, proved of invaluable help in the initial stages of the work in this field at Harvard. In his handbook on underwater sound technique

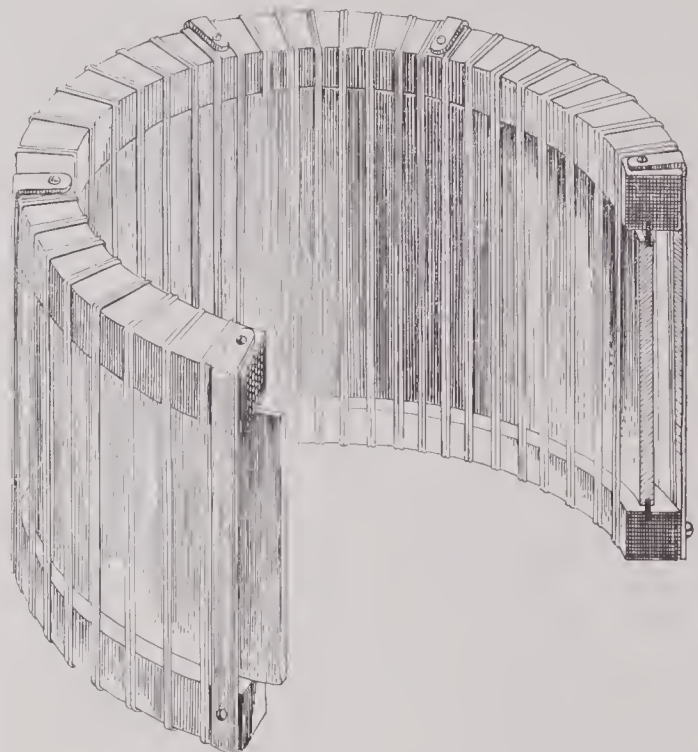


FIGURE 12. Early example of radially vibrating cylinder.

published in 1922, Aigner¹⁸ makes no mention of underwater devices operating on this principle. The small amplitude attainable makes possible only small amounts of radiated power at audible frequencies. Since the radiated power is proportional to the square of the product of the amplitude and frequency, it is generally necessary to go to supersonic frequencies to realize acoustic powers of useful magnitude. Prior to the development of vacuum-tube oscillators and amplifiers, electric oscillations in the supersonic range were not easily obtained. Moreover, the earlier use of piezo-electric crystals for the production of high-frequency mechanical vibration pretty well pre-empted the field.¹⁷

CONFIDENTIAL

In a patent application filed January 3, 1927, Pierce^{21,24} disclosed a magnetostrictive oscillator consisting essentially of a magnetostrictive tube or rod



FIGURE 13. A. An underwater sound magnetostrictive device to be operated at a frequency of about 18 kc. It was toroidally wound on a nickel tube about 4 in. in diameter and oil-filled with an outer jacket of rubber. B. Stacks of magnetostrictive laminations toroidally wound for supersonic applications.

clamped at the midpoint and excited by means of an alternating current superimposed on a direct polarizing current. He suggests a means of generating sound waves in water by attaching a magnetostrictive rod to the steel plates on the opposite

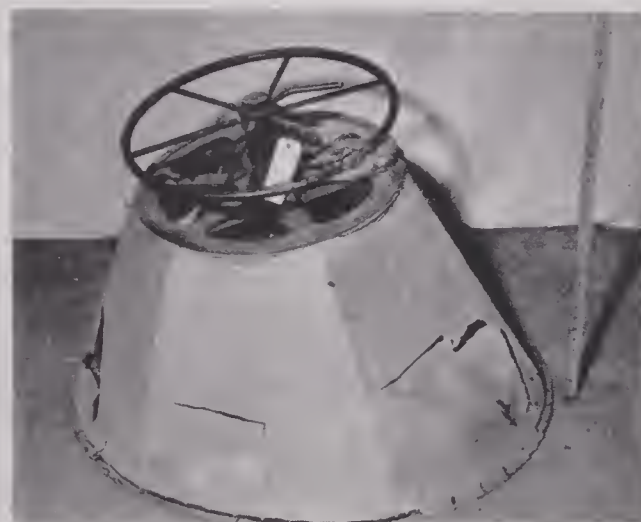
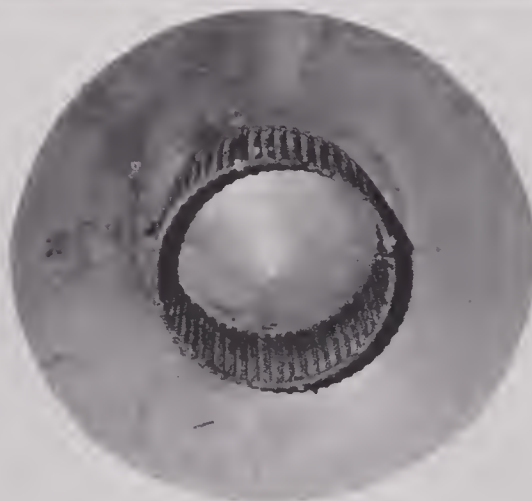
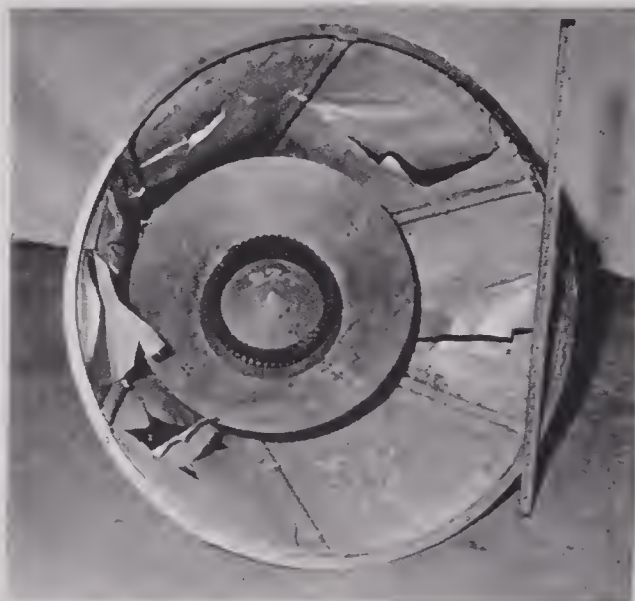


FIGURE 14. Magnetostrictive unit designed for altidrift measurements on the dirigible USS *Akron*. It was designed to operate at about 8 kc. A similar unit about one foot in diameter surrounded by a metal cone was also tried for underwater echo ranging (N933-34).

sides of a ship's hull and exciting the rod with tuned alternating current in a coil surrounding the rod.

One of the earliest experimental studies of magnetostrictive vibrations was reported in 1928 by K. C. Black,²² working with Professor Pierce. These studies were made on samples clamped at their mid-point within a magnetizing solenoid and free to vibrate longitudinally as half-wave oscillators, using

electric energy or the reverse. The most efficient types of magnetostrictive transducers are those operating at or near a resonant frequency of the magnetostrictive driving member. Two general types have been developed: (1) those employing the longitudinal vibrations of rods, tubes, or laminae, and (2) those employing the radial vibrations of tubes or rings. For a transfer of power from the

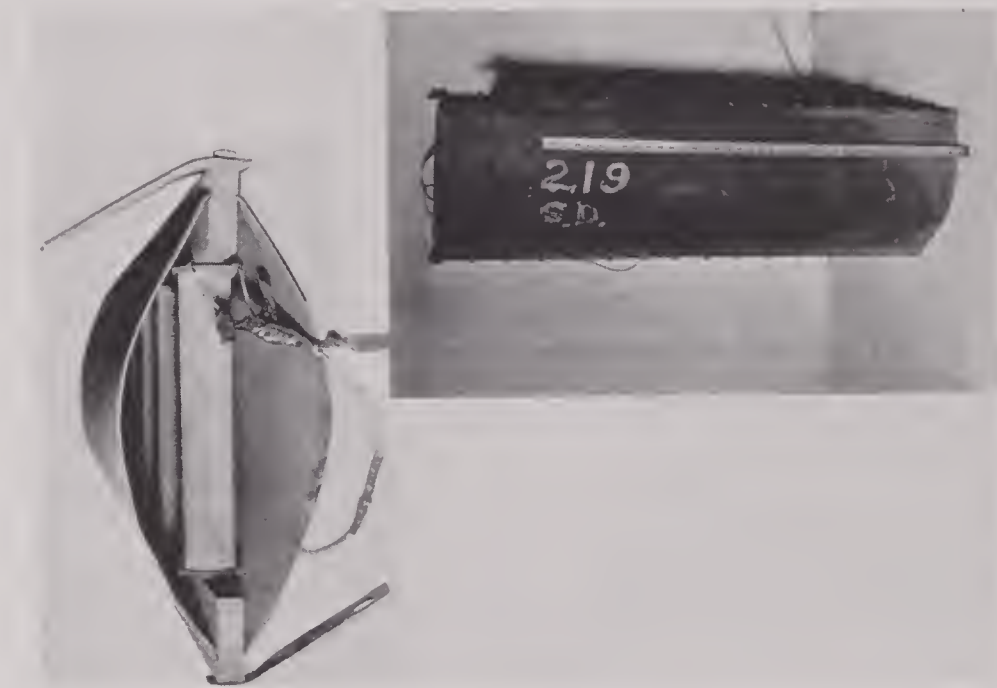


FIGURE 15. Air horns built at NRL in May 1929. The individual tubes, driven longitudinally, were anchored to the vertical members of the vibrating system. The shape of the vibrating area was such as to produce mechanical amplification of the magnetostrictive displacement.

the impedance methods developed by Kennelly and Pierce³² for the study of telephone receivers. Samples of Invar, stainless steel, and nickel were studied. Under applied alternating fields at resonance, vibrational amplitudes were produced several hundred times as great as the static displacement by a d-c field of equal strength. The motional impedance in annealed nickel was found to reach a maximum with a polarizing field of about 30 oersteds.

The resistive component of the motional impedance at resonance and the lag between the magnetic flux and applied current were greater in rods than in tubes. The flux change due to the vibration was found to be greatest at the motion node. All these findings are of importance in the design of transducers for underwater signaling.

1.9 TYPES OF MAGNETOSTRICTIVE TRANSDUCERS

For the purpose of this volume, a transducer may be defined as a device for transforming acoustic to

driving element into the medium, it is essential that the medium present the proper acoustic resistance to the motion of the driver. One of the means employed to this end is the *tube-and-plate*, illustrated in one of its earliest forms in Figure 11.³⁰ Here the driving elements are magnetostrictive tubes whose length is approximately a quarter of the wave length, in the metal, of the sound to be radiated. These are set in massive blocks tuned to the same frequency and are driven in phase by the alternating currents in the coils. Polarizing fields for the magnetostrictive tubes are supplied either by a d-c component of the current or by permanent magnets. The alternating pressure exerted on the plate by the driving elements is transmitted over the entire area of the opposite face. A variant of the tube-and-plate is the *tube-and-cone*. Here the force of the driving element is applied at the apex of the cone, which operates in a manner somewhat analogous to the horn of a loud-speaker as an impedance transforming device.

The radially vibrating tube is illustrated in one of

its earlier forms in Figure 12.²⁹ Here the energizing coil is wound toroidally and the polarizing and alternating flux is circumferential. The lowest radial resonant vibration occurs at a frequency for which the wave length in the metal is equal to the circumference of the tube. A variant of the tube type is the *consolidated stack of ring laminations*. Internal windings on diametral cores of highly permeable

The preceding illustrations, Figures 13 to 16, are photographs of a number of early experimental magnetostrictive transducers made at the Anacostia Naval Research Laboratory.^b

Ring stacks of half-annealed 2V-Permendur (iron-cobalt-vanadium alloy) have been found to be operable at high levels and with relatively high efficiency on remanence.

Figure 17 shows a prototype of laminations which have received considerable attention in the development of *laminated stack* transducers. The lamination

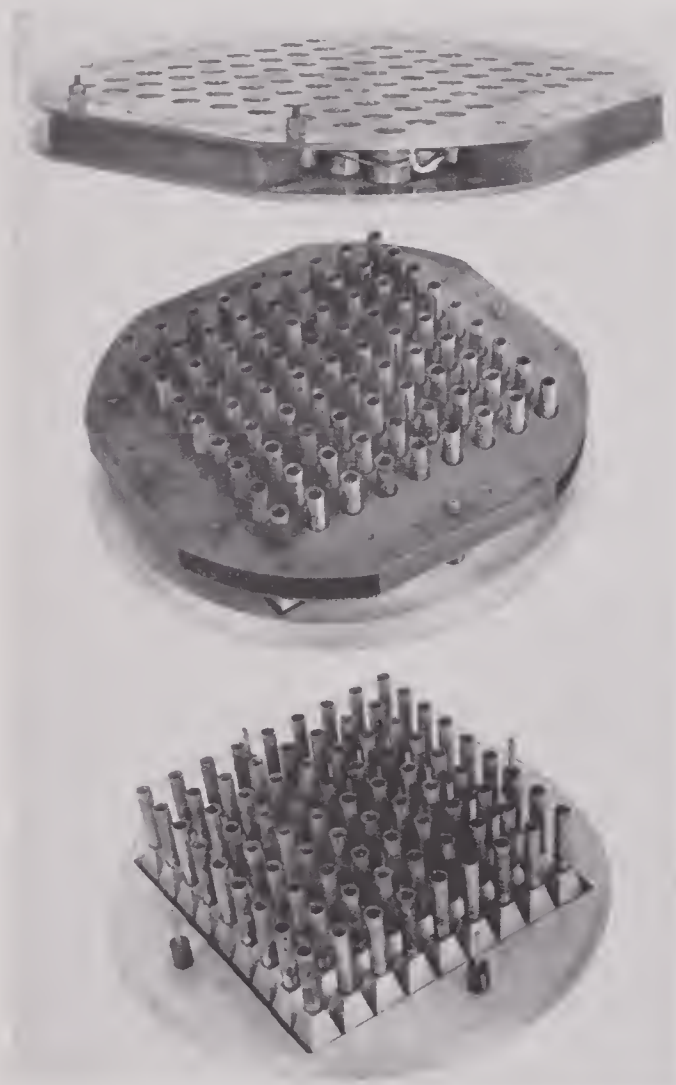


FIGURE 16. Production model of the XQC projectors.

material and armature-type windings on nonmetallic core forms have been used. Since the radially vibrating tube transducers afford a closed magnetic circuit, they may for certain uses be operated on magnetic remanence. Tubes of unannealed and of half-hard nickel with remanent polarization have found extensive use in underwater listening devices. Permanent-magnet polarization of annealed-nickel tubes has been effected by means of Alnico magnets placed on a diameter or inserted in the circumference.

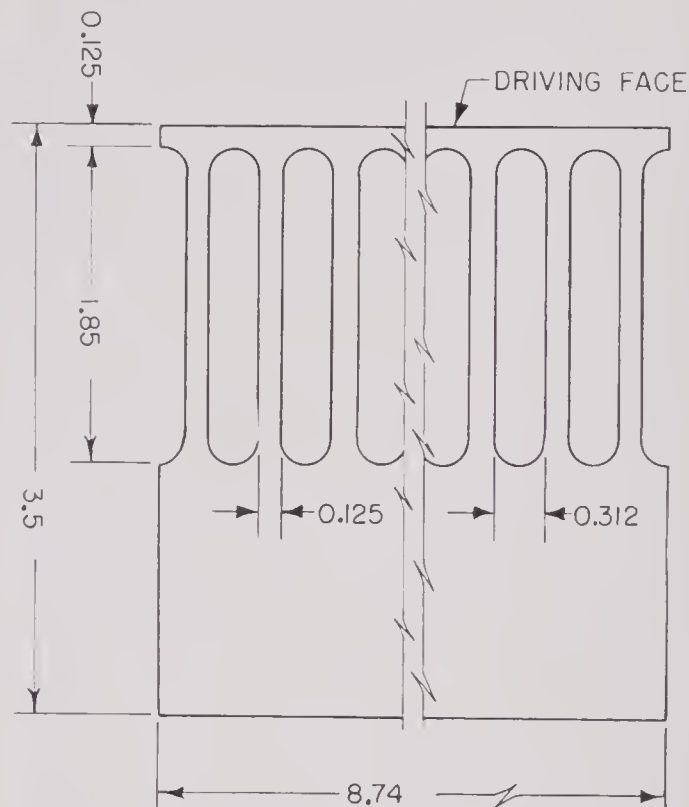


FIGURE 17. Lamination of asymmetrical stack transducer.

is a strip of metal whose width is approximately one-half the wave length in the metal of the frequency to be radiated. Winding slots are cut in one half of the lamination. The legs between windows, around which are the coils for alternating and direct current,

^b These photographs were supplied through the courtesy of Dr. Harvey C. Hayes, Naval Research Laboratory, Anacostia, Maryland. They illustrate some of the early work on magnetostrictive acoustic devices done at NRL. The covering letter from Dr. E. D. Klein, Associate Superintendent of the Sound Division, states:

"These and various other devices which dealt with magnetostrictive elements were worked on progressively from 1927 to 1935. Only a limited few were tested in service for echo-ranging purposes, due to their being replaced by crystals in our development program."

constitute the driving elements. The thickness of the legs and of the arches of the window is designed to secure the proper impedance match with the water. The HP type of laminations used in the magnetostrictive scanning sonar transducers is a developed form.⁸ All the various transducers designed for special uses and described hereafter will be seen to be modifications of one of the general types listed above.

1.10 CHARACTERISTICS OF SOUND WAVES

Any variation in the physical properties of a medium that is propagated through the medium is called a *wave*. A sound wave in water consists of a propagated change in particle displacement, particle velocity, and pressure. The velocity of propagation c is given by the familiar equation $c = \sqrt{E/\rho}$, where E is the volume elasticity and ρ the density of the medium. The velocity of sound in sea water is approximately 1,500 meters per second.

The intensity of sound in a plane or spherical wave is the rate at which vibrational energy is transmitted across a unit area of cross section normal to the direction of propagation. If the particle displacement is a sinusoidal function of time, then the intensity of sound I_s at any point on the wave is given by the equations

$$I_s = 2\pi^2\rho c A^2 f^2 = \frac{1}{2}\rho c U^2 = \frac{P^2}{2\rho c}, \quad (13)$$

where A , U , and P are the amplitudes of the displacement, the velocity, and the pressure respectively. Denoting the root-mean-square (rms) values of velocity by u and pressure by p ,

$$\begin{aligned} I_s &= \rho c u^2 = \frac{p^2}{\rho c} \text{ (ergs/sec/cm}^2\text{)} \\ &= \frac{p^2}{\rho c} \times 10^{-7} \text{ watts/cm}^2. \end{aligned} \quad (14)$$

In a free field, p is the rms force in dynes per square centimeter exerted on a thin lamina of the medium, and u is the rms particle velocity in centimeters per second. The *acoustic resistance* of the medium defined as p/u equals ρc .

1.11 DECIBEL NOTATION

The decibel scale is used to express the ratio of amounts of power and energy, as well as other

quantities proportional thereto. It is a logarithmic scale in which the numerical values corresponding to successive, equally spaced graduations on the scale bear a fixed ratio one to another. One decibel difference on the scale corresponds to a ratio whose logarithm is 0.1 (1.259:1). The decibel level referred to unity for any quantity which varies directly as a power or an energy is numerically 10 times the logarithm of the numeric of the quantity. Thus:

$$\text{Power level} \left\{ \begin{array}{llll} 1 \text{ watt} & = 10 \log 1 & = 0 \text{ db ref. 1 watt} \\ 10 \text{ watts} & = 10 \log 10 & = 10 \text{ " " " "} \\ 20 \text{ " } & = 10 \log 20 & = 13 \text{ " " " "} \\ 40 \text{ " } & = 10 \log 40 & = 16 \text{ " " " "} \\ 100 \text{ " } & = 10 \log 100 & = 20 \text{ " " " "} \end{array} \right.$$

Since the power in an electric circuit of fixed impedance varies as the square of the applied voltage or as the square of the current and since the intensity of sound is proportional to the square of the acoustic pressure, the decibel level of these quantities is 20 times the logarithm of the numeric of the quantity in each case:

$$\text{Voltage level} \left\{ \begin{array}{llll} 1 \text{ volt} & = 20 \log 1 & = 0 \text{ db ref. 1 volt} \\ 10 \text{ volts} & = 20 \log 10 & = 20 \text{ " " " "} \\ 20 \text{ " } & = 20 \log 20 & = 26 \text{ " " " "} \\ 40 \text{ " } & = 20 \log 40 & = 32 \text{ " " " "} \\ 100 \text{ " } & = 20 \log 100 & = 40 \text{ " " " "} \end{array} \right.$$

Similarly, the pressure level of acoustic pressure referred to 1 dyne per square centimeter is 20 times the logarithm of the pressure.

1.12 CHARACTERISTICS OF TRANSDUCERS

Most magnetostrictive transducers are reversible. They may be used to produce an electric signal in response to an alternating acoustic pressure. When so used they will be spoken of as *hydrophones*. When used in the reverse manner, to radiate acoustic energy under electric driving, they will be referred to as *projectors*, or sometimes simply as transmitters.

The performance of a transducer, either as a hydrophone or as a projector, may be described in a variety of ways. Imagine, for example, the existence of a uniform sound field consisting of plane waves traveling in a certain direction in open water. Let the rms pressure due to the waves be p . This pressure is assumed to be measurable by means of a standard so small that its presence does not appreciably distort the field. Now suppose that an unknown transducer is inserted into the sound field,

so oriented as to obtain a maximum electric output. Let E be the rms voltage developed at the output terminals of the transducer when no current is drawn from it. The ratio E/p is now defined as the open-circuit (voltage) sensitivity. Notice that p is the rms pressure in the sound field before the introduction of the hydrophone. The sound field will be more or less distorted by the hydrophone, but the pressure calculated from a known sensitivity and open-circuit voltage will, by definition, still be the correct value for the undisturbed field.

Other definitions of sensitivity are sometimes useful. Suppose, for example, that the hydrophone is short-circuited instead of open-circuited, other conditions being the same as specified above. Let the rms current which flows be I . Then the short-circuit (current) sensitivity is defined as the ratio I/p . The open-circuit voltage E and the short-circuit current I are related by Ohm's law — $E = I|Z|$ where Z is the electric impedance of the transducer (in water). Thus the open-circuit (voltage) sensitivity is just $|Z|$ times the short-circuit (current) sensitivity. Under other conditions of measurement, it may be convenient to define additional sensitivities which will be rather simply related to the two already used. In this report, the first definition will be most frequently used and the term "sensitivity," unless otherwise qualified, will refer to the open-circuit (voltage) sensitivity.

In practical applications the sensitivity is usually expressed in decibels relative to a sensitivity of one volt per dyne per square centimeter. Sometimes a distinction is made between sensitivity expressed in volts per dyne per square centimeter and 20 times the logarithm of this quantity, which is then called the (open-circuit) receiving response. However, the terms "sensitivity" and "receiving response" shall be considered interchangeable and shall be expressed either in volts per dyne per square centimeter or in decibels relative to one volt per dyne per square centimeter.

The *threshold* of a hydrophone is expressed in terms of the pressure level in a uniform plane-wave free sound field parallel to the acoustic axis of the device, in decibels vs reference pressure (1.0 dyne per sq cm) which produces a signal voltage equal to the inherent noise voltage. This noise voltage is taken in a band width of one cycle when the device is in a matched tuned circuit. For magnetostrictive transducers, the inherent noise is the thermal noise, and it can be shown that the threshold, as defined above,

of a transducer of this type whose resistance is R is given by the equation

$$\text{Threshold} = 10 \log R - 194.9 - \text{sensitivity.}^6 \quad (15)$$

(Sensitivity here is expressed in decibels.)

1.13 RESPONSES OF PROJECTORS

To observe the performance of a transducer in transmitting (as a projector), suppose that it is placed in open water with no near-by obstructions which could reflect sound energy. When electric power is supplied to the transducer, acoustic power is radiated. The direction in which the intensity is greatest is the same as the direction in which the sensitivity is greatest and will be called the *acoustic axis*. Except at points very close to the transducer, the pressure falls off as the inverse first power of the distance. Let p_1 be the rms pressure one meter from the transducer, assuming that the pressure in this vicinity is already falling off inversely with the distance. Otherwise p_1 is defined as the pressure on the axis at some great distance multiplied by the ratio of this distance to one meter.

Now, the transmitting performance of the transducer can be specified by giving the ratio of p_1 to some appropriate quantity connected with the electric input to the transducer. The *current-transmitting response* will be defined as the ratio of p_1 to the rms current delivered to the transducer. Likewise, the *voltage-transmitting response* is the ratio of p_1 to the rms voltage across the transducer. As in receiving, other responses may be defined in terms convenient for certain instances.

The various responses in transmission and reception are connected by relations which will be given shortly.

The *efficiency of a projector* is defined as the ratio of the total acoustic power delivered by the projector to the electric power input into the projector. Since this is the ratio of two powers, it may naturally be expressed in decibels:

$$\text{Efficiency (decibels)} = 10 \log \frac{P_a}{P_e}, \quad (16)$$

where P_a and P_e are the acoustic power output and the electric power input respectively. Efficiency is expressed in decibels rather than as a simple ratio or percentage because sound-measuring equipment is generally calibrated in decibels, hence measured values are averaged in logarithmic rather than in

linear units, and probable errors should properly be expressed in decibels.

The acoustic power output is found by integrating the energy-flux density ($= p^2/\rho c$) over a sphere of radius r .

Let ρ = density of the medium (gm per cu cm),
 c = velocity of sound (cm per sec),
 p = rms acoustic pressure (dynes per sq cm).

$$P_a = \frac{1}{\rho c} \int_{\text{sphere}} p^2 d\sigma = \frac{4\pi r^2}{\rho c} p'^2 D \text{ (ergs/sec)} \quad (17)$$

$$= \frac{4\pi r^2}{\rho c} p'^2 D \times 10^{-7} \text{ (watts),}$$

p' is the value of the acoustic pressure measured at the principal maximum of the radiation pattern, and D is the *directivity ratio*, defined as the ratio of the average value of p^2 over the entire sphere to its value at the principal maximum. The precise evaluation of the value of D is in general a matter of some difficulty, since it involves the integration of p^2 over the entire sphere. The experimental data required are obtained by placing a measuring hydrophone, connected to recording equipment, in the water at a distance from the projector — great in comparison with projector dimensions. If the projector is rotated about an axis, the relative pressures in all directions in a plane perpendicular to that axis are recorded. Depending upon the geometry of the radiating face, patterns in one or more planes will be required to give the needed information for evaluating D .

The electric power input is obtained directly from the measured value of the input voltage E_i and the impedance $Z_i = R_i + jX_i$ of the transducer,

$$P_e = \frac{|E_i|^2 R_i}{|Z_i|^2} \quad (18)$$

From equations (17) and (18),

$$\text{Eff} = \frac{P_a}{P_e} = \frac{4\pi r^2 \cdot p'^2 D \cdot |Z_i|^2 10^{-7}}{\rho c \cdot R_i |E_i|^2} \quad (19)$$

For sea water, $\rho c = 1.55 \times 10^5$. With the numerical values inserted and r expressed in meters,

$$\text{Eff (decibels)} = 20(\log r + \log p' - \log E_i + \log Z_i) + 10(\log D - \log R_i) - 70.9. \quad (20)$$

If the power input P_e can be directly measured, then equation (20) may be written:

$$\text{Eff (decibels)} = 20(\log r + \log p') + 10(\log D - \log P_e) - 70.9.$$

1.14

RECIPROCITY

Most of the transducers to be considered in this report are linear, passive, reversible systems and satisfy a reciprocity theorem. The reciprocity theorem states that the performance of the transducer, in a sense to be specified more completely below, is the same in transmitting as in receiving. Whether or not any particular system is reciprocal can be decided only by experiment. It may, of course, be proved explicitly that an ideal transducer, employing a particular type of electromechanical coupling, is reciprocal by making use of the basic laws governing the coupling. Thus, for example, the experimental laws of magnetostriction will be used in Chapter 3 to show that magnetostrictive transducers satisfying the conditions of linearity, etc., are also reciprocal. On the other hand, it is quite possible to construct mongrel transducers which satisfy all the other conditions but are still not reciprocal.

Later in this book reciprocity in electromechanical systems will be discussed by regarding them as analogous to purely electric systems. It will be understood that no proof of reciprocity²⁶ will be undertaken but that the purpose of the discussion will be to establish the meaning of reciprocity and to show its connection with the same term as applied to electric systems. The usual statement of reciprocity applicable to an electric circuit composed of invariable reversible elements is as follows:

"If any electromotive force E is applied in any branch and the current I is measured in any other branch, then their ratio (frequently called the transfer impedance) E/I is equal in magnitude and phase to the ratio obtained if the positions of E and I are interchanged."¹⁹

In Chapter 2, a slightly different form will be used, equating mutual impedances instead of transfer impedances. For the purpose at hand, the reciprocity theorem for a circuit is stated in a less common form: First, let an electromotive force E'_a be applied in any branch a and the open-circuit voltage E'_b be measured at a pair of terminals b formed by breaking any other branch. Second, let a generator be connected at b which produces a current I''_b in this branch and let I''_a be the resulting current in branch a . Then the ratios E'_a/E'_b and I''_b/I''_a are equal in both phase and magnitude. An analogous statement of reciprocity in an electromechanical system can be obtained immediately by replacing the

voltage and current at the terminals b by a force and velocity respectively, or other suitable quantities in the mechanical system. Consider the arrangement in Figure 18A, which shows a voltage E' applied to a transducer and a pressure p' produced at a point O in the sound field. The ratio E'/p' is analogous to the ratio E'_a/E'_b above. Here, instead of force and velocity, pressure and volume velocity will be considered as being analogous to voltage and current

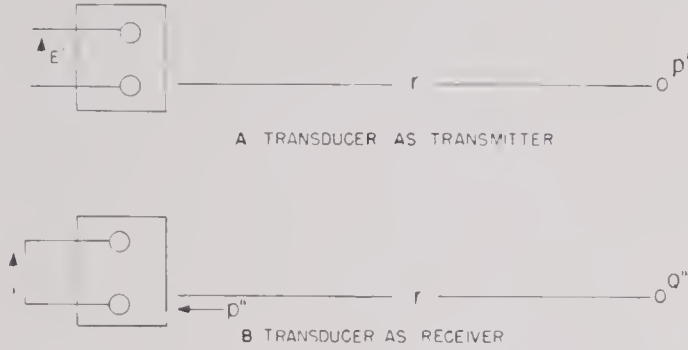


FIGURE 18. Transducer in transmission and reception.

respectively. Pressure and volume velocity are conjugate in the sense that their product represents power. Figure 18B shows the transducer in reception. A small spherical sound source Q'' is placed at the point where p' was previously measured. The source has a strength (rms volume velocity) Q'' and it produces a current I'' in the transducer, which is now short-circuited. The ratio Q''/I'' is analogous to our previous I''_b/I''_a . Thus, by comparison with the purely electric systems, the electromechanical system is said to be reciprocal if

$$\frac{E'}{p'} = \frac{Q''}{I''}. \quad (21)$$

Ideal electromechanical transducers employing electrostatic or piezoelectric coupling do satisfy equation (21). On the other hand, if the coupling is electromagnetic or magnetostrictive, equation (21) holds in magnitude but the two sides are of opposite sign. Therefore, generalizing equation (21) the statement of reciprocity is taken to be

$$\frac{E'}{p'} = \pm \frac{Q''}{I''}. \quad (21a)$$

Generally, a transducer utilizing both types of coupling, one with positive and the other with negative sign, will not satisfy the reciprocity theorem.

The statement of reciprocity for an electromechanical system, in the simple form of equation (21) is valid only if a consistent system of units

is used with the same unit of power throughout. Cross multiplication in equation (21) yields an equality between two quantities with the dimensions of power. One of these is electrical and the other mechanical. In practice, the mechanical unit of power is the erg per second while the electric unit is the watt equal to 10^7 ergs per sec. Thus, for common usage,

$$\frac{E'}{p'} = \pm \frac{Q''}{I''} \times 10^{-7}, \quad (21b)$$

where E' and I'' are measured in volts and amperes and p' and Q'' are measured in dynes per square centimeter and cubic centimeters per second respectively.

1.15 VOLTAGE SENSITIVITY AND EFFICIENCY

To develop the relationship between voltage sensitivity and efficiency, the value of the acoustic pressure in a medium at a distance r cm from a simple source of strength Q must be found. For the full mathematical treatment, the reader should consult any of the standard texts on the theory of sound.²⁰

The rate at which energy is supplied to the sound field by a source of strength Q'' located at the center of a sphere of radius r is

$$4\pi r^2 I_s = \frac{\pi \rho c Q''^2}{\lambda^2} = \pi \rho f \frac{Q''^2}{\lambda}, \quad (22)$$

where I_s is the intensity of sound as defined in equation (14), Q'' is the strength of the source (= rms volume velocity), and λ is the wave length. Then

$$I_s = \frac{p''^2}{\rho c} = \frac{\rho c Q''^2}{4r^2 \lambda^2},$$

$$|p''| = \frac{\rho c}{2r\lambda} |Q''| = \frac{\rho f}{2r} |Q''|. \quad (23)$$

Eliminating Q from equations (21b) and (23),

$$\left| \frac{I''}{p''} \right| = \frac{2r}{\rho f} \left| \frac{p'}{E'} \right| 10^{-7} = J \left| \frac{p'}{E'} \right|. \quad (24a)$$

The expression $2r/\rho f \times 10^{-7} = J$ is the *reciprocity parameter* involving the frequency of the sound, the distance r in centimeters, and the density of the medium. If r be taken as 1 meter, $\rho = 1.03$,

$$J_1 = \frac{2 \times 10^{-5}}{\rho f} = \frac{1.94 \times 10^{-8}}{f_{kc}}. \quad (24b)$$

Multiplying both sides of equation (24a) by $|Z_i|$, the impedance of the transducer,

$$\left| \frac{E''}{p''} \right| = S = J \left| \frac{p'}{E'} \right| |Z_i| = J \frac{p'}{I'}. \quad (24c)$$

In equation (19),

$$\text{Eff} = \frac{4\pi r^2 D \times 10^{-7}}{\rho c R_i} \times \left| \frac{p'}{E'} \right|^2 |Z_i|^2.$$

From equation (24c)

$$\left| \frac{p'}{E'} \right|^2 |Z_i|^2 = \frac{S^2}{J^2} = \frac{\rho^2 c^2 S^2 \times 10^{14}}{4r^2 \lambda^2},$$

$$\text{Eff} = \frac{\pi \rho c S^2 D \times 10^7}{\lambda^2 R_i}. \quad (25)$$

$$\text{Eff (decibels)} = 20(\log S - \log \lambda) + 10(\log D - \log R_i) + 127. \quad (25a)$$

It will be obvious that agreement between the values of the efficiency as computed from equations (19) and (25) will depend upon strict linearity between the electric and acoustic powers over a wide range, since the actual magnitude of the electric power involved in sensitivity measurements is very small compared with that used in measuring transmitting response.

1.16 RECEIVING AND TRANSMITTING RESPONSE

If in equations (24a) and (24c) $J = J_1$, the value corresponding to a value for r of 1 meter, then equation (24a) can be read:

$$\begin{aligned} & \text{(Short-circuit [current] sensitivity)} \\ & = J_1(\text{voltage transmitting response}). \end{aligned} \quad (26)$$

Similarly, equation (24c) reads:

$$\begin{aligned} & \text{(Open-circuit [voltage] sensitivity)} \\ & = J_1(\text{current transmitting response}). \end{aligned} \quad (27)$$

Since the value of J_1 varies inversely with frequency, a transducer having a sensitivity uniform with frequency over a certain range will have a rising current transmitting response proportional to frequency over this range.

The change in sensitivity near resonance in a highly resonant transducer will be large compared with the change in frequency. Hence, over a small frequency range near resonance, change in J_1 will be relatively small; current transmitting response will be nearly proportional to open-circuit sensitivity; and the frequency variation of the two will be nearly the same.

ABSOLUTE RECIPROCITY CALIBRATION

The measurement of the sensitivity or efficiency of an electromechanical transducer usually requires a calibrated standard whose sensitivity or transmitting response is known. A transducer known to satisfy the reciprocity theorem can be calibrated without reference to any other electromechanical standard. The principle underlying the method is most easily illustrated by visualizing two identical transducers which are both reciprocal. The

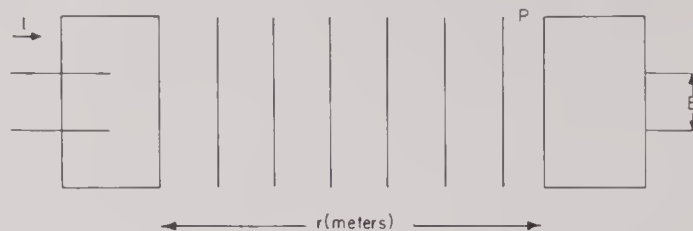


FIGURE 19. Reciprocity calibration with two identical transducers.

practical case in which there is only one reciprocal transducer is discussed later in this chapter. In Figure 19, the transducers are arranged in water so that one is a projector and the other a hydrophone. The first is driven by a current I , producing a pressure p at distance r meters (before the other transducer is introduced). The pressure is given by

$$p = \frac{T_I I}{r}$$

where the current transmitting response T_I is the pressure produced at one meter when the driving current is one ampere. When the second hydrophone is introduced, an open-circuit voltage E is generated, which is related to p and the open-circuit sensitivity S_V by

$$E = S_V p.$$

Eliminating p from the two equations,

$$S_V T_I = \frac{Er}{I}. \quad (28)$$

Since both transducers are the same and reciprocal, the receiving and transmitting responses are connected by

$$S_V = J_1 T_I,$$

where J_1 is the reciprocity parameter for one meter, as defined previously. Solving for S_V , we find

$$S_V = \sqrt{\frac{E}{I}} J_1 r = \sqrt{\frac{J E}{I}},$$

where J is the reciprocity parameter at distance r . Obviously the method as outlined is of no practical use because of the grave restriction to two identical transducers.

This limitation may be removed as follows: Consider three transducers labeled A , B , and C . Transducer A is to be used only as a transmitter, B only as a receiver, but C is to be used both in transmission and reception and is assumed reciprocal. All three transducers are assumed linear, but A and B need not be reciprocal. B and C will be compared as receivers (using A as a transmitter), then A and C

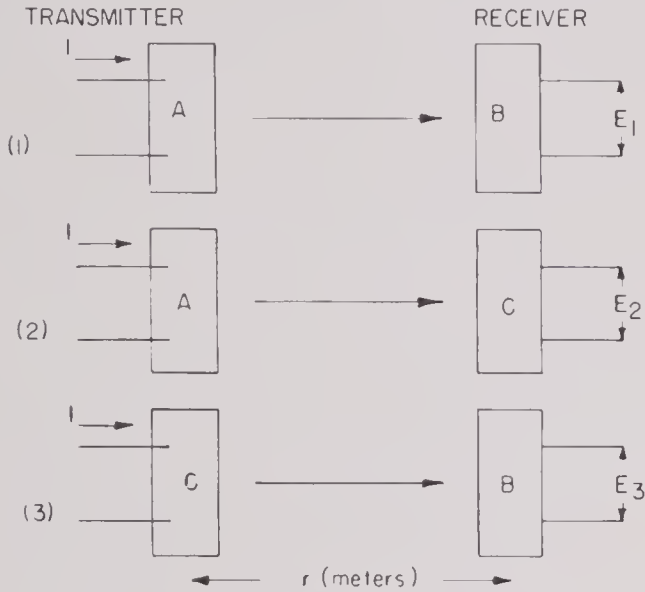


FIGURE 20. Reciprocity calibration using three transducers, one of which is reciprocal.

compared as transmitters (using B as a receiver), and finally an equation will be developed similar to (28) for A and B . Figure 20 shows the experimental arrangement schematically. For the sake of simplicity, suppose that the same current I is delivered to the transmitters in each of the three experiments and that the spacing of the transmitting and receiving transducers is also the same. The quantities E_1 , E_2 , and E_3 are the open-circuit voltages produced in the three situations. Conditions (1) and (2) give an immediate comparison of the receiving performances of B and C . Thus

$$S_V^{(B)} = \frac{E_1 S_V^{(C)}}{E_2} \quad (29)$$

Similarly (1) and (3) give a relation between the transmitting performance of A and C :

$$T_I^{(A)} = \frac{E_1 T_I^{(C)}}{E_3} \quad (30)$$

Considering experiment (1) by itself,

$$S_V^{(B)} T_I^{(A)} = \frac{E_1 r}{I} \quad (31)$$

Substituting equations (29) and (30) in (31) results in:

$$S_V^{(C)} T_I^{(C)} = \frac{E_2 E_3 r}{E_1 I},$$

which is essentially the same as equation (28) found previously for two identical transducers. Treating it in the same way as equation (28),

$$S_V^{(C)} = J_1 T_I^{(C)} = \sqrt{\frac{J E_2 E_3}{E_1 I}} \quad (32)$$

Equation (32) can be used in combination with equations (29) and (30) to obtain $S_V^{(B)}$ and $T_I^{(A)}$.

Sometimes, in making a reciprocity calibration, it will not be convenient to maintain the same current in the three experiments in Figure 20. If these currents are taken as I_1 , I_2 , and I_3 respectively, and if the three distances are made r_1 , r_2 , and r_3 , it is found that equations (29), (30), and (32) become

$$S_V^{(B)} = \frac{E_1 I_2 r_1 S_V^{(C)}}{E_2 I_1 r_2} \quad (29')$$

$$T_I^{(A)} = \frac{E_1 I_3 r_1 T_I^{(C)}}{E_3 I_1 r_3} \quad (30')$$

and

$$S_V^{(C)} = J_1 T_I^{(C)} = \sqrt{\frac{J' I_1 E_2 E_3}{E_1 I_2 I_3}} \quad (32')$$

where J' is the reciprocity parameter evaluated for the distance $r_2 r_3 / r_1$.

The simplest experimental procedure is as follows: The projector A (Figure 20) is located at a fixed position in the water and the transducers B and C are in turn located at a second point at a distance r from A . A fixed current I is maintained in A and the voltages generated in B and in C are measured. C is kept in position and A is replaced by B . The same current I drives C and the voltage generated in B is measured. In general, the measurement of the current I is the least accurate factor and therefore the choice for the reversible unit of a transducer of low impedance and fairly uniform response is desirable. Thin-walled tube-type magnetostrictive hydrophones meet these requirements to a fair degree and have proved extremely useful for calibration purposes as well as for secondary standards.

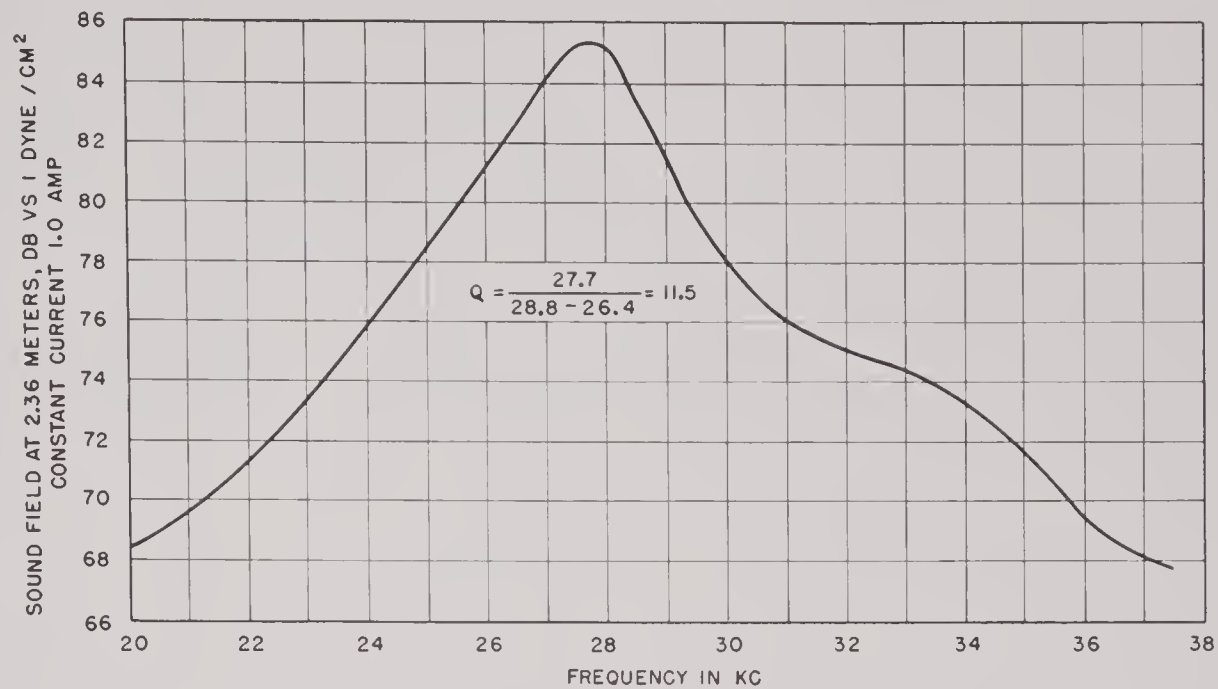


FIGURE 21. Transmitting response of magnetostrictive unit.

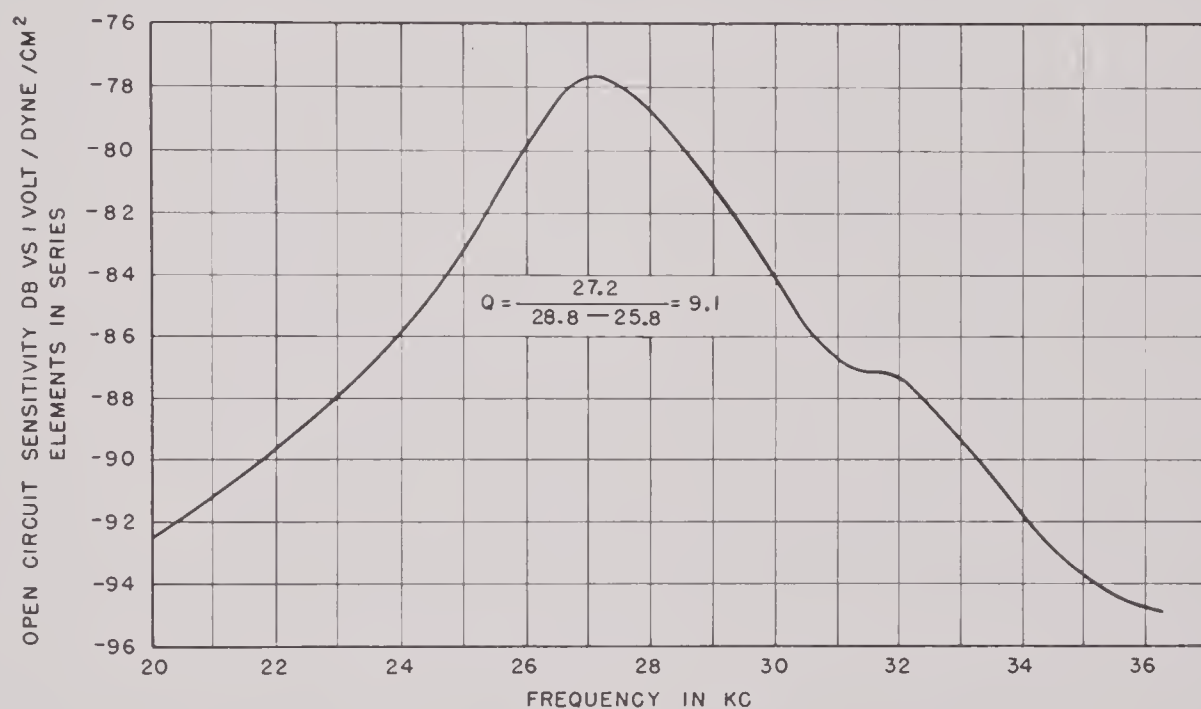


FIGURE 22. Receiving response of magnetostrictive transducer.

1.18 MEASUREMENT OF TRANSDUCER PERFORMANCE

Details of the measuring technique will not be considered here. Simply to illustrate the various relations deduced in the preceding sections, the results of measurements on an experimental magnetostrictive unit are presented in Figures 21 and 22.

The unit is sketched in Figure 23. It consisted of four stacks of nickel laminations 0.010 inch thick. Each stack was 3 inches high and was polarized with permanent magnets. From Figure 22 and from impedance and pattern measurements, the following data are taken:

Resonant frequency = 27.2 kc.

Z_i (elements in series) = $102 + j160$ (ohms).

CONFIDENTIAL

Sensitivity at resonance = -77.8 db ref 1 volt per dyne per sq cm (all elements in series).

The value of D computed from pattern measurements was 0.0157.

The efficiency calculated from these data, using equation (25a) is -3.6 db = 0.43.

The efficiency at resonance may also be computed from data obtained by driving the unit as a projector (see Figure 21). In this case, the four ele-

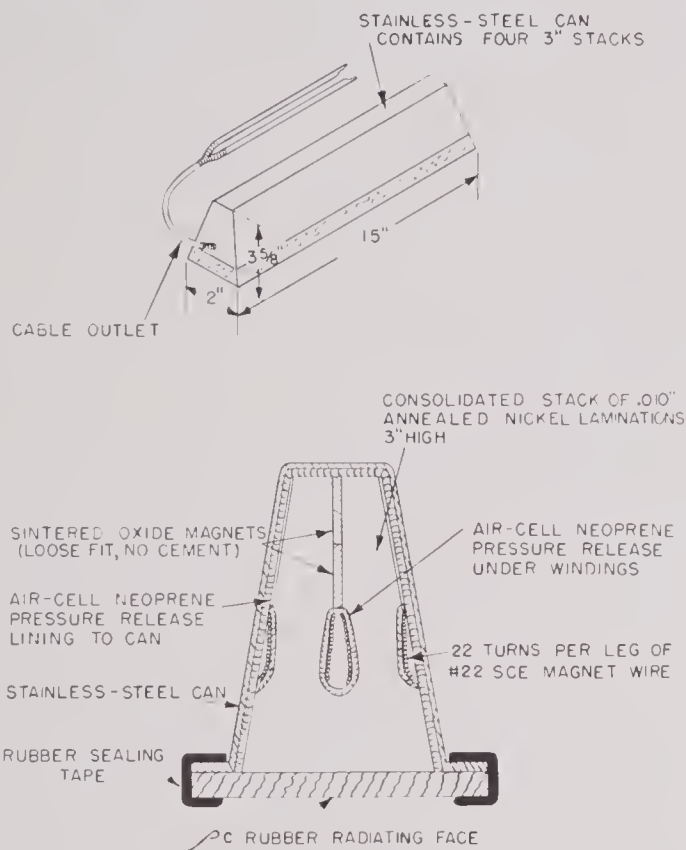


FIGURE 23. Sketch of magnetostrictive transducer.

ments were connected in parallel. The measured quantities needed for this computation, using equation (20) were as follows:

$$20 \log p' = 85.2,$$

$$r = 2.36 \text{ meters.}$$

$$Z_i = 6.4 + j10 \text{ (ohms).}$$

$$\text{Driving current } I = \frac{|E|}{|Z|} = 1.0 \text{ ampere.}$$

The efficiency computed from equation (20) is -4.3 db = 0.37. It should be said that the agreement in the computed values of the efficiency from receiving and transmitting response data is better than is usually found in comparisons of this sort. Because of the number of factors involved in each of the two equations and the fact that measurement

errors, although fairly small when expressed in decibels, are large numerically, differences as great as 3.0 decibels (or a factor of 2 to 1) may reasonably be expected to appear, unless all measurements are made with extreme care and under the best experimental conditions.

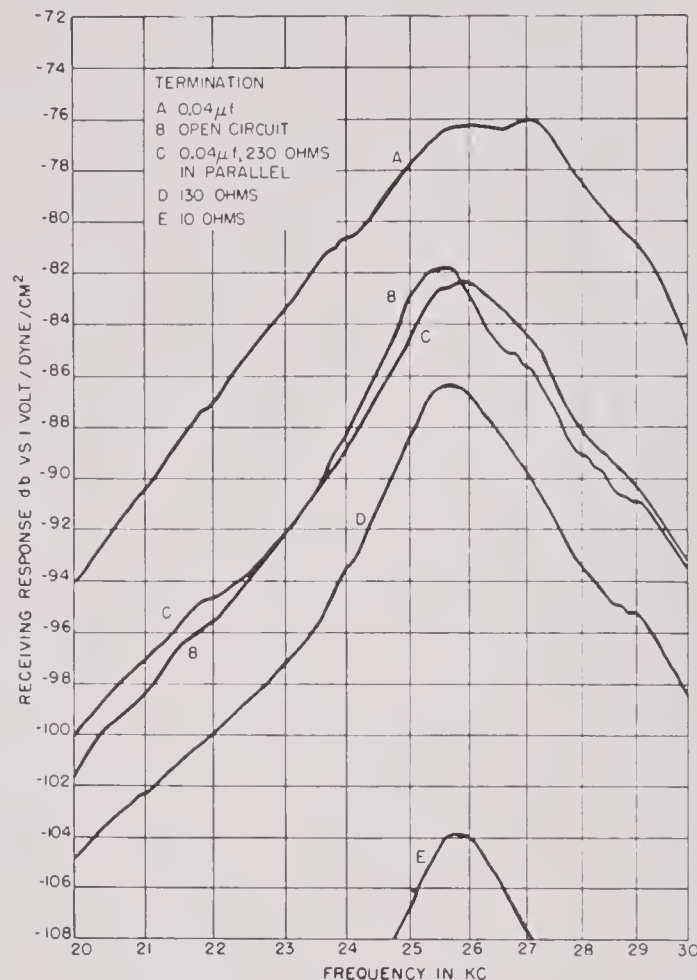


FIGURE 24. Effect of termination on receiving response of transducer.

1.19 BAND WIDTH: SHARPNESS OF RESONANCE

As has already been stated, the various frequency response curves of a resonant transducer will show peaks at or near mechanical resonance. It is customary to speak of the band width as the interval between the two frequencies at which the response has fallen to $\sqrt{1/2}$ ($= -3$ db) relative to its peak value. It should be emphasized that the several responses which have been defined here may show large differences with respect to band width, both in magnitude and in dependence on frequency. The situation is illustrated in Figure 24, where voltage sensitivities are shown for a particular transducer

with several electric terminations. The band width may be expressed as the frequency interval or as a fraction by taking the ratio of the interval to the central frequency. By analogy with the current-voltage relation in a simple resonant circuit, it is common to speak of the Q of the response curve as the reciprocal of the fractional band width. Thus

$$Q = \frac{f_0}{f_2 - f_1}, \quad (33)$$

where f_2 and f_1 are the “ -3 db points” and $f_0 = \sqrt{f_2 f_1}$ is the center frequency. As can be seen from

Figure 24, the Q ranges from 7.2 to 13.5, depending on which of the responses measured is used in equation (33). Care must therefore be taken to specify the conditions of measurement of the response in quoting a Q determined in this way.

In addition to the foregoing sending and receiving data needed for the intelligent use of transducers designed to serve both as projectors and hydrophones, special types call for other kinds of measurements. It is also possible to secure much useful information on transducer performance from the purely electric measurements covered in Chapter 11.

Chapter 2

TRANSDUCERS AS MULTITERMINAL NETWORKS

2.1

ELECTRIC SYSTEMS

In approaching the theoretical treatment of magnetostrictive transducers, a purely electric four-terminal network as shown in Figure 1 is considered. The network is assumed to be composed of linear passive elements. Then the relations between the potentials and currents on the two sides of Figure 1 can be written (see glossary for definitions)

$$\begin{aligned} E_1 &= Z_1 I_1 + Z_{12} I_2, \\ E_2 &= Z_{21} I_1 + Z_2 I_2, \end{aligned} \quad (1)$$

with

$$Z_1 Z_2 - Z_{12} Z_{21} \neq 0.$$

The impedances Z_1 and Z_2 are the impedances on the two sides when the opposite circuits are open, whereas Z_{12} and Z_{21} are known as mutual impedances. For a purely electric system with linear passive elements, the reciprocity theorem states that

$$Z_{12} = Z_{21}. \quad (2)$$

If the network of equation (1) is to be physically realizable with passive elements, the resistive parts of Z_1 and Z_2 must be positive, although there is no such condition on Z_{12} . Thus,

$$\begin{aligned} Z_1 &= R_1 + jX_1 \quad R_1 \geq 0, \\ Z_2 &= R_2 + jX_2 \quad R_2 \geq 0, \\ Z_{12} &= R_{12} + jX_{12}. \end{aligned} \quad (3)$$

An application of the network is in transferring power from a source to a load as shown in Figure 2. Then, in addition to equations (1),

$$E_2 = -Z_L I_2, \quad (4)$$

and by eliminating E_2 and I_2 between equations (1) and (4) it is found that the input impedance with the load connected is

$$Z_i = R_i + jX_i = Z_1 - \frac{Z_{12}^2}{Z_2 + Z_L}. \quad (5)$$

The efficiency of the four-terminal network (the ratio of the power output at terminals 2 to the power input at terminals 1) is

$$\text{Eff} = \frac{R_L}{R_i} \left| \frac{Z_{12}}{Z_2 + Z_L} \right|^2 = \frac{R_1 R_L (R_{12}^2 + X_{12}^2)}{[R_1(R_2 + R_L) - R_{12}^2][R_1(R_2 + R_L) + X_{12}^2] + [R_1(X_2 + X_L) - R_{12}X_{12}]^2}. \quad (6)$$

Equation (6) has a maximum with respect to X_L when

$$R_1(X_2 + X_L) - R_{12}X_{12} = 0, \quad (7)$$

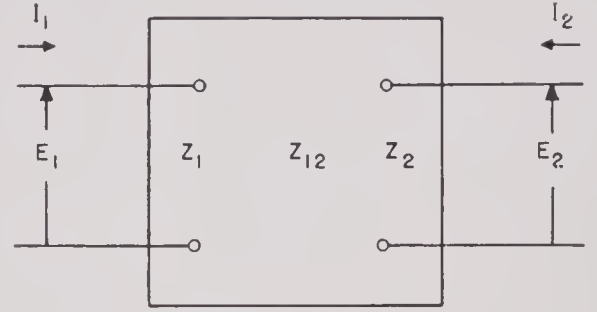


FIGURE 1. Electric four-terminal network.

and a maximum with respect to R_L when

$$R_1^2 R_L^2 = (R_1 R_2 - R_{12}^2)(R_1 R_2 + X_{12}^2) + [R_1(X_2 + X_L) - R_{12}X_{12}]^2. \quad (8)$$

If equations (7) and (8) hold simultaneously, the value of equation (6) is

$$\text{Pot eff} = \frac{\sqrt{R_1 R_2 + X_{12}^2} - \sqrt{R_1 R_2 - R_{12}^2}}{\sqrt{R_1 R_2 + X_{12}^2} + \sqrt{R_1 R_2 - R_{12}^2}}. \quad (9)$$

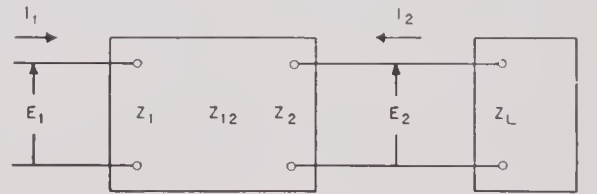


FIGURE 2. Four-terminal network connected to load, $Z_L = R_L - jX_L$.

The potential efficiency is thus the highest efficiency that a four-terminal network can exhibit in transferring power from one pair of terminals to the other when both the resistance and the reactance of the load are considered variable.

It can be shown that the necessary and sufficient

condition that must be satisfied if equation (6) is to remain less than unity for all Z_L with $R_L \geq 0$ is

$$R_1 R_2 - R_{12}^2 \geq 0. \quad (10)$$

This equation must be satisfied by any four-terminal network which is made up of linear, passive, physically realizable elements. The equality in equation (10) gives a maximum efficiency of unity according to equation (9).

It is interesting to compare equation (10) with the equations satisfied by special types of four-terminal networks. Consider, for example, the T network shown in Figure 3. It is easily found that

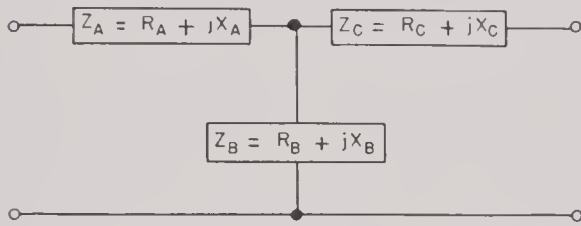


FIGURE 3. T network.

the impedances of equations (1) are related to those of Figure 3 by the equations

$$\begin{aligned} Z_1 &= Z_A + Z_B, \\ Z_2 &= Z_B + Z_C, \\ Z_{12} &= Z_{21} = Z_B. \end{aligned} \quad (11)$$

To be physically real the elements of the T network must satisfy

$$R_A \geq 0, R_B \geq 0, R_C \geq 0. \quad (12)$$

Hence, from equation (11),

$$\begin{aligned} R_1 &\geq R_{12}, \\ R_2 &\geq R_{12}. \end{aligned} \quad (13)$$

Equation (10) is, therefore, satisfied by the T network, but note that the conditions in equation (13) are stronger than in (10). Thus not all physically realizable four-terminal networks can be obtained as T networks. It is quite easy to find, for example, a feasible π network which can be represented by a T network only with the help of negative resistance elements.

2.2 ELECTROMECHANICAL SYSTEMS

Linear passive four-terminal networks are considered (Figure 4) in which two of the terminals are electrical and two mechanical. In the figure, F is the force of the (water) load on the radiating surface

of the transducer, while v is its velocity. The convention on directions is such that the transducer is receiving energy from the load when F and v are in phase. Equations (1) hold for the electromechanical network if appropriate changes are made in the impedances.

$$\begin{aligned} E &= Z_e I + Z_{em} v, \\ F &= Z_{me} I + Z_m v, \\ Z_e Z_m - Z_{em} Z_{me} &\neq 0. \end{aligned} \quad (14)$$

In equations (14), $Z_e = R_e + jX_e$ is the electric impedance of the electromechanical transducer or network when the mechanical side is rigidly clamped

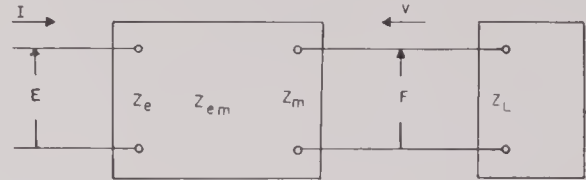


FIGURE 4. Electromechanical four-terminal network of transducer with attached mechanical load.

($v = 0$), and Z_m is the mechanical impedance (F/v) of the transducer when the electric terminals are open-circuited. The electromechanical mutual impedances are Z_{em} and Z_{me} . The system is taken to involve only one type of electromechanical coupling. Then a reciprocity theorem holds for the system and $Z_{em} = \pm Z_{me}$ according to the type of coupling:

$$Z_{em} = +Z_{me} \quad (\text{electrostatic or piezoelectric coupling}). \quad (15)$$

$$Z_{em} = -Z_{me} \quad (\text{electromagnetic or magnetostrictive coupling}). \quad (16)$$

A system incorporating types of coupling corresponding to both (15) and (16) may not satisfy the reciprocity theorem.^a

With electrostatic or piezoelectric coupling, equation (15), the analysis of equations (3) to (13) applies, if the obvious changes in subscripts are made. On the other hand, for electromagnetic or magnetostrictive coupling, when equation (16) holds, some further changes must be made. The rest of this section is restricted to this case. By rewriting equation (14) and employing equation (16) it is found that

$$\begin{aligned} E &= Z_e I + Z_{em} v \\ F &= -Z_{em} I + Z_m v \end{aligned} \quad \left. \begin{array}{l} \text{electromagnetic or} \\ \text{magnetostrictive} \end{array} \right\} \quad (17)$$

$$Z_e Z_m + Z_{em}^2 \neq 0.$$

^a For a linear transducer system that does not satisfy the reciprocity system, see reference 1.

As before, for a physically realizable passive system

$$\begin{aligned} Z_e &= R_e + jX_e, & R_e &\geq 0, \\ Z_m &= R_m + jX_m, & R_m &\geq 0, \\ Z_{em} &= R_{em} + jX_{em}. \end{aligned} \quad (18)$$

Since the mechanical load in Figure 4 has impedance $Z_L = R_L + jX_L$,

$$F = -Z_L v, \quad (19)$$

and the electric input impedance with the mechanical termination is

$$Z_i = R_i + jX_i = Z_e + \frac{Z_{em}^2}{Z_m + Z_L}. \quad (20)$$

The efficiency of the transducer in converting electric power into mechanical power is then

$$\text{Eff} = \frac{R_L}{R_i} \left| \frac{Z_{em}}{Z_m + Z_L} \right|^2 \quad (21)^b$$

The maximum of equation (21) with respect to X_L occurs when

$$R_e(X_m + X_L) + R_{em}X_{em} = 0, \quad (22)$$

and that with respect to R_L when

$$R_e^2 R_L^2 = (R_e R_m + R_{em}^2)(R_e R_m - X_{em}^2) + [R_e(X_m + X_L) + R_{em}X_{em}]^2. \quad (23)$$

The value of equation (21) at the maximum with respect to both variables is

$$\text{Pot eff} = \frac{\sqrt{R_e R_m + R_{em}^2} - \sqrt{R_e R_m - X_{em}^2}}{\sqrt{R_e R_m + R_{em}^2} + \sqrt{R_e R_m - X_{em}^2}}. \quad (24)$$

The potential efficiency is the highest efficiency that the four-terminal electromechanical network can exhibit in transferring power from its electric to its mechanical terminals or vice versa. The necessary and sufficient condition that potential efficiency always remain less than unity is

$$R_e R_m - X_{em}^2 \geq 0. \quad (25)$$

It will be noticed that the only difference between equations (10) and (25) is exchange of real and imaginary parts of the mutual impedance.

2.3 EXAMPLE — LOUDSPEAKER

The preceding general theory will be illustrated by an application to an electromagnetic transducer or loudspeaker of the dynamic type. The essential components are shown in Figure 5A.

The cone assembly is taken to be perfectly stiff, so that the motion is everywhere the same and lumped constants can be used. The system has a mass M , a stiffness K , and a certain internal mechanical damping resistance R_m which does not include the radiation load. The voice coil consists of N turns of

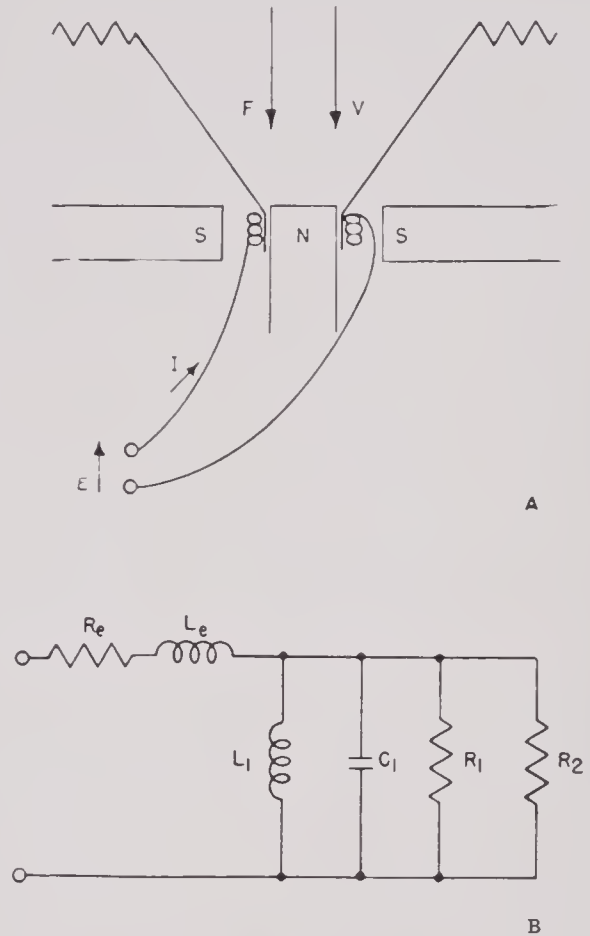


FIGURE 5. A. Dynamic-type loudspeaker. B. Equivalent circuit of loudspeaker.

radius a with a resistance R_e and inductance L_e . The induction in the gap where the coil lies is B . The force F is applied on the system by some external mechanical agency, such as air, and the positive direction of v is the same as for F . An alternating potential E is applied to the terminals of the coil and a current I flows through it. For definiteness, it is assumed that a positive current circles the coil in the counterclockwise sense when viewed from the front of the speaker (top of Figure 5A).

$$^b \text{Eff} = \frac{R_L}{R_i} \left| \frac{Z_{em}}{Z_m + Z_L} \right|^2 = \frac{R_e R_L (R_{em} + X_{em}^2)}{[R_e(R_m + R_L) + R_{em}^2][R_e(R_m + R_L) - X_{em}^2] + [R_e(X_m + X_L) + R_{em}X_{em}]^2}.$$

In the following, unless otherwise stated, electric units are measured in the electromagnetic system. The reason for this is that the practical system of electric units uses the watt as the unit of power, whereas the cgs power unit is the erg per second ($= 10^{-7}$ watt). The reciprocity theorem in the simple form of equations (15) and (16) holds only when the electric and mechanical power units are the same.

Let the system be acted on by an applied force F of which the angular frequency is ω , with the coil open so that no current flows. Then motion takes place with velocity v given by

$$F = Z_m v = \left[j\omega M + \frac{K}{j\omega} + R_m \right] v. \quad (26)$$

If a current I flows through the voice coil and it is required that the same motion be maintained, an additional force must be applied. This is equal and opposite to the force produced on the coil by the interaction of I and B and can be calculated without regard to the motion of the coil. Then

$$F = -2\pi a N B I + Z_m v, \quad (27)$$

with the mechanical impedance Z_m as in equation (26).

On the other hand, it is possible to start from the electric side and apply a potential E to the coil, with the system clamped mechanically so that its velocity is zero. Then a current I flows, given by

$$E = Z_e I = (R_e + j\omega L_e) I. \quad (28)$$

If now the coil is allowed to move with velocity v and the same current must be maintained, then E must be altered by the emf generated in the coil by the motion. Then

$$E = Z_e I + 2\pi a N B v, \quad (29)$$

with the electric impedance Z_e as in equation (28).

Equations (27) and (29) are of form (17) with

$$Z_{em} = 2\pi a N B. \quad (30)$$

2.3.1 Two-Terminal Equivalent Circuit of Loudspeaker

In normal operation the loudspeaker is fed electric power and radiates acoustic power. The normal load Z_L (see Figure 4) is thus the radiation impedance of the air to the cone. For simplicity, assume that this is a pure resistance R_L . The electric impedance

seen at the coil terminals is given by equation (20) and can be written

$$Z_i = R_e + j\omega L_e + \frac{4\pi^2 N^2 a^2 B^2}{R_m + R_L + j\omega M + \frac{K}{j\omega}}. \quad (31)$$

With the help of the abbreviations

$$\begin{aligned} R_1 &= \frac{4\pi^2 N^2 a^2 B^2}{R_m}, & R_2 &= \frac{4\pi^2 N^2 a^2 B^2}{R_L}, \\ L_1 &= \frac{4\pi^2 N^2 a^2 B^2}{K}, & C_1 &= \frac{M}{4\pi^2 N^2 a^2 B^2}. \end{aligned} \quad (32)$$

equation (31) can be written as

$$Z_i = R_e + j\omega L_e + \frac{1}{\frac{1}{R_1} + \frac{1}{R_2} + j\omega C_1 + \frac{1}{j\omega L_1}}. \quad (33)$$

The impedance at the electric terminals of the loudspeaker is thus the same as the impedance of the circuit shown in Figure 5B. The series elements R_e , L_e are purely electric, whereas the shunt elements R_1 , R_2 , L_1 , and C_1 are the elements reflected into the electric circuit by the mechanical system. When the mechanical impedance is made very large, as by blocking the cone, the shunt impedance becomes very small and the impedance reduces to that of the electric elements alone. The additional impedance due to the mechanical system is known as motional impedance, designated Z_{mot} . From equations (20) and (33)

$$\begin{aligned} Z_{\text{mot}} &= Z_i - Z_e = \frac{Z_{em}^2}{Z_m + Z_L} \\ &= \frac{1}{\frac{1}{R_1} + \frac{1}{R_2} + j\omega C_1 + \frac{1}{j\omega L_1}}. \end{aligned} \quad (34)$$

2.3.2

Impedance Diagram

In this work it will often be found convenient to plot an impedance such as the motional impedance (34), regarding $Z_{\text{mot}} = R_{\text{mot}} + jX_{\text{mot}}$ as a vector with horizontal and vertical components R_{mot} and X_{mot} respectively. Since Z_{mot} is not constant but depends on the frequency, it will plot out a locus as the frequency is changed. This locus will be spoken of as the impedance diagram. In the particular case of equation (34), it will now be shown that the motional impedance diagram is a circle, as pictured in Figure 6. The easiest way to do this perhaps is

to put equation (34) into polar coordinates. The following abbreviations are used:

$$D = \frac{R_1 R_2}{(R_1 + R_2)}, \quad Q = \frac{\sqrt{MK}}{(R_m + R_L)} = D \sqrt{\frac{C_1}{L_1}} \quad (35)$$

$$\omega_0 = \sqrt{\frac{K}{M}} = \frac{1}{\sqrt{L_1 C_1}}, \quad p = \frac{1}{2} \left(\frac{\omega}{\omega_0} - \frac{\omega_0}{\omega} \right) \simeq \frac{\omega - \omega_0}{\omega_0}.$$

Then equation (34) becomes

$$Z_{\text{mot}} = Z_i - Z_e = \frac{D}{1 + j2Qp}. \quad (36)$$

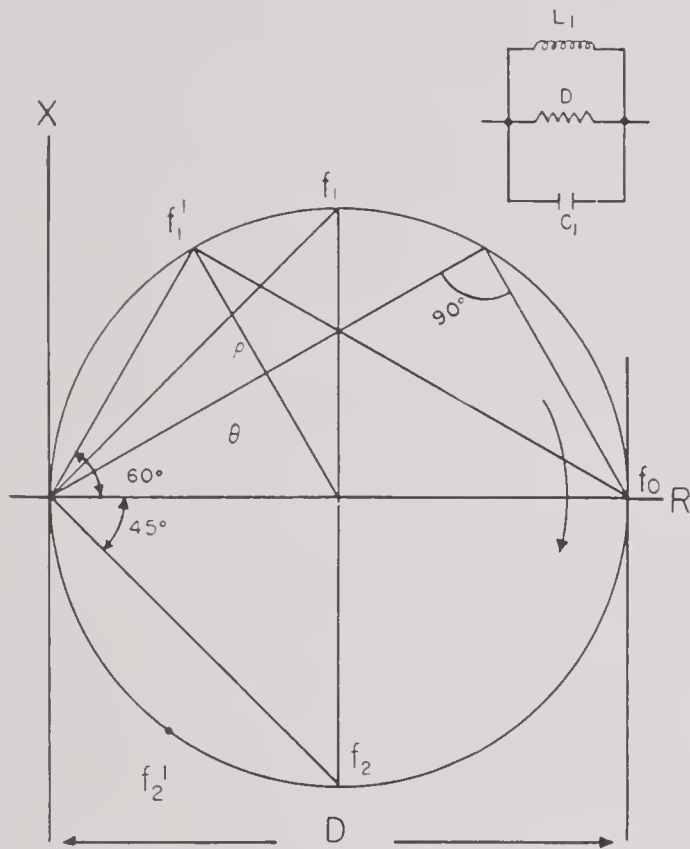


FIGURE 6. Motional impedance diagram.

The quantity p measures the departure of the frequency from resonance, which occurs when $\omega = \omega_0$. At resonance the motional impedance is a pure resistance equal to D . To convert (36) to polar coordinates ρ, θ , note that

$$\tan \theta = \frac{X}{R} = -2Qp, \quad (37)$$

$$\rho = \sqrt{R^2 + X^2} = \frac{D}{\sqrt{1 + 4Q^2 p^2}}.$$

By eliminating $2Qp$ between these two equations,

$$\rho = D \cos \theta, \quad (38)$$

which is the polar equation of the circle with diameter D shown in Figure 6. As the frequency increases

from zero, the impedance locus, starting at the origin, traces out the circle in the clockwise sense indicated by the arrow, finally returning to the origin when the frequency becomes infinite.

Resonance occurs at the frequency $f_0 (= \omega_0/2\pi)$ where the circle crosses the resistance axis. The diameter joining the origin with the point f_0 is known as the resonance diameter. The points marked with the frequencies f_1 and f_2 are of special interest. They lie at the ends of the diameter perpendicular to the resonance diameter. At these points, θ , the phase angle of the impedance, is $\pm 45^\circ$, and ρ , the magnitude of the impedance, is $\sqrt{1/2}$ of its maximum value D at resonance. These are also sometimes known as the 3 db points, since a constant current through the circuit will develop across it a voltage 3 db less at f_1 or f_2 than its value at f_0 . It is easy to show that $f_1 f_2 = f_0^2$, so that f_1, f_0 , and f_2 are uniformly spaced on a logarithmic scale. The relation

$$Q = \frac{f_0}{(f_2 - f_1)} \quad (39)$$

is easily deduced.

As has been stated earlier, the blocked impedance is the impedance due to the purely electric elements and is given by

$$Z_e = R_e + j\omega L_e. \quad (40)$$

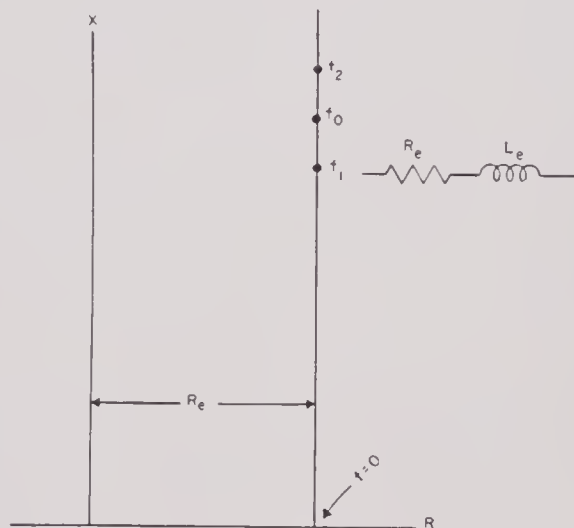


FIGURE 7. Blocked impedance diagram.

The impedance diagram for equation (40) is shown in Figure 7. The locus is a straight line, parallel to the reactance axis and R_e to the right. Frequency increases upward along the line, $f = 0$ being the point on the resistance axis. The point f_0 lies at the height $X_0 = \omega_0 L_e = 2\pi f_0 L_e$, with similar formulas for f_1, f_2 .

The total impedance as given by equation (33) is the vector sum of the blocked and motional impedance and can be obtained by combining Figures 6 and 7. The result is shown in Figure 8.

The measured impedance of a small permanent-magnet loudspeaker (Utah 4PZ), suspended in air without baffle, is shown in Figure 9. It will be noted that the observed curve has the same general characteristics as the theoretical one. In Figure 9 the motional impedance is somewhat larger, compared with the blocked impedance, than that assumed in drawing Figure 8, so that the impedance becomes capacitive over a range of frequencies.

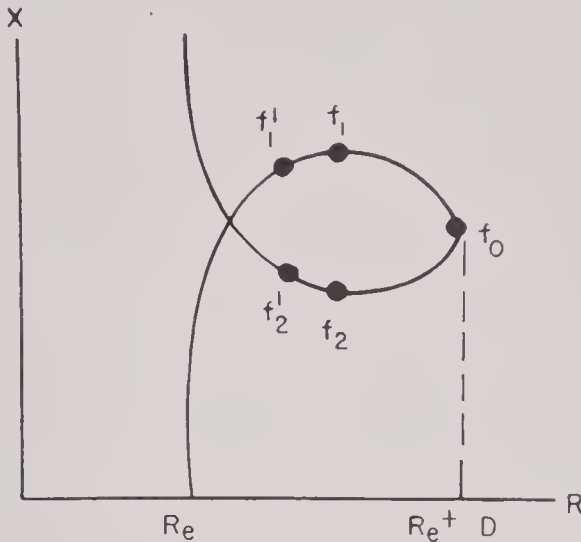


FIGURE 8. Total impedance diagram.

From Figure 9 the following set of values can be deduced:

$$\begin{aligned} R_e &= 3.0 \text{ ohms,} \\ L_e &= 150 \mu\text{h,} \\ D &= 3.5 \text{ ohms,} \\ f_0 &= 234 \text{ c,} \\ f_1 &= 214 \text{ c,} \\ f_2 &= 256 \text{ c,} \\ Q &= 5.6 \\ L_1 &= 425 \mu\text{h,} \\ C_1 &= 1090 \mu\text{f.} \end{aligned} \quad (41)$$

The assumptions made and the data obtained are not sufficient to determine the efficiency. However, a formula can be derived that will be instructive for later applications. Consider formula (21) as applied to the present case. In the first place, according to equation (30), Z_{em} is real, so that $X_{em} = 0$. Now, as the frequency is varied, the only term in (21) which changes is $X_m + X_L$. Actually it has been assumed that $X_L = 0$, but in any

case X_m and X_L can be lumped. Also R_L is assumed to be constant. Then the maximum of efficiency with respect to frequency is the maximum with respect to $X_m + X_L$, as given by equation (22). Since $X_{em} = 0$, this maximum occurs at f_0 , the frequency of resonance. From equation (21) its value is found to be

$$\text{Eff}_{\text{resonance}} = \frac{1}{\left[1 + \frac{R_e(R_m + R_L)}{R_{em}^2}\right]} \cdot \frac{R_L}{R_m + R_L} \quad (42)$$

Comparison of equations (30), (32), and (35) shows that

$$\frac{R_m + R_L}{R_{em}^2} = \frac{1}{D}, \quad (43)$$

where D is the diameter of the motional impedance circle. Equation (42) then becomes

$$\text{Eff}_{\text{resonance}} = \frac{D}{R_e + D} \cdot \frac{R_L}{R_m + R_L} \quad (44)$$

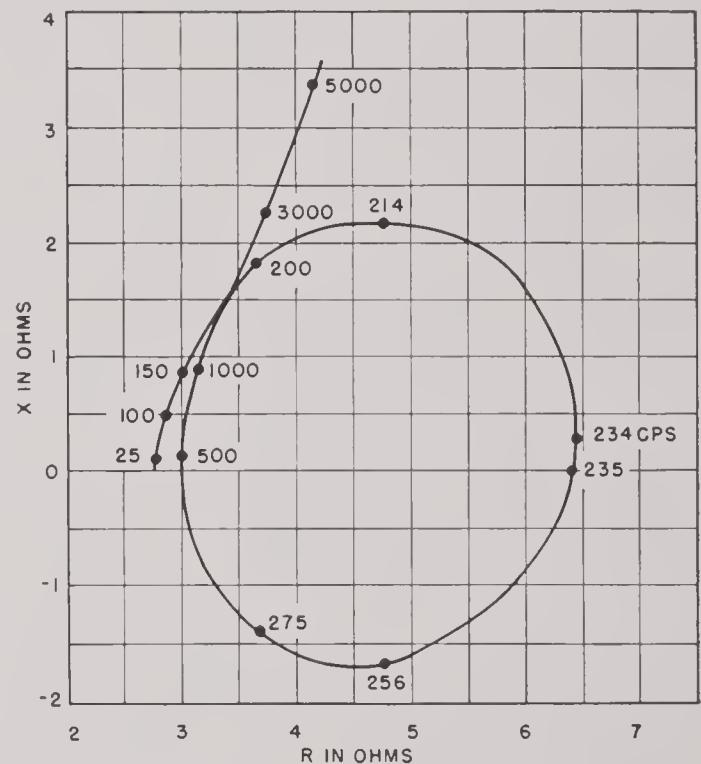


FIGURE 9. Measured impedance of 4-in. PM speaker (Utah 4PZ).

So far, no way of obtaining the second factor in this equation has been proposed. This will be temporarily disregarded here. The first factor, however, can be directly found from Figures 8 or 9. In the latter, it is equal to 0.54. The two factors in (44) can be given a very simple interpretation. The first factor can be regarded as a gross electromechan-

ical conversion efficiency whereas the second can be thought of as a purely mechanical efficiency which gives the fraction of total mechanical power that the speaker delivers to the useful load (radiation resistance of air). It is seen that both factors are less than unity, so that the above interpretation is reasonable. A word of caution is necessary, however, since later transducers will be considered in which the equivalent of the first factor may exceed unity, although the product of the two never does.

2.3.3 Four-Terminal Equivalent Circuit for Dynamic Speaker

The circuit already obtained in Figure 5 is equivalent to the speaker as a two-terminal electric network; that is, the circuit represents correctly the reflection into the electric circuit of the masses, stiffnesses, and resistances which are parts of the speaker or coupled to it. It cannot be seen from the circuit just what the velocity of the cone is when a known voltage is applied nor what force is developed between the cone and the air. The circuit does give the correct disposition of power among internal electrical and mechanical losses and useful radiation, and this information is frequently sufficient.

However, slightly more complicated equivalent circuits can be constructed which represent the loudspeaker as a four-terminal network, so that force and velocity appear at the mechanical terminals as well as voltage and current at the electric terminals. The mutual impedances have already been shown to be of opposite sign in an electromagnetic or magnetostrictive system and of the same sign in electrostatic, piezoelectric, and purely electric systems. It is clear, therefore, that an electric four-terminal network cannot be obtained equivalent to an electromagnetic or magnetostrictive system, when *force* is replaced by *voltage* and *velocity* by *current*. However, by replacement of *force* by *current* and *velocity* by *voltage*, such a representation can be made. By rewriting equations (17) to obtain E and v as linear combinations of I and F ,

$$\begin{aligned} E &= \left(Z_e + \frac{Z_{em}^2}{Z_m} \right) I + \left(\frac{Z_{em}}{Z_m} \right) F, \\ v &= \left(\frac{Z_{em}}{Z_m} \right) I + \left(\frac{1}{Z_m} \right) F. \end{aligned} \quad (45)$$

Notice that the cross coefficients are now equal not only in magnitude but also in sign. Thus, if F is

regarded as a current and v as a voltage, a purely electric network equivalent to equations (45) can be formed. The simplest is shown in Figure 10,

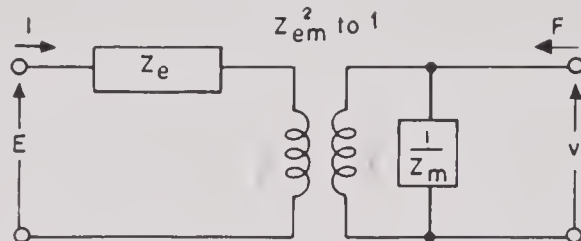


FIGURE 10. Equivalent four-terminal network for electromagnetic transducer.

where the transformer shown is ideal with impedance ratio Z_{em}^2 to unity. If a resistance $1/R_L$ is connected across the mechanical terminals, with the help of equations (30) and (32) it is found that Figure 10 becomes the same as Figure 5. With Figure 10, of course, the current (force) flowing in and the voltage (velocity) developed across the mechanical load can be determined.

Consider a simple example of the use of Figure 10, here using low frequencies, for which the wave length

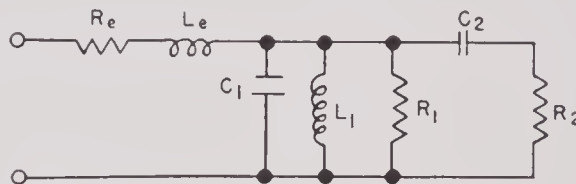


FIGURE 11. Equivalent circuit of dynamic speaker at low frequencies.

is greater than the circumference of the speaker considered as a vibrating disk. It can be shown then that the load to be connected to the right terminals in Figure 10 consists of a resistance and con-



FIGURE 12. Equivalent circuit of dynamic speaker at intermediate frequencies.

denser in series, in order to represent the radiation impedance of the air. This is equivalent to inserting a condenser in series with R_2 in Figure 5, yielding the circuit of Figure 11.

The symbols used are for the most part the same

as in Figure 5. When the speaker is driven electrically, power dissipated in R_2 represents useful radiation of sound. For further restriction of the frequency range, consider only frequencies above resonance. Thus for the speaker whose impedance was shown in Figure 9, frequencies are limited to those between 400 and about 1,500 c. In this range the circuit reduces to Figure 12, where the omitted elements are negligible. Furthermore, the various impedances are related by

$$R_e \gg \frac{1}{j\omega C_1} \gg \frac{1}{j\omega C_2} \gg R_2,$$

and thus the power delivered to R_2 (useful radiation) is approximately

$$\text{Radiated power} = \left(\frac{E}{R_e} \frac{j\omega C_2}{j\omega C_1} \right)^2 R_2,$$

which is independent of frequency.

2.4 MOTIONAL IMPEDANCE

Before an explicit consideration of magnetostriction is developed, some of the results already found for the dynamic loudspeaker will be generalized. Methods will be obtained by which the impedance and particularly the motional impedance of a transducer to operate in water can be used to determine its potential and actual efficiency.

As already stated, the motional impedance of a transducer is that part of its electric impedance arising from the motion of its mechanical terminals. In representing the motional impedance by Z_{mot} ,

$$Z_{\text{mot}} = Z_i - Z_e = \frac{Z_{em}^2}{(Z_m + Z_L)} \quad (46)$$

can be written, as in equation (34).

In this equation, Z_i and Z_e are impedances measured at the electric terminals, the first when the transducer is free to move under mechanical load Z_L and the second when the transducer is blocked so that no motion is possible at its mechanical terminals. The second equality in equation (46) comes from the previous expression (20) for Z_i . According to equation (46), the motional impedance is the vector difference between the loaded and blocked impedance. If the loaded and blocked impedances have been measured and plotted as two curves in an impedance diagram, the motional impedance can immediately be determined through a point-by-point subtraction of the two curves.

Frequently in underwater sound, the mechanical system, consisting of the mechanical parts of the transducer and the load, is resonant at some frequency. Usually, if this resonance is pronounced, the transducer is useful only in a certain frequency range near resonance. The methods to be developed in this section are particularly useful for resonant transducers and get into difficulty in application when the mechanical resonance becomes very broad. The total mechanical impedance (internal plus load) will be assumed to be resonant at the frequency f_0 . When the frequency is in this vicinity this impedance will be written in the usual form

$$Z_m + Z_L = (R_m + R_L) + j\left(\omega M - \frac{K}{\omega}\right). \quad (47)$$

Here R_m (internal) and R_L (load) are mechanical resistances, M is the equivalent lumped mass, and K the equivalent lumped stiffness of the system. These quantities, R_m , R_L , M , and K , are constant over the interval to which equation (47) applies. The angular frequency ω_0 at resonance is given by

$$\omega_0 = 2\pi f_0 = \sqrt{\frac{K}{M}}. \quad (48)$$

Just as in electric systems, it is convenient to define a mechanical Q which measures the sharpness of mechanical resonance and may be taken as the ratio at resonance of the mass or stiffness reactance to the resistance:

$$Q = \frac{\sqrt{MK}}{(R_m + R_L)}. \quad (49)$$

The total mechanical impedance (47) may now be rewritten

$$Z_m + Z_L = (R_m + R_L)[1 + j2Qp], \quad (50)$$

where, as in equation (35), the abbreviation

$$p = \frac{1}{2} \left(\frac{\omega}{\omega_0} - \frac{\omega_0}{\omega} \right) \quad (51)$$

has been used.

The frequencies at which the phase angle of $Z_m + Z_L$ is $\pm 45^\circ$ are f_2 and f_1 , and the relations

$$f_2 f_1 = f_0^2, \quad Q = \frac{f_0}{(f_2 - f_1)} \quad (52)$$

exist. The motional impedance can now be written as

$$Z_{\text{mot}} = Z_i - Z_e = \frac{Z_{em}^2}{R_m + R_L} \cdot \frac{1}{[1 + j2Qp]}, \quad (53)$$

which is very similar to the motional impedance found in equation (36) for the loudspeaker. The only difference is that there the coefficient D was real, whereas here the coefficient $Z_{em}^2/(R_m + R_L)$ in general is complex. Assume that Z_{em} is independent of frequency or at least that it varies slowly enough compared with $Z_m + Z_L$ so that it can be considered constant in the neighborhood of resonance. Then the motional impedance (53) is a circle whose resonance diameter is inclined to the horizontal at an angle equal to twice the phase angle of Z_{em} , and whose diameter is

$$D = \frac{|Z_{em}^2|}{(R_m + R_L)}. \quad (54)$$

The motional impedance circle is illustrated in Figure 13 for the case where Z_{em} has a small negative-phase angle. It will be noticed that the resistive part of the motional impedance is negative over a certain

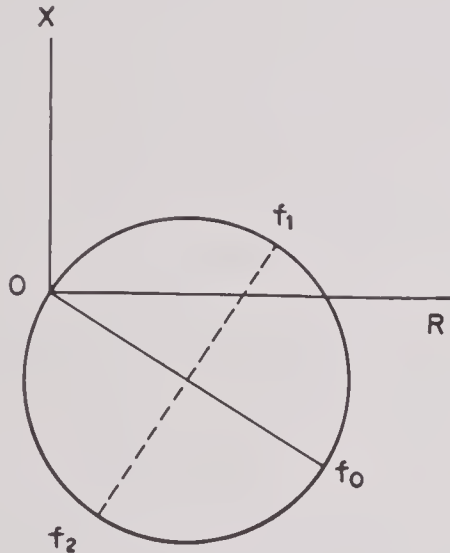


FIGURE 13. Motional impedance of a resonant transducer.

part of the impedance circle in Figure 13. This does not represent a violation of energy conservation, however, since condition (25) insures that total input resistance R_i and clamped electric resistance R_e are always positive.

Equations (49) and (54) give the mechanical Q and the diameter of the motional impedance circle when the transducer is loaded with the mechanical resistance R_L . When the transducer is placed in water, R_L is the radiation resistance of the water to motion of the face of the transducer. A subscript W on Q and D will be used to denote that these quantities are measured with the normal radiation load of the water on the transducer.

Similarly, if the transducer is removed from the water and measured in air, the radiation load R_L is effectively zero. The subscript A will be taken to denote measurements of Q and D made under these conditions. Note that the same formulas, (49) and (54), give both Q_W and Q_A , and D_W and D_A ; R_L is set equal to zero when the transducer is in air. In general, Z_L , the radiation impedance of the water, will not be a pure resistance. There will then be differences in M and K between measurements in water and air. The most noticeable effect will be a change in the frequency of resonance, as given by (48), between air and water. Whenever the dimensions of the transducer are large in comparison with the wave length, the radiation impedance will be almost purely resistive and change in resonance will not occur.

2.4.1 Efficiency at Resonance

The efficiency of the transducer, which was given by equation (21) can be rewritten with the use of equation (20) in the form

$$\text{Eff} = \frac{|Z_i - Z_e|}{R_i} \cdot \frac{R_L}{|Z_m + Z_L|}. \quad (55)$$

At resonance, $|Z_i - Z_e|$ becomes equal to D_W , the diameter of the motional circle in water. Further, $|Z_m + Z_L|$ becomes $R_m + R_L$, in accordance with equation (47). Also, from equation (54)

$$\frac{R_L}{R_m + R_L} = \frac{D_A - D_W}{D_A}. \quad (56)$$

Thus, the efficiency at resonance becomes

$$\frac{D_W}{R_i} \left(1 - \frac{D_W}{D_A} \right), \quad (57)$$

where R_i = resistance at resonance in water,
 D_W = diameter of motional circle in water,
 D_A = diameter of motional circle in air.

The first and second factors in equation (57) may be interpreted respectively as a gross electro-mechanical efficiency and a pure mechanical efficiency. The separation into electrical and mechanical losses is not unambiguous, however, and it is possible to have the first factor greater than unity, although the product is always less.

2.4.2 Potential Efficiency

The potential efficiency of an electromechanical transducer is its maximum efficiency in converting electrical to mechanical power, when both the mechanical load resistance and reactance are varied. The expression (24) has already been deduced for this quantity; however, it depends on quantities not directly known or measurable. The following formula is one from which, in a great many cases, the potential efficiency can be found at once from impedance data.

Equation (24), rewritten with slight alteration, gives

$$\text{Pot eff} = \frac{\left| \sqrt{R_e + \frac{R_{em}^2}{R_m}} - \sqrt{R_e - \frac{X_{em}^2}{R_m}} \right|}{\left| \sqrt{R_e + \frac{R_{em}^2}{R_m}} + \sqrt{R_e - \frac{X_{em}^2}{R_m}} \right|}. \quad (58)$$

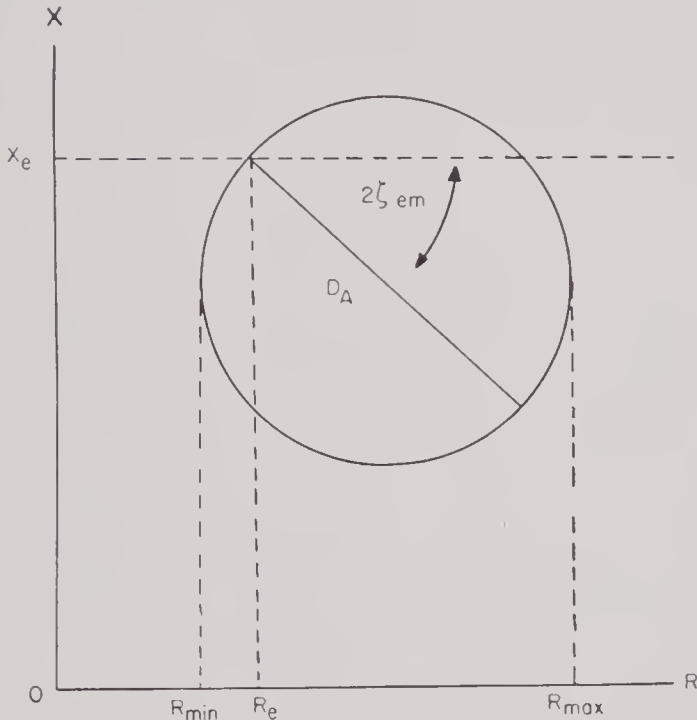


FIGURE 14. Impedance diagram for transducer in air.

Consider now the impedance diagram for the transducer in air. The diameter of the impedance circle, obtained from equation (54), is

$$D_A = \frac{|Z_{em}^2|}{R_m} = \frac{(R_{em}^2 + X_{em}^2)}{R_m}, \quad (59)$$

since $Z_{em} = R_{em} + jX_{em}$. In general, R_m is several times smaller than $R_m + R_L$. Thus the diameter of the air circle is several times larger than the water circle and, in addition, the resonance in air is sharper than in water. These facts frequently combine to

make it a good approximation to assume that the blocked impedance is constant while the motional impedance is traversing the greater part of the circle. The impedance diagram is shown in Figure 14 and consists simply of the motional circle displaced by the constant Z_e . As noted after equation (53), the inclination of the resonance diameter is $2\zeta_{em}$, or twice the phase angle of Z_{em} and it is found from simple geometrical considerations (when blocked impedance may be considered constant) that

$$R_{\max} = R_e + \frac{D_A}{2}[1 + \cos 2\zeta_{em}] = R_e + D_A \cos^2 \zeta_{em},$$

$$R_{\min} = R_e - \frac{D_A}{2}[1 - \cos 2\zeta_{em}] = R_e - D_A \sin^2 \zeta_{em}, \quad (60)$$

where R_{\max} and R_{\min} are the maximum and minimum resistances around the circle, as shown in Figure 14. From equation (60) and the fact that

$$|\tan \zeta_{em}| = \left| \frac{X_{em}}{R_{em}} \right|,$$

$$R_{\max} = R_e + \frac{R_{em}^2}{R_m}, \quad (61)$$

$$R_{\min} = R_e - \frac{X_{em}^2}{R_m}.$$

These are just the quantities needed for the potential efficiency in equation (58). Thus, finally,

$$\text{Pot eff} = \frac{\sqrt{R_{\max}} - \sqrt{R_{\min}}}{\sqrt{R_{\max}} + \sqrt{R_{\min}}}. \quad (62)$$

As already stated, the principal condition for the validity of equation (62) is that the blocked impedance can be considered constant over the motional loop. This implies that the motional loop is very close to a circle.

Equation (62) is very easy to apply and gives a figure of merit for the transducer without requiring measurements in water.

2.4.3 Application to Actual Transducer

The idea of motional impedance and its representation by the motional impedance circle can best be illustrated by data obtained from measurements on an actual transducer. In Figure 15 are shown impedance diagrams for a stack of nickel laminations,

punched in the form of circular rings from 5-mil sheet and wound toroidally. The total reactance X_i is plotted against the total resistance R_i for both air and water measurements, over a range of frequencies including resonance. The characteristic loop produced by the motional impedance is evident. The loops are not perfect circles, since the blocked impedance is not strictly constant over the frequency range corresponding to the major portion of the loop.

The transducer illustrated in Figure 15 is particularly favorable in this respect since both loops are close to circles, implying rather small changes in the blocked impedance. The loops are flattened slightly in the direction of the change in the blocked impedance, which is approximately the direction of a line drawn between points at 30 kc and 80 kc. The diameters of the air and water circles may be estimated from Figure 15 with reasonable accuracy; thus, $D_A = 7.8$ ohms, $D_W = 2.35$ ohms. In addi-

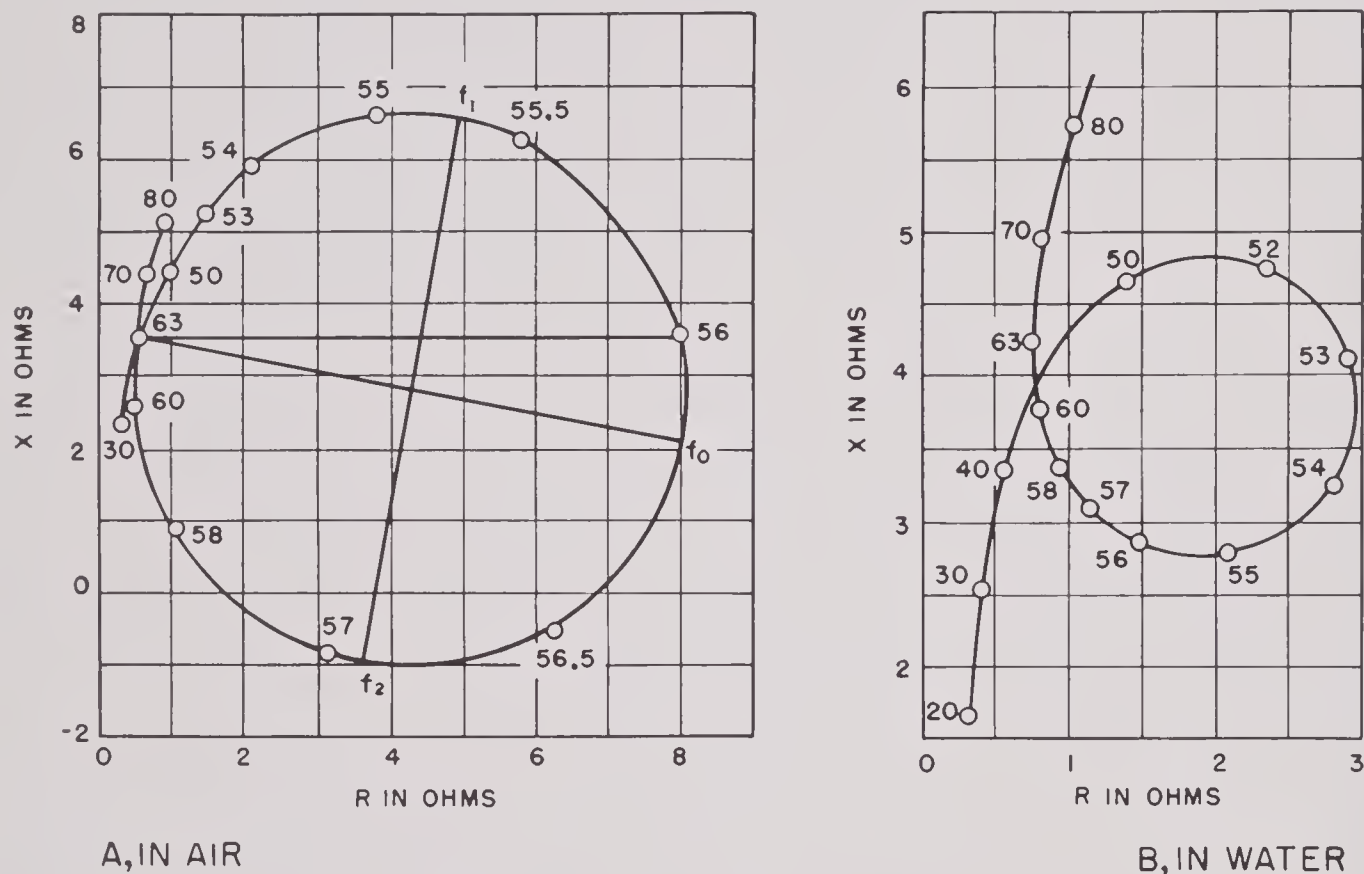
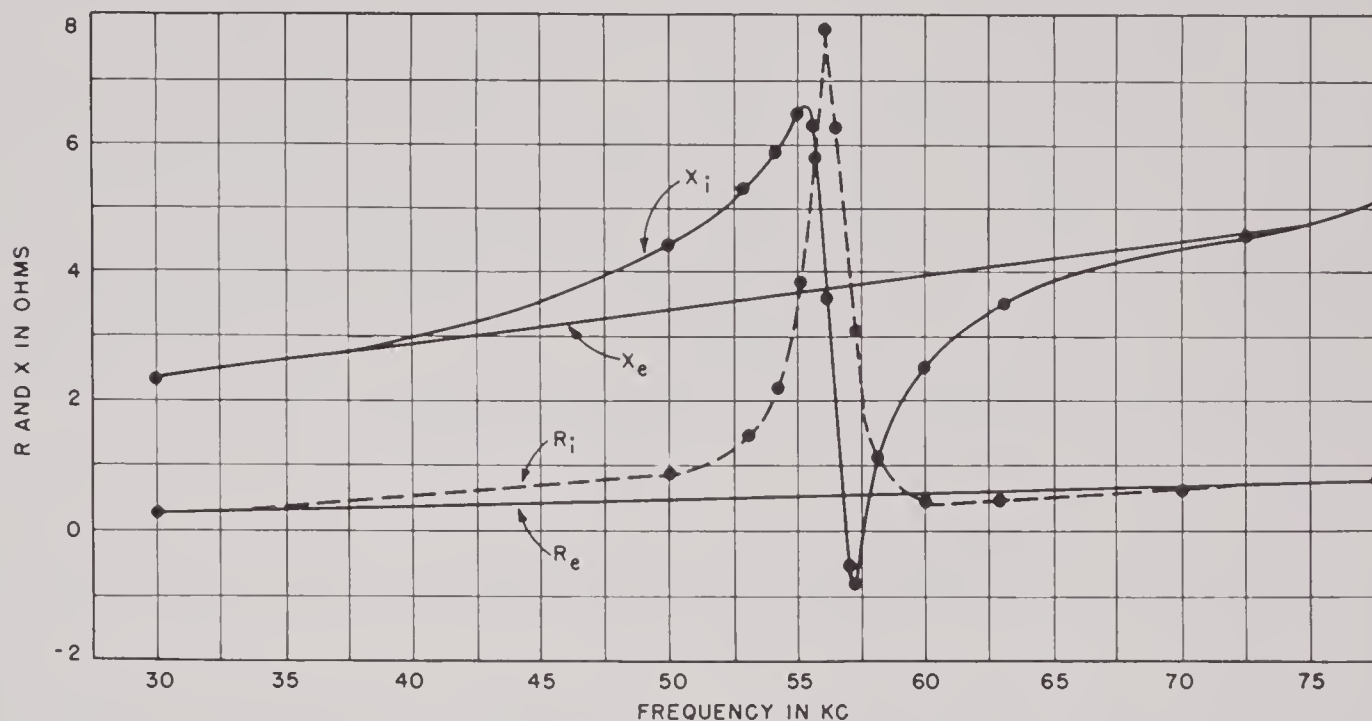


FIGURE 15. Air and water impedance diagrams.

It is not feasible to try to obtain the blocked impedance by direct measurement on a transducer for use in water, since it is virtually impossible to find a large enough mechanical load Z_L . What must be done is to estimate the blocked impedance by interpolation between two frequencies sufficiently above and below resonance so that the motional impedance can be assumed small. Various procedures are available, but it is clear that the accuracy with which the locus of the blocked impedance can be estimated and the accuracy with which the motional impedance can be determined will depend on how much the blocked impedance changes over the greater part of the motional loop.

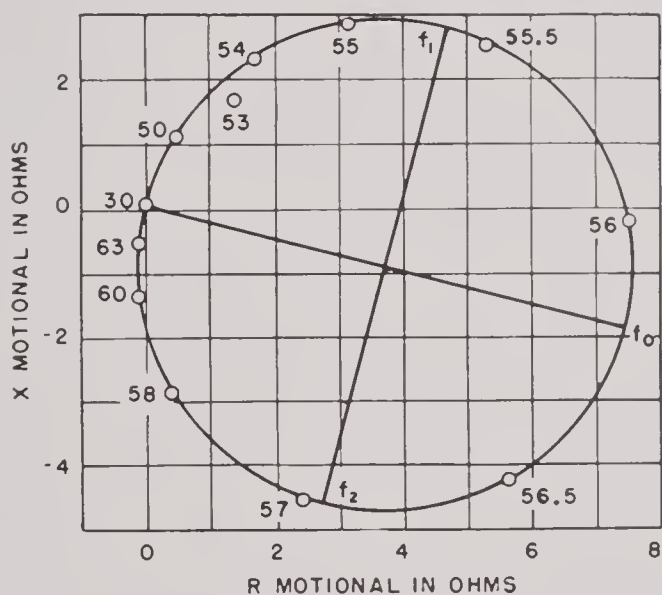
tion, the resistance in water at resonance is about 2.9 ohms. The last figure is less certain, since the point of resonance has not been located accurately. By use of equation (57), 0.57 is found to be the efficiency at resonance. The maximum and minimum resistances in Figure 15A are 8.1 and 0.5 ohms. The potential efficiency determined from equation (62) is therefore 0.60.

When the blocked impedance changes more rapidly with frequency compared with the motional impedance than it does in the present example, it is necessary to obtain the motional impedance explicitly. Far enough from resonance, the motional impedance will be small, so that the blocked and total imped-



A

FIGURE 16A. Resistance and reactance of transducer in air.



B

FIGURE 16B. Motional impedance diagram for transducer in air.

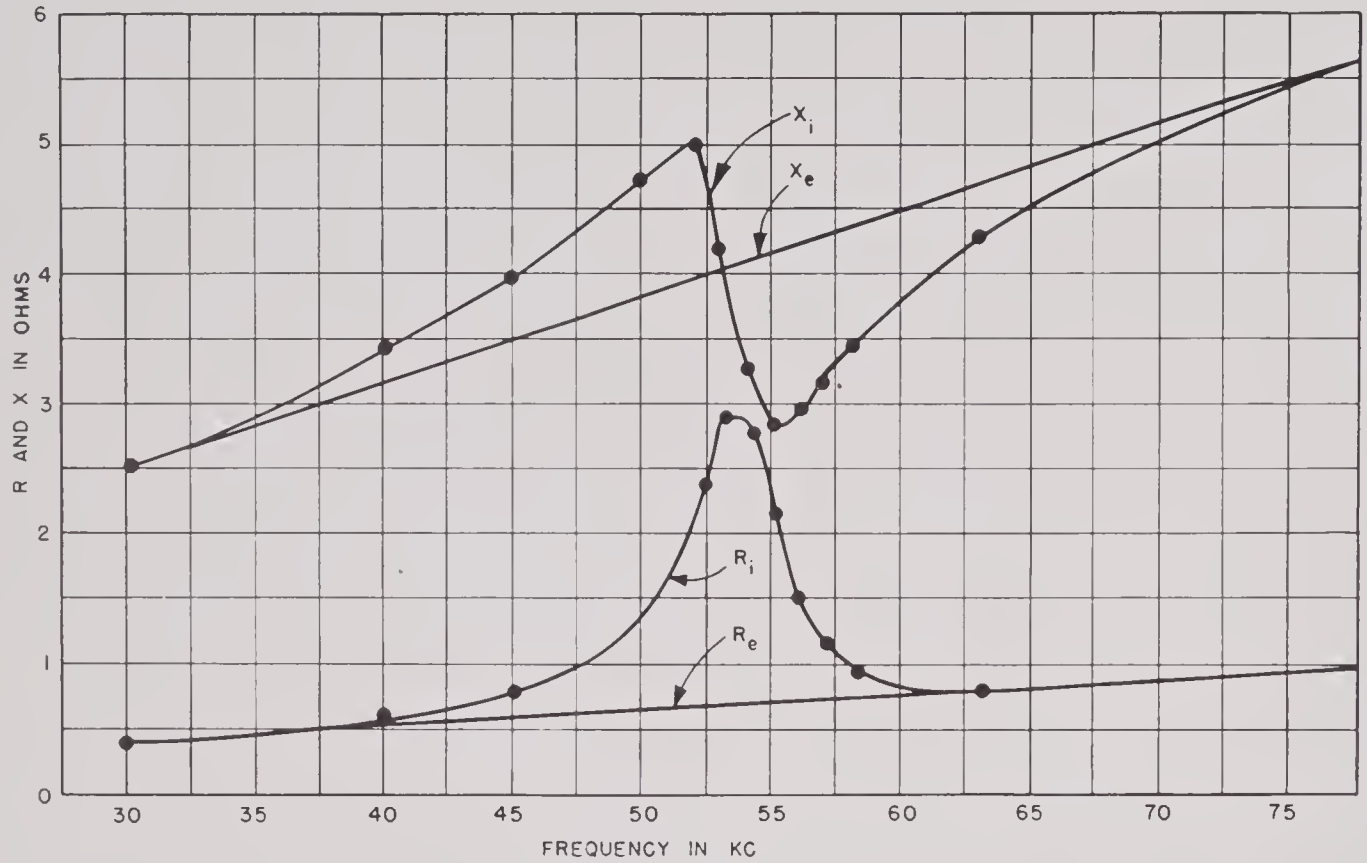
30 and 70 kc. Theoretically, the curve for this transducer should be the arc of a circle, as will be seen in Chapter 3. Once the blocked curve has been chosen, the motional impedance is obtained by vector subtraction (graphically) from the total impedance. The success of the method is measured by the closeness of the motional loop to a circle.

TABLE 1

	Air	Water
f_0	56.2 kc	53.6 kc
$Q = f_0/(f_2 - f_1)$	33	11
D	7.60 ohms	2.34 ohms
R_e (resonance)	0.52 ohm	0.61 ohm
X_e (resonance)	3.82 ohms	4.00 ohms
R_i (resonance)	7.90 ohms	2.90 ohms
R_i (max)	8.00 ohms
R_i (min)	0.40 ohm
Efficiency (resonance)	57%
Potential efficiency	63%

ance curves will come together. The course of the blocked impedance may, therefore, be estimated by drawing a smooth curve between a point well below and another well above resonance. The choice of an interpolation curve will be governed by the appearance of the impedance diagram and by theoretical considerations dependent on the nature of the transducer. In Figure 15, good results are obtained if the blocked impedance is taken as a straight line with a uniform frequency scale joining the points at

A different interpolation method of somewhat greater complexity is shown in Figures 16 and 17. Here the total resistance R_i and reactance X_i are plotted against frequency for both air and water data. Interpolation curves, which in the present case are straight, are shown for the blocked quantities R_e and X_e . Finally the components of the motional impedance are the differences $R_i - R_e$ and $X_i - X_e$, which are plotted as the circles in Figures 16 and 17. Pertinent data obtained from the curves are given in Table 1.



A

FIGURE 17A. Resistance and reactance of transducer in water.

2.4.4 Motional Reactance at Resonance and at the Point of Maximum Efficiency with Optimum Loading

The motional reactance of a transducer at *resonance in air*, found from equation (53), is

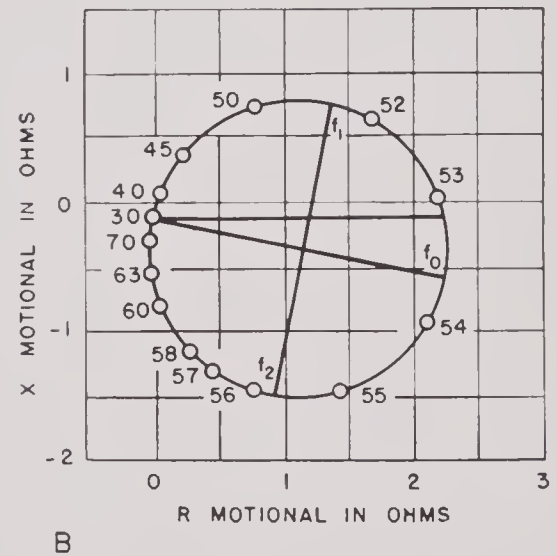
$$X_{\text{mot}} = \frac{2R_{em}X_{em}}{R_m} \quad (63)$$

This is very simply related to the reactance of the same transducer with optimum loading and at the frequency which gives maximum efficiency (under the conditions for obtaining the potential efficiency). From equation (46),

$$X_{\text{mot}} = \frac{2R_{em}X_{em}(R_m + R_L) - (R_{em}^2 - X_{em}^2)(X_m + X_L)}{(R_m + R_L)^2 + (X_m + X_L)^2} \quad (64)$$

With the help of equations (22) and (23) it can be shown that equation (64) is

$$X_{\text{mot}} = \frac{R_{em}X_{em}}{R_m} \quad (65)$$



B

FIGURE 17B. Motional impedance diagram for transducer in water.

Thus the motional reactance under optimum conditions for efficiency is one-half the motional reactance at resonance in air. This fact will be used in Chapter 3 in discussing the geometry of the impedance diagram.

Chapter 3

MAGNETOSTRICTIVE VIBRATORS AND EQUIVALENT CIRCUITS

3.1 EDDY CURRENTS

At ultrasonic frequencies, losses due to eddy currents in the magnetostrictive material may be quite large, even with laminated cores, and it is necessary to consider them in setting up the magnetostrictive equations. It can be shown that eddy-current losses can be taken into account by multiplying the permeability μ by a complex eddy-current factor χ . This factor depends on the geometry of the magnetostrictive material and on a characteristic length,

$$d = \sqrt{\frac{10^9 \rho_e}{\mu f}} \text{ (cm)}, \quad (1)$$

where ρ_e = resistivity in ohm-centimeter,
 μ = magnetic permeability,
 f = frequency of applied field.

The physical significance of d is that a magnetic field, applied tangentially to a thick sheet, is reduced to $e^{-2\pi}$ times its value at the surface in penetrating through a depth d . It is the same characteristic length which occurs in the general theory of penetration of an electromagnetic wave into a conducting medium (see glossary for definitions).

For a large flat sheet of thickness t or a stack of such flat laminations insulated from one another, the eddy-current factor χ depends on the ratio d/t . It is convenient to introduce a characteristic frequency f_c defined by

$$\frac{d}{t} = \pi \sqrt{\frac{2f_c}{f}} \quad (2)$$

or

$$f_c = \frac{10^9 \rho_e}{2\pi^2 \mu t^2}.$$

The eddy-current factor χ can now be shown to be

$$\begin{aligned} \chi &= \chi_0 e^{-j\zeta} = \chi_R - j\chi_I \\ &= \frac{\tanh \sqrt{\frac{jf}{f_c}}}{\sqrt{\frac{jf}{f_c}}}. \end{aligned} \quad (3)$$

Graphs of the magnitude χ_0 and the phase ζ , as well as the real and imaginary parts χ_R and χ_I of χ , are shown in Figure 1. They can be used for curved sheets, where the magnetic field lies parallel to the sheets, provided the radius of curvature is large compared to d and provided the sheet does not form a closed electric loop, linked with the magnetic field. The field and current distributions in a sheet are shown in Figure 2 for the case $f/f_c = 2.5$ ($t/d = 0.36$).

From equation (3) the relations

$$\begin{aligned} \chi_R &= 1 - \frac{2}{15} \left(\frac{f}{f_c} \right)^2 + \frac{62}{2835} \left(\frac{f}{f_c} \right)^4, \\ \chi_I &= \frac{1}{3} \left(\frac{f}{f_c} \right) - \frac{17}{315} \left(\frac{f}{f_c} \right)^3 \end{aligned} \quad (4)$$

apply at low frequencies and

$$\chi_R \rightarrow \chi_I \rightarrow \frac{1}{\sqrt{\frac{2f}{f_c}}}, \quad \zeta \rightarrow 45^\circ \quad (5)$$

is valid when the frequency is sufficiently high.

The eddy-current factor χ can be used to determine the core impedance of a coil with laminated core of magnetic material. The core impedance is that part of the total impedance resulting from the magnetic flux that traverses the core which is assumed to have no gap. The total impedance consists of the core impedance plus the leakage impedance, the latter being composed of the copper resistance and the leakage reactance arising from the flux which links the winding without entering the core. Obviously, the splitting of the total flux into two mutually exclusive parts, one of which lies completely in the core and the other completely outside the core, is quite arbitrary. It is, however, a very convenient simplification and does not introduce serious error in well-designed magnetic circuits.

If the core inductance, calculated without taking account of eddy currents, is L_0 , then the actual core impedance is given by

$$Z_c = R_c + jX_c = j\omega L_0 \chi. \quad (6)$$

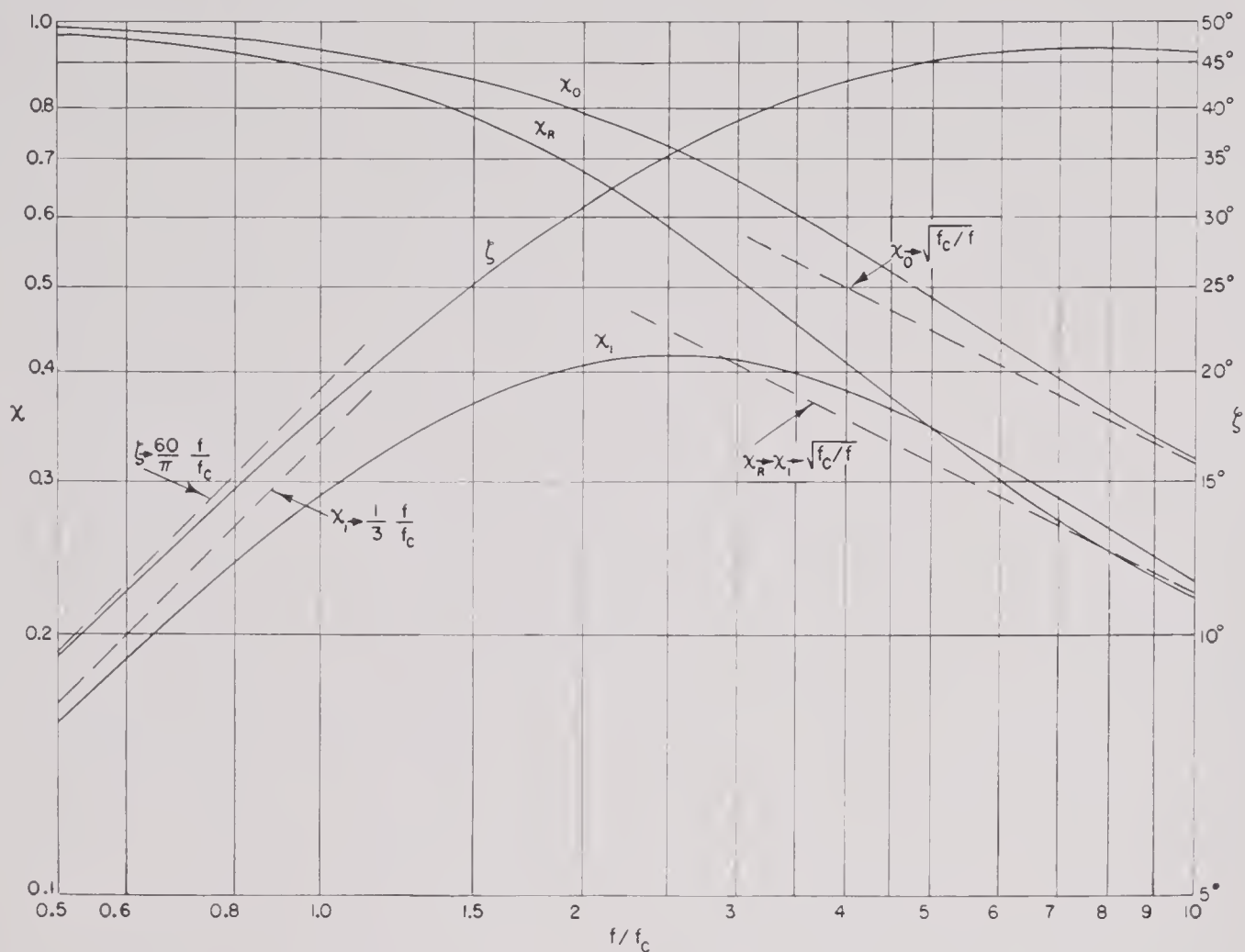


FIGURE 1. Eddy-current factors for flat lamina.

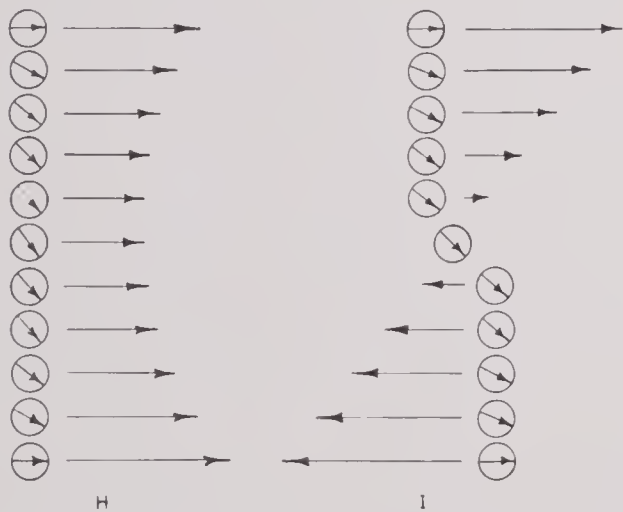
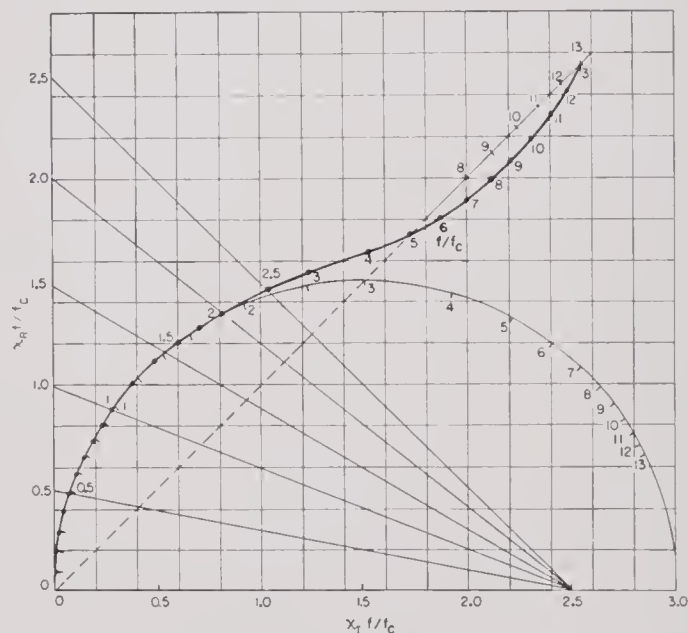
FIGURE 2. Field and current distribution in a plane sheet with $f/f_c = 2.5$. The encircled arrows show the lag in phase. H and I are mutually perpendicular.

FIGURE 3. Theoretical impedance of core composed of flat laminations.

The dependence of equation (6) on frequency is shown in Figure 3, where $\chi_R f/f_c = X_c/2\pi f_c L_0$ is plotted against $\chi_I f/f_c = R_c/2\pi f_c L_0$, with f/f_c as a

parameter. When the frequency is low, the locus follows a circle with radius 1.5. In this region, the frequency scale along the curve can be easily found,

since lines drawn from the point 2.5 ($5/2$ times the radius) on the horizontal axis through points on the curve produce intercepts on the vertical axis equal to the values of f/f_c on the curve. The frequency scale in this construction is therefore linear on the vertical axis. This is useful in frequency interpolation on an experimental curve. This rule is only approximate, but the error in frequency is less than 1 per cent up to $f/f_c = 2.5$ and less than 5 per cent if f/f_c is less than 4.0.

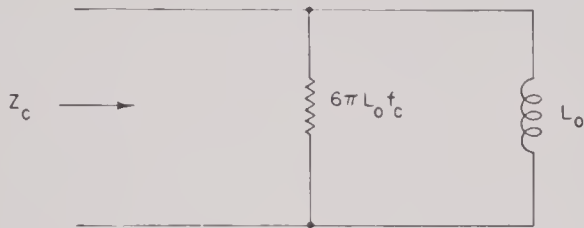


FIGURE 4. Approximate representation of core impedance.

At low frequencies, the core impedance (6) can be represented by the circuit shown in Figure 4, consisting of the inductance L_0 in parallel with a constant resistance $6\pi L_0 f_c$. The impedance of this circuit divided by the factor $2\pi f_c L_0$ is the semicircle in Figure 3. The approximation is quite accurate up to $f = f_c$, but beyond this point there are increasing deviations, particularly in the resistance.

The characteristic frequency f_c which was defined in equation (2) gives a rough indication of eddy-current losses, which are large when the actual frequency f is greater than f_c but small otherwise. In most of the magnetostrictive transducers which have been designed for high efficiency, f/f_c has been kept less than unity through the operating range. Graphs of the characteristic frequency in terms of thickness of the sheet are shown in Figure 5 for nickel and 2V-Permendur. These are included only as a guide, since other factors in equation (2) depend on conditions of polarization and anneal. The constants assumed in Figure 5 are $\rho_e = 8 \times 10^{-6}$ ohm-cm, $\mu = 30$ for nickel, and $\rho_e = 35 \times 10^{-6}$, $\mu = 50$ for 2V-Permendur.

When the magnetic sheet does form a closed electric loop, linking the magnetic field, equation (3) must be modified. This would be necessary, for example, if the sheet were in the form of a tube with its axis parallel to the magnetic field. Then eddy currents flow around the circumference of the tube and shield the interior from the applied magnetic field.

The magnetic field can be visualized as penetrating from only one side of the sheet (the outside of the tube), whereas in a flat sheet the field penetrates from both sides. The situation is illustrated in Figure 6 in which the field and current distributions are shown for a closed cylindrical sheet. This figure

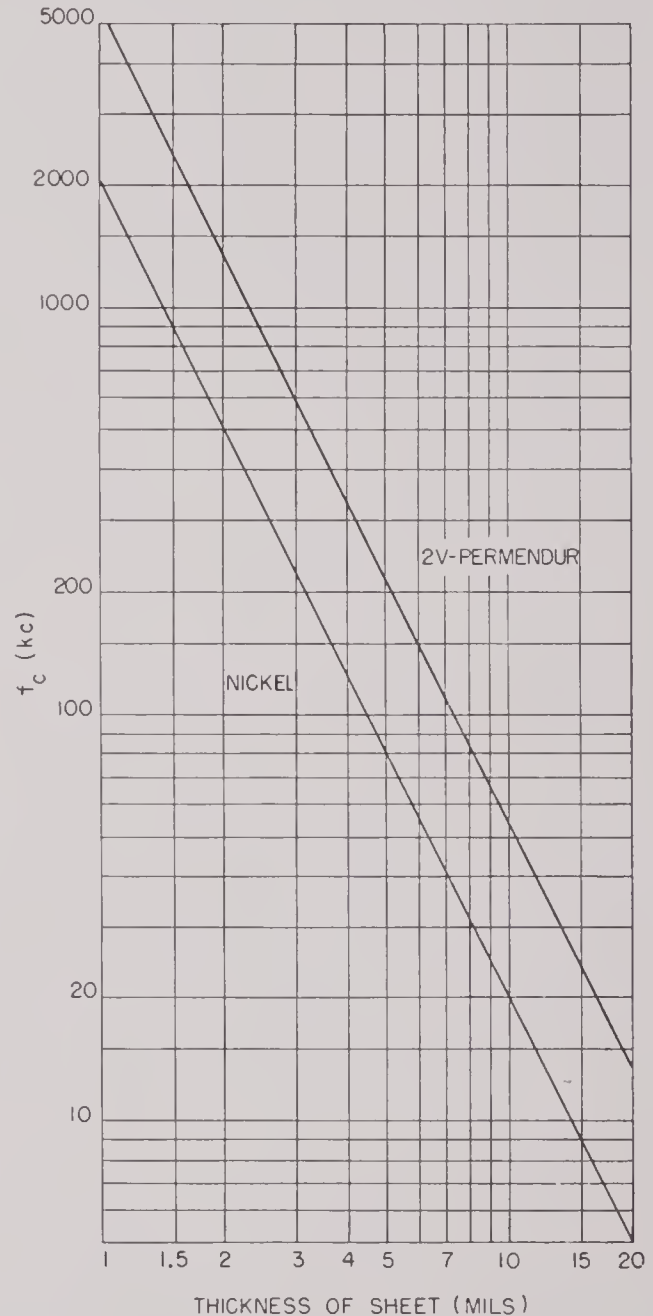


FIGURE 5. Eddy-current parameter f_c for nickel and 2V-Permendur.

is drawn for the same parameters as Figure 2. The lower edge of the sheet in the figure represents the inside of the cylindrical loop or tube, and the shielding of the inside by the circulating currents is illustrated by the decreasing field and current density.

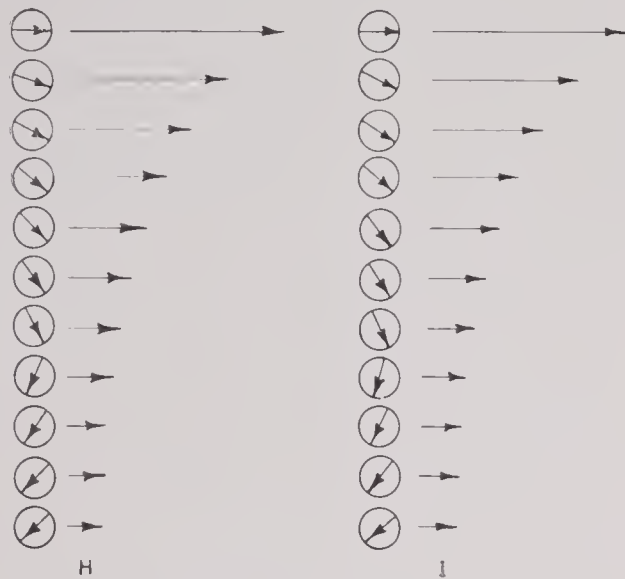


FIGURE 6. Field and current distributions in a cylindrical sheet with $f/f_c = 2.5$. The field is parallel to the axis of the cylinder, which has a large radius in comparison with d .

The eddy-current factor in this case is given by

$$\chi = \frac{e^{-\sqrt{jf/f_c}} \sinh \left| \frac{\sqrt{jf}}{f_c} \right|}{\left| \frac{\sqrt{jf}}{f_c} \right|} \quad (7)$$

and is plotted in Figure 7.

3.2 THEORY OF MAGNETOSTRICTION

Suppose that the total magnetic and mechanical potential energy associated with unit volume of the magnetostrictive material can be written in the form

$$W = \left(\frac{1}{4\pi} \right) \int_0^B H dB - \epsilon B^2 s + \frac{Es^2}{2}, \quad (8)$$

where W = potential energy per unit volume,

H = (total) magnetic field,

B = (total) magnetic induction,

s = longitudinal strain (H , B , s in same direction),

ϵ = magnetostrictive coefficient,

E = Young's modulus for unmagnetized material.

The longitudinal stress P and the externally applied field H_e are given by the partial derivatives

$$\begin{aligned} P &= \left(\frac{\partial W}{\partial s} \right)_B = -\epsilon B^2 + Es, \\ H_e &= 4\pi \left(\frac{\partial W}{\partial B} \right)_s = H - 8\pi\epsilon Bs. \end{aligned} \quad (9)$$

It should be noticed that H , H_e , B , s , and P are total quantities. In general, interest will be centered on small changes in these quantities. For example, according to equations (9), the stress produced by induction B when the strain is zero varies as the square of B . It is therefore customary to apply a static polarizing induction B_0 and superpose on this an incremental induction, which for our purposes will vary sinusoidally with the time. The incremental equations are obtained from equation (9) by differentiation. By now using the same letters for incremental quantities which previously stood for total quantities,

$$P = -\lambda B + Es, \quad (10)$$

$$H_e = H - 4\pi\lambda s, \quad (11)$$

where

$$\lambda = 2\epsilon B_0 \quad (12)$$

is the usual magnetostrictive constant. As shown explicitly by equation (12) it has been assumed in equation (8) that λ is proportional to the polarizing induction B_0 . Evidence verifying this point for nickel within the accuracy of experiment will be presented later.

Since now B and H (incremental values) are presumed small,

$$B = \mu H$$

may be taken as applying in the static case and

$$B = \mu\chi H \quad (13)$$

when eddy currents are present. Here μ is the incremental permeability at the induction B_0 . Use of equations (11) and (13) allows equation (10) to be rewritten

$$P = -\lambda\mu\chi H_e + (E - 4\pi\lambda^2\mu\chi)s. \quad (14)$$

The value of Young's modulus, when the flux density is held constant, is E , as in equation (10); its value in a constant applied field, according to equation (14), is

$$E' = (E - 4\pi\lambda^2\mu\chi) = E(1 - k^2\chi), \quad (15)$$

where $k = \sqrt{4\pi\lambda^2\mu/E}$ is the electromechanical coupling. Since, as stated in equation (12), λ is zero when the polarizing flux is zero, (15) can be interpreted as the value of Young's modulus with polarizing flux, whereas its value without polarization is simply E . Maximum values of k for nickel are of order 0.2 to 0.3, depending upon heat treatment and polarization.

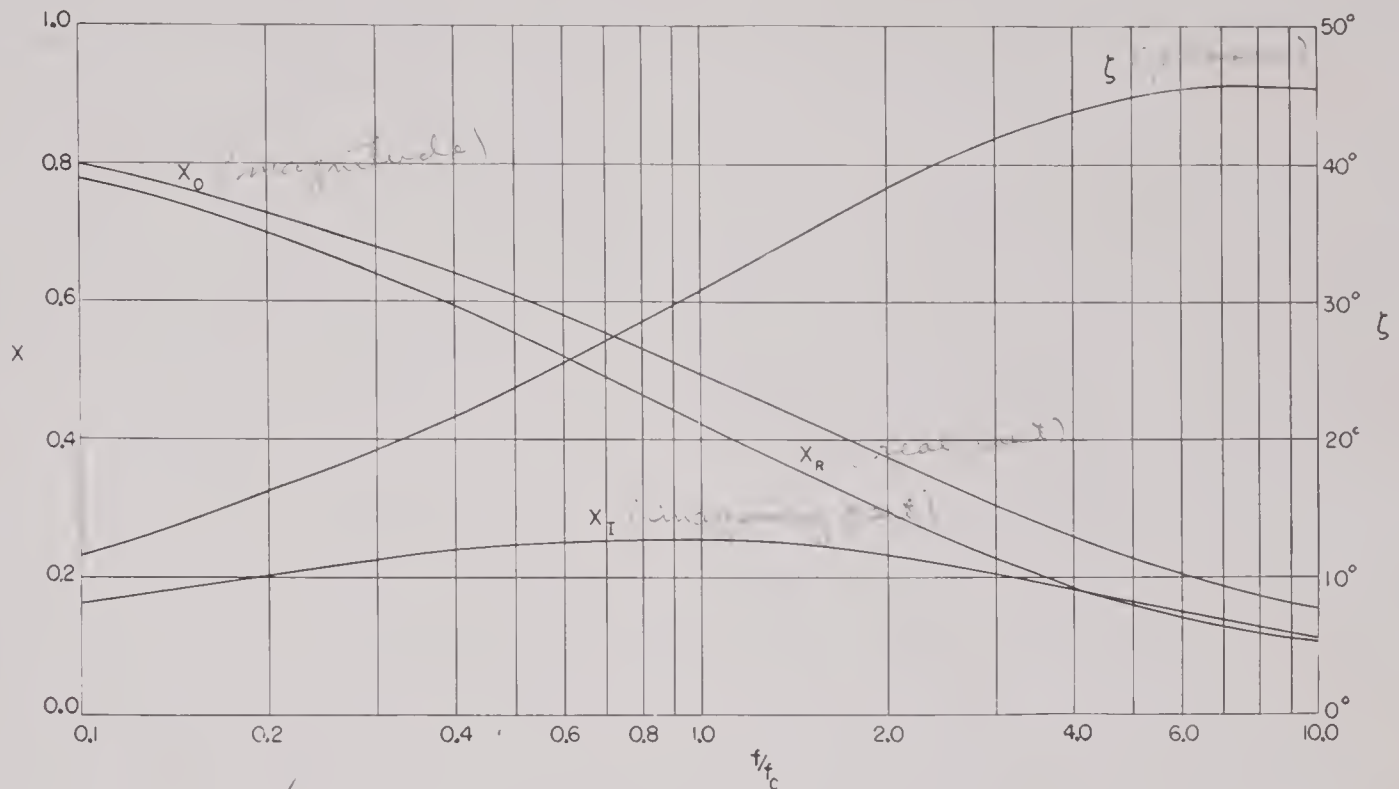


FIGURE 7. Eddy-current factors for large cylindrical lamina.

3.3 RADIAL VIBRATION OF MAGNETOSTRICTIVE RING

Theoretically the simplest type of magnetostrictive transducer consists of a core of magnetostrictive material in the form of a cylindrical shell. The coil is wound toroidally about this core. Two types of construction are shown in Figure 8.

3.3.1 Mechanical Impedance of Ring

The impedances of this transducer are readily obtained. Let F be the scalar pressure integrated over the cylindrical surface. Consider the motion in which all parts of the surface have the same radial component of velocity. The mechanical impedance is

$$Z_m = R_m + jX_m = R_m'' + j\left(\omega M - \frac{K}{\omega}\right), \quad (16)$$

where M is the mass of the cylindrical shell and K is its stiffness. The reason for the double primes on the resistive component on the right will become evident in a moment. The mass M is

$$M = 2\pi ab l \rho_m, \quad (16a)$$

where ρ_m is the density of the magnetostrictive core material and the dimensions a , b , and l are shown in

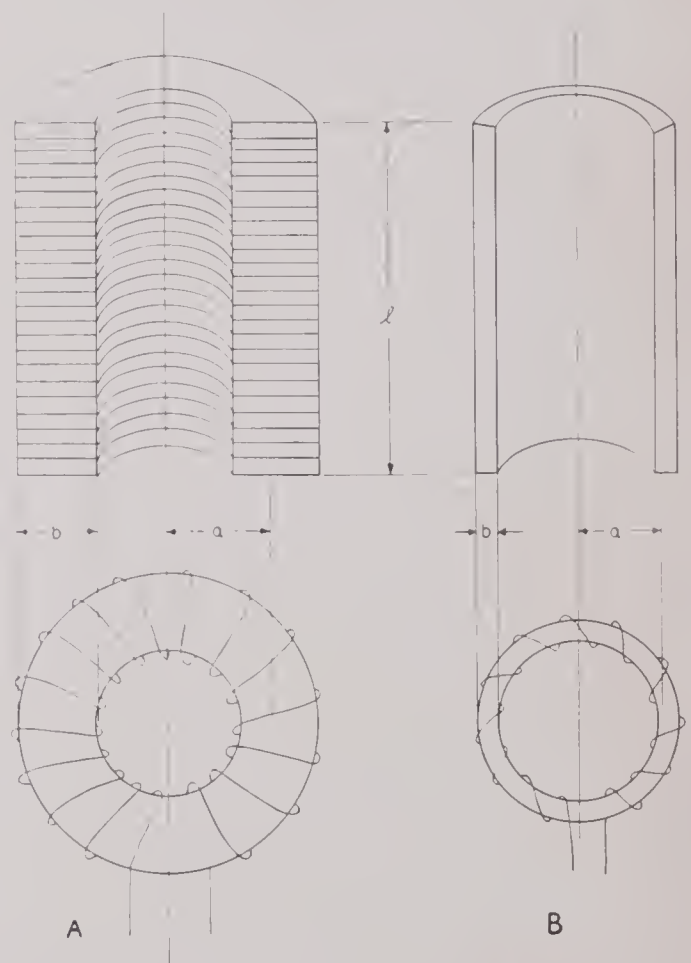


FIGURE 8. Two cores for cylindrical magnetostrictive transducers. A. Core consisting of a stack of rings, B. Core consisting of a thin-walled tube.

Figure 8. If the core were not magnetostrictive, the stiffness could properly be written as

$$K_0 = \frac{2\pi b l E}{a}, \quad (17)$$

where E is the Young's modulus of the material. However, it has just been shown in equation (15) that even under static conditions a magnetostrictive core has a Young's modulus E or E' , according as the induction B or the applied field H_e is held constant. Further, E' depends on the permeability μ , which in the dynamic problem must be replaced by $\mu\chi$ where χ is the eddy-current factor. Thus E' depends on the frequency, because of eddy currents, and is complex, since χ has an imaginary part. This means that the term $K/j\omega$ in equation (16) is not purely imaginary and therefore represents resistance as well as reactance when magnetostriction is present.

The presence of an additional resistive part of the mechanical impedance due to magnetostriction and eddy currents can be understood rather easily. Consider the dissipation of power when a sinusoidal force is applied to the magnetostrictive core. First, of course, the velocity v produced by the force causes power loss $R_m''v^2$ on account of the purely mechanical resistance present. Second, the velocity, being attended by an alternating strain, sets up an alternating field through the inverse magnetostrictive (Villari) effect. The magnetic field and the associated induction then produce eddy currents which dissipate power because of the electric resistivity of the core. Thus there must be an additional mechanical resistance R_m' such that the second dissipation of power is $R_m'v^2$. Clearly R_m' depends on the magnetostrictive constant λ or the coefficient of coupling k and is zero when λ and k are made zero by removing the polarizing flux. The total resistance R_m is the sum of the two resistances R_m' and R_m'' .

Returning to the stiffness of the cylindrical shell, magnetostriction can be included in equation (17) by replacement of E by E' as given by equation (15). This also takes account of eddy currents through the eddy-current factor χ , giving an effective permeability $\mu\chi$ in equation (15). Here

$$K = K_0(1 - k^2\chi), \quad (18)$$

where K and K_0 are the stiffnesses with and without magnetostriction respectively; k is the coefficient of electromechanical coupling; and χ is the eddy-

current factor. The mechanical impedance given in equation (16) can now be split into two parts,

$$Z_m = Z_m' + Z_m'', \quad (19)$$

of which the second is of purely mechanical origin and is given by

$$Z_m'' = R_m'' + jX_m'' = R_m'' + j\left(\omega M - \frac{K_0}{\omega}\right), \quad (20)$$

while the first, resulting from the electromechanical coupling of the core material, is given by

$$Z_m' = R_m' + jX_m' = \left(\frac{k^2 K_0}{\omega}\right)(\chi_I + j\chi_R). \quad (21)$$

3.3.2 Electric Impedance of Ring

The blocked electric impedance of the transducer can be considered in two parts. The first, Z_c , called the core impedance, is due to the magnetic flux in the core material. It consists of resistance as well as reactance, because of eddy-current losses, and has already been discussed at the beginning of this chapter. The second, denoted Z_l , consists of the resistance of the winding and the reactance due to the flux that does not pass through the core. In the simple cylindrical transducer, the core flux and the leakage flux are distinct. The core impedance is

$$Z_c = j\omega L = j\omega L_0\chi = \frac{j\omega 2N^2 b l \mu \chi}{a} \quad (22)$$

in electromagnetic units. Here N is the number of turns linking the core of length l , radius a , and thickness b , as shown in Figure 8. Equation (22) has the same form as equation (6) and its dependence on frequency is shown in Figure 3. The total blocked electric impedance is

$$Z_e = Z_l + Z_c. \quad (23)$$

3.3.3 Mutual Impedance of Ring

The mutual impedances Z_{em} and Z_{me} remain to be determined. In this first example, particular attention will be given all signs and directions in order to show that $Z_{me} = -Z_{em}$. Ordinarily this relation would be assumed. The actual sign of Z_{em} , as distinct from relative signs of Z_{em} and Z_{me} , rarely is of much consequence, since it depends on conventions chosen for directions of current and velocity, which are usually not specified. It should be noted that important formulas like equations (20), (21), (24), and (25) of Chapter 2 are not affected by reversing the signs of Z_{em} and $Z_{me} = -Z_{em}$.

To consider Z_{me} first, according to equation (14) of Chapter 2,

$$Z_{me} = \left(\frac{F}{I} \right)_{v=0}, \quad (24)$$

where $v = 0$ in the evaluation of the ratio of force to current. The conventions adopted here as to signs and directions can be made clear with the help of Figure 9. The positive direction of the (incremen-

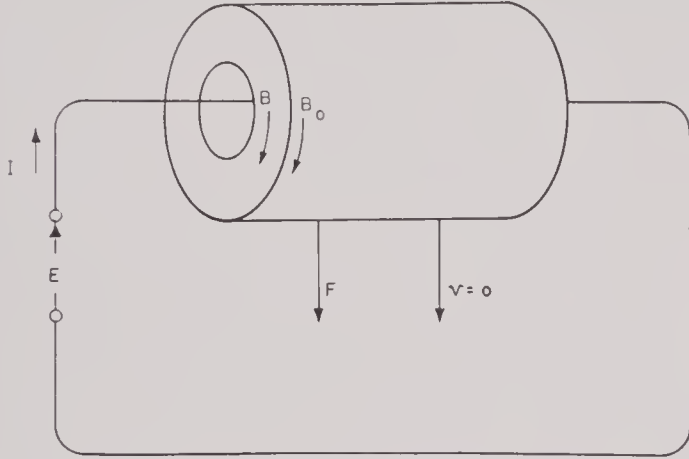


FIGURE 9. Force produced by blocked transducer excited with current I .

tal) induction B is the same as the polarizing induction B_0 in the core. This also fixes the positive direction of current if positive I is taken to produce positive B . Positive E is then determined as shown by the previous convention that E/I should have a positive real part when the transducer is passive. Finally, a radially outward force over the cylindrical surface applied *on the transducer* and an outwardly directed radial velocity will be called positive. Suppose now that a positive current, in the direction shown in Figure 9, is passed through the winding. There is then an induction

$$B = \frac{2N\mu\chi I}{a}$$

through the core in the direction shown and by the convention assumed here this is positive. Since the transducer is blocked ($v = 0$), $s = 0$ in equation (10), and the circumferential stress set up in the core may be written

$$P = -\lambda B = \frac{-2\lambda N\mu\chi I}{a}.$$

The corresponding total radial force is

$$F = 2\pi b l P = \frac{-4\pi\lambda N b l \mu\chi I}{a}.$$

It should be noted that P is negative (compression) and that F is also negative (radially inward). Finally, from equation (24),

$$Z_{me} = \frac{-4\pi\lambda N b l \mu\chi}{a}. \quad (25)$$

Consider now the other mutual impedance,

$$Z_{em} = \left(\frac{E}{v} \right)_{I=0}. \quad (26)$$

The surface of the transducer is set in motion with velocity v . The strain, which is proportional to the integrated velocity, is

$$s = \frac{v}{j\omega a}.$$

Since $I = 0$, there is no externally applied magnetic field (disregarding static polarizing fields) and equation (11) gives

$$H = 4\pi\lambda s = \frac{4\pi\lambda v}{j\omega a}$$

for the magnetic field produced by the motion. The direction of this field is shown in Figure 10. The flux in the core as a result of the field H is

$$\Phi = \frac{4\pi\lambda b \mu\chi v}{j\omega a},$$

and the generated open-circuit voltage

$$E = N \frac{d\Phi}{dt} = j\omega N \Phi = \frac{4\pi\lambda N b l \mu\chi v}{a}, \quad (27)$$

where the direction of E is shown in Figure 10.

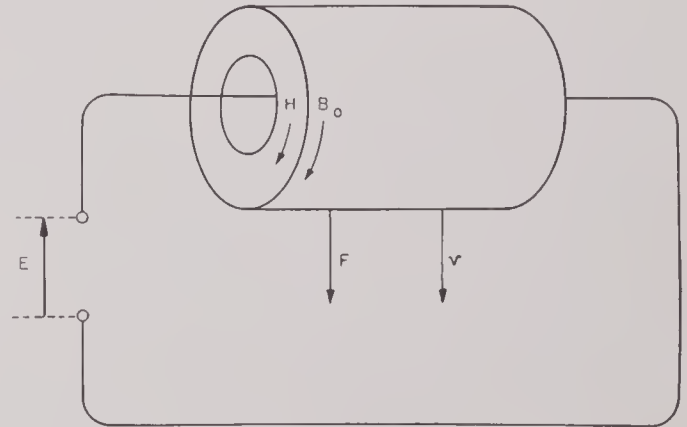


FIGURE 10. Open-circuit voltage produced by transducer driven with velocity v .

Comparison of equations (26) and (27) allows the conclusion

$$Z_{em} = \frac{4\pi\lambda N b l \mu\chi}{a}. \quad (28)$$

Thus the mutual impedances as given by equations (25) and (28) are equal in magnitude but opposite in sign, in accord with equation (17) of Chapter 2.

3.3.4 Relation Between Z'_m and Z_c

Some relation might reasonably be expected between the part Z'_m of the mechanical impedance and the core impedance Z_c , involving also the mutual impedance Z_{em} . This follows, since Z'_m is, in a manner of speaking, the reflection of the core impedance in the mechanical system. From equations (21), (22), and (28), it can easily be found that

$$Z'_m = -\frac{Z_{em}^2}{Z_c} = \left(\frac{jZ_{em}}{Z_c}\right)^2 Z_c. \quad (29)$$

Equations for the four-terminal, electromechanical network may be written, therefore, as

$$\begin{aligned} E &= (Z_l + Z_c)I + Z_{em}v, \\ F &= -Z_{em}I + \left(Z'_m - \frac{Z_{em}^2}{Z_c}\right)v, \end{aligned} \quad (30)$$

where Z_l is the leakage (and copper) impedance, Z_c is the core impedance given by equation (22), Z_{em} is the mutual impedance given by equation (28), and Z'_m is the mechanical impedance in the absence of magnetostrictive coupling, represented by equation (20).

3.3.5 Equivalent Electric Circuits for Ring

It has been stated previously that an equivalent circuit is unobtainable for an electromechanical transducer of the electromagnetic or magnetostrictive type when *forces* are replaced by *voltages* and *velocities* by *currents*. The reason for this is that these two types of coupling lead to mutual impedances equal but opposite in sign, while purely electric circuits always lead to the same sign. In the dynamic speaker, this difficulty was avoided by replacement of *forces* by *currents* and *velocities* by *voltages*, since then the cross coefficients [equation (45) in Chapter 2] had the same sign and could be represented as mutual impedances in an equivalent electric circuit. Although the same process can be carried through for magnetostrictive transducers,^a it is more convenient to use a different approach. The reason for

^a This is the method used by Mason.⁴⁶ He has omitted losses due to eddy currents in his treatment.

this concerns the term $-Z_{em}^2/Z_c$ in the mechanical impedance. An analogous term Z_{em}^2/Z_m in equation (45) of Chapter 2 provided a basis for representing these equations by the L section (and transformer) of Figure 10 of Chapter 2. In general, a T section would have been required. Here too, through use of the term $-Z_{em}^2/Z_c$, the number of elements required in the equivalent circuit can be reduced by one.

A voltage e and a current i are introduced through the relations

$$F = jc, \quad v = ji, \quad (31)$$

which imply that e and i are 90 degrees out of phase with F and v respectively. Equations (30) become

$$\begin{aligned} E &= (Z_l + Z_c)I + jZ_{em}i, \\ e &= jZ_{em}I + \left(Z'_m - \frac{Z_{em}^2}{Z_c}\right)i. \end{aligned} \quad (32)$$

Since the new mutual impedances are both jZ_{em} with no difference of sign, equation (32) can be represented formally by an equivalent electric circuit.

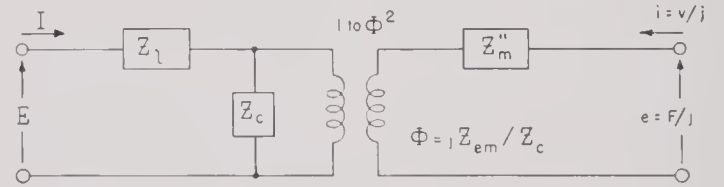


FIGURE 11. Equivalent circuit for cylindrical magnetostrictive transducer.

This circuit is shown in Figure 11, where the transformer is ideal and has the impedance ratio $\Phi^2 = (jZ_{em}/Z_c)^2$ in the direction indicated. From equations (22) and (28) for the cylindrical transducer,

$$\Phi = \frac{jZ_{em}}{Z_c} = \frac{\lambda}{Nf} \quad (33)$$

as the turns ratio of the ideal transformer. Here N is the number of turns on the core, f is the frequency,

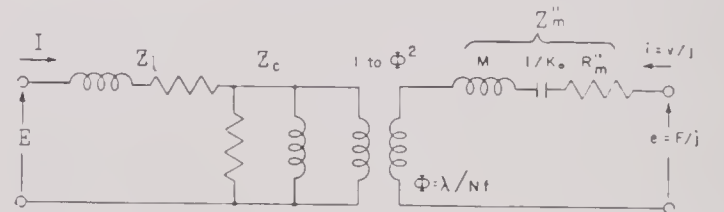


FIGURE 12. Approximate equivalent circuit for cylindrical magnetostrictive transducer.

and λ the magnetostrictive constant. The fact that the turns ratio is dependent on frequency is unorthodox here, but it introduces no formal difficulty. By

use of the forms already found for Z_L , Z_c , and Z_m'' , the more explicit equivalent circuit shown in Figure 12 is obtained. The parallel representation for Z_c has already been discussed (Section 3.1).

3.3.6 Efficiency of Ring

Some additional information can be extracted from equations (29) and (33). With these equations rewritten,

$$Z_m' = \left(\frac{jZ_{em}}{Z_c} \right)^2 Z_c,$$

$$\frac{jZ_{em}}{Z_c} = \frac{\lambda}{Nf}.$$

If these equations are split into their real and imaginary parts,

$$\frac{R_m'}{R_c} = \frac{X_m'}{X_c} = \left(\frac{\lambda}{Nf} \right)^2,$$

$$\frac{X_c}{R_{em}} = \frac{-R_c}{X_{em}} = \frac{Nf}{\lambda}.$$

These can be combined to give

$$\begin{aligned} R_c X_m' &= -R_{em} X_{em}, \\ R_c R_m' &= X_{em}^2. \end{aligned} \quad (34)$$

Consider equation (21) of Chapter 2 the general formula for efficiency obtained previously. If it is assumed that leakage inductance and copper resistance are negligible so that $Z_e = Z_c$, this equation can be written

$$\text{Eff} = \frac{R_c R_L (R_{em}^2 + X_{em}^2)}{AB + C}, \quad (35)$$

where $A = R_c (R_m + R_L) + R_{em}^2$,

$$B = R_c (R_m + R_L) - X_{em}^2,$$

$$C = [R_c (X_m + X_L) + R_{em} X_{em}]^2.$$

Remember that $R_m = R_m' + R_m''$ and $X_m = X_m' + X_m''$, where the double-primed quantities are of purely mechanical origin and the single-primed are reflections of the core impedance into the mechanical system by the magnetostrictive coupling. Then equations (34) can be used to eliminate R_m' and X_m' from equation (35), with the result:

$$\text{Eff} = \frac{R_L (R_{em}^2 + X_{em}^2)}{DF + G}, \quad (36)$$

where $D = R_c (R_m'' + R_L) + R_{em}^2 + X_{em}^2$,

$$F = R_m'' + R_L,$$

$$G = R_c (X_m'' + X_L)^2.$$

3.3.7 Frequencies of Maximum Efficiency and Resonance

It has previously been shown in equation (22) of Chapter 2 that maximum efficiency, with respect to X_L , occurs when the squared bracket in the denominator of equation (35) is zero (according to equation (36), when $X_m'' + X_L = 0$). If frequency is considered the variable instead of X_L , it is still true that maximum efficiency occurs for $X_m'' + X_L = 0$ provided, as is usually the case, that a variation of factors other than $X_m'' + X_L$ can be neglected. On the other hand, resonance occurs when the total mechanical reactance is zero. Denoting by f_E and f_R the frequencies of maximum efficiency and resonance, respectively,

$$\begin{aligned} X_m'' + X_L &= 0 \text{ at } f_E, \\ X_m' + X_m'' + X_L &= 0 \text{ at } f_R. \end{aligned}$$

Note that f_E is constant, independent of the magnetostrictive coupling, whereas f_R is variable, depending on this coupling. If the magnetostrictive coupling is small, X_m' is small and f_R approaches f_E . In other words, f_E is the value of f_R without coupling. As the coupling is increased, X_m' increases and f_R is depressed below f_E . Later in this chapter it will be shown that this relation can be expressed in terms of an effective coupling coefficient k_{eff} by

$$\frac{f_R}{f_E} = \sqrt{1 - k_{\text{eff}}^2}.$$

At f_E , the frequency of maximum efficiency, equation (36), reduces to

$$\text{Eff}_{\text{max}} = \frac{1}{1 + \frac{R_c (R_m'' + R_L)}{R_{em}^2 + X_{em}^2}} \cdot \frac{R_L}{R_m'' + R_L}. \quad (37)$$

For the cylindrical transducer, equation (37) can be simplified by the use of forms that have been found for the various impedances. By substituting equations (22) and (28) into (37),

$$\text{Eff}_{\text{max}} = \frac{1}{1 + \left[\frac{f_E a \chi_I (R_m'' + R_L)}{4\pi \lambda^2 b l \mu \chi_0^2} \right]} \cdot \frac{R_L}{R_m'' + R_L}, \quad (38)$$

where f_E = frequency of maximum efficiency,

a, b, l = dimensions as shown in Figure 8,

χ_I, χ_0 = eddy-current factors (Section 3.1),

μ = permeability,

λ = magnetostrictive constant,

R_m'' = internal mechanical resistance of purely mechanical origin,

R_L = mechanical load resistance.

3.4 LONGITUDINAL VIBRATIONS

The magnetostrictive rod in longitudinal vibration is essentially more complex than the cylinder or ring just considered. At any instant, different points in the rod have different velocities and different stresses, in contrast to the ring, where radial velocities and longitudinal stresses are the same for all parts of the ring. This is another way of saying that the ring is a lumped system but the rod is a distributed system.

3.4.1 Rod as a Six-Terminal Network

If forces are allowed to act at both ends of the rod (or tube) shown in Figure 13 the system can be considered to have two pairs of mechanical terminals and one pair of electric terminals. Positive direc-

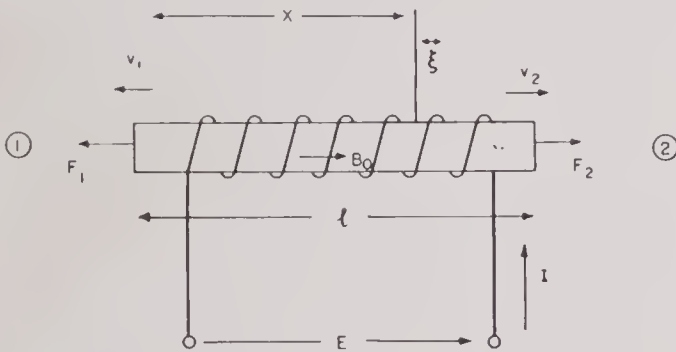


FIGURE 13. Magnetostrictive rod in longitudinal vibration.

tions of the velocities and the forces applied to the rod are shown. A polarizing induction B_0 is supposed to exist in the direction which corresponds to positive incremental induction B and to positive voltage and current. Distance from the left end of the rod is measured by the variable x , and the displacement of the point with equilibrium position at x is $\xi(x, t)$ measured to the right. Thus the values of x at the left and right ends, (1) and (2) in Figure 13, are respectively $x = 0$ and $x = l$. Also

$$v_1 = -\dot{\xi}_{x=0}, \quad v_2 = \dot{\xi}_{x=l},$$

where the dot denotes a partial differentiation with respect to time. The rod will be taken to be long and thin, so the demagnetization can be ignored. The induction B is then given by $B = \mu\chi H$, where H is the average field along the rod, produced by

current in the winding and by strain in the rod. According to equation (11),

$$H = H_e + 4\pi\lambda s,$$

where H_e is due to the current, s is the strain, and λ is the magnetostrictive constant. In terms of the variable ξ , the average strain is

$$\bar{s} = \frac{\xi_2 - \xi_1}{l},$$

so that the induction B can be written

$$\begin{aligned} B &= B_e + 4\pi\lambda\mu\chi\bar{s}, \\ &= \mu\chi H_e + \frac{4\pi\lambda\mu\chi(\xi_2 - \xi_1)}{l}. \end{aligned} \quad (39)$$

The stress P in the rod is found from equation (10), thus,

$$P = -\lambda B + Es,$$

in which E is Young's modulus. With the help of equation (39),

$$P = -\lambda B_e - \frac{4\pi\lambda^2\mu\chi(\xi_2 - \xi_1)}{l} + E\frac{\partial\xi}{\partial x} \quad (40)$$

is evolved, in which $\partial\xi/\partial x$ has been written for the strain s . The equation of motion is then simply

$$\rho_m \ddot{\xi} = \frac{\partial P}{\partial x} = E \frac{\partial^2 \xi}{\partial x^2}, \quad (41)$$

since the first two terms in equation (40) do not depend on x . The solution of equation (41) is used in the form

$$\xi = e^{j\omega t}(C_1 \cos kx + C_2 \sin kx), \quad (42)$$

in which $k = \omega\sqrt{\rho_m/E} = \omega/c_m$ is the wave number when the induction is held constant, or when the magnetostrictive constant is zero.

The boundary conditions remain to be defined. These are

$$\begin{aligned} P &= \frac{F_1}{\sigma}, \quad \dot{\xi} = -v_1 \quad \text{at } x = 0, \\ P &= \frac{F_2}{\sigma}, \quad \dot{\xi} = v_2 \quad \text{at } x = l, \end{aligned} \quad (43)$$

where σ is the cross section of the rod.

Equations (40) to (43), with a little manipulation, yield

$$\begin{aligned} F_1 &= -\lambda\sigma B_e - \frac{4\pi\lambda^2\sigma\mu\chi(v_2 + v_1)}{j\omega l} \\ &\quad - j(\rho c\sigma)_m(v_1 \cotan kl + v_2 \operatorname{cosec} kl), \\ F_2 &= -\lambda\sigma B_e - \frac{4\pi\lambda^2\sigma\mu\chi(v_2 + v_1)}{j\omega l} \\ &\quad - j(\rho c\sigma)_m(v_1 \operatorname{cosec} kl + v_2 \cotan kl). \end{aligned} \quad (44)$$

The induction B_e due to the externally applied field is

$$B_e = \left(\frac{4\pi N \mu \chi}{l} \right) I.$$

It is convenient to let

$$G = \frac{4\pi \lambda \sigma N \mu \chi}{l}, \quad (45)$$

so that the terms $\lambda \sigma B_e$ in equations (44) are expressed merely as GI . By neglecting demagnetization, the core impedance can be written

$$Z_c = \frac{j\omega 4\pi N^2 \sigma \mu \chi}{l}. \quad (46)$$

Then the voltage across the winding is found with the aid of equations (39) and (43):

$$\begin{aligned} E &= Z_l I + N \sigma B \\ &= (Z_l + Z_c) I + G v_1 + G v_2, \end{aligned} \quad (47)$$

where Z_l represents copper resistance and leakage inductance. Equations (44) can be rewritten with the abbreviations (45) and (46)

$$\begin{aligned} F_1 &= -GI - \left[j(\rho c \sigma)_m \cotan kl + \frac{G^2}{Z_c} \right] v_1 \\ &\quad - \left[j(\rho c \sigma)_m \operatorname{cosec} kl + \frac{G^2}{Z_c} \right] v_2, \end{aligned} \quad (48)$$

$$\begin{aligned} F_2 &= -GI - \left[j(\rho c \sigma)_m \operatorname{cosec} kl + \frac{G^2}{Z_c} \right] v_1 \\ &\quad - \left[j(\rho c \sigma)_m \cotan kl + \frac{G^2}{Z_c} \right] v_2. \end{aligned}$$

Equations (47) and (48) are the final results for the magnetostrictive rod as a six-terminal network. Notice that the mutual impedances G appear with opposite signs. Later the system will be reduced to a four-terminal network by appropriately terminating one end of the rod.

3.4.2 Six-Terminal Equivalent Networks for Rod

Equivalent electric circuits for the rod can be obtained by the same methods as were used previously for the ring. Let

$$\begin{aligned} F_1 &= j e_1, & F_2 &= j e_2, \\ v_1 &= j i_1, & v_2 &= j i_2. \end{aligned} \quad (49)$$

Equations (47) and (48) become

$$\begin{aligned} E &= (Z_l + Z_c) I + j G i_1 + j G i_2, \\ e_1 &= j G I - \left[j(\rho c \sigma)_m \cotan kl + \frac{G^2}{Z_c} \right] i_1 \\ &\quad - \left[j(\rho c \sigma)_m \operatorname{cosec} kl + \frac{G^2}{Z_c} \right] i_2, \\ e_2 &= j G I - \left[j(\rho c \sigma)_m \operatorname{cosec} kl + \frac{G^2}{Z_c} \right] i_1 \\ &\quad - \left[j(\rho c \sigma)_m \cotan kl + \frac{G^2}{Z_c} \right] i_2. \end{aligned} \quad (50)$$

These equations are satisfied by the voltages and currents of the networks shown in Figures 14 to 16.

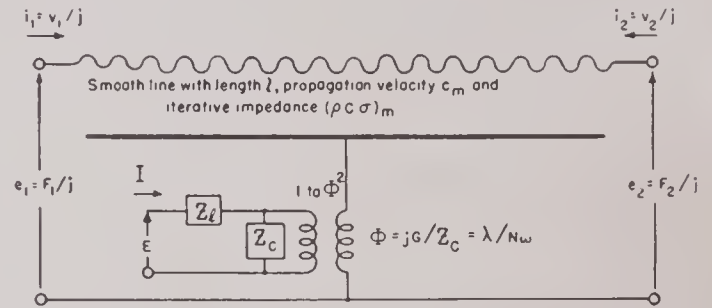


FIGURE 14. Equivalent circuit for magnetostrictive rod.

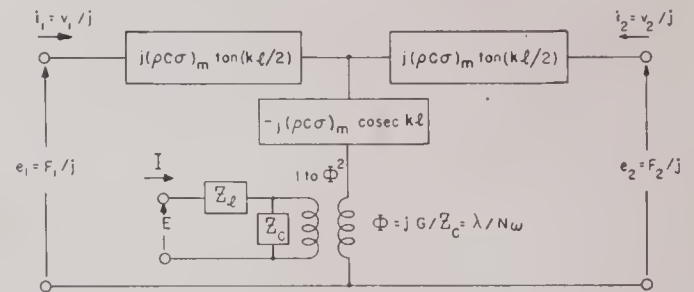


FIGURE 15. Equivalent T circuit for magnetostrictive rod.

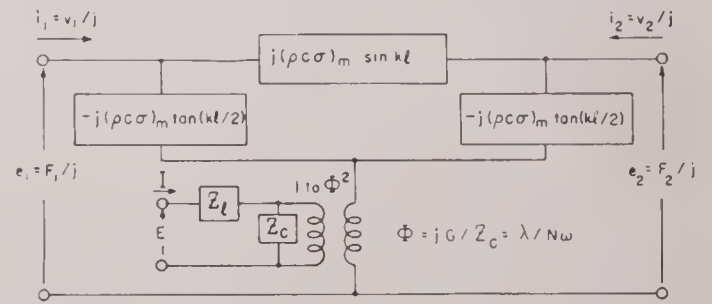


FIGURE 16. Equivalent π circuit for magnetostrictive rod.

Note that the ideal transformer here has a turns ratio Φ differing by a factor of 2π from that found for the ring. For any narrow range of frequency, the equivalent circuit can be simplified by introducing lumped constants to replace the smooth line. The

error made in doing this is small if the frequency range over which it is used is small. For example, when the rod is close to half a wave in length, the circuit is as shown in Figure 17. Here the induct-

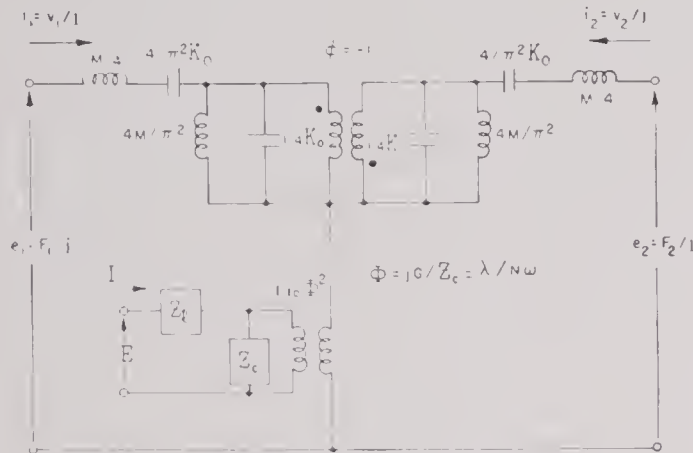


FIGURE 17. Equivalent lumped circuit for half-wave magnetostrictive rod.

ances and condensers in the mechanical part of the circuit have been marked with their values in terms of the mass of the rod $M = l\sigma\rho_m$ and its static stiffness $K_0 = E\sigma/l$ (E = Young's modulus) without magnetostrictive coupling. The ideal transformer marked $\phi = -1$ takes account of the phase inversion produced by a half-wave transmission line. (The black dots indicate corresponding ends of the two windings.)

3.4.1.3 Rod with One End Free; Equivalent Circuits

The equivalent circuit for a rod which is free on one end can be obtained by shorting that end (Figure 15). The result is shown in Figure 18, in which the subscripts on the mechanical voltages and

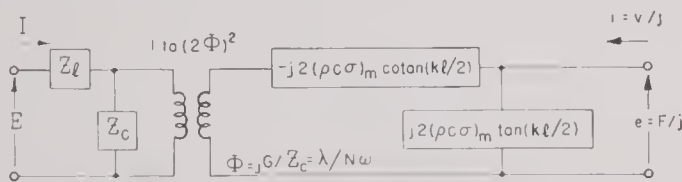


FIGURE 18. Equivalent circuit for magnetostrictive rod free on one end.

currents have been dropped, since the system has now reduced to a four-terminal network. The circuit can be put in more useful form by transforming the T network of mechanical elements into an L network with the help of the equivalence shown in Figure 19.

In the present case, A and B are equal, so that the impedance ratio of the transformer in Figure 19 is 1 to 4. After use of Figure 19 the two series-arm impedances can be combined and the circuit shown in Figure 20 results.

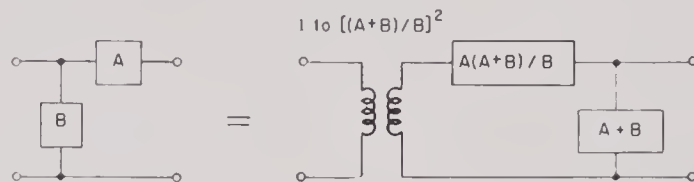


FIGURE 19. Equivalence used in transforming the T circuit of Figure 18 into the L circuit of Figure 20.

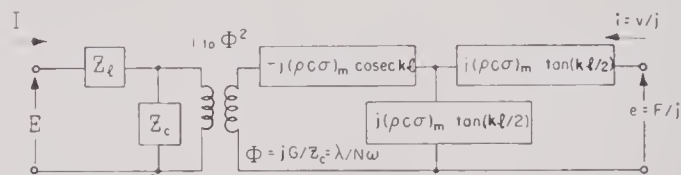


FIGURE 20. Equivalent circuit for magnetostrictive rod free on one end.

As before in Figure 17, the mechanical impedances can be represented by lumped inductances and capacities if the frequency range is restricted. If the frequency is near $f_1 = c_m/2l$, which makes the rod half a wave in length, the series arm is accurately represented by a resonant circuit and the shunt arm by an antiresonant circuit. The frequencies of resonance and antiresonance are both f_1 . The circuit constants are shown in Figure 21 in which M

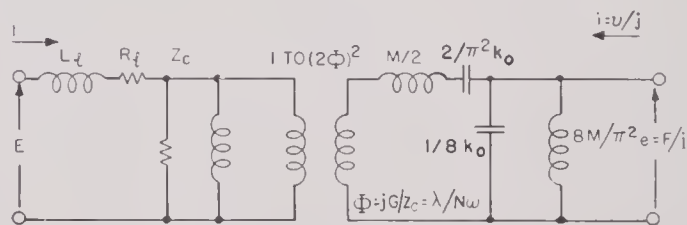


FIGURE 21. Equivalent circuit for half-wave magnetostrictive rod free on one end.

is the mass of the rod and K_0 is the static stiffness without magnetostrictive coupling. At f_1 both the magnitude and the frequency dependence of the two mechanical arms are correct.

The circuit shown in Figure 22 gives the correct impedances at f_1 , where the rod is a quarter wave in length. This circuit does not give quite the right variation of the reactances with frequency since it has only one component in each arm. It is sufficiently accurate for many purposes, however, and

has the advantage of simplicity. If necessary, more complicated circuits can be drawn or Figure 20 can be consulted. Both Figures 21 and 22 show the

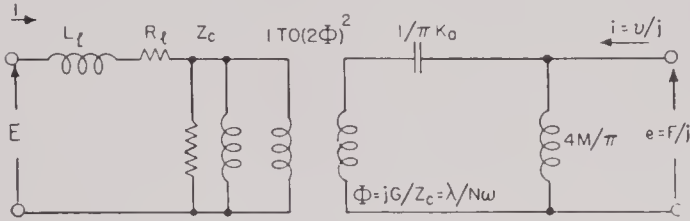


FIGURE 22. Equivalent circuit for quarter-wave magnetostrictive rod free on one end.

core impedance as a fixed inductance and the resistance in parallel, in accordance with the approximation discussed in this chapter in the section on eddy-current theory.

3.1.4 Rod with One End Free and the Other Loaded with Mass and Resistance

One type of magnetostrictive transducer consists of a heavy steel plate with longitudinally vibrating nickel tubes mounted on one side. The other side of the plate is in contact with the water and is thus loaded with the radiation impedance of the water. Usually this impedance is a pure resistance equal to the specific resistance ρc per unit area over the frequency range of the device. The principal effect of the plate is to introduce a mass in series with the radiation resistance as the load on the individual tube.

In order to examine this situation it is convenient to make a transformation of the equivalent circuit

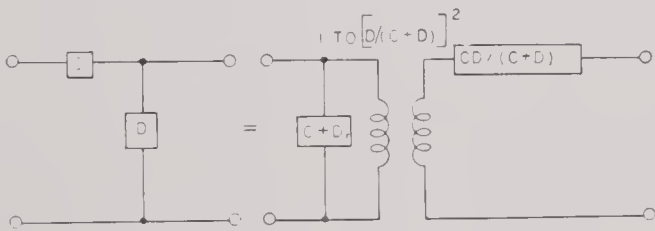


FIGURE 23. Equivalence used in transforming Figure 18 into Figure 24.

shown in Figure 18. In Figure 20, by means of the equivalence of Figure 19, a circuit was obtained in which the mechanical elements were represented by an L section with the open end of the L facing the electric terminals. The transformation will now be made in such a way that the L faces in the opposite direction. For this the equivalence given in Figure 23 is required.

By starting either from Figure 18 or Figure 20, it is found that the circuit of Figure 24 results. Here

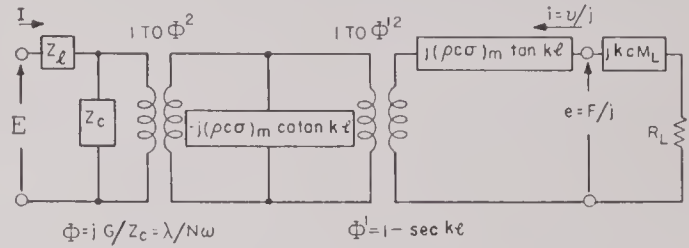


FIGURE 24. Equivalent circuit for magnetostrictive rod with load consisting of series mass and resistance.

the mechanical load consisting of $j\omega M_L = jkcM_L$ in series with R_L has been shown. The equivalent circuit to the left of the mechanical terminals is correct no matter what the mechanical termination. It will be noticed that the second transformer has a turns ratio Φ' which depends on frequency. In fact, when the rod approaches a quarter wave in length, Φ' becomes indefinitely large. In actuality this circuit is useful only over a narrow range, sufficiently removed from the frequency of quarter wave length so that Φ' can be regarded as constant. The frequency range of consequence lies about the point where the series mechanical elements $j(\rho c \sigma)_m \tan kl$ and $jkcM_L$ are resonant. This is the resonance of the mechanical system when the magnetostrictive coupling is zero. Also, if the leakage impedance is small, as assumed previously for the ring, it is the frequency of maximum efficiency which was denoted by f_E . Here a subscript 0 will be used to designate this frequency in order not to compromise Z_L . Whenever Z_L is sufficiently small, f_0 can be identified with f_E . Look first at the circuit for the one frequency f_0 and ignore for the moment what happens in its vicinity. As stated, the reactance of the series mechanical arm becomes zero. This condition may be written as

$$(\tan k_0 l) = -\frac{M_L}{m_0},$$

where $k_0 = 2\pi f_0/c_m$ is the wave number at frequency f_0 , and $m_0 = (\rho \sigma)_m/k_0$ is the mass of a section of the tube $1/2\pi$ times a wave length (one radian). Also the shunt element is

$$-j(\rho c \sigma)_m \cotan k_0 l = j(\rho c \sigma)_m \frac{m_0}{M_L}.$$

The turns ratio Φ' is given by

$$\Phi' = 1 - \sec k_0 l = 1 + \sqrt{1 + \left(\frac{M_L}{m_0}\right)^2}.$$

With the use of these equations, we find that Figure 24 reduces to Figure 25 at frequency f_0 . The mechanical transformer has been removed and the load resistance divided by the impedance ratio Φ'^2 .

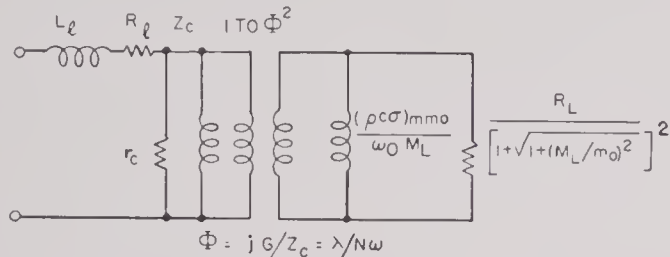


FIGURE 25. Equivalent circuit of Figure 24 at resonance of series arm.

In Figure 25, it is seen that current flowing into the transducer has four competing shunt paths. Only two of these are dissipative, namely, the core re-

R_l , since they increase the total current. If the efficiency is to be high, it is necessary for the transformed load resistance to be low compared with r_c . Thus either the core must be well laminated, which raises r_c , or M_L/m_0 must be large in order to reduce the transformed load. It is not feasible to increase M_L/m_0 indefinitely, since eventually the load resistance becomes less than the copper resistance R_l and also since there are always internal mechanical losses, some of which increase with M_L/m_0 (see next section). However, it is possible to obtain a material increase in efficiency by this device when the eddy-current losses would otherwise be excessive.

Figure 26 shows two of the important quantities connected with the circuit of Figure 25. The parameter M_L/m_0 against which the curves are drawn is the ratio of the mass of the plate associated with

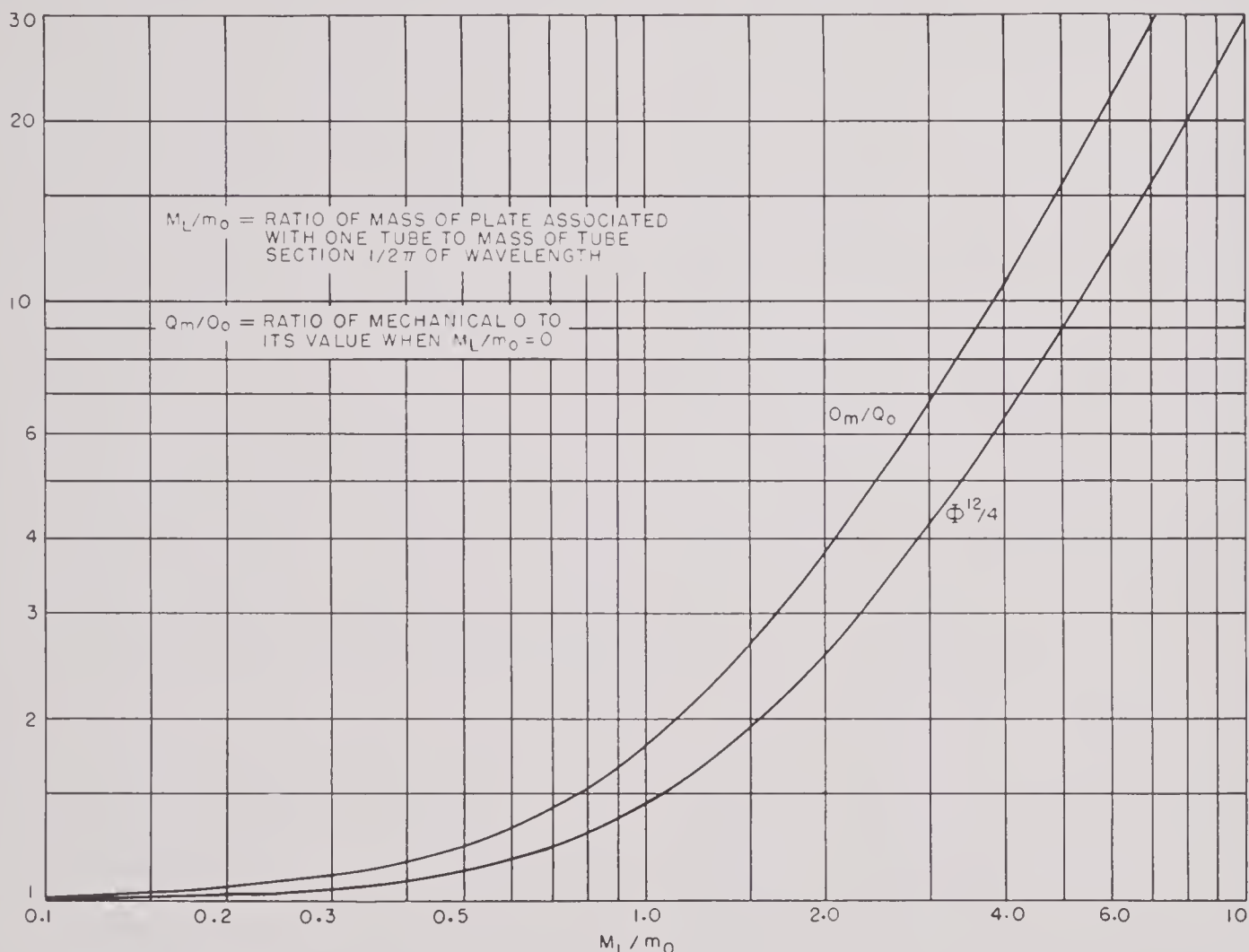


FIGURE 26. Mechanical impedance transformation and mechanical Q for transducer of tube-and-plate construction.

sistance representing eddy-current losses and the mechanical load resistance. The other two paths, of course, increase the losses in the copper resistance

one tube to the mass of a section of tube $1/2\pi$ times a wave in length. The impedance ratio Φ'^2 is shown by the lower curve. The quantity actually plotted

is $\Phi'^2/4$, since $\Phi' = 2$ when $M_L = 0$ and the tube is a half wave in length. The upper curve gives the Q of the mechanical system expressed in multiples of the $Q = Q_0$, which obtains when the mass of the front plate M_L is zero. Then

$$\frac{Q_m}{Q_0} = k_0 l \frac{\left[1 + \left(\frac{M_L}{m_0}\right)^2\right]}{\pi} + \frac{M_L}{\pi m_0}.$$

Figure 26 shows that Q_m increases rapidly as more mass is attached to the tube. The breadth of response which is inversely proportional to Q_m decreases correspondingly.

Until now the frequency has been considered as being held constant at f_0 . If the frequency is allowed to vary slightly in either direction from f_0 , the element in the circuit of Figure 24 that varies most rapidly is the series mechanical arm, provided that Q_m is large. When this is assumed to be so, the turns ratio $\Phi' = 1 - \sec k_0 l$ may be regarded as constant and equal to $\Phi'_0 = 1 - \sec k_0 l$. The shunt mechanical arm, too, usually has a high impedance

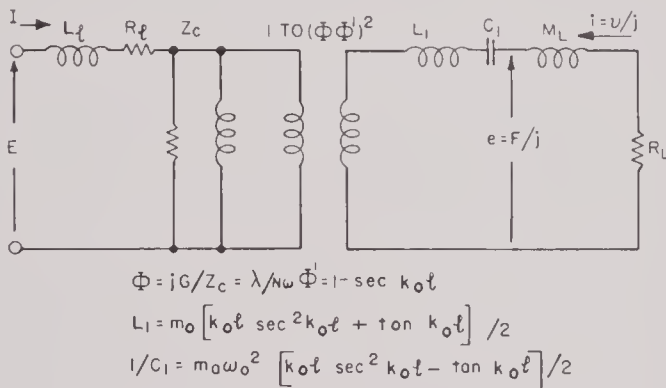


FIGURE 27. Approximate equivalent circuit for magnetostrictive rod with load consisting of series mass and resistance.

compared with other shunt paths, especially when M_L/m_0 is large. Thus it will be omitted entirely, so that Figure 24 in the vicinity of f_0 can be represented by the approximate circuit shown in Figure 27.

It will be observed that Figure 27 has been reduced to the same form as the circuit for the simpler case of the ring as shown in Figure 12.

3.4.5 Internal Mechanical Losses

It is apparent that no allowance was made for internal mechanical resistances in the preceding sections that treated the longitudinal vibrations of a rod. Such a resistance was included in the treatment of

the ring described earlier. There the mechanical system was simple enough so that a reasonably accurate representation could be expected by insertion of a constant mechanical resistance in series with the mass and stiffness of the ring. Furthermore, elaborate transformations of the system were not required in examining its behavior so that the addition of this resistance introduced no great complication. With the magnetostrictive rod, however, matters are somewhat different. In Figure 14, series resistance may be inserted along the smooth transmission line to simulate frictional resistance opposing the velocity at points along the rod. In addition, lumped resistances may be added at the ends to represent, for example, dissipation in supporting members. These resistances greatly complicate transformations in the system. They may be represented approximately by adding an equivalent internal resistance in series with the load. It should be remembered, however, that such an equivalent resistance will not, in general, be constant either with changes of frequency or conditions of loading. Take, for example, the problem just investigated of the mass-loaded tube of Figures 24 or 27. Resistance introduced anywhere except at the loaded end of the tube will not be transformed by the same mechanical transformer shown in Figure 24. The equivalent resistance, introduced in series with the load, will therefore not remain constant as M_L/m_0 is increased but will also increase. Eventually this increase will cause the efficiency to fall off as already noted.

3.5 GEOMETRY OF THE IMPEDANCE DIAGRAM

In this section some of the more important geometrical relations which hold in the impedance diagram for a magnetostrictive transducer will be given. Of necessity, numerous restrictions and approximations are made in the interests of simplicity. Thus the idealized impedance diagram to be discussed will be only an approximation of the actual one but will still be valuable as a guide in interpretation.

The case considered explicitly will be the cylindrical shell or ring for which the equivalent circuit was obtained in Figure 12. This is not so great a specialization as it would seem at first sight, since other systems can be approximately represented by the same equivalent circuit. The half-wave magneto-

strictive rod as shown in Figure 21 is the same if the shunt antiresonant elements are omitted. If, as will usually be true for this system, the load resistance is not large, these elements will present a comparatively high impedance, and their omission will introduce no serious error. Another case, in which the equivalent circuit is almost the same as for a ring, is the example just investigated of the mass-loaded tube (Figure 27).

The core will be assumed to be composed of flat sheets, the flux lying in the plane of the sheets. As long as circulating eddy currents do not flow, the sheets can be curved. Thus slotted tubes are included. Eddy-current effects will be considered small in the sense that f/f_c is less than 2, for instance. According to Figure 3, the core can then be represented as a parallel resistance and inductance. If leakage inductance and copper resistance are now negligible, the impedance of the transducer is the same as that of the circuit in Figure 28. Here the

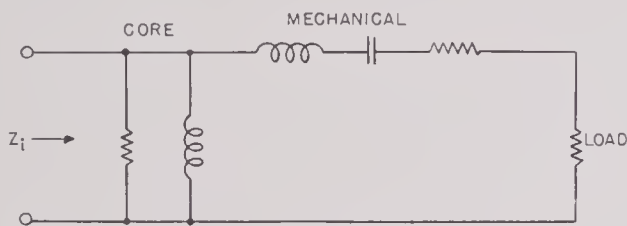


FIGURE 28. Circuit representing loaded impedance of transducer.

electromechanical transformer has been omitted by multiplying the mechanical elements by the proper impedance ratio $1/\Phi^2$. The mechanical Q will be considered to be very high. Then there is a comparatively slow change of the blocked (core) impedance, and the loop in the locus of the loaded impedance will be nearly a circle. Also, the variation of Φ with frequency can be ignored.

Figure 29 shows the idealized impedance diagram. The locus of the blocked impedance is the circular arc OO' with radius r and with center at C on the resistance axis. The large motional circle with diameter D_A is obtained with the transducer in air, that is, with the load resistance in Figure 28 short-circuited. Resonance occurs at point R_A (in air), so that the resonance diameter passes through C and meets the blocked impedance line at right angles. Angle ζ whose tangent is χ_I/χ_R is the complement of the phase angle of the blocked impedance at resonance and also, from equations (53) of Chapter 2 and (28), is one-half the angle between the

resonance diameter and the horizontal. Here χ_R , χ_I are the eddy-current factors.

The smaller motional circle is the motional impedance of the transducer in water, that is, with the load resistance in Figure 28. Larger or smaller circles can be drawn to correspond to smaller or larger load resistances respectively. The circle actually drawn represents the optimum mechanical loading, so that the maximum efficiency, which occurs at point E , is equal to the potential efficiency. The optimum circle may be found by the following geometrical construction. Draw the auxiliary circle which passes through O and O' and has its center on the reactance axis. This circle has radius $r \tan \zeta$ and is the locus of the points of maximum efficiency. This is most easily seen by noting that the suscept-

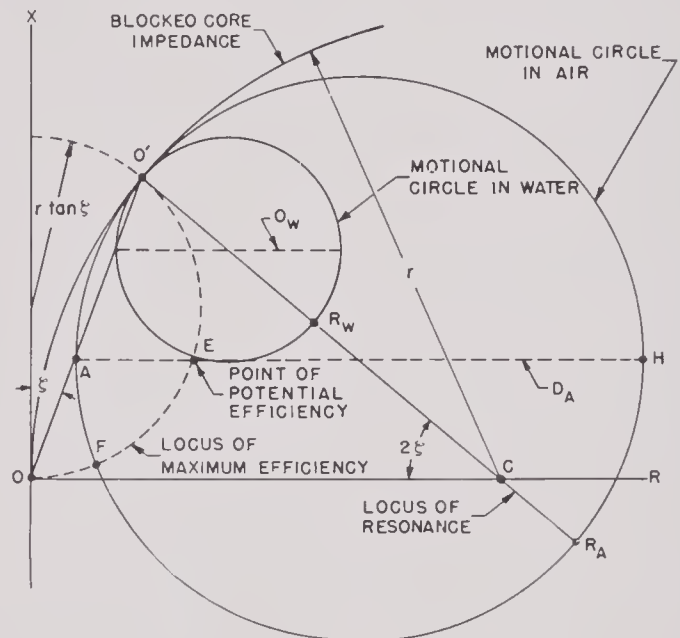


FIGURE 29. Idealized impedance diagram for transducer in air and water.

ance at maximum efficiency is equal to the core susceptance, since the mechanical arm is resonant. The locus of constant susceptance is a circle passing through the origin and having its center on the reactance axis. The auxiliary circle must intersect the motional circle in water, whatever its size, and so must pass through O' . To find the optimum water circle, draw the horizontal diameter of the motional circle in air. This diameter, incidentally, intersects the air circle on the line OO' at the point A . Now the point of maximum efficiency E on the optimum water circle must lie on the horizontal diameter, since there is then a motional reactance at E equal to one-half the motional reactance at R_A , in accordance with

equations (63) and (65) of Chapter 2. The point E , therefore, lies at the intersection of the auxiliary circle and the horizontal diameter. The optimum circle in water may now be constructed, since it passes through O' and has its center on $O'R_A$. As an aid in construction, it may be noted that the auxiliary circle intersects all motional circles at right angles.

In Figure 29A the construction for an actual transducer is carried out, using the data presented in Figures 15, 16, and 17 of Chapter 2. These were for a ring stack of annealed nickel laminations 0.005-inch

thick, toroidally wound and polarized by direct current. The center of the clamped impedance are OO' was determined by the three points representing the impedances at 0, 30, and 80 ke. Point O' corresponding to the clamped impedance at 55 ke (approximately the resonance frequency) was fixed by interpolation along the arc between 30 and 80 ke. The motional-impedance circles of Figures 16 and 17 of Chapter 2 were drawn tangent to the clamped-impedance arc at point O' . The center of the auxiliary circle is the point of intersection of the bisector of the angle 2ζ with the reactance axis. It will be noted that the radius r of the clamped impedance arc passes nicely through the center of the air circle, but not through the center of the water circle. This represents a small departure from the idealized transducer. The point E which lies at the intersection of the auxiliary

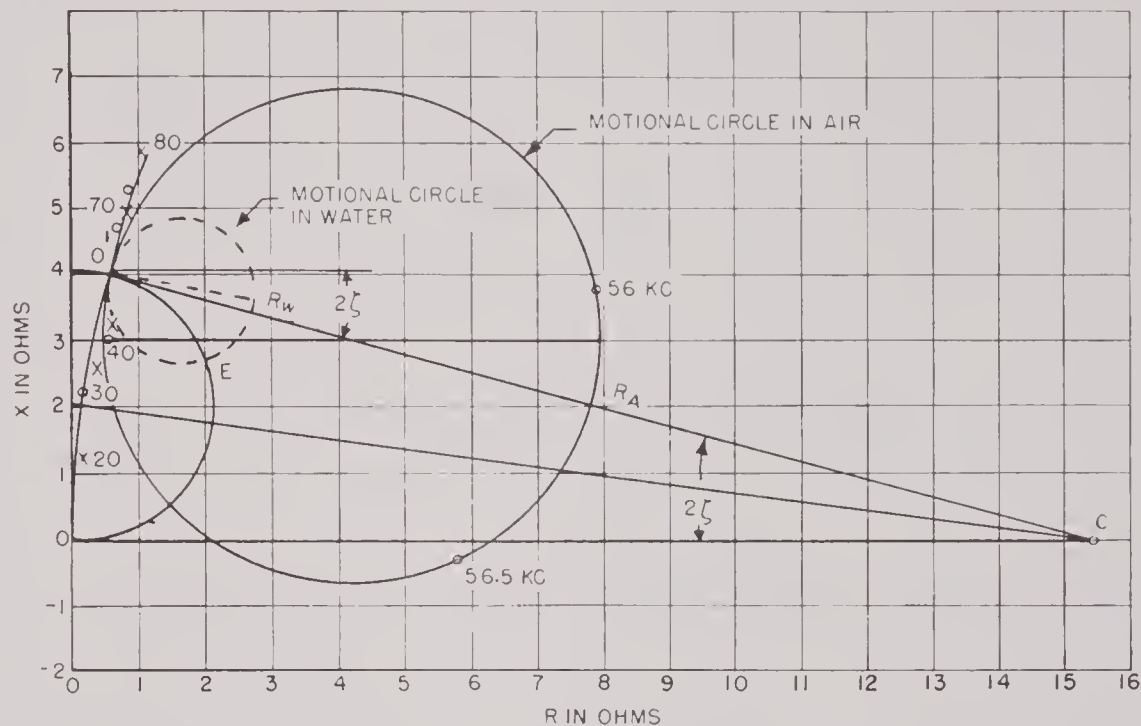


FIGURE 29A. Analysis of impedance diagram for an actual transducer. (See Figures 16 and 17 of Chapter 2.)

thick, toroidally wound and polarized by direct current. The center of the clamped impedance arc OO' was determined by the three points representing the impedances at 0, 30, and 80 ke. Point O' corresponding to the clamped impedance at 55 ke (approximately the resonance frequency) was fixed by interpolation along the arc between 30 and 80 ke. The motional-impedance circles of Figures 16 and 17 of Chapter 2 were drawn tangent to the clamped-impedance arc at point O' . The center of the auxiliary circle is the point of intersection of the bisector of the angle 2ζ with the reactance axis. It will be noted that the radius r of the clamped impedance arc passes nicely through the center of the air circle, but not through the center of the water circle. This represents a small departure from the idealized transducer. The point E which lies at the intersection of the auxiliary

leakage in a toroidally wound ring stack with dc polarization is extremely small. The slight difference between the potential efficiency and the efficiency at resonance as computed from equation (57) of Chapter 2 indicates that the ideal conditions assumed in Figure 29 are closely approximated in the actual case.

Although the ideal construction will not in general be found to apply so well as in the foregoing example, frequently it will prove a useful tool in analyzing transducer performance.

3.6 MOTIONAL ADMITTANCE

The impedances — self and mutual — of a transducer, its motional impedance, and impedance diagram have already been examined quite thoroughly.

There are some advantages, with respect both to measurement and to interpretation, which may be gained by the use of admittance instead of impedance. The comparison between admittance and impedance bridges will be found in Chapter 11. From the standpoint of interpretation, it should be remembered that the impedances of several series elements are additive, while the admittances are combined in more complex fashion. Thus, in the dynamic speaker, according to Figure 5 of Chapter 2, there is a purely electric impedance in series with a group of elements of mechanical origin, representing the motional impedance. Since the two are in series, their impedances are additive and will be more easily separated in an impedance diagram than an admittance diagram. Contrast with this the equivalent circuits of Figures 11 and 12 for the magnetostrictive ring. Here the two important impedances Z_c and Z_m''/Φ^2 are in parallel when viewed from the electric terminals, the mechanical terminals being short-circuited. It is true that Z_l representing the leakage inductance and copper resistance is in series with the combination, but in many cases Z_l will be negligibly small, as was assumed in Figure 28 in the discussion of the impedance diagram. If Z_l is omitted, the admittances $Y_c = 1/Z_c$ and $\Phi^2 Y_m'' = \Phi^2/Z_m''$ are additive and are easily separated in the admittance diagram. When, as in Figure 28, the mechanical terminals are not shorted but are connected to a load Z_L , the admittance Y_m'' is replaced by

$$Y_M = \frac{1}{Z_m'' + Z_L}. \quad (51)$$

By making use of equation (6) the core admittance may be written

$$Y_c = G_c - jB_c = \frac{1}{Z_c} = \frac{1}{j\omega L_0 \chi}, \quad (52)$$

where G_c and B_c are the core conductance and susceptance respectively and L_0 is the core inductance at low frequencies. Throughout this report, susceptance B will be taken as the negative imaginary part of the admittance. The signs of reactance X and susceptance B are then the same. In Figure 30,

$$\frac{f_c \chi_R}{f \chi_0^2} = 2\pi f_c L_0 B_c$$

is plotted against

$$\frac{f_c \chi_I}{f \chi_0^2} = 2\pi f_c L_0 G_c,$$

with f/f_c as parameter. Figure 30 shows the variation of core admittance with frequency. When $f/f_c < 2$, G_c is nearly constant, since Figure 30 is close to a vertical straight line. This straight portion is the geometrical inversion of the circle which the core impedance followed at low frequencies in Figure 3.

In examining the geometry of the admittance diagram for a transducer the same restrictions are made as were made for the impedance diagram. The equivalent circuit is the same, then, as that

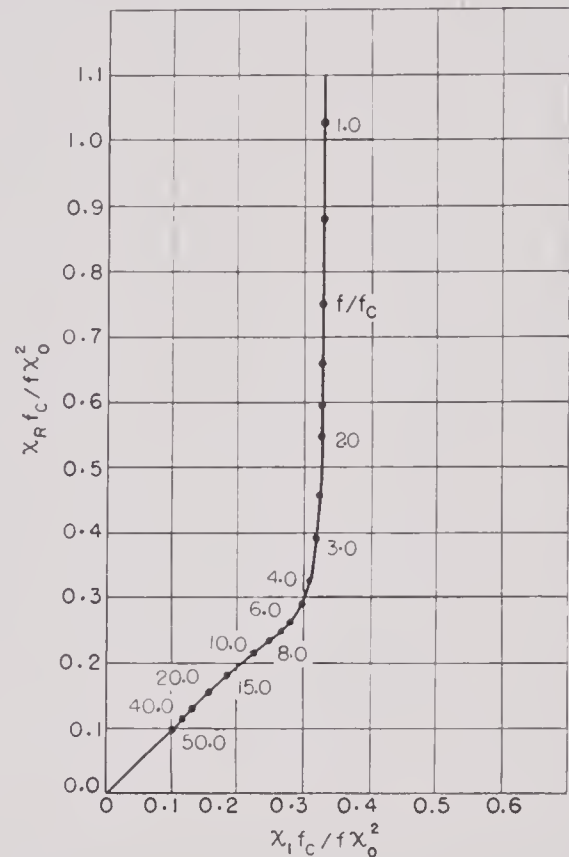


FIGURE 30. Theoretical admittance of core composed of flat laminations.

drawn in Figure 28. The admittance diagram is shown in Figure 31. It represents the same idealized transducer whose impedance was plotted previously, since it was obtained by geometrical inversion of Figure 29. The same letters have been used to designate corresponding points in both figures. Note that the locus of points of maximum efficiency, which was previously the arc of a circle, is now the horizontal straight line $O'EF$. This is an important advantage of the use of admittance, since maximum efficiency is usually more important than resonance. Similarly, the locus of points of resonance, which was previously the straight line $O'R_{II}R_A C$ (the

efficiency. In the special case of the circuit of Figure 28 and the simplified admittance diagram, Figure 31, the efficiency given is equal to the maximum efficiency. The general formula for the motional admittance is $Y_{\text{mot}} = Y_i - Y_e$. Here $Y_i = 1/Z_i$ is the loaded admittance of the transducer and $Y_e = 1/Z_e$ is the blocked admittance. With the help of equation (20) of Chapter 2 it is found that

$$Y_{\text{mot}} = Y_i - Y_e = \frac{-\frac{Z_{em}^2}{Z_e^2}}{Z_m + Z_L + \frac{Z_{em}^2}{Z_e}}. \quad (55)$$

Similarly, from equation (21) or (55) of Chapter 2,

$$\begin{aligned} \text{Eff} &= \frac{|Z_i - Z_e|}{R_i} \cdot \frac{R_L}{|Z_m + Z_L|} \\ &= \frac{|Y_i - Y_e|}{G_i} \cdot \frac{R_L}{Z_m + Z_L + \frac{Z_{em}^2}{Z_e}}. \end{aligned} \quad (56)$$

Equations (55) and (56) are identical in form with equations (46) and (55) of Chapter 2. The blocked electric impedance Z_e and the mutual impedance Z_{em} are assumed to be slowly varying compared with $Z_m + Z_L$, which goes through a simple resonance at frequency f_R . The denominator of equation (55) is real (resonant) at a slightly different frequency f'_E . Here at f'_E , Y_{mot} has its maximum magnitude equal to D_Y , the diameter of the admittance circle. By the same process that leads from equations (46) and (55) to (57) of Chapter 2, it is found that efficiency at f'_E is

$$\begin{aligned} \text{Eff}'_E &= \left(\frac{\text{Diameter admittance circle in water}}{\text{Conductance at } f'_E \text{ in water}} \right) \\ &\times \left(1 - \frac{\text{Diameter admittance circle in water}}{\text{Diameter admittance circle in air}} \right). \end{aligned} \quad (57)$$

Note the similarity between equation (57) and equation (57) of Chapter 2. In general the admittance formula gives a somewhat higher efficiency than the impedance formula, since f'_E is usually closer to f_E (maximum efficiency) than is f_R (resonance). From equation (22) of Chapter 2 it is found that

$$X_m + X_L = \left| \frac{Z_{em}^2}{Z_e} \right| \frac{\sin 2\zeta_{em}}{2 \sin \zeta_e} \quad (\text{at } f_E), \quad (58)$$

where the phases ζ_e and ζ_{em} are defined through

$$Z_e = j e^{-j\zeta_e} |Z_e|, \quad Z_{em} = e^{-j\zeta_{em}} |Z_{em}|. \quad (59)$$

The reason for choosing the phases in this particular way is that they both become equal to the eddy-current angle ζ when the transducer under consideration is a ring with negligible leakage inductance and copper losses. At frequency f'_E

$$X_m + X_L = \left| \frac{Z_{em}^2}{Z_e} \right| \cos(\zeta_e - 2\zeta_{em}) \quad (\text{at } f'_E). \quad (60)$$

At resonance, of course,

$$X_m + X_L = 0 \quad (\text{at } f_R).$$

The ratio of equation (60) to (58) is

$$\frac{(X_m + X_L)'_E}{(X_m + X_L)_E} = 1 + \frac{\sin 2(\zeta_e - \zeta_{em})}{\sin 2\zeta_{em}}.$$

Thus E' may lie above or below E . When $\zeta_e = \zeta_{em}$, E' and E are coincident and equation (57) gives the maximum efficiency. This will happen, in general, only when leakage inductance and copper resistance can be ignored and when there are no important shunt elements except the core impedance. In most of the applications here, ideal conditions will be assumed and equation (57) will be interpreted as the maximum efficiency. An easy test which tells whether f'_E and f_E are close together is to note the inclination of the principal diameter of the admittance circle. According to equation (55),

$$\begin{aligned} \text{Inclination of principal admittance diameter} \\ = 2(\zeta_e - \zeta_{em}). \end{aligned} \quad (61)$$

Thus, when the principal diameter is horizontal, ζ_e and ζ_{em} are equal and equation (57) gives the maximum efficiency.

3.7 COMPARISON OF IMPEDANCE AND ADMITTANCE METHODS

In this section the principal differences between the impedance and admittance methods are outlined. In what follows it has been assumed that the mechanical system goes through a simple resonance and that the blocked electric impedance and the mutual impedance are constant in comparison. A further specialization is made in that ζ_e and ζ_{em} of equation (59) are taken as equal. This is tantamount to omitting leakage inductance and copper resistance and using the circuit of Figure 28 in which the mechanical arm has high Q .

3.7.1 Principal Points of Difference between Impedance and Admittance Methods

1. The core admittance in the region of small eddy currents is a straight line; the core impedance is the arc of a circle.

2. The principal diameter of the motional admittance circle is horizontal; the principal diameter of the motional impedance circle is inclined.

3. The principal diameter of the motional admittance circle ends in the point of maximum efficiency, which is the efficiency most readily obtained by the admittance method. The principal diameter of the motional impedance circle ends in the point of resonance and it is the efficiency at resonance which is most easily found by the impedance method.

4. The mechanical Q found from the admittance diagram does not include damping from eddy currents; the Q from the impedance diagram does include this damping.

5. For small eddy currents, core conductance is constant and the diameter of the motional admittance circle is a good index of potential efficiency. Since core resistance does change with frequency, the diameter of the motional impedance circle is not an index of potential efficiency.

6. If copper resistance and leakage reactance are not negligible, it is more difficult to take them into account in the admittance method than in the impedance method.

7. If copper resistance is neglected, zero frequency falls at infinity in the admittance diagram and at origin in the impedance diagram.

3.7.2 Summary of Formulas for Impedance Diagrams

1. Potential efficiency

$$= \frac{\sqrt{R_{\max}} - \sqrt{R_{\min}}}{\sqrt{R_{\max}} + \sqrt{R_{\min}}}, \quad (62)$$

where R_{\max} , R_{\min} are the maximum and minimum resistances on the impedance circle.

2. The Q of the mechanical system *including* damping due to eddy currents (Q_z) is

$$Q_z = \frac{\text{Frequency of resonance}}{\text{Difference between frequencies at ends of diameter perpendicular to resonance diameter}}. \quad (63)$$

3. Efficiency at resonance

$$= \frac{D_W}{R_i} \cdot \frac{D_A - D_W}{D_A}, \quad (64)$$

where R_i = resistance at resonance in water,

D_W = diameter of *impedance* circle in water,

D_A = diameter of *impedance* circle in air.

3.7.3 Summary of Formulas for Admittance Diagrams

1. Potential efficiency

$$= \frac{\sqrt{G_{\max}} - \sqrt{G_{\min}}}{\sqrt{G_{\max}} + \sqrt{G_{\min}}}, \quad (65)$$

where G_{\max} , G_{\min} are the maximum and minimum conductances on the admittance circle. G_{\min} is also the core conductance G_c , and G_{\max} is $G_c + D_Y$, the sum of the core conductance and the diameter of the admittance circle.

2. The Q of the mechanical system *excluding* damping due to eddy currents (Q_Y) is

$$Q_Y = \frac{\text{Frequency of maximum efficiency}}{\text{Difference between frequencies at ends of diameter perpendicular to efficiency diameter}}. \quad (66)$$

3. Maximum efficiency

$$= \left(\frac{D_W}{G_i} \right) \cdot \left(\frac{D_A - D_W}{D_A} \right), \quad (67)$$

where D_A and D_W are the diameters of the *admittance* circles in air and water, and $G_i = G_c + D_W = G_{\max}$ is the maximum conductance in water.

3.7.4 Relation between Impedance and Admittance Diagrams

In the following, R_c , X_c are respectively the core resistance and reactance, with leakage impedance assumed to be negligible; G_c and B_c are respectively the core conductance and susceptance; D_Z and D_Y are the diameters of the motional circles in the impedance and admittance diagrams respectively; and Q_z , Q_Y , are the Q 's for the motional circles in the impedance and admittance diagrams respectively. It is assumed that the principal diameter of the admittance circle is horizontal, i.e., that equation (61) is zero.

1. Diameters of circles: The diameter of the admittance circle is related to quantities in the *impedance* diagram by

$$D_Y = \frac{D_Z}{R_c^2 + X_c^2 - R_c D_Z}. \quad (68)$$

The diameter of the impedance circle is related to quantities in the admittance diagram by

$$D_Z = \frac{D_Y}{G_c^2 + B_c^2 + G_c D_Y}. \quad (69)$$

2. Mechanical Q 's: The Q measured from the admittance circle Q_Y , which excludes damping due to eddy currents, is related to impedance data by

$$Q_Y = \frac{Q_Z(R_c^2 + X_c^2)}{R_c^2 + X_c^2 - R_c D_Z} \sqrt{1 + \frac{D_Z X_c}{Q_Z(R_c^2 + X_c^2)}}. \quad (70)$$

The Q measured from the impedance circle, which includes damping due to eddy currents, is related to admittance data by

$$Q_Z = \frac{Q_Y(G_c^2 + B_c^2)}{G_c^2 + B_c^2 + D_Y G_c} \sqrt{1 - \frac{D_Y B_c}{Q_Y(G_c^2 + B_c^2)}}. \quad (71)$$

3. Frequencies of resonance and maximum efficiency:

$$\begin{aligned} \frac{f_R}{f_E} &\cong \sqrt{1 - \frac{D_Z X_c}{(R_c^2 + X_c^2) Q_Z}} \\ &\cong \sqrt{1 - \frac{D_Y B_c}{(G_c^2 + B_c^2) Q_Y}} \\ &\cong \sqrt{1 - k_{\text{eff}}^2} \end{aligned} \quad (72)$$

where f_R is the frequency of resonance, f_E is the frequency of maximum efficiency, and k_{eff} is the effective coefficient of electromechanical coupling.

4. Effective electromechanical coupling:

$$k_{\text{eff}} = \sqrt{\frac{D_Z}{X_c Q_Z}} = \sqrt{\frac{D_Y}{B_c Q_Y}}. \quad (73)$$

Effective coupling will be discussed in the next section.

5. Relation between efficiency at resonance and maximum efficiency:

$$\begin{aligned} \text{Eff}_{\text{max}} &= \frac{R_c(R_c^2 + X_c^2) + (X_c^2 - R_c^2)D_Z}{R_c(R_c^2 + X_c^2) + X_c^2 D_Z} \\ \frac{R_c^2 + X_c^2}{R_c^2 + X_c^2 - R_c D_Z} \cdot \text{Eff}_{\text{res}} &\cong \frac{R_c^2 + X_c^2}{R_c^2 + X_c^2 - R_c D_Z} \text{Eff}_{\text{res}}, \end{aligned} \quad (74)$$

where all quantities refer to the *impedance* diagram in water.

$$\begin{aligned} \text{Eff}_{\text{res}} &= \left(\frac{(G_c + D_Y)(G_c^2 + B_c^2)}{G_c(G_c^2 + B_c^2) + B_c^2 D_Y} \right) \\ &\quad \left(\frac{G_c^2 + B_c^2}{G_c^2 + B_c^2 + G_c D_Y} \right) \text{Eff}_{\text{max}} \\ &\cong \left(\frac{G_c^2 + B_c^2}{G_c^2 + B_c^2 + G_c D_Y} \right) \text{Eff}_{\text{max}} \end{aligned} \quad (75)$$

where all quantities refer to the *admittance* diagram in water.

3.8 TRANSDUCER AS BAND-PASS FILTER: EFFECTIVE COUPLING

The circuit used previously in the discussion of impedance and admittance diagrams is reproduced in Figure 32. Its elements are simply related to

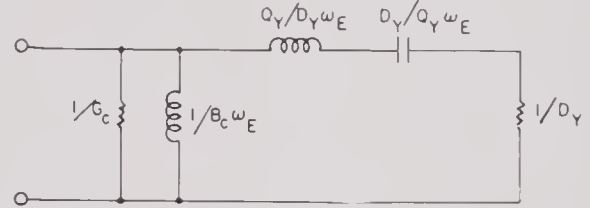


FIGURE 32. Elements of equivalent circuit from admittance data.

quantities easily found from the admittance diagram and have been labeled. If only impedance data are available, Figure 32 may still be used with the help of conversion formulas given in the previous section. In Figure 33, a shunt condenser with capacity B_c/ω_E , together with a generator, has been connected to the electric terminals. The portion of the circuit

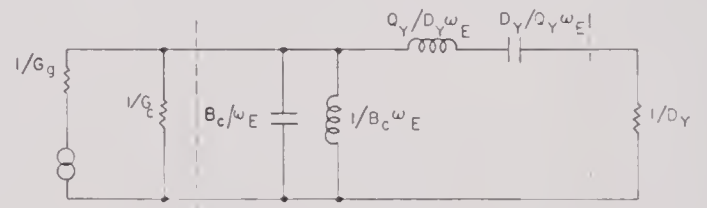


FIGURE 33. Transducer as band-pass filter.

between the dotted lines is seen to be a band-pass L section, which, since the resonance of the series arm and the antiresonance of the shunt arm coincide, is of the constant- K type. The width of its pass band is given by

$$\frac{(f_2 - f_1)}{f_E} = \sqrt{\frac{D_Y}{Q_Y B_c}} = k_{\text{eff}}, \quad (76)$$

where f_2 and f_1 are the nominal cutoff frequencies and where k_{eff} will be called the effective coefficient

of electromechanical coupling for the transducer. The image impedance at midband frequency $f_E (= \sqrt{f_1 f_2})$ is

$$K = \sqrt{\frac{Q_Y}{D_Y B_c}} = \frac{1}{B_c k_{\text{eff}}}.$$

Now the best band-pass behavior of the filter will be obtained if it is terminated on both ends with a resistance close to K . (A slight mismatch may be deliberately introduced in the right direction in order to hold up the response near cutoff.) The termination on one end consists of the resistance $1/D_{YW}$ (the reciprocal of the admittance diameter in water). Therefore, it is desirable that

$$D_{YW} \simeq B_c k_{\text{eff}}.$$

On the electric end, the filter is terminated by the resistance $1/G_c$ in parallel with the generator. If the generator resistance is $1/G_g$, proper termination indicates

$$G_g \simeq B_c k_{\text{eff}} - G_c.$$

The efficiency when the transducer is terminated for optimum characteristics as a filter is less than the potential efficiency which would be obtained if the termination were optimum for efficiency. The two efficiencies can be found from equations (65) and (67). They refer to the transducer itself and do not include any losses incurred in the generator. Thus

Band-pass eff
Potential eff

$$= \frac{1}{1 + \frac{G_c}{B_c k_{\text{eff}}}} \cdot \frac{1 - \frac{B_c k_{\text{eff}}}{D_A}}{1 + \frac{2G_c}{D_A} - 2\sqrt{\frac{G_c}{D_A} + \frac{G_c^2}{D_A^2}}}. \quad (77)$$

When the transducer has small mechanical losses, D_A is large and the second factor is close to unity. If eddy-current losses are also small, B_c/G_c is large and the first factor is near unity. If both conditions apply, the loss in efficiency is small.

The effective coefficient of electromechanical coupling defined by

$$k_{\text{eff}} = \sqrt{\frac{D_Y}{B_c Q_Y}} = \sqrt{\frac{D_Z}{X_c Q_Z}} \quad (78)$$

is a useful and important quantity which can be obtained directly from impedance or admittance data. Note that D/Q remains constant as the load resistance is varied, so that equation (78) can be applied

to measurements either in air or water, provided, as has been assumed, the water adds a purely mechanical resistance. The effective coupling is closely related to k , the coupling coefficient for the magnetostrictive material. From equation (15)

$$k = \sqrt{\frac{4\pi\lambda^2\mu}{E}},$$

where λ is the magnetostrictive constant, μ the permeability, and E Young's modulus. For the cylindrical transducer,

$$k_{\text{eff}} = k \sqrt{\frac{\chi_0^2}{\chi_R}}.$$

The factor $\chi_0/\sqrt{\chi_R}$ is within 1 per cent of unity if the frequency f is less than f_c , the characteristic frequency for eddy currents, and if the departure does not reach 10 per cent until f/f_c is greater than 3. Thus, in any reasonably well-designed cylindrical transducer, k_{eff} is nearly as large as k .

For other forms than the toroid, the relation becomes more complicated, since such effects as demagnetization and leakage, as well as the geometrical form, introduce numerical factors which reduce k_{eff} with respect to k . With good design, this reduction is not large and the nearness of k_{eff} to k is one of the criteria of excellence for a transducer.

3.8.1 Representation of Force by Current and Velocity by Voltage

It will be recalled that there is a fundamental difficulty in obtaining an equivalent electric circuit for an electromagnetic or magnetostrictive transducer when forces are replaced by voltages and velocities by currents. This arises from the opposite signs of the mutual impedances with these types of electromechanical coupling. The difficulty was avoided in the magnetostrictive case by the device of rotating the phase of the force and velocity through 90 degrees before converting them to voltage and current.

Earlier in this chapter it was noted that an alternative method is to represent force by current and velocity by voltage. The chief objection to doing this is that complex mutual impedances are very difficult to include, since an ideal transformer whose impedance ratio is complex is required. However, when the phase of the mutual impedance is small it can, without much error, be set equal to zero.

With this simplification, the impedance of the transducer can be represented by the circuit of Figure 34. The series arm represents the blocked impedance, including both leakage and core impedances. This is in contrast to Figure 32, where

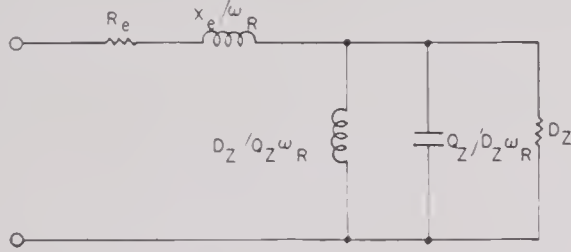


FIGURE 34. Elements of equivalent circuit from impedance data.

leakage had to be omitted. On the other hand, while Figure 32 gives a motional impedance circle with inclined resonance diameter, the resonance diameter for Figure 34 is horizontal. Thus, Figure 34 will be the better representation if leakage is large but the eddy-current angle and, hence, dip-of-resonance diameter are small. When these conditions are reversed, Figure 32 is superior.

The band-pass properties of a transducer can be shown with Figure 34 by much the same method that was used with Figure 32. Since the blocked and motional impedances are in series and thus additive in Figure 34, it is convenient here to use impedance data, and the elements of the circuit have

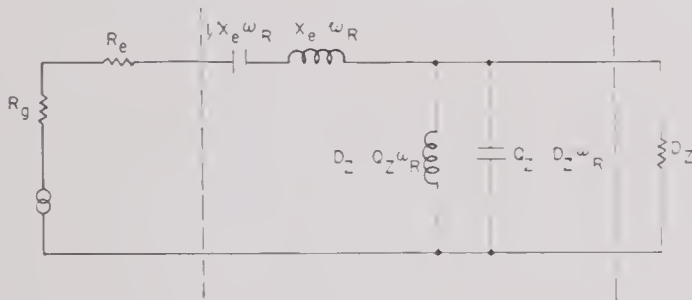


FIGURE 35. Transducer as band-pass filter.

been so labeled. In Figure 35 a series-tuning condenser, with capacity $1/\omega_R X_e$, has been added, and the transducer has been attached to an electric generator of resistance R_g . The portion of the circuit between the dotted lines is a constant- K , band-pass filter section. Its band width is

$$\frac{f_2 - f_1}{f_R} = \left| \frac{D_Z}{Q_Z X_e} \right| = k_{\text{eff}}, \quad (79)$$

where f_1, f_2 are the frequencies of cutoff and the center of the pass band is at resonance $f_R = \sqrt{f_1 f_2}$.

Thus equations (76) and (79) are in agreement in predicting a band width equal to the coefficient of coupling. The image impedance at midband is

$$K = \left| \frac{D_Z X_e}{Q_Z} \right| = X_e k_{\text{eff}},$$

and the filter is properly terminated when

$$D_{ZW} = X_e k_{\text{eff}}$$

and

$$R_g = X_e k_{\text{eff}} - R_e.$$

The efficiency is less than the potential efficiency by the factor

$$\frac{\text{Band-pass eff}}{\text{Potential eff}}$$

$$= \frac{1}{1 + \frac{R_e}{X_e k_{\text{eff}}}} \cdot \frac{1 - \frac{X_e k_{\text{eff}}}{D_A}}{1 + \frac{2R_e}{D_A} - 2 \left| \sqrt{\frac{R_e}{D_A} + \frac{R_e^2}{D_A^2}} \right|},$$

which is similar in form and interpretation to equation (77).

3.3.2 Relation Between Maximum Efficiency and Effective Coefficient of Electromechanical Coupling

Maximum efficiency with respect to frequency is given by

$$\text{Eff}_{\text{max}} = \frac{D_{YW}}{G_i} \left(1 - \frac{D_{YW}}{D_{YA}} \right), \quad (80)$$

where D_{YW} and D_{YA} are the diameters of the admittance circles in water and air respectively, and G_i is the total conductance in water at the frequency of maximum efficiency f_E . Equation (80) is obtained from equation (57) under the assumption that E and E' are coincident, that is, the principal diameter of the admittance circle is horizontal. Then, also,

$$G_i = G_c + D_{YW},$$

where G_c is the core conductance. Thus, equation (80) can be written

$$\text{Eff}_{\text{max}} = \left(\frac{1}{1 + \frac{G_c}{D_{YW}}} \right) \cdot \left(1 - \frac{D_{YW}}{D_{YA}} \right).$$

With the help of equation (75)

$$\frac{G_c}{D_{YW}} = \frac{1}{k_{\text{eff}}^2 Q_{YW} Q_c}$$

can be written where the abbreviation $Q_c = B_c/G_c$ has been used. Also, with the assumption that the water load is a purely mechanical resistance,

$$\frac{D_{YW}}{D_{YA}} = \frac{Q_{YW}}{Q_{YA}}.$$

Finally

$$\text{Eff}_{\max} = \left(\frac{1}{1 + \frac{1}{k_{\text{eff}}^2 Q_{YW} Q_c}} \right) \cdot \left(1 - \frac{Q_{YW}}{Q_{YA}} \right). \quad (S1)$$

This formula is essentially the same as equation (38) previously obtained for the ring. The first factor can be regarded as a gross electromechanical efficiency and the second as a mechanical efficiency. Note that the first factor increases with increasing Q_{YW} , while the second decreases. The formula gives an insight into the conflict between the requirements of high efficiency and low Q_{YW} in magnetostrictive transducers where the effective coupling is low ($k_{\text{eff}}^2 \cong 0.05 \text{ max}$).

3.9 IMPEDANCE-ADMITTANCE DATA AND RESPONSE DATA

In Chapter 1 it was shown that the responses of a transducer in transmitting and receiving are simply related when the transducer satisfies the reciprocity theorem and is linear in the range of operation involved. The connections which were found earlier can be written

$$\begin{aligned} S_I &= J_1 T_V, \\ S_V &= J_1 T_I, \\ J_1 &= \frac{200}{\rho f} 10^{-7} = \frac{1.94 \times 10^{-8}}{f_{kc}}, \end{aligned} \quad (S2)$$

where S_V = open-circuit (voltage) sensitivity (volts/dyne/cm²),

S_I = short-circuit (current) sensitivity (amperes/dyne/cm²),

T_V = voltage transmitting response (dynes/cm² at one meter/volt),

T_I = current transmitting response (dynes/cm² at one meter/ampere),

J_1 = reciprocity parameter appropriate to distance of test of one meter, as used in transmitting response.

The sensitivities S_V and S_I will be expressed in terms of the self and mutual impedances of the trans-

ducer in order that they may be compared with the motional impedance and motional admittance (see Figure 36). The transducer has electric impedance Z_e when open-circuited ($v = 0$) on the mechanical end; mechanical impedance Z_m when open-circuited on the electric end; and mutual impedance Z_{em} . The relations involving these impedances have already been discussed in Chapter 2. The impedance

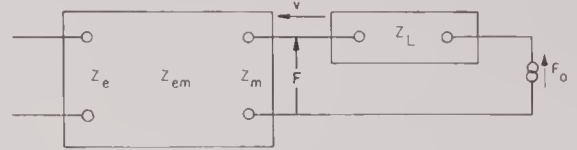


FIGURE 36. Transducer as hydrophone.

Z_L in Figure 36 represents the radiation impedance presented to the face of the transducer by the water. The generator F_0 represents the equivalent mechanomotive force acting in the circuit when the transducer is placed in a sound field. With the circuit equations (17) of Chapter 2, the open-circuit voltage at the terminals of the transducer is found to be

$$E_0 = \frac{Z_{em} F_0}{Z_m + Z_L}, \quad (S3)$$

and the current generated by the transducer when it is short-circuited is

$$I_S = - \left(\frac{Z_{em}}{Z_e} \right) \frac{F_0}{Z_m + Z_L + \frac{Z_{em}^2}{Z_e}}. \quad (S4)$$

Equations (S3) and (S4) could be used at once to determine S_V and S_I if the connection between F_0 and the pressure in the sound field (before the transducer is placed there) were known. In order to find this relation, the reciprocity theorem will be applied to the water between the transducer and a simple source placed in front of the transducer and at a sufficient distance to produce approximately plane waves. The arrangement is shown in Figure 37. The two pairs of terminals at which connection is made to the water consist, first, of the face of the transducer (denoted by the subscript 1), and second, of the surface of the simple source (designated 2), which may be taken as a small sphere of area σ_2 . Suppose that 1 transmits through the water to 2 and that 2 is stiff, so that its surface velocity is zero ($v'_2 = 0$). The mutual impedance is

$$\frac{F'_2}{v'_1} = - \frac{\sigma_2 p'_2}{v'_1}, \quad (S5)$$

where F'_2 is the force applied to the medium at 2 when its velocity at 1 is v'_1 . The pressure in the water at 2 is p'_2 . This is the same whether or not 2 is present, since it is assumed small and stiff. Now let the transmission take place in the reverse direction, from 2 to 1. This time the velocity at 1 is

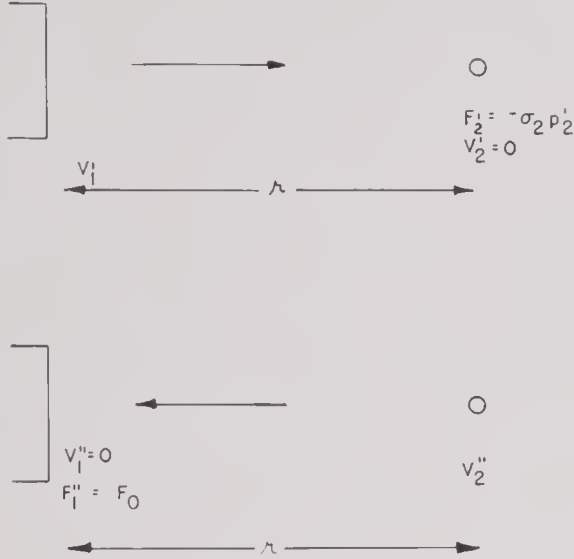


FIGURE 37. Reciprocity applied to transmitting medium.

taken to be zero ($v''_1 = 0$). Then the force F''_1 which 1 exerts on the water is the same as F_0 , the mechanomotive force at 1 due to source 2 in the water. The mutual impedance here is

$$\frac{F''_1}{v''_2} = \frac{F_0}{v'_2}. \quad (86)$$

According to the reciprocity theorem, the quantities in equations (85) and (86) are equal. Thus,

$$F_0 = - \frac{\sigma_2 p'_2 v''_2}{v'_1}. \quad (87)$$

Now let the transducer 1 be removed and let the source 2 continue to transmit with surface velocity v''_2 . Pressure p at the position which the transducer previously occupied is, apart from phase,

$$|p| = \left| \frac{\rho c v''_2 \sigma_2}{2r\lambda} \right|, \quad (88)$$

where ρc is the characteristic acoustic resistance of the medium, r is the distance between the two positions 1 and 2, and λ is the wave length in the medium. Combining equations (87) and (88),

$$|F_0| = \frac{2r\lambda}{\rho c} \cdot \left| \frac{p'_2}{v'_1} \right| \cdot |p|. \quad (89)$$

When transducer 1 is radiating, the power transmitted is

$$|v'_1|^2 R_L = \frac{4\pi r^2 D |p'_2|^2}{\rho c}, \quad (90)$$

where R_L is the radiation resistance for the transducer and D is its directivity ratio. Equations (89) and (90) give the relation

$$|F_0| = 2\sigma' |p|, \quad (91)$$

with

$$\sigma' = \sqrt{\frac{\lambda^2}{4\pi D} \cdot \frac{R_L}{\rho c}}. \quad (92)$$

The area σ' is an effective area of the transducer. It can be shown that σ' is equal to the actual area for any transducer whose radiating face is plane and lies in an infinite plane, stiff baffle. If the baffle conditions are not met but the radiating face is still plane, it can be shown that σ' approaches the actual area σ as the ratio of the dimensions to the wave length is increased.

Combination of equation (91) with equations (83) and (84) allows the receiving sensitivities to be written

$$S_V = \left| \frac{E_0}{p} \right| = 2\sigma' \left| \frac{Z_{em}}{Z_m + Z_L} \right| \times 10^{-8} \quad (93)$$

and

$$S_I = \left| \frac{I_s}{p} \right| = 2\sigma' \left| \frac{\frac{Z_{em}}{Z_e}}{Z_m + Z_L + \frac{Z_{em}^2}{Z_e}} \right| \times 10, \quad (94)$$

where the factors 10^{-8} and 10 take into account that the impedances Z_{em} and Z_e make use of electromagnetic units, while S_V and S_I are expressed in terms of practical units. Equations (93) and (94) can also be obtained from equations (27) of Chapter 1, (17) and (21) of Chapter 2, with proper attention to units.

The motional impedance and admittance of a magnetostrictive transducer are given by equations (46) of Chapter 2 and (76), namely,

$$Z_{mot} = \frac{Z_{em}^2}{Z_m + Z_L} \quad (95)$$

$$Y_{mot} = \frac{-\frac{Z_{em}^2}{Z_e}}{Z_m + Z_L + \frac{Z_{em}^2}{Z_e}}. \quad (96)$$

With the assumption that σ' and $|Z_{em}|$ vary slowly with respect to frequency in comparison to $|Z_m + Z_L|$, it is seen that equation (93) and the magnitude of equation (95) change with frequency in the same way. Thus, the Q determined from the open-circuit receiving response S_r or the current-

transmitting response T_I is approximately that obtained from the impedance diagram Q_Z . Similarly, comparison of equations (94) and (96) shows that Q_r is approximately the same as the Q obtained from the short-circuit receiving response or the voltage transmitting response.

Chapter 4

MAGNETIC AND MAGNETOSTRICTIVE PROPERTIES OF MATERIALS

4.1 INTRODUCTION: TYPES OF MEASUREMENT

This chapter is an account of the magnetic and magnetostrictive properties of a number of ferromagnetic materials, as obtained from experiments carried out at the Harvard Underwater Sound Laboratory [HUSL]. Since the laboratory did not have facilities for making special alloys, studies were made only on materials available commercially and on small samples supplied through the courtesy of the International Nickel Company.

Information was obtained in considerable detail for materials that were widely used at HUSL. It should be emphasized, however, that only a few samples were measured of each material subjected to a given type of heat treatment, making it somewhat difficult to judge how consistently a certain set of desirable properties can be reproduced in a given batch of material. For this reason the results described in this chapter should be regarded as representative rather than definitive.

Three types of measurements were employed to obtain information about the characteristics of the materials. The first consisted of magnetic measurements of the usual kind by the induction method. Normal magnetization curves (commutation curves), major and minor hysteresis loops, and the reversible permeability at various intensities of polarization are obtained from this type of measurement. Such data are needed for the design of transducers that employ somewhat complicated magnetic circuits, for a preliminary study of the losses in magnetostrictive transducers, and for checking the theory of a magnetostrictive transducer of simple construction.

The second type is a static study of magnetostriction and is employed only when the material cannot be obtained in the form of rolled sheets of suitable width. In measurements of this type observation is made of the change in polarization at a steady magnetic field for a given change in applied stress with the

sample in static equilibrium before and after each measurement.

In the third type, which may be referred to as dynamic measurements, a ring sample, together with the primary coil wound on it, forms a transducer, and evaluation is made of the various coefficients from impedance or admittance bridge measurements, using the theory of a ring transducer.

The electric resistivities of the various materials were measured and in certain cases a simple determination of the density was also made.

A comprehensive survey of magnetostrictive materials has been made at the Bell Telephone Laboratories Inc.^{35, 36} Their results should be compared with those described in the present chapter.

4.2 FUNDAMENTAL MAGNETO-MECHANICAL RELATIONS

The phenomenon of magnetostriction has been discussed in some detail in Chapter 1, while the relation among stress, strain, and an applied magnetic field has been used extensively in the discussions of Chapter 3. In this section rigorous derivations of the fundamental magnetomechanical relations will be made in order to clarify the definitions of the various quantities obtained in the different types of measurements and the relations among these quantities.

Under the action of a magnetic field H , the shape of a magnetostrictive body and its intensity of magnetization I are functions of H . Therefore, when external forces are applied to the body, both its shape and intensity of magnetization are functions of H and of the applied forces.

For present applications, discussions will be limited to the change of linear dimension in the direction of I when the body is isotropic and when both I and the stress P in the material are parallel to H . In general, a change in linear dimension in

the direction of I is accompanied by similar changes of the opposite sign in the perpendicular directions, hence the change in volume can be neglected. Thus only the length L , which is measured parallel to H and P of the body, will be considered and the equations of the state of the body can be written in the form:

$$s = s(H, P, T) \quad B' = B'(H, P, T). \quad (1)$$

If equations (1) can be solved, we can also write

$$H = H(B', s, T) \quad P = P(B', s, T), \quad (2)$$

where T = the absolute temperature, $B' = 4\pi I = B - H$, and $s = \delta L / L_0$ is the strain in the material.

The L_0 can be taken as the length of the body when it is demagnetized and free from magnetic field and stress or as the length of the body under the equilibrium action of a steady field H_0 and a steady stress P_0 .

From equations (2) the total differentials may be written as

$$\begin{aligned} dH &= \left(\frac{\partial H}{\partial B'} \right)_{s,T} dB' + \left(\frac{\partial H}{\partial s} \right)_{B',T} ds + \left(\frac{\partial H}{\partial T} \right)_{s,B'} dT, \\ dP &= \left(\frac{\partial P}{\partial B'} \right)_{s,T} dB' + \left(\frac{\partial P}{\partial s} \right)_{B',T} ds + \left(\frac{\partial P}{\partial T} \right)_{s,B'} dT. \end{aligned} \quad (3)$$

Here $(\partial P / \partial s)_{B',T}$ is Young's modulus at constant temperature and constant polarization and will be denoted by E ; $(\partial P / \partial B')_{s,T}$ will be defined as the magnetostrictive constant and denoted by $-\lambda$.

When B' is increased to $B' + dB'$ and s to $s + ds$ by small changes in H and P , the work (dW) done on unit volume of the material is given by

$$dW = H \frac{dB'}{4\pi} + P ds.$$

From the fundamental law of thermodynamics, we have

$$dU = TdS + H \frac{\partial B'}{4\pi} + Pds,$$

where U is the internal energy and S the entropy per unit volume. Hence the differential of the free energy F is given by

$$dF = -SdT + H \frac{dB'}{4\pi} + Pds.$$

As dF is a total differential, it follows that for an isothermal change,

$$\left(\frac{\partial H}{\partial s} \right)_{B',T} = 4\pi \left(\frac{\partial P}{\partial B'} \right)_{s,T} = -4\pi\lambda. \quad (4)$$

Equations (1) state: If an increase in magnetizing field should accompany a stretching (positive s) of the material in order to keep the polarization constant, a tension (positive P) must accompany an increase in polarization in order to keep the length constant. Hence λ has the same sign as magnetostriction in the usual sense, namely, the change of length with polarization. The sign of λ is immaterial for most applications, but a distinction must be made whenever two different materials are used in the construction of one transducer.

Using equations (3) together with the differentials of equations (2) and setting $dT = 0$, we can solve for dB' and ds in terms of dP and dH . Thus

$$\begin{aligned} dB' &= \left[\left(\frac{\partial P}{\partial s} \right)_{B',T} dH - \left(\frac{\partial H}{\partial s} \right)_{B',T} dP \right] \frac{1}{\Delta}, \\ ds &= - \left[\left(\frac{\partial P}{\partial B'} \right)_{s,T} dH - \left(\frac{\partial H}{\partial B'} \right)_{s,T} dP \right] \frac{1}{\Delta}, \end{aligned} \quad (3a)$$

or,

$$\begin{aligned} \left(\frac{\partial B'}{\partial H} \right)_{P,T} &= \left(\frac{\partial P}{\partial s} \right)_{B',T} \frac{1}{\Delta}, \quad \left(\frac{\partial B'}{\partial P} \right)_{H,T} = - \left(\frac{\partial H}{\partial s} \right)_{B',T} \frac{1}{\Delta}, \\ \left(\frac{\partial s}{\partial H} \right)_{P,T} &= - \left(\frac{\partial P}{\partial B'} \right)_{s,T} \frac{1}{\Delta}, \quad \left(\frac{\partial s}{\partial P} \right)_{H,T} = \left(\frac{\partial H}{\partial B'} \right)_{s,T} \frac{1}{\Delta}, \end{aligned} \quad (5)$$

where

$$\begin{aligned} \Delta &= \begin{vmatrix} \left(\frac{\partial H}{\partial B'} \right)_{s,T} & \left(\frac{\partial H}{\partial s} \right)_{B',T} \\ \left(\frac{\partial P}{\partial B'} \right)_{s,T} & \left(\frac{\partial P}{\partial s} \right)_{B',T} \end{vmatrix} = \begin{vmatrix} \left(\frac{\partial H}{\partial B'} \right)_{s,T} & -4\pi\lambda \\ -\lambda & E \end{vmatrix} \\ &= E \left(\frac{\partial H}{\partial B'} \right)_{s,T} - 4\pi\lambda^2. \end{aligned} \quad (6)$$

From the second and third parts of equation (5) and from equation (4), it follows that

$$\left(\frac{\partial B'}{\partial P} \right)_{H,T} = 4\pi \left(\frac{\partial s}{\partial H} \right)_{P,T}, \quad (6a)$$

which can be independently obtained from a consideration of the Gibbs' thermodynamic potential G which satisfies:

$$dG = -SdT - \frac{B'}{4\pi} dH - sdP.$$

In the equations of state (1) and (2), H and P enter symmetrically. However, it is an experimental fact that an unmagnetized or demagnetized body cannot be magnetized simply by stretching or compression. In other words, stress has the sig-

nificance of direction but not of sense. Therefore, at the point $B = H = 0$, $(\partial B'/\partial P)_{H,T} = 0$. It follows from (6a) that $(\partial s/\partial H)_{P,T} = 0$, and from the third part of equation (5) that $\lambda = 0$. Thus, for an unmagnetized body, small variations in B' do not set up any macroscopic stress in the body.

Since, in the present applications, the active material of the transducer is subjected to no steady stress, $P = 0$, and it may be said that $(\partial B'/\partial H)_{P,T} = (\mu' - 1)$, where μ' is the reversible permeability at constant stress, as is usually observed. In order to take account of hysteresis, μ' is here defined as the reversible rather than the differential permeability. The permeability at constant strain shall be denoted as $\mu - 1 = (\partial B'/\partial H)_{s,T}$. With these abbreviations, it is found from the first, second, and last of equations (5) and (6) that

$$\begin{aligned} \mu - 1 &= \left(\frac{\partial B'}{\partial H} \right)_{s,T} = \frac{1}{\left(\frac{\partial H}{\partial B'} \right)_{s,T}} \\ &= (\mu' - 1) \cdot \left\{ 1 - \frac{4\pi\lambda^2(\mu' - 1)}{E} \right\}, \end{aligned} \quad (7a)$$

$$\begin{aligned} E' &= \left(\frac{\partial P}{\partial s} \right)_{H,T} = \frac{1}{\left(\frac{\partial s}{\partial P} \right)_{H,T}} \\ &= E \left[1 - \frac{4\pi\lambda^2(\mu' - 1)}{E} \right], \end{aligned} \quad (7b)^a$$

$$\text{and} \quad \Lambda = \left(\frac{\partial B'}{\partial P} \right)_{H,T} = \frac{4\pi\lambda(\mu' - 1)}{E}. \quad (7c)$$

In the above equations, μ may be called the clamped core reversible permeability and E' Young's modulus at constant magnetic field. Experimentally it is always μ' and E' that are directly observed, since it is not practical to clamp the sample or to keep the magnetization constant. Moreover, it is Λ that is observed in static measurements, while λ is of special interest in transducer theory.

It will be seen that in the above discussions all the differential coefficients considered should be called isothermal coefficients. In acoustic experiments, however, we deal with adiabatic conditions rather than isothermal. By a consideration of the internal energy and the enthalpy (total heat), it can be

shown that relations similar to those of equations (4) and (6a) also exist in the adiabatic case. Therefore, all the equations derived above are true for the adiabatic case if the subscript T of the differential coefficients is replaced by S .

Experimentally, static measurements are made under isothermal conditions, while dynamic measurements are made under adiabatic conditions. However, the adiabatic changes of temperature in practical cases are usually very small. Thus the difference between the isothermal and the adiabatic Young's moduli for metals is usually about half of one per cent, while the magnetocaloric effect of a ferromagnetic material at a temperature far below its Curie point is scarcely larger than 1 per 1000 C. Such small effects are well within experimental error and it may be said that the adiabatic coefficients are approximately equal to the respective isothermal coefficients.

In deriving the equation of motion of a transducer, it is necessary to find a relation between the change of stress dP , the change in field dH and the change in strain ds . This can be found from equations (3) ($dT = 0$) and (7). Thus,

$$\begin{aligned} -dP &= \lambda dB' - Eds \\ &= \lambda(\mu' - 1)dH + 4\pi\lambda^2(\mu' - 1)ds - Eds \\ &= \lambda(\mu' - 1)dH - E'ds. \end{aligned} \quad (8)$$

In the second form of $-dP$ in the last expression, the change of polarization dB' is divided into two parts, one due to the change of field dH and one due to the change of strain ds . In the case of a transducer, dH is an alternating field. Since the first part is in phase with dH , it is the second that provides a transfer of electric energy into mechanical energy, or vice versa. Therefore, the coefficient $4\pi\lambda^2(\mu' - 1)/E$ is of fundamental importance. In practice, μ' is much greater than unity, hence the latter may be neglected and we may write $k = \sqrt{4\pi\lambda^2\mu'/E}$. Equation (8) is then similar to equation (14) of Chapter 3.

In the third form of $-dP$, the effect of magnetostriction is taken account of in the modified Young's modulus E' , which should be used in calculating the resonant frequency of a transducer.

It is clear from the above discussions that the reversible permeability that enters into the theory of magnetostrictive transducers is the clamped-core reversible permeability μ' . This fact should be kept in mind when a comparison is made between the reversible permeability deduced from impedance

^a This equation is in agreement with equation (11) of Chapter 1, if it is recalled that μ is usually large compared to unity, so that $\mu - 1$ is approximately equal to μ .

measurements at supersonic frequencies, by the help of transducer theory, and that directly measured by the d-c method, since the latter is μ' rather than μ . The difference between the two is usually small, but it can amount to more than 10 per cent when k is large.

The foregoing discussions are based upon the assumption that the polarization of a material is entirely reversible. Actually this is not true, owing to magnetic hysteresis. At high frequencies, the eddy-current effect also changes the nature of the induction in the material. As Chapter 3 states, these effects are usually taken account of by replacing μ by $\mu\chi_0e^{-j(\zeta+\eta)}$, where χ_0 and ζ are eddy-current parameters and η is the hysteretic loss angle. It is obvious that such a replacement in the first part of $-dP$ in equation (8) introduces an electric loss in the clamped core, and in the second part it introduces a mechanical loss to the motion. That part of the mechanical loss which is due to magnetic hysteresis appears as elastic hysteresis. Thus, a magnetostrictive material would normally have an additional elastic hysteresis caused by its magnetic hysteresis. Note also that the Young's modulus E' observed will be affected by the hysteresis and eddy-current effects.

Because of its importance, the coefficient $k = \sqrt{4\pi\lambda^2\mu'E}$ is frequently used as a criterion in the selection of magnetostrictive materials. It will be seen later that E and λ are not affected to any significant degree by the structural changes of the material, while the value of μ at a given value of magnetization depends greatly upon the previous history (heat treatment and mechanical working) of the material. In seeking large values of k , therefore, the choice of material is mainly based on the value of λ rather than of μ .

Prior to the development of the theory of magnetostrictive transducers, experimental study of magnetostriction was generally made with three different types of observations: (1) the variation in the length of a free specimen with its magnetization, (2) the effect of constant stress on the magnetization curve, and (3) the so-called ΔE effect. As can be seen from the above discussions, the relations between such phenomena and λ are not very simple. Therefore, in using existing literature as a guide, the reservation should be made that a material which appears to have the largest magnetostriction as judged from the results of previous studies may not be the best material for magnetostrictive transducers.

4.3

SAMPLES MEASURED

4.3.1

Nickel and Nickel Alloys

The first group of materials measured in the course of experimentation consisted of pure nickel and its alloys. These included A-nickel, Z-nickel, and D-nickel, manufactured by the International Nickel Company, and an alloy of nickel and iron containing 45 per cent of nickel by weight, commonly called 45-Permalloy and produced by Western Electric Company, Inc.

Chemical analyses were made only of the A-nickel. However, D-nickel is known to contain 4.65 per cent manganese,⁴⁵ with the remaining impurities presumably the same as those of A-nickel. The composition of Z-nickel is not available but it is known to contain more carbon and certain other elements than A-nickel, so that it is correspondingly more sensitive to mechanical working and heat treatment. Moreover, Z-nickel can be age-hardened. Table 1 shows four sets of analyses made on different stocks of A-nickel, including two samples that had been subjected to the regular oxide-annealing treatment frequently used in this laboratory. It will be seen from the table that the oxide-annealed treatment re-

TABLE 1. Analysis of different stocks of A-nickel.

Elements	0.005-in. sheets as received	2½-in. tubing* as received	0.005-in. sheets oxide annealed	1½-in. tubing* oxide annealed
Ni	98.89%	98.71%	98.70%	98.69%
Co†	0.6	0.6	0.6	0.6
Si	0.04	0.04	0.04	0.03
Cu	0.07	0.09	0.08	0.11
Mn	0.34	0.32	0.31	0.35
Fe	0.09	0.07	0.08	0.09
S	0.004	0.004	0.005	0.005
C	0.04	0.1	0.02	0.01

*0.035-in. wall thickness.

†Approximate; spectroscopic analysis.

moved some of the carbon from the nickel, which was to be expected. Further discussion of the composition and quality of these A-nickel samples will be made in the next section.

A nickel rod 1/8 in. in diameter and 22 cm long, believed to be similar in quality to the A-nickel, was used in the static measurements.

4.3.2

Iron-Cobalt Alloys

The second group of materials used in the experiments consisted of iron-cobalt alloys containing small

amounts of vanadium as a third alloying element. Chemical analyses of these samples were not made, but their nominal compositions are as follows:

1. 2V-Permendur: 49% Fe, 49% Co, and 2% V by weight.
2. 6.5V-vicalloy: 41% Fe, 52% Co, 6.5% V, and 0.5% Mn by weight.
3. 8V-vicalloy: 40% Fe, 52% Co, and 8% V by weight.

A sample of an iron-cobalt alloy $\frac{1}{8}$ in. in diameter and 22 cm long containing 70% cobalt was also procured for the tests. This sample consisted of electrolytic iron of high purity together with cobalt of commercial quality (99.8% Co, with Fe and Ni constituting a major portion of the impurity).

4.4

HEAT TREATMENT

One of two types of heat treatment, depending on the design of the unit, should be used for the magnetostrictive material of the transducer. Since the magnetostrictive coefficient is zero at zero polarization and the stress set up in the material by a variation of the magnetizing field does not vary with the sense of the field if the material is operated at zero polarization, the active material of a magnetostrictive transducer must be operated at a certain steady polarization B_0 , unless it is to be driven by large a-c magnetic fields at half of the resonant frequency. This steady polarization can be obtained by a d-c field, a permanent magnet, or by previously magnetizing the active material to saturation and bringing the polarization back to the remanence B_r .

When d-c polarizing fields or permanent magnets are used, the material obviously should be as soft as possible magnetically so as to save d-c power. Annealing at 900 C to 1000 C for one hour is generally sufficient for this purpose. The oxide-annealing treatment is particularly beneficial for nickel, since it forms a thin oxide film of very high electric resistivity on the surface of the material.

Regular laboratory practice is to anneal in air at 900 C for 20 minutes. But since annealing in air forms no insulating film, high-temperature annealing of other materials is generally done in hydrogen, an atmosphere which usually improves the magnetic properties of the materials.

When the material is to be operated at remanence it is desirable that the remanence be at least as great

as half of the saturation value and that the coercive force and the reversible permeability at remanence be as large as possible. It is well known that many materials exhibit small remanence either in the cold-worked or the well-annealed state, while annealing at a temperature close to the recrystallization point gives the maximum remanence and somewhat higher reversible permeabilities than can be obtained in the cold-worked state, without at the same time reducing the coercive force too much. This type of treatment is called half hard.

A detailed study of the proper temperature for this half-hard treatment was carried out on 2V-Permendur because the stock made available to HUSL was believed to be from the first large-scale production of this material in the form of rolled sheets. This treatment was generally carried out in hydrogen, although for nickel a hydrogen atmosphere is not necessary.

The vicalloys are ternary alloys which form homogeneous solid solutions at high temperatures. At temperatures below 700 C, marked precipitation begins to take place. By controlling the degree of precipitation, the mechanical and magnetic hardness of the material can be controlled. In extreme cases these alloys can be made hard enough magnetically to become permanent-magnet materials. The heat treatment then becomes a hardening rather than a softening operation.

Annealing was carried out in a partly muffled furnace with automatic temperature control. The samples were enclosed in a stainless-steel box through which hydrogen could be passed when necessary. In general, the temperature was accurately measured by a chromel-alumel thermocouple and the temperature fluctuation was about 5 C. With the exception of the nickel rod and the hydrogen-annealed 5-mil. A-nickel samples, however, the cooling was not always done in hydrogen.

4.5 EXPERIMENTAL PROCEDURE

4.5.1

Form of Sample

The samples measured were in the form of strips or rods and stacks of punched rings consolidated by an insulating cement, usually Vinylseal or Cycle-Weld. Strips were employed only for auxiliary studies of magnetic properties along the direction of rolling and for resistivity measurements. The two

rods previously mentioned were used in the static measurements. These were made from $\frac{5}{16}$ -in. rods of the metals by swaging. Ring stacks were used in both magnetic and dynamic measurements. With the exception of the 8V-vicalloy and the D- and Z-nickel samples, each stack contained more than 25 laminations. Two 6.5V-vicalloy samples were in the form of scrolls, which were made by rolling up a long $\frac{3}{8}$ -in. rolled strip and consolidating it with bakelite after heat treatment. The results obtained on these samples represent characteristics along the direction of rolling, while those obtained on ring stacks represent average characteristics in the plane of rolling.

4.5.2 Magnetic Measurements

METHOD USED

Magnetic measurements were made by the well-known induction method, using a ballistic galvanometer with 24-second periods and a sensitivity of 0.003 microcoulomb per mm at 1 meter. A 50-mh standard mutual inductance was used to calibrate

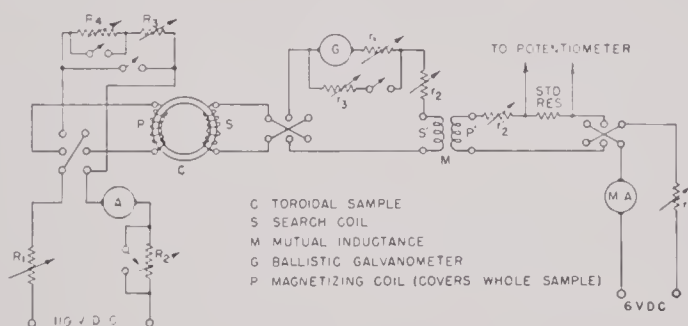


FIGURE 1. Circuit used in static magnetic measurements.

the galvanometer. For this purpose the secondary of the mutual inductance was permanently connected in the galvanometer circuit and the current used in the primary of the mutual inductance was measured with a 1-ohm standard resistance and a potentiometer. A simple circuit of the whole arrangement is shown in Figure 1.

For magnetizing rod or strip samples, an air-core solenoid was used, measuring about 80 cm in length, with an air-core 3.7 cm in diameter, and capable of producing a maximum field for continuous operation of 1,320 oersteds at 10 amperes. Two similar search coils were connected in opposition and placed side by side at the center of the magnet. Before the sample was introduced into one of these coils, their relative

positions were adjusted until a reversal of field gave no deflection of the galvanometer coil. In this way the directly measured quantity was $4\pi I = B'$, rather than B .

The demagnetizing factors of cylindrical rods are known⁴⁷ and hence the static measurements could be corrected, but there seems to be no existing literature on the demagnetizing factors of strips, so that data obtained on them are to some extent erroneous. These errors are believed to be small, however, since the lengths of the strips tested were generally large compared with their thicknesses.

Measurements on ring samples were made in the following way. The sample was first covered smoothly by a thin silk tape. Secondary coils made of a fine insulated wire (No. 35 to No. 39 B & S) were tightly wound on top of the tape. In most cases the sample had a cross section of 0.15–0.55 sq cm, so that a secondary of less than 30 turns gave sufficient sensitivity for measuring B while one of less than 200 turns was adequate for measuring the reversible permeability. The secondaries were again protected by silk tape and a primary of two layers of No. 22 or No. 20 insulated wire was wound on top. The ring samples were particularly well adapted to this type of measurement, but coils had to be wound on each sample, and it was not possible to use large enough fields to saturate the sample completely so that information ordinarily obtainable from the saturation value was lacking. Corrections for leakage flux were usually estimated and applied.

The magnetic properties of a sample are generally studied by measuring three curves: the normal B - H or commutation curve, a major hysteresis loop, and the reversible permeability as a function of field along the normal curve. Before measurement, the sample was first magnetized to near saturation and then demagnetized by continuously decreasing an alternating field to zero.

The normal curve was then traced by increasing H in steps and measuring the B by a single reversal of H . Each reading was repeated after a few reversals of the field. The normal curve is therefore the locus of the tips of the hysteresis loops traced out by maximum fields of varying magnitude.

A major hysteresis loop is one obtained by the reversal of a maximum field that is large compared with the coercivity. It can be most readily measured when it is possible to change the primary current in steps in a single series of operations. This method was used with the circuit of Figure 1.

INTERPRETATION OF RESULTS

The term reversible permeability needs further explanation. First consider the initial portion of the magnetization curve. Lord Rayleigh⁴¹ found that if a small induction B_1 is obtained at a small field H_1 by increasing or decreasing the field, then the change in B by varying the field by a small amount ΔH in the backward direction can be given by

$$\Delta B = \mu'_1 \Delta H \pm \frac{1}{2} \alpha (\Delta H)^2,$$

where μ'_1 and α are constants and the second term is positive or negative according as ΔH is positive or negative. It is obvious that the first term in the above expression represents the reversible part of ΔB and that μ'_1 is the initial reversible permeability, while the second term represents the irreversible part of ΔB . If $H_1 = B_1 = 0$ and ΔH is an alternating field of amplitude ΔH_1 , then the magnetization curve traced out is a small lance-shaped loop which is symmetrical with respect to the origin and in which the major axis has a slope $\mu'_1 + \frac{1}{2} \alpha \Delta H_1$. The remanence is simply $\frac{1}{2} \alpha \Delta H_1$. The same situation is presumably true for any point in the B - H plane, provided that ΔH is very small. In this general

ments the current through the transducer is also not infinitesimal.

When the material is polarized by a steady field H_0 and an alternating field of amplitude ΔH_1 is superposed, then, as ΔH_1 becomes large, an unsymmetrical loop is traced out. Such a loop is defined here as a minor loop.

4.5.3 Static Measurements

For the static magnetostriction measurements, the air-core solenoid mentioned in the foregoing section was used. A pair of spools were installed side by side in the central portion of the solenoid. Each spool had two sets of coil windings, one over the other. The first pair of coils, with 5,625 turns, were used for measuring μ' and Λ ; the second pair, with 319 turns, measured B . The arrangement was such that any emf generated by changes in an externally applied field were balanced out. An endpiece was soldered to each end of the cylindrical sample under test, so that when the sample was properly inserted in one of the spools, one endpiece could be rigidly clamped with respect to the solenoid and the spool.

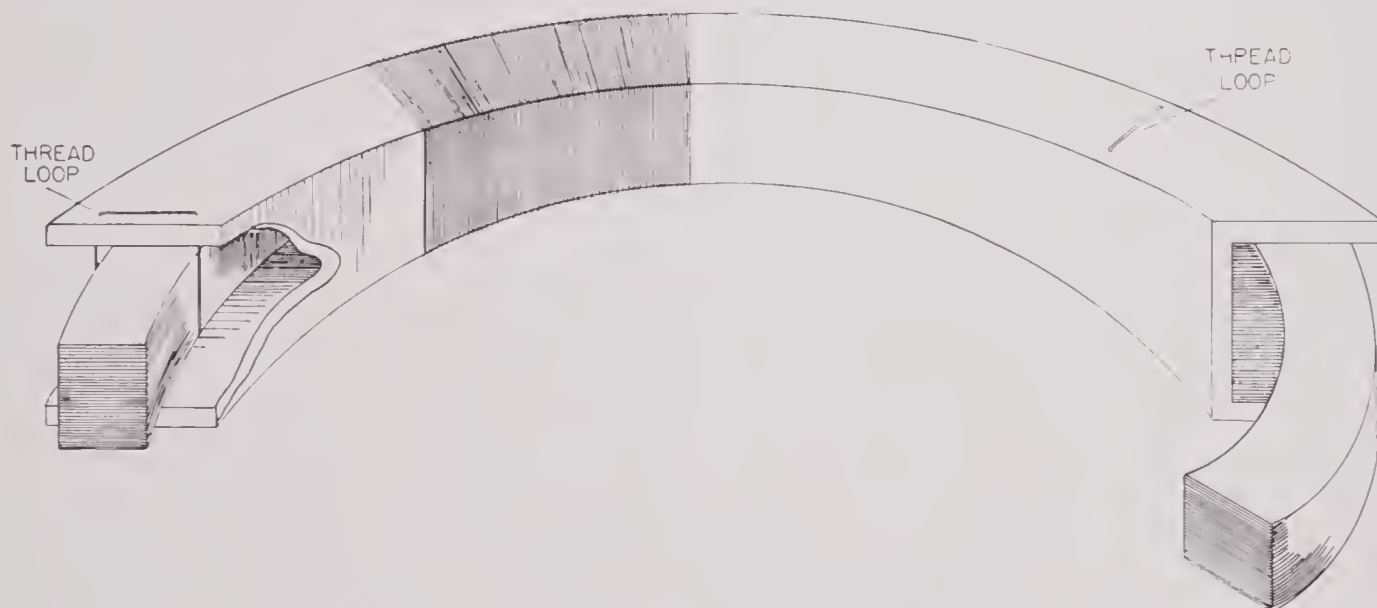


FIGURE 2. Mounting of sample for dynamic measurement.

case, however, μ' and α both decrease with increasing B . The μ' is thus a limiting value, and any measured value with a finite ΔH gives the slope $\mu' + \frac{1}{2} \alpha \Delta H$ of the corresponding lance-shaped loop. However, for practical purposes such measured values are accurate enough if ΔH is small. In the present measurements, $2\Delta H$ seldom amounted to 10 per cent of the main field. Note that in the bridge measure-

On the other endpiece was attached a flexible wire which passed over a pulley to support an aluminum pan. Change of magnetization was observed by loading or unloading the pan.

Weights of 100, 200, and 500 grams were used in measuring Λ . In general, hysteresis effect was present and increased with the increased size of the load. Each reading was accordingly taken by loading and

unloading the sample several times until a steady change of magnetization was obtained.

4.5.4 Dynamic Measurements

After magnetic measurements had been made on a ring stack, the primary and secondary coils were removed. The sample under test was then freely suspended by three equally spaced loops of silk thread in a toroidally wound frame made of wood (see Figure 2). A primary coil was then wound on the wooden frame and the sample was ready for dynamic measurements by an impedance or admittance bridge. It is seen from the theory of toroidal transducers that any external mechanical resistance acting uniformly on the toroidal core does not affect the values of the fundamental quantities λ , μ , and E . The fact that this method of suspension reduces external mechanical resistances does, however, make possible increased precision of measurement.

The dynamic measurements reported here were made in the Electrical Measurements Department. For a detailed account of the procedure and the apparatus, see Chapter 11.

4.5.5 Resistivity and Density

Both strips and punched rings were used for measuring resistivity. When a strip was used, two leads were soldered or welded to each end. Through one pair of leads a measured current of 0.50 to 1.00 ampere was sent through the strip and the potential across the other pair of leads was measured with a potentiometer. In the case of a punched ring, the leads were soldered or welded at two diametrically opposite points on the ring so that the two halves of the ring formed two equal resistances in parallel. Owing to the small thickness of the samples, the absolute values of the resistivities are accurate to about 2 to 3 per cent, but the relative accuracy is in general about 1 per cent.

The densities of A- and D-nickel are known. For the rest of the materials, approximate estimations were made by weighing a number of punched pieces, the dimensions of which were accurately known.

4.6 EVALUATION OF FUNDAMENTAL QUANTITIES

Before presenting the results it will be helpful to summarize some of the formulas of Chapter 3 for the

special case of a toroidal transducer of which the magnetostrictive core has a radius a , length l , and wall thickness b , and the winding consists of N turns. From these formulas μ , k , and λ can be readily evaluated from impedance or admittance data.

1. For impedance data:

a. Clamped-core impedance $Z_c = \frac{j\omega 2N^2 b l \mu X}{a}$.

b. Frequency of resonance $f_R = \frac{1}{2\pi} \sqrt{\frac{K'}{M}}$,

where M = total mass of toroidal core,

$$K' = \text{stiffness factor} = \frac{2\pi b l}{a} E'$$

$$= \frac{2\pi b l}{a} E (1 - \chi_R k^2).$$

c. Diameter of motional-impedance circle

$$D_Z = \frac{|Z_{cm}^2|}{R_m + R_L}.$$

d. $Q_Z = \frac{\sqrt{MK'}}{R_m + R_L}.$

e. The electromechanical coupling coefficient

$$k = \frac{4\pi\lambda^2\mu}{E} \text{ is given by}$$

$$\frac{D_Z}{Q_Z X_c} = \frac{k^2}{1 - \chi_R k^2} \cdot \frac{\chi_0^2}{\chi_R}.$$

With a knowledge of the density of the core material, Young's modulus E' at constant field can be immediately calculated. If the effect of magnetic hysteresis is neglected, then χ_R and χ_0 can be read from the curves in Figure 1 of Chapter 3, since the eddy-current loss angle ζ is determined from the dip angle ($= 2\zeta$) of the resonance diameter of the motional-impedance circle. Thus k can also be calculated immediately.

Calculation of λ calls for a knowledge of μ , which may either be obtained from d-c measurements or calculated from the clamped-core impedance at resonance, provided the effect of magnetic hysteresis is again neglected. A better method is to apply the theory described in the first section of Chapter 3 to a whole series of values of the clamped-core impedance. This method can be applied to data obtained at a given frequency for various intensities of polarization as well as for those obtained at a fixed polarization.

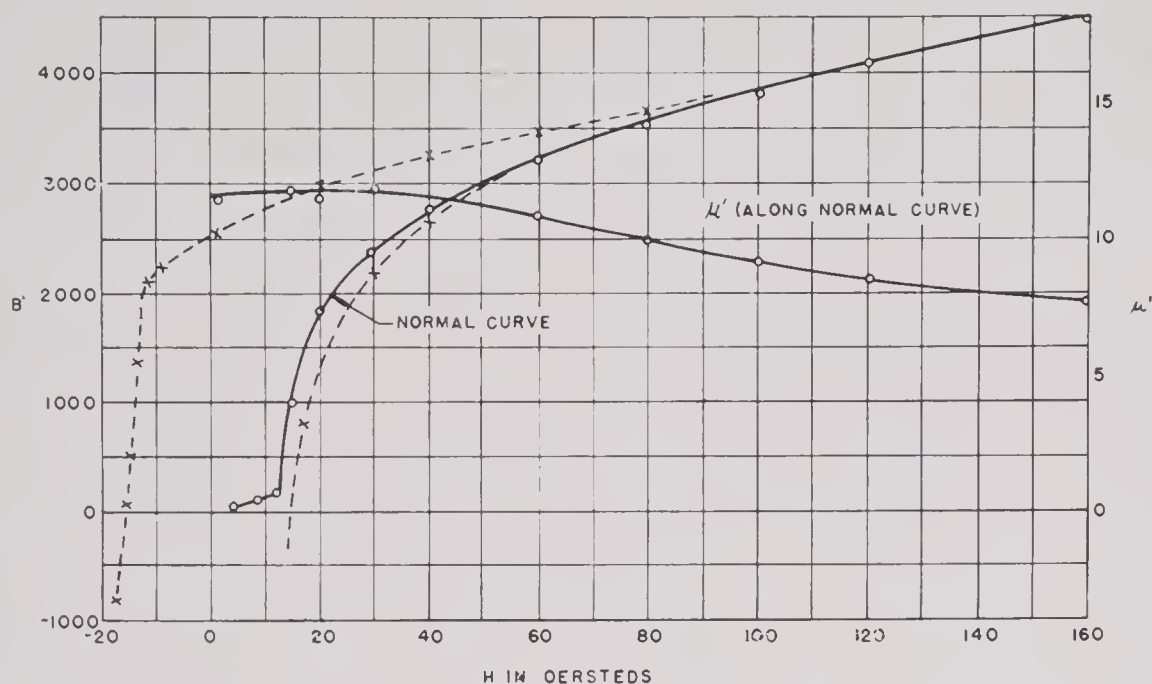


FIGURE 3. Magnetization and permeability of hard-drawn A-nickel tubing, 1.5-in. diameter, 0.035-in. wall. Magnetized circumferentially.

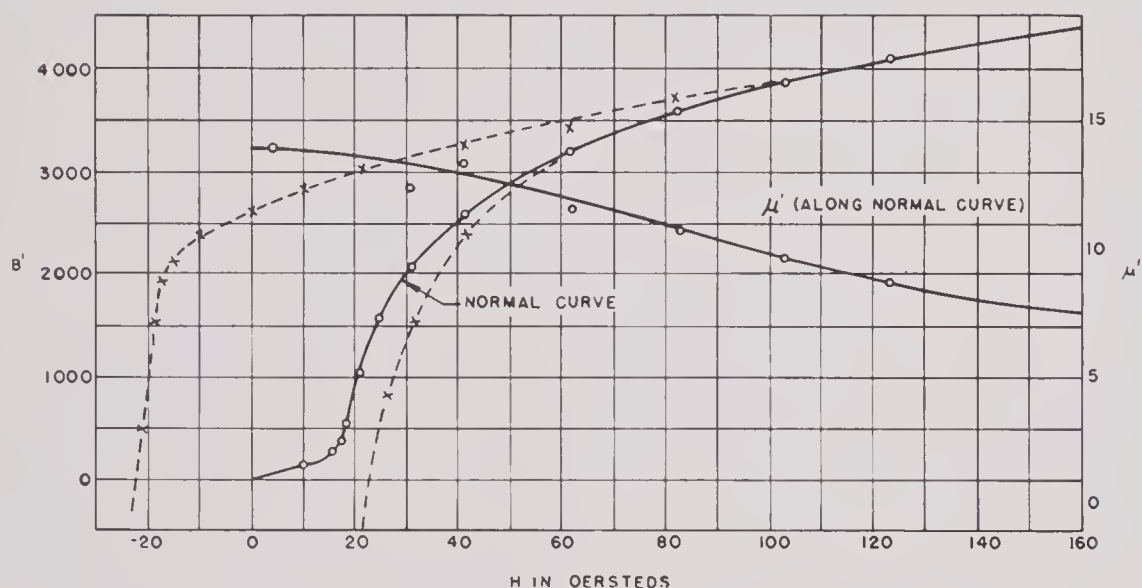


FIGURE 4. Hard-drawn A-nickel tubing, 2½-in. diameter, 0.035-in. wall, magnetized circumferentially.

tion for various frequencies. Also, it furnishes somewhat independent values of the resistivity and the reversible permeability. A quite different value of the resistivity is frequently obtained by this method as compared to that directly measured.

2. For admittance data:

- a. Frequency of maximum efficiency

$$f_E = \frac{1}{2\pi} \sqrt{\frac{K}{M}}$$

where K = stiffness factor = $\frac{2\pi bl}{a} E$.

- b. Diameter of motional admittance circle

$$D_Y = \frac{\frac{-Z_{em}^2}{Z_c^2}}{R_m'' + R_L}$$

c. $Q_Y = \frac{\sqrt{MK}}{R_m'' + R_L}$

- d. The coefficient of electromechanical coupling k is given by

$$k = \sqrt{\frac{D_Y}{Q_Y} \frac{B_c}{(G_c^2 + B_c^2) \chi_R}}$$

In this case, χ_R can be determined by the type of geometrical construction shown in Figure 3 of Chapter 3 or from the clamped-core admittance Y_c at the frequency of maximum efficiency. The effect of magnetic hysteresis is again neglected. The values of μ can also be found by a study of the clamped-core admittance.

4.7 DISCUSSION OF RESULTS

4.7.1 Method of Presentation

The results obtained in these investigations are

presented in Figures 3 through 48. These figures form two groups, one showing the general magnetic properties and the other the magnetostrictive properties of the various materials. There are more samples shown in the first category than in the second, but for every sample that appears in the magnetostrictive group, there is a corresponding set of curves for the magnetic group. In order to facilitate comparison, curves for several samples are sometimes plotted in a single figure, but curves for one sample are sometimes repeated in several figures.

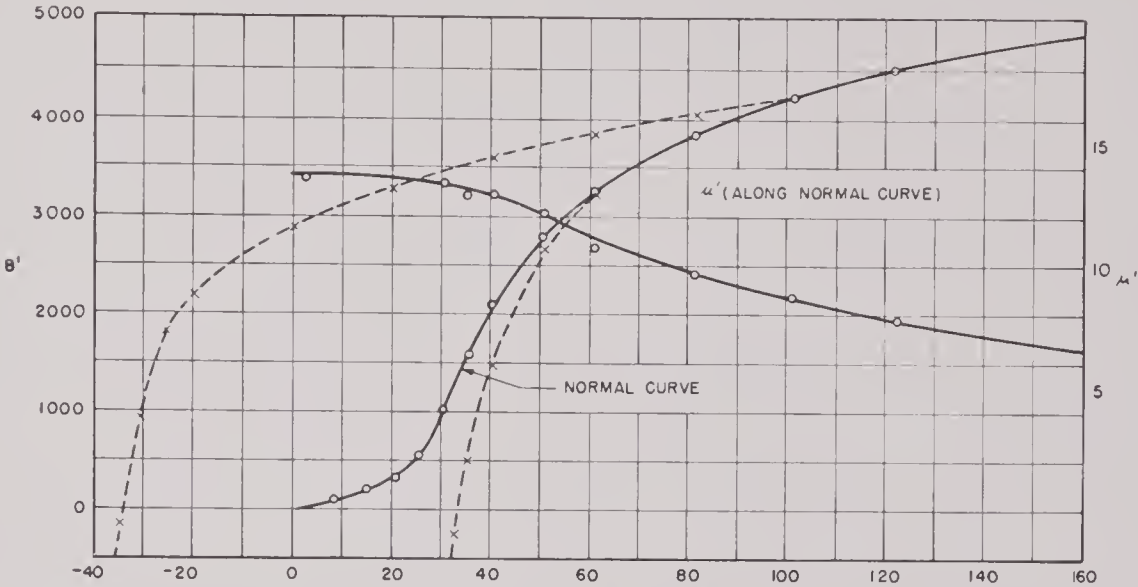


FIGURE 5. Cold-rolled A-nickel sheets 0.005 in. thick.

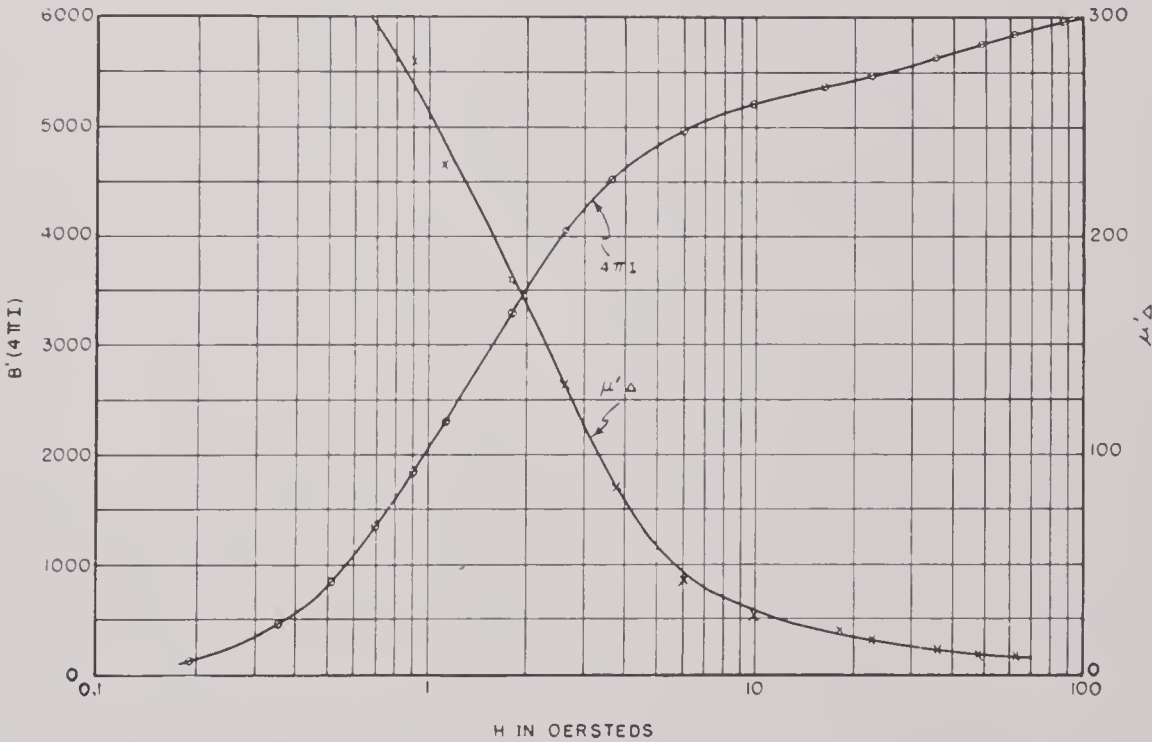


FIGURE 6. A-nickel rod annealed for 1 hour in hydrogen at 1000 C, slowly cooled.

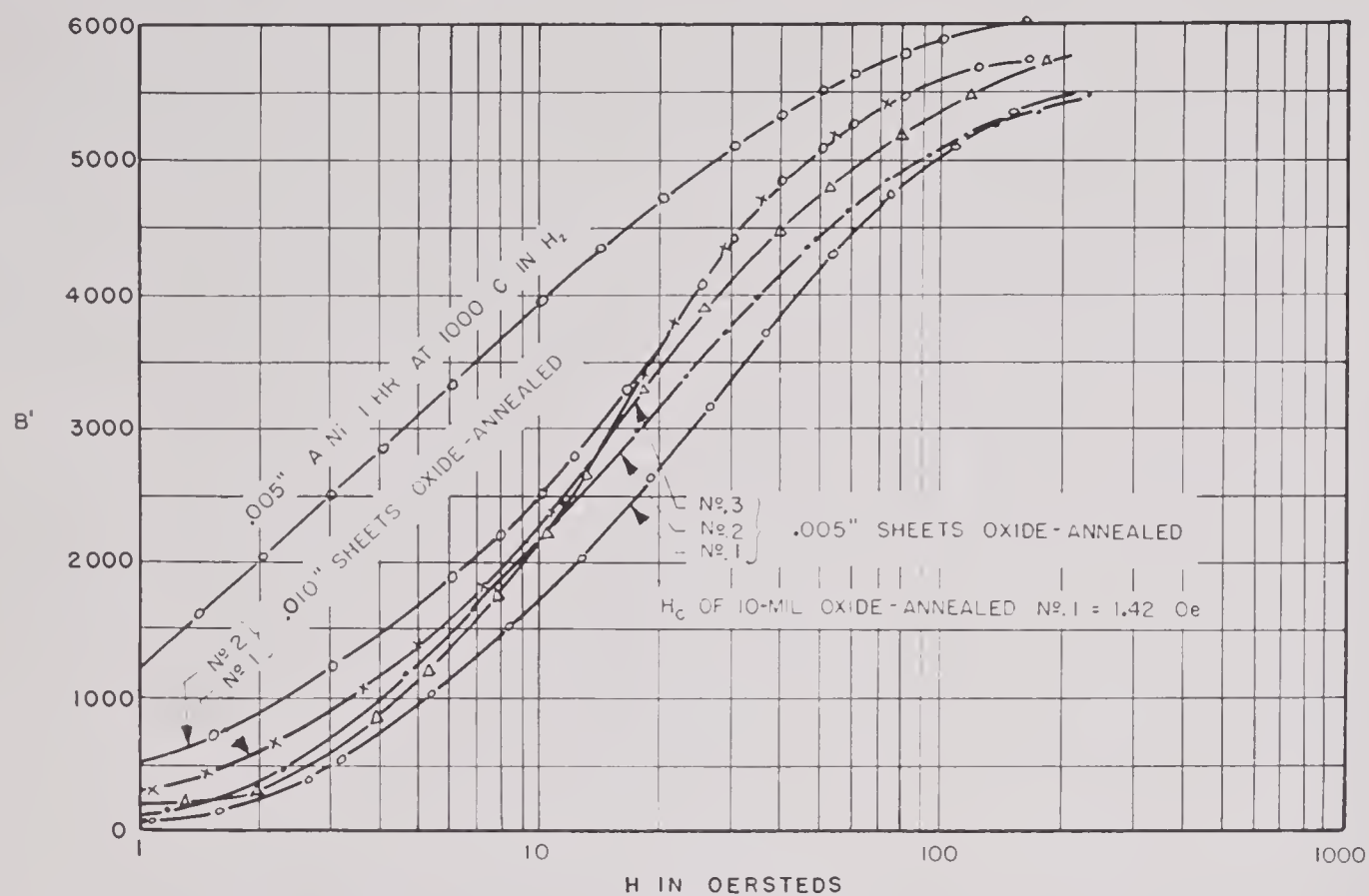


FIGURE 7. Magnetization of A-nickel sheets as affected by thickness and annealing conditions.

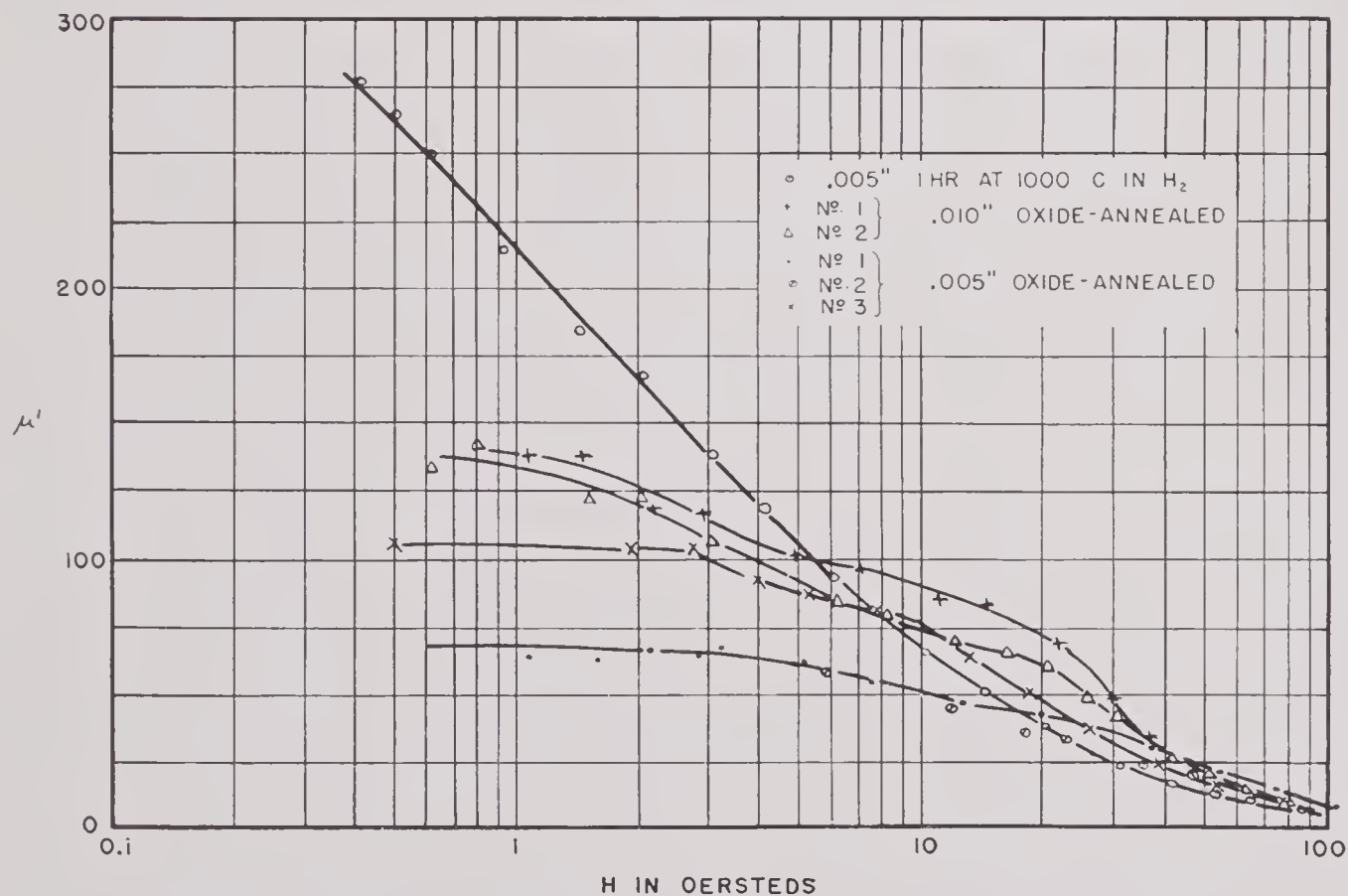


FIGURE 8. Reversible permeability of A-nickel sheets as affected by thickness and annealing conditions.

CONFIDENTIAL

Since the figures represent the properties of the various samples in sufficient detail, it will not be necessary to discuss all of them individually. Supplementary explanations will be made of details that cannot be shown in the figures, and special attention will be given to the consistency with which results can be reproduced and to the agreement between experiment and theory.

4.7.2 Magnetic Measurements

NICKEL

As will be seen by the three A-nickel samples shown in Figures 3, 4, and 5, different stocks of the same material do not have identical magnetic properties. Judging by the initial values of the reversible permeability, these samples are seen to have approximately the same magnetic hardness. The coercive forces are markedly different, however, causing variations in low-induction permeability. Differences in high-induction permeability also appear. These differences are presumably due to differences in previous history,

and one of the 5-mil A-nickel ring stacks of Figures 7 and 8. These samples were annealed one hour at 1000 C in hydrogen, cooled to 400 C at an approximately uniform rate in 10 hours, and then removed from the furnace. The rod had an initial permeability of 370 and was practically saturated at a field of 20 oersteds. Probably because of differences in size and orientation of grain, the sheet sample did not become as soft as the rod.

There is a limit to the degree of annealing to be done in reducing internal strains in order to soften a magnetostrictive material, since in cooling the material through its Curie point internal strains are set up spontaneously by virtue of magnetostriction. According to Becker and Kersten's theory,⁴⁶ the maximum value of initial permeability $\mu'_{i\max}$ can be estimated from

$$\mu'_{i\max} = 1 + \frac{8\pi}{9} \frac{I_s^2}{s_s^2 E},$$

where I_s is the saturation magnetization, E Young's modulus, and s_s the total fractional change of length at saturation of a free sample as a result of magnetostriction. Taking $I_s = 510$, $E = 2 \times 10^{12}$, and the somewhat uncertain value of 30×10^{-6} of s_s for nickel yields $\mu'_{i\max} = 405$. Thus the nickel rod approaches the limit of magnetic softness.

If the nickel rod is taken as standard for fully annealed nickel, the oxide-annealed samples shown in Figures 7 to 11 appear to be only partially annealed. This is probably due to the short time during which the latter samples were held at the high temperature.

In Figures 7 to 11, No. 3 of the 5-mil samples was actually annealed 30 minutes in hydrogen and 10 minutes in air at 900 C. All other samples went through the regular oxide-annealing process (20 minutes at 900 C in air). The two 10-mil samples were actually from a single batch of punched rings annealed at the same time. It can be seen that the five oxide-annealed samples differ magnetically among themselves. However, one point seems to be quite definite: the 10-mil stock becomes magnetically softer than the 5-mil stock after the oxide-annealing treatment.

The research laboratories of the International Nickel Company³⁸ made chemical and physical tests for HUSL on four batches of oxide-annealed 10-mil A-nickel stampings which showed differences in magnetic properties similar to those in Figures 7 to 11. Abnormality of chemical composition was absent,

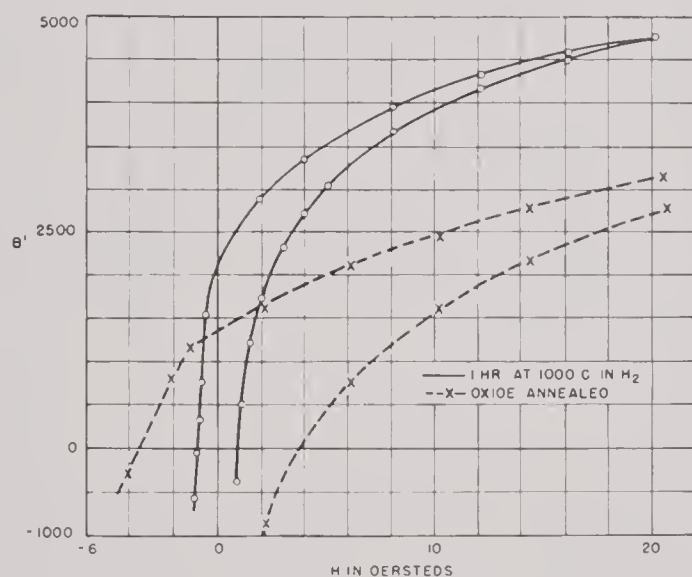


FIGURE 9. Ring laminations 0.005 in. thick of A-nickel.

since chemical analyses of the samples as shown in Table 1 are markedly uniform. In any case, it must be expected that similar differences will exist to some extent after heat treatment, particularly when samples are not fully annealed.

It is well known that nickel can be made magnetically very soft by high-temperature annealing in hydrogen. Examples are the nickel rod of Figure 6

thickness of the oxide film varied from 0.00006 in. to 0.00025 in., and the Vickers hardness number varied from 63.1 to 82.6. It would seem, then, that the differences in mechanical and magnetic hardness of the

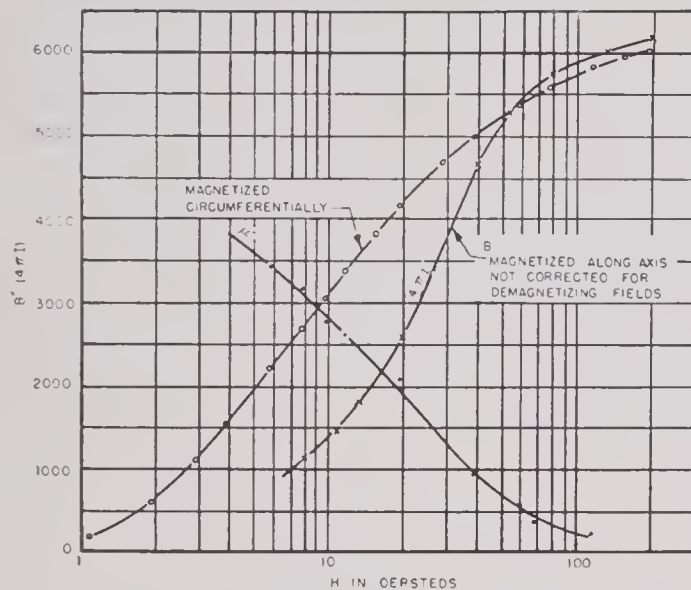


FIGURE 10. A-nickel tube, 1.5-in. diameter, 6.0 in. long, 0.035-in. wall, magnetized longitudinally and circumferentially.

oxide-annealed samples are largely due to differences in the previous history of the stock materials. Moreover, the short annealing period probably makes the control of heat-treatment conditions difficult and this causes small differences.

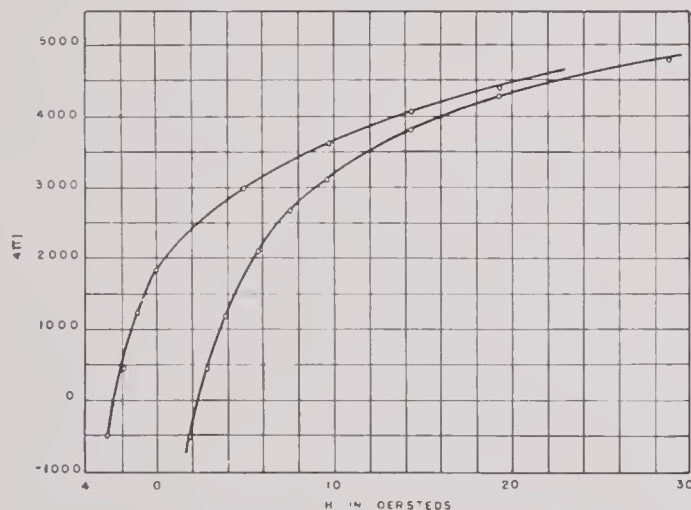


FIGURE 11. Hysteresis of A-nickel tube, magnetized circumferentially.

Differences apparent in the two 10-mil samples (Figure 7) indicate that small differences will almost always be present in different samples because of slight nonuniformity in the stock itself. These differences seem to occur at low inductions so that they

are relatively unimportant and will affect the transducer only when it is driven hard, since in actual practice the active material of a transducer is generally polarized to a high intensity ($B_0 \simeq 4,000$ for Ni).

Evidence of the effect of preferred orientation is exhibited by the data obtained on the tubing shown in Figures 10 and 11. The two normal curves cross at $B' = 5,300$. When corrected for demagnetizing fields, the curve for longitudinal magnetization should have a larger portion lying above the curve for circumferential magnetization than is shown by Figure 10.

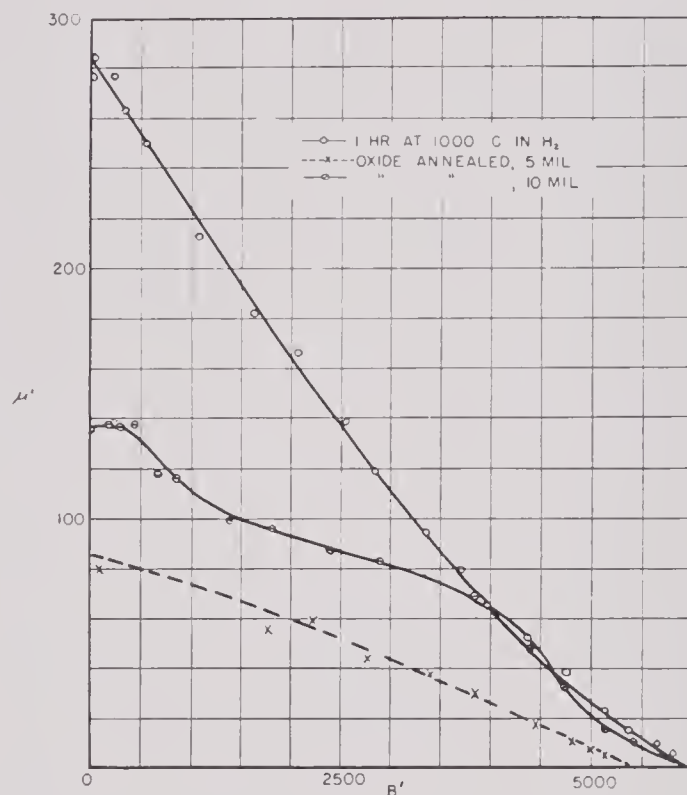


FIGURE 12. Permeability of 0.005-in. A-nickel ring laminations.

Thus magnetization at high induction is easier along the axis, which means that the direction of easy orientation of the crystallites tends to coincide with the axis of the tubing. A similar effect presumably exists in the sheet samples, but, since measurements were made on ring samples containing a large number of laminations, the effect would be averaged out.

It is generally accepted that the reversible permeability μ is a function only of the magnetization I , so that for a given value of I , μ should have the same value whether measured at a point on the normal curve or on either branch of a major hysteresis loop. This should certainly be true for well-annealed materials since hysteresis is small in such materials. For

hard and half-hard materials, however, peculiar hysteresis effects exist as exemplified by Figure 17. Smith⁴⁰ has also found that if μ is plotted against $B-H$ the result approximates a straight line. Such an approximate relationship may sometimes be useful for practical purposes. As Figure 12 indicates, this seems to be true for the cases of the hydrogen-annealed and oxide-annealed 5-mil A-nickel, but con-

magnetization, even though the Curie point lowers at the same time.³⁹

As can be seen by comparing Figures 14 and 15 with Figure 5, the 20-mil D-nickel sample in the hard-rolled state is magnetically softer than the 5-mil A-nickel sheets. But this may not mean that D-nickel cannot be made harder. On the other hand, the 1000 C annealing made the material extremely soft with an

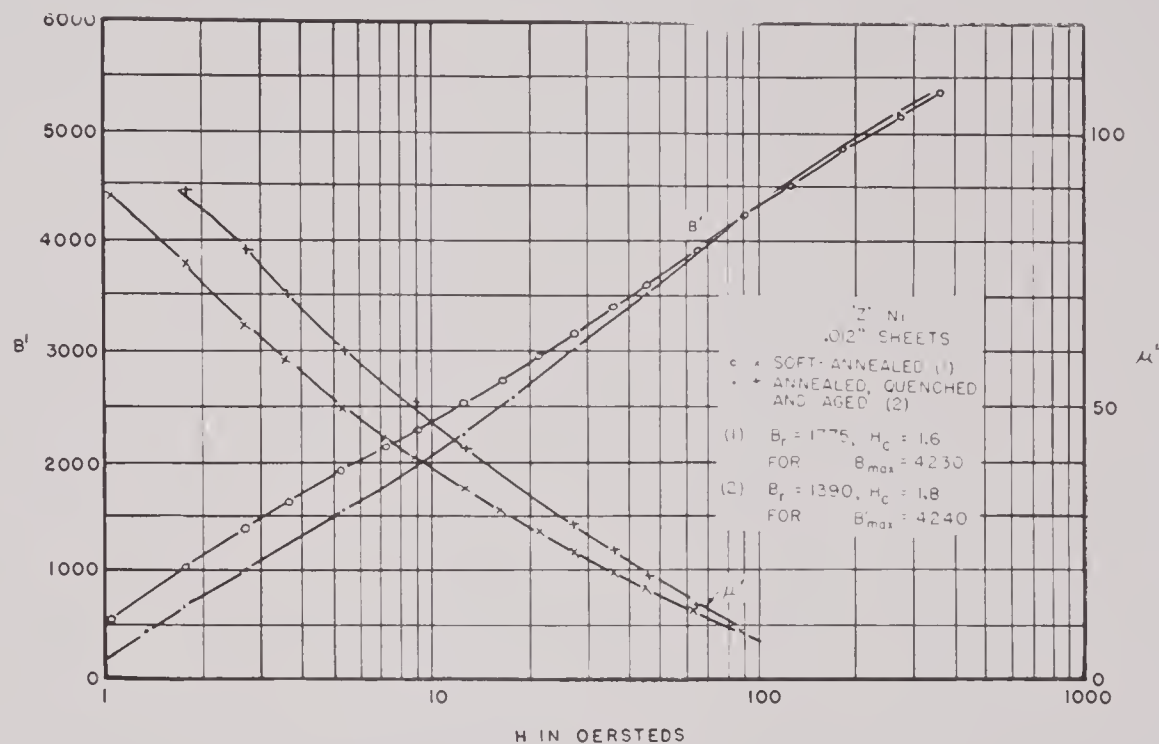


FIGURE 13. Magnetization and permeability of Z-nickel.

siderable deviation is present in oxide-annealed 10-mil A-nickel.

From correspondence with E. M. Wise of the International Nickel Company, it was learned that the special features of Z-nickel are its higher mechanical hardness (20 to 35 Rockwell C) obtainable by mechanical work and aging and its higher resistivity. The maximum coercive force obtainable in this material is about 48 as compared with 42 in A-nickel.

The annealed sample of Z-nickel shown in Figure 13 was treated at 1050 F and quenched from that temperature. The other sample in the figure was quenched from the same temperature and aged at 485 F for 10 hours. As seen from the curves, the aged sample, presumed to be mechanically harder, shows a higher reversible permeability than the quenched sample.

The D-nickel is of particular interest because previous investigations showed that small amounts of dissolved manganese in nickel increase its saturation

initial permeability close to 700. As the saturation value was only about 10 per cent greater than that of A-nickel, Becker and Kersten's theory already cited⁵ predicts that the magnetostrictive effect has been reduced. It will be seen later that this is true.

The laboratory's primary interest in half-hard materials was their usefulness for transducers operated at remanence. For this purpose, the remanence should be fairly high since the magnetostrictive coefficient generally increases with increasing polarization. At the same time, the coercive force and the reversible permeability at remanence should also be large so that the remanence can be kept permanent and the electromechanical coupling coefficient can be large. These requirements are in some respects conflicting, because the various quantities cannot be controlled independently. In general, an increase in coercive force or in remanence is accompanied by a drop in the reversible permeability at remanence. Therefore, the practice has been to anneal at such a tem-

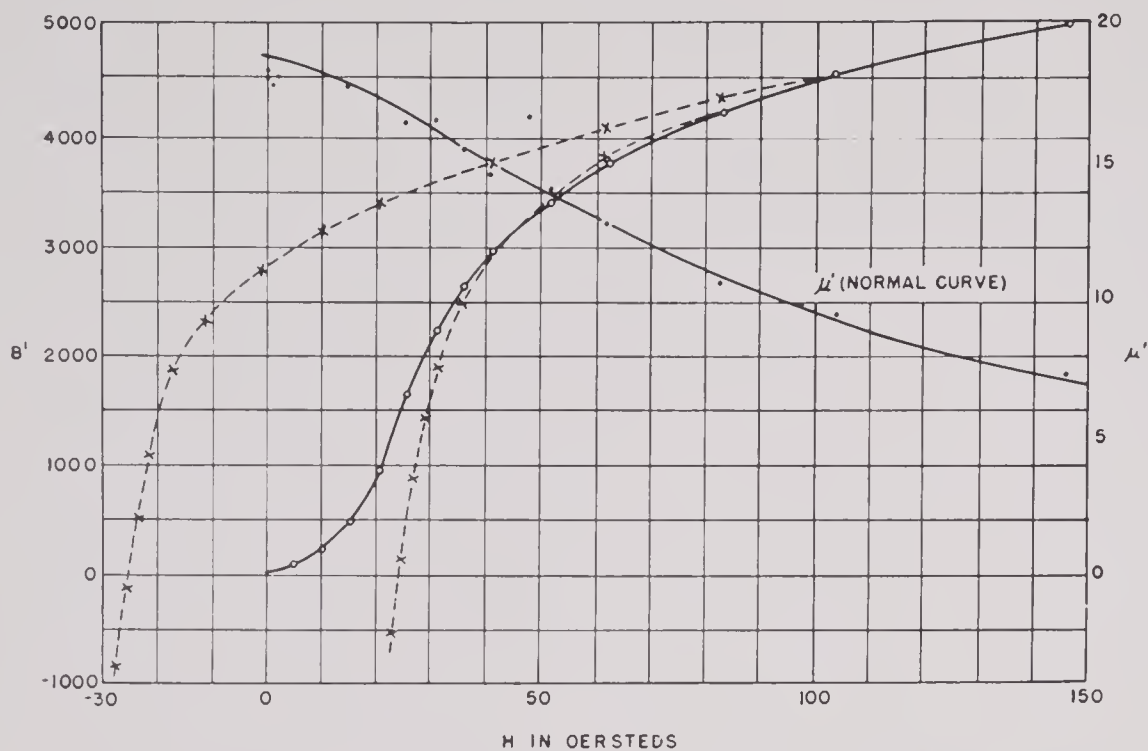
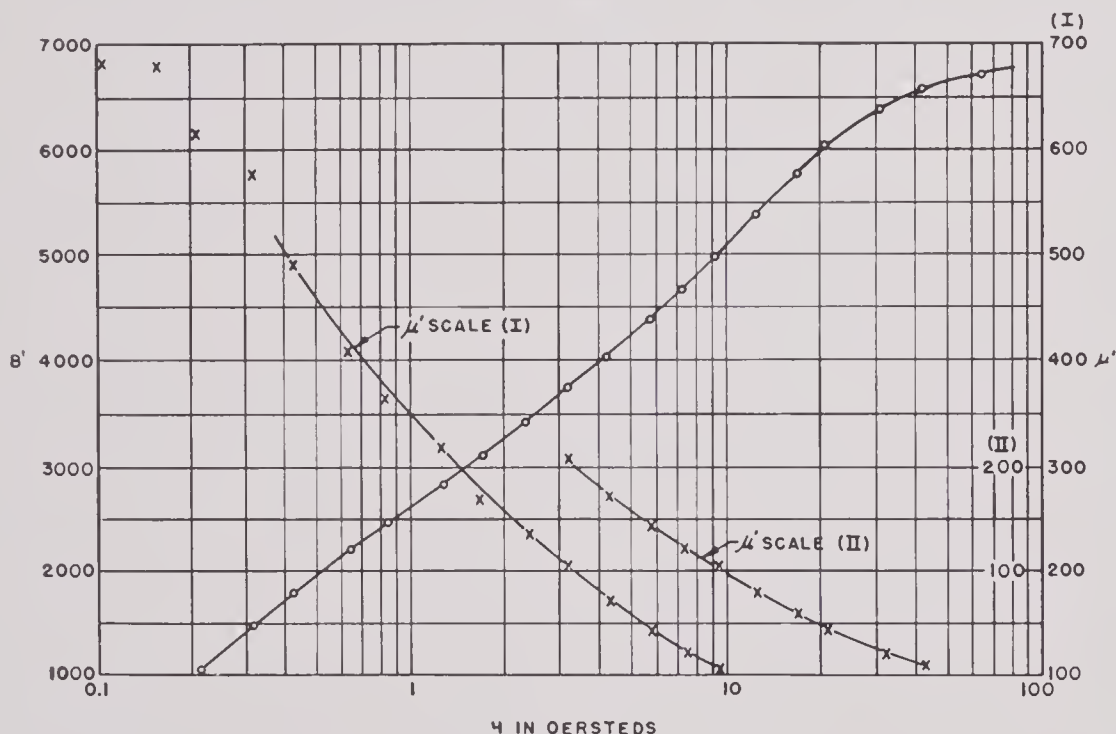


FIGURE 14. Hysteresis and permeability of D-nickel as received.

FIGURE 15. Magnetization and permeability of D-nickel annealed 1 hour in hydrogen at 1000 C. $B_r = 2,330$, $H_c = 0.24$.

perature that the remanent magnetization is high without too great a sacrifice in coercive force.

Figures 16 and 17 show that the range of annealing temperatures for 5-mil A-nickel within which the remanence increases is rather narrow. A comparison with Figure 5 shows that only a slight change from the unannealed state results from annealing for one

hour at 550 C. On the other hand, annealing at 620 C for one hour gives a lower value of the remanence than for the 600-degree anneal and reduces the coercive force to below 20. The critical temperature must therefore be very close to 600 C. One hour at this temperature increases the remanence by more than 10 per cent and the reversible permeability by more

CONFIDENTIAL

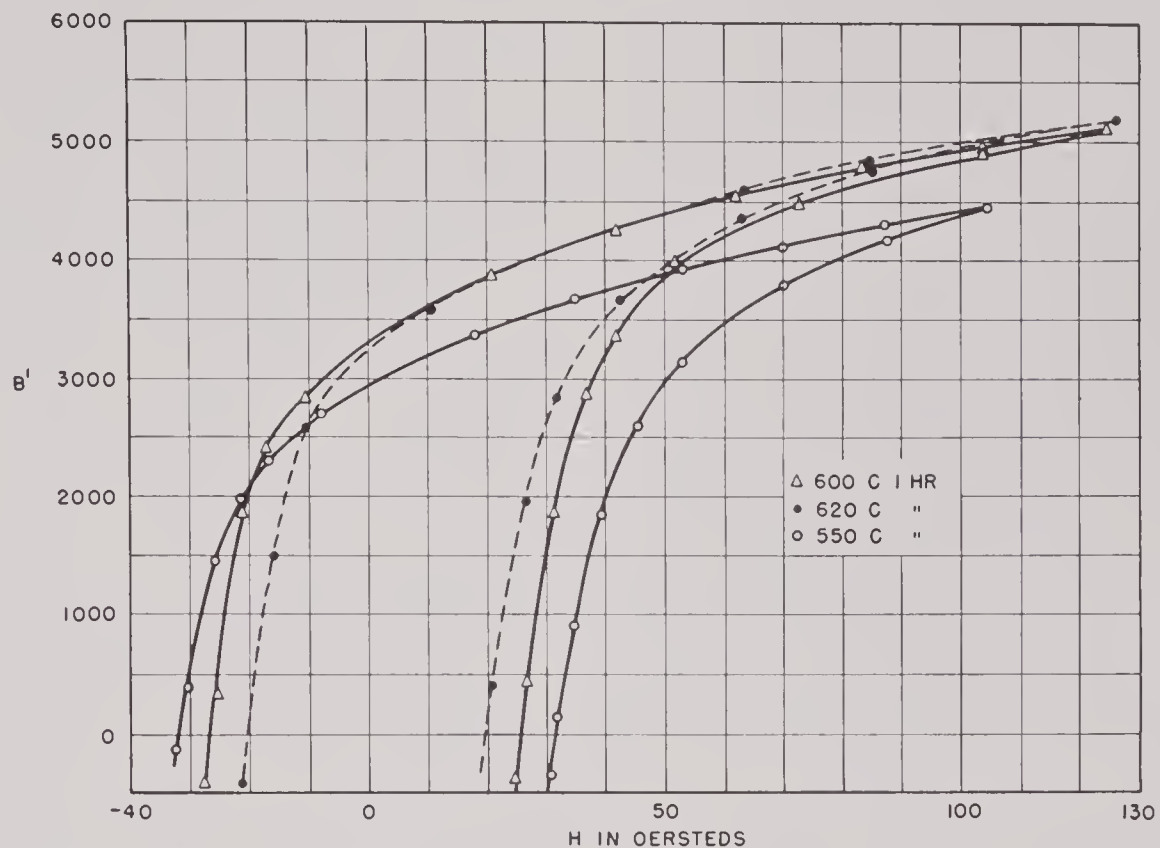


FIGURE 16. Half-hard A-nickel sheets 0.005 in. thick.

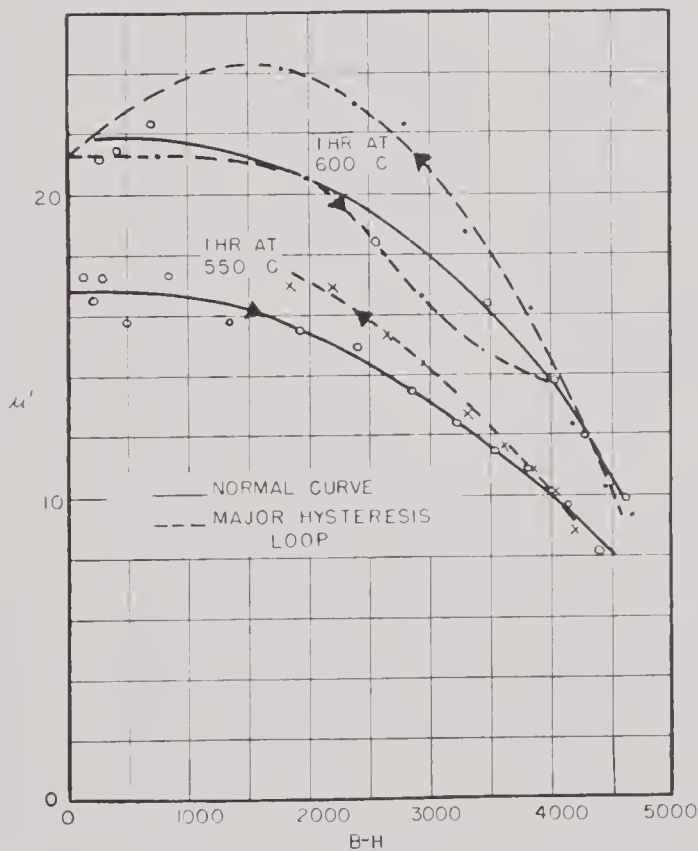


FIGURE 17. Permeability of half-hard A-nickel sheets 0.005 in. thick.

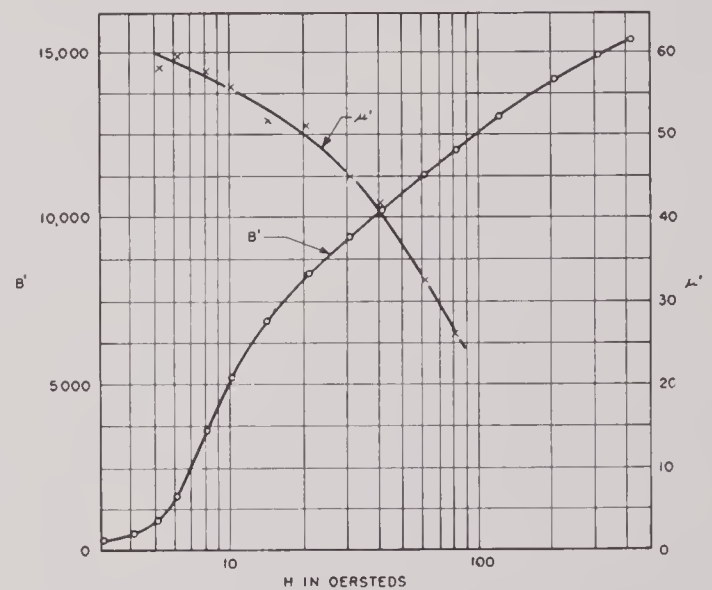


FIGURE 18. Magnetization and permeability of hard-rolled 45-Permalloy sheets 0.005 in. thick.

hour anneal at 600 C does improve the overall effectiveness of the material for operation at remanence. Data on 45-Permalloy are presented in Figures 18, 19, and 20.

IRON-COBALT ALLOYS

Previous investigations on the fractional change of length as a function of magnetization show that iron-cobalt alloys with about 40 to 70 per cent cobalt con-

than 30 per cent, and decreases the coercive force by about 20 per cent. It will be seen later that the one-

tent have the largest magnetostriction. According to Masiyama,⁴⁸ the maximum occurs at a cobalt content of about 70 per cent. However, these alloys are known

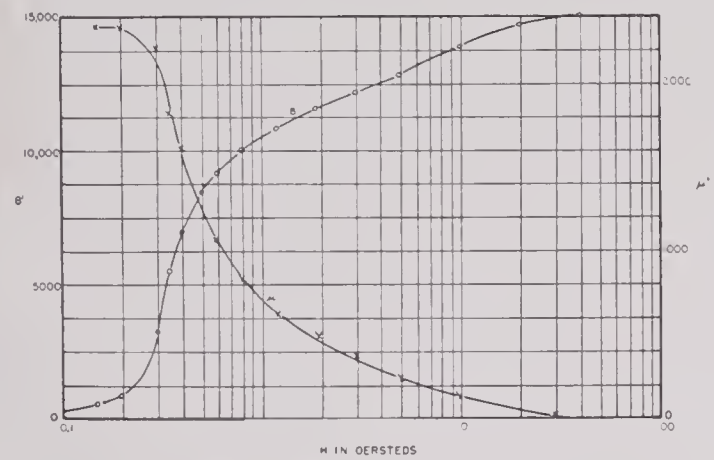


FIGURE 19. Magnetization of 0.005-in. 45-Permalloy annealed in hydrogen 1 hour at 1000 C.

to be magnetically hard and mechanically very difficult to work. Furthermore, it is difficult to reproduce magnetic properties in the high-cobalt alloys. These

in. in diameter. In spite of high-temperature annealing (identical with that for the nickel rod), the reversible permeabilities seemed to be rather low for a material with such a high saturation value. The peculiar manner in which the reversible permeability of this sample varied with polarization was not observed in any of the other materials.

Previous investigators found that the addition of a small amount of vanadium improves the mechanical workability of the iron-cobalt alloys. With special heat treatment, the magnetic properties of some of these ternary alloys can also be improved.⁴³ These are the reasons for the development of 2V-Permendur, although this material was not originally developed for magnetostrictive transducers.

For the ternary alloys with a constant cobalt content of 50 per cent, Koester and Lang⁴⁴ found that the α - γ transformation temperature lowers with increasing vanadium content. When the vanadium content increases beyond 2 per cent, temperature hysteresis in the α - γ transformation becomes quite

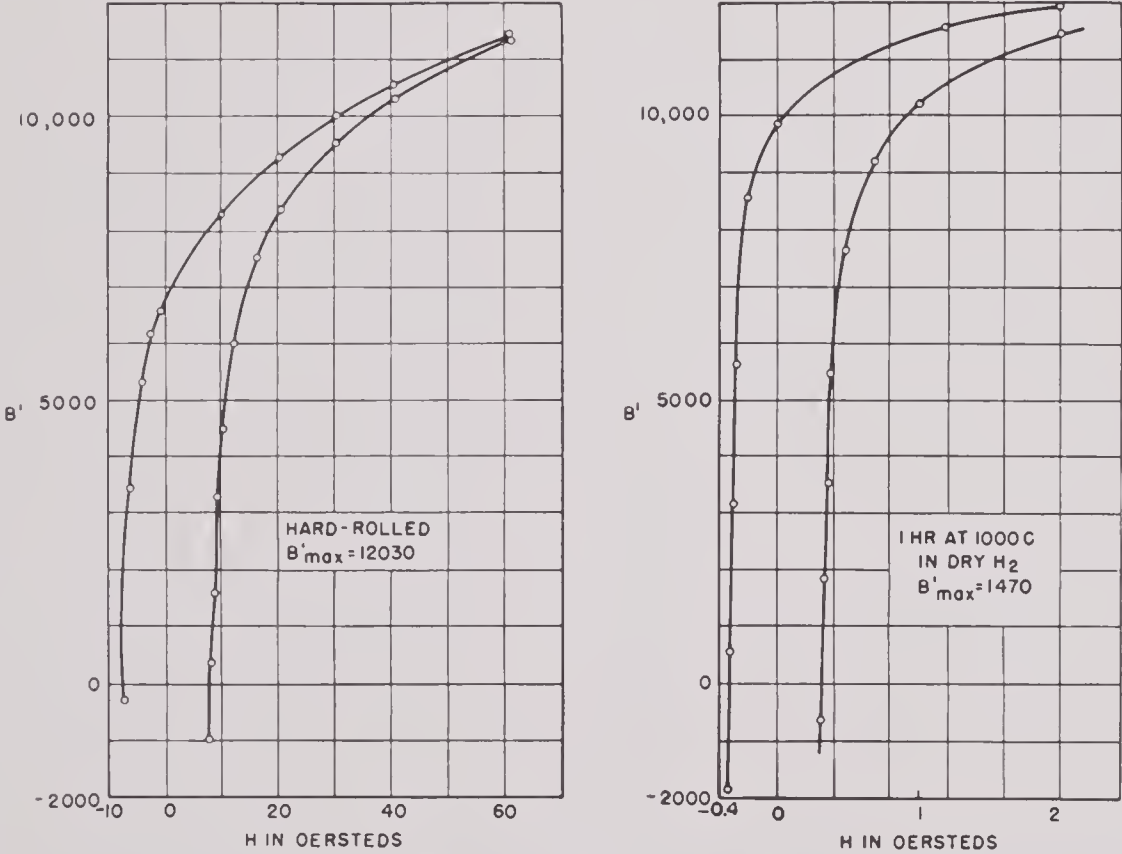


FIGURE 20. Hysteresis of 0.005-in. 45-Permalloy sheets.

empirical facts seem to be borne out in the 70% Co, 30% Fe rod seen in Figure 21. The original test sample, 1/8 in. in diameter and 22 cm long, was made with considerable difficulty by swaging from a piece 5/16

large. For this reason, the high-vanadium alloys can be hardened by partial precipitation, whereas well-annealed 2V-Permendur is soft because it contains a single α phase.

Of the 2V-Permendur samples measured, those shown in Figures 22 through 27 were made from the first batch of 0.006-in. sheets obtained from BTL, while the remainder were made from a larger stock supplied by Western Electric Company, Inc. In this case, the normal curves of the soft-annealed samples again show considerable differences which are somewhat exaggerated by the large differences in the coercive force. (Compare Figures 24 and 28.) In contrast, the two ring samples annealed at 500 C (Figures 27 and 31) are in close agreement. It would seem that magnetic properties can be more easily reproduced in half-hard than in fully annealed samples of this material.

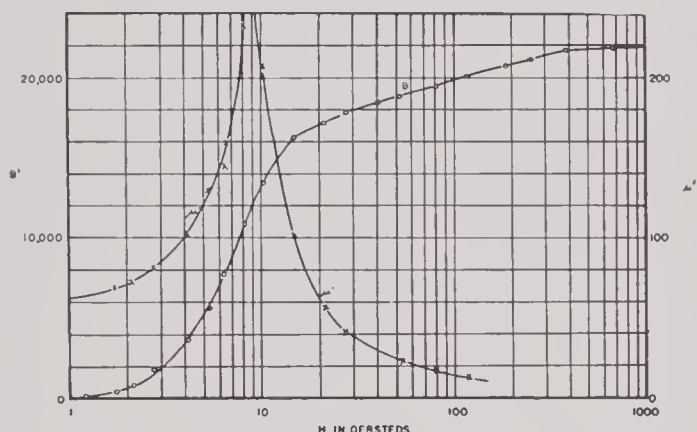


FIGURE 21. Magnetization and permeability of Fe 30%, Co 70%, reannealed and slowly cooled.

A detailed series of measurements for determining the proper annealing temperature for half-hard 2V-Permendur is shown in Figures 31A, 31B, and 32. It can be seen that the characteristics of the resulting material do not vary significantly if the annealing temperatures are in the range 450 to 625 C. For practical purposes, annealing at 500 C, or even 450 C, is better than at higher temperatures since a larger coercive force is obtained.

A comparison between 2V-Permendur rings of varying thicknesses after a 450 C annealing is also shown in Figure 33. It will be seen that the various samples have the same coercive force but not quite the same remanence.

VICALLOYS

The vicalloys were studied in the hope of finding a material comparable to 2V-Permendur but with a larger coercive force. These include the 8 per cent and 6.5 per cent V-alloys, both of which can be precipitation-hardened by annealing at about 600 C for one or two hours. The major hysteresis loops of three

samples are shown in Figures 34 through 36. The coercive forces obtained in these samples are certainly of satisfactory magnitude. Unfortunately, none of these samples has large reversible permeability at the remanence point.

The 6.5V-vicalloy scrolls are unsatisfactory in another respect. The peculiar shape of the demagnetization curves (Figure 35) shows immediately that the samples actually contain two *phases*, one of which has a coercive force of about 70 oersteds and the other (present in lesser amount), a coercive force of 30 to 35 oersteds. For this reason, if an a-c field is applied to the material at remanence, minor hysteresis loops of large area will be traced out when the amplitude of the a-c field approaches 30 oersteds. This point is illustrated by the minor loops in the same figures. Such loops in an actual transducer would cause excessive hysteresis losses (the small minor loop in Figure 36 corresponds to about 10 watts per cc at 20 kc per sec) and distorted wave forms of the acoustic output.

Further studies on another batch of 6.5V-vicalloy sheets, which were also supplied by BTL, show that the heterogeneous nature of the scroll samples is not inherent in the precipitation process. Thus the three hysteresis loops in Figure 37 are normal. Because of the sluggishness of the precipitation process, an increase in the time of annealing or in the annealing temperature pushes the coercive force to still higher values. The reversible permeabilities at remanence of these three loops are also more than double those of the scrolls. Unfortunately, all three samples have rather small values of remanence so that the increases in reversible permeability do not represent any real improvement. Because of large hysteresis, the remanence will be reduced further under a large a-c field. This last point is illustrated by the minor loops in Figure 37.

4.7.3 Static Measurements of Magnetostrictive Properties

The results of static measurements on the nickel and the 30% Fe, 70% Co rods are shown in Figures 38 to 41. As previously noted, the observations were made by loading the sample with weights of 100, 200, and 500 grams. The relation between the load and the change of magnetization was not quite linear, and along the steep portion of the normal curve there was also a hysteresis effect which was rather pronounced in the case of the iron-cobalt sample. No attempt was

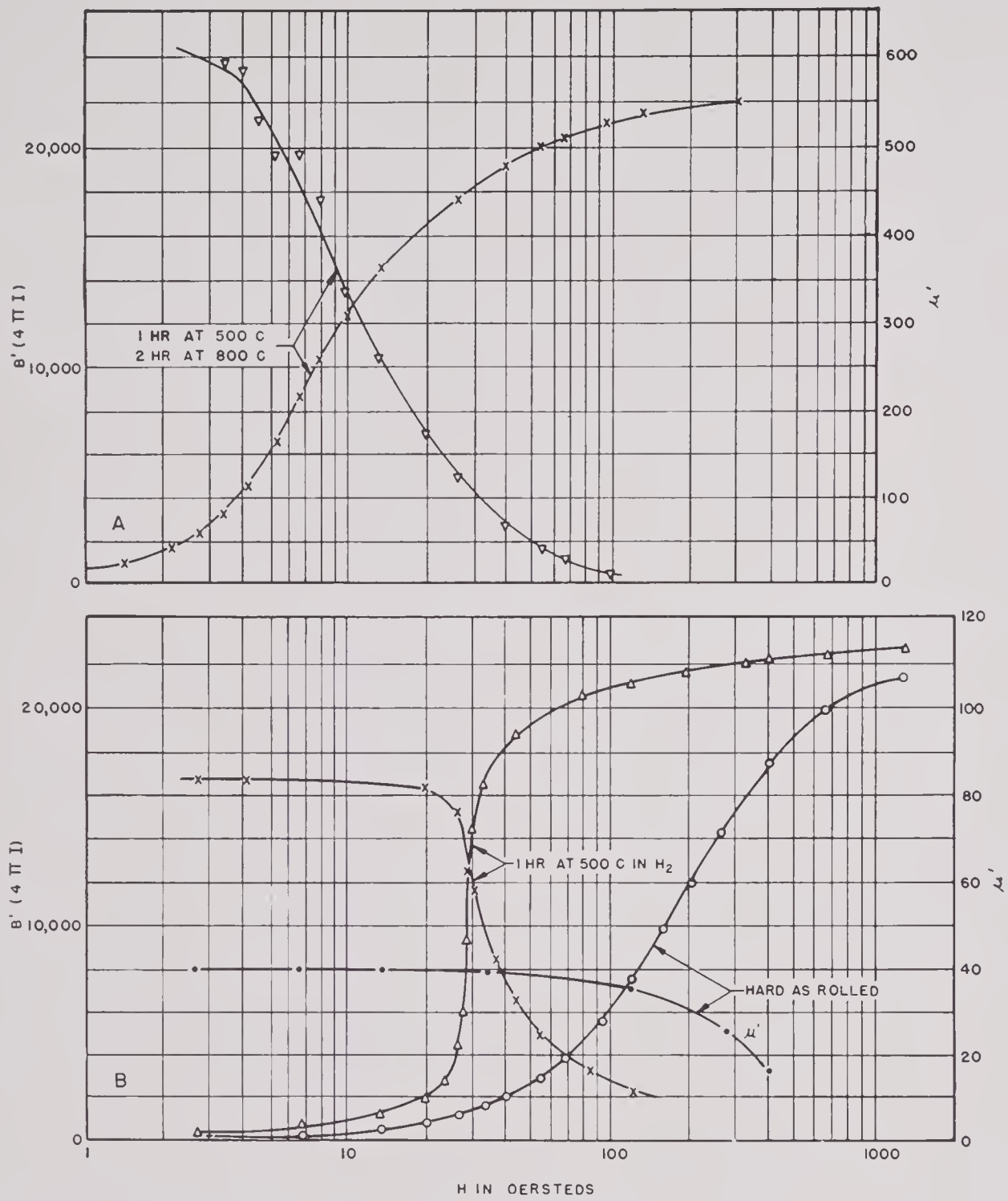


FIGURE 22. A. Magnetization and permeability of 0.006-in. 2V-Permendur strip in rolling direction, annealed. B. Magnetization and permeability of 0.006-in. 2V-Permendur strip in rolling direction, hard and annealed.

made to study these effects in detail and only the reversible part of the change of magnetization with tension was recorded. The data presented for the nickel sample are those obtained with the 100-gram load, since both nonlinearity and hysteresis are small for this sample. For the iron-cobalt alloy, extrapolation to zero load has been carried out for each value of Λ .

From equation (7c) we have the relation

$$\lambda = \frac{E}{4\pi} \left(\frac{\Lambda}{\mu' - 1} \right).$$

From this and the relation shown in (7a) we get the relation

$$k \simeq \frac{E}{4\pi} \frac{\Lambda}{\sqrt{\mu' - 1}}.$$

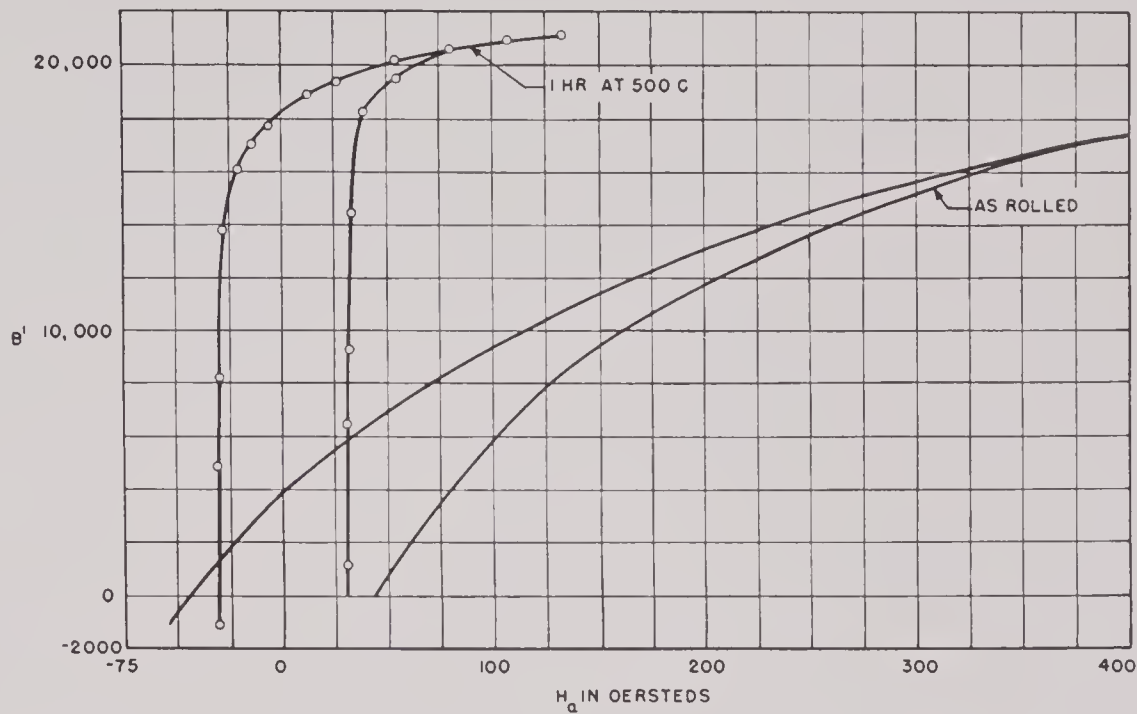


FIGURE 23. Hysteresis in rolling direction of hard and annealed 2V-Permendur strip 0.006 in. thick.

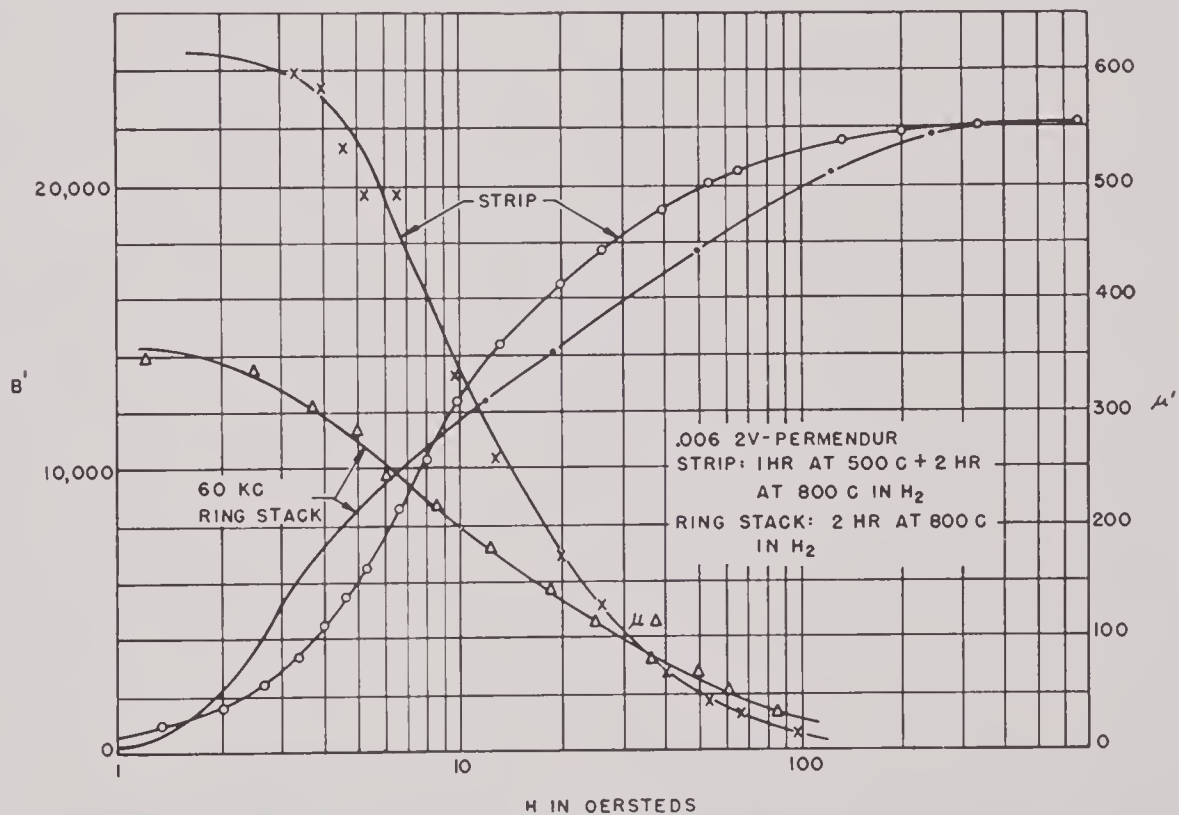


FIGURE 24. Magnetic properties of 2V-Permendur as affected by annealing conditions.

The curves $\lambda/\sqrt{\mu' - 1}$ vs $4\pi I$ are readily converted to curves of λ and k vs $4\pi I$, since E is practically constant with respect to varying values of $4\pi I$. Taking 2.2×10^{12} for the value of E for both samples, the maximum values of λ are -3.5×10^4 , and 1.6×10^4 for the nickel and the iron-cobalt samples respec-

tively. The maximum values of k are 0.40 and 0.25. It will be seen later that the value 0.40 is the largest so far found for k . However, this is due to the unusually high reversible permeabilities of the nickel rod rather than any abnormality in the values of λ .

The $\lambda/\sqrt{\mu' - 1}$ vs $4\pi I$ curve of the iron-cobalt

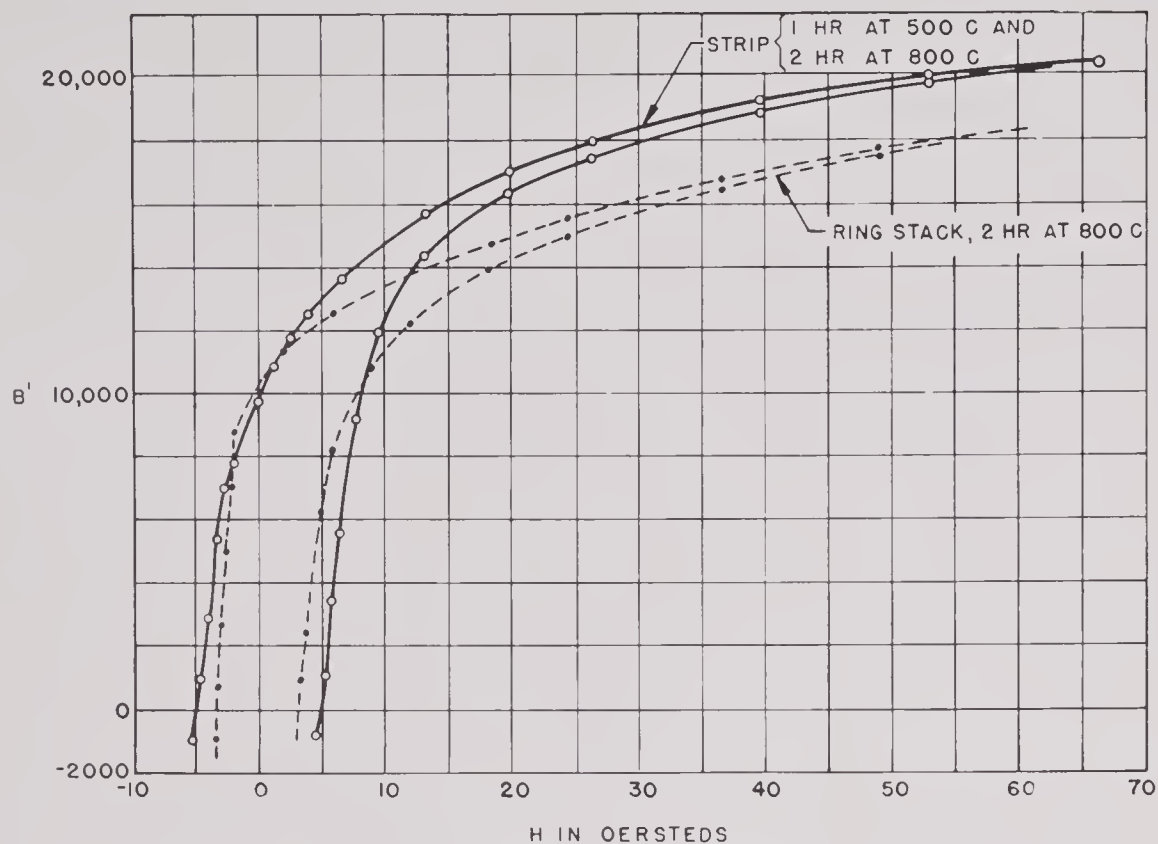


FIGURE 25. Hysteresis of 0.006-in. 2V-Permendur rings and strip.

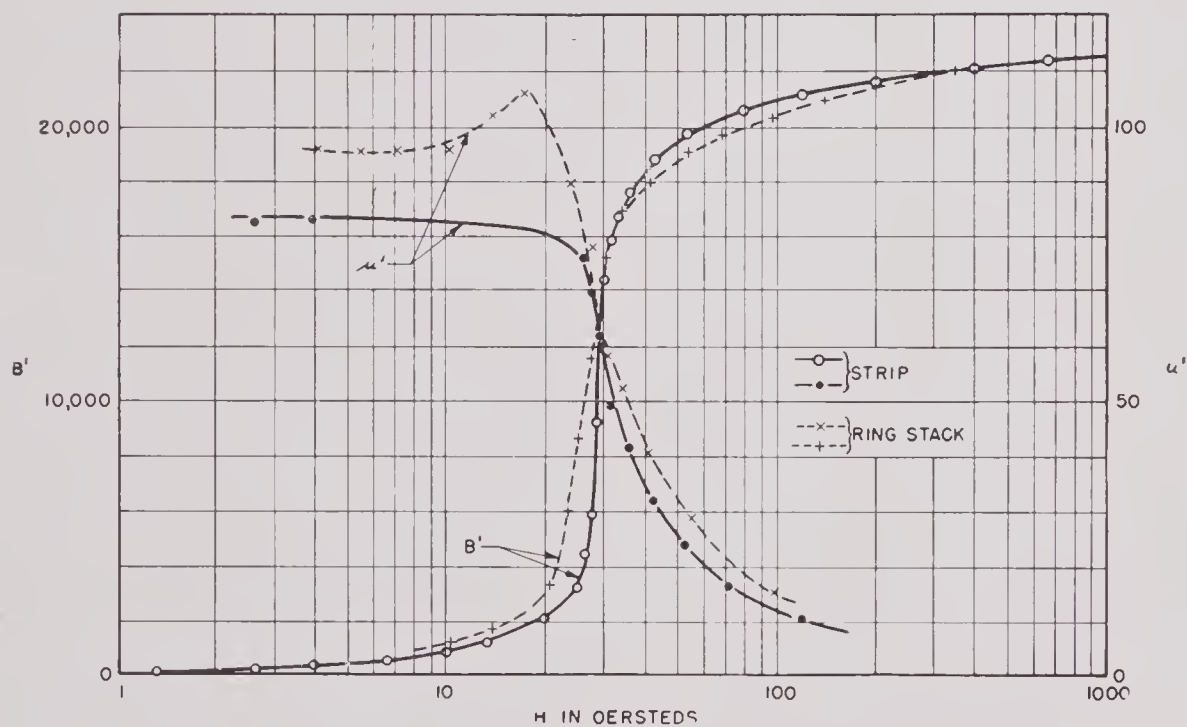


FIGURE 26. Magnetization and permeability of two samples of 2V-Permendur annealed 1 hour in hydrogen at 500 C.

sample contains a number of irregularities which have not been observed in any other sample. However, it is certain that these irregularities are not

caused by errors in the measured values of μ' since rather small variations of the field were used in determining μ' .

CONFIDENTIAL

A further study of the data just presented will throw light on the phenomenon of magnetostriction. From equation (6a),

$$\left(\frac{\partial s}{\partial H}\right)_{P,T} = \frac{\Lambda}{4\pi}. \quad (9)$$

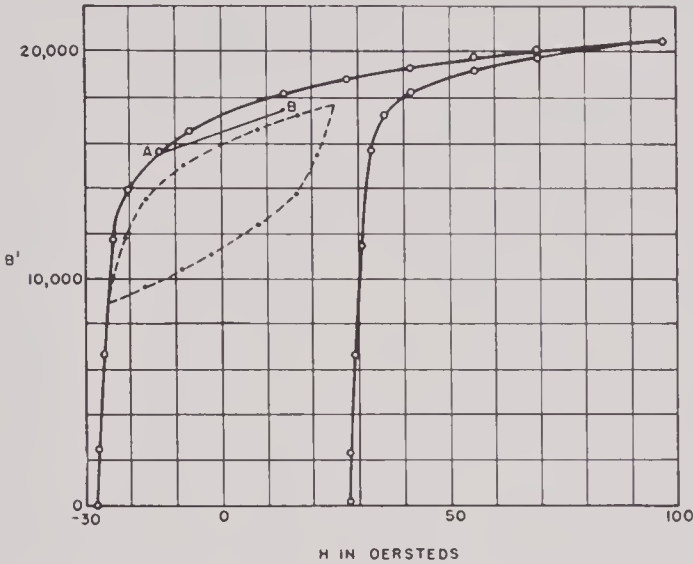


FIGURE 27. Hysteresis of 2V-Permendur rings 0.006 in. thick annealed 1 hour in hydrogen at 500 C.

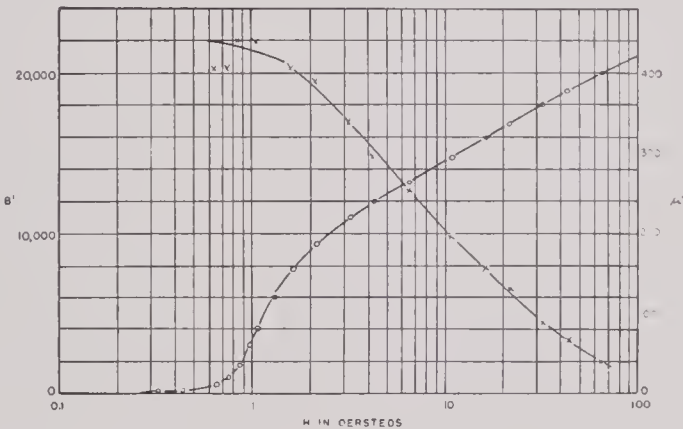


FIGURE 28. Magnetization and permeability of 2V-Permendur rings 0.006 in. thick annealed 1 hour in hydrogen at 500 C.

In Figures 38 and 40, Λ is plotted as a function of H , and the total strain s for any value H_0 of H is $\frac{1}{4\pi}$ times the area under the curve from $H = 0$ to $H = H_0$. Carrying out the integration graphically,

$$s = -16.1 \times 10^{-6} \text{ for nickel for } H = 100, \quad (10)$$

$$s = 26 \times 10^{-6} \text{ for 30\% Fe, 70\% Co for } H = 100.$$

These values of s are much lower than those found by direct measurement of the quantity. However, the above values represent only the reversible parts of the fractional change in length, since mechanical hysteresis is neglected both in the theory and in the measure-

ment of Λ . A similar situation exists when the area under the μ' vs H curve is taken to determine the reversible portion of the magnetization. Thus, using the data shown in Figures 6 and 21, we find:

$$B'(\text{rev}) = 1,790, \text{ for } B'_{\text{max}} = 6,000 \text{ for nickel rod.} \quad (11)$$

$$B'(\text{rev}) = 4,725, \text{ for } B'_{\text{max}} = 20,000 \text{ for 30\% Fe, 70\% Co.}$$

Thus the *reversible* portion of the magnetization is less than 30 per cent of the total.

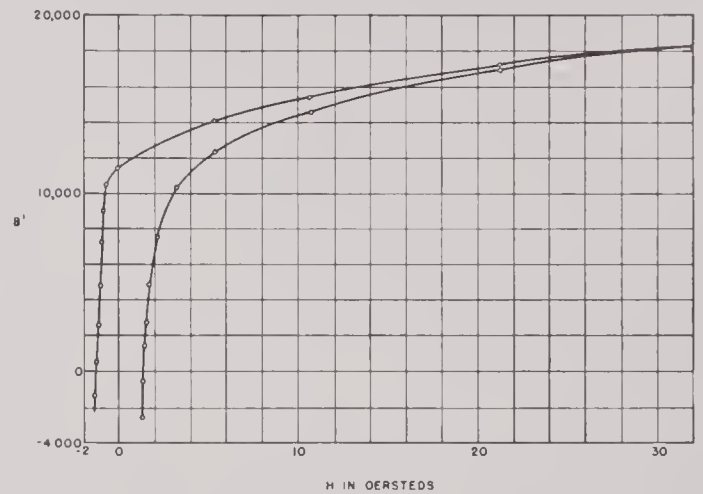


FIGURE 29. Hysteresis of 2V-Permendur rings 0.006 in. thick annealed for 2 hours in hydrogen at 800 C. $B_{\text{max}} = 20,000$.

To find the total fractional change of length, it is necessary to consider the change of length due to the total change of magnetization. This is done by integrating the curves of Figures 39 and 41 from 0 up to the values of B' corresponding to $H_0 = 100$ and $H_0 = 117$. These values of B' are 6,000 and 20,000 respectively. By a slight transformation, equation (9) becomes

$$\left(\frac{\partial s}{\partial B}\right)_{P,T} = \frac{\Lambda}{4\pi(\mu' - 1)}. \quad (12)$$

Therefore, the area under the curve of $\Lambda/(\mu' - 1)$ vs B' will give 4π times the total fractional change of length for the maximum value of B' . The computed areas under the two curves give

$$s_{\text{total}} = -34.9 \times 10^{-6} \text{ for nickel, } B'_{\text{max}} = 6,000.$$

$$s_{\text{total}} = 63.7 \times 10^{-6} \text{ for 30\% Fe, 70\% Co,}$$

$$B'_{\text{max}} = 20,000.$$

Since the samples were not quite saturated, these calculated values of s are in good agreement with previous observations.

Since it can be safely assumed that the samples used in the HUSL experiments were comparable to those used by previous authors, the foregoing discussion leads to the conclusion that irreversible as well as reversible polarization contributes stresses in a clamped sample. This conclusion is of considerable

importance, since it implies that $\lambda dB'$ should be integrated in calculating the power output of a magnetostrictive transducer when it is driven by a large a-c field.

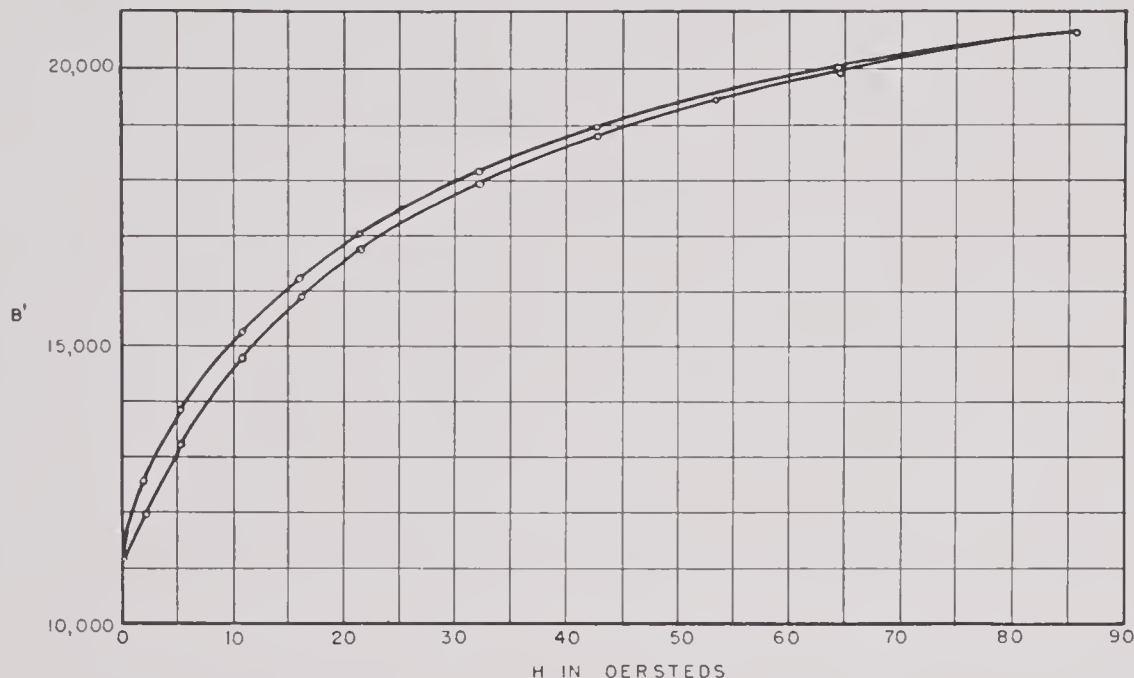


FIGURE 30. Minor hysteresis loop, 2V-Permendur 0.006 in. thick annealed for 2 hours in H_2 at 800 $^{\circ}C$.

importance, since it implies that $\lambda dB'$ should be integrated in calculating the power output of a magnetostrictive transducer when it is driven by a large a-c field.

4.7.4 Dynamic Measurements

CLAMPED-CORE IMPEDANCE AND RELATED FACTORS

The procedures for separating the clamped-core impedance and the motional impedance circle have already been described in Chapter 2, and earlier in the present chapter formulas have been summarized relating the fundamental coefficients μ , λ , E , and the various quantities determined from the clamped-core impedance and the motional impedance or admittance circle. In the following paragraph complete sets of data will be set down and discussed in order to show the degree to which experimental results agree with theory.

A complete analysis of impedance data, taking into account the effect of magnetic hysteresis, is somewhat complicated. Fortunately, the effect of hysteresis is usually so small compared with the effect of

eddy currents at the small d-c fields used in bridge measurements that it can be neglected. With this approximation, the clamped-core reversible permeability μ and the resistivity ρ_c can be estimated from the clamped-core impedance and the dip angle 2ζ of the resonance diameter of the motional impedance circle.

In this way, μ , ρ_c , and the eddy-current factors are determined; all the other quantities can be calculated by the formulas given in the last section.

Owing to the variation of magnetic softness across the sheets⁴² and perhaps to the imperfect insulation between the laminations, the value of the resistivity thus obtained often appears erratic when compared with the directly measured value. In order to be certain of the correctness of the eddy-current theory, an improved procedure is to obtain effective values of the resistivity ρ_c and the reversible permeability μ by making use of all the values of the clamped-core impedance in the data. This involves (1) correcting the clamped-core impedance for leakage impedance, which can be estimated with fair accuracy and (2) plotting the clamped-core resistance against the clamped-core reactance. Since the corrected clamped-core impedance is proportional to the product of z^2 (the eddy-current parameter) and χ , the plotted points for various frequencies and various reversible permeabilities, corresponding to various magnetizations, lie on a single locus that is similar to the one shown in Figure 3 of Chapter 3. The initial portion of

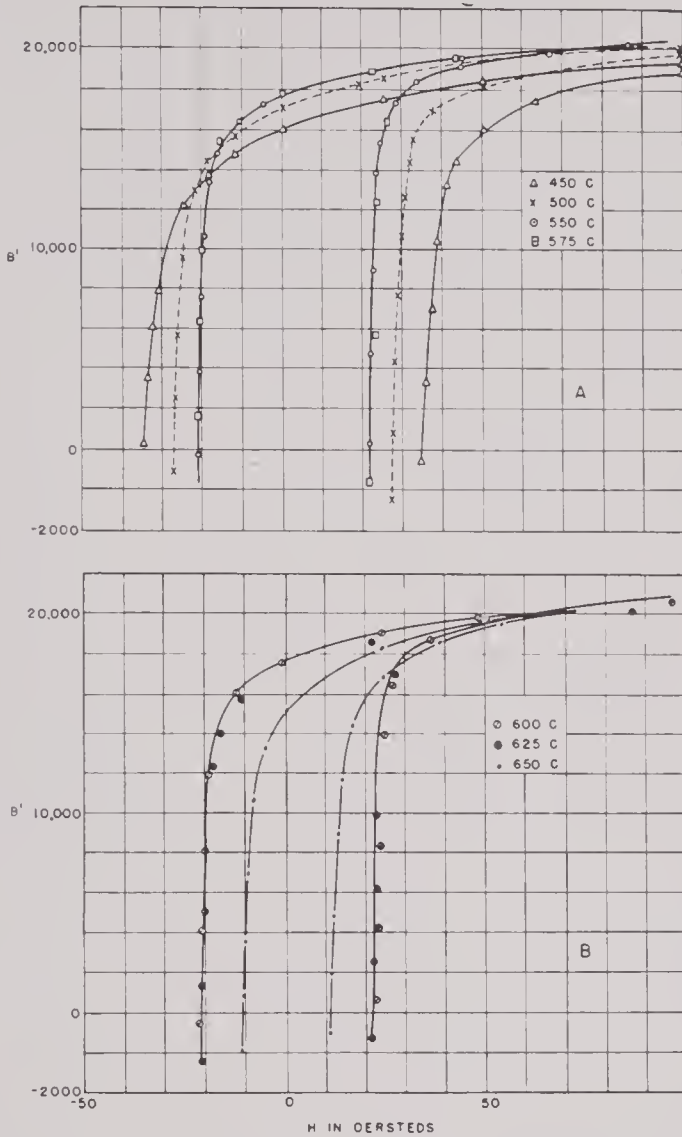


FIGURE 31. A. Hysteresis, remanence, and coercive force of 2V-Permendur annealed for 1 hour in hydrogen at different temperatures. B. Hysteresis, remanence, and coercive force of 2V-Permendur annealed for 1 hour in hydrogen at different temperatures.

the locus, then, is an arc of a circle of which the radius is

$$r = 1.5 \times \frac{2N^2lb\rho_e}{\pi at^2}, \quad (13)$$

where t is the thickness of the laminations, ρ_e the resistivity, and other quantities are as defined in the previous section. Since all the quantities except ρ_e in the last expression are known, it is a simple matter to find the radius from the locus and evaluate ρ_e .

Next, a point is located on the horizontal diameter of the circle that is at a distance equal to two-thirds the radius to the right of the center. By using this point as a pole and projecting the points on the initial

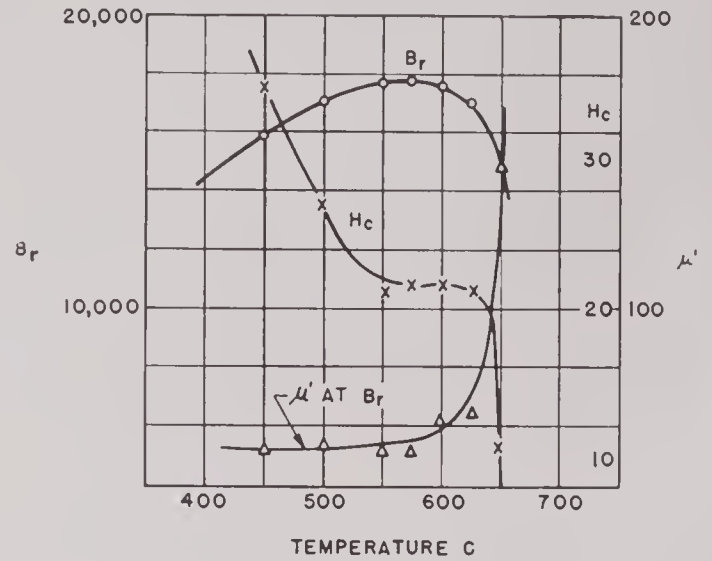


FIGURE 32. Remanent magnetization and coercive force of hydrogen-annealed 2V-Permendur sheets 0.006 in. thick, as function of ambient temperature.

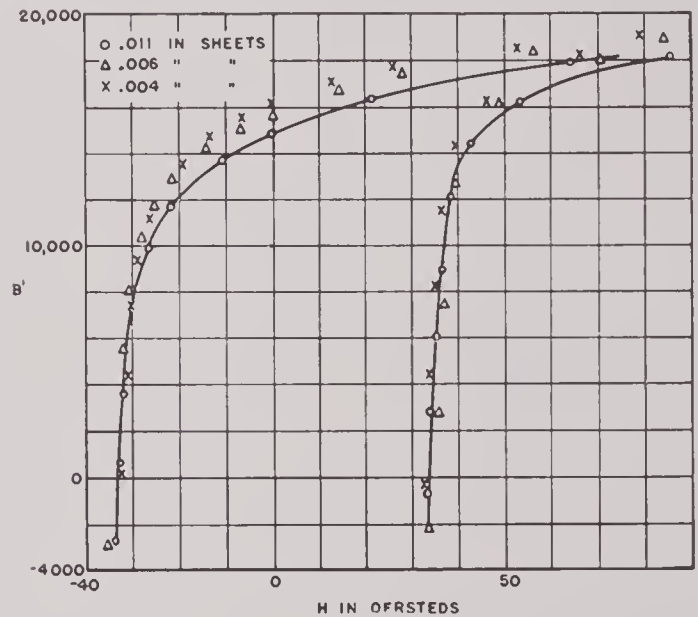


FIGURE 33. Hysteresis of 2V-Permendur rings of varying thickness annealed at 450 C.

portion of the locus onto the vertical axis, the intercepts thus obtained will be equal to

$$\omega L_0 = \frac{2\omega N^2bl\mu}{a},$$

where values of L_0 are the clamped-core inductances free from eddy-current effect. Knowing the frequency, the values of μ can again be independently calculated.

The procedure just described is illustrated in Figure 42 by the data for the soft-annealed 2V-Permendur ring stack which will be discussed presently. The val-

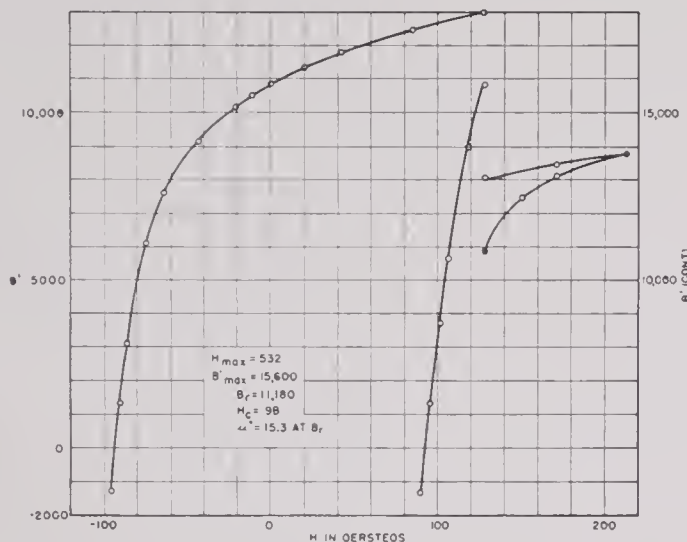


FIGURE 34. Hysteresis of SV-vicalloy laminations 0.014 in. thick.

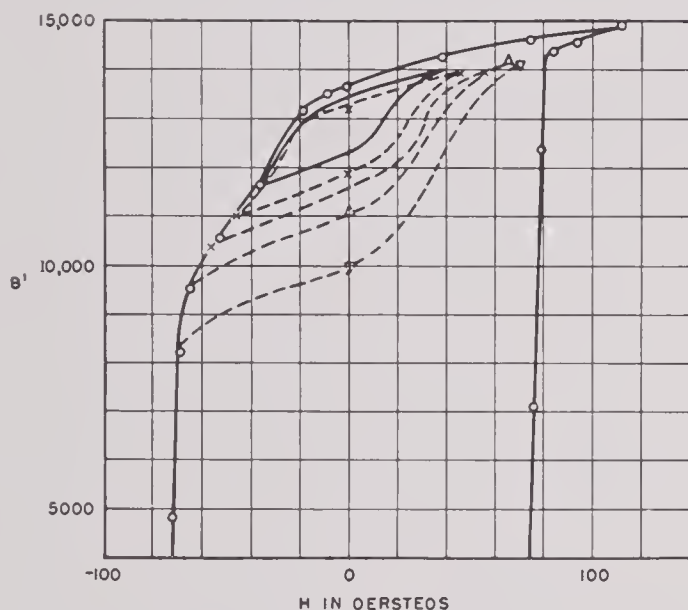


FIGURE 35. Scroll of 6.5-vicalloy 0.002 in. thick, annealed 2 hours at 605 C.

ues plotted in this case are the clamped-core impedances at resonance for various polarizing fields and hence for various reversible permeabilities, neglecting small differences in the resonant frequency. Since the copper resistance of the winding and the leakage impedance are constant, it is not necessary to correct the clamped-core impedance before plotting. Instead, the corrections are determined by the location of the circle.

Four complete sets of data are shown in Tables 2 to 5 for soft-annealed A-nickel, 45-Permalloy, 2V-Permendur, and half-hard A-nickel. The 2V-Permendur sample is the one from which the curve of Figure 42 was derived. The measurements were made with the

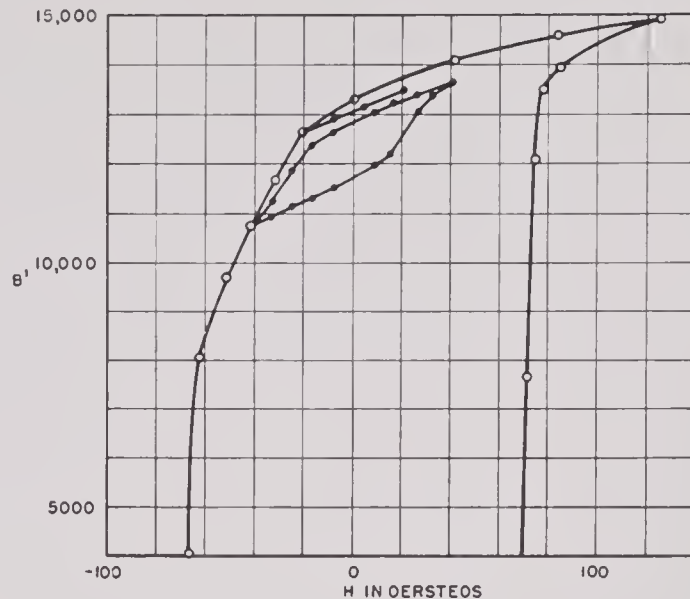


FIGURE 36. Effect of two phases in 6.5-vicalloy on minor hysteresis loops at remanence.

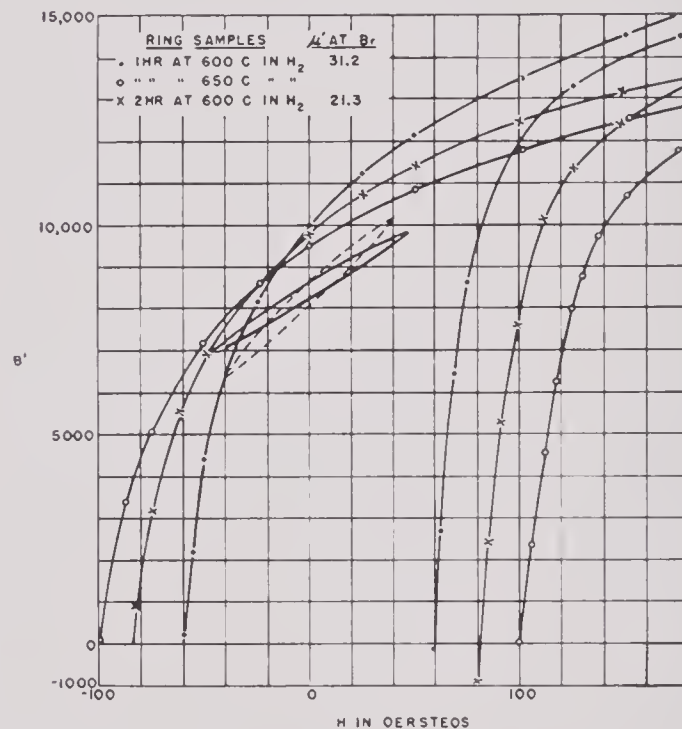


FIGURE 37. Hysteresis curves for 6.5-vicalloy for different anneals.

samples polarized to various intensities I_0 by various d-c fields H_0 . In accordance with the usual practice, the values of I_0 were obtained along the normal curve for soft samples and along the demagnetizing branch of a major hysteresis loop for half-hard or hard samples. The upper columns of each table give an overall check of the eddy-current theory and the lower columns the values of the important quantities determined from the motional impedance circle and those

of the electromechanical coupling coefficient k , etc., calculated therefrom.

The quantities listed in the upper columns of Tables 2 to 5 are defined as follows:

- μ' = reversible permeability obtained from magnetic measurements,
- 2ζ = dip angle of the resonance diameter of motional impedance circle equal to twice the eddy-current loss angle, neglecting hysteresis,
- $R_c + jX_c$ = corrected clamped-core impedance obtained by interpolation from clamped-core impedance curves,
- μ = reversible permeability computed by the method just described.

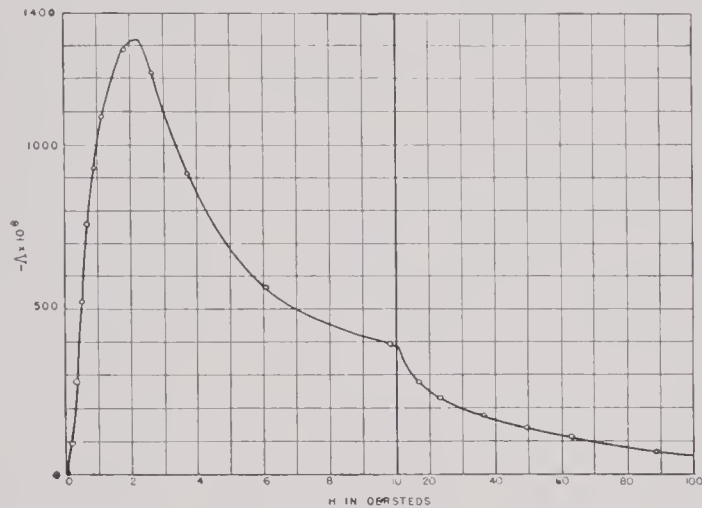


FIGURE 38. Nickel rod annealed 1 hour at 1000 C in hydrogen.

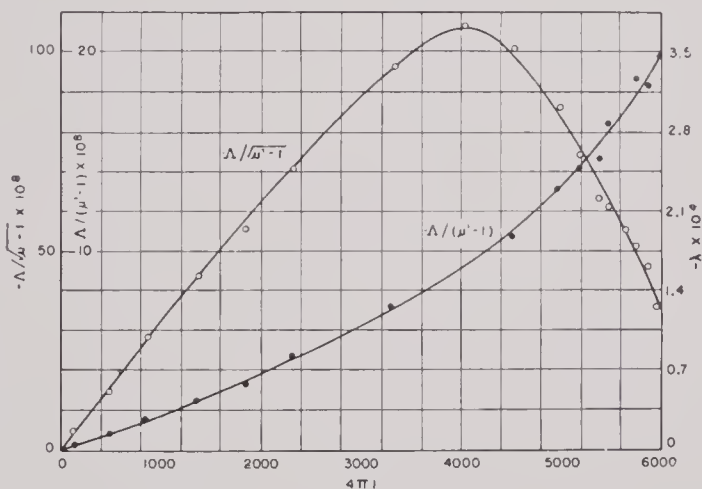


FIGURE 39. Nickel rod, annealed 1 hour at 1000 C in hydrogen and slowly cooled.

The value of μ and the simultaneously determined value of the resistivity are, in turn, used to calculate ζ , R_c , and X_c by the formulas of eddy-current theory. These calculated values provide a check on the con-

sistency of the series of analyses and are shown in the last three upper columns in each table.

In earlier discussions, emphasis has been placed on the difference in meaning of μ' and μ . As can be seen from equation (7a), the numerical difference between the two is practically equal to the square of the electromechanical coupling coefficient k . In the cases of the soft-annealed A-nickel and 45-Permalloy samples of Tables 2 and 3, the values of μ do seem to be smaller than the corresponding values of μ' , but in general the pairs of values fail to show consistently the existence of the electromechanical coupling coefficient. In the case of the Permendur sample, the

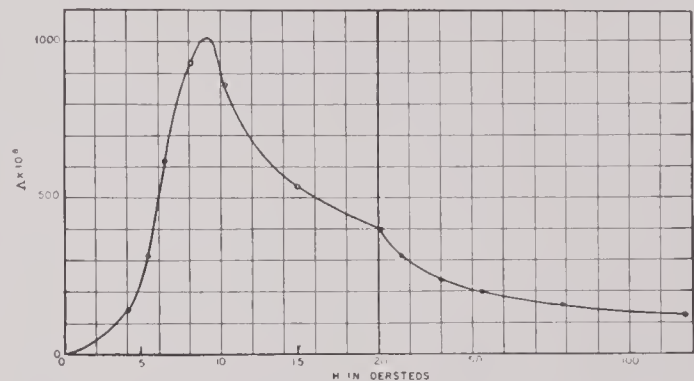


FIGURE 40. Iron-cobalt rod annealed 1 hour at 1000 C in hydrogen and slowly cooled.

data only show that μ' and μ are of the same order of magnitude. The discrepancy between experiment and theory is due mainly to the large errors in the graphically determined values of μ , and to some extent to errors in the polarizing field. (The meters used to measure the polarizing currents during the course of impedance measurements were not so accurate as those used for magnetic measurements.)

The agreement between the observed and calculated values of ζ and X_c in the tables is generally good. Large discrepancies are present, however, in the case of R_c . This is largely due to the fact that R_c cannot be interpolated as accurately as X_c . Also, for small total resistances, the dissipations in the condensers used in the bridge cause some errors in R_c .

For the half-hard A-nickel sample, there is no need to evaluate μ , since the values of k are small for this sample. Accordingly, the measured values of μ' and ρ have been used to calculate the theoretical values of ζ , R_c , and X_c in checking the theory. Table 5 shows the agreement in this case to be excellent.

From the above discussions it can be concluded that the eddy-current theory is on the whole fairly

TABLE 2. Measurements for soft-annealed A-nickel (0.005 in.). Test conditions: 1 hr at 1000 C in H₂; 50 laminations; Vinylseal consolidated; OD, 3.31 in.; ID, 2.65 in.; turns of winding, 336.

H_0 oersted	$4\pi I_0$ gausses	μ'	ζ degrees	R_c ohms	X_c ohms	μ	ζ_{calc} degrees	$R_{c\ calc}$ ohms	$X_{c\ calc}$ ohms
3.0	2520	137	24.6	183	449	122	21.3	156	399
5.0	3105	105	20.3	119	370	98.5	17.8	109	340
7.1	3530	84	15.8	78.8	302	81.5	15.0	79.0	291
10.0	3930	66.5	14.4	59.3	272	69.4	12.7	58.1	253
14.1	4335	50.7	9.6	24.1	197	48.1	9.2	28.6	181
19.6	4680	39	7.7	14.6	166	38.4	7.4	18.4	146
30.3	5110	26	4.2	6.6	102	25.5	5.0	8.5	98.3

H_0 oersted	f_r ke/sec	D ohms	Q	k	$E' \cdot 10^{-12}$ dynes/cm ²	$E \cdot 10^{-12}$ dynes/cm ²	$-\lambda \cdot 10^{-4}$ dynes/gauss cm ²	$\frac{R'_m}{R_m}$	Pot eff
3.0	19.58	1015	30.1	0.272	1.92	2.04	0.94	0.86	0.75
5.0	19.48	1023	28.6	0.304	1.90	2.06	1.20	0.88	0.80
7.1	19.46	1027	32.4	0.312	1.90	2.08	1.39	0.88	0.83
10.0	19.46	1032	36.3	0.310	1.90	2.08	1.55	0.86	0.84
14.1	19.53	1080	52.0	0.310	1.91	2.10	1.78	0.95	0.93
19.6	19.64	1120	78.6	0.282	1.93	2.10	1.85
30.3	19.83	1133	142	0.271	1.97	2.13	2.18	0.98	0.98

TABLE 3. Measurements for soft-annealed 45-Permalloy (0.005 in.). Test conditions: 1 hr at 1000 C in dry H₂; 50 laminations; Vinylseal consolidated; OD, 3.31 in.; ID, 2.65 in.; turns of winding, 296.

H_0 oersted	$4\pi I_0$ gausses	μ'	ζ degrees	R_c ohms	X_c ohms	μ	ζ_{calc} degrees	$R_{c\ calc}$ ohms	$X_{c\ calc}$ ohms
2.9	11,960	375	7.0	90	1045	396	7.6	140	1060
4.9	12,770	245	4.7	37	670	244	4.7	54.2	664
9.7	13,830	131	3.2	13.7	367	121	2.4	13.8	335
15.5	14,420	70	0	6.7	193	65	1.3	4.21	183
23.3	14,790	32	1.8	2.3	83	28.5	0.65	0.88	82
38.9	15,020	9.4	0.5	0.89	26.2	9.6	0.3	0.134	28

H_0 oersted	f_r ke/sec	D ohms	Q	k	$E' \cdot 10^{-12}$ dynes/cm ²	$E \cdot 10^{-12}$ dynes/cm ²	$-\lambda \cdot 10^{-4}$ dynes/gauss cm ²	Pot eff
2.9	17.15	6200	81.7	0.259	1.37	1.47	0.45	0.87
4.9	17.17	5900	99.2	0.287	1.37	1.49	0.63	0.91
9.7	17.36	5250	174	0.288	1.40	1.53	0.91	0.94
15.5	17.63	3800	315	0.249	1.45	1.55	1.08	0.95
23.3	17.936	1345	478	0.182	1.50	1.55	1.20	0.96
38.9	18.190	193.5	1040	0.082	1.54	1.55	0.93	0.95

satisfactory and that the assumption of negligible hysteresis effect is justified.

In the lower columns of Tables 2 to 5, f_r and D are accurate to within 1 per cent. The precision to which Q is determined depends upon the magnitude of Q , but in general the error is not greater than 5 per cent. The interpolated values of X_c are precise to about the same degree. Therefore k should generally be precise to about 5 per cent. Because of the high accuracy of f_r and the small magnitude of k^2 , both E' and E have high relative accuracy. On the other hand, the values

of λ may have errors considerably higher than 5 per cent, because, in determining these values, the values used for μ were those deduced from eddy-current theory.

The ratio of that part of motional resistance, R'_m , which is due to eddy-current effect to the total motional resistance R_m , and the potential efficiency given in Tables 2, 3, and 5 have no bearing on the determination of the fundamental coefficients. The actual values of these quantities merely indicate that highly efficient transducers can be realized by reducing external mechanical resistances.

TABLE 4. Measurements for soft-annealed 2V-Permendur (0.006 in.). Test conditions: 2 hr at 800 C in H₂; 40 laminations; Vinylseal consolidated; OD, 2.86 in.; ID, 2.42 in.; turns of winding, 162.

H_0 oersted	$4\pi I_0$ gausses	μ'	ζ degrees	R_c ohms	X_c ohms	μ	ζ_{calc} degrees	$R_{c calc}$ ohms	$X_{c calc}$ ohms
3.6	11,400	325	26.7	102	195	327	26.7	99	198
6.9	13,370	247	22.4	72	171	260	22.0	69.6	172
12.8	15,190	178	16.6	40	134	187	16.5	40.1	134
25.2	17,230	110	10.3	16	85.0	112	10.5	15.6	85.5
46.6	19,070	60.5	4.5	4.7	45.4	57.6	5.4	4.34	45.9
66.5	20,010	38	4.4	2.4	31.3	39	3.7	2.1	31.8

H_0 oersted	f_r kc/sec	D ohms	Q	k	$E' \cdot 10^{-12}$ dynes/cm ²	$E \cdot 10^{-12}$ dynes/cm ²	$-\lambda \cdot 10^{-4}$ dynes/gauss cm ²
3.6	23.50	390	42.0	0.220	2.01	2.09	0.49
6.9	23.40	422	32.1	0.274	1.99	2.12	0.72
12.8	23.34	432	34.8	0.294	1.98	2.15	0.91
25.2	23.48	422	53.4	0.292	2.01	2.19	1.16
46.6	23.78	265	79.3	0.261	2.06	2.21	1.41
66.5	24.12	267	156	0.227	2.11	2.23	1.55

TABLE 5. Measurements for half-hard A-nickel (0.005 in.). Test conditions: 1 hr at 600 C in H₂; 50 laminations; Vinylseal consolidated; OD, 3.31 in.; ID, 2.65 in.; turns of winding, 339.

H_0 oersted	$4\pi I_0$ gausses	μ'	ζ degrees	R_c ohms	X_c ohms	ζ_{calc} degrees	$R_{c calc}$ ohms	$X_{c calc}$ ohms
-15.6	2490	23.0	2.55	5.23	92.4	2.90	4.74	96.0
0	3280	19.5	2.55	4.23	80.9	2.46	3.45	81.3
27.0	3975	14.7	1.8	2.63	61.9	1.82	1.95	61.3
61	4450	10.8	1.1	2.02	46.9	1.3	1.04	44.6
110	4890	7.8	0.95	1.29	32.5	1.0	0.57	32.6

H_0 oersted	f_r kc/sec	D ohms	Q	k	$E' \cdot 10^{-12}$ dynes/cm ²	$E \cdot 10^{-12}$ dynes/cm ²	$-\lambda \cdot 10^{-4}$ dynes/gauss cm ²	Pot eff
-15.6	20.64	859	898	0.099	2.16	2.19	0.86	0.91
0	20.61	1080	711	0.140	2.16	2.20	1.32	0.93
27.0	20.57	1064	761	0.149	2.15	2.20	1.63	0.94
61	20.49	1146	1078	0.152	2.13	2.18	1.94	0.96
110	20.64	943	1453	0.140	2.17	2.21	2.10	0.97

THE MAGNETOSTRICTIVE CONSTANT AND THE COEFFICIENT OF ELECTROMECHANICAL COUPLING

Values of λ and k obtained by dynamic measurements on various samples, including those of Tables 2 to 5, are plotted as functions of the intensity of polarization in Figures 43 to 48. The values of λ for the nickel rod as deduced from the values of $\lambda/\mu' - 1$ in Figure 39 are also shown in Figure 43 for purposes of comparison. Figures 43 and 44 also contain the results obtained at 22 and 48 C from sample No. 1 of the 10-mil oxide-annealed A-nickel sheets of Figure 7. These latter results are part of a series to be discussed in some detail at the end of this chapter.

For hydrogen-annealed nickel, the fair agreement between the λ vs $4\pi I$ curve obtained by static measurements and that obtained by dynamic measurements tends to confirm the correctness of the thermodynamic relations as well as the transducer theory. However, differences definitely exist among the λ vs $4\pi I$ curves of the variously treated A-nickel samples. Since the longitudinal magnetostriction in single nickel crystals is anisotropic, such differences can be expected if, in the polycrystalline samples, perfect random orientations of the grains are not always obtained. On the other hand, it is not clear whether internal stresses in the samples can also affect the magnitude of λ .

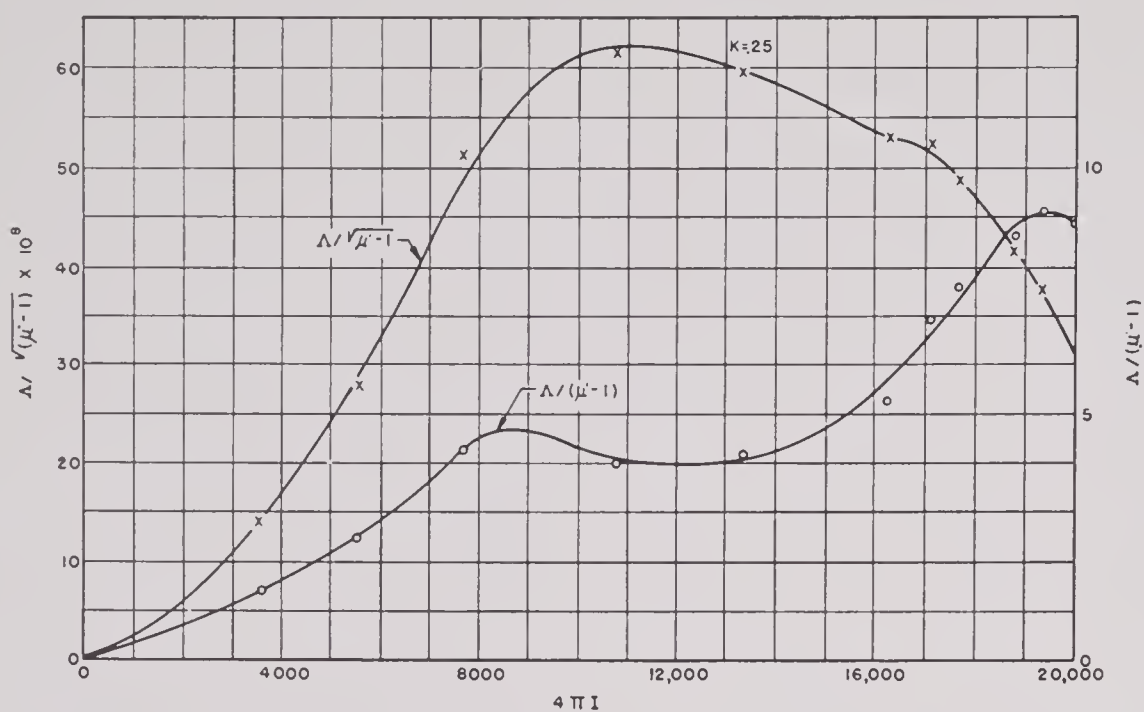


FIGURE 41. Iron-cobalt rod annealed 1 hour at 1000 C in hydrogen and slowly cooled.

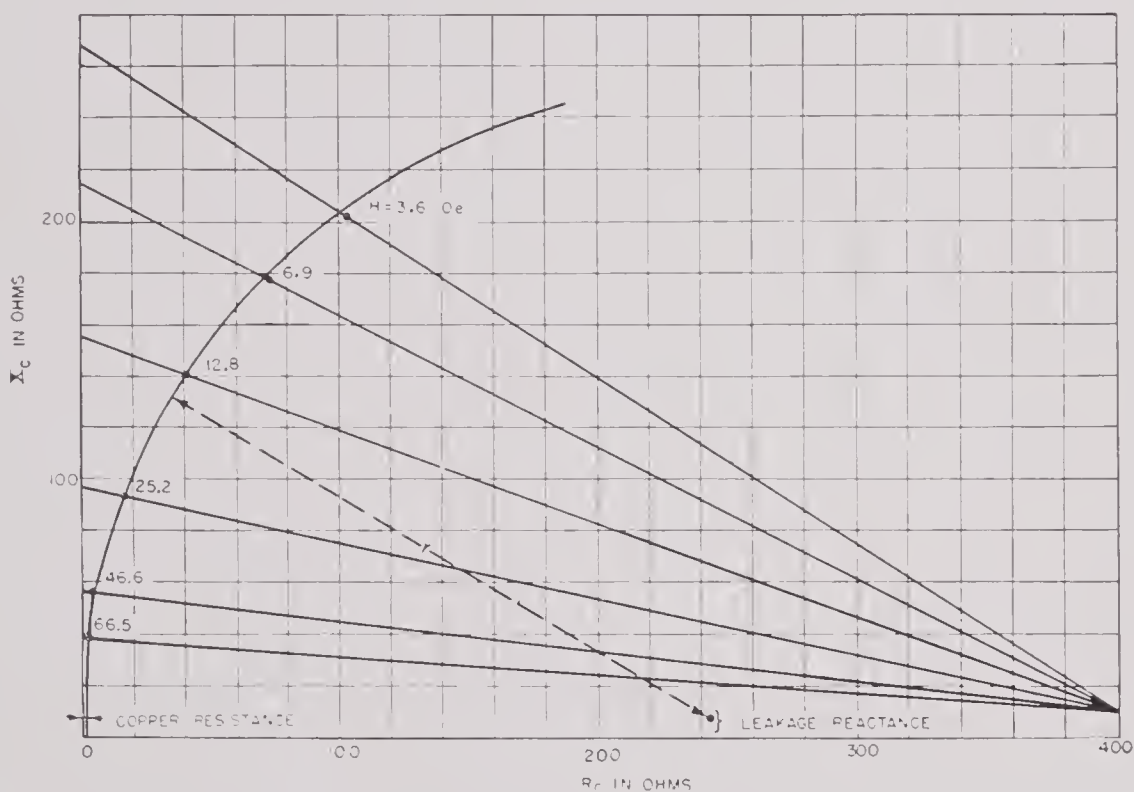


FIGURE 42. Locus of clamped-core impedance at resonance of 0.006-in. 2V-Permendur ring stack annealed for 2 hours in hydrogen at 800 C.

It is not known whether the saturation magnetization of Z-nickel is considerably smaller than that of A-nickel. On the basis of Figure 43, annealed Z-nickel has about the same values of λ as oxide-annealed A-nickel. Because of the small reversible permeabil-

ities of the particular sample chosen for dynamic measurements, the values of k shown in Figure 44 for Z-nickel appear rather small. Actually, the aged Z-nickel sample of Figure 13 shows considerably larger reversible permeabilities and therefore is ex-

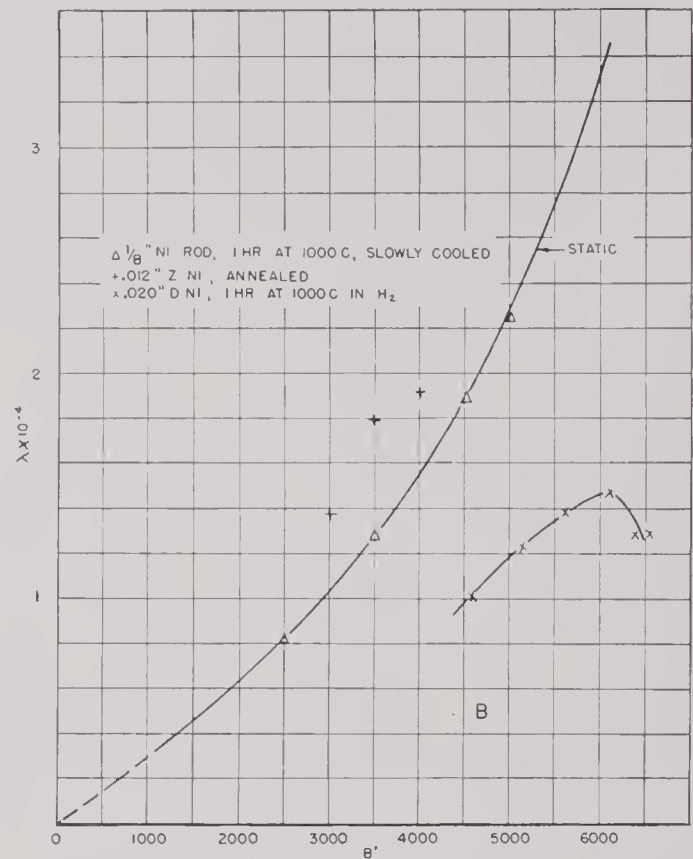
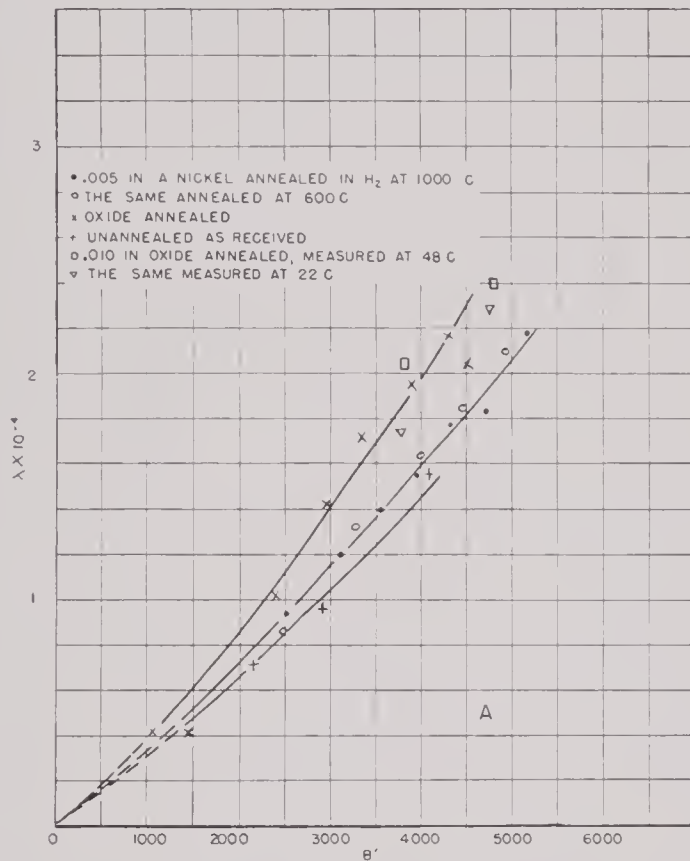
CONFIDENTIAL

pected to have as large k values as oxide-annealed A-nickel, although the maximum value of k comes at a higher field intensity. In view of its higher resistivity and superior mechanical properties, the Z-nickel may yet prove superior to A-nickel.

The results obtained from D-nickel are interesting but rather disappointing. As may be seen from Figure 43, the 5 per cent of dissolved manganese has reduced

TABLE 6. Dynamic measurements at remanence.

	B_r	μ'	k	λ
6.5V-vicalloy scroll No. 1	13,750	13	0.082	1.01×10^4
8V-vicalloy ring stack	11,180	15.3	0.086	0.93×10^4

FIGURE 43. Magnetostrictive coefficients for various nickel samples as function of B' .

the value of λ in nickel at high inductions by more than 50 per cent. This was the only case investigated in which nickel was alloyed with a considerable percentage of a nonmagnetic element.

Further experiments on nickel with small additions of other elements might well be made.

MEASUREMENTS ON THE VICALLOYS

Only two sets of dynamic measurements have been made on the vicalloys. The results of these measurements are shown in Table 6.

In the foregoing discussions no mention has been made of the value of the resistivity as derived from impedance data by applying eddy-current theory. Using the actual thickness of the laminations, the derived value of the resistivity departs considerably from the measured value in many cases and therefore

deserves particular attention. A comparison of the values of resistivity derived from impedance data with those directly measured is shown in Table 7, in which the values of density ρ_m and of Young's moduli E' and E are also listed.

The measured values of the resistivity are shown in the third column of Table 7. These values are only accurate to within 1 to 3 per cent in absolute magnitude because of the small thicknesses of the samples, but their relative accuracy is about 1 per cent. For A-nickel, the small differences in the several values can be explained by the differences in the amount of cold work remaining in the variously treated samples. The large influence of heat treatment on the resistivity is, of course, expected in the vicalloys, since in these cases a partial phase transformation is involved. The considerable differences among the values ob-

tained on 2V-Permendur indicate that even in this low-vanadium alloy the phase transformation is not always complete; yet it is still not clear why, in this case, the heat treatment tends to change the resistivity in the direction opposite to that observed for the vicalloys.

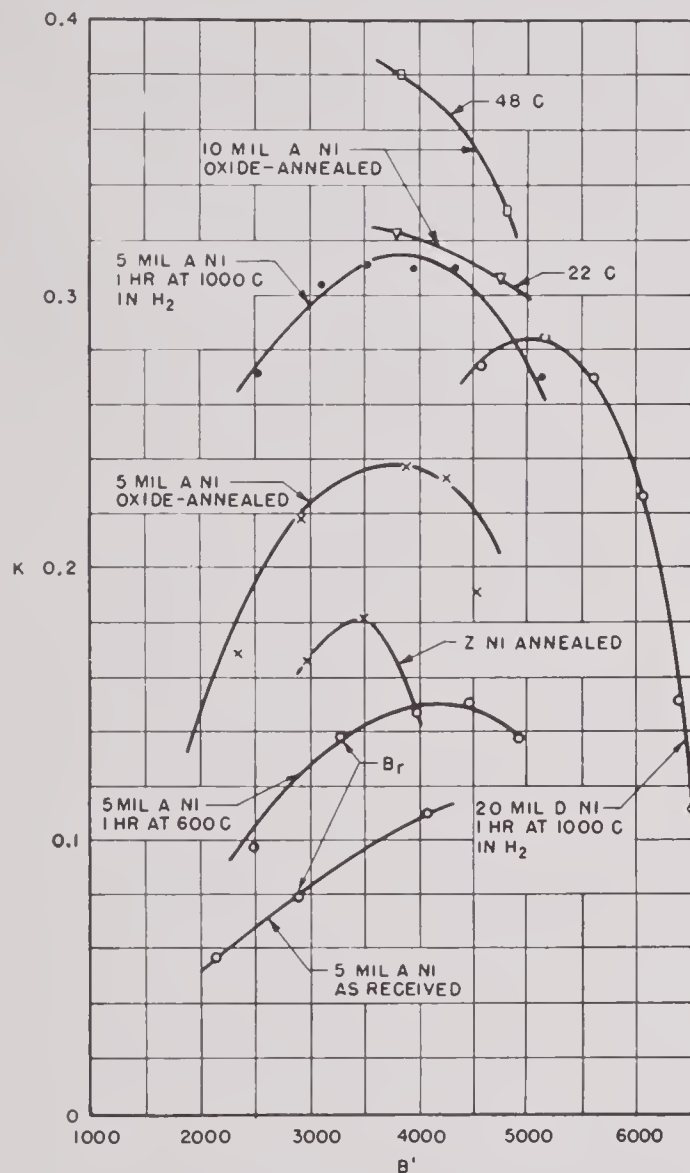


FIGURE 44. Electromechanical coupling coefficients of samples of nickel as function of B' .

The fourth column of Table 7 shows the values of resistivity derived from impedance data. Among these values a few are enclosed in parentheses because they were obtained by the method illustrated in Figure 42. With the exception of a few samples, the value of the resistivity that fits impedance data is seen to be 15 to 40 per cent smaller than the measured value. As there is no consistency in these discrepancies, the most plausible explanation for them is

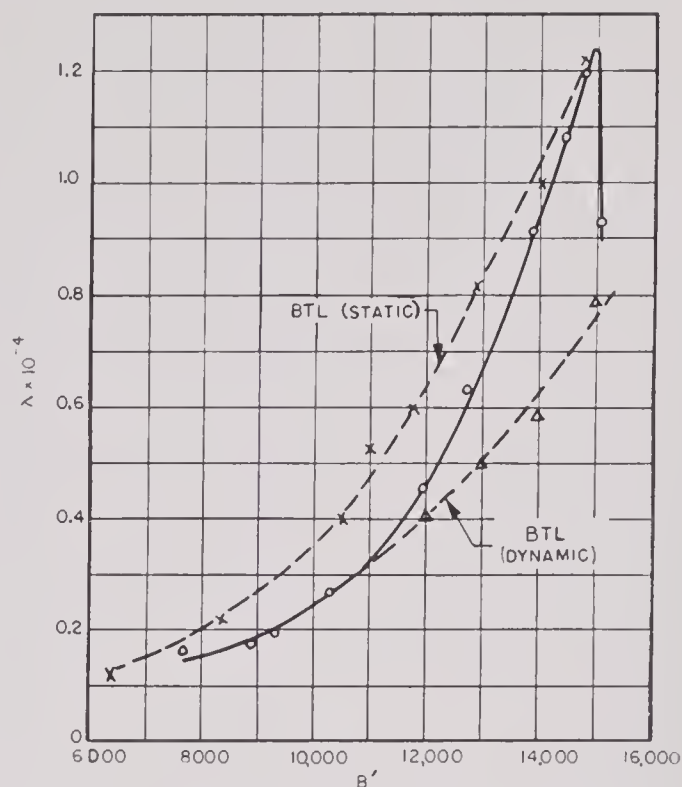


FIGURE 45. Magnetostrictive coefficient of hydrogen-annealed 45-Permalloy as function of B' (Bell Telephone Laboratories, Inc.).

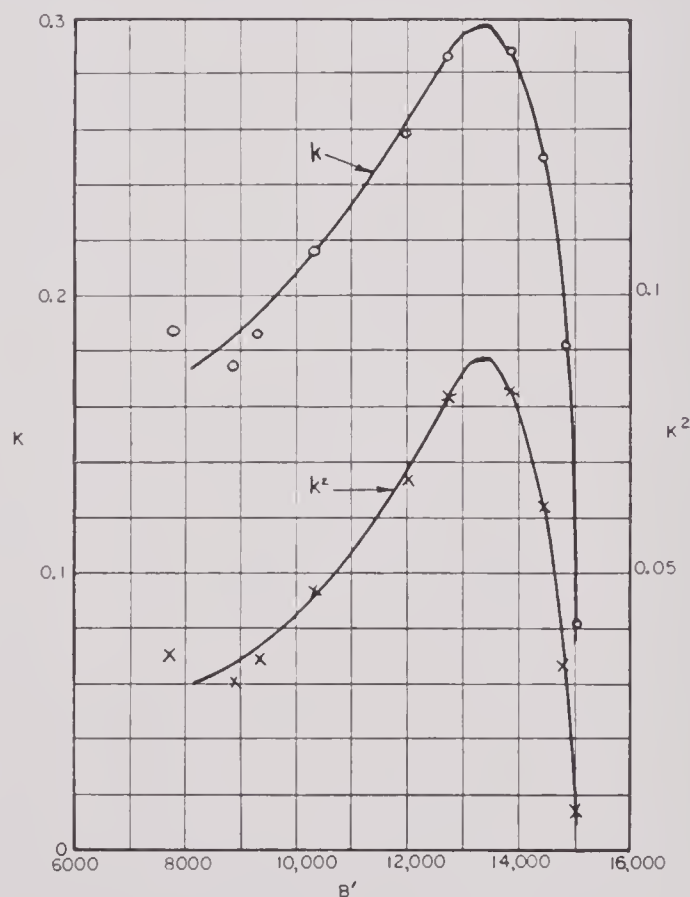


FIGURE 46. Electromechanical coupling coefficient of 45-Permalloy (Bell).

TABLE 7. A comparison of resistivity, density, and Young's modulus of magnetostrictive materials under various conditions. Values enclosed in parentheses were obtained by the method illustrated in Figure 42.

Material	Treatment	$\rho_{e \text{ obs}}$ ohm-cm	$\rho_{e \text{ calc}}$ ohm-cm	ρ_m grams/cc	E' dynes/cm ²	E dynes/cm ²
A-nickel	5-mil, unannealed	$10.4 \cdot 10^{-6}$	$10.4 \cdot 10^{-6}$	8.9	$2.16 \cdot 10^{12}$	$2.17 \cdot 10^{12}$
A-nickel	5-mil, oxide-annealed	10.0	(7.2)	8.9	2.05	
A-nickel	10-mil, oxide-annealed	9.1	9.1	8.9	1.99	2.15
A-nickel	5-mil, 1 hr at 1000 C in H ₂	9.4	(6.2)	8.9	1.90	2.08
A-nickel	5-mil, 1 hr at 600 C in H ₂		10.0	8.9	2.16	2.20
Z-nickel	14-mil, annealed, quenched, aged	14.3		8.86		
Z-nickel	annealed, quenched		14.3	8.86	2.06	2.13
D-nickel	20-mil, unannealed	20.5		8.79		
D-nickel	1 hr at 1000 C in H ₂		15.0	8.79	2.06	2.11
45-Permalloy	unannealed	54.4		8.16		
45-Permalloy	1 hr at 1000 C in dry H ₂		(53.9)	8.16	1.40	1.53
2V-Permendur	2 hr at 800 C in H ₂	38.9	30.2; 26;	8.18	1.98	2.15
		39.4	29.8; (24)			
2V-Permendur	1 hr at 500 C in H ₂	35.4	28.8; 33.5;	8.18	2.26	2.36
			28.2			
2V-Permendur	unannealed	31.1		8.18		
6.5V-vicalloy	unannealed	89.9				
6.5V-vicalloy	1 hr at 600 C in H ₂	71.3		8.1	2.46	2.48
8V-vicalloy	unannealed	90.1				
8V-vicalloy	2 hr at 600 C in H ₂	60.3	53.8	7.75	2.22	2.24

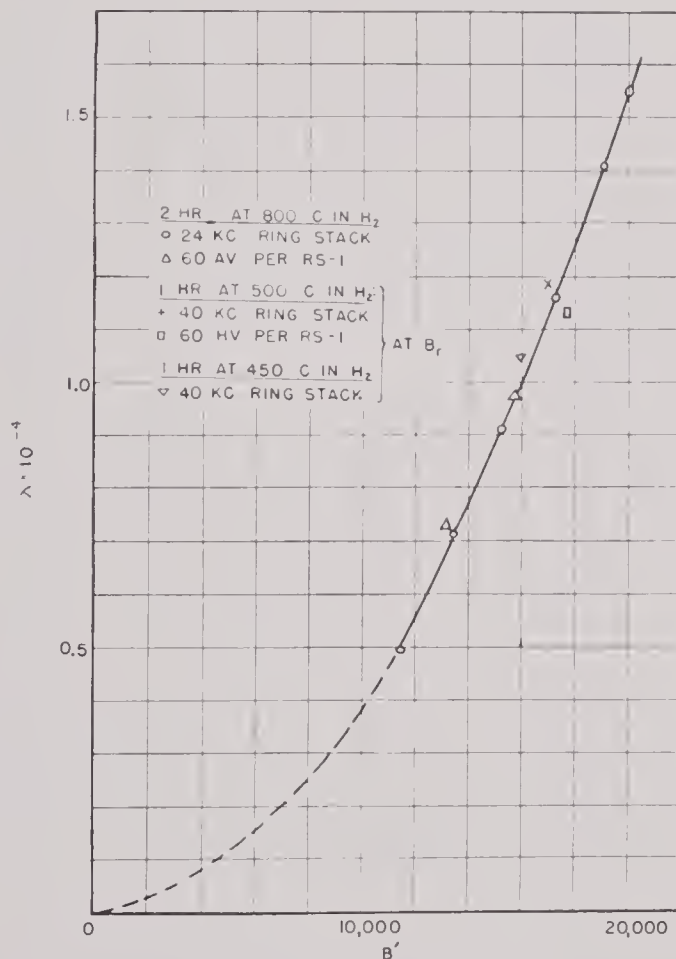


FIGURE 47. Magnetostrictive coefficients of various samples of 2V-Permendur.

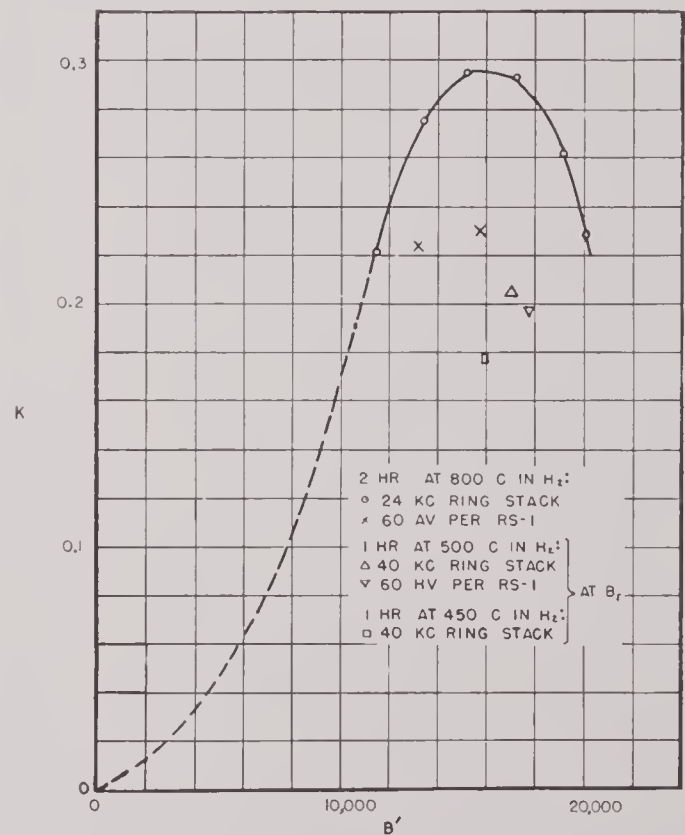


FIGURE 48. Electromechanical coupling coefficients of samples of 2V-Permendur.

CONFIDENTIAL

the nonuniformity of the reversible permeability across the sheet or on occasional improper consolidation.

In Table 7, the values of ρ_m are either taken from previous authors or determined by weighing. The values of E' for the soft-annealed samples are actually the minimum values approximately corresponding to the maximum values of k . Those for the half-hard and hard samples are taken at the remanence point. It might be remarked again that E' is the Young's modulus to be used in calculating the actual velocity of sound in the material.

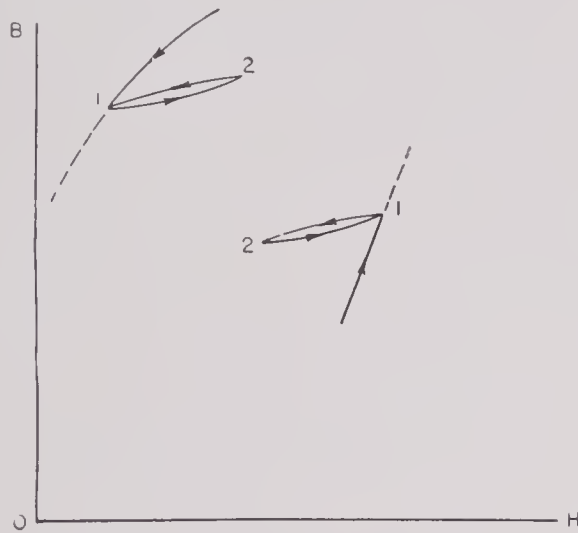


FIGURE 49. Minor loops.

It should be pointed out that the steady increase of Young's modulus E with increasing B' in the cases of the soft-annealed materials and the falling-off of λ after it has reached a maximum in the cases of D-nickel and 45-Permalloy are phenomena that are not very well understood.

SIGNIFICANCE OF RESULTS FOR TRANSDUCER DESIGN

Some comparison of the various materials can now be made from the standpoint of transducer design. As can be seen from equations (28) and (83) of Chapter 3 the open-circuit sensitivity of a magnetostrictive transducer operated as a receiver below resonance is approximately proportional to $\lambda\mu$. The open-circuit sensitivity for a given total impedance is, however, proportional to $\lambda\sqrt{\mu}$ or the electromechanical-coupling coefficient k . Also, as discussed in Chapter 3, the possible width of response of a transducer operating at resonance is approximately proportional to k .

Although the increase of λ and the decrease of μ

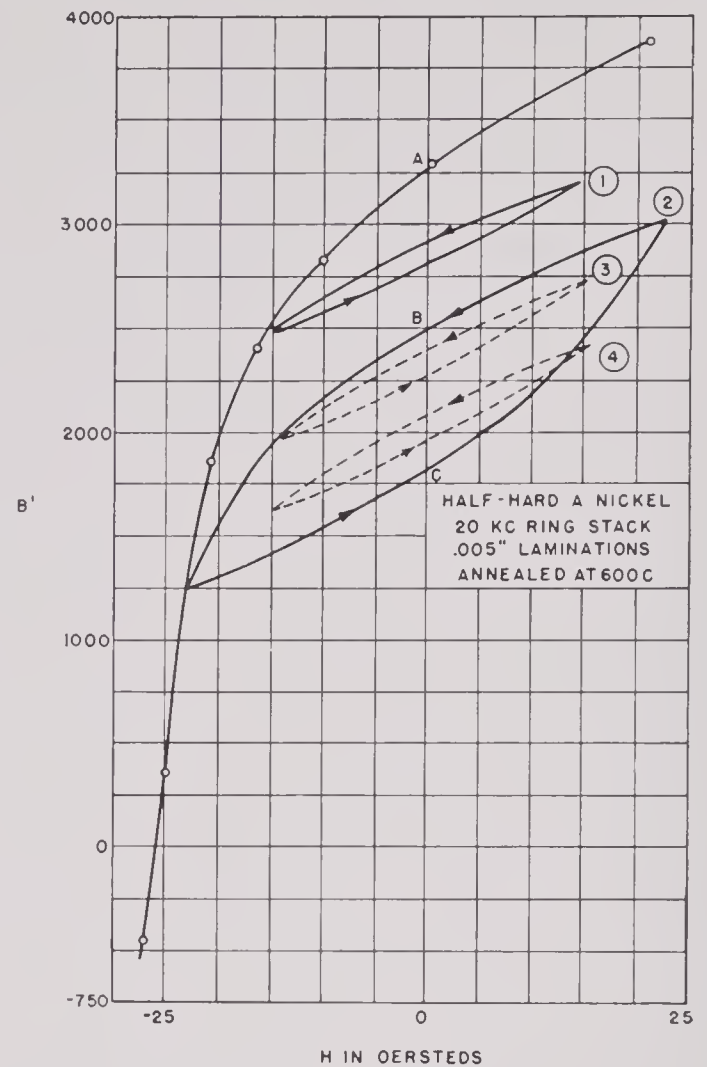


FIGURE 50. Variation under alternating field of half-hard ring laminations 0.006 in. thick, annealed at 600 C.

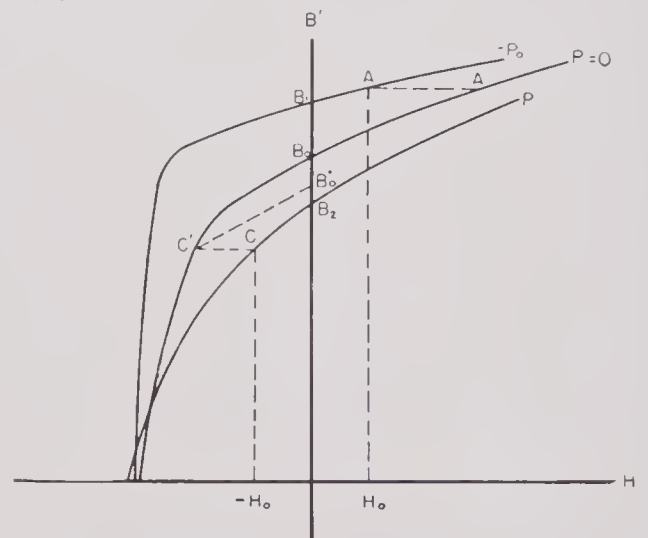


FIGURE 51. Illustrating joint effect of field and stress variation on magnetization.

with increasing intensity of polarization make the theoretical efficiency higher at higher intensities of polarization, it is desirable to operate the transducer

at the maximum value of k . For, as the electromechanical coupling decreases, the impedance becomes quite small, and copper losses and leakage flux will play an ever increasing part in determining the efficiency. For these reasons, the most important single quantity that can be used as a criterion of the magnetostrictive material is the maximum value of the coefficient of electromechanical coupling.

A second quantity of importance is the depth d , characteristic of the penetration of the magnetic field into the material. According to equation (1) of Chapter 3, d is proportional to the square root of the ratio of the resistivity, ρ_e to the reversible permeability μ . The thickness of the sheets which can be used for specified eddy-current losses is proportional to d . Thus, when other factors remain the same, a high value of $\sqrt{\rho_e/\mu}$ allows thicker laminations to be used, with consequent reductions in manufacturing cost and difficulty of construction.

Numerical values of the quantities under discussion

TABLE 8. A quantitative comparison of materials used in transducer design. Values used are from the data plotted in Figures 6 to 49 and the measured values of μ' and ρ_e .

<i>At Optimum Polarization</i>				
Material	Treatment	k_{\max}	μ'	$\sqrt{\rho_e/\mu'} \times 10^3$
5-mil A-nickel	1 hr at 1000 C in H ₂	0.315	70	0.38
5-mil A-nickel	oxide-annealed	0.240	30	0.58
10-mil A-nickel	oxide-annealed	> 0.32	> 60	< 0.41
20-mil D-nickel	1 hr at 1000 C in H ₂	0.286	100	0.45
5-mil 45-Permalloy	1 hr at 1000 C in H ₂	0.298	195	0.53
6-mil 2V-Permendur	2 hr at 800 C in H ₂	0.296	150	0.51
5-mil A-nickel	1 hr at 600 C	0.152	12	0.91
<i>At Remanence</i>				
Material	Treatment	k	μ'	$\sqrt{\rho_e/\mu'} \times 10^3$
5-mil A-nickel	1 hr at 600 C	0.14	19	0.72
6-mil 2V-Permendur	1 hr at 500 C in H ₂	0.204	54	0.85

are reproduced for several materials in Table 8. Hydrogen-annealed 5-mil A-nickel and oxide-annealed 10-mil A-nickel are seen to be superior to the other

materials in respect to k_{\max} but are inferior from the standpoint of $\sqrt{\rho_e/\mu}$. Oxide-annealed 5-mil A-nickel is inferior to Permalloy and Permendur with regard to k_{\max} , but the three are almost equivalent in $\sqrt{\rho_e/\mu}$. It is to be noted that a higher value of k_{\max} may be achieved for oxide-annealed 5-mil A-nickel by increasing the annealing temperature or time. The value of k_{\max} of annealed D-nickel is comparable to that of A-nickel, but the corresponding value of $\sqrt{\rho_e/\mu}$ is not large. It will also be noted that D-nickel and Permalloy are somewhat more critical with respect to polarizing flux than nickel, as shown by the k vs $4\pi I$ curve in Figures 44 and 46. Annealed Z-nickel has not been included in Table 8 because the small amount of information obtained on this material was not conclusive.

The cost of Permendur sheets and of 45-Permalloy is very much greater than that of nickel. Furthermore, both these alloys have to be heat-treated in a reducing atmosphere, whereas the oxide coating formed on nickel by air annealing is a good insulator which obviates any extra precautions to prevent electric contact between laminations. For general use nickel is therefore believed to be superior, on the whole, to the two alloys.

The rather small value of the k of half-hard nickel at remanence, shown in Table 8, already indicates that nickel is inferior to Permendur for operation at remanence. But for this latter purpose other factors, to be discussed in the next section, must also be taken into account.

For transducers to be used at high levels, the maximum power output must be taken into consideration. Because of the complicated nature of the problem, only the maximum stresses that can be practicably set up in the materials by magnetostriction will be indicated. These can be obtained by integrating the areas under the λ vs $4\pi I$ curves. From Figures 43, 45, and 47, we find:

$$P_{B'=6,000} = 70 \times 10^5 \text{ dynes per sq cm for A-nickel,}$$

$$P_{B'=15,000} = 40 \times 10^5 \text{ dynes per sq cm for 45-Permalloy,}$$

$$P_{B'=20,000} = 105 \times 10^5 \text{ dynes per sq cm for 2V-Permendur.}$$

Permendur would accordingly seem to be superior to the other materials in this respect.

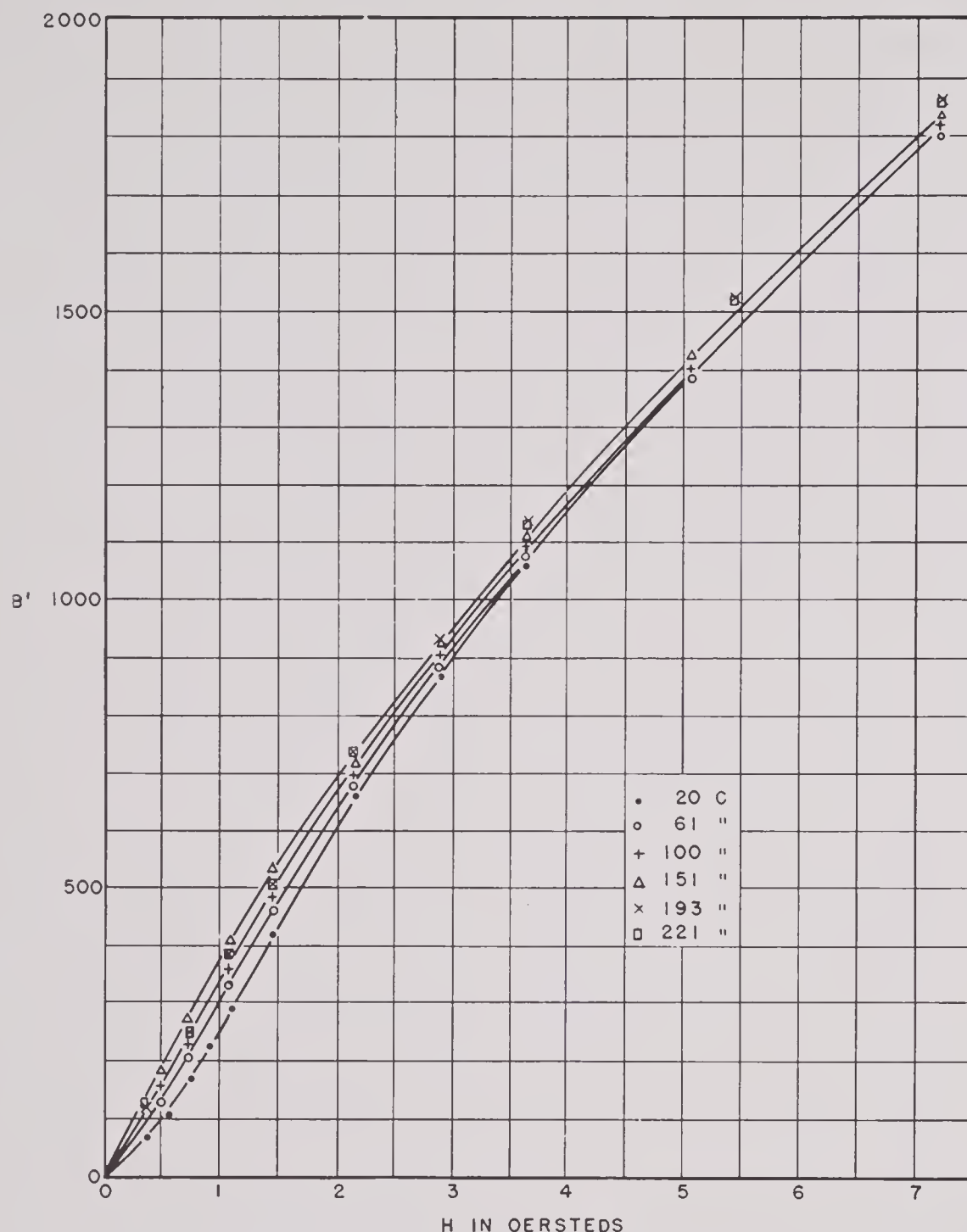


FIGURE 52. Variation of normal magnetization of oxide-annealed A-nickel, with temperature for small values of H .

4.8 TRANSDUCERS OPERATED AT REMANENCE

The half-hard materials used in transducers operated at remanence have, in general, large magnetic hysteresis. Once the active material of such a transducer is demagnetized its remanence will remain small. Demagnetization results from the application of too large an a-c field as well as from severe strains

or mechanical vibrations. This section will first describe some experimentally obtained data from which it is possible to estimate the maximum a-c field that can be used for a given material from its major hysteresis loop. The demagnetizing effect of mechanical vibrations will then be qualitatively explained. The maximum magnetostrictive stresses to be obtained in half-hard A-nickel and Permendur will be estimated and some experimental tests described.

CONFIDENTIAL

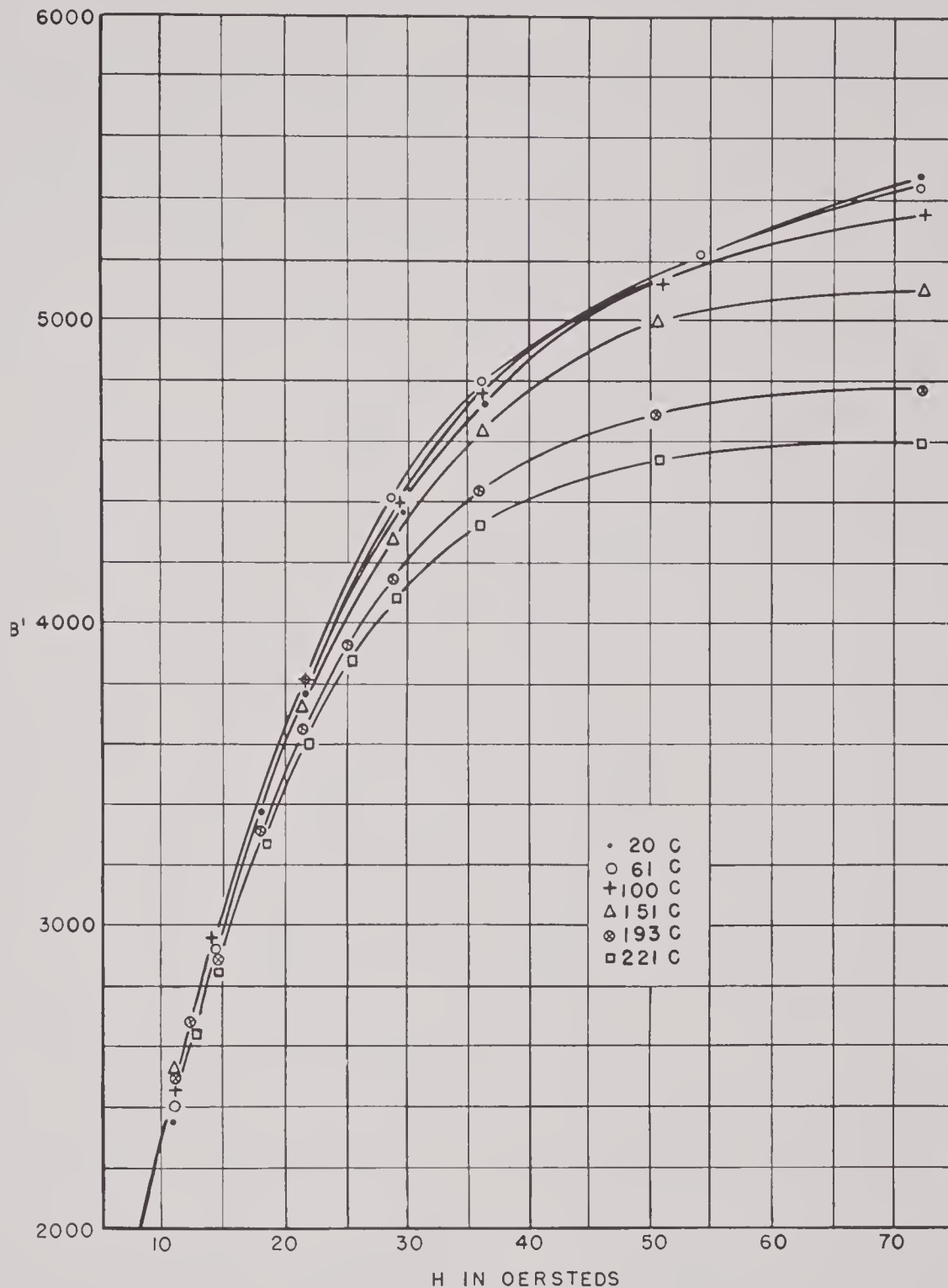


FIGURE 53. Variation of normal magnetization of oxide-annealed A-nickel, with temperature for higher values of H .

4.8.1 Some General Rules about Minor Hysteresis Loops

Suppose the material is magnetized by a d-c field which can be slowly increased, decreased, or reversed. Any variation of the field will trace out a path in the B vs H plane. A number of tests and measurements show that the following rules hold.

When the field is increased to such an extent that point 1 (H_1, B_1) is reached, magnetization will not in general retrace the original path when the field decreases (Figure 49). Subsequently, if the field reverses on reaching point 2 (H_2, B_2), the succeeding path will again be different from that used in going from 1 to 2 but will reach point 1 if the field does increase to the value H_1 .

CONFIDENTIAL

If, on reaching point 1 the second time, the field turns to decrease again, the path followed in going from 1 to 2 the first time will be retraced. Similarly if, on reaching point 2 the second time, the field turns from decreasing to increasing again, the path followed in going from 2 to 1 the first time will also be retraced. Thus a minor loop is stabilized by a complete cycle of variation of the field from H_1 to H_2 and back to H_1 .

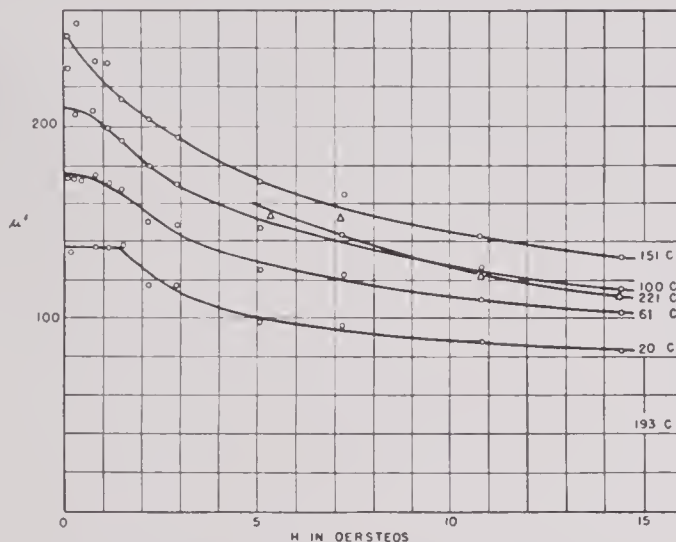


FIGURE 54. Variation in reversible permeability of oxide-annealed A-nickel, with temperature for small values of H .

If, in an intermediate stage, the field does not turn to decrease on reaching point 1 but continues to increase, the path traced out will be the continuation of the original path, as if the minor loop had not been traced.

The same holds true if point 1 is reached not by an increasing but by a decreasing field.

These rules are illustrated schematically in Figure 49. It will be noticed that the above rules are merely a generalization of Rayleigh's law described previously. With these rules the following inferences can be drawn:

1. All minor loops are wholly enclosed by the major loop obtained by reversals of a field that is strong enough to saturate the material.
2. Successive applications to the material of a field which varies cyclically between the extreme values H_1 and H_2 will retrace the same minor loop no matter at what point of a cycle the field is removed after each application.
3. If a field varying cyclically between the extreme values H_1 and H_2 is first applied to the material

to trace out a primary minor loop, subsequent arbitrary variations of the field within the range H_1 to H_2 will trace out secondary minor loops that are wholly enclosed by the primary minor loop.

The half-hard A-nickel sample of Figure 16 may be taken as an example. The descending branch of the major hysteresis loop and four minor loops are reproduced in Figure 50. Minor loops 1 and 2 were obtained by a cyclically varying field of ± 15.4 oersteds and ± 22.7 oersteds respectively, the initial magnetization being the retentivity marked by A . Loops 3 and 4 were obtained by cyclically varying the field between $+15.4$ and -15.4 oersteds, starting from the remanences B and C respectively. In obtaining these minor loops, the field can start to change either in the positive or in the negative direction, in accordance with the rules given above.

If the rules applied strictly, loop 1 should have its lower tip on the major loop and loop 4 should have its upper tip on loop 2. Failure in this respect is due to observational errors, fluctuations of the field, and transient mechanical vibrations.

The effect on a sample of an a-c field of low frequency should be the same as that of cyclically varying a d-c field. Thus an a-c field of amplitude 22.7 oersteds, when applied to the nickel sample of Figure 50, will also trace out the minor loop 2. However, an a-c field cannot be controlled with the same accuracy as a d-c field. After removing the a-c field, therefore, the remanence may be at any point on the line BC , depending on the exact point of a cycle at which the a-c field is removed. This point should be remembered, as it often causes confusion in certain types of magnetic experiments.

4.8.2 Demagnetization Effect of Strains

The foregoing discussions are based on the assumption that the sample is in static equilibrium. In the actual case of a transducer driven at resonance, the active material is alternately strained by the vibrations of the transducer. The strain amplitude is proportional to the mechanical Q , as well as to the amplitude of the exciting magnetostrictive stress, so that it can be much larger than the natural change of length arising from magnetostriction. Since hysteresis is something inherent in the material, changes of magnetization caused by strains are also partly irreversible. When a transducer polarized at retentivity

is first set into vibration by an a-c field, the phase relations between the transient vibrations and the field are somewhat complicated. In any case, during part of the first few cycles, a demagnetizing field is aided by a demagnetizing strain, so that the total demagnetization is actually larger than that estimated from measurements of the type shown in Figure 50.

The joint effect of a field and a stress on magnetization is further qualitatively elucidated in Figure 51,

will not return to state B_0 after removal of the tension and the field but will go along part of a minor loop to B'_0 . The sample is therefore demagnetized by an amount $B_0 - B'_0$. If at some instant the transients set up by a sudden application of an a-c field on a transducer bring the active material to some such state as C , the transducer will be demagnetized by about the same amount.

It is clear from the foregoing that the requirement

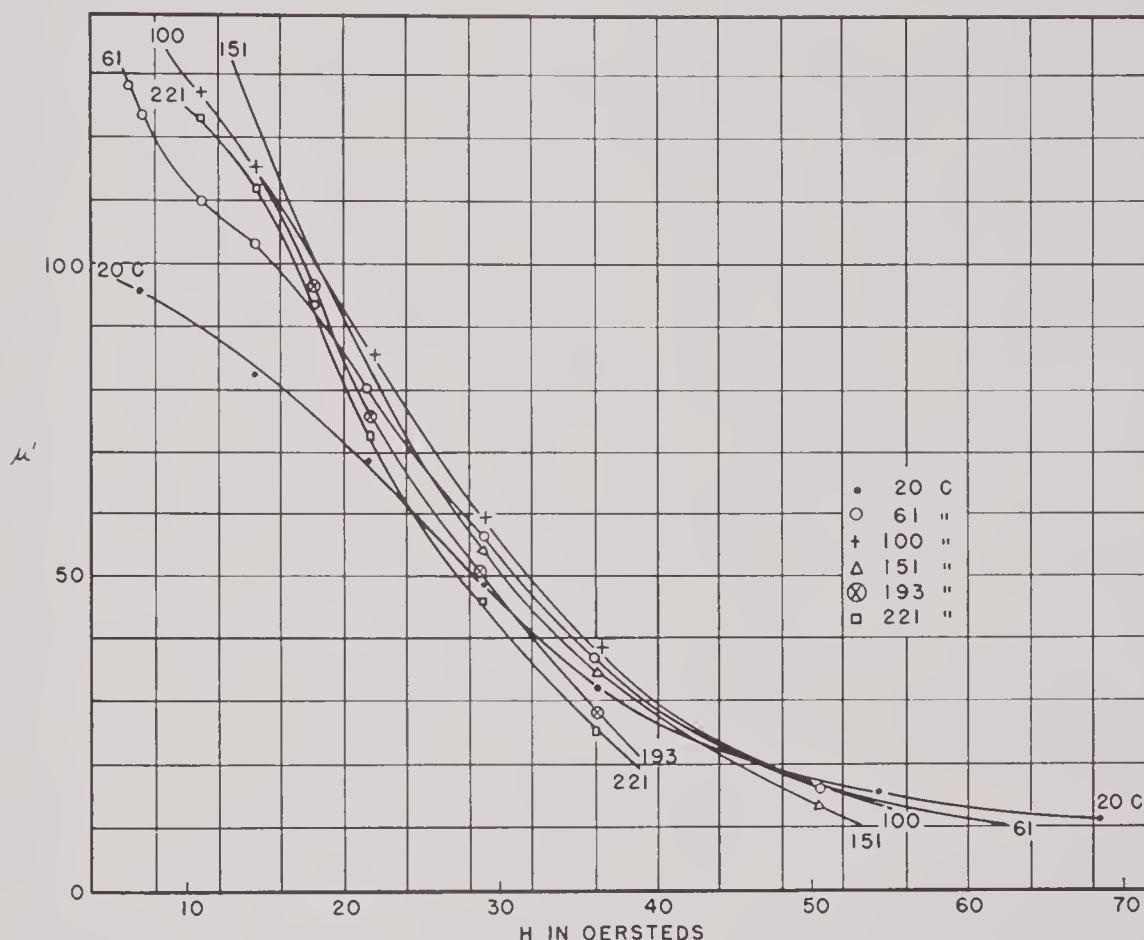


FIGURE 55. Variation in reversible permeability of oxide-annealed A-nickel, with temperature for higher values of H .

which shows the descending branches of the major hysteresis loops of a nickel sample under various static stresses. Suppose the sample is originally at the retentivity B_0 . A compression and a positive field H_0 bring the sample to state A . Since a stress is equivalent to a field, state A is magnetically equivalent to state A' . According to the rules, the sample will return to state B_0 after the compression and the field are removed, unless the former is so large as to deform the sample plastically. On the other hand, a tension P_0 and a field $-H_0$ bring the sample to the state C which is equivalent to C' . In this case, the sample

calling for small demagnetization of a transducer operated at retentivity limits the magnitude of the driving field, the exciting stress, and the mechanical Q . When detailed experimental data are available, it is possible to set an upper limit to the extent of demagnetization and find the optimum values of Q and of the maximum exciting stress, on condition that the available acoustic output is a maximum. Without detailed data it is more advantageous to choose a small Q , since the output of a given transducer is proportional to Q and to the square of the amplitude of the exciting stress.

CONFIDENTIAL

4.8.3 Some Experimental Tests on Half-Hard A-Nickel and 2V-Permendur

Consideration can now be devoted to the maximum exciting stresses that can be set up in half-hard A-nickel and 2V-Permendur transducers without too much demagnetization, assuming that the mechanical Q 's are small. For half-hard A-nickel, Figure 50 shows that the maximum safe peak field is about 15.4 oersteds, corresponding to minor loop 1. Some minor loops for 2V-Permendur have already been shown in Figure 17. The minor loop at the top of that

minor loop differ to a small extent. Taking the rms values of the integrals as P_0 ,

$$P_0 = 3.94 \times 10^6 \text{ dynes per sq cm for half-hard A-nickel,}$$

$$P_0 = 8.45 \times 10^6 \text{ dynes per sq cm for half-hard 2 V-Permendur.}$$

Thus the maximum available power output of a transducer made of half-hard 2V-Permendur is about 4.5 times as large as that of a similar unit made of half-hard A-nickel.

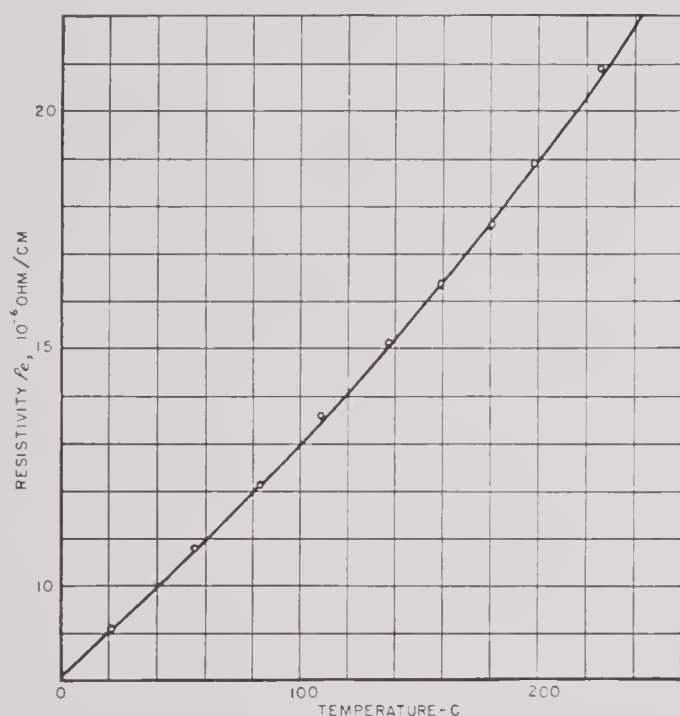


FIGURE 56. Variation with temperature in resistivity of oxide-annealed A-nickel.

figure is about as large as can safely be used. Thus a maximum peak field of 14 oersteds is obtained. To find the corresponding peak-exciting stresses P_0 , loop 1 in Figure 50 and the small loop in Figure 17, together with the data in Figures 43 and 47, are used to integrate $\lambda dB'$ along half of each minor loop. Theoretically, the clamped-core minor loops should be used to calculate the exciting stresses. However, because of the small values of the electromechanical coupling coefficient of the half-hard materials, the minor loop of a free sample is only a little different from the corresponding loop of the clamped sample. Therefore the approximation is justified. Because of the presence of terms proportional to the square of B' , the values of $\int \lambda dB'$ for the two halves of each

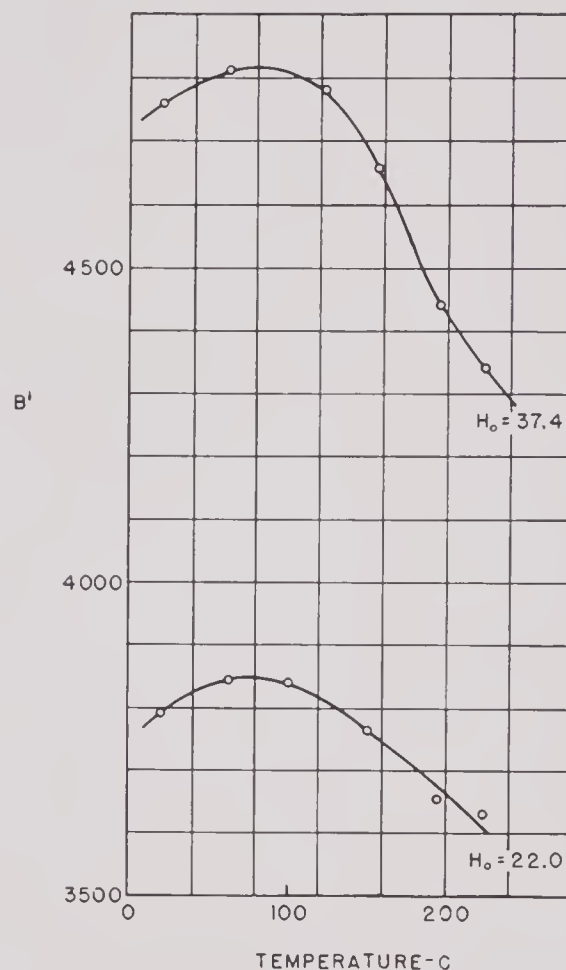


FIGURE 57. Variation in B' with temperature of annealed A-nickel.

Because it is not known how small the mechanical Q should be, some tests of prolonged "driving" in water at a peak field of 16.5 oersteds were made on half-hard A-nickel (0.005-in. laminations, 1 hour at 600 C) and 2V-Permendur (0.006-in., 1 hour at 500 C). The samples used were 60-kc ring stacks with 1.04-in. mean diameters and 0.165-in. wall thicknesses. The mechanical Q 's of these stacks in water were of the order of 6. Each sample was first magnetized to the retentivity and then subjected to continuous reversals of a decreasing d-c field, starting

from 16.5 oersteds, so that the remanence was brought to the middle of the minor loop that was traced out by the first few reversals of a field of 16.5 oersteds. Impedance measurements were then made with both samples in air. Next, each sample was immersed in water in an absorbent-lined tank and driven by alternating current at resonance, with the current increasing slowly from zero to a value corresponding to a peak field of 16.5 oersteds.

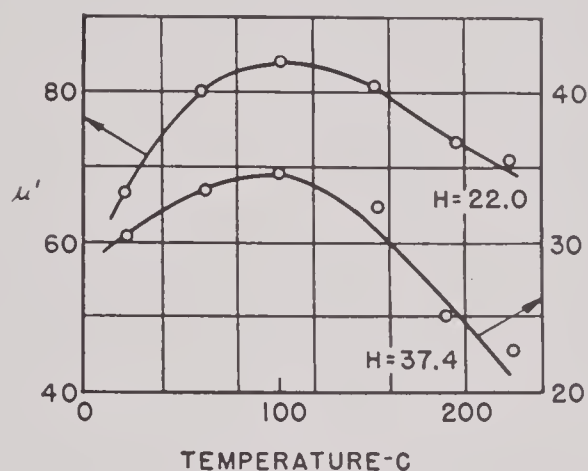


FIGURE 58. Variation in reversible permeability with temperature of A-nickel.

In the case of the Permendur sample, pronounced cavitation was noticed from the noise and gas bubbles created by the vibrations of the sample at the higher fields. In the case of the nickel sample, cavitation was barely noticeable at 16.5 oersteds. In general, cavitation did not seem to be a good criterion for estimating the output power, because it depended greatly on whether the sample was in the tank, which simulated an open field, or in an enclosed vessel where standing waves caused cavitation to set in at a much lower power level.

After about thirty minutes' driving, the alternating current was slowly decreased to zero and the sample was taken out of water, dried, and checked by impedance measurements. For the Permendur sample, the motional impedance circle was practically the same as that obtained before driving, indicating that the remanence of the core had not changed. In the case of the nickel sample, the diameter of the motional impedance circle decreased by about 10 per cent, indicating that the sample had been demagnetized slightly by the driving. Since the diameter of the motional impedance circle is proportional to $\mu^2\lambda^2$ and since μ does not vary significantly for a small variation in B' (see Figure 17), an estima-

tion made with the help of Figure 43 shows that remanence had decreased by about 100 gauss.

The relative acoustic output as a function of driving field was also observed. It was found that up to the maximum peak field of 16.5 oersteds the sound pressure was very nearly proportional to the square of the peak field and had practically no harmonic distortions. This should be the case, since for driving fields of such magnitude the minor loops are short, straight, and almost parallel to one another and the variation of λ with B' is also linear.

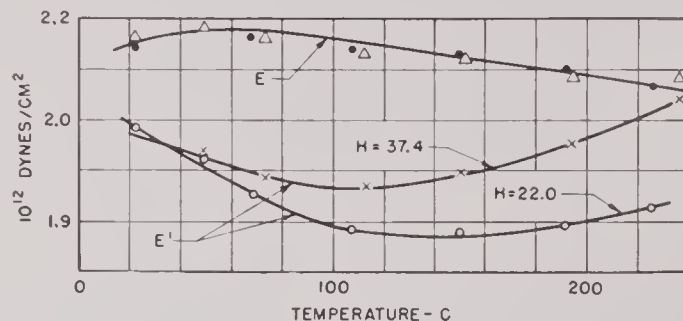


FIGURE 59. Young's Moduli of A-nickel as affected by temperature and imposed magnetic field.

4.9 EFFECT OF TEMPERATURE ON PROPERTIES OF A-NICKEL

In testing elements of various magnetostrictive multielement transducers in this laboratory, it was frequently noticed that the characteristics of the elements varied to a certain extent with fluctuations in room temperature. This phenomenon was most conspicuously exhibited by variations in the resonant frequency, which was often measured to within 2 to 3 c. Since some of the transducers had to meet a number of close specifications for satisfactory operation, it became desirable to study the phenomenon in more detail under controlled conditions. The problem is also of importance for two other reasons. First, a transducer used as a high-powered projector has numerous internal losses which tend to raise the temperature of the transducer and change its characteristics. Second, previous investigations⁴² have shown that the E effect (change in E with magnetization) in nickel becomes large as the temperature increases and reaches a maximum at about 180°C, indicating that the electromechanical coefficient may be much higher at elevated temperatures than at room temperatures. For this reason, some detailed measurements were carried out on A-nickel.

The sample used for these measurements was No. 1 of the 0.010-inch oxide-annealed samples of which the magnetization curves at room temperature are shown in Figure 7. It contained 26 laminations of the same mean diameter and wall thickness as those listed in Table 2. The laminations were loosely tied up at three points by thin glass-fiber cords to form a composite ring, with oxide films the only insulating material between the laminations.

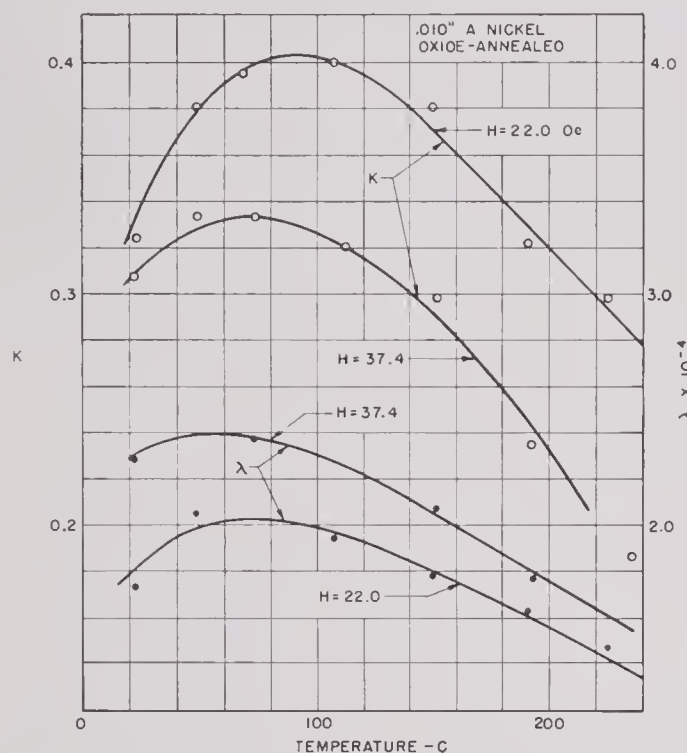


FIGURE 60. Magnetostrictive coefficient and coefficient of electromechanical coupling of A-nickel as affected by temperature.

The sample was installed in a somewhat different manner from that described earlier in this chapter. A toroidal brass cup, which had a cross section about $1\frac{1}{2} \times 1\frac{1}{2}$ in. and wall thickness $1\frac{1}{32}$ in., replaced the wood frame. The nickel ring stack was freely suspended inside the toroidal cup by No. 35 copper wire, which formed three loops supported by horizontal glass rods held across the top of the toroidal cup by a high-temperature cement.

The outside of the cup was then coated with a layer of Insalute cement. When this coating was dry, two coils (10 and 120 turns respectively) of No. 35 bare copper wire were wound on the toroidal cup. These served as search coils for measuring B' and μ' and were also coated with Insalute so that both were well insulated and protected turn by turn. The leads of these coils came out through alundum tubes.

A primary coil consisting of 136 turns of No. 14 bare copper wire was wound uniformly on the toroid to serve as magnetizing coil in the magnetic measurements and as a-c driving coil in the dynamic measurements. This coil was also partly coated by Insalute to insure good insulation. The whole assembly was then baked at 300 F for a day to dry and harden the Insalute cement.

Before the measurements were carried out various tests were made to be sure that the coils were insulated from one another and that each was insulated from the brass cup. The whole assembly was then placed in an oven which was capable of maintaining a maximum temperature of about 250 C. The leads of the three coils were protected by alundum tubes and were led out of the oven through small openings.

The temperature was measured both by a mercury thermometer and a copper-constantan thermocouple whose hot junction was located close to the nickel ring stack. In general, the temperature was accurate to about 1 C. In the magnetic measurements, however, the temperature sometimes fluctuated by as much as 4 C because of the heating effect of the magnetizing currents.

Resistivity measurements were made on a single ring lamination in the manner already described.

The normal magnetization curves and the μ' vs H curves are shown on different scales in Figures 52 to 55. From these curves it can be seen that at a given field both the intensity of magnetization and the reversible permeability vary with temperature. The sense and magnitude of the variations are, however, greatly dependent upon the strength of the field. This is due to the fact that different quantities which vary with temperature are in predominant control of the intensity of magnetization and the reversible permeability in different ranges of the field.

In addition to the intensity of magnetization and the reversible permeability, the coercive force was also observed. It was found to decrease steadily from 1.4 oersteds at 22 C to 0.79 at 221 C, indicating that the hysteresis decreased steadily with increasing temperature. This decrease in hysteresis accounted partly for the increase in the reversible permeability.

The variation of the resistivity with temperature is shown in Figure 56. It is seen that its value at 200 C is just double that at 20 C.

Impedance measurements were made at various temperatures for two polarizing fields, 22.0 and 37.4 oersteds. At 22 C, a field of 22 oersteds is close to that at which the electromechanical coupling coefficient

is a maximum. Figures 57 and 58 show the induction B' and the reversible permeability μ' as functions of temperature at these two values of the field. These

ρ_c of Figure 55, the effective thickness of laminations that fits the experimental values of ζ is 0.012 in. as against the actual value of 0.010 in.

TABLE 9. A summary of impedance and magnetic measurements for oxide-annealed 10-mil A-nickel, with H_0 equal to 22.0 oersteds.

Temp, C	$4\pi I_0$ gausses	μ'	ζ degrees	R_c ohms	X_c ohms	μ	f_r kc/sec	D_A ohms	Q_A	Pot eff per cent
22	3795	67.8	31.7	18.6	27.3	58.4	19.91	51.1	18.1	56
48	3830	77.0	29.9	17.4	29.0	60.1	19.73	67.5	15.5	82.9
67	3850	81.3	30.0	18.6	32.3	66.5	19.58	73.1	14.0	87.6
107	3835	84.0	28.5	19.5	36.0	71.9	19.38	84.2	13.8	87.9
149	3770	80.8	26.0	19.0	40.1	75.9	19.33	98.2	15.9	92.0
190	3690	75.6	22.8	17.6	41.6	73.8	19.38	113.4	22.0	86.9
224	3615	69.6	20.1	16.1	40.2	68.0	19.47	122.2	32.5	79.1

TABLE 10. A summary of impedance and magnetic measurements for oxide-annealed 10-mil A-nickel, with H_0 equal to 37.4 oersteds.

Temp, C	$4\pi I_0$ gausses	μ'	ζ degrees	R_c ohms	X_c ohms	μ	f_r kc/sec	D_A	Q_A	Pot eff per cent
22	4760	30.7	16.4	5.8	19.7	31.0	19.84	62.3	31.0	79
49	4800	32.9	18.5	6.8	20.5	33.3	19.79	64.7	26.4	88
73	4820	34.2	17.8	6.5	21.0	33.9	19.67	68.7	27.0	94
112	4800	34.6	16.8	6.7	22.3	35.7	19.60	75.7	30.6	87
151	4660	32.3	15.5	5.9	22.4	35.2	19.67	81.2	37.8	93
193	4440	26.4	11.8	4.1	19.1	28.8	19.80	88.0	79.2	87
235	4300	18.4	7.5	2.3	13.5	19.5	19.98	86.6	175	82

last figures are derived from the curves in Figures 52 to 55.

The data obtained from impedance measurements, together with those obtained from magnetic measurements, are summarized in Tables 9 and 10. In these tables, $4\pi I_0$ and μ' are interpolated from the curves of Figures 57 and 58. All the other quantities in these tables, except μ and the potential efficiency, are experimentally determined and have appeared in preceding tables, so that no further explanation is needed. The values of the clamped-core reversible permeability μ are calculated from X_c , ζ_c , and f_r . A comparison of the values of μ with the corresponding values of μ' and a calculation of the values of the electromechanical coupling coefficient show that several values of μ in Table 8 are somewhat too small, while those in Table 9 are in general too large. However, these discrepancies are believed to be due largely to errors in the polarizing fields rather than to errors in ζ and the interpolated values of X_c .

As in the case of several of the samples discussed in Section 8, the calculated values of μ do not check with the eddy-current theory without discrepancy. Taking the calculated values of μ and the values of

The values of the potential efficiency in the last columns of Tables 9 and 10 are calculated from R_c , ζ , and D_A . Owing to large errors in the interpolated values of R_c , these are only approximate. However, the potential efficiency shows a general tendency to increase with increasing temperature, reaching a maximum at about 150 C, and then to decrease again.

The Young's moduli E' and E , the electromechanical coupling coefficient k , and the magnetostrictive coefficient λ are plotted as functions of temperature in Figures 59 and 60.

All the data are now available from which a conclusion may be reached as to what takes place in a nickel magnetostrictive transducer when it is heated up. It will be assumed that the transducer is polarized at room temperatures by a constant field to an intensity corresponding to the maximum of k . From previous calculation it is known that both μ and λ increase as the temperature is raised. Consequently, the electromechanical coupling coefficient increases, but its increase is largely due to the increase of μ . The rapid increase of the electric resistivity more than compensates for the increase of μ , so that the potential efficiency increases rather than decreases. But

the potential efficiency does not tell the whole story, since it applies only to low power levels. We know from the magnetic measurements that the rapid in-

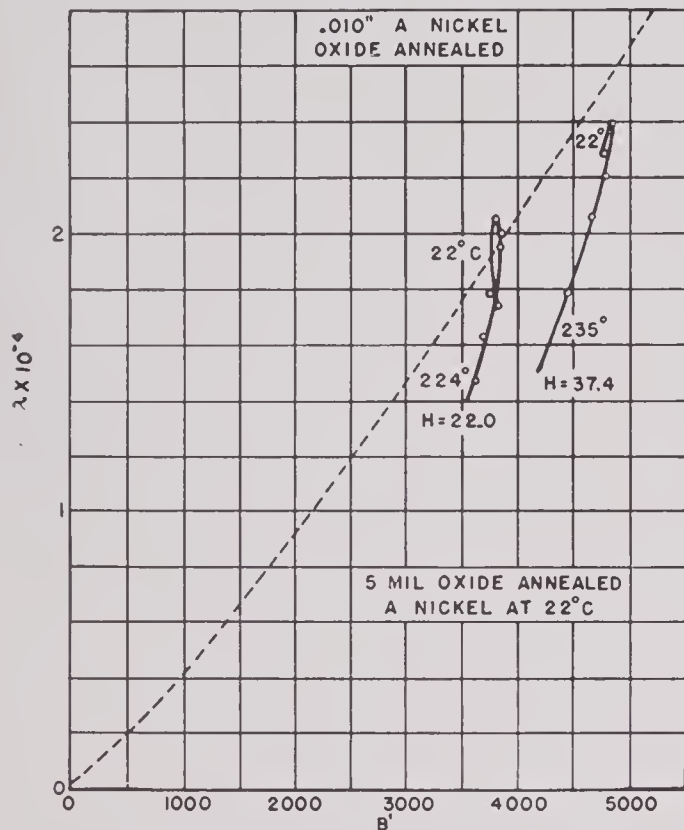


FIGURE 61. Variation of magnetostrictive constant of A-nickel with B' and temperature.

crease in resistivity is also accompanied by a decrease of hysteresis. Therefore, for a transducer operating at high power levels, an increase in temperature will probably reduce the losses appreciably.

As a result of the increase in electromechanical coupling, Young's modulus E' , and therefore the resonant frequency, decreases since E does not vary noticeably until the temperature is well beyond 100 C. In general, the effect of thermal expansion also tends to decrease the resonant frequency, but the effect is small. For nickel, the coefficient of thermal expansion between 0 and 200 C is about 14×10^{-6} . Thus, for our ring stack at 200 C, thermal expansion alone reduces the resonant frequency by about 0.3 per cent. The values of E' in Tables 9 and 10 have been corrected for this effect. Taking both of these effects into account, results show that for a 10-mil oxide-annealed A-nickel transducer polarized to about the optimum intensity at room temperature the resonant frequency decreases by about 0.035 per cent per degree centigrade between 20 C and 50 C.

The variation of λ with temperature is not entirely clear theoretically. In any case, results show that it increases slightly between 20 and 50 C. Beyond 50 C it begins to decrease steadily. The values of λ are also plotted against $4\pi I$ in Figure 61, in which the curve for 5-mil oxide-annealed A-nickel is reproduced for comparison. It should be noted that the values of λ are calculated from k^2 , E , and μ , so that errors in the values of μ are also introduced into the values of λ .

At the two values of the polarizing field used, μ reaches a maximum at about 150 C. Beyond 150 C, the simultaneous decrease of λ and μ causes the electromechanical coupling to drop sharply. For this reason the potential efficiency begins to decrease even though μ decreases and ρ_e continues to increase.

Chapter 5

DIRECTIVITY PATTERNS

5.1 INTRODUCTION

The pressure field of a sound source depends on the condition of the medium through which the sound is propagated, the disposition and surface condition of the baffles, and the shape, size, and physical characteristics of the source itself. The medium, usually water, is assumed to be uniform, that is, of constant density and velocity of sound transmission. The baffle conditions will always be stated; in most of the cases treated here, there is either no baffle or an infinite-plane baffle. Under certain conditions, such as when the dimensions of the source are large compared with the wave length of the signal, the pattern may be independent of the source baffle conditions.

5.1.1 The Problem

Here the main concern is with the dependence of the pressure field on the shape and size of the source and with the effect of varying the amplitude and phase of different portions of the active surface of the radiator.

5.1.2 Definition of Pattern

Throughout this discussion, the distance between the source of sound and the point of reception will be assumed to be large compared with the dimensions of the source. This allows considerable simplification in the analysis and is the usual practice. The distribution in angle of pressure amplitude at a large fixed distance from the source is called the pressure amplitude pattern or directivity pattern of the source. There is some occasion for referring to the distribution of the phase of the pressure at a large fixed distance from the source; this is called the pressure phase pattern of the source. Since primary interest here centers in the relative amplitude of the pressure, it is convenient to disregard factors depending on distance and to normalize the amplitude pattern to unity in some direction, usually the direction of maximum sound amplitude.

5.2 RECIPROCITY THEOREM

An acoustic reciprocity theorem applies to all the calculations shown in this chapter, that is, the directional pattern in transmission is the same as that in reception, provided the term directional pattern is understood in the proper sense. The reciprocity theorem in its most general form may be stated as follows:

Let an enclosed region have bounding surfaces S_1, S_2, \dots , and let the two distributions, generally different, of normal velocities v' and v'' over the bounding surfaces produce pressure fields p' and p'' respectively in the enclosed region. Then

$$\int_{S_1, S_2, \dots} (p''v' - p'v'')dS = 0.$$

To obtain the reciprocity theorem in the simple form usually used, take as two of the bounding surfaces a microphone or transmitter with associated baffles and a spherical source with radius a that is small compared with the wave length of the signal. Furthermore, let v' be zero except at the microphone, and let v'' be zero except at the spherical source, where it is the radial velocity of the surface. The quantity $4\pi a^2 v''$ is called the strength of the spherical source and is denoted by Q_s . Then the equation above becomes

$$\int_M p_M'' v' dM = Q_s p_s',$$

where p_M'' is the pressure on the microphone M when the simple source is used as a transmitter, and p_s' is the pressure on the simple source when the microphone is used as a transmitter. This equation states that the pressure at any point S caused by a given velocity distribution on a microphone is the same as the total pressure on the microphone (diaphragm held rigid) caused by a source of unit strength at S , the elements of area of the microphone being weighted in accordance with the original velocity distribution.

5.2.1 Constant Velocity Source

If a microphone with constant velocity over the diaphragm is used as transmitter,

$$\frac{1}{Q_s} \int_M p_M'' dM = \frac{p_s'}{v'}.$$

Thus reciprocity holds if (1) the directionality in transmission is taken as the pressure at distant points in various directions caused by unit velocity of vibration of the transducer-microphone, and (2) the directionality in reception is taken as the total force on the rigid diaphragm caused by sound incident on the microphone from distant sources of unit strength in various directions.

In applying the theorem of reciprocity, care must be taken to use it only for conjugate quantities, for example, the normal velocity in transmission and the weighted total force on a rigid diaphragm in reception.

There is no simple relation between the *motion* of the diaphragm in transmission and in reception. If the mechanical impedance of the diaphragm is not large compared with the acoustic impedance of the medium, there is no longer justification for applying the reciprocity theorem directly to velocity and pressure, as was done above, because the diaphragm is then not rigid. Instead, it must be applied to the whole electromechano-acoustic system, including the electric circuits and mechanical connections of the microphone.

Ballantine⁶⁰ has extended the reciprocity theorem to general electromechano-acoustic systems. As a further illustration, consider the application of his theorem to a microphone. If a voltage E' applied to the microphone produces a pressure P_s' in the sound field and a source of strength Q_s'' at the same point produces a current I'' when the microphone output is *short-circuited*, then Ballantine's theorem gives the result that

$$\frac{P_s'}{E'} = \pm \frac{I''}{Q_s'}.$$

Again, only open-circuit voltage and short-circuit current are conjugate in the sense of the reciprocity theorem. The voltages in transmission and in reception cannot be related without a more detailed knowledge of the terminating impedances of the circuits involved.

Ballantine's theorem applies to any linear passive system, even when it includes damping forces, provided they are linear.

5.3

POINT SOURCES

A small sphere whose radius expands and contracts sinusoidally has a pattern uniform in all directions. The source described is commonly called a simple point source. If the radius is not small compared with the wave length of the signal, the pattern is still uniform in direction. Uniformity of pattern holds approximately for a radiator of any shape, provided its dimensions are small compared with the wave length of the signal, and provided its various portions are not too badly out of phase with one another. This is illustrated by considering the pattern of two point sources. If the point sources are equal in strength and have a phase difference of 2ψ , the pattern is given by

$$P = \cos \left(\frac{\pi a}{\lambda} \sin \gamma + \psi \right),$$

where a is the distance between sources, λ is the wave length of the signal, and γ is the angle between the direction of observation and the normal to the line joining the sources (see Figure 1). The patterns when $\psi = 0$ and $a = \lambda/4$, $\lambda/2$, λ , and 2λ are shown in Figure 2. It is clear that if $2\psi \neq 180^\circ$, then as a becomes smaller the pattern becomes independent of

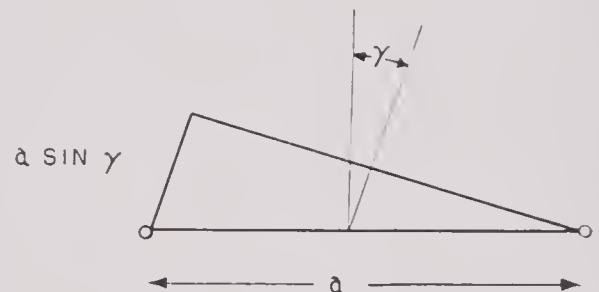


FIGURE 1. Relation between point sources and direction of observation.

γ and therefore uniform. For example, if the point sources are in phase ($\psi = 0$), and if $a = \lambda/20$, then the pressures in the two directions $\gamma = 0$ and $\gamma = 90^\circ$ differ by only 1 per cent. If the same two point sources are out of phase by 90 degrees ($2\psi = 90^\circ$), then the pressures in the two directions differ by 18 per cent. This illustrates that uniformity of pattern depends upon the relative phases of the parts of the source.

5.3.1

Dipole Sources

In fact, if $2\psi = 180^\circ$, so that the point sources are of opposite phase, for small a ,

$$P = \frac{\pi a}{\lambda} \sin \gamma,$$

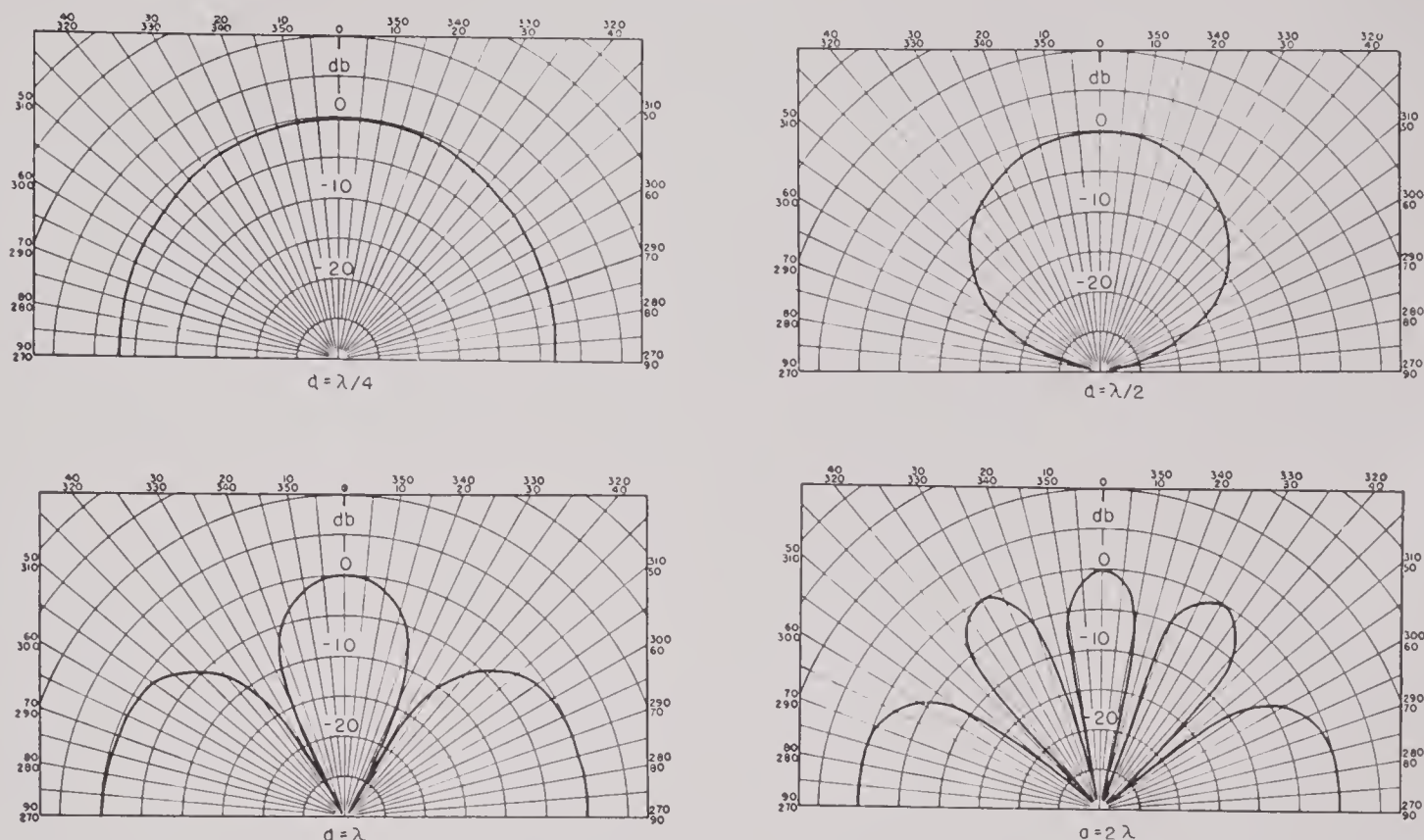


FIGURE 2. The pattern of two point sources separated by distance a for various values of a . λ is the wave length of the signal.

which is not uniform in angle no matter how small a is. This source, consisting of two near-by point sources which are 180 degrees out of phase, is called a dipole source. The normalized pattern of a dipole source in a plane through the dipole is shown in Figure 3. It has the property of having zero pressure in the plane normal to the line of the dipole. The directivity ratio of a dipole is $1\frac{1}{2}$ as compared with 1 for a simple point source.

5.3.2 Pattern of Array of Point Sources

To obtain the pattern of an array of N simple point sources in a baffless space, let the positions of the point sources be determined by the radius vectors $\mathbf{r}_1, \mathbf{r}_2, \dots, \mathbf{r}_N$ drawn from an arbitrary origin O . Then the directivity pattern of this array of sources is

$$P = P_0 \sum_{n=1}^N Q_n e^{j[k(\mathbf{u} \cdot \mathbf{r}_n) + \psi_n]}, \quad (1)$$

where Q_n and ψ_n are the strength and phase respectively of the n th source, \mathbf{u} is the unit vector in the direction of observation, and P_0 is a normalizing factor which will usually be chosen to make P unity in the direction in which it is a maximum. The quan-

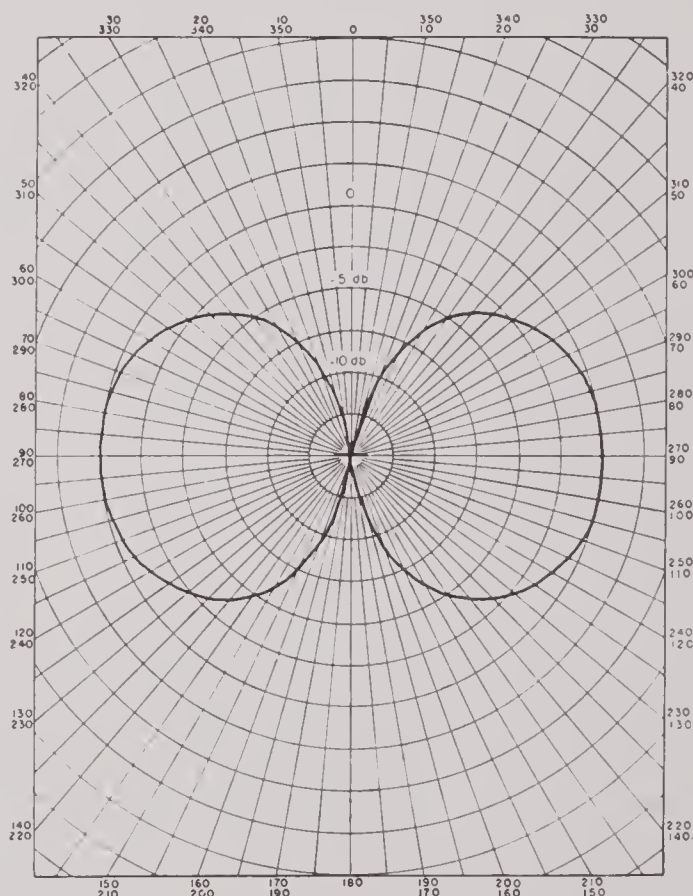


FIGURE 3. Pattern of a dipole source.

tity k is one that occurs quite often in the theory of patterns; it is called the wave number of the signal and is given by

$$k = \frac{2\pi}{\lambda},$$

where λ is the wave length of the signal. The usual vector dot product notation is used in writing $\mathbf{u} \cdot \mathbf{r}_n$.

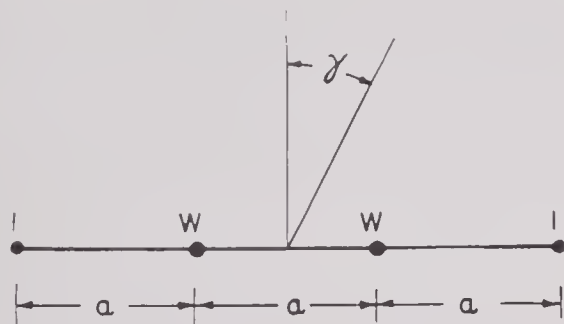


FIGURE 4. Relation between point sources and direction of observation.

PATTERN PARAMETERS

It is evident from equation (1) that there are three independent variables (parameters) which determine the pattern of an array of point sources:

- (1) the configuration of the array itself as determined by the relative distance between point sources, etc.,
- (2) the relative strengths of the point sources, and
- (3) the relative phases of the point sources.

SHADING

To show how each of these variables affects the resulting pattern, consider four point sources on a line. Suppose first that they have the same phase and are equally spaced a distance a apart, but that the middle two point sources are stronger than the outer two in the ratio of w to 1. The resulting normalized pattern is given by

$$P = \frac{1}{w+1} \left[w \cos \left(\frac{ka}{2} \sin \gamma \right) + \cos \left(\frac{3ka}{2} \sin \gamma \right) \right], \quad (2)$$

where γ is the angle between the direction of observation and the normal to the line of the sources (see Figure 4). A family of patterns is shown in Figure 5 for $a = \lambda/2$, or $ka = \pi$, and $w = \frac{1}{2}, 1, 2$, and 4. Notice that as w is increased, the minor lobes decrease and the major lobe becomes broader.

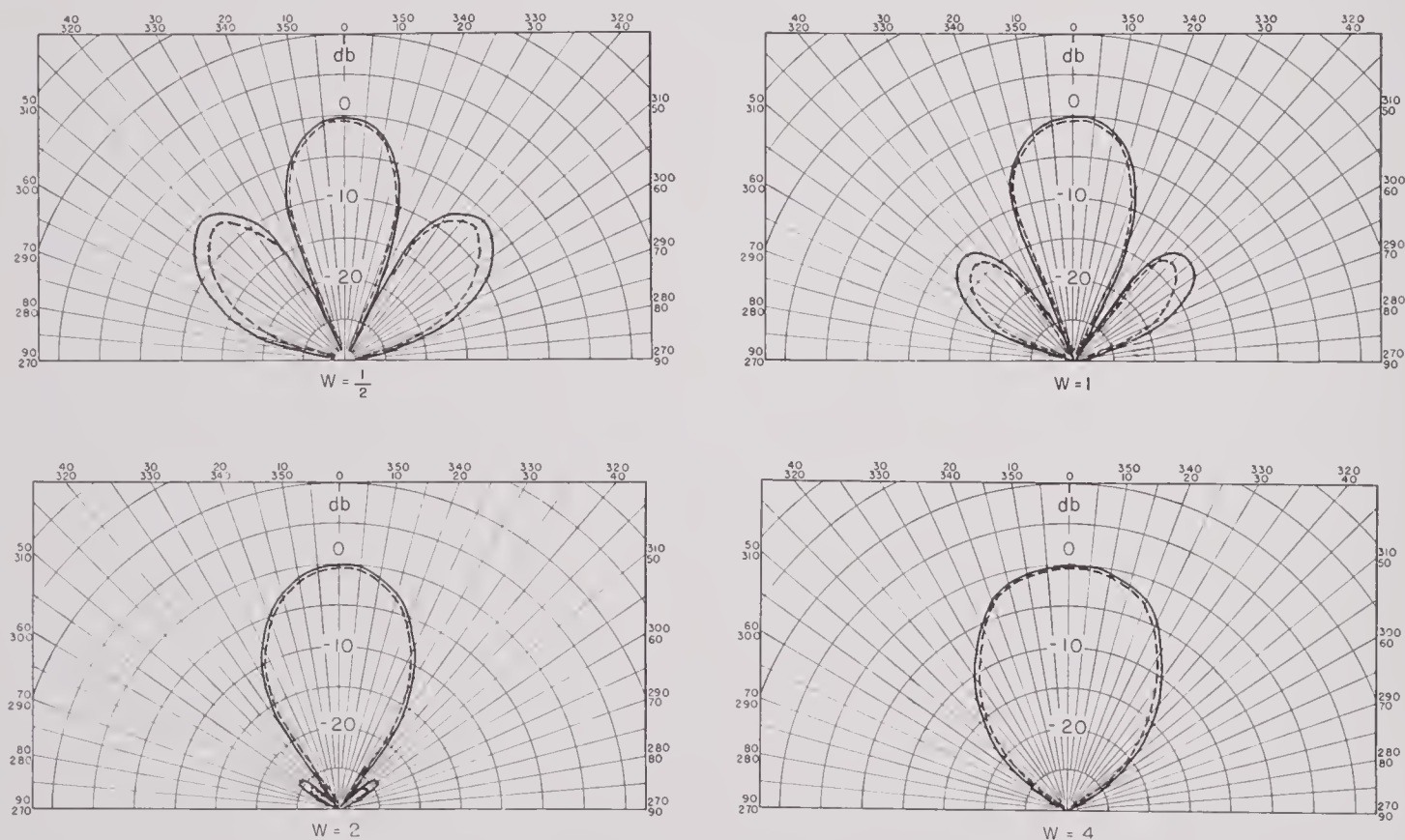


FIGURE 5. The pattern of four sources, equally spaced one-half wave length apart and having the same phase. W is the ratio of the strengths of the middle two sources to the two outer sources (see Figure 4). The solid curve is for point sources, the dotted curve for line sources one-half wave length long.

SPACING AND PHASING

Next suppose that the four point sources have equal strengths and phases but that the distances between successive points are a_1 , a_2 , and a_1 (see Figure 6). Then the pattern is

$$P = \frac{1}{2} \left[\cos \left(\frac{ka_2}{2} \sin \gamma \right) + \cos \left(\frac{k(a_2 + 2a_1)}{2} \sin \gamma \right) \right].$$

In Figure 7, patterns are drawn in which $a_2 + 2a_1$ is held constant at $3\lambda/2$, and the quantity

$$w = \frac{a_2}{a_2 + 2a_1}$$

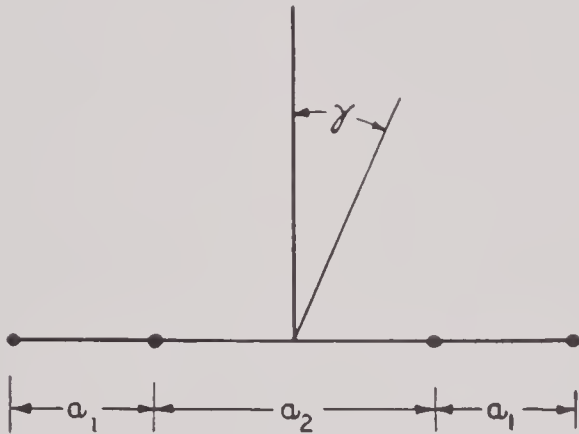


FIGURE 6. Relation between point sources and direction of observation.

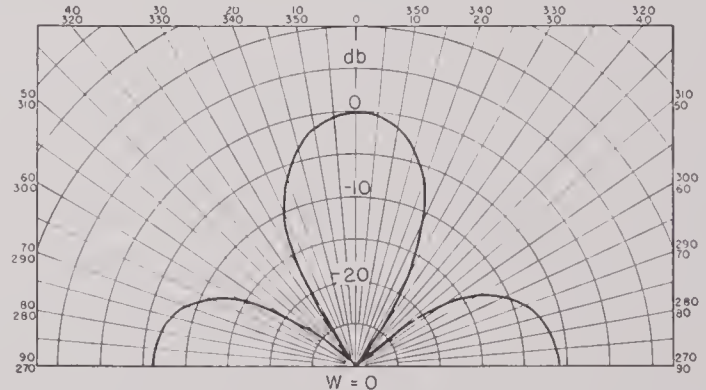
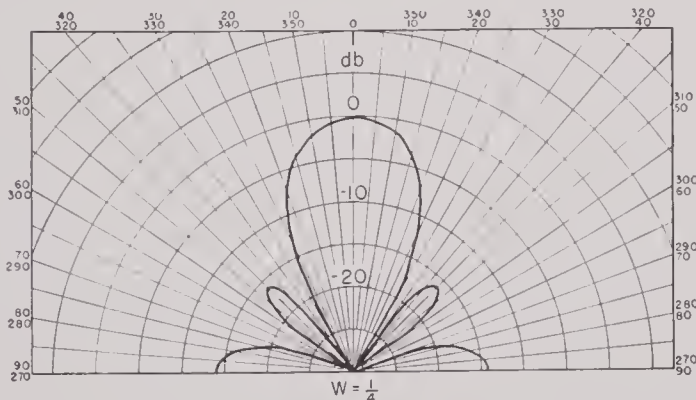
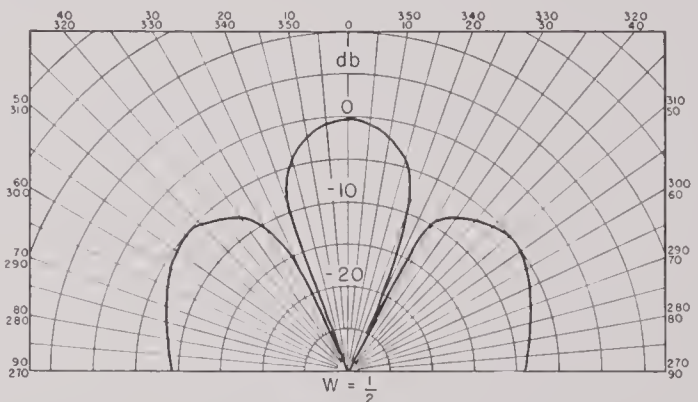
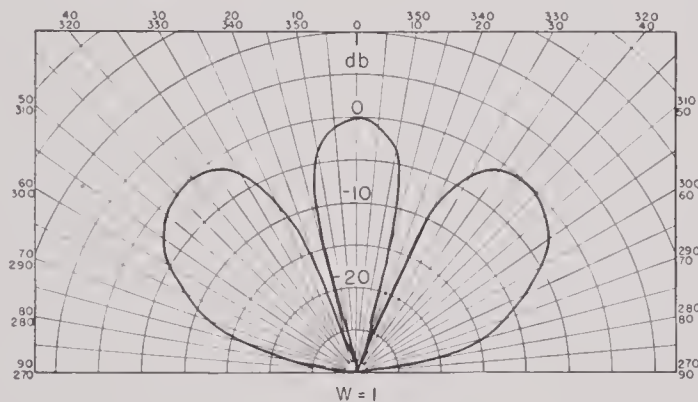


FIGURE 7. The pattern of four point sources of equal strength and phase, symmetrically spaced on a line. W is the ratio of the distance between the inner point sources to the distance between the outer point sources, the latter being assumed fixed at one and one-half wave lengths (see Figure 6).

has the values 1, $\frac{1}{2}$, $\frac{1}{4}$, and 0. Again it will be noticed that as the strength density increases at the center of the line of sources the major lobe becomes broader and the minor lobes become smaller.

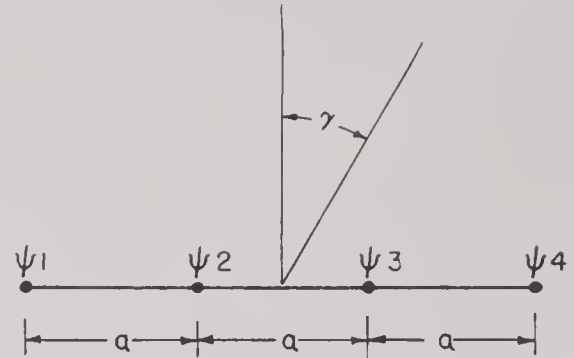


FIGURE 8. Relation between point sources and direction of observation.

Finally, suppose the point sources have equal strength and are equally separated by a distance a , but the phases are not the same (see Figure 8). If ψ_1 , ψ_2 , ψ_3 , and ψ_4 are the phases of the successive point sources, the pattern is given by

$$P = P_0 \left[e^{-j \left(\frac{3ka}{2} \sin \gamma - \psi_1 \right)} + e^{-j \left(\frac{ka}{2} \sin \gamma - \psi_2 \right)} + e^{j \left(\frac{ka}{2} \sin \gamma + \psi_3 \right)} + e^{j \left(\frac{3ka}{2} \sin \gamma + \psi_4 \right)} \right].$$

Consider the case in which there is progressive phasing, so that $\psi_1 = 3\psi$, $\psi_2 = \psi$, $\psi_3 = -\psi$, and $\psi_4 = -3\psi$. Then the pattern is

$$P = 2P_0 \left[\cos \left(\frac{3ka}{2} \sin \gamma - 3\psi \right) + \cos \left(\frac{ka}{2} \sin \gamma - \psi \right) \right].$$

The amplitude pattern of P is shown in Figure 9 when $a = \lambda/2$ and $\psi = 30^\circ, 45^\circ, 60^\circ$, and 75° . It will be noticed that the pattern is somewhat the same as one in Figure 5, except that the major lobe is shifted by an amount approximately $2_3\psi$.

where $\phi = ka \sin \gamma$, and γ is the angle between the direction of observation and the normal to the line of the sources. P_0 is given by

$$\frac{1}{P_0} = \sum_n Q_n,$$

and the directivity ratio (see Section 5.7) of the pattern is

$$D = P_0^2 \sum_m \sum_n Q_m Q_n \frac{\sin ka(m+n)}{ka(m+n)}.$$

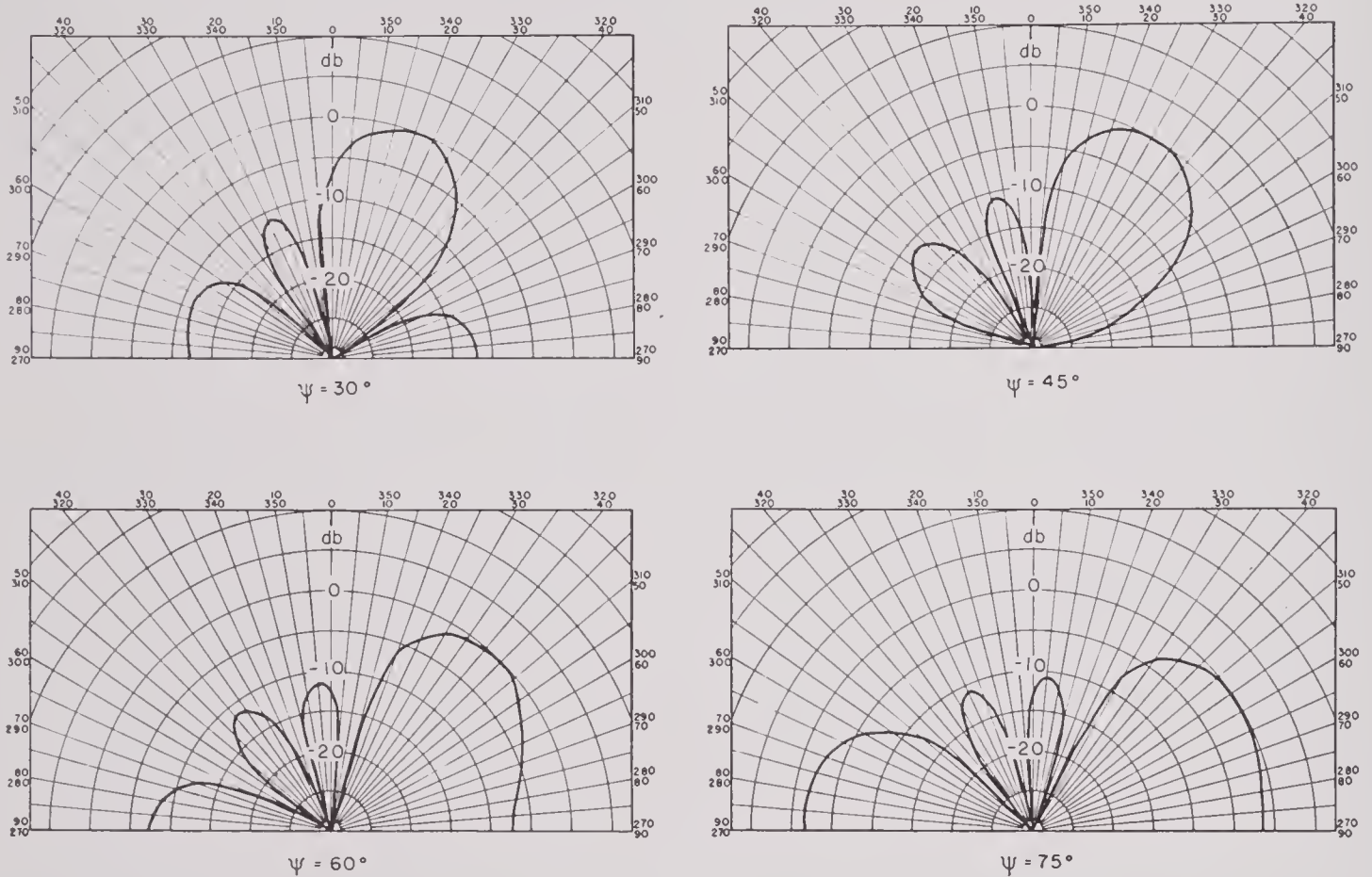


FIGURE 9. The pattern of four point sources of equal strength equally spaced one-half wave length apart and progressively phased by an amount 2ψ (see Figure 8).

5.3.3 Equally Spaced Point Sources on a Line

Suppose that N point sources are equally spaced a distance a apart on a line and that all the sources have the same phase. The pattern is then given by

$$P = P_0 \sum_n Q_n e^{jn\phi}, \quad (3)$$

FOURIER RELATION BETWEEN SOURCE STRENGTHS AND PATTERN

It is clear that equation (3) gives the expansion of the pattern P in a finite Fourier series. Thus the coefficients Q_n , which are the strengths of the point sources, are related to the pattern by the formula

$$Q_n = \frac{1}{2\pi} \int_{-\pi}^{\pi} \left(\frac{P}{P_0} \right) e^{-jn\phi} d\phi. \quad (4)$$

If the source is symmetrical ($Q_n = Q_{-n}$), it is more convenient to use the cosine form

$$P = P_0 \left[Q_0 + 2 \sum_{n=1}^{(N-1)/2} Q_n \cos n\phi \right] \quad (5)$$

for the case where the center of symmetry falls at one of the point sources, and

$$P = 2P_0 \left[\sum_{n=1}^{N/2} Q_{n-\frac{1}{2}} \cos \left(n - \frac{1}{2} \right) \phi \right] \quad (6)$$

for the case where the center of symmetry falls midway between two of the point sources. In the former case N is odd, in the latter case N is even. In either P is symmetrical and

$$Q_n = \frac{2}{\pi} \int_0^\pi \left(\frac{P}{P_0} \right) \cos n\phi d\phi. \quad (7)$$

The importance of the Fourier relationships between P and Q_n is that they permit "designing" for a given pattern P without recourse to a long trial-and-error procedure which may or may not be successful. That is, for any given pattern P , equation (4) gives the required strengths of the point sources directly. Of course, for an arbitrary P , Q_n will not be zero for large n , so that in general an infinite number of point sources are required to fit a given pattern. This requires that a compromise be made in choosing the pattern P to be approximated or in choosing N large enough so that the contribution of the neglected point sources is below some prescribed amount.

DESIGNING FOR GAUSSIAN PATTERN

To illustrate the above, find the line of equally spaced points which will produce the radiation pattern

$$P = e^{-(\phi/\Delta)^2} \quad (8)$$

where $\phi = ka \sin \gamma$ and Δ is a parameter determining the width of the pattern. From equation (7),

$$Q_n = \frac{2}{\pi} \int_0^\pi e^{-(\phi/\Delta)^2} \cos n\phi d\phi.$$

If $e^{-(\pi/\Delta)^2}$ is small compared with unity, the integration may be extended to infinity, with the result that

$$Q_n = \frac{\Delta}{\sqrt{\pi}} e^{-(n^2\Delta^2/4)} = -\frac{1}{n} \left[\frac{\Phi_2\left(\frac{n\Delta}{2}\right)}{2} \right] \quad (9)$$

where the notation in Jahnke and Emde⁶³ has been used for the second derivative of the error integral. In this equation n is either an integer or half an odd integer, according as the center of symmetry coincides with one of the point sources or is midway between two of them. Since Q_n is not zero for finite n , the Gaussian pattern (8) requires an infinite number of point sources for its exact representation. However, only a reasonable approximation of this pattern is required, therefore terms beyond a certain point in the series are omitted. This introduces minor lobes into the pattern. Minor lobes can be made sufficiently small if care is taken not to omit terms in (3) which contribute a significant amount. Because the coefficients in (9) fall off so rapidly with increasing n , the first omitted term is by far the most important and the height of the minor lobes can be said to be about twice the first omitted coefficient.

This procedure will be illustrated by a numerical example. Suppose that a radiator is desired with six point sources and with total width of two and one-half wave lengths, that is, the distance between adjacent point sources is $\lambda/2$. The minor lobes must be no higher than -30 db compared with the central lobe. The width of the major lobe cannot be specified, as enough quantities have already been fixed to determine it. Since there are an even number of point sources (six), the pattern is given by

$$P = 2P_0 \left[Q_{1/2} \cos \left(\frac{\pi}{2} \sin \gamma \right) + Q_{3/2} \cos \left(\frac{3\pi}{2} \sin \gamma \right) + Q_{5/2} \cos \left(\frac{5\pi}{2} \sin \gamma \right) \right],$$

where Q_n is given by equation (7). Only three terms of the series have been used, each term corresponding to two point sources of the radiator. The coefficient $Q_{1/2}$ is the amplitude of the central two point sources, $Q_{3/2}$ of the next pair, and $Q_{5/2}$ of the outside pair. The first omitted coefficient is $Q_{7/2}$ and this must be small enough so that its omission will not reintroduce minor lobes higher than -30 db (3.16 per cent). It is desirable to make $2Q_{7/2}$ no smaller than 0.0316, because a smaller value would reduce the minor lobes unnecessarily below -30 db and, at the same time, broaden the central lobe, that is, require a larger Δ . Also the maximum power which could be radiated would be smaller because of the

smaller amplitude on the outside point sources. Since

$$Q_{7/2} = -\frac{2}{7} \left[\frac{\Phi_2\left(\frac{7\Delta}{4}\right)}{2} \right],$$

Δ must be found so that

$$\frac{1}{2} \Phi_2\left(\frac{7\Delta}{4}\right) = -\frac{7}{2} (0.0316) = -0.1106.$$

From Jahnke and Emde,^{63a} $7\Delta/4$ is found to be 1.687, so that Δ is 0.964. Further calculations show that

$$Q_{1/2} = 0.514, Q_{3/2} = 0.322, Q_{5/2} = 0.128$$

and

$$\frac{1}{2P_0} = Q_{1/2} + Q_{3/2} + Q_{5/2} = 0.964.$$

The pattern (see Figure 10) is then

$$P = 0.533 \cos\left(\frac{\pi}{2} \sin \gamma\right) + 0.334 \cos\left(\frac{3\pi}{2} \sin \gamma\right) + 0.133 \cos\left(\frac{5\pi}{2} \sin \gamma\right).$$

It is 32 degrees wide, 6 db from the peak, and satisfies the imposed minor-lobe requirement.

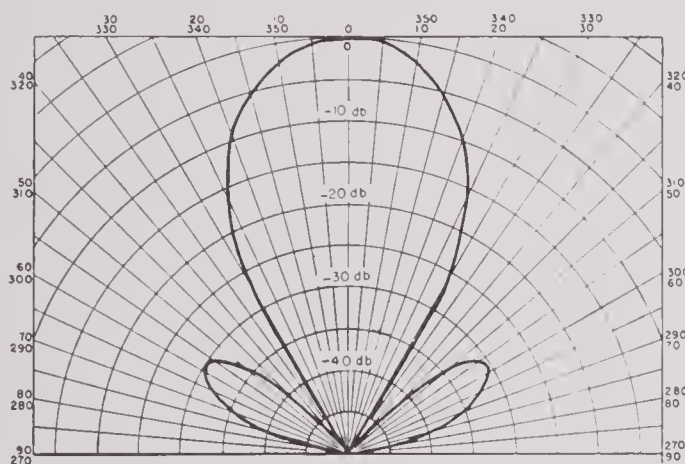


FIGURE 10. The pattern of six point sources spaced one-half wave length apart and shaded to have minor lobes lower than 30 db below the peak of the major lobe.

In the pattern just discussed, the distance between adjacent point sources was arbitrarily taken to be $\lambda/2$. In the design of a radiator of point sources, spacing must be selected for the point sources. Theoretically the *maximum spacing is one wave length*, but in *practice it must be considerably less*. Consider the Fourier series (5) and (6); the first has a period 2π in ϕ , whereas the second has a period of 4π in ϕ , but at the point $\phi + 2\pi$ it has the negative of the value at

ϕ (see Figure 11). Thus, in both cases, the intensity pattern which is proportional to the square of the pressure has a period of 2π . In the physical problem only a finite rather than an infinite range of ϕ must now be considered. In fact, since $\phi = (2\pi a/\lambda) \sin \gamma$, ϕ ranges between the limits $\pm 2\pi a/\lambda$ as γ is varied between its limits of $\pm \pi/2$. If $2\pi a/\lambda > 2\pi$, that is, if $a > \lambda$, it is clear that the physical range of ϕ includes not only the central major lobe at $\phi = 0$ but also the two major lobes at $\phi = \pm 2\pi$. Since this is a situation which should be avoided, the relation $a < \lambda$ must be maintained. Actually, the spacing a should be enough smaller than λ so that the physical range of ϕ does not go beyond the point A which marks the beginning of the second lobe in Figure 11.

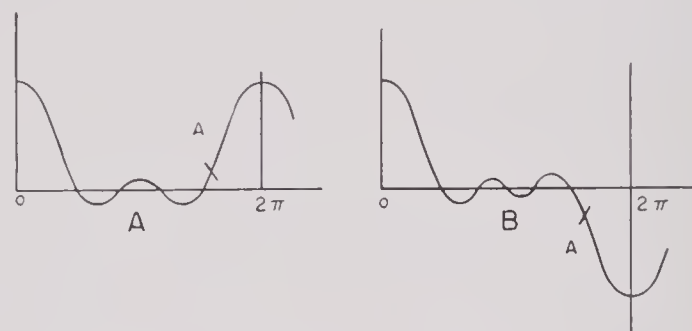


FIGURE 11. Illustrating pattern for equally spaced point sources on a line, A for the odd number of sources, B for the even number of sources.

The above analysis can be applied with minor modifications to a line of equally spaced point sources with a progressive shift in phase of an amount ψ between points. There is the same pattern of equations (3), (5), or (6) but with

$$\phi = \frac{2\pi a}{\lambda} \sin \gamma - \psi.$$

The preceding discussion makes use of the fact that with $\psi = 0$ the physical range of ϕ is between $\pm 2\pi a/\lambda$. With phase shift ψ , the limits are $\pm 2\pi a/\lambda - \psi$. The largest value of ψ to be used is $\psi = 2\pi a/\lambda$, corresponding to a shift of 90 degrees in γ . For this shift the limits on ϕ are 0 to $-4\pi a/\lambda$ which, as in the preceding section, must be within $\pm 2\pi$. Hence *when a large progressive phase shift is to be used, $a < \lambda/2$ must be true*.

Apply equation (1) to obtain the pattern of N point sources equally spaced on a line, assuming that all the point sources have the same strength and phase. Let the origin 0 be on the line of the sources

a distance a_0 from the first source, and let the distance between successive sources be a . Then

$$P = P_0 \sum_{n=1}^N e^{jk[a_0 + (n-1)a] \sin \gamma},$$

where γ is the angle between the direction of observation and the normal to the line of the sources. This expression can be summed up to give

$$P = P_0 \frac{\sin \left(N \frac{ka}{2} \sin \gamma \right)}{\sin \left(\frac{ka}{2} \sin \gamma \right)} e^{jk[a_0 + a(N-1)/2] \sin \gamma}.$$

Thus, if $a_0 = -(N-1)a/2$, which places 0 midway

indefinitely while keeping $(N-1)a = l$ constant. Thus the pattern of a uniform line source of length l is

$$P = \frac{\sin \left(\frac{kl}{2} \sin \gamma \right)}{\frac{kl}{2} \sin \gamma}. \quad (11)$$

This pattern is shown in Figure 13 plotted against the universal parameter $(l/\lambda) \sin \gamma$. This pattern is important since, as will be seen later, it is also the pattern of a square in a normal plane parallel to the side of the square. The highest minor lobe is 13.5 db

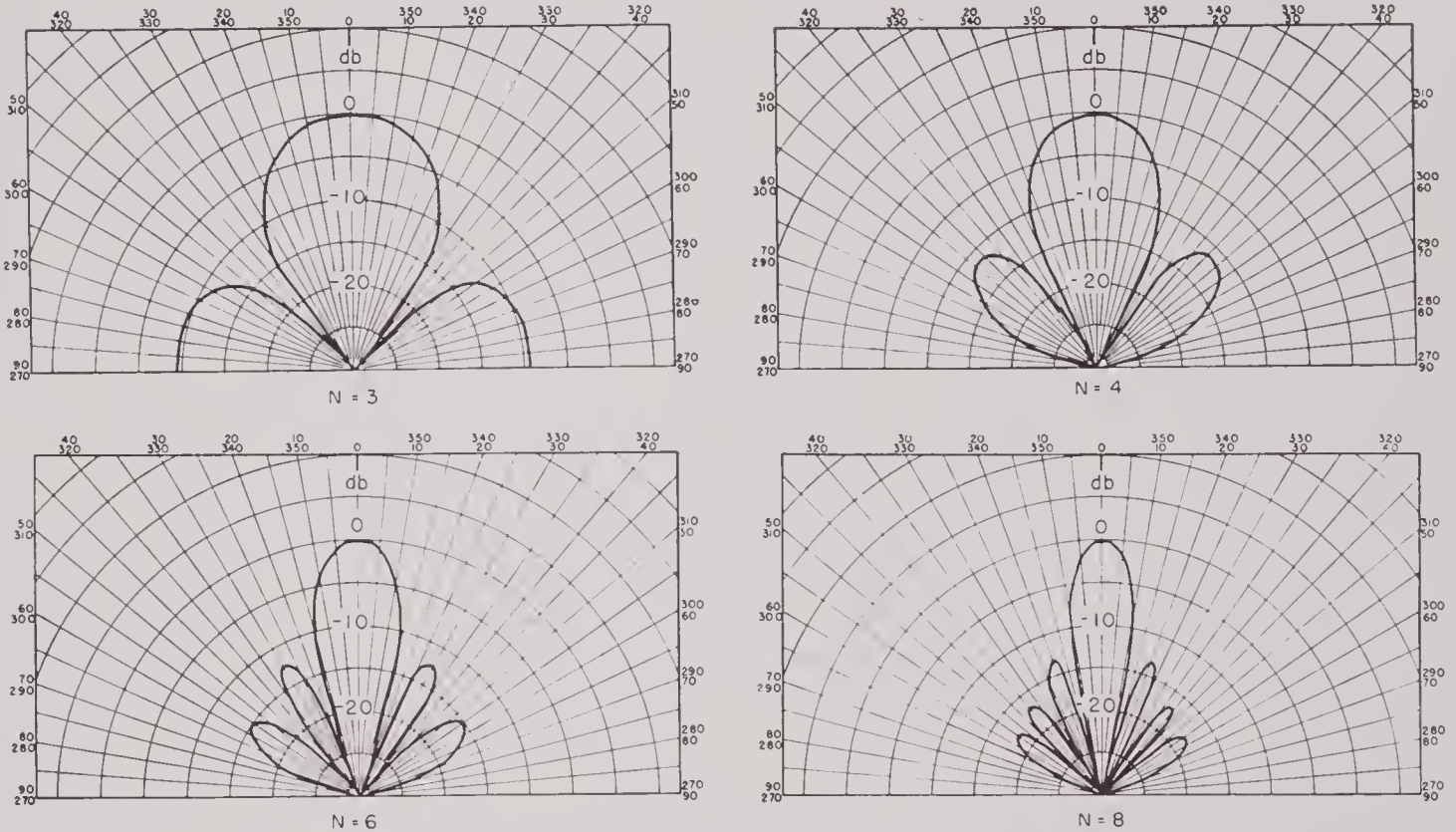


FIGURE 12. The pattern of N point sources of equal strength and phase equally spaced one-half wave length apart on a line.

between the two end-point sources, and $P_0 = 1/N$, which normalizes the pattern,

$$P = \frac{\sin \left(N \frac{ka}{2} \sin \gamma \right)}{N \sin \left(\frac{ka}{2} \sin \gamma \right)}. \quad (10)$$

In Figure 12, this pattern is shown with $a = \lambda/2$ and $N = 3, 4, 6$, and 8 .

5.4 LINE SOURCES

The pattern of a line source can be obtained from equation (10) by letting N increase and a decrease

below the major lobe, and the width 2γ of the major lobe 6 db down is determined approximately by

$$\sin \gamma = \frac{3\lambda}{5l}$$

so that, if $\lambda/l \ll 1$,

$$2\gamma = 68.8 \frac{\lambda}{l} \text{ degrees.}$$

For example, if $l = 5\lambda$, the major lobe is approximately 13.8 degrees.

5.4.1 Directivity Ratio of Line Source

The directivity ratio of a line source is shown in Figure 14 plotted against l/λ . When $l/\lambda \gg 1$, it is given by

$$D = \frac{\lambda}{2l}.$$

In Figure 15 the directivity ratio of a line source is shown as a function of the width of the pattern 3, 6, and 10 db from the peak. These curves are useful when the pattern is available and the exact effective dimensions of the line source are not known.

A general formula for the pattern of a line source can easily be obtained from equation (1). Thus by letting

$$Q_n = f(x_n)dx$$

so that $f(x_n)$ is the strength per unit length of the line source at $x = x_n$ (the origin of x is taken at the midpoint of the line source), and then by permitting N to increase indefinitely

$$P = P_0 \int_{-l/2}^{l/2} f(x) e^{j(kx \sin \gamma + \psi)} dx \quad (12)$$

is obtained where l is the length of the line source; γ is the angle between the direction of observation and the normal to the line source; and the normalizing factor, when $\psi \equiv 0$, is determined by

$$\frac{1}{P_0} = \int_{-l/2}^{l/2} f(x) dx.$$

Equation (11) can be easily verified for the pattern of a uniform line source by taking $P_0 = 1/l$, $f(x) \equiv 1$, $\psi = 0$, and integrating.

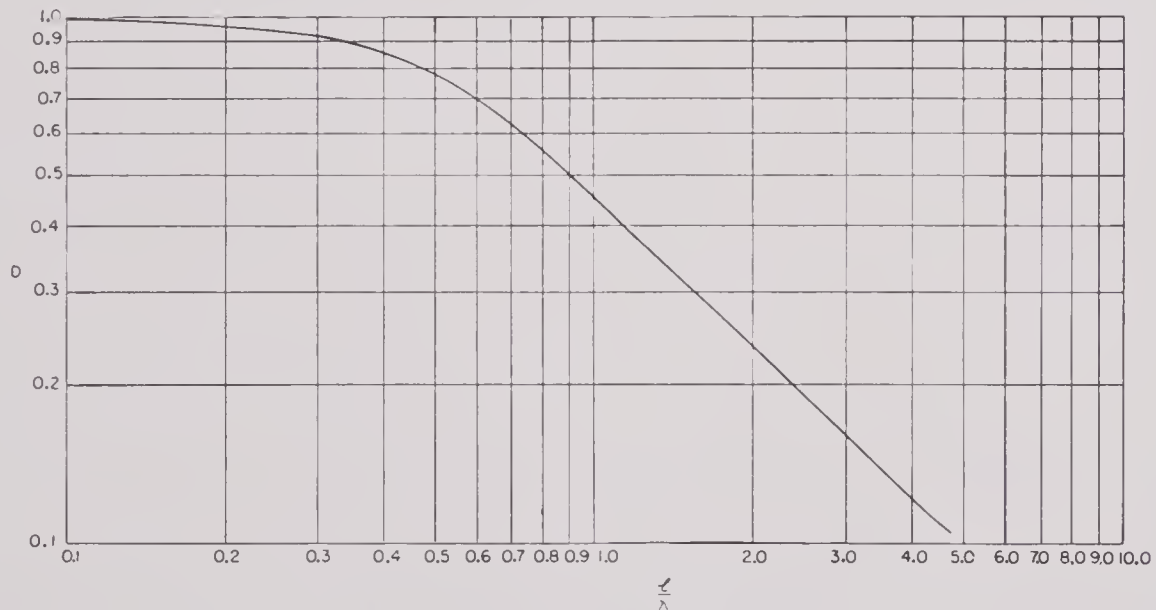


FIGURE 14. Directivity ratio D of a line source of length l to a signal of wave length λ . When $l/\lambda \gg 1$, then $D = \lambda/2l$.

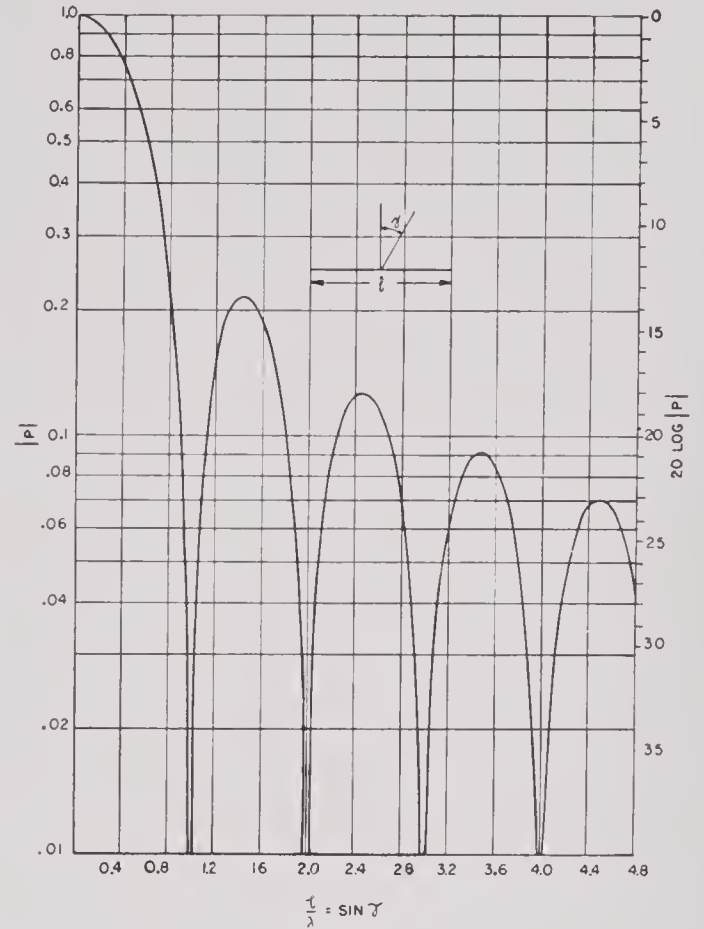


FIGURE 13. The pattern of a line source of length l in terms of the dimensionless parameter $(l/\lambda) \sin \gamma$, where λ is the wave length of the signal and γ is the angle between the normal to the line source and the direction of observation.

5.4.2

Shading

DISCRETE SHADING

The effect of shading on the pattern of line sources when $\psi = 0$ will be illustrated by considering two cases. First suppose that a line source of length l is divided into four equal segments, and suppose $f(x) = 1$ on the outer two segments and $f(x) = w$, a constant, on the inner two segments. The pattern of such a shaded line source is

$$P = \frac{2}{w+1} \left[\frac{\sin \phi}{\phi} + \frac{(w-1)}{2} \frac{\sin \frac{\phi}{2}}{\frac{\phi}{2}} \right],$$

so that the shading is parabolic; w is the ratio of the strength at the midpoint to that at the ends of the line source. The pattern is given by

$$P = j_0(\phi) + 2 \left(\frac{w-1}{w+1} \right) j_2(\phi),$$

where $\phi = (kl/2) \sin \gamma$ and $j_n(\phi)$ is the n th spherical Bessel function.⁶² These patterns for $w = 1, 2, 4, \dots, \infty$ are shown in Figure 18 and the corresponding directivity ratio curves are shown in Figure 19. Again it is clear that as the shading is increased the major lobe broadens while the minor lobes decrease and the directivity decreases, that is, the directivity ratio increases.

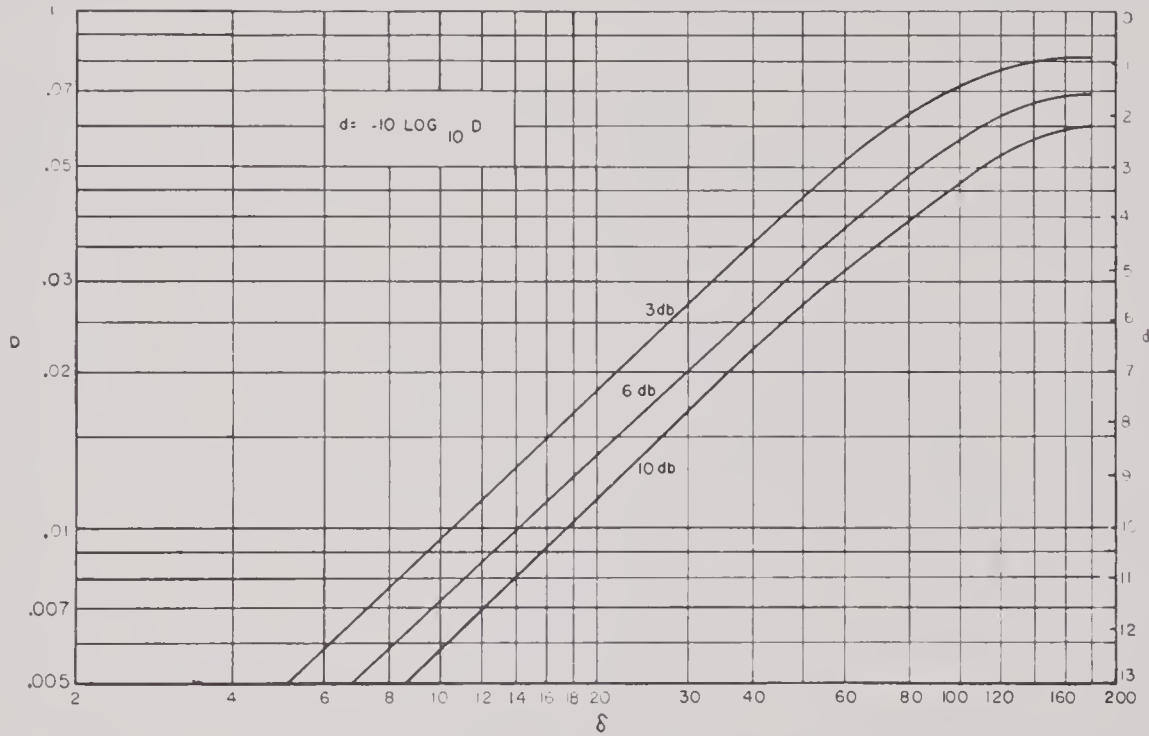


FIGURE 15. Directivity ratio D and directivity index d of a line source as a function of width δ of a pattern 3, 6, and 10 db from peak.

where $\phi = (kl/2) \sin \gamma$, and γ is the angle between the direction of observation and the normal to the line source. A family of patterns is shown in Figure 16 for $w = 1, 2, 3$, and 4. As w increases, the major lobe widens, while some minor lobes decrease as others increase. When $w = 1\frac{1}{2}$, the minor-lobe energy is almost equally distributed among the first three minor lobes. Figure 12 shows the patterns when $l = 2\lambda$. The directivity ratios of the patterns in Figure 16 are shown in Figure 17.

CONTINUOUS SHADING

Next suppose the line source of length l is continuously shaded and that

$$f(x) = 1 - \left(\frac{w-1}{w} \right) \left(\frac{2x}{l} \right)^2,$$

5.4.3 Product Theorem for Line Sources

Suppose a line source of length L is divided into N equal segments of length l and that $f(x)$ and ψ are constant on each segment, say $f(x) = Q_n$ and $\psi = \psi_n$ on the n th segment. By applying equation (12) to obtain the resultant pattern, it is found that

$$P = \frac{\sin \left(\frac{kl}{2} \sin \gamma \right)}{\left(\frac{kl}{2} \sin \gamma \right)} P'_0 \sum_n Q_n e^{j(nkl \sin \gamma + \psi_n)},$$

where P'_0 differs from P_0 by a simple constant factor. In the summation, n is integral if N is odd and is half an odd integer if N is even. It has just been shown

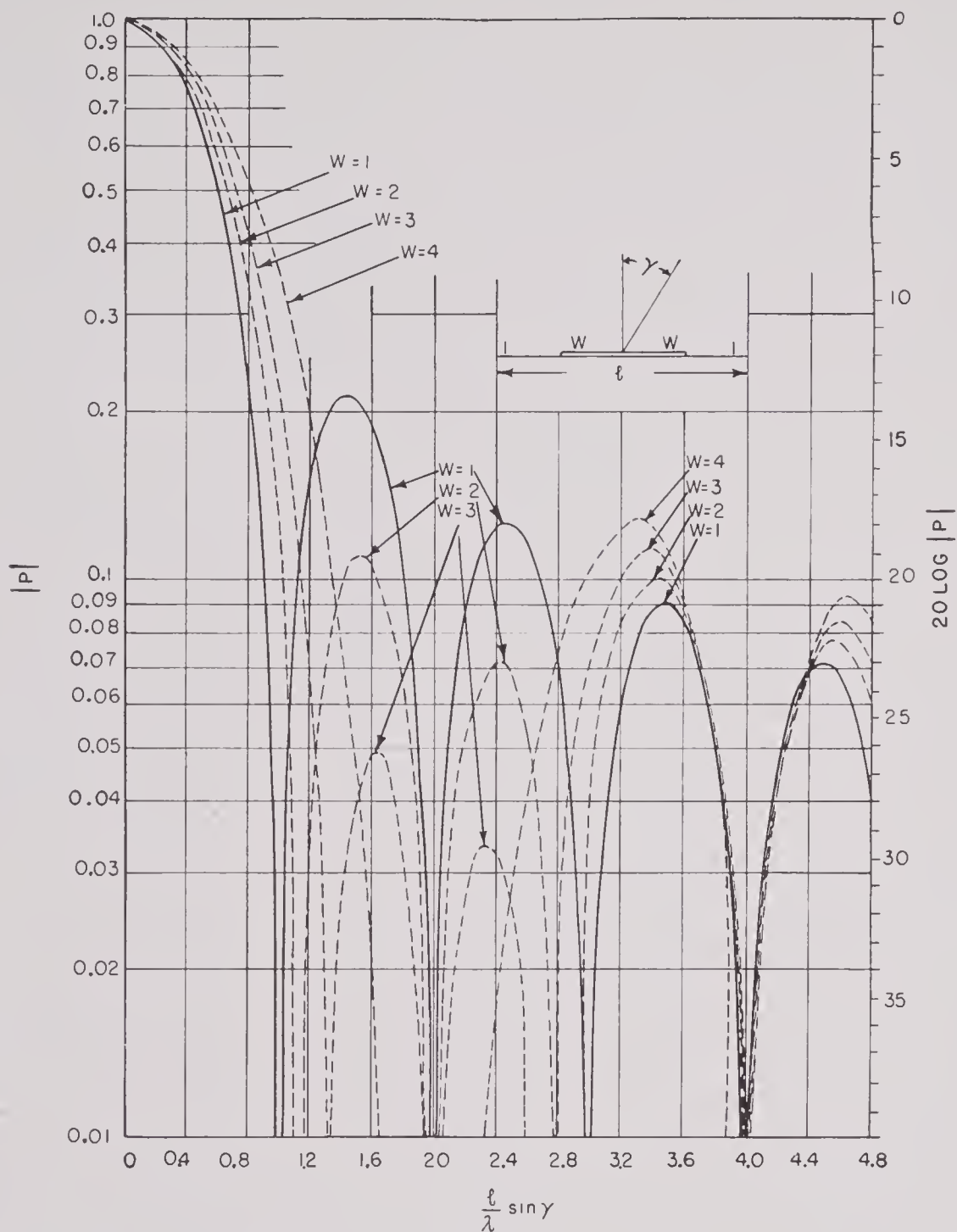


FIGURE 16. The pattern of a shaded segmented line source of length l in terms of the dimensionless parameter $(l/\lambda) \sin \gamma$. λ is the wave length of the signal and γ is the angle between the normal to the line source and the direction of observation. W is the ratio of the amplitude of the two middle elements to that of the two end elements.

that the pattern of a segmented line source is the product of the pattern of a single segment with the pattern of point sources having the strengths and phases of the segments and situated at similar points of corresponding segments. This is a special case of the more general product theorem discussed later in the chapter.

For example, the pattern of a line source consisting of four equal segments each of length a , all of the same phase but with the center two segments being w times as strong as the end two, is simply the pattern of equation (2) multiplied by the pattern of a line source of length a , or

$$P = \frac{\sin\left(\frac{ka}{2} \sin \gamma\right)}{\left(\frac{ka}{2} \sin \gamma\right)} \cdot \frac{1}{w+1} \left[w \cos\left(\frac{ka}{2} \sin \gamma\right) + \cos\left(\frac{3ka}{2} \sin \gamma\right) \right]$$

This pattern is shown in Figure 5 for $a = \lambda/2$ and $w = 1/2, 1, 2$, and 4 (the same cases as for the point sources). The improvement of the segmented line source pattern over the corresponding point source pattern is apparent.

responds to the Fourier series relation between the pattern of a line of point sources and the strengths of the point sources. It follows that

$$g(\mathbf{u}) = \frac{1}{2\pi} \int_{-\infty}^{\infty} e^{-j\phi \mathbf{u}} \frac{P(\phi)}{P_0} d\phi. \quad (14)$$

This permits prescribing the pattern $P(\phi)$ and finding the shading $g(\mathbf{u})$ of the line source to obtain the pattern. In general $g(\mathbf{u})$ will not be 0 for $|\mathbf{u}| > kl/2$, no matter how large kl , so that the effect on the pattern of having a line source of finite length must be evaluated; that is, the contribution of the neglected part of the line source must be below prescribed limits. This is similar to the procedure followed for a

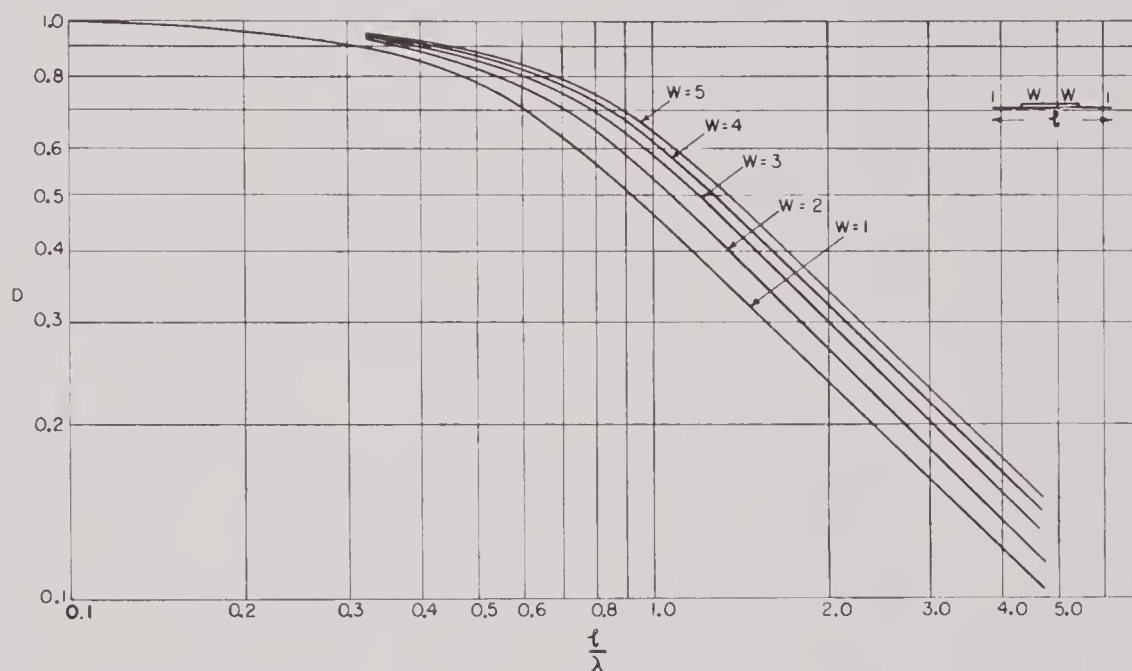


FIGURE 17. The directivity ratio of a shaded, segmented line source of length l to a signal of wave length λ . W is the ratio of amplitude of the two middle elements to that of the two outer elements.

5.4.4 Fourier Integral Relation between Pattern and Strength Function

If ψ is considered to be zero in equation (12) and a simple change of variable is made inside the integral sign,

$$P(\phi) = P_0 \int_{-kl/2}^{kl/2} g(\mathbf{u}) e^{j\mathbf{u}\phi} d\mathbf{u},$$

where $\phi = \sin \gamma$, $\mathbf{u} = kx$, $g(\mathbf{u}) = f(\mathbf{u}/k)$. If $g(\mathbf{u})$ is set equal to zero when $|\mathbf{u}| > kl/2$,

$$P(\phi) = P_0 \int_{-\infty}^{\infty} e^{j\mathbf{u}\phi} g(\mathbf{u}) d\mathbf{u}. \quad (13)$$

This Fourier integral relation between the pattern of a line source and the shading of the line source cor-

responds to the Fourier series relation between the pattern of a line of point sources; the method is illustrated in the following example.

5.4.5 Designing for a Gaussian Pattern

Consider the Gaussian pattern

$$P = e^{-(\phi/\Delta)^2}, \quad (15)$$

where $\phi = \sin \gamma$. For small Δ this is sharply peaked at $\gamma = 0$ and the breadth of the peak increases with increasing Δ . By substitution and integration in equation (14),

$$g(\mathbf{u}) = \frac{\Delta}{2\sqrt{\pi}} e^{-(\Delta \mathbf{u}/2)^2}. \quad (16)$$

It is clear that the source required to give a true

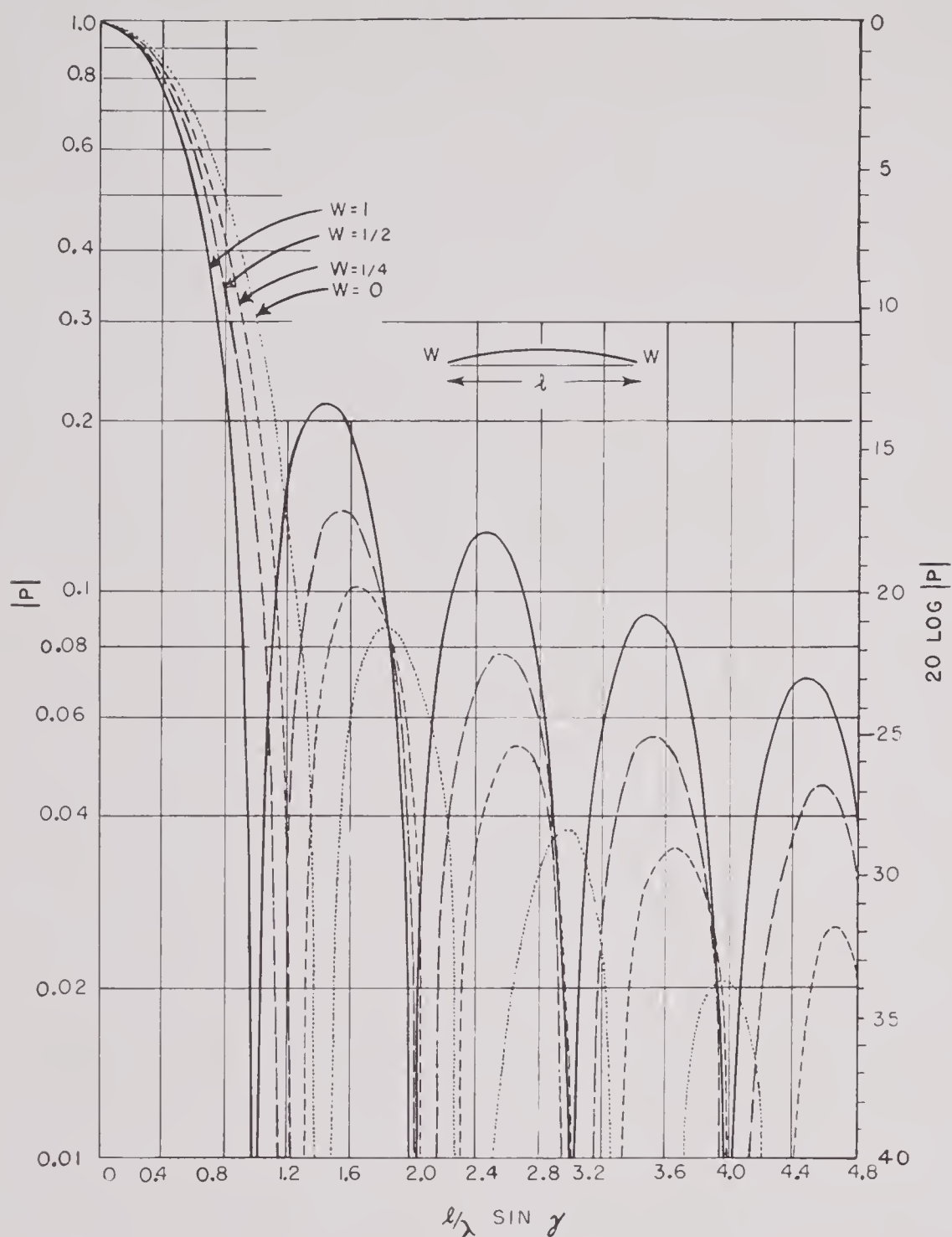


FIGURE 18. The pattern of a parabolically shaded line source of length l in terms of the dimensionless parameter $(l/\lambda) \sin \gamma$. λ is the wave length of the signal and γ is the angle between the normal to the line source and the direction of observation. W is the ratio of the amplitude at the ends to the amplitude at the midpoint of the line source.

Gaussian pattern is infinitely broad, since the equation above gives a nonzero value of $g(u)$ for all finite values of u . However, as u increases above the value 2Δ , $g(u)$ falls very rapidly and the effective part of the radiator is quite limited. The question then is where the radiator can be chopped off without materially affecting the pattern. This can be answered by substituting $g(u)$ into equation (13) and inte-

grating between the finite limits, say $u = \pm kl/2$. Then

$$\begin{aligned}
 P(\phi) &= \frac{\Delta}{2\sqrt{\pi}} \int_{-kl/2}^{kl/2} e^{-(\Delta u)^2 + ju\phi} du \\
 &= e^{-(\phi/\Delta)^2} - \frac{2}{\sqrt{\pi}} \int_{\Delta kl/4}^{\infty} e^{-t^2} \cos\left(\frac{2\phi}{\Delta} t\right) dt.
 \end{aligned}$$

CONFIDENTIAL

The alteration in the Gaussian pattern introduced by cutting off the radiator at $u = \pm kl/2$, or $x = \pm l/2$, is measured by the second term of the equation above. This term is never larger than

$$E = \frac{2}{\sqrt{\pi}} \int_{\Delta kl/4}^{\infty} e^{-t^2} dt = \text{Erfc}\left(\frac{\Delta kl}{4}\right).$$

The quantity $1 - E$ is tabulated in Jahnke and Emde,⁶³ and Peirce.⁶¹ For example, consider the three

while the height of the minor lobe is

$$h = \frac{E}{1 - E}.$$

Further, if w is the ratio of the width of the resulting major lobe to the width of the major lobe of a uniform line source,

$$w = \frac{10}{11} \left(\frac{\Delta kl}{4} \right).$$

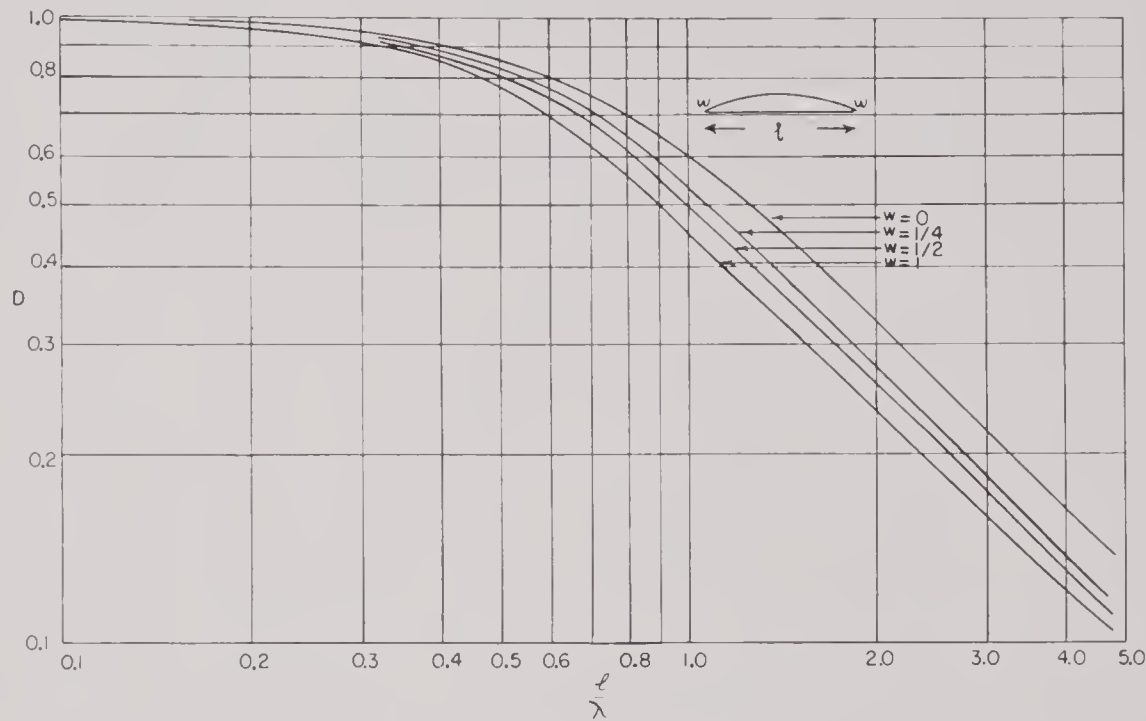


FIGURE 19. Directivity ratio of a parabolically shaded line source of length l to a signal of wave length λ . W is the ratio of the amplitude at the ends to the amplitude at the midpoint of the line source.

cases in which the minor lobe is required to be 30 db, 40 db, and 50 db below the major lobe, which means that E must be 0.0316, 0.0100, and 0.0032 respectively. Then $\pi/2 \cdot l/\lambda \cdot \Delta$ must have the values 1.520, 1.821, and 2.084 respectively. To illustrate, a radiator 3 wave lengths long with 30-db minor lobes gives $\Delta = 0.323$, which is a pattern whose major lobe is approximately 38 degrees wide across the $1/e$, or 8.68 db points.

From the analysis above, a relationship may be obtained between the amplitude at which the radiator is cut off and the height of the first minor lobe. The ratio of the amplitude at the cutoff to that at the center of the line source is

$$r = \frac{f\left(\frac{l}{2}\right)}{f(0)} = e^{-(\Delta kl/4)^2},$$

Thus h and w may be considered functions of r and are plotted in Figure 20. The above relations for h and w hold only when r is small. When r is large, say between $1/10$ and 1, the shading is close to parabolic shading, for which the patterns have already been obtained (see Figure 18). These patterns were used to get h and w for large r .

5.5

RADIATING SURFACES

Thus far simple arrays of point and line sources have been discussed and it may have seemed that undue emphasis has been placed on the patterns of such sources, since actual radiators involve vibrating surfaces. However, the results on point and line sources have much greater applicability than heretofore indicated; in particular, it will be shown that the pattern of a flat source in any plane normal to the

surface of the source is the same as the pattern of a line source with an appropriately chosen line-strength function.

5.5.1 Baffle Conditions

Three kinds of baffle conditions will be considered: (1) that in which the source is set in an infinite-plane stiff baffle, (2) that in which the source is set in an infinite-plane release baffle, and (3) that in which the source has no baffle. A surface is called *stiff* if its normal velocity is zero and *release* if the pressure at all points of the surface is zero.

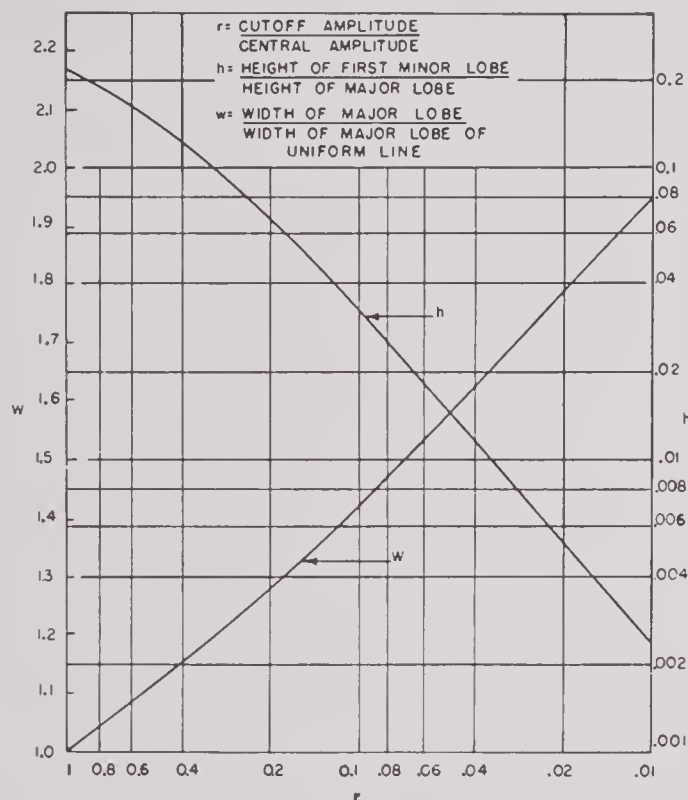


FIGURE 20. The relation between the cutoff amplitude, height of first minor lobe, and width of major lobe of a Gaussian shaded line source.

5.5.2 Nonbaffle Conditions

The nonbaffle condition also requires a word of explanation. It is clear that the body of a transducer will always act as a self-baffle, so that it is not possible to escape some sort of baffle condition in any case. Such baffle conditions are extremely difficult to analyze. J. K. L. MacDonald¹⁶ has considered the case in which a vibrating circular disk is set in the end of a semi-infinite cylinder; the cylinder is supposed to be an idealized approximation to the body of the transducer. He found that when the radius of

the disk is of the order of λ to 4λ (with λ the wave length of the signal) the pattern obtained is the same as that in which the disk is set in an infinite-plane stiff baffle multiplied by the factor $\frac{1}{2}(1 + \cos \gamma)$, where γ is the angle between the direction of observation and the normal to the disk. This rule has been adopted in the following to obtain patterns under the nonbaffle condition even when the face of the

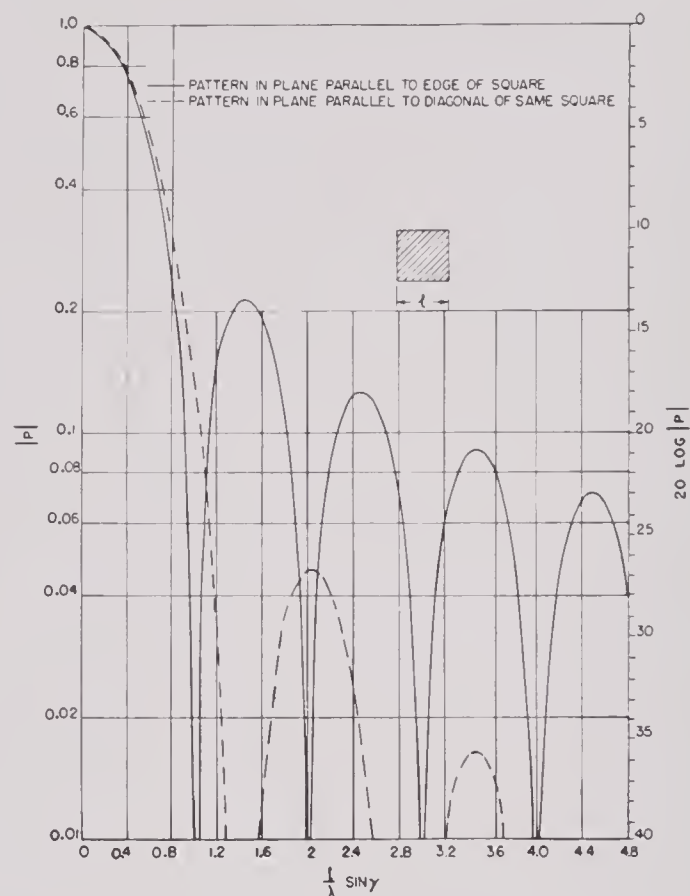


FIGURE 21. The pattern of a square source of side l as a function of the dimensionless parameter $(l/\lambda) \sin \gamma$. λ is the wave length of the signal and γ is the angle between the normal to the surface of the source and the direction of observation.

transducer is not circular. It places the nonbaffle condition between the stiff- and release-baffle conditions, since the pattern of a radiator in an infinite-plane release baffle may be obtained from the pattern in a stiff baffle by multiplying by the factor $\cos \gamma$.²¹

5.5.3 Patterns

The patterns produced by plane surface radiators are a little more complex than those of line sources. This is so because line sources have an axis of symmetry (the line itself), whereas plane sources in general do not. In dealing with line sources the pattern

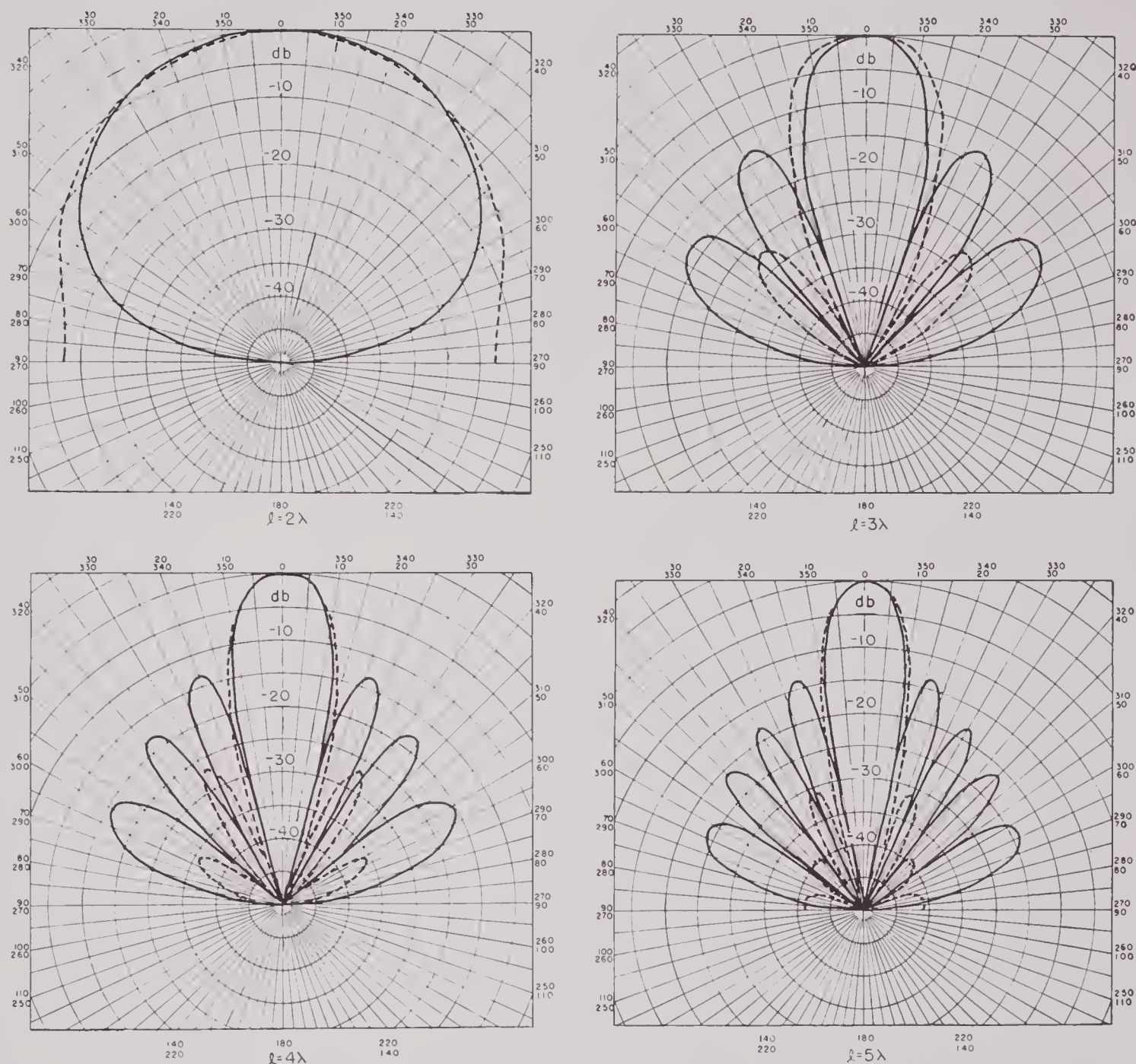


FIGURE 22. The pattern of a square of length l for a signal of wave length λ . The solid curve is the pattern in a plane parallel to a side, the dotted curve is the pattern in a plane parallel to the diagonal of the square.

was considered only for directions lying in the plane, including the line source. In dealing with plane sources, on the other hand, the pattern in all directions must be observed. A complete representation requires a three-dimensional graph of the pattern. In practice only those directions lying in some plane including the normal to the active surface will be examined at one time. For example, in examining the pattern produced by a square radiator, consider first the pattern in a plane parallel to an edge, then in a plane parallel to a diagonal, and finally the patterns in intervening planes.

The pattern of a plane-faced radiator set in an infinite-plane stiff baffle is given by

$$P(\mathbf{u}) = P_0 \int_S F(\mathbf{r}) e^{jk(\mathbf{r} \cdot \mathbf{u})} dS. \quad (17)$$

Here dS is an element of the active surface S ; \mathbf{r} is the vector from an arbitrarily chosen origin O in S to dS ; \mathbf{u} is a unit vector in the direction of observation with origin at O , and k is the wave number of the signal, that is $k = 2\pi/\lambda$, λ being the wave length of the

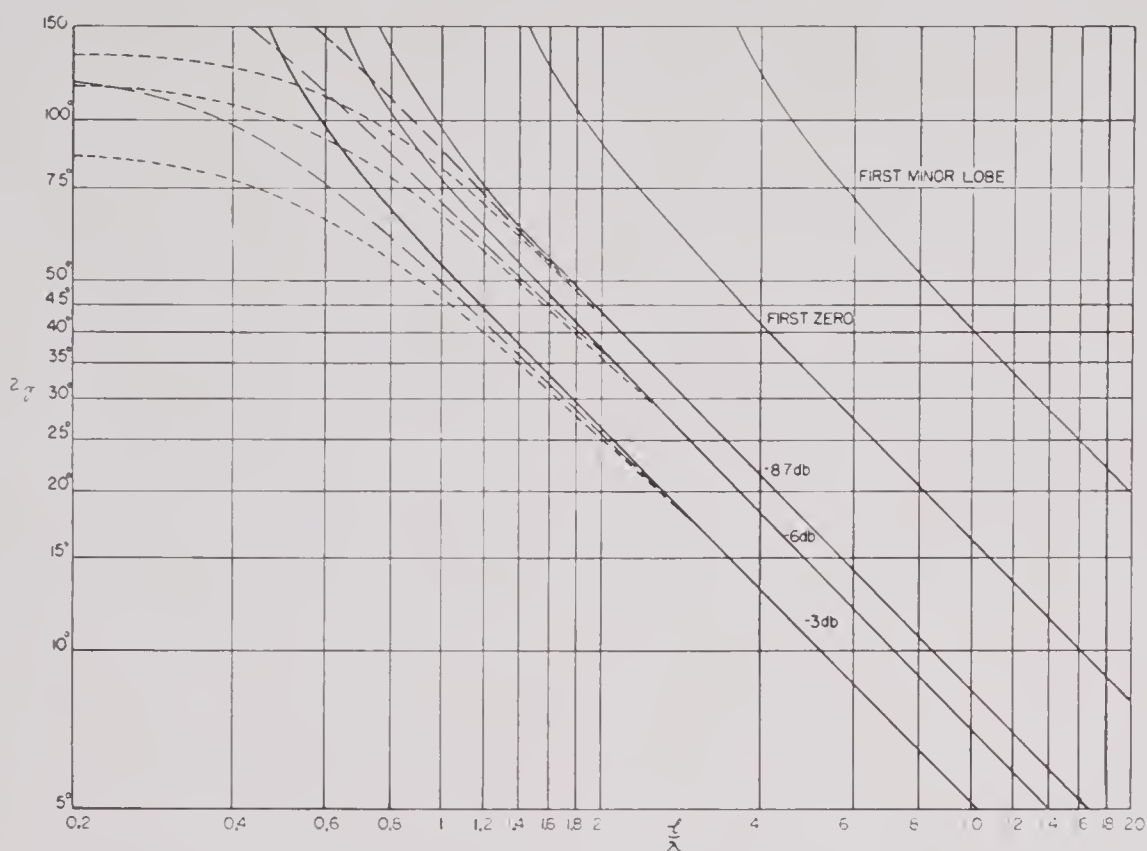


FIGURE 23. The total pattern width 2γ of a square source in a plane parallel to an edge; l is the length of a side of the square source and λ is the wave length of the signal. The baffle conditions are: ——— stiff baffle; - - - no baffle; - - - - pressure-release baffle.

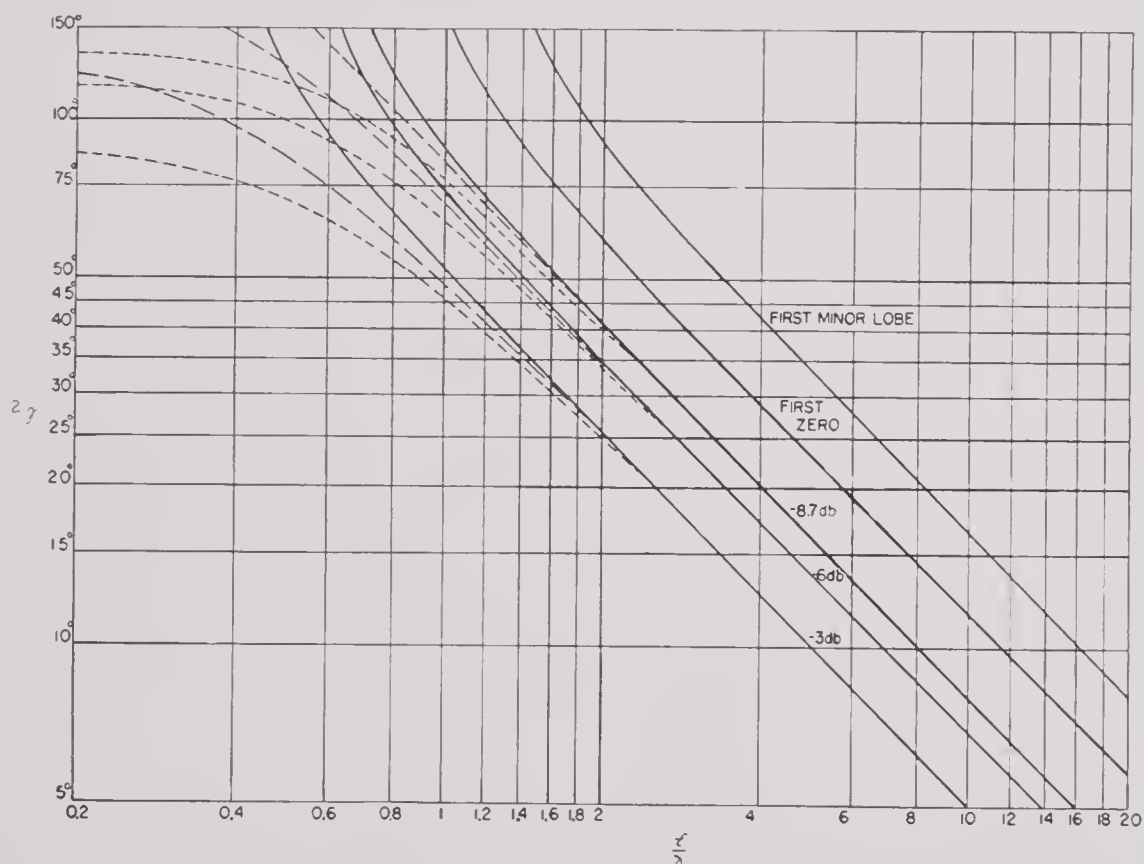


FIGURE 24. The total pattern width 2γ of a square source in a plane parallel to a diagonal. l is the length of a side of the square source and λ is the wave length of the signal. Baffle conditions are indicated in the same manner as for Figure 23.

CONFIDENTIAL

signal. $F(\mathbf{r})$ is the velocity of the element of surface dS and may be complex, since portions of S may be out of phase. P_0 is a normalizing factor.

Let a rectangular coordinate system be set up whose axis is normal to the face of the source and whose x and y axes lie in the face of the source. The unit vector \mathbf{u} has the components $\cos \alpha$, $\cos \beta$, $\cos \gamma$, where α , β , and γ are the angles between the direction of observation and the coordinate axes x , y , z , respectively. Equation (17) can now be written

$$P(\alpha, \beta, \gamma) = P_0 \iint_S F(x, y) e^{jk(x \cos \alpha + y \cos \beta)} dx dy. \quad (18)$$

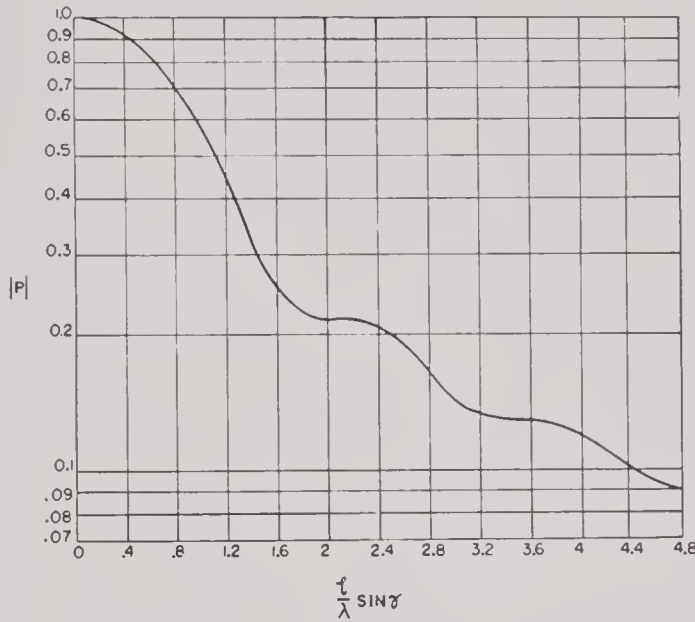


FIGURE 25. The amplitude pattern of an isosceles right triangle in a plane normal to the hypotenuse in terms of the dimensionless parameter $(l/\lambda) \sin \gamma$. l is the length of a side of the triangle, λ is the wave length of the signal, and γ is the angle between the normal to the source and the direction of observation.

Consider, for example, the pattern in the $x - z$ plane (the plane $\beta = 90^\circ$, $\cos \beta = 0$). By writing

$$f(x) = \int F(x, y) dy,$$

then

$$P = P_0 \int f(x) e^{jkx \sin \gamma} dx,$$

where the proper limits of integration must be taken. Comparison with equation (12) justifies the previous assertion concerning the equivalence of line source patterns and patterns of flat-surface sources in planes normal to the surface.

To prove even more, suppose the strength function $F(x, y)$ has the form

$$F(x, y) = g(x) h(y).$$

Then equation (18) takes the form

$$P = P_0 \int g(x) e^{jkx \cos \alpha} dx \int h(y) e^{jky \cos \beta} dy.$$

The first integral is the radiation pattern produced by a line source of strength $g(x)$ along the x axis and the second is the pattern of a source of strength $h(y)$ along the y axis. Since $g(x)$ and $h(y)$ are arbitrary

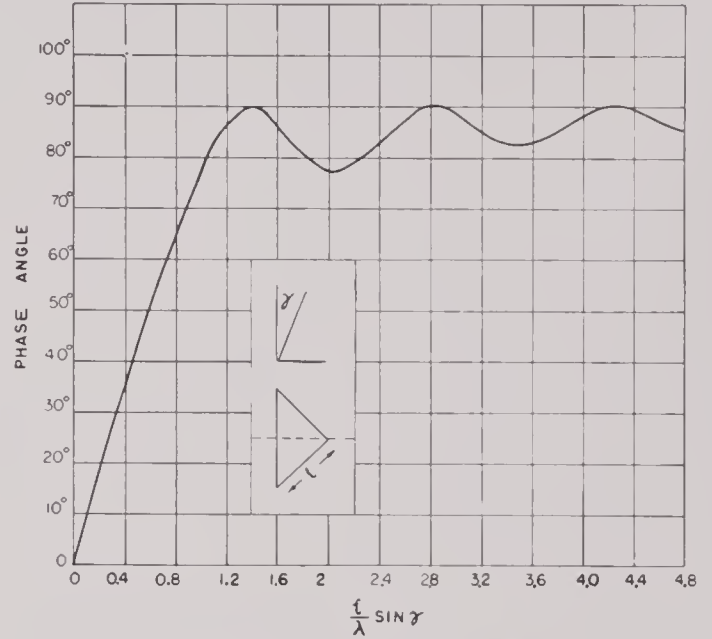


FIGURE 26. The phase pattern of an isosceles right triangle in a plane normal to the hypotenuse in terms of the dimensionless parameter $(l/\lambda) \sin \gamma$. l is the length of a side of the triangle, λ is the wave length of the signal, and γ is the angle between the normal to the source and the direction of observation.

and since the pattern in the $x - z$ plane is determined by $g(x)$ alone and the pattern in the $y - z$ plane by $h(y)$ alone, it has been shown that *it is possible to prescribe the pattern of a flat radiator in two normal planes*. For example, suppose the same Gaussian pattern of equation (15) is desired in two planes. Then both $g(x)$ and $h(y)$ must have the form of equation (16); therefore

$$\begin{aligned} F(x, y) &= f(kx) f(ky) \\ &= \frac{\Delta^2}{4\pi} e^{-(\Delta kx/2)^2 - (\Delta ky/2)^2} \\ &= \frac{\Delta^2}{4\pi} e^{-(\Delta r/2)^2} \end{aligned}$$

where $\mathbf{r}^2 = x^2 + y^2$. The source distribution in this case has circular symmetry in the $x - y$ plane.

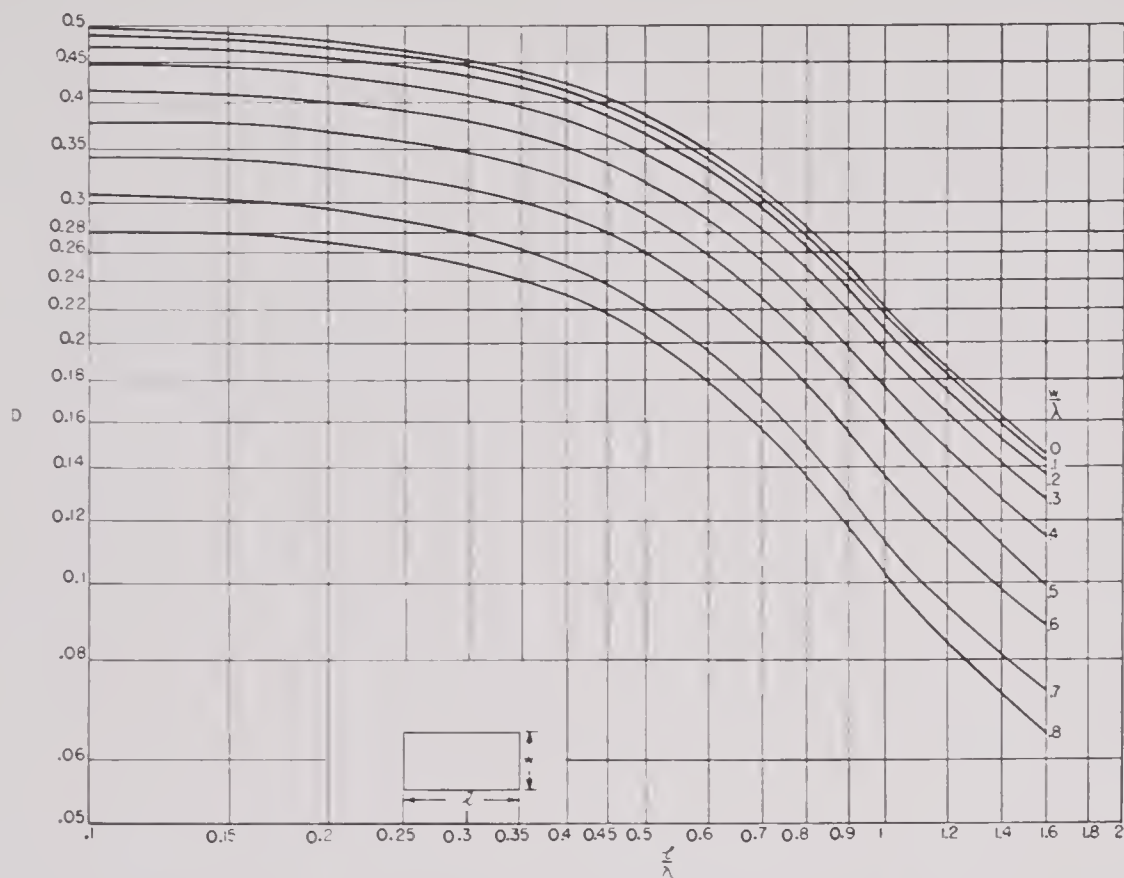


FIGURE 27. The directivity ratio D of a flat rectangular source of sides l and w in a stiff baffle. λ is the wave length of the signal.

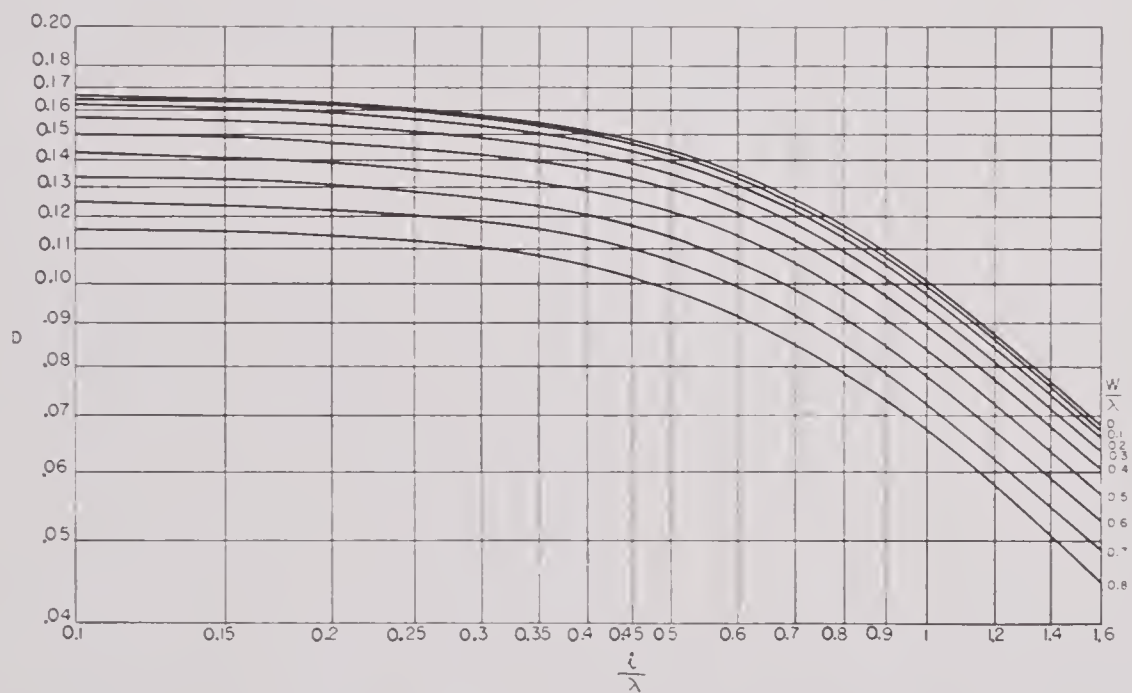


FIGURE 28. The directivity ratio of a flat rectangular source of sides l and w in a release baffle. λ is the wave length of the signal.

CONFIDENTIAL

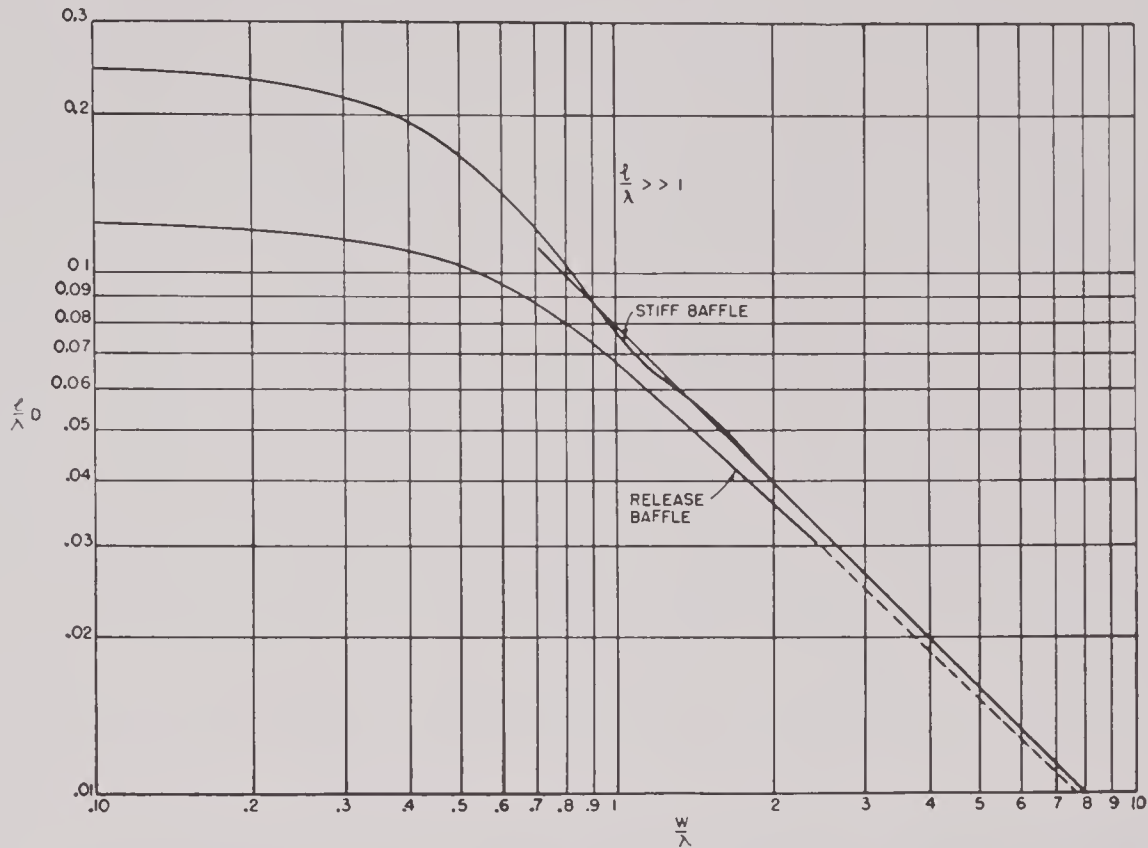


FIGURE 29. The directivity ratio D of a long rectangular source of length l and width w to a signal of wave length λ .

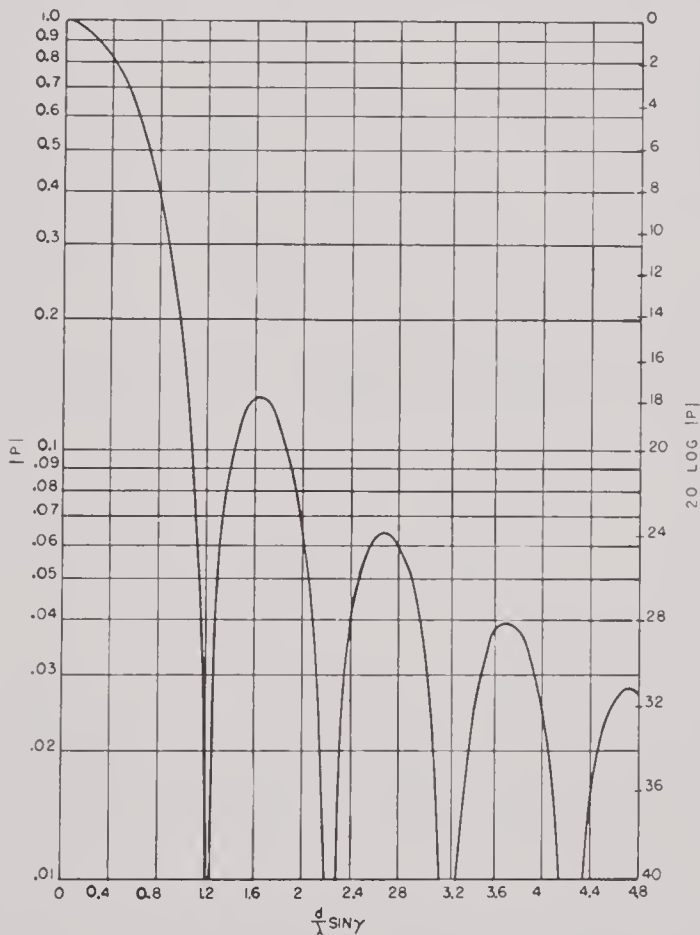


FIGURE 30. The pattern of a flat circular source of diameter d in terms of the dimensionless parameter $(d/\lambda) \sin \gamma$. λ is the wave length of the signal and γ is the angle between the normal to the plane of the source and the direction of observation.

5.5.4

Product Theorem

Before a discussion of particular patterns is started, the product theorem, a general and useful result of research on directivity patterns,² should be stated. Consider a number of radiators of the same frequency and of identical pattern and orientation in space but possibly with different strengths and phases of motion. Then, if the reaction of one radiator on the other is neglected, the pattern produced by the aggregate of the radiators is the pattern produced by an aggregate of point sources having the same distribution in space and the same strengths and phases of motion as the actual radiators, multiplied by the pattern of a single radiator.

5.5.5

Various Sources

RECTANGULAR SOURCES

It is a simple matter to apply equation (18) to obtain the pattern of a rectangular source of uniform amplitude and phase in a stiff baffle. The x, y coordinate axes are taken parallel to the sides of the rec-

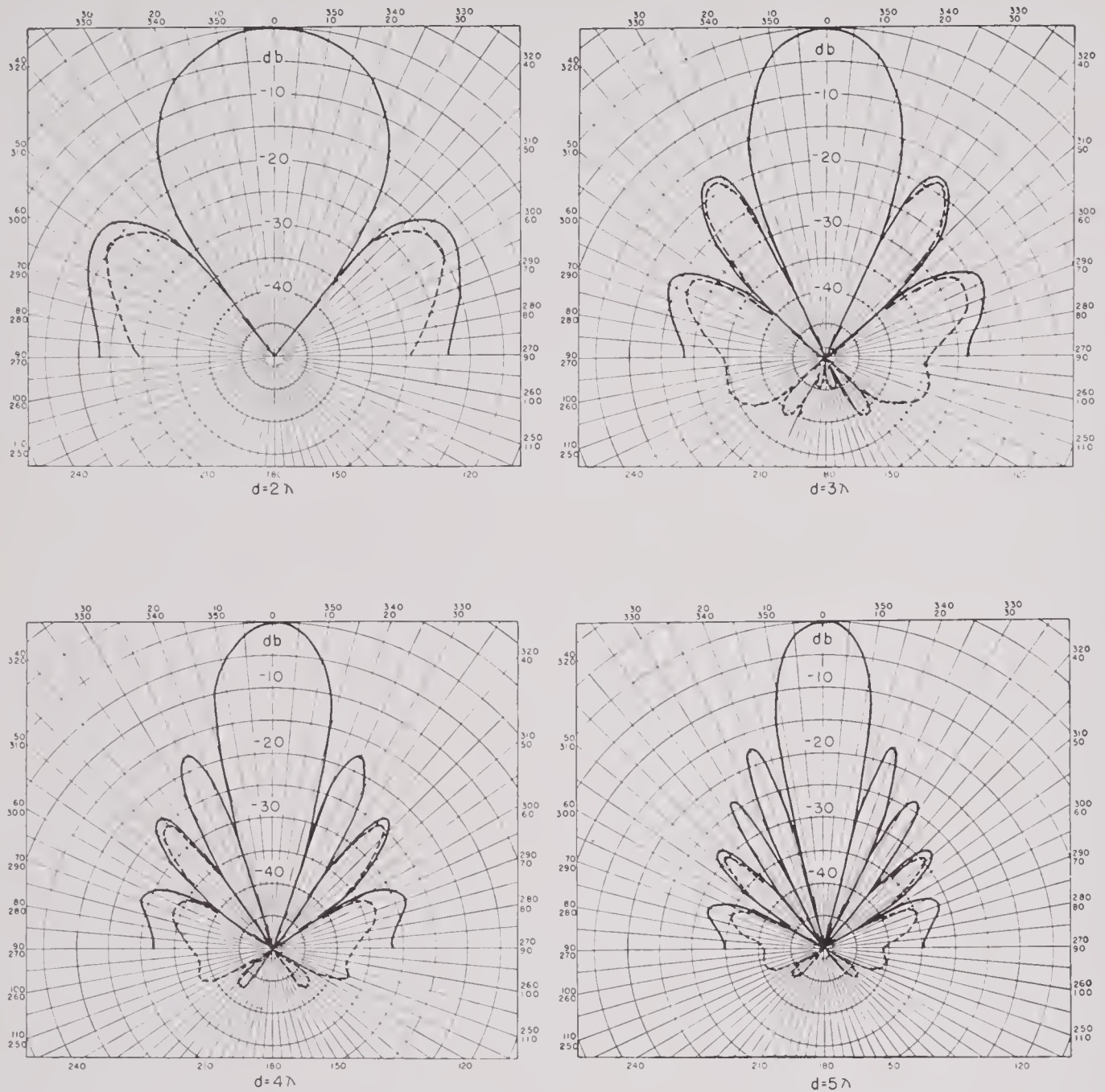


FIGURE 31. The pattern of a circular disk of diameter d in stiff (solid curve) and release (dotted curve) baffles. λ is the wave length of the signal.

tangle with origin at the center. By putting $F(x,y) = 1$ and $P_0 = 1/lw$, where l is the length and w the width of the rectangle, it is found that

$$P = \frac{\sin\left(\frac{kl}{2} \cos \alpha\right)}{\left(\frac{kl}{2} \cos \alpha\right)} \frac{\sin\left(\frac{kw}{2} \cos \beta\right)}{\left(\frac{kw}{2} \cos \beta\right)}.$$

SQUARE SOURCES

In a plane parallel to an edge of the rectangle, say the length, $\beta = 90^\circ$, $\cos \beta = 0$, and $\cos \alpha = \sin \gamma$, so that

$$P = \frac{\sin\left(\frac{kl}{2} \sin \gamma\right)}{\left(\frac{kl}{2} \sin \gamma\right)}. \quad (19)$$

By comparison with equation (11) this pattern is seen to be the same as that of a uniform line source of length l and is shown in Figure 13. Thus all the results on uniform line sources and segmented line sources of variable strength and progressive phasing may be carried over to segmented rectangular or square sources.

minor lobe as a function of the size of the transducer (l/λ). For this purpose the curves on Figures 23 and 24 have been drawn. The first gives the pattern structure of a square in a plane parallel to an edge, and the second, in a plane parallel to a diagonal under three baffle conditions. It will be noticed that only when $l/\lambda < 2$ is the effect of the baffle appreciable.

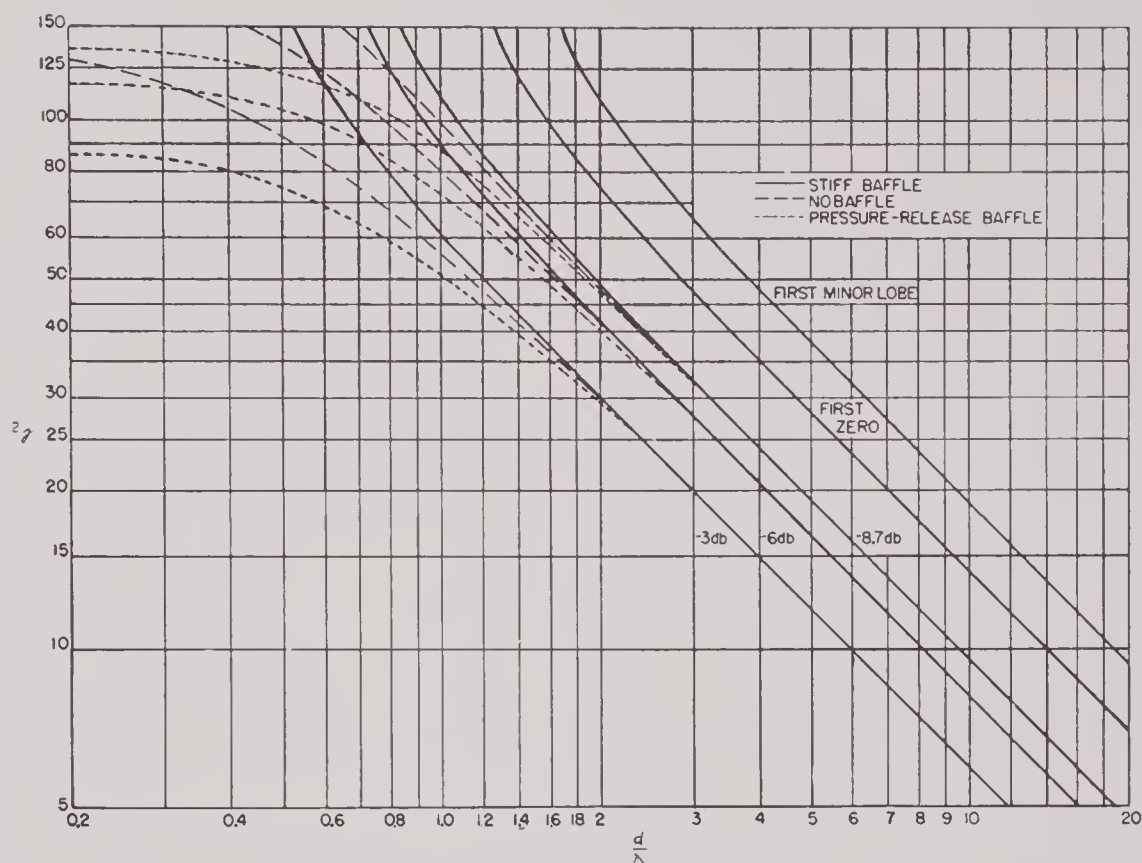


FIGURE 32. Total pattern width 2γ of a circular disk of diameter d to a signal of wave length λ .

If the radiator is a square, in a plane parallel to the diagonal of the square, $\alpha = \beta$ and

$$\cos \alpha = \cos \beta = \frac{1}{\sqrt{2}} \sin \gamma,$$

so that

$$P = \frac{\sin^2 \left(\frac{kd}{4} \sin \gamma \right)}{\left(\frac{kd}{4} \sin \gamma \right)^2}, \quad (20)$$

where $d = \sqrt{2}l$ is the length of the diagonal of the square. Patterns (19) and (20) are plotted in Figure 21 against the parameter $(l/\lambda) \sin \gamma$. The patterns for the particular dimensions $l = 2\lambda$, 3λ , 4λ , and 5λ are shown in Figure 22.

It is sometimes desirable to study the width of the major lobe and the height and position of the first

A square radiator is sometimes split along a diagonal and the two halves phased differently to form a shifted lobe pattern. It then becomes of interest to know the pattern of each half of the split square. The pattern of one of the halves in a plane perpendicular to the diagonal is given by

$$P = \frac{1}{2} \frac{\sin^2 \left(\frac{kd}{4} \sin \gamma \right)}{\left(\frac{kd}{4} \sin \gamma \right)^2} + \frac{j}{\left(\frac{kd}{2} \sin \gamma \right)}.$$

$$\left[1 - \frac{\sin \left(\frac{kd}{2} \sin \gamma \right)}{\left(\frac{kd}{2} \sin \gamma \right)} \right],$$

where d is the length of the diagonal of the square and γ is the angle between the direction of observation and the normal to the face of the square; it is taken as positive when the direction of observation

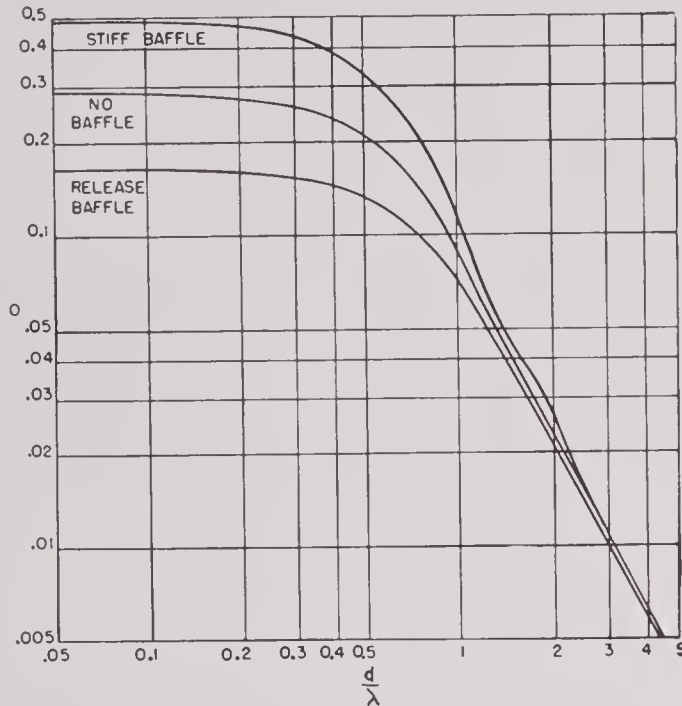


FIGURE 33. The directivity ratio D of a flat circular source of diameter d for a signal of wave length λ under various baffle conditions.

makes an acute angle with the source and as negative in all other cases. The complex time factor is assumed to be $e^{j\omega t}$. The pattern of the other half of the square is the conjugate complex quantity P^* . Figures 25 and 26 show the amplitude and phase patterns of P plotted against $(l/\lambda) \sin \gamma$, where $l = 1/\sqrt{2} d$ is the length of the side of the square.

The directivity ratio of a rectangular transducer with long length (l) and large width (w) is simply

$$D = \frac{\lambda^2}{4\pi lw} = \frac{\lambda^2}{4\pi_{(\text{area})}}. \quad (21)$$

However, when either l or w or both are small compared with λ , this formula for D , which is independent of baffle conditions, does not hold.

In Figures 27 and 28 the directivity ratio of a rectangular source when both dimensions are small is given under stiff- and release-baffle conditions. The directivity ratio when only one of the dimensions is small is given in Figure 29.

DISKS

The pattern of a circular disk vibrating as a piston in a stiff baffle can be obtained from equation (18)

by first changing to polar coordinates with the origin at the center of the disk. When the shading is circularly symmetric,

$$F(x, y) = f(r),$$

where $r^2 = x^2 + y^2$, and

$$P = 2\pi P_0 \int_0^{d/2} f(r) J_0(kr \sin \gamma) r dr.$$

Here d is the diameter of the disk and γ is the angle between the direction of observation and the normal to the disk. $J_n(z)$ is the n th order Bessel function of argument z and is tabulated in Jahnke and Emde.⁶³

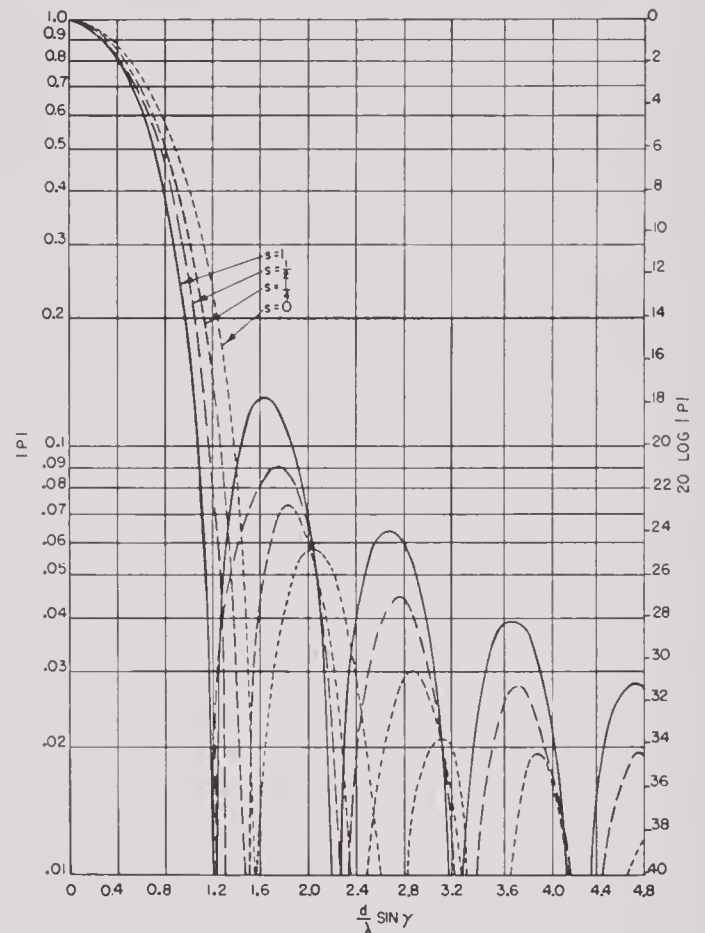


FIGURE 34. The pattern of a parabolically shaded circular source of diameter d in a stiff baffle in terms of the dimensionless parameter $(d/\lambda) \sin \gamma$. λ is the wave length of the signal and γ is the angle between the normal to the plane of the source and the detection of observation. s is the ratio of the amplitude at the edge to the amplitude at the center of the source.

When the disk has uniform strength and phase ($f(r) \equiv 1$), and if P_0 is chosen appropriately,

$$P = 2 \frac{J_1\left(\frac{kd}{2} \sin \gamma\right)}{\left(\frac{kd}{2} \sin \gamma\right)}.$$

This pattern is shown in Figure 30, plotted against the parameter $(d/\lambda) \sin \gamma$. The particular patterns when $d = 2\lambda$, 3λ , 4λ , and 5λ are shown in Figure 31 for stiff- and non-baffle conditions. The structure of the pattern of a circular disk is shown in Figure 32, where the width of the major lobe and the position of the first minor lobe are shown as a function of d/λ under three baffle conditions.

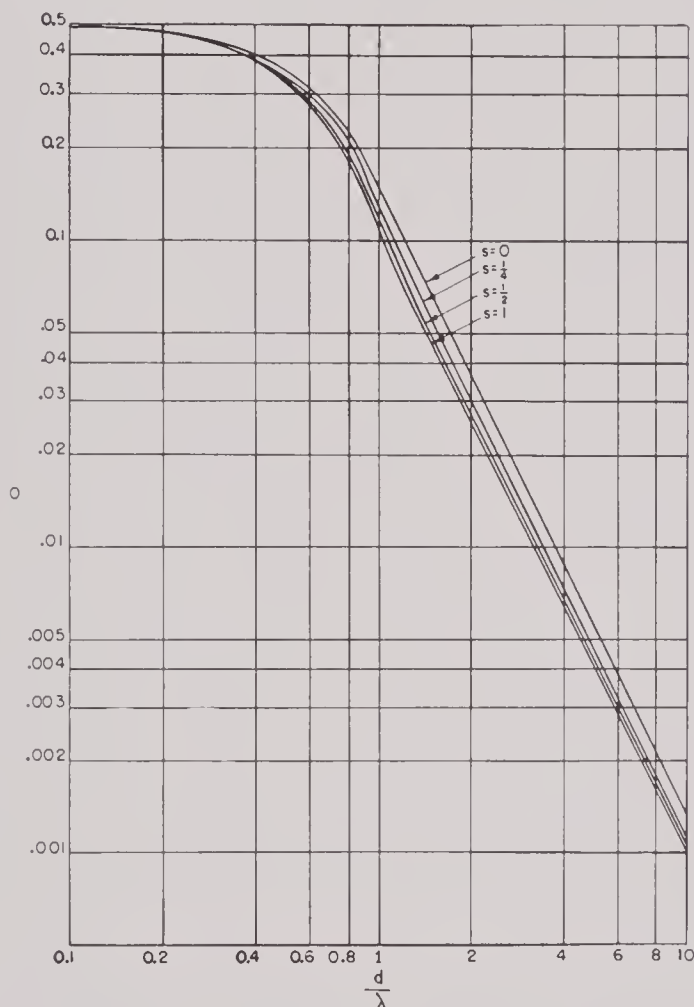


FIGURE 35. The directivity ratio of a parabolically shaded circular source of diameter d in a stiff baffle for a signal of wave length λ . s is the ratio of the amplitude at the edge to the amplitude at the center of the source.

The directivity ratio of the pattern of a circular disk in a stiff baffle is given by

$$D = \left(\frac{2}{kd}\right)^2 \left[1 - 2 \frac{J_1(kd)}{kd} \right].$$

When there is no baffle or the baffle is pressure release (the pressure over the surface of the baffle is zero), the expression for D is more complicated. In Figure 33 the D of a circular disk is plotted against d/λ under three baffle conditions. When the diameter

of the disk is large compared with the wave length of the signal,

$$D = \left(\frac{2}{kd}\right)^2,$$

which agrees with the general result of equation (21).

The pattern of a circular disk with parabolic shading has been computed. The shading function is

$$f(r) = 1 - (1 - s) \left(\frac{2r}{d}\right)^2,$$

where d is the diameter of the disk and s is the ratio of the amplitude of vibration at the edge to that at the center of the disk. The normalized pattern of such a source in a stiff baffle is

$$P = \frac{4}{1+s} \frac{J_1(z)}{z} + 4 \left(\frac{1-s}{1+s} \right) \frac{J_3(z)}{z},$$

where

$$z = \frac{kd}{2} \sin \gamma.$$

These patterns for $s = 1, \frac{1}{2}, \frac{1}{4}$, and 0 are shown in Figure 34, plotted against the parameter $(d/\lambda) \sin \gamma$. The effect of shading on minor lobe heights and on the width of the major lobe is clearly shown. The directivity ratio of these patterns and the corresponding patterns when the baffle is release are given in Figures 35 and 36.

Another type of radiator is a circular flexible diaphragm fixed at its edges and vibrating in its fundamental mode. Patterns for this case are given by Stenzel,⁵⁹ who finds that the central lobe is somewhat broader and the minor lobes lower than for a uniform piston, as is to be expected.

Sometimes a circular disk is split along a diameter so that the two halves may be phased separately to form a shifted lobe pattern. It is therefore of interest to find the pattern of a semicircular piston. In a plane normal to the diameter of the semicircle, the pattern in a stiff baffle is given by

$$P = \frac{J_1(z) + j[S_1(z)]}{z},$$

where

$$z = \frac{kd}{2} \sin \gamma,$$

d is the diameter of the semicircle, and γ is the angle between the direction of observation and the normal to the face of the source. $S_n(z)$ is the n th order

Struve function (see Jahnke and Emde^{63b} and Watson,⁶⁴ who denotes the Struve function by a boldface **H**). The amplitude and phase patterns of P are shown in Figures 37 and 38.

NOISE SIGNALS

All the pattern calculations above have been based on the assumption that the signal consisted of a single frequency. Excitation of a transmitter or microphone by a single frequency signal has some disadvantage on account of the standing-wave pat-

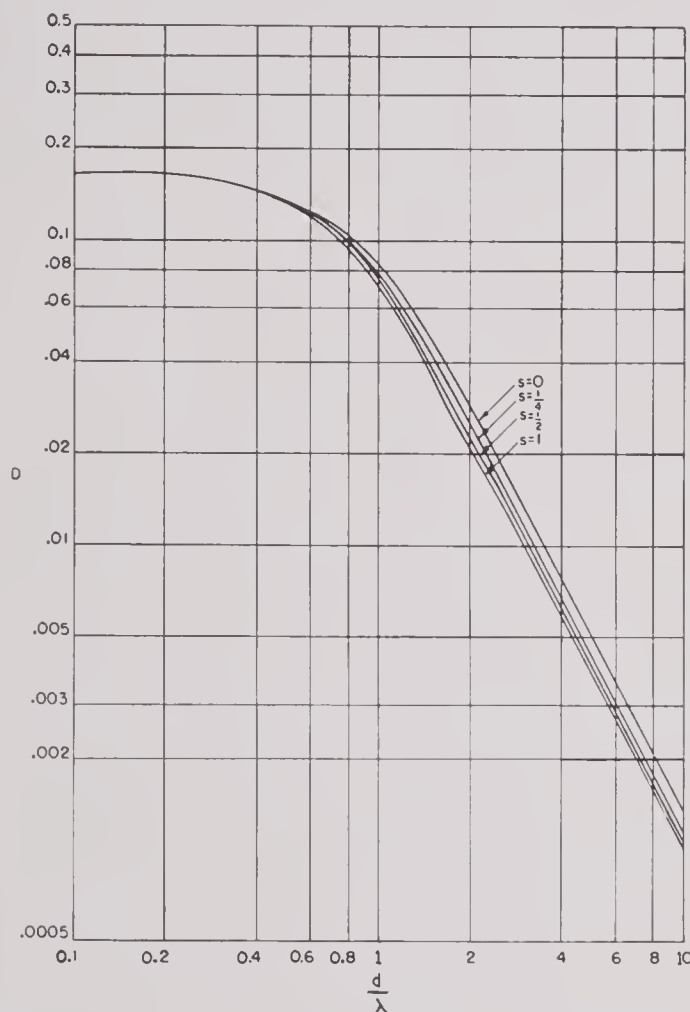


FIGURE 36. The directivity ratio of a parabolically shaded circular source of diameter d in a release baffle for a signal of wave length λ . s is the ratio of the amplitude at the edge to the amplitude at the center of the source.

tern which may be set up in the surrounding medium. To obviate this difficulty, a signal may be applied which has a band of frequencies with roughly uniform amplitude between the two limiting frequencies. This would produce a different standing-wave pattern for each frequency, so that the observed result is the average over the frequency band and hence does not

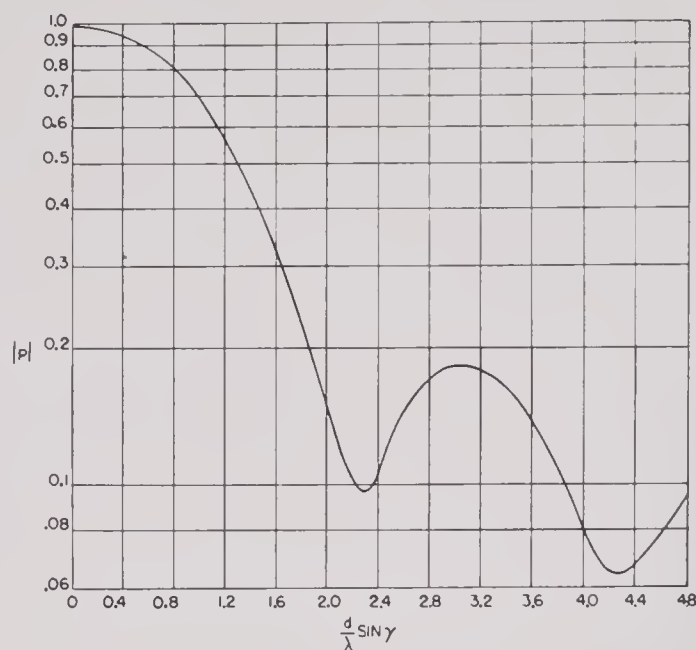


FIGURE 37. The amplitude pattern of a semicircular source of diameter d in a plane normal to the diameter in terms of the dimensionless parameter $(d/\lambda) \sin \gamma$. λ is the wave length of the signal and γ is the angle between the normal to the source and the direction of observation.

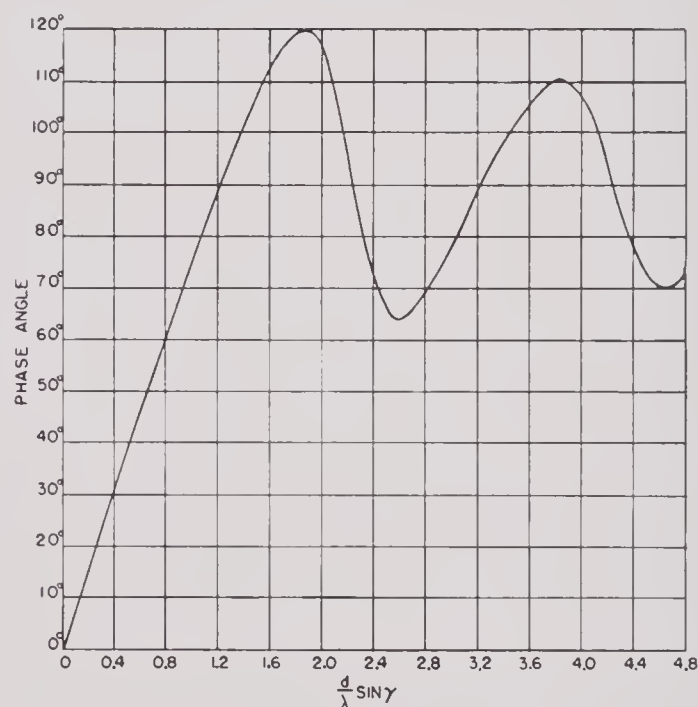


FIGURE 38. The phase pattern of a semicircular source of diameter d in a plane normal to the diameter in terms of the dimensionless parameter $(d/\lambda) \sin \gamma$. λ is the wave length of the signal and γ is the angle between the normal to the source and the direction of observation.

have such large fluctuations in space. The directional pattern for such excitations is also modified. Since the different frequencies are not related in phase, the

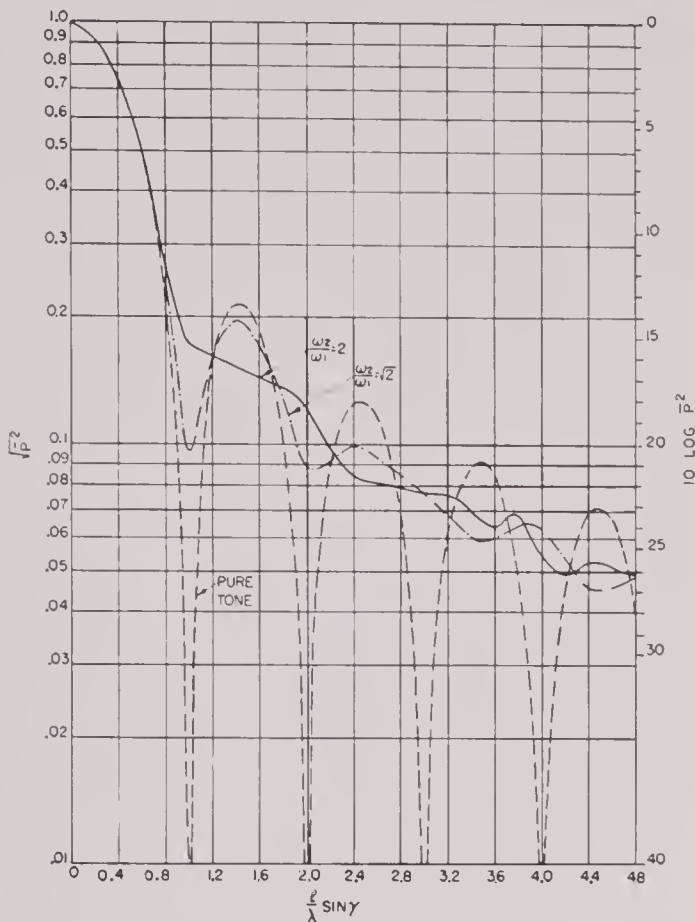


FIGURE 39. The intensity pattern of a line source of length l to a signal consisting of a band of frequencies from ω_1 to ω_2 . λ_0 is the wave length of the midband frequency $\omega_0 = \sqrt{\omega_1 \omega_2}$ and γ is the angle between the normal to the line source and the direction of observation.

intensity rather than the amplitude must be averaged to obtain the intensity pattern:

$$\bar{P}^2 = P_0^2 \int |A(\omega)|^2 |P(\omega)|^2 d\omega,$$

where $A(\omega)$ is the excitation amplitude at the angular frequency ω , $P(\omega)$ is the pattern of the source as a function of ω , and P_0^2 is a normalizing factor. For a line source

$$P(\omega) = \frac{\sin\left(\omega \frac{l \sin \gamma}{2c}\right)}{\left(\omega \frac{l \sin \gamma}{2c}\right)},$$

where c is the velocity of sound. Assume

$$|A(\omega)| = \begin{cases} 1, & 0 \leq \omega_1 < \omega \leq \omega_2 \\ 0, & \text{elsewhere} \end{cases}$$

Then it is found that

$$\bar{P}^2 = \frac{1}{r^2 - 1} \left[\frac{\sin^2\left(\frac{\pi u}{r}\right)}{\left(\frac{\pi u}{r}\right)^2} - r^2 \frac{\sin^2(\pi u r)}{(\pi u r)^2} + \frac{S_i(2\pi u r) - S_i\left(\frac{2\pi u}{r}\right)}{\left(\frac{\pi u}{r}\right)} \right],$$

where $\omega_2 = r\omega_0$, $\omega_1 = \omega_0/r$, $r, \lambda_0\omega_0 = 2\pi c$, and $u = (l/\lambda_0) \sin \gamma$. $S_i(x)$ is the incomplete sine integral tabulated

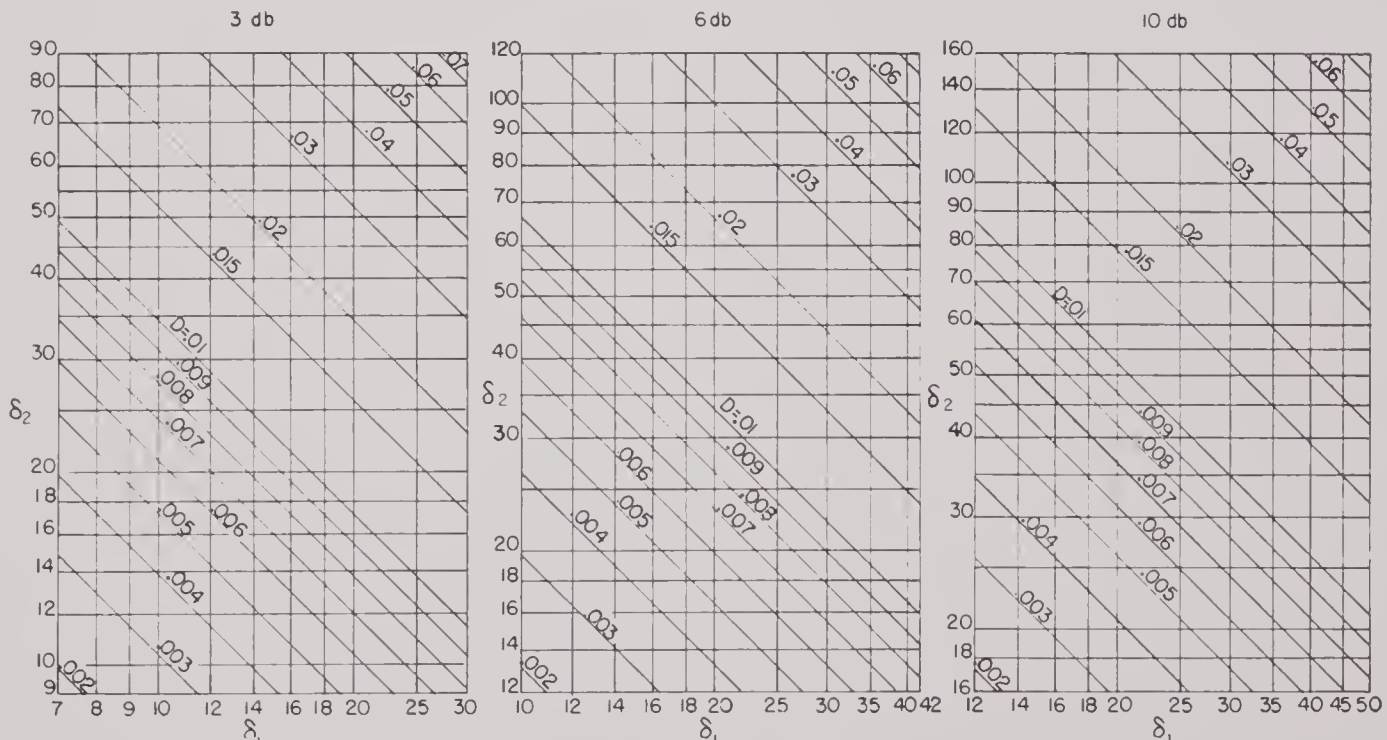


FIGURE 40. Directivity ratio D in terms of total pattern widths δ_1 δ_2 in degrees between points 3, 6, and 10 db below maximum.

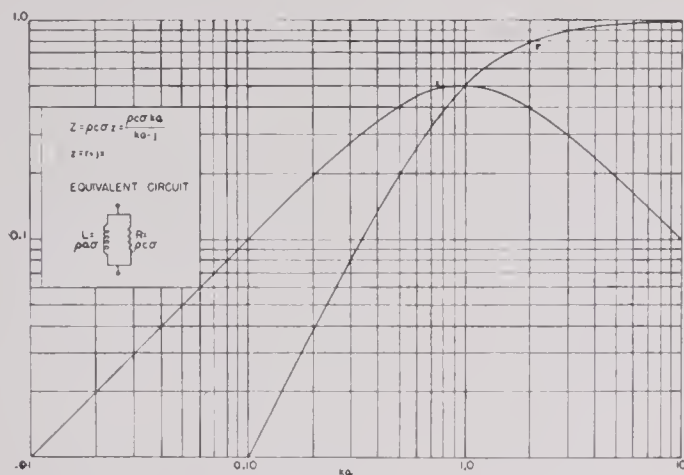


FIGURE 41. Radiation impedance of sphere.

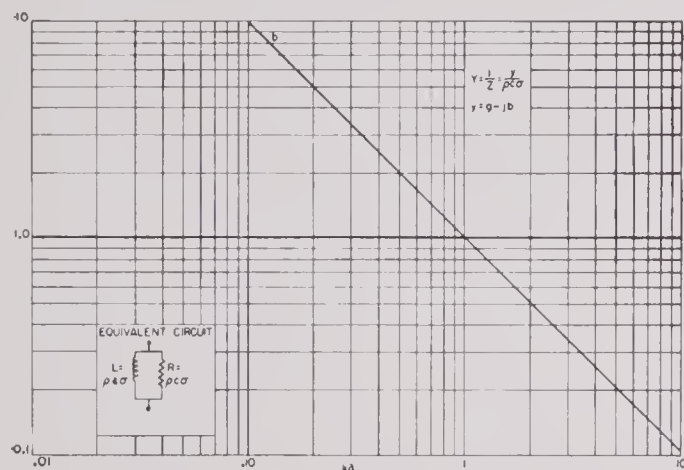


FIGURE 42. Radiation admittance of sphere.

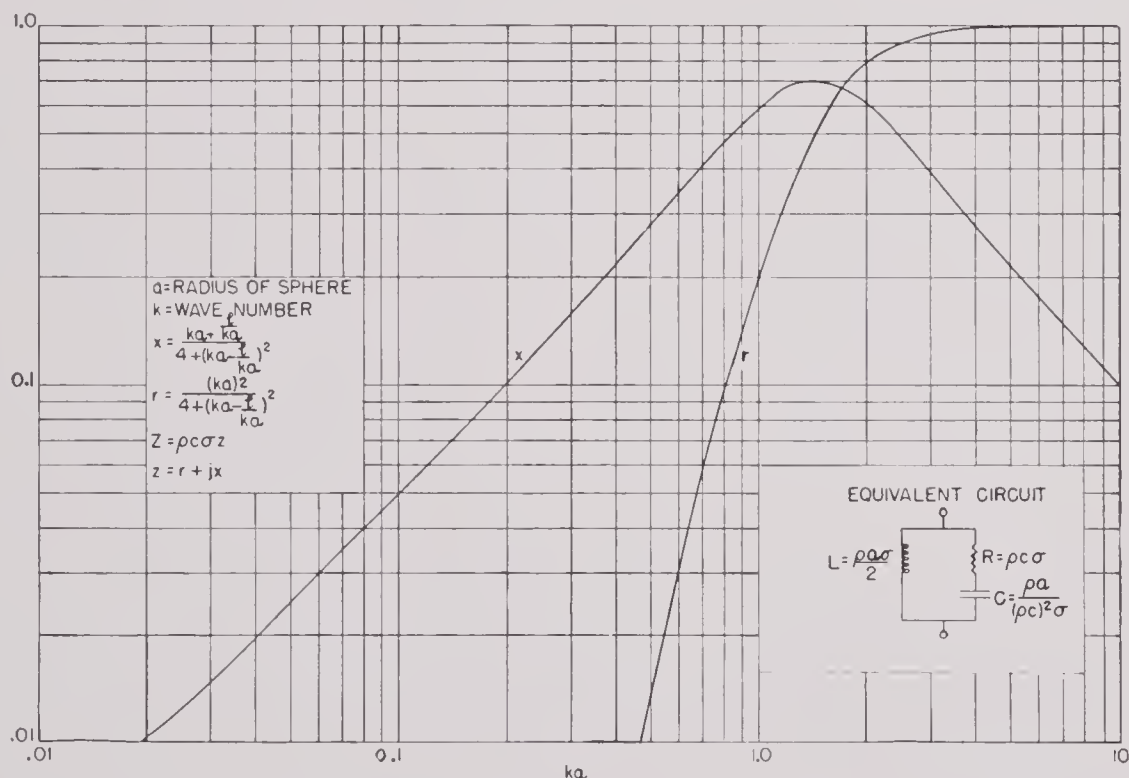


FIGURE 43. Radiation impedance of a spherical dipole source.

in Jahnke and Emde.⁶³ This pattern is plotted in Figure 39 for the cases in which the band width is an octave and a half-octave, and the results are compared with the pattern of a pure frequency signal. It will be noticed that the principal difference is a smoothing out of the minima and a slight decrease of the maxima. For other radiators, like behavior would be expected.

DIRECTIVITY RATIOS OF GIVEN PATTERNS

In various instances the directivity ratio of a pattern has already been shown to be a function of the transducer (its shape, size, and shading). However, it often happens that these properties of the transducer are known only inaccurately or not at all, though the pattern of the transducer may have been measured quite accurately. It then becomes of interest to know the directivity ratio of a pattern as a function of the properties of the pattern itself (its type of symmetry, width of major lobe, height of minor lobes, and so on).

If there is no sort of symmetry or regularity to the pattern, some form of numerical integration is needed to obtain the directivity ratio. Actually the pattern is seldom known in more than two perpendicular planes so that it is necessary to assume that the overall pattern is the product of the two known patterns. If the minor lobes are lower than 25 db, the

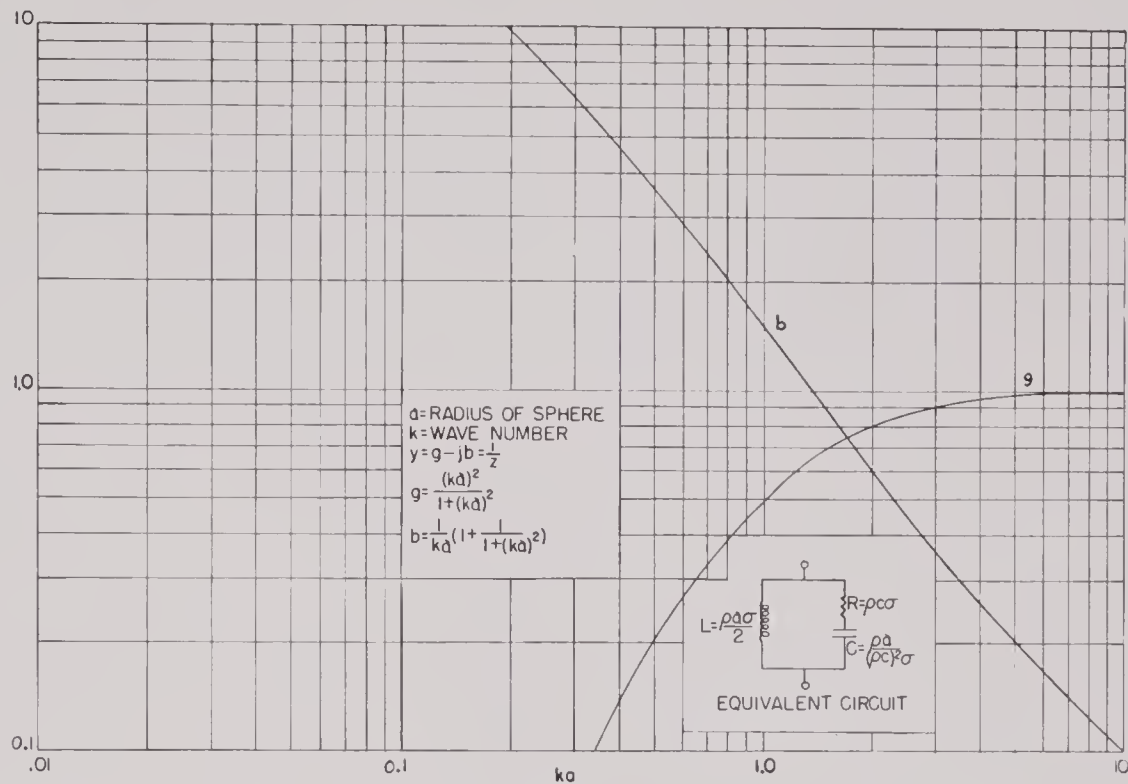


FIGURE 44. Radiation admittance of a spherical dipole source.

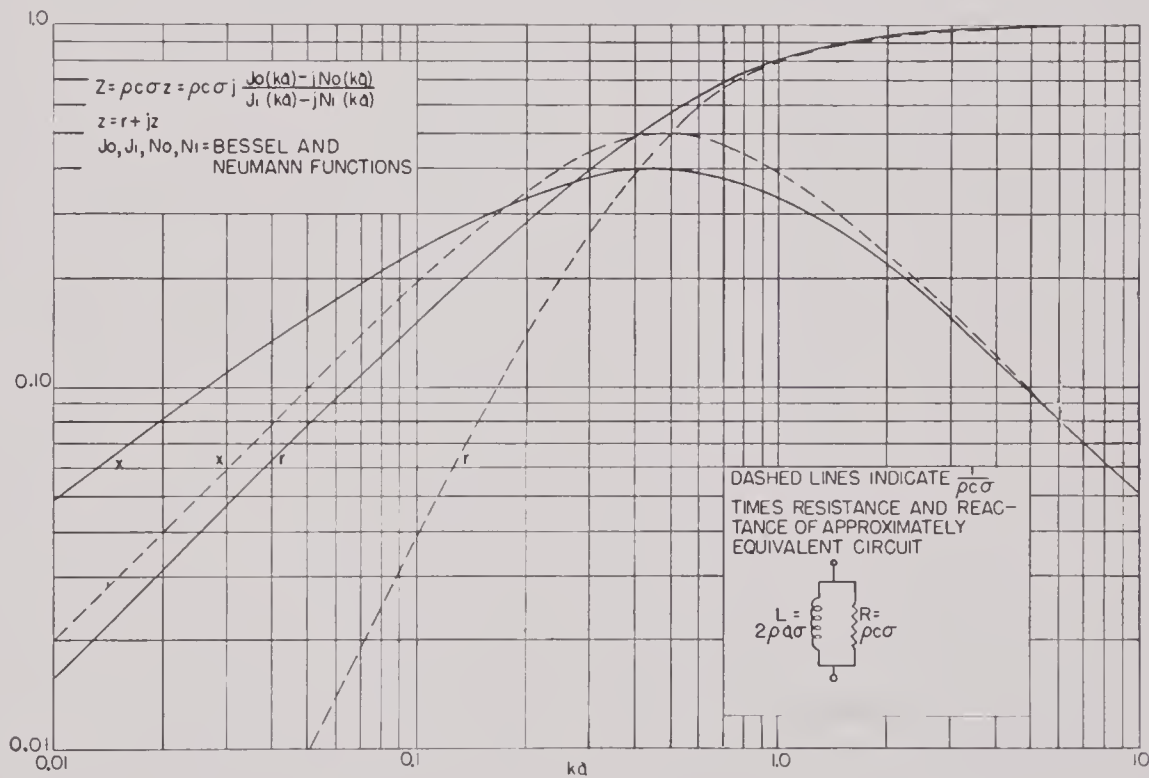


FIGURE 45. Radiation impedance of infinitely long circular cylinder.

directivity ratio of the pattern is given quite closely by

$$D = \frac{3}{2} \delta_1 \delta_2 10^{-5},$$

where δ_1, δ_2 are the widths in degrees, 6 db below the peak of the patterns in two perpendicular planes.

In Figure 40 the directivity ratio is given as a function of the widths δ_1, δ_2 when measured 3 db, 6 db, and 10 db from the peak of the pattern. The 6-db case is based on the formula above. A check is afforded by comparing the three values of D given by the three parts of Figure 40. The average of the

CONFIDENTIAL

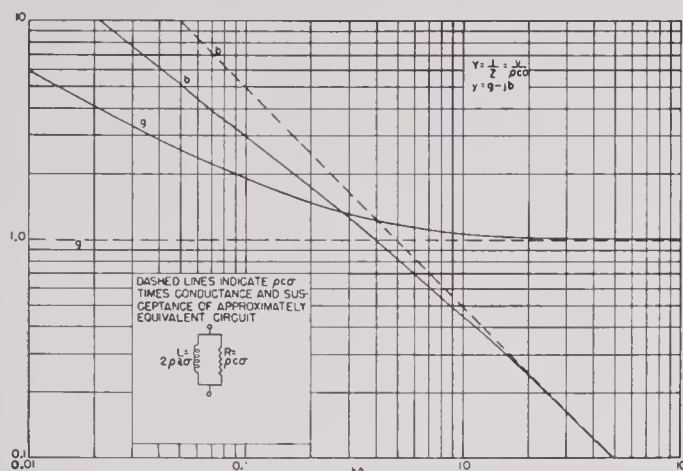


FIGURE 46. Radiation admittance of infinitely long circular cylinder.

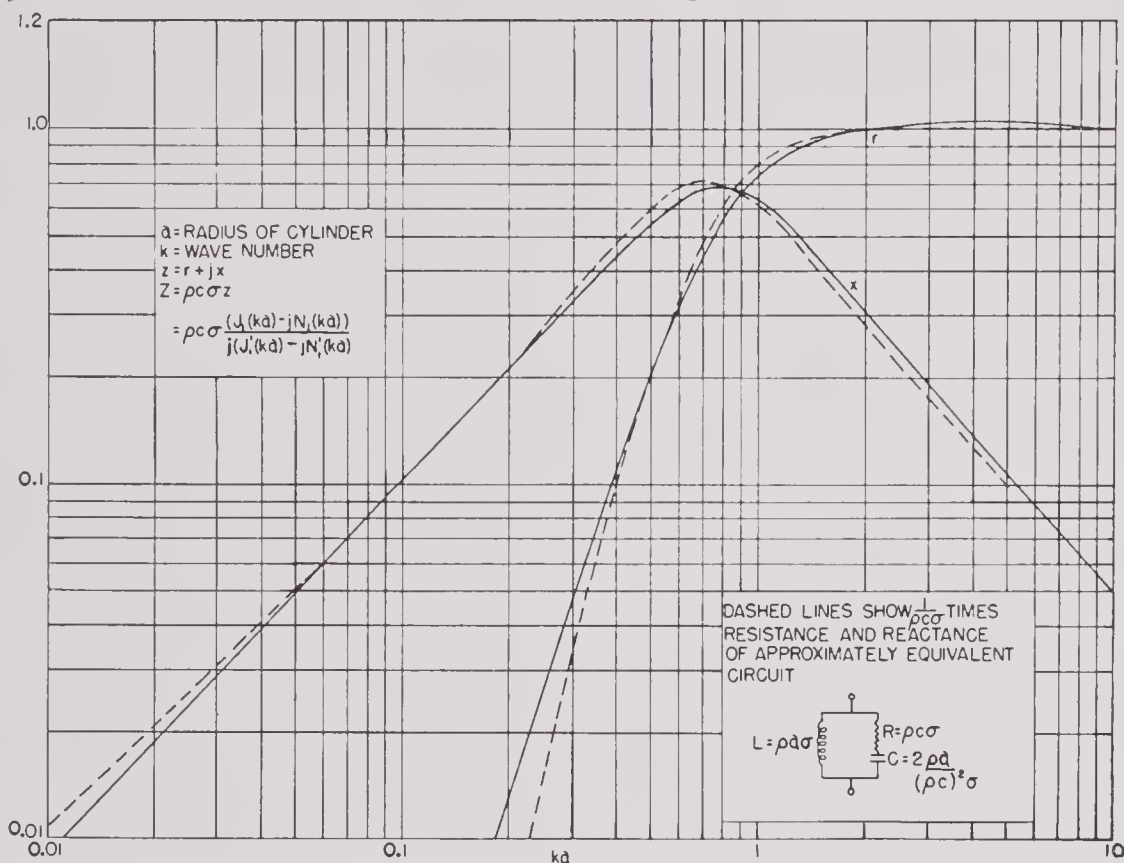


FIGURE 47. Radiation impedance of a cylindrical dipole source.

three values of D is probably the best value to use. A rough correction term to account for ordinary minor lobes may be applied as follows: add $\frac{1}{2}$ db to the directivity index given in Figure 40 for each 5 db that the minor lobes exceed -25 db. This should give the directivity index to within a decibel.

5.6 RADIATION IMPEDANCE

5.6.1 Introduction

If a sinusoidal force is applied to a surface, the surface vibrates and radiates sound into the sur-

rounding medium. In considering this problem, attention is focused on the action of the force and the reaction of the medium on the applied force. In general, this reaction depends, in an extremely complicated manner, on the disposition and condition of constraining surfaces (impedance), including the active surface of the transducer itself. The problem can be stated mathematically as a general boundary value problem requiring solutions of the wave equation. Except in a few simple cases, it involves a knowledge of higher analysis; therefore, the detailed derivations will not be given here. The results will be simply formulated in an elementary manner, making use of electromechanical analogies.

5.6.2 Energy Radiated

The average energy radiated from the active surface σ of a transducer is given by

$$E = \operatorname{Re} \frac{1}{2} \int_{\sigma} p v^* d\sigma,$$

where p is the sinusoidally varying pressure and v is the normal particle velocity of the radiating surface at the element of surface $d\sigma$. Re is an abbreviation for "real part of" and v^* is the conjugate complex value of v . Assume the complex time factor of p and v to be $e^{j\omega t}$, where ω is the angular frequency of the vibration.

5.6.3 Radiation Impedance and Admittance

If the face of the transducer moves like a rigid piston, that is, with a uniform velocity v , then

$$E = \operatorname{Re} \frac{1}{2} v^* \int_{\sigma} p d\sigma, \quad \text{then}$$

while if the pressure p over the face of the transducer is uniform,

$$E = \operatorname{Re} \frac{1}{2} p \int_{\sigma} v^* d\sigma.$$

After writing

$$Z = R + jX$$

$$Y = G - jB,$$

$$E = \frac{1}{2} R v v^*,$$

$$E = \frac{1}{2} G p p^*.$$

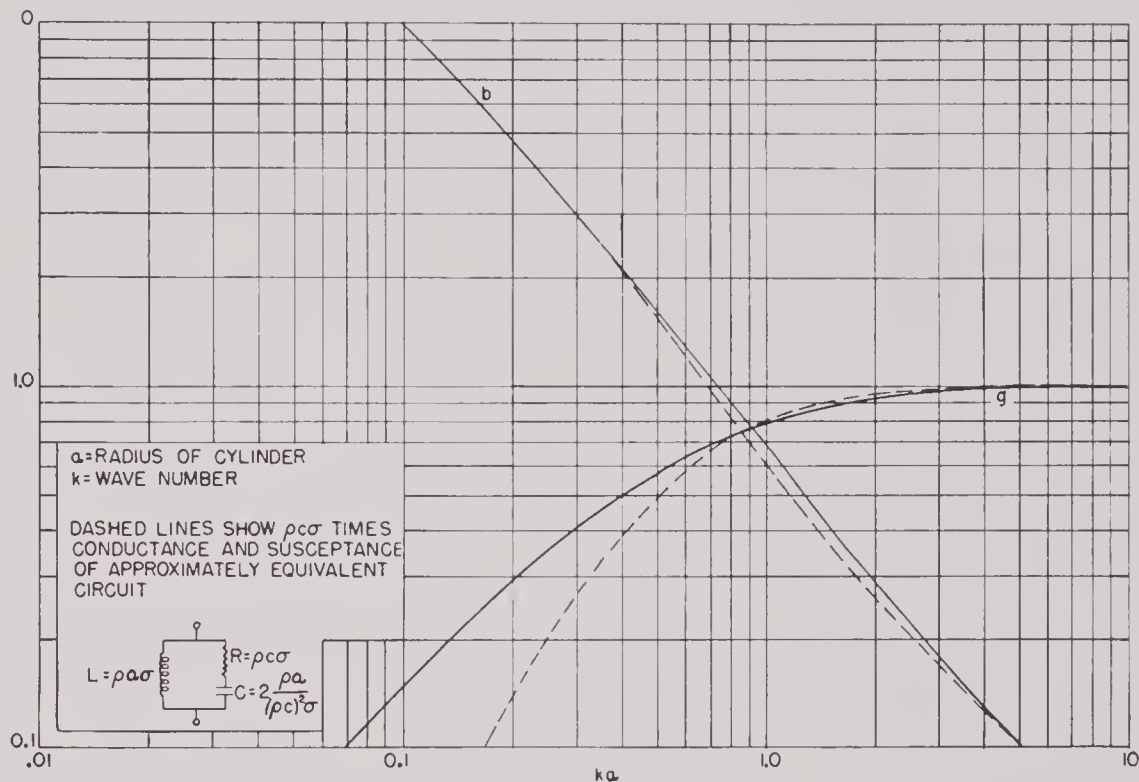


FIGURE 48. Radiation admittance of a cylindrical dipole source.

In the former case the complex radiation impedance is defined as

$$Z = \frac{1}{v} \int_{\sigma} p d\sigma,$$

and in the latter case the complex radiation admittance is defined as

$$Y = \frac{1}{\sigma^2 p} \int_{\sigma} v d\sigma.$$

Both definitions coincide when both p and v are uniform over σ and therefore

$$Z = \frac{p\sigma}{v} = \frac{1}{Y}.$$

SPECIFIC IMPEDANCE AND ADMITTANCE

The quantity Z/σ is called the specific radiation impedance, and σY the specific radiation admittance. It is usually convenient to plot the real and imaginary parts of

$$z = r + jx,$$

$$y = g - jb,$$

$$z = \frac{Z}{\rho c \sigma},$$

$$y = \frac{\sigma Y}{\rho c}.$$

ρ is the density of the medium and c the velocity of sound in the medium. The ρc is commonly called the

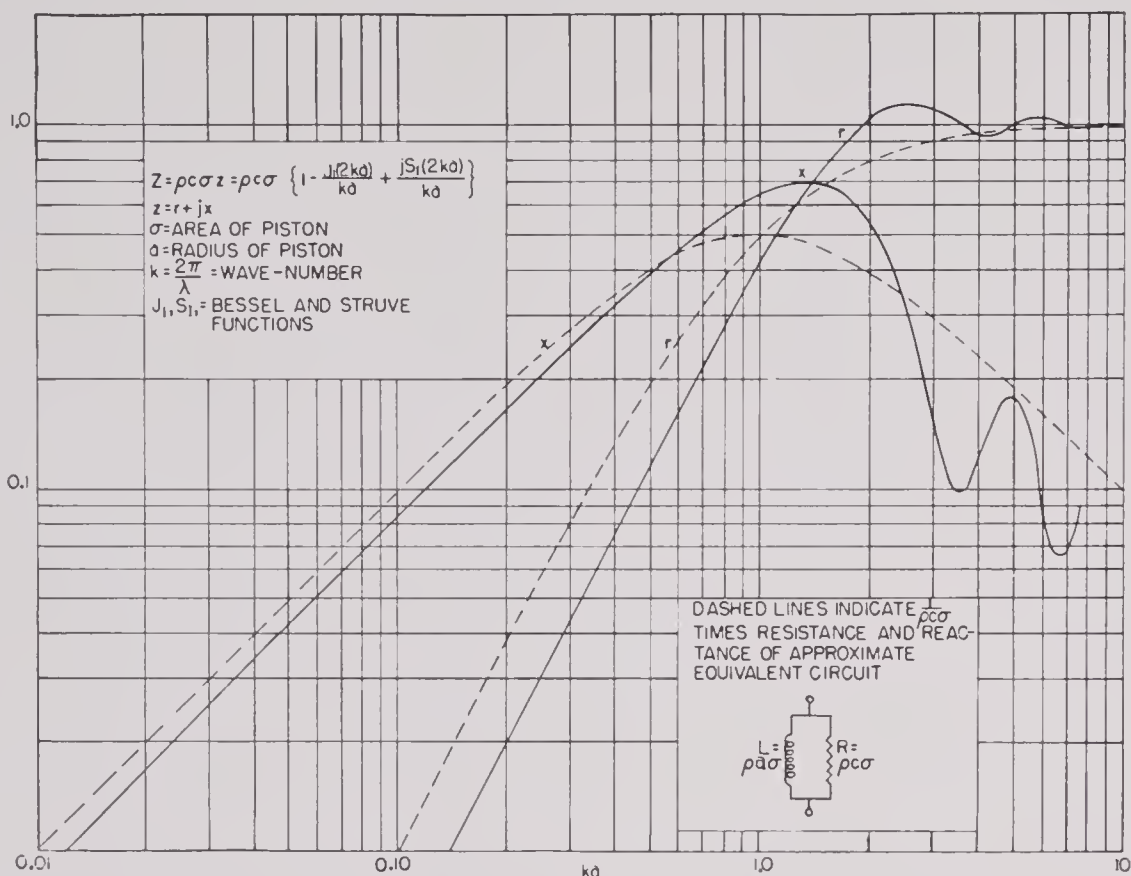


FIGURE 49. Radiation impedance of circular piston in stiff infinite plane baffle.

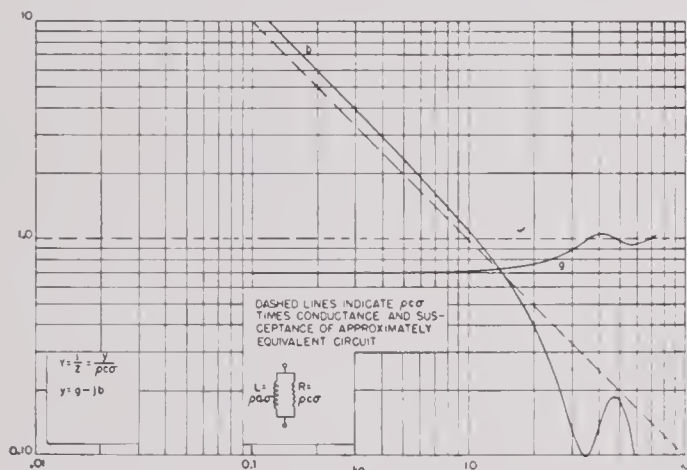


FIGURE 50. Radiation admittance of circular piston in stiff infinite plane baffle.

specific acoustic resistance of the medium; it has the value 42 in air and 150,000 in water when the units are grams per square centimeter second, or bars seconds per centimeter.

In Figures 41 to 52, the quantities z and y are plotted for various radiators. The independent variable is a dimensionless quantity involving the wave number k , given by

$$k = \frac{\omega}{c} = \frac{2\pi}{\lambda},$$

λ being the wave length of the signal.

FOR A PULSATING SPHERE

The radiation impedance and admittance of a pulsating sphere of mean radius a are plotted in Figures 41 and 42. It is seen that a parallel combination of resistance $pc\sigma$ and inductance $pa\sigma$ can simulate the radiation impedance and admittance where σ is the mean area of the sphere.

FOR A DIPOLE SPHERE

The radiation impedance and admittance of an oscillating dipole sphere of fixed radius a are shown in Figures 43 and 44. In this case there is again an exactly equivalent circuit which is shown on the graphs.

FOR A PULSATING CYLINDER

Figures 45 and 46 show the radiation impedance and admittance per unit length of a long pulsating cylinder of mean radius a . The inductance required in the equivalent circuit in order to give a good approximation for large ka is twice that needed in the case of the pulsating sphere.

FOR A CYLINDRICAL DIPOLE

The radiation load per unit length of a long oscillating cylinder (cylindrical dipole) of fixed radius a with approximately equivalent circuits is shown in Figures 47 and 48.

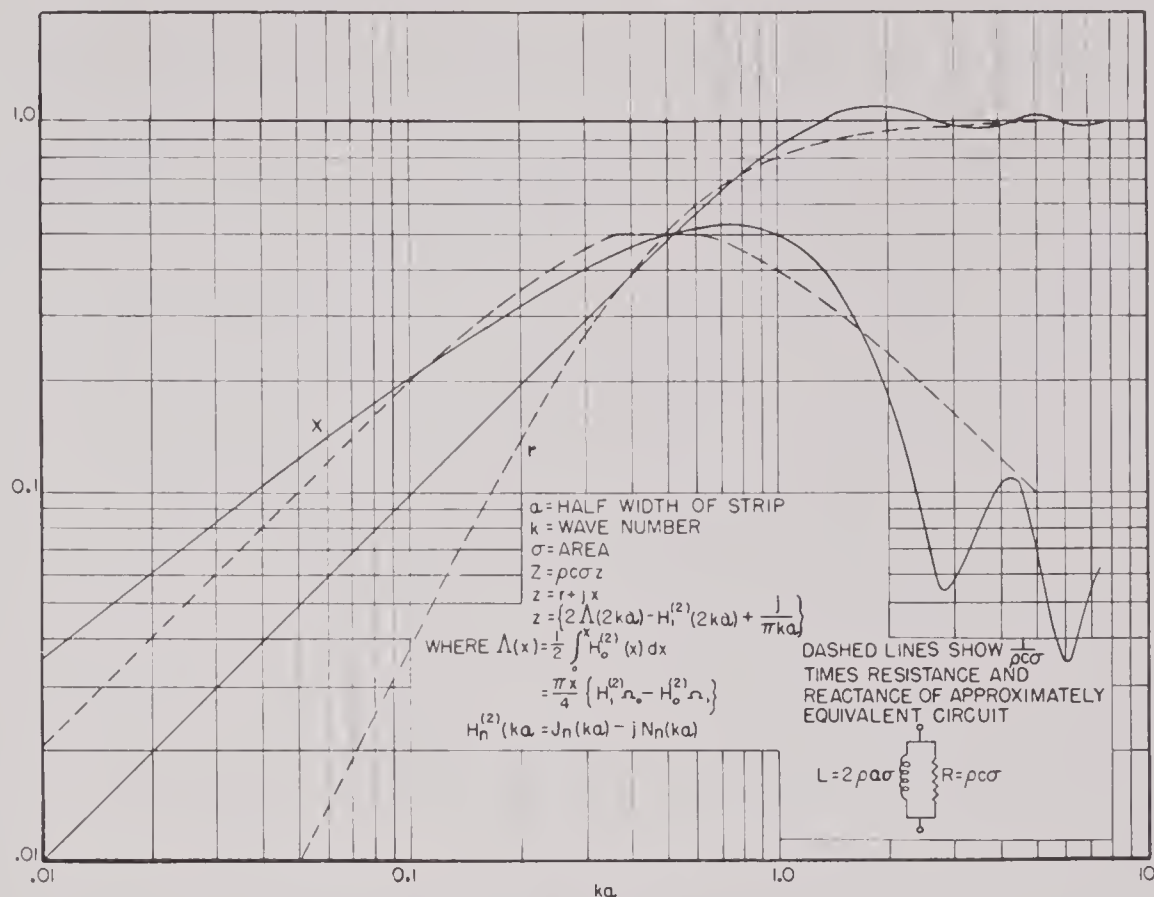


FIGURE 51. Radiation impedance of long strip in stiff plane baffle.

FOR A CIRCULAR PISTON

The radiation, impedance, and admittance of a circular piston of radius a set in an infinite-plane, stiff baffle are shown in Figures 49 and 50. It is evident that no simple series or parallel combination of resistance and inductance exhibits similar frequency variation. However, the same parallel combination as for the sphere, for which the impedance and admittance are shown in dashed lines on Figures 49 and 50, gives a fairly good approximation.

FOR A LONG, FLAT STRIP

The radiation load per unit length of an oscillating long strip of width $2a$ set in a large stiff-plane baffle is shown in Figures 51 and 52. The approximately equivalent circuit is the same as that of a long pulsating cylinder.

FOR A RADIATOR OF LARGE DIMENSIONS

In every case above it will be noticed that when the dimensions of the radiator are large compared with the wave length of the signal, the radiation impedance is resistive and is very closely given by

$$R = \rho c \sigma,$$

where σ is the active area of the radiator.

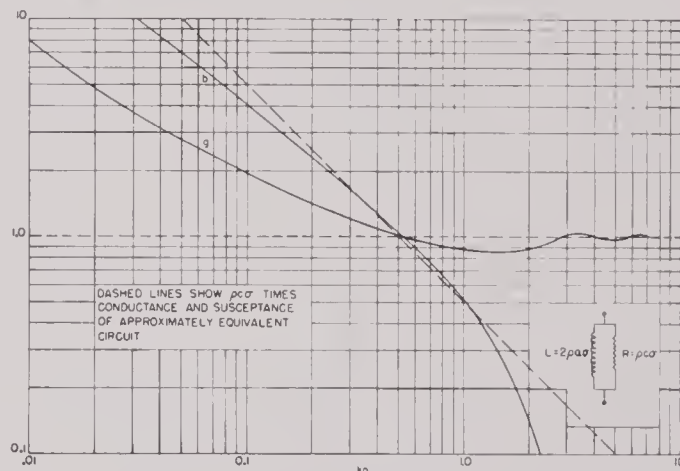


FIGURE 52. Radiation admittance of long strip in stiff plane baffle.

5.7

DIRECTIVITY RATIO

The intensity of a sound beam is defined as the average energy passing through a unit area and is given by

$$I = \operatorname{Re} \frac{1}{2} p v^*.$$

Thus the total energy passing through a surface S is given by

$$E = \int_S I dS.$$

Let I_0 be the sound intensity a large distance a from the source in the principal direction of propagation. If the intensity in all directions were I_0 , the average energy radiated would be

$$E_0 = 4\pi a^2 I_0.$$

The directivity ratio D is defined as

$$D = \frac{E}{E_0} = \frac{1}{4\pi a^2} \int_S \frac{I}{I_0} dS,$$

where S is a sphere of large radius a centered at the radiator.

When I_0 is the maximum I , as is generally the case, D is a number between 0 and 1. The more directive the sound field, the smaller is D . A uniform sound field, such as that of a point source, has a D of 1.

The directivity index d is defined as

$$d = -10 \log_{10} D \text{ db.}$$

This number has the desirable property of increasing with the directivity of the sound beam.

At large distances from the source the pressure p and the normal particle velocity v are related by

$$p = \rho c v.$$

If the pressure p at a large fixed distance from the source, commonly called the pressure pattern of the source, is normalized to be 1 in the principal direction of propagation, then the directivity ratio may be written

$$D = \frac{1}{4\pi} \int p p^* d\Omega,$$

where Ω is a solid angle ($d\Omega = dS/a^2$).

By using the expressions previously obtained for the average energy E radiated from the source, it is found that

$$R = \frac{4\pi a^2}{\rho c} \left(\frac{p_0}{v} \right) D,$$

$$\sigma^2 G = 4\pi a^2 \rho c \left(\frac{v_0}{p} \right) D,$$

where R is the radiation resistance of a source having a uniform velocity v and G is the radiation conductance of a source of area σ exerting a uniform pressure p . The pressure and particle velocity of the sound

field at a large distance a from the source in the principal direction of propagation are represented by p_0 and v_0 respectively.

The quotients p_0/v and v_0/p that occur in the above equations can be evaluated in certain simple cases,

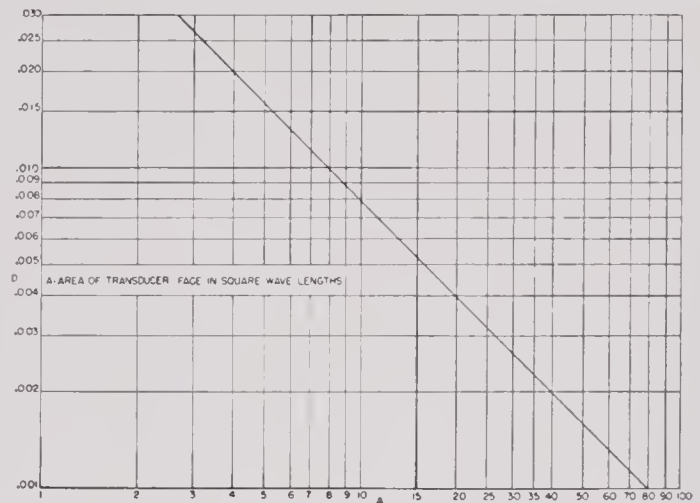


FIGURE 53. Directivity ratio of flat-faced transducer when dimensions are large.

for example, when the active face of the radiator is a flat surface set in an infinite-plane baffle. When the source has a uniform velocity v the baffle is assumed stiff, that is, the surface velocity of the baffle is zero. Then

$$\frac{p_0}{v} = \frac{\rho c \sigma}{a \lambda},$$

so that

$$R = \rho c \sigma \cdot \frac{4\pi \sigma}{\lambda^2} \cdot D.$$

When the source exerts a uniform pressure p , the baffle is assumed to be pressure release. Then

$$\frac{v_0}{p} = \frac{\sigma}{\rho c \sigma \lambda},$$

and

$$G = \frac{1}{\rho c \sigma} \cdot \frac{4\pi \sigma}{\lambda^2} \cdot D.$$

In either case, when the dimensions are large,

$$D = \frac{\lambda^2}{4\pi \sigma}.$$

Figure 53 is a plot of D against σ when σ is expressed in square wave lengths.

Chapter 6

RADIALLY VIBRATING TRANSDUCERS

6.1

INTRODUCTION

Reference has already been made in Chapter 1 (see Figure 13) to the early use of the radial vibration of a cylindrical shell of magnetostrictive material in the generation of sound waves. A mathematical theory of the phenomenon appears in Chapter 3. From equations (16), (16a), and (18) of Chapter 3, the resonant frequency of the first radial mode is easily found to be

$$f_0 = \frac{1}{2\pi a} \sqrt{\frac{E}{\rho_m}} = \frac{c_m}{2\pi a}, \quad (1)$$

where c_m is the velocity of sound in the magnetostrictive material and a is the mean radius of the cylindrical shell. Equation (1) is equivalent to saying that the lowest resonant frequency of a tube or cylindrical shell is the frequency at which the wave length in the shell material is equal to the mean circumference of the shell. Hence for a given value of a the resonant frequency is independent of the radial thickness.

The shell thickness is, however, an important factor in determining the sharpness of the mechanical resonance as the following elementary analysis shows. It is assumed that internal mechanical resistance and damping due to eddy currents are small in comparison with the radiation resistance of the water. The latter assumption implies that at least one dimension of the shell is not small in terms of the wave length in water of the radiated sound. With these simplifying assumptions, the shell may be considered a radial vibrator with radiation damping $\rho_w c_w$ per square centimeter of radiating surface. From equation (15) of Chapter 3 the mass reactance of the shell per unit area of radiating surface may be written:

$$\text{Mass reactance} = m\omega = b\rho_m\omega \quad (2)$$

$$\text{At resonance, } \omega = \omega_0 = 2\pi f_0 = \frac{c_m}{a}.$$

Then

$$Q_{\text{mech}} = \frac{b\rho_m c_m}{a\rho_w c_w}, \quad (3)$$

where b is the radial thickness of the shell.

With the values of $\rho_m c_m$ and $\rho_w c_w$ for nickel and water respectively, the approximate equation is:

$$Q_{\text{mech}} = 29.6 \frac{b}{a}. \quad (3a)$$

In thin-walled drawn commercial tubing the radiation resistance is large in comparison with the mass reactance, giving low values of Q . Standard 1.5-in. nickel tubing has a wall thickness of 0.035 in. The computed value of $Q = 0.035/0.75 = 0.047$. Impedance measurements on transducers made from such tubing show no measurable radial resonance in water, with the result that the response varies only slightly

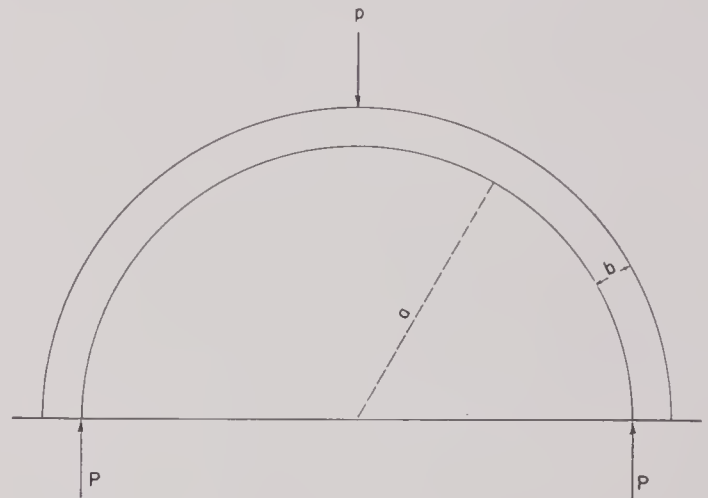


FIGURE 1. Radial and tangential stresses in cylindrical tube.

with frequency over a wide range. The efficiency is correspondingly low, so that applications of radially vibrating thin-walled tubes have been almost wholly limited to their use as hydrophones rather than projectors. Ring stacks, on the other hand, have been designed to have a fairly high efficiency over a comparatively narrow frequency range and have been used extensively for both transmission and reception.

An inherent virtue of the radially vibrating tube lies in the fact that the area exerting pressure on the water is increased over that carrying the magnetostrictive stress by a factor a/b , the ratio of tube radius to the wall thickness. This is easily shown by refer-

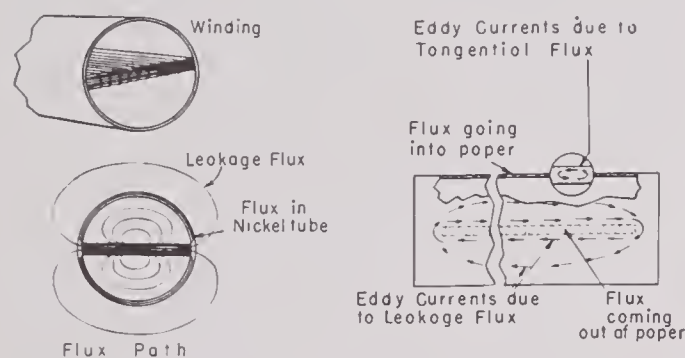
ence to Figure 1. Consider a diametral section of the tube, subjected to a hydrostatic pressure p . Then the component of the externally applied force per unit length normal to the section is $2ap$. This is in equilibrium with the force due to the stress P over an area $2b$, so that

$$2ap = 2bP$$

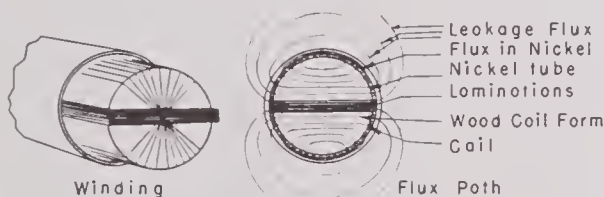
or

$$\frac{P}{p} = \frac{a}{b}.$$

It is evident that in the radially vibrating tube one problem in transducer design, namely, that of securing proper acoustic loading of the vibrating surface, is in a measure automatically solved by the inherent geometrical configuration of the tube.



A ORIGINAL STRAIGHT HYDROPHONE



B WOOD CORE OF JP-1 HYDROPHONE



C TOROIDALLY WOUND HYDROPHONE

FIGURE 2. Types of New London tubular hydrophones.

6.2 THIN-WALLED TUBULAR HYDROPHONES: NEW LONDON DEVELOPMENT

Except for the early limited use of the thin-walled cylindrical sonic device shown in Figure 13 of Chapter 1, no references to this type of magnetostrictive vibrator appear in the literature prior to World

War II. The development of the possibilities of magnetostrictively driven tubes stems from the pioneer work of A. L. Thuras at the New London laboratory. The present account of the work carried on there is taken from the New London report.¹⁷⁴ The original report should be consulted for the extremely valuable mass of detailed information it contains.

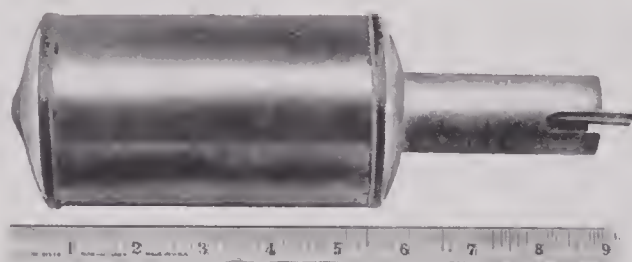
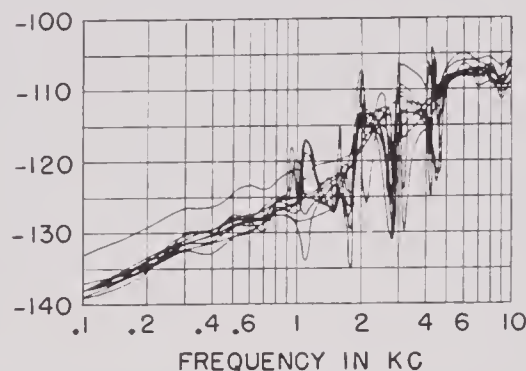


FIGURE 3. D-16 Mark IVE hydrophone (sensitivity given in decibels versus 1 volt per dyne per square centimeter).

The earliest interest of the New London group in tubular hydrophones was in connection with directional sonic listening devices when they attempted to duplicate, with a feasible design in the sonic-frequency range, the directional listening patterns then available in the supersonic range using crystal hydrophones. However, like most fertile ideas, it soon found other important applications, notably in the *New London expendable buoy* [ERSB] hydrophone and the *depth charge direction indicator* [DCDI] hydrophones as well as in the sound-gear monitoring hydrophones developed at HUSL. Hydrophones of this type range in size from units 5 ft and more in length, used in the JP listening systems,¹⁵² down to midget units with tubes $\frac{3}{4}$ in. in diameter and 1 in. long.

6.2.1 Sonic Listening Hydrophones

The desired properties of a sonic listening hydrophone are (1) a broad-band frequency response below 10 kc and (2) a sharp beam pattern with much lower sensitivity in the direction of the minor lobes than in the direction of the main beam. As already stated, the thin-walled magnetostrictive tube meets the first requirement. The second requirement calls for at least one dimension that is several times the wave length in water of the signal. At 5 kc, a frequency well up in the sonic range, the wave length is 11.2 in. Tubular hydrophones intended for sonic listening evidently must be sizable affairs.

The earlier hydrophones built at the New London laboratory were designed to operate on magnetic remanence. For this use, it was found that partial annealing of hard-drawn commercial nickel tubing led to improved efficiency and greater uniformity. The annealing schedule adopted after extensive experimentation was three hours at 600 C. This treatment was found to increase the remanent permeability from 22 (unannealed tubing) to about 30. (These values are appreciably higher than those given for 5-mil nickel laminations in Chapter 4. The difference is probably to be explained by the greater hardness, which is due to the cold working of the thin sheets of the HUSL measurements. However, the optimum annealing temperature was practically the same as that found in the Harvard measurements.)

Since the remanence anneal was carried out at a temperature at which the permeability of the nickel varies rapidly with temperature and since annealing at this temperature does not fully erase the previous history, nickel tubing so annealed was found to vary widely in its properties. For this reason, a method was developed for point-to-point measurement of the permeability of the long tubes used for sonic listening hydrophones. The elimination of tubes with non-uniform permeability was found to be a necessary precaution.

The sensitivity of a listening hydrophone is of secondary importance, since the result desired is discrimination between water noise and the noise whose source is to be detected. An increase in sensitivity cannot increase the detection range, but a high sensitivity means that less gain and noise reduction are necessary in the listening amplifier.

The directivity index D plays an important role in the performance of a sonic listening device. It determines the ratio of the response to sound coming

from the direction of maximum response to the total response to sound arriving from all directions. Since water noise is a controlling factor, it is desirable to have response to sound arriving in random directions that are low in comparison with response in the direction of the main lobe. Taken alone, this calls for the reduction of minor lobes, which in general can be achieved only at the expense of an increase in the width of the main beam. This latter, however, decreases the directional discrimination, so that the

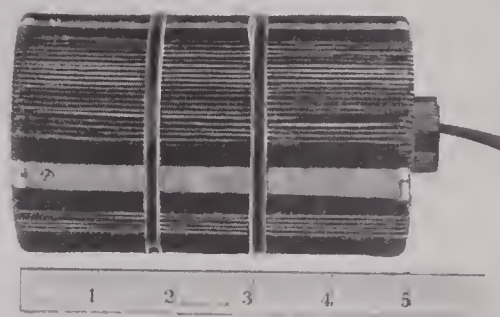
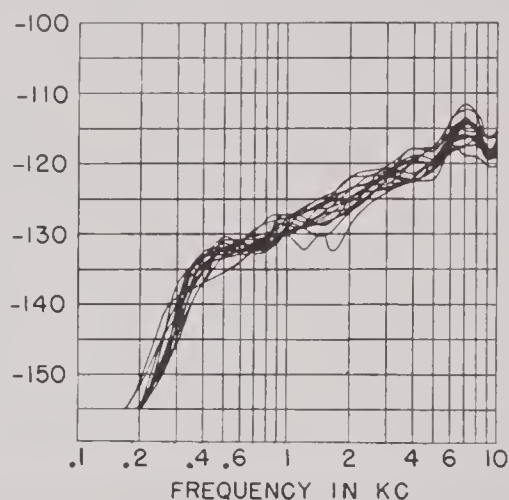


FIGURE 4. M-7/CRT-1A hydrophone (sensitivity given in decibels versus 1 volt per dyne per square centimeter).

optimum pattern for a sonic listening hydrophone is necessarily a compromise between that for maximum variation of response with angle and that for minimum interference from random noise. From a theoretical study of the problem, the authors of the New London report conclude that for a line hydrophone of given length the minimum directive index (maximum directional discrimination) is that given by a uniform velocity everywhere on the radiating surface, provided the contributions from all points of the surface

add in phase on the main beam. For a line source, this latter condition holds at distances several times the length of the source. It is stated on theoretical grounds that a 5-ft line hydrophone would be expected to show approximately 6 db greater discrimination against random noise originating on the horizon than would a 15-in. circular piston and should give greater discrimination against spatially random sound at frequencies below 6,000 c. Above this frequency, the 15-in. piston should be better. The relative merits of particular patterns, however, are dependent upon conditions of use.

6.2.3 Expendable Radio Sono Buoy Hydrophones

The requirements of this use were (1) cheapness, lightness, and ease of construction; (2) nondirectionality; (3) ruggedness; (4) voltage response that rises with frequency in the range from 0.1 to 10 kc.

Since the submerged life of the hydrophone was intended to be only a matter of a few hours, protection against the prolonged action of sea water was not needed. The earlier hydrophone developed for this use was a nickel tube 3 in. in diameter, 5 in. long



FIGURE 5. Toroidal sonic listening hydrophone.

6.2.2 Construction Types

The general types of tubular hydrophones developed at New London are shown in Figure 2. In construction A, there is considerable leakage flux inside the tube that does not contribute to the hydrophone output. Moreover, external leakage at the extremities of the core generates eddy currents in the tube. In B, the wood core carrying the windings close to the inner surface of the tube was found to reduce internal leakage and to produce a 6-db rise in the sensitivity. When the coil was wound toroidally about the tube wall, as shown in C, the eddy currents were reduced to the longitudinal currents caused by the circumferential flux. In this construction, eddy-current losses can be reduced by lamination of the tube, a method that cannot be usefully employed with the diametral core.

(Figure 3). The internal construction consisted of the diametral, magnetically permeable core with windings as shown in Figure 2A. The core consisted of twelve laminations of soft iron totaling about $\frac{1}{4}$ in. in thickness, wound with 265 turns of No. 20 double cotton-covered wire with an impedance of about 50 ohms in the sonic-frequency range.

A later model was of the type shown in Figure 4. In this, 120 turns of No. 22 Vinylite-covered wire were wound toroidally on a half-hard, open-ended nickel tube to an impedance of about 2 ohms. A layer of air-cell rubber (pressure release) was inserted between the windings and the inner surface of the tube to prevent cancellation of sound pressure on the outer surface by the sound entering the open ends; this was a necessary provision, since the length of the tube was not great in terms of the wave length.

CONFIDENTIAL

Although the voltage sensitivity of the toroidally wound type was considerably lower than that of the earlier model, the improved frequency response together with the lower impedance resulted in marked overall improvement in performance.

The hydrophone developed concurrently with an improved *directional radio sono buoy* [DRSB] was

large area included gave rise to serious leakage flux. In a later development, the windings were forced to the inner surface of the tube by means of a flexible fibrous core. The electric closure of the ring, the easiest mode of construction, resulted in a short-circuited turn producing high eddy-current losses. Tests made at the Underwater Sound Reference Laboratories showed that the pattern did not depart materially from the theoretical pattern of a uniform circle of equal size. The open-circuit sensitivity in the frequency range from 0.5 to 2 kc was about -110 db referred to 1 volt per dyne per sq cm. Listening tests conducted on a submarine moving at three to six knots at periscope depth gave ranges on surface ships of 4 to 5 miles and bearings to within 2 degrees.

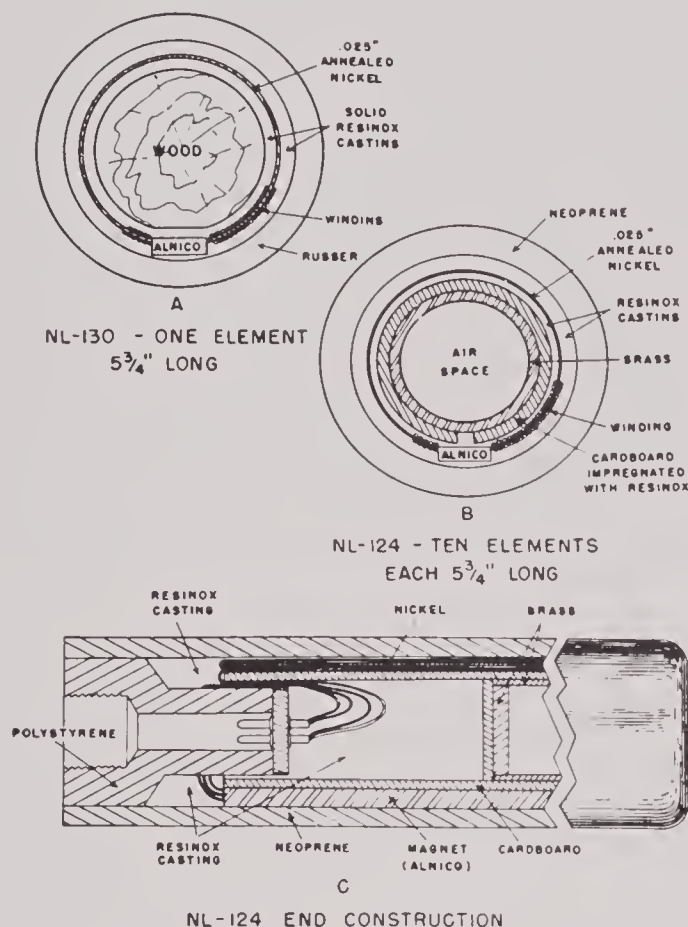


FIGURE 6. Section and assembly of NL-130 and NL-124.

a folding 2-ft, straight toroidally wound magnetostriction unit. It consisted of two 12-in. nickel tubes, 1 3/4-in. in diameter, with a 0.025-in. wall, annealed for three hours at 1100 F. These two elements fall into a line when the buoy is dropped into the water.¹⁷²

6.2.4 Sonic Listening Hydrophones: Production Models

The first production hydrophone constructed early in 1942 was toroidal or doughnut shaped (Figure 5). It consisted of a hard-nickel tube with a 2-in. diameter and 0.035-in. wall, bent into a ring having a 24-in. internal diameter and initially not completely closed. A coil of 100 turns of No. 20 insulated wire was fed into the ring. No internal core was used, and the

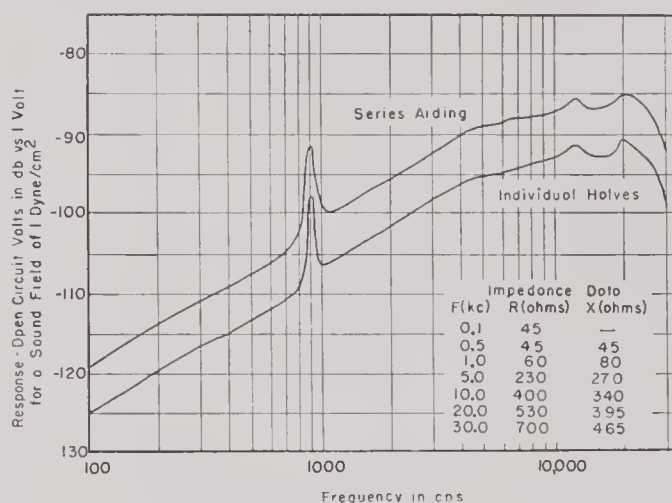


FIGURE 7. Response of NL-124.

The unexpectedly high directional properties of the device have been explained by the marked change in sound quality of a broad band source when the hydrophone is swung past the target. Owing to differences in the spacing of the maxima and minima in the receiving pattern with a difference in frequency, the quality as well as the intensity of the audible signal changes with the angle. It is a well-known phenomenon of hearing that the ear makes much finer discriminations in the quality than in the intensity of complex sounds. The toroidal hydrophone was the first rather than the last word in sonic listening hydrophones, but it had sufficient merit to arouse interest in sonic listening as an effective means of detection and location of underwater sources of sound.

Both because of greater simplicity of construction and better performance, the straight tube soon replaced the toroidal hydrophone. The earlier forms

used are shown in Figure 2. A later development, the NL-130, was the toroidally wound tube with permanent-magnet polarization shown in Figure 6. It consisted of an annealed nickel tube $1\frac{3}{4}$ in. in diameter, $5\frac{3}{4}$ in. long, with a 0.025-in. wall. A longitudinal slot was cut the full length of the tube, in which was soldered an Alnico magnet $\frac{3}{16} \times \frac{1}{2}$ in. The tube was wound toroidally, leaving a gap in the winding in which the Alnico strip was centered. The whole assembly was cast in plastic.

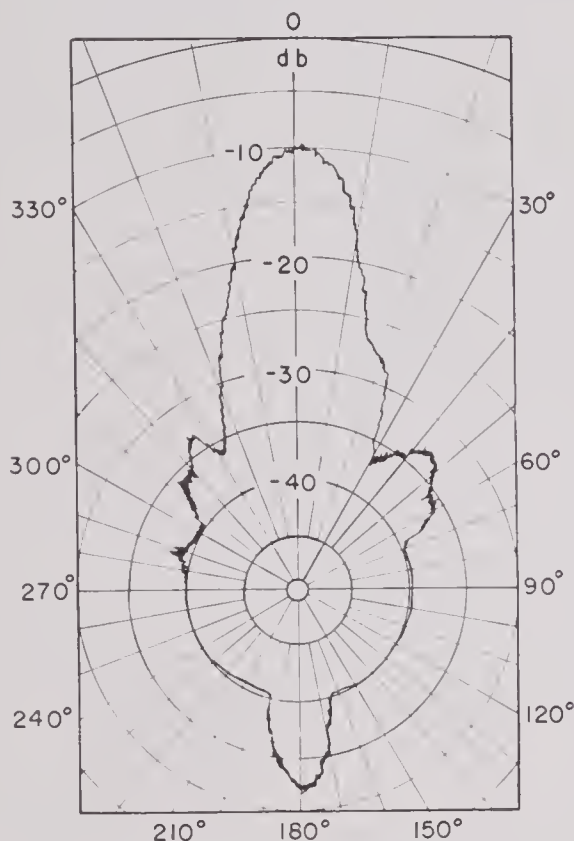


FIGURE 8. Pattern of 5-ft NL-124 in baffle, series aiding 5- to 9-kc noise band.

Before assembly, the polarizing element was magnetized by using an electromagnet which gave a flux density of about 15,000 gauss in the Alnico. Thus magnetized, the Alnico yielded a flux density of 2,000 to 4,000 gauss in the nickel.

An extended investigation was made of materials and techniques for casting. Of the large number of plastics tried, only one or two proved to have the qualities requisite for this application. These are:

1. Permanently high electric resistance and low moisture absorption.
2. Perfect adhesion to the windings and tube, with freedom from voids.
3. Chemical stability in sunlight.

4. A processing technique that can be carried out in factory production.

Consideration of the known properties of various plastics reduced the field of possibilities to three: (1) styrene, (2) methacrylates, and (3) phenol-formaldehyde compounds. Experiments eliminated the first two. The phenolic chosen, a commercial product known as Resinox,^a meets the requirements of mechanical strength and ease of handling, but its specific resistance (10^9 ohms per cm) is too low, its

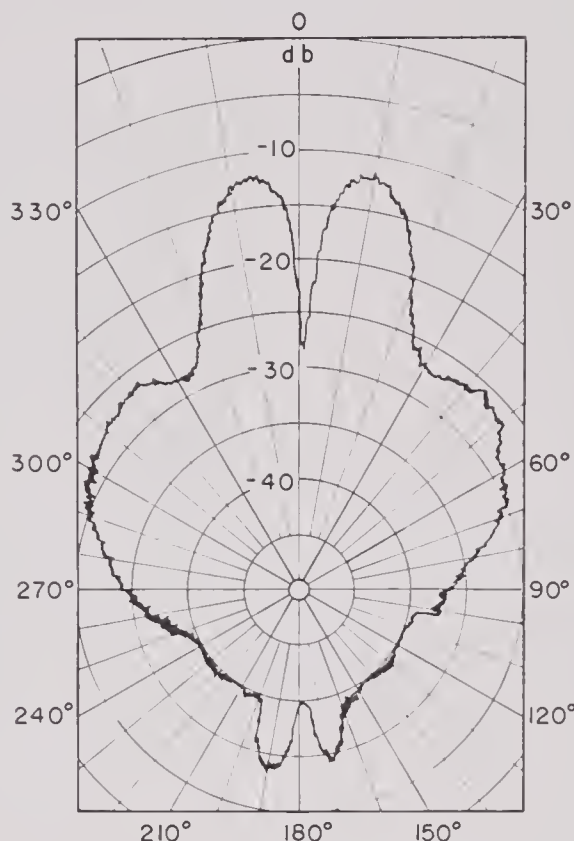


FIGURE 9. Pattern of 5-ft NL-124 in baffle, series opposing 5- to 9-kc noise band.

water absorption (0.1 per cent) is too high, and it was judged not to be sufficiently stable chemically to stand indefinite exposure to sea water without a protective coating. This protective coating consisted of a polystyrene tube coated with a black polystyrene composition.

The NL-130 was used as a basic unit for the construction of 3-, 4-, and 5-ft listening hydrophones, the NL-124 series. The 5-ft units contained ten of the

^a Cast phenolic Resinox (Monsanto 4200) 100 parts, dibutyl phthalate 6 parts, ethyl phosphoric acid 5.5 parts, cured 72 hours at 60 C. Resin and dibutyl phthalate are mixed together at a temperature of 60 to 80 C, and ethyl phosphoric acid is added while mixture is cooling.

NL-130 elements, which were sometimes shaded to give lobe reduction or were of uniform winding without taper. Figures 7, 8, and 9 give typical performance data for a 5-ft model.

The development and improvement in tubular hydrophones for sonic listening can best be summarized by the table supplied by W. B. Snow of the New

February 1944

NL-124. Straight-tube annealed nickel; permanent Alnico magnet, toroidally wound; cast in plastic, rubber covered. +16.0 db

June 1944

Experimental a-c polarized, toroidally wound, annealed nickel. +22.0 db

August 1944

Experimental hydrophone of NL-124 construction with 2V-Permendur tube. +20.0 db



FIGURE 10. Underwater loudspeaker.

London laboratory. The numerical values shown are the relative sensitivities in decibels averaged over the frequency band 0.5 to 10 kc and corrected to a 3-ft length and a common impedance; all values refer to the first production hydrophone of the HP-1 listening system.

Date	Relative sensitivity
<i>January 1942</i>	
Straight, core wound, hard-drawn nickel tube.	-11.0 db
<i>June 1942</i>	
Production model ring hydrophone; internal winding, no core; hard-drawn nickel tube.	+7.0 db
<i>September 1942</i>	
Original toroidally wound, straight hydrophone; hard-drawn nickel tube, without permanent covering.	+5.0 db
<i>November 1942</i>	
JP-1 straight tube, wood core; hard-drawn nickel tubes for installation on submarine.	0 db
<i>October 1943</i>	
Toroidally wound, straight tube; half-hard nickel, plastic cast cover.	+12.0 db

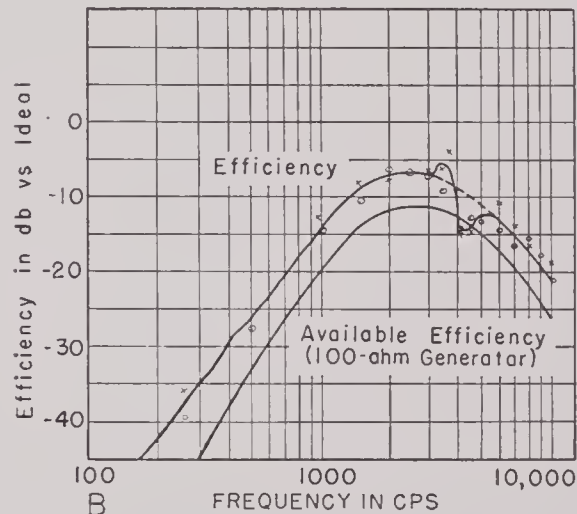
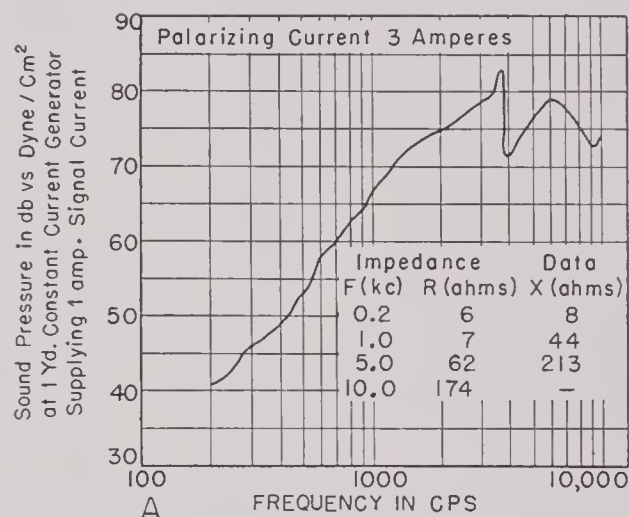


FIGURE 11. Response and efficiency of NL loudspeaker for A, transmitting response and B, computed efficiencies.

6.2.5 Underwater Voice Frequency Loudspeaker

A beginning was made at the New London laboratory on the design and production of a loudspeaker for an underwater communications system operating at sonic frequencies. The low attenuation in this fre-

CONFIDENTIAL

quency region promised considerably greater ranges than could be obtained in a heterodyne system using a carrier frequency in the supersonic range. The sonic frequency projector could be used in connection with the sonic listening gear. Efficient conversion of electric energy into sound energy over a wide band of frequencies requires a loudspeaker with a radiating area comparable in its dimensions to the wave length of sound in the transmitting medium. Thus, to operate in water at voice frequencies, a large transmitter is necessary. The toroidally wound, cylindrical hydrophone scaled up in dimensions would best meet the requirements; accordingly, the unit shown in Figure 10 was constructed. It was composed of three concentric, fully annealed laminations 0.015 in. thick, 18 in. long, formed into a cylinder 9.5 in. in diameter. The laminations were consolidated with Du Pont hot-melt cement. The windings were of No. 16 formex insulated wire, wound over an inside lining of air-cell rubber to neutralize pressures set up within the cylinder. The whole assembly was covered by BTL with a coating of 60 per cent butyl and 40 per cent methyl-methacrylate. With a d-c polarizing current of 3.0 amperes, this speaker gave the measured characteristics shown in Figure 11. The efficiency is seen to be greatest in the frequency range between 2,000 and 3,000 cycles, which is desirable for high intelligibility of speech. To compensate for the lowered output at 1 kc, it was recommended that the amplifier circuit be resonated at that frequency, using a 4- μ f condenser. Although the results with this model were very encouraging, the development had not been completed at the termination date.

6.3

HARVARD MODELS

The interest at HUSL in tubular-type transducers was focused on two prime objectives. The first was the possible development of special transducers for sonar use, but this idea was abandoned early in that program. The second grew out of a widespread need for means of tuning and aligning the projectors used in sound-ranging systems. The requirements for this latter use are not widely different from those for the sonic listening devices in which the New London group was interested except for the difference in the frequency range in which they were designed to operate. The features desired for *sound gear monitor*¹⁸¹ [SGM] hydrophones are: relatively simple construction, mechanical ruggedness, smooth frequency response, a radiation pattern uniform in azimuth, and

a sensitivity unaffected by mechanical shocks or temperature variation. All these qualities are potentially inherent in the tubular hydrophone. The B-19B hydrophones used in the OAX monitor, with a frequency range from 15 to 26 kc, and the B-19H used in the OCP extended-range monitor, 10 to 70 kc, were the end products of this development.¹⁸¹ They were widely used and were manufactured in quantity by commercial firms under Navy contracts.

6.3.1

Early Experiments

Experimental work on the tubular-type hydrophone was begun at HUSL in the first half of 1942. Some of the numerous variants of the vibrating tube that were tried in the earlier months are shown in Figure 12. Results of the measurements on these units may be summed up by saying that in general they were useful in showing what to avoid in building magnetostrictive transducers. At that time the necessity for delicacy of mechanical construction was not recognized. For example, in the light of later experience it is easy to see that soldering the joints of S-1 was sufficiently bad practice to cause nonuniform radiation in a plane at right angles to the axis of the cylinder.

S-4 will be recognized as an elongated version of the New London toroidal hydrophone. It was made of $\frac{3}{8}$ -in. nickel tubing, 18 in. long. The windings were without core. With an impedance of 1,000 ohms, sensitivity was relatively high for this type of transducer, -80 db vs 1 volt per dyne per sq cm, but the efficiency was low, something like 0.05 per cent. The elimination of the short-circuit path in the unbroken metal construction of S-4 by the introduction of the insulating gaskets shown in S-7 resulted in a threefold increase in sensitivity and served to give early emphasis to the necessity for avoiding a conducting path shunting the windings of the transducer.

S-6 consisted of four annealed nickel tubes each 8 in. long and 2 in. in diameter. The four tubes contained three coils. The two middle tubes contained one leg of each of two coils while the outer pair contained only the return legs of a single coil. The response and radiation patterns of this unit are shown in Figure 13. Theoretically, the radial resonance frequency of a tube 2 in. in diameter is 31 kc. The peak response shown is at 29 kc, and the sensitivity at resonance transformed to a 5,000-ohm impedance is -86 db referred to 1 volt per dyne per sq cm. The measured efficiency was 2.0 per cent, an unusually high

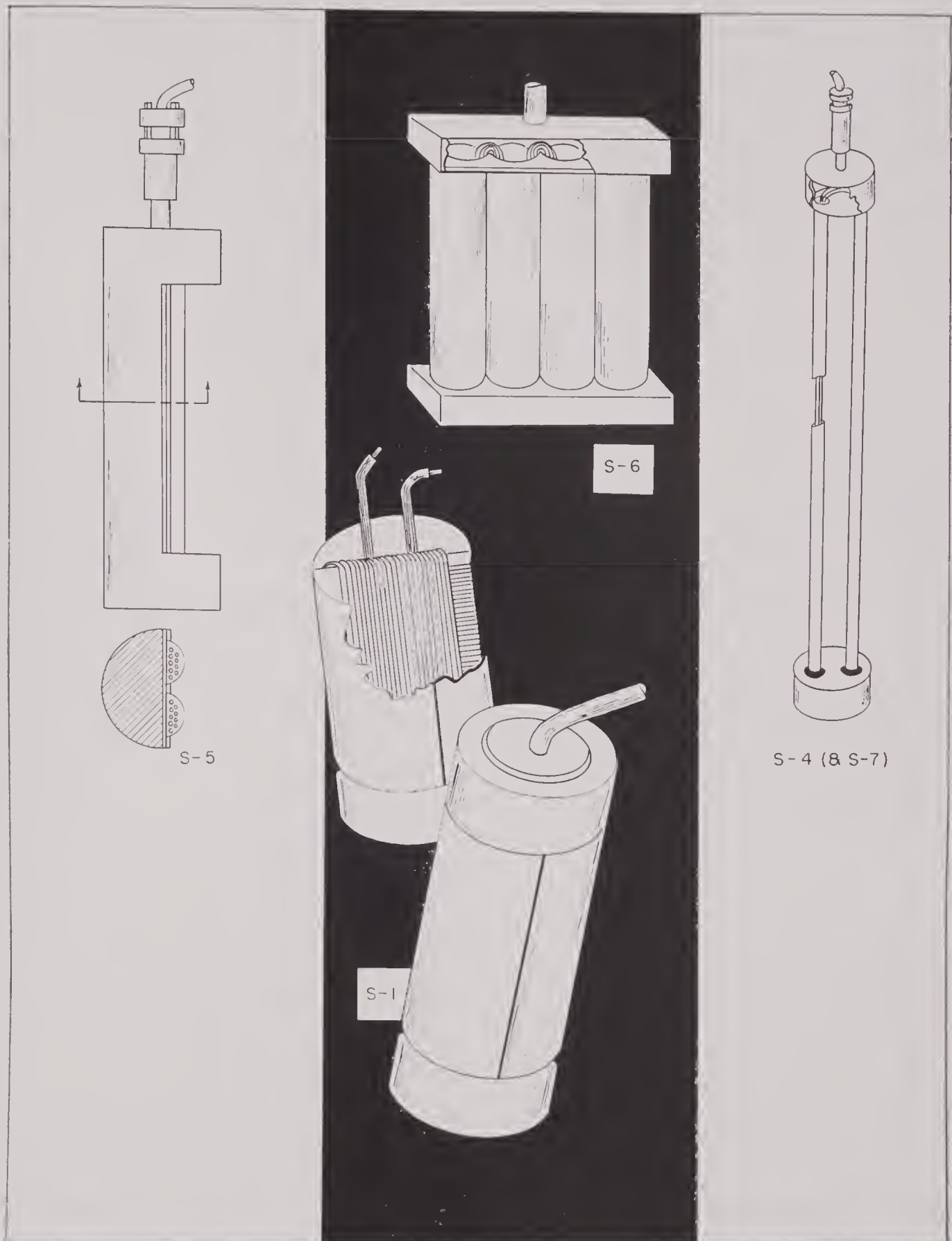


FIGURE 12. Four S-type transducers.

CONFIDENTIAL

value for this type of transducer. The pattern was equivalent to the theoretical pattern for a rectangular flat plate 8 in. high by 4.2 in. wide. Since the efficiency was low and the construction of this type of hydrophone did not lend itself to production methods, further development as a possible projector for sonar use was abandoned. It is of interest to note, however, that the idea of an array of tubular hydrophones with their axes parallel and all lying in the same plane was carried out quite successfully in the *QP* projector, developed for measurement use, which is described later.

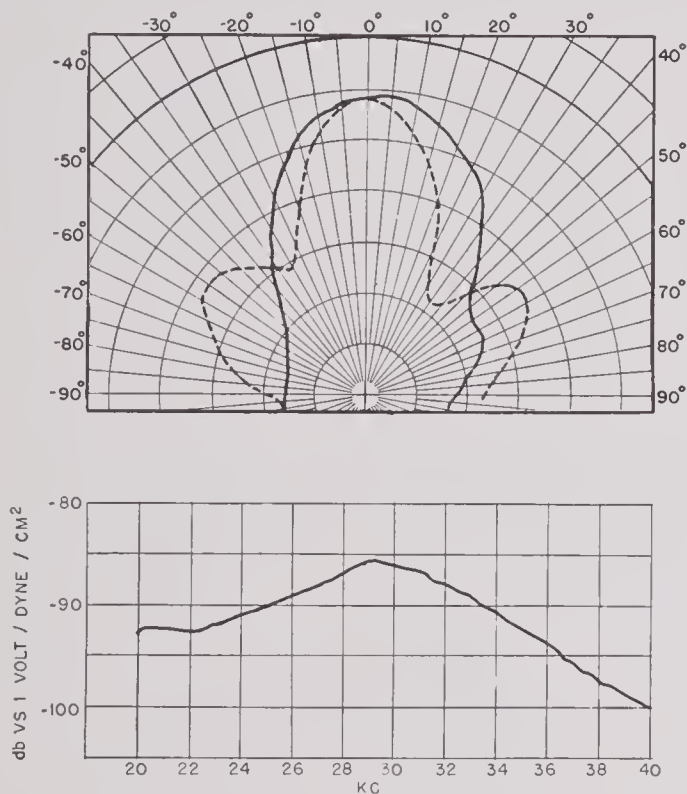


FIGURE 13. Pattern and response of four-tube hydrophone.

The S-6 marked the close of attempts to produce an efficient, radially vibrating, cylindrical projector. About the middle of 1942 attention was turned to the development of laminated stack transducers for this use, and work on tubular hydrophones was concentrated on producing a transducer that would meet the requirements of the overside sound gear monitor.

6.3.2 B-Series Hydrophones

OPERATING ON REMANENCE

In the early stages, development of laminated stack transducers was along lines which were being followed at New London in the sonic listening hydro-

phones, using unannealed nickel tubes with internal windings operating on remanent magnetization.

Figure 14 illustrates this development. The lens-shaped hydrophone A represents an attempt to realize the increased sensitivity that theoretically is possible from an increased radius of curvature without an increase in periphery.¹ The measured performance of this unit was disappointing. The frequency response was quite irregular and the average sensitivity low (-140 db referred to 1 volt per dyne per sq cm) over the frequency range from 10 to 50 kc. The straight tube with return winding passing through a brass tube B gave good patterns and a smooth frequency response (-131 db referred to 1 volt per dyne per sq cm, impedance 180 ohms at 20 kc), but it was difficult to wind and was not a practical construction for open-water use. It found use later in an early form of the installed monitor. In C is shown the prototype of the B-6A hydrophone. It differed from the New London straight-tube hydrophones in having a quadrant instead of a diametral core of Permalloy. Similar units in which sextant cores were used were built but showed no marked improvement over the quadrant or Maltese cross type of core. The large brass end caps were an early and unsatisfactory solution of the difficulty of sealing the ends of the tube and making the cable connections without burning the insulation off the windings in the soldering process. In B-6A, shown at D, the soldering problem was solved by providing the water seal for the cable connection shown at the top and by making the core shorter than the tube, so that the bottom could be soldered in without heating the insulation. The first and the final forms of suspension rig for the B-6 hydrophones are shown in Figure 15. In the final form soldered joints were completely eliminated by providing circular grooves in each of the stainless-steel end caps. The nickel tube fits in these grooves against neoprene gaskets, the assembly being held together by the six tie rods shown. This type of mounting has proved entirely satisfactory for hydrophones using $1\frac{1}{2}$ -in. nickel tubes. The B-6C, shown in Figure 16, was supplied with the early units of the 5D sound gear monitor model but was subsequently replaced by the B-19B permanent-magnet type.

A monitor transducer must be used both as projector and as hydrophone. The use of a polarizing current in a portable monitor is objectionable because of the bulk and weight of the rectifier and blocking chokes needed in the electric circuit. Heavy a-c driving may alter the sensitivity of a hydrophone operat-

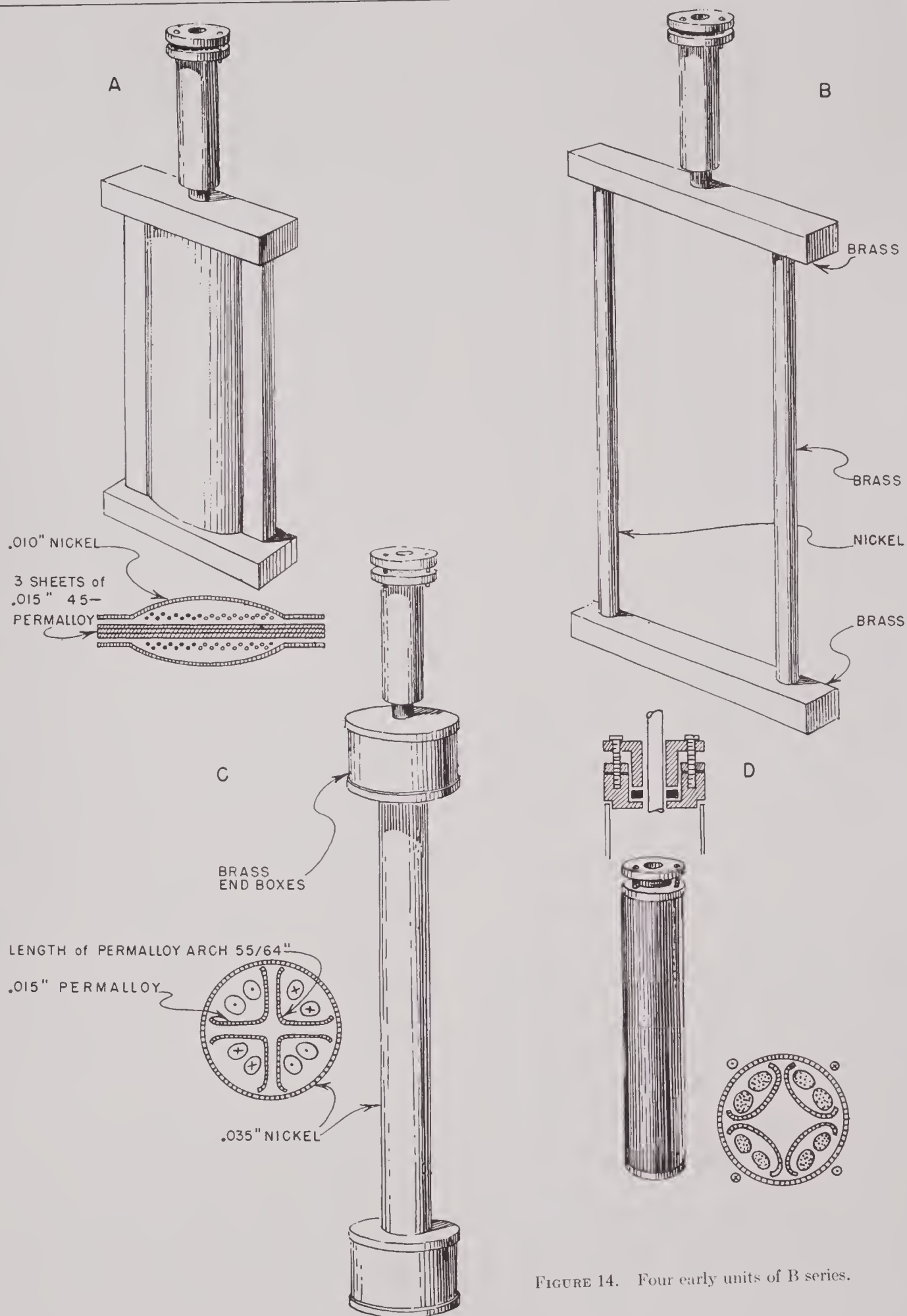


FIGURE 14. Four early units of B series.

CONFIDENTIAL

ing on remanence by partially depolarizing the magnetostrictive element.

In Figures 17 and 18 the sensitivities of a B-6A (unannealed) and a B-6B (annealed) hydrophone are shown as a function of the polarizing current. It will be noted that the sensitivity of the hydrophone with the unannealed tube is much less dependent on the polarizing current than is the one with the annealed tube. The effect of a-c driving on sensitivities is shown in Figure 17B.

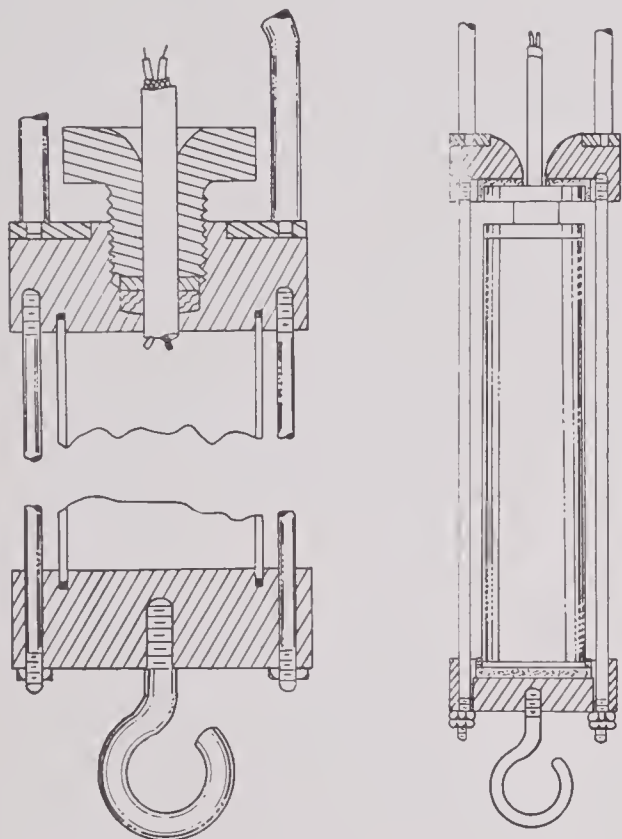


FIGURE 15. Two types of B-6 mounts.

TUBULAR HYDROPHONES WITH PERMANENT MAGNET POLARIZATION: B-19

The foregoing limitation of the tubular hydrophone operating on remanence emphasized the desirability of permanent magnetization when constancy of response is essential. The greater stability of the unannealed over the annealed tube was offset by its lower sensitivity, which called for greater amplification in the monitor amplifier. The annealed tube with permanent magnetization proved capable of meeting both requirements of greater sensitivity and permanent calibration.

Two experimental models, B-19 and B-19A, were built before the final design for the B-19B was adopted. In the B-19, polarization was supplied by



FIGURE 16. B-6C hydrophone.

20 small Alnico magnets each $\frac{1}{8}$ in. in diameter by $1\frac{1}{4}$ in. long set in holes in the solid wood core, which carried the windings on its circumference. The design of B-19A was identical except that 40 magnets were used. The first of the latter type to be built was used for a period of six months as a secondary standard at HUSL's Charles River barge. During this time,

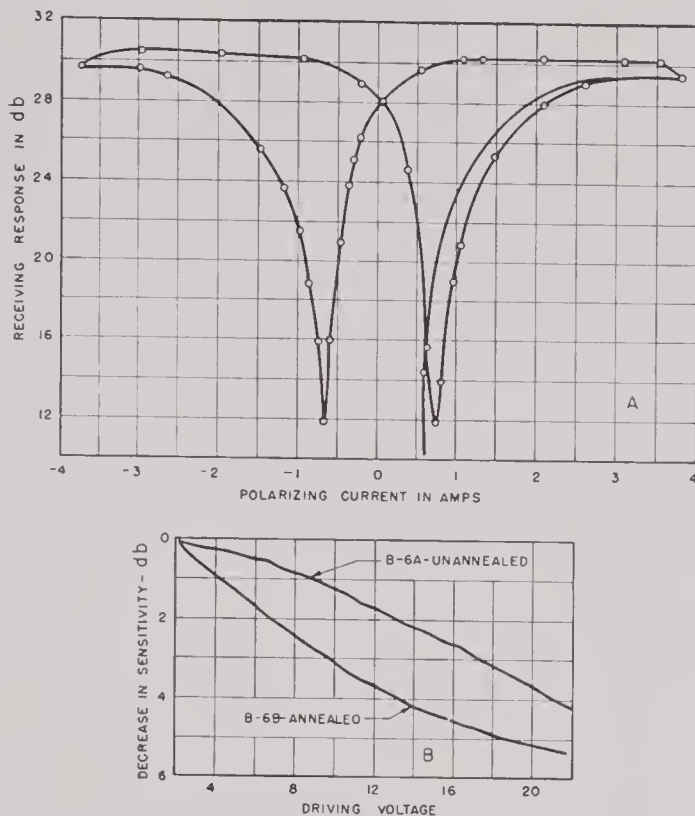


FIGURE 17. Hysteresis and depolarizing effect of driving on B-6 hydrophones.

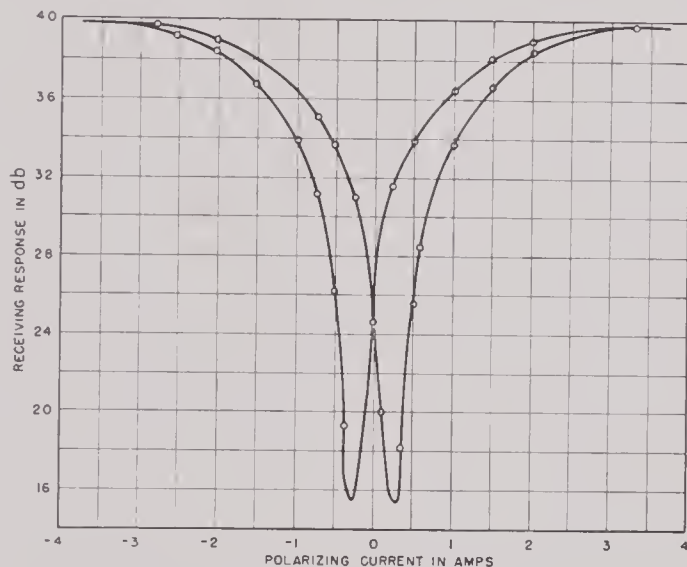


FIGURE 18. Hysteresis of annealed tube hydrophone.

eleven independent calibrations were made using BTL's pressure gradient standards. Water temperatures ranged from 5 C to 23 C. Although this hydrophone experienced rough handling in field use during this period, no significant sensitivity variations were observed. The increased magnetomotive force of the 40 magnets in B-19A over the 20 in B-19 produced an increase of 12 db in sensitivity, suggesting the possibility of still further improvement by the use of more

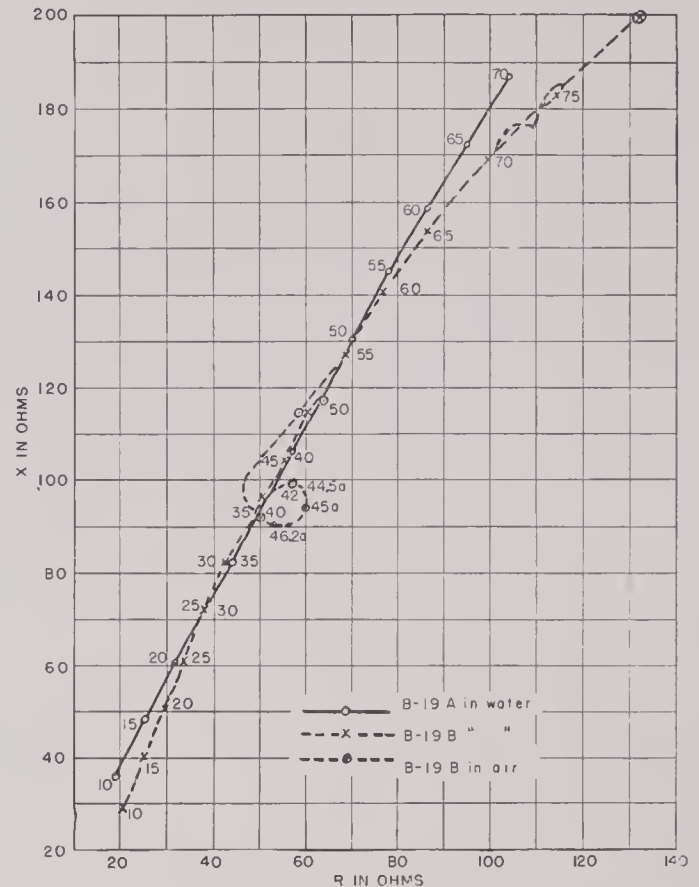


FIGURE 19. Impedance of B-19 hydrophones.

permanent magnet material. In the B-19B the separate magnets were replaced by two prisms of Alnico II, each $\frac{5}{16}$ in. thick by 1.40 in. wide. Pertinent electric and acoustic data on B-19A and B-19B hydrophones are shown in Figures 19, 20, and 21. The higher sensitivity of B-19B, even though it has a slightly lower impedance, indicates a closer approximation of the optimum polarization.

Polarization and Aging of Magnets. The demagnetization curve of Alnico II is shown in Figure 22. The optimum value of B for magnetostrictive response in annealed nickel is between 3,500 and 4,000 gauss. Experience has shown that a close approximation of this value gives both maximum sensitivity and permanence of calibration. The procedure used to obtain this value in the B-19B hydrophone is as follows: The Alnico prism is left unmagnetized until the core assembly is complete. The core piece is then placed between the poles of a large electromagnet and a field of at least 2,000 oersteds is applied. A magnetomotive force of about 10,000 ampere turns per inch of air gap is required. By proper rheostat control, the field is gradually reduced to zero and the core is removed from the air gap of the electromagnet. This treatment leaves the Alnico magnetized to full

strength, which is too great for maximum sensitivity and stability. Partial depolarization is effected by connecting the core windings to the output of a 250-volt Variac and allowing an a-c current of 7 to 9 amperes to flow through it for a short time. Care is taken to decrease the depolarizing current to zero smoothly to prevent the possibility of heavy transients when the circuit is broken. The field produced

series-parallel across the condensers serve to remove any residual charge. The 10,000-ohm, 4-watt variable resistor is a means of adjusting the d-c voltage output of the rectifier, and the 1- μ f, 1,500-volt condenser provides some filtering of the rectifier output. Operation of the device is as follows: The FG-57 thyratron (a slow, indirectly heated cathode type) preheats for 5 minutes; otherwise, damage to the tube will result.

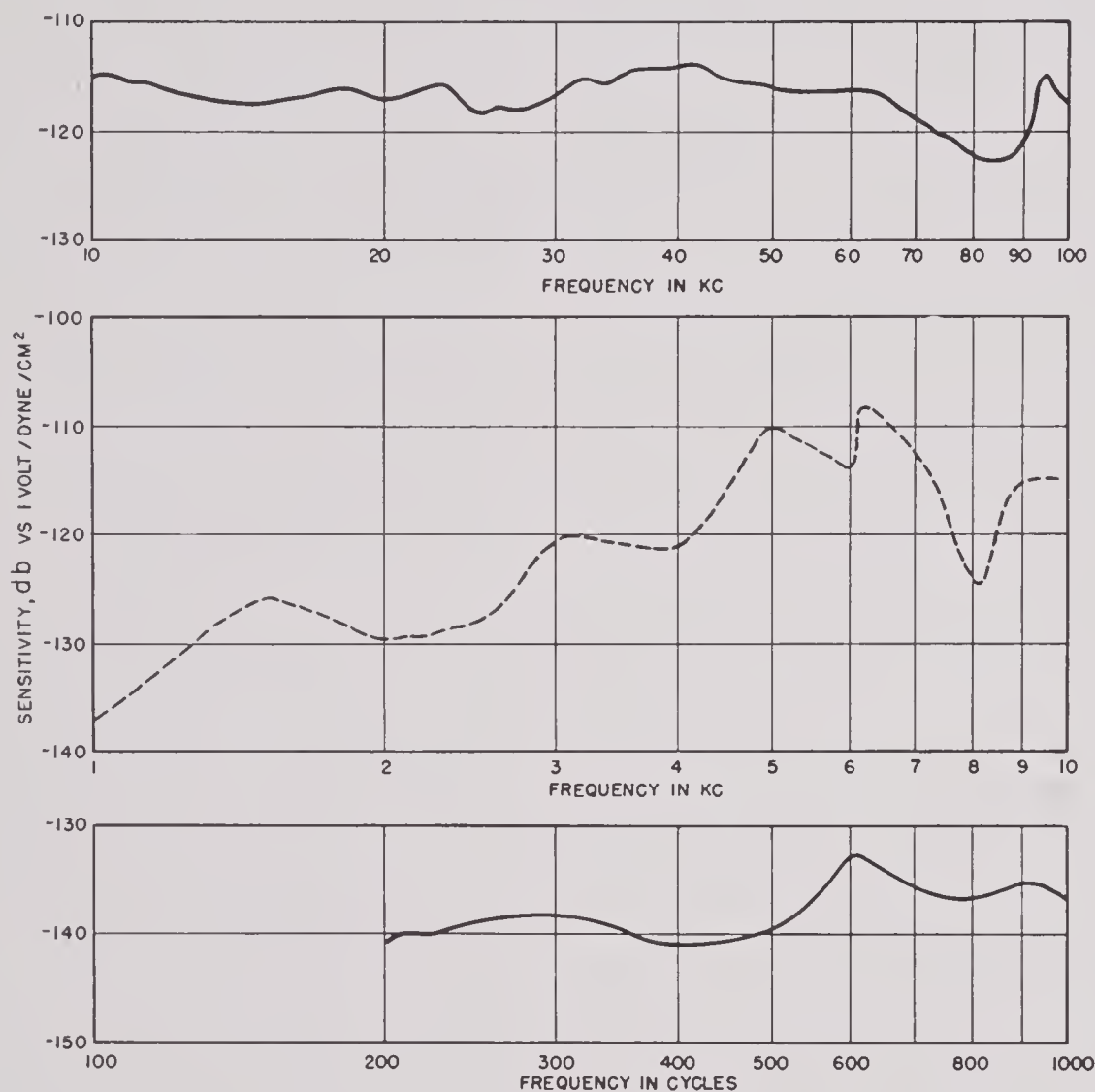


FIGURE 20. Sensitivity of B-19A hydrophone.

by the magnet after this treatment should be 200 egs units at a distance of 7.0 mm from the pole face.

An alternative means of polarizing the Alnico magnet is shown in Figure 23. A stock power transformer (Thordarson 13R16) supplies 800 volts of alternating current (400 each side C'T) to the plates of the 5R4GY half-wave rectifier tube and also 5 volts to filament. A second transformer (Thordarson 19F83) furnishes 5 volts at 4.5 amperes for the FG-57 thyratron filament. Two 0.15-megohm, 2-watt resistors in

After the FG-57 cathode is preheated, the "push switch" is closed, lighting the 5R4GY filament and applying the a-c plate voltage to the half-wave rectifier. The d-c output of the rectifier is utilized as the charging voltage of the 150- μ f bank of condensers. During the charging time, a voltage drop appears across the 20,000-ohm, 10-watt resistor, due to the charging current flowing through it. This voltage negatively biases the grid of the FG-57 thyratron and prevents the tube from conducting. When the 150- μ f

condenser bank has been charged to a voltage equal to that of the power supply, the charging current ceases to flow and hence the biasing voltage on the thyatron drops to zero. The latter becomes a conductor and discharges the 150- μ f condensers through the core winding. The cycle will repeat if the push button is held down long enough.

The variations in receiving response and patterns among different units are indicated in Table 1. These values were obtained from measurements on 13 hydrophones picked at random from 140 made at HUSL.

When the transducer was used as a projector, the sound pressure set up at a distance of 1 meter with 8

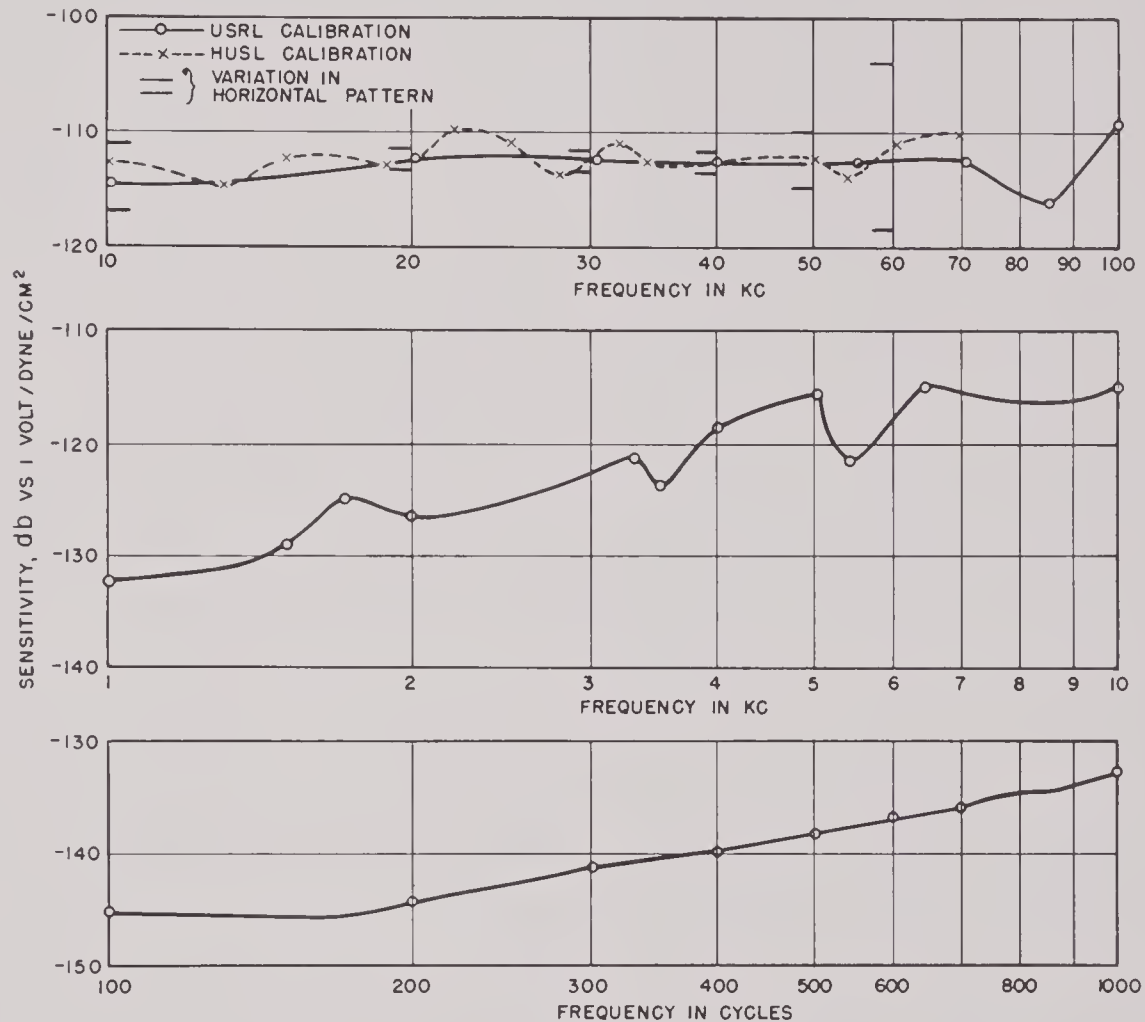


FIGURE 21. Sensitivity of B-19B hydrophone.

Various safety devices such as interlocks, a shorting relay across the condensers, and careful protection of the output terminals (marked B-19B) should be incorporated to protect the operator from the high voltages and heavy current built up in the operation of the device.

The dependence of the impedance and the sensitivity on the state of magnetization of the Alnico is shown in Figure 24. The upper graphs show the effect on the frequency response produced by the application of a 4-ampere depolarizing current to a fully magnetized core. The lower curve shows the change in sensitivity at 20 kc caused by depolarizing currents of increasing magnitudes up to 10 amperes.

volts applied across the terminals varied between 43 and 51 db above 1 dyne per sq cm over the frequency range from 10 to 40 kc. No appreciable change in sensitivity was found to result from driving at supersonic frequencies up to voltages as high as 20.

With the cooperation of members of the New London laboratory, rigorous tests for possible effects of shock waves have been made. A B-19B hydrophone was mounted on the deck of a submarine submerged at 100 ft. No measurable change in sensitivity resulted from 16 successive explosions of 300-lb depth charges at a distance of 300 yd.

Construction Details of B-19B Hydrophones. Figures 25, 26, and 27 give the assembly details of the produc-

tion model. The permanent magnet is made from two cast sections of Alnico II, each $0.312 \times 1.40 \times 2.5$ in. The core halves are made of wood impregnated with phenolic resin and cemented to the magnet. The coil consists of 130 turns of No. 26 single cotton-

frequency response and pattern are affected to a considerable degree by the delicacy of mechanical details. (Successful commercial production of B-19B hydrophones for use with the OAX overside sound-gear monitor was carried out on a large scale by the

TABLE 1. Variations of sensitivity and receiving patterns of thirteen B-19B hydrophones.

Frequency (kc)	10	15	20	25	30	35	40
Sensitivity (db ref. 1 volt / dyne/cm ²)							
Max	-114	-112	-112	-111	-111	-112	-110
Min	-119	-114	-114	-117	-114	-114	-113.5
Avg	-116	-113	-113	-114	-112.5	-113	-111.5
Pattern variation							
Max	...	2.0	3.0	2.5	1.5	2.0	...
Min	...	0.3	0.7	0.5	0.6	0.7	...
Avg	...	1.3	1.8	1.7	1.1	1.0	...

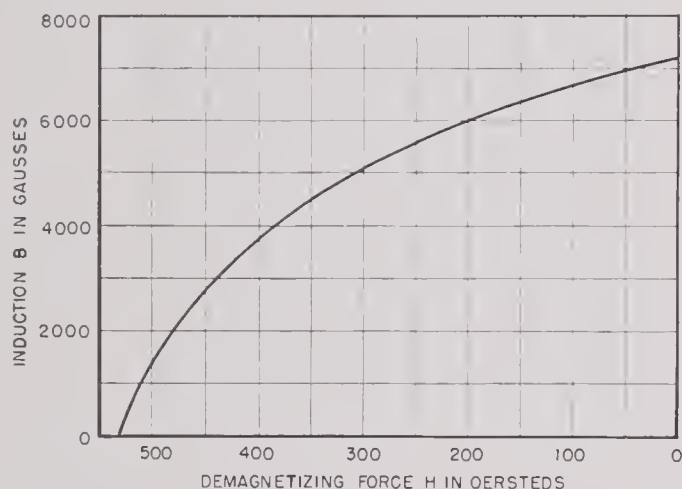


FIGURE 22. Demagnetization curve of Alnico II.

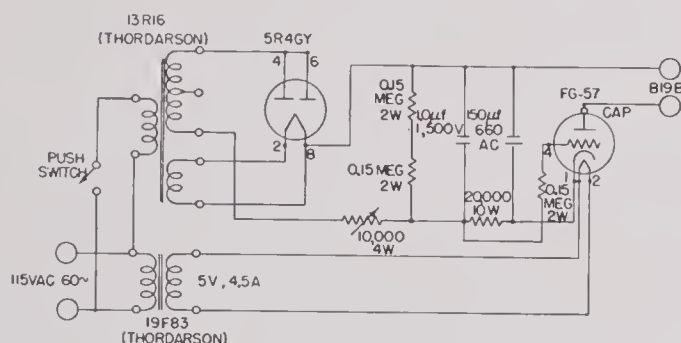


FIGURE 23. Circuit for polarizing magnets.

covered wire and is wound in two halves on specially designed jigs to fit nicely on the wooden core pieces to which they are cemented. The whole core assembly is cemented and baked into a compact unit that makes a sliding fit in the nickel tube. Both

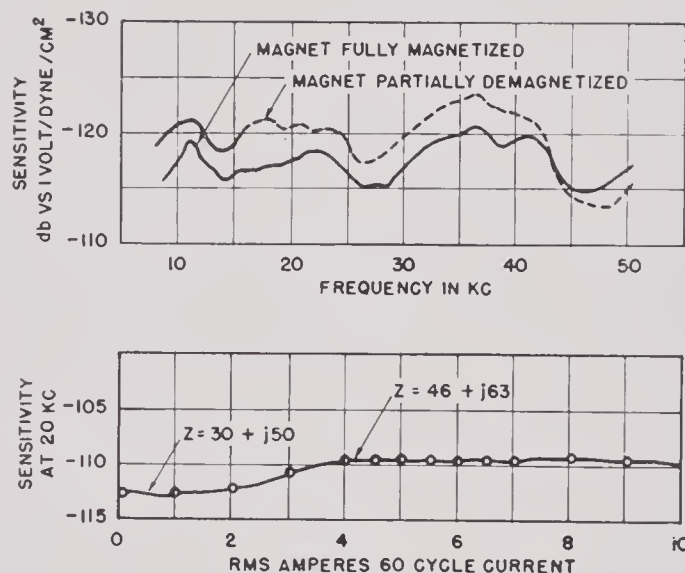


FIGURE 24. Effect of partial depolarization on sensitivity of B-19B hydrophone.

Presto Recording Corporation of New York and the Harvey Radio Laboratories of Cambridge.)

B-19H Hydrophone. The B-19B meets the requirements of monitor use up to 40 kc, approximately the frequency of the first radial resonance of a 1.5-in. nickel tube. Above this frequency, the horizontal pattern is no longer uniform, and the response varies widely with the orientation of the hydrophone. The B-19H (Figure 28), which is essentially a miniature reproduction of the B-19B, has a $\frac{3}{4}$ -in. tube and is polarized by a Cunico diametral magnet. The resonance frequency is 83 kc. Curve 1 of Figure 29 gives the sensitivity of the bare hydrophone. Impedances in air and water are shown in Figure 30. The vari-

ation in horizontal pattern was found to be not greater than 2.0 db at frequencies from 10 to 70 kc.

The efficiency of B-19H is relatively low. The directivity indices and efficiencies, computed from sensitivity data by equation (25) of Chapter 1, are as follows:

Frequency	20 kc	30 kc	60 kc
Directivity index	0.225	0.193	0.104
Per cent efficiency	0.084	0.25	0.36

In the earliest units the end caps were simply brass plugs soldered into the ends of the nickel tube, after the fashion of the B-6A type. But when the tube was

posed between tube and end cap gave a smooth frequency response, but this type of mount was too fragile to be practical.

After considerable experimentation with mounting in a protective cage, the production model shown in

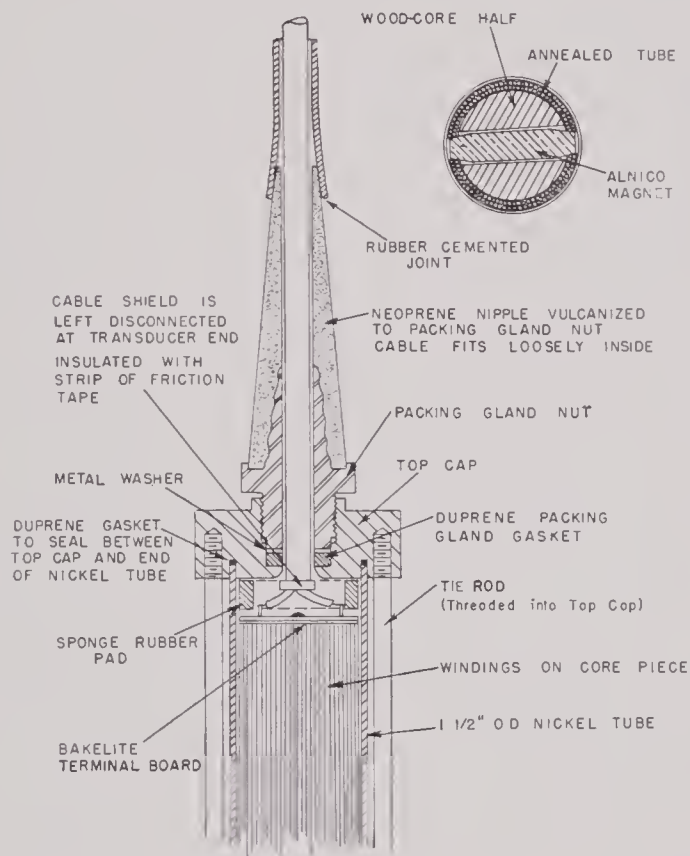


FIGURE 25. Sections of B-19B hydrophone.



FIGURE 26. Preamssembly of B-19B.

mounted in the lantern-type mount, a sharp irregularity in response, accompanied by a large variation in the horizontal pattern, occurred at 21 kc, as shown on curve 2, Figure 29. The smaller diameter tubes of the B-19H proved much more susceptible to undesired vibrational modes than were the larger tubes of the B-19B. Electric measurements on the mounted hydrophone in air (Figure 30) gave no evidence of a motional impedance circle at 21 kc. This anomalous behavior has not been fully explained, but it involves mechanical coupling between the tube and the end caps. Tubes mounted in end caps with corprene (cork-neoprene) washers inter-

Figures 31 and 32 was evolved. The protecting cylinder (*H*) of expanded stainless steel is hydrogen-welded to the stainless-steel end rings. The flange of the upper end cap (*A*) is bolted to the upper ring of the protective cage, with a corprene washer (*I*) separating the two metal surfaces.

The lower end of the tube (*B*) fits snugly into a ring of butyl rubber (*F*), which isolates it from the protective cage. This method of mounting largely eliminates the spurious resonance at 21 kc and reduces the strain on the soldered joint between the tube and the upper end cap. Both soldered joints are protected from corrosion by painting with Amercoat

33, a water-resisting polyvinyl-chloride-based paint. Soldered joints painted with this material and exposed for 200 hours to hot salt spray showed no sign of deterioration. The receiving and transmitting response and pattern data for five units presented in Figure 33 are typical.



FIGURE 27. Coil and magnet assembly of B-19B.

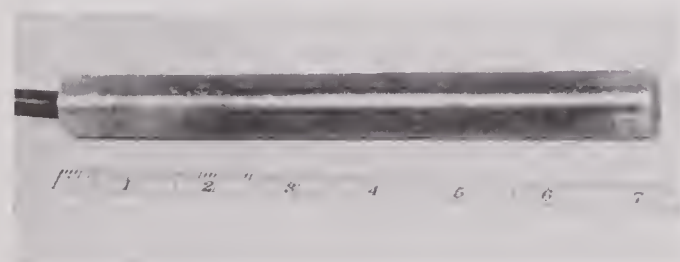


FIGURE 28. Unmounted B-19H hydrophone.

Variants of the B-19 Type Hydrophone. Several hydrophones of the B-19 type have been built for special uses. The B-19K was built to serve as a projector for monitor use in the octave from 5 to 10 kc to supplement the B-19H, which is unsatisfactory as a projector below 13 kc. The oxide-annealed nickel tube was 2.5 in. in diameter and 6.5 in. long. Internally it was a 2.5-in. version of the B-19B. Its characteristics are shown in Table 2.

The B-19L (Figure 34) is an 11-in. modification of the B-19B and was intended for the use in locating submerged stationary sound sources. Since it was to

be used with its long axis lying in the horizontal plane, it was designed to have a sharp azimuthal pattern. For this reason, the three-coil construction proved preferable, since the desired pattern could be obtained by shading the two half-length sections at the end. One half of the circumference of the tube was

TABLE 2. Characteristics of the B-19K hydrophone.

Frequency (kc)	5	10	15	20
Impedance	$28 + j28$	$33 + j49$	$38 + j70$	$43 + j85$
Sensitivity (db vs 1 volt/dyne/cm ²)	-112	-110	-110	-110
Field at 1 meter, 10 volt driving (db vs 1 dyne/cm ²)	41	48	48.5	48.5
Horizontal pattern variation (db)	5	4.5	1.0	1.0
Efficiency (per cent)	0.12	0.29

covered with pressure-release material (air-cell neoprene) to control the pattern in the median plane perpendicular to the axis. When it is used in searching, the hydrophone is mounted in a streamlined housing (Figure 35) made of molded Lucite, with pro-

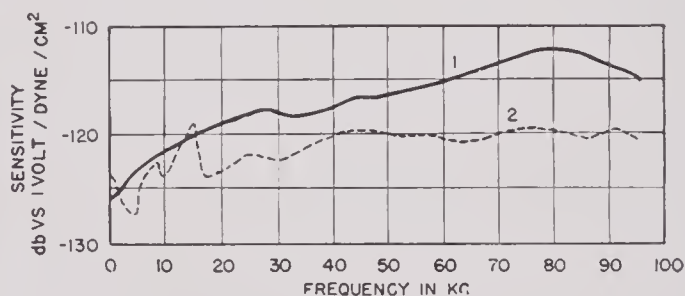


FIGURE 29. Sensitivity of B-19H, (1) without mounting and (2) with lantern-type mount.

vision for rotating the hydrophone about its length. Rotation of the transducer with its dome about the axis rotates the beam in azimuth. The patterns at 25 kc in the two planes are shown in Figures 36 and 37.

A number of B-19H units 2 in. long have been built. These have proved to be more subject to individual variations in response and pattern. Well-behaved units, however, showed theoretically predictable characteristics, namely, sensitivities about 8 db below the 5-in. B-19H and patterns corresponding to the theoretical for a 2-in. line source.

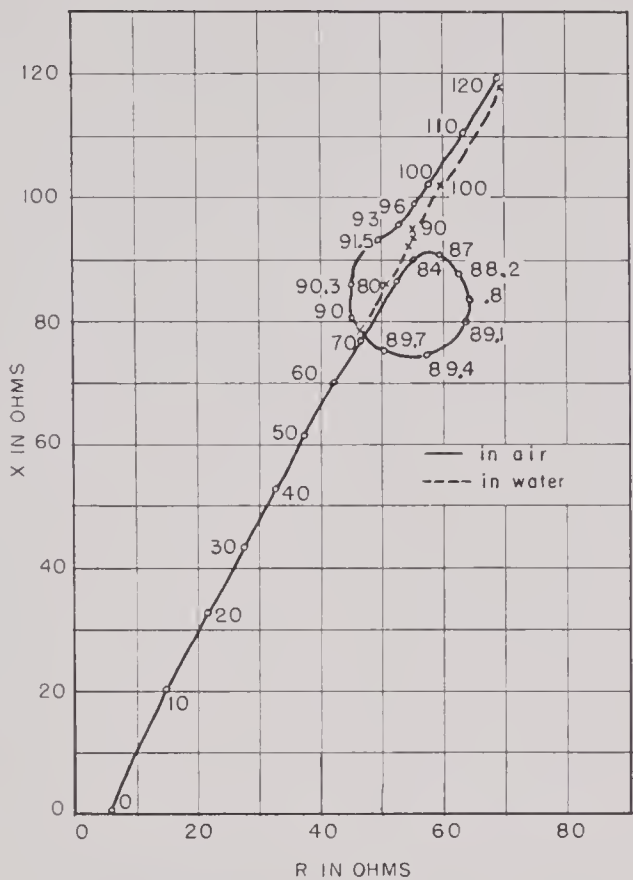


FIGURE 30. Impedance of B-19H.

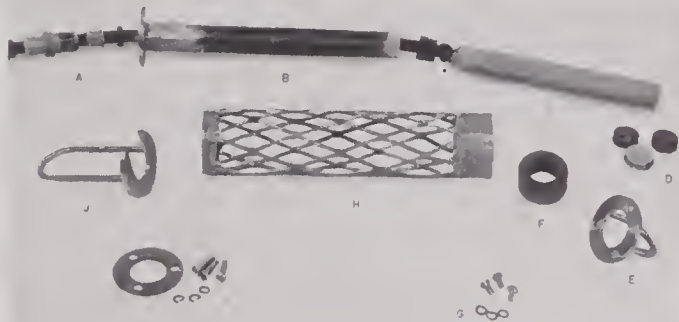


FIGURE 31. Preassembly of B-19H (production model).

6.3.3 Installed SGM Hydrophones

A hydrophone intended to be permanently installed for monitoring use must be enclosed in some form of streamlined housing. Various mountings have been tried, which are briefly described as follows.

1. Thin-walled stainless steel of "teardrop" cross section enclosing a B-6A hydrophone. The form was filled with outgassed castor oil. Because of poor response and patterns, this was replaced by a free-flooding housing of expanded metal, covered with thin stainless-steel sheet (0.020 in.). This was used

satisfactorily on the USS *Galaxy* for a period of more than a year.

2. A hollow rubber form reinforced internally with expanded metal, with a tubular transducer inserted in a cylindrical cavity in the rubber. Difficulty was experienced in getting an assembly free from air between the transducer and the rubber, as well as in molding rubber which would be free from voids around the expanded metal. One satisfactory unit was produced in this way.

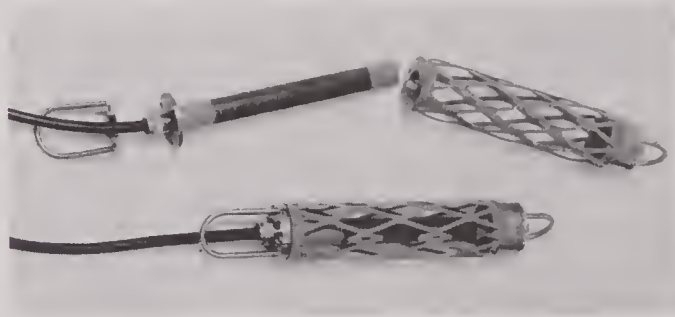


FIGURE 32. Production model B-19H.

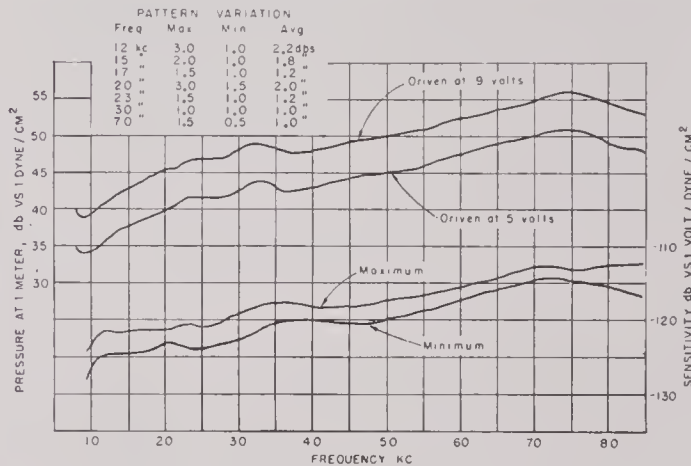


FIGURE 33. Transmitting and receiving response of B-19H.

3. Transducers mounted in the pitometer log strut.^b Several different types of mounting were tried. The most successful is shown in Figures 38 and 39. A B-19H hydrophone was inserted in a cylindrical hole in a rubber casing vulcanized into the window in a bronze frame of pitometer log cross section. The effect of the bronze casing on sensitivity and pattern is shown in Figure 40, but since, in the use intended, the orientation of the installed unit relative to the projector would be fixed, the rather large variation in the

^b Pitometer log equipment, developed by the Pitometer Log Corporation includes a streamlined strut with two tubes for measuring the static and dynamic pressure of the water.



FIGURE 34. B-19L listening hydrophone.

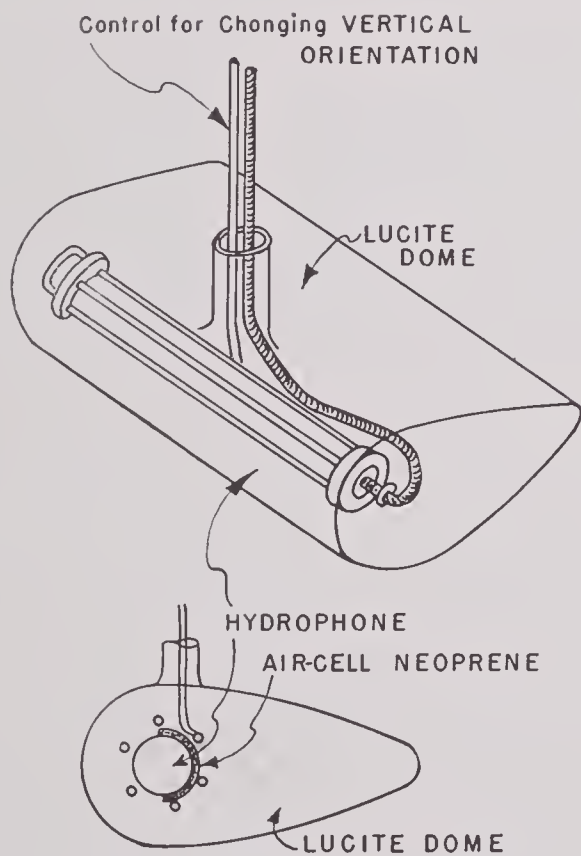


FIGURE 35. Mount for B-19L.

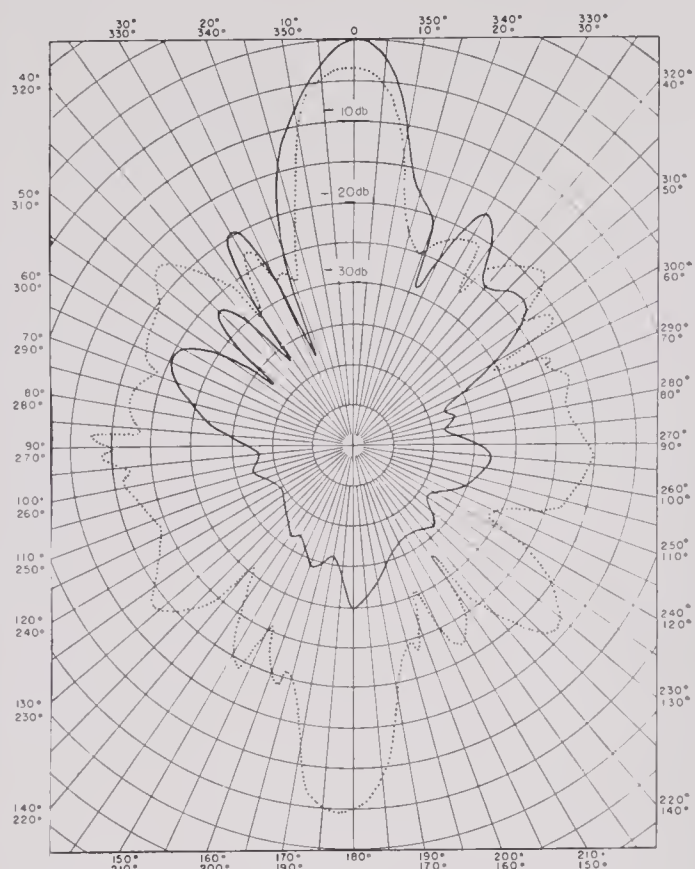


FIGURE 36. Pattern of B-19L in plane of the axis. Solid line, with pressure-release backing; broken line, without backing.

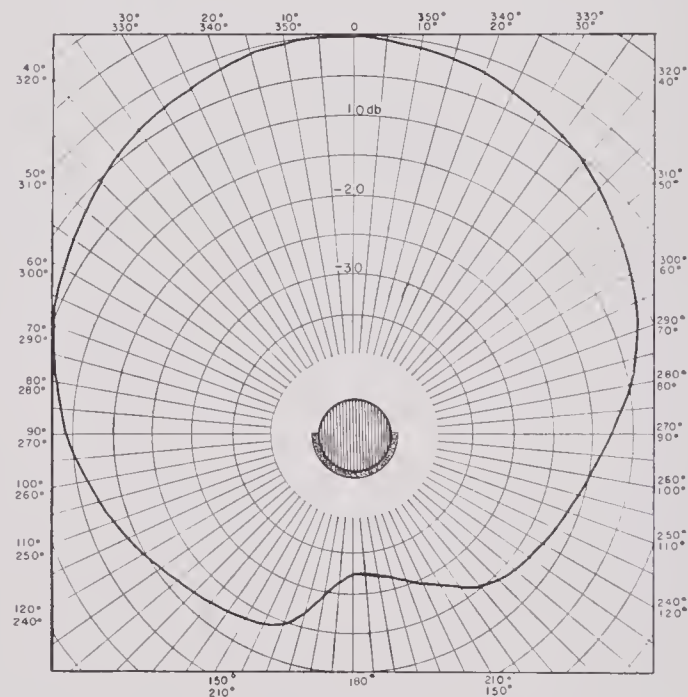


FIGURE 37. Pattern of B-19L in plane perpendicular to the axis.

pattern would not rule out this hydrophone for monitor use. Four of these units were built and two gave satisfactory monitoring service on Navy ships for periods of more than six months.

CONFIDENTIAL

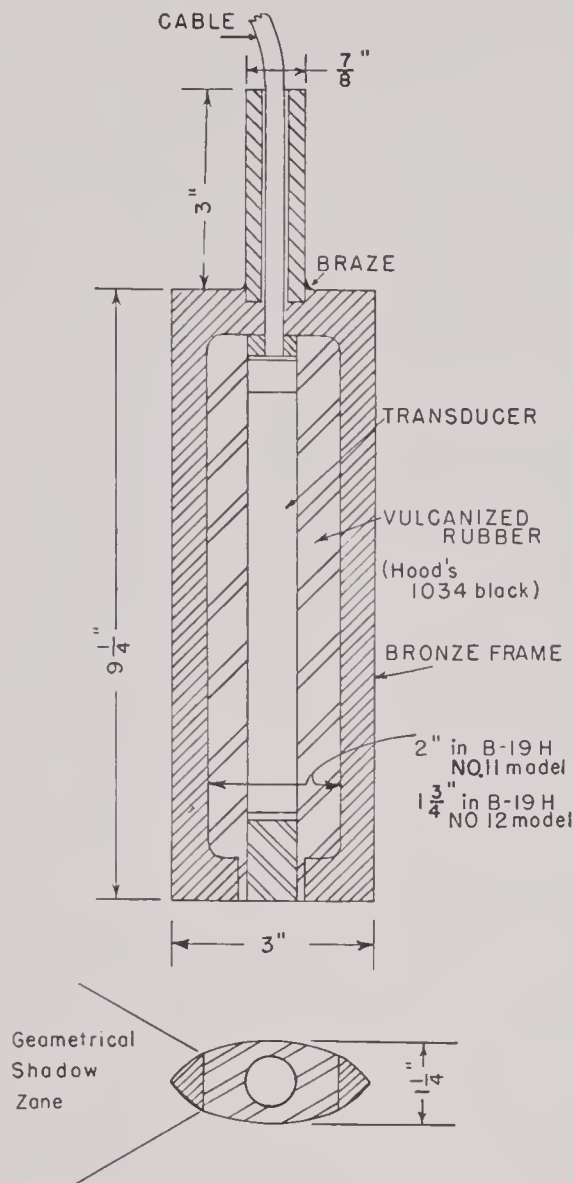


FIGURE 38. Installed SGM in pitometer log strut.

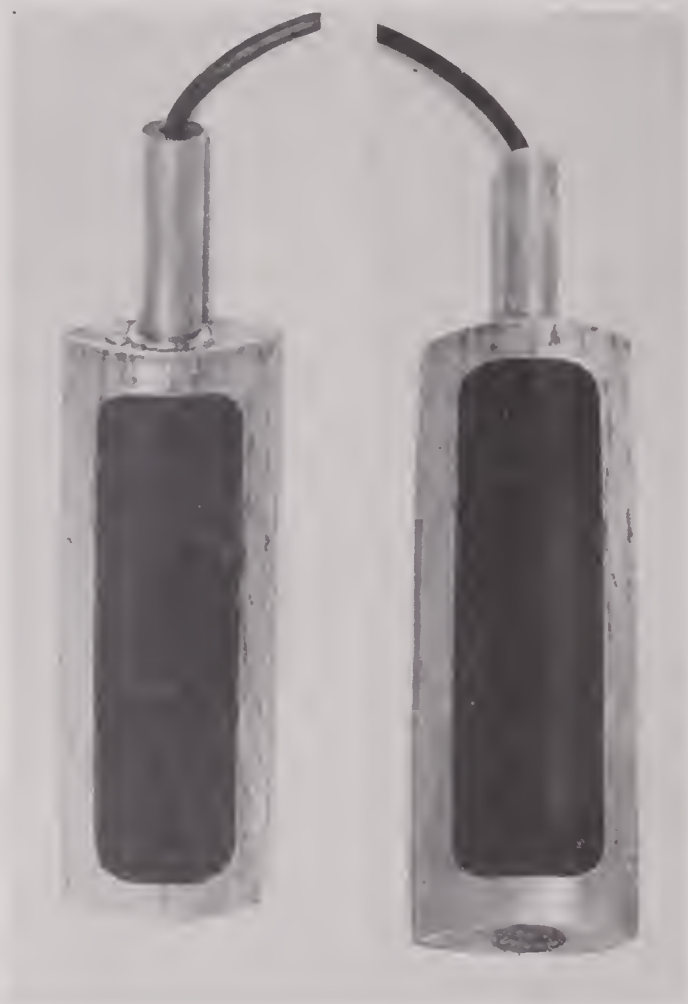


FIGURE 39. Production model of installed SGM hydrophone.

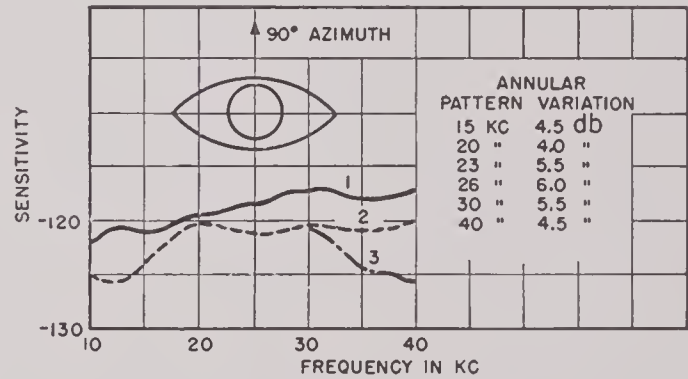


FIGURE 40. Sensitivity of installed SGM hydrophone: (1) unmounted hydrophone, (2) at 90 degrees azimuth, (3) at 0 degrees azimuth.

6.3.4 Laminated Tube Transducers

HARVARD EXPERIMENTAL UNITS

Attempts at HUSL to get higher efficiencies in tube transducers by laminated construction were not very successful. Efforts in this direction were limited to laminated tubes built of thin nickel stock rolled into scrolls or built up in layers, with the successive layers bonded together with an adhesive. Sections of several types tried are shown in Figure 41.

The form shown at A was made by winding layers of nickel sheet 0.003 in. thick on each half of a split mandrel to form a double D, giving a diametral core on which the coil was wound. Forms at B and C were provided with diametral wooden cores with peripheral windings.

In B, the magnetostrictive tube was formed by winding the thin annealed-nickel sheet on a mandrel under constant tension. The scroll thus formed was reannealed to remove winding strains and then consolidated with adhesive.

The laminations of the layer-built tubes shown at C were annealed and the composite tube was formed by placing the first layer on a mandrel and coating it with Vinylseal resin. After the coating was partly dried, the second layer was applied. The process was repeated until the seven split tubes had been built up into a solid unit. This was placed in a compression mold and baked under pressure for half an hour at 150 C.

ber of cements and consolidating techniques were tried in cooperation with the Westinghouse Electric Company's laboratory in Sharon, Pennsylvania. The methods employed were those used in building split-core transformers. A defect, now obvious, in the units with wooden cores and peripheral internal winding lies in the fact that no advantage accrues from the laminated structure. This is due to the magnetic shielding of the outer by the inner layers. One

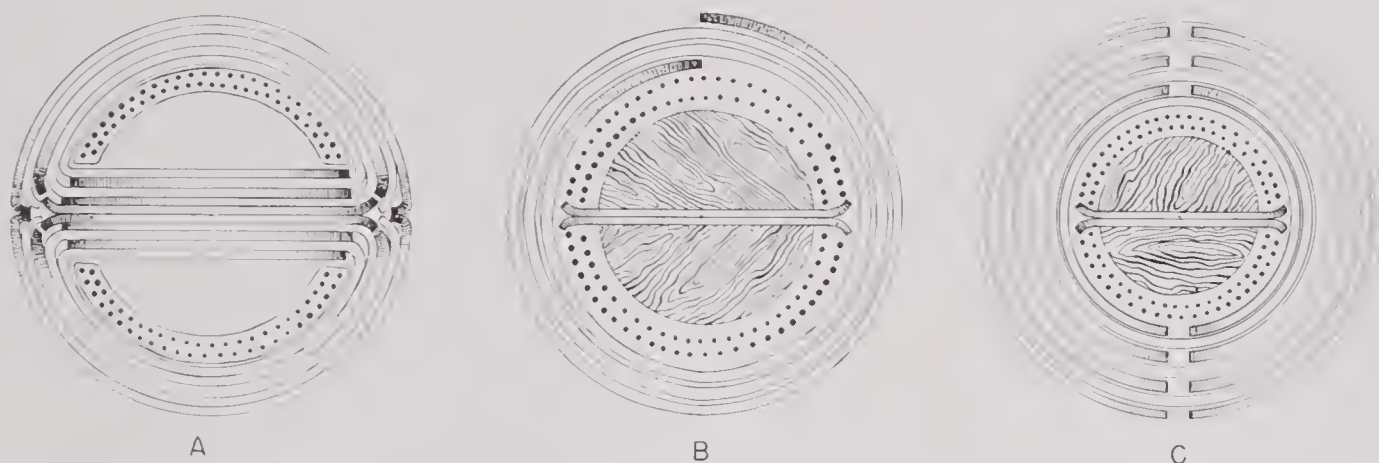


FIGURE 41. Cross sections of three types of laminated tubes.

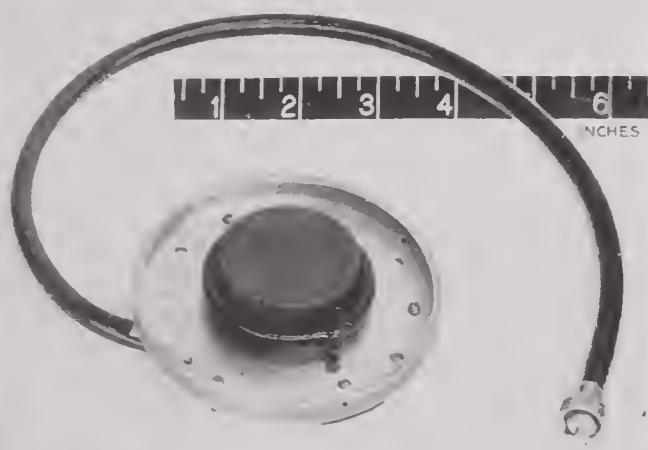


FIGURE 42. Bell Telephone Laboratories' MKX laminated scroll hydrophone.

Six of the scroll and three of the layer-built tubes were made, all 1 in. in diameter and $4\frac{1}{2}$ in. long. None of these showed sensitivities as great as that of a control unit with a solid annealed-nickel tube 0.035 in. thick of the same dimensions and wound to approximately the same impedance. The chief difficulty was in getting a uniform mechanical structure. With a single exception, the patterns of all the laminated tubes were poor. In consolidating the scrolls, a num-

ber of the layer-built units was subsequently rewound toroidally and gave a resonant response with a Q of 2.8 and a measured efficiency of 20 per cent. All things considered, however, the laminated ring stacks with toroidal winding presented fewer mechanical difficulties and greater promise than the laminated tubes. Further development of these tubes was accordingly abandoned at HUSL late in 1943.

RING SCROLLS BY BELL TELEPHONE LABORATORIES

An account of work at BTL in the development of a nondirectional transducer includes a description of a spirally wound ring of Permalloy tape 0.002 in. thick and 0.375 in. wide. This was wound to give a ring with outside diameter of 2.36 in. and wall thickness of 0.197 in., designed for maximum response at 24 kc.¹⁸⁴ The surface of the Permalloy was insulated by applying a thin layer of silica by cataphoresis while the ring was being wound. The ring was annealed and vacuum-impregnated with bakelite resin. It was wound with a layer of cotton tape over which was wound a single layer (320 turns) of No. 28 enameled, silk-covered wire and again impregnated with bakelite resin, bonding the winding to the ring. This construction would be expected to give a much more compact assembly than the method used for the

tubes at HUSL. However, the frequency response proved to be far from smooth and the pattern in the plane of the ring was only fairly uniform. This irregularity, observed in all the tape-wound models, was explained by the probable presence of low-frequency modes superimposed on the radial mode of vibration. An account of later and more successful experiments at BTL with specially wound tape rings will be found in the final section of this chapter.

A somewhat unusual application of the radial vibrator was made by BTL in the MKX hydrophone designed for the transmission of acoustic energy to the water through an intervening shell of steel.¹⁸³ This hydrophone is shown in Figure 42. In this case the ring was 0.002-in. nickel tape annealed at 600 degrees to operate on a remanent flux density of 3,600 gaussses and a coercive force of $H_0 = 14$ oersteds. The construction of the ring was otherwise similar to that just described. A 1.25-in. rubber cylinder with diameter greater than the inside diameter of the ring was forced into the ring. The rubber cylinder was cemented to the steel backing plate. The latter carried a cupped rim that served to center the hydrophone in the desired position with the free end of the rubber cylinder in contact with the inner surface of the shell through which sound was to be transmitted into the water. The backing plate was drawn down, compressing the rubber cylinder so that its clamped length was about 85 per cent of its free height. The radial vibrations of the ring excited longitudinal alternating stresses in the rubber that were transmitted through the metal shell into the water.

6.4 RING STACKS

The ring stack transducer is composed of ring laminations which vibrate radially. In toroidal winding, the electroacoustic transformation is effected by the magnetostriction of the laminae. The design of a ring stack is a fairly straightforward job. If there is mechanical uniformity in the plane of the ring, then the pattern in this plane will be uniform. Since the mean circumference of the stack is one wave length of sound at the resonant frequency in the magnetostrictive material, and since the wave lengths in water and metal are proportional to the velocities of sound in the two media, it is easy to show that the mean diameter of the stack is about 1.1 wave lengths of sound at the resonant frequency in water. Hence the pattern in a plane containing the axis will be approxi-

mately that of a line source of length equal to the height of the stack. The resonant frequency and the patterns are thus determined by the mean diameter and the height of the stack respectively. The mechanical Q is given by equation (3) and involves only the ratio of the radial thickness to the mean radius.

6.4.1

Design Features

The ring stacks built at HUSL were generally designed to have a Q of about 5, which from equation (3) calls for the ratio of radial thickness to radius of about 0.17. In Table 3 are shown the dimensions and

TABLE 3. Dimensions of ring dies.

Nominal freq. of ring stack in kc/sec.	Lami- nation thickness (inches)	ID (inches)	b/a	OD (inches)	Material die was designed to punch
20	0.010	2.652	0.22	3.308	Nickel
23.5	0.010	2.315	0.228	2.745	Nickel
24	0.010	2.42	0.167	2.86	2V-Permendur
26	0.010	2.23	0.172	2.65	2V-Permendur
28	0.010	1.94	0.169	2.30	Nickel
31	0.010	1.87	0.164	2.20	2V-Permendur
36	0.075	1.61	0.171	1.91	2V-Permendur
40	0.075	1.42	0.19	1.72	2V-Permendur
54	0.005	1.006	0.17	1.194	Nickel
58	0.005	0.875	0.16	1.205	Nickel
60	0.005	0.97	0.18	1.15	2V-Permendur

materials of the various ring stacks that were built at the laboratory. In general, the measured resonance frequencies agreed well with computed values. As would be expected, the value of Q shown by measurement of the completed transducer was affected by a number of factors besides the ratio of radial thickness to radius. Thus, a stack with the height of a wave length or less in water showed a Q higher than the computed value because the water loading was not wholly resistive, as it was assumed to be in deriving the formula for Q . Impregnating and plasticizing a stack resulted in lowering the resonance frequency as well as in reducing the sharpness of the response. Experimental stacks with a b/a value considerably less than 0.17 were built and showed almost uniform response over a wide frequency range. All told, the ring stack has proved a quite flexible electroacoustic transducer. An efficiency of 40 to 50 per cent was realized repeatedly with a Q of 5. It was possible to build a thin-walled stack of 2V-Permendur with a

thickness-to-radius ratio of only 0.06 and a Q of less than 2 that showed a measured efficiency of 15 to 25 per cent over the frequency range from 40 to 60 ke.

6.4.2 Thickness and Heat Treatment of Laminations

As Chapter 3 showed, eddy-current loss is a function of both frequency and lamination thickness. The thicknesses of the laminations used in the ring stacks listed in Table 3 will be seen to lie below the critical thickness for the various frequencies as shown in equation (3). Hard, half-hard (600 C), and fully annealed (1000 C) nickel rings have been built, the first two designed to operate on remanence, the last requiring d-c polarization. The 2V-Permendur was annealed at 500 degrees for one hour in hydrogen.

The half-hard nickel has lower coercive force than the hard but has a higher remanent magnetization and greater coefficient of electromechanical coupling. After flash polarization either with a heavy d-c or a nonoscillatory condenser discharge, ring stacks of either hard or half-hard nickel will stand being driven at low levels without depolarization. So used, driving efficiency as high as 40 per cent has been realized. The 2V-Permendur is decidedly superior for operation on remanent magnetization. It can be driven with alternating current giving a depolarizing field as great as 12 oersteds without being demagnetized. A Permendur stack was driven continuously for half an hour at cavitation pressure without being depolarized in any measurable degree.

6.4.3 Consolidations of Stacks

The consolidation of ring stacks presents no particular difficulties. In the case of unannealed and half-hard nickel and Permendur, the bonding agent should provide electric insulation between laminations. The oxide layer that forms on fully annealed nickel serves this purpose. Numerous cements were used successfully at HUSL, but, on the whole, C-3 Cycle-Weld, made by the Chrysler Corporation, proved the most satisfactory. Cycle-Weld 55-6 does not furnish the necessary insulation for nonoxidized laminations, although it produces strong stacks. Very little difficulty was encountered with parasitic resonances in ring stacks, in contrast with longitudinally vibrating stacks. In consolidating with C-3 Cycle-Weld, the rings are laid out on wire mesh, sprayed on

both sides, and either air-dried at room temperatures for a period of a few hours or at a temperature of 120 C for 20 minutes. They are stacked on a mandrel turned accurately to the inside diameter of the ring and baked under pressure at a temperature of 320 C for 20 minutes. Oxide-coated rings may be stacked on the mandrel and 55-6 Cycle-Weld brushed on the outer surface of the stack.

6.4.4 Winding: Turns and Wire Size

The number of turns and the size and type of wire used will depend on the impedance desired, the allowable d-c resistance, the ease of winding the various sizes of wires, and the type of mounting used. The impedance is determined by the specific use intended. At HUSL the most commonly used value of impedance for ring stacks was approximately 125 ohms. Ordinarily, the choice between meeting a specified impedance by either parallel or series tuning was made so that the transducer could be wound with the most convenient size of wire and number of turns. For example, the 24.5-ke 2VP *Spherical Source* transducer,¹⁵⁸ which was made up of stacks 1½ in. high, would have required a large number of turns of fairly small wire if it had been series-tuned to the desired impedance. However, when the stacks were wound with about 140 turns of No. 19 wire, an easy size to wind, these transducers could be parallel-tuned to the necessary value of impedance.

If no polarizing current is used, transducers operating at magnetic remanence can be wound with what amounts to only a partial layer. Full winding of d-c polarized stacks is needed to get optimum polarization without burning out the wire.

The choice between a plastic-covered or an enameled wire was usually determined by the type of mounting and by whether or not the toroidal windings were to be exposed directly to the water. If the windings were to be exposed, plastic-covered wire was necessary, but the plastic covering takes up a considerable amount of space, so that many fewer turns can be put on than of enameled wire. Moreover, plastic-covered wire is quite easily punctured or abraded in use.

Since the d-c resistance of the wire varies inversely as the square of the wire diameter, whereas the number of turns per linear inch varies directly as the wire diameter, the total number of ampere turns per inch for a given d-c voltage increases with wire size. Wire size was usually determined by the ease of

winding. It was found that No. 19 enameled wire was about the largest size that could be conveniently used in most applications.

A very large number of turns of small wire wound on a ring stack tends to tune the transducer electrically because of the distributed capacity of the turns. Under these conditions, cable capacity may contribute appreciably to the total impedance as measured at the cable terminals. For most uses low-impedance windings were found to be preferable.

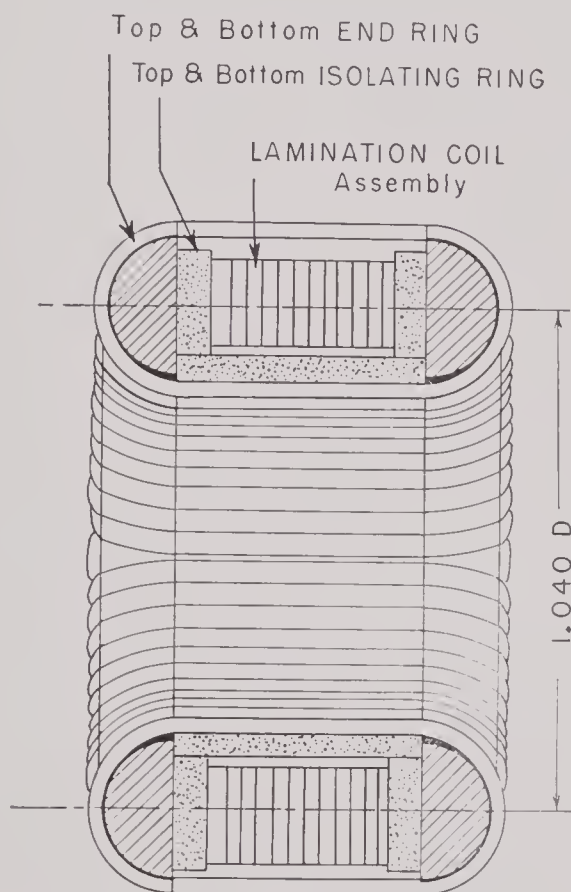


FIGURE 43. Coil assembly of ring stack.

After the laminations were consolidated and before the winding was added, the insides of the stacks were lined with pressure-release material, such as corprene or Cell-Tite neoprene (made by Sponge Rubber Products Company). Washers of the same material were usually cemented to the ends of the stacks to prevent any interference by the windings. A bakelite or Lucite end cap of the shape of a half doughnut was added to each of the washers. This end cap projected slightly over the inside and outside walls of the stack so that when the winding was pulled tight there was no danger of the wire being injured by coming into contact with the laminations, nor of the vibrations of

the ring stack being inhibited by the wire. These details can be clearly seen in Figure 43.

6.4.5 Types of Stack Mounting

In the first ring stack transducers the windings were left exposed to the water. The disadvantages of this procedure have already been noted. The next step was to encase the transducer in a rubber or neoprene boot filled with castor oil. This process involved out-

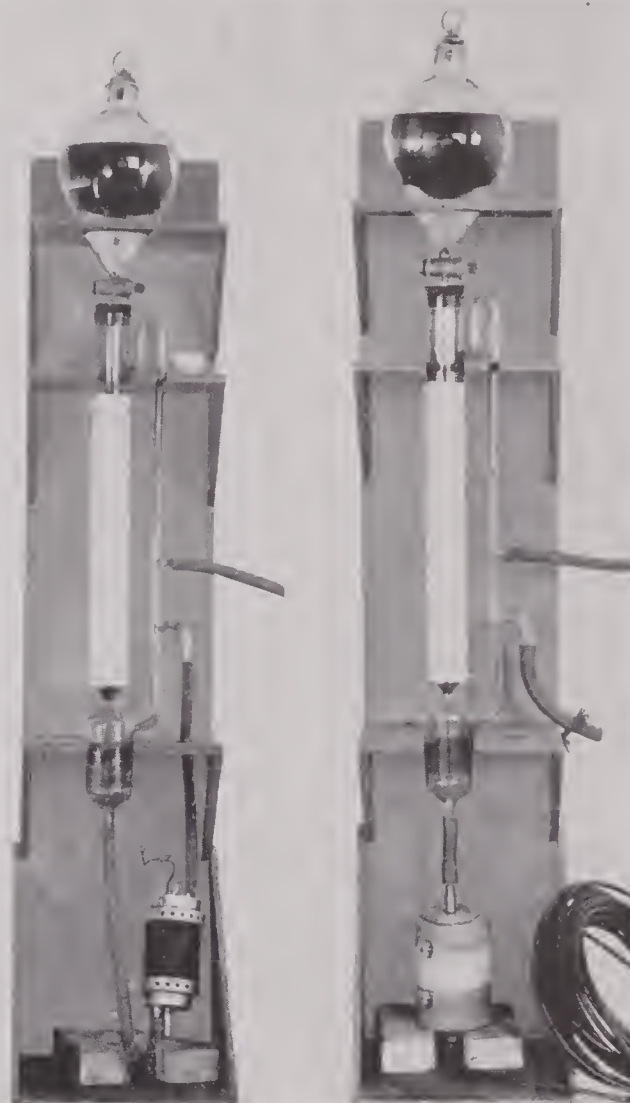


FIGURE 44. Apparatus for oil-filling of transducers under vacuum.

gassing of the oil and evacuation of the transducer to insure that no air would be trapped in the rubber container. The vacuum requirements entailed many complications, since the mountings had to be carefully constructed in order to maintain a good seal. When properly built, however, ring stacks mounted in rubber and castor oil gave satisfactory performance.

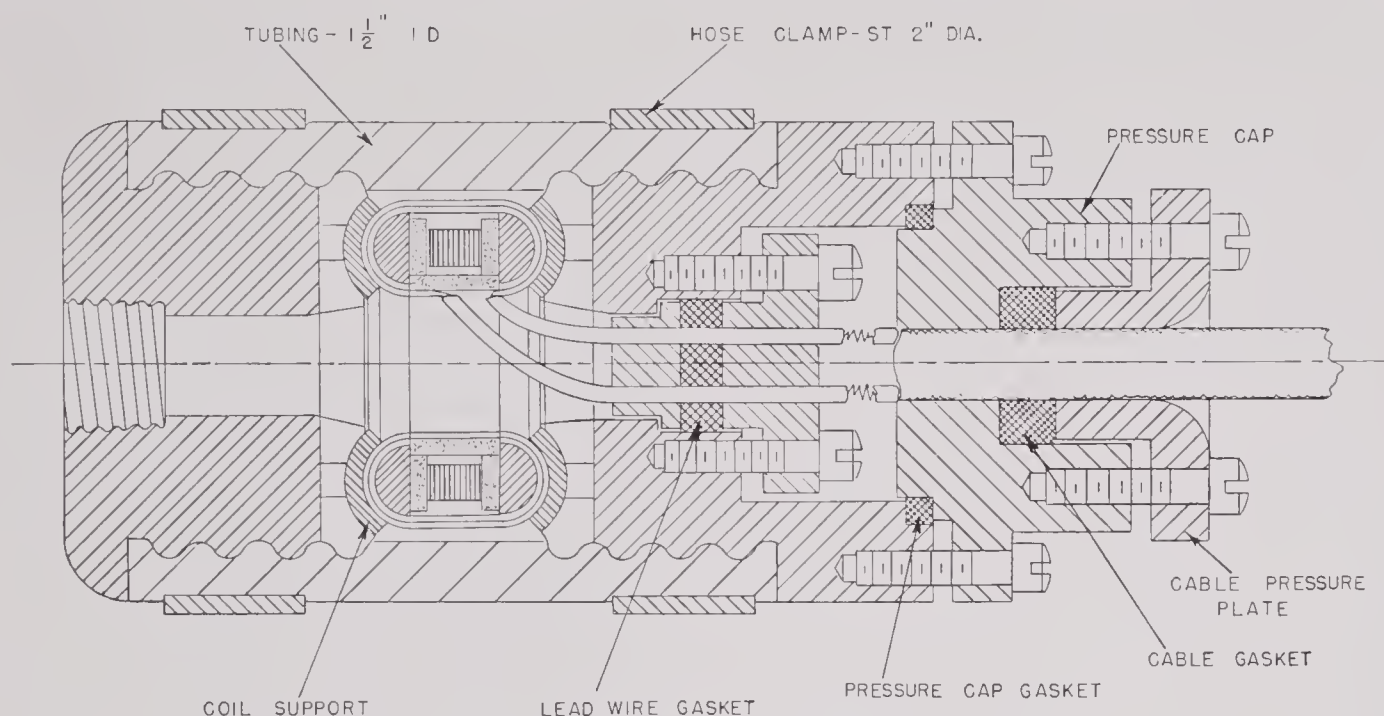


FIGURE 45. Section of 60-ke spherical pattern transducer.

Figure 44 shows the method that was used to fill transducers with oil under vacuum. If the transducer has two oil connections, the oil should be introduced through the lower connection while the upper connection remains under vacuum.

The castor oil was passed through a chamber loosely filled with rubber chips, thus exposing more surface area to the low pressure. This increased the efficiency of the outgassing process. While in the chamber the oil was heated to approximately 80 C by means of a nichrome heating coil wound around the outside of the chamber. This heating decreased the viscosity of the oil so that it flowed more rapidly into the transducer and the many small holes and crevices inside. A surplus of oil was taken care of in the small reservoir just below the outgassing chamber.

Many of the ring stacks were mounted in a housing consisting of metal supporting parts and a rubber tubing or boot which was vacuum-filled with oil. The boot was usually $\frac{1}{4}$ inch thick and was made of good-quality rubber or neoprene. The boots fitted smoothly over grooved end caps and were cemented to them with a cold-setting rubber-to-metal cement such as Vulcalock, Miracle adhesive, or Bostik 410D.

A junction box was usually provided to avoid the necessity for evacuating the cable, which had a porous filler, and to allow for changing the cable without removing the castor oil. If the transducer was to be

driven at high voltages, the junction box was completely lined with some insulating material such as fish paper or empire cloth.

Figure 45 is a section and Figure 46 a photograph of a 60-ke spherical-pattern transducer which was

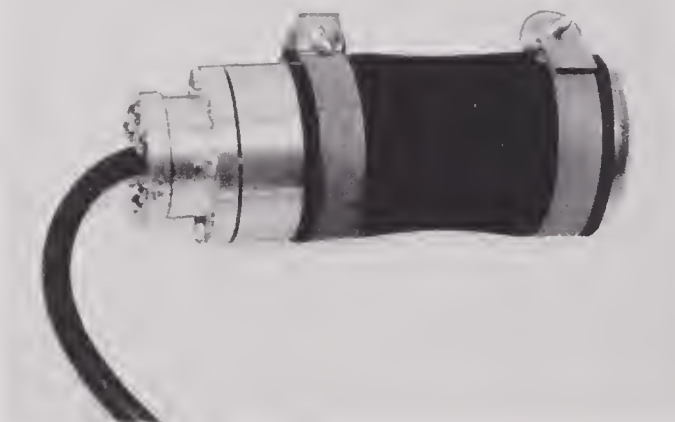


FIGURE 46. A 60-ke spherical pattern ring stack in oil and rubber mounting.

constructed in this manner. The details of the rubber boot and of the junction box can be seen clearly.

When long ring stacks are mounted in this manner, it is usually necessary to increase the strength by adding a center rod or pipe. This pipe should be well insulated from the windings of the transducer. If the

oil is introduced through this pipe, there must be enough holes in the wall to allow free passage of the oil.

If there is good electric contact with the water at each end of the rod, then an electrically conducting center section and the water form a shorted turn around the core. Such a shorted turn alters the impedance of the transducer, reduces the sensitivity, and may increase the noise pickup. The difficulty may be avoided either by insulating one of the end caps from the water or by breaking the center pipe or rod and inserting an insulating piece.

The idea of casting a ring stack in plastic was attractive and a large number of experiments were performed to find a suitable casting medium.

TABLE 4. Experiments in coating transducers.

Materials	Difficulties
Marblette resin casting	Too hard and brittle; too high a coefficient of expansion.
Latex rubber dipping and baking	Very unsatisfactory; not waterproof.
Lucite (methyl methacrylate resin) casting	Resin attacks the wire insulation.
Lucite monomer impregnating, then polymerizing	Very unsatisfactory; reduces the Q and the efficiencies.
Successive dippings in Harvell 612-C (cashew-base) varnish	Very satisfactory; it must be coated with a waterproofing material.
Neoprene paint	Difficult to coat in a sufficiently thick layer and in such a way as to prevent air bubbles from forming.

Table 4 gives a synopsis of the various compounds tried at HUSL and the difficulties encountered. Of these the most promising was cashew-base varnish, but investigation of it was dropped because of the superiority of phenol-formaldehyde resin.

A number of ring stacks were cast in phenol-formaldehyde resin. The technique employed was essentially the one used at New London in casting the tubular listening hydrophones. Usually the casting was done in a glass beaker or other container, which was later removed by breaking if necessary. The ring stack was suspended in the glass container (Figure 47), and the phenolic (Resinox), at a temperature between 60 and 70 C, was allowed to run in slowly but usually not under vacuum. When the phenolic



FIGURE 47. Illustrating method of plastic casting of ring stacks.



FIGURE 48. Plastic cast 23.5-ke ring-stack transducer.

was poured slowly, no difficulty with entrapped air was encountered. The plastic material was allowed to polymerize at a temperature of 60 C for 48 hours. Figure 48 is a photograph of a 23.5-ke spherical-pattern receiver cast in phenol-formaldehyde resin.

When wooden molds were used, the inside walls of the mold were coated with two smooth coats of Amercoat 33 Vinylite so that the casting would not adhere to the wood.

The polymerized phenolic resin was sometimes made more waterproof by coating with an alkyd resin prime coat (such as GE's Glyptal or American Cyanamid Company's Rezyl) followed with a coating of polystyrene paint (thick type: 100 parts styrene monomer, 25 parts polystyrene, 1 part benzoyl peroxide). This paint sets in 24 hours at 60 C.

Most of the phenolic (Resinox) cast ring stacks were coated with Amercoat 33. This paint was easy to apply, had good adhesion to the phenolic, but was not particularly tough or resistant to abrasion. However, it was so convenient that it was used for most of the ring stacks built in this way. Amercoat 23 is said to be similar but tougher.

6.4.6 Four Typical Ring-Stack Transducers

A large number of ring stack transducers were constructed during the history of HUSL. Of these, four models selected as typical and considered in detail are described as follows:

1. An oxide-annealed (1000 C) nickel ring stack made of 0.005-in. laminations; 5.0 in. high, with exposed windings; polarized with 8-ampere d-c current; ID = 2.65 in.; OD = 3.31 in.; mean radius, $a = 1.49$ in.; radial thickness $b = 0.33$ in.; $b/a = 0.22$.

2. Half-hard (550 C anneal) nickel stack 0.625 in. high, made of 0.010-in. laminations; cast in Resinox,

TABLE 5. Characteristics of four ring stack transducers.

	1	2	3	4
Impedance at resonance				
(a) In air	30 + j70	127 + j80*	720 + j50	...
(b) In water	...	44 + j270	125 + j270	6.0 + j45
Resonant frequency (f_0)				
(a) In air	20 kc	24.1 kc	59.3 kc	59.1 kc
(b) In water	...	22.3 kc	58.0 kc	56.0 kc
$Q = f_0 / (f_1 - f_2)^\dagger$				
(a) In air	60
(b) In water	5.0	6.4	2.7	1.3
Per cent efficiency				
(a) Potential	64	33	61	55
(b) Computed from impedance	68	26	30	...
(c) Computed from acoustic data	55	15-25
Sensitivity at resonance				
Dbs ref. 1 volt/dyne/cm ²	-92	-102	-97.5	-111
Patterns				
(a) In plane normal to axis	Uniform	Max. var. 3.5 db	Uniform	Uniform
(b) In plane containing axis	Approximates line source $l = 0.7\lambda$...	Approximates line source $l = 1\lambda$	Approximates line source $l = 1\lambda$
(c) Directivity ratio	0.28	...	0.45	0.44

* Impedances of bare transducer.

† f_1 and f_2 are frequencies 3 db down from resonance.

All things considered, the plastic casting of ring stacks proved a more satisfactory method of protecting the toroidal windings than encasing in rubber and castor oil. The casting technique, once mastered, is relatively simple and does not require any machined parts for mounting. Only a single water seal (for the cable) is needed. The resonant frequency of the stack is generally lowered a little by thick walls of plastic, and at the same time the Q is reduced. For many uses, the extended band width more than compensates for the loss in efficiency.

operated on remanence from a 10-ampere flash polarization; ID = 2.315 in.; OD = 2.745 in.; $a = 1.29$ in.; $b = 0.215$; $b/a = 0.17$.

3. A 2V-Permendur stack, 1 in. high, half hard (500 C anneal), made of 0.005-in. laminations mounted in castor oil and rubber; operated on remanence from 15- to 20-ampere flash polarization; ID = 0.97 in.; OD = 1.15 in.; $a = 0.53$ in.; $b = 0.09$ in.; $b/a = 0.17$.

4. Thin-walled stack, 1 in. high, 2V-Permendur, made from 0.005-in. laminations (500 C anneal)

CONFIDENTIAL

mounted in rubber and castor oil; operated on remanence from 15- to 20-ampere flash polarization; $a = 0.53$ in.; $b = 0.030$ in.; $b/a = 0.056$.

The significant data on these four transducers are collected in Table 5. Unfortunately, no direct comparison among the different types can be made, since the wide variation in the different uses to which these transducers were to be put necessitated equally wide variations in their construction. In Figure 49

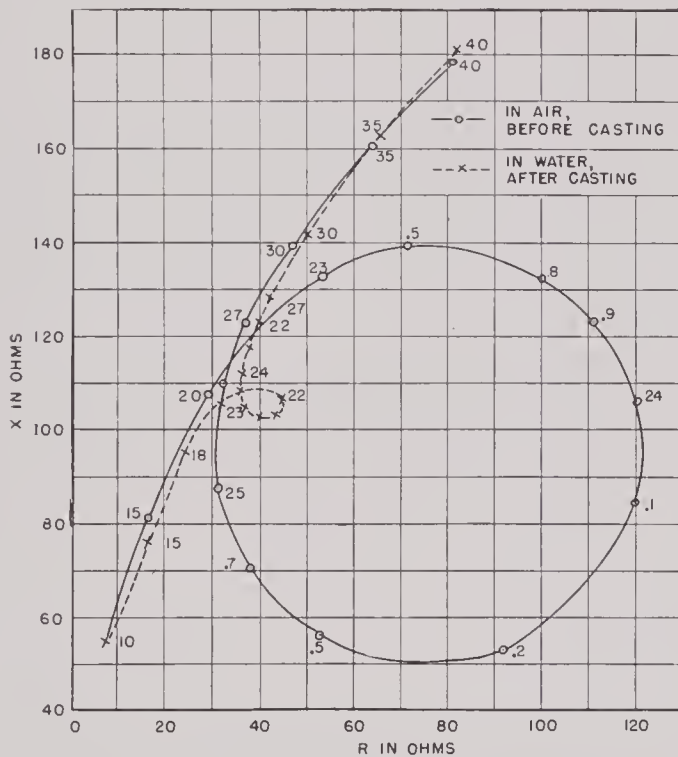


FIGURE 49. Impedance curves of 23.5-ke ring stack before and after plastic casting.

are shown the impedance curves of the 23.5-ke stack in air before casting and in water after casting. These curves are not significantly different from similar curves taken on bare transducers in air and in water. The relatively low potential efficiency of 33 per cent deduced from measurements in air before casting indicates that the low measured efficiency of 26 per cent shown by the cast transducer in water is not to be attributed to the casting. The effect on the 60-ke 2V-Permendur stack of mounting in castor oil and rubber is indicated in Figure 50.

A comparison of the sensitivities of the two 60-ke ring stacks is shown in Figure 51. It should be noted that the thin-walled stack was wound to a much lower impedance than the other. This, together with its much greater band width, accounts for its lower sensitivity. However, analysis of the original data

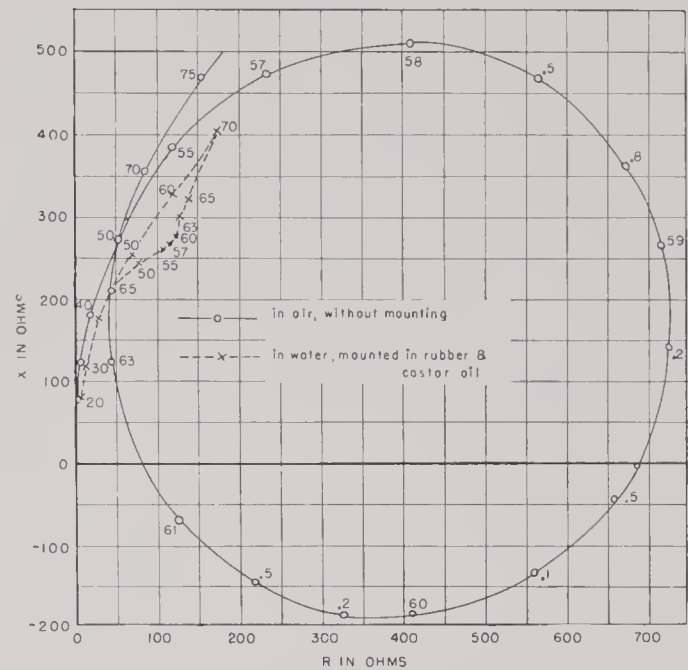


FIGURE 50. Impedance of thick-walled 2V-Permendur ring stack.

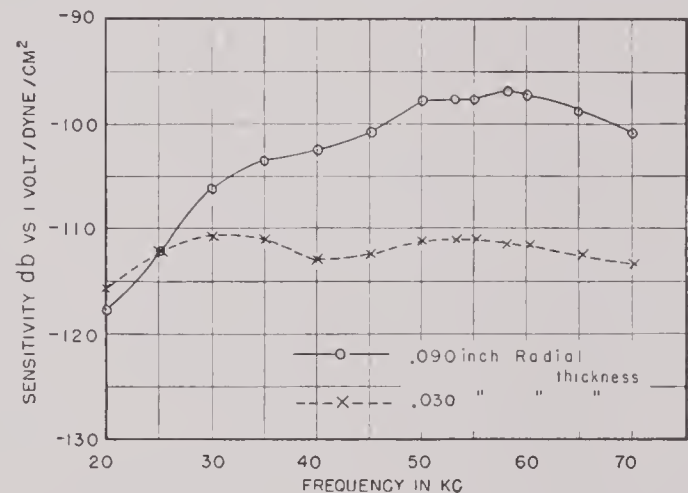


FIGURE 51. Sensitivities of thick-walled and thin-walled 2V-Permendur ring stacks.

indicated that the efficiency of the thin-walled stack was at least as great as 15 per cent over the entire frequency range from 25 to 70 ke. It was found that when this stack was used as a projector, a driving voltage as great as 20 volts, corresponding to an input power of 1.8 watts, would give an undistorted wave form for frequencies above 25 ke. The magnetizing field in the stack was about 15 egs units, and it was found that the acoustic power output was proportional to electric input up to a peak driving current of 0.8 ampere or about 12 egs units of magnetizing field. This puts an upper limit on the electric power input which the 2V-Permendur stacks, operating on remanence, will handle without being

subject to variations resulting from partial depolarization by the a-c driving current. Experiments with a 23-kc thin-walled stack of the same material showed that it could be driven continuously at a level that would produce cavitation at atmospheric pressure without depolarization. However, transients set up by the sudden making or breaking of the driving current at high levels were found to produce changes as great as 18 db in the acoustic power output.

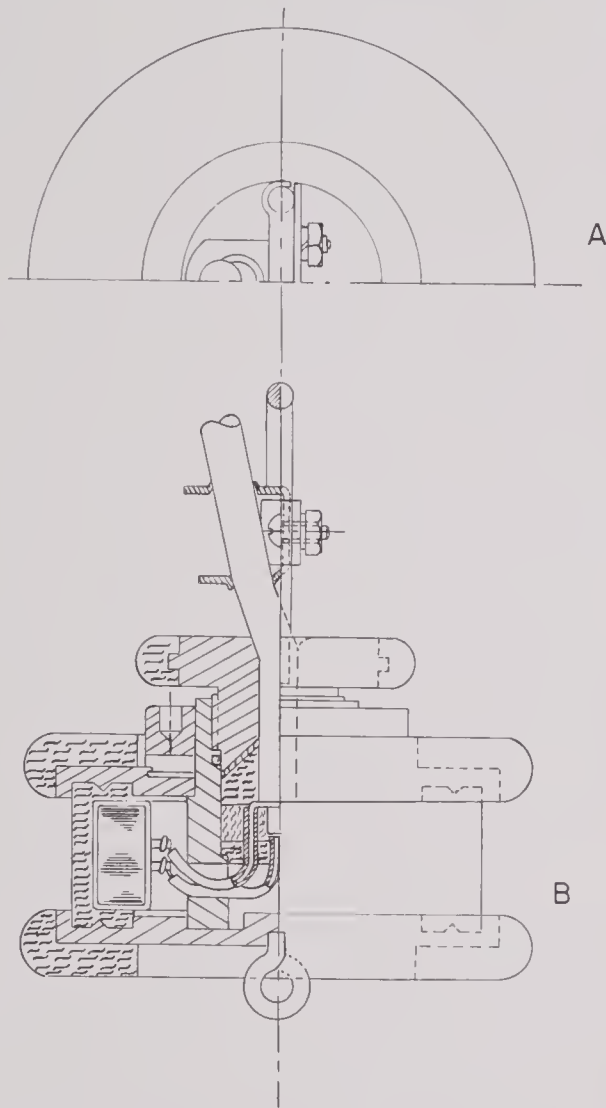


FIGURE 52. Nondirectional ring-stack transducer, BTL design.

The highly desirable qualities of thin-walled stacks of 2V-Permendur laminations are offset by the practical difficulties of building such stacks. The only procedure so far developed has been to machine down thick-walled stacks after consolidation, a rather delicate and not very satisfactory operation from a practical point of view. Comparison of the 15 to 25 per cent efficiency of thin-walled, toroidally wound

stacks with the 0.3 per cent efficiency shown by solid tubes of the B-19 type makes it seem desirable to develop further the possibilities of laminated radial vibrators with low eddy-current losses.

6.4.7 Nondirectional Ring Stack: Bell Telephone Laboratories' Design

The mounting developed at BTL for ring stacks designed to have an approximately spherical pattern is shown in Figure 52. For a resonant frequency of

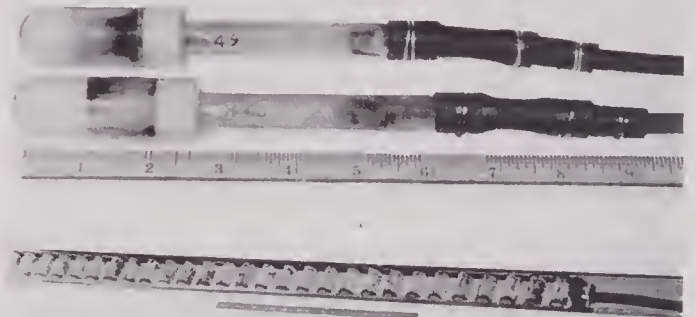


FIGURE 53. A. New London "thimble" hydrophone. B. Twenty-eight element perpendicular arrangement of 3-ft hydrophone assembly.

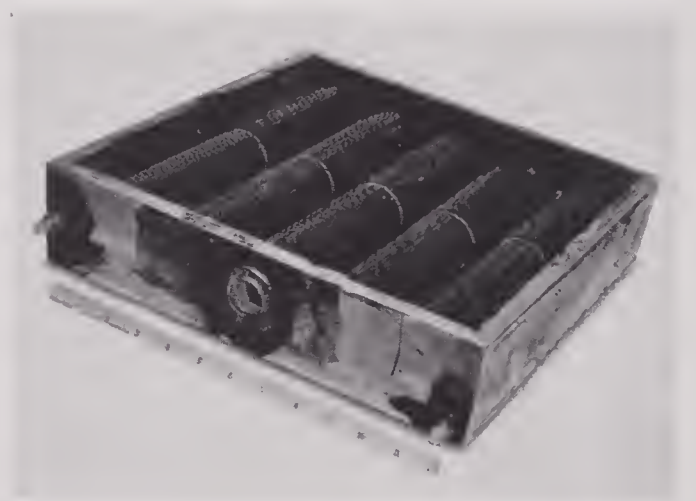


FIGURE 54. New London 12 × 12-in. transducer.

24 kc, the rings were of half-hard nickel 0.004 in. thick, with ID of 2 in., OD of 2.75 in., and stacked to a height of 1.0 in. The laminations were cleaned, coated with silica by cataphoresis, and annealed, then vacuum-impregnated with bakelite resin. After the curing process, the winding was applied and the wound ring was then impregnated with the same resin and cured. Sound-transparent rubber was cemented

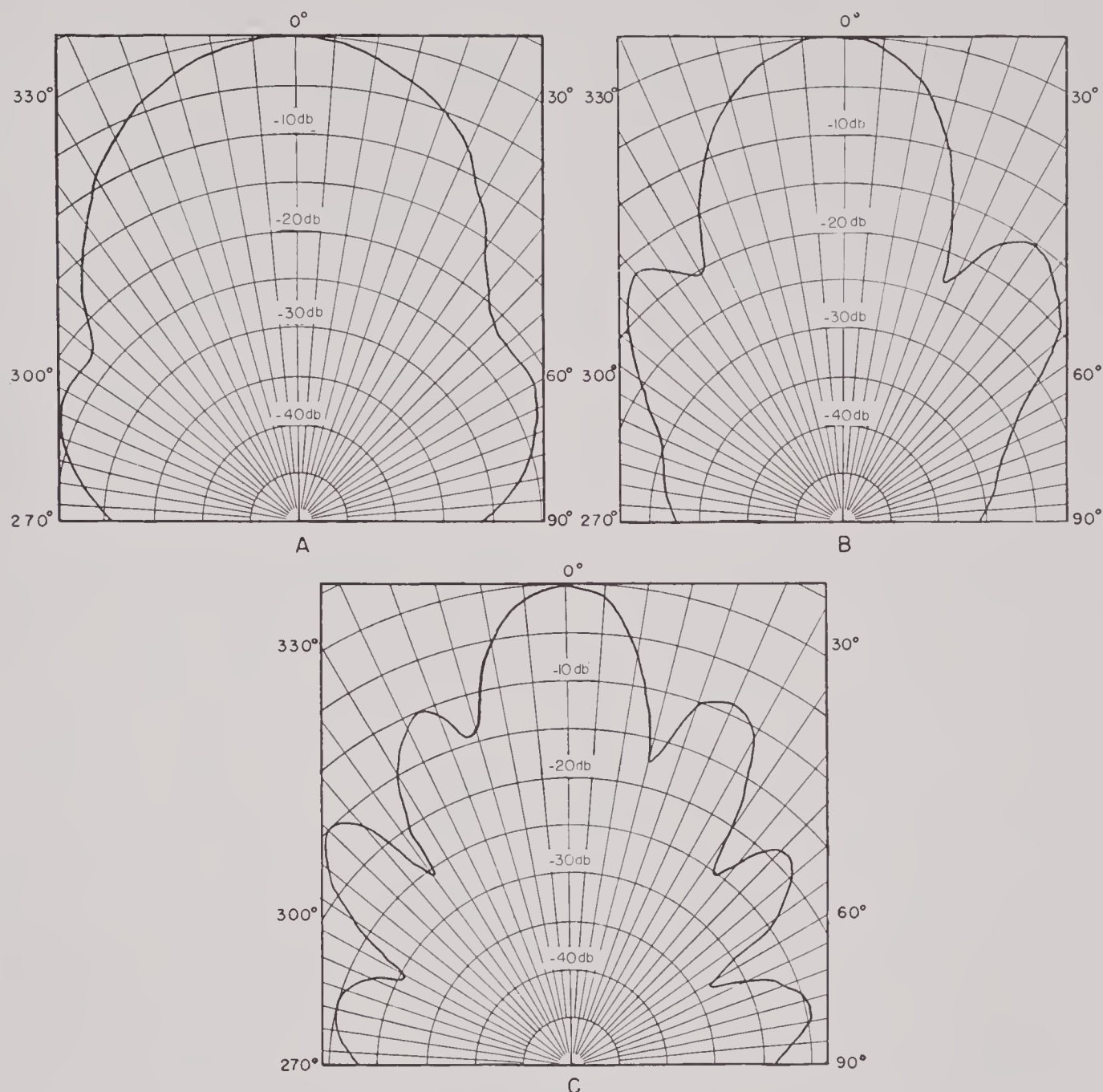


FIGURE 55. Radiation patterns of QP projector at A, 25 kc; B, 40 kc; and C, 60 kc.

with Tri-ply cement to the outer surface and to the top and bottom of the stack as shown in Figure 52B. The mounting parts are indicated in Figure 52A. Measurements showed that a unit of this type had a Q of about 6.0 when used as a projector. The radiation in the plane of the ring was practically uniform and showed a maximum departure from uniformity of 9 db in a plane passing through the axis. The impedance in water at 24 kc was $46 + j192$ ohms. The acoustic output was linear with input up to a value of 10 watts of electric input power. The reported efficiency was of the order of 70 per cent.

6.5 MULTIELEMENT TUBULAR TYPE: NEW LONDON MODELS

The possibility of fabricating transducers built up from an array of small radial vibrators was explored both at New London and at HUSL. Figure 53A shows two of the thimble hydrophones made at New London for monitoring use.⁷⁶ These consisted of hard-nickel cylinders, 1 in. long by $\frac{3}{4}$ in. in diameter, toroidally wound, with wood-dowel filling cast in plastic cylinders. Directional hydrophones were built using large numbers of similar midget elements cast

CONFIDENTIAL

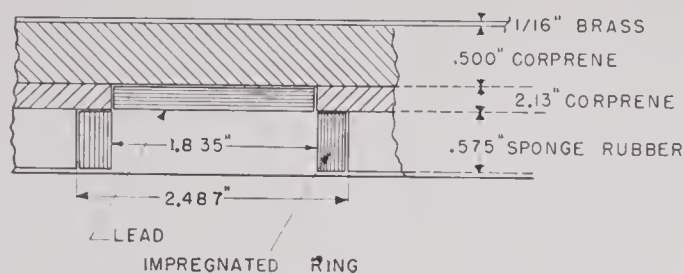


FIGURE 56. Section of single element of M-5 transducer.

in solid plastic. A 28-element array with element axes perpendicular to the length of the assembled hydrophone is shown in Figure 53B.

The advantage of this construction over the NL-130 type lies in its higher efficiency in the upper sonic

Figure 54. This was built at the New London laboratory for field studies comparing a square array with a 5-ft straight hydrophone using the same amount of sensitive material. It consisted of a bronze box with an open side, containing ten permanent-magnet tubular elements similar to those used in the NL-124. The elements were cast in solid plastic and faced with sound-transparent neoprene. The impedance and frequency responses were roughly the same as the NL-124; the directivity in the sonic-frequency range was much poorer than for the 5-ft NL-124.

6.6 QP PROJECTOR (HUSL)

The QP transducer described in Chapter 10 was built at HUSL for use as a projector at the measuring stations. It consisted of five B-19H hydrophones

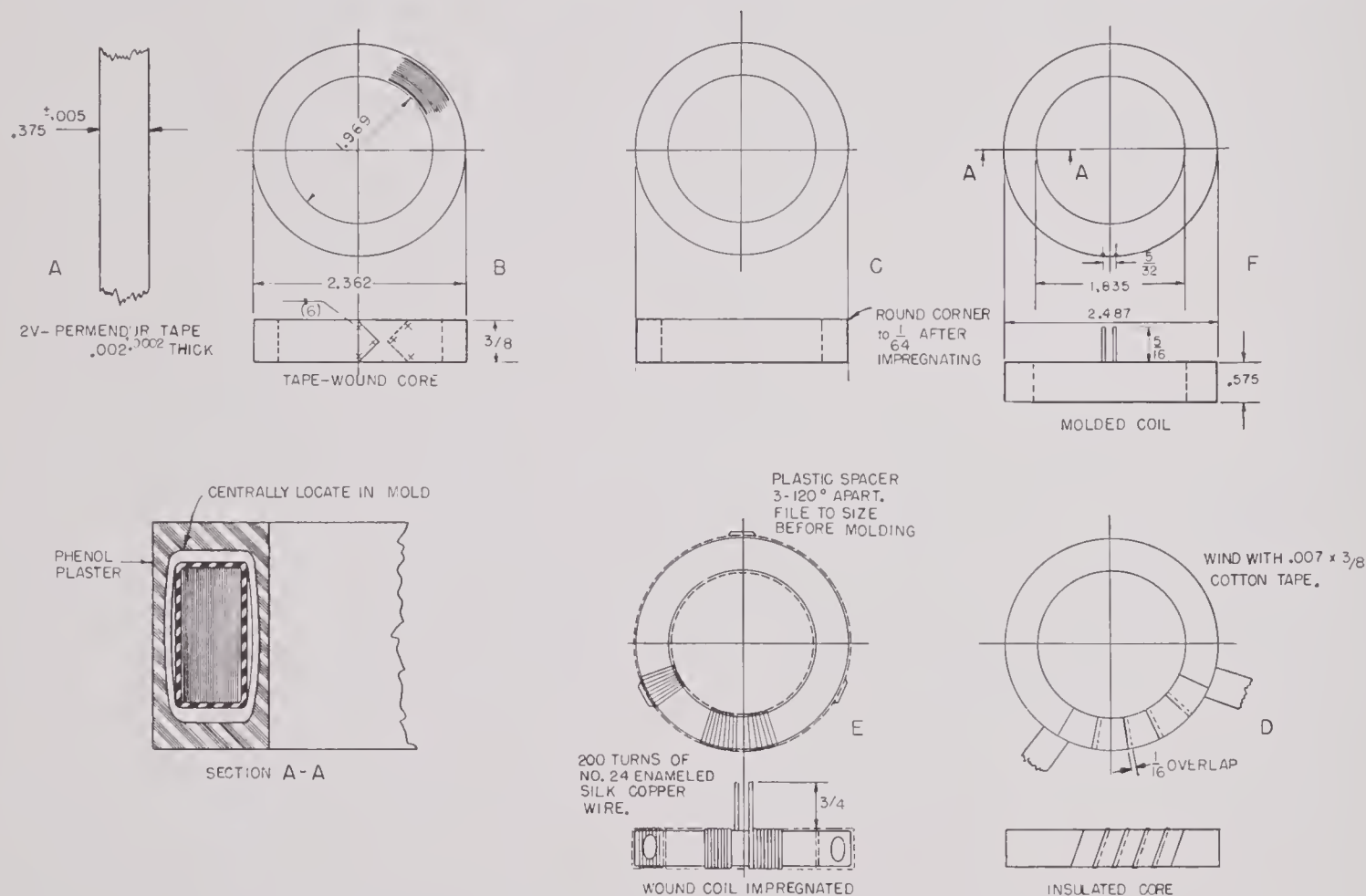


FIGURE 57. Details of construction of magnetostrictive element of M-5 transducer.

and supersonic range of frequencies. The smaller diameter and thinner walls of the midjet elements make for greater sensitivity and lower eddy-current losses in the higher frequencies than prevails in the larger, thicker-walled tubes.

A 12-in. by 12-in. square transducer is shown in

mounted in a flat array inside an open-faced aluminum case. These were connected in series inside a junction box at the rear of the case and were parabolically shaded to reduce side lobes. Impedances were in the ratio of 25 to 22 to 13 from the center to the outside hydrophones. The back surface and sides

of the case were surfaced with air-cell rubber. The radiation patterns at 25, 40, and 60 kc in a plane at right angles to the length of the tubes are shown in Figure 55. It will be noted that at the two lower frequencies the patterns are roughly those of a single-plane surface source with lobe reduction. At 60 kc, however, where the distance between the centers of the tubes becomes about three-fourths of a wave length, the pattern appears as that of a series of

transducer has proved the most satisfactory of the considerable number of projectors used in transducer measurement at HUSL.

6.7 RING MAGNETOSTRICTIVE TRANSDUCER BY BTL

The *broad band magnetostriction projector* developed at BTL may be cited as a further example of the use

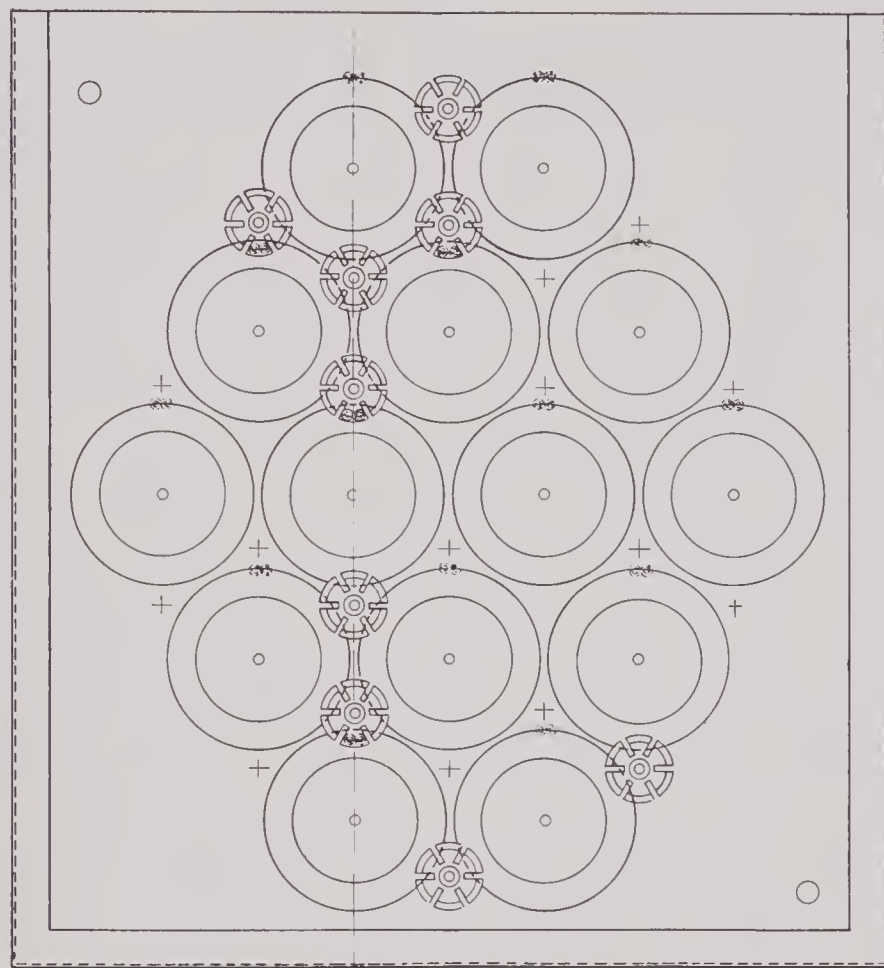
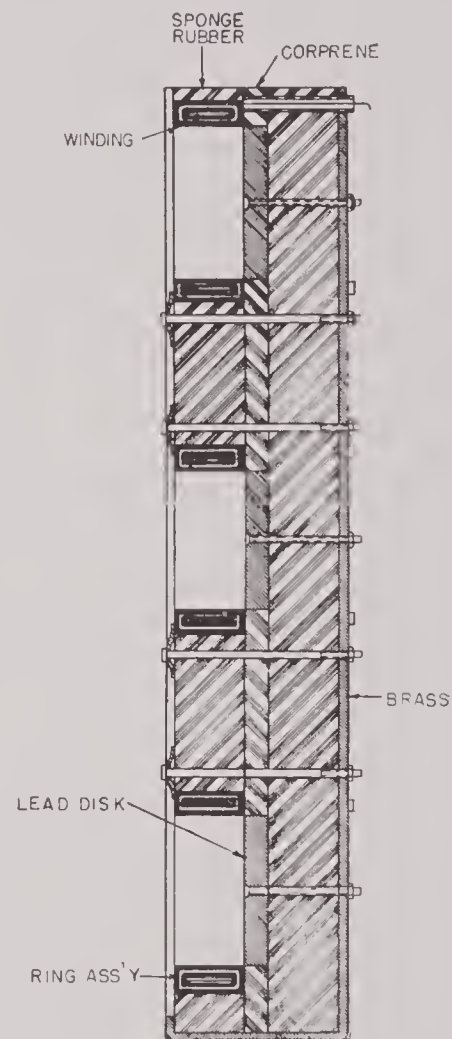


FIGURE 58. Assembly of 14-element array in M-5 transducer.

separate line sources. A similar situation occurs with an array of line sources on the surface of a cylinder with phase retardations to give the directional patterns of a flat surface. In the case of the QP, the pattern is also modified by the reflection with change of phase from the pressure-release backing. Receiving and transmitting response curves are given in Chapter 10. For constancy of response over long periods of time, freedom from temperature effects, and smoothness of response over a wide frequency range, the QP

of vibrating rings in a multielement sharp-beam transducer.¹⁸⁵ The purpose of the assignment of this task was to "determine the possibilities of developing a magnetostrictive transducer for sonar use to approach the broad frequency range and efficiency characteristics of the Rochelle salt type QBF projector." The transducer developed is designated as the *M-5 ring-type magnetostrictive projector* and is described in detail in reference 9.

The operation of this device is essentially different



from that of the tubes and ring stacks hitherto considered, in that radiation of energy occurs from the inside surface of the ring. In the earlier models, one end of the ring was closed with a pressure-release material from which reflection with change of phase occurred. In later models, a lead disk was used for

The individual magnetostrictive element of the 14-element array was a spirally wound ring of vanadium-Permendur tape (0.002×0.375 in.), insulated with a very thin deposit of silica dust and wound upon itself to have inside and outside diameters of approximately 5 cm and 6 cm respectively. The Permendur was heat-treated to give maximum remanent magnetization to permit operation at low and intermediate levels without d-c polarization. For driving

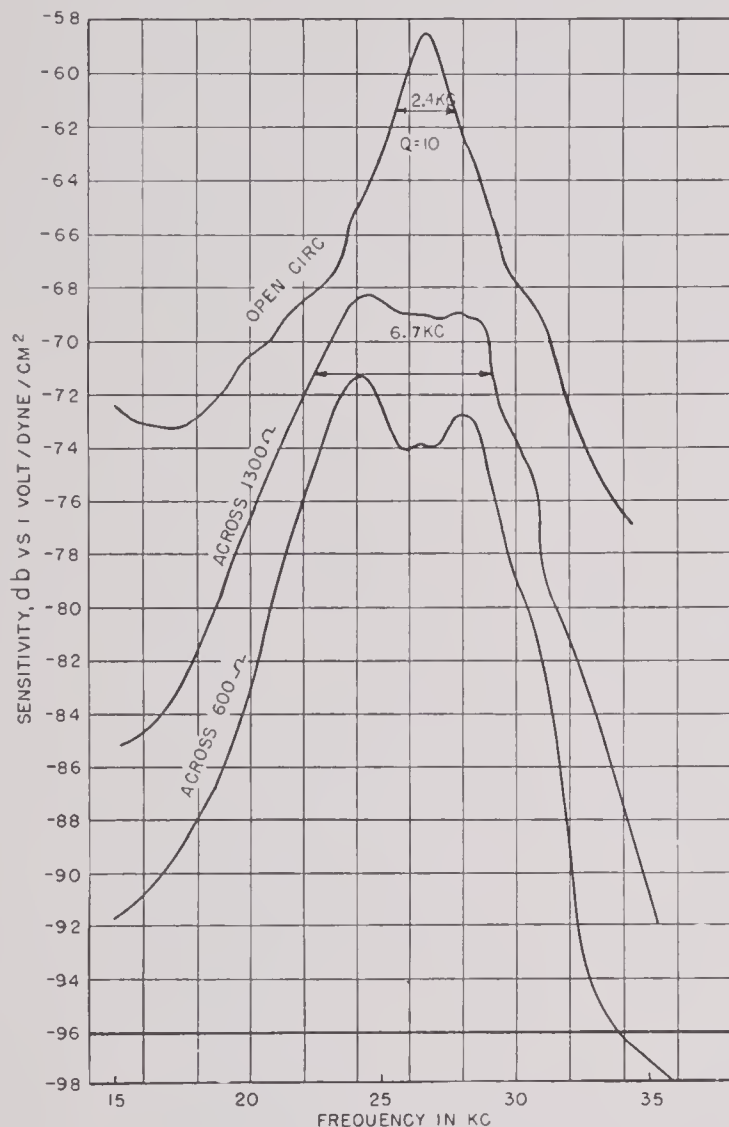


FIGURE 59. Receiving response of M-5.

closure of this end. The change produced a measurable increase in efficiency. The radial vibration of the ring produces a to-and-fro movement of the liquid partially enclosed within it, causing it to vibrate somewhat like a liquid piston, thus radiating energy from the open end of the ring. The outer surface of the ring moves against a highly compliant material which gives no external acoustic loading. The situation is thus seen to be just the reverse of the more usual case in which the outer surface of the ring is acoustically loaded. The essential features of a single element are shown in Figure 56.

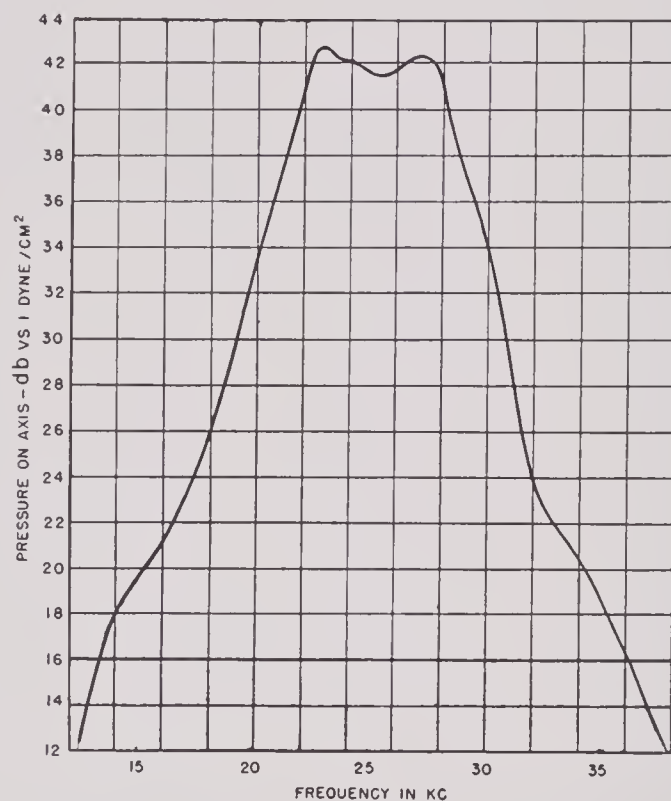


FIGURE 60. Sound pressure level at 10 ft generated by M-5, input 1 volt.

at higher levels, a polarizing current of 1 ampere in the windings was required. The rings were impregnated with bakelite resin, insulated with cloth tape, and wound with silk-covered enameled wire. A protective sheath was molded over the ring and winding. The details of construction are shown in Figure 57.

The assembly of the 14-element array of these rings in a diamond-shaped pattern is shown in Figure 58. A backing plate of corprene is laid against a mounting frame of thin brass. A second sheet of corprene, the core plate, is cemented to this. The core plate is $\frac{1}{4}$ in. thick and has circular holes cut in it to accommodate the lead disks that act as the bottoms of the resonating cavities formed by the magnetostrictive rings. A mounting plate of sponge rubber $\frac{5}{8}$ in. thick is cemented to the core plate.

The mounting plate has 14 holes, 2.510 in. in diameter, in which the molded rings are loosely fitted. Substitution of sponge rubber in the final model in place of the corprene mounting plate proved advantageous. With the corprene, the rings fitted rather loosely in the holes, and shrinking or swelling of the corprene caused binding of the rings, resulting in poor acoustic characteristics. The compliance of the rubber proved to be great enough to offer no restraint to the freedom of motion of the rings, and the transducer gave acceptable patterns with spacing between elements as great as a wave length of the radiated sound. In use, the transducer was mounted, by means of suitable brackets, in a QBF housing, which was filled with castor oil under a slight vacuum.

6.7.1 Consolidation of Spirally Wound Rings

Earlier in this chapter, the poor performance of impregnated scroll-wound rings was mentioned. This resulted from the tendency of radial vibrators of this type to develop flexural modes of vibration with two, four, or even six nodes. A detailed study of the problem at BTL showed this effect to be due, in the main, to the relatively large spacing (0.0002 in.) between adjacent turns of the spirally wound tape. A solution of the difficulty was found in a special technique whereby this space was reduced to 0.00005 inch, with adequate insulation maintained between turns. By using the improved method of consolidation, the 80 to 90 per cent of rejected rings made by the earlier process was reduced to a negligible fraction, and the efficiency was increased by about 3 db. Bakelite resin (BR-0014) applied in vacuo was used in consolidating the rings.

The impregnated rings were wound with 200 turns of black-enameled, silk-covered wire, and the windings were impregnated following the same procedure as was used in consolidating the rings themselves. The protecting sheath was of phenol plastic composed of 15 per cent cotton flock, 15 per cent wood flour, and 70 per cent bakelite resin (BR-15055), molded about the wrapped coil at a pressure of 600 pounds per square inch. Forms thus molded withstood temperature cycles down to -40°C without crackling and with no impairment of their transmission characteristics. Detailed directions for the various processes involved are given in the BTL report.

6.7.2 Electric and Acoustic Characteristics

The *receiving response* of the M-5 14-element transducer with three different terminating resistances is shown in Figure 59. The curve for the 600-ohm load was measured, while those for the open circuit and 1,300-ohm load were computed from the 600-ohm curve and the impedance data. The dependence of

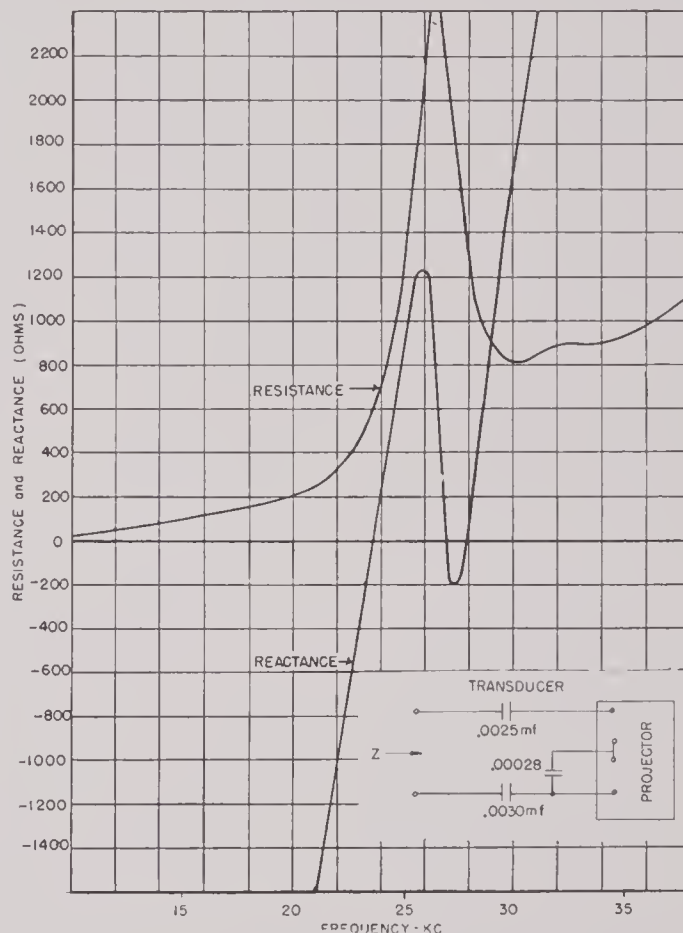


FIGURE 61. Impedance of M-5 with tuning condensers shown.

band width on the load resistance is to be noted. (Compare with Figure 20 of Chapter 1.) For the open-circuit condition, the frequency range between the -3 db points is about 2.4 kc, with a Q of 10, while for the 1,300-ohm load the band width is about 6.7 kc, with a corresponding Q of 4.7. The efficiency at resonance given in the report was computed from the equation

$$\text{Eff}_R = R_r - 10 \log A - \log r + 115.9,$$

where $R_r = -58.9$ db, open-circuit sensitivity,

$$A = \text{area in sq cm of equivalent circular piston} = \pi \times 10.5^2,$$

$$r = 2,700 \text{ ohms.}$$

The efficiency thus computed was -2.7 db, or 53 per cent.

By using the same data and a value -21.1 for the directivity index ($10 \log D$), the computed efficiency comes out -2.5 db, or 63 per cent.

The transmitting response of the M-5 is shown in Figure 60. Here a band width of 7 kc is shown with a nominal Q of 3.9. Impedance curves measured with the tuning condensers shown are given in Figure 61.

$$\begin{aligned} r &= 3.05 \text{ meters, } 20 \log r = 9.7, \\ 20 \log p &= 44, \\ \log E_i &= 0, \\ Z_i &= 2,700 + j1200, \\ |Z_i| &= 2,950 \text{ ohms, } 20 \log |Z_i| = 69.4, \\ 10 \log D &= -21.1, \\ -10 \log R_i &= -34.3, \\ 10 \log \text{ constant} &= -70.9, \\ \text{Eff (decibels)} &= -3.2 \text{ db, or 48 per cent.} \end{aligned}$$

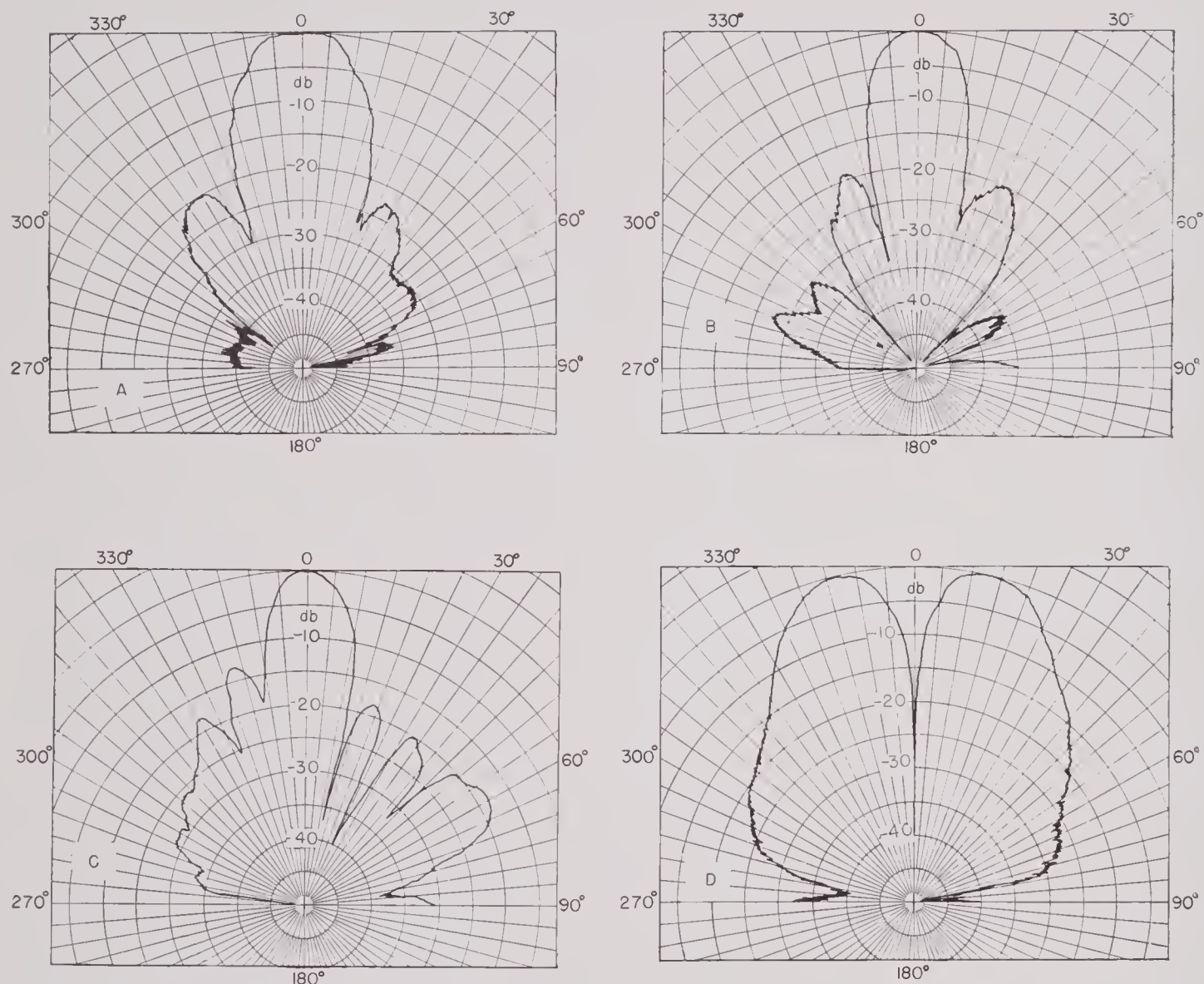


FIGURE 62. Radiation patterns of M-5. A. In horizontal plane at 25 kc. B. In horizontal plane at 30 kc. C. In vertical plane at 25 kc. D. In horizontal plane, halves opposing for BDI operation.

The computed efficiency of the transducer when driven by a 600-ohm generator, as given in the report, was -2.8 db, or 52 per cent. The efficiency at 26 kc may be computed from equation (20) of Chapter 1, using the following data:

6.7.3

Radiation Patterns

Figure 62 gives the patterns in various planes and also the pattern when the right and left groups of rings are connected opposing for BDI operation.

In the last case, balance between the two halves was obtained by a small trimmer condenser placed across the left half of the transducer. These patterns indicate that the multiple array of ring-type elements radiated sound in the direction of their axes in a manner quite comparable to a circular piston of approximately the same overall area.

TABLE 6. Constants of 2V-Permendur magnetostrictive ring.

Circuit constant	Definition or formula	Value of circuit constant
R_d	Damped-core resistance (ohms)	4.05
L_d	Damped-core inductance (mh)	1.27
s	Stiffness of ring (dynes/cm)	2.44×10^{12}
r	Mechanical resistance (ohms)	0.0155×10^6
m	Mass of ring (grams)	62.5
R	Water load (mech. ohms)	3.09×10^6
G	Force factor (dynes/abamp.)	3.76×10^8
L_m	Motional inductance $\frac{G^2}{s} \times 10^{-9}$ (mh)	0.0579
R_m	Motional resistance $\frac{G^2}{r} \times 10^{-9}$ (ohms)	9120
C_m	Motional capacity $\frac{m}{G^2} \times 10^9$ (μ f)	0.442
R_L	Load resistance $\frac{G^2}{R} \times 10^{-9}$ (ohms)	45.8
C_d	Tuning condenser $\frac{1}{w^2 L_d}$ (μ f)	0.0201
C	$\frac{C_d C_m}{C_d + C_m}$ (μ f)	0.0192
C_1	$\frac{C_d^2}{C_d + C_m}$ (μ f)	0.000875
L_1	$L_m \frac{(C_d + C_m)^2}{C_d}$ (mh)	30.6

6.7.4 Characteristics of Individual Rings

The preceding sections constitute little more than an abstract of that portion of the BTL report that deals with the assembled transducer and its salient characteristics. Succeeding sections of the report contain technical details of construction both of the individual elements and of the assembled transducer. The section dealing with the consolidation of the

vanadium-Permendur tape cores is of particular importance, since it appears that the desired behavior of the individual rings and hence of the whole transducer depends in large measure upon the degree to which the core, its winding, and the protecting sheath are consolidated into a rigid unit.

As has been shown to be the case in other multi-element devices, the realizable efficiency of the combination of rings falls considerably below that of a single component. Table 6 is instructive as showing the physical and electric characteristics of a spirally wound ring of vanadium-Permendur tape 0.002 in. thick, as well as the potential efficiency of electro-mechanical transformation of energy.

Table 7 gives a comparison of the coefficient of elec-

TABLE 7. Comparison of electromechanical coupling of 2V-Permendur tape-wound ring with those of crystal transducers.

	$\frac{C_0}{C_1}$	k
Magnetostrictive ring J-892 (vanadium-Permendur tape-wound ring)	22	0.23
Z-cut ADP crystal transducer	13.5	0.29
Y-cut Rochelle salt transducer	12.5	0.30
X-cut quartz-crystal transducer	133	0.096

tromechanical coupling of the vanadium-Permendur ring with those of crystals now in use in underwater transducers.

The development of the M-5 14-ring projector was not carried beyond the laboratory stage. However, the work done on it demonstrated the possibility of making a beam-radiating projector from an array of radially vibrating rings radiating energy from their open ends. The chief difficulty inherent in the idea seems to be the limitation that the geometry of such an array imposes on the radiation pattern. Satisfactory consolidation of the rings under manufacturing conditions would seem to be the major technical difficulty to be expected. Simplicity of design and economy in the use of a magnetostrictive material that can be operated at fairly high levels on magnetic remanence recommend this transducer for further development.

Chapter 7

LONGITUDINALLY VIBRATING LAMINATED STACKS

7.1 GENERAL CONSIDERATIONS

7.1.1 Definitions

A longitudinally vibrating laminated stack is a stack of laminations which vibrates in such a way that all the particle velocity vectors are parallel to a given line that lies in the plane of the laminations. Usually the laminations are longer along one axis than any other and usually the direction of the particle velocities is parallel to this long axis. In nearly all cases the laminations are made symmetrical on each side of the principal axis of the particle velocity and unsymmetrical on each side of the nodal plane.

7.1.2 General Types

UNIFORM BARS

Types of Structures. Examples of uniform bar types of laminated stacks are shown in Figures 1A, B, C, and D. In these cases the stacks are of uniform cross section along the principal axis of the particle velocity. In each sketch the position of the nodal plane and the direction of the particle velocities are shown for the first mode of free vibration. The direction of magnetic polarization should be parallel to the particle velocity. When the bars vibrate the greatest mechanical strain occurs in the region of the nodal plane and consequently the windings that surround the bars should be centered or concentrated in this region to give the maximum linkage with the flux that is most effective magnetostrictively.

Bars of the type shown in Figures 1B, C, and D are made from laminations formed to a channel-like cross section by a die-stamping operation. Laminations of this type are stiff and easy to handle even though the metal is thin. The advantage of the X-shaped cross section of the bar shown in Figure 1C is that the high-frequency magnetic flux emanating from the edges of the laminations when the bar vibrates magnetostrictively is distributed over a greater cross section of air path; thus the magnetic reluctance of the air-path part of the magnetic circuit is appreci-

ably less than that for the bars shown in Figure 1A and B.

To give the optimum mechanical and magnetic performance, the dimensions of the bars in the nodal plane (lateral) should be small relative to their dimensions along the principal axis (longitudinal); that

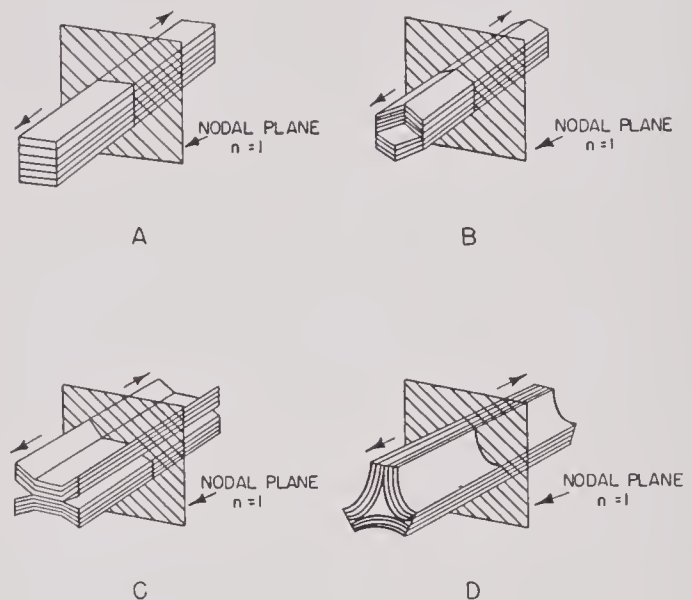


FIGURE 1. Some typical forms of laminated magnetostrictive bars of uniform cross section.

is, the bars should be long and slender. If the lateral dimensions were made approximately the same as the longitudinal dimension, the natural frequencies of vibration in the lateral direction would approach those of the longitudinal direction and the two or more modes of vibration would become coupled, due to the Poisson ratio effect. Such coupled modes of vibration could easily cause shifts in the frequencies of resonance and spoil all attempts to maintain close frequency tolerances on the vibrating elements. For magnetization, long slender bars are also superior because the demagnetizing field produced by the free magnetic poles at the ends is less than that for bars with large cross sections, and the ratio of the area of the exposed edges of the laminations to the cross-sectional area is greater. Thus the high-frequency flux density in the air path adjacent to the exposed

edges of the laminations is less, and as a result the reluctance of the high-frequency magnetic circuit is less.

Simple bars of this type cannot be used conveniently to couple directly to water or a similar acoustic medium because the dimensions of the ends of the bars are usually small in comparison to the wave length in water, and under these circumstances the water radiation impedance has a high reactive component and a small resistive component. If the end of the bar is used as the radiating face and if this face is more than a wave length square, the water radiation impedance becomes nearly resistive, with a value of ρc . Under these conditions the mechanical Q for the first mode of vibration of the system is $\pi/2$ times the ratio of the ρc of the bar material to the ρc of water. Usually, however, bars of this type are attached to pistons or diaphragms which present to the water radiating areas larger than the cross section of the bar.

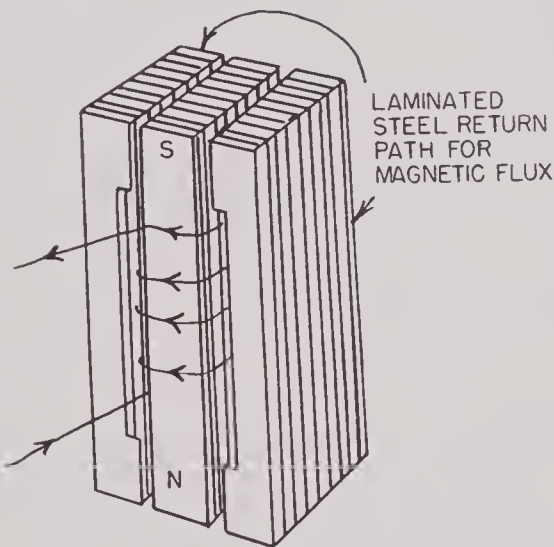


FIGURE 2. Single uniform bar with a pair of laminated steel return paths for the magnetic flux.

Frequencies and Modes of Vibration. In the first mode of longitudinal vibration of a uniform bar the node is midway between the free ends, and the distance from the nodal plane to each free end is just a quarter of the wave length in the bar, hence the frequency of resonance is

$$f_1 = \frac{c}{2L}. \quad (1)$$

In general, the frequency in the n th mode of vibration is

$$f_n = \frac{nc}{2L}. \quad (2)$$

In all these modes of vibration the distribution of the particle velocity along the bar is sinusoidal and consequently the kinetic energy of the vibrating bar is the same as that of a lumped mass of one-half the total mass of the bar vibrating with the same velocity and amplitude as the free end of the bar. (This mass is defined as the effective or equivalent mass of the vibrating system and will be designated by the symbol M^* .) If the cross-sectional area of the bar is A , then the radiation resistance of the water against the motion of the end of the bar is $A(\rho c)_w$ and the mechanical Q of the system with this radiation damping is

$$Q_n = \frac{\omega_n M^*}{A(\rho c)_w} = \frac{2\pi f_n A \rho L}{2A(\rho c)_w} = \frac{n\pi}{2} \frac{(\rho c)_{bar}}{(\rho c)_w}. \quad (3)$$

Thus the mechanical Q for the n th mode of vibration is n times that for the first mode.

The magnetic polarization of single uniform laminated bars can be accomplished by use of a component of direct current in the windings or by use of permanent magnets. The degree of perfection of the magnetic circuits is determined by the density and distribution of the polarizing flux in the bar and by the distribution of the reluctance in the high-frequency magnetic circuit. The polarizing flux should be parallel to the direction of the particle velocity in the most active magnetostrictive regions and should have a magnitude sufficient to develop the maximum electromechanical coupling in the magnetostrictive material. In a well-designed polarizing flux circuit more than half of the total magnetic reluctance should be due to that portion of the circuit made up of the bar itself. This means that any air gaps in the circuit should be short in length and large in cross section. The same is true of the high-frequency magnetic circuit, and it must be remembered that in this circuit eddy-current shielding can contribute a large amount to the reluctance.

The simplest possible magnetic circuit for uniform bars consists of the bar itself and the air return path. Such a circuit is satisfactory only if the cross-sectional area of the bar is very small in comparison to that of the air return path. Some magnetic circuits which may be used when the cross-sectional area of the magnetostrictive bars is relatively large are illustrated in Figures 2 and 7.

A design is shown in Figure 2 for the magnetostrictive bar surrounded by the winding and a laminated-steel magnetic return path. This type of element requires the use of polarizing current, but the magnetic

reluctance for both the polarizing flux and the high-frequency flux is relatively low. There are several alternative ways in which the return flux path of this

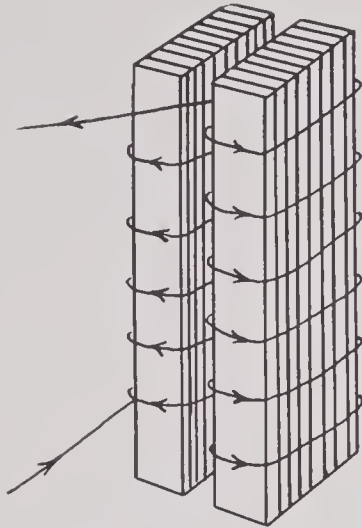


FIGURE 3. Uniform bars polarized with direct current.

type can be constructed. One of the most economical would be to make the "half shells" from a nest of thin sheets bent into a shallow U-shaped cross section. This general type is not very practical because of the difficulty of keeping the bar mechanically free of the coil and magnetic return assembly.

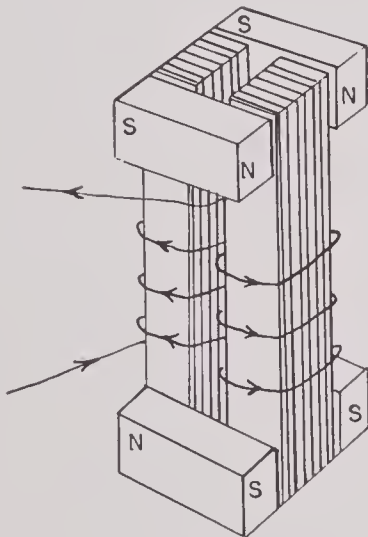


FIGURE 4. Uniform bars polarized with Alnico V permanent magnets.

Figure 3 shows a simple arrangement in which one bar serves as the magnetic return for the other so that all parts of the magnetic flux path are active magnetostrictively except the relatively small air gaps at the top and bottom ends. These gaps can be made as narrow as the thickness of the coil permits. This

design is quite satisfactory except for the need of polarizing current.

Figure 4 shows a method by which a pair of uniform rectangular bars can be polarized with small bars of Alnico V or any other similar magnetic material which has a coercive force of over 500 oersteds and sufficient flux density. In this case the polarizing flux path and the alternating flux paths are separate at the bottom and top ends of the bars. The polarizing flux goes through the Alnico magnets while the high-frequency flux goes across the air gap in one direction at the top end and the other direction at the bottom end between the exposed edges of the lamina-

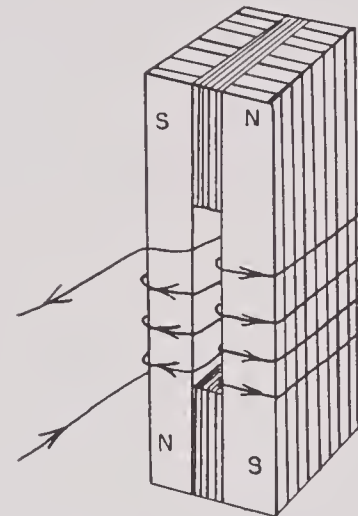


FIGURE 5. Uniform bars polarized with sintered-oxide permanent magnets.

tions. The width of the gap between the two laminated bars is determined by the coercive force and flux density of the Alnico magnets and by the amount of polarizing flux leakage occurring between the two bars. In the actual construction of an assembly of this type, arrangements must be made to keep the two bars mechanically free of the coil and polarizing magnet assembly and yet hold them in the proper relative positions. The best way is to make the coil and magnet assembly into a solid mechanical unit and support the bars on this assembly by means of cushioning material placed near their nodal regions.

Figure 5 shows a pair of uniform bars arranged to be polarized with sintered-oxide permanent magnets. The very high resistivity of sintered oxide makes it possible for the high-frequency flux to traverse it without any eddy-current losses or shielding. As the reversible permeability of the sintered oxide is only 1.15, it acts almost as a simple air gap to the high-frequency flux. The cross-sectional area of each of

the sintered-oxide blocks (measured in a plane perpendicular to the direction of the flux through it) should be 4 to 6 times the cross-sectional area of one leg, and the thickness of magnets from the N pole face to the S pole face should be adjusted so that the demagnetizing force on the magnets is less than 500 oersteds when the flux density in the magnetostrictive material is up to the optimum value. To give a numerical example as an illustration, suppose the bars are made of oxide-annealed nickel, that the frequency of resonance is 28 kc, the width of the laminations is one-twelfth their length, and the nickel must be polarized to 4,000 lines per sq cm. Then the

tubes or heavily electroplated with copper to prevent any appreciable amount of alternating flux from traversing the magnets. The best magnet material for this application is Alnico V. The coil surrounds the entire stack and magnet assembly. The high-frequency flux return is through small packets of thin silicon steel laminations cemented to the outside of the coil. These packets should be placed as far as possible from the polarizing magnets to prevent them from drawing an excessive amount of polarizing flux and thus losing a considerable amount of their reversible permeability.

There are many possible variations of the design indicated in Figure 6. An example is the alternative bar-and-magnet cross section sketched in the lower right-hand corner of Figure 6. Whatever the variations may be, it is essential that the exposed edges of the laminations point outward so that the high-frequency flux can leave the inner laminations without having to cross through the outside laminations, with the consequent eddy-current shielding.

Figure 7 shows a design in which the alternating flux path is enclosed entirely within the polarizing flux path. The polarizing flux is produced by radially polarized Alnico magnets which are placed in the annular spaces between the laminated bar and the steel tube which serves as the return path for the flux. The solid copper rings placed at each end of the coil assembly serve as high-frequency flux shields to prevent the flux from going to the regions beyond the ends of the coil. This design is inherently strong and compact. All the parts can be readily supported on the steel tube housing.

SIMPLE BARS WITH PISTONS OR DIAPHRAGMS

Types of Structures. Any of the simple uniform bars shown in Section 12 can be attached to a piston or diaphragm of some kind. Each bar may be attached to its individual piston or a group of bars may be attached to a single large piston or diaphragm. If two or more bars are to operate together in the same transducer, all must satisfy the usual phase and frequency tolerance requirements so that they vibrate together in close enough unison to give good acoustic patterns.

The active area of the piston associated with a single bar is generally made several times as great as that of the cross section of the bar. This allows a greater radiation resistance for each bar and consequently a lower mechanical Q , if the mass of the piston is not too great. The greater area of the piston

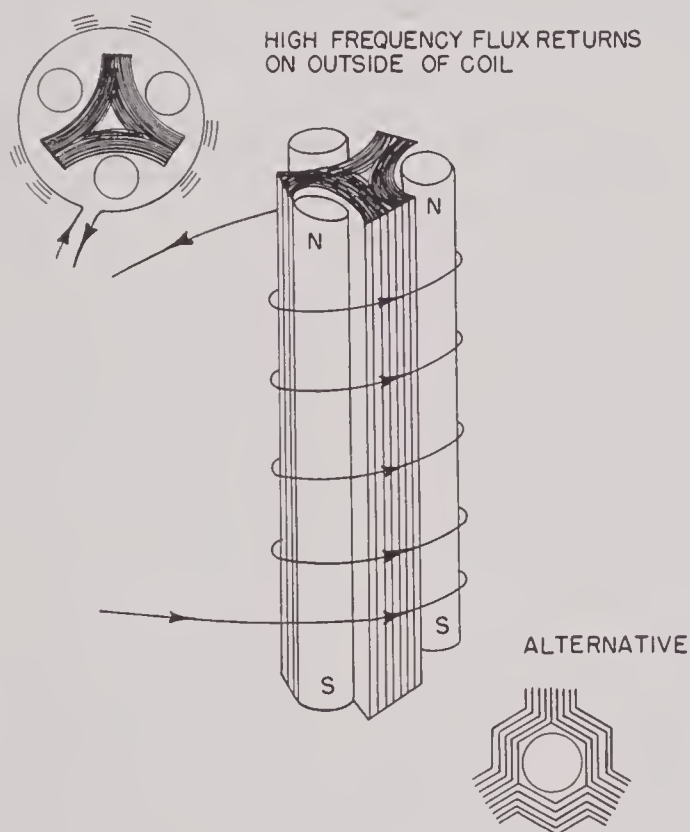


FIGURE 6. Single bar polarized with longitudinal permanent magnets.

length must be 3.5 in., the width about 0.3 in., the height of the magnets about 1.25 in., and the thickness of the magnets about 0.188 in. This leaves 1 in. of the center portion of the stacks available for the coils. This would be a fairly practical design.

Figure 6 shows a design in which a single uniform bar is polarized by means of long rod-shaped Alnico magnets placed parallel with it. It is necessary to prevent the magnets from rubbing against the vibrating parts of the stack. The magnets should also be surrounded with sleeves of thin-walled copper

also allows room around the sides of the magnetostrictive bar for the coil, the flux return paths, and in some cases the polarizing magnets. Thus the active faces of the pistons can present a continuous large active face to the water without crowding the magnetostrictive bars and their auxiliary parts excessively.

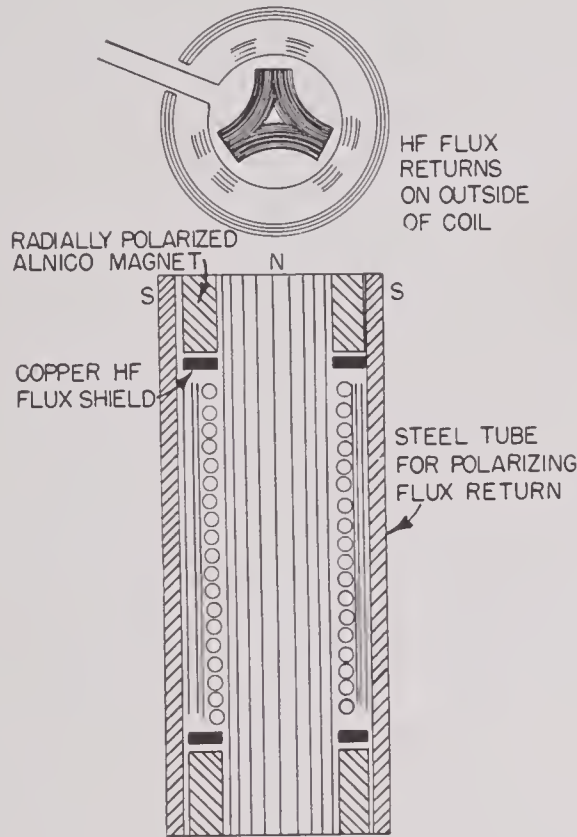


FIGURE 7. Uniform bar polarized by radially polarized ring-shaped Alnico magnets, with alternating flux path enclosed entirely within the polarizing flux path.

The attachment of the laminated bars to the pistons or diaphragm presents some difficult practical problems because each lamination must be attached perfectly to give satisfactory results. Some of the materials which have been used for pistons and diaphragms are steel, brass, bronze, aluminum, magnesium, polystyrene, molded bakelite, and bakelite-impregnated glass fiber. Soft or hard solders may be used to attach the bars to steel, brass, or bronze. Some of the various strong thermosetting cements are usually best for attaching bars to aluminum, magnesium, or plastic diaphragms. An alternative method is to solder the laminated bar to a thin steel button and cement the flat face of the button to the diaphragm. The button may also be made with a short threaded stud which screws into a threaded hole in the diaphragm.

Supporting the coil and magnets in a practical transducer of this type also presents some difficult design problems. The two most successful methods are, first, to support them on some compliant material (such as Cell-Tite neoprene), which is cemented to the laminated stack in the nodal region, or, second, to support them by a compliant member from the piston or diaphragm. Illustrations of these methods will be given later in Section 7.2.2.

Modes and Frequencies of Vibration. When a mass is attached to the end of a uniform bar the positions of the nodes are no longer symmetrical with respect to the bar. In general, the nodes are shifted toward the weighted end and the frequency of any given mode of vibration is lower than that for the corresponding mode in the bar alone.

If the thickness of the piston is less than one-eighth of a wave length of sound in the piston material and if the piston is stiff in a flexural sense, then it may be considered as a lumped mass M_L . The frequencies of resonance occur when the mass reactance of this lumped mass is the conjugate of the stiffness reactance of the uniform bar at the point of attachment. Figure 8 shows a sketch of a uniform bar with a face mass attached at one end and graphs showing qualitatively the distribution of particle velocity and mechanical reactance along the length. The cross-sectional area of the laminated bar is σ and the distance from the free end is x . The mechanical reactance is

$$j\rho c\sigma \tan \frac{2\pi f}{c}x = j2\pi f m \tan \frac{2\pi f}{c}x \quad (4)$$

where m is the mass of a length of the bar, which is $1/2\pi$ times the wave length in the bar material. The condition for resonance is

$$j2\pi f M_L + j2\pi f m \tan \frac{2\pi f}{c}L = 0$$

or

$$\tan \frac{2\pi f}{c}L = -\frac{M_L}{m} = \frac{-2\pi f M_L}{\rho c\sigma} \quad (5)$$

The values of f_n which satisfy this equation are the frequencies of resonance. If m_1 and m_2 represent the values of m for the first and second modes of vibration respectively, the ratio of the particle velocity at the free end of the bar to that of the active face for the first mode is

$$\left(\frac{v_1}{v_0}\right)_1 = \sec k_1 L = -\left[\left(\frac{M_L}{m_1}\right)^2 + 1\right]^{1/2} \quad (6)$$

and for the second mode is

$$\left(\frac{v_1}{v_0}\right)_2 = \sec k_2 L = \left[\left(\frac{M_L}{m_2}\right)^2 + 1\right]^{\frac{1}{2}} \quad (7)$$

where $k_1 = 2\pi f_1/c$ and $k_2 = 2\pi f_2/c$ are the wave numbers or radians of phase angle per centimeter of length of the bar.

Radiation Loading and Q's. If the area of the radiating face is A and the extent of the face is great enough so that the impedance of the water load is al-

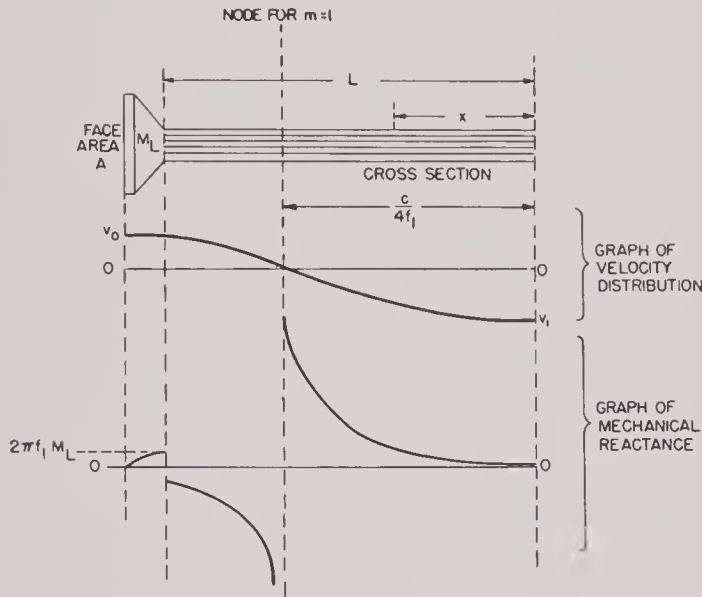


FIGURE 8. Fundamental vibrational characteristics of a uniform bar mass-loaded at one end. The cross-sectional area of the laminated bar is σ .

most purely resistive, then the radiation resistance for each bar is $\rho c A$ dynes per cm per second. The equivalent mass of the bar for the n th mode of vibration is

$$\frac{m}{2} \sec^2 k_n L [k_n L + \sin k_n L \cos k_n L] \quad (8)$$

and the total equivalent mass is this plus the mass of the face. Thus

$$M_n^* = M_L + \frac{m_n}{2} \sec^2 k_n L [k_n L + \sin k_n L \cos k_n L]. \quad (9)$$

Consequently the Q for the n th mode of vibration is

$$Q_n = \frac{2\pi f_n M_n^*}{\rho c A}, \quad (10)$$

and this is roughly proportional to n because M_n^* remains almost equal to one-half the mass of the bar for all the modes of vibration.

Magnetic Circuits and Polarization. The magnetic circuit and polarization details of elements of this type are almost identical with those for the symmetrical uniform bar discussed above. The only important difference is in the position of the nodes in the vibrating bar. The position of the magnets and coils should be made to center as closely as possible around the primary node. If it is intended that the units be used at either of the first two modes of vibration, the coil assembly should be shifted slightly toward the free end of the bar to include as well as possible the node of the first mode of vibration and the node nearest the free end for the second mode of vibration.

DOUBLE OR MULTIPLE BARS WITH SYMMETRICAL CLOSED ENDS

Types of Structures. Several lamination forms of this type are illustrated in Figure 9. All the forms except that shown in D have perfectly closed magnetic circuits and consequently give the highest possible

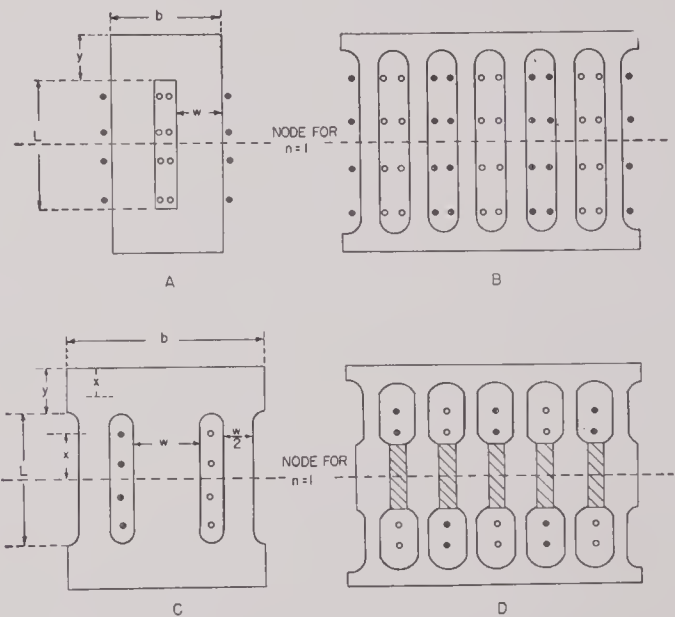


FIGURE 9. Typical forms for laminated bars with symmetrical closed ends.

electromechanical coupling coefficients for the particular magnetostrictive material used as a longitudinal vibrator. However, these forms must be polarized by the magnetic remanence flux alone or with the aid of a component of direct current in the windings. The form shown in D is arranged to be polarized by sintered-oxide permanent magnets. The advantage of this form is that it can use coils preformed over the magnets and slipped into the

slots. The other forms must be wound by threading wire back and forth through the winding slots.

Laminations of this type are punched from flat sheets with good dies so that a negligible burr is produced. The thickness of the flat sheets from which the laminations should be punched is determined by the reversible permeability, the resistivity, and the frequency of operation. Reference to Figure 5 of Chapter 3 can be made to select a lamination thickness that gives a characteristic frequency f_c , which is well above the range of frequencies at which the transducer is to be used. For example, if the material is oxide-annealed nickel, 0.010-in. material is satisfactory up to 25 ke, 0.005-in. material up to 60 ke.

Modes and Frequencies of Vibration. The most important mode of vibration is the first, in which the one node is at the center as shown in Figure 9. This mode of vibration is perfectly symmetrical, so that the particle velocities at the two faces are equal in amplitude and opposite in direction. The second mode of vibration is sometimes of practical importance; it is not symmetrical and the particle velocities of the two opposite faces are in the same direction and have the same amplitude. It is relatively easy to calculate the characteristics of the first mode of vibration but the second mode is more complicated, since some of the lamination forms and some of the cases require special analytical treatment. Therefore the discussion here will be limited to the first mode of vibration.

Frequencies for forms A, B, and C of Figure 9 may be calculated in the same way, since these forms are essentially alike. At the frequency of resonance, the reactive component of the mechanical impedance at the node is infinite and at the active face is zero. If the distance measured from the node is denoted by x , the reactive mechanical impedance per unit height of pile-up of stack is

$$j\rho c 2w \cot kx, \quad (11)$$

where $k = 2\pi f/c$, as before.

If the distance measured from the active face inward toward the node is x' , the reactive mechanical impedance is

$$j\rho e b \tan kx'. \quad (12)$$

At resonance these reactances must be equal at the junction between the leg portion and the face portion. Therefore,

$$2w \cot \frac{2\pi f_1}{c} \left(\frac{L}{2} \right) = b \tan \frac{2\pi f_1}{e} y \quad (13)$$

is the relationship between the principal dimensions and the frequency of resonance. This is a transcendental equation which can be solved graphically or by successive approximation to any degree of accuracy desired.

With x and x' used to denote the same variable distances as above, and the rms particle velocity at the active face denoted by v_0 , the particle velocity in the face section is

$$v' = v_0 \cos k_1 x', \quad (14)$$

and that in the leg portion is

$$v = \frac{v_0 \cos k_1 y}{\sin k_1 \left(\frac{L}{2} \right)} \sin k_1 x. \quad (15)$$

Therefore the kinetic energy of the leg section (on one side of the node) per unit height of stack is

$$\frac{w\rho v_0^2 \cos^2 k_1 y}{k_1 \sin^2 k_1 \left(\frac{L}{2} \right)} \left[k_1 \left(\frac{L}{2} \right) - \cos \left(\frac{L}{2} \right) \sin \left(\frac{L}{2} \right) \right] \quad (16)$$

and that of the face section is

$$\frac{b\rho v_0^2}{2k_1} [k_1 y + (\sin k_1 y)(\cos k_1 y)]. \quad (17)$$

It follows that the equivalent mass of both halves of the lamination per unit height of the stack is

$$M^* = \frac{2w\rho \cos^2 k_1 y}{k_1 \sin^2 k_1 \left(\frac{L}{2} \right)} \left[k_1 \left(\frac{L}{2} \right) - \cos \left(\frac{L}{2} \right) \sin \left(\frac{L}{2} \right) \right] + \frac{b\rho}{k_1} [k_1 y + (\sin k_1 y)(\cos k_1 y)], \quad (18)$$

and, as before, the mechanical Q due to full resistive water radiation loading is

$$Q = \frac{2\pi f_1 M^*}{b\rho c}. \quad (19)$$

Magnetic Circuits and Polarization. The magnetic circuits and polarization of laminated stacks of this type will not be considered further here except to point out that the thickening of the sections at the centers of the legs of the lamination form shown in D of Figure 9 serves two purposes; first, it improves the magnetic circuit, and second, it improves the electromechanical coupling by moving the region of maximum mechanical strain from the node to the junction of the slender leg with the thickened center section where the polarizing flux is parallel with the direction of the strain.

DOUBLE OR MULTIPLE BARS WITH SYMMETRICAL CLOSED ENDS AND ATTACHED DIAPHRAGM

Stacks of any of the lamination types shown in Figure 9 can be attached to a metal or plastic diaphragm. If the diaphragm material has a ρc which is considerably greater than that of water and if the diaphragm thickness is less than one-eighth of a wave length of sound in the diaphragm material, it

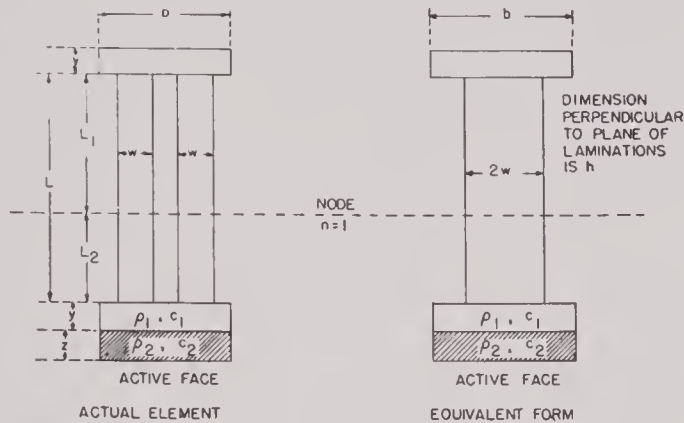


FIGURE 10. Element of a laminated stack of double uniform bars with symmetrical closed ends and attached to a thin diaphragm of different material.

may be considered as an additional lumped mass on the face. If the thickness of the diaphragm is considerably greater than one-eighth wave length, it must be considered as an elastic part of the vibrating system. In general, it is good practice to keep the diaphragm as small in mass as possible consistent with maintaining its flexural stiffness. For this reason it is preferable to make the diaphragms from light materials such as aluminum alloys, magnesium alloys, or certain stiff plastic laminates. There may be rare cases in which high Q 's are desired and in which the diaphragm should be made massive and thick in the direction of vibration. Recent experiments indicate that some interesting modes of vibration and unusual frequency responses can be obtained from laminated stacks attached to relatively thick diaphragms of materials of low density. The possibilities of vibrating systems of this kind should be explored rather thoroughly in the future.

The problems of attaching the laminated stacks to the diaphragm are essentially the same as those for laminated uniform bars, which have been discussed in this section; the problems of supporting the windings and polarizing magnets are usually not difficult. The coils and magnets usually can be attached to the laminated stack itself through thin compliant layers of material, such as Cell-Tite neoprene.

Modes and Frequencies of Vibration. The simplest case to consider is the first mode of vibration of a system of the type shown in Figure 10 in which the face sections attached at each end of the legs may be considered as lumped masses. In such a case

$$\cot k_1 L_1 = \frac{k_1 M_1}{2\rho_1 w h} \quad (20)$$

and

$$\cot k_1 L_2 = \frac{k_1 M_2}{2\rho_1 w h},$$

where h is the dimension perpendicular to the plane of the laminations, where

$$M_1 = \rho_1 b y h, \quad (21)$$

$$M_2 = h b (\rho_1 y + \rho_2 z),$$

and where $k_1 = 2\pi f_1 / c_1$ is the wave number for the frequency of the first mode of vibration. Therefore,

$$L_1 = \frac{1}{k_1} \tan^{-1} \left(\frac{2\rho_1 w h}{k_1 M_1} \right) \quad (22)$$

$$L_2 = \frac{1}{k_1} \tan^{-1} \left(\frac{2\rho_1 w h}{k_1 M_2} \right)$$

serve to determine the length of the legs when the frequency, leg width, and face masses are specified. The inverse problem of finding the frequency when the dimensions and face masses are given may be solved by finding the solution to the transcendental equation

$$k = \frac{1}{L} \left[\tan^{-1} \frac{2\rho_1 w h}{k M_1} + \tan^{-1} \frac{2\rho_1 w h}{k M_2} \right] \quad (23)$$

by graphical or successive approximation methods.

The ratio of the velocity of the back face to the velocity of the active face is

$$\frac{v_1}{v_0} = \frac{\sin k_1 L_1}{\sin k_1 L_2}. \quad (24)$$

The effective mass of the system is

$$M^* = \frac{\sin^2 k_1 L_1}{\sin^2 k_1 L_2} M_1 + \frac{\rho_1 w h}{k_1 \sin^2 k_1 L_2} \cdot \quad (25)$$

$$[k_1 L_1 - (\cos k_1 L_1) (\sin k_1 L_1)] + M_2$$

$$+ \frac{\rho_1 w h}{k_1 \sin^2 k_1 L_2} [k_1 L_2 - (\cos k_1 L_2) (\sin k_1 L_2)].$$

If the active face is large enough to allow full resistive radiation loading and if internal mechanical damping is negligible, then the mechanical Q of the system is

$$\frac{2\pi f M^*}{b h (\rho c)_w}.$$

If the face portions of the laminations are considerably thicker than one-eighth of a wave length and if the diaphragm is also very thick, the modes of vibration become so numerous and complicated that no attempt at a general analysis of them will be made here. As was pointed out above, a considerable amount of theoretical and experimental research work should be done on vibrating systems of this kind.

The magnetic circuits and polarization of elements of this type are the same as those for the symmetrical laminations without mass-loading diaphragms, except for a shift in the position of the nodes.

DOUBLE OR MULTIPLE BARS WITH UNSYMMETRICAL CLOSED OR NEARLY CLOSED ENDS

Types of Structures. Several laminations of this type are shown in Figures 11 and 12. Those in A and B of Figure 11 have legs of uniform width that are parallel, whereas the others have legs of uniform width (except for the center portions of the legs of B in Figure 12) that converge toward a common center. Those with converging legs find application in cylindrical sonar transducers. Several kinds of transducers with plane faces have been constructed using stacks made of laminations of the general forms indicated in A and B of Figure 11. The depth of the heavy end portion may vary from about one-eighth wave length to over one-quarter wave length in the lamination material. Hence this part acts as a compressible bar, not as a lumped mass.

The problems of stacking, consolidating, mounting, and making provision for acoustic contact with the water are the same as for the other types already discussed.

Modes and Frequencies of Vibration. Laminated stacks of this type are capable of vibrating in many different modes. The most important of these modes in actual cases are the first two longitudinal ones. In the discussion that follows, the details of only the first mode of longitudinal vibration of laminations of the type shown in A and B of Figure 11 will be presented. The frequencies of resonance and the mechanical Q 's of laminations of the general form shown in Figures 11 and 12 when vibrating in the second mode are roughly twice those for the first mode.

Figure 13 shows a simplified equivalent form of the two-legged laminations which will be used as a basis for design considerations. In practical designs b is usually of the order of a half wave length in water at the desired frequency, w and y are made approxi-

mately $\frac{1}{6}b$, and $2W$ is made equal to or less than b . The exact selection of values of y , w , W , and L_3 depends largely on the value of the mechanical Q desired. For the sake of clearness, three special cases will be considered, (1) where the node lies in the thin leg section, (2) where the node lies at the junction of

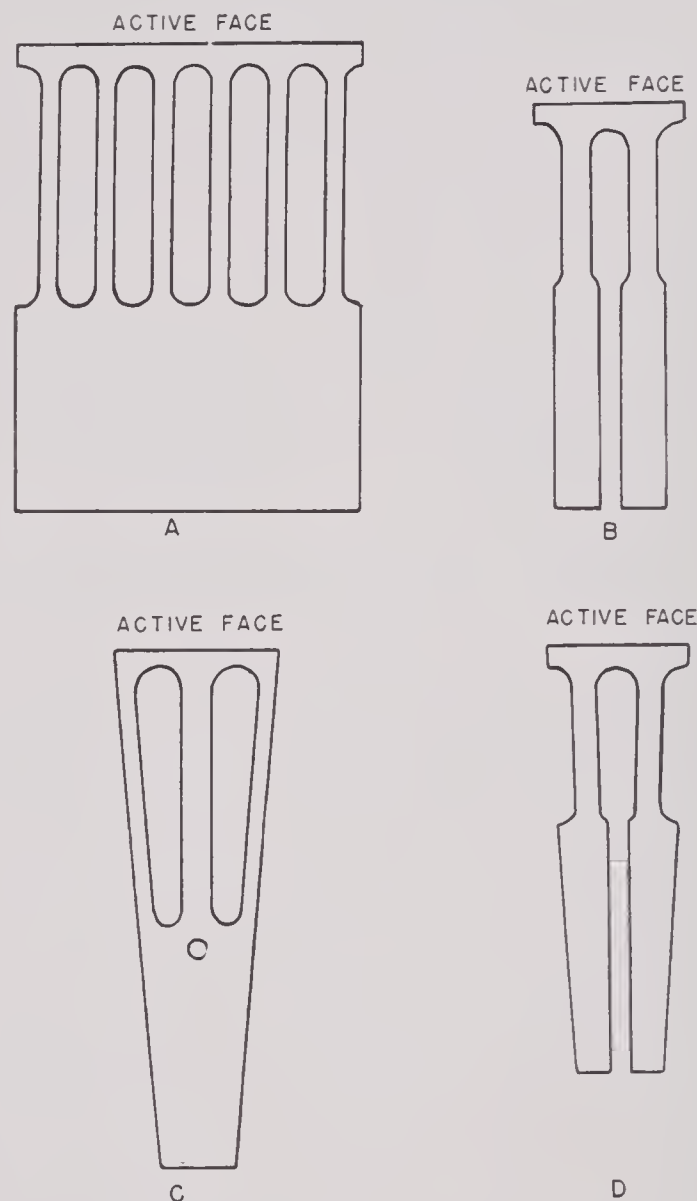


FIGURE 11. Types of laminations consisting of two or more uniform bars with unsymmetrical closed ends.

the thin legs and the wide backing section, and (3) where the node lies in the thick backing section.

Case 1: Node in the thin leg section. The conditions for resonance are

$$\begin{aligned} \tan k_1 y \tan k_1 L_1 &= \frac{2w}{b}, \\ \tan k_1 L_3 \tan k_1 L_2 &= \frac{w}{W}. \end{aligned} \quad (26)$$

where $k_1 = 2\pi f_1/c$ as before. If the rms particle velocity of the active face is v_0 , then the velocity in the face portion is

$$v(x') = v_0 \cos k_1 x', \quad (27)$$

where x' is the distance from the active face, the particle velocity in the slender leg section is

$$v(x_1) = v_0 \frac{\cos k_1 y}{\sin k_1 L_1} \sin k_1 x_1, \quad (28)$$

where the distance x_1 is measured from the node and is considered positive in the direction of the active face. The particle velocity in the thick leg portion is given by

$$v(x_3) = -v_0 \frac{\cos k_1 y}{\sin k_1 L_1} \frac{\sin k_1 L_2}{\cos k_1 L_3} \cos k_1 x_3, \quad (29)$$

where x_3 is the distance measured from the free end of the thick leg section. From this distribution of particle velocity the effective mass of the vibrating system referred to the velocity of the active face is found to be

$$M^* = \rho h \left\{ \frac{b}{2k_1} [k_1 y + \sin k_1 y \cos k_1 y] + \frac{\cos^2 k_1 y}{\sin^2 k_1 L_1} \cdot \frac{w}{k_1} \right. \\ \left. [k_1 L - \cos k_1 L_1 \sin k_1 L_1 - \cos k_1 L_2 \sin k_1 L_2] \right. \\ \left. + \frac{\cos^2 k_1 y}{\sin^2 k_1 L_1 \cos^2 k_1 L_3} \frac{W}{k_1} [k_1 L_3 + \sin k_1 L_3 \cos k_1 L_3] \right\}. \quad (30)$$

The mechanical Q is therefore

$$Q_1 = \frac{2\pi f_1 M^*}{(\rho c)_w b h} = \frac{(\rho c)_{\text{lam}}}{(\rho c)_w} \left\{ \frac{1}{2} [k_1 y + \sin k_1 y \cos k_1 y] \right. \\ \left. + \frac{w}{b} \cdot \frac{\cos^2 k_1 y}{\sin^2 k_1 L_1} [k_1 L - \cos k_1 L_1 \sin k_1 L_1 - \cos k_1 L_2 \sin k_1 L_2] \right. \\ \left. + \frac{W}{b} \cdot \frac{\cos^2 k_1 y}{\sin^2 k_1 L_1 \cos^2 k_1 L_3} [k_1 L_3 + \sin k_1 L_3 \cos k_1 L_3] \right\}. \quad (31)$$

Case 2: Node at junction of the thin leg section and the thick backing section. In this case the conditions for resonance are

$$\tan k_1 y \tan k_1 L_1 = \frac{2w}{b}, \quad (32)$$

$$\tan k_1 L_3 = \infty.$$

The second condition means simply that the heavy backing section should be just one-quarter wave length long. The distribution of particle velocity in

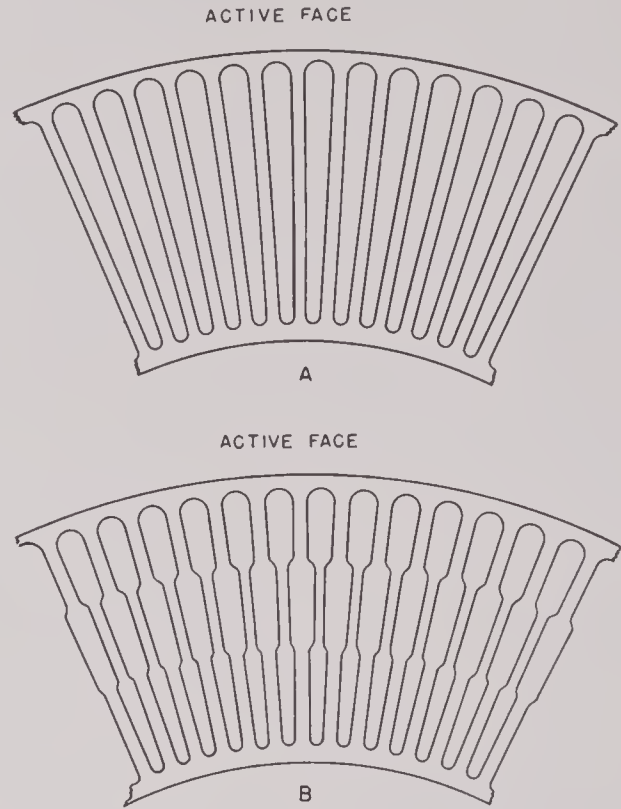


FIGURE 12. Ring-shaped laminations which are essentially longitudinally vibrating bars with unsymmetrical closed ends.

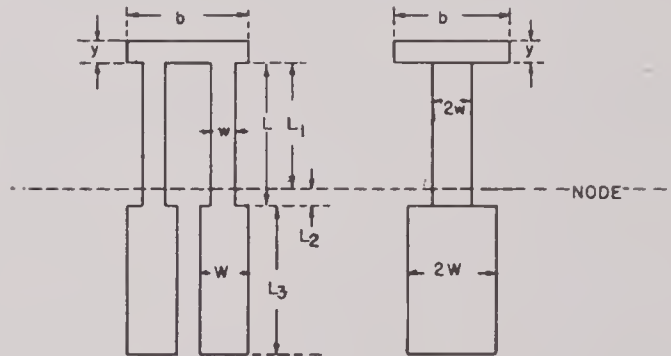


FIGURE 13. Equivalent form for laminations of the form shown in A and B of Figure 11.

the front half of the lamination is the same as in case 1 above. The particle velocity in the thick backing portion is

$$v(x_3) = -v_0 \frac{w}{W} \frac{\cos k_1 y}{\sin k_1 L_1} \cos k_1 x_3, \quad (33)$$

where x_3 is measured from the free end of the thick section. The effective mass referred to the velocity of the active face is

$$M^* = \rho h \left\{ \frac{b}{2k_1} [k_1 y + \sin k_1 y \cos k_1 y] + \frac{\cos^2 k_1 y}{\sin^2 k_1 L_1} \cdot \frac{w}{k_1} \right. \\ \left. [k_1 L_1 - \cos k_1 L_1 \sin k_1 L_1] + \frac{w^2}{W^2} \cdot \frac{\cos^2 k_1 y}{\sin^2 k_1 L_1} W L_3 \right\}. \quad (34)$$

The mechanical Q is

$$Q_1 = \frac{(\rho c)_{\text{lam}}}{(\rho c)_w} \left\{ \frac{1}{2} [k_1 y + \sin k_1 y \cos k_1 y] + \frac{w}{b} \cdot \frac{\cos^2 k_1 y}{\sin^2 k_1 L_1} \cdot [k_1 L_1 - \cos k_1 L_1 \sin k_1 L_1] + \frac{w^2 L_3 k_1}{W b} \cdot \frac{\cos^2 k_1 y}{\sin^2 k_1 L_1} \right\}. \quad (35)$$

Case 3: Node in thick backing section. In this case the condition for resonance in the first mode is

$$\frac{\tan k_1 L_3}{\tan k_1 (L + x_0)} = -\frac{w}{W}, \quad (36)$$

where

$$x_0 = \frac{1}{k_1} \tan^{-1} \left(\frac{b}{2w} \tan k_1 y \right). \quad (37)$$

If the particle velocity at the active face is v_0 , then the particle velocity at the free end of the heavy backing section is

$$(v_3)_0 = -v_0 \frac{\cos k_1 y}{\cos k_1 x_0} \cdot \frac{\cos k_1 (L + x_0)}{\cos k_1 L_3}. \quad (38)$$

The effective mass, referred to the particle velocity of the active face, is

$$M^* = \frac{\rho h}{k_1} \left\{ \frac{b}{2} [k_1 y + \sin k_1 y \cos k_1 y] + \frac{\cos^2 k_1 y}{\cos^2 k_1 x_0} \cdot \frac{\cos^2 k_1 (L + x_0)}{\cos^2 k_1 L_3} W [k_1 L_3 + \sin k_1 L_3 \cos k_1 L_3] + \frac{\cos^2 k_1 y}{\cos^2 k_1 x_0} w [k_1 L + \sin k_1 (L + x_0) \cos k_1 (L + x_0) - \sin k_1 x_0 \cos k_1 L_3] \right\}, \quad (39)$$

and the mechanical Q is

$$Q_m = \frac{(\rho c)_{\text{lam}}}{(\rho c)_w} \frac{1}{b} \left\{ - + - + - \right\}, \quad (40)$$

where the brace is the same as that in equation (39).

The mechanical mounting and the magnetic polarization of laminated stacks of this type can be made essentially the same as those for the types discussed earlier in this chapter.

DOUBLE OR MULTIPLE BAR WITH UNSYMMETRICAL CLOSED ENDS AND DIAPHRAGMS

In some types of transducers that use unsymmetrical laminated stacks it is desirable to use a strong diaphragm plate for mechanical strength. In these cases it is usually desirable to cement the active faces of the stacks directly to the diaphragm in order to make good acoustic contact and the diaphragm becomes a definite part of the vibrating system and consequently influences its vibration characteristics.

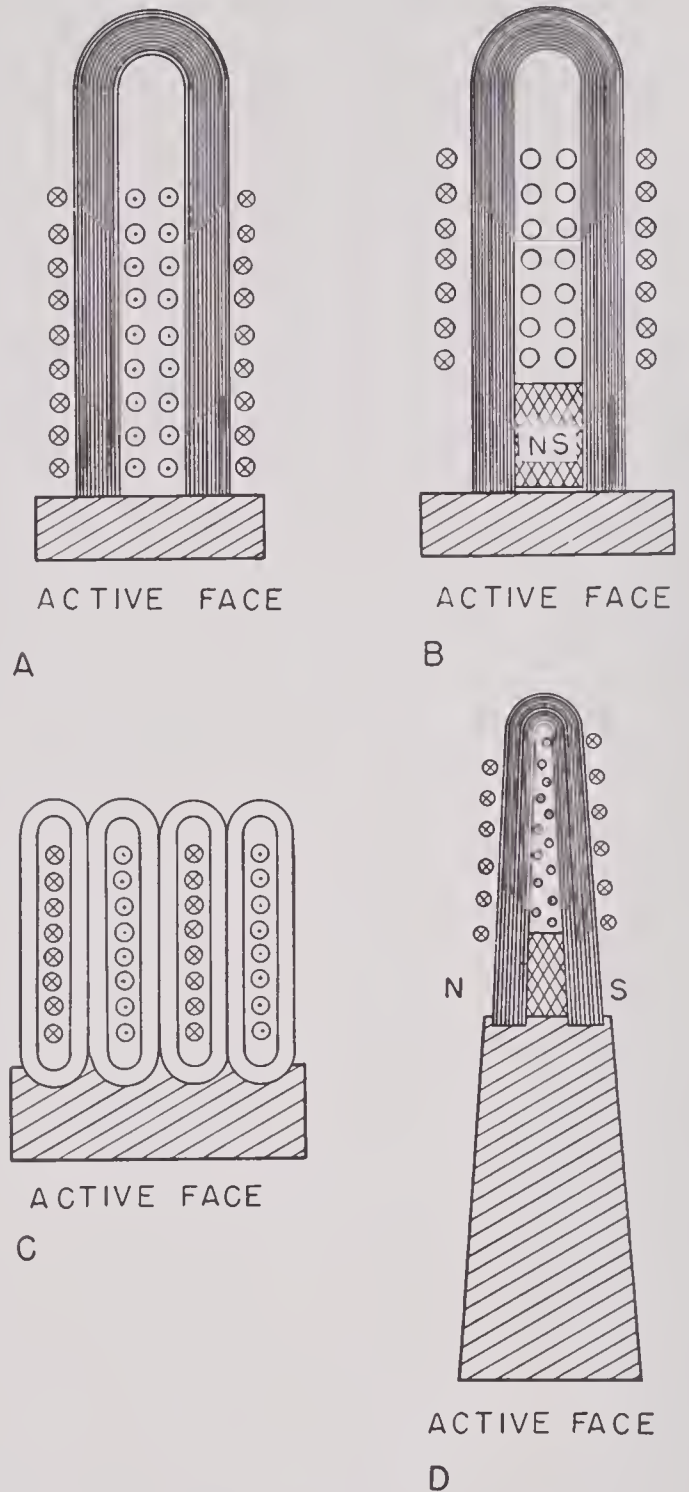


FIGURE 14. Miscellaneous forms of laminated longitudinally vibrating transducer elements.

The complete theory of the modes of vibration of systems of this type has been worked out, but the results of the few experimental models constructed indicate that some unusual mechanical filter action occurs, giving rise to unusual frequency responses. It is possible that further experimental investigation of transducers of this type might yield some units with a flat band-pass type of frequency responses.

MISCELLANEOUS FORMS

There are several miscellaneous forms of laminated, longitudinally oscillating transducers that are not included in the classifications above. Some of these are illustrated in Figure 14. These all make use of consolidated scroll-type elements made by the same process used for commercial Hipersil transformer cores. The forms shown in A and C of Figure 14 require the use of direct current for magnetic polarization but those shown in B and D are polarized by means of permanent magnets.

7.2 EXPERIMENTAL TRANSDUCERS

7.2.1 Simple Uniform Bars

Simple uniform bars have not been used as practical transducers because of the relatively small radiation loading on the available face area and because of the impossibility of making a continuous active face. However, a great many simple uniform bars have been made and used as half-wave oscillators for testing the magnetostrictive properties of sample ma-

TABLE 1. Performance characteristics of experimental bookphone elements.

Model	Stack length (in.)	Diaphragm	Polarization	Polariz. current (amp)	f_r in ke	Max OC sensitivity in db (v/b)	Mech Q	Efficiency		
								Poten-tial	From air & water	From acoustic measurements
1A	4.5	Steel	DC	0.6	18.2	- 79	12
2A	4.5	Steel	DC	0.6	19.0	- 80	15	High	...	0.10
2B	4.5	Steel; rubber face	DC	0.7	18.9	- 82	6	0.55
3A	3.5	Steel	DC	0.8	23.5	- 85	10	0.43
4A	2.5	Steel	DC	1.0	32.0	- 90	5.5	0.13	...	0.04
5B	4.5	Steel; no flanges; rubber face	Alnico magnet at top, plus DC	0.75	17.5	- 85	11	0.26	0.25	0.275
13A	4.5	Polystyrene	Alnico magnets top & bottom	None	18.0	- 86	7	0.065	0.066	0.05
14A	4.5	Brass	Alnico magnet at bottom, plus DC	0.7	17.0	- 80	24	0.45	0.43	0.33
17A	4.0	Steel	DC	2.0	19.0	- 96.5	3	0.13	0.15	0.07
18A	4.0	Cu-plated Alnico II	Alnico magnet diaphragm plus DC	0.7	31.2 (2nd mode?)	- 86.5	24	0.14	...	0.16
20A	4.0	Steel; no flanges; rubber face	DC	1.0	19.4	Not tested	25	0.61	0.42	...

In all the cases shown in Figure 14 the laminated structure must be cemented, soldered, or brazed to the face plates. Also, in all the types shown, the free ends of the vibrators consist of the rounded portion of the wrapped scrolls. The mass and elastic characteristics of these rounded ends are difficult to hold constant in practice and to analyze theoretically. The stiffness of the arches depends to a considerable extent on the degree of consolidation. The variations in the degree of consolidation that normally occur in practice cause the frequency variations among supposedly identical units to be undesirably large. No attempt will be made here to present an analysis of the modes and frequencies of vibration.

Several experimental transducers of this type were made and tested at HUSL. These will be described and discussed later in this chapter.

materials or the mechanical losses in laminated stacks consolidated with various cementing materials. Freely supported laminated bars have also been used as secondary frequency standards because their different modes of vibration give sharp resonances, indicated by sharp changes in their impedance. Correction for the change of frequency with temperature may be applied in those cases in which extreme accuracy is required.

7.2.2 Uniform Bars with Pistons or Diaphragms

BOOKPHONES

Several experimental transducer elements of this type were made at HUSL, where they were commonly referred to as bookphones because of their re-

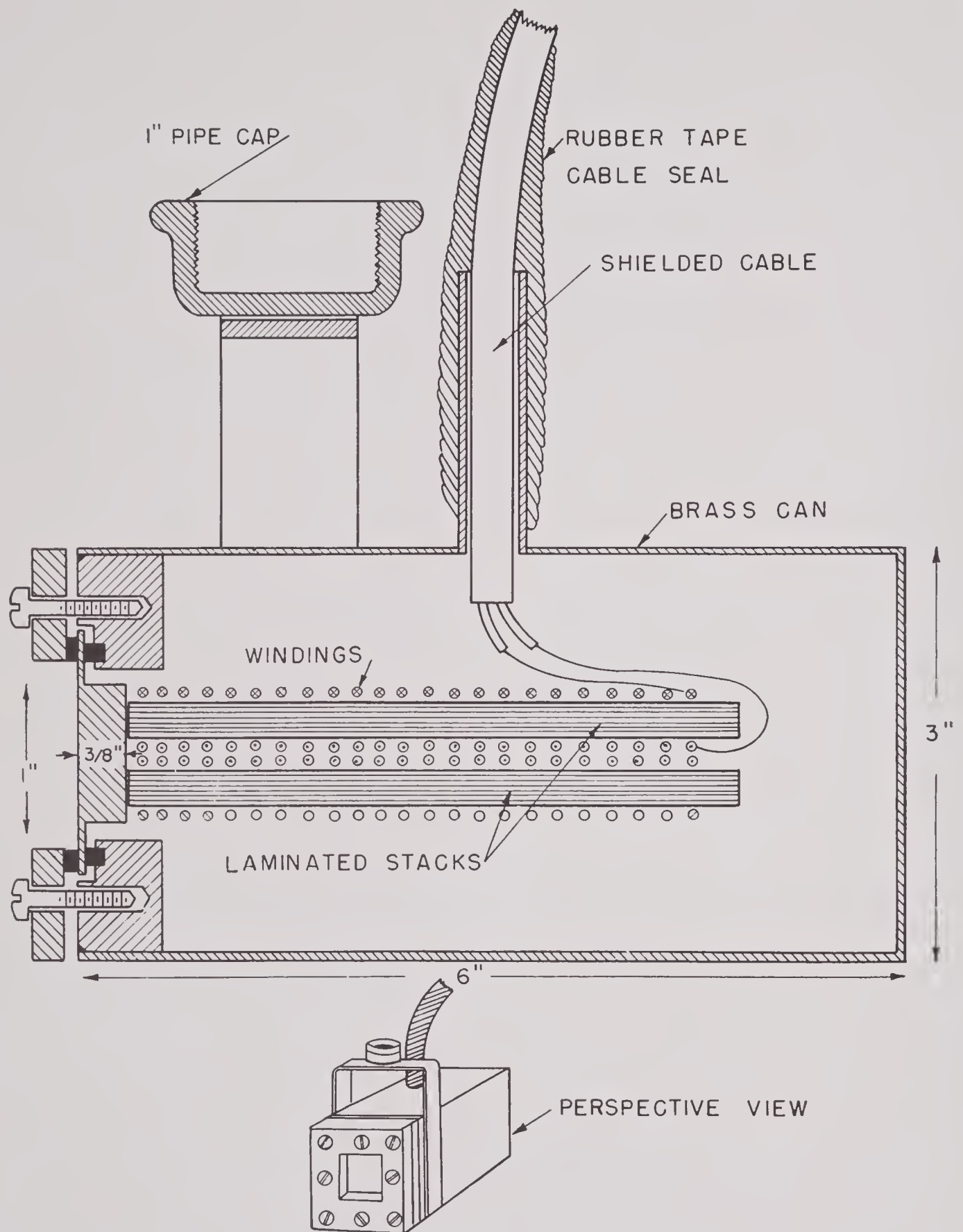


FIGURE 15. Special housing for testing bookphone elements.

CONFIDENTIAL

semblance to books standing on a shelf. An extensive series of tests on single elements was made by using a special housing in which the elements could be changed easily. The housing is shown in section and in perspective in Figure 15. The simple bar-shaped laminated stacks were made from flat nickel laminations consolidated with bonding materials such as Vinylseal resin, phenol-formaldehyde cements, and Cycle-Weld cement. The same materials were used to bond the laminated stacks to the diaphragm, which was made of steel or brass. The moving part of each of the diaphragms was $\frac{3}{8}$ in. thick and 1 in. square. The entire vibrating element assembly was fastened to the housing through the thin compliant rim of the diaphragm. The windings were supported on the laminated stacks by thin pads of Cell-Tite neoprene. The lengths of the stacks ranged from $2\frac{1}{2}$ in. to $4\frac{1}{2}$ in. The earliest models were polarized with direct current while some of the later models were polarized by placing Alnico magnets between the two stacks at the two ends.

The results of experiments on cementing the laminated stacks to the diaphragms showed that Bostik T46M cement (made by the Boston Blacking and Chemical Company) had the greatest strength. Du Pont 4646 and Cycle-Weld C-3 or 55-6 made bonds that were strong enough to be quite satisfactory. All these joints, when properly made, showed tensile strengths of a few thousand pounds per square inch. Because the high-frequency alternating magnetic flux from the laminated stacks cannot penetrate far into the solid diaphragm owing to eddy-current shielding, very little is gained by using a cement that electrically insulates the laminated stacks from the diaphragm. Some rather unsuccessful attempts were made to solder the laminated stacks to the diaphragms.

Results of measurements on some of the experimental elements tested are summarized in Table 1. Results of measurements on elements found to be defective are not listed. Most of the elements were polarized by use of direct current in the windings. Some were made with Alnico II magnet inserts between the two laminated bars, somewhat as illustrated in Figure 5. Element 18A was made by using a piece of Alnico II magnet material for the diaphragm and bonding the laminated bars to it. In no case did the magnets give optimum magnetic polarization.

The best elements were those made with steel diaphragms with rubber faces but without flanges. The poorest unit (aside from those that were mechan-

ically defective) was the 13A, which was made by polymerizing styrene around one end of the assembly, as shown in Figure 16. The polystyrene diaphragm apparently did not have sufficient stiffness to transmit the force of the magnetostrictive stacks to the

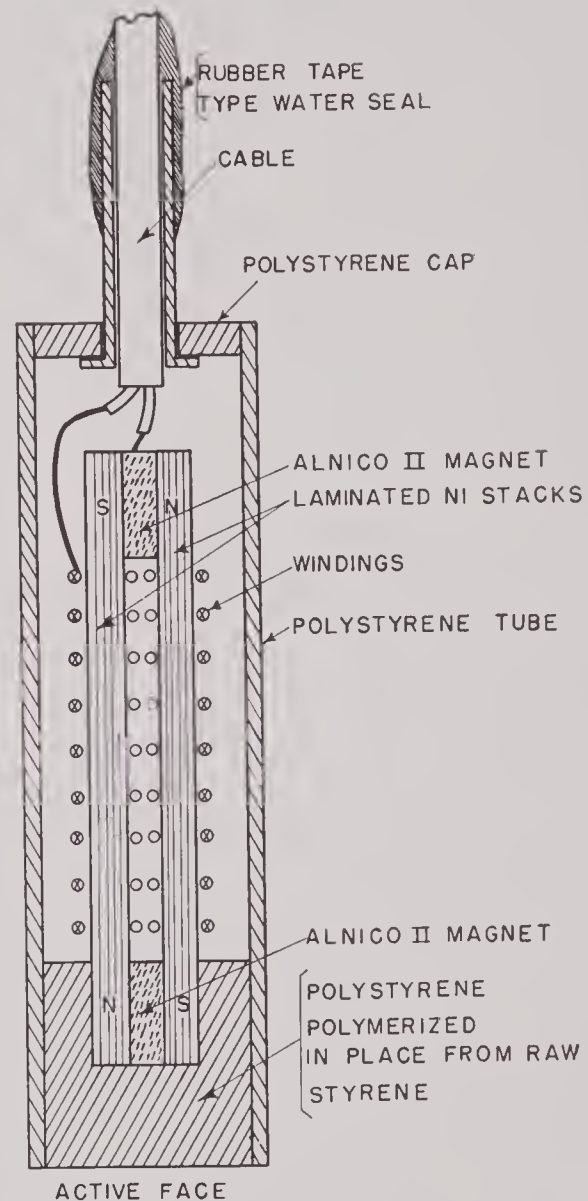


FIGURE 16. Laminated double-bar magnetostrictive element with Polystyrene diaphragm and housing.

full face area and, in addition, introduced a considerable amount of mechanical damping. This has been the usual result when polystyrene and similar plastic materials have been used as diaphragms for elements of this general type.

The theoretical frequency for the first mode of vibration of the $4\frac{1}{2}$ -in. elements as given by equation (5) is 18.6 ke. By equation (9) the effective mass is 211 grams, and by equation (10) the mechanical Q should be 26. Differences in the observed frequencies

of resonance from the values expected theoretically are probably due to slight variations in the lengths of the bars and the thicknesses of the diaphragms. In several instances the general shapes of the frequency responses were rather ragged, due to imperfect joints between the laminated bars and the diaphragm and to mechanical coupling between the housing and the diaphragm.

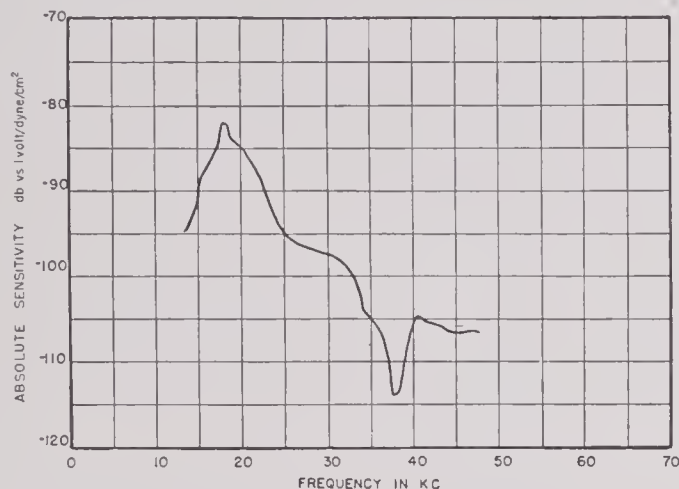


FIGURE 17. Open-circuit frequency response of book-phone, Model 2B No. 1.

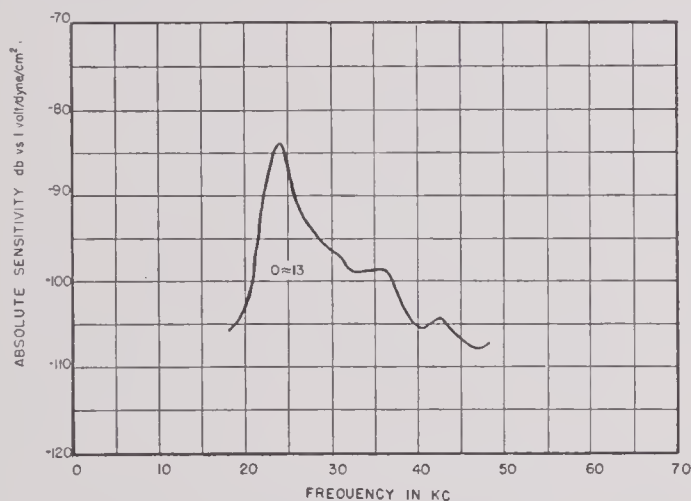


FIGURE 18. Open-circuit frequency response of book-phone, Model 3A No. 1.

Some of the observed open-circuit frequency responses are shown in Figures 17 to 21 inclusive. No acoustic measurements were made on element 20A. However, the impedance diagrams shown in Figures 22 and 23 show that it was a very efficient element and free from spurious resonances.

Only one attempt was made to make a multielement transducer of the bookphone type. This one was known as the *line source bookphone*. It was made with six pairs of laminated bars $\frac{1}{4} \times 1 \times 4$ in. Each pair

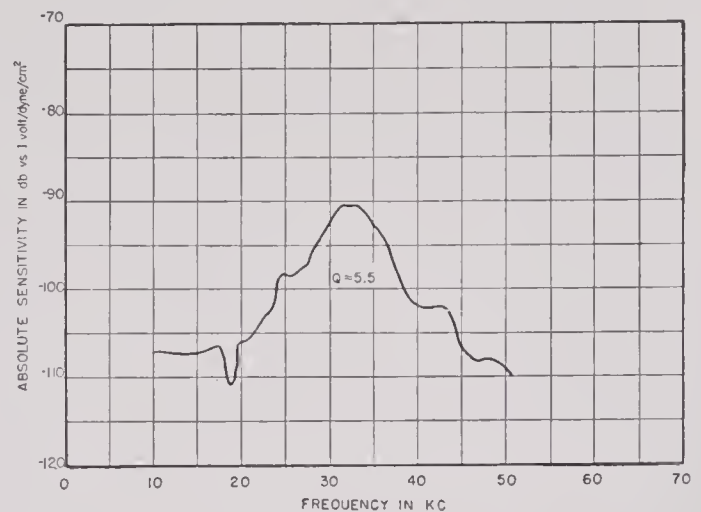


FIGURE 19. Open-circuit frequency response of book-phone, Model 4A No. 1.

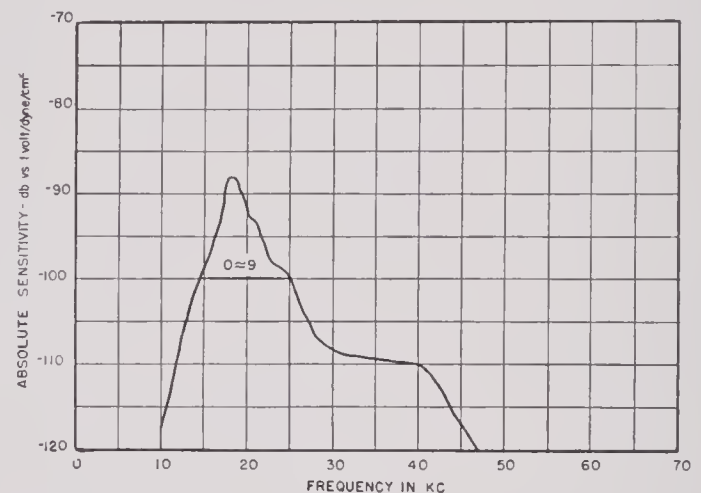


FIGURE 20. Open-circuit frequency response of book-phone, Model 13A No. 1.

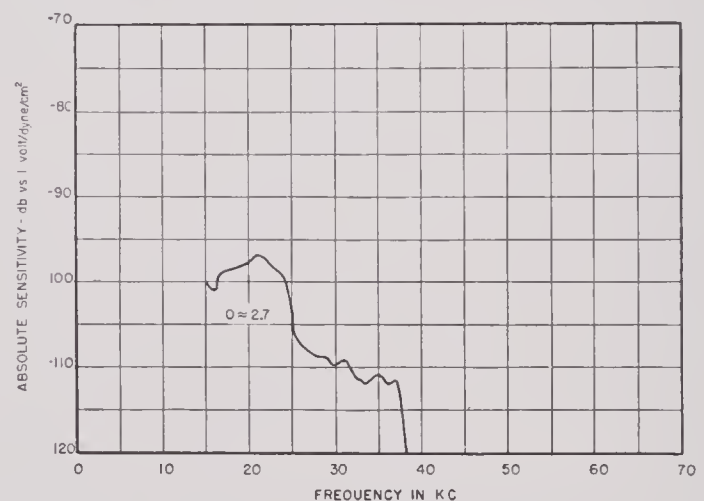


FIGURE 21. Open-circuit frequency response of book-phone, Model 17A No. 1.

was cemented together to form an element, with Alnico II magnets between the bars at the top and bottom ends. The six elements were bonded to a

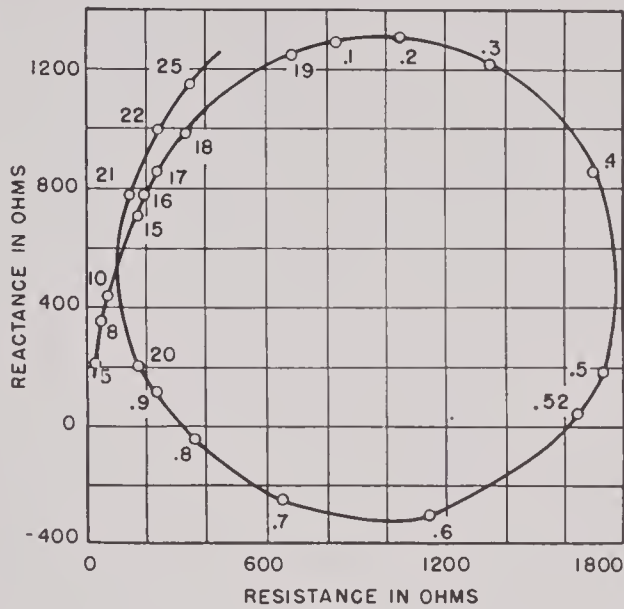


FIGURE 22. Impedance diagram of bookphone, Model 20A No. 1 in air.

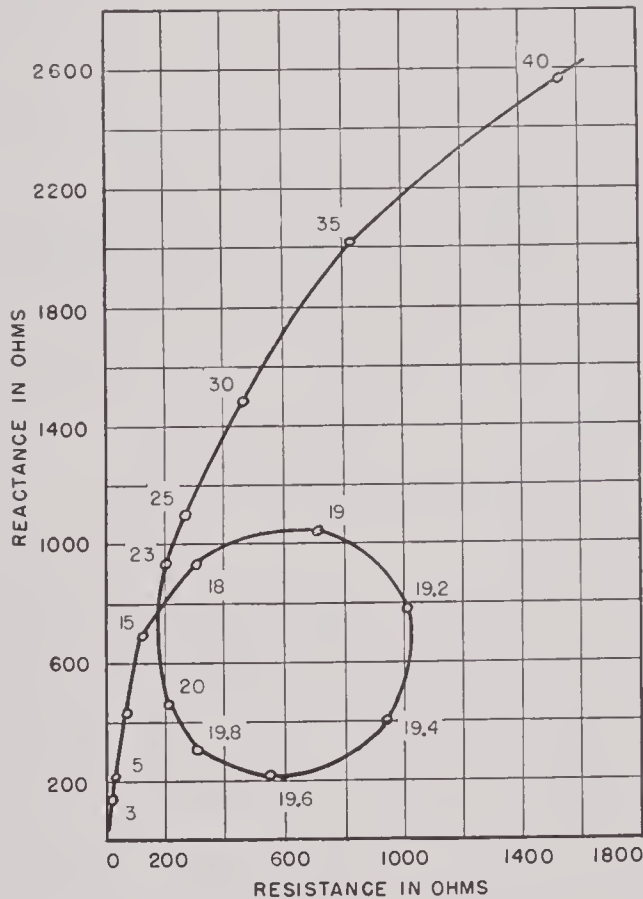


FIGURE 23. Impedance diagram of bookphone, Model 20A No. 1 in water.

brass diaphragm $\frac{3}{8} \times 1 \times 10\frac{1}{4}$ in. with Bostik T46M cement. The length of the diaphragm was divided into six sections by five grooves $\frac{1}{4}$ in. wide and $\frac{1}{4}$ in. deep to provide some compliance between the diaphragm sections to which the elements were

bonded. The diaphragm was attached to the housing by a compliant strip of ρc rubber. The housing consisted of a long narrow brass box lined with pressure-release material. The entire unit proved to be mechanically strong and watertight.

The open-circuit frequency response of the line source bookphone is shown in Figure 24, when the polarization due to the Alnico magnets was augmented by 1.4 amperes of d-c polarizing current. The primary resonance should occur in the region of 20 kc and the second resonance in the region of 40 kc. The latter appears but the former seems to be smothered

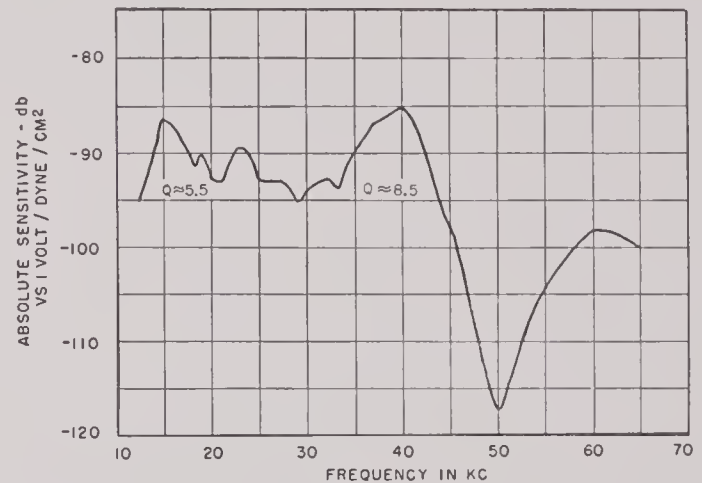


FIGURE 24. Receiving response of line source bookphone.

out by internal damping and spurious mechanical resonances of other types. The patterns had high minor lobes which indicated considerable variation of phase and amplitude among the elements along the diaphragm strip. Results indicated that refinement in the methods of constructing bookphones is required before they can be used in multielement transducers where matching of phase and amplitude among the elements is of great importance.

TRANSDUCER WITH T-SHAPED LAMINATIONS

A second kind of transducer made at HUSL, in the class of laminated bars with diaphragms, was one which employed T-shaped laminations of the form shown in Figure 25A. The laminations were consolidated to form stacks of the size shown in Figure 25B. One multielement transducer was made in which the elements were arranged in the pattern shown in Figure 25C. The crossbar part of the T served as the diaphragm and the stem of the T as the longitudinally vibrating bar. The faces of the stacks were Cycle-Welded to a circular, flat disk face. The rubber face

was stiffened by cementing it to a grill of parallel bars lying between the rows of stacks without touching them. The ends of the bars were attached to a strong steel ring which surrounded the elements and was fastened to the steel face ring which held the rubber face. Figure 26 shows the two sectional views

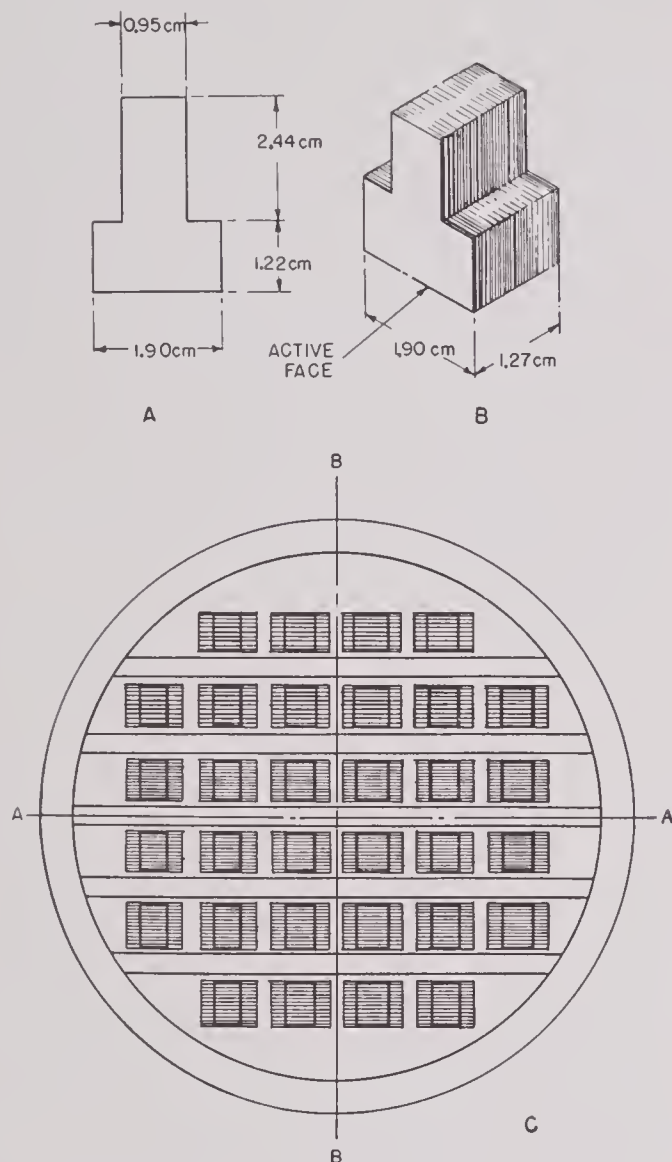
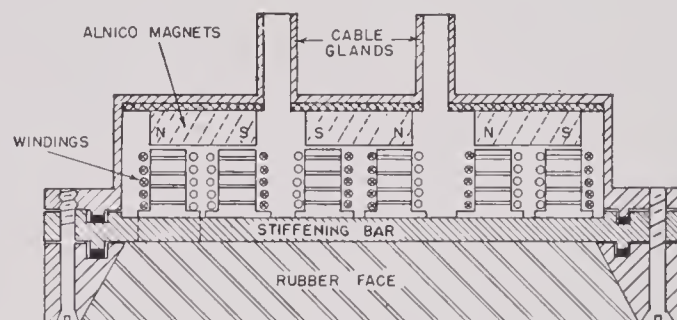


FIGURE 25. Multielement transducer built from T-shaped laminations.

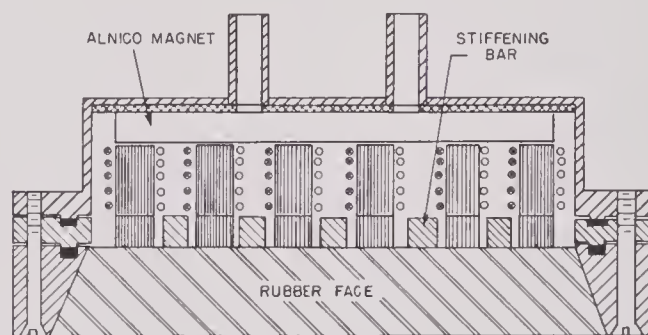
indicated by AA and BB in Figure 25C. The stacks and their windings were supported entirely by the thick rubber face. The windings were made up as pre-formed consolidated coils which fitted closely on the stacks but did not touch them.

The magnets were cemented to a nonmagnetic supporting plate. The supporting plate was in turn supported by the case in such a position that the clearance between the magnets and the free ends of the stacks was of the order of 0.020 in. Three large

slablike Alnico magnets were used to polarize the stacks in pairs, as indicated in Figure 26A. This arrangement made it possible to polarize the nickel stacks to a little below the optimum flux density. The high-frequency alternating flux paths also linked pairs of stacks but jumped across the large air gap between pairs because of the shielding effect of eddy currents in the solid Alnico magnets.



A SECTION A-A FROM FIG. 25 C



B SECTION B-B FROM FIG. 25 C

FIGURE 26. Section of the T transducer shown in Figure 25C.

In this transducer design the cross section of the air path was not much greater than the cross section of the nickel stacks, consequently most of the reluctance of the high-frequency flux path was due to the air path. This decreased the effective reversible permeability of the magnetic circuit and so the electro-mechanical coupling coefficient was much lower than that for better designs.

Open-circuit frequency response of this transducer is shown in Figure 27. On the assumption that the crossbar of the T would act as a lumped mass, the frequency of resonance was calculated to be about 63 kc. The observed frequency was about 56.3 kc. This variation from the calculated frequency is greater than can be accounted for by any error in the velocity of sound in the nickel or by transverse flexibility of the face bar. The mechanical Q from the

observed frequency response was about 32, as compared to the theoretical value of 70, indicating that internal mechanical damping was a little greater than water radiation damping. The impedance circle measurements verified this conclusion. The acoustic patterns for this transducer were about as expected theoretically, that is, the main lobe was about 17 degrees wide at -6 db and the first minor lobes were about 15 db below the peak.

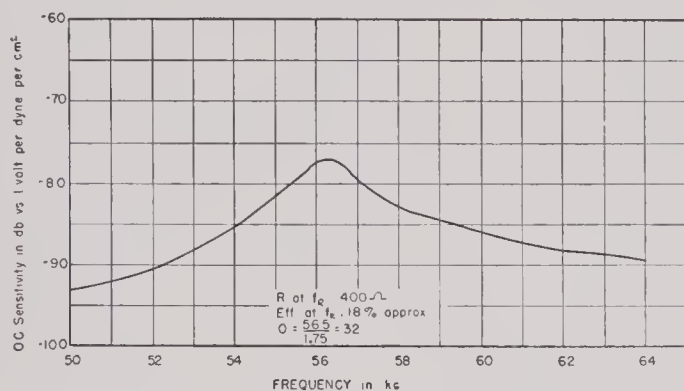


FIGURE 27. Receiving response of the 56-ke T transducer.

This type of transducer was abandoned because (1) it was difficult to polarize satisfactorily, (2) the high-frequency magnetic circuit was inefficient and, (3) the mechanical Q was higher than desired.

BELL TELEPHONE LABORATORIES' MOX TRANSDUCER

A third kind of transducer of this type, called the MOX hydrophone, was made and tested by the Bell Telephone Laboratories.⁸² The general shape of the laminations used in this hydrophone is shown in Figure 28A and a diagrammatic representation of the essential features of the magnetic circuits and methods of mechanical mounting are shown in Figure 28B. The 0.004-in. 45-Permalloy laminations were annealed in a hydrogen atmosphere at a temperature of 1050 C. They were consolidated with mineral-filled bakelite cement (BC-12996) to form a mechanically solid stack. The thickness of the cement between laminations was about 0.001 in.

The rubber face made acoustic contact with the water through a thin metal shell (not shown). The laminated stack was mounted in two saddle-like recesses in the main brass supporting ring. A layer of pressure-release rubber was inserted between the laminated stack and the brass support ring to isolate the vibrating stack from the support ring and to transmit mechanical pressure from the laminated

stack to hold the rubber face against the watertight metal shell referred to above.

The Alnico V permanent magnet provided a polarizing flux of approximately 12,000 gauss in the legs of the laminated stack. The air gap between the pole

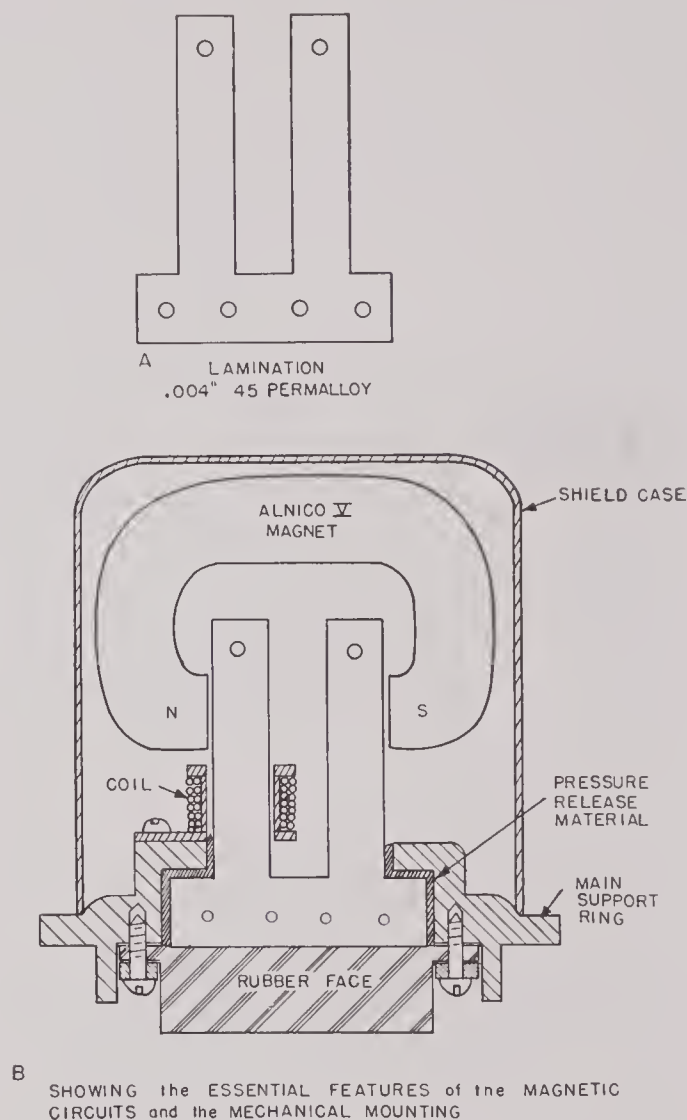


FIGURE 28. MOX hydrophone made by Bell Telephone Laboratories, Inc. [BTL].

faces of the Alnico magnet was about $1\frac{1}{32}$ in. The high-frequency flux traversed the air gap between the two legs instead of going through the solid magnet. In the actual transducer the plane of the Alnico magnet was parallel to that of the face, not in the position shown in Figure 28B.

No data on the open-circuit frequency response and patterns of this transducer are available. The results given in the BTL report indicated approximately 50 per cent efficiency at resonance. This transducer was well designed both magnetically and mechanically. Magnetostrictive elements of this kind,

however, cannot be usefully applied in making multi-element transducers because the polarizing magnet requires too much interelement space.

7.2.3 Double or Multiple Bars with Symmetrical Closed Ends

BELL TELEPHONE LABORATORIES' CI-100 TRANSDUCERS

Early in the war the Bell Telephone Laboratories were given a contract by the Bureau of Ships to develop some improved magnetostrictive-type transducers which could be substituted for the standard

satisfy the requirements. Various test models were made to determine the best method of mounting the laminated stacks to permit one end to radiate into the water while the rest of the element was sealed from the water. The first method tried was to bond one end of the element to a thin ($1\frac{1}{32}$ -in.) steel diaphragm. Soldering and cementing with various adhesives were tried without much success. Models were then made in which the ends of the elements were imbedded in an acoustic rubber face. Results were sufficiently satisfactory so that a full-sized multiple-element transducer was made in this way. Later experiments indicated that even better results could be obtained by using plastic diaphragms and improved methods of consolidating the laminations into stacks.

The general assembly drawing of the CI-100 transducer is shown in Figure 30. Forty laminated stack elements were cemented to the large, thick rubber face. The back ends of the stack elements were held in place by a wire grill with rubber cushions. The housing for the laminated stack elements was made to fit in a standard QC projector case.

The laminations were made of 0.004-in. thick, half-hard, A-nickel strip. To flatten the burrs, the individual laminations were bumped between hardened and polished steel plates. The outside dimensions of the laminations were $1\frac{1}{4}$ in. by $3\frac{1}{2}$ in. and the dimensions of the window were $\frac{1}{2}$ in. by 2 in. The laminations were coated with a layer of silica gel insulation and consolidated with BR-0014 bakelite resin. The windings were concentrated in the nodal region and were bonded firmly to the stack with bakelite cement.

The general wiring diagram is shown in Figure 31. The stacks marked "1" each had two coils of 45 turns, while those marked "2" each had two coils of 32 turns each. This decrease of turns on the outer stacks was used to give some lobe reduction in addition to that due to the diamond-shaped array. The left and right halves of the array were wired separately for BDI applications. The stacks were polarized by a component of direct current in the windings. This made necessary the use of a filter junction box with the equipment. A 3-ampere polarizing current in each winding was necessary to give optimum performance. The complete transducer was polarized by a 6-ampere, 12-volt source of direct current when the two halves were connected in parallel.

Figure 32 shows a plot of the acoustic pressure produced on the main axis at a distance of one meter per watt of electric input power versus the frequency.

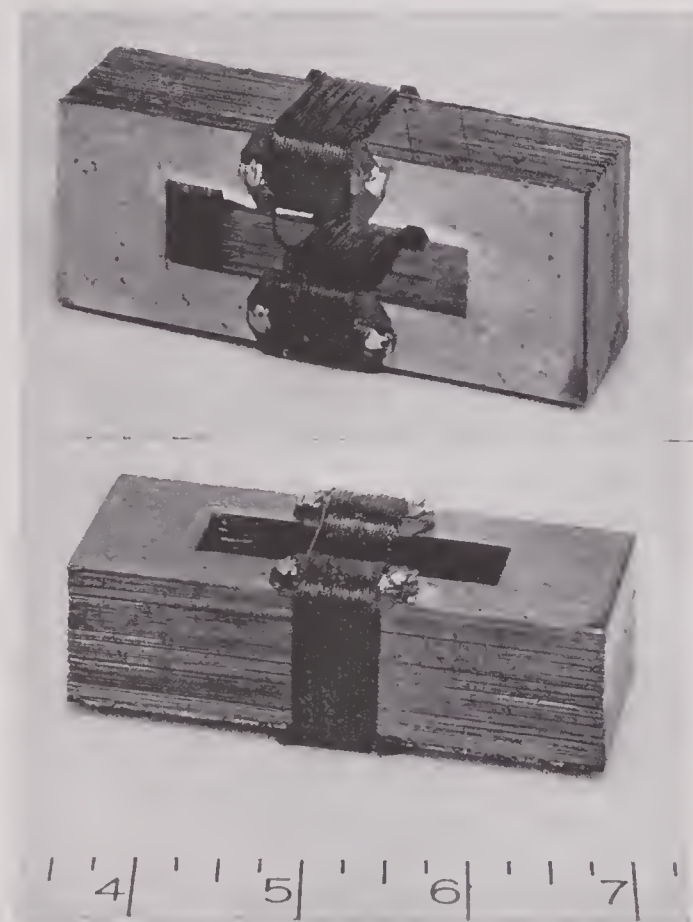


FIGURE 29. Laminated block element for BTL's CI-100 transducer.

QC type. Improvements in acoustic patterns, efficiency, and useful frequency band width were desired. The first model proposed by BTL for development was one made up of an array of laminated stack elements, each element consisting of a pair of half-wave bars with connecting endpieces forming a closed magnetic circuit, as shown in Figure 29.⁸³ Impedance tests on sample elements indicated that they would

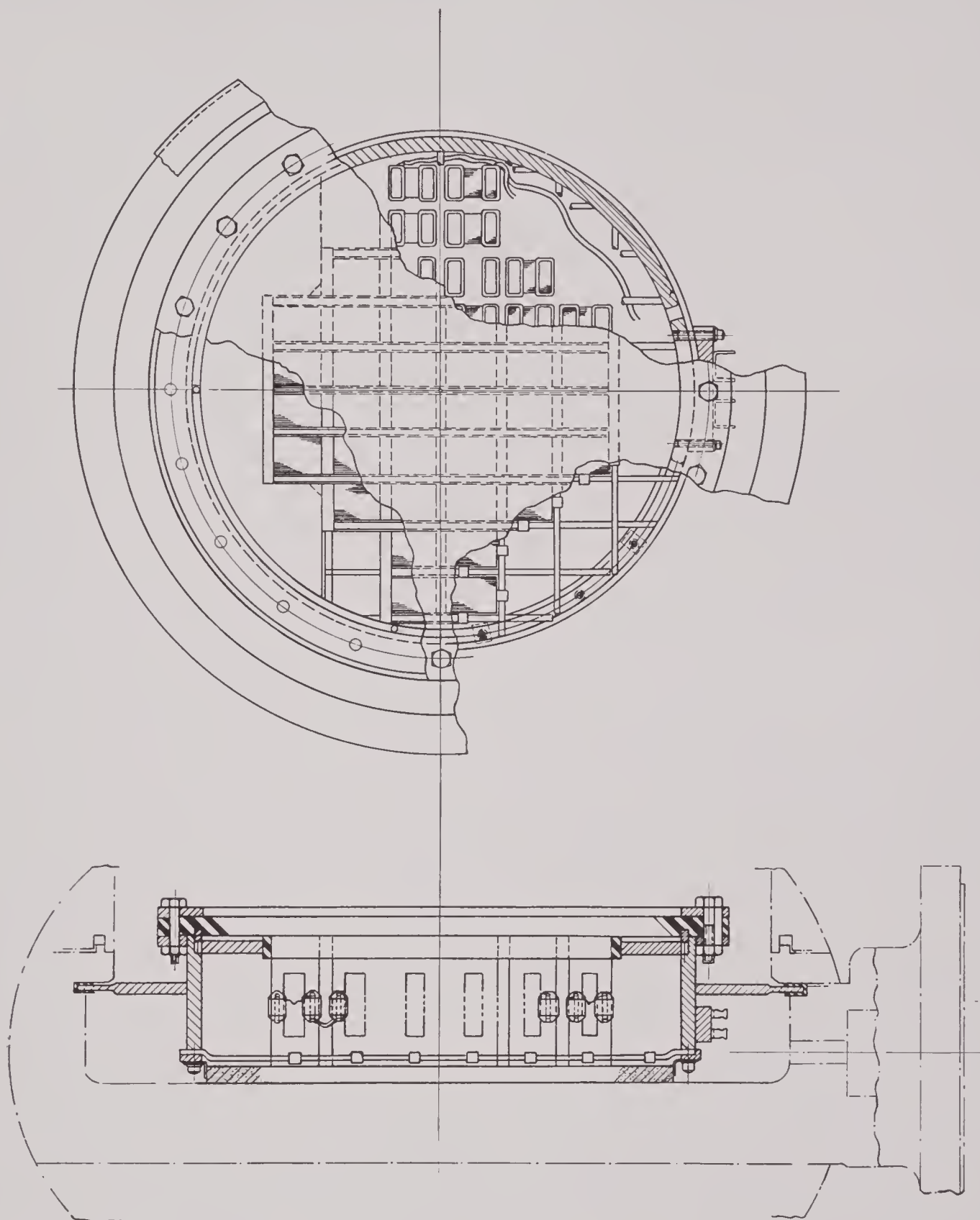


FIGURE 30. General assembly drawing of BTL's CI-100 transducer.

CONFIDENTIAL

This is essentially a plot of efficiency against frequency. Actually impedance varied rapidly with frequency in the region of resonance, so that the open-circuit frequency response curve would be much sharper than the curve shown in Figure 32. The band width over which the efficiency is greater than one-half its maximum value is about 4 kc. Other tests

types developed at about the same time. Therefore, the CI-100 type was not adopted as standard equipment.

SUBMARINE SIGNAL COMPANY'S 20-KC FATHOMETER TRANSDUCER

The transducer for the 20-kc Fathometer system, manufactured by the Submarine Signal Company, consists of a stack of laminations with windings around the legs, as shown in Figure 34; the stack is housed in a case that is partially filled with castor oil. The laminations are punched from pure nickel strip 0.010 in. thick and annealed in air at about 1250 F. They are stacked without consolidation and held in alignment by two lugs projecting from the laminations at the nodal line. The bottom part of the transducer case is made of a thin piece of stainless steel, which comes in contact with the water on the outside and with castor oil on the inside. The laminated

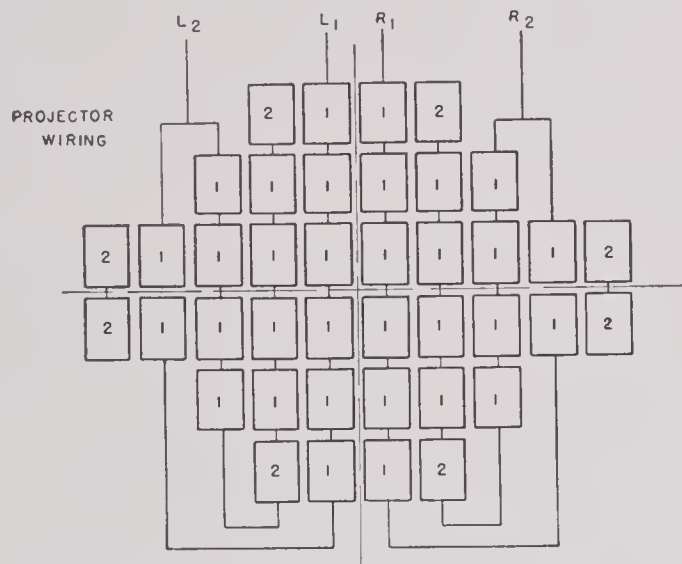


FIGURE 31. Wiring diagram for BTL's CI-100 transducer.

showed that the acoustic output was linear up to an input of 400 watts. For comparison, the efficiency curve for the QCU transducer (one of the best tube-and-plate types) and the X1-100 transducer (a special tube-and-plate transducer built for wide band by BTL) are also shown in Figure 32. The maximum efficiency of the CI-100 transducer occurred at 22 kc and had a value of about 40 per cent.

The acoustic pattern in the horizontal plane, taken at 22 kc, is shown in Figure 33. The main lobe was about 21 degrees wide at -6 db and 27 degrees wide at -10 db. The higher of the first minor lobes was -28 db and the highest of all the minor lobes was -26 db relative to the major lobe. The directivity index was about 0.007. The diamond-shaped active face area and the amplitude shading of the outer stacks were obviously effective in reducing the height of the minor lobes.

This transducer was a definite improvement over the standard QC transducer in efficiency, band width, acoustic patterns, and power-handling capacity. However, the required use of polarizing current made it less desirable for practical use than some of the permanent-magnet polarized tube-and-plate QC

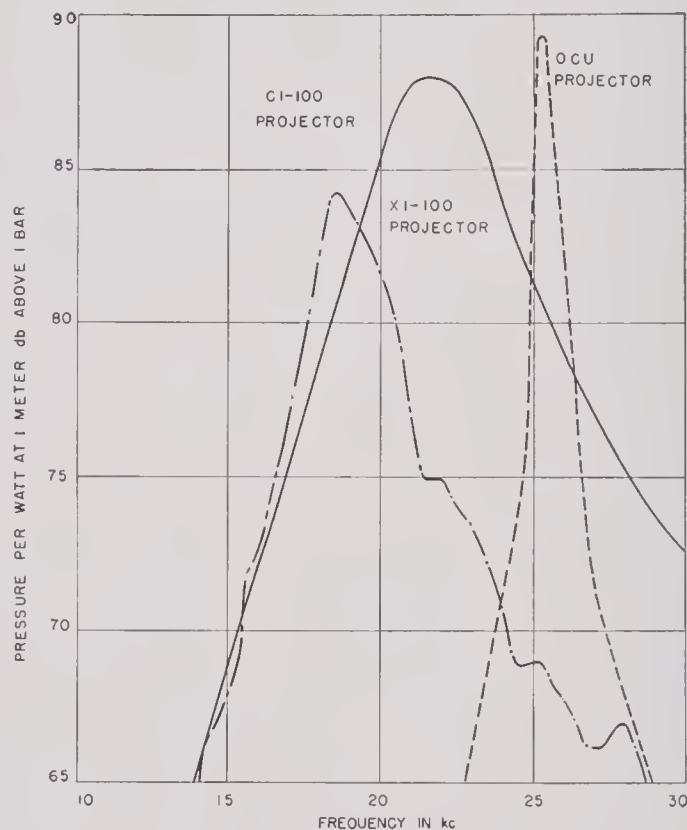


FIGURE 32. Transmitting response per watt input of BTL's CI-100 transducer.

stack is supported in the case with one of the faces near and parallel to the stainless-steel bottom. The case is filled with enough castor oil to insure that the space between the bottom active face of the laminated stack and the stainless-steel bottom sheet of the case is always full of oil to allow for any reason-

able degree of roll or pitch of a ship. The windings consist of a few heavy conductors encircling each of the two heavy center legs.

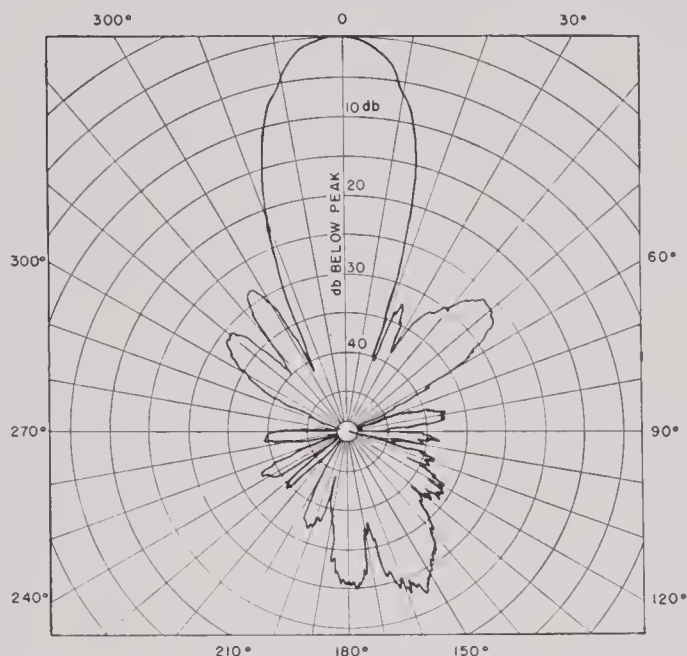


FIGURE 33. Horizontal pattern of BTL's CI-100 transducer at 22 kc.

During the summer and autumn of 1943, HUSL made several model transducers that used such laminations to test the effect on mechanical damping resulting from consolidation of laminations and from immersion of the laminated stacks in oil and in water.³¹ Each of the experimental laminated stacks consisted of 250 laminations (2½ in.). A housing with a rubber face was made into which any one of the experimental stacks could be placed for testing. Four different models were constructed:

1. Hydrogen-annealed laminations, unconsolidated, with the entire assembly vacuum-filled with castor oil.
2. Oxide-annealed laminations, unconsolidated, with the entire assembly vacuum-filled with castor oil.
3. Oxide-annealed laminations, consolidated with Vinylseal resin, with the housing filled with water.
4. Oxide-annealed laminations, consolidated with Vinylseal resin, with the laminated-stack face Cycle-Welded to the rubber face and the stack assembly surrounded by air.

Electric impedance measurements were made with these models with and without water-radiation loading. The "cleanness" of the mechanical resonance,

the potential efficiency, and the actual efficiency were determined from the impedance vs frequency curves. Conclusions drawn from the results of the tests were that (1) loose stacking of the laminations encourages spurious minor resonances and increases the internal mechanical damping; (2) a castor oil film is effective in providing electric insulation between bright hydrogen-annealed laminations; (3) immersion of a stack in castor oil or water causes increased mechanical damping even though the nonradiating surfaces are surrounded by pressure-release material, such as corprene; and (4) the best method of mounting laminated-stack transducers is to cement the active face of the stack directly to the rubber face and have the stack surrounded by air.

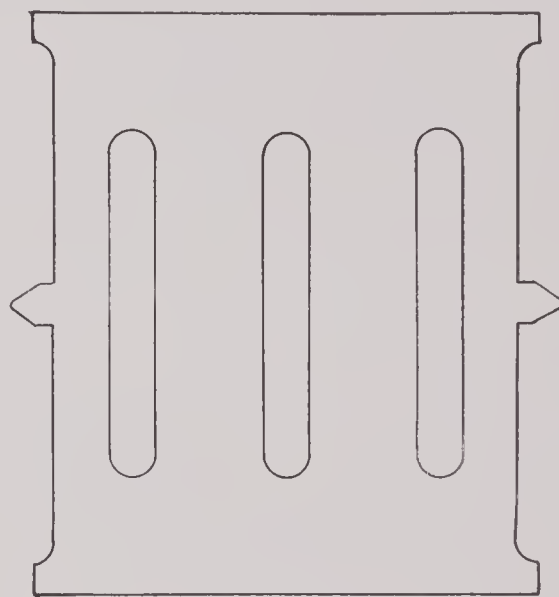


FIGURE 34. Lamination of Submarine Signal Company's 20-ke Fathometer.

LADDERPHONE TRANSDUCERS

Early in 1944, some symmetrical multiple-bar, laminated-stack transducers were made at HUSL to determine the effect of mechanical coupling from bar to bar due to stiffness of the face sections of the laminations.³⁹ The laminations had the general form shown in Figure 9B and were made of nickel 0.005 in. thick, oxide-annealed at 1000 C. They were bonded together with C-3 Cycle-Weld resin to form solid stacks 2 in. high. Each stack had ten bars or legs. One of the stacks was left as a solid unit while the other was cut into five sections, each containing a pair of bars. Perspective views of the two laminated stacks are shown in Figure 35. Separate windings were placed on each pair of bars and a pair of lead wires was

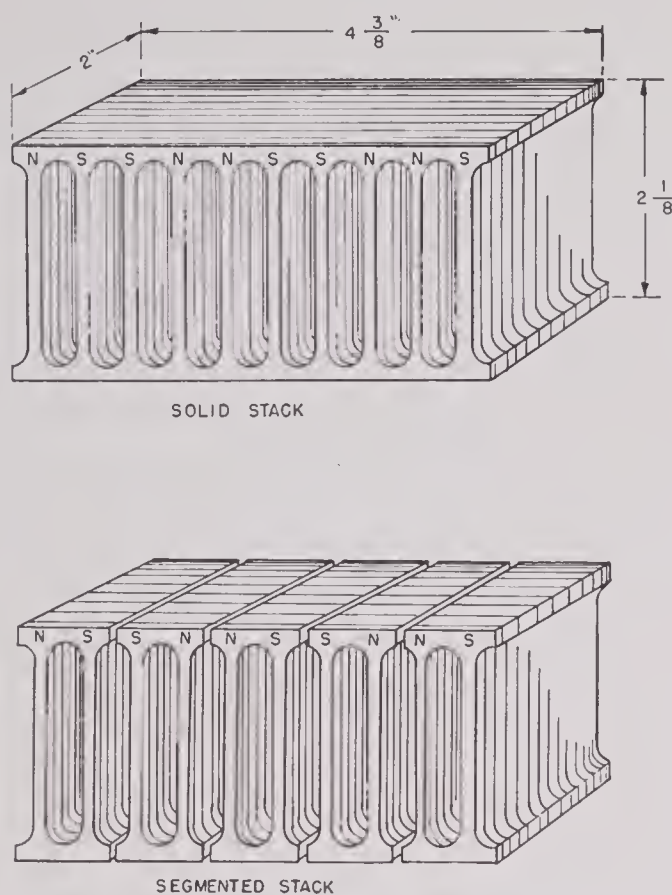


FIGURE 35. Ladderphone stacks for measurement on mechanical coupling.

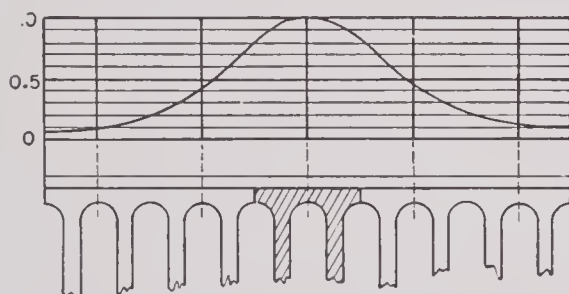


FIGURE 36. Possible distribution of particle velocity along the face of the solid ladderphone stack, center section driven.

brought out through the cable from each of the windings. The direction of the windings was such as to make the magnetic polarities of the bars N-S, S-N, N-S, etc., as shown in Figure 35. Each of the transducer stack assemblies was Cycle-Welded to a ρ c rubber face and each was housed in a watertight rectangular box. Every precaution was taken to isolate mechanically the laminated stack structures from the housings so that there would be no spurious coupling effects.

Electric and acoustic measurements were made to estimate the degree of coupling between the sections

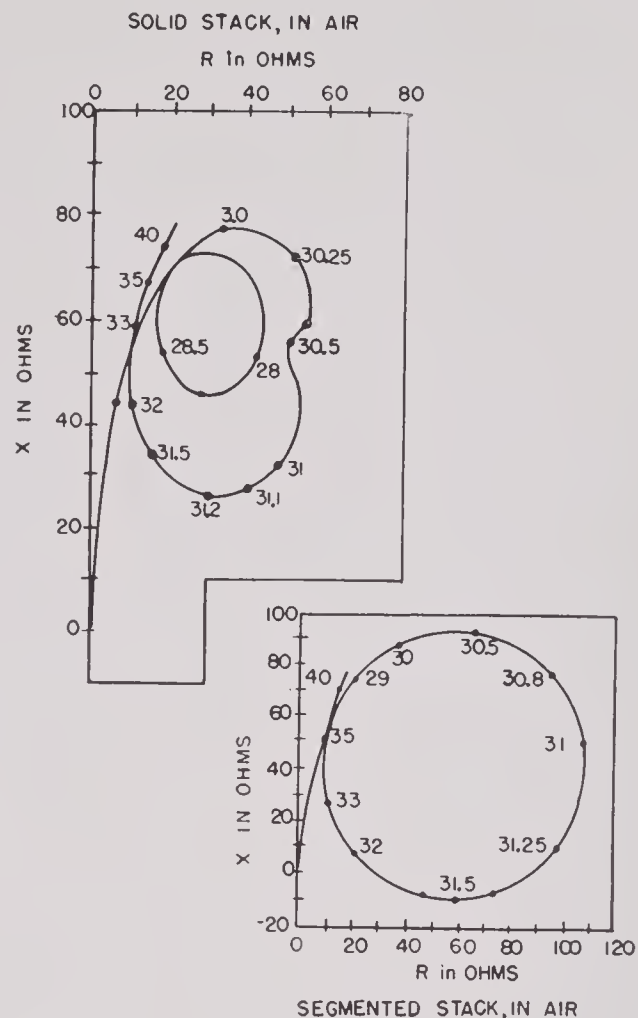


FIGURE 37. Impedance curves for solid and segmented ladderphone transducers in air, center section driven.

within each transducer. The results of the impedance vs frequency measurements indicated that when all sections were driven together in phase both transducers performed alike. However, when only the center section was driven, the effects of mechanical coupling were very obvious in the unsegmented stack, whereas they were absent in the segmented stack. An analysis of the acoustic pattern of the unsegmented stack transducer showed that if the distribution of velocity along the face was gaussian when only the center section was driven, the shape of the gaussian distribution curve would be about as shown in Figure 36. The effect of the mechanical coupling of the center section to the remainder of the unsegmented stack was also shown clearly by the secondary resonances which were induced. This effect is shown in Figure 37, where the impedance circles of the center sections of the unsegmented and segmented transducers are compared.

To investigate further the effect of coupling be-

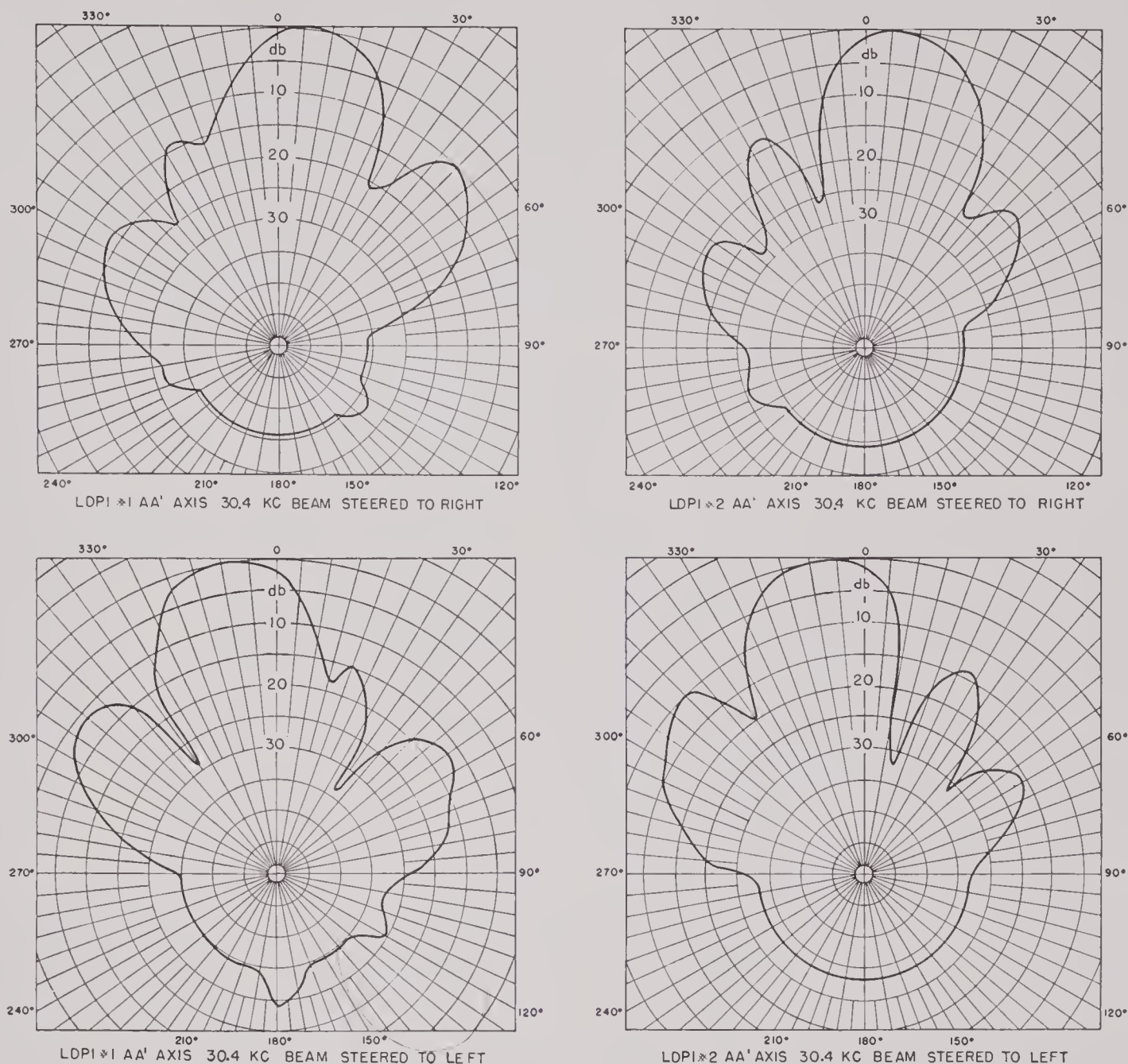


FIGURE 38. Electrically steered acoustic patterns for solid and segmented ladderphone transducers.

tween the segments, an electric phase-delay line was constructed and connected to the windings of the segments so that a phase delay of about 40 degrees was introduced in the electric signal between successive segments. The phase-delay line used was designed to steer the acoustic beam to the left or to the right by 10 degrees, depending on which end of the line was connected to the source of the signal. Experimental results are shown in Figure 38. They indicate that the acoustic patterns of each transducer can be steered about equally well by the electric phase-delay network. The only significant difference between the patterns of the two transducers is that

the null positions caused by cancellation of the signals from the different sections are more pronounced for the segmented stack. This was to be expected because each of the small faces of the segments of the segmented stacks moved as a unit whereas there was probably a smooth change of phase of the particle velocity from one end to the other of the face of the unsegmented stack. The principal conclusion drawn from the results of these tests was that the mechanical, magnetic, and electric coupling between neighboring pairs of legs of the unsegmented type of *ladderphone* is sufficiently low to make its use feasible in a multielement sonar transducer.

CONFIDENTIAL

7.2.4 Double or Multiple Bars with Symmetrical Closed Ends and a Diaphragm

EXPERIMENTAL MODELS MADE BY BELL TELEPHONE LABORATORIES

Several small test models of this type were made by BTL.² Their general characteristics are listed in Table 2 and a photograph of Model CI-50 is shown in

a stiff diaphragm with a resulting increase in the face mass and the radiation resistance.

Model IJ-10 is shown in Figure 42. Model IJ-20 was the same except that the diaphragm was made of Lucite instead of polystyrene. The stacks in each of these model transducers were built up of nickel laminations 0.002 in. thick. The frequency response of Model IJ-10, plotted as efficiency (in decibels) vs frequency, is shown in Figure 43. The frequency response of Model CI-65 is also shown in the same

TABLE 2. Characteristics of BTL laminated block models with diaphragms.

Model	Diaphragm material	Block elements				Freq. (kc)	Band width (kc)	Efficiency (db from ideal)
		No.	Type*	Material	Anneal (degrees C)			
CI-50	Rubber	4	A	Nickel	800	22.0	3.0	- 3.9
CI-60	Lucite	4	A	Nickel	800	21.0	5.5	- 7.9
CI-61	Polystyrene	4	A	Nickel	800	23.0	3.0	- 8.4
CI-63	Lucite	4	A	2V-Permendur	550	25.5	5.4	- 5.1
CI-64	Bakelite	4	A	Nickel	800	21.0	3.7	- 3.1
CI-65	Lucite	6	B	Nickel	750†	21.5	6.5	- 6.3
IJ-10	Polystyrene	12	C	Nickel	800	35.0	6.0	- 8.1
IJ-20	Lucite	12	C	Nickel	750†	38.0	9.4	- 11.0

* Type A: Laminations $1\frac{1}{4} \times 3\frac{1}{2}$ in. with window $\frac{1}{2} \times 2$ in.; laminations stacked $\frac{7}{8}$ in. high.

Type B: Laminations $1\frac{1}{4} \times 3\frac{1}{2}$ in. with window $\frac{1}{2} \times 2$ in.; laminations stacked $\frac{1}{2}$ in. high.

Type C: Leg section $\frac{1}{4} \times \frac{1}{4}$ in.; end section $1 \times \frac{1}{4}$ in.

† Air anneal; thin cement bonding.

Figure 39. The four stack elements were cemented to a rubber diaphragm $\frac{1}{2}$ in. thick and the stacks were imbedded in it to a depth of $\frac{3}{8}$ in. Models CI-61 and CI-64 were similar to Model CI-60 except for the diaphragm material, which was polystyrene in Model CI-61 and clear bakelite in Model CI-64. Model CI-63 was the same as Model CI-60 except that the blocks were built up of laminations of 2V-Permendur 0.006 in. thick and annealed at 550 C for operation on magnetic remanence without polarizing current.

Model CI-65, shown in Figure 40, had six nickel stack elements, each $\frac{1}{2}$ in. thick, but otherwise the dimensions were the same as the stacks used in the other models. The laminations were insulated with a thin layer of nickel oxide produced by annealing the laminations in an air atmosphere at 750 C. They were consolidated with an unusually thin layer (0.0001 in.) of bakelite cement. The spacing between the stacks was larger than on the other models. The frequency response plotted as efficiency (in db) vs frequency is shown in Figure 41. It has lower peak efficiency and lower frequency of resonance but greater band width than Model CI-50. This result was to be expected if the Lucite diaphragm acted as

figure for comparison. The frequency response of Model IJ-20 was similar to that of Model IJ-10 but had a slightly lower peak frequency. These models were designed on the assumption that the dominant mode would be that in which the diaphragm would be driven as a piston, acting as a substantial mass load on the lower end of the laminated stacks. This mode of vibration is present (21 kc) but the mode actually dominant is that at about 34 kc, which is near the natural frequency of the free laminated stack.

Some measurements were made of the variation of efficiency with input power for the Model CI-60 test transducer. Results are shown in Figure 44, where the sound pressure for five different frequencies near resonance is plotted against the electric input power. In this figure the origin of the decibel ordinate scale is arbitrary. The curves indicate that the response is nearly linear for an input of 10 watts or less. For greater inputs the response falls off from linearity. At a 150-watt input the response is about 4 db below the value corresponding to linearity. These results indicate that a full-sized QC-like transducer made up of 40 such stacks should be linear up to a

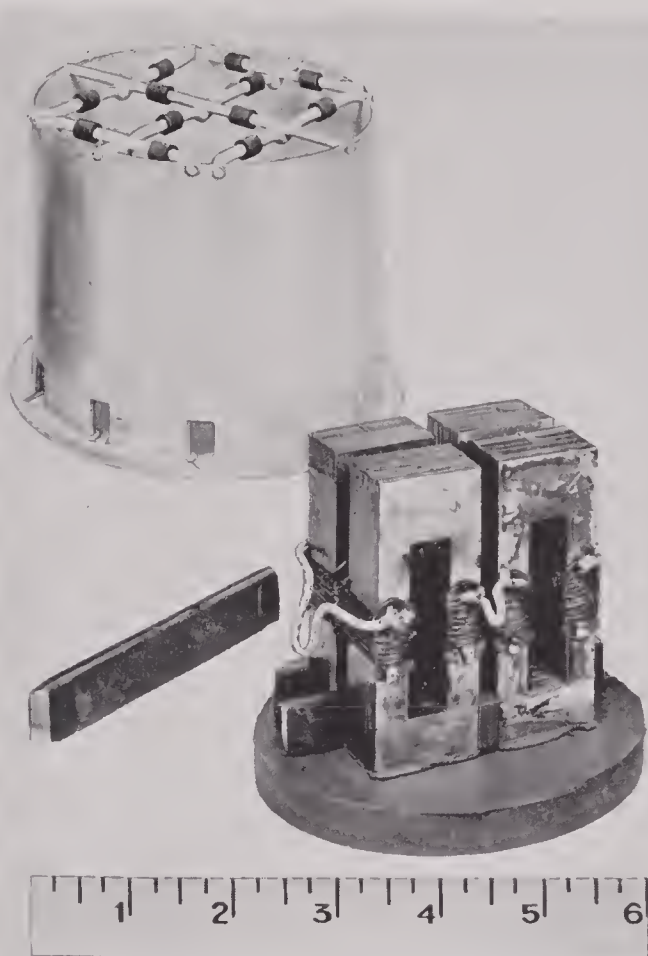


FIGURE 39. Working parts of BTL's Model CI-50 test transducer.

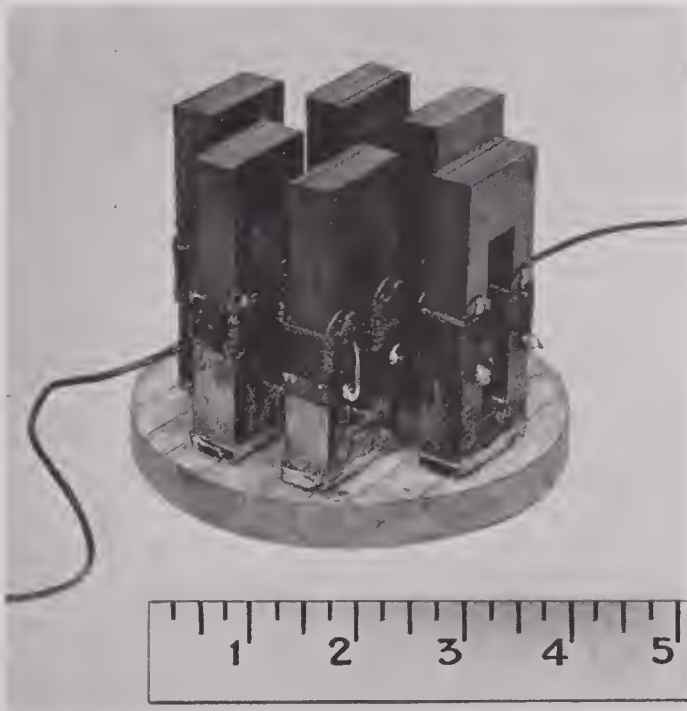


FIGURE 40. Active parts of BTL's Model CI-65 test transducer.

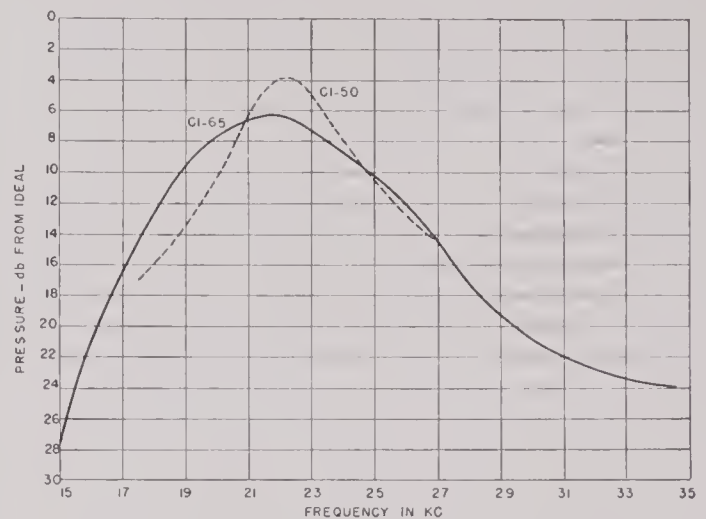


FIGURE 41. Receiving responses of BTL's test transducers, Models CI-50 and CI-65.

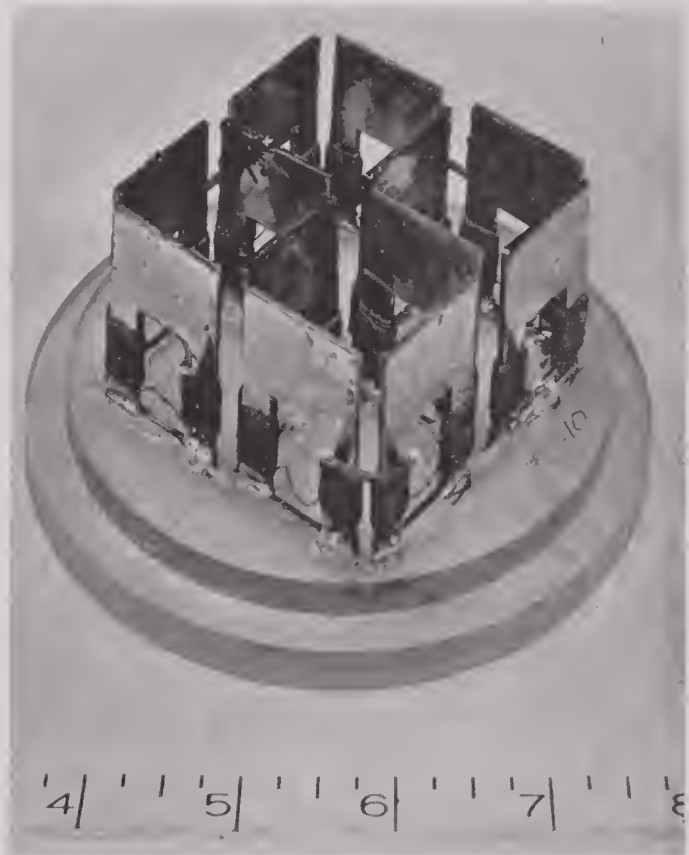


FIGURE 42. Active parts of BTL's Model IJ-10 test transducer.

400-watt input and should be only 4 db below linearity for an input power of 6 kw. Thus if the CI-100 transducer (see Section 7.2.3) were driven with 6-kw input it should produce about 1 kw of acoustic power.

Similar efficiency vs frequency measurements were made on the Model CI-63 transducer (2V-Permendur

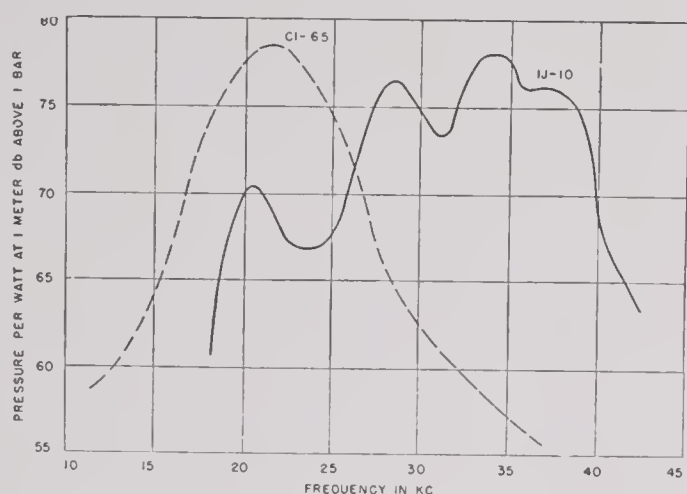


FIGURE 43. Receiving responses of BTL's test transducers, Models IJ-10 and CI-65.

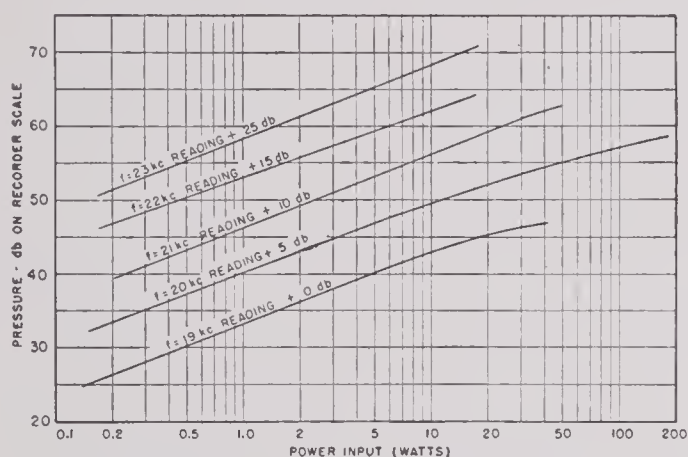


FIGURE 44. Sound pressure vs electric power input for BTL's Model CI-60 single-stack element.

stack operating on magnetic remanence). There was no apparent demagnetization for power inputs up to 25 watts per stack element because the response at the lower input levels could be repeated after the higher level tests were performed. Tests made at input levels greater than 25 watts per stack, using polarizing current to maintain the magnetization, indicated a decrease in efficiency similar to that observed for Model CI-60.

7.2.5 Double or Multiple Bars with Unsymmetrical Closed Ends

ASYMMETRIC STACK TRANSDUCERS, 9×9 IN.

Two transducers of the asymmetric laminated type with active faces 9×9 in. were made at HUSL. The laminations used in Model 1 and Model 2 units are

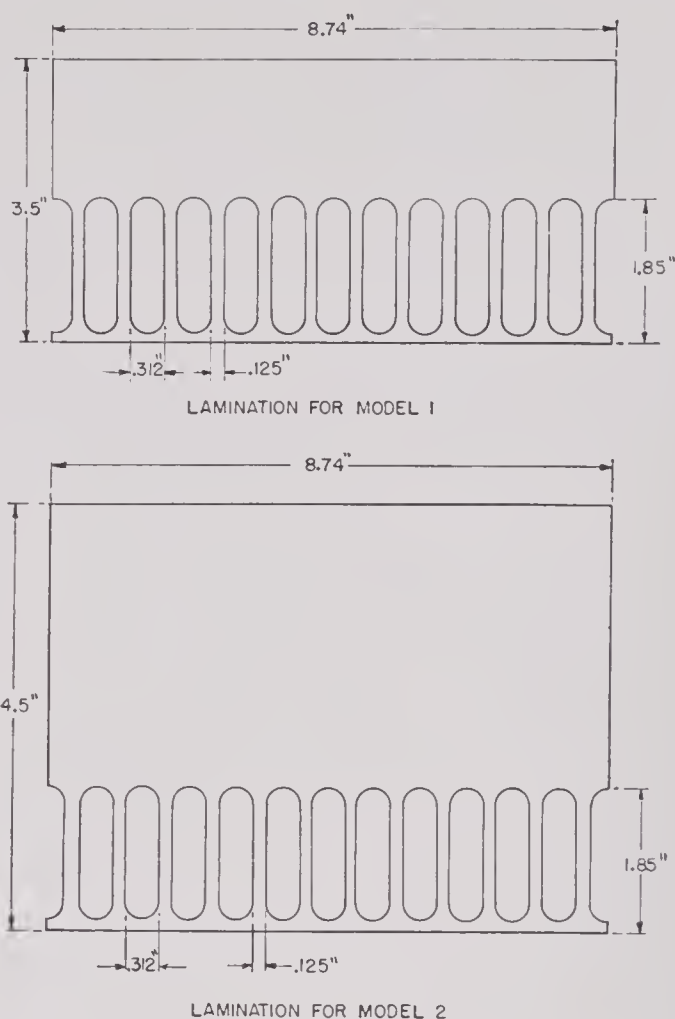


FIGURE 45. Laminations of Models 1 and 2, 9×9 -in. asymmetrical stack transducers.

shown in Figure 45. These transducers were originally designed for use with an early experimental sonar that proved unsatisfactory and consequently was never adopted or put into service use. However, a laboratory version of the Model 1 transducer was used as an experimental unit for transducer development. One of the goals of this development was to produce a magnetostrictive transducer that would be an improvement over the conventional tube-and-plate type QC transducer. The Model 2 unit was also used as an experimental transducer of lower frequency than the Model 1.

Model 1 Unit. Laminations for the Model 1 unit were punched from 0.007-in. nickel, annealed in a neutral atmosphere at 1000 C, and consolidated with General Electric No. 7000 resin to form a stack $8\frac{3}{4}$ in. high. Bakelite end plates $\frac{1}{8}$ in. thick and the same shape as the laminations were cemented to each end of the stack to serve as winding caps and mounting plates.

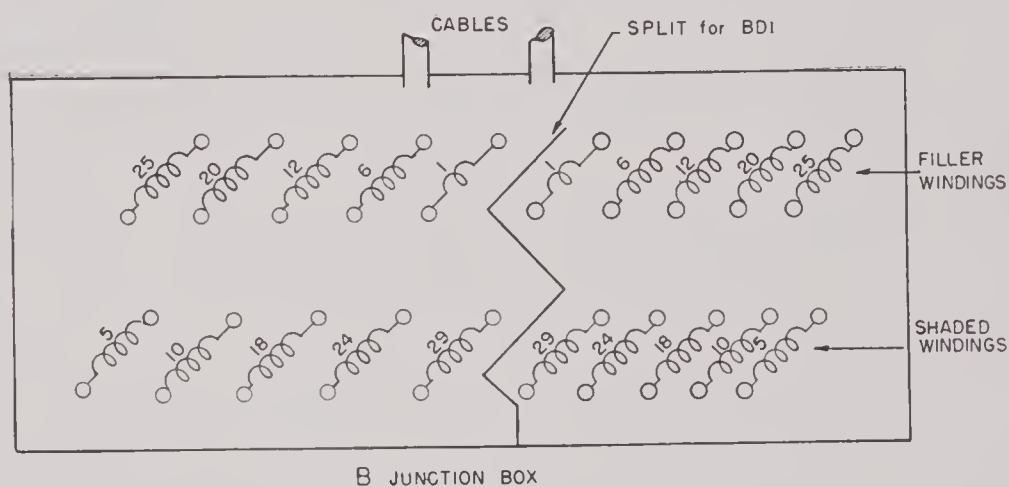
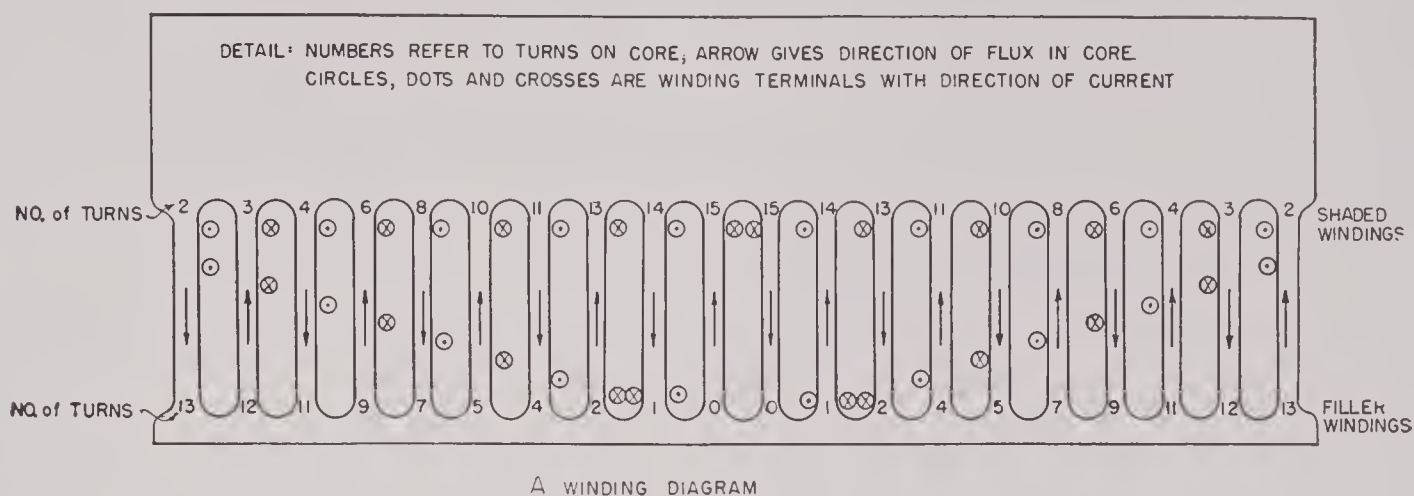


FIGURE 46. Details of windings on 9 x 9-in. stack and connections in terminal box.

The legs of the Model 1 transducer were wound with No. 16 stranded wire with Gencaseal insulation. It was necessary that this insulation be watertight because the entire stack and winding assembly was to be submerged directly in sea water. The windings were divided primarily into left and right halves for BDI applications. Each of the half windings was divided into so-called shaded and filler windings. The shaded windings were used for both alternating current and direct current, but the filler windings were used for direct current only. Each leg of the stack was wound with a total of 15 turns of wire. Some of the turns belonged to the shaded winding and the remainder to the filler winding. The number of turns belonging to the shaded winding was greatest for the legs at the center of the stack and least for the legs near the edges of the stack. This shading of the windings in which the alternating current passed was to reduce the heights of the minor lobes of the acoustic

pattern taken in the plane of the laminations. The direct current for polarizing the stack passed through both the shaded and filler windings so that all legs were equally polarized. Figure 46A shows a lamination on which are indicated the direction of the polarizing flux, direction of current flow in the windings, and the number of turns on each leg devoted to the shaded and filler windings. Figure 46B diagrams the layout of terminals in the terminal box. The coils shown between pairs of terminals represent the windings on the laminated stack that are connected to those terminals. Each pair of terminals was connected to the lead wires from the coils of either the shaded or filler winding on two adjacent pairs of legs of the stack. The number of turns of wire between each pair of terminals is indicated.

A rough diagram of the assembled transducer is shown in Figure 47. A rectangular metal frame supported the laminated stack and terminal box. The

laminated stack assembly rested on rubber pads and the terminal box was fastened in the upper part. The side of the terminal box which faced in the same direction as the active face of the stack contained 40 water seals through which the wires of the windings entered. The top side of the terminal box contained two water seals through which the two main cables entered. The side of the terminal box opposite the active face was removable so that the necessary connections could be made within the terminal box after all wires and cables were sealed into place.

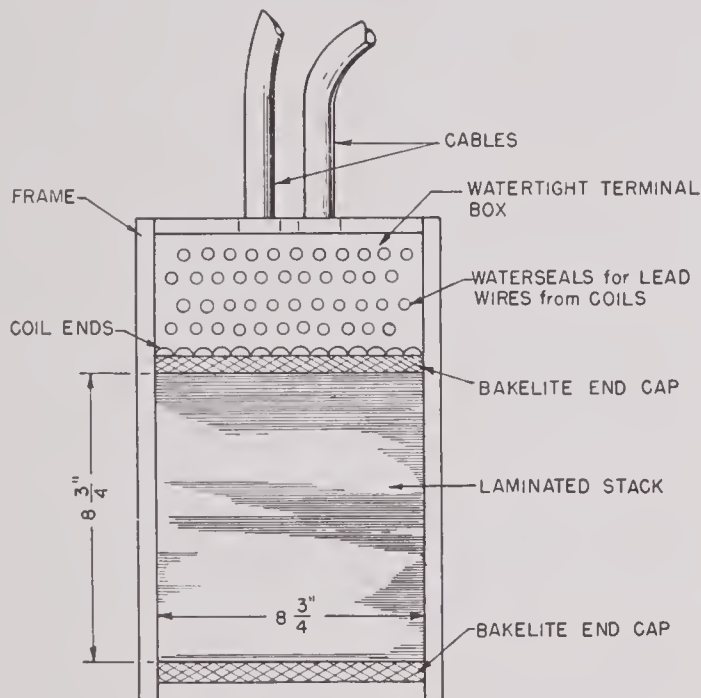


FIGURE 47. Sketch of front view of Model 1, 9 x 9-in. asymmetrical stack transducer.

Many experiments were performed with this transducer, some of which will be described to illustrate several important effects of design and construction of laminated stack transducers.

The effect of polarizing current on the open-circuit receiving sensitivity is shown in Figure 48. The magnetizing field in the legs was about 5.7 oersteds per ampere. Full receiving sensitivity was obtained for a polarizing current of 4 or more amperes, which corresponds to 15 or more oersteds of magnetizing field. The sensitivity at magnetic remanence was about 5 db below the maximum, but the remanence flux density was easily reduced by jarring the stack or by driving it lightly with alternating current. This was shown by the fact that at the start of the polarizing test the sensitivity was 20 db below maximum although the unit had been polarized during a previous test.

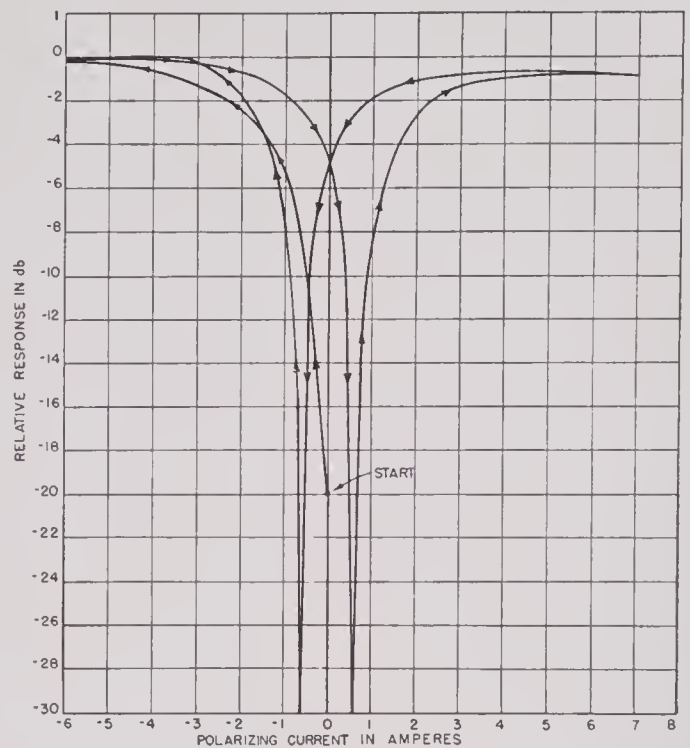


FIGURE 48. Receiving response vs polarizing current, Model 1, 9 x 9-in. asymmetrical stack transducer.

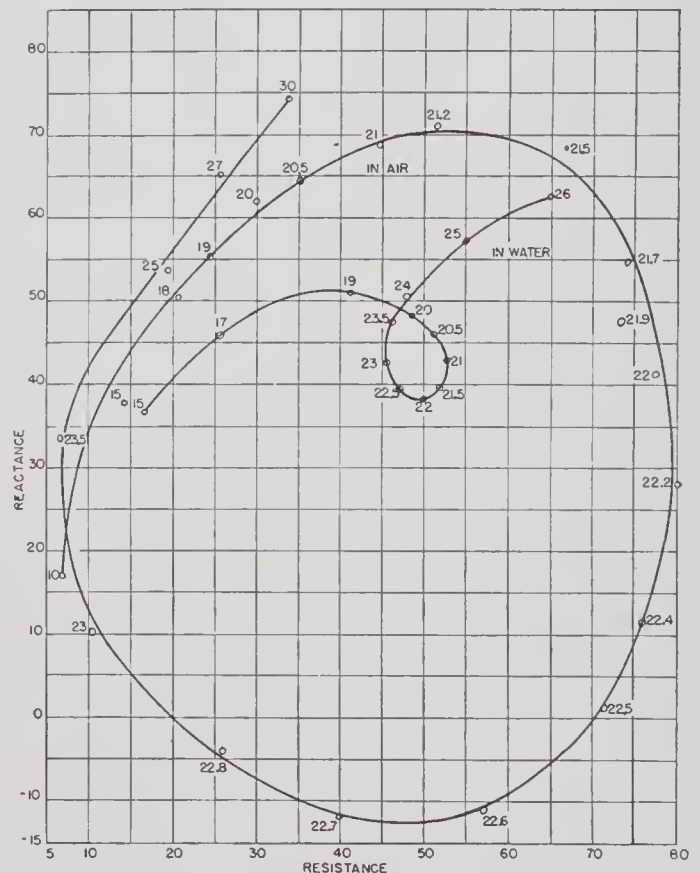


FIGURE 49. Impedance in air and in water, Model 1, 9 x 9-in. asymmetrical stack transducer.

The first acoustic measurements were made with the windings and both front and back faces exposed to the water. The impedance curves of Figure 49 reveal an important fact: Under these conditions, at frequencies away from resonance, the impedances (clamped core) when the transducer is in water are markedly different from those when the transducer is in air. This effect is attributed to the distributed capacity of the windings to water, which effects partial electric tuning of the circuit and thus renders detailed interpretation of impedance data impossible.

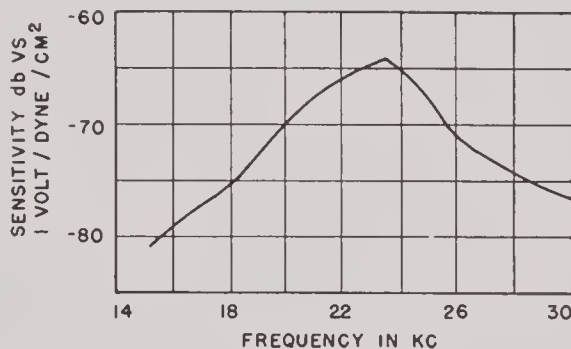


FIGURE 50. Model 1, 9 x 9-in. transducer; open-circuit receiving response, both faces exposed to the water, and no pressure-release material in the winding slots.

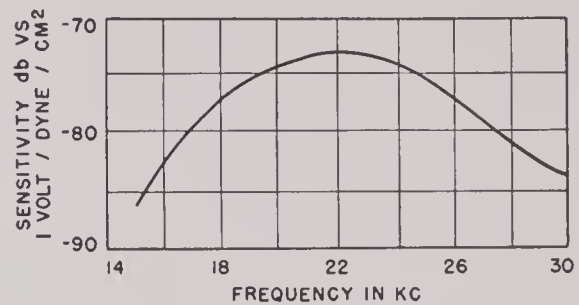


FIGURE 51. Receiving response with connections as shown in Figure 52.

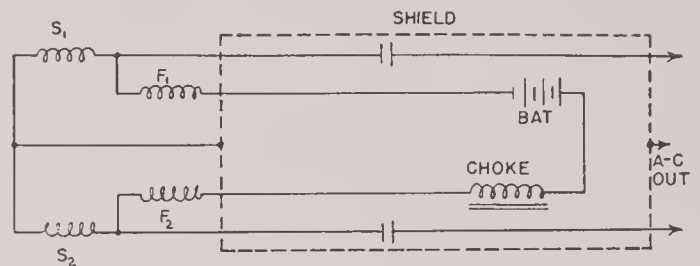


FIGURE 52. Connection for direct current in all windings and alternating current in shaded windings only, Model 1, 9 x 9-in.

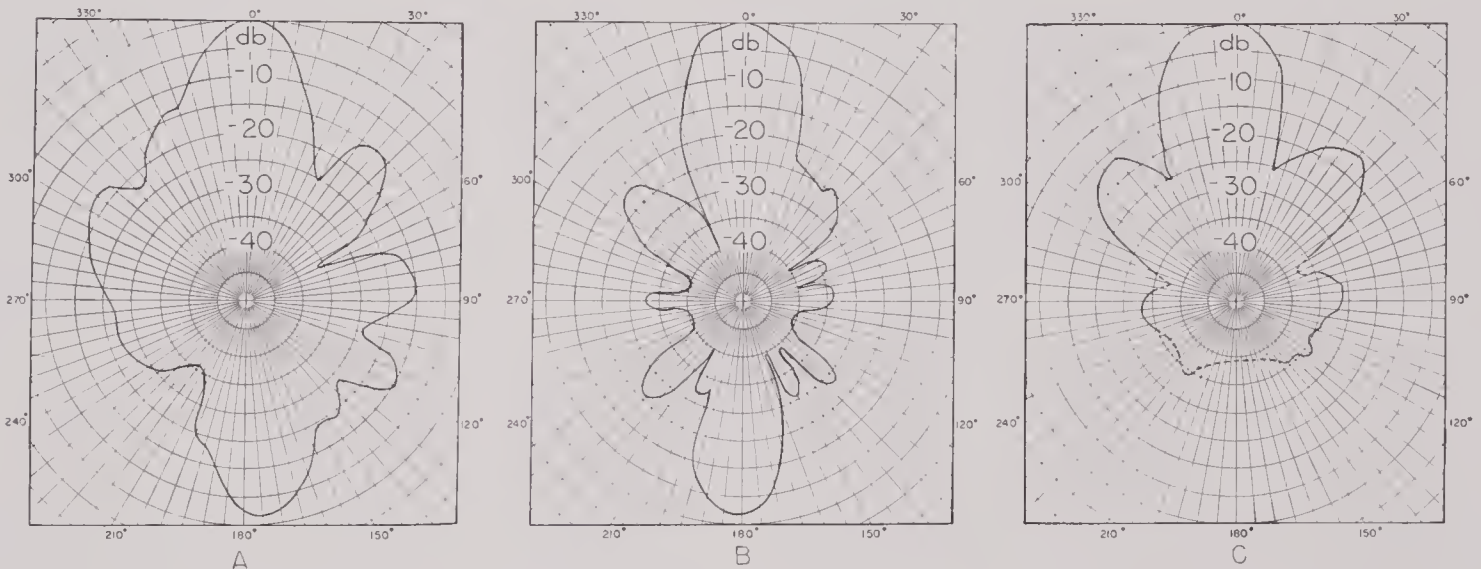


FIGURE 53. A. Pattern at resonance, same conditions as in Figure 50 of Model 1, 9 x 9-in. transducer. B. Horizontal pattern taken under the conditions of Figure 52. C. Horizontal pattern at frequency of resonance of Model 1, 9 x 9-in. asymmetric stack with corprene on back face and signal from shaded winding.

The open-circuit sensitivities of the transducer with the halves connected in series aiding and with windings and both faces exposed to the water are shown in Figure 50, where both shaded and filler windings were in the a-c and polarizing circuits. In Figure 51 the polarizing current passed through all the windings, but the a-c signal was picked up on the shaded windings only. Figure 52 shows wiring con-

nections for the shaded windings. In the first case, the Q was 6.5, only about half what it should have been if damping had been due only to radiation resistance from the front face. The still lower Q of about 3 in the second case indicates an unusually high degree of damping due to the "pumping" action in the winding slots and the radiation from the back face.

In Figure 53A and B the radiation patterns at

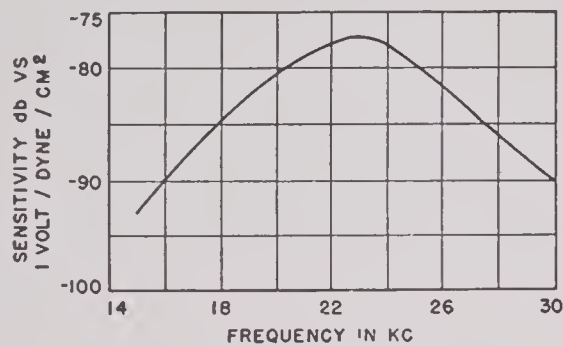


FIGURE 54. Receiving response of 9 x 9-in. asymmetrical stack after grinding active face.

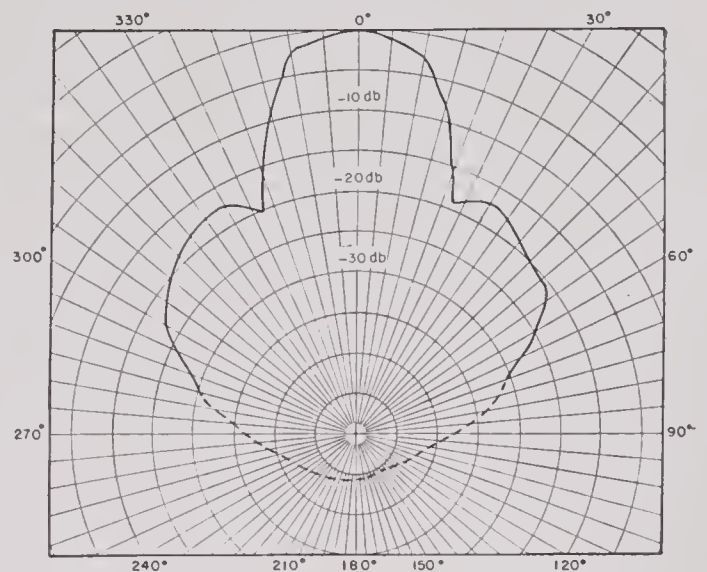


FIGURE 55. Pattern at 23 KC of 9 x 9-in. asymmetrical stack after grinding active face.

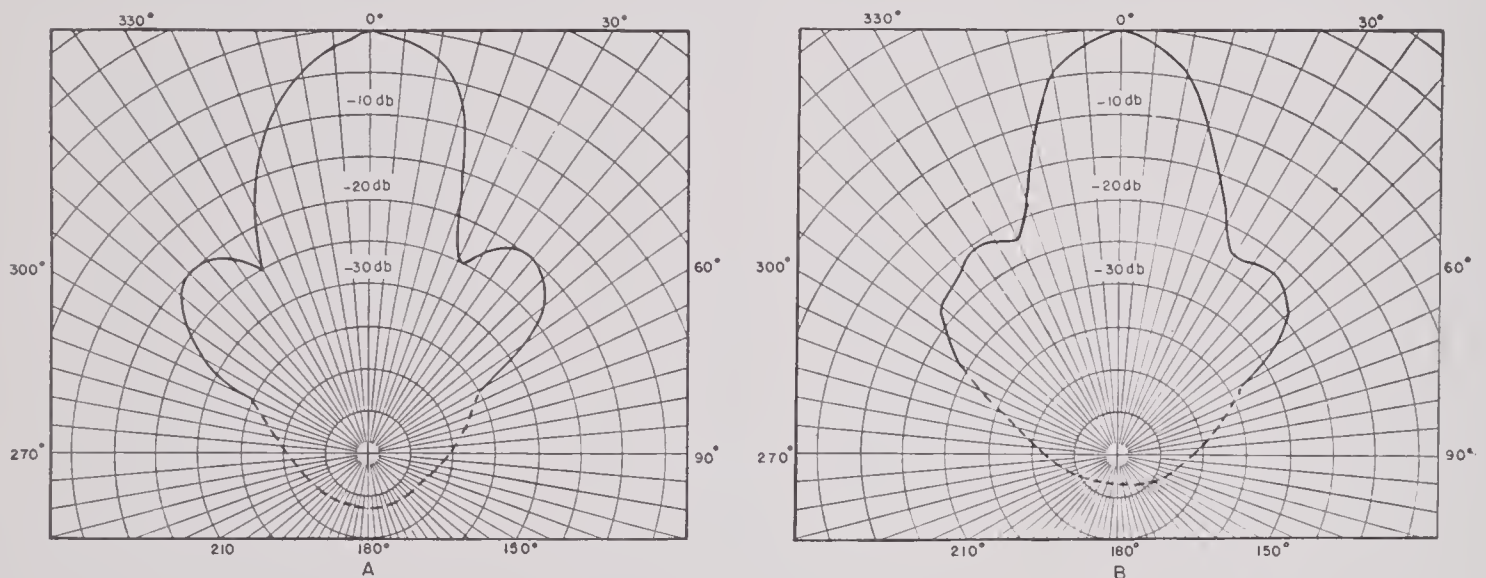


FIGURE 56. A. Pattern at 23 KC of 9 x 9-in. asymmetrical stack with rubber face. B. The same as A but with transducer completely enclosed.

peak frequency are shown for the two conditions just mentioned. The effect of a layer of corprene on the back face in reducing back radiation is shown in Figure 53C. Some reduction of the side lobes produced by shading is apparent, though not so much as would be expected from theory. This and the absence of widening of the main lobe, which would be anticipated on theoretical grounds, could be caused by coupling between the center and the edges of the stack through the stiffness of the back portion.

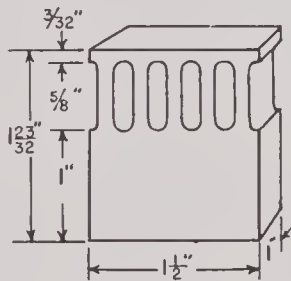
The sharp, exposed edges of the laminations in the foregoing experiments facilitated the collection of bubbles on the face of the transducer, so that it was impossible to determine whether the radiating face

was uniformly wet. Grinding the transducer face smooth proved a partial remedy, and as a result the behavior of the transducer was much less erratic and more in accord with theory. Figure 54 shows the receiving response, after grinding, with the two halves in parallel and the signal only on shaded windings. The increase in sensitivity is seen by comparison with Figure 51. In the latter, the halves were connected in series, and when the same performance is assumed for the two cases the sensitivity in Figure 51 should be 6 db higher than in Figure 54. Actually, it was only 4 db higher, showing a 2-db improvement as a result of the grinding. The improvement in pattern is shown in Figure 55.

Still further improvement in patterns is shown in Figure 56. The pattern in A was obtained after a $\frac{1}{8}$ -in. sheet of rubber was cemented closely to the ground face of the transducer but with the windings still exposed to the water. The whole transducer was then enclosed in a watertight rubber box with the edges cemented to the rubber face so that the windings were no longer in contact with the water. In this condition the radiation pattern was as shown in Figure 56B, in which reduction of the height of the side lobes is to be noted. The peak open-circuit sensitivity was increased, with an increase in Q from 5 to 8.7. Thus enclosed, the clamped-core impedance proved to be the same in air as in water.



A SAMPLE OF PRINTER'S INK IMPRESSION MADE ON NICKEL SHEET PREPARATORY TO CUTTING OUT THE LAMINATIONS BY ELECTROLYTIC ETCHING.



B STACK MADE FROM THE ELECTROLYTIC ETCHED LAMINATIONS.

FIGURE 57. Laminated stack used in small experimental 51-kc transducer.

Experience with this transducer indicated the necessity for keeping the windings of laminated stacks free from contact with the water and thus influenced the construction of all subsequent transducers.

Model 2 Unit. The laminations of Model 2, 9×9 -in. stack transducer were punched from pure nickel stock 0.005 in. thick and $4\frac{1}{2}$ in. wide. The face and leg structures were the same as in the Model 1 unit, so that the solid backing section of Model 2 was 1 in. deeper than that of Model 1. The laminations were annealed at 1000 C in an atmosphere of hydrogen. They were consolidated into a solid block with

General Electric No. 7000 resin. The stack was mounted in a rectangular frame in much the same way as in Model 1 and the windings were also made in the same way.

Results of tests were not widely different from those on Model 1. They showed that the mechanical coupling caused by the transverse stiffness of the thick backing section nearly eliminated the effect of the shaded windings and also introduced an additional mode of vibration, which had a frequency near that of the principal mode. This complication of the modes of vibration was probably enhanced by the node lying within the solid backing-block section which coupled the transverse motion with the normal longitudinal motion by the Poisson effect. These difficulties indicated that it is poor design practice to make either the face plate or the backing plate so thick that it includes the node of the principal mode of vibration. No further experiments were made with the Model 2 transducer.

51-KC STACK OF ELECTROLYTICALLY CUT LAMINATIONS

The production of small detailed laminations from magnetostrictive sheet material 0.003 in. or less in thickness by use of punch-and-die techniques is very difficult because punches and dies used on such material must fit with unusual precision. An alternative to this method is electrolytic etching. Experiments in producing thin laminations by this method were tried, since it had been used with considerable success in cutting templates from steel sheets for use in marking out airplane parts.

An accurate, enlarged drawing of the lamination boundaries is made with a wide black line. From the drawing a photograph is made and reduced to the exact size of the finished lamination. This is used in etching a copper printing block with the boundary lines of the lamination etched in such a way that when the block is inked and set in contact with the nickel sheet it makes an ink print of the exact lamination surrounded by a narrow band of unprinted area (Figure 57A). While the ink is still damp, powdered dried resin called dragon's blood is sifted on and sticks to the printed portions of the sheet. This is then baked to form an impervious, lacquer-like covering on the inked portions of the sheet. The opposite side of the sheet is also coated with a layer of impervious lacquer. The nickel sheet is then suspended in a salt solution and serves as the anode, while a

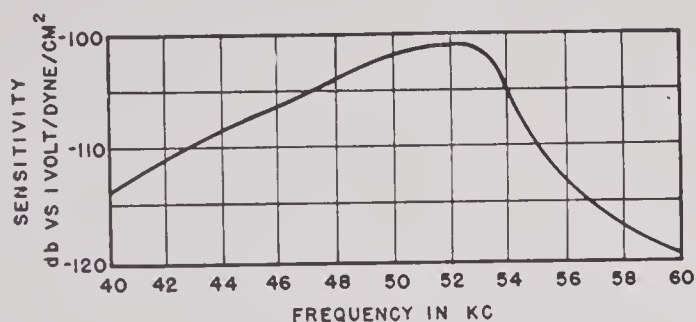


FIGURE 58. Receiving response of 51-kc transducer made from electrolytically etched laminations.

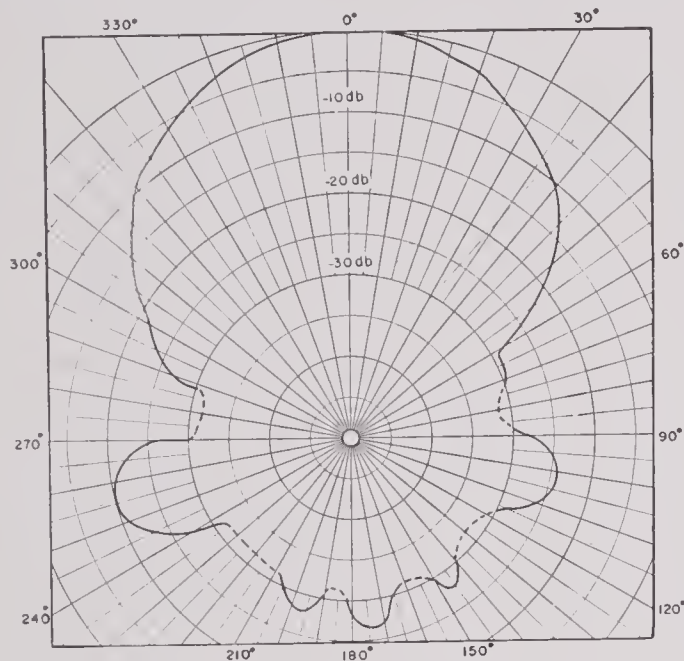


FIGURE 59. Pattern at 51-kc of transducer made from electrolytically etched laminations.

submerged lead sheet serves as the cathode. Nascent chlorine deposited on the exposed parts of the nickel sheet rapidly etches the nickel and in a few minutes eats completely through the sheet, so that the newly formed lamination is suspended only by the layer of lacquer on the back side. The exposed edges of laminations produced in this way are surprisingly square and free of burrs. It is technically possible to set up an assembly in which this process could be made to work continuously on long lengths of thin sheet stock.

Laminations of 0.003-in. nickel were made in this way for a small 51-kc stack of the shape and dimensions shown in Figure 57B. The nickel strip was soft-annealed before the laminations were etched. The lacquer coatings were left on after etching to serve as insulating layers, and the laminations were consolidated into a solid stack with Vinylseal resin. The legs of the stack were covered with compliant layers of

air-cell neoprene before the windings were put on. The complete stack assembly was mounted in a watertight rubber box with the active face of the stack Cycle-Welded to one face of the box and the other surfaces lined with air-cell neoprene for pressure release.

The open-circuit frequency response of the unit is shown in Figure 58. The sensitivity was about -100 db vs 1 volt per bar and the Q was about 12. The acoustic pattern at 51 kc, taken in the plane of the laminations, is shown in Figure 59. Efficiency at resonance as given by acoustic measurements was 30 per cent, and as given by impedance circle measurements, 39 per cent. The performance of this unit was good enough that larger multielement transducers using similar stacks and mounting were developed. These larger transducers were known as SPEP transducers. They will be described in some detail later in this chapter.

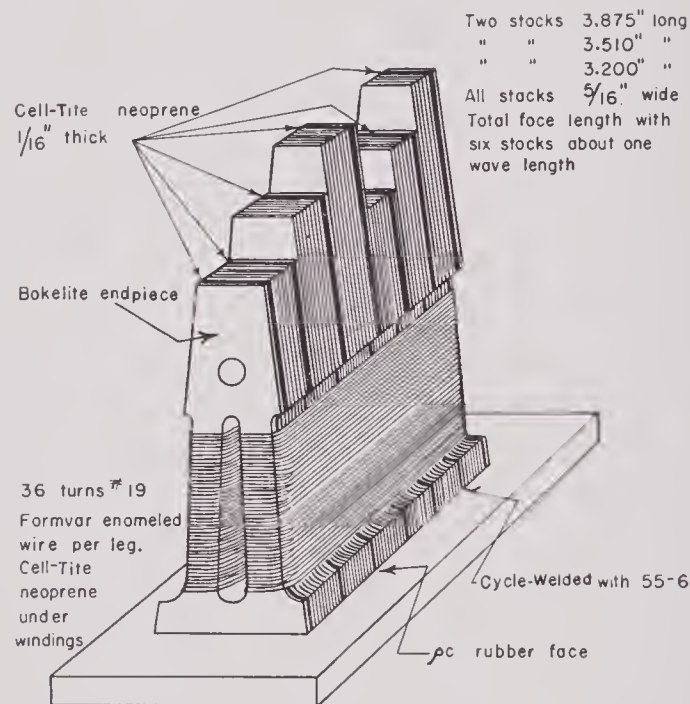


FIGURE 60. Experimental stepped-frequency transducer.

STEPPED-FREQUENCY TRANSDUCER ⁴⁶

From the earliest days of transducer design at HUSL attempts were made to get broad frequency response and small rate of change of phase shift with frequency by having the vibrating system consist of elements which have two or more natural frequencies of resonance spaced rather close together. In most cases these attempts were unsuccessful because of too close mechanical coupling between the various vibrating elements or improper coupling with the water.

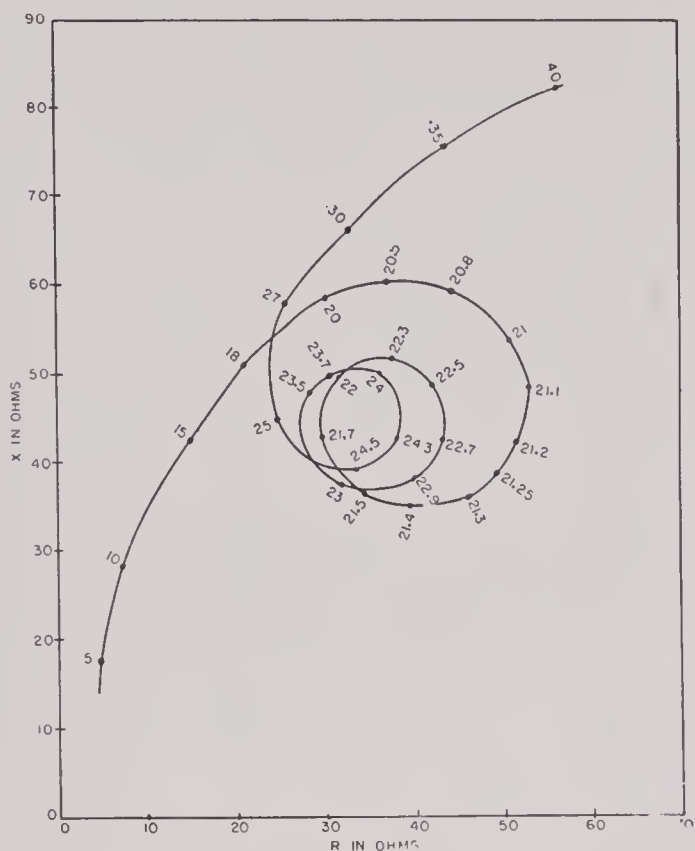


FIGURE 61. Vector impedance diagram for the stepped-frequency transducer in air.

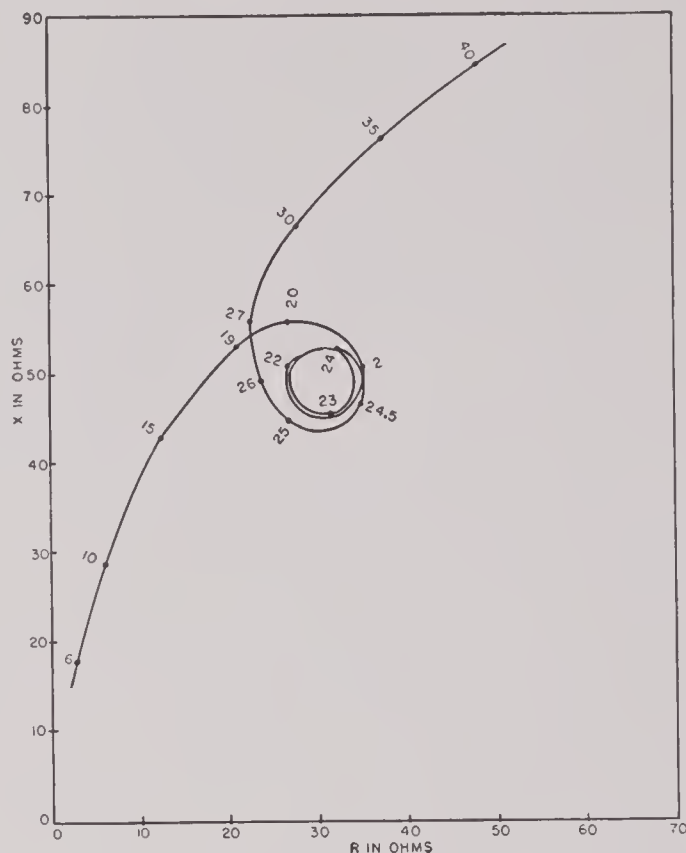


FIGURE 62. Vector impedance diagram for the stepped-frequency transducer in water.

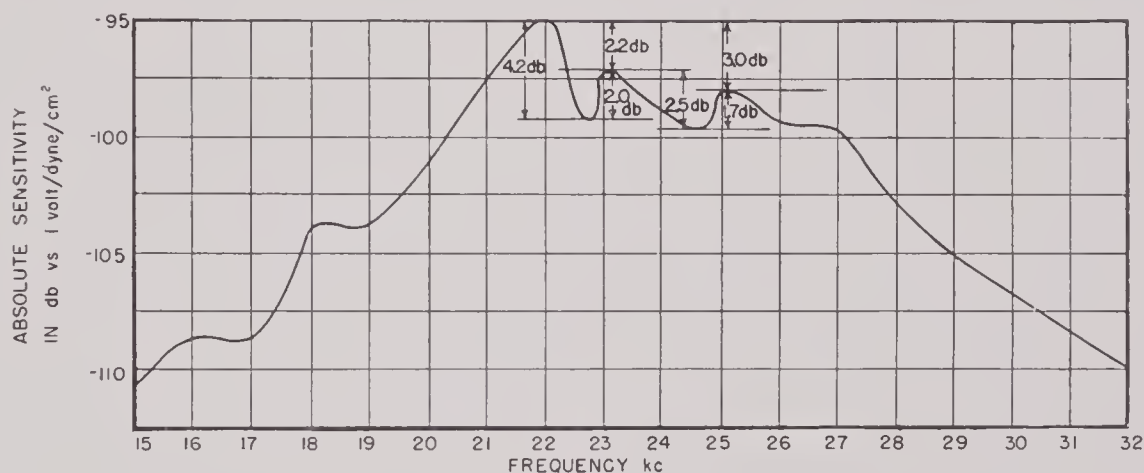


FIGURE 63. Receiving response of the stepped-frequency transducer.

In an attempt to make a transducer with broad frequency response, an experimental unit containing elements having three different natural frequencies, all linked by the same winding, was made and tested at HUSL. The essential parts of the transducer are shown in Figure 60. The assembly was mounted in a watertight metal box with the ρc rubber face in contact with the water. The individual stack elements each had faces that were a small fraction of a wave length wide (in water) and were mechanically isolated from one another by thin layers of air-cell neoprene.

The vector impedance diagram for the assembled transducer in air (unloaded) is shown in Figure 61, and that for the transducer in water is shown in Figure 62. The motional impedance circles corresponding to the three different frequencies of resonance stand out clearly in both the air and water measurements. The open-circuit frequency response of the unit is shown in Figure 63. The three resonances at 21.5 kc, 23 kc, and 25 kc are pronounced and have the general effect of holding the response to a uniform value over the frequency range from 20 kc to 27 kc.

CONFIDENTIAL

While this transducer was being given acoustic tests in water, the phase difference between the electric signal generated in the windings and the sound signal in water was measured. The results are given in Figure 64. In the general design of the transducer, the mechanical phase angle (relative to the sound signal) of one of the elements was expected to be nearly canceled by that of another of the elements,

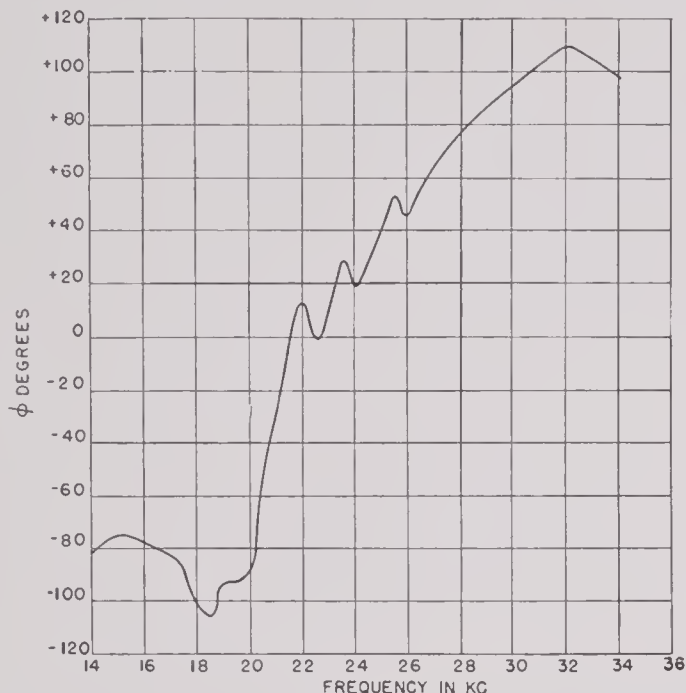


FIGURE 64. Phase difference between electric signal and acoustic signal as a function of frequency for the stepped-frequency transducer.

since one would be above its frequency of resonance while the other would be below; therefore, the mechanical phase angles of the two sections would be about equal in magnitude but opposite in direction. Figure 64 shows that this effect was nearly attained. It appears that if the stack sections that resonated at 23 kc and 25 kc had been made a little thicker in comparison with the 21.5 kc sections the desired phase behavior would have been more nearly obtained.

The acoustic measurements indicated that the efficiencies at 21.5 kc, 23 kc, and 25 kc were about 9 per cent, 6 per cent, and 5 per cent, respectively. These efficiencies were approximately one-third of those for similar transducers made of single-frequency stacks. This lowered efficiency was primarily due to the fact that only about one-third of the total stack contributed to the generated signal at any one frequency, while the whole structure contributed to the core losses. This result is in agreement with the general

principle that any broadening of the band width of frequency response can be obtained only at the expense of the efficiency. Thus in practical applications the best compromise between the band width of response and the efficiency must be chosen.

DIRECT-CURRENT POLARIZED SPEP TRANSDUCER²⁹

Following the success of the small experimental 51-kc laminated stack transducer described above, a multielement, flat-faced transducer containing 32 small laminated stacks designed for about 60 kc was made. The laminations had the shape and dimensions shown in Figure 65A and were punched out of 0.005-in. nickel strip. These laminations were cleaned, annealed in air at 1000 C, and consolidated with C-3 Cycle-Weld resin to form stacks $9\frac{1}{16}$ in. high,

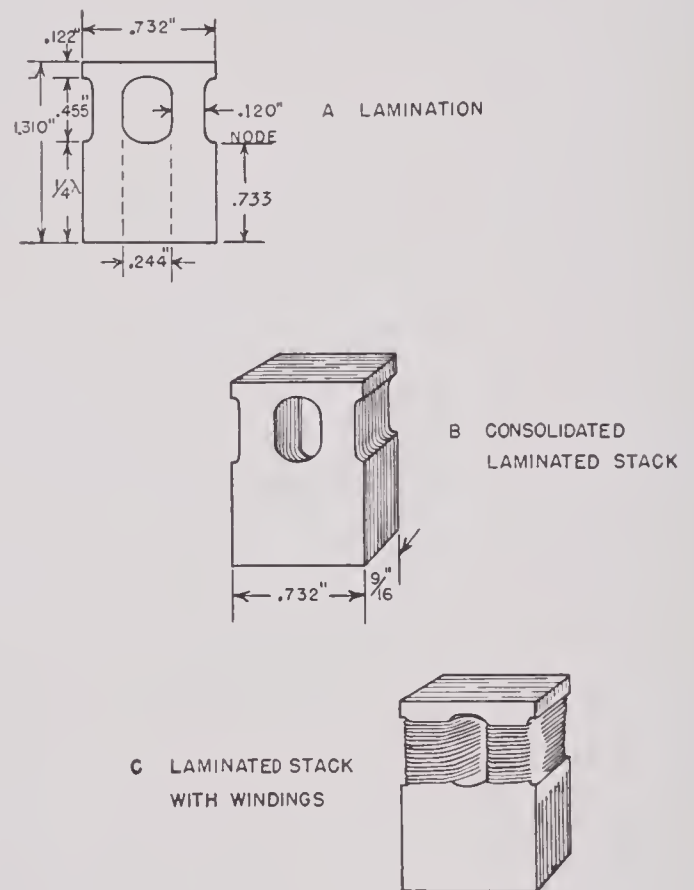


FIGURE 65. Nickel laminations and stacks of the 60-kc, d-c polarized, SPEP transducer.

as shown in Figure 65B. Windings were placed around each of the two legs with thin layers of air-cell neoprene to isolate mechanically the winding from the laminated stack. The direction of the windings was such as to make the magnetic flux go up one leg and down the other. In this way the entire magnetic circuit for both the polarizing flux and the high-fre-

quency flux lay entirely within the nickel laminations; consequently, the electromechanical coupling coefficient approached the maximum possible for nickel.

The active faces of the laminated stacks were Cycle-Welded to a flat disk-shaped *pc* rubber face 1 in. thick, as indicated in Figure 66. The array of stacks was as shown in Figure 67. The planes of the laminations in neighboring stacks were placed at right angles to each other to minimize magnetic coupling between stacks and to make the inactive space between stacks equal on all sides of the stacks. The

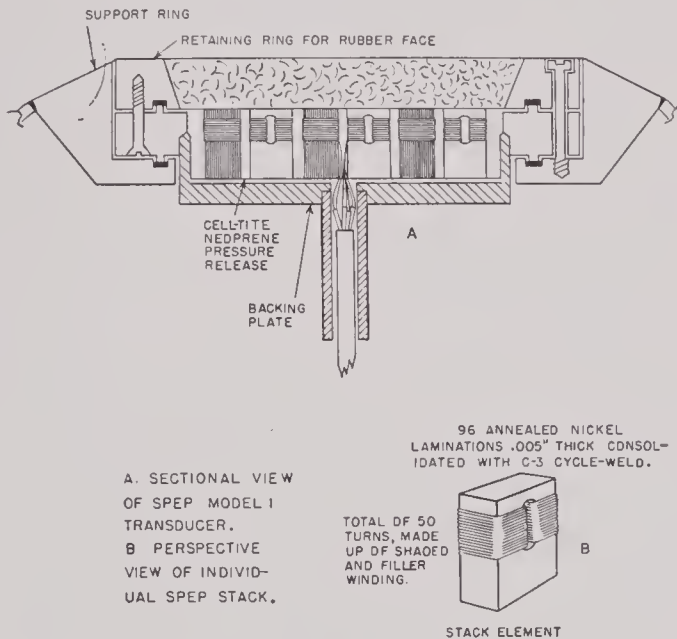


FIGURE 66. Section of Model 1 d-c polarized 60-ke SPEP transducer.

windings were divided into four quadrants corresponding to the geometrical quadrants to the transducer. To minimize the heights of the minor lobes of the transducer's acoustic pattern, the number of turns of the windings devoted to the high-frequency current in the outer stacks was fewer than for the center stacks. These windings were called the shaded windings. However, in order to produce equal polarization of all the stacks, an additional filler winding was placed on each stack to make the total number of turns the same. The polarizing current was allowed to flow in both the shaded and the filler windings. On each stack the total turns devoted to the shaded and filler windings are indicated in Figure 67 by the numbers following the *S*'s and *F*'s marked on each stack. Three wires were brought out from each quadrant, the + wire of the *S* winding, the common - of the *S* winding and + of the *F* winding, and the - of the *F* winding.

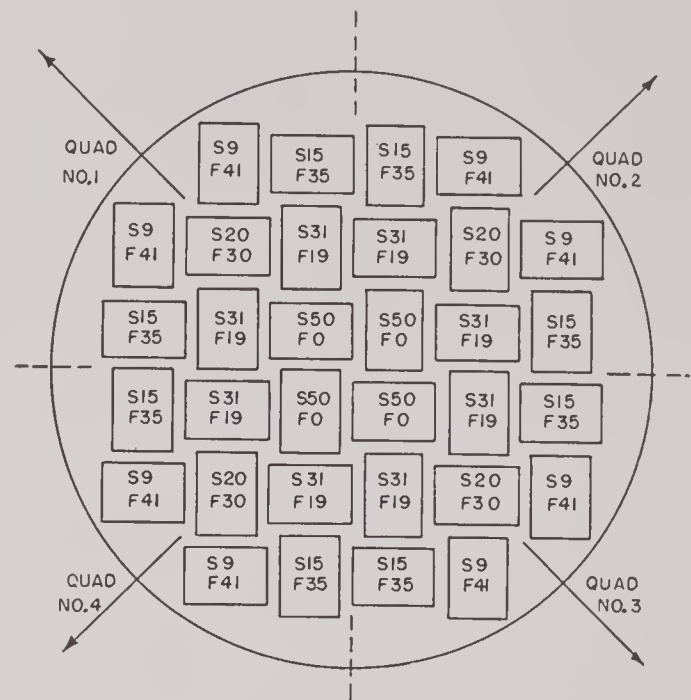


FIGURE 67. Stack arrangement viewed from the rear in SPEP Model No. 1 transducer. *S* figures are the turns of shaded winding (a-c and d-c). *F* figures give filler winding turns (d-c only).

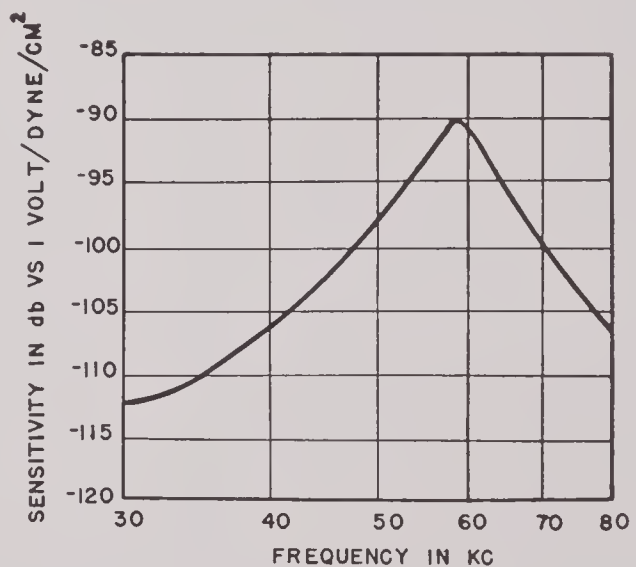


FIGURE 68. Receiving response of the Model 1, d-c polarized, 60-ke SPEP transducer, all quadrants in parallel.

The rubber face shown in Figure 66 was Cycle-Welded into the steel face ring before the laminated stacks were Cycle-Welded to the rubber face. Both these Cycle-Welding operations required the use of special jigs to hold the various parts in place during the curing process.

The back part of the hydrophone case was constructed so that it made a watertight seal against the steel face ring and also supported the back ends of the

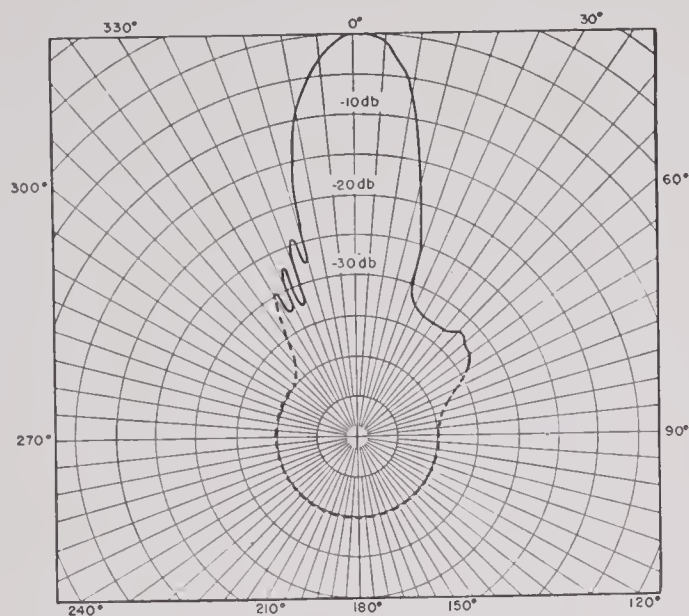


FIGURE 69. Pattern at 58.4 kc of Model 1, d-c polarized, 60-kc SPEP transducer, signal from shaded windings, axis of rotation parallel to one side of the square array.

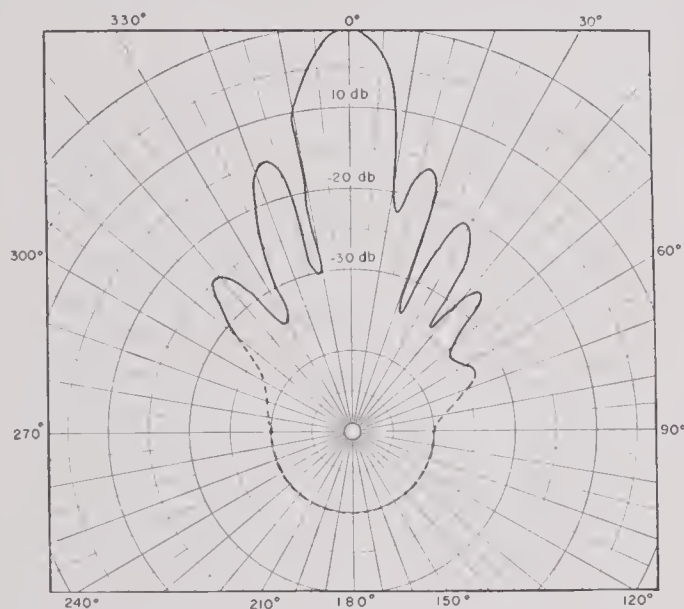


FIGURE 70. Pattern at 58.4 kc of Model 1, d-c polarized, 60-kc SPEP transducer, signal from full windings, axis of rotation parallel to one side of the square array.

laminated stacks through a thin layer of air-cell neoprene. The entire transducer was made to fit in a recess in a special hemispherical baffle of approximately 9-in. radius.

The electric and acoustic performance of this transducer was unusually good. The open-circuit frequency response for all four quadrants connected in parallel is shown in Figure 68. The Q was about 9 and the efficiency about 25 per cent. Figure 69 shows the

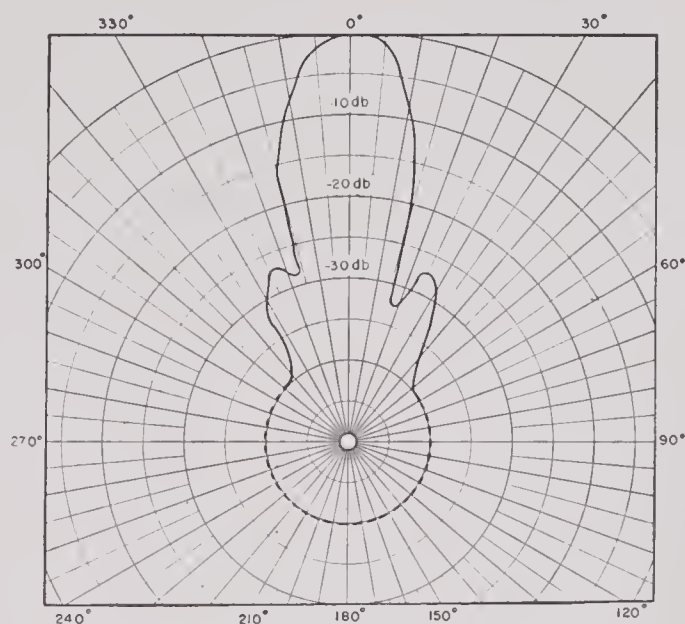


FIGURE 71. Transmitting pattern at 58.4 kc of Model 1, d-c polarized, 60-kc SPEP transducer with 40-watt input to shaded windings, axis of rotation parallel to one side of square array.



FIGURE 72. Rear view of stack assembly in SPEP Model No. 2.

pattern of the transducer as a receiver at 58.4 kc taken about an axis parallel to one side of the square array when the signal was taken from the shaded windings. When the axis of rotation was parallel to a diagonal of the square array, the side lobes were even lower than those shown in Figure 69. Figure 70 shows the pattern of the unit as a receiver at 58.4 kc taken

about an axis parallel to a side of the square array when the signal was taken from the full windings. This shows that the effect on the height of the minor lobes due to shading of the windings on the stacks is pronounced, as predicted by theory. Figure 71 shows the pattern of the unit as a projector at 58.4 kc when the input power on the shaded windings was 40 watts and the axis of rotation was parallel to one side of the square array. The measured efficiency of the unit under these conditions was about 30 per cent.

As soon as it became evident that the SPEP trans-

ducer made with special steel cases, special molded rubber faces with spherical curvature, and special aluminum grillwork to help support the back ends of the stacks. Figure 72 shows the array of stacks Cycle-Welded to the rubber face. The rubber faces for these units were molded from natural rubber compounds. The finished moldings had durometer hardnesses of about 35 to 45 and were as free as possible from porosity.

Model 3 was the same as Model 2 except that the aluminum grillwork used to support the back ends of the stacks in Model 2 was replaced by snugly fitting

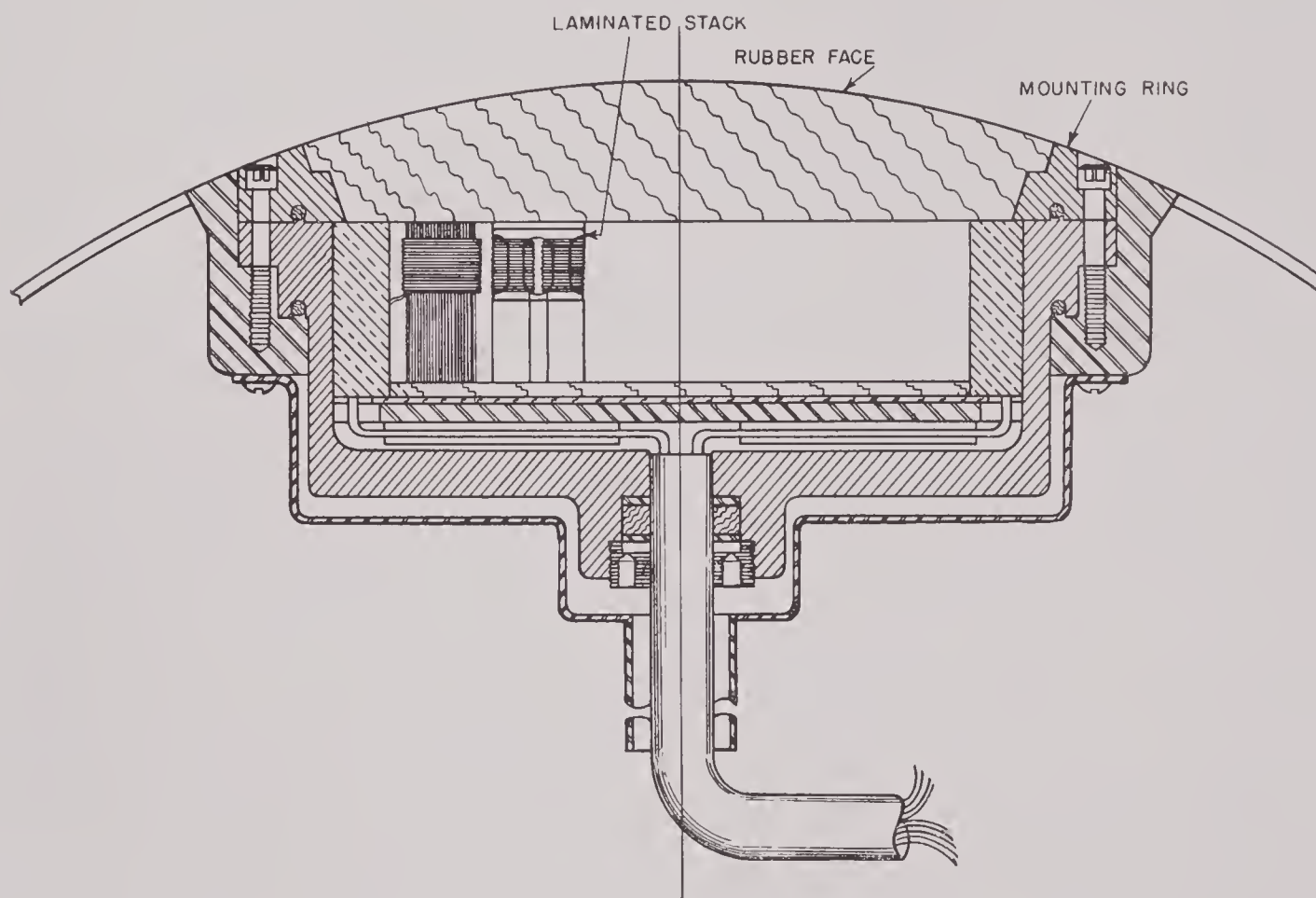


FIGURE 73. Section of SPEP Model No. 6 (PM-polarized).

ducer would satisfy the various acoustic and electric specifications required, design work for a more rugged and better-engineered unit was begun. Six different types, Models 1 through 6, were made. Models 1 through 5 used laminated stacks polarized with direct current, while Model 6 used stacks polarized with sintered-oxide permanent magnets.

The two Model 1 units were similar to the original SPEP described above.

The nine Model 2 units constructed and tested were

pads of corprene. This made the array of stacks more resilient, so that the units could withstand severe mechanical shocks better than the Model 2 units.

In Models 4 and 5 attempts were made to construct rubber faces that had thin metal reinforcement plates either cemented to the outside of the face or molded inside the rubber. On Model 4 the reinforcement consisted of a 0.010 in. thick, stainless-steel spinning, with the same radius of curvature as the outside face of the rubber, which was Cycle-Welded to the front

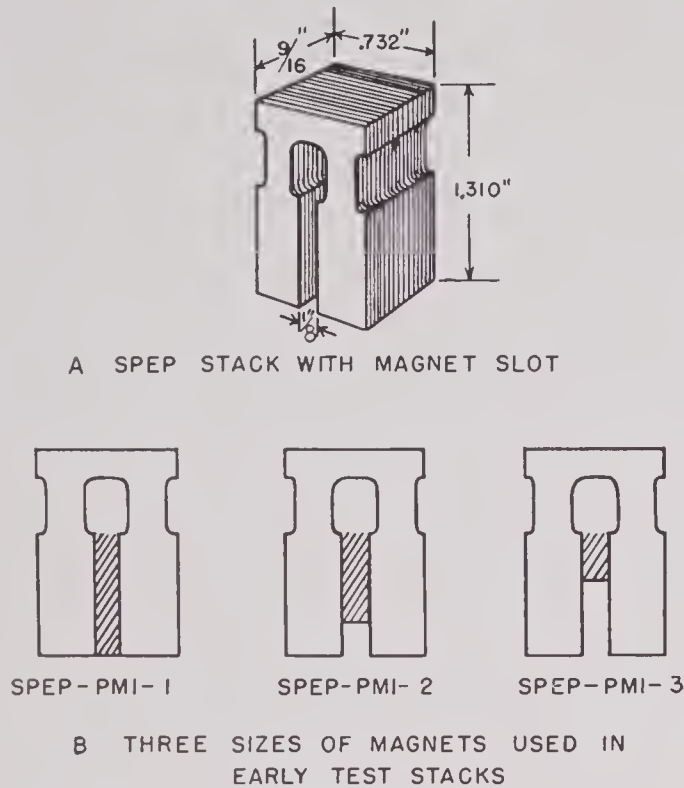


FIGURE 74. SPEP stacks modified for polarization by sintered-oxide magnets.

was molded in the rubber face when it was made. This unit proved to be entirely unsatisfactory because of poor acoustic transmission through porous places in the rubber face next to the metal, where gas bubbles were trapped. It was eventually found that rubber faces with a durometer hardness of about 70 and without any metal reinforcement were more satisfactory.

PERMANENT MAGNET (PM) POLARIZED SPEP TRANSDUCER

The Model 6 SPEP transducers were essentially the same as Model 3 except that the laminated stacks were polarized with sintered-oxide permanent magnets. A cross section of this model is shown in Figure 73. Twenty-seven units of the Model 6 SPEP transducers were made and tested. From the point of view of transducer design and development the most important feature of this model was the PM polarization.

The first tests on the use of sintered oxide as a permanent magnet material for polarizing laminated transducer stacks were made on SPEP stacks of the

TABLE 3. Results of impedance measurements for permanent magnet polarized stacks SPEP-PMI No. 1, SPEP-PMI No. 2, SPEP-PMI No. 3, and a standard direct-current polarized stack.

	No. 1, full magnet, 0 pol cur	No. 2, $\frac{3}{4}$ magnet		No. 3, $\frac{1}{2}$ magnet		DC pol SPEP stack, 1.25 amp pol cur element No. 2
		0 pol cur	1.5 amp pol cur	0 pol cur	2.0 amp pol cur	
Z clamped @ f_r	$2.2 + j19.8$	$3.0 + j23.6$	$1.71 + j16.25$	$5.5 + j31.4$	$2.45 + j19.7$	$13.6 + j51$ $14.1 + 53 @ 60 \text{ ke}$
D_a	10.7	7.8	3.6	11.7	4.4	58
f_r	59.96	60.75	61.2	59.30	61.50	57.43
$Z_a @ f_r$	$12.4 + j16.6$	$10 + j20$	$5.0 + j15$	$17 + j29.5$	$5.1 + j17.5$	$63 + j20.5$
Q_a	34	15.6	22.6	16	16	37
$k = \sqrt{D_a/Q_a}X$	0.127	0.146	0.099	0.152	0.117	0.176
$2\xi_{cm}$	17.5°	27°	20.5°	9.0°	30.5°	31°
$Z_{\max}/Z_{\min} \text{ (air)}$	1.625	1.38	1.19	1.34	1.18	3.40
Pot eff	0.412	0.327	0.277	0.275	0.258	0.445
Area of magnet	6.06	4.55	4.55	3.03	3.03	No magnet
Area of one leg						
Quality of stack	Good	Mediocre	Mediocre	Mediocre	Mediocre	Good

surface of the rubber face. This unit was unsuccessful because perfect bonding was not obtained between the metal and rubber. The frequency response and the acoustic patterns were therefore unsatisfactory.

In Model 5, the reinforcement consisted of a 0.015 in. thick, dish-shaped piece of stainless steel which

form shown in Figure 65B, which was modified by cutting a $\frac{1}{8}$ -in. slot in the backing portion to make stacks of the form shown in Figure 74A. The first three experimental test stacks had three different sizes of magnets, as shown in Figure 74B. Results of impedance tests on these three stacks, as compared

to a conventional d-c polarized stack, are given in Table 3. All the stacks had a standard 50-turn winding. Impedance measurements were also taken on PM stacks No. 2 and No. 3 when the polarization was increased by some direct current in the windings.

Comparison of the electromechanical coupling coefficients k , listed in Table 3, indicates that stacks 1 and 2 were somewhat overpolarized by the magnets, since the highest k was found for stack 3 without polarizing current. The gap in the magnetic path in the PM polarized stacks decreased the effective reversible permeability of the stacks, with a consequent decrease in k as compared with the d-c polarized stack that had a complete magnetic circuit.

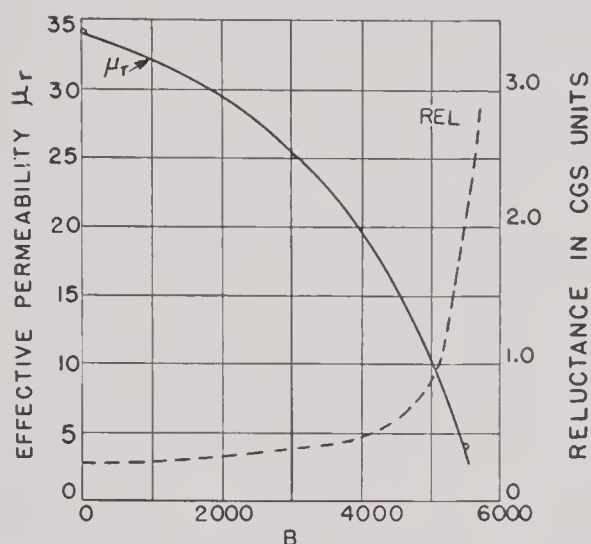


FIGURE 75. Effective reversible permeability and reluctance vs flux density in the legs of a PM-polarized SPEP stack.

The clamped-core impedance of the stacks was considered to be a better criterion of the actual degree of magnetic polarization of the stacks than the electromechanical coupling coefficients. The effective reversible permeability of the PM polarized stacks was calculated from the geometry of the stacks and the results of static magnetic measurements on samples of similar nickel. The reluctance and effective permeability are plotted against the flux density in the nickel legs of the stacks in Figure 75. At high flux densities the permeability decreases rapidly, due to saturation of the nickel. Figure 76 shows the clamped-core impedance diagrams for PM-polarized SPEP stacks which were calculated from the μ_r 's given in Figure 75. Observed values of the clamped-core impedances for the various PM stacks are indicated on the same graph. The fact that the observed values lie

so near the calculated curve indicates the correctness of the theory. The positions of the observed values along the line are a good indication of the degree of polarization of the stacks. These results indicated that the three-quarter sized magnet would give the proper degree of polarization for maximum efficiency.

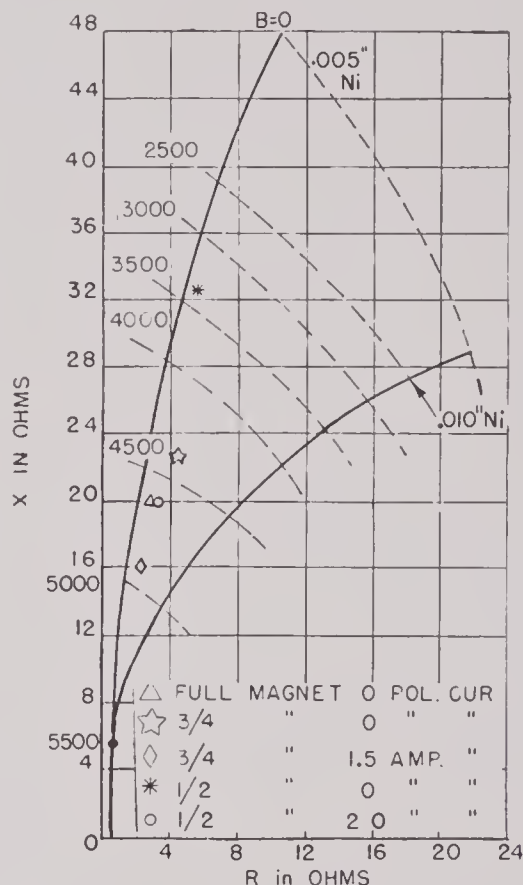


FIGURE 76. Calculated and observed clamped core impedance of PM-polarized SPEP stacks at 60 kc for various degrees of polarization (50-turn winding).

However, these magnets were magnetized to their highest value and it was pointed out that the final transducer would be more stable if the full-sized magnets were used and partially depolarized while in place in the nickel stack. Consequently, all the subsequent PM polarized SPEP stacks were equipped with magnets which filled the entire magnet slot.

Figure 77 shows the clamped-core impedance diagram for d-c polarized SPEP stacks made of 0.005-in. oxide-annealed nickel where the flux density is the parameter. The observed clamped-core impedance for a stack polarized with a 1.2-ampere polarizing current is shown on the same graph. The position of the observed point indicates that the stack was underpolarized ($B = 3,200$) and that 2.4 amperes would be required to polarize it for optimum efficiency. The most outstanding difference between the

impedances of the d-c and PM polarized stacks is that the magnitude of impedance for the d-c polarized stacks in the region of $B = 4,000$ is roughly twice that of the PM polarized ones. This means that for the region of $B = 4,000$ the introduction of the magnet slot in the stack decreases the effective reversible permeability to about one-half the value for the unslotted stacks.

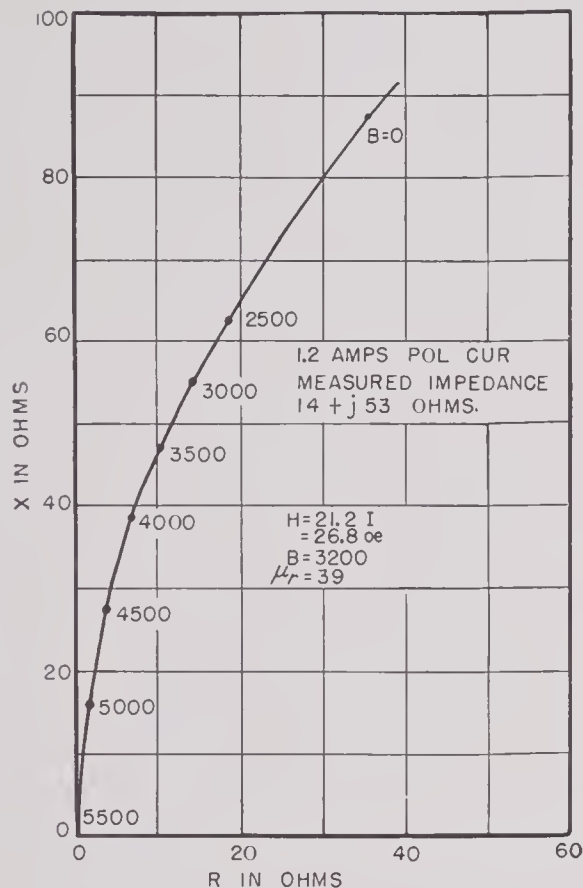


FIGURE 77. Calculated clamped-core impedance of a d-c polarized SPEP stack with 50-turn winding.

Because the electromechanical coupling coefficient and the eddy-current factor vary with the degree of polarization, the size of the motional impedance circle on the vector impedance diagram is zero for zero polarization, increases to a maximum size for the polarization which gives maximum coupling, then decreases in size for greater polarization. Figures 78 and 79 show in graphical form the loci of the ends of the resonance diameters of the motional impedance circles when they are added vectorially to the corresponding points (same polarization) on the clamped-core impedance lines. Figure 78 is for the PM polarized stacks and Figure 79 for the direct-current polarized stack. If it is assumed that all the mechanical power loss in the stacks is due to acoustic

radiation, then the efficiency is given by the ratio of the water impedance circle diameter divided by the resistance at resonance. The efficiencies for the two kinds of stacks are plotted against the polarizing flux density in Figure 80.

The PM polarized SPEP stack which contained the full-sized magnet was inserted in a watertight rubber housing so that electric and acoustic tests

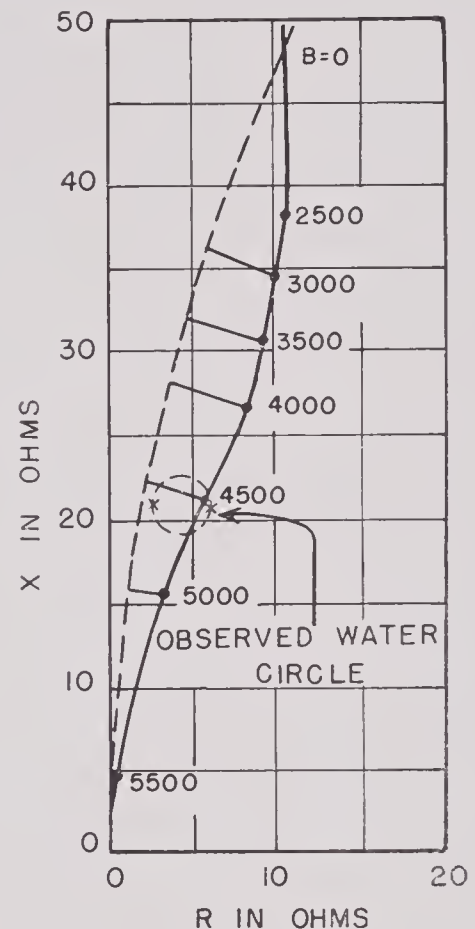


FIGURE 78. Total impedance at resonance of PM-polarized SPEP stack, 50-turn coil, in water for various degrees of polarization.

could be made in water as well as in air. The tests showed it to have a Q of 37 in air and a Q of 7.5 in water. The efficiency was 0.43, as determined from the diameters of the air and water motional impedance circles and the total resistance at resonance in water. Considering that some of the mechanical power loss was in the stack itself, this result was in good agreement with the value of 0.63 indicated in Figure 80.

The use of PM polarized stacks in the SPEP transducer simplified its construction to a considerable extent because only a single winding was needed on each stack and only two lead wires from each quad-

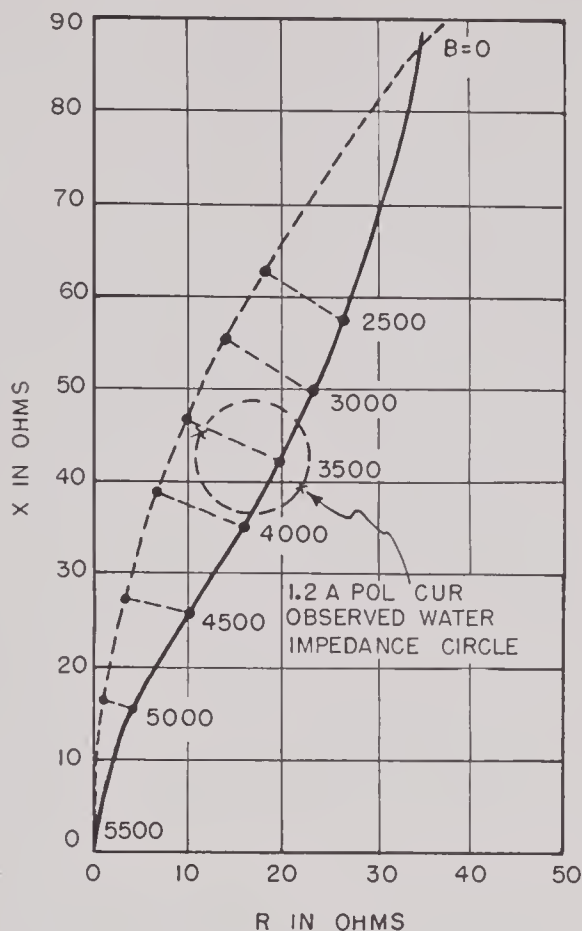


FIGURE 79. Total impedance at resonance in water for various degrees of polarization of d-c polarized SPEP stack, 50-turn coil.

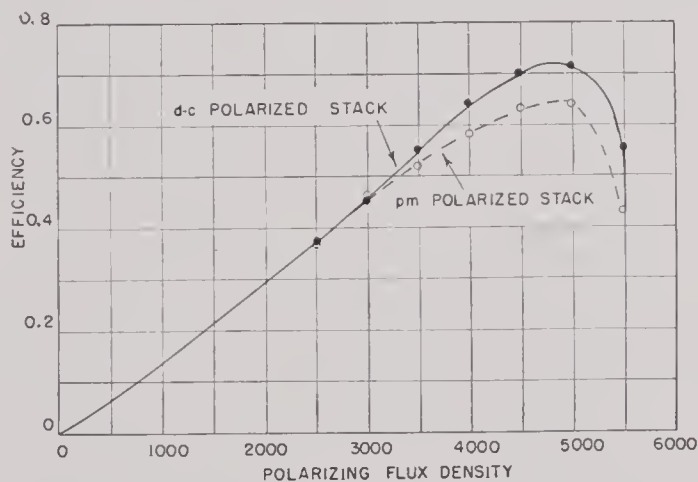


FIGURE 80. Efficiency of SPEP stacks as a function of the degree of polarization.

raut. Typical vector impedance plots in air and in water for a complete Model 6 SPEP transducer are shown in Figures 81 and 82. These impedance data show the mechanical Q of the unit to be about 12.5 when it is loaded by water radiation and the efficiency at resonance to be about 54 per cent. Both these values are nearly up to the theoretical values

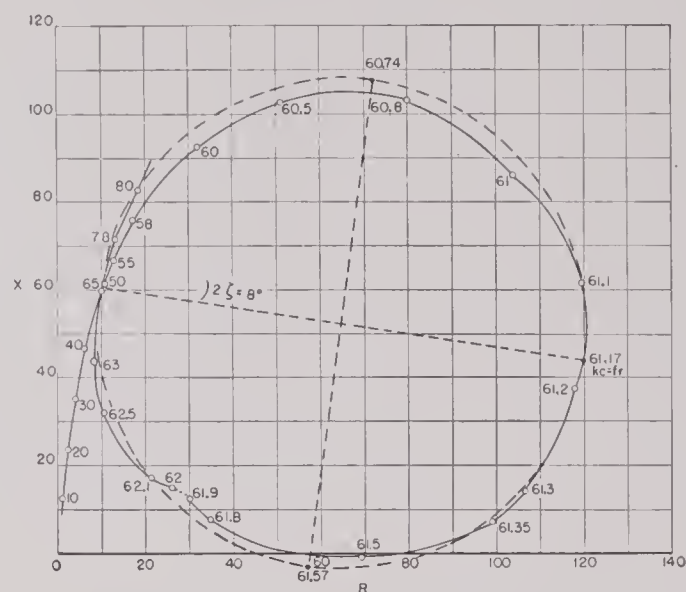


FIGURE 81. Vector impedance curve for SPEP No. 6 in air.

for a perfect transducer of this type. Figure 83 shows the acoustic pattern of a good SPEP 6 transducer, taken at 60 kc about an axis parallel to one of the diagonals of the square array of stacks. The response in the directions for which the curve is not given was below the -40 db level. This pattern approximates very closely the gaussian pattern (without side lobes) which was originally desired for this transducer.

To investigate the performance of the SPEP transducer at high electric input power levels, measurements were made on some single PM polarized SPEP stacks mounted in rubber housings.^{64,71,73} Steady state measurements at very high levels were impractical because of damage to the stack from overheating. The measurements were made with power pulses approximating 0.015 second in length, 2½ pulses per second. Driving currents up to 3.84 rms amperes were used, corresponding to input powers up to 150 watts. The wave form of the acoustic output remained sinusoidal for all the input powers used. This was attributed to the mechanical Q of the system being high enough to give a mechanical filter effect. The acoustic output power was nearly linear up to 60 watts of electric input but dropped below linearity for higher input powers. No cavitation effects were observed at the active face of the stack during the short pulses, despite the fact that the acoustic power flux was as great as 15 watts per sq cm, which corresponds to about seven atmospheres of acoustic pressure. The maximum possible acoustic power output is limited by magnetic saturation and is about 30 watts per

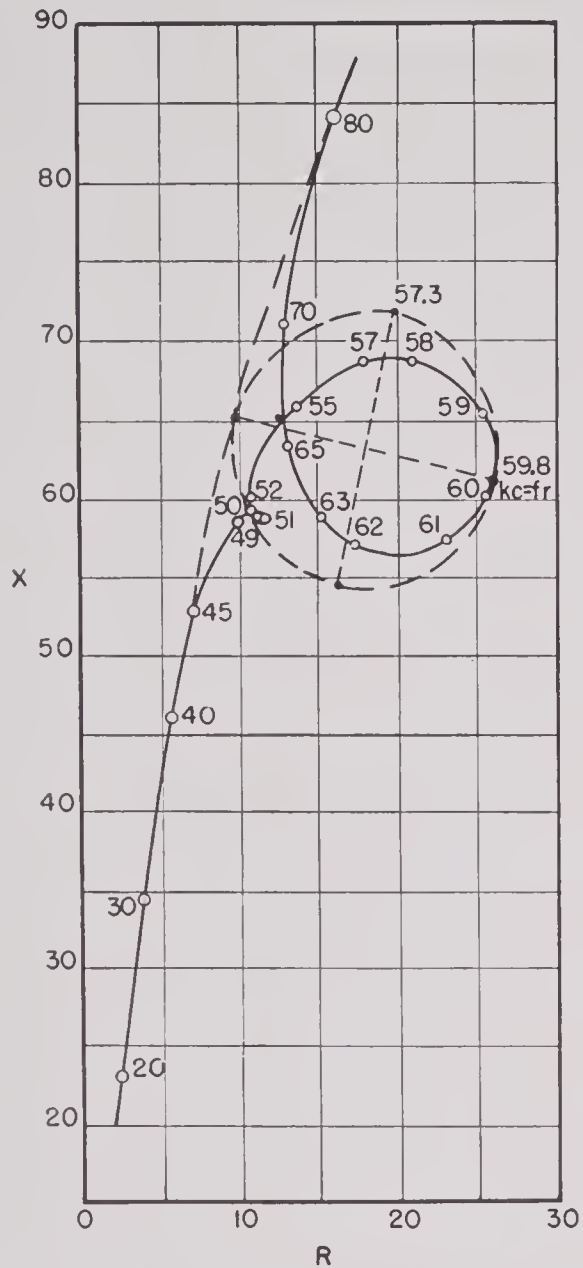


FIGURE S2. Vector impedance curve for SPEP No. 6 in water.

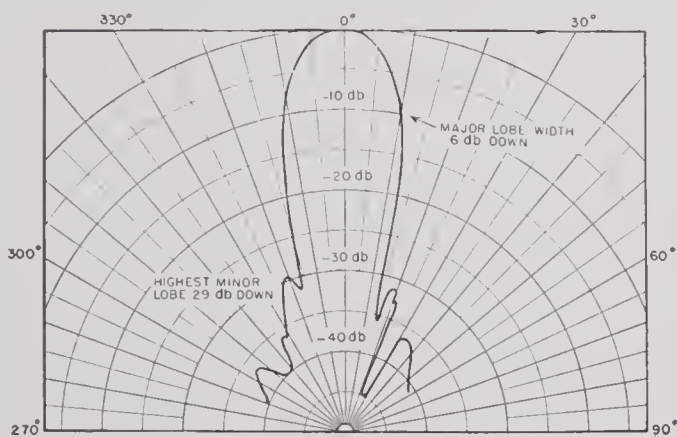


FIGURE S3. Acoustic pattern at 60-ke of an SPEP 6 transducer taken about an axis parallel to a diagonal of the square array of stacks.

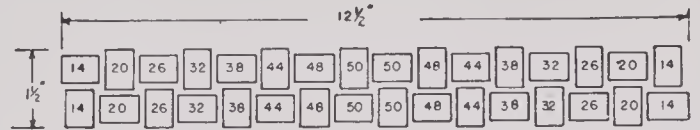


FIGURE S4. Layout of SPEP stacks in sword-arm depth-angle transducer showing the total number of turns of winding on each stack.



FIGURE S5. Completed 60-ke sword-arm depth-angle transducer.

CONFIDENTIAL

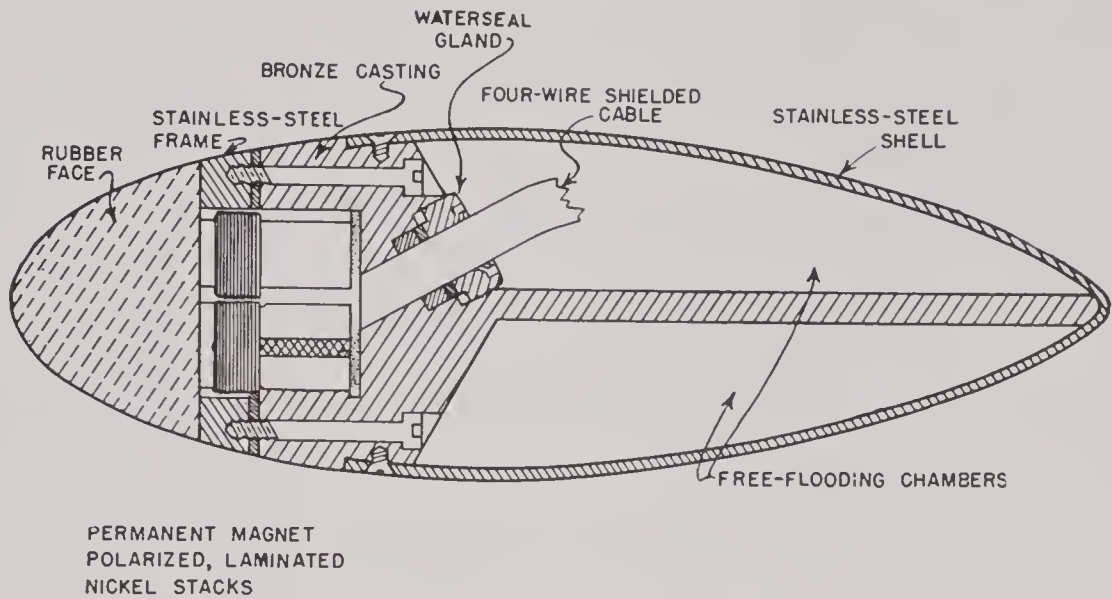


FIGURE 86. Section in place perpendicular to long axis midway along the length of a 60-ke sword-arm depth-angle transducer.

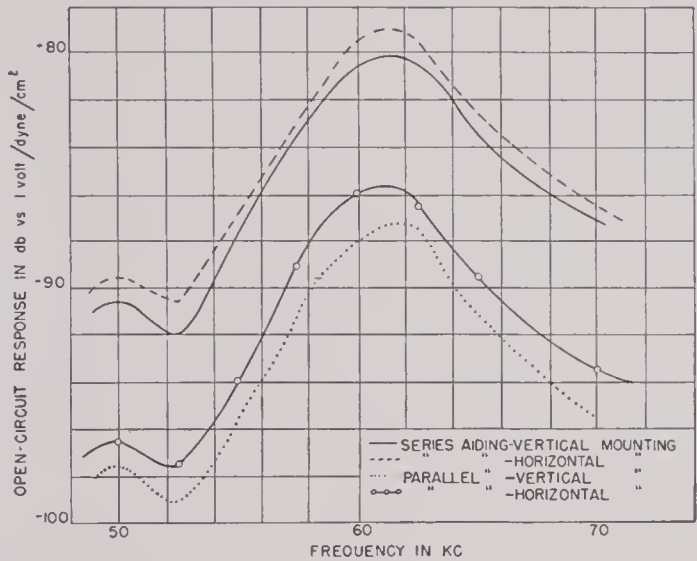


FIGURE 87. Open-circuit frequency response for series and parallel connections of 60-ke sword-arm depth-angle transducer.

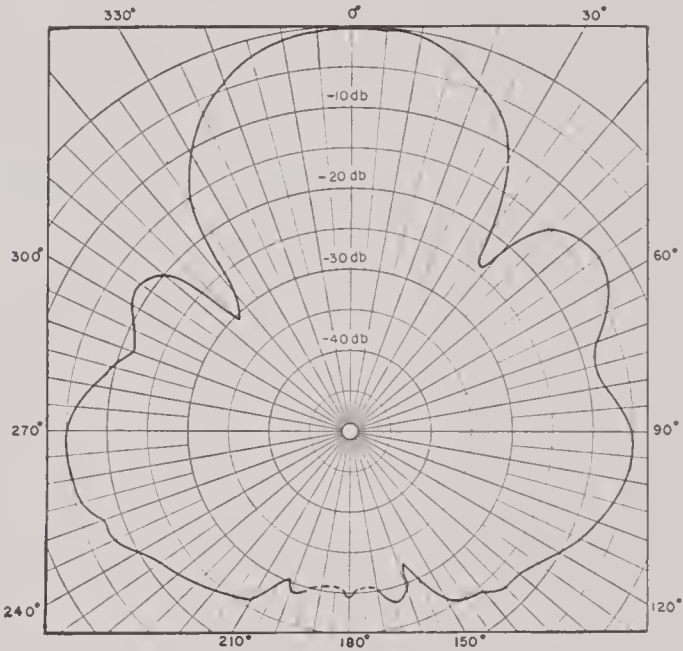


FIGURE 88. Pattern in horizontal plane at 61.2 ke, parallel-aiding connection of 60-ke sword-arm depth-angle transducer.

stack. For a whole SPEP transducer this corresponds to a total input power of about 1,500 watts to produce about 250 watts of acoustic output. This has been verified experimentally in high-power pulsing tests on full-sized SPEP transducers.

60-KC SWORD-ARM DEPTH-ANGLE TRANSDUCER

During the first half of 1944, a special sword-arm depth-angle transducer was designed and made at HUSL to be used as an echo-ranging transducer to determine the depth angle of deep underwater targets. The active part of the transducer consisted of a long, narrow array of thirty-two 60-ke PM polarized

SPEP stacks arranged as shown in Figure 84. The long axis of the transducer was in the vertical direction so that the acoustic pattern in the vertical plane was sharp while that in the horizontal plane was broad. A photograph of the completed transducer is shown in Figure 85. The molded rubber face to which the laminated stacks were Cycle-Welded appears on the lower front edge. The top section of the structure was a stainless-steel sleeve used in attaching the transducer to the streamlined strut mounting. A sec-

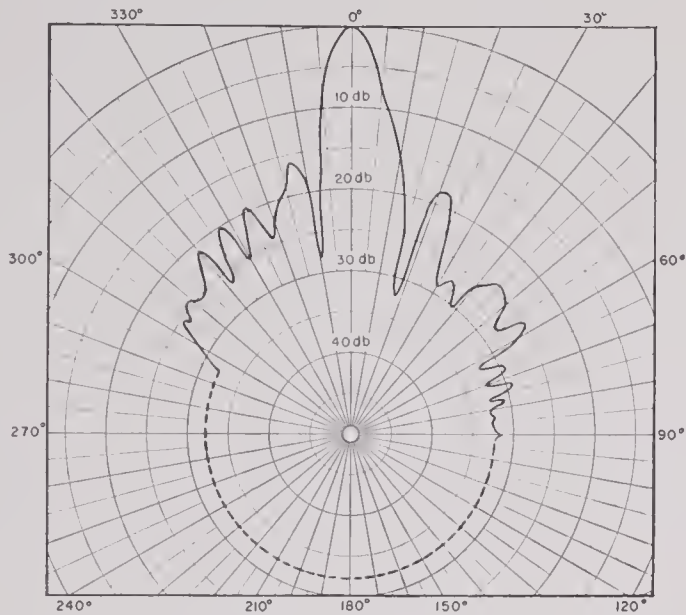


FIGURE 89. Pattern in vertical plane at 61.2 kc, parallel-aiding connection of 60-kc sword-arm depth-angle transducer.

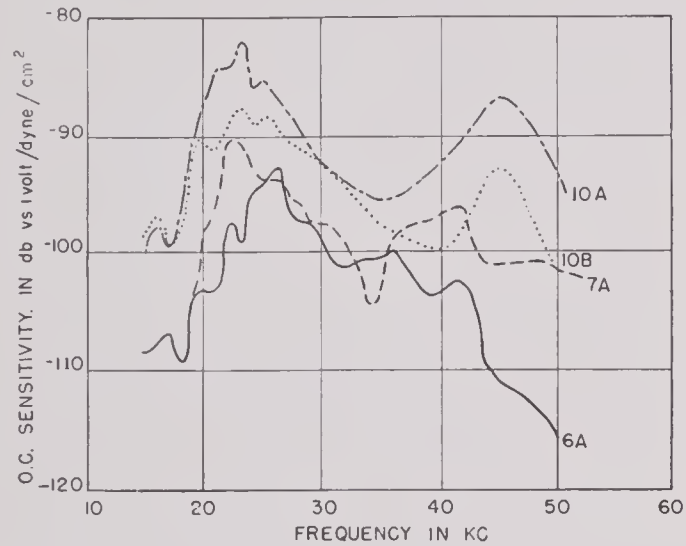


FIGURE 90. Receiving response of Models 6A, 7A, 10A, and 10B hairpin transducer units.

tion of the transducer taken at the center of the length of the active portion is shown in Figure 86.

All the stacks in both upper and lower halves were connected in series aiding. Separate lead wires were brought out through the cable from each of the halves so that the transducer could give BDI operation in the vertical plane. The number of turns on the stacks was decreased parabolically from 50 at the center to 14 at the ends in order to give minor lobe suppression.

Results of impedance measurements on the transducer in air and water are listed in Table 4. These

show that the bottom half was not so good as the top half. The impedances of the two halves, separately or in parallel, were consistent, but the impedance of the two halves in series differed widely from the expected value of four times that of the two halves in parallel. The variation was caused by electric tuning due to distributed capacity in the windings and the cable.

TABLE 4. Analysis of impedance measurements on the 60 kc sword-arm depth-angle transducer.

	Top half alone	Bottom half alone	Two halves parallel	Two halves in series
f_r	59.98	60.20	60.00	60.20
Q_A	35	35	35	21
Z_c	$87 + j351$	$110 + j350$	$43 + j171$	$1080 + j480$
D_A	245	174	114	620
k	0.14	0.12	0.14	0.15
Pot eff	0.34	0.25	0.34	0.20
<hr/>				
$f_r(\text{water})$	59.7	59.9	59.9	61.2
Q_W	11.0	10.0	10.3	11.1
Z_c	$95 + j342$	$94 + j340$	$46 + j171$	$920 - j125$
$Z \text{ at } f_r$	$180 + j297$	$172 + j300$	$87 + j149$	$73 + j0$
D_W	97	75	47	230
k	0.16	0.16	0.16	0.15
Eff	0.32	0.25	0.32	0.20

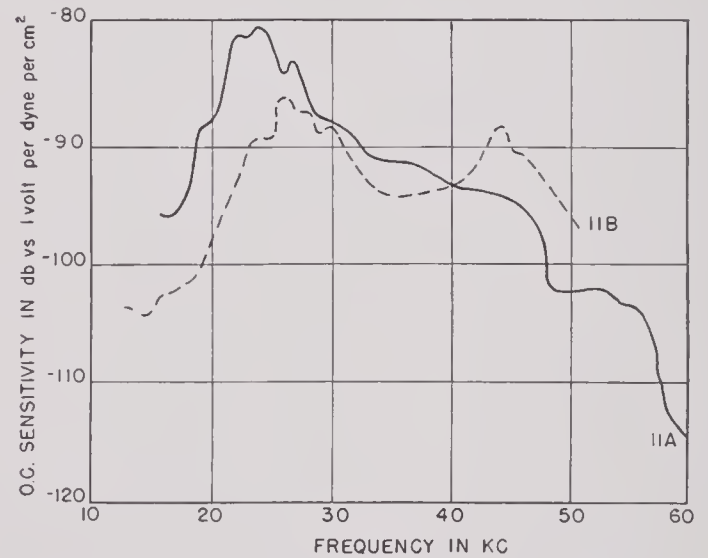


FIGURE 91. Open-circuit frequency response of Models 11A and 11B hairpin transducer units.

The open-circuit frequency responses of the unit for the parallel and series connections are shown in Figure 87. The difference between the responses for the series and parallel connections should be exactly 6 db, but the actual difference is more than this, due to the electric tuning effect for the series connection.

The pattern in the horizontal plane at 61.2 kc is shown in Figure 88 and for the vertical plane in Figure 89. The heights of the side lobes in the horizontal plane pattern were approximately as expected, while those in the vertical plane pattern were considerably higher than they should have been for the degree of shading used. The only explanation that has been

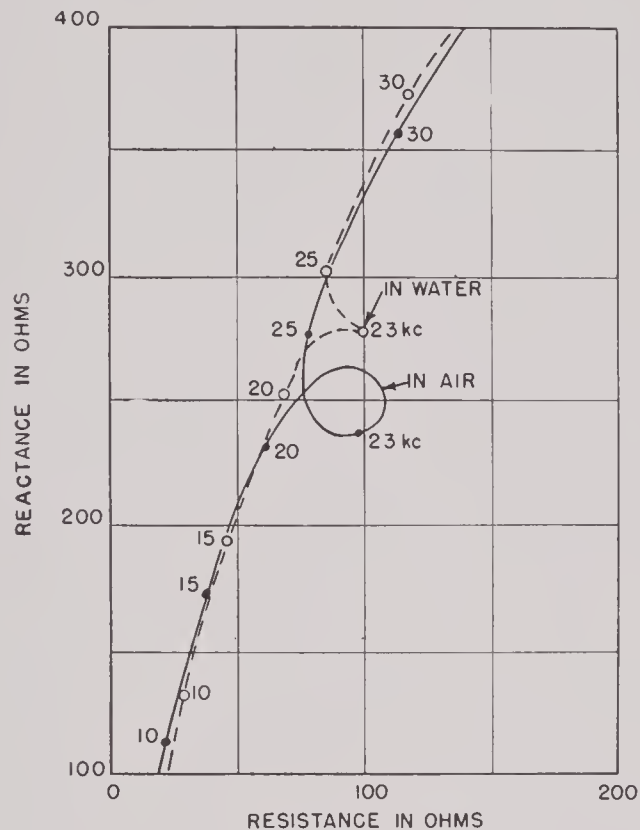


FIGURE 92. Vector impedance locus plot for hairpin transducer Model 10B.

given for this deviation from theory is that there may have been some phase variation along the length of the array of stacks, due to distributed capacity in the windings.

Only one unit of this type was made because a crystal transducer developed by BTL to serve the same purpose was demonstrated and accepted before this magnetostrictive unit was completed.

SONAR TRANSDUCER ELEMENTS

The elements of most of the magnetostrictive sonar transducers made at HUSL consisted of stacks of laminations of the form shown in Figure 11C and D. The models actually made and tested were HP-1, HP-2, HP-3, HP-5, and HP-8.

7.2.6

Miscellaneous Forms

Some of the miscellaneous forms of laminated longitudinal vibrators have been shown above in Figure 14 and discussed generally in Section 12. All four of the forms illustrated in Figure 14 have been investigated experimentally to some extent at HUSL. None of them showed any promise of giving stable reproducible frequencies of resonance, high efficiency, or uniform acoustic patterns. As pointed out in Section 12, one cause of trouble is the variation in the exact shape and degree of consolidation of the arched portion of the laminated structure. A second is the

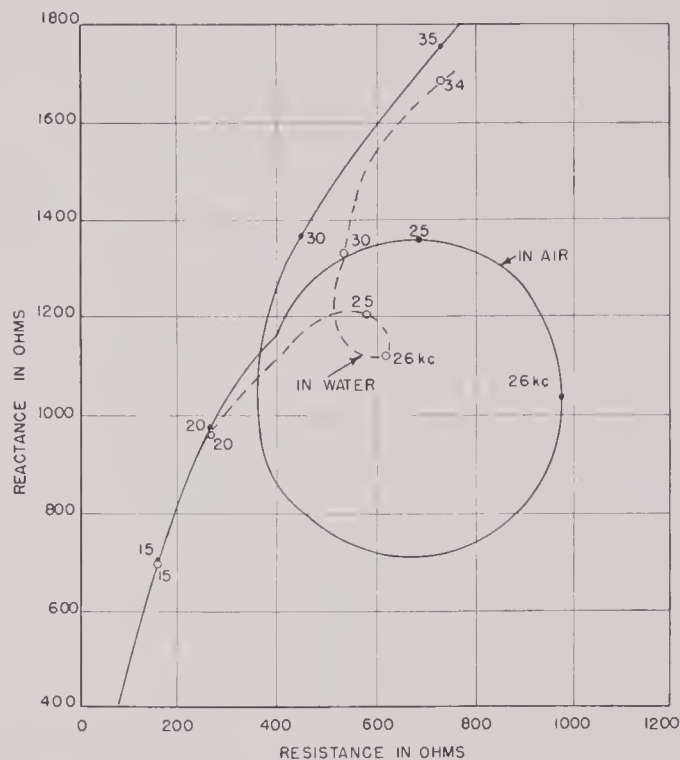


FIGURE 93. Vector impedance locus plot for hairpin transducer Model 11B.

mechanical joint between the laminated structure and the face plate, and a third is the relatively poor high-frequency magnetic circuit between the free ends of the laminated structures of the types shown in Figure 14A, B, and D. In these cases the high-frequency flux cannot pass freely between the two arms of the laminated structure because of eddy-current shielding in the inner laminations. The type shown in Figure 14C does not suffer from this difficulty.

Eight experimental models of the forms shown in Figure 14A and B were constructed and tested. The hairpin-shaped laminations were made from oxide-annealed nickel 0.005 in. thick by 1 in. wide by the Westinghouse Electric Company, using the same

process as for commercial Hipersil transformer cores. The thickness of the stack of laminations was $\frac{1}{4}$ in. and the distance from the flat open end to the outside of the arch end was $2\frac{1}{2}$ in. These laminated structures were cemented to diaphragm pieces $1 \times 1 \times \frac{3}{8}$ in. thick and were mounted in the housing used for testing the bookphone transducer models (Figures 15 and 16).

principal one. Some of the units also showed considerable response at the second principal mode of vibration in the region of 45 kc. The vector impedance locus plots for Model 10B, one of the poorest of the units, are shown in Figure 92, and for comparison the same type of plots are shown in Figure 93 for Model 11B, one of the best.

On the whole, the performance of the hairpin type

TABLE 5. Performance characteristics of experimental "hairpin" laminated stacks.

Model	Stack length (inches)	Diaphragm	Polarization	Polarizing current (amp)	f_r (kc)	Max OC sensitivity db (b/v)	Mech Q	Efficiency		
								Potential (per cent)	From air and water impedance (per cent)	From acoustic meas. (per cent)
6A	$2\frac{1}{2}$	Steel, double slots	DC	0.8	26.5	- 92	8.5
7A	$2\frac{1}{2}$	Steel, double slots	Alnico magnet at bottom	None	23	- 90	8	Low	Low	9
9A	$2\frac{1}{2}$	Brass, single slot	Alnico magnet at bottom	None	24	- 95	5	Low	Low	2
10A	$2\frac{1}{2}$	Brass, single slot, spread hairpin	Alnico magnet at bottom	None	22	- 85	5	15	15	19
10B	$2\frac{1}{2}$	Brass, single slot, spread hairpin	Alnico magnet at bottom	None	23	- 87.5	4	13	10	9
11A	$2\frac{1}{2}$	Plane steel	DC	0.5	25	- 83	6	27	29	17
11B	$2\frac{1}{2}$	Plane steel, rubber face	DC	0.5	26	- 86	7	25	24	8
19A	$2\frac{1}{2}$	Polystyrene, polymerized in place	DC	0.7	25.1	- 97	30	6

The general construction characteristics and test results of these eight models are listed in Table 5. None of the units was outstandingly good. Open-circuit frequency responses are shown in Figures 90 and 91. Most responses were ragged, indicating that there were several minor resonances associated with the

of laminated longitudinal vibrators did not equal that of well-constructed laminated stacks of the more conventional type. It is concluded, therefore, that unless some way can be devised for overcoming its natural weaknesses, it cannot compete with the conventional forms.

CONFIDENTIAL

Chapter 8

TUBE-AND-PLATE TRANSDUCERS

The theory of the magnetostrictive half-wave tube or rod vibrator has been treated in an earlier chapter. The problem of applying this type of vibrator to underwater signaling has been in part a matter of securing the proper acoustic loading on the vibrating member. A similar problem arises in ordinary loud-speaker design; the coil-driven cone and/or the tapered horn are the devices most usually employed to give efficient coupling of the vibrating member to the air. In the loudspeaker, the desired condition is effective coupling over a wide frequency range to insure undistorted acoustic output. Pattern requirements are in general secondary. The problem in underwater sound signaling, on the other hand, has been largely one of securing high efficiency over a limited frequency range with a sharp beam radiation pattern.

Theoretical considerations presented in earlier chapters indicate that the first requirement, high efficiency, calls for a mechanically resonant system. The half-wave tube or rod meets this requirement. The sharp beam pattern requires a surface whose dimensions are large compared with the wave length of the radiated sound vibrating as an acoustic piston, that is, with the motion of all parts of the surface in phase.

The device illustrated in Figure 11 of Chapter 1 is an early example of the tube-and-plate idea for increasing the area of the radiating surface. Here the drivers are magnetostrictive tubes, each tube attached to a block or cylinder of metal the height of which is a half wave length in the metal of the radiated frequency. The elements are connected by thin webs located in a plane that is relatively stationary with reference to the driver and radiating faces. The suggested dimensions for a cylindrical block of aluminum to resonate at 30 kc are a 2-in. diameter and a height of approximately 3 in. The specifications state that theoretically the driving tube and the driven block should have the same natural frequency. The formula²⁵ given for the length of the magnetostrictive tube is

$$L = \frac{C_n}{f_0} \cdot \frac{\phi}{2\pi} + \frac{k}{4} \quad (1)$$

where C_n = velocity of sound in the metal of the tube,

f_0 = resonance frequency,

k = the odd integers 1, 3, 5, etc.,

$$\phi = \tan^{-1} \frac{C_n}{2\pi f} \cdot \frac{M_0}{M}.$$

M_0 is the mass per unit length of the tube and M the mass of the cap plate in which the tube is threaded into the resonator block. Note that, if M is small compared to M_0 , $\phi/2\pi$ approaches $1/4$. This means that if the attaching means has a negligible mass compared with a unit length of the driving tube the latter should be a half wave length when driving a half-wave resonator.

8.1 TUBE-AND-CYLINDER FULL-WAVE OSCILLATOR

Two experimental transducers embodying the idea suggested in Figure 11 of Chapter 1 were built at Harvard Underwater Sound Laboratory [HUSL]. However, instead of relying on deep slots in a half-wave plate to afford mechanical isolation between elements, as in Figure 11 of Chapter 1, each element consisting of a half-wave magnetostrictive tube vibrator and a half-wave brass cylinder was built separately. These elements were supported at the nodes of the half-wave cylinders by being press-fitted and soldered into holes in a $1/16$ -in. steel plate. Nineteen of these elements were assembled in a circular array to which a rubber face was molded, as shown in Figure 1. The transducer was designed to have a resonant frequency of about 64 kc and to have a radiation pattern whose main lobe was 20 degrees wide 6 db down from the maximum with side lobes at least 30 db below the maximum of the main lobe.

These units did not meet the particular need for which they were designed but their construction yielded certain useful information on the behavior of composite elements intended to operate as full-wave oscillators. The single elements, one of which is shown in detail in Figure 2, were carefully tuned by turning

down the brass cylinder to the same resonant frequency, 65.25 kc, to within 0.1 kc. A second mode of vibration appeared with maximum response at 50 kc. Impedometer measurements on the separate elements showed a potential efficiency at this latter frequency of about 34 per cent, with a mechanical Q of 31.

The assembled unit, however, showed an efficiency of only 5 per cent. This loss is ascribable partly to lack of exact phase-matching among the elements in the steel plate and partly to the damping action of the rubber that intruded into the crevices between the brass cylinders.

the high values of the mechanical Q and their relatively low efficiencies.

3.2 TUBE-AND-CONE HYDROPHONE

Figure 3 shows a hydrophone of this type, which was developed for a special use at HUSL. It consisted essentially of a cone of brass or aluminum, the base of which was the radiating surface. The cone was driven by means of a magnetostrictive tube attached to its vertex. Specifications called for a radiation pattern 90 degrees wide 6 db down from the maximum,

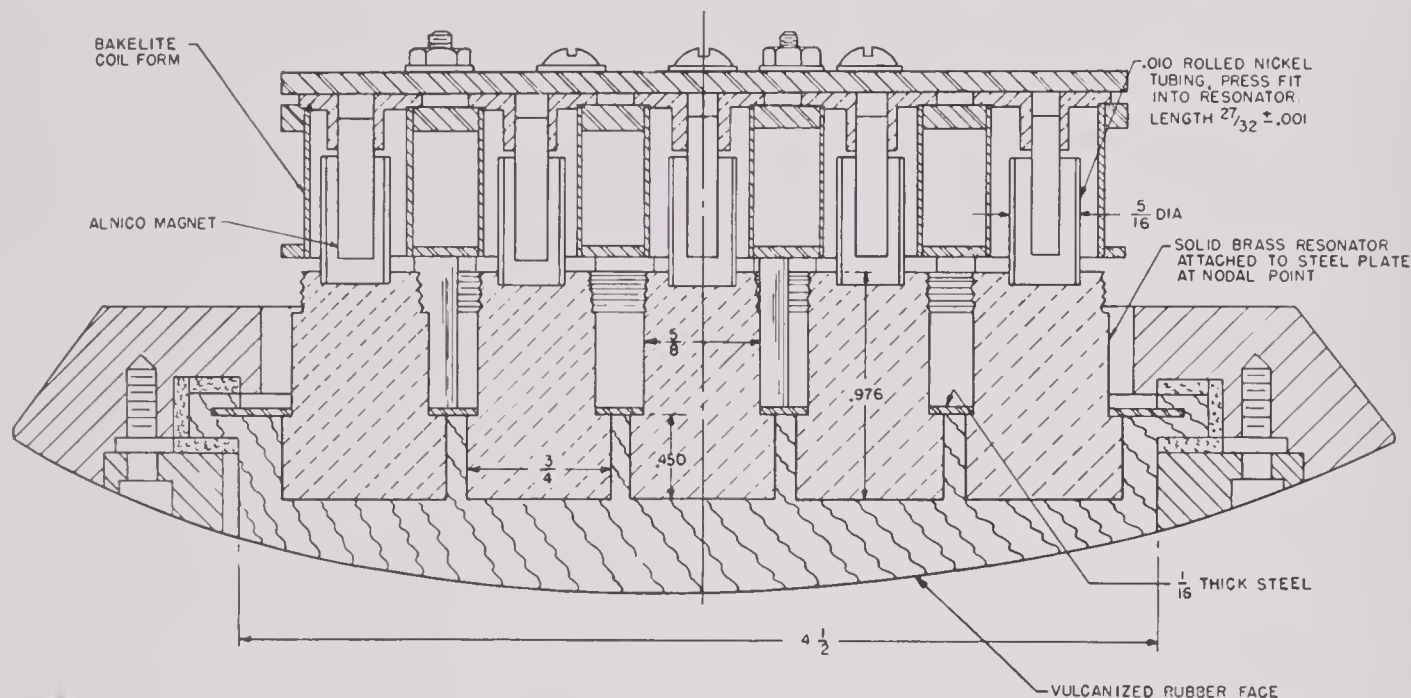


FIGURE 1. Experimental transducer, nineteen full-wave oscillator elements.

The main lobe of the radiation pattern met the design requirement of 20-degree width at the 6-db point, but the side lobes were down only about 15 db.

As was to be expected, it was found that the resonance frequencies of the individual elements were dependent more on cylinder length than on the length of the nickel tube. Even the variations in the mechanical properties of different samples of brass were great enough to make quite appreciable differences in the resonant frequencies of different elements, though these were made to the same dimensions with all possible accuracy. In addition to high mechanical losses in this particular design, the practically open magnetic circuit resulted in magnetization of the nickel tubes by the Alnico magnets considerably below the optimum.

Other experimental units of the full-wave oscillator type tried at HUSL proved disappointing, because of

with a maximum sensitivity in the neighborhood of 20 kc. The pattern requirement dictated a diameter of about 3 in. for the base of the cone, and space limitations dictated a cone height of $2\frac{1}{2}$ in. The driving tube had a $\frac{3}{8}$ -in. OD with a wall thickness of 0.015 in. and was made of soft-annealed nickel. Its permeability was 40 to 50 when polarized with an Alnico I or Alnico II magnet $\frac{3}{16}$ in. in diameter, $1\frac{3}{4}$ in. long, with a pole strength of about 40 cgs units. The tube was slotted to reduce eddy-current losses and the magnet was placed about midway within the tube. A cone of these general dimensions has a resonance at 27 kc in addition to the 20-ke resonance.

In the particular use for which this hydrophone was intended, a maximum voltage output was desired to be fed to the grid of an amplifier input tube. The pickup coil consisted of 5,000 turns of single cotton-covered No. 33 enameled copper wire. The high side

of this was connected in series with a loading coil of 0.23-h inductance at 1,000 cycles. The distributed capacity of the 2.5 feet of two-conductor shielded-cable connection to the amplifier served to parallel-tune the loading coils at a peak frequency of 20 kc. The open-circuit sensitivity of the hydrophone thus terminated was of the order of -55 to -60 db vs 1 volt per dyne per sq cm. With brass cones, the measured Q was about 60, whereas an aluminum cone giving approximately the same sensitivity showed a Q as low as 30.

In Table 1 are shown computed values of sensitiv-

TABLE 1. Computed values of sensitivity and efficiency for different combinations of brass cones and driver. Resonance frequency 19 kc; radiating face 3 in. in diameter.

Height of cone (inches)	Frequency (kc)	Driver	Sensitivity db/1 volt / dyne/cm ²	Q	Eff
2.75	19	0.015-in. slotted tube 2.32 in. long	- 65	44	0.16
2.75	19	0.010-in. slotted tube 2.35 in. long	- 66	37.5	0.075
2.75	19	0.005-in. laminations 0.2 cm ² cross section 2.22 in. long	- 50	85	0.30
2.75	19	0.005-in. laminations 0.62 cm ² cross section 1.83 in. long	- 44	80	0.62

ity and efficiency for different combinations of brass cones and driver, all designed to have a resonance frequency of 19 kc, with radiating face 3 in. in diameter in each case.

Figure 4 shows a breakdown of a typical cone hydrophone into its components. The radiation pattern of the hydrophone set in a pressure-release baffle is given in Figure 5.

3.3 FOUR-TUBE HYDROPHONE

A later development at HUSL of a hydrophone embodying the tube-and-plate idea is shown in Figure 6. Specifications called for a peak frequency of 24.5 kc with an effective band width of 2 kc and a reception pattern having a single beam 120 degrees to 140 degrees wide 10 db down from the maximum. The unit was to feed into the grid of the first amplifier stage, producing a voltage of -60 db vs 1 volt for a field pressure of 1 dyne per sq cm at peak frequency. The radiating face was $2\frac{1}{2}$ in. in diameter.

It was found that the peak response was nearly independent of diaphragm thicknesses between $\frac{1}{2}$ in.

and $\frac{3}{4}$ in. The length of the driving tubes was 2.03 in., approximately one-fourth of the wave length in nickel of sound of the resonant frequency. Slotted seamless tubing with 0.015-in. wall or rolled tubes made from 0.010-in. sheet were used. The diaphragm was suspended by a thin, relatively compliant web

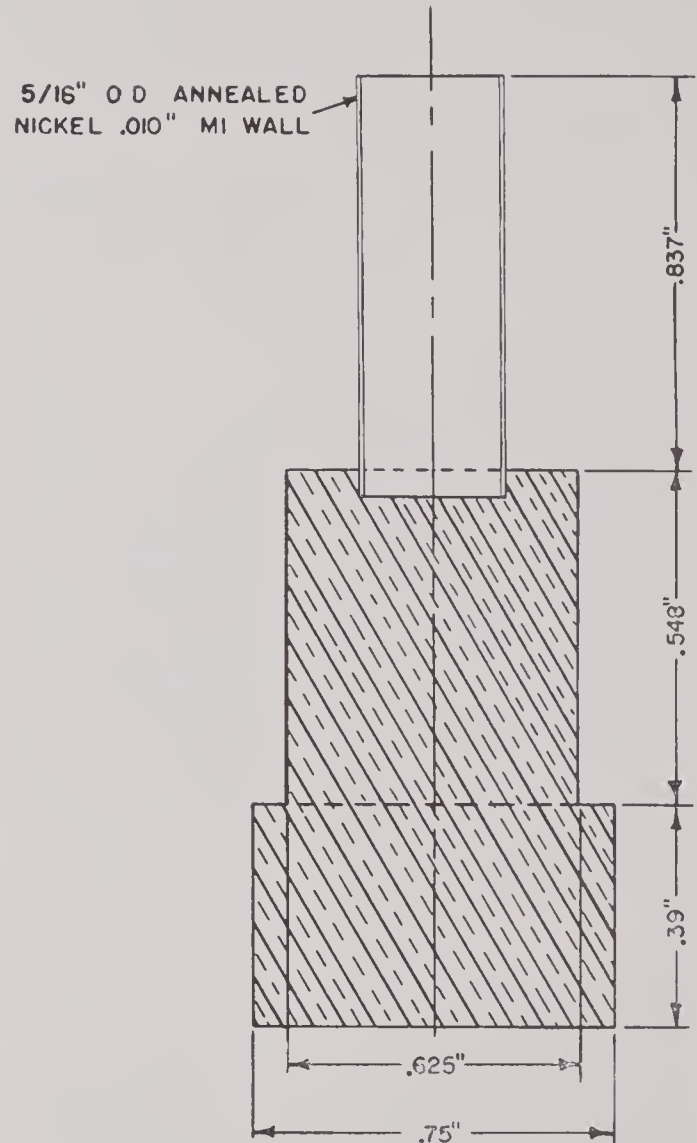


FIGURE 2. Detailed single element of Figure 1.

at the periphery in order to produce true piston motion. This web was $\frac{1}{16}$ in. thick and extended for $\frac{1}{4}$ in. beyond the diaphragm. Higher sensitivity was shown when the compliance ring projected from the lower rather than the upper edge of the diaphragm.

In order to get the desired frequency band width, small variations were made in the effective lengths of the four tubes. Units having equal length tubes had effective band widths of about 800 cycles; units with tubes that varied by steps of $\frac{1}{64}$ in. from $3\frac{1}{32}$ in.

had band widths of 1,200 cycles and, with twice this variation, the band width was increased to 2,000 cycles.

Experience with the cone hydrophones led to the use of silver solder instead of soft solder. With time, hydrophones in which soft solder was used frequently showed changes in their sensitivity that were believed to be due to the crystallization of the lead in the solder. Tubes were of uniform length but their effective lengths were varied by counterboring holes of different depths in the diaphragm. The tubes were annealed in hydrogen at a temperature of 900–1000 C for one hour and polarized with Alnico magnets $3\frac{1}{16}$ in. in diameter, magnetized to a pole strength of 40 cgs units.

The special termination of the hydrophone in the particular use for which it was designed is of interest. It was specified that the unit should operate into an input panel originally designed to terminate a crystal

served to match the input impedance to the characteristic impedance of the crystal transducers. The method by which a fairly respectable match was secured between the magnetostrictive transducer with its inductive impedance and the input provided at the panel is shown in Figure 7. The condenser C_1 parallel-tuned the inductance of the four coils to elec-

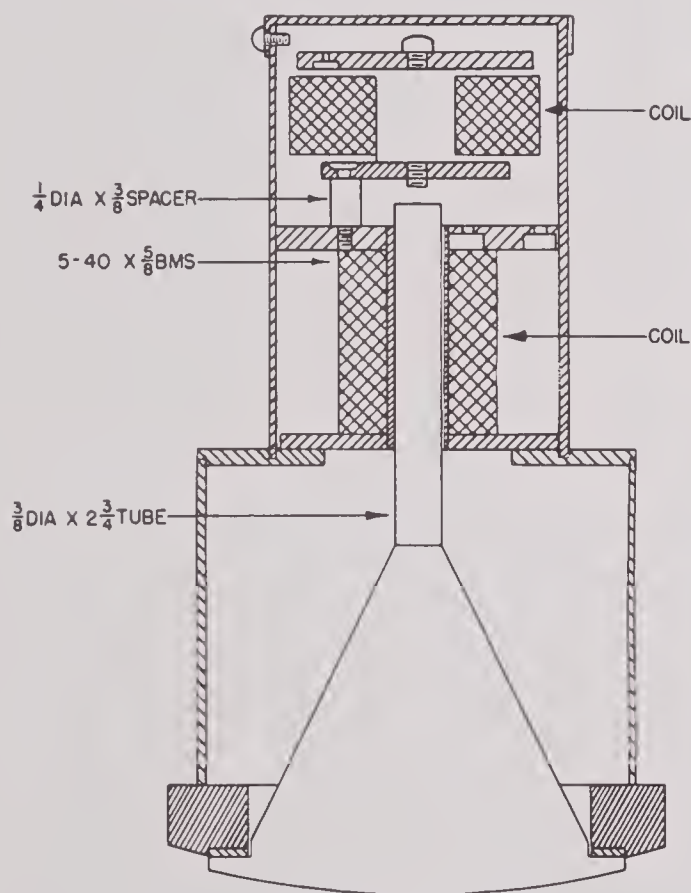


FIGURE 3. Tube-and-cone hydrophone.

hydrophone with high capacitive impedance. This panel consisted essentially of a 225-mh toroidally wound coil and an 0.82-megohm resistor shunting the grid of a 6SH7 tube. The choke parallel-tuned the capacity of the crystal and the high shunt resistor



FIGURE 4. Parts of tube-and-cone hydrophone.

tric resonance at peak frequency, giving an output impedance, mainly resistive, of about 30,000 ohms. The capacitance C is due to the cable (50 to 60 $\mu\mu f$), which reduced the effective inductance of the 225-mh input coil. The series condenser C_2 located inside the microphone case served both to block a low-frequency switching voltage that was impressed across the first stage and to effect the complete tuning of the input coil. This termination was not ideal, but even with the loss of sensitivity due to the broadened response, the four-tube hydrophone gave a voltage sensitivity into the grid of the first amplifier stage of from 60 to

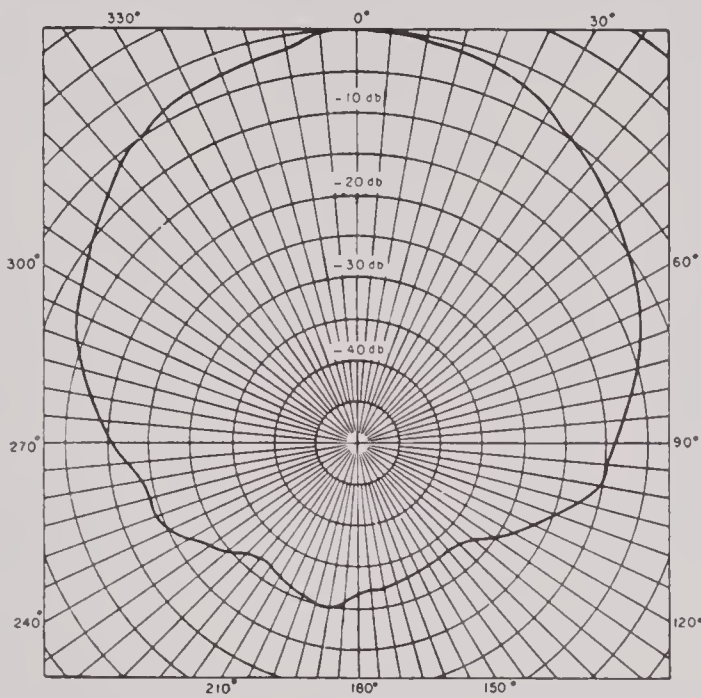


FIGURE 5. Pattern at 20 ke of tube-and-cone hydrophone in pressure-release baffle.

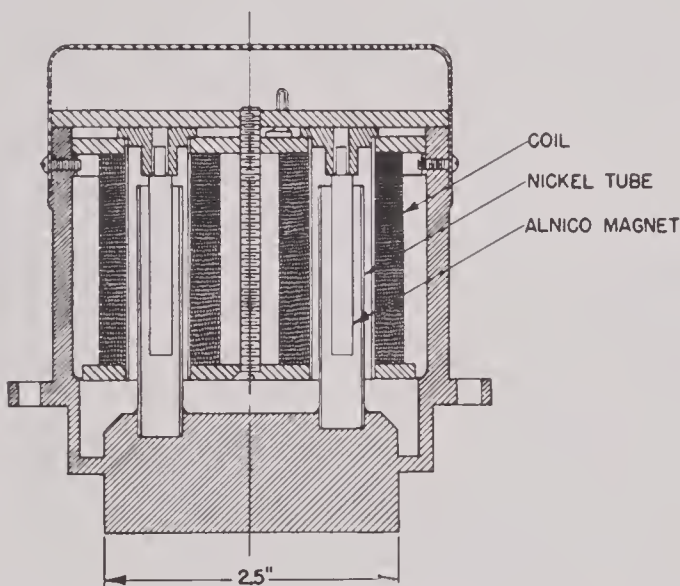


FIGURE 6. Section of four-element tube-and-plate hydrophone.

65 db below 1 volt for a sound field of 1 dyne per sq cm, only slightly less than that of the crystal hydrophone designed for the same use.

This case exemplifies a fact that is constantly encountered, namely, proper electric termination is a prime requisite for satisfactory transducer performance and this problem for magnetostrictive units that are relatively low inductive impedance devices is fundamentally different from that for high-impedance capacitive crystal hydrophones.

The construction of this four-tube hydrophone is indicated by the photographs, Figures 8 and 9. These

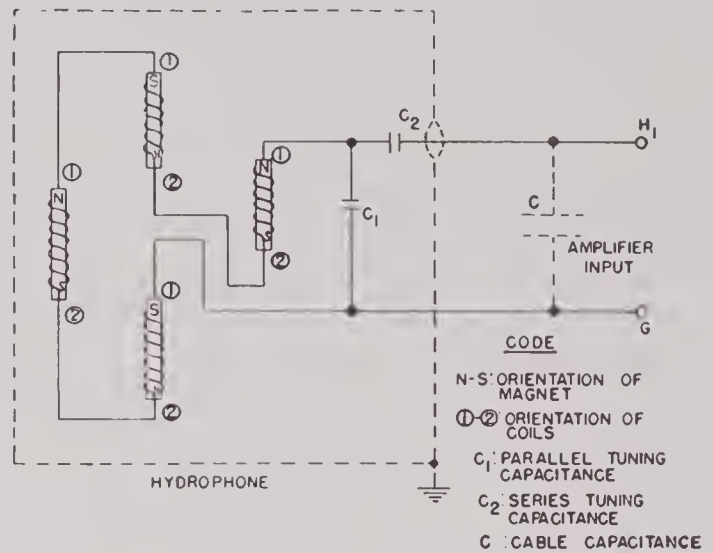


FIGURE 7. Termination of four-tube magnetostrictive hydrophone when replacing a high-impedance crystal hydrophone.

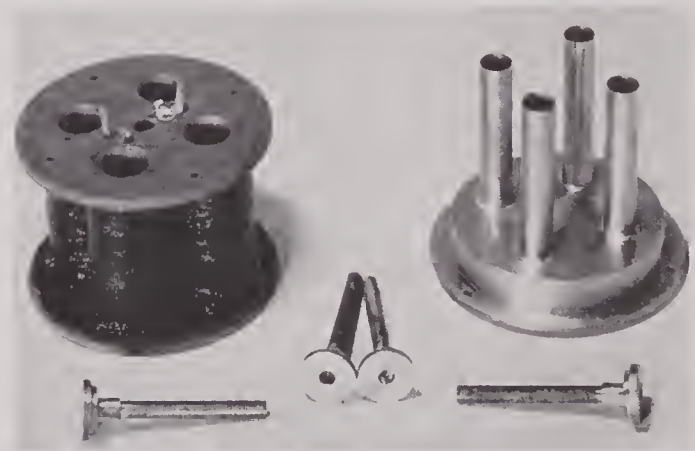


FIGURE 8. Components of four-tube hydrophone.

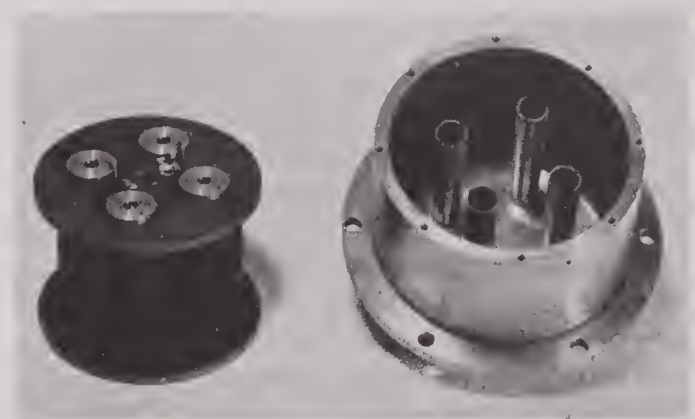


FIGURE 9. Subassembly of four-tube hydrophone.

units were fairly rugged and could stand a reasonable amount of abuse without change in their performance. Pattern and receiving response curves are shown in Figures 10 and 11.

3.1 TUBE AND SLOTTED-PLATE PROJECTOR

Early in the history of the sonar program at HUSL, the need arose for a sharp beam transducer to use as a mechanically rotated receiver. The sharp beam requirement called for dimensions that were large in comparison with the wave length in water of the sound to be received. The existing equipment designed to be used with this transducer operated at about 14 kc, corresponding to a wave length in water of approximately 4 in. A 12×12 -in. radiating surface was thought to be sufficiently large to meet the

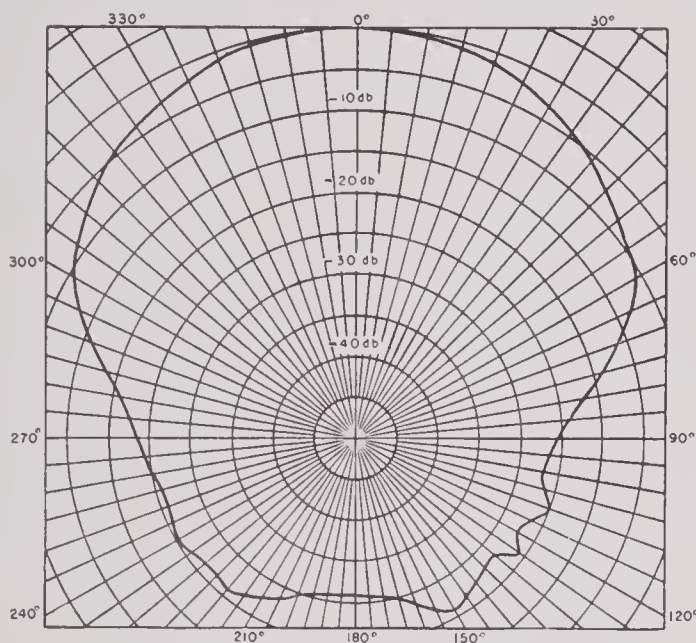


FIGURE 10. Pattern at 24.5 kc of four-tube hydrophone.

pattern requirement. Considerations of weight suggested a relatively light tube-driven plate. In earlier experiments with plates less than $\frac{1}{2}$ in. thick driven at distributed points, the tendency of such plates to break into segmented vibrations had been noted. These partial vibrations resulted in bad patterns and ragged frequency response. To avoid this difficulty while still using a relatively light construction, the plate was divided into small segments and each segment was driven by its own tube and coil assembly.

The detailed construction of the unit built is shown in Figure 12. The steel diaphragm was $\frac{3}{8}$ in. thick, with diagonal slots $\frac{1}{16}$ in. wide and $\frac{5}{16}$ in. deep milled in the back surface, producing 112 square segments each 1 in. on a side. A nickel tube $\frac{3}{8}$ in. in diameter, 3.7 in. long with 0.010-in. wall, was soldered to each segment. The tubes were polarized with Alnico mag-

nets. Each magnet was held in a wood dowel carried in the frame that supports the coils. Each coil consisted of 104 turns of No. 20 wire and the coils in each half were connected in series. Separate leads were brought out from each half.

On the assumption that the $\frac{1}{16}$ -in. web between the segments effects mechanical isolation between sections, each tube may be treated as a quarter-wave vibrator mass loaded at one end, and the analysis given in Chapter 3 should apply. If the coupling between segments is negligibly small, all parts of the

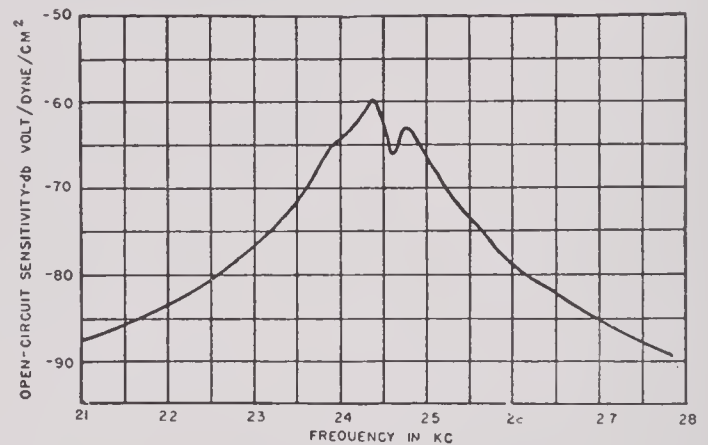


FIGURE 11. Frequency response of four-tube hydrophone.

plate should be driven in phase, and true piston motion should result. If these conditions are realized, the pattern and frequency response should be unaffected by segmental vibrations. From Figure 17 in Chapter 5 this transducer, which is 3 wave lengths on a side, would be expected to show a pattern with the main lobe 17 degrees wide at the -3 db points and 22 degrees wide at the -6 db points, with the minor lobes down 13 db from the main lobe. The measured pattern of Figure 13 shows a fair agreement with the theoretical values, although the pattern as a whole is not gratifying. The 12×12 -in. tube and slotted-plate projector was the first attempt of HUSL to build a projector of this type. Though its performance was not outstanding, it served a very useful purpose in the general development program, since it was the first transducer on which an analysis was made based on both impedance and acoustic measurements. Impedance curves in air and in water are shown in Figures 14 and 15, and the derived motional impedance circles in Figures 16 and 17. The rather large deviations of the measured points from the plotted curves will be noted. This is explained by two sources of experimental error that were not recognized in the

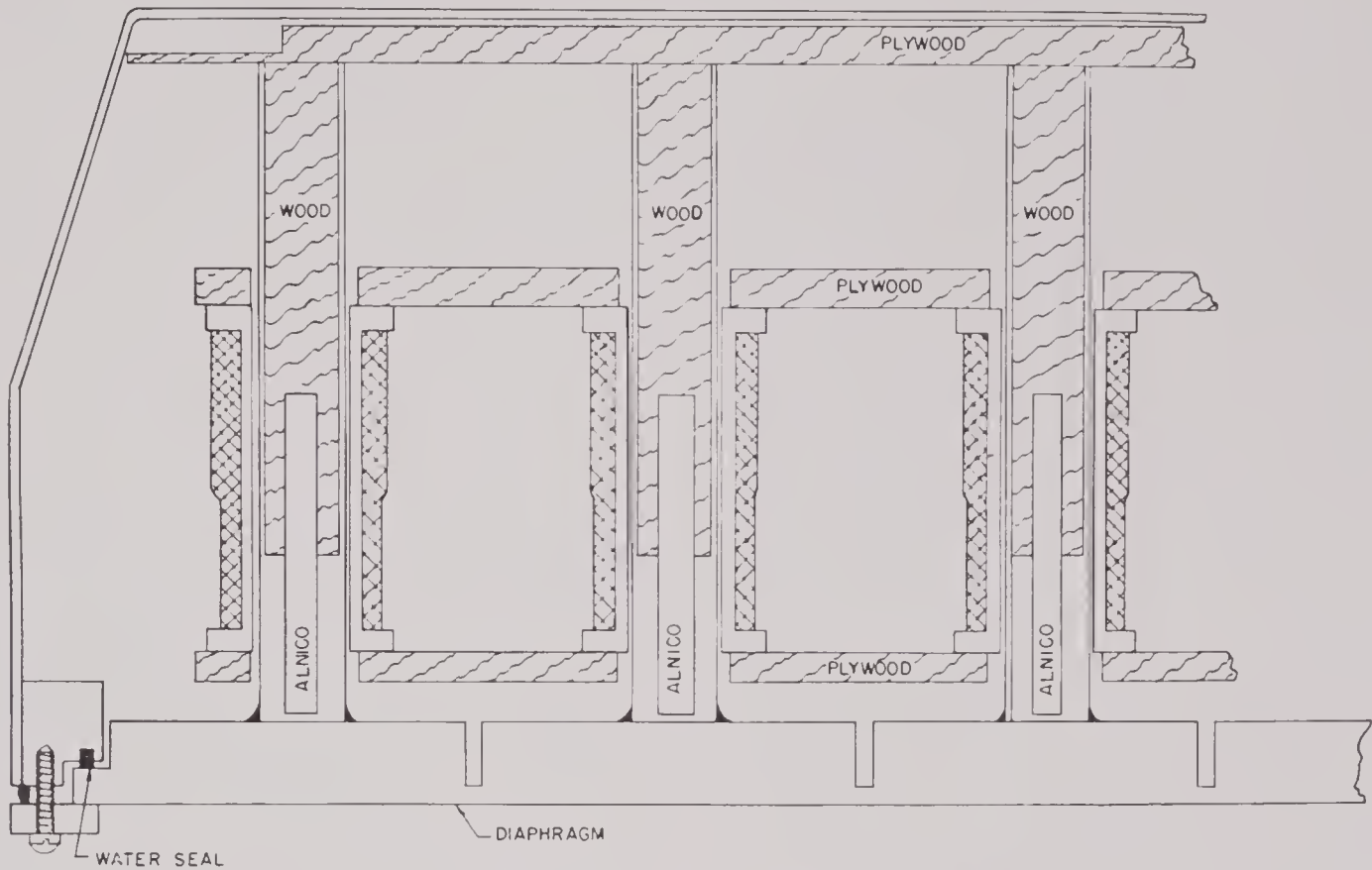


FIGURE 12. Section of the 12 x 12-in. tube and slotted-plate transducer.

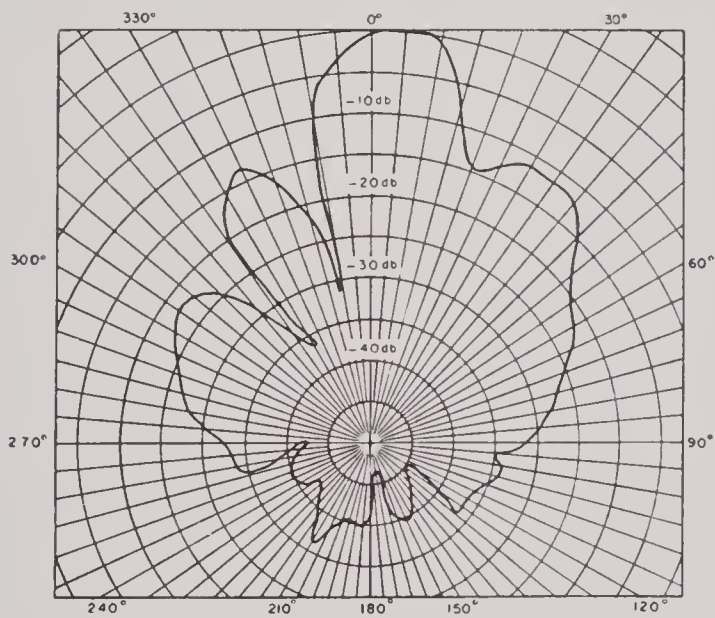


FIGURE 13. Pattern of 12 x 12-in. transducer.

early stages of this work. The first was due to lack of precision in the assigned value of the frequencies, and the second arose from the variation with frequency of water-loading due to the standing waves in the tank.

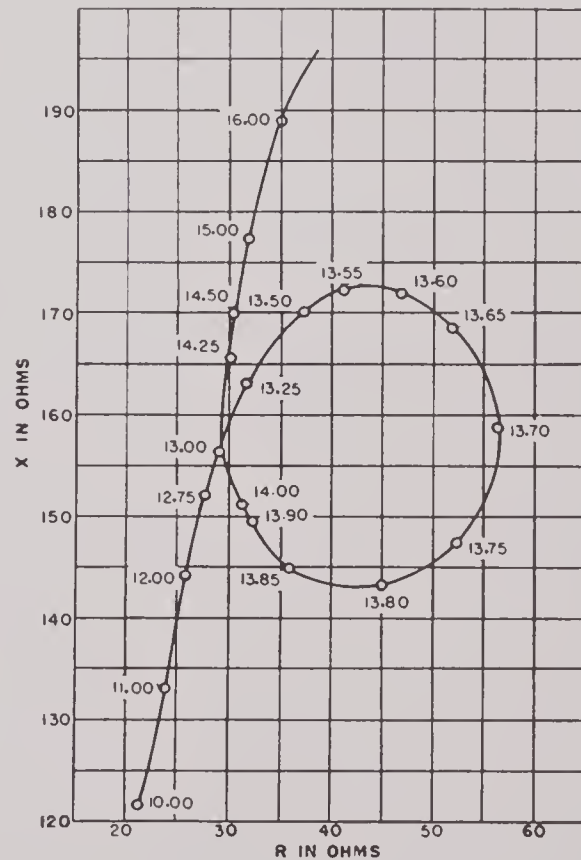


FIGURE 14. Impedance curve of 12 x 12-in. transducer in air.

CONFIDENTIAL

3.5

QC PROJECTORS

The tube-and-plate projectors used by the Navy for echo-ranging are designated as the QC type; in this classification are included a large number of subtypes all operating on the same general principle but with various modifications in detail. The QCL illustrates the construction used. It is designed to operate at 20 kc and is housed in a spherical chamber

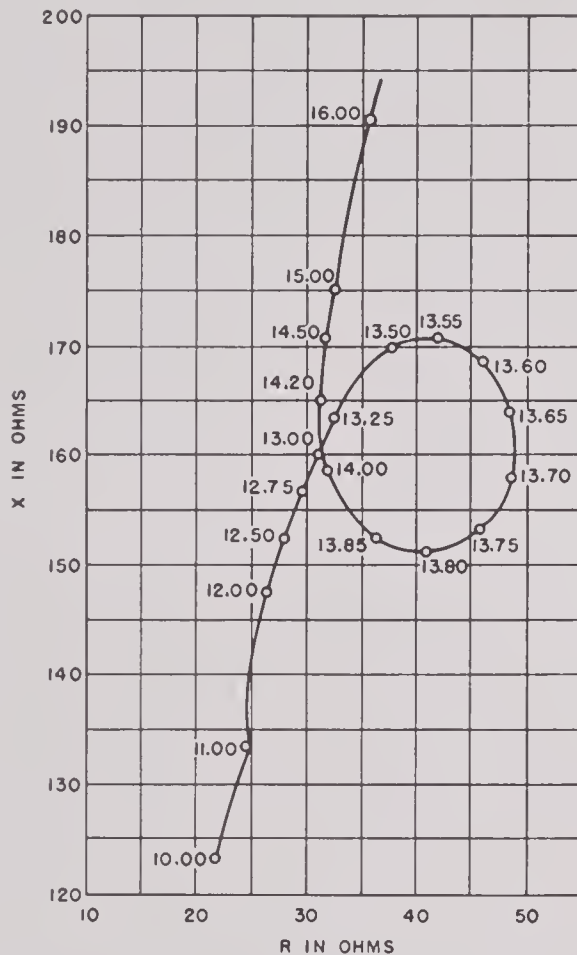


FIGURE 15. Impedance curve of 12 x 12-in. transducer in water.

19 in. in diameter with a front half of stainless steel 0.040 in. thick. The rear portion of the housing is of heavy cast iron with internal ribs. Both front and back portions are fastened to a heavy midsection of cast iron in which the projector itself is mounted. The latter is a steel plate 1 in. thick and 16 in. in diameter to which are firmly attached 608 nickel tubes each 0.25 in. in outside diameter with 0.025-in. wall. Each tube extends 2.563 in. from the face of the plate. The diaphragm is held in the housing by a gasketed clamping ring. The space between the front face of the diaphragm and the thin front cover of the hous-

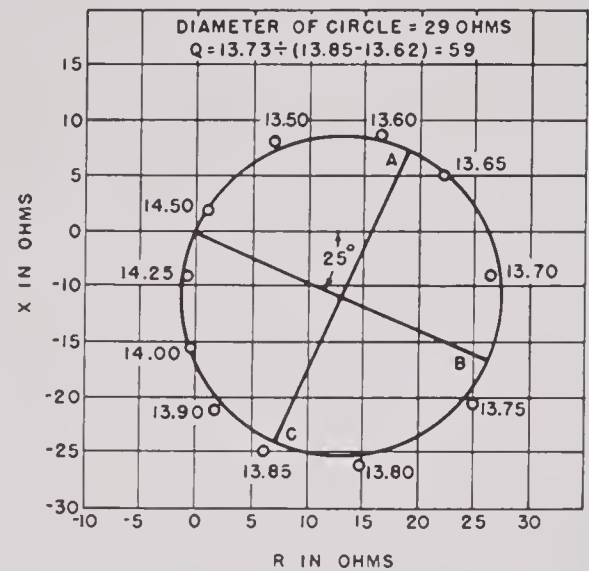


FIGURE 16. Motional impedance circle of 12 x 12-in. transducer in air.

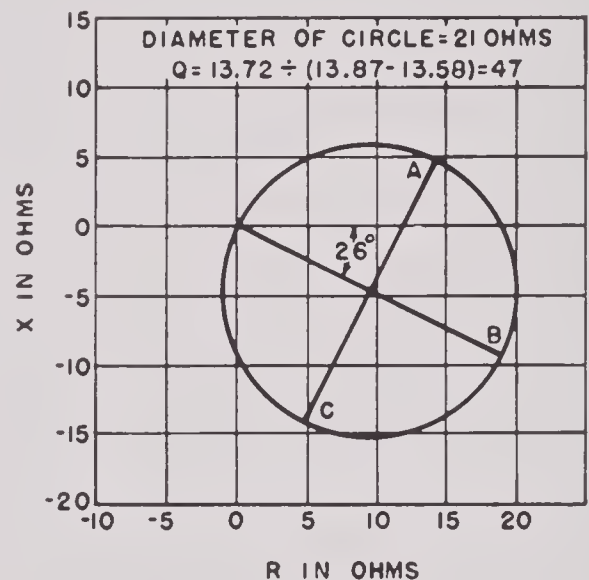


FIGURE 17. Motional impedance circle of 12 x 12-in. transducer in water.

ing is filled with a mixture of ethylene glycol and water.

All the tubes in each vertical row have coils with the same number of turns, but the number of turns per coil increases from a minimum for the outer rows to a maximum for the center rows. The coils on each half are connected in series, with the two halves connected in parallel. A 75-volt d-c power source supplies 6.8 amp of polarizing current through a choke coil in a filter junction box. Tuning condensers tune out the reactive component of the impedance, giving a pure resistance of approximately 100 ohms at 20-ke resonance.

CONFIDENTIAL

3.6 STUDIES AT BELL TELEPHONE LABORATORIES

A study of the QCL transducer was made at the Bell Telephone Laboratories²⁴; results appear in a final report to the Bureau of Ships on Task No. 4B. The work on this task was directed to the development of a magnetostrictive projector unit interchangeable with the standard QC projector but with greater band width in order to eliminate the sharp tuning required for efficient operation of a highly resonant transducer. A comprehensive theoretical study of the

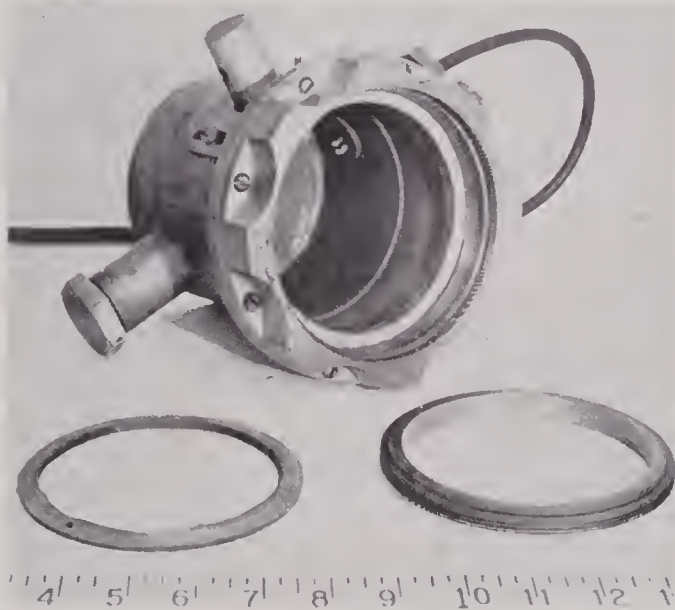


FIGURE 18. Mounting for small-scale tests of tube-and-plate transducers (BTL).

tube-and-plate type of transducer was made. This was supplemented by the construction and testing of a considerable number of small-scale model units and ultimately by a full-sized unit, XI-100, embodying the results of the theoretical and experimental studies.

For the small-scale tests the models were mounted in a test chamber of the type shown in Figure 18. This accommodated a diaphragm 4 $\frac{5}{8}$ in. in diameter, mounted in the front flange and clamped between rubber gaskets by means of the clamping ring shown. Measurements were made in an absorbent-lined tank.²³ The power input was either 1 watt or 0.1 watt, and response and pattern measurements were made at a distance of about 14 in., using a calibrated pressure gradient hydrophone. A typical model is shown in Figure 19. The tube-and-plate assembly for the full-scale unit is shown in Figure 20.



FIGURE 19. Small-scale experimental model tube-and-plate transducer (BTL).

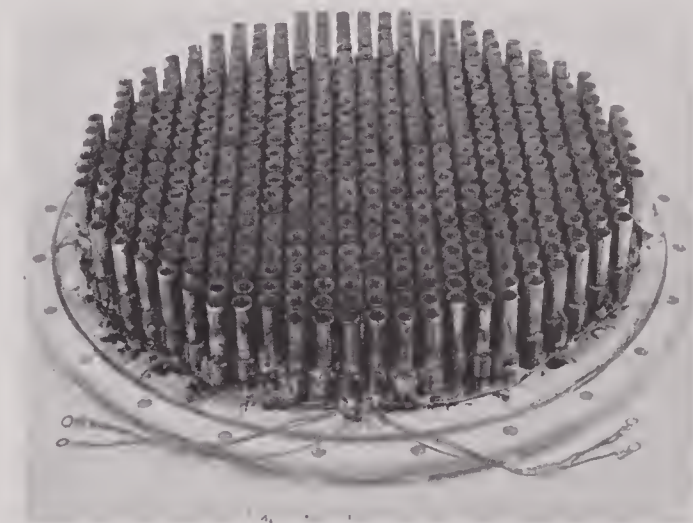


FIGURE 20. Tube-and-plate assembly for XI-100 experimental QC projector (BTL).

Descriptive data with measurements of performance are given in Table 2. Construction details, which may materially affect performance, are given in Figure 21. Note that the tubes were force-fitted into the thicker plates by means of taper plugs and were brazed onto the thin steel plate. The coils, impregnated with bakelite resin, were bonded directly to the tubes. In the QCL the coils are wound on thin-walled bakelite tubes, which slip loosely over the nickel

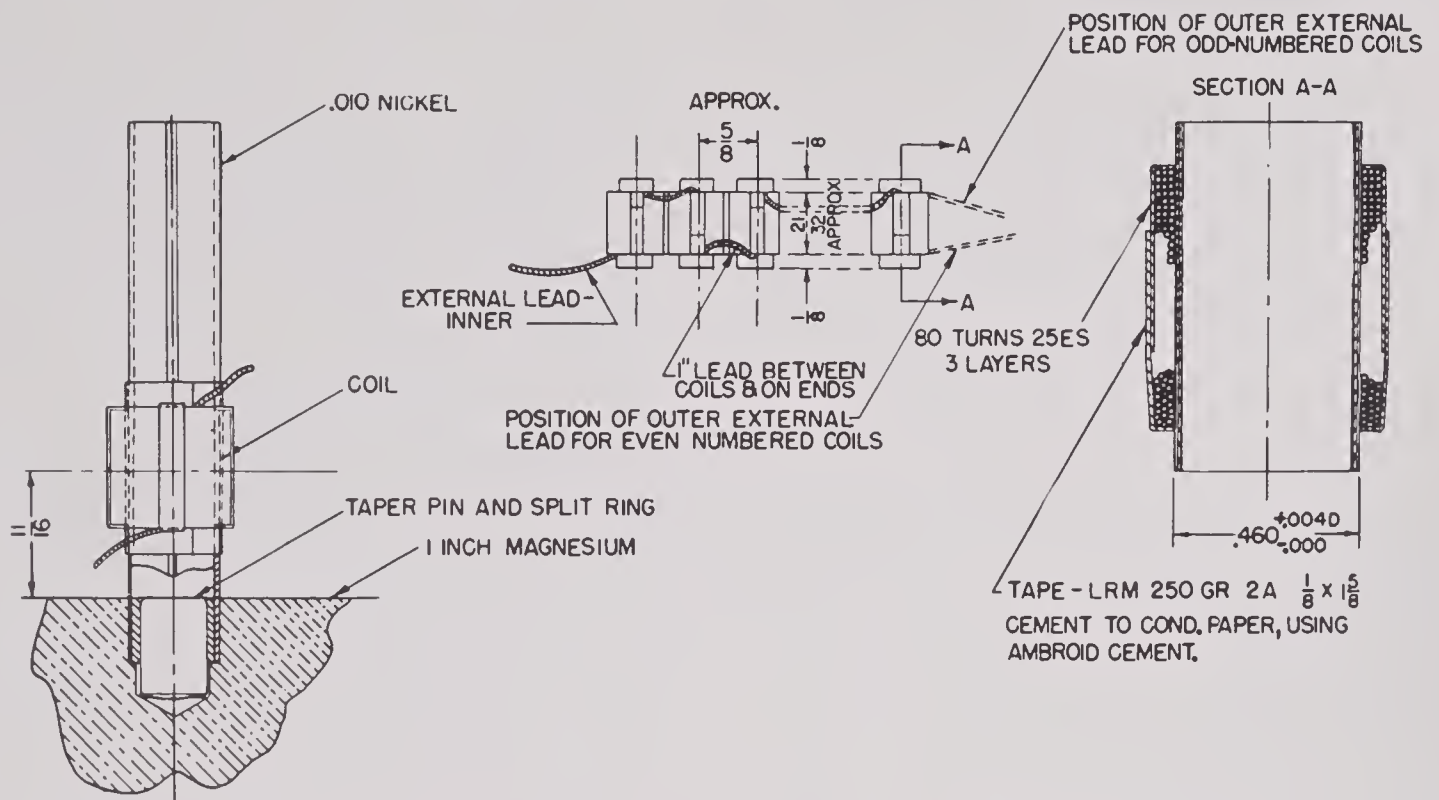


FIGURE 21. Details of tube-and-plate assembly for XI-100 (BTL).

TABLE 2. Data on BTL tube-and-plate experimental model projectors.

Model	Material	Thick- ness (inches)	No.	Ma- terial*	Wall (inches)	OD (inches)	$\frac{A_1}{A_2}$ †	Bias‡	Freq	Band- width§	Eff (db)	Eff (per cent)
XI-10	Magnesium	1	21	Ni	0.010	$\frac{1}{2}$	0.026	DC	18.5	1.9	-9.4	11.5
								PM	18.5	1.7	-8.5	14.
XI-15	Magnesium	$\frac{3}{4}$	21	V-P	0.010	$\frac{1}{2}$	0.026	DC	24.0	3.2	-10.0	10.
XI-20	Magnesium	1	44	Ni	0.006	$\frac{5}{16}$	0.021	DC	19.0	2.0	-12.6	5.5
XI-30	Magnesium	1	21	Py	0.010	$\frac{1}{2}$	0.026	DC	20.0	2.2	-7.4	18.
XI-40	Magnesium	$\frac{1}{2}$	21	Ni	0.006	$\frac{1}{2}$	0.016	DC	17.2	3.2	-12.7	5.5
XI-50	Steel	$\frac{1}{8}$	21	Ni	0.010	$\frac{1}{2}$	0.026	DC	25.0	3.0	-9.6	11.
XI-60	Magnesium	$\frac{3}{4}$	21	Ni	0.010	$\frac{1}{2}$	0.026	DC	23.0	2.8	-8.3	15.
								PM	23.5	3.5	-9.7	10.5
XJ-20	Polystyrene	$\frac{9}{16}$	12	Ni	0.012¶	$\frac{1}{2}$	0.036	DC	28.0	10.0	-12.7	5.5
								PM	28.0	10.6	-13.0	5.
XJ-30	Polystyrene	$\frac{3}{4}$	12	Ni	0.006	$\frac{1}{2}$	0.009	DC	22.0	...	-17.2	1.7
XJ-40	Lucite	$\frac{3}{4}$	12	Ni	0.006	$\frac{1}{2}$	0.018	DC	22.5	7.0	-11.8	6.5

* Ni: nickel; V-P: vanadium-Permendur.

† A_1/A_2 : ratio of cross-sectional area of tubes to that of diaphragm.

‡ DC: direct current; PM: permanent magnet.

§ 3 db below peak response.

|| Diameter of radiating surface is 2.84 inches; for other models, 4 inches.

¶ 6 layers of tape 0.002 in. thick.

tubes and rest directly on the plate. In the experimental models, the loading of the tubes by the coils lowered the resonant frequency appreciably and quite possibly had some effect on increasing the band width. Various inferences are drawn from the data. Models XI-10 and XI-20 differ in wall thickness of the tubes, 0.010 in. and 0.006 in. respectively, but the closer spacing of the latter yields about the same ratio of cross-sectional area of nickel to cross-sectional

tional area of the diaphragm as in the former. The band width was the same for the two, but the efficiency of the thin-walled model was about 3 db (50 per cent lower). The efficiency of both units is lower than the efficiency computed for a closed magnetic return path. It was concluded that flux leakage materially reduces the effective value of the magnetostrictive constant and that this reduction is greater for thin-walled than for thicker-walled tubes. A wall

CONFIDENTIAL

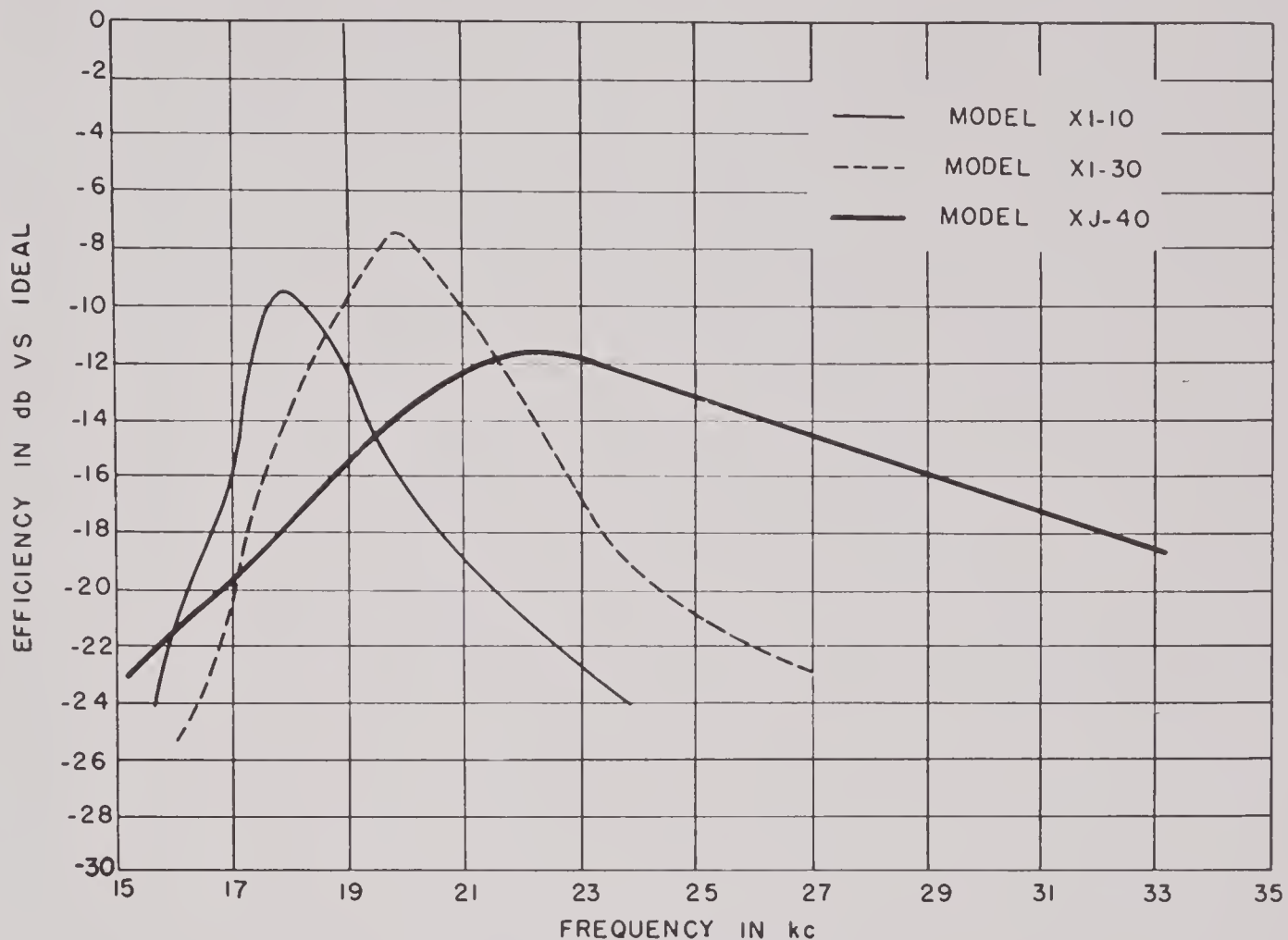


FIGURE 22. Efficiency of three experimental projector models (BTL).

thickness of 0.010 in. was suggested as a good compromise between the low eddy-current requirement calling for thin tubes and the desideratum of low flux leakage, which calls for thicker walls.

Model XI-40 represents a second attempt to use the 0.006-in. tubes. Here the tubes are larger, the spacing greater than in XI-20, and the decreased mass of nickel is partly offset by a diaphragm of half the thickness. The efficiencies of XI-20 and XI-40 are similar, as they should be theoretically, but lower than that of the units with the 0.010-in. tubes.

Model XI-60 is like XI-10 but has a thinner diaphragm. It shows a somewhat greater band width but similar efficiency. BTL ascribes this variation to a difference in coil design. In Model XI-10 the coil was concentrated near the node, whereas in XI-60 the coil extended over the lower half of the tube.

There may be a question as to whether increased band width without loss of efficiency is to be ascribed wholly to the change in coil design. Increased band width with decreased plate thickness is to be expected from both theory and experiment. Decrease

in the diaphragm thickness moves the nodal plane of the tube towards the free end, raising the resonant frequency. The maximum change of magnetization in the tube occurs at the node; therefore, to extend the coil along the tube away from the conducting surface of the diaphragm would tend to increase the alternating flux leakage through the coil, hence increase the electromechanical coupling and the efficiency. To follow this line of reasoning, the greater band width of XI-60 as compared with XI-10 would be ascribed to decreased plate thickness, and its undiminished efficiency to the change in coil design. Before conclusions are drawn, however, experiments in which the parameters are varied one at a time are desirable.

Magnetostrictive tubes of nickel, Permalloy, and vanadium Permendur were used. In comparing XI-10 and XI-30, increases in both bandwidth and efficiency are noted with the Permalloy tubes. BTL suggests that some slight improvement might be expected in the performance of transducers of the XI-100 type with the use of 45-Permalloy, which has

CONFIDENTIAL

higher permeability and a resulting reduction in leakage flux. Analysis of impedance data, however, indicates that this improvement would be very slight.

A very close agreement is shown between the performance data of XI-15 with a $\frac{3}{4}$ -in. magnesium diaphragm and XI-50 with a diaphragm of $\frac{1}{8}$ -in. steel, which indicates that a projector similar in performance to the XI-100 with a thin steel diaphragm is a possibility. However, there is the possibility that flexural modes of vibration would be excited in a $\frac{1}{8}$ -in. steel plate of QC diameter.

Of the three plastic models, the best performance is that of the XJ-40. This is a transducer of simple construction with wide-band response, but its efficiency is somewhat low for an echo-ranging projector. Responses of three of these experimental models are shown in Figure 22.

8.7 QC-TYPE PROJECTOR WITH MAGNESIUM PLATE

The full-scale model XI-100 was similar in tube-and-plate construction to the small model XI-10. The diaphragm was of cast magnesium alloy 4, ASTM specification B-80. The split tubes were made from formed sheet A-nickel 0.10 in. thick, annealed at 1000 C. Each tube had a $\frac{7}{16}$ -in. inside diameter. Tubes, 448 in all, were arranged in square pattern on $\frac{5}{8}$ -in. centers and were secured in the plate by means of a forced fit, using tapered pins. Coils were impregnated with bakelite resin BR-0014 and bonded to the tubes. Each coil had 80 turns of No. 25 es wire. The housing was essentially the same as that of the QCL. Transmitting responses of the XI-100, the QCL, and the QCU projectors are shown in Figure 23.

8.8 COMPARISON OF DIFFERENT QC MODELS

Tables 3 and 4 contain data on QC projectors that have been used by the Navy as well as experimental modifications of some of them. Structurally they all bear a close family resemblance to the QCL described in an earlier section. A similar resemblance is to be noted in their performance data.

The coils in the QGA^a units are carried free from the tubes and plates, with the windings crowded close to the motion nodes of the tubes. The permanent magnets are tightly fitted at one end within a soft-

^a Information on QCA projectors furnished by E. E. Turner, Jr., of the Submarine Signal Company, Boston, Mass.

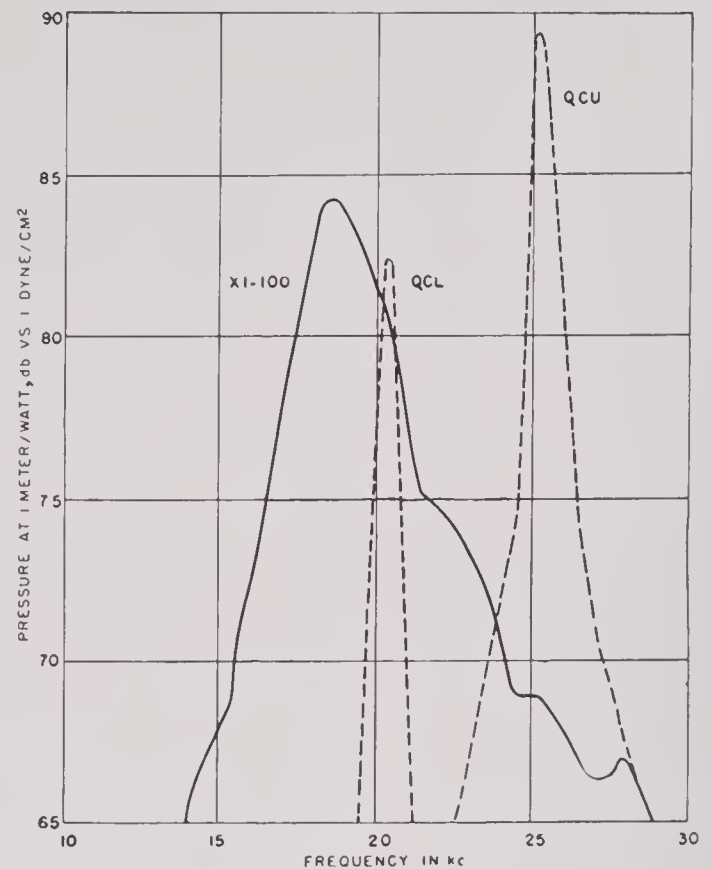


FIGURE 23. Transmitting response of three QC-type projectors (BTL).

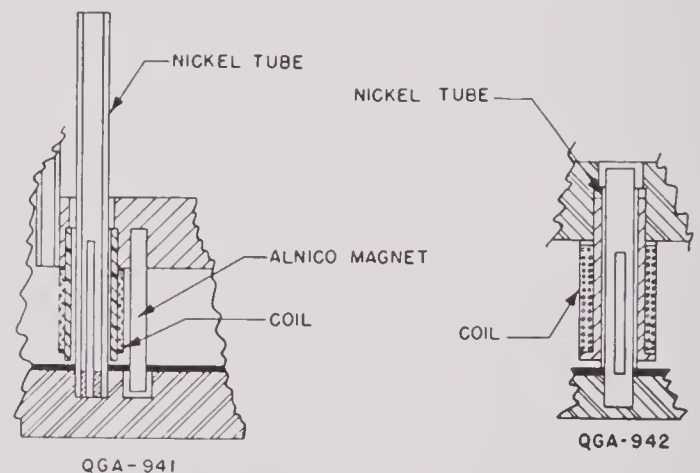


FIGURE 24. Assembly detail of tube, coil, and magnet in the QGA projectors (Submarine Signal Company).

iron distributing plate with the opposite ends projecting into recesses in the diaphragm plate, allowing a small radial air gap between magnets and plates. The arrangement is shown in Figure 24.

In the QCU units,²⁰ the biasing magnetization is supplied by heavy Alnico slabs backing the soft-iron distributing plate. The return magnetic path is by way of the plate and the steel of the supporting ring.

TABLE 3. Descriptive data on tube-and-plate projectors.

Projector	Plate			Tubes			
	material	thickness (inches)	effective diameter (inches)	number	length (inches)	OD (inches)	wall (inches)
1. QCL	Steel	1	15	608	2.5	0.25	0.025
2. QGA Type 941	Steel	$\frac{3}{4}$	16	424	3.58	0.25	0.025
3. QGA Type 942	Steel	$\frac{3}{8}$	12	256	1.69	0.25	0.025
4. QCU Production	Steel	$\frac{5}{8}$	$11\frac{7}{8}$	182	2.04
5. QCU No. 1 Experimental	Steel	$\frac{3}{4}$ (?)	$11\frac{7}{8}$	152 laminated stacks $0.15 \times 0.15 \times 2.04$, diaphragm slotted			
6. QCU No. 2 Experimental	Steel	$\frac{3}{4}$ (?)	$11\frac{7}{8}$	Same as No. 5, but diaphragm not slotted			
7. QCU No. 3 Experimental	Steel	$\frac{7}{8}$	$11\frac{7}{8}$	182	2.04
8. XI-100	Magnesium	1	15	448*	2.5	0.63	0.010

* Split tubes; all others slotted.

TABLE 4. Performance data of QC-type projectors.

Type	Resonant frequency (kc)	Impedance at resonance	Sensitivity (db)	Directivity (db)	Q	$\frac{A_1}{A_2}$	Bandwidth (kc)	Efficiency as projector (db)	Efficiency (per cent)
QCL*	20.4	$34 + j69.5$	- 85	- 21	41	0.066	0.5	- 9.5	11
QGA Type 941†	14.8	$120 + j285$	- 76	- 18.2	38	0.037	0.4	- 8.0	16
QGA Type 942‡	30.5	$130 + j235$	- 76.4	- 23.2	24	0.04	1.27	- 7.5	18
QCU Production§	25.4	$33.8 + j117$	- 80.5	- 22.5	80	...	0.3	- 3.8	42
QCU No. 1 Experimental	24.3	$98 + j218$	- 69.8	- 23.6	81	0.031	0.3	- 3.0	50
QCU No. 2 Experimental	24.2	$103 + j235$	- 68.2	- 23.3	97	0.031	0.24	- 2.5	56
QCU No. 3 Experimental	25.4	...	- 81.5	- 22.5	100	...	0.25	- 4.5	35
XI-100 Experimental	18.5	- 23.2	7.4	0.026	2.5	- 9.7	10.7

* NDRC Report Sec. 6.1 sr 20-889.

† NDRC Report Sec. 6.1 sr 1130-1626.

‡ NDRC Report Sec. 6.1 sr 1130-1379.

§ NDRC Report Sec. 6.1 sr 1130-2138.

|| BTL Report on Task 4B, BuShips No. NX sr 46932.

Sensitivity: ref. 1 volt/dyne/cm².Directivity (db): $10 \log D$.A₁, A₂: ratio of area of nickel to area of plate.

It will be observed that in all projectors of this type the reluctance of the magnetic path for the a-c flux is high, because of the low permeability of Alnico. Moreover, high losses are to be expected because of eddy currents induced in the massive metal of the plates.

Experimental QCU Models 1 and 2 (Figure 25) had laminated stacks instead of tubes as the driving elements. These were soldered to lugs that screwed into the diaphragm plate. In Model 1, the plate was divided by milled slots into square segments each about $1\frac{1}{2} \times 1\frac{1}{2}$ in. Each segment carried four stacks, to which coils were cemented directly. In Model 2 the diaphragm was not slotted.

As has been noted, the XI-100 experimental variant is distinguished by having a 1-in. magnesium plate and thinner-walled tubes with attached coils. The magnetizing bias was given by d-c current.

Inspection of Table 4 discloses a fairly definite correlation between sharpness of resonance and efficiency. For Q 's of 40 or less, efficiencies at resonance

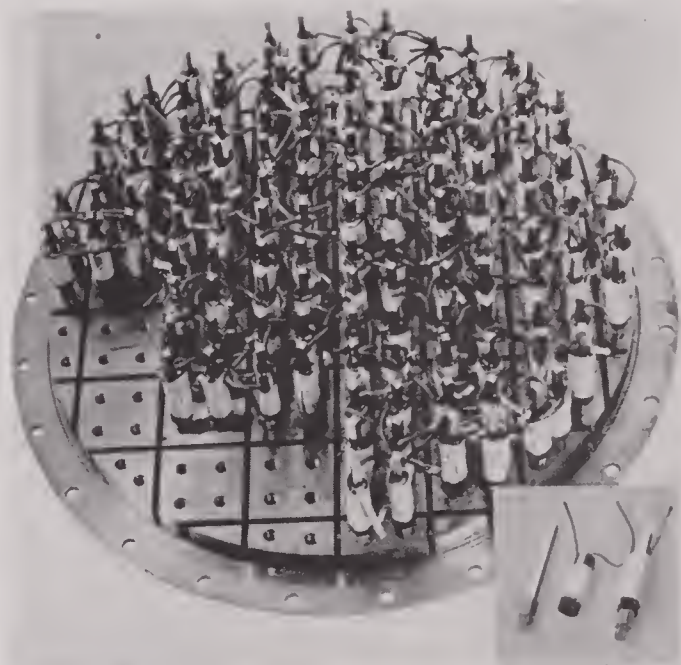


FIGURE 25. Plate and laminated stack assembly of experimental QCU projectors.

CONFIDENTIAL

lie between 10 and 20 per cent, while the higher efficiencies are associated with Q 's of 80 to 100. These values are typical of the general performance of projectors of this type and would seem to be inherent in the low electromechanical coupling of the design. Calculations cited in the BTL report indicate values for this quantity one-tenth to one-third as great as would be shown if a closed magnetic circuit were assumed.

8.9 MAGNETIC CIRCUIT IN TUBE-AND-PLATE TRANSDUCERS

Various methods of producing the biasing magnetization of the magnetostrictive tubes have been indicated in previous sections. Perhaps somewhat more detailed consideration should be given to the magnetic circuits of these methods.

In the earliest tube-and-plate transducers, magnetic polarization was secured by passing d-c current through the windings. In the simplest case, the return path was through the air outside the tube. The reluctance of the thin-walled tube and the air path is consequently high, and more than 80 ampere turns per inch of tube are needed to give the required d-c magnetization of the nickel. This may be reduced by allowing the free ends of the tubes to project into holes in a steel plate (without touching it), so that the d-c path consists of all the tubes in parallel, the steel sides of the housing, and the steel diaphragm plate. This method has the added advantage that the polarizing flux is parallel to the direction of strain in the region of the node near the plate where the strain is maximum.

When the polarization is supplied by small permanent magnets placed inside the tube, the pole nearest the plate should extend as far as possible below the

nodal plane, so that the polarizing flux at the node may be as large as possible and parallel to the axis of the tube. Eddy-current losses in the magnet can be made negligible by copper coating to supply an eddy-current shield.

Another method of using small magnets is indicated in Figure 24. Here a single magnet is placed at the center of the square array of the four driving tubes that surround it. The extension of the magnets into the recesses in the diaphragm plate decreases the reluctance of the d-c flux path and also reduces the eddy currents that would otherwise be generated in the plate due to its high frequency motion.

Where the polarization is supplied by Alnico slabs as in the QCU, the Alnico is polarized in the direction of the tube length after the transducer is assembled. The polarizing flux threads through all the tubes in parallel, through the distributing plate, the Alnico magnet, the steel housing of the transducer, the steel diaphragm, and back through the tubes again. Obviously the distributing plate must be magnetically isolated from the steel housing, otherwise only a small portion of the total flux would pass through the tubes.

Because of the shielding effect of eddy currents in the tubes, at high frequencies their effective cross-sectional area is less than their actual cross section. This effect has been discussed in Section 3.1 of Chapter 3, where it is shown that slotting the tubes gives a higher degree of electromechanical coupling from a given cross section of nickel. It has been suggested that some decrease in the reluctance of the return path for the a-c flux can be effected by attaching small packets of thin laminations of highly permeable material, such as silicon steel, to the outside of the windings with the length of the packet parallel to the tubes.

Chapter 9

MEASUREMENT OF ELECTRICAL CHARACTERISTICS

9. 1

INTRODUCTION

Much of the performance data of a mechanically resonant transducer can be most readily obtained from the locus of its vector impedance or admittance. With a large program of developmental work on transducers such as the Harvard Underwater Sound Laboratory has carried on, facilities for making reliable electrical measurements should be maintained. This chapter includes the measurement techniques employed and the design and construction of the electrical measuring equipment used at HUSL.

In the fall of 1942, several of the HUSL staff were assigned the task of making electrical measurements on the various transducers being developed. This work consisted mainly of the measurement of the electric impedance of these transducers with both air and water loading. The water loading was effected by immersing the transducer in water in a steel tank 9 ft long, 4 ft wide, and 2½ ft deep. General Radio Company's Type 516-C radio-frequency bridge with considerable accessory apparatus was first used in making these measurements. Under these conditions two sources of large error appeared. The wide range of impedances to be measured required the use of external variable resistance and capacitance standards with the bridge, and the capacities of these boxes to ground could not be compensated. Furthermore, reflections occurring at the steel walls of the tank gave rise to standing wave patterns that caused significant error in the apparent impedance of the transducer.

In June 1943, an absorbent-lined tank was received from the Bell Telephone Laboratories and proved to be a considerable improvement over the steel tank.²⁹ Simultaneously, an impedance bridge designed to replace the GR bridge was constructed and assembled in a console. Completed in August 1943, this bridge was of the series-tuned arm, equal-ratio arm, Wheatstone type. Since some error and inconvenience (especially in the measurement of impedance with negative phase angles) are inherent in this bridge circuit, a similar bridge with a parallel-

tuned arm was built. This bridge was finished in March 1944.

When the absorbent-lined tank was received, the necessary measuring equipment for obtaining patterns, frequency responses, and sensitivities of hydrophones was built with the hope of taking some of the work load from the HUSL Charles River barge. However, the tank proved too small for most of the transducers being tested, so that it was used chiefly in making measurements on developmental elements and transducers.

When HUSL began the construction of several types of multi-element transducers, it became necessary to test each of the individual elements. The *conductometer* was devised in October 1944 to provide a quick and accurate measurement of the impedance and resonant frequency of each element in air. The *vector impedance locus plotter* [VILP],²⁵ built in February 1945, grew out of the experience gained in building the conductometer. This device traces on a cathode-ray tube the vector impedance locus of a transducer (or any other impedance). It was hoped that with experimentation it could be made accurate enough to replace the bridges for impedance determination in all except the most precise measurements.

9. 2

IMPEDANCE MEASUREMENTS

9. 2. 1

General Requirements

Determination of the locus of the terminus of the vector impedance $Z = R + jX$ requires measurement of R and X at a number of frequencies; similarly the determination of the locus of the vector admittance $Y = G + jB$ requires the measurement of G and B . The value of information derived from these loci is proportional to the accuracy, reliability, and rapidity achieved in measurements of the quantities R , X , G , and B .

The nature of the loci and the information to be obtained therefrom, as well as the physical characteristics of the transducers and the conditions under

which they are to be measured, impose certain requirements on the method of making satisfactory measurements. These requirements are listed as follows.

Impedance Range. Measurements must be made of both resistance and reactance from 0.1 ohm to 10,000 ohms. The impedance loci of Figures 1, 2, and 3 illustrate the manner in which R and X may vary with frequency.

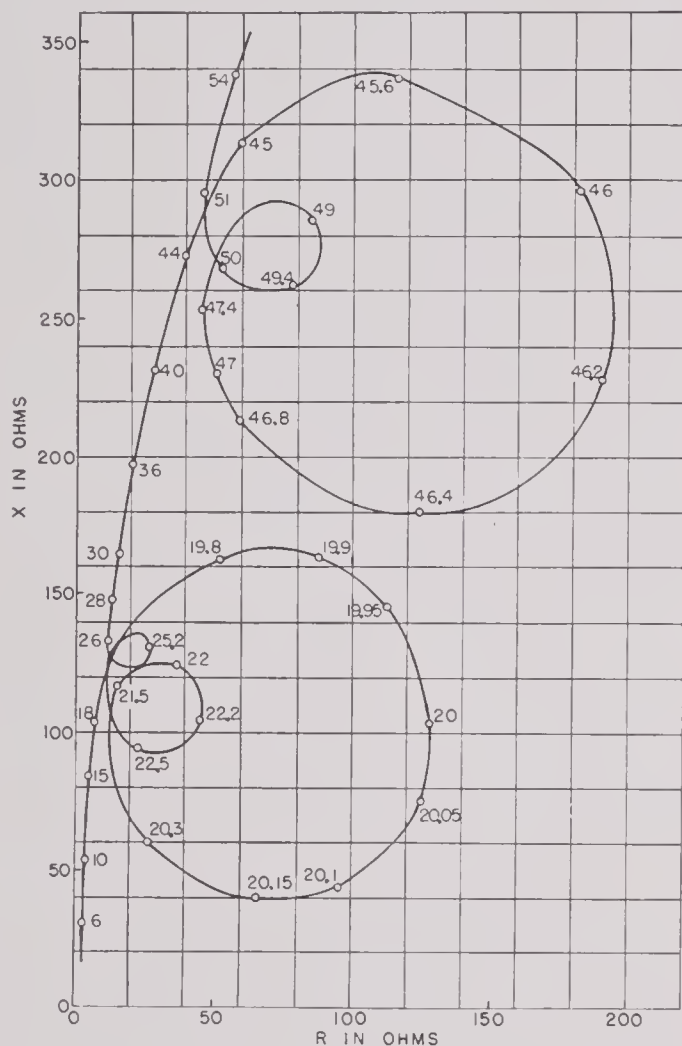


FIGURE 1. Impedance locus of magnetostrictive transducer in air.

Reactance Sign. Measurements must be made of both positive and negative reactances over the above range. With a change in frequency the reactance of a given transducer may remain positive, as shown in the magnetostrictive transducer of Figure 1; or may remain negative, as shown in the crystal transducer of Figure 3; or may change from positive to negative, as shown in the transducer of Figure 2. Because of the frequent occurrence of such a change in sign, the

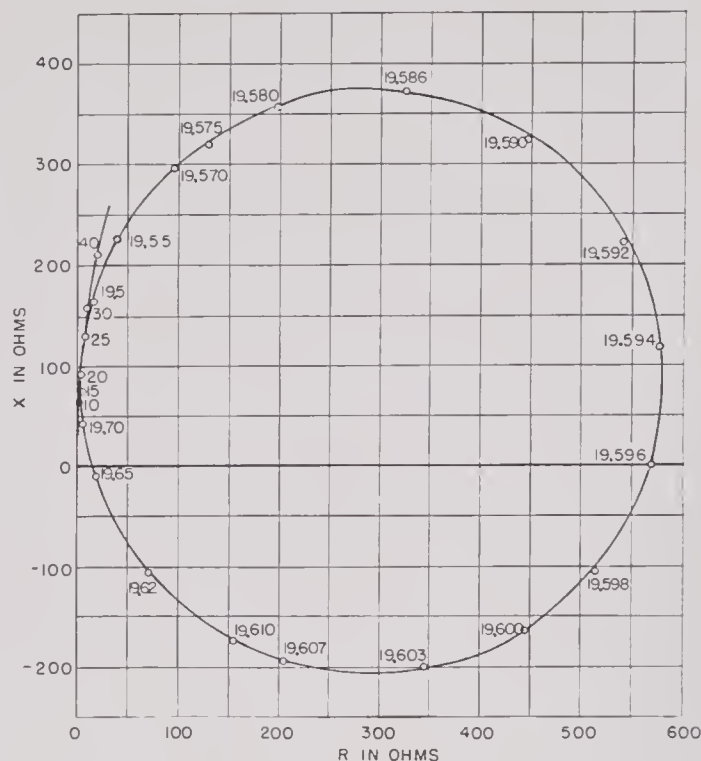


FIGURE 2. Impedance locus of magnetostrictive ring stack in air.

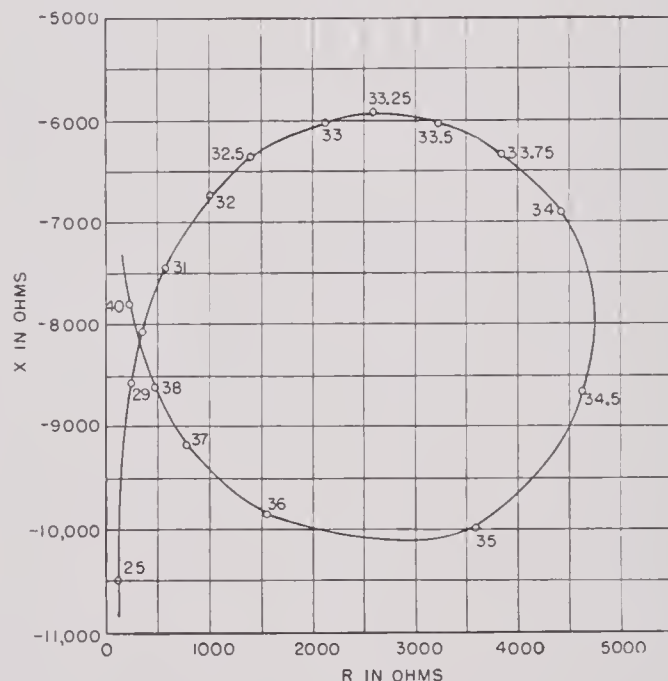


FIGURE 3. Impedance locus of mechanically resonant crystal transducer in air.

operations required to change from the measurement of inductance to the measurement of capacity should involve a minimum of alterations in method and apparatus with no loss in time or accuracy.

Frequency Range. Measurements must be made over the frequency range from 1 kc to 100 kc. Al-

though the resonant frequencies of most of the transducers fall within a smaller range, the determination of the core or clamped impedance requires measurements at frequencies considerably above and below resonance.

Accuracy. The measurements of both R and X must involve errors no greater than 1 per cent.

Ease of Operation and Computation. The measurements must be made easily and rapidly, and the

transducer in water. The conditions of measurements can be stated definitely enough to insure reproducible results only if one terminal of the transducer is grounded.

Superposed Direct Current. The measurements must sometimes be made with direct currents as high as 20 amp flowing through the transducers. This necessitates grounding one terminal.

Several methods of measurement can be found

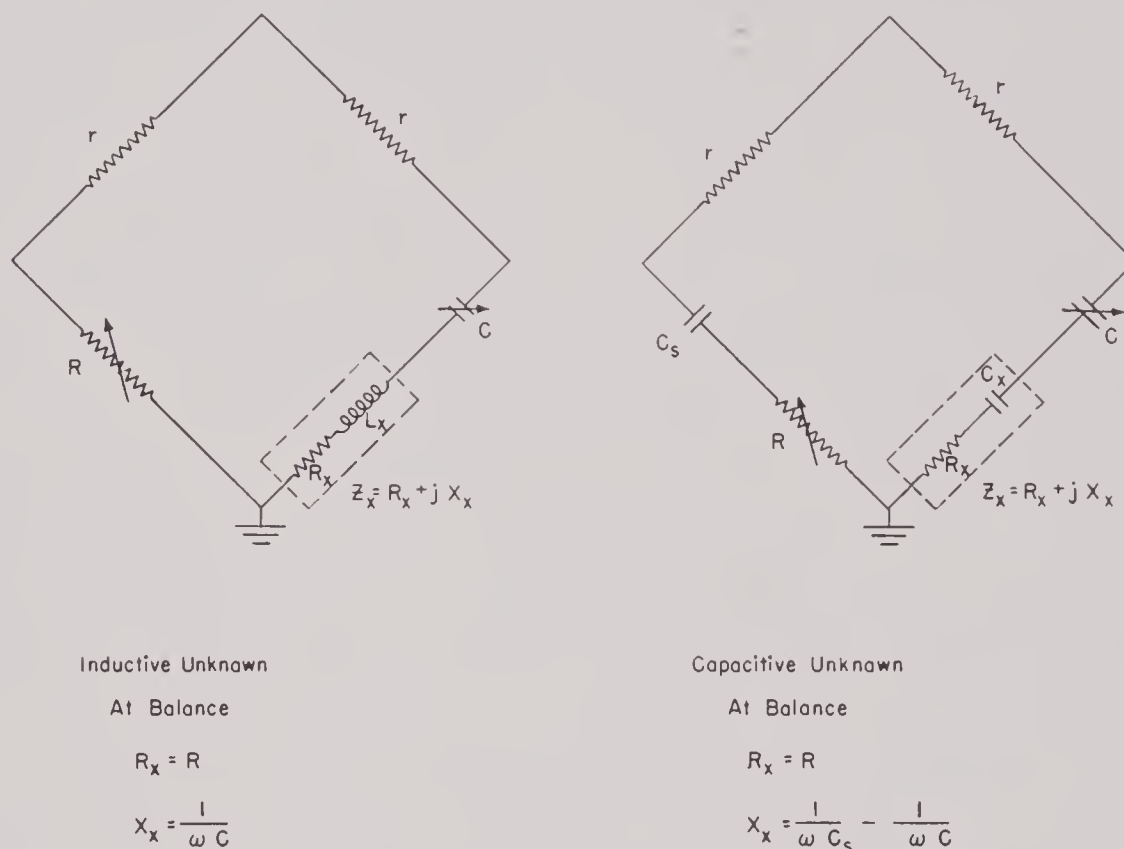


FIGURE 4. Impedance bridge.

operations involved in obtaining R and X from the observed data must require little time and effort and no sacrifice in accuracy. Because of the complexity of the loci (Figure 1), it is necessary to plot the locus as the measurements are made, in order to select those frequencies which will best define the locus with a minimum of measurements. For this reason, the ease and speed with which the loci can be determined are dependent on both the measuring operations and the computation and plotting operations.

Grounding the Unknown. The measurements must be made with one terminal of the unknown impedance grounded. The capacity to ground is not only large but variable, because of the large physical size of many transducers, the use of long cables with them, and the necessity for measurements with the

that satisfy these requirements in part, but it is difficult to satisfy all the requirements by a single method.

9.2.2. Measurement by Null Methods

BRIDGE METHODS

Types of Bridges. Consideration of the foregoing requirements results in the following choice of methods. The use of a null rather than a deflectional method is demanded by the accuracy required over a wide impedance range. Conventional bridge methods are applicable if considerable care is taken to remove sources of error. The superiority of variable capacitors over variable inductors both in range and in the magnitude and variation of residuals suggests that

reactances be measured in terms of a capacitance standard; satisfactory standards of capacitance and resistance are available to cover the required range of impedance and frequency. Measurements at supersonic frequencies, as well as easy operation, require that the bridge network be simple and symmetrical in order that the residuals may be controlled or eliminated. This involves the use of a ratio bridge rather than a product bridge and, in particular, an

attention must be paid to the residuals in order to obtain accurate values of resistance and reactance with the resonance bridge.

For the measurement of the impedance of inductive unknowns, the series-resonance bridge of Figure 4 is convenient. Here three of the branches are resistances and the fourth is a series-resonant circuit composed of the unknown and a variable condenser. When the ratio arms r are equal and balance is ob-

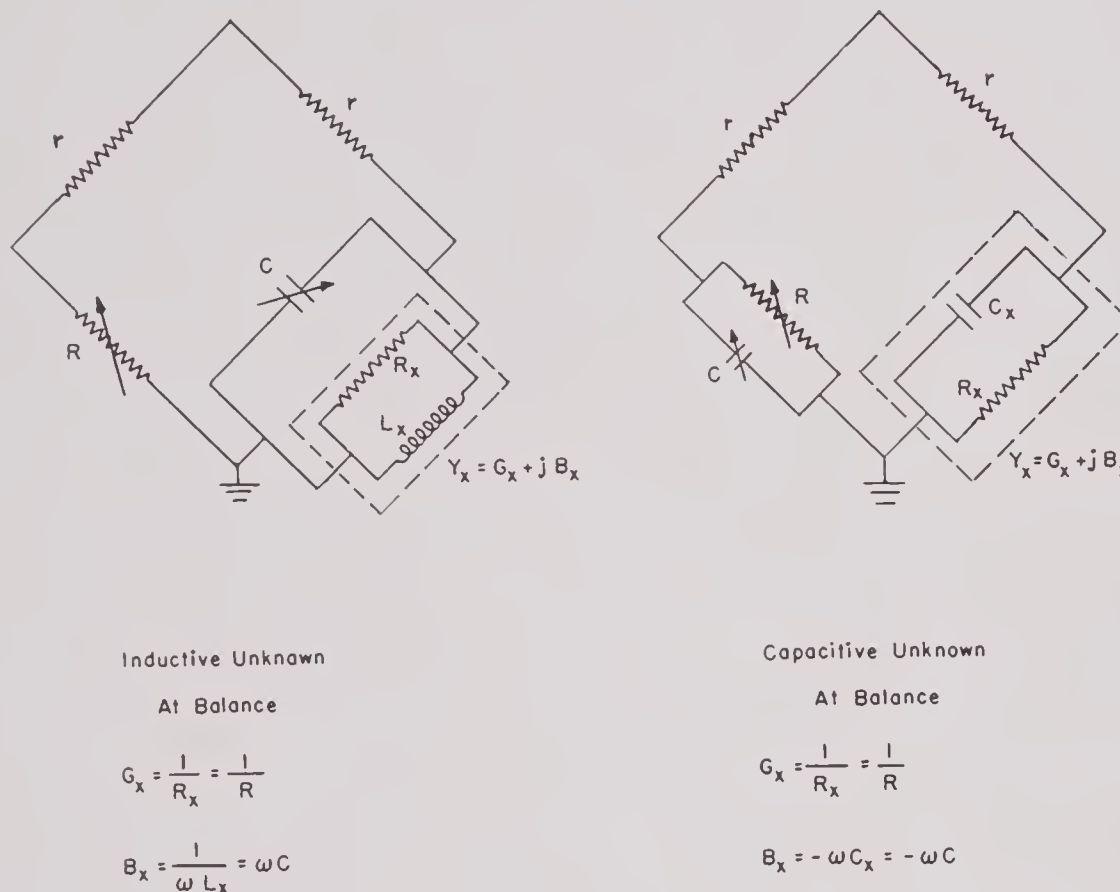


FIGURE 5. Admittance bridge.

equal-arm ratio bridge. In such a bridge circuit the unknown is compared directly with the standard, so that the bridge can be made direct-reading in terms of a resistance and capacitance equivalent to the unknown. Most of the residuals can be counterbalanced simply and permanently so that they do not affect the reading of the bridge; the others can be made negligibly small or can be offset by a constant correction.

The requirement that both resistance and reactance be measured to the same accuracy and preferably with a single balance of a bridge network requires the use of a resonance bridge. Since the residuals of a bridge network have more effect on the resistance measurement than on reactance, careful

tained by adjusting R and C , the variable standard resistor R reads directly the series resistance R_x of the unknown, while the reactance of the variable condenser C is equal to that of the unknown X_x . Thus only the calculation of the reactance from the value of C is necessary to determine the reactance of the unknown. Even though the ratio arms r are equal, the bridge network is not actually symmetrical because there is no point in the branch containing the variable resistor R to correspond to the junction point of the variable condenser C and the unknown. Stray capacities from this junction point may cause large errors, and, because of the lack of symmetry, compensation for these capacities is difficult. The form of bridge is convenient for measurements with

superposed direct current, since the tuning condenser C serves to block the direct current from other branches of the bridge network.

For the measurement of capacitive unknowns the series-resonance bridge becomes a form of capacity bridge by the addition of a condenser C_s in series with the variable resistor R . The balance is still obtained with R and C and the resistor R still reads the series resistance R_x of the unknown, but the reactance X_x of the unknown is the difference between the reactance of C_s and that of C . This requires two calculations and involves a loss in accuracy when the difference in the reactance is small compared to the magnitude of either C_s or C . Although there is in this network a junction point in the branch containing R , the network still lacks symmetry because the junction points in the two lower branches are not equivalent when the bridge is balanced. Since the branch containing the unknown suffers no alterations in the change from inductance to capacitance measurements, this form of capacity bridge is convenient because it retains the advantage of the series-resonance bridge for measurements with superposed direct current, and the change in bridges can be made without interrupting such a current.

If the unknown impedance is tuned by a parallel condenser instead of a series condenser, the network becomes the parallel-resonance bridge of Figure 5. The balance is still obtained by varying R and C , but at balance the value of R is now equal to the effective parallel resistance of the unknown. Since this bridge measures in terms of parallel equivalents, it is convenient to express the measurements in terms of admittance rather than impedance. For this reason the name *admittance bridge* has been applied to the parallel-resonance bridge and that of *impedance bridge* to the series-resonance bridge. The measurements obtained from either bridge, of course, can be expressed as impedance or admittance and the locus plotted in either form as desired.

For the measurement of capacitance the tuning condenser C has merely to be connected across the resistor R instead of across the unknown. This change is easily made and involves no additional components in the network. The condenser C reads directly the capacitance of the unknown with the same accuracy obtained in inductance measurements. Although, as in the impedance bridge, the change from measurement of inductance to measurement of capacitance involves no changes in the connections of the unknown, the admittance bridge in either

form provides no condenser to block direct current flowing through the unknown from entering the other network branches. Special provisions must be made for measurements with superposed direct current.

The parallel-resonance or admittance bridge has the great advantage of permitting one terminal of both R and C , as well as one terminal of the unknown, to be grounded. This eliminates the junction point which was the cause of asymmetry and the resulting

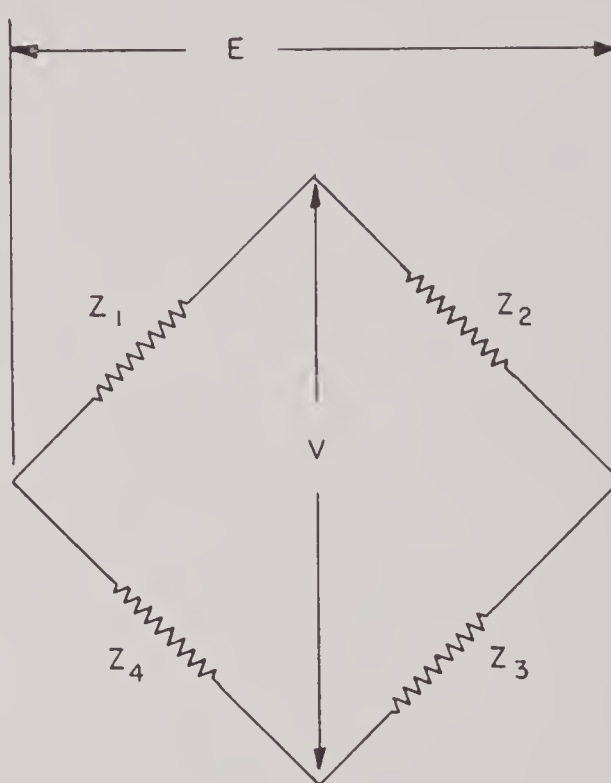


FIGURE 6. Wheatstone network.

difficulties in the impedance bridge network. As connected for the measurement of either inductance or capacitance, the parallel-resonance bridge network with equal ratio arms is truly symmetrical, with all the attendant advantages of symmetry. The chief advantage of a symmetrical bridge network is that all the residuals (but not the changes in residuals with a change in R or C) can be eliminated from the measurement by means of a preliminary balance of the bridge with the unknown disconnected. Thus all measurements become, in effect, substitution measurements, with accuracy limited by the accuracy of the variable standards.

In the measurement of inductance with either the impedance or admittance bridge, the lower limit of inductance that can be measured at a given frequency is determined by the maximum capacity available to tune the inductance; this maximum is

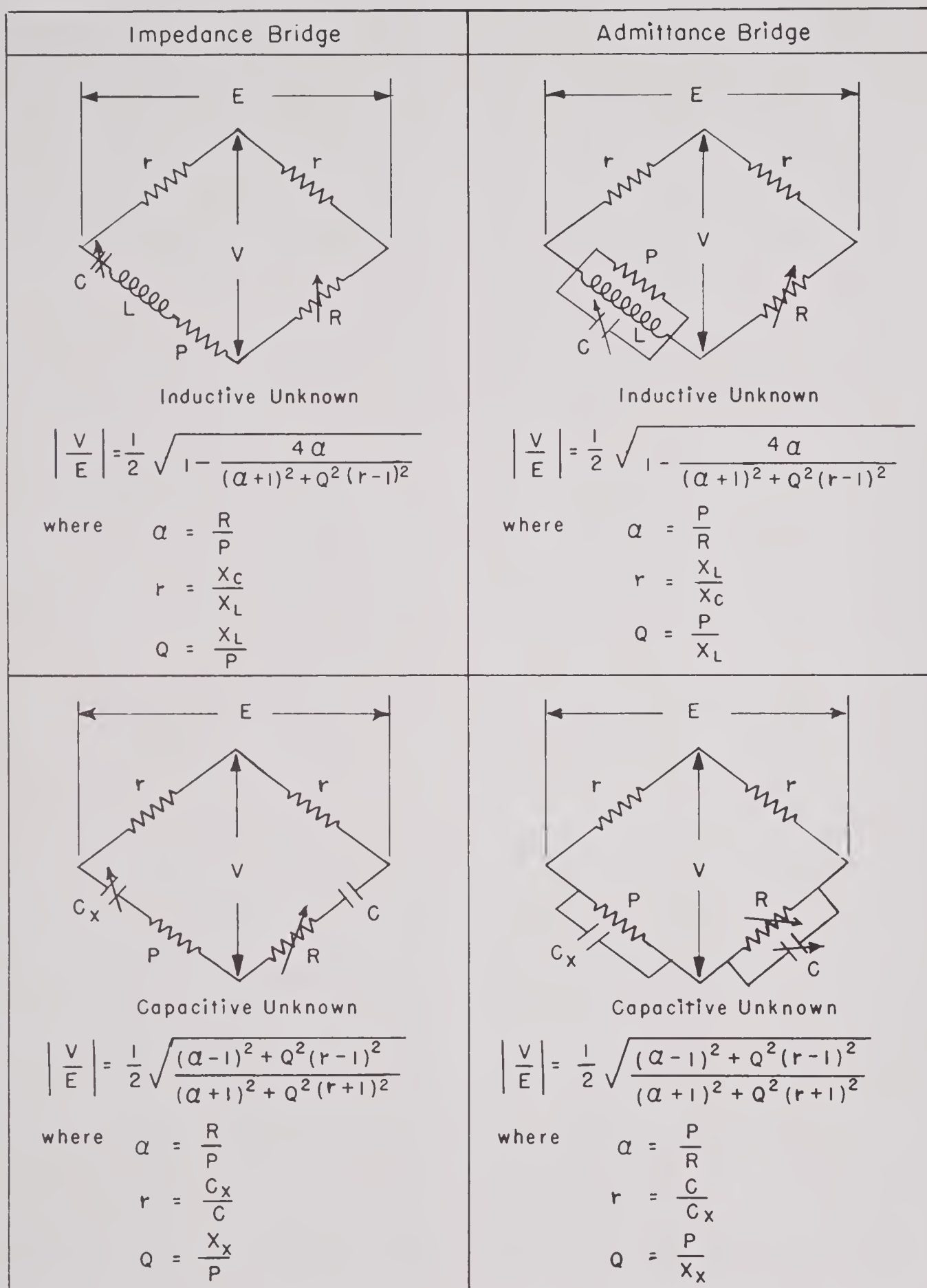


FIGURE 7. Equation applied to four bridge networks for determination of impedance and admittance loci.

CONFIDENTIAL

limited to a few microfarads since condensers of low dissipation are required. The upper limit of reactance, inductive or capacitive, is fixed in the impedance bridge by the errors due to residuals that cannot readily be eliminated from that network; in the admittance bridge this limit is determined by the accuracy of the standards employed. In both bridges the resistance is limited by the range of the decade resistor. In the impedance bridge the limit imposed by error due to dissipation in the condensers may set

source, and the detector are all equal to the impedance being measured. However, large deviations from this optimum condition can be tolerated in practice, since by the use of amplification in the detector the sensitivity of the bridge can be made more than adequate for the required accuracy of measurement. Hence the magnitude of the ratio arms need not be varied, and fixed resistors with accurately matched impedances can be used effectually as the equal-ratio arms.

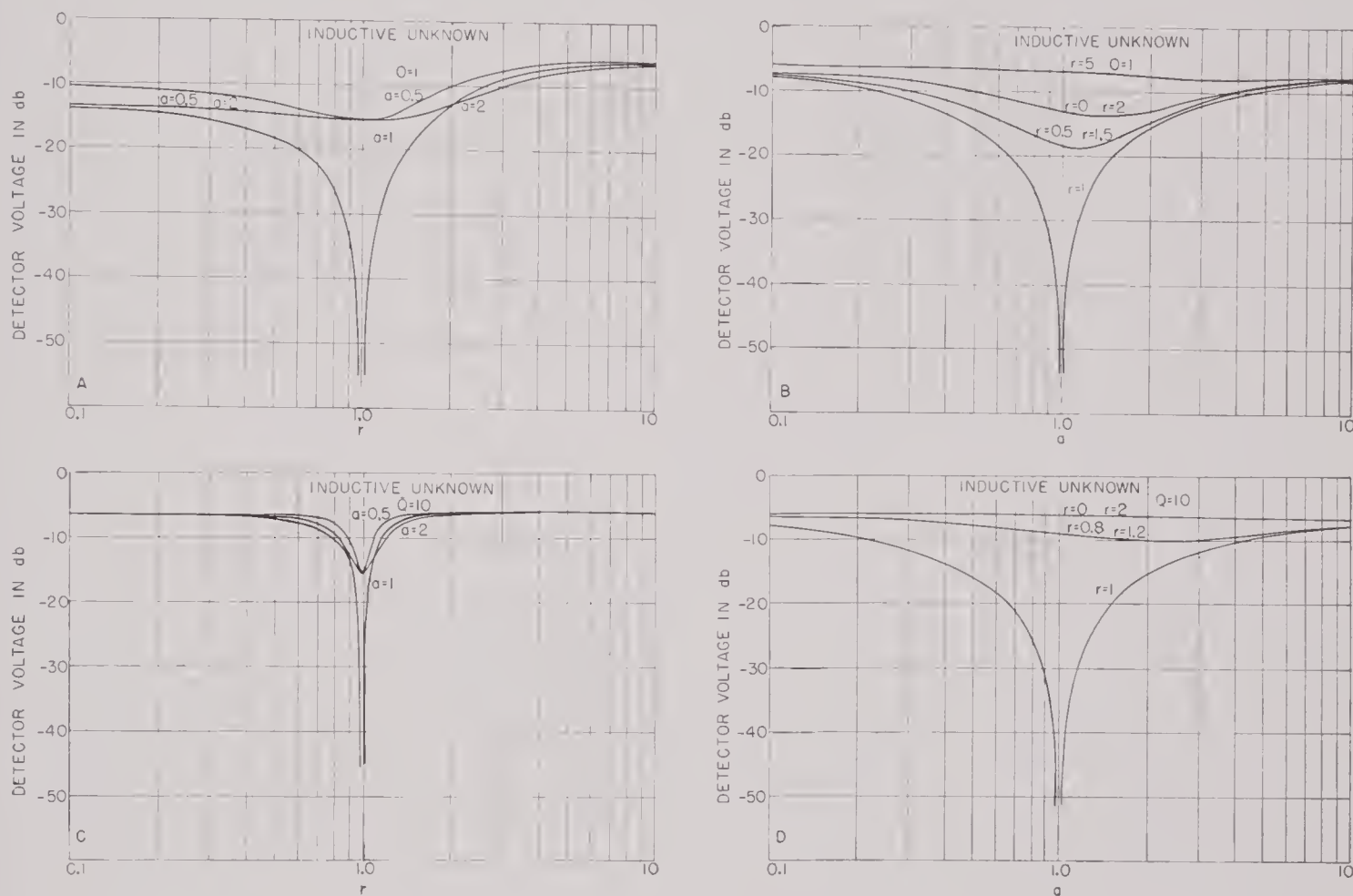


FIGURE 8. Detector voltage vs bridge unbalance ratios (inductive unknown).

the lower limit of accurate resistance measurement above that imposed by the range of the decade. In the admittance bridge, which measures equivalent parallel resistance, the upper limit of the decade may not be sufficiently high, but the useful range can be extended by shunting the unknown with a known value of resistance.

With either the admittance or impedance form of equal-ratio bridge network, the sensitivity is maximum when the impedances of the ratio arms, the

Convergence of Balance. Since the ease and speed with which bridge measurements can be made depends upon the manner in which the detector voltage varies with adjustment of the bridge elements, it is worth while to investigate the process by which balance is attained in the two forms of bridges employed for transducer measurements. It is particularly important to determine the manner in which the detector voltage responds to the balance adjustments when the bridge is not near balance, in order that the

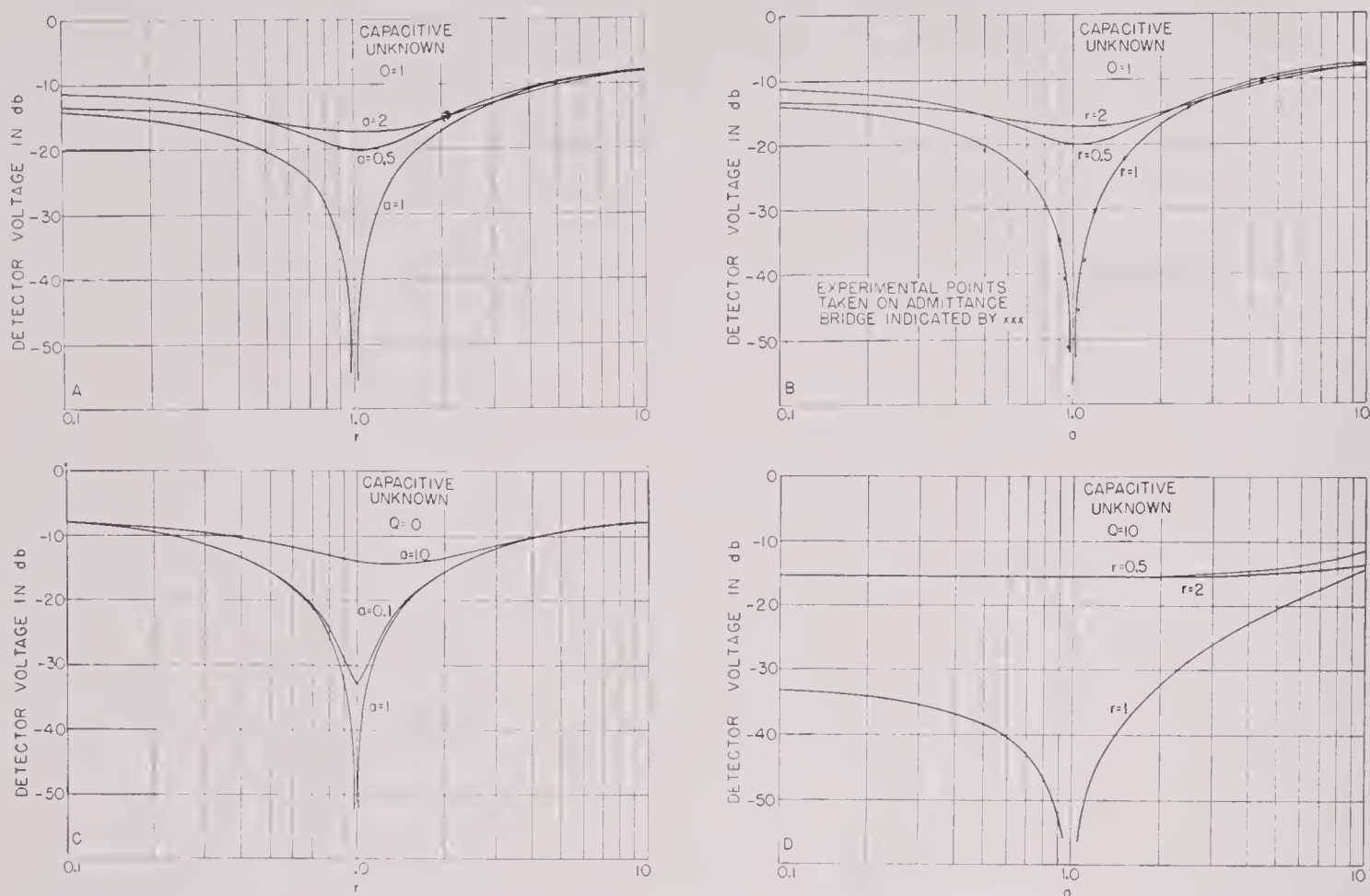


FIGURE 9. Detector voltage vs bridge unbalance ratios (capacitive unknown).

successive adjustments required to attain balance may be made in the right order to cause the detector voltage to converge towards zero rapidly.

By assuming that the detector has infinite impedance, as is closely approximated in practice by a vacuum-tube voltmeter, for the Wheatstone network of Figure 6 the ratio of the detector voltage V to the applied voltage E is

$$\frac{V}{E} = \frac{Z_1 Z_3 - Z_2 Z_4}{(Z_1 + Z_2)(Z_3 + Z_4)}.$$

For an equal-arm ratio bridge $Z_1 = Z_2$ and

$$-\frac{V}{E} = \frac{1}{2} \frac{Z_3 - Z_4}{Z_3 + Z_4}.$$

This equation, applied to the four bridge networks used for the determination of impedance and admittance loci, gives the results tabulated in Figure 7. The formulas for the magnitude of V/E are the same for both impedance and admittance bridge networks, but the parameters α , r , and Q are inverted in going from one form of bridge to the other. Note that the

unknown is represented as its series equivalent in the impedance bridge network and as its parallel equivalent in the admittance bridge network.

The parameter α represents the resistance unbalance ratio and the parameter r the reactance unbalance ratio. The parameter Q for both networks is the usual ratio of series reactance to resistance. In Figures 8 and 9 the detector voltage, expressed in a logarithmic voltage ratio as $20 \log V/E$, is plotted as a function of these parameters. The detector voltage is plotted logarithmically because the voltmeter used as a detector has variable gain and is in effect a logarithmic voltmeter, that is, the meter sensitivity is inversely proportional to the applied voltage. The values of 1 and 10 have been chosen for the parameter Q as sufficient to illustrate the effect of the Q of the unknown on the convergence.

The conclusions to be drawn from the curves of Figures 8 and 9 are as follows:

The reactance adjustment should be made first, since there is a better minimum of detector voltage when the reactance is varied with a resistance un-

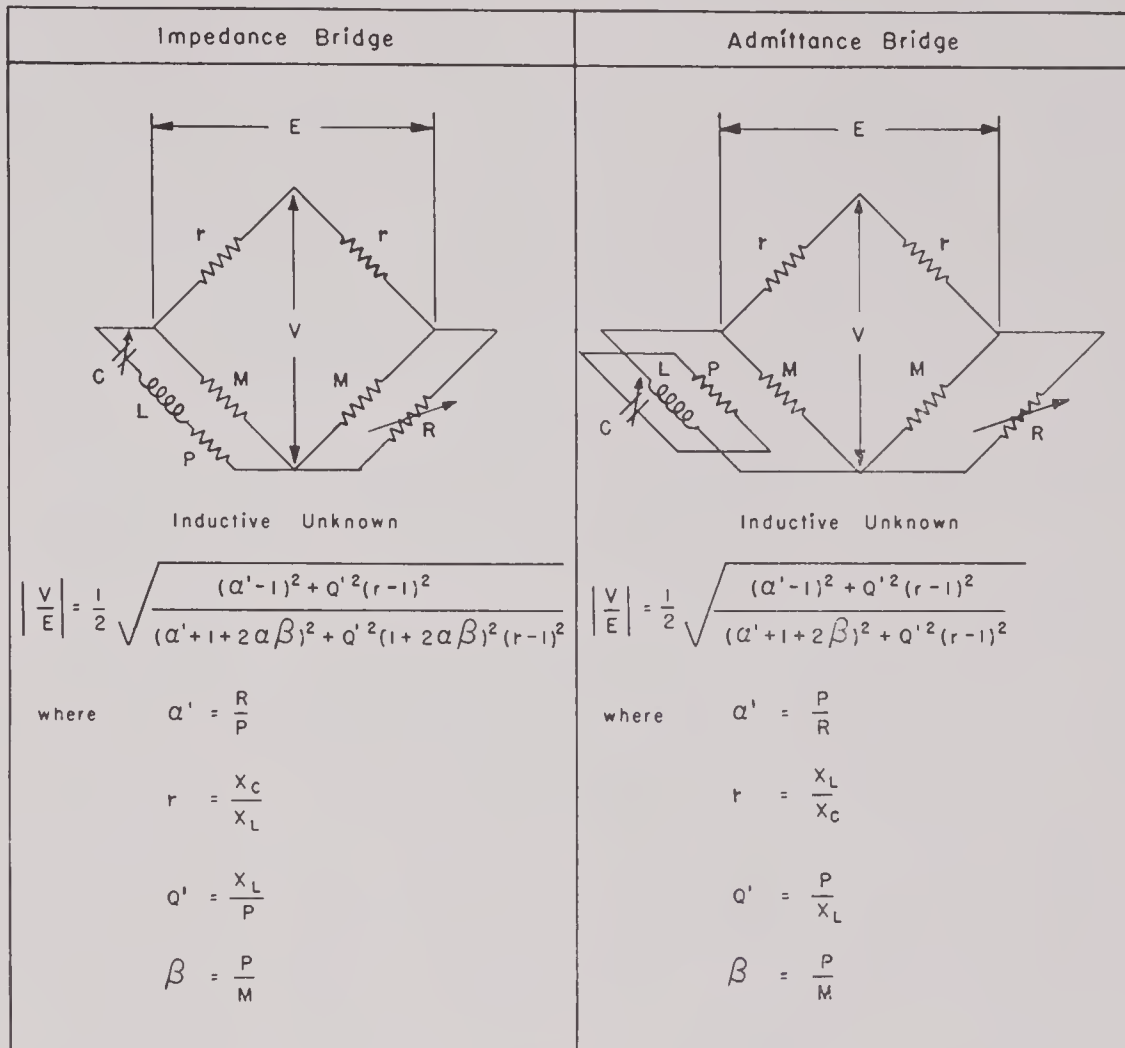


FIGURE 10. Tabulation of convergence equations for actual bridge networks.

balance than when the resistance is varied with a reactance unbalance, especially with a high Q .

The initial value of α should be less than unity rather than greater for rapid convergence. This means that if the initial setting of R is not close to the balance value, that is, to the resistance P , then for the impedance bridge the setting of R should preferably be less than P and for the admittance bridge the setting of R should be greater than P .

The actual bridge circuits of Figures 12 and 16 differ somewhat from the simple networks of Figure 7. The principal difference is due to the shunting of the two lower branches of the bridge networks by the resistances contained within the Leeds & Northrup ratio box for the purpose of obtaining a conductance balance. The bridge networks for inductive unknowns become those of Figure 10 if these shunting resistances are included. The value of the resistors M in the L & N ratio box is 4,000 ohms.

If the resistors M are equal they do not affect the balance conditions for the network, but their effect

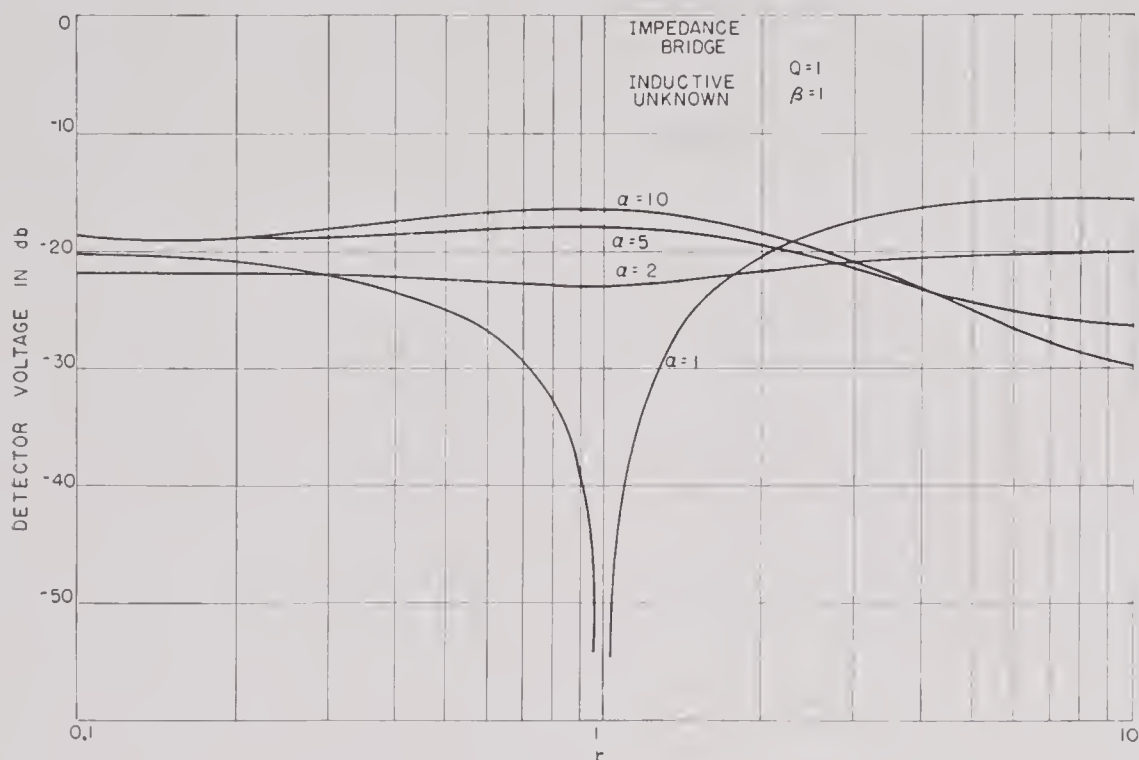
on the convergence is apparent in the appearance of the factor β in equations for the magnitude of V/E . The admittance bridge network of Figure 10 can be simply reduced to the form of Figure 7 by considering the resistors M as parts of P and R . The curves of Figures 8 and 9 can thus be applied if the primed values of α and Q are converted to the unprimed values for which the curves are plotted through the relations

$$\alpha = \frac{\alpha' + \beta}{\beta + 1}$$

and

$$Q = \frac{Q'}{\beta + 1}$$

The effect of M on the impedance bridge network is more complex, since the shunt resistor M cannot be considered as a constant series-equivalent resistance added to P if the reactance is varied. As the magnitude of P becomes comparable to M , that is, $\beta \rightarrow 1$, the effect on the convergence is considerable,

FIGURE 11. Detector voltage vs bridge unbalance ratios ($B = 1$).

as shown in Figure 11. However, if the use of the bridge is confined to unknowns of such low impedance that P is small compared to M , that is, $\beta \ll 1$, the effect of M is negligible and the curves of Figures 8 and 9 are applicable.

An apparent advantage of the impedance bridge network over the admittance bridge is the ease of obtaining initial balance. This can be attributed to the fact that the concept of impedance is more familiar to the operator than that of admittance and that the series-equivalent low-frequency a-c resistance is close to the value of the d-c resistance. These combine to make it easier, with the impedance bridge, to set the initial value of the decade resistor R close to the balance value. For rapid convergence, the decade setting should be low rather than high in the impedance bridge. This condition is readily fulfilled, since the decade range extends down to zero. In the admittance bridge the reverse should be true. This latter condition is not so readily obtained, because the decade range is limited to 10,000 ohms at the upper end. The parallel-equivalent resistance of the unknown impedance is often above 10,000 ohms, so that unless the unknown is shunted down to the range of the decade resistor the setting of the decade must necessarily be low and the bridge cannot be brought into balance by adjustment of the decade alone.

The HUSL Impedance Bridge. An impedance

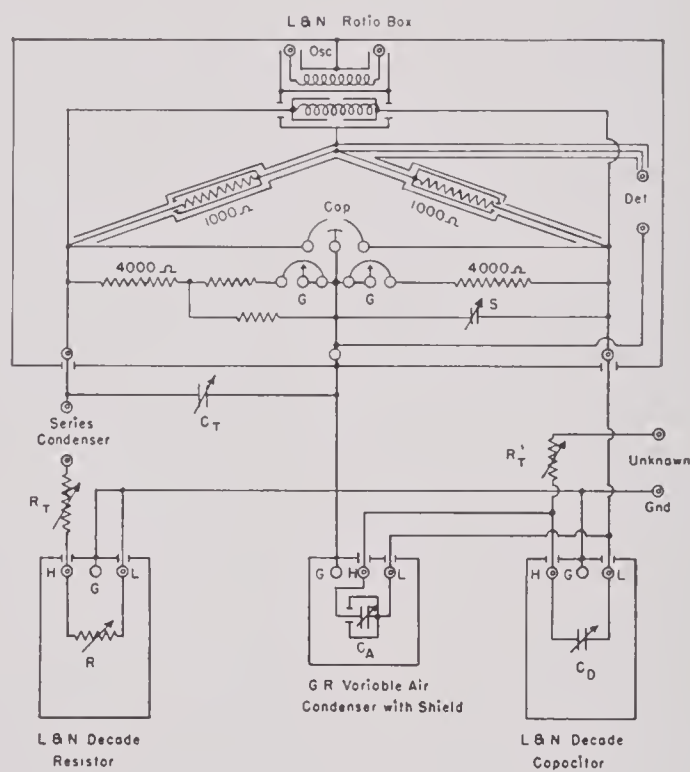


FIGURE 12. Circuit of impedance bridge.

bridge of the type shown in Figure 4 was built at HUSL. A complete circuit diagram of this bridge is shown in Figure 12, a sketch of the bridge console showing the arrangement of components in Figure 13, and a photograph of the bridge console and accessory apparatus in Figure 14.

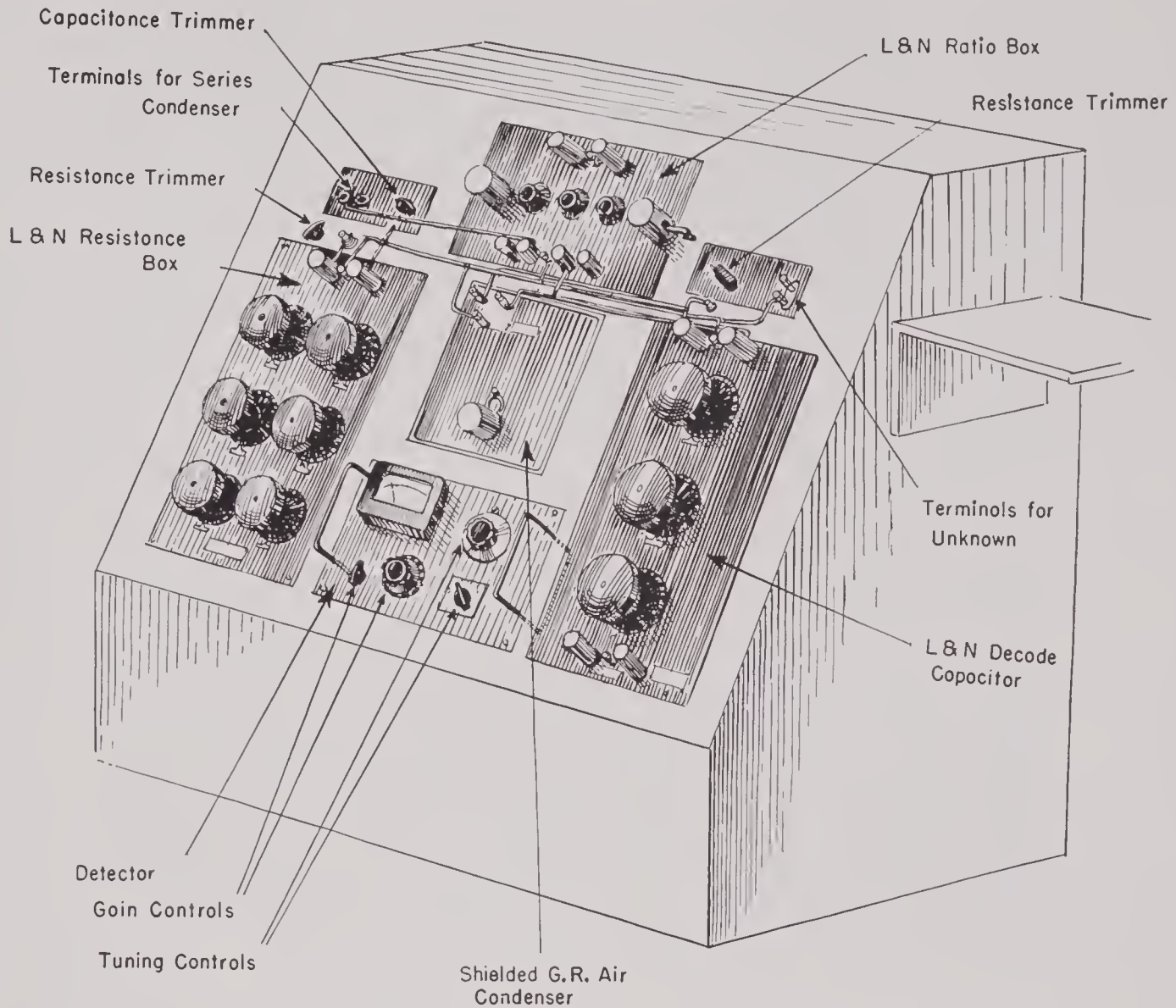


FIGURE 13. Sketch of impedance bridge console.

A Leeds & Northrup, Campbell-Shackelton shielded ratio box (No. 1553) contains the two shielded and accurately balanced 1,000-ohm resistors that comprise the ratio arms r , a double-shielded input transformer, and capacitance (Cap and S) and resistance (G) trimmers for obtaining an initial balance. The connections to the other two bridge arms, to the oscillator, and to the detector are conveniently made from shielded terminals on the ratio box. The variable resistance R is a Leeds & Northrup six-dial shielded resistance box (No. 4764) with a range of 11,111.1 ohms in 0.01-ohm steps. The variable capacitance C is composed of the parallel capacitors C_D , an L & N three-dial shielded mica capacitor (No. 1071) with a range of $1.11 \mu\text{f}$ in $0.001\text{-}\mu\text{f}$ steps, and C_A , a General Radio variable air condenser Type 539-C with a nominal capacitance of 60–2000

μf . The GR condenser has been provided with a second shield for reasons to be discussed below. The trimmer condenser C_T consists of a $200\text{-}\mu\text{f}$ fixed mica condenser in parallel with a $300\text{-}\mu\text{f}$ variable air condenser. The trimmer resistor R_T' is a variable resistor with a range of 0 to 10 ohms in 1-ohm steps constructed from $\frac{1}{2}$ -watt 1-ohm resistors and an 11-position rotary switch. The other trimmer resistor R_T is a GR Type 669 compensated slide-wire resistor, continuously variable from 0 to 1.1 ohms. The terminals marked "series condenser" permit the insertion of a GR Type 509 standard condenser in series with the resistance R as the capacitance C_S required for the measurement of capacitive unknowns. For the measurement of inductive unknowns these terminals are shorted. These bridge components, together with a tuned amplifier de-

CONFIDENTIAL



FIGURE 14. Impedance bridge console and auxiliary apparatus.

tor, were assembled in a console, as shown in Figures 13 and 14. Connections between components have been made with unshielded bus wires.

The necessity for operating the variable condensers with both terminals off ground requires that considerable care be taken in the control of stray capacities from these components to ground. The capacity from the high side of the condenser to ground (C_A in Figure 15A) shunts the whole arm of the bridge, while that from the low side C_B shunts only the unknown, Z_X . It is easy to compensate for C_A by an equal capacity C_T shunting the opposite arm (Figure 15B), but C_B causes an error in the apparent value of Z_X . Hence it is desirable to have the value of C_B known, constant, and as small as possible in order to correct this error or to make it negligible. If the shield of the condenser is connected to one side of the condenser, as it is in the GR variable air con-

denser, and the condenser is connected as in Figure 15A, the large capacity from the shield to ground is C_B , which shunts the unknown. The connection shown in Figure 15B makes the capacity from shield to ground C_A , which can be compensated by C_T , leaving only a small value of C_B across the unknown. However, in making adjustments of the capacitance C , the operator's hand varies the capacity C_A , which makes a fixed compensation of C_A impossible and the process of determining balance very difficult. To make the capacity C_A definite regardless of the position of the operator's hand, a second, grounded shield can be added to the condenser, as in Figure 15C. Such a shield has been added to the GR variable air condenser used in the impedance bridge. No alterations were made in the GR condenser other than to enclose it in a Dural box, which required adding a longer shaft to the vernier control, removing the

knob from the dial, and providing terminals on the outer case. Since the vernier shaft is electrically connected to the inner shield, the control knob had to be provided with a shield insulated from the shaft but connected to the outer shield of the condenser by a spring contactor. With the condenser thus shielded, the capacity C_A is $>195 \mu\mu\text{f}$ and C_B is only $5 \mu\mu\text{f}$.

The L & N decade condenser has three terminals, so that it is possible to ground its case to prevent hand-capacity troubles. The high terminal of the condenser, since it has the smaller capacity to the grounded case, is connected to the unknown. With this condenser in parallel with the shielded GR condenser in the bridge, the effective shunt capacity

To compensate for wiring resistance, R_T and R'_T are adjusted for balance with the terminals "series condenser" and "unknown" shorted, the condensers C_A and C_D shorted, and R set at zero. The series resistance of the condensers can be offset only by adjusting the trimmers when an inductance having a known value of resistance is connected to the "unknown" terminals. Since the accurate determination of the resistance of an inductor is difficult, compensation for the condenser resistance cannot be achieved with any accuracy. With the bridge connected for the measurement of capacitive unknowns a partial compensation is possible, because the trimmers can be adjusted with C equal to C_S , the "unknown" terminals shorted, and R set at zero. Of

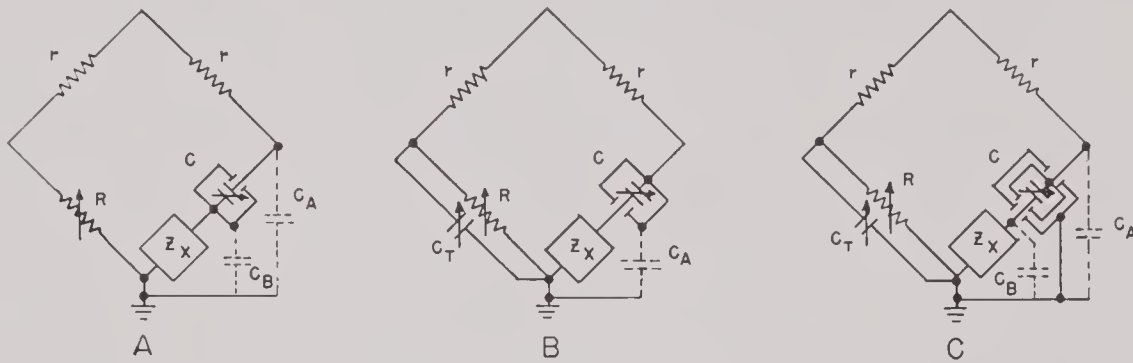


FIGURE 15. Shielding of variable condenser.

across the entire arm C_A has been found by measurement to be $297 \mu\mu\text{f}$, whereas the effective shunt capacity across the unknown C_B is $38 \mu\mu\text{f}$. The $297 \mu\mu\text{f}$ capacity is compensated by C_T , but the $38 \mu\mu\text{f}$ capacity appears as part of the unknown. Except for unknowns of high impedance, this small capacity is negligible; it is the equivalent of only a few inches of shielded cable added to a transducer.

The proper adjustment of C_T to compensate for the capacity C_A is made by adjusting C_T for a minimum reading of the detector when the terminals "series condenser" and "unknown" (Figure 12) are open and the decade and air condensers C_D and C_A are set at their lowest values. The capacity trimmers in the ratio box may be used as a fine adjustment of C_T , and the resistance trimmer in this box must be used to obtain a sharp balance. If the range of this resistance trimmer is not sufficient to obtain balance, it may be necessary to shunt C_T with a resistor to compensate for conductance shunting of C_A .

The series resistance trimmers R_T and R'_T are included to permit compensation of wiring resistance and the equivalent series resistance of the condensers.

course, the compensation is made only for C set at a value equal to C_S ; the variations in the series resistance with a change in C remain uncompensated. For many measurements the errors due to the uncompensated equivalent series resistance of the condensers are negligible.

The change from measurement of inductance to that of capacitance requires a realignment of the bridge. Addition of the capacitor C_S changes the value of the trimmer C_T required for balance, since the stray capacity from the series condenser C_S to ground is added to C_T . The added resistance of C_S also requires a readjustment of the resistance trimmers for balance.

The impedance bridge has several major disadvantages.

1. There is a fixed capacity, which cannot be offset, shunting the impedance being measured. This causes an error in the apparent value of the unknown that is a function both of frequency and of the magnitude of the unknown impedance. The mathematical subtraction of this shunt capacity is tedious and time-consuming, especially for the

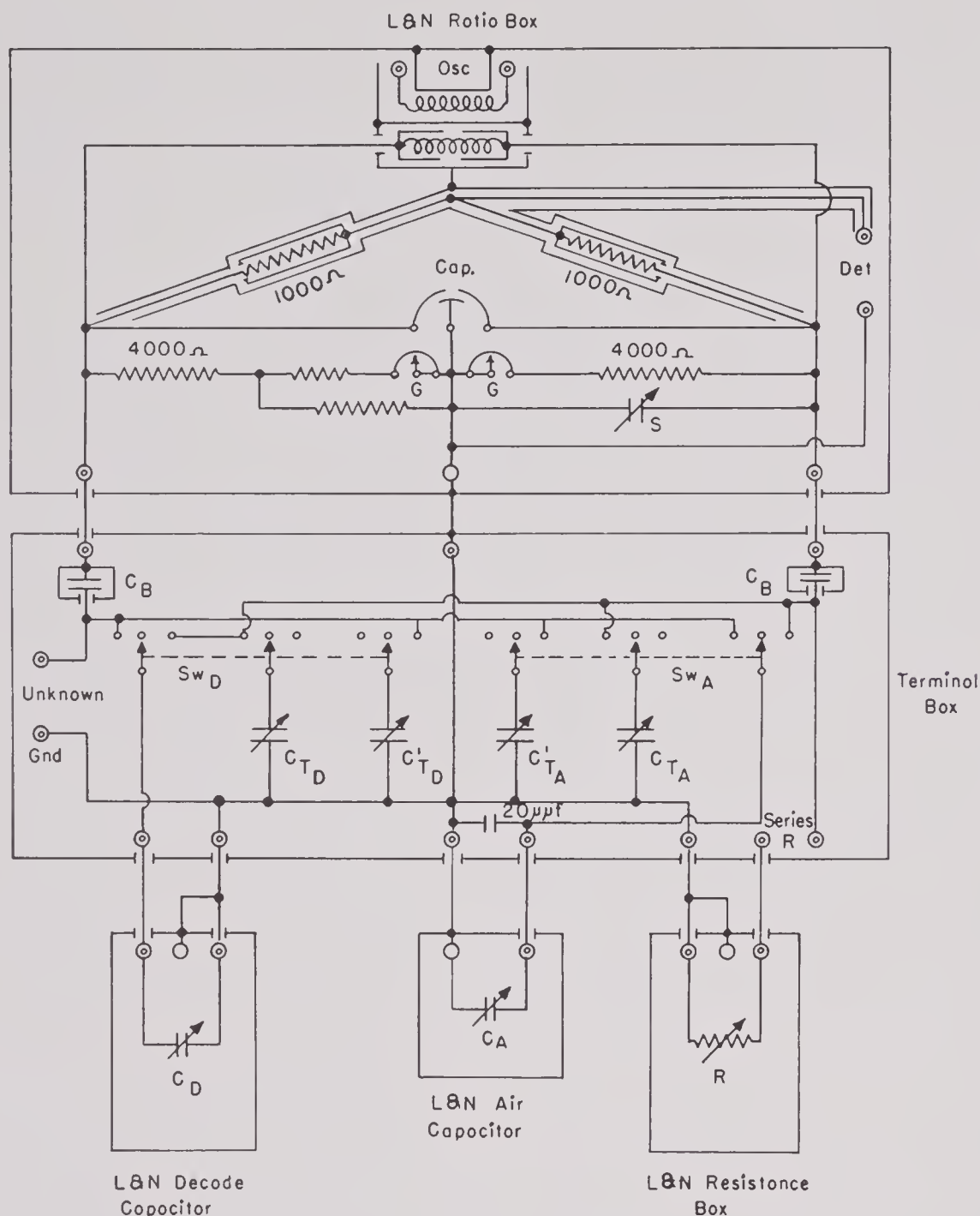


FIGURE 16. Circuit of admittance bridge.

series of measurements required to determine an impedance locus.

2. It is impossible to align the bridge accurately without the use of an external inductance standard for which the equivalent series resistance is accurately known over a wide frequency range. The lack of such standards makes the measurement of small resistive components with this bridge subject to considerable errors.

3. The change from measurement of inductance to measurement of capacitance cannot be made

rapidly because of the necessity for realigning the bridge whenever the change is made.

4. The measurement of capacitance with this form of bridge is inconvenient and often inaccurate, because the unknown reactance is balanced by the difference between two reactances $X_x = 1/\omega C_s - 1/\omega C$. This means that the series condenser C_s must be chosen so that its reactance at all the frequencies to be measured is greater than the reactance of the unknown and, for accuracy, preferably about twice the reactance of the unknown. Since the

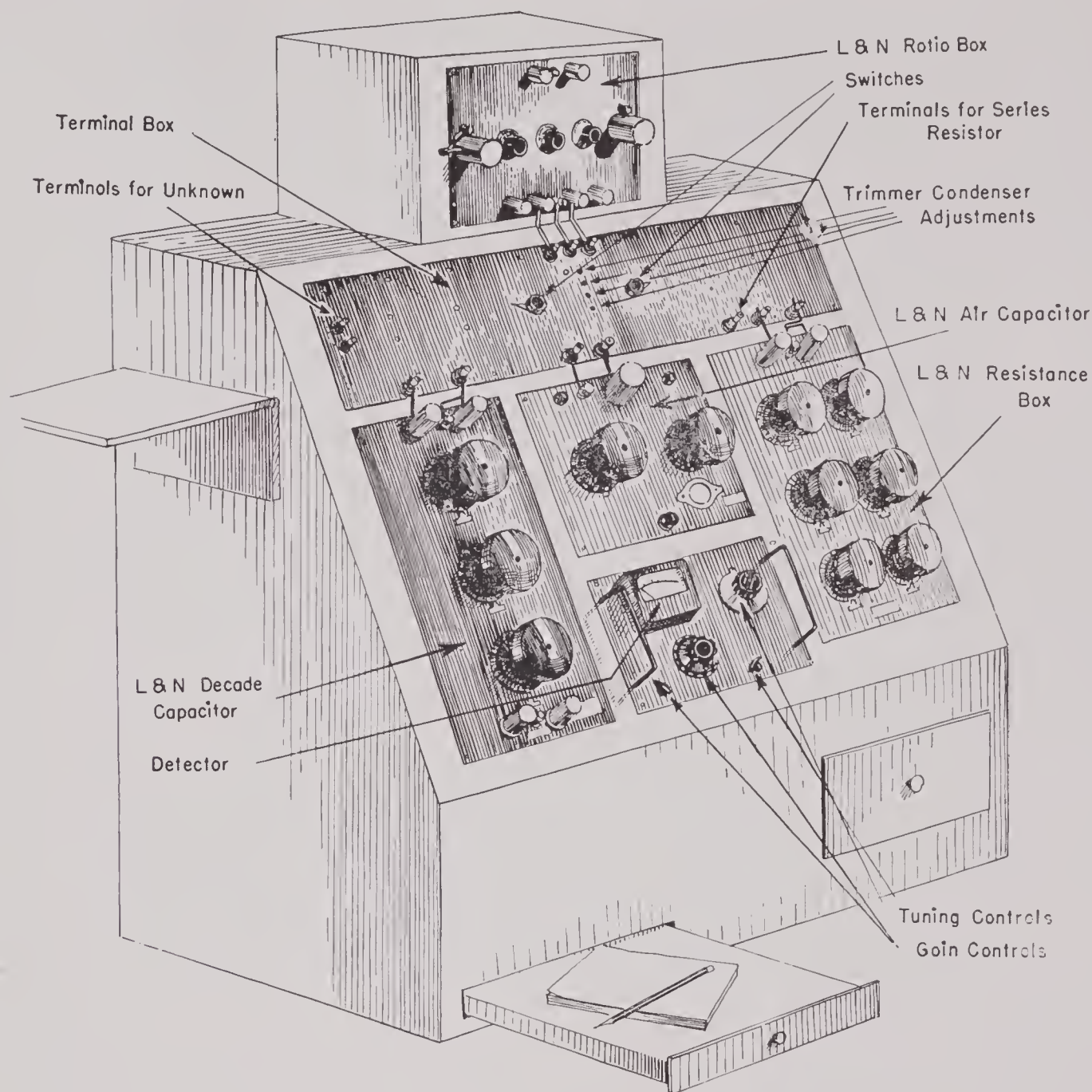


FIGURE 17. Sketch of admittance bridge console.

amount of negative reactance occurring in an impedance locus can seldom be predicted, the choice of C_S is usually a trial-and-error process, which is time-consuming. If a single value of C_S is used for the measurement of a range of reactances, the accuracy of some of the measurements may be poor.

Despite these disadvantages, the impedance bridge is very useful in the measurement of impedances lying within the range in which the effect of the shunt capacity in the bridge is negligible and errors due to inaccurate resistance alignment are small. Where results expressed as impedance rather than admittance

or impedance loci rather than admittance loci are preferred, the advantage of the impedance bridge is that the resistance R_x and the series-tuning capacity for an inductive unknown are read directly and the reactance X_x can be easily calculated.

The impedance bridge, however, fails in several respects to fulfill satisfactorily the requirements established for a method of measurement of those quantities required to determine the impedance loci of transducers. The range of impedances within which accurate measurements can be made is insufficient. The operations required to change the bridge



FIGURE 18. Admittance bridge console and auxiliary apparatus.

from the measurement of inductance to the measurement of capacitance are time-consuming and involve both the use of additional standards and a loss in accuracy. The measurement of capacitance with this bridge is less convenient and less accurate than that of inductance.

The HUSL Admittance Bridge. Because of the advantage of a symmetrical bridge network and because the information obtainable from the vector admittance locus is as useful as that obtainable from the impedance locus, an admittance bridge of the form shown in Figure 5 was also constructed at HUSL. The complete circuit diagram of the bridge is shown in Figure 16, a sketch of the bridge console showing the arrangement of components in Figure

17, and a photograph of the bridge console and accessory apparatus in Figure 18.

As in the impedance bridge, a Leeds & Northrup, Campbell-Shackelton shielded ratio box (No. 1553) supplies the 1,000-ohm ratio arms, the double-shielded input transformer, and the capacitance (C_p and S) and conductance (G) trimmers. The variable resistance R is an L & N six-dial shielded resistance box (No. 4764) with a range of 11,111.1 ohms in 0.01-ohm steps. The variable capacitance C is composed of the parallel capacitors C_D , an L & N three-dial shielded mica capacitor (No. 1071) with a range of 1.11 μf in 0.001- μf steps and C_A , and L & N adjustable air capacitor (No. 1188) with a range of 50 to 1,300 μf (see Figure 16).

CONFIDENTIAL

A blocking condenser C_B has been connected in series with the unknown impedance to permit the use of superposed direct current to polarize the transducer without passing this current through any of the other branches of the bridge network. To preserve the symmetry of the network, an identical condenser has been placed in the opposite arm. These two condensers, C_B , are GR Type 509 standard condensers each having a calibrated capacitance of $0.9991 \mu\text{f}$. Since one terminal of these condensers is connected to the case of the condenser, this terminal has been connected to the corner of the bridge rather than to the unknown so that the capacity from the case to ground would fall across the whole arm of the bridge. If the two condensers are similarly mounted, their capacities to ground should balance each other.

In order to change from the measurement of inductance to that of capacitance, the capacitance C of Figure 5 must be switched from one arm to the other. The operation is performed by two rotary-action three-pole, double-throw switches with a center off position, Sw_D and Sw_A , one for each of the condensers C_D and C_A . These switches are GR Type 339-A four-pole, double-throw switches, with one pole unused. One pole of each switch is used to shift the high side of its condenser to either arm of the bridge or, in the center position of the switch, to disconnect the condenser. Thus the condensers can be used in any combination in either arm of the bridge.

Compensation for residual capacities in the variable resistor and capacitors and wiring capacities must be made by equal capacities in the opposite arm of the bridge to maintain symmetry and keep the bridge direct reading. The residual capacities of the condensers C_A and C_D are balanced by the trimmer condensers C_{TD} , C'_{TD} , C_{TA} , and C'_{TA} . Differences in wiring capacities cause the residuals of C_A or C_D to vary as the condenser is switched from one arm to the other; for this reason a separate capacity trimmer is provided for each position of both condensers. Two poles of each of the switches are used to connect the proper trimmer to the opposite arm of the bridge as the connections of the condensers are changed. Because the residual of the L & N decade capacitor (C_D) with the case connected to the low terminal is of the order of $70 \mu\text{mf}$, the trimmers C_{TD} and C'_{TD} are Centralab ceramic trimmer condensers (823AN) with a range of 20 to $125 \mu\text{mf}$. Since the L & N air capacitor has two terminals rather than three like the L & N decade, its calibration includes the residual, so that

only the wiring capacity needs be counterbalanced. Because this wiring capacity is smaller than the 7 to $45 \mu\text{mf}$ range of the Erie ceramic trimmer condensers (TS2B) used for C_{TA} and C'_{TA} , a $20\text{-}\mu\text{mf}$ fixed ceramic condenser has been connected in parallel with C_A to bring its residual within the range of the trimmers.

The blocking condensers C_B , the switches, the trimmers, and the associated wiring are mounted on a metal panel and shielded by an aluminum case. The panel also provides the terminals for the connection of the unknown, the ratio box, and the variable resistor and capacitors. This terminal box is shown in Figure 19. The blocking condensers and the

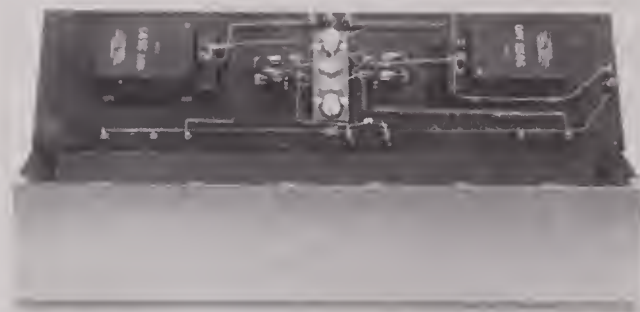


FIGURE 19. Interior of terminal box for admittance bridge.

trimmer condensers are insulated from the panel by being mounted on polystyrene. The terminals are polystyrene insulated, GR Type 138-UL binding posts, which afford a very high leakage resistance. An extra terminal is provided on the panel above the resistance box to permit the insertion of a fixed resistor in series with the variable resistor to extend its range. If no series resistor is used, the terminals marked Series R in Figure 16 are connected.

The adjustment of the trimmers to align the bridge is made as follows. The high terminal of resistor R is disconnected. This is conveniently done by removing the short from the two terminals provided for a series resistor. With the switches Sw_D and Sw_A in the center position and with the "unknown" terminals open, the bridge is then aligned by adjusting the trimmers G , Cap , and S in the ratio box for a minimum detector reading.

With the decade capacitor C_D set at 0.000, the switch Sw_D is thrown first to one side and then the other, and the corresponding trimmers C_{TD} and C'_{TD} are adjusted for a minimum detector reading. With C_D set at $0.001 \mu\text{f}$ and C_A set at $1,000 \mu\text{mf}$, the switches Sw_A and Sw_D are thrown to connect C_A and

C_D to opposite arms of the bridge. One of the trimmers C_{TA} and C_{TD} is then adjusted for a minimum detector reading. The positions of C_A and C_D are next reversed by means of the switches and the other trimmer is adjusted. The adjustments of these trimmers are made by means of a screwdriver through the top of the terminal box. This alignment should be practically independent of frequency.

The reconnection of the resistor R makes the bridge ready for use. However, the connection of the resistance box introduces across the arm of the bridge a small reactance, which varies in magnitude and sign with the setting of the dials. With the box set at 10,000 ohms, the resistance is shunted by a capacity of about 10 μf . This introduces a small susceptance error into the bridge, but for measurements in which the sum of C_D and C_A amounts to more than 1,000 μf , this error is negligible.

For measurements involving smaller capacities, an additional alignment procedure is used. With the bridge aligned as just described, the resistance box is connected and set at 10,000 ohms and a 10,000-ohm L & N secondary standard a-c resistor (No. 4640) is connected to the "unknown" terminals. The condenser C_D set at 0.001 μf is connected across one arm of the bridge and the condenser C_A set at 1,000 μf across the opposite arm. The bridge is then aligned by adjustment of the trimmers in the ratio box. This alignment compensates the reactance of the resistance box at the 10,000-ohm setting, but does not compensate for changes in that reactance as R is varied. The impedance to be measured is connected in parallel with the 10,000-ohm standard resistor. For the measurement of inductance-tuning with a small capacity, C_D is connected across the unknown and C_A across the opposite arm, while for the measurement of small capacities, C_A is connected across the unknown and C_D opposite. If R is disconnected or aligned at 10,000 ohms as above, small capacities with low dissipation can be readily compared to the air capacitor C_A by a substitution method.

For the measurement of impedances having an equivalent parallel resistance above the 11,111.1-ohm range of the resistance box R , (that is, admittances having a conductance G less than 0.09 millimho) the 10,000-ohm standard resistor is again used to shunt the unknown. It is easy to subtract the 0.1-millimho conductance of this standard resistor from the measured conductance to obtain that of the unknown. The bridge is aligned with this resistor and the resistance box connected as before, with

the capacitors either disconnected by the switches being in the center position or connected to opposite arms, depending on the magnitude of the capacities used.

Although a fixed resistor in series with the resistance box can be used to extend its range, this method is not recommended because it may alter the symmetry of the bridge and introduce unbalanced residuals, necessitating a large number of calibrated fixed resistors to cover the added range. Moreover, the adjustment of the resistance is not convenient when the resistance box covers only a portion of the total resistance of R . With a 10,000-ohm shunt resistor across the unknown, parallel resistance up to 1 megohm can be measured conveniently and with errors within 1 or 2 per cent.

The advantages of this admittance bridge are:

1. The bridge can be accurately aligned without the use of external standards. This alignment is independent of frequency and of the magnitude of the unknown.

2. The accuracy of the bridge is limited only by the accuracy of the variable resistance and capacitance employed. Within the range of the resistor and the capacitors used in the bridge, errors in measurements are less than 0.1 per cent up to at least 50 kc. With the range of the resistor extended by shunting the unknown with 10,000 ohms, the errors may rise to 1 or 2 per cent.

3. The change from the measurement of inductance to that of capacitance is made very simple by means of the switches Sw_D and Sw_A . No realignment of the bridge is necessary when the change is made, no additional standards are required, and there is no loss in accuracy. The calculation of susceptance from the reading of the bridge capacitors is the same for both while the sign of the calculated susceptance is determined by the position of the switches.

4. The effect of an impedance, such as that of a cable or other connecting wires, shunting the unknown can be readily eliminated from the reading of the bridge. This can be done by aligning the bridge with the shunting impedance but not the unknown connected to the bridge; when the unknown is connected, the bridge reads directly its parallel equivalents. Alignment of the bridge to balance out the shunting impedance need be made at only one frequency and can usually be made by means of the trimmers in the ratio box alone.

5. The fact that the unknown and all the variable components in the bridge have one terminal grounded

considerably simplifies the shielding of the components and the control of residuals.

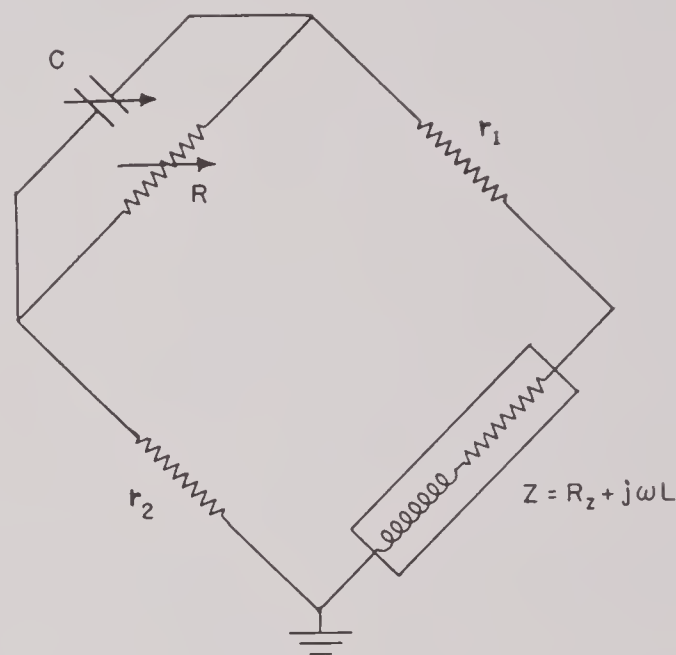
This admittance bridge satisfactorily fulfills the requirements previously listed for a method of measuring those quantities needed to determine the admittance or impedance loci of transducers. It has, however, the one disadvantage that when an impedance locus is preferred or series equivalents rather than parallel equivalents are desired additional computations are required to convert from admittance to impedance. Since the concept of impedance is more familiar, although not more useful, than that of admittance, conversion of the admittance to impedance data is required far more often than is conversion in the opposite sense.

Bridges Developed at BTL. Subsequent to the construction of the admittance bridge, it was found that a bridge that satisfies many of the requirements indicated in preceding sections had been developed at the Bell Telephone Laboratories. This is the W-10125 impedance bridge^{36, 48} covering the carrier-frequency range from 200 to 150,000 cycles and the impedance range of 1 μ h to 100 h and 0.01 ohm to 10 megohms with an accuracy of the order of 0.25 per cent. The bridge will allow potentials up to 100 volts and currents up to 0.2 amp to be applied to the impedance being measured.

For the measurement of inductance, this bridge takes the form of a Maxwell bridge, shown in Figure 20, in which inductance is measured in terms of a capacitance standard. This is a product-arm bridge and hence lacks the advantages of a symmetrical ratio bridge. The shielding problem is more complex, since the standards are operated off ground. However, it has the advantage that it can be made direct-reading in both inductance and series resistance, since the conditions of balance are independent of frequency. The variable resistor R is a conductance decade with its resistors connected in parallel and calibrated directly in equivalent series resistance. This type of decade has the further advantage that its capacitance stays relatively constant as the conductance is varied. For the measurement of capacitance, the bridge is changed to the same form of ratio bridge used in the admittance bridge (Figure 5). In both forms the resistors r are varied to change the range of the bridge.

Since the determination of impedance loci requires the measurement of reactance, the use of a bridge that is direct-reading in inductance has no particular advantage. A symmetrical bridge, with all its at-

tendant advantages, can better be used in such measurements for inductances as well as capacitors. However, the Bell Laboratories' bridge does suggest that the admittance bridge might be improved by the incorporation of a conductance decade rather than a resistance decade.^{32, 33, 41} A decade calibrated directly in conductance would eliminate the necessity for calculating conductance from the reading of a resistance decade. The conductance decade might also be more readily compensated so that its residual reactance does not change with setting.



$$\text{At balance: } L = r_1 r_2 C$$

$$R_2 = r_1 r_2 \frac{1}{R} = r_1 r_2 G$$

FIGURE 20. Maxwell bridge.

AUXILIARY EQUIPMENT

1. *Oscillators.* The oscillators used in connection with the impedance and admittance bridges have been the GR Type 713-B beat-frequency oscillator shown in Figure 18 and the Western Electric 17B oscillator³⁷ shown in Figure 14. Occasionally a Hewlett-Packard Model 205-A special oscillator has been used to supplement the GR oscillator.

The GR oscillator is very satisfactory for impedance measurements so far as stability and harmonic content of the output are concerned, but its dial frequency range and scale are not well adapted to this work. For measurements above 40 kc another oscillator or a frequency doubler must be used. For

the accurate determination of frequency the oscillator output must be compared to a frequency standard. An extra frequency control has been added to the GR oscillator shown in Figure 18 in the form of another variable condenser in parallel with the "cycles increment" condenser and located to the right of that condenser. This control was added to permit use of the wide frequency spread at the lower end of the dial (0 to 1,000 or 20 kc to 21 kc) at other frequencies

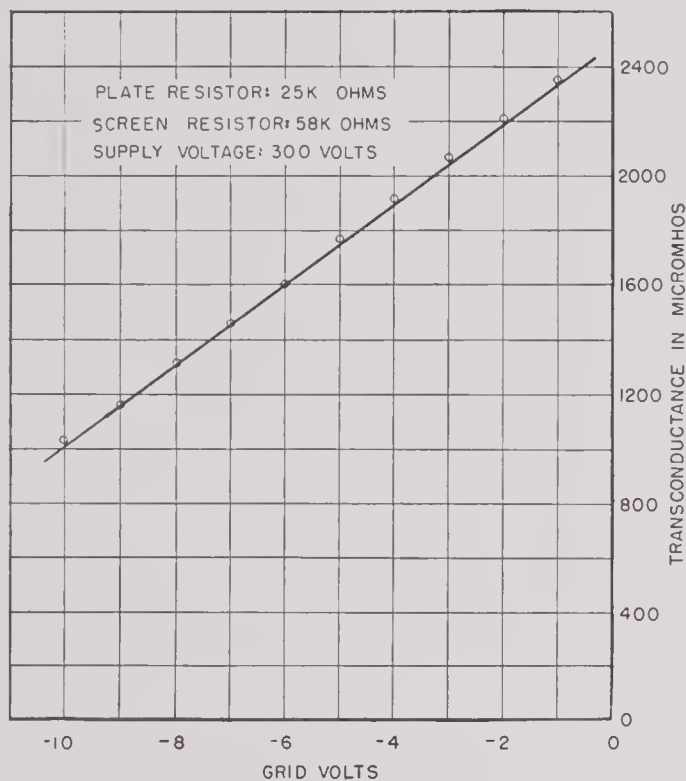


FIGURE 21. Characteristic curve of a 6SK7.

by setting 17 kc, 18 kc, 19 kc, 20 kc, etc. at the 21-kc point on the main dial. When an adequate frequency standard is employed, there is little need for this extra control. The input to the bridge transformer is usually connected to the 50-ohm output terminals of the oscillator, and the output voltage is set at approximately 1.5 volts.

The WE 17B oscillator has an adequate frequency range and scale calibration for use with these bridges. However, the oscillator shown in Figure 14 proved less stable than the GR oscillator. It shows a random frequency variation of a few cycles, which interfered with a sharp balance. The bridge transformer is connected to the 135-ohm output of this oscillator, and the output is usually set at about 3 volts.

The Hewlett-Packard Model 205-A Special has

good stability and frequency range but is difficult to use where small increments of frequency are required, since its increment control effects a percentage deviation in frequency rather than a fixed number of cycles deviation. It proved useful, however, for measurements where the frequency increments were not less than 500 cycles.

2. *Frequency Doubler.* In order to extend the frequency range of the GR 713-B oscillator, a device with an output of twice the frequency of its input over a range of input frequencies was built. Its operation requires a circuit having the nonlinear characteristic to be described. If sinusoidal voltage $e = E \cos \omega t$ is applied to a circuit having the parabolic voltage-current characteristic

$$i = Ae + Be^2,$$

then

$$i = AE \cos \omega t + BE^2 \cos^2 \omega t,$$

which can be expressed as

$$i = \frac{BE^2}{2} + AE \cos \omega t + \frac{BE^2}{2} \cos 2\omega t.$$

The current thus contains components of both the input frequency and double that frequency. If another voltage $e' = -E \cos \omega t = E \cos (\omega t + \pi)$, which is phase-inverted with respect to e , is applied to a circuit with the same characteristics, the current is

$$i' = AE \cos (\omega t + \pi) + BE^2 \cos^2 (\omega t + \pi)$$

or

$$i' = \frac{BE^2}{2} - AE \cos \omega t + \frac{BE^2}{2} \cos 2\omega t.$$

Thus, by adding the two currents,

$$i + i' = BE^2 + BE^2 \cos 2\omega t,$$

the term containing the input frequency is eliminated, leaving only a d-c component and the second harmonic component.

The desired parabolic characteristic can be closely approximated by vacuum tubes. By a proper choice of operating conditions, the i_p vs e_g characteristic can be made parabolic over a range of values of e_g . This is equivalent to a linear g_m vs e_g characteristic. The characteristic curve of a 6SK7 is shown in Figure 21. Triodes can also be made to have the desired characteristic,⁴⁶ as shown in Figure 22. The elimination of the input frequency from the output is achieved by using two tubes with a common load but with a push-pull input, as in Figure 23. By using

closely matched tubes, the component of the input frequency in the output can be made very small.

The circuit of Figure 24 shows a frequency doubler and power amplifier of the type constructed to extend the range of the GR oscillator. The input range was 20 to 40 kc, corresponding to an output of 40 to 80 kc, with a constant input voltage of about 1.5 volts. The power amplifier was designed to work into a bridge input transformer. A 6SC7 double triode operated as shown with a 300-volt plate supply and a fixed bias of about 6.8 volts was used as the nonlinear element.

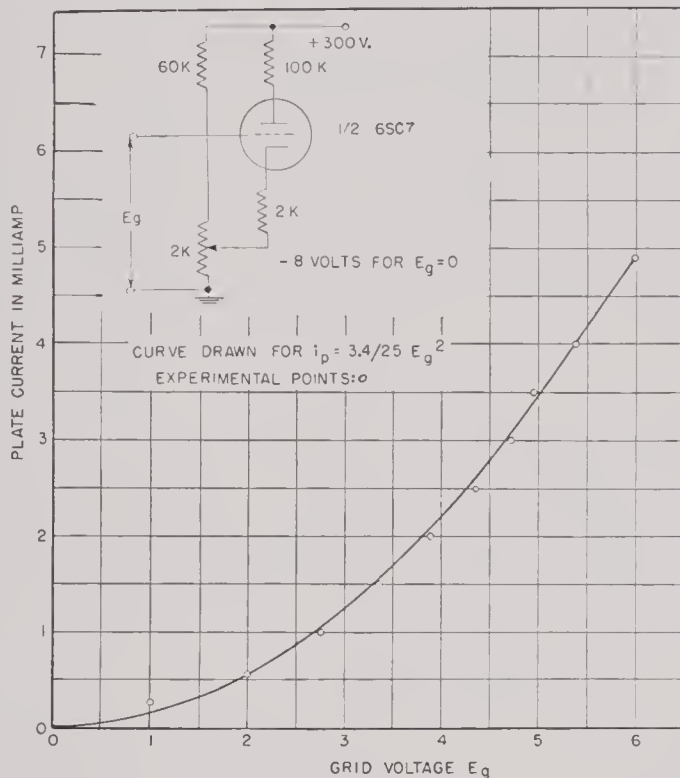


FIGURE 22. Characteristic curve of 6SC7.

The circuit could be balanced so that the input frequency component in the output was about 45 db below the second harmonic. This is not sufficient for good bridge balance but it is usable. The harmonic content of the output could be improved by the use of octave filters or, if another tuning control be tolerated, by a tuned filter. The frequency range could be extended by the elimination of transformers. Development work, however, is impeded by the lack of harmonic analyzers for this range of frequencies.

3. *Frequency Standards.* The determination of impedance and admittance loci requires that measurements be made at a number of accurately known frequencies over the range from 1 kc to 100 kc. Because of the rapid variation in impedance with a change in frequency in the neighborhood of reso-

nance, measurements in this region must be made at frequencies that differ by very small amounts. The need for frequency increments as small as 10 cycles in the region around 20 kc is not uncommon (Figure 2). This requires an oscillator with wide frequency range and, at the same time, stability and calibration such that small and accurate increments of frequency can be obtained within that range.

Although an oscillator is available that almost satisfies these requirements,^a one with the range and stability but without such an accurate scale^b can be employed if a suitable standard of frequency is used

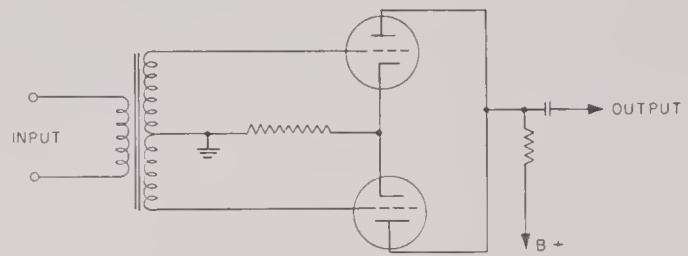


FIGURE 23. Basic circuit of frequency doubler.

to check the output of the oscillator. The frequency of the standard is compared with that of the oscillator by use of Lissajous figures on a cathode-ray oscilloscope. If a low-frequency standard is employed, a large number of frequencies in the oscillator range can be checked by the use of the Lissajous figures. The ratio of frequencies corresponding to a particular Lissajous figure need not be identified, since the calibration of the oscillator should indicate which multiple of the standard is being checked. The spacing between the frequencies which can be checked against the standard should be such that a dial on the oscillator can be used to interpolate any desired frequency within that interval.

Because of its convenience and availability, a standard frequency of 1 kc has been used. The standard was derived from a General Radio primary frequency standard Class C-21-HLD located in the Cruft Laboratory, Harvard University, and carried to the location of the impedance measurements on telephone lines. This standard alone has been adequate for use with a WE 17B oscillator, which has a

^a The Western Electric 17B oscillator covers the frequency range from 50 c to 150 kc with a scale calibrated every 100 c and an accuracy of 25 c at any scale setting.

^b Such as the Hewlett-Packard Model 205-A Special or the General Electric Type 713-B, although the latter has a maximum of 40 kc.

The necessary high Q can be obtained from a tuned circuit employing a coil of lower Q by the addition of a negative resistance to the tuned circuit. Such a negative resistance can be produced across the input of an amplifier by the use of feedback.^{39, 42, 44, 45} Since the tuned circuit has to be followed by amplification in order to obtain sufficient output, this method of increasing Q is convenient and economical. The

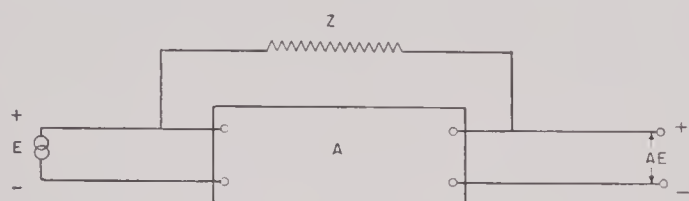


FIGURE 26. Negative resistance circuit.

method of obtaining a negative resistance is shown in Figure 26. For conditions shown in the figure, the input impedance is

$$Z_{in} = \frac{E}{I} = \frac{E}{\frac{E - AE}{Z}} = \frac{Z}{1 - A}.$$

Thus, if A is greater than 1, Z_{in} is negative. Since $dZ_{in}/Z_{in} = dA/(1 - A)$, the gain A of the amplifier must not be close to unity for stability. The gain of the amplifier can be made stable by use of negative feedback.

If the feedback impedance Z is a resistance R , then $R_{in} = R/(1 - A)$. The tuned circuit of Figure 27 has a

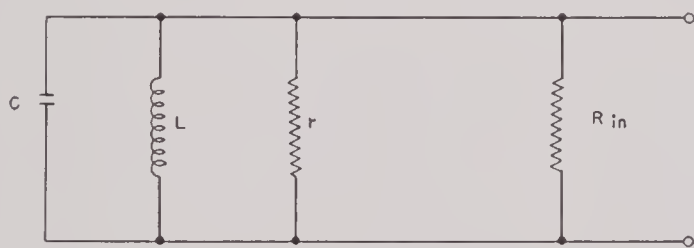


FIGURE 27. Tuned circuit with negative resistance.

Q of $r/\omega L$ without the feedback; with the addition of the resistance R_{in} , the Q becomes $rR_{in}/(r + R_{in}/\omega L)$. The Q has been changed by the ratio

$$R_{in}/(r + R_{in}/\omega L).$$

The circuit of the complete multiplier is shown in Figure 28. The 1,000-cycle input is twice amplified, clipped, and differentiated by the stages containing the first four tubes to produce the pulses. These pulses are applied to the parallel-tuned circuit, which is followed by a two-stage amplifier and a cathode-

follower output tube. The two-stage amplifier that provides the negative resistance uses negative feedback and a regulated power supply for stability and a fairly low impedance output to avoid trouble with wiring capacities in the feedback controls. The cathode-follower output stage provides a low impedance output and isolates the amplifier stages from the load. The tuned circuits, switches, trimmers, and feedback adjustments are housed in a separate box for both electric and thermal isolation. For stable operation, considerable care must be taken in the arrangement of components and wiring.

The coils used are Western Electric toroids wound on molybdenum-Permalloy cores ($\mu' \doteq 125$). Higher Q 's could probably have been obtained at the desired frequencies by using cores of lower permeability ($\mu' \doteq 26$). Three inductances are used to keep the capacity required to tune the coils to the 12 frequencies within a convenient range. A pushbutton switch selects the inductance, capacitance, and feedback required for the frequency desired. The use of a pushbutton instead of a rotary switch permits the selection of frequencies in any order without the necessity for switching through intervening positions. A door on the front panel gives ready access to the trimmer condenser and feedback adjustments for each frequency. These adjustments do not have to be made frequently. The pushbutton switch on the input circuit permits a momentary disconnection of the 1,000-cycle input to determine whether the feedback circuit is causing oscillation.

The output of this multiplier is satisfactorily stable at a level of about 10 volts and frequencies of 7, 8, 9, 10, 11, 12, 13, 17, 19, 23, 29, and 31 kc with a 1-kc input of about 5 volts. The selectivity of the tuned circuit is sufficient at any of these frequencies to attenuate the adjacent harmonics at least 26 db so that the output is more than satisfactory for the production of Lissajous figures. The effective Q 's of the tuned circuits range from 100 to 400; they are greater for the higher frequencies because of the need for greater selectivity at high frequencies of resonance in order to attenuate a frequency 1 kc off resonance.

4. *Frequency-Comparison Oscilloscopes.* The frequency of the oscillator output is compared with a standard frequency by means of the Lissajous figure on the screen of a cathode-ray tube, to the deflection plates of which are applied signal voltages of the two frequencies. An oscilloscope for this purpose requires only the cathode-ray tube, amplifiers to supply sufficient voltage to the deflection plates, and a power

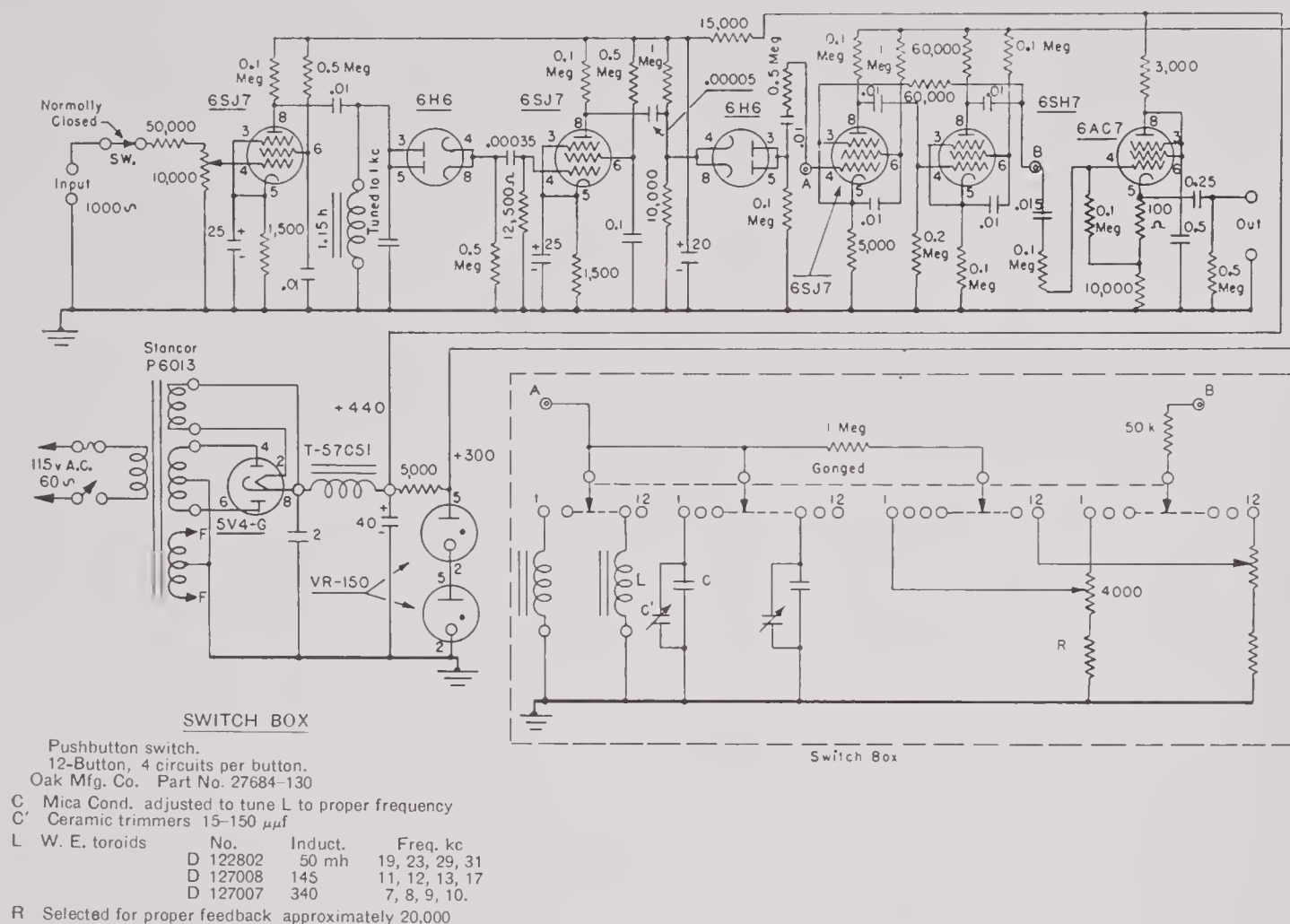


FIGURE 28. Frequency multiplier.

supply. Two such oscilloscopes have been constructed for use with the impedance and admittance bridges.

The oscilloscope shown with the impedance bridge in Figure 14, just below the WE oscillator in the right-hand rack, contains a single 2-in. 2AP1 cathode-ray tube. The upper row of knobs controls the focus, intensity, vertical and horizontal centering. The lower three knobs are gain controls for the oscillator and 1-ke and 10-ke inputs. Two toggle switches permit the horizontal deflection amplifier to be connected to either the 1-ke or 10-ke input and the vertical deflection amplifier to be connected to either the 10-ke or the oscillator input. Thus the oscillator output can be compared to either the 1-ke or 10-ke standard, and the 10-ke output of the frequency multiplier can be checked against the standard 1 ke. The oscilloscope input, together with the bridge input, is connected across the 135-ohm output of the WE oscillator.

The oscilloscope shown with the admittance bridge in Figure 18, just above the GR oscillator in the

right-hand rack, contains two 2-in. 2AP1 cathode-ray tubes. The oscillator output is applied to the vertical deflection plates of both tubes, but the 1-ke standard is applied to the horizontal plates of one tube, while the output of the frequency multiplier is applied to the horizontal plates of the other. This permits a continuous comparison with the 1-ke standard and a simultaneous comparison with one of the standard frequencies from the multiplier. The three knobs on the panel are gain controls for the oscillator, 1-ke and multiplier inputs. The intensity, focus, and centering controls for the cathode-ray tubes are located behind the panel. The oscillator input to the oscilloscope is connected to the 5,000-ohm output terminals of the GR oscillator.

5. *Detectors.* Because of the frequency range over which the bridge must operate and the occasion for continuous operation over long periods, an aural indication of balance such as that used in a telephone is not practical, and a pointer indicator is preferable. A simple form of visual detector is, of course, the a-c

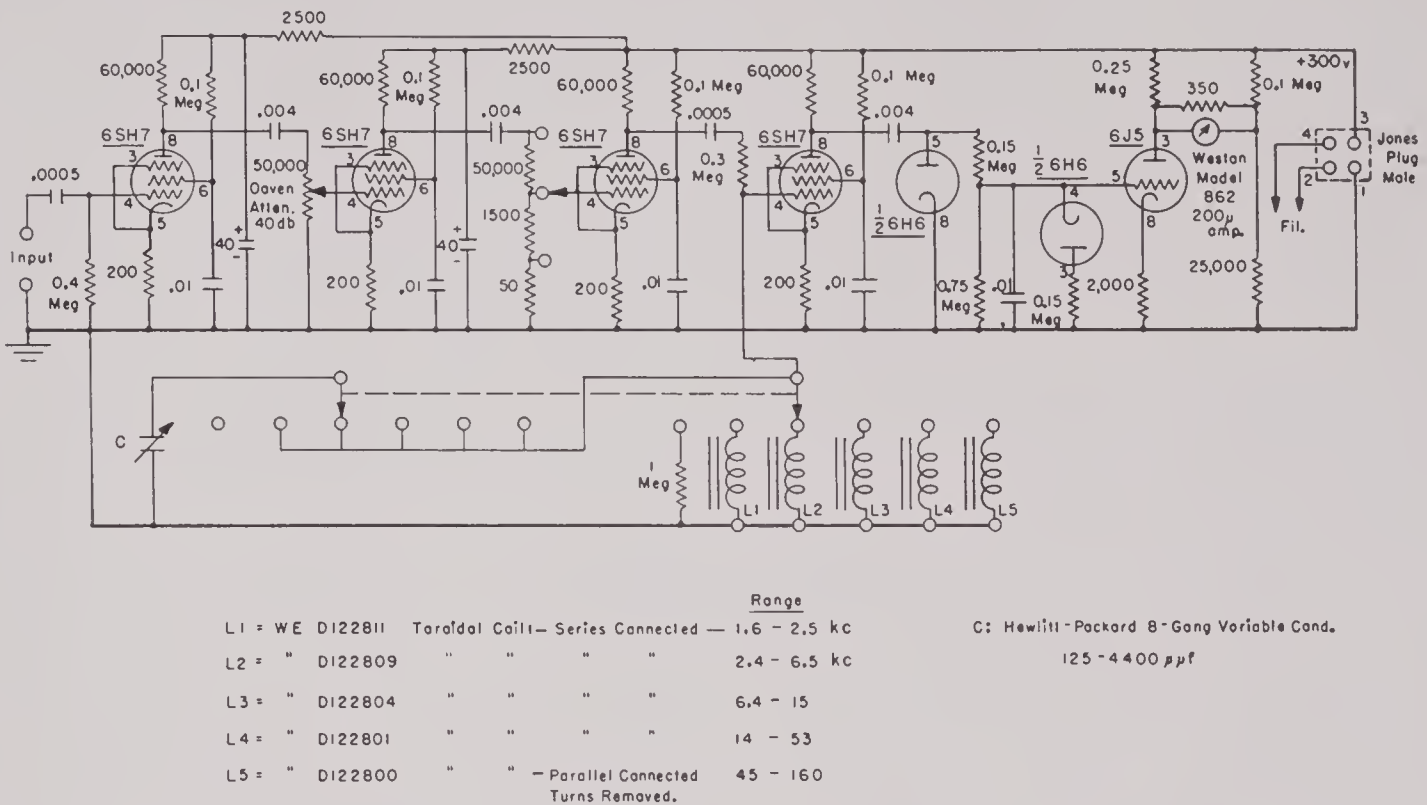


FIGURE 29. Tuned amplifier bridge detector.

voltmeter. A voltmeter can be made to operate over the required frequency range and, by the use of vacuum-tube amplifiers, can be made very sensitive. By varying the gain of the amplifiers, the sensitivity of the voltmeter can be altered, so that the response of the indicator to the bridge voltage is effectively logarithmic and changes in that voltage are easily detected, even though the magnitude of the voltage varies over a wide range.

The use of a tuned detector is advantageous. The maximum usable sensitivity of a detector is limited by the noise level due to harmonics in the oscillator output, tube noise in the amplifiers, and pickup in the bridge wiring and the unknown. With a tuned detector this noise can be reduced and the signal-to-noise ratio considerably improved, so that the indication of the detector is positive and steady, even though the sensitivity is high. Very small voltages can be detected with a tuned voltmeter, thus making possible a very sharp balance at the bridge.

A tuned-amplifier vacuum-tube voltmeter for use as a detector with the impedance and admittance bridges is shown in the circuit diagram of Figure 29. The detector is designed to fit the bridge consoles but it is made portable so that it can be readily removed from the console for use with other bridges and for measurements at field stations. The detector is shown

in position in the bridge consoles in Figures 13, 14, 17, and 18. Its panel contains the meter, a tuning control, a band-changing switch for the tuner, and coarse and fine gain controls. The connections of the external, voltage-regulated power supply and the input are made at the rear of the chassis.

The detector of Figure 29 uses three pentode stages of a-c amplification, followed by a parallel-tuned circuit across the input of a fourth stage. This fourth stage feeds a shunt-type diode rectifier. One half of the 6H6 double-diode is used to balance out the current due to contact-potential effect in the rectifier, so that there is no d-c output when no signal is applied to the rectifier. A negative voltage from the rectifier is applied to the grid of the 6J5.

The triode 6J5 forms one branch of the Wheatstone bridge network of Figure 30. When no d-c voltage from the rectifier is applied to the grid of the triode, the bridge arms are so adjusted that the bridge is balanced and no current flows through the meter. If the triode is further biased by a negative voltage on its grid, the bridge is unbalanced, and a current passes through the meter. When the negative voltage on the grid reaches the cutoff point of the tube, the current through the meter is a maximum, and further increases in the signal have no effect on the meter. By choosing the values of the bridge components so

that this maximum current through the meter causes full-scale deflection, the meter can be protected against overloading, regardless of large changes in the input signal. This type of meter circuit is very useful in detectors, since large and rapid changes in signal level occur in the process of balancing the bridge. The relation of meter deflection to a-c input for this meter circuit and rectifier is shown in Figure 31.

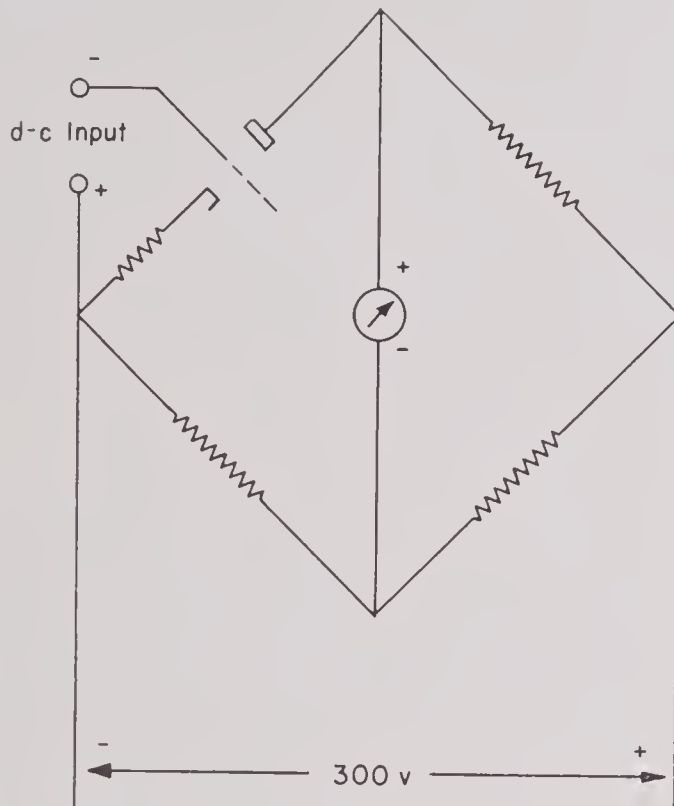


FIGURE 30. Voltmeter bridge.

The meter actually used in construction of the detectors was a Weston Model 862-VU meter, because it has a large illuminated scale and was available at the time. The internal copper-oxide rectifier is disconnected for this application. With the 350-ohm shunt shown in Figure 29, the damping of the meter is very satisfactory for use in the detector. The first gain control in the amplifier is a 50,000-ohm Daven attenuator Type P-621-S having a 40-db range in 2-db steps, with the detent mechanism removed to make its operation easier. This attenuator was used because of its positive reliable action. The second gain control has three steps, giving attenuations of approximately 0, 32, and 65 db.

With the detector tuned to 20 kc and set at maximum gain, the input required for 75 per cent of full-scale meter deflection is -106 db vs 1 volt. The frequency response without the tuned circuit is flat

within ± 1 db from 2 to 100 kc. The sharp balance obtainable with this tuned detector is evident from the experimental curves shown in Figure 9B; the minimum measurable voltage was over 100 db below the signal voltage applied to the bridge.

The amplifier is tuned by means of the parallel inductance and capacitance across the input of the fourth amplifier stage. The frequency to which the amplifier is tuned can be varied continuously over a

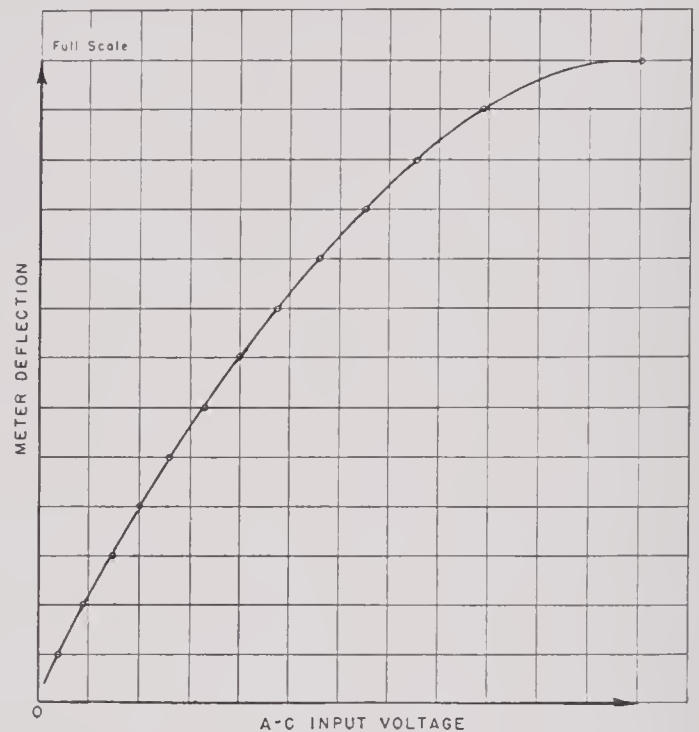


FIGURE 31. Relation of meter deflection to a-c input.

range by means of the variable condenser C whereas the tuning range can be changed by a selector switch that chooses one of the five inductances L_1 to L_5 . One position of the range-selector switch disconnects the tuned circuit wide-band operation of the detector. The detector is tuned to the frequency of the signal applied to the bridge by adjusting the tuning controls for a maximum deflection of the detector meter when the bridge is not balanced. Although this adjustment must be made whenever the frequency is changed, thus lengthening the process of measurement, experience has proved that the advantages of a tuned detector more than offset the inconvenience of having to tune it.

Although this type of detector has been very satisfactory, the use of a detector with phase selectivity would facilitate attainment of balance by discriminating between the effects of reactance and resistance

NAME _____			REMARKS _____			DATE _____		
POLARIZING CURRENT _____			_____			BY _____		
AIR OR WATER _____			_____			FOR _____		
TEMPERATURE _____			_____			_____		

F	R	C	ADMITTANCE		G^2	B^2	$G^2 + B^2$	IMPEDANCE	
			G	B				R	X

FIGURE 32. Block diagram of BTL's cathode-ray detector.

bridge adjustments. Phase-selective detectors⁴³ have been considered for use with the impedance and admittance bridges, but none has been tried. However, the development of the vector impedance locus plotter in this laboratory²⁵ has suggested the application of this device as a detector. With slight modifications, the VILP circuit could be used to plot the vector voltage appearing across the detector terminals of the bridge, indicating both phase and magnitude. This vector could be plotted on the screen of a cathode-ray tube, or two meters could be used to indicate the magnitudes of the components of the vector voltage. The only adjustment necessary would be that of a gain control in the amplifiers, since the circuit is inherently frequency-selective and requires no tuning. This gain control might conveniently be foot-operated, leaving the operator's hands free for the manipulation of the bridge components.

Another useful type of phase-sensitive detector is that described by Lamson.³⁴ The balance is indicated by an ellipse on the screen of a cathode-ray tube. When the bridge is unbalanced the ellipse has its major axis tilted from the horizontal, and the adjustment of either bridge control will simultaneously change both the tilt and the length of the minor axis. By varying the phase of the voltage from the oscillator applied to the horizontal sweep of the tube, the reactive adjustment of the bridge can be made to alter only the tilt and the resistive adjustment only the length of the minor axis, so that the detector is phase-selective. When the bridge is balanced the ellipse becomes a horizontal straight line on the screen.

This type of detector is employed by the Bell Telephone Laboratories in their D-169459 and D-170369

cathode-ray detectors⁴⁷ for use with their W-10135 and W-10125 impedance bridges. These detectors use a tuned amplifier but employ a selective feedback network for tuning³⁵ instead of the L - C circuit used in the detectors designed for the impedance and admittance bridges. A block diagram of these detectors is shown in Figure 32. The detectors differ only in the frequency range for which they are designed; D-169459 covers the range 20 to 20,000 cycles; D-170369, 200 to 200,000 cycles. Provision is made for the use when desired of a meter instead of a cathode-ray tube. The cathode-ray tube can also be used to check frequency if the horizontal plates are switched to a standard frequency instead of to the bridge oscillator. Some *automatic volume control* [AVC] is used to prevent overloading when the bridge is off balance.

The use of selective feedback for tuning could provide better selectivity than that used in the detector of Figure 22, but sharper tuning does not seem to be necessary, hence the more exact adjustment required is an unnecessary complication. Whether the additional adjustment of the phase-shifting network required for phase-sensitive detection can be justified by the advantages gained thereby has not been determined, since this type of detector was never tried with the admittance bridge or impedance bridge.

6. *Polarizing Equipment.* The direct current sometimes required to polarize magnetostrictive transducers is supplied by a 168-volt storage battery. This battery is divided into 14-volt sections, which can be connected in any series or parallel combination by means of a plug-and-jack system. The current drawn from this battery is controlled by the rheostats and meters mounted on a panel located beside the bridge.

Two such polarizing panels are shown mounted in the racks to the left of the bridge consoles in Figures 14 and 18. The d-c circuit containing the battery and polarizing panel components as used to polarize a transducer is shown in Figure 33.

Since the impedance of the source of direct current is in parallel with the transducer, the choke shown in Figure 33 is connected in series with the high side of this source to increase the impedance shunting the transducer. The effect of this shunt impedance can be made negligible by using a choke with an impedance great enough compared with that of the transducer. However, the choke must also be capable of carrying large direct currents for relatively long periods. The

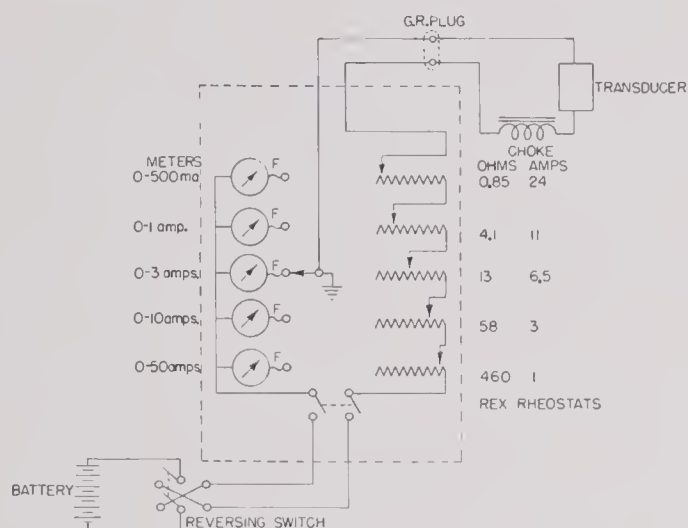


FIGURE 33. Polarizing circuit.

chokes shown on the shelves above the polarizing panels in the left-hand racks of Figures 14 and 18 are satisfactory for most measurements. These have an inductance of about 170 mh and are self-resonant at about 40 ke. There is a powdered iron core inside the solenoidal coil, but the effects of saturation are negligible even with direct currents over 6 amp. When higher current or impedance is required, a special choke must be used and may be parallel-tuned for maximum impedance.

Since the rotor of the switch used to change meters is not insulated, one side of the polarizing circuit is grounded to the polarizing panel, but because one side of the transducer is generally grounded, this causes no trouble. A single meter with a variable shunt could have been used in this circuit instead of the five ammeters, but this would have required more complex switching.

Treatment of Data. Data are obtained from the impedance bridge for an inductive unknown in the

form of a resistance and a capacitance, and for a capacitive unknown in the form of a resistance and two capacitances. The resistance read from the bridge is the series-equivalent resistance required to plot the impedance locus. The required reactance, however, must be calculated from the value of capacity obtained from the bridge by use of the equations $X = 1/\omega C$ for an inductive unknown and $X = 1/\omega C_s - 1/\omega C$ for a capacitive unknown. The data obtained from the bridge and the results of the calculations are conveniently recorded on a data sheet of the form shown in Figure 34. The calculation of reactance can be made on a slide rule in the following manner. The value of the frequency on the C scale is set above 159 on the D scale. With the hairline of the indicator set at the value of the capacity on the CI or CIF scale, the reactance is read under the hairline on the corresponding D or DF scale.

The data obtained from the admittance bridge are in the form of a resistance and a capacity for both inductive and capacitive unknowns. The resistance is the equivalent parallel resistance of the unknown, and the reciprocal of this resistance value must be computed to determine the conductance. The susceptance must be calculated from the capacity by use of the relation $B = \omega C$, where B is positive when the capacity is across the same arm of the bridge as the unknown. The data obtained from the bridge and from the calculations are conveniently recorded on a data sheet of the form shown in Figure 35. When the unknown is shunted by a 10,000-ohm resistor, the reading of the resistance box is recorded as R , but the 0.1-millimho conductance of this resistor is mentally subtracted from the calculated reciprocal of R , so that the recorded conductance G is that of the unknown. The susceptance can be conveniently calculated on a slide rule in the following manner. The hairline on the indicator is set to twice the value of the frequency on the D scale. The capacity value of the CIF scale is set under the hairline. The susceptance is then read on the D scale under the index of the C scale or on the DF scale above the index of the CF scale.

When an impedance locus is to be plotted directly from the admittance bridge data, the data sheet of Figure 36 is convenient. Admittance data are converted to impedance by use of the relations

$$R = \frac{G}{G^2 + B^2} \quad \text{and} \quad X = \frac{B}{G^2 + B^2}.$$

DATA ON _____

DATE _____

BY _____

POLARIZING CURRENT _____

FOR _____

REMARKS _____

TEMPERATURE _____

FREQUENCY	RESISTANCE	CAPACITY	REACTANCE	STD. CAP'Y	REACTANCE	REACTANCE

FIGURE 34. Impedance data form.

NAME _____

REMARKS _____

POLARIZING CURRENT _____

DATA _____

LOADING _____

BY _____

D.C. RESISTANCE _____

FOR _____

TEMPERATURE _____

F	R	C			G	B

FIGURE 35. Admittance data form.

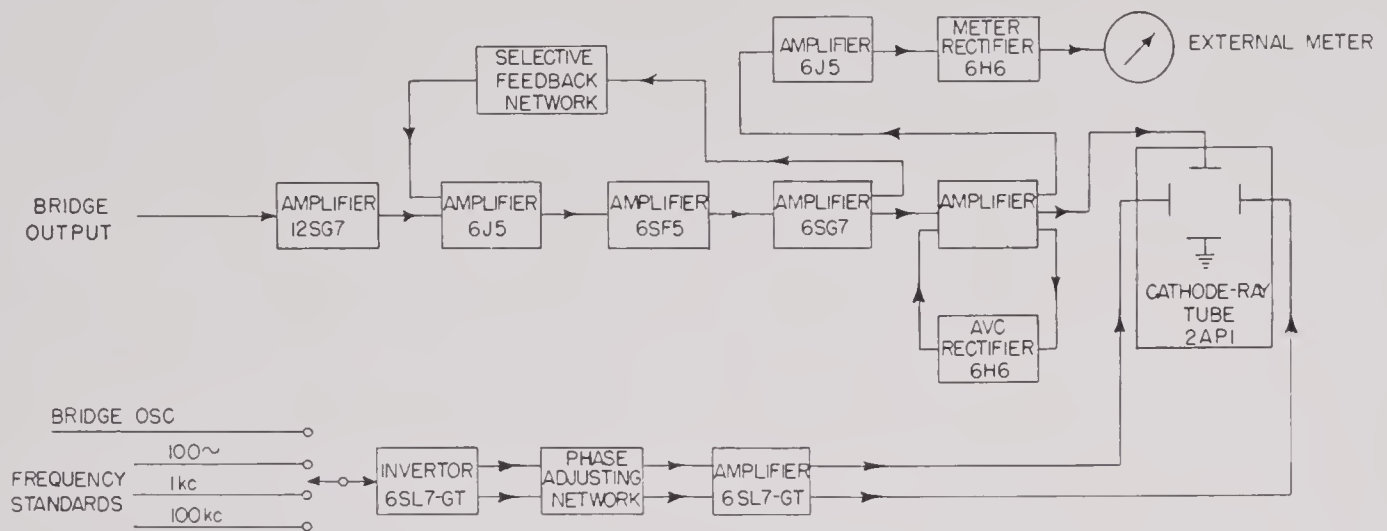


FIGURE 36. Admittance-impedance data sheet from Tank Department.

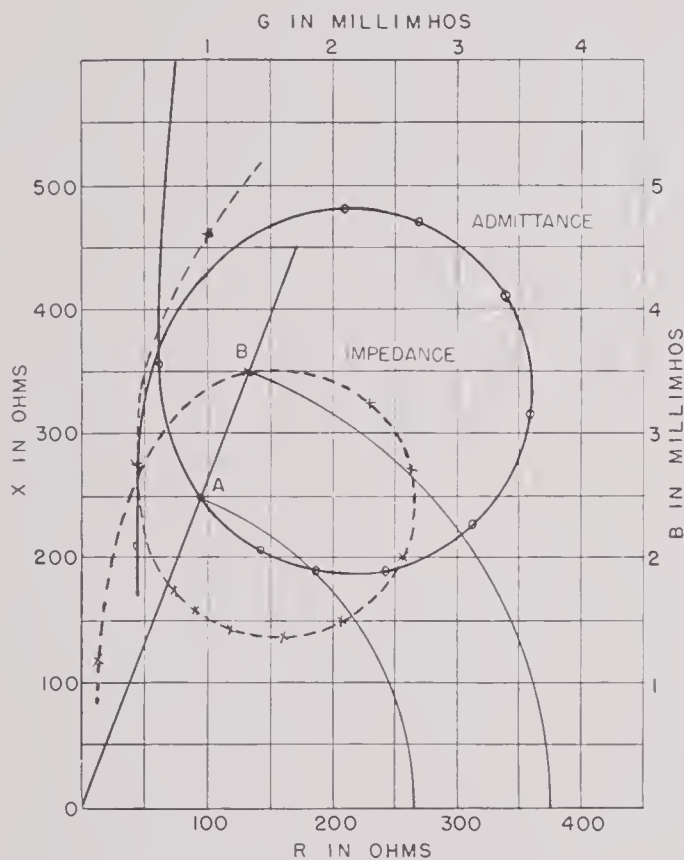


FIGURE 37. Conversion of admittance locus to impedance locus.

The conversion of an admittance locus to the corresponding impedance locus or vice versa can be made by a simple semigraphical method.^c Admittance has been so defined that the admittance vector has the same phase angle as its corresponding impedance vector but a magnitude that is the reciprocal of

^c For a discussion of a graphical method of conversion, see reference 11.

that of the impedance vector. Hence the admittance and impedance vectors corresponding to a given frequency lie along the same line through the origin. Thus in Figure 37, if a line is drawn from the origin through any point on the admittance locus, such as A, this line must also contain the point on the impedance locus corresponding to the point A. To locate this point along the line through A, the length of the vector from the origin to A can be measured with a compass in terms of the scale of the G or B axis. In Figure 37 the magnitude of the admittance vector with tip A is 2.67 millimhos. By computing the reciprocal of the admittance magnitude thus determined, the magnitude of the impedance can be found. The impedance corresponding to the admittance of point A is 374 ohms. If then, a length equivalent to this impedance measured along the scale of the R or X axis is laid out with the compass from the origin along the line through A, the point B on the impedance locus corresponding to A on the admittance locus will be determined. By repeating this process for other points on the admittance locus, the corresponding impedance locus can be drawn. The scale of the impedance axes can, of course, be chosen arbitrarily and need not be so simply related to that of the admittance axes as is the case in Figure 37.

T Networks. A null method for the measurement of impedance can employ T networks instead of bridge networks.⁴⁰ However, the T networks are not well adapted to the routine measurement of transducers because their ranges of frequency and impedance are not sufficient at the low end, they cannot readily be used to measure capacitance, and their operation is difficult. They can be used to advantage

for particular measurements within their range where the peculiar characteristics of these networks can be utilized for higher accuracy than that obtainable with a bridge network.

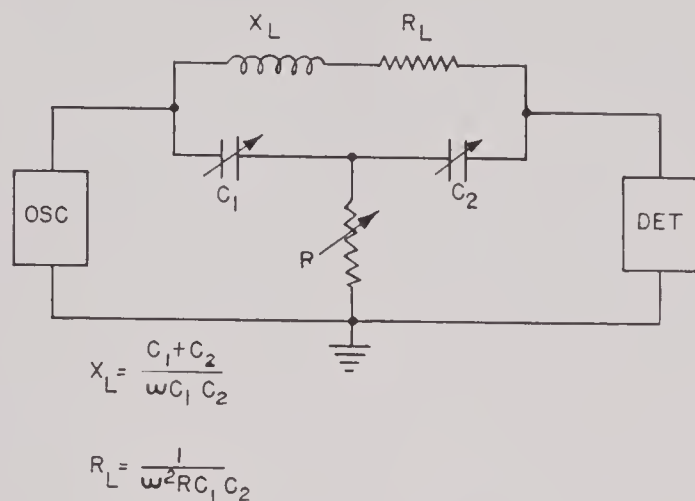


FIGURE 38. Bridged-T network.

Bridged-T. The bridged-T network shown in Figure 38 is useful in measuring fairly high inductances with superposed direct current. The balance conditions of this network are independent of the impedances of the source and the detector. Hence a battery can be connected in series with either source or detector to superpose a direct current on the inductance being measured, if the source and detector are capable of carrying the desired direct current. Usually the source and detector must be shunted by chokes to by-pass the direct current, but the size of these chokes is not critical since they do not affect the accuracy of measurement. No transformer is required because one terminal of both source and detector can be grounded. One terminal of the variable resistance can also be grounded, and one terminal of each of the condensers is effectively at ground potential since capacities across the source and detector do not affect the measured quantities.

A practical circuit used for the measurement of the impedance of polarizing chokes is shown in Figure 39. The chokes CH are used to provide a d-c path without passing direct current through the oscillator or detector. A decade resistor is used for the resistance R , a decade capacitor for C_2 , and a fixed GR standard condenser for C_1 . The condensers are connected so that most of their capacity to ground falls across the source or detector rather than across R , where it would become a source of error. Care must be taken to avoid coupling between the choke being measured and the other two chokes. Balance is at-

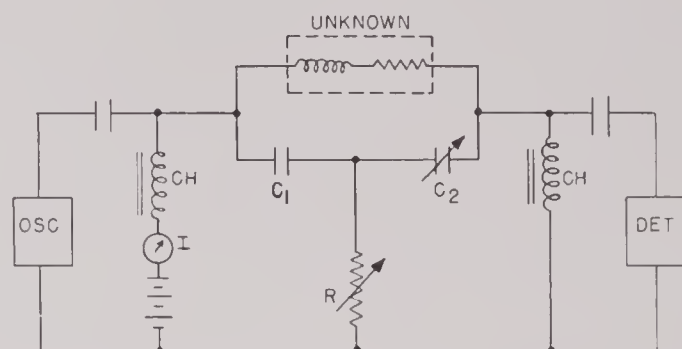


FIGURE 39. Bridged-T circuit for measurement of choke impedance.

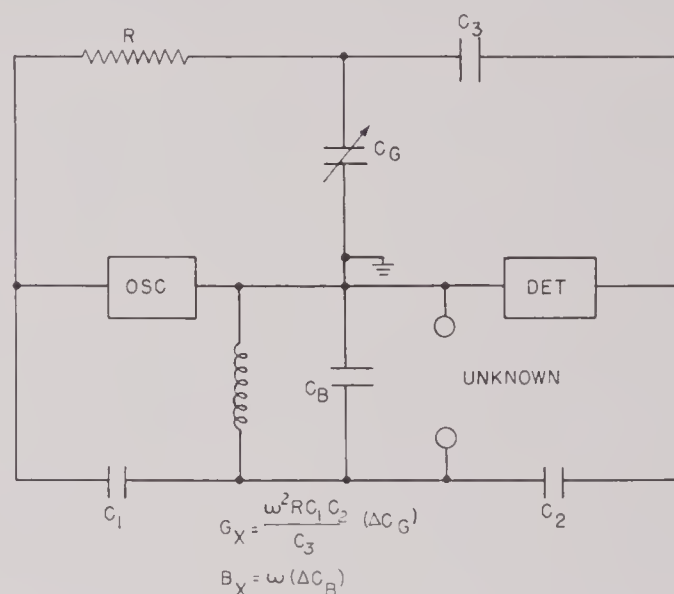


FIGURE 40. Parallel-T or twin-T network.

tained by varying R and C_2 for a minimum reading of the detector. The magnitude of C_1 must be chosen so that the value of C_2 for balance is within the range of the decade, but C_1 can be varied by plugging in different sizes of standard condensers.

Parallel-T. The parallel-T, or twin-T network, shown in Figure 40 is useful for the measurement by an accurate substitution method of relatively large inductances (150 mh) having a high Q (200). As in the bridged T, one terminal of both source and detector can be grounded, but in this network one terminal of each of the variable standards and of the unknown can also be grounded. The conductance of the unknown is measured in terms of a variable condenser, so that difficulties with the variation of reactive residuals in variable resistance standards are avoided. By use of a substitution method in which an initial balance is obtained without the unknown and a second balance with the unknown connected, the accuracy of the measurement of sus-

ceptance is limited only by the precision of the variable standards, while that of the conductance is limited only by the accuracy of the fixed and variable standards or by the exactness with which the conductance condenser can be calibrated with a known conductance.

This network has been used to check the measurements made on the admittance bridge of the Q of some toroidal coils, since these coils had a conductance beyond the accurate range of the bridge standards (about 0.2 micromho). Two GR precision air condensers were used for the variable condensers C_B and C_G . The other components were so chosen that the initial balance and the balance with the unknown connected both fell within the range of these condensers. Very reliable measurements of susceptance have been obtained with this network, but the accuracy of the conductance measurements has been limited by the lack of conductance standards of sufficiently small magnitude.

9.2.3 Measurement by Deflection Methods

The complete and accurate determination of an impedance or admittance locus is often unnecessary. An indication of the existence, relative size, and approximate resonant frequency of the motional

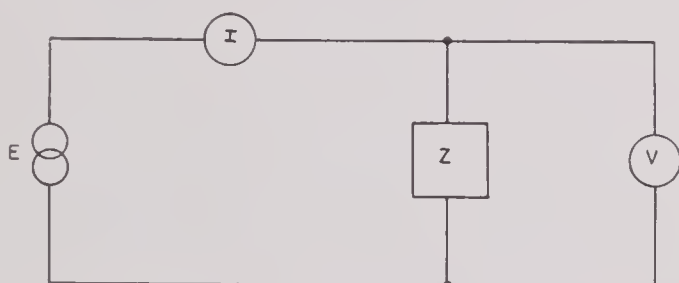


FIGURE 41. Voltmeter-ammeter method for impedance measurements.

circle is in many cases sufficient. It is also useful to determine only the maxima, such as the maximum resistance or maximum conductance and their associated frequencies. For the measurement of these quantities the accuracy of a null method is not required, and the use of point-by-point bridge measurements is needlessly time-consuming. A deflection method of measuring impedance can be used to advantage where high accuracy and a wide range of impedance and frequency can be sacrificed for a gain in speed and ease of operation. Another advantage of a deflection method is that the effect on the imped-

ance of changes made in the device being measured, such as a change in loading, polarization, and tuning, can be observed continuously as these variations are being made.

1. *Impedometer*. A simple method of obtaining a meter deflection proportional to impedance is the voltmeter-ammeter method shown in Figure 41. If the current is held constant while the frequency is varied, the voltage V is proportional to the magnitude of the impedance Z . The voltmeter can be calibrated to read impedance.

A form of this circuit employed for impedance measurements is shown in Figure 42. This has been called an *impedometer*. A constant current is obtained by using a resistance, which is large compared to the

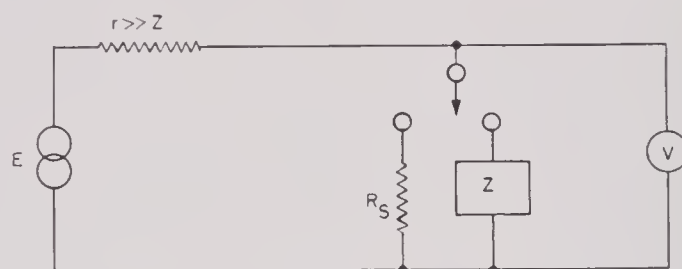


FIGURE 42. Impedometer circuit.

impedance being measured, in series with a constant-voltage generator. The voltage across the unknown impedance Z is measured with a sensitive vacuum-tube voltmeter, such as the Ballantine Model 300 electronic voltmeter. The voltmeter is calibrated to read impedance by comparing the deflection produced by the unknown to that produced by a known impedance, such as the resistor R_s . With the voltmeter across the known impedance, the current can be adjusted to produce a convenient deflection of the voltmeter by varying the voltage E .

The same circuit can be used to measure impedance by a comparison method, if higher accuracy than that obtainable by the deflection method is desired. The voltmeter is switched alternately to the unknown and to a variable standard impedance, such as a decade resistor. If the standard is varied until the same deflection of the voltmeter is produced by both impedances, the magnitude of the unknown is equal to that of the standard. The accuracy of the voltmeter calibration does not affect this measurement.

The impedometer circuit has been useful for rough measurements of impedance magnitudes. It has also found application in determining the relative diameters of motional impedance circles and the approximate resonant frequencies. The resonant frequency

can be approximated by finding the average of the two frequencies that produce the minimum and maximum impedance in the region of resonance. This average frequency is useful as a criterion for the comparison of the resonant frequencies of the transducer elements in multielement transducer production.

2. *Admittometer.* In a manner similar to that used for impedance, a deflection proportional to admittance can be produced with the circuit of Figure 43. Since $I = EY$, if the voltage is held constant the current I is proportional to the admittance Y . The ammeter I can be calibrated directly in admittance.

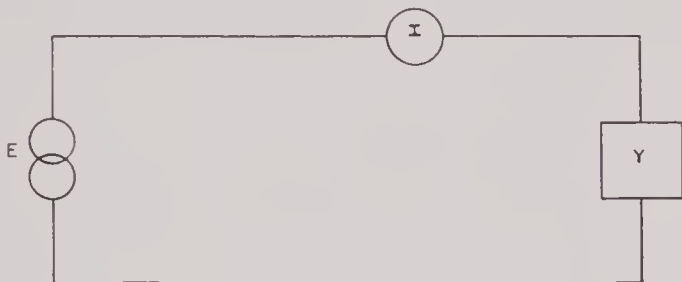


FIGURE 43. Voltmeter-ammeter method for admittance measurements.

An *admittometer* circuit is shown in Figure 44. A constant voltage generator is used to supply the voltage E . The current is measured by a sensitive voltmeter connected across a small resistance r in series with the unknown. The admittance of r should be large compared with that of the unknown. The voltmeter is calibrated by connecting a known admittance, such as a resistor R , in place of the unknown.

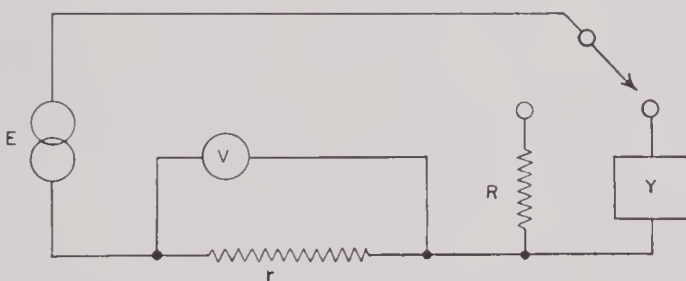


FIGURE 44. Admittometer circuit.

3. *Resolving Circuits.* In both the impedometer and admittometer the meter deflection indicates only the magnitude of the vector impedance or admittance. The characteristics of the impedance or admittance loci could be better determined if the phase of these vectors was also indicated. One method of indicating both the phase and magnitude of the vectors is to

obtain meter deflections proportional to both the resistive and reactive components of the impedance vector or to the conductive and susceptive components of the admittance vector. To produce such deflections, voltages proportional to the desired components must be obtained from the device being measured.

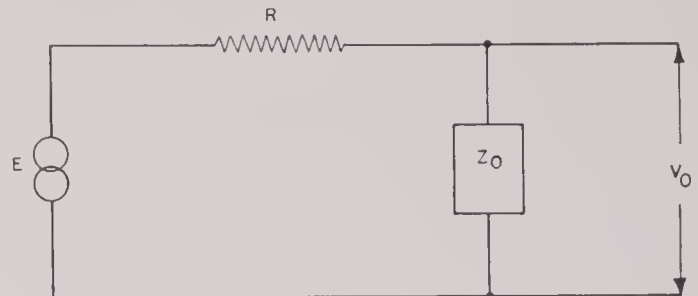


FIGURE 45. Impedometer circuit.

In the impedometer circuit of Figure 45, with the resistance R sufficiently greater than the impedance Z_0 to make the current through Z_0 independent of the changes in Z_0 and to make that current have the same phase as the voltage E , the voltage V_0 appearing across Z_0 is proportional in magnitude to Z_0 and differs in phase from the current and hence the voltage E by $\Phi = \arctan X_0/R_0$, the phase angle of Z_0 . Similarly in the admittometer circuit of Figure 46,

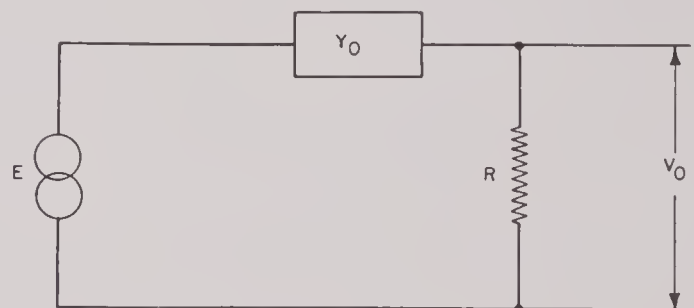


FIGURE 46. Admittometer circuit.

with the conductance of the resistor R so large compared to the admittance of Y_0 that the current through Y_0 is proportional to Y_0 , the voltage V_0 appearing across the resistance R is proportional to the magnitude of Y_0 and differs in phase from the voltage E by $\phi = \arctan B_0/G_0$, the phase angle of Y_0 . Hence in both circuits there appears a vector voltage V_0 which is proportional in magnitude to the vector impedance or admittance and has a phase angle with respect to another voltage E which is the same as the phase angle of the impedance or admittance.

The two components of V_0 , one, $|V_0| \cos \phi$, in phase with E and the other, $|V_0| \sin \phi$, in quadrature with E , are therefore proportional respectively to the real and imaginary components of the vector impedance or admittance.

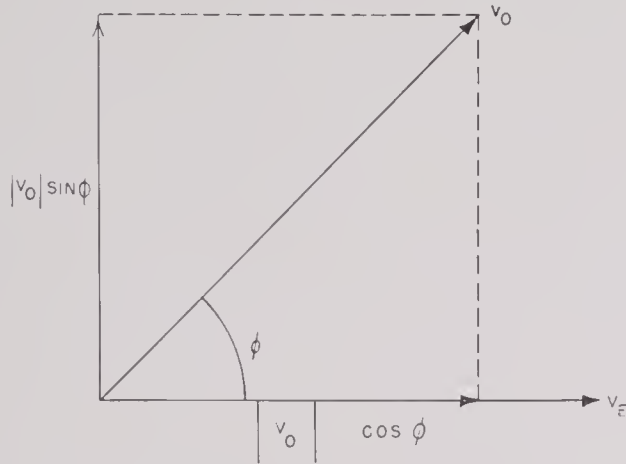


FIGURE 47. Vector diagram of voltages.

The resolution of such a vector voltage V_0 into two components, one in phase and the other in quadrature with a voltage E (Figure 47), can be accomplished electrically with the following component-taking or "resolver" circuit (also known as a phase-sensitive detector circuit). The switch in Figure 48 is controlled by the polarity of the voltage E .

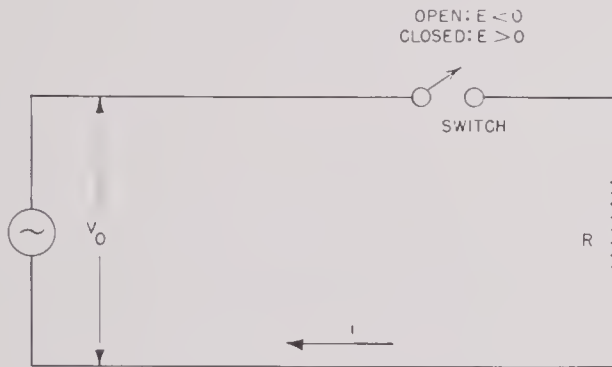


FIGURE 48. Resolver circuit.

For example, when E is positive the switch is closed, when E is negative the switch is open. The voltage E does not appear in the circuit of Figure 48; it merely operates the switch. When the frequency of E is the same as that of V_0 but the phase difference is ϕ , these voltages may be expressed as

$$\begin{aligned} V_0 &= |V_0| \sin \theta \\ E &= |E| \sin (\theta - \phi), \end{aligned}$$

and the current i through the circuit is

$$i = \frac{V_0}{R} = \frac{|V_0|}{R} \sin \theta \quad (E \text{ positive, switch closed})$$

$$i = 0 \quad (E \text{ negative, switch open}).$$

The average current through R is (Figure 49)

$$i_{\text{avg}} = \frac{1}{2\pi R} \int_{\phi}^{\phi + \pi} |V_0| \sin \theta d\theta$$

or

$$i_{\text{avg}} = \frac{|V_0|}{\pi R} \cos \phi.$$

Hence, the d-c voltage appearing across R is proportional to $|V_0| \cos \phi$, which is the desired component of V_0 in phase with E .

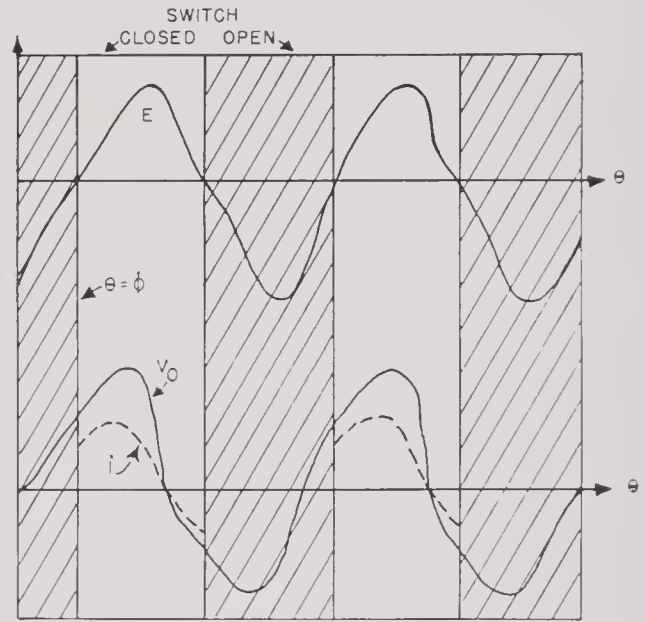


FIGURE 49. Phase diagram with E in phase with V_0 .

To obtain the quadrature component, the phase of E is shifted 90 degrees, so that

$$E = |E| \sin \frac{\theta - \phi - \pi}{2}.$$

The average current through R is now (Figure 50)

$$i_{\text{avg}} = \frac{1}{2\pi R} \int_{\phi + \pi/2}^{\phi + 3\pi/2} |V_0| \sin \theta d\theta$$

or

$$i_{\text{avg}} = \frac{-|V_0|}{\pi R} \sin \phi.$$

The d-c voltage across R is thus proportional to $V_0 \sin \phi$, which is the component of V_0 in quadrature with E .

Since the switch of Figure 48 must operate at switching frequencies up to 100 kc without phase error, any mechanical switch is impractical. One type of switch that can be used in the resolver circuit is an electronic switch in which the plate current of a multielectrode vacuum tube is cut off by a change

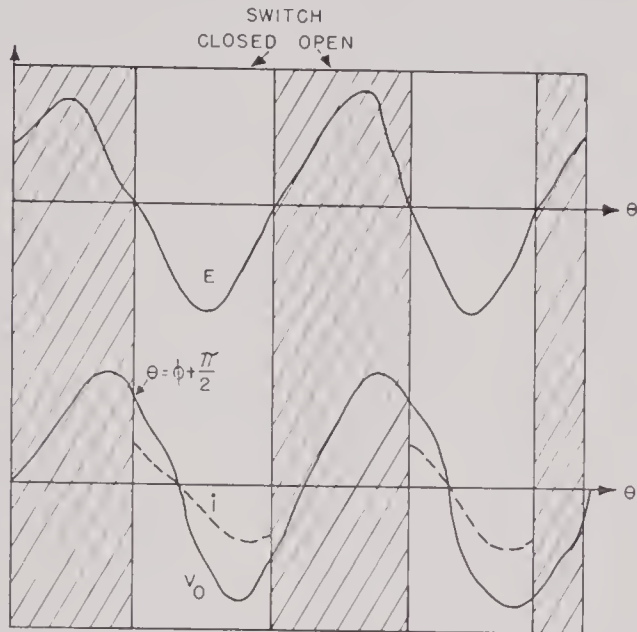


FIGURE 50. Phase diagram with phase of E shifted 90 degrees.

in the potential applied to one of the electrodes. The switching voltage can be applied to the plate, to any one of the grids, or to the cathode. With a signal voltage applied to the control grid, the tube functions as a normal amplifier of that signal for one polarity of the switching potential but cuts off the signal for the opposite polarity. This implies that the wave form of the switching voltage must be square in order to maintain proper electrode potentials during the half-cycle when the tube is to function as an amplifier and to cut off the plate current completely during the other half-cycle.

Another type of switch that can be used in this resolver circuit is the biased rectifier, illustrated in Figure 51. If the rectifier is assumed to be ideal and the switching voltage E is greater than V , the current through R is a function of V for one polarity of E and is zero for the opposite polarity. When the rectifier conducts, there is, of course, a component of current due to the switching voltage E . This can be eliminated from the output by using a balanced circuit, as shown in Figure 52. If the a-c switching voltage E is large compared with the signal voltage V , the cutoff of the rectifiers is sharp and the switch

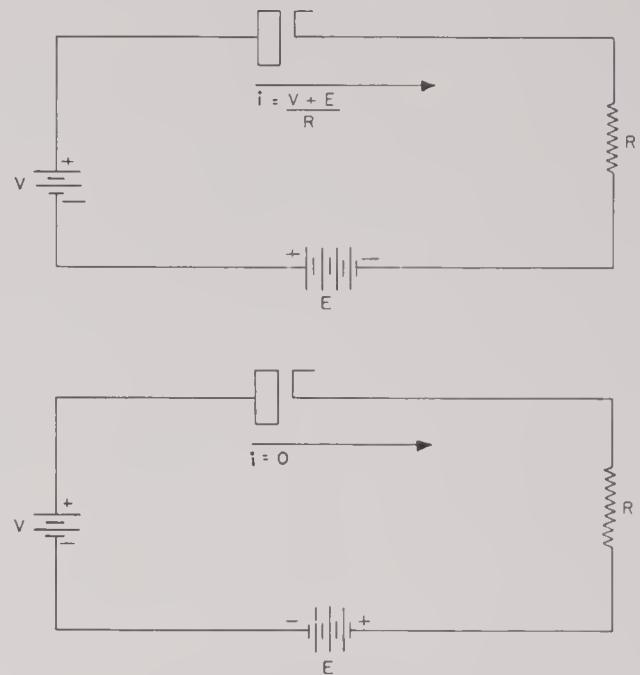


FIGURE 51. Biased rectifier switch.

is effectively open for one half-cycle of E . The rectifiers can be either varistors or diodes.³⁸

4. *Conductometer*. The point of maximum conductance on the admittance locus of a resonant transducer is useful as a criterion of both the potential efficiency and the frequency of maximum efficiency of the transducer because the principal diameter of the motional admittance circle is for many transducers nearly parallel to the conductance axis. The determination of the frequency and the value of the maximum conductance by bridge methods is too tedious and time-consuming to be applicable in

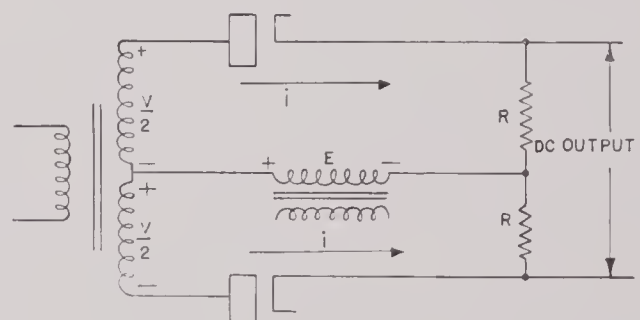


FIGURE 52. Balanced switch circuit.

production testing of large numbers of transducer elements. A deflection method combining the admittometer circuit with a resolving circuit in an instrument known as a *conductometer* is very useful for such measurements. The conductometer indicates on a meter the magnitude of the conductance of a transducer as a function of frequency.

The circuit of a conductometer is shown in Figure 53. This circuit is a combination of the circuits of Figures 46 and 52. The source of constant voltage required by the admittometer circuit is the feedback amplifier shown in Figure 54, which has an output impedance of less than 0.1 ohm. Since the resistance r , across which the voltage V appears, adds to the effective impedance of the source, this resistance must be kept small to maintain a constant voltage

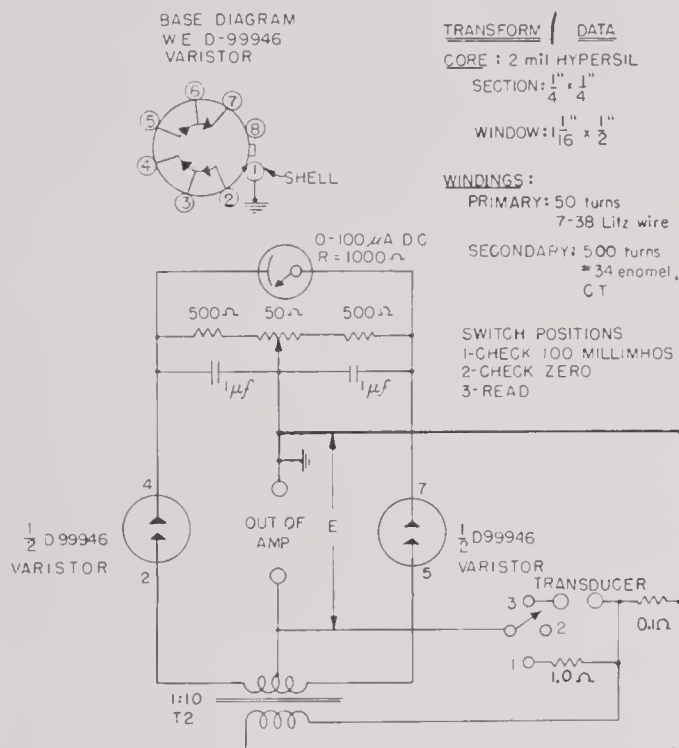


FIGURE 53. Conductometer circuit diagram.

across the transducer but must also be large enough to provide a usable voltage. With a 0.1-ohm resistor in series with the source, the total source impedance is about 0.2 ohm. In consequence, the amplifier can maintain an a-c output voltage constant within 4 per cent across a load whose admittance may vary from 0 to 200 millimhos.

The resolver circuit uses varistors as the rectifiers. The switching voltage is the same voltage from the amplifier output that is applied to the conductometer circuit. The signal voltage V is obtained from the 0.1-ohm series resistor through a 10-to-1 step-up transformer. The maximum usable switching voltage is limited by the 2-volt maximum allowable voltage on the varistors. With an amplifier output voltage of 1.5 volts, the conductance of the unknown can rise to 200 millimhos before the signal voltage ceases to be less than one-tenth of the switching voltage.

In the circuit shown, with an input voltage of 1.5 volts a conductance of 100 millimhos produces a 40-μa current through the meter.

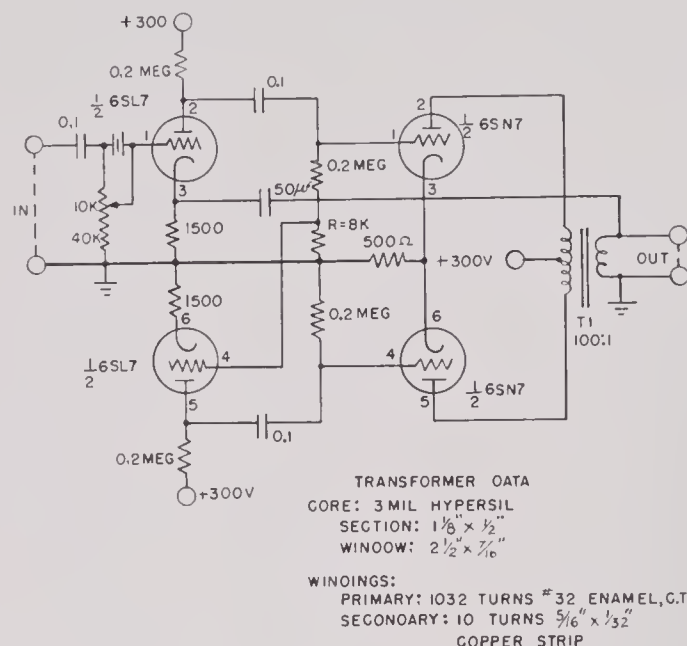


FIGURE 54. Conductometer amplifier diagram.

This conductometer is used as follows. An oscillator and power supply are connected to the amplifier. The input to the amplifier should be about 1.5 volts. With the switch on position 2 (Figure 53), the resolver circuit is balanced by adjusting the 50-ohm potentiometer so that the meter reads zero. With the switch thrown to position 1, the meter is calibrated by adjusting the input voltage, using the potentiometer on the amplifier input as a fine adjustment, so that the meter reading corresponds to a conductance of 100 millimhos. With the switch thrown to position 3, the meter reads the conductance of the unknown admittance connected to the terminals.

This conductometer circuit cannot be used over a wide range of frequencies because of the difficulty in maintaining the balance of the resolver circuit, which prevents the switching voltage from appearing in the output, and because of the difficulty in designing the transformer T_2 so that it has no phase shift as a function of frequency. However, the conductometer circuit was very useful in the production testing of laminated-stack transducer elements. In testing HP-3 stacks it was possible to determine easily and quickly the frequency of maximum conductance in air to within 0.02 per cent and the maximum conductance within 5 per cent.

5. *Vector Impedance Locus Plotter [VILP]*. The use of deflection methods of measuring a vector impedance or admittance can be extended ultimately to the automatic plotting of the locus of the vector. Since a combination of the impedometer or admittometer circuit and two resolver circuits can provide d-c voltages proportional to the two components of the vector impedance or admittance, these voltages can be used to operate a mechanical plotter or can be applied to the deflection plates of a cathode-ray tube to produce a trace of the locus on the screen of the tube, thus providing a very quick and easy method of measuring transducer characteristics.

A VILP was constructed for this purpose. It traces the locus of the tip of an impedance vector $Z = R + jX$ by plotting X against R on the face of a cathode-ray tube as the frequency of the applied signal is varied. This action is produced by the use of the impedometer circuit to provide a voltage V (Figure 45) across the impedance Z , which is proportional to the magnitude Z and has a phase angle with respect to the input voltage E equal to the phase angle of Z . Two resolver circuits are used to obtain d-c voltages proportional to the components of V that are in phase and in quadrature with the voltage E . These d-c voltages proportional to the real and imaginary components of Z are applied to the horizontal and vertical deflection plates of a cathode-ray tube. A transparent screen that bears suitable rulings is mounted in front of the cathode-ray tube and provides the coordinate axes.

The resolver circuits of the VILP employ an electronic switch because it is more suitable than the rectifier switch at high frequencies and at the high voltage and impedance levels required for cathode-ray deflection. As stated in the discussion of resolver circuits, the electronic switch requires a square-wave switching voltage. To obtain a square wave form from a sinusoidal switching voltage, a peak-clipping or limiting circuit can be used. The switching tube can itself serve to clip one of the peaks by use of the cutoff point of the electrode to which the switching voltage is applied. Since the rectangularity of the wave form increases with the proportion of the peak that is clipped, the voltage swing required on that electrode to cut off the tube should be small, so that a satisfactorily rectangular wave can be obtained without the application of an unduly large amplitude sine wave. The amplitude of the sine wave applied to the clipper must be sufficient to produce a satisfactorily rectangular wave but must not ex-

ceed the value that will cause distortion of that wave in the circuits in which it is generated or in those circuits to which it is applied. Within these limits, the effect of variations in the amplitude of the switching voltage upon the rectangularity and amplitude of the square wave, and hence upon the switching action, will be small.

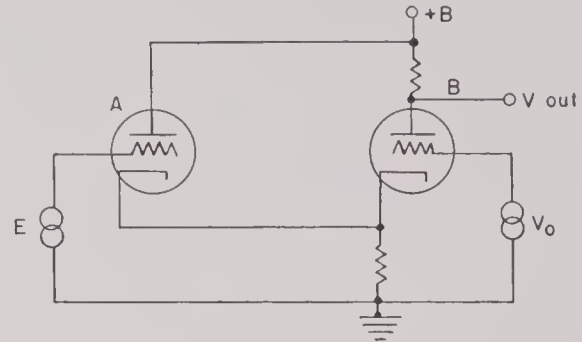


FIGURE 55. Electronic switch.

A sharp cutoff at a relatively low voltage can be obtained by applying the switching voltage to the cathode of a triode.^d A second triode (Figure 55), which has its cathode connected to that of the switching tube, is used to bias the switching tube to cutoff and, at the same time, to clip the other peak of the switching voltage. When the voltage E swings positive, the increase in cathode current cuts off tube B ; when E swings negative, tube A is cut off. The biases of the two tubes are so adjusted that the output of tube B with no signal V_0 is a symmetrical square wave and with tube A cut off tube B is properly biased to amplify V_0 . The voltage at the plate of B as a function of time is shown in Figure 56.

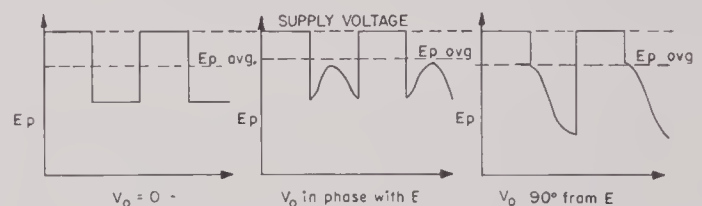


FIGURE 56. Plate voltage wave forms.

As Figure 56 shows, the output due to V_0 is in the form of half-wave pulses, which must be filtered to produce an average d-c output proportional to $|V_0| \cos \phi$. Less filtering is necessary with the full-wave circuit of Figure 57 and the d-c output for a given input V_0 is also doubled. In this circuit both the signal and the switching voltage are phase-inverted

^d The DuMont Type 185-A electron switch and square-wave generator employs a similar method of switching.

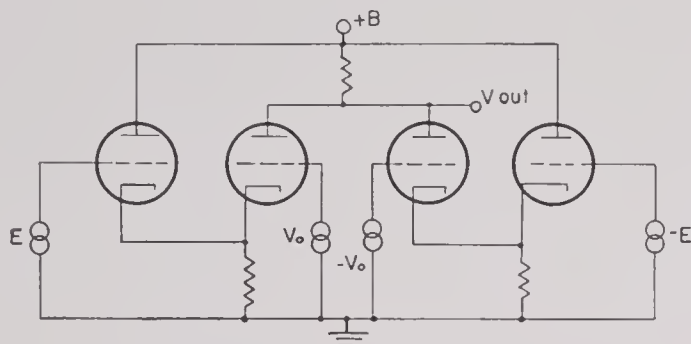


FIGURE 57. Full-wave switching circuit.

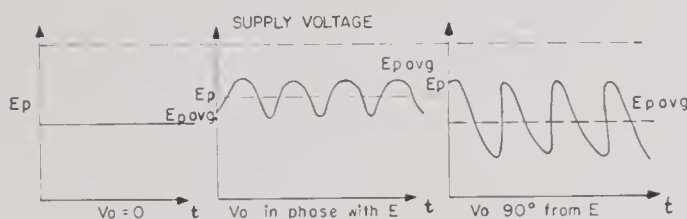


FIGURE 58. Plate voltage wave forms.

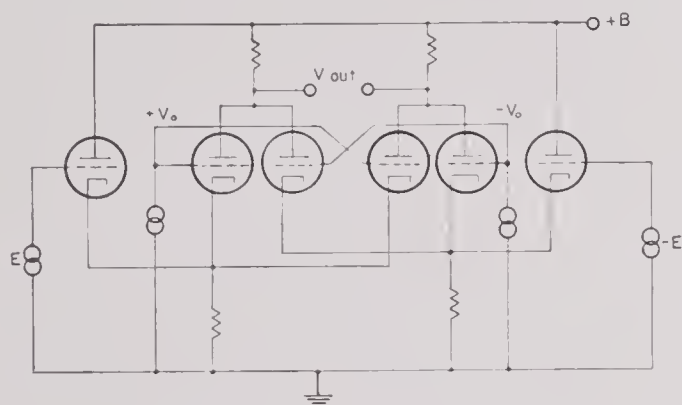


FIGURE 59. Balanced full-wave switching circuit.

and fed into two switching tubes with a common plate load. Since one tube is always conducting while the other is cut off, the plate remains at a constant potential when no signal V_0 is applied. The plate voltage as a function of time is shown in Figure 58. A further advantage of this circuit is the fact that the permissible d-c plate voltage swing due to the signal is doubled, since the average plate voltage with no signal V_0 is the operating plate potential of the tube (Figure 58) for this circuit, while for the half-wave circuit it is the mean value of the plate supply voltage and the operating potential (Figure 56).

For a balanced d-c output, two of the circuits of Figure 57 can be combined, as shown in Figure 59. The output of this resolver can be connected directly to the plates of a cathode-ray tube, since the output

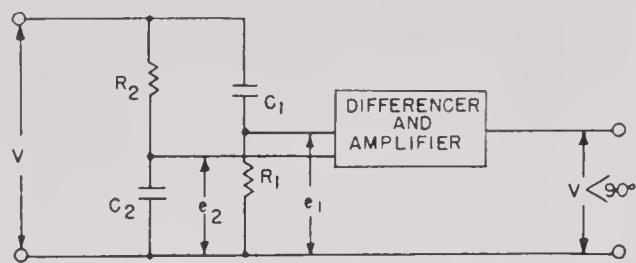


FIGURE 60. 90-degree phase shifter.

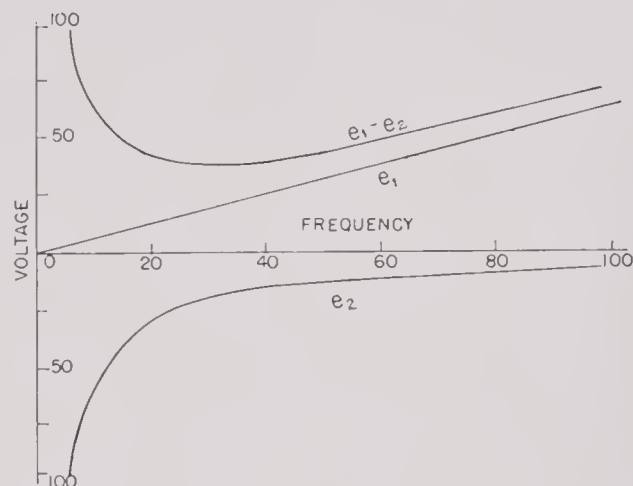


FIGURE 61. Frequency response of phase shifter.

voltage swing of the resolver tubes can be made large enough for cathode-ray tube deflection. Connection of the deflection plates directly to the resolver is not convenient because of the difficulty of adding to the resolver circuit a positioning control for the beam of the cathode-ray tube. For this reason, a cathode-coupled push-pull amplifier stage, directly coupled to the output of the full-wave, unbalanced-output resolver of Figure 57, best serves to provide balanced deflection voltages, together with a means of initially positioning the spot.

It was noted above that the switching voltage E must be shifted 90 degrees in phase in order to obtain the sine component of V_0 . Therefore a circuit is required that will give 90 degrees of phase shift over a wide range of frequency. A further requirement is that the magnitude of the output voltage of this circuit should be nearly constant with frequency, since changes of more than approximately 6 db in the switching voltage cannot be tolerated by the resolver circuits. These requirements can be met by a circuit consisting of two constant-resistance, all-pass, lattice networks whose outputs differ in phase by 90 degrees when they are fed from a common source.²⁴ However, the usable frequency range is limited to two octaves, and the networks are relatively complex, requiring the

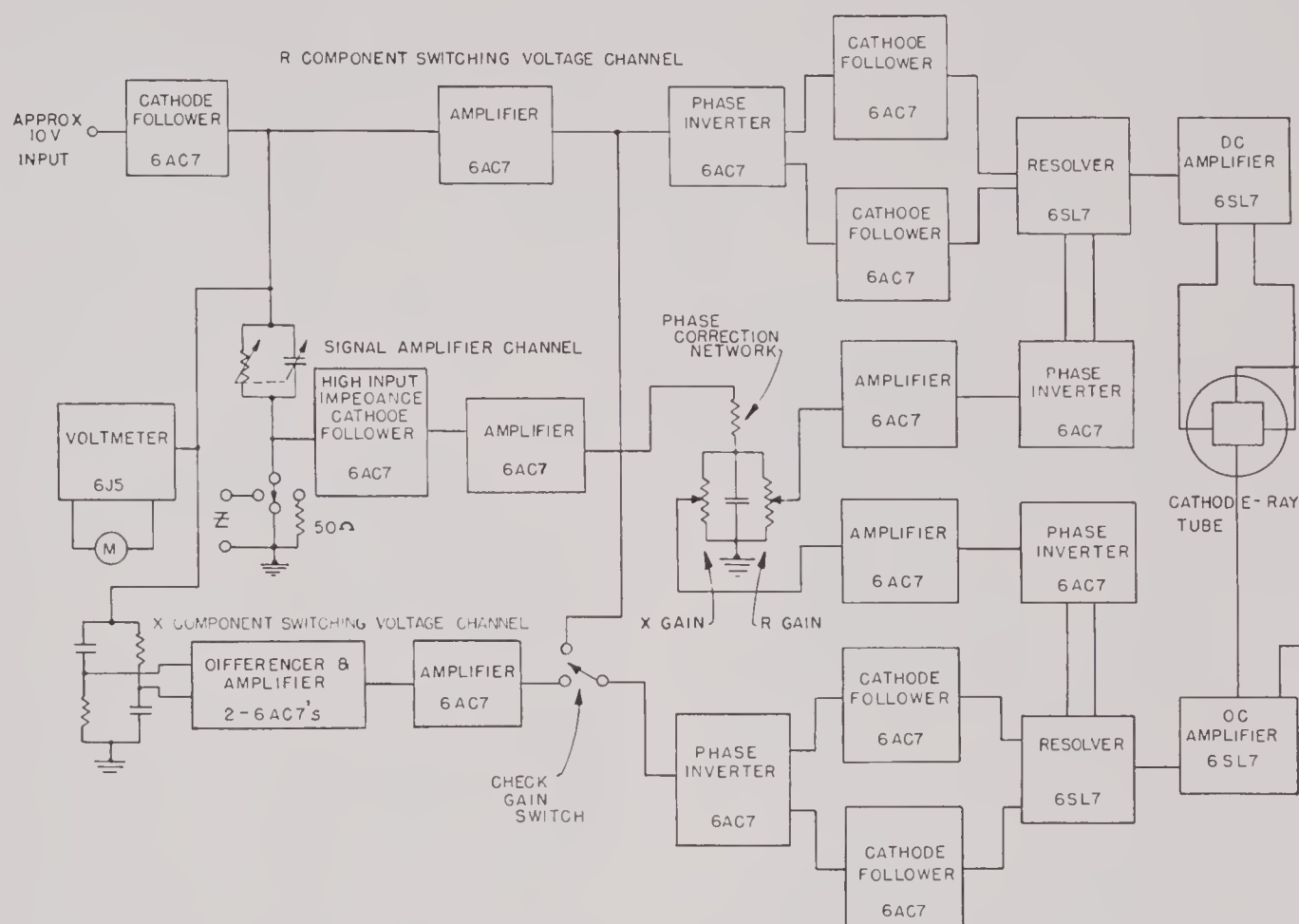


FIGURE 62. Complete block diagram of first vector impedance locus plotter.

careful adjustment of numerous components. A much simpler circuit (Figure 60) can be made to perform the required functions over a wider frequency range with very small phase error and amplitude variation. If $\omega R_1 C_1 \gg 1$, the voltage e_1 in Figure 60 leads V by 90 degrees and its amplitude increases linearly with frequency, while if $\omega R_2 C_2 \gg 1$, the voltage e_2 lags V by 90 degrees and its amplitude varies inversely with frequency. As Figure 61 shows, by taking the difference of these two voltages (note that e_2 is 180 degrees out of phase with e_1 and is therefore plotted as a negative voltage), their amplitude variations can be made to compensate each other partially, so that the difference varies less than ± 2.5 db over a decade range of frequency. The minimum value of $e_1 - e_2$ occurs approximately at the frequency at which $\omega R_1 C_1 = 1/\omega R_2 C_2$. The output voltage of this circuit can be kept as nearly in quadrature with the input V as desired by the choice of the products $\omega R_1 C_1$ and $\omega R_2 C_2$, with a limit imposed by the permissible attenuation of the network.

A complete block diagram of the first VILP is shown in Figure 62 and the complete circuit dia-

gram in Figure 65. A cathode-follower stage is placed at the signal input to prevent any possible loading of the oscillator and to present a low impedance to the various circuits of the VILP. A voltmeter is included in order that the voltage E upon which the constant current depends may be easily adjusted to the correct value to preserve the calibration of the instrument. The constant-current resistor is variable in eleven steps from 2,000 ohms to 5 megohms, corresponding to plotting impedances with maximum values of 20 to 50,000 ohms respectively. The self-capacity of the 5-megohm resistor is sufficient to cause considerable phase error and some amplitude error in the constant current at 100 kc. The phase-correction network in the signal amplifier channel is designed to correct this defect. Hence capacities are added in parallel with all lower values of constant-current resistors so that their RC time constants are all equal and the one phase-correction network will serve for all values of the constant-current resistor. Since this network is a relatively low-impedance circuit, the potentiometers controlling the gain in the two channels R and X are included here. The check-gain

switch in the X component switching voltage channel allows the R component switching voltage to be applied to both channels. The switch at the input to the signal amplifier channel allows the selection of zero impedance, 50 ohms, or connection to the terminals of the impedance to be plotted. If the check-gain switch is thrown so that the R com-

ponent switching voltage is applied to both channels, the screen bearing the coordinate axes is movable to allow the first and fourth quadrants of the impedance plane to be centered on the screen. No provision is allowed for plotting in the second and third quadrants.

The amplifier and phase-inverter stages in the signal and switching-voltage channels have been compensated for phase shift due to capacity from the plate circuit to ground. The proper value of inductance to be placed in series with the plate resistor was determined by observing the phase shift of the stage



FIGURE 63. First model of VILP.

ponent switching voltage is applied to both resolvers, and if the 50-ohm resistor is selected, the deflection should correspond to $50 + j50$ ohms. (Each channel is in this instance taking the same component of that impedance and should show equal deflections.) The instrument can be calibrated by adjusting the gain controls in each channel to show a deflection of exactly $50 + j50$ ohms when the voltmeter indicates the proper value of input signal. The amplitude of the switching voltage applied to the cathode followers in the R channel is 25 volts and that in the X channel has a minimum of 20 volts. Wire-wound resistors (100-ohm BW $\frac{1}{2}$) are placed in series with many of the grids of the phase-shift compensated amplifier tubes. This has proved an effective method of preventing parasitic oscillations. Controls on the d-c amplifiers allow an initial positioning of the spot before an impedance locus is plotted. The transparent

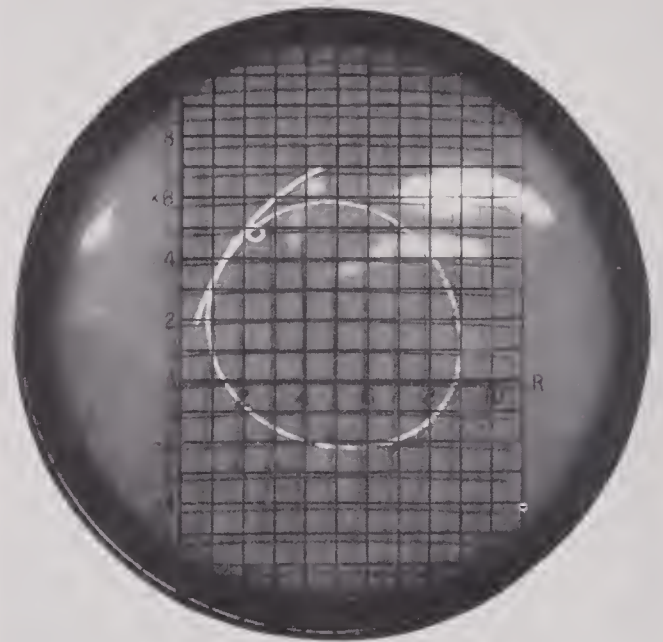


FIGURE 64. Photograph of impedance locus on VILP.

as a variable inductance was adjusted. A ladder attenuator having a low characteristic impedance was constructed of BT-1 (metallized) resistors and it was assumed that this attenuator was free from phase defects. The signal from this attenuator was amplified by the stage being tested, and the output of the stage was compared with the input signal to the attenuator on a cathode-ray oscilloscope. A cathode follower was used as a high-input impedance stage to take the signal from the plate circuit, since even small added capacities affect the phase shift seriously. It was found necessary to have the following stage connected and operating before this phase-shift correction could be made. When the proper inductance value was determined, coils were wound on small Western Electric toroidal cores, making very compact inductors. An amplifier with zero phase shift and cathode-follower input and output stages was constructed for comparing the phase of the relatively

small V_0 signal at the input of the resolvers with the switching voltage in the same manner. These numerous custom-tailoring phase-shift adjustments made the construction of the first VILP a slow process.

The first model of the VILP is shown in Figure 63. The rack contains the cathode-ray tube chassis, the VILP chassis, and the power supply for the VILP. An oscillator, such as the H-P Model 200-D, is used to supply the variable frequency voltage to the VILP chassis. An example of an impedance locus traced on the screen of the cathode-ray tube is shown in Figure 64. The impedance locus shown is that of a magnetostrictive transducer element in air over a frequency range of 10 to 50 ke.

The first model of the VILP (Figure 65) still has many defects. The upper limit of the impedance it can plot is established by the size of the constant-current resistors and their shunt capacity. Even the 5-megohm resistor, which is the highest value now used, has phase defects that indicate that it cannot be considered as a pure resistance shunted by a capacity but as a much more complicated network. The phase correction network should, therefore, be much more elaborate. Perhaps the development of some sort of vacuum-tube constant-current generator would serve to eliminate these difficulties and allow the plotting of impedances up to 1 megohm. The output voltages of the resolver tubes are not entirely independent of the amplitude of the switching voltage and some motion of the spot occurs in the X direction, as the frequency is varied even when the selector switch is on zero impedance. This is due to the change in shape of the square wave as the amplitude of the X switching voltage varies with frequency. A bias voltage is applied to the grids of the cathode-follower switching tubes by means of a battery so that tube A in Figure 55 will cut off at the proper point for the production of a good square wave. The motion of the spot on the cathode-ray tube which is due to changes in the amplitude of the switching voltage is critically dependent upon the value of this bias voltage. It is hoped that this difficulty can be overcome in some way. The operation of the first two tubes of the signal amplifier channel from an a-c filament supply generated so much noise that the spot on the cathode-ray tube screen was unduly large. A d-c filament supply is, therefore, used for these two tubes. Perhaps the use of a different tube with better noise characteristics than the 6AC7 will allow use of the a-c filament supply for all tubes.

The VILP could be converted to a *vector admittance*

locus plotter [VALP] by using the admittometer circuit instead of the impedometer circuit to obtain the vector voltage V from the device being measured. The VALP would eliminate the troubles with phase angles of the large resistors required to produce a constant current through high impedances in the VILP circuit, since the VALP circuit employs a constant voltage source and a small series resistor. Use of a series resistor to measure current, however, makes it impossible to ground at the same time one terminal of the voltage source, of the impedance being measured, and of this series resistor. The VALP would be useful in plotting the high impedances that cause trouble in the VILP circuit, but the VILP is more applicable to low impedances.

The resolving circuits of the VILP can, of course, be used to plot the locus of any vector voltage V . One such application is the plotting of the transfer impedance of a four-terminal network. This was tried with the present VILP circuits with encouraging results.

The VILP proved very useful in the measurement of impedance loci, both as a substitute for, and a complement to, the bridges. In many cases the VILP trace can supply all the desired information very quickly. This is particularly true in experimental work where an indication of the effect of changes in the transducer on the impedance locus is sufficient. The effect of such changes can be observed on the VILP screen as the changes are made. This was particularly useful in determining and eliminating the effects on impedance loci of reflections in the absorbent-lined tanks. A preliminary measurement on the VILP can save much time and effort, even when bridge measurements are required, by indicating the approximate size and complexity of the locus and the resonant frequencies and by indicating defects in the transducers, such as short or open circuits, which can be remedied before time is wasted on bridge measurements.

9.2.4

Loading

Analysis of transducers by the use of impedance loci requires that the impedance of the transducer be measured with the transducer radiating into a water load. In addition to the electrical problems involved in measurements with the transducer under water, the problem of obtaining the proper load on the face of the transducer is encountered. The radiation impedance into which the transducer is working may differ from the ideal radiation load of water because

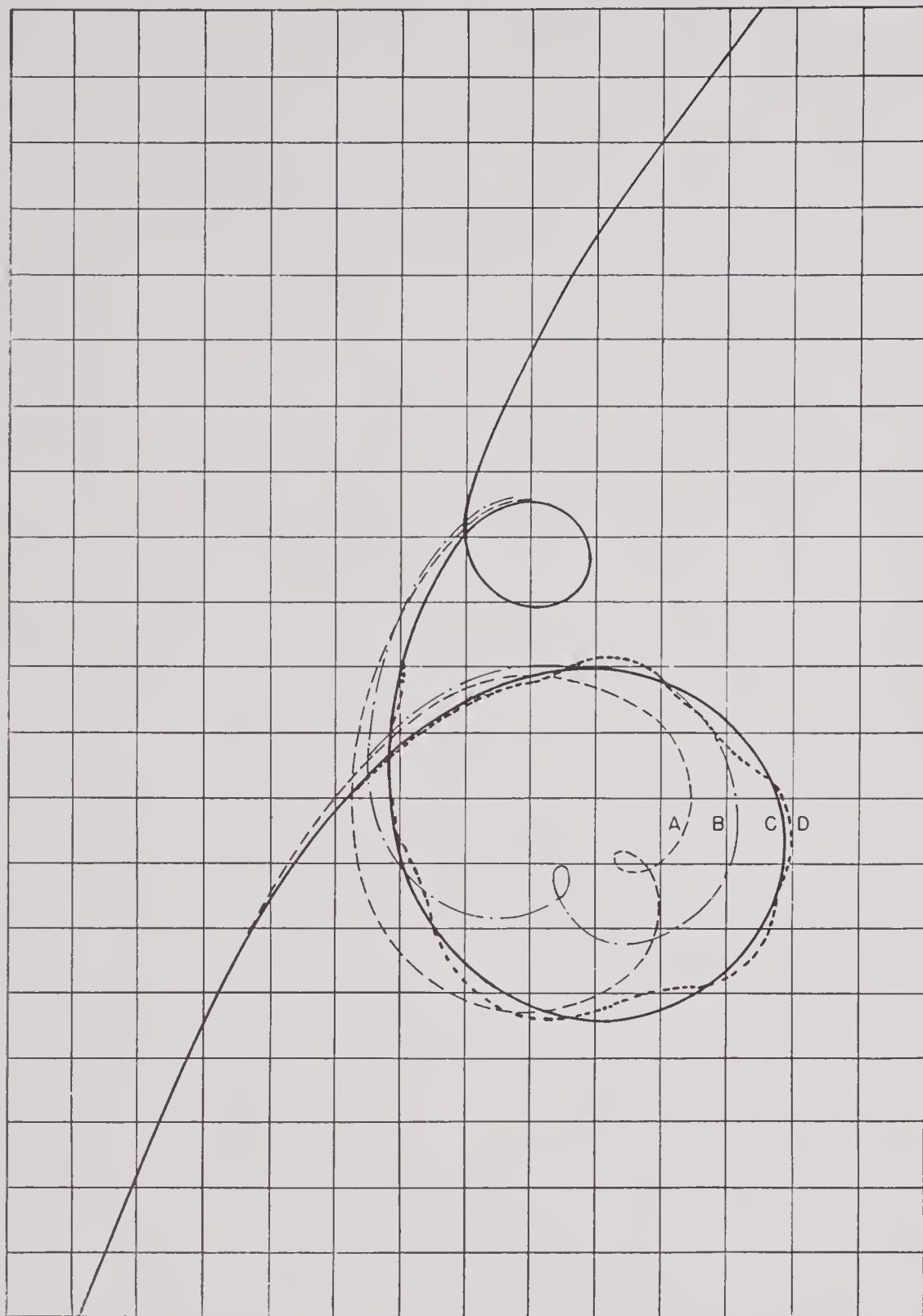


FIGURE 66. Effect of reflection on impedance locus.

of the formation of air bubbles on the transducer face or the return of energy to the transducer which results from reflections.

The presence of large quantities of air in the water results in the formation of a layer of minute bubbles on the surface of an immersed transducer. Such

CONFIDENTIAL

formation is particularly rapid and troublesome if the temperature of the transducer is higher than that of the water, as is often the case when the transducer is polarized with several amperes of direct current. The solubility of air in water in contact with the heated transducer face is reduced, so that some air comes out of solution and collects on the transducer face in the form of small bubbles. The load on the transducer then approaches that of air alone. Water from the city mains was found to contain a large quantity of air, so that a tank filled with this water is practically useless for impedance measurements until the dissolved air has been removed. The water will become sufficiently air-free after being in the tank for a week or more, but heating the water by the use of electric immersion heaters or by releasing live steam into the tank will speed up the process. For maximum effect the water should be boiled, but this is difficult with large quantities.

To hasten the wetting of the transducer face, a wetting agent such as Aerosol OT, in a 25 per cent water solution is usually applied. Even with the use of a wetting agent, it is sometimes necessary to allow the transducer to soak for hours before it is thoroughly wet. This is particularly true of laminated stacks without rubber faces, where the consolidating material on the face apparently is difficult to wet.

The presence of reflections causes the radiation impedance into which the transducer is working to be a function both of frequency and transducer position, so that the conditions of measurement are not only difficult to reproduce but also are not those of open water. The changes in radiation impedance due to reflections are evident in measurements of the electric impedance of the transducer. The magnitude of the changes in electric impedance resulting from reflections is proportional to the efficiency of the transducer and is shown in Figure 66. The heavy curve *C* is the impedance locus in the absence of reflections; the curves *A* and *B* show the effect of reflection from an almost perfectly reflecting surface, with the distance of the transducer face from the surface very slightly different for the two loci. The curve *D* shows the effect of reflections from a surface that absorbs most of the incident energy. The dimensions of the face of the transducer used for these loci were 1.67×0.48 wave lengths at 26 kc. A transducer whose face is small compared with a wave length shows only a change in the diameter of the impedance circle as the result of reflections, instead of

small circles, cusps, or indentations. A transducer whose face is two or more wave lengths in either dimension may exhibit more than one re-entrant circle or cusp on the impedance circle, as in Figure 68, where one dimension of the face was about 6 wave lengths.

Reflections can, of course, be avoided by working in open water where there are no reflecting surfaces, but it is more convenient to work in a tank where water conditions can be controlled. In a tank with steel walls the reflections are such that impedance measurements are practically impossible, but these reflections can be reduced by lining the tank with an absorbing material. Such a tank was built by the Bell Telephone Laboratories³¹ and proved useful in making impedance measurements with water loading.

Since the walls of the absorbent-lined tank do not absorb all incident sound, measurements in the tank are subject to some troubles with reflections. At normal incidence the sound reflected from the surface of the tank walls is 17 or 18 db below the incident sound at 30 kc.¹⁹ The effect of this on one transducer has been illustrated in curve *D* of Figure 66, where the transducer was facing the bottom of an absorbent-lined tank. Figure 67 shows the changes in the

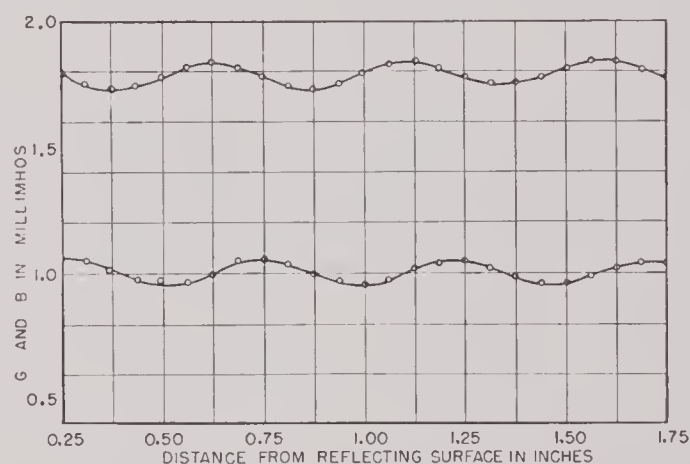


FIGURE 67. Graph of *G* and *B* vs distance from reflecting surface.

admittance of another transducer at its frequency of maximum efficiency as the distance of the transducer face from the bottom of the tank was varied. From the magnitude of these changes and other data obtainable from the air and water admittance loci of the transducer, the reflection coefficient of the reflecting surface can be computed.¹⁸ The reflection coefficient computed for the tank bottom at 62 kc

is about 0.1, in agreement with the data given above.

Effects of reflections in the tank can usually be eliminated by orienting the transducer in the tank so that most of the radiation must be reflected more than once before it can return to the transducer, with a resulting increase in attenuation with each reflection. The directional discrimination of the transducer can be utilized to attenuate reflections further. However, it is sometimes impossible to orient the transducer at a skew angle with respect to all the reflecting surfaces. For example, when only the face of the transducer can be immersed, the reflections from the bottom of the tank return normal to the transducer face after only one reflection, resulting in a distortion of the impedance locus of a transducer having fairly

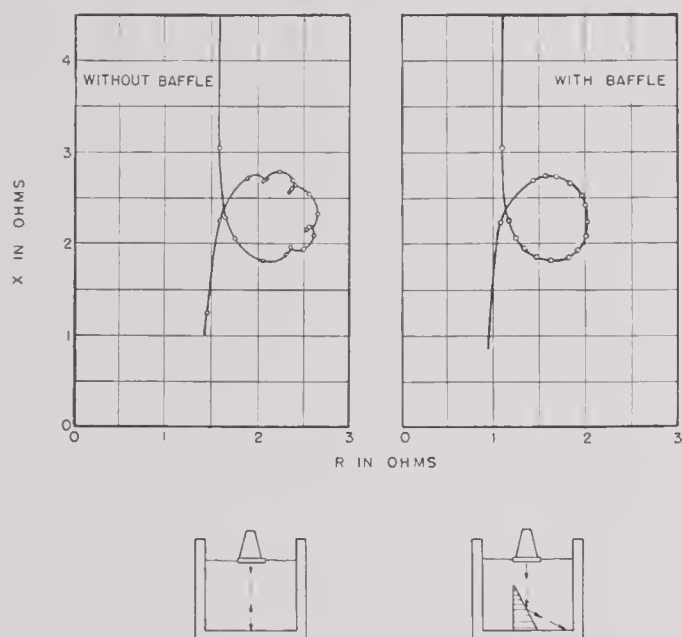


FIGURE 68. Effect of reflections in tank on admittance circle.

high efficiency. Figure 68 shows the effect of such reflections. A remedy for this trouble is the use of a tank with a bottom that is not parallel to the surface of the water. The same effect can be obtained with a false bottom or reflecting baffle under the transducer, so that the radiated sound is deflected against several absorbing surfaces before it can return to the transducer. The improvement effected by a reflecting baffle, consisting of an air-filled metal box, is also shown in Figure 68. The efficiency of the baffle could be improved by incorporating in it some additional attenuation of the incident sound instead of simply using the nearly perfect reflection from a water-air interface to divert the sound beam.

9.2.5

Field Measurements

When transducers were too large to be placed in the absorbent-lined tanks for impedance measurements with water loading, these measurements had to be made at the HUSL field stations. For this purpose a portable admittance bridge was constructed. The circuit is essentially that of the admittance bridge of Figure 16, but the terminal box with its switches, trimmers, and blocking condensers is omitted. The L & N resistor and capacitors are connected directly to the ratio box's A and C' terminals, and the unknown to the A or C terminal, according to whether it is inductive or capacitive. The change from inductive to capacitive measurement is made by switching the connection of the unknown from one terminal to the other.

The bridge components were mounted in a wooden frame and connected with bus wire. One of the detectors used with the admittance and impedance bridges was removed from the bridge console and used with this portable bridge. The field stations provided suitable oscillators.

The alignment of this bridge was similar to that of the admittance bridge, except that the only trimmers were those in the ratio box. When these trimmers did not have sufficient range, external resistors or capacitors had to be added to the bridge, but this was seldom necessary. When the decade capacitor was used, its residual capacity of about $70 \mu\text{f}$ had to be offset by a slightly different alignment procedure than that used for the admittance bridge, since there is no separate trimmer for this compensation. The alignment was made by means of the trimmers with the resistance box disconnected and the decade capacitor set at $0.001 \mu\text{f}$ across one arm of the bridge and the air capacitor set at $1,000 \mu\text{f}$ across the opposite arm. The air capacitor was then connected in parallel with the decade capacitor for the measurements. If a 10,000-ohm resistor was used across the unknown to bring the conductance within the range of the bridge, the alignment was made with this resistor and the resistance box set at 10,000 ohms connected to opposite arms of the bridge.

The accuracy of this bridge was equal to that of the admittance bridge used in the laboratory, but it was not so convenient to use because of the necessity for changing the connections and realigning the bridge when a change was made from inductive to capacitive operation. The lack of blocking condensers in the bridge was not a serious disadvantage

because polarizing current was seldom required in the field measurements.

9.3 PATTERN AND FREQUENCY RESPONSE MEASUREMENTS IN ABSORBENT-LINED TANKS

9.3.1 Methods

The methods of calibrating transducers and measuring their frequency responses and patterns in absorbent-lined tanks are the same methods as those used in open water at the field stations, and the equipment is similar.⁶ Differences between tank measurements and open-water measurements result from the small separation of source and receiver imposed by the tank dimensions and from reflections from the tank walls.

9.3.2 Equipment

The tanks used for acoustic measurements in water were the absorbent-lined tanks constructed by the Bell Telephone Laboratories.^{5, 31} One is shown in Figure 69. To the cover of the tank, as received from BTL, was added the apparatus for suspending and rotating the devices under test. At one end of the cover is a shaft which can be rotated by hand or at two speeds by motor. This shaft can be raised or lowered by a hand crank but cannot be moved along the slit in the tank cover. At the other end of the tank is a similar shaft which can be raised or lowered, rotated by hand, and moved back and forth along the opening in the cover. The maximum possible separation of the two shafts is about 18 in. Both shafts are terminated in a standard 1-in. male pipe fitting. The shafts are hollow and a transducer may be supported by feeding its cable through the shaft. The left-hand transducer shown with the tank in Figure 69 is an example. Special adapters have been made to attach transducers to the fittings on the shafts and to permit offsetting the transducer from the axis of the shaft.

The equipment used with the tanks in calibration, frequency-response, and pattern measurements is shown in Figure 70. The left-hand rack contains, from top to bottom, a New London measuring amplifier, a calibration amplifier, a heterodyne re-

ceiver, and the power supplies for the two amplifiers. The left center rack contains an oscilloscope, with shelf space for additional instruments, such as the decade amplifier shown beside the oscilloscope in the photograph, a 10-kc frequency multiplier, and a 1-kc isolation amplifier, the lower part of the rack being

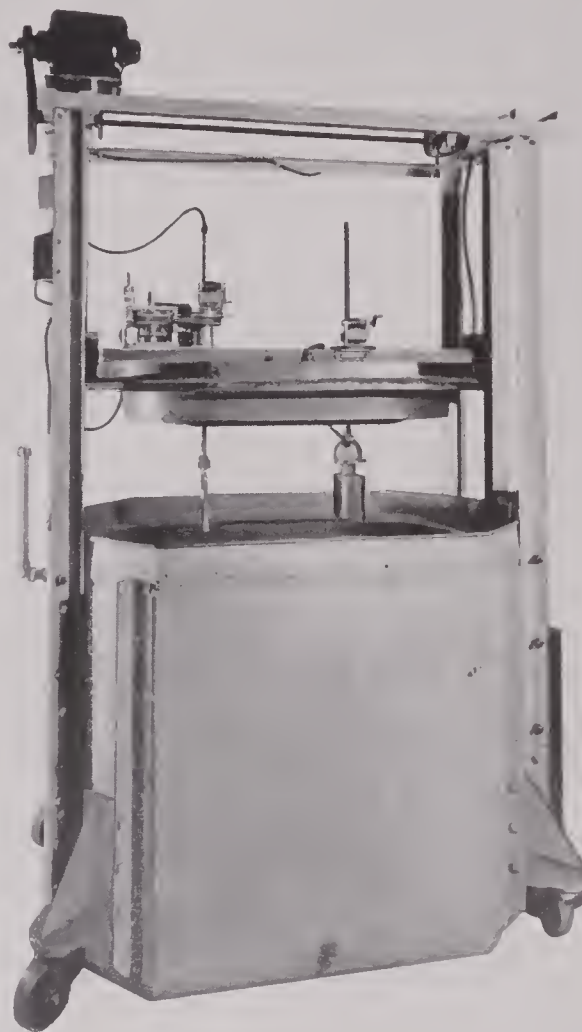


FIGURE 69. BTL absorbent-lined tank.

filled with blank panels. The right center rack contains a meter panel, an H-P oscillator Model 200-D, a Sound Apparatus Company's automatic voltage level recorder, and the regulated power supplies for the oscillator and recorder. The right-hand rack contains an H-P oscillator Model 200-CR, a noise generator, a push-pull parallel 6L6 power amplifier, an output transformer panel, a cathode-follower power amplifier, and a space for storing standard hydrophones and projectors.

The New London measuring amplifier was constructed for HUSL by the New London Underwater

⁶ Only steady-state measurements have been made at HUSL. For the application of pulse methods to such measurements, see reference 19.

Sound Laboratory. It is an excellent low-noise amplifier^{7, 8, 9, 12, 13} with a maximum gain of 80 db and provision for inserting a calibrating voltage, but it was used only occasionally to supplement the calibration amplifier.

The calibration amplifier was designed and built at HUSL for use in calibration measurements. It has a high-impedance input into a grid circuit and a low-impedance (100-ohm) input into a transformer. The transformer input can be either balanced or unbalanced with respect to ground. A calibration voltage can be inserted in series with any of the input circuits.

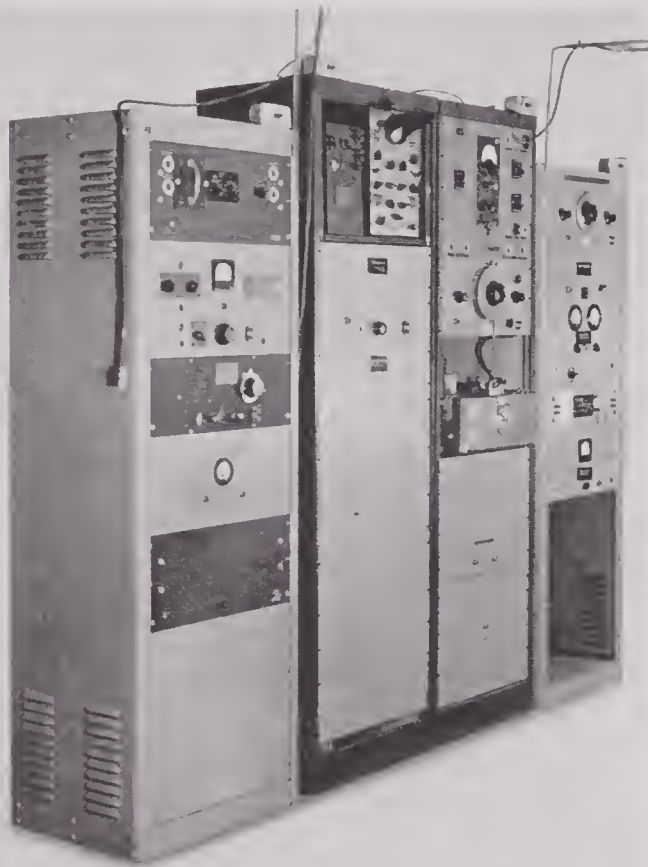


FIGURE 70. Racks containing calibration equipment.

The maximum voltage gain with the high-impedance input is 116 db, with the low-impedance input 109 db. The frequency response is shown in Figure 71 and the circuit of the amplifier in Figure 72. An external electronically regulated power supply is used with this amplifier.

The heterodyne receiver is one of those constructed at HUSL. It was used occasionally for listening to the output of hydrophones.

The shelf at the top of the left center rack can be

used to support two Du Mont Type 224 oscilloscopes or other apparatus.

The 10-kc frequency multiplier supplies the tenth harmonic of the 1,000-cycle standard signal for use in checking frequency. The circuit is similar to that of the multiplier used with the bridges shown in Figure 28.

The 1-kc isolation amplifier was designed to eliminate the interaction between other circuits throughout the laboratory connected to the 1,000-cycle line and the measuring equipment. An amplifier with a tuned circuit and several cathode-follower outputs was used to isolate the equipment using the 1,000-cycle signal from the line. The subsequent introduction of a low-impedance 1,000-cycle line throughout the building with isolating resistors at each outlet made this isolation amplifier unnecessary.

The meter panel provided a convenient means of switching a Ballantine VTVM to any of the circuits used in calibration or to external circuits. It also provided a switch for connecting the oscillator output to either the power amplifier or the calibration input of the calibration amplifier and for simultaneously connecting the voltmeter to the proper circuit. Another switch permitted the selection of either frequency or rotation indexing controls for the marker circuit in the recorder. On the meter panel are mounted two 10 K resistors, the use of which will be discussed in connection with the use of the power amplifier to supply constant current to a projector. The circuit of the meter panel is shown in Figure 73.

The H-P Model 200-D audio oscillator was modified for use in calibration work. A dial drive was provided to permit the rotation of the oscillator dial by the recorder drive in plotting a frequency response automatically. The dial could be rotated at either of two speeds by changing the connection of the flexible shaft to the recorder gear box. The two speeds correspond to the frequency range of 7 to 70 kc spread over either 15 or 24 in. of recorder paper. A frequency indexing signal is supplied to the marker circuit of the recorder by a relay in the recorder which is operated by a photocell. A disk of the same size as the oscillator dial, mounted on the dial shaft behind the panel, and with small holes drilled around its circumference to correspond to the dial calibration marks, acts as a shutter between the photocell and a light source, so that the photocell operates the relay as these holes permit the light to strike the photocell. The photocell circuit is shown in Figure 74. Its sensitivity can be adjusted by a shaft through the bottom

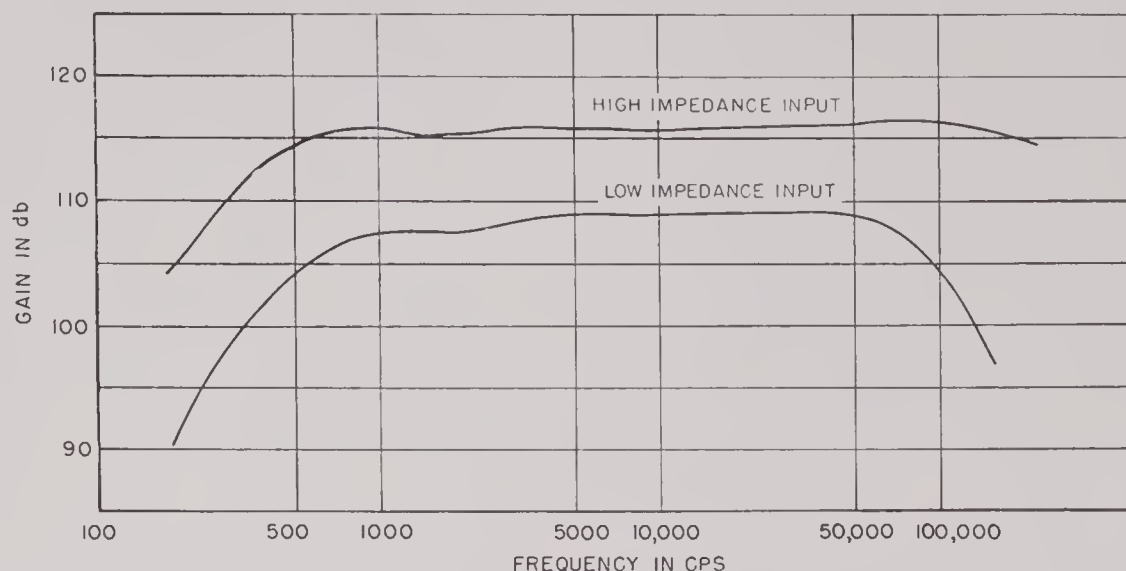


FIGURE 71. Frequency response of calibration amplifier.

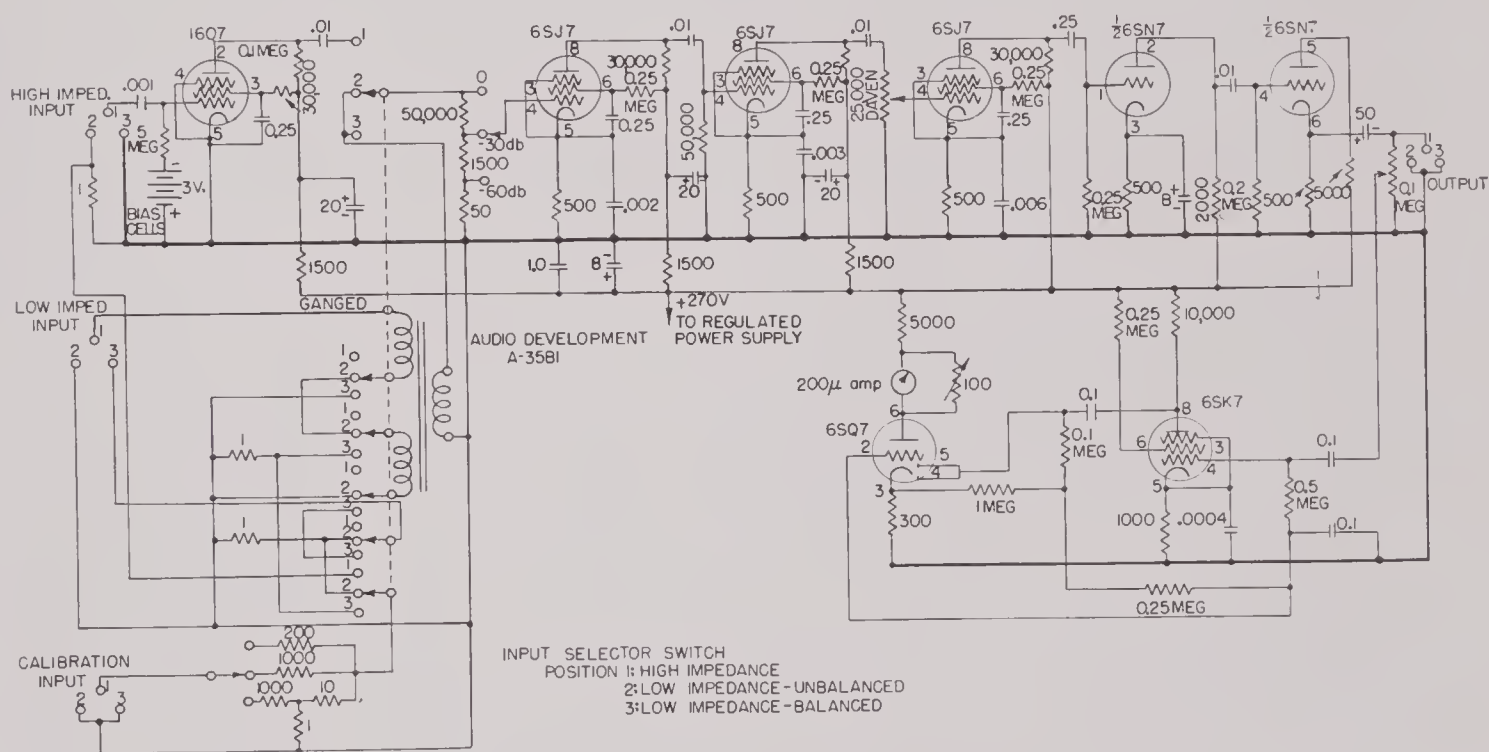


FIGURE 72. Circuit of calibration amplifier.

of the oscillator to the left of the dial. The leads to the relay-operated switch appear at the rear of the oscillator as a two-pronged Jones plug. The plate voltage of the photocell circuit can be turned off and on with the switch at the lower left corner of the oscillator panel. A limit switch operated by the photocell disk shuts off the recorder motor when the high-frequency end of the dial is reached. The connection of the switch to the recorder is made by a cable emerging from the right side of the oscillator.

The voltage control of the oscillator was altered to permit a finer control of the output voltage. The single potentiometer used in the original oscillator was replaced by the circuit of Figure 75. The two-position switch and the potentiometer with a logarithmic taper (Centralab N-115) permit the voltage to be set at any level without difficulty. These two controls are located at the upper right of the panel. The output voltage can also be varied by the insertion of a 35-db attenuator across the output termi-

CONFIDENTIAL

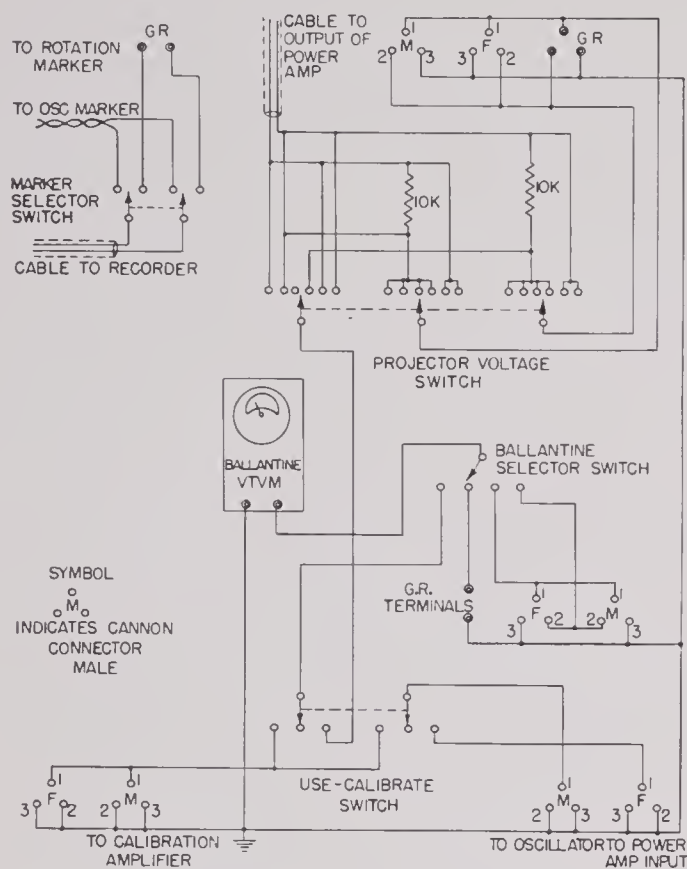


FIGURE 73. Circuit of meter panel.

nals, controlled by the switch beside the output terminals on the panel. This attenuator is shown in Figure 76. The oscillator's original power supply has been disconnected, and an external electronically regulated power supply is used for greater stability.

The circuit of Sound Apparatus Company's voltage level recorder was changed considerably to improve its operation and extend its frequency range. The changes made in this instrument are discussed in Chapter 10, and circuit diagrams of the original and modified forms are given in Figures 32 and 33 respectively of that chapter.

The H-P Model 200-CR oscillator is used occasionally when frequencies above the 70-ke maximum of the other oscillator are desired.

The noise generator is a source of broad-band thermal noise but was used very rarely in measurement work in the tanks.

The push-pull parallel 6L6 power amplifier was used largely to drive a Brush Model C 13-2, 4 × 4-in. crystal transducer as a projector. Its high-impedance balanced output can, however, be used for other purposes, or by the use of an output transformer, such as the Western Electric W-28562, it can be used to drive lower impedances. The circuit of the amplifier

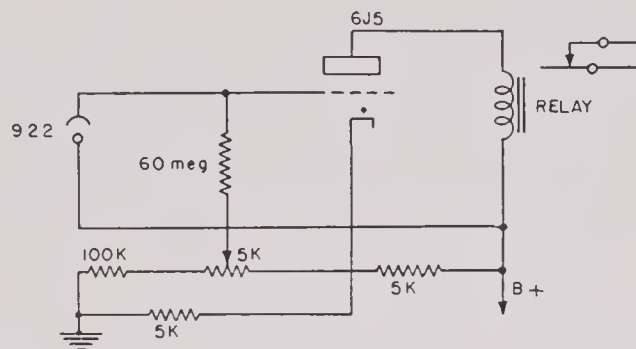


FIGURE 74. Photocell marker circuit.

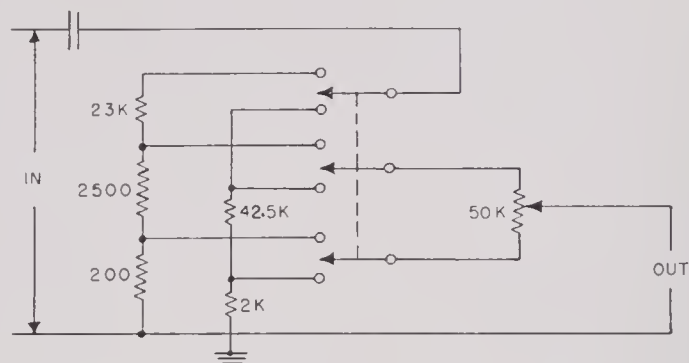


FIGURE 75. Voltage control circuit in oscillator.

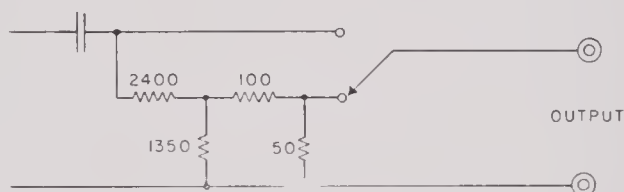


FIGURE 76. Attenuator pad in oscillator.

is shown in Figure 77. In order to drive the Brush C 13-2 at a constant current as the frequency varies with a constant voltage input to the amplifier, a compensating circuit had to be used in the input of the amplifier. The male Cannon connector permits the input to pass through the compensating circuit, while the female connector feeds the following stage of the amplifier and permits the use of the amplifier with a relatively flat frequency response. To obtain a constant current through the Brush C 13-2, two 10 K resistors are connected in series with it, as in Figure 78, so that variations in its impedance with temperature have little effect on the load on the amplifier. These resistors are mounted on the meter panel and can be removed from the circuit by the top switch. These 10 K resistors also permit the current through the transducer to be measured with the Ballantine VTVM. This is done by measuring the voltage drop across either of the two resistors. The top right-hand switch on the meter panel connects

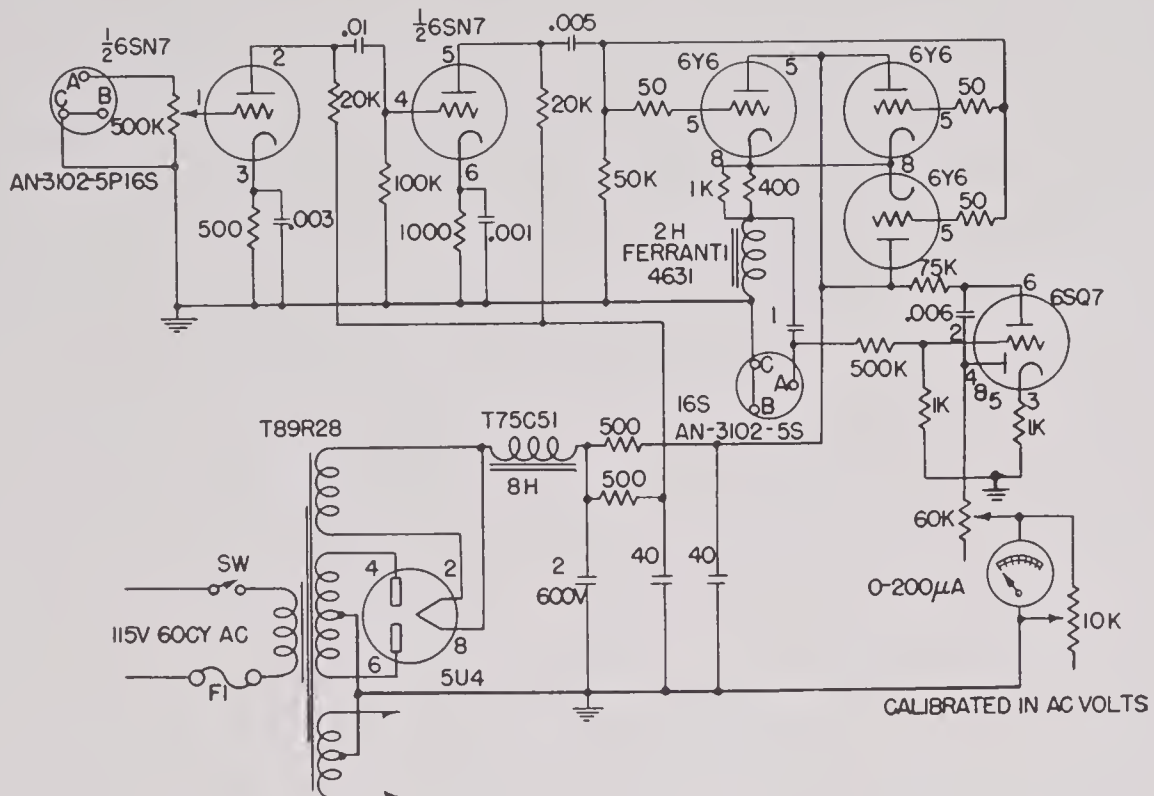
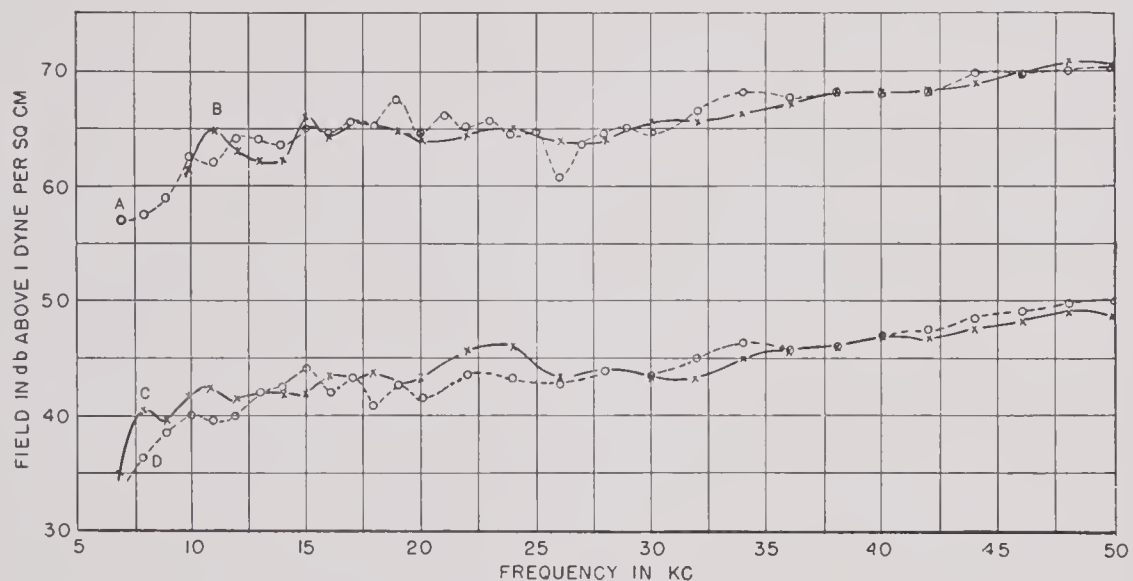


FIGURE 80. Power amplifier for Brush 4×4-in. microphone, 6Y6 output.

FIGURE 81. Sound field vs frequency in absorbent-lined tank. *A* and *B*. Measured in tank under supposedly identical conditions. *C*. Measurements made at barge at 92 in. *D*. Measurements made in tank at 18 in.

Some care was taken in the grounding of this equipment to avoid troubles with ground loops in measurements at low levels. The frame of the tank in Figure 69 is grounded to the main laboratory ground bus bar. The two outside racks, containing the calibration and power amplifiers, are grounded to the tank by two metal strips (Figure 70), which also serve to support cables running from the tank to the racks.

The two center racks are grounded only through the cables connecting their apparatus to that of the other racks.

9.3.3

Results

Calibrations made in the absorbent-lined tank closely approximate those made in open water. The

CONFIDENTIAL

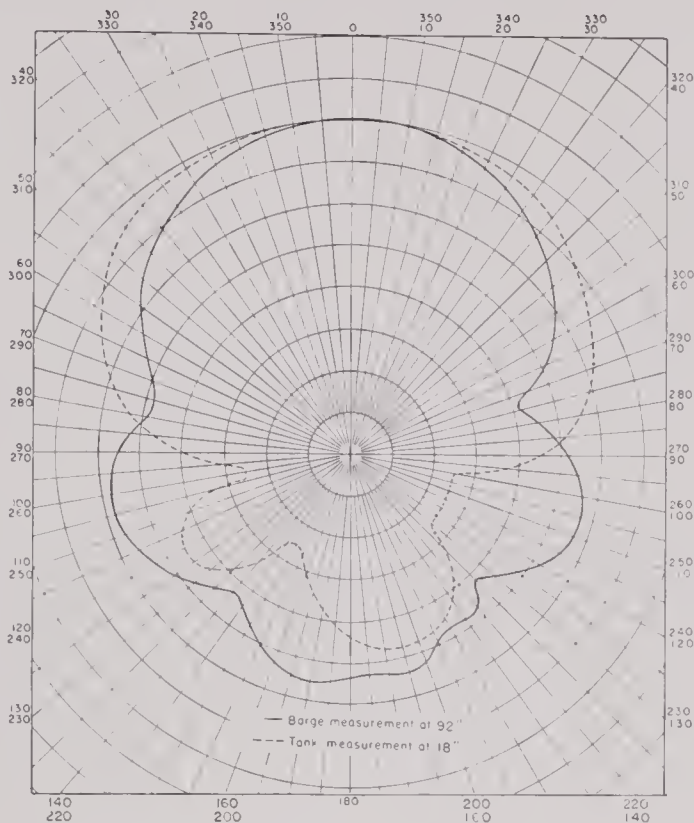


FIGURE 82. Directivity pattern of Brush C 13-2 at 20 kc.

agreement depends on frequency, separation, and the hydrophone and projector used in the measurement; the more directional the transducers used, the smaller the effect of reflections in the tank. Figure 81 shows some typical sound fields as a function of frequency measured in the tank (curves *A*, *B*, and *D*) and one (curve *C*) measured in open water at the barge with the same equipment used in the tank measurements. Measurements in the tank were not made under optimum conditions for the reduction of fluctuations in the field because of reflections, since a bi-directional pressure gradient hydrophone was used as a reference standard and the receiving hydrophone was located at the focus of reflections from the curved end of the tank. The open-water measurement was also made at a greater distance than that possible in the tank. However, even under these conditions, the maximum fluctuations amount to only 2 or 3 db. The reduction in fluctuations with an increase in frequency may be attributed both to an increase in the

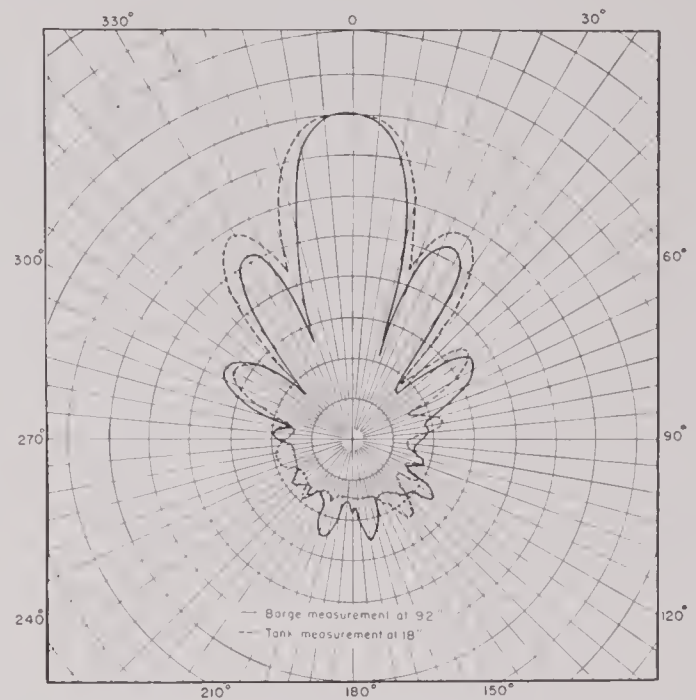


FIGURE 83. Directivity pattern of Brush C 13-2 at 60 kc.

attenuation of the tank walls and an increase in the directionality of the Brush C 13-2 transducer used as the projector (Figures 82 and 83). These curves also show the extent to which a flat field was achieved by driving the Brush C 13-2 at a constant current.

The effect of both reflections and the small separation of source and receiver are more evident in the measurement of directional patterns than in that of frequency response. The distortion of the patterns taken in the tank is considerable, particularly in the minor lobes and the rear radiation, as shown in Figures 82 and 83, and such measurements have only relative significance. However, in the development of transducers, the qualitative information obtainable from tank measurements of directivity is useful in determining faults in construction, such as air bubbles in the castor-oil filling, before time is wasted in more accurate measurements at field stations.

The use of the tank for pattern and frequency response measurements was confined largely to obtaining qualitative data rapidly, since field stations were available for more accurate and more reliable measurements in open water and at distances sufficiently large to approximate those used in practice.

Chapter 10

OPEN-WATER MEASUREMENT AT HUSL

10.1

INTRODUCTION

A complete investigation of the acoustic and electric properties of transducers can be made only if facilities are available for testing the products of transducer research under conditions duplicating as nearly as possible those encountered in actual operation. The realization of such conditions requires supporting a transducer at any desired depth in water and at any orientation with respect to a free sound field. The production of a free field at the region of measurement is accomplished in practice by a transmitter in open water at sufficient distance from that region so that nonuniformity in the wave caused by shape and directional selectivity of the transmitter is ineffective and at sufficient depth to prevent disturbances from reflections from the surface of the water. The facilities and procedures at HUSL for the determination of the acoustic characteristics of transducers are described in this section.

Measurements of transducer performance in open water were first made at various Boston Harbor piers or on the USS *Galaxy*. Neither arrangement proved satisfactory. Because of various inconveniences, the decision was made to build a field station with permanent installations for testing. A barge rather than a pier was chosen partly as a result of the experience of the New London Laboratory with its barge and partly in the expectation of having a measuring station that could be towed out into Boston Harbor away from noise and other disturbances.

10.2

CHARLES RIVER BARGE

10.2.1

Locations

The Charles River barge was built by the Hodge Boiler Works of Boston, Massachusetts, and launched at the Hodge pier on March 31, 1942. The barge was first tied there and measurements were made in the water at this location for five months, but the site was very unsuitable because of noisy surroundings and rough waters. On September 3, 1942, the barge

was moved to the lower Charles River Basin and located 150 ft off shore and about 500 ft upstream from the Charles River Dam.

The exterior of the barge and of an auxiliary craft known as "Tippecanoe" is shown in Figure 1. The barge itself was 61×21 ft, fabricated from $\frac{1}{4}$ -in. tank steel, with about 18-in. draft and a displacement of 47 tons. It carried a cabin approximately 40×18 ft, with laboratory space 28×18 ft and living quarters for the crew of three. The hold provided a limited amount of storage space for equipment not in constant use. Shore power (110 volts a-c) and telephone connections were supplied by means of a submarine cable. A well 10×3 ft provided access to the water. At the bottom of the well were a pair of hinged steel doors which could be closed when the barge was being towed.



FIGURE 1. Charles River barge and "Tippecanoe."

Figure 1 shows davits for hoisting heavy equipment on board and the 6-in. I beam which extended inside the cabin over the full length of the well. A half-ton electric hoist, traveling along the I beam, made the handling of the heaviest transducers a fairly simple matter. An interior view of the laboratory is given in Figure 2.

10.3

"TIPPECANOE"

This craft is shown alongside the Charles River barge in Figure 1. It was originally built for develop-

ment work and was nothing more than a barrel float with a shed on it. A wood deck 31×15 ft was strapped to three cylindrical tanks 12 ft long by 3 ft in diameter. The deck house was $18 \times 10 \times 8$ ft. Its equilibrium was unstable, hence its name. Two openings through which transducers could be lowered into the water were cut in the floor 6 ft apart.

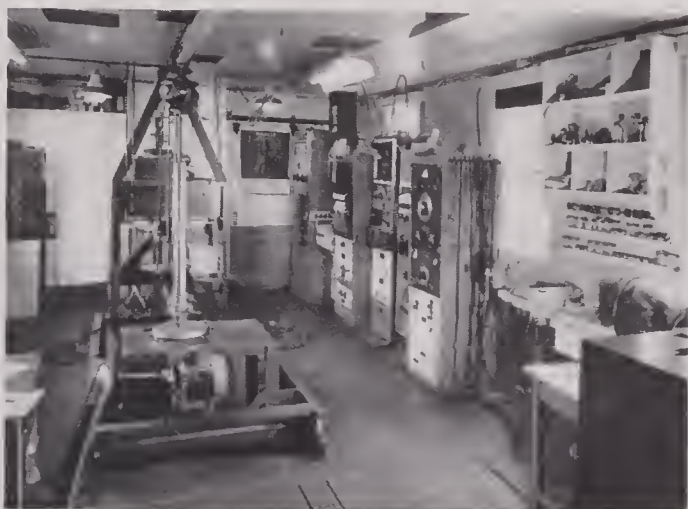


FIGURE 2. Interior of the barge laboratory.

It also served a useful purpose for the demonstration of *projector test gear* [PTG].²⁷ For this use, a hoist gear similar to the standard QC hoist, by means of which the projector to be tested was lowered into the water, was built over one of the wells. Pattern and response measurements were made with the *sound gear monitor* [SGM].⁷⁴ During 1944 "Tippy" served a useful purpose in training Navy personnel in the technique of projector testing.

10.4

SPY POND STATION

After about a year of operation at the barge, the expanding program at HUSL called for increased measuring facilities. The size of the barge well and the awkward means of getting very large units on board imposed a serious limitation on the size of devices that could be tested. No object greater than 19.5 in. in diameter could be put in the sound field without considerable difficulty, and measurements at distances greater than 8 ft could be made only by temporary rigging of the sound source from the barge deck outside the cabin. In order to meet the requirements of the ordnance division of the laboratory, a measuring station to which equipment could be delivered directly from trucks was desirable. A number of lakes and ponds within a radius of 16 miles of

HUSL were investigated and fortunately the one best suited for the purpose was found at Spy Pond in Arlington Center, only $3\frac{1}{2}$ miles away.



FIGURE 3. Map of Spy Pond.

A rough sketch of the pond is given in Figure 3. Soundings of the pond showed that the eastern shore and the shore of the island drop off sharply to a depth of 40 ft. The remaining shore has a more gradual slope. A contour of the bottom and an elevation of the station as finally built are shown in Figure 4. No serious acoustic difficulties due to reflection of sound from the adjacent shore were encountered during the two years of the station's operation.

Plans for the station were based on experience with the limitations of the barge facilities as well as on ideas solicited from the various HUSL groups interested in acoustic measurements. The specifications for the building called for a frame structure 20×32 ft, with two 16-in. 50-lb steel I beams, spaced 4 ft apart, running on either side of the centerline the full length of the building. The lower flanges of these beams served as a track for the dolly on which transducers were carried along the well and from which they could be mounted on the vertical shaft for lowering into the water. A structural feature consisted of two 12-in. I beams running across the ceiling, spaced 12 ft apart, each carrying a one-ton electric hoist. A platform 2 ft wide extended across the water front of the building. An apron of planking nailed to the bottom, framing timbers around the whole outside of the building and extending 6 in. below the surface of the water, served as a windbreak for the space between the water and the floor.

The general layout of the station is shown in

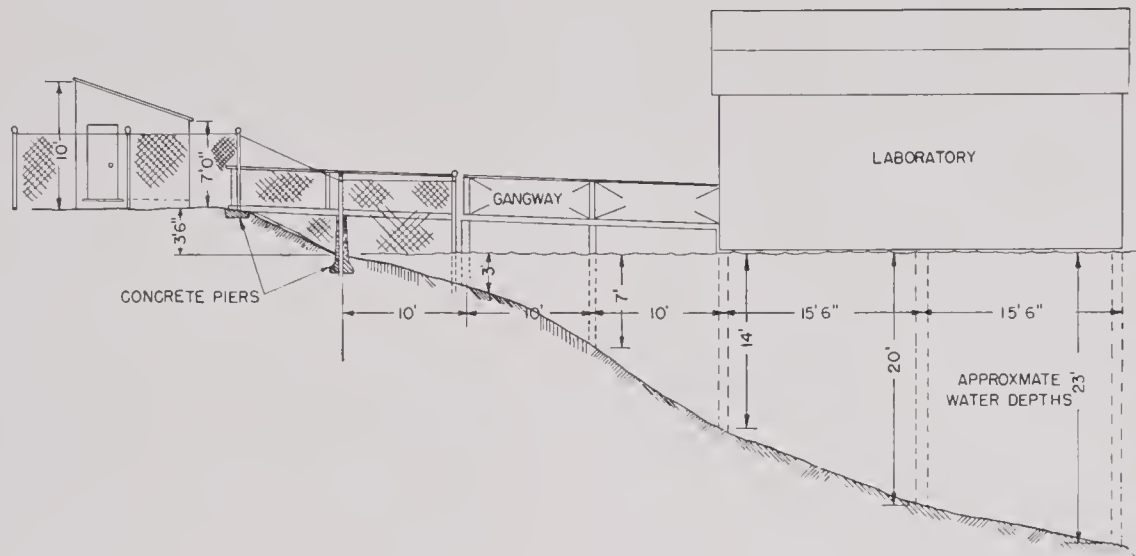


FIGURE 4. Elevation of Spy Pond station.

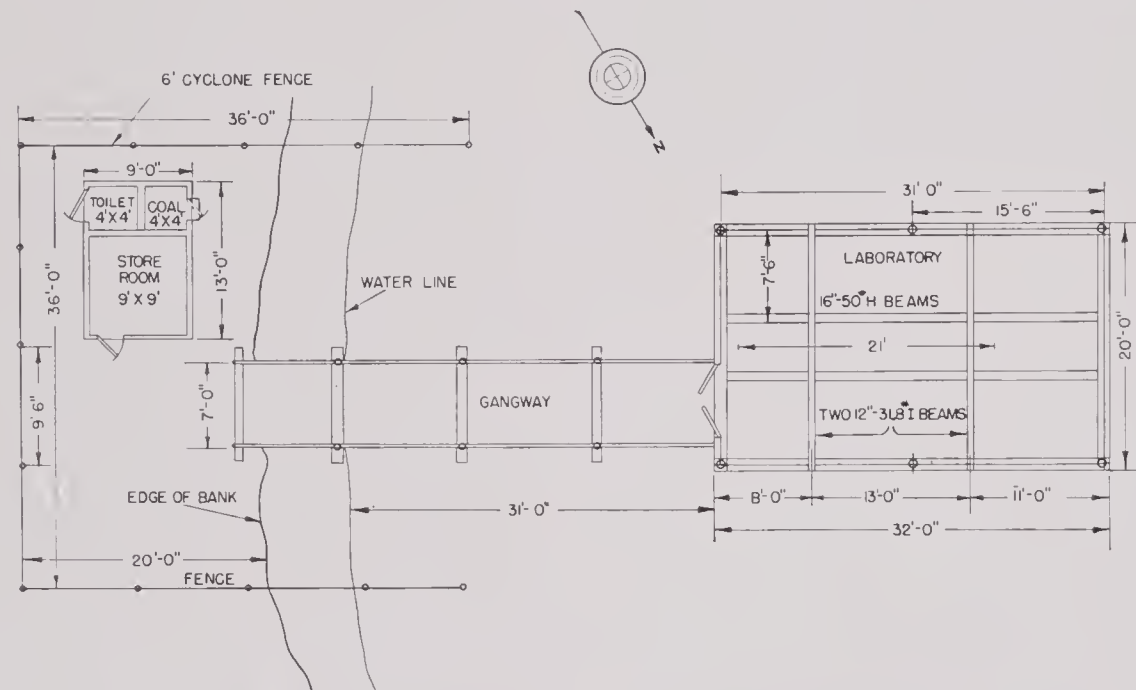


FIGURE 5. Floor plan of Spy Pond station.



FIGURE 6. General view of Spy Pond laboratory.



FIGURE 7. Front view of Spy Pond laboratory.

CONFIDENTIAL

Figure 5. Heavy equipment up to 24 ft in length could be handled with comparative ease by means of dollies running on the ramp from the shore to the station. Photographs of the exterior are shown in Figures 6 and 7.

10.5 HANDLING EQUIPMENT

Good measurement technique involves setting up a sound field in the water and placing the transducer to be measured at a known fixed point in this field. For this purpose precise means are needed to determine the depth and orientation of the sound source and of the receiver and their exact location in the water relative to each other. In the early days at the barge, this was done in somewhat primitive fashion by mounting projector and receiver at ends of 1-in. pipe. The depth of the projector was determined by direct measurement from a fiducial mark on the supporting pipe to the transducer. The depth of the receiver was adjusted accordingly by means of a collar clamped to its pipe support, with the collar set in a pipe clamp fastened on the edge of the well. In the summer of 1943 an improved gear for the barge was developed which, with the necessary modification, was essentially the same as that installed at Spy Pond. The 1-in. pipes, which quite often proved not to be straight, were replaced by 14 ft sections of selected nickel-plated tubing $2\frac{3}{4}$ in. in diameter, each terminated by a 6-in. flange with four slots and hinged bolts for attaching a shorter flanged section that carried the transducer. The arrangement is clearly shown in Figure 8, which is the receiver mount at Spy Pond.

A number of special adapters and clamps to take care of the different types of transducer mountings were designed. Some of these are shown in Figure 9. The shaft was raised and lowered by means of a half-ton electric hoist in the peak of the roof. (The steeple on the barge in Figure 1 was added to permit this arrangement.) The hoist was controlled by light cables running down from the motor switch. The shaft was graduated in half-inch intervals about 9 ft of its length. The zero point was 5 ft above the bottom surface of the flange when the latter was at the surface of the water. The distance from the bottom of the shaft flange to the midpoint of the transducer was measured directly, so that the submersion depth was the reading on the scale on the shaft plus this measured distance. A scale giving the distances be-

tween the transmitter and receiver shafts was marked on the track that carried the transmitter shaft.

The transducer was oriented with reference to a fiducial mark on the shaft running along its length and a fixed mark on the sleeve through which the shaft passed. Alignment of the face of the transducer with the fiducial mark could be made by eye with a precision of ± 2 degrees. A more precise orientation of a transducer with reference to a circular scale on

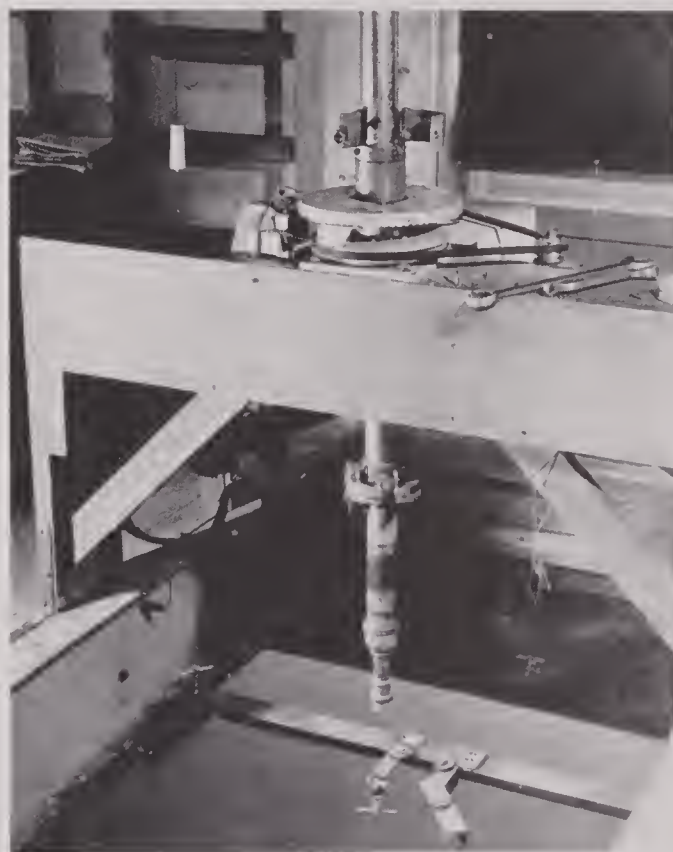


FIGURE 8. Transducer mount at Spy Pond.

the disk that is shown in the illustration, which could be clamped to the shaft, could be made by acoustic means provided the transducer gave a sharp beam radiation pattern. The shaft was rotated by clamping it to the disk-and-pulley assembly, which was belt-connected to a $\frac{1}{10}$ -hp motor. The rotational speed was one revolution in 98 sec.

A similar but somewhat simpler arrangement for the projector mounting is shown in Figures 10 and 11. Here the raising and lowering were effected by means of a hand winch and steel cable. The cable was attached to the bottom rather than to the top of the shaft. In Figure 10 a steady bearing may be seen down close to the water, while at Spy Pond vertical alignment of the shaft was insured by bearings at the top and bottom of the pyramidal frame that carried

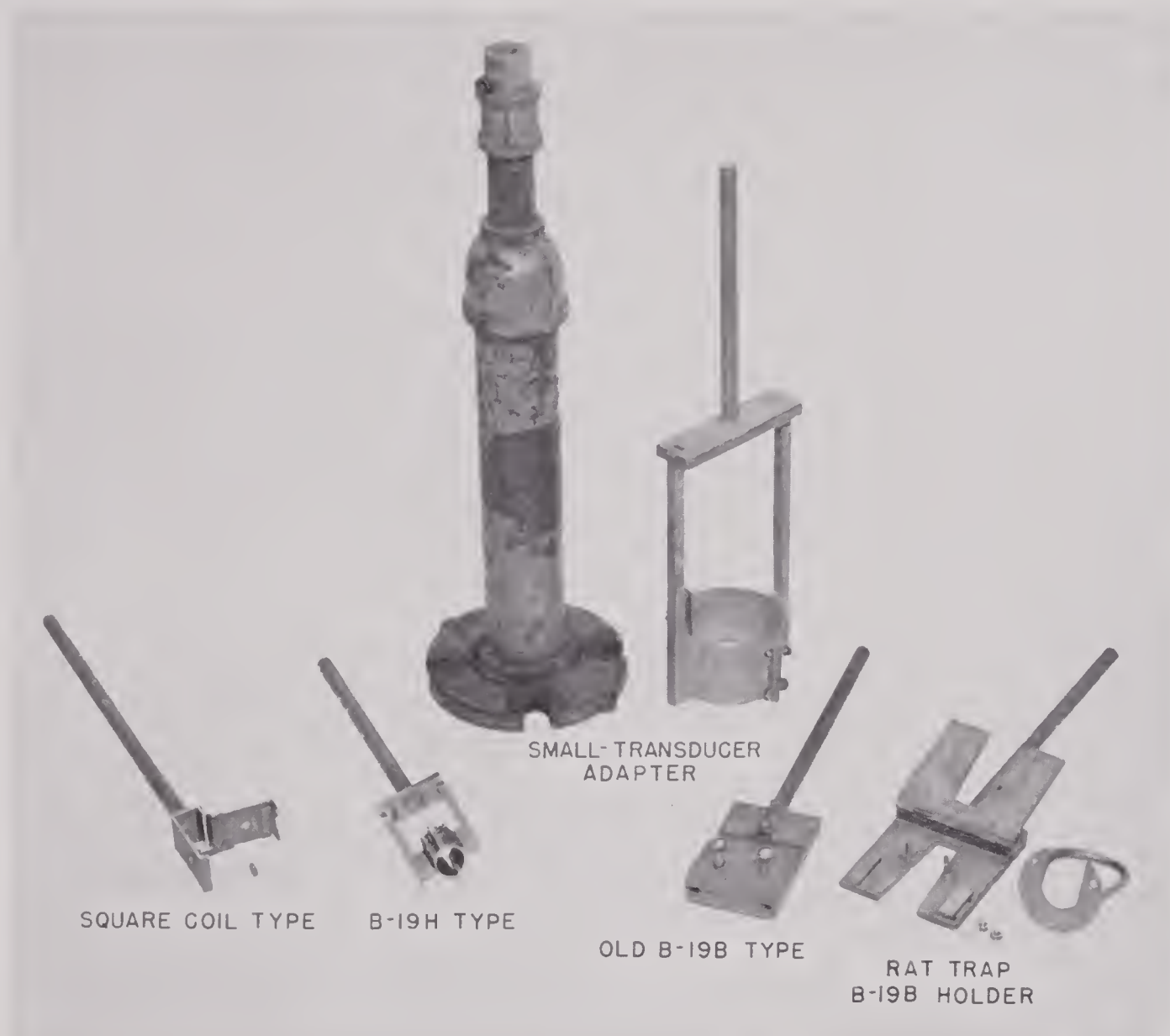


FIGURE 9. Transducer clamps and adapters.

the shaft. The means for controlling the depth and orientation were the same as in the mounting for the receiver.

In Figure 12 is shown the device used at Spy Pond for making pattern measurements on a hydrophone that is offset from the axis of the body in which the hydrophone is mounted. A sturdy 3.5×4 -ft frame made from steel angles supports a coordinate pair of carriages, movable in directions at right angles to each other. The inner carriage carries a flange supporting the body in which the hydrophone is mounted. By adjustment of the positions of the carriages, the face of the hydrophone can be brought into the axis of rotation, thus giving a true radiation pattern of the mounted hydrophone.

10.6 MEASUREMENT OF TRANSDUCER CHARACTERISTICS

For full knowledge of the performance of a transducer used as a receiver, the following data are needed: (1) open-circuit sensitivity, (2) receiving response, (3) impedance, and (4) radiation pattern.

For a transducer used as a projector, the *transmitting response*, that is, the sound pressure set up at a standard distance (usually 1 meter) for a stated electric input, is also required. The meanings of the above terms are discussed in Chapter 1, where it has been shown that the efficiency (ratio of acoustic power output to electric power input) can be computed from the measured values of these quantities.

CONFIDENTIAL

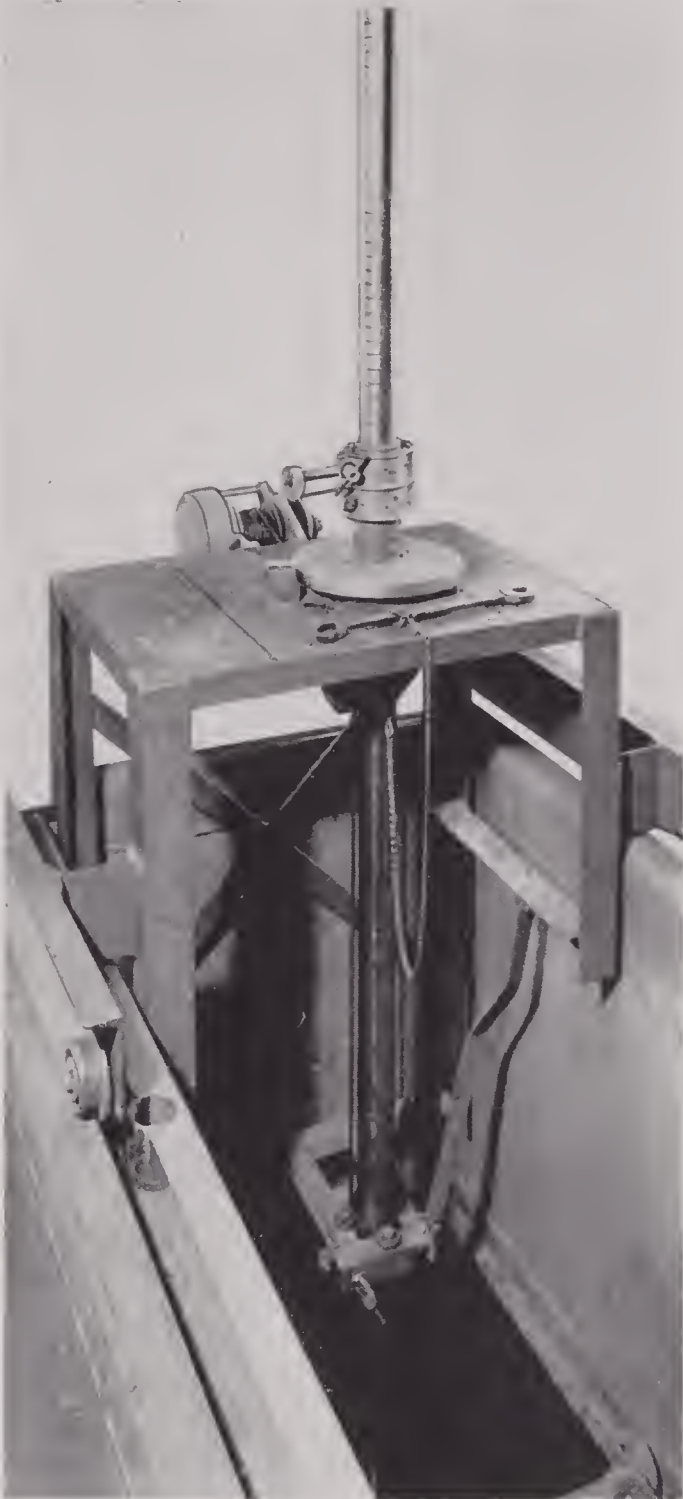


FIGURE 10. Projector shaft and carriage at the barge.

Sensitivity is ordinarily expressed in decibels referred to a unit sensitivity of 1 volt per dyne per sq cm and sound pressure level in decibels referred to 1 dyne per sq cm.

10.6.1 Measurement of Sound Field with Standard Hydrophone

The fundamental measurement for the determination of all the foregoing is the measurement of in-



FIGURE 11. Projector shaft and carriage at Spy Pond.

tensity of the sound at a given point in the sound field. Since all the characteristics of a transducer are functions of the frequency of the sound, knowledge of the frequency is also essential. An approach to the general procedure followed in acoustic measurements at HUSL can best be made by a detailed account of the measurement of the sound-pressure level by means of a calibrated hydrophone, that is, one of known sensitivity. The arrangement is shown schematically in Figure 13.

The electric signal is supplied by a continuous frequency oscillator through a variable-gain amplifier and output transformer to the standard transmitter, which generates a pure-tone acoustic signal whose frequency can be varied by movement of the frequency dial of the oscillator. The sound is picked up by the calibrated hydrophone, and the generated voltage is amplified by the variable-gain receiving amplifier, the output of which feeds into the voltage-level recorder. Certain preliminary adjustments are first made. The transmitting and receiving hydrophones are varied in depth and azimuth until a



FIGURE 12. Off-center transducer mount.

maximum output is shown on the vacuum-tube voltmeter V_1 at some convenient frequency in the range to be covered. Next, the gain controls of the transmitting and receiving amplifiers are set so that the recorded voltage level will fall within the 40-db range on the recorder tape over the entire frequency range. Gain-control settings on both transmitting and receiving amplifiers are not changed during the further course of the measurements.

The recorder driving mechanism is then mechanically connected to the frequency control dial of the oscillator, initially set at the lower end of the frequency range to be covered. The recorder is turned on, driving the oscillator dial through the desired range of frequency and giving a trace on the recorder tape (*response curve* shown in Figure 14A). The curve recorded on the tape is a function not only of the pressure level of the sound field but of the gains of the receiving amplifier and the recorder. The shape of the response curve depends upon the frequency

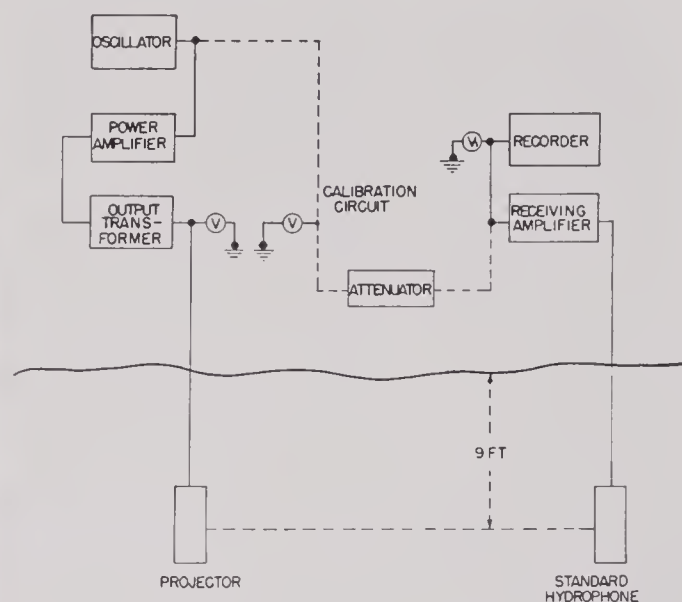


FIGURE 13. Schematic of arrangement for measurement of field.

characteristics of both, as well as upon variation of the field with frequency.

A voltage calibration of the amplifier and recorder is needed to find the actual voltage level of the standard hydrophone output. In Figure 15A the transducer is represented as a voltage generator E_T with internal impedance Z_T terminated by the high-input impedance Z_L of the receiving amplifier. In making the voltage calibration, the sound is turned off and a calibrating resistor R_c is inserted in the transducer circuit, as shown in Figure 15B.

The resistance R_c is much smaller than Z_T . The calibrating voltage is measured by first reading the voltage output of the oscillator on a vacuum-tube voltmeter and then connecting the oscillator through the attenuating network, whose attenuation has been previously measured, across the resistor R_c . The attenuator pad is designed to give a range of attenuations in 10-db steps, so that the applied calibrating voltage level in decibels is known from the measured voltage of the oscillator and the attenuator setting. The calibrating voltage is chosen to give a recorder trace either above or below the response curve when the oscillator dial is moved over the frequency range of the response curve. The calibration curve on Figure 14A was obtained in this way and is the locus of points on the recorder tape corresponding to an applied voltage level of -75 db vs 1 volt at the indicated frequencies.

The voltage level generated by the sound in the standard hydrophone is obtained from the two curves. The horizontal spaces on the tape correspond

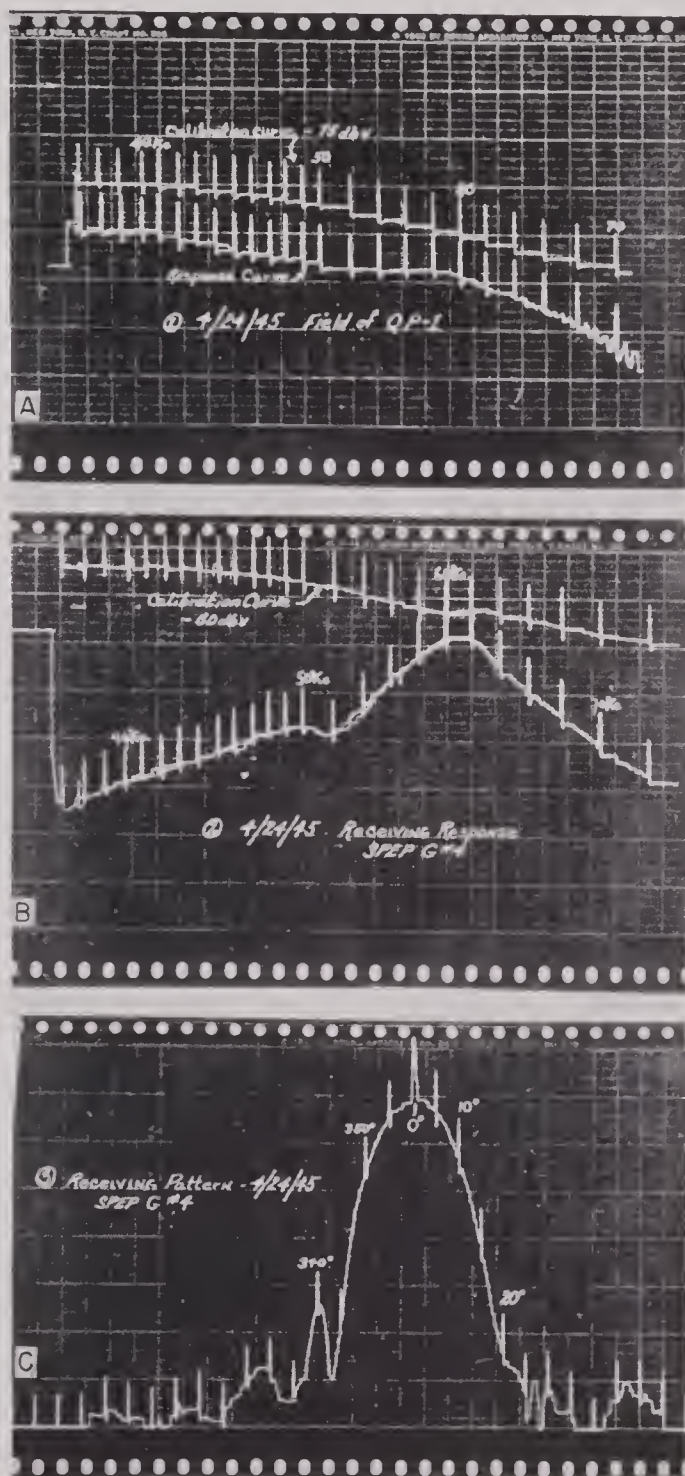


FIGURE 14. A. Response and voltage calibration of standard in measurement field. B. Receiving response and voltage calibration of test transducer. C. Receiving pattern of test transducer.

to a 1-db difference in the voltage level. Thus the voltage level of the response at 40 kc is $-75 - 5 = -80$ db referred to 1 volt. By carrying out the subtraction for the series of frequencies, data are obtained for the voltage response curve of the standard transducer in the sound field. It should be re-emphasized that no change is made in the gain in the receiving

circuit between the taking of the response and the voltage calibration curves.

When the voltage response of the calibrated hydrophone is known, the sound-pressure level is easily obtained from this and the known sensitivity of the hydrophone.

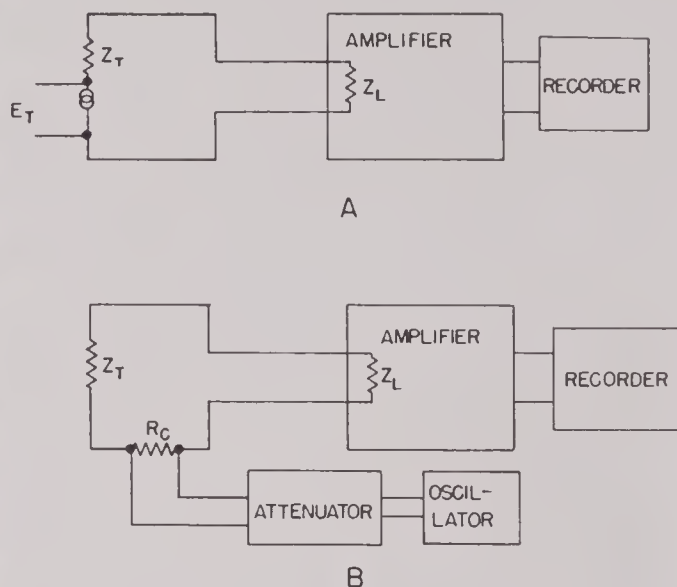


FIGURE 15. Schematic of voltage calibration.

The sensitivity = volts per dyne per sq cm

Sensitivity (db) = voltage level (db) - pressure level (db)

Pressure level = voltage level - sensitivity (db)

The sensitivity of the standard used in this particular case at 40 kc was -112.9 db. Hence the sound-pressure level was $-80 - (-112.9) = 32.9$ db vs 1 dyne per sq cm. Since the pressure level equals $20 \log p$, the pressure at 40 kc is $\log^{-1} 1.645$, or 43 dynes per sq cm.

The frequency at each point of both the response and calibration curves is given by the vertical breaks in the curves. These are made by electric signals originating at the frequency dial of the oscillator as it moves over the frequency range. Details of some of the frequency marker circuits used will be given later.

10.6.2 Transmitting Response Curve

Definitions of the various transmitting responses of interest were given in Chapter 1. The procedure followed in measuring the field is essentially the same as would be used in measuring the transmitting response of a projector. For example, the *current transmitting response* of the projector, used in obtaining the curves of Figure 14A, could be found if the value

of the current supplied to the projector to produce the field and the distance from projector to hydrophone were known. By definition,

$$\text{Current transmitting response} = \frac{p_1}{I},$$

where p_1 is the rms sound pressure produced at 1 meter when a current of I amp flows through the transducer windings. The pressure is assumed to vary inversely as the distance from the source. If p is the pressure measured at a distance r , then

$$\text{Current transmitting response} = \frac{pr}{I}.$$

Similarly, the *voltage transmitting response* can be measured by making simultaneous measurements of the input voltage across the projector and the field

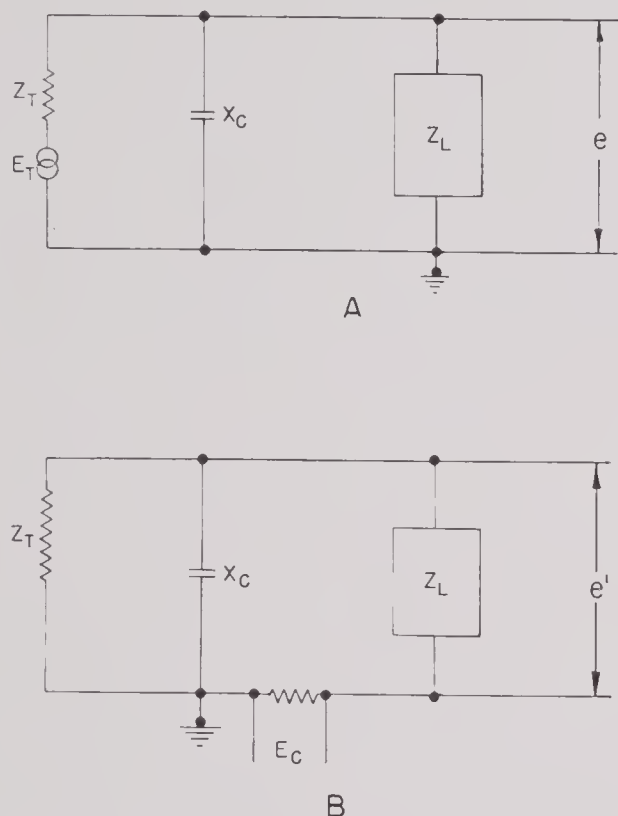


FIGURE 16. Equivalent circuits of transducer and cable.

at a known distance. If, for example, the voltage across the terminals of the projector had been maintained at a constant known value as the frequency varied, a voltage transmission curve for the projector could be deduced from the curves of Figure 14A.

10.6.3 Measurement of Receiving Sensitivity

Determination of the receiving sensitivity of a transducer involves a further set of measurements with the unknown transducer placed at the same point in the sound field as was occupied by the standard. Conditions at the transmitting end are to be kept unchanged, and response and calibration curves are to be taken exactly as in the case of the standard. Such curves for a transducer having a resonance peak at 60 kc are shown in Figure 14B. The voltage level generated in the windings of the unknown is computed from the calibrating voltage and the difference of level on the tape between the response and calibration curves. Again the sensitivity of the unknown transducer is obtained by dividing the generated voltage by the sound pressure producing it or, expressing the sensitivity in decibels, by subtracting the pressure level in the field from the voltage level generated in the transducer windings. To illustrate the calculation procedure, the sensitivity at 60 kc of the transducer for which the response is shown on Figure 14B is computed in detail.

R_s (Resp. of stand.)	=	16	db	R_x (Resp. of hyd.)	=	31	db
C_s (Cal. of stand.)	=	20	db	C_x (Cal. of hyd.)	=	33.5	db
$R_s - C_s$	=	-4	db	$R_x - C_x$	=	-2.5	db
C_{rs} (Cal. volt.)	=	-75	db	C_{rx}	=	-50	db
$R_s - C_s + C_{rs}$	=	-79	db	$R_x - C_x + C_{rx}$	=	-52.5	db
Sens. of stand.	=	-112.4	db	- Field	=	-33.4	db
Field (db vs 1 dyne per cm ²)	=	33.4		Sens. (db vs 1 volt per dyne per cm ²)	=	-85.9	

The effect on the receiving response curve of the impedance in which the receiver is terminated has been indicated in Chapter 1. In the measurements just described, the open-circuit sensitivity of the standard was used and since in all the measurements the receivers were terminated in the high input impedance of the receiving amplifier, it was the open-circuit sensitivity that was measured. A further point to be noted is that voltages are measured not at the transducer terminals but at the end of the measuring amplifier.

In general, magnetostrictive transducers have relatively low impedances, so that the shunted capacity of the leads produces a negligible error in the measurements at frequencies below 70 kc. Crystal transducers, on the other hand, have high impedances and the voltage measured across the cable terminals may differ materially from that generated by the trans-

ducer. In such cases, a measuring amplifier with a very high impedance ($Z_L > 17 Z_T$) may be used. If under these conditions the calibrating voltage is applied directly across the input terminals of the amplifier, with the transducer shorted out, the error is less than 0.5 db. When it is necessary to measure the open-circuit voltage developed by a high impedance transducer with no cable attached, the procedure indicated in Figure 16 may be followed. The impedance of the cable is X_c .

Figure 16A is the equivalent circuit of the transducer and cable when sound is being received from the water. When a series-calibrating voltage E_c is introduced, the situation is as shown in Figure 16B, and

$$e' \approx E_c.$$

If $Z_L \gg Z_T$ or Z_c , and E_c is adjusted to give the same output from the measuring amplifier as given by the sound signal, then $e = e'$. From Figure 16A,

$$e = e' = E_T \frac{X_c}{Z_T + X_c} = E_c$$

or

$$E_T = E \frac{Z_T + X_c}{X_c}.$$

To evaluate E_T both the cable capacity and the transducer impedance must be known by independent measurements.

10.6.1 Pattern Measurements

Receiving patterns are usually taken while the receiver and projector are still oriented as in taking the frequency response. The gain control of the receiving amplifier is set to give a maximum level of about 35 db on the tape with the oscillator set at the frequency at which the pattern is to be measured. The graduated disk is clamped to the rotor shaft with the zero of the scale at the fixed index. The shaft and transducer are then rotated slightly more than 180 degrees from this position. The recorder-marking circuit is switched to the microswitch, operated by notches cut in the edge of the rotor disk so that markings on the recorder tape now correspond to angles measured from the initial orientation of the transducer. The recorder and the motor driving the rotor are turned on simultaneously and allowed to run through a complete revolution of the transducer. The receiving pattern is thus recorded as a function

of the angle of orientation measured from the position of maximum response (Figure 14C).

The transmitting pattern is similarly measured, starting from the arrangement of projector and receiver for getting the transmitting frequency response. The transmitting pattern is obtained by rotating the transducer and recording the electric output of the receiving standard hydrophone, which remains stationary.

10.7 MEASURING EQUIPMENT

The bare essentials of equipment needed for acoustic measurement and transducer calibration are indicated in Figure 13. The original equipment at the Charles River barge was little more than this. The elaboration of the transducer development program, the necessity for time-saving devices, and the designing of special apparatus for specific types of measurements resulted in the addition of considerable accessory equipment. In general this was the same in the two stations, with minor variation dictated by the division of labor between the two.

An idea of the overall final arrangement at the Charles River barge is obtained by reference to Figure 17. The essential features, with certain additions, were duplicated at Spy Pond (Figure 18). An important detail not shown in the photographs is that all the racks at the barge were on Lord resilient mounts. At both stations, difficulties with spurious grounds and resulting ground loops were encountered. These were particularly troublesome at the barge. The provision of a positive common ground, consisting of a mass of metal resting on the pond bottom and connected by a heavy cable to a brass plate mounted on the wall behind the racks, gave the versatility of grounding needed to eliminate ground loops at Spy Pond. The electric isolation of the racks from one another and from the steel hull was an additional requirement at the barge. A second feature of importance in the precision of measurement was the installation of a voltage regulator to control fluctuations of the main 110-volt 60-cycle power supply. This, together with electronically regulated power supplies for the separate oscillators (Figure 19), gave the measuring systems a high degree of stability.

The individual elements of the final complete system at the barge are listed below Figure 17. Description in detail will be given only of such elements as contain special features.

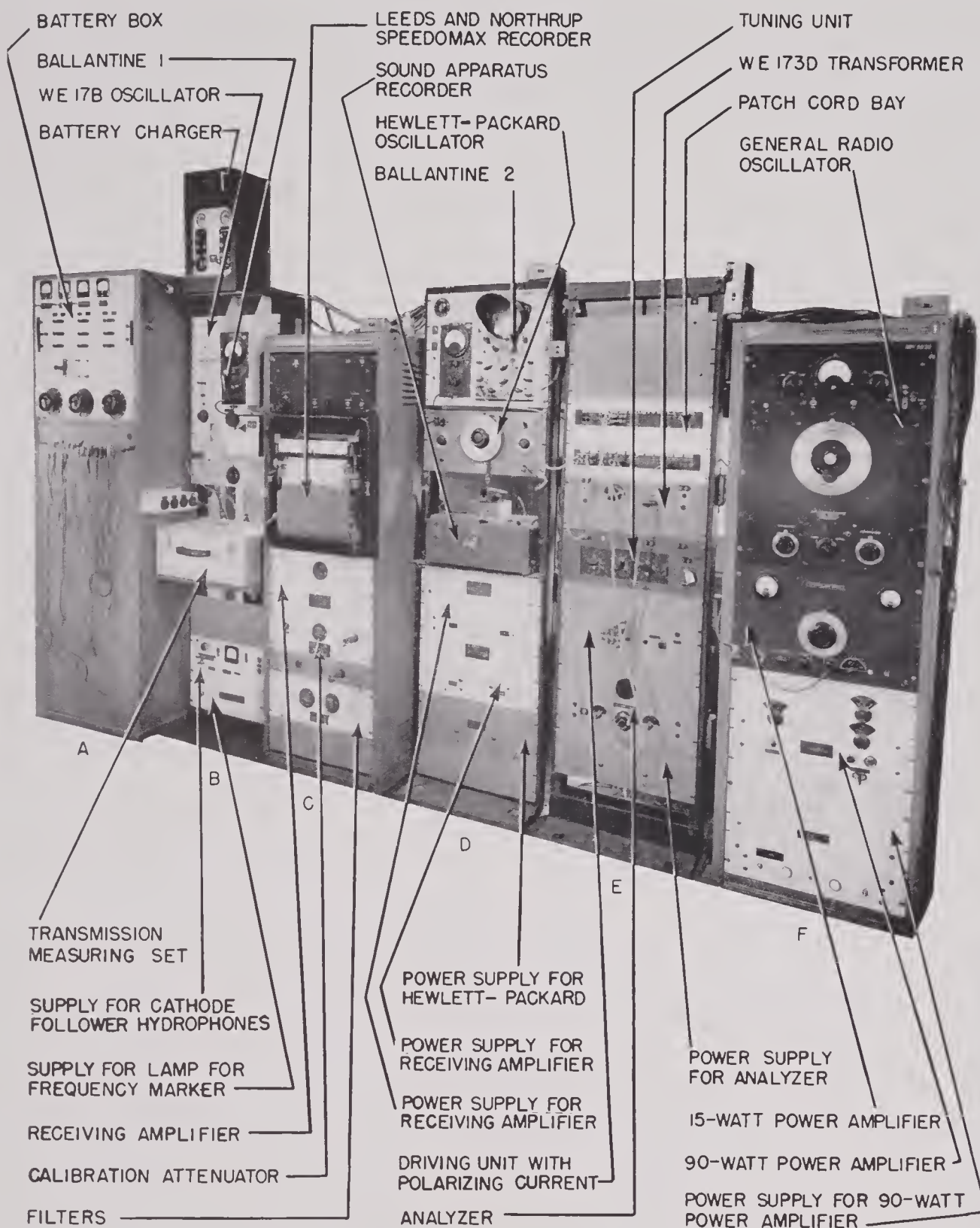


FIGURE 17. Complete measuring equipment at the barge. (Note: Ballantine 2 is somewhat to left of arrow.)

10.7.1 Sound Generating System

The source of a-c current for frequencies up to 72 kc originally used at the barge and throughout at Spy Pond was the Hewlett-Packard 200-D oscillator.

The H-P 200-C (20-200,000 cycles) was a standby source for occasional measurements above 70 kc. The latter was not rack-mounted. In the early days, the markings of the frequency dial of the oscillator were taken at their face value. Where greater frequency

CONFIDENTIAL

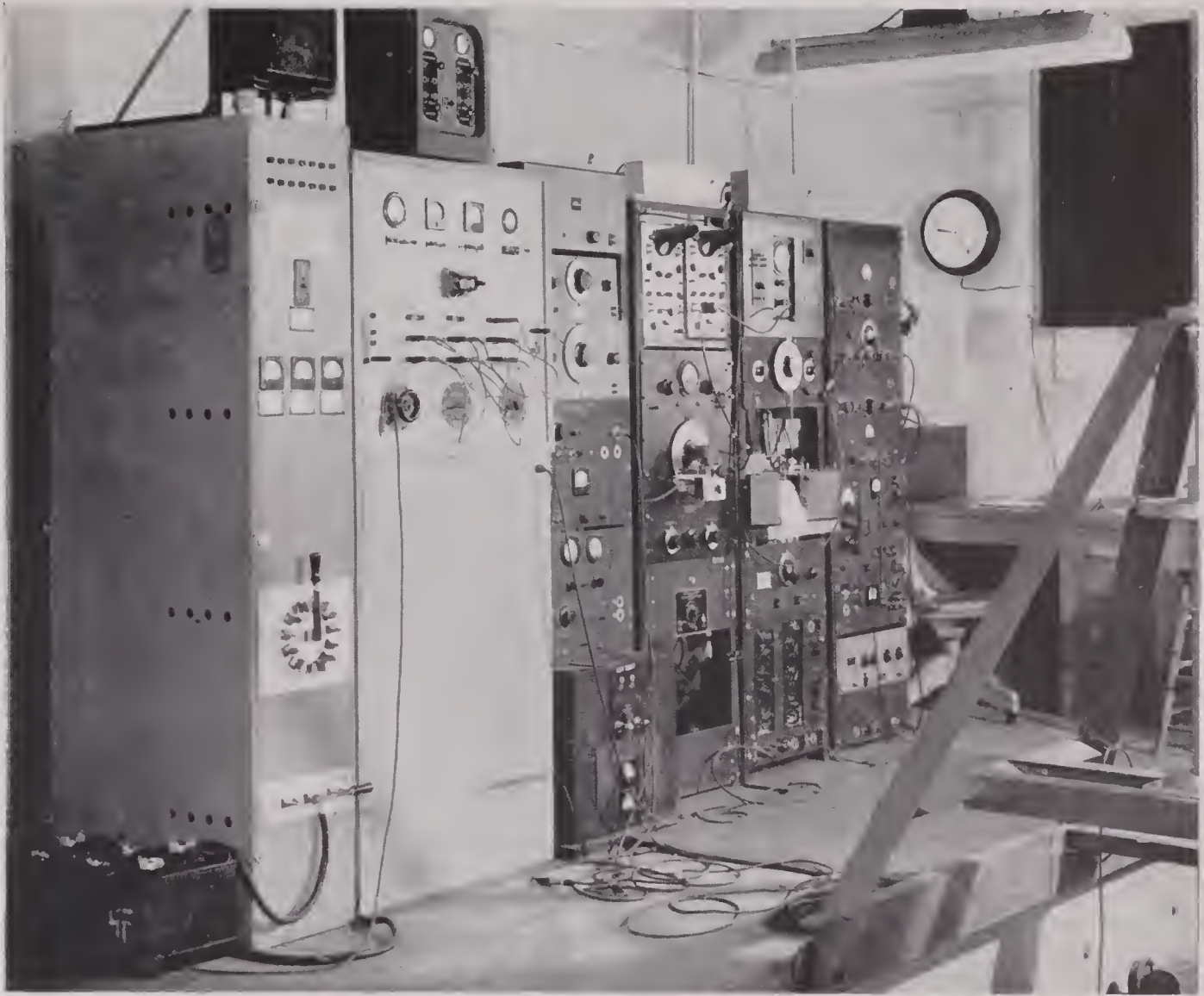


FIGURE 18. Complete measuring equipment at Spy Pond.

precision was required, the General Radio 713-B oscillator was used for frequencies up to 40 kc. Early in 1944, Western Electric 17B oscillators became available and one of these was installed at the barge but not at Spy Pond. A very precise tuning-fork frequency standard (described later) was installed for frequency checking at both stations.

Modifications of the oscillators were made to adapt them to our use. The first was designed to provide means for marking the frequency of the signal on the recorder tape. Various mechanical and electric devices, more or less satisfactory, were tried, but the photoelectric device described here and used at Spy Pond proved the most reliable.

It was necessary to move the frequency dial a few inches out in front of the chassis to allow room for the frequency indexing mechanism. A brass disk, slightly larger than the main tuning dial, was mounted on the

tuning shaft between the panel and the chassis. Small holes were bored near the edge of the disk coinciding with the frequency index marks on the main tuning dial. A pinhole lamp was mounted on one side of the disk so that when the disk rotated a flash of light was directed at a Type 922 photoelectric cell, which was mounted on the opposite side of the disk, every time a frequency index mark was passed. The impulse from the cell operated a relay that jogged the recording pen, thus making a frequency indication on the recorder tape.

To obtain a finer control of the power output of the H-P oscillator the gain-control potentiometer was replaced by a voltage divider. An attenuator pad designed to give an additional attenuation of 35 db was also built into the output of the oscillator to serve when a very small amount of power was desired.

CONFIDENTIAL

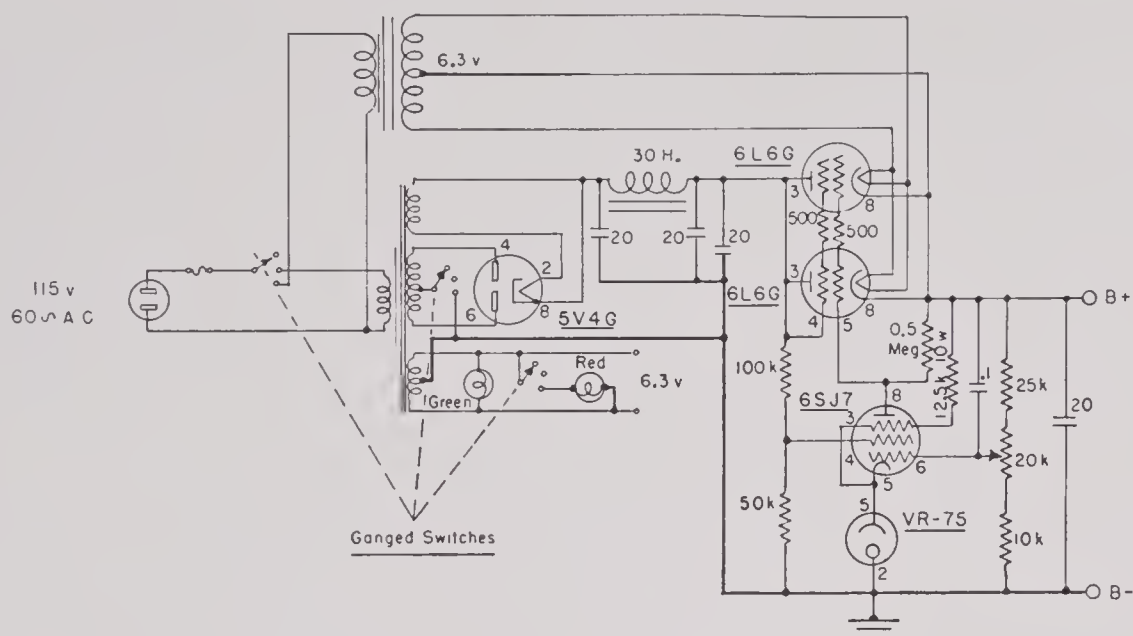


FIGURE 19. Electronically regulated power supply.

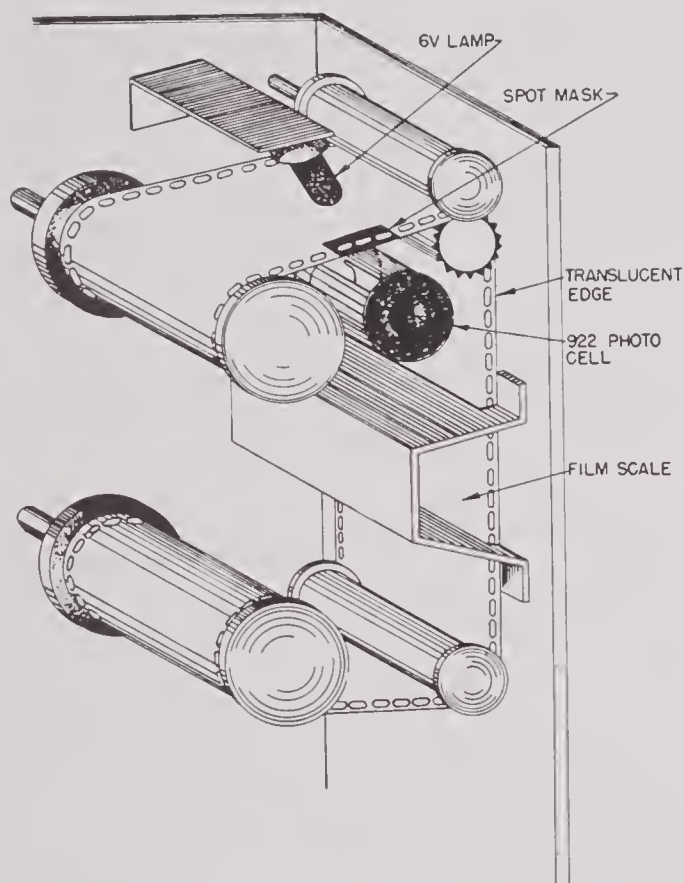


FIGURE 20. Frequency marking device on WE 17B oscillator.

The mechanism for continuously varying the frequency of the oscillator consisted of a worm gear, driven by a flexible shaft from the *sound apparatus recorder* (described later), that engaged a gear mounted on the tuning condenser shaft of the oscil-

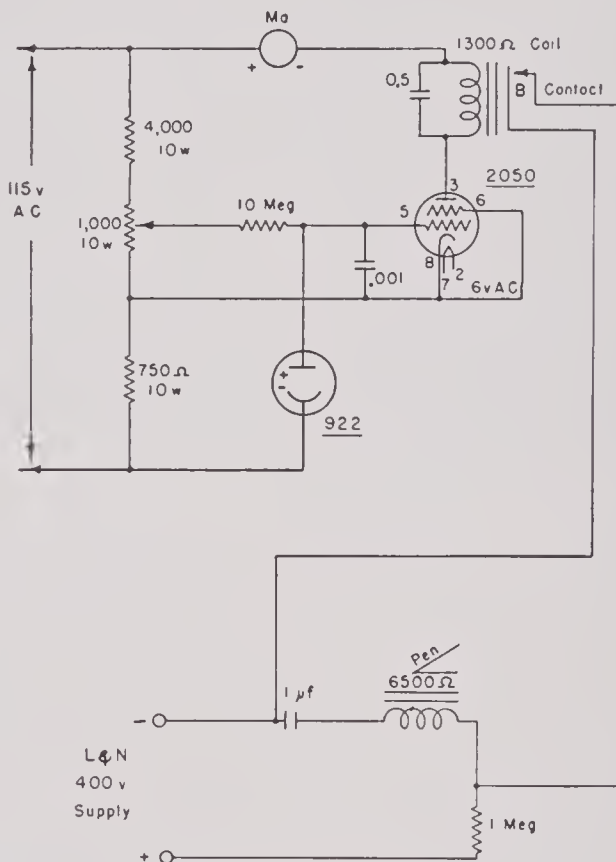


FIGURE 21. Thyatron circuit for frequency marking on 17B oscillator.

lator directly behind the tuning dial. The worm gear was mounted on a pivoted support so that it could be engaged or not as desired. A limit microswitch actuated by a projection on the frequency indexing dial stopped the motor drive of the recorder at the upper frequency limit of the oscillator. The mechan-

Motor Switch Diagram

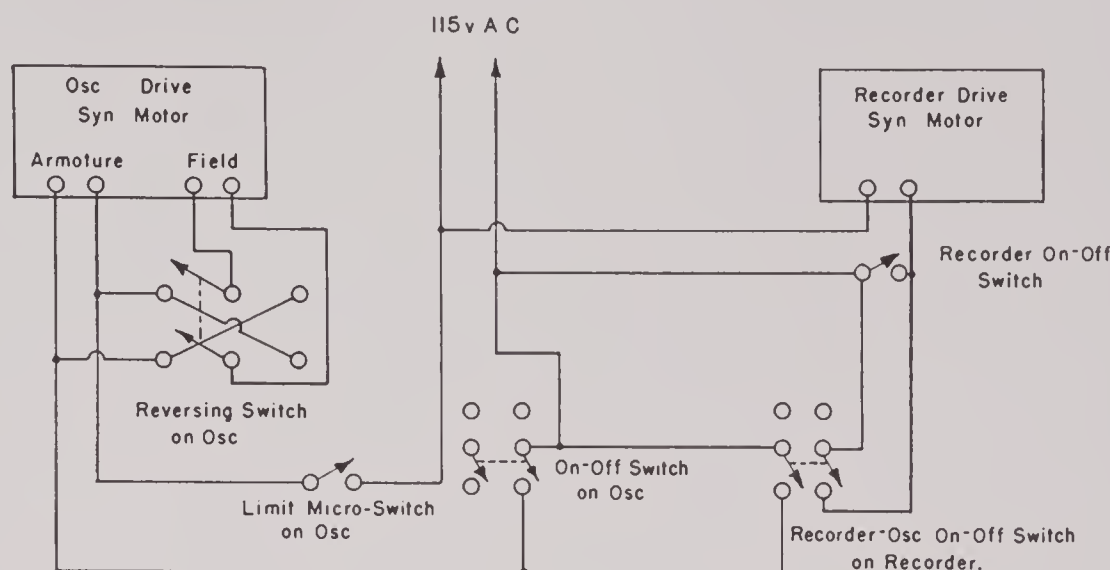


FIGURE 22. Circuit for synchronizing 17B oscillator and Speedomax recorder.

ical connection between the oscillator and recorder is shown in Figure 17.

The power supply of the oscillator was removed and replaced by the external voltage-regulated supply shown in Figure 19. The supply of the oscillator as furnished was found to be too unstable to give the desired frequency stability. The oscillator and its power supply had to be isolated from the racks electrically by plastic grommets placed over the mounting screws so that the oscillator would not introduce a second ground in calibration procedures.

The installation of the frequency marker in the 17B oscillator was somewhat more complicated than in the Hewlett-Packard. The frequency scale in the former is approximately linear and is etched on a celluloid tape illuminated from behind. The photoelectric scheme used is indicated in Figure 20. A 6-volt bulb and a 922 photocell were mounted inside the oscillator on opposite sides of the frequency tape, all parts being blacked out so that only a narrow beam of light passed through one edge of the tape onto a small patch of the active surface of the cell. Small spots or masks of Movietone film lacquer were painted on the frequency film in order to intercept the light at the points where frequency signals were to be given. Details of the thyatron circuit that activated the marker pen are shown in Figure 21.

Synchronism of the Western Electric oscillator with the Leeds & Northrup voltage level recorder used at the barge was effected by means of the arrange-

ment shown in Figure 22. The shaft of a small synchronous motor, connected as shown to the driving motor of the recorder, were geared to the frequency control shaft of the oscillator. The speed with which the frequency varied was thus controlled by the recorder speed. In order to reduce the normal output of the oscillator (0.7 to 21 volts at 20 kc) two 20-db attenuating pads were built into the oscillator output circuit.

10.7.2

Driving Amplifiers

For most of the measurements the power supplied by the HUSL Type 33 15-watt amplifier was sufficient. A circuit diagram is shown in Figure 23. The input impedance is approximately 0.1 megohm and the output at 35 kc about 10,000 ohms. The barge equipment included in addition a 90-watt amplifier, shown in Figure 17. The circuit diagram of the amplifier, with its power supply, is shown in Figure 24. Ordinarily it was driven by the Type 33 unit. A third special amplifier was designed and built by the Spy Pond crew, primarily to give constant-current driving to the crystal projectors that were originally used in measurement. Owing to the decrease with frequency in the impedance, the transmitting response of a crystal transducer has a rising frequency characteristic. The nominally constant-current amplifier (Figure 25) supplied a current to the Brush C-13 X-cut crystal transducer that varies by only about 20 per cent from 8 to 70 kc.

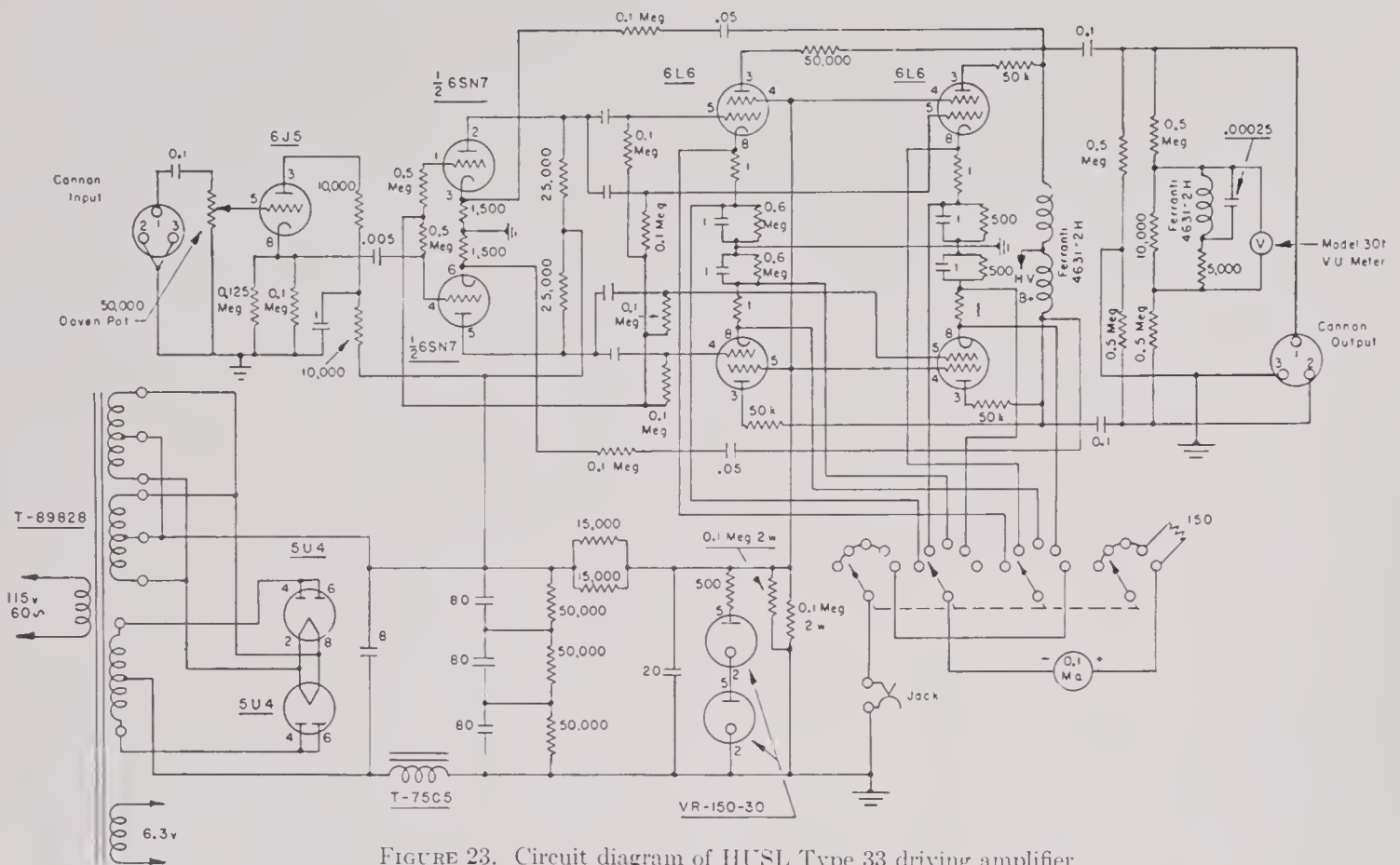


FIGURE 23. Circuit diagram of HUSL Type 33 driving amplifier.

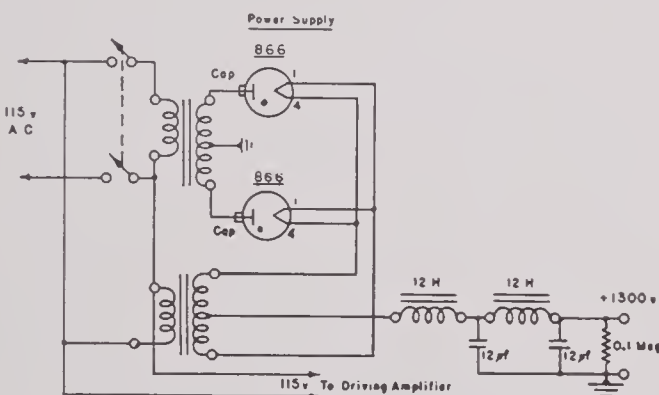
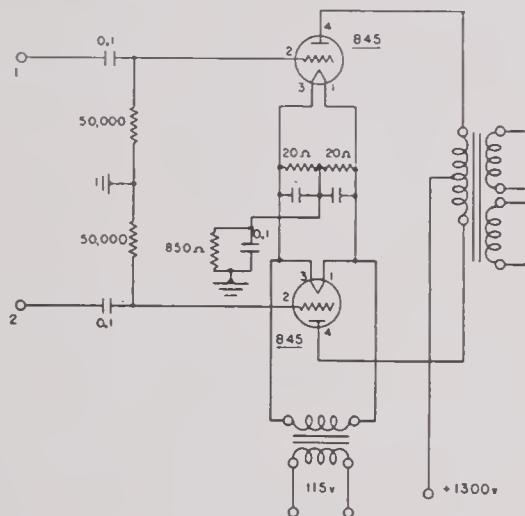


FIGURE 24. Circuit diagram of the barge's 90-watt amplifier.

10.7.3 Output Transformer

For the efficient transfer of electric power from the amplifier to the projector, the Western Electric 173-D output transformer was used with the lower-powered amplifier. This is designed to match push-pull parallel 6L6 tubes to various loads. Its rated frequency range is from 35 to 15,000 cycles, but it is down by a matter of only a few decibels at 70 kc. The transformer with switching arrangements was rack mounted (Figure 17). Nominal impedances of 7.5, 17, 30, 125, and 500 ohms could be selected. A 1-ohm resistor inserted in the transducer circuit allowed driving current measurements to be made.

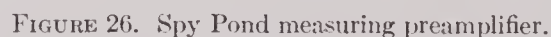
Three output transformers for the 90-watt amplifier provided six possible output impedances of 2, 8, 20, 80, 200, or 800 ohms. The secondary of each transformer had two sections. They showed impedances of 2, 20, or 200 ohms connected in parallel, and 8, 80, or 800 ohms in series.

10.7.4 Receiving Systems

In the original installation at the barge and in the final installation at Spy Pond, a preamplifier giving a 40-db gain and a final amplifier with a 70-db gain



The single 110-db amplifier designed and built for final installation at the barge is shown in Figure 30.



Both high and low impedance input circuits were balanced to ground, and the calibrating voltage was injected at the midpoint. The high impedance input was mounted in a separate chassis not carried on the relay rack. With certain transducers, there was at

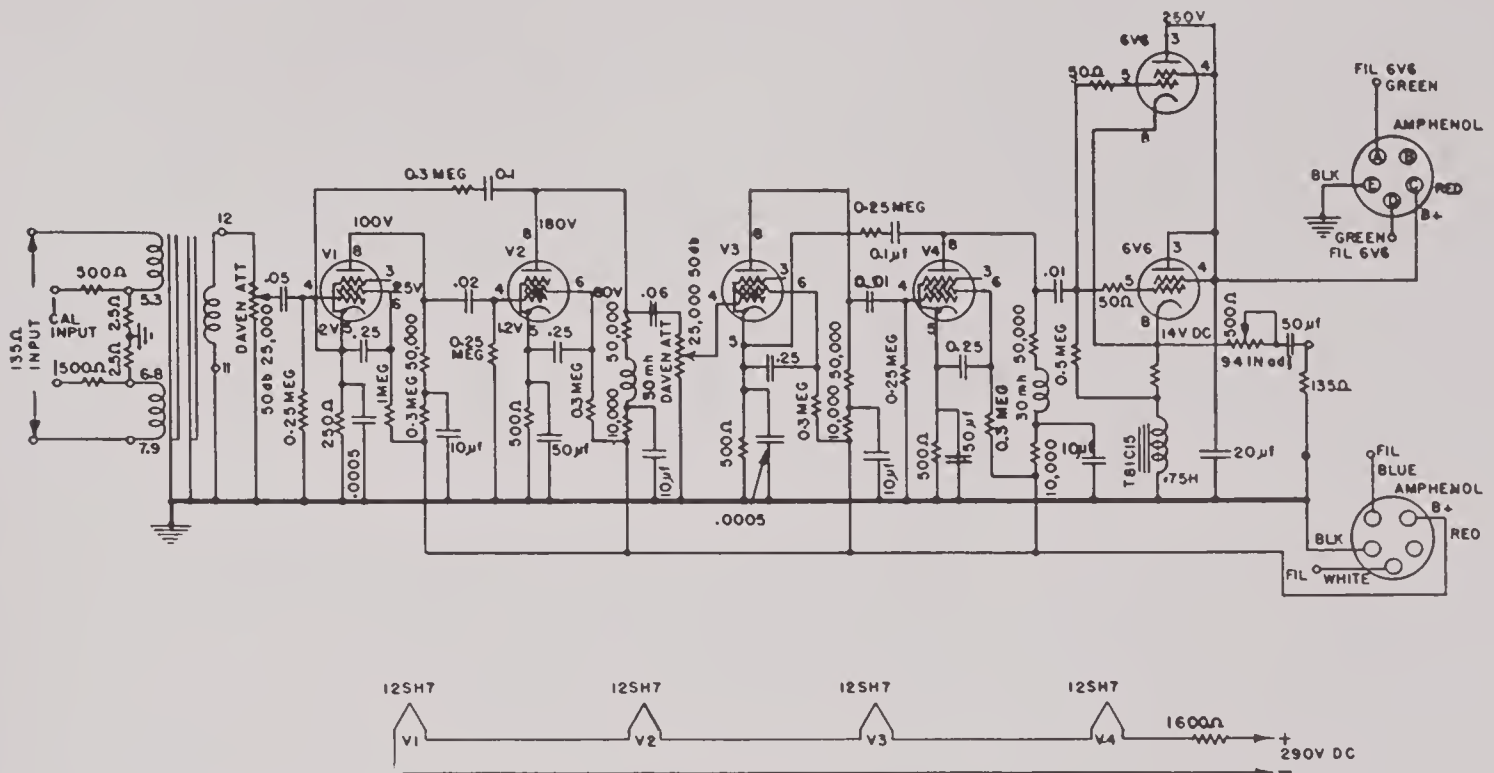


FIGURE 30. Barge's 110-db receiving amplifier.

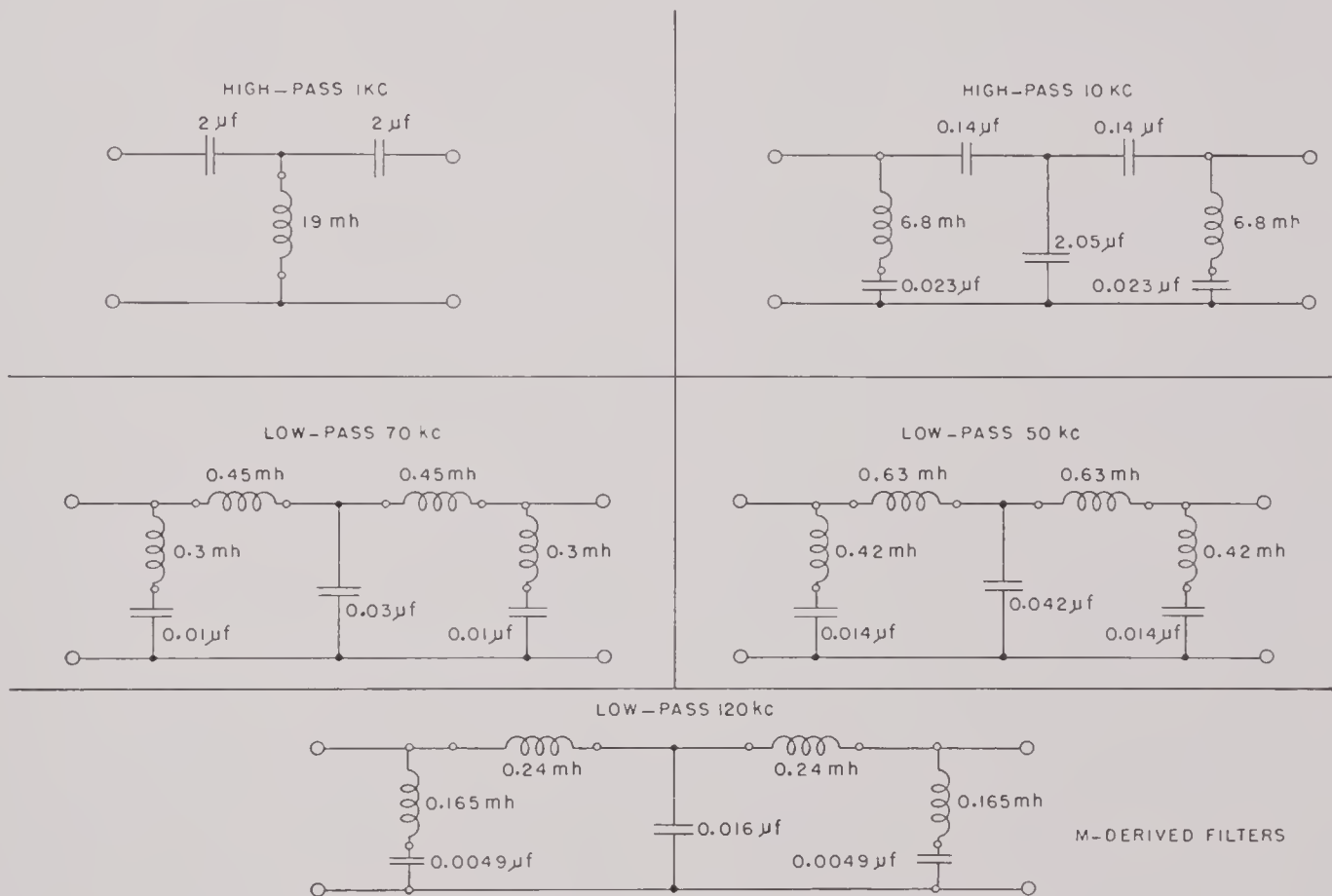


FIGURE 31. High- and low-pass filters used at the barge.

CONFIDENTIAL

times serious interference from long-wave radio signals originating at a nearby station. This was eliminated by a set of filters designed to be inserted in the receiving circuit between the receiving amplifier and the recorder. Included in it were two high-pass filters with cutoff at 1 kc and 10 kc to suppress low-frequency noise originating on the barge or in the water, and three high-frequency filters cutting off frequencies above 50, 70, and 120 kc and thus eliminating noise of radio origin. Components of these filters are shown in Figure 31 and the location of the rack-mounted assembly in Figure 17.

10.7.5 Voltage Level Recorders

Until early in 1944, the recorders used at the measuring stations were Type FR, manufactured by the Sound Apparatus Company of New York. This instrument is designed to cover a voltage level range of 40 db over a frequency range from 20 to 20,000 cycles. As supplied by the manufacturer, its performance in the supersonic-frequency range leaves much to be desired.³⁰ The recording pen is coupled to a contact that moves over a logarithmic potentiometer in such a manner as to keep the power input to the recorder constant under varying applied voltages. The movement of the pen carriage is produced by a magnetic clutch that couples the pen carriage to the proper side of a disk rotating at constant speed in a manner to maintain a constant input. The rotational speed of the wheel is such as to give a maximum speed of pen motion of 40 db per second. For supersonic work the outstanding defects of the recorder in its original state were a marked decrease in response above 50 kc and erratic behavior of the magnetic clutch. Figure 32 shows the circuit diagram of the recorder in its original form plus a stage of d-c amplification to increase the ratio of the d-c output voltage to the a-c input.

The modified circuit shown in Figure 33 represents contributions of the HUSL staff to the improved performance of this instrument in the desired frequency range. Thus modified and with a certain amount of nursing, it was used at Spy Pond with a reasonable degree of satisfaction. The coupling device to the 200-D oscillator is shown in Figure 17. The gearbox is shown on the top of the recorder. It contains a gear train by means of which two ratios of oscillator speed to recorder-tape speed can be obtained. Samples of the recorder traces of the *sound apparatus recorder* trace have already been shown.



FIGURE 34. Leeds & Northrup recorder mounted in rack.

The Leeds & Northrup Speedomax power level recorder used in the final installation at the barge is shown in Figure 34. Voltage levels are recorded on a tape 10 in. wide, covering a 40-db range of variation of the recorder input. It is designed to operate between 150 and 150,000 cycles and over this range is accurate to 0.5 per cent of full scale. The 0-decibel input level corresponds to a voltage of about 5 mv and can be adjusted over a range of approximately 10 db about this value. The input impedance is approximately 165 ohms. The speed of response of the recorder is such that the pen will traverse any part of the 10-in. chart and arrive at complete balance, without overshooting, in approximately 1.5 sec. The

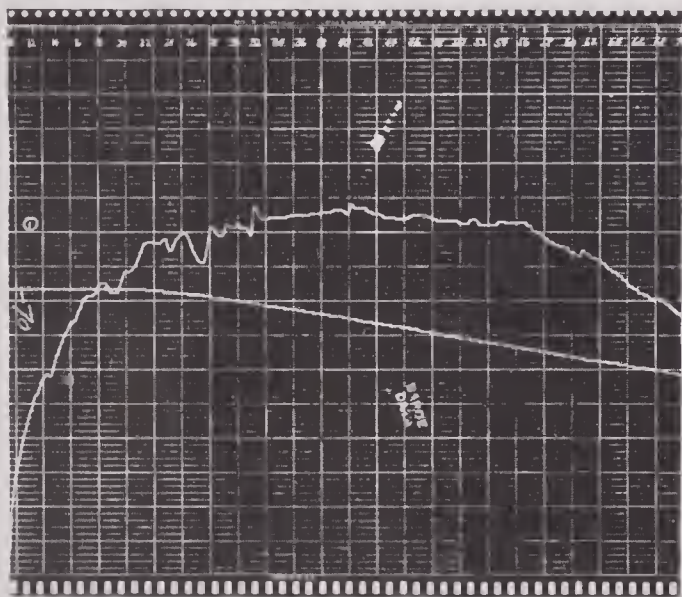


FIGURE 35. Response calibration from L & N recorder.

paper is driven 6 in. per minute by a synchronous motor. An extra pair of spiral gears is supplied with the accessories so that paper speeds of 3 in. per minute or 6 in. per hour may be obtained in place of the standard speed. A switch permits "continuous" or "limited" paper drive; when it is on "limited," the drive stops if the pointer reaches either extreme of the scale. The frequency marker pen at the left end of the chart is operated by the circuit shown in Figure 20. The recorder itself operates from a standard 115-volt 60-cycle supply. A response curve and voltage calibration curve are shown in Figure 35.

10.3 PROJECTORS AND STANDARD HYDROPHONES

10.3.1 Projectors

Several projectors, both crystal and magnetostrictive, have been used for measurements at the field

stations. The first were the HUSL 1 × 1-in. X-cut Rochelle salt crystal hydrophones made in the laboratory. These were quite similar in construction to the HK series developed at the Massachusetts Institute of Technology.²⁰ The main point of difference between the two was the substitution in the Harvard units of glass for the metal faces — and later rubber — of the MIT model. Units known as "Harvard 6 × 6" projectors were built later. These were similar in mechanical construction to the 1 × 1's, with a 6 × 6-in. radiating surface divided into four quadrants with connections for operating the quadrant in series, parallel, or series-parallel. Driven at constant voltage, these units showed a rising frequency characteristic due to the drop in impedance with increasing frequency.

Later, the Brush Model C-13-2 X-cut crystal hydrophone became standard equipment at both stations. This has a 4 × 4-in. radiating area of Rochelle salt crystals surfaced with a rubber face and mounted on heavy metal backing plate. For HUSL use, the front-to-back discrimination was increased by cementing a ¼-in. layer of corprene on the back surface. These units showed good patterns up to 80 kc, with the frequency response typical of crystal projectors. The data for Figures 36 and 37 were supplied by the manufacturers, the Brush Development Company, Cleveland, Ohio.

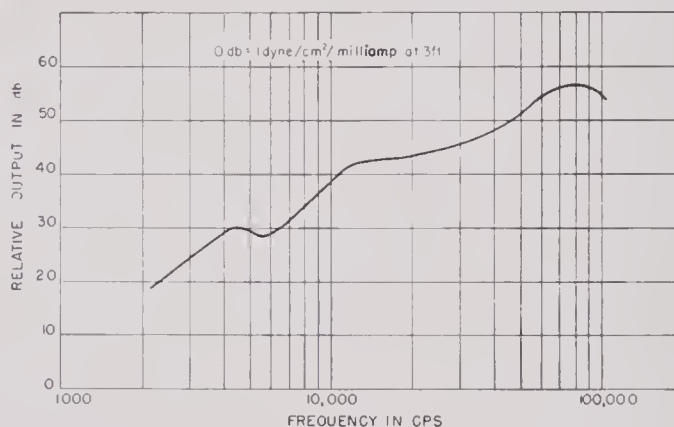


FIGURE 36. Transmitting response of Brush C 13-2 transducer.

At frequencies below 10 kc the crystal hydrophones gave relatively low outputs, with distorted wave forms. In this range, the Type 1K low-frequency electrodynamic projector developed by the Bell Telephone Laboratories was used.^{19, 76} The somewhat ragged frequency characteristic in the 6- to 10-kc range proved an objectionable feature of this projector. The XPA 3 × 12-in. crystal unit developed

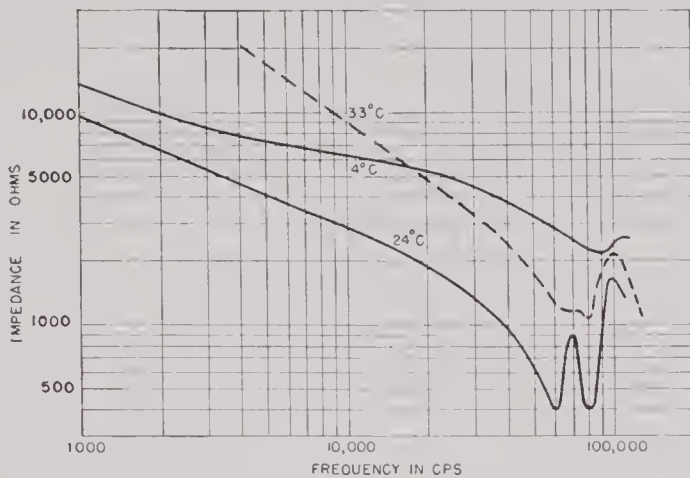


FIGURE 37. Impedance characteristics of Brush C 13-2 transducer.

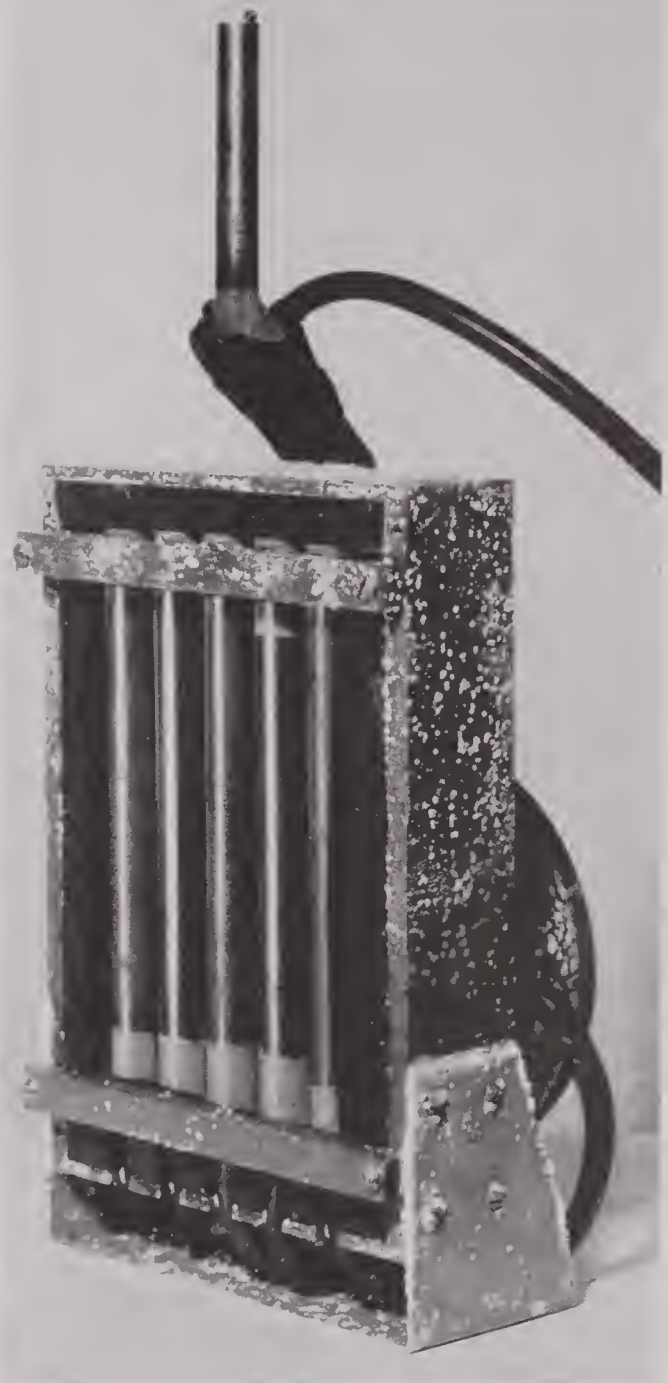


FIGURE 39. QP projector.

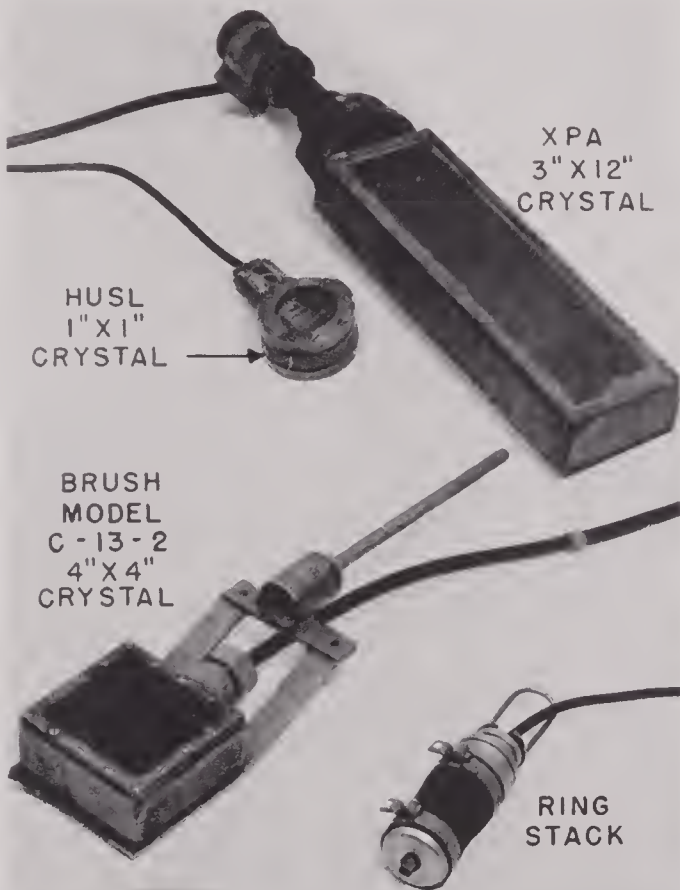


FIGURE 38. Projectors used at field stations.

by MIT²³ proved more satisfactory for low-frequency measurements.

The temperature dependence of the X-cut crystal projectors, particularly when the water temperature approaches the Curie point of Rochelle salt, is an inherent defect of this type for measurement purposes. Magnetostrictive transducers, while relatively free

from temperature effects, have low efficiency at frequencies far from resonance, but they have proved extremely useful in many types of measurement. Thus the B-19B's, though designed primarily for use as hydrophones, have been used as projectors in the frequency range from 15 to 40 kc where fields of the order of 35 db vs 1 dyne per sq cm at 2 meters have sufficed. The B-19K (see Chapter 6, Section 6.3.2) has proved satisfactory for measurements between 5

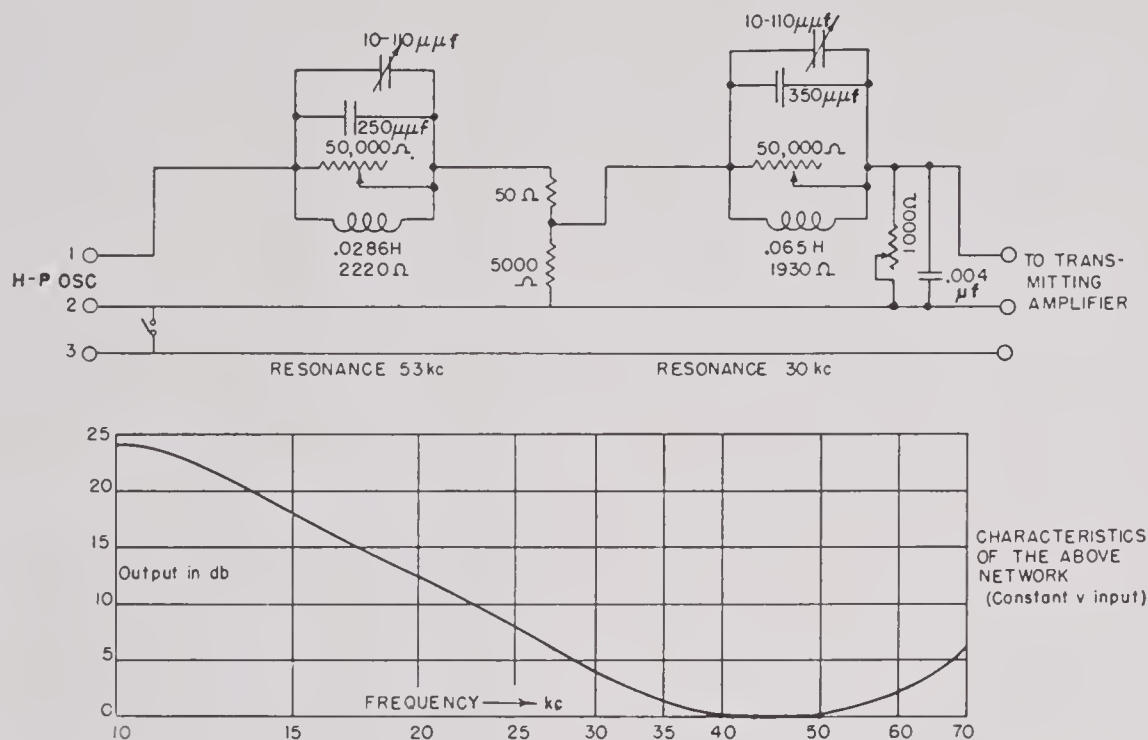


FIGURE 40. Inverse network to give flat field with QP projector.

and 10 kc. The thin-walled 60-kc ring stack, less than a wave length in height (see Chapter 6, Section 6.4.6) has been used as a spherical source over the testing range from 10 to 70 kc. Some of the projectors mentioned above are shown in Figure 38.

The QP projector (Figure 39), described in Chapter 6, Section 6.6, has proved more satisfactory for most measurements in the range from 10 to 100 kc than any other projectors used. The average of 30 measurements of field shown in Figure 41 was obtained with the compensating network shown in Figure 40 inserted between the oscillator and the constant current amplifier. The constancy is shown by the maximum deviations from the average of these measurements made over a period of almost four months.

10.3.2 Standard Hydrophones

An equally diversified list of standard hydrophones has been used. The earliest standards used were the Bell Telephone Laboratories 1A and 2A "square coil" pressure gradient hydrophones.^{18, 75}

In a 1A unit a rectangular coil is movable in the field of a permanent magnet. It has a fairly flat response from 0.1 to 50 kc, with a sensitivity of approximately -140 db vs 1 volt per dyne per sq cm and an impedance of about 60 ohms at 20 kc. The similar

but smaller model, 2A,²² designed for use up to 100 kc, has an impedance of about 9 ohms at 20 kc and a sensitivity of -152 to -162 db vs 1 volt per dyne per sq cm over the measuring frequency range. Because of their low sensitivity and rather fragile construction, these hydrophones were not the ideal instruments for many of the measurements required. The original calibrations were supplied by the Underwater Sound Reference Laboratories of Columbia University Division of War Research [USRL].

The development of the B-19B and later the B-19H hydrophones met the need for sturdier and more sensitive standards. Reciprocity calibrations of selected units of these types, which were found to check very closely with USRL calibrations of similar units, gave reliable standards for field measurements for frequencies between 10 and 100 kc.⁴⁵

A relatively small proportion of the measurements made at HUSL was in the range of audible frequencies. The standard hydrophones used were the 3A and the 5E crystal hydrophones designed for NDRC by the Bell Telephone Laboratories. These were all crystal units with the preamplifier incorporated in the hydrophone housing. Description and performance data are given in references 17, and 77, 21 and 80. With all these crystal transducers a separate battery power supply for the preamplifier must be provided. The battery box, which was designed as a special unit,

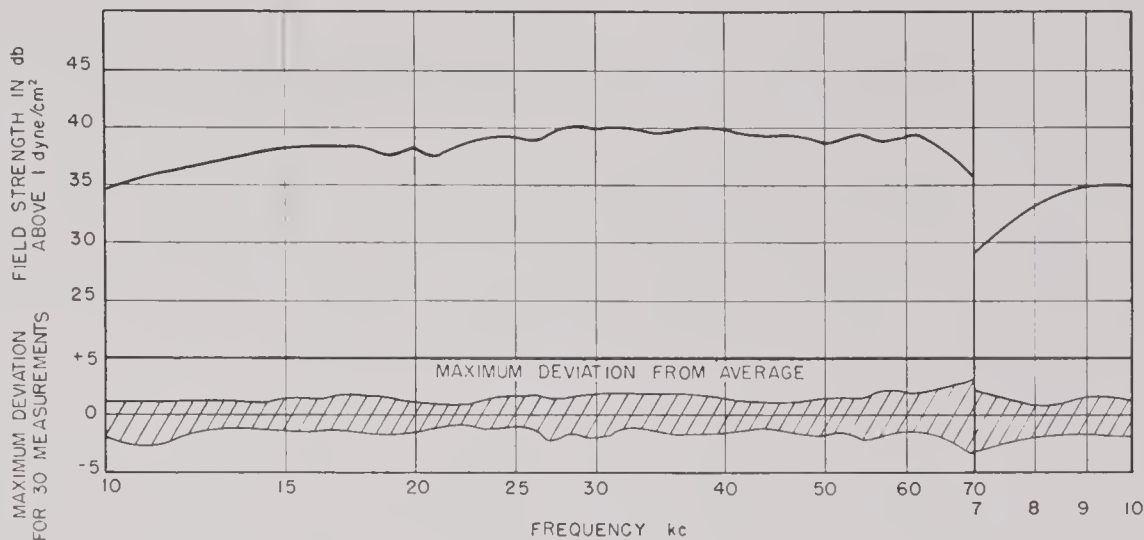


FIGURE 41. Field of QP-1 with constant current amplifier and inverse network.

is shown in Figure 17 and the circuit in Figure 42. The unit is supplied with a meter for measuring filament and plate voltages and amphenol plugs to fit the terminals of the crystal hydrophones. The 135-ohm resistor across the signal leads from the hydrophone provides the proper termination for the 5E pre-amplifier.

The hydrophones mentioned in the foregoing paragraph are illustrated in Figure 43.

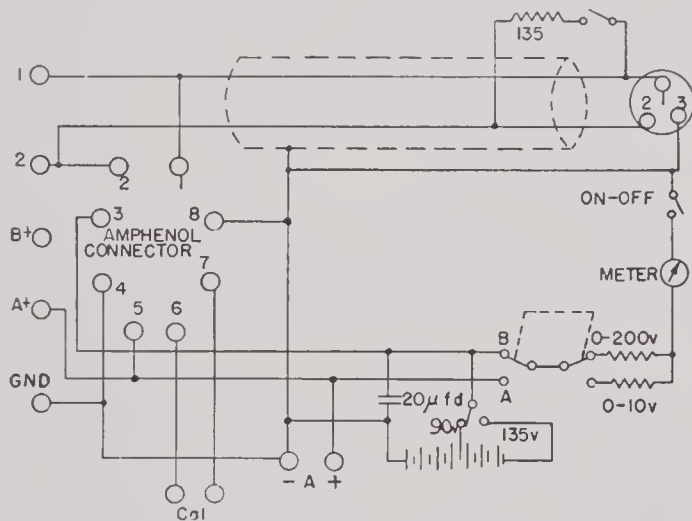


FIGURE 42. Battery power supply for standard crystal transducers.

10.9 ABSOLUTE CALIBRATION OF HYDROPHONES

The theory underlying the absolute calibration of a linear reversible transducer appears in Chapter 1. In making reciprocity calibrations at HUSL, the

measurements were made in such a way that equation (32) of Chapter 1 could be used in calculating the sensitivity of the reversible transducer C , used both in transmission and reception. To repeat equation (32)⁵ of Chapter 1,

$$S_v^C = \left(\frac{J E_2 E_3}{E_1 I} \right)^{\frac{1}{2}}, \quad (1)$$



FIGURE 43. Standard hydrophones used at HUSL.

where J is the reciprocity parameter $2r/\rho f \times 10^{-7}$, r being the constant distance between transmitter and receiver at which the three sets of voltage and cur-

rent measurements shown in Figure 20 of Chapter 1 were made and I the constant value of the transmitting current. E_1 and E_3 are voltages generated in transducers B and C respectively by a current $I_1 = I_2$ in transducer A , while E_3 is the voltage generated in B by the current I in transducer C . By reference to the right-hand member of the equation, it is apparent that the absolute value of the current in transducer A when E_1 and E_2 are being measured need not be known. It is only necessary that the current be the same in the two cases, since it is the ratio of E_2 to E_1 that enters into the expression and this ratio is independent of the magnitude of the driving current in transducer A . A is used only as a transmitter and B only as a receiver, so that neither need be reciprocal. Transmitter C is used in both transmission and reception and a linear relation must exist between current and generated pressure and between pressure and voltage over the whole range covered in the measurements. A corollary of this last is the requirement that the acoustic output of C shall be undistorted.

The sensitivity of a transducer is recorded in decibels referred to 1 volt per dyne per square cm. With equation (1) put into logarithmic form,

$$20 \log S_c = 10 \log J + 10 \log E_2 + 10 \log E_3 - 10 \log E_1 - 10 \log I. \quad (2)$$

Since the voltages are recorded in decibels referred to 1 volt, ($20 \log E$), logarithms of the E 's can be obtained by dividing the measured voltage levels by 2.

The actual measurement procedure followed in making a reciprocity calibration may be illustrated by the calibration of a B-19 hydrophone.

The Brush 4×4 was used as transducer A , a B-19H as transducer B , and the B-19B as transducer C . The driving level of A was fixed by adjusting the gain of the driving amplifier to a given voltage at some definite frequency, in this case 10 volts at 10 kc. The response of the B-19H placed at a definite point in the field was recorded. A calibrating voltage was injected from which the voltage level $20 \log E_1$ could be measured. The B-19B was then put down in the same position as that occupied by the B-19H and, with the driving conditions unchanged, the voltage level $20 \log E_2$ was measured. With the B-19B maintained in its position, the Brush 4×4 was replaced by the B-19H. The B-19B was then driven, the driving current being kept at a constant value, which was measured by means of a Ballantine vacuum-tube

voltmeter [VTVM] across a calibrated 1-ohm resistor inserted in the leads of the B-19B. The voltage level generated at the output of the B-19H is $20 \log E_3$, the value of which is determined from the response and calibration curves in the usual manner. The values obtained from measurements made in this manner can all be inserted in logarithmic form of the equation for the sensitivity of the B-19B. (Half the voltage levels of E_1 , E_2 , and E_3 must, of course, be used.)

The reciprocity parameter J is a function of frequency and may be computed for each frequency. A preferable procedure, however, is to reduce the expression for J to the logarithmic form

$$10 \log J = 10 (\log 2 + \log r - \log \rho - \log f - 7) \\ = 10 \log r - 10 \log f - 66.9. \quad (3)$$

Tables of values of $10 \log J$ for the needed values of r and f may be prepared. A simpler procedure, however, is to plot on semilog paper $10 \log J$ as a function of f with r as a parameter, r being measured in centimeters, since the density of water is taken as 1 gm per cubic cm. So plotted, $10 \log J$ appears as a family of parallel straight lines from which its value for any given values of r and f can be taken.

The sensitivity of the reciprocal transducer having been determined, the sensitivity of transducer B can be deduced by direct comparison of the measured voltage levels of E_1 and E_2 , since both were generated by the same sound field. The sensitivity of transducer A , however, cannot be derived from the measurements described.

10.9.1 Results of Reciprocity Calibrations

Measurements for the first absolute calibration of a transducer at HUSL were made on April 20, 1943, on a laminated stack transducer, HP-4. The results of those measurements were used to evaluate the sensitivity of the HP-4 and also to check the calibration of the BTL standard 1A No. 17 supplied with the instrument.¹¹

The sensitivity of the latter as deduced from the measurements agreed to within 1 db with the values given by BTL over the frequency range from 10 to 40 kc. From 40 to 70 kc, differences were no greater than 3 db.

Since that date, refinements in measuring technique have been made, with periodic checks of the

various standards used at the field stations. In most of these, a Ballantine VTVM has been used for response and voltage calibration in place of the level recorder. The degree of reproducibility in the results

TABLE 1. Absolute sensitivity of B-19B, in db vs 1 volt per dyne/sq cm. Average from 13 reciprocities.

Freq. in kc	Sensitivity	Deviation from Ebaugh	0.675 of rms error
7	- 117.4	- 0.2	0.7
8	- 115.0	+ 1.0	0.9
9	- 114.4	+ 0.2	0.2
10	- 115.2	+ 0.1	0.4
11	- 115.0	+ 0.3	0.5
12	- 114.1	+ 0.3	0.6
13	- 113.2	+ 0.3	0.6
14	- 115.1	0	0.5
15	- 113.3	+ 0.3	0.5
16	- 113.3	+ 0.2	0.4
17	- 112.8	+ 0.1	0.3
18	- 112.6	- 0.1	0.5
19	- 113.3	- 0.2	0.5
20	- 113.9	- 0.4	0.5
21	- 113.4	+ 0.2	0.4
22	- 112.4	+ 0.1	0.3
23	- 111.6	0	0.2
24	- 111.3	- 0.3	0.4
25	- 111.9	0	0.5
26	- 111.3	- 0.1	0.4
27	- 111.8	+ 0.3	0.5
28	- 112.7	- 0.2	0.7
29	- 113.3	+ 0.5	0.4
30	- 113.2	+ 0.7	0.5
32	- 112.0	- 0.1	0.7
32.2	- 116.4	...	0.8
34	- 112.8	- 0.3	0.5
36	- 112.7	- 0.4	0.3
38	- 113.1	- 0.4	0.3
40	- 112.9	- 0.2	0.2
42	- 113.2	- 0.2	0.2
44	- 113.5	- 0.5	0.3
46	- 113.6	- 0.3	0.4
48	- 113.5	- 0.5	0.4
50	- 113.6	- 0.3	0.5
52	- 113.4	- 0.4	0.5
54	- 113.7	- 0.7	0.7
56	- 113.5	- 0.6	0.6
58	- 112.8	- 0.6	0.5
60	- 113.3	- 0.5	0.5
62	- 114.0	- 0.6	0.5
64	- 114.4	- 0.7	0.5
66	- 114.5	- 0.4	0.5
68	- 114.8	- 0.5	0.5
70	- 115.1	- 0.6	0.6

the precision there shown should naturally be greater than might be expected in routine measurements. From the same analysis it was concluded that 95 to 98 per cent of single measurements made under routine conditions would fall within a range of ± 1.5 db from the statistical mean of a number of measurements made under carefully controlled conditions.⁶⁷

10.10 AUXILIARY MEASURING EQUIPMENT

10.10.1 Current Supply for D-C Polarization

To provide means for introducing direct current into the windings of transducers requiring d-c polarization, a storage battery with charger was installed in both the barge and Spy Pond laboratories. The front of the battery box, on which were mounted meters, switches, and rheostat controls, is shown in Figure 17.

Eighteen 6-volt storage batteries, housed in a wooden box with three shelves, provided a direct-current source for operation of d-c motors, polarization of transducers, and numerous other uses. Two batteries were connected in series, each pair being wired to Giant insulated jacks mounted on a Transite switching panel on the front of the battery box. Therefore, each pair of jacks on the front panel supplied 12 volts. Any combination of the 12-volt sections could be connected to the output circuit by plug connectors, thus providing a means for controlling the current output of the battery up to a maximum value of 25 amp. The output was wired directly to d-c input terminals on the impedance-measuring and d-c polarizing panels. A General Electric Tungar battery charger, capable of charging any combination up to 12 batteries, was mounted on top of the battery box and wired to the Giant insulated jacks on the Transite panel.

10.10.2 Polarizing-Current and Impedance-Measuring Panels

At Spy Pond, a special panel was installed which served a dual purpose of introducing polarizing current into a transducer in the water and/or providing means for making impedance measurements on a transducer in the water. The wiring diagram is shown

of such measurements can be inferred from Table 1. A careful analysis of the data from a large number of measurements indicates that fluctuations in the sound field between the source and the receiver constitute the chief source of error in single measurements.⁵⁸ The individual calibrations, which are averaged in Table 1, were made with considerable care, so that

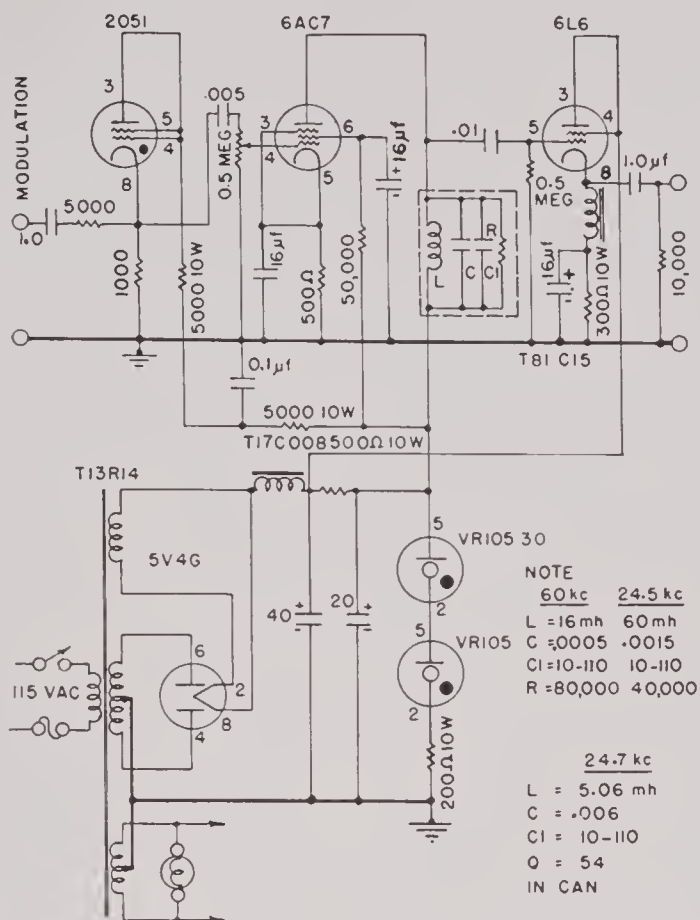


FIGURE 47. Band noise generator, 24.5 kc and 60 kc.

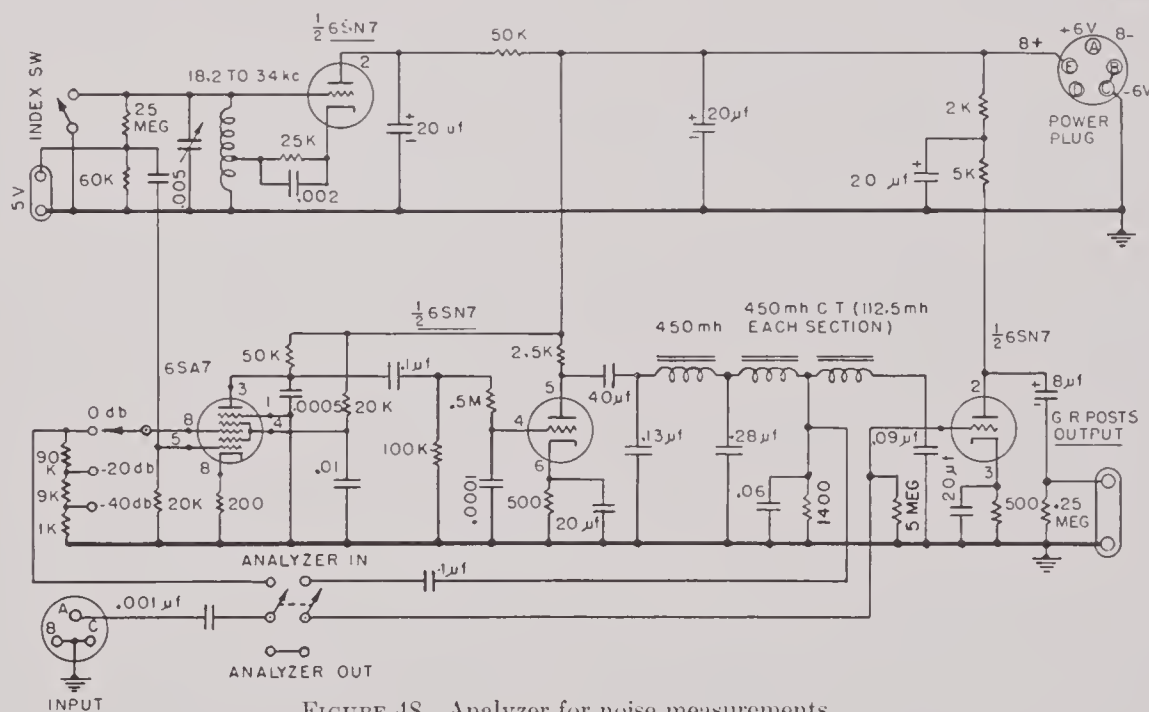


FIGURE 48. Analyzer for noise measurements.

ators were built for this use. The one shown in Figure 46 gave two narrow band outputs, from 15 to 30 and 55 to 75 kc, and a third wide band from 15 to 75 kc.

The generator shown in Figure 47 was designed to give two bands centering at 24.5 kc and at 60 kc, frequencies on which interest was particularly centered.

10.10.1 Analyzer for Noise Measurements

Most tests involving noise measurements were made with the analyzer, the circuit for which is shown in Figure 48. Any noise or pure-tone signal voltage appearing across the input terminals is heterodyned with a pure-tone signal from a local oscillator, the difference voltage from the mixer tube being amplified and passed through a low-pass filter to the output. The pass band of the analyzer simulated that in the receiving circuit of the transducer under study and thus provided a means of measuring hydrophone response to noise under the same conditions as those under which the hydrophone would be operated in practice. Since the pass band of the analyzer (1,960 cycles) was known, the results of measurements through the analyzer could be evaluated in terms

10.10.3

Noise Generators

Certain types of measurements at Spy Pond called for knowledge of the response of transducers to noise lying within a specified frequency band. Two gener-

of "spectral sensitivity," that is, the sensitivity to continuous spectrum noise, referred to a band width of one cycle and to a pressure of 0.0002 dyne per sq cm.

Several changes in the analyzer increased its use-

was part of an oscillator that contained enough feedback to keep it from oscillating. The purpose of the tube ($\frac{1}{2}$ 6SN7) was to improve the Q of the tuned circuit by introducing a negative resistance into it. This high Q circuit oscillated only at harmonics of the pulsing frequency when sufficient feedback was present to keep it from oscillating by itself. Its output was fed to a cathode follower to isolate the circuit and give a low impedance output for the device. The tuned circuit consisted of a three-section variable condenser, 150 μmf per section, with the sections in parallel and a Bell Telephone Laboratories toroidal coil with molybdenum-Permalloy core, having an inductance of 450 mh and a Q of approximately 80. This combination gave outputs from 7 to 14 ke with only the harmonics of 1,000 cycles appearing. The unit delivered $7\frac{1}{2}$ volts at 1 ke and from 7 to 3 volts from the harmonic generator, depending on the setting of the feedback potentiometer.

The unit was calibrated against Harvard's Cruft Laboratory 1,000-cycle standard throughout several eight-hour continuous running periods. The frequency did not vary perceptibly. The fork was 0.1 cycle below the Cruft Laboratory standard at 1,000 cycles.

10.10.6 Portable Polar Chart Recorder

Some use has been made of a *direction pattern tracer* (*portable polar chart recorder* [PPC'R]) designed in the laboratory.^{31, 73} This device plots directional patterns on polar-coordinate paper. A gear mounted on the shaft rotating the transducer drives a CT synchro-motor which in turn controls a second CT synchro-motor within the recorder. The recorder motor controls a servomotor that drives the recorder turntable in synchronism with the rotating shaft. The electronic part of the recorder consists of a cathode-follower input followed by a low-impedance logarithmic attenuator, the output of which feeds into an amplifier, followed by a rectifier and differencing circuit to obtain a d-c output. The d-c output is modulated with 60 cycles and the result is amplified and fed to a 60-cycle motor that drives the recorder pen.

10.10.7 Four-Channel Amplifier

Some of the measurement work at Spy Pond called for the comparison of four hydrophones mounted in a single cylindrical body. To insure identical conditions for both the acoustic signal applied to each of

the transducers and the electric output to the measuring amplifier, it was desirable to make the measurement on each hydrophone in turn without the time-consuming job of removing the body from the water and opening it. A further desideratum was to make the measurements at the output panel of the pre-amplifier, located within the submerged body, and thus eliminated the effect of the twenty feet of cable needed for connection to the regular receiving amplifier. The conditions of measurement thus became identical with those that would prevail in the actual operation of the transducers. Figure 50 shows the amplifier with the four preamplifier circuits designed and built for this purpose. The power supply was contained in a separate chassis mounted in the relay racks. The final amplifier with switching control for the channels was also built in a separate chassis mounted in the racks. The four-channel preamplifier was contained in a boxlike chassis placed inside the cylindrical body in which the hydrophones were mounted. Connection from the preamplifier to the main amplifier was through three braided six-wire shielded cables about 20 ft long which passed through water seals in the back plate of the cylinder. With this combination it was possible to calibrate four separate hydrophones without taking off the back-plate to change from one hydrophone to another. A switch on the amplifier panel controlled three relays in the preamplifier so that any one of the four hydrophones and preamplifier tubes could be switched into the d-c cathode-follower output channel of the pre-amplifier.

10.10.8 Special Apparatus for Measurements on Multielement Transducers

In addition to the apparatus already described as standard equipment of the field stations, a portable impedance bridge (see Chapter 9) was required. The measurement of the phase relations of the responses of the different transducer elements to the incident sound called for a specially designed phasemeter, which consisted essentially of twin channels, each of which comprised the following elements. (1) A phase inverter, with a two-position switch, allowed the transmission of the signal with phase inverted or uninverted as desired. (2) A series of amplifying tubes terminated in a twin diode clipped both halves of the incoming sine waves. These diodes were biased so that they clipped when the amplitude of the amplified

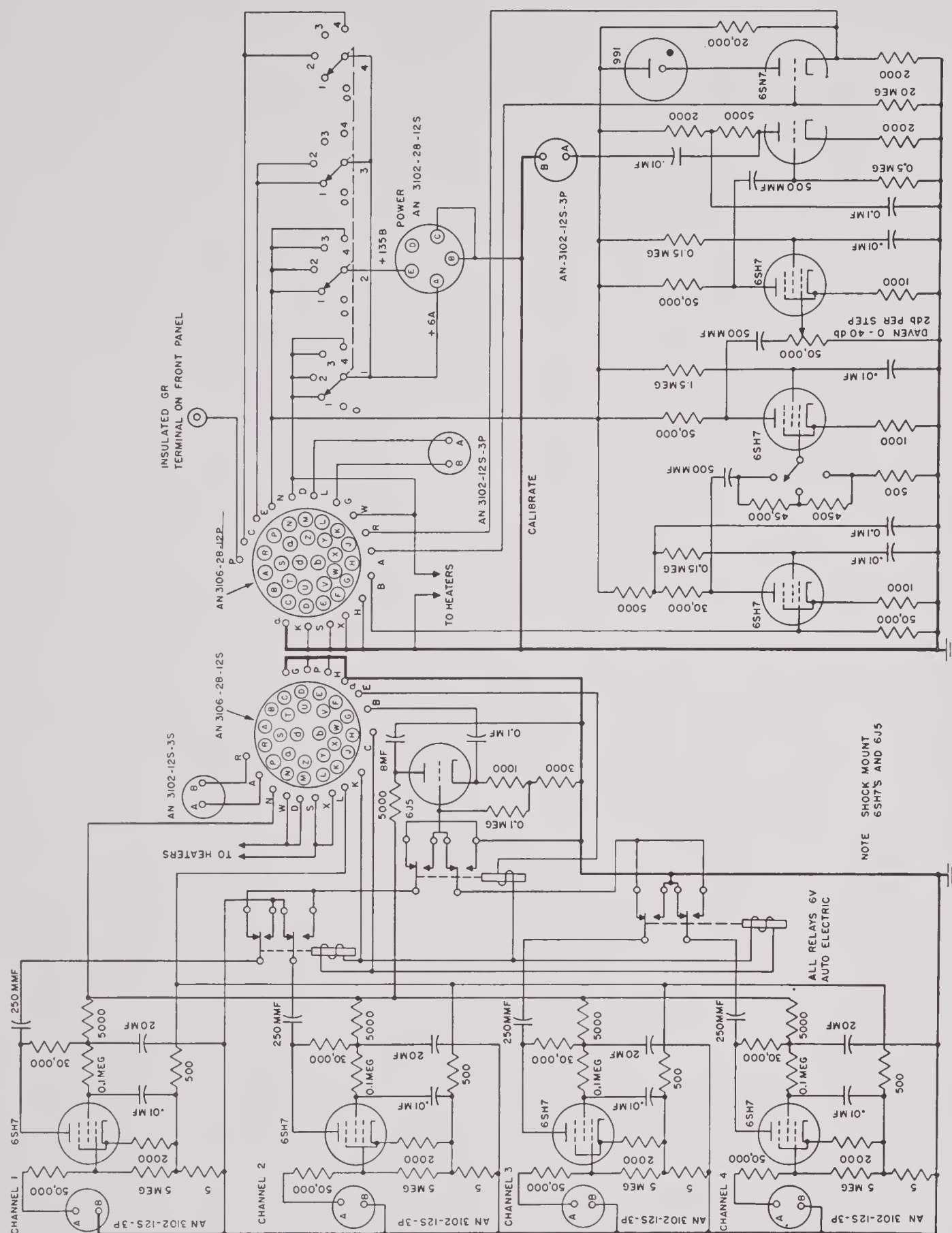


FIGURE 50. Four-channel amplifier used at Spy Pond.

CONFIDENTIAL

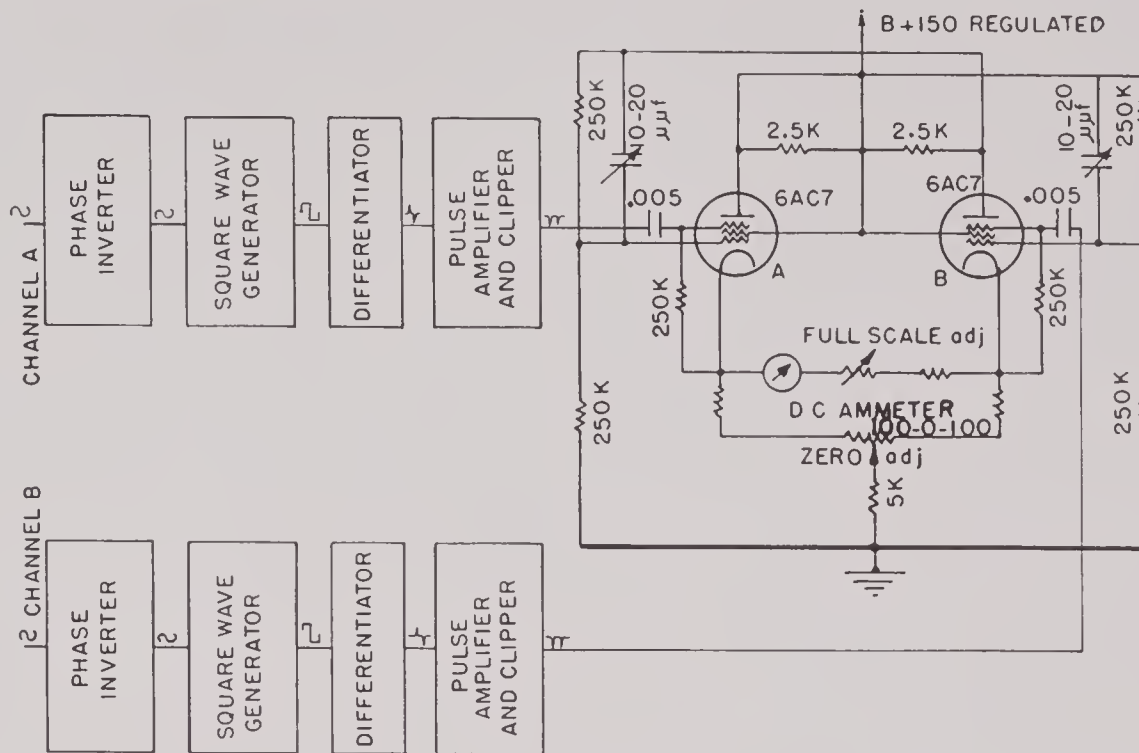


FIGURE 51. Block diagram of phase meter.

signal exceeded 1.5 volts. Amplifying and clipping were repeated until the wave form was approximately "square." (3) A differentiator using a conventional RC circuit gave a series of pulses, one at each crossing of the voltage axis by the original sine wave. These pulses were passed through a two-stage pulse amplifier, the last stage of which clipped off the positive pulse, leaving the negative pulse to excite the suppressor grid of the tube in the trigger circuit. Shown

in Figure 51 is a block diagram of the circuit just described, together with a wiring diagram of the trigger circuit, by which phase differences in the signals received at the inputs of the two channels were indicated on a zero-center d-c meter.

As designed, the phasemeter required between 0.4 and 1.2 volts input, which for most measurements required amplification of the signals from the transducer elements. A two-channel amplifier designed to give identical phase shifts in the two channels was built for this purpose. The usual arrangement for measuring phase differences between the outputs of individual elements is shown in Figure 52. It will be noted that in this arrangement the phasemeter is used simply as a null indicator. The setting of the standard lag line needed to give a null indication gives the phase difference between the outputs of the two elements.

10.11 SPECIAL TESTS: CALIBRATION OF SOUND GEAR MONITOR

A wide variety of special tests was required from time to time during the life of the field stations. Generally these could be carried on with improvised gear supplementing the standard equipment already described. One of the more important routine jobs was the calibration of the *sound gear monitor* [SGM].

A large number of preproduction units of this de-

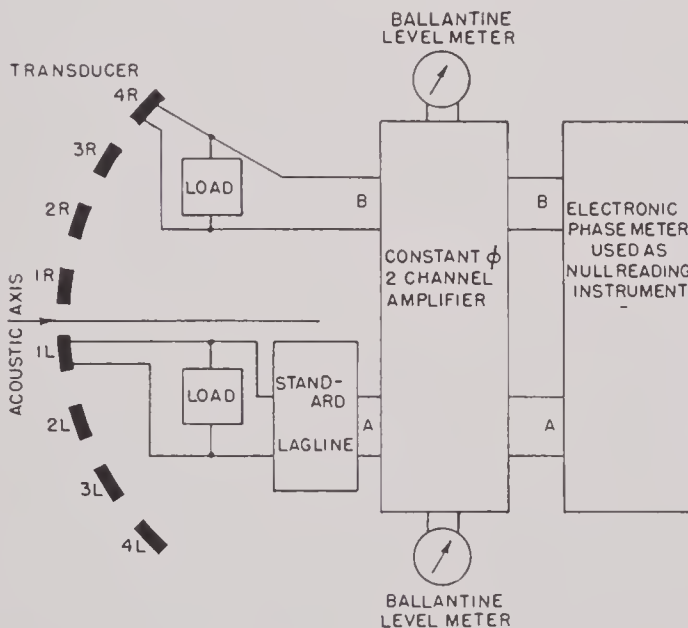


FIGURE 52. Block diagram illustrating phase-difference measurements.

DATA SHEET FOR S.G.M ASSEMBLY MEASUREMENTS

DEPTH.....9'
 DISTANCE.....5'
 MEAS. HYDROPHONE B19B #18
 SOURCE 4x4 VOLTAGE 10v AT 10kc

DATE 10/14/43
 OBSERVERS Mueser Ebaugh
 CHASSIS 5C #5
 HYDROPHONE B19B #27

FIELD MEASUREMENTS

FREQUENCY	17	18	19	20	21	22	23	24	25	26
I. Response of standard (Att = 30 ± 30 db)	-16	-15.2	-16.8	-15	-15.2	-12.7	-12.9	-10.4	-11.1	-9.7
Calibration (-60 db vs. 1 volt)	-9.7	-9.8	-9.9	-10.0	-10.2	-10.3	-10.2	-10.0	-9.8	-9.8
* Voltage response										
* Sens. of Standard										
* Field db vs. 1 bar	46.2	47	46	48	48	50	49.3	51.5	50.5	52
S.G.M. Receiving 60' cable	40	40	40	40	40	40	40	40	40	40
a. "Read direct"	-9	-6.9	-7.4	-6.7	-5.8	-5.0	-3.2	-2.9	-1.6	-5
b "Subtract 30"	67 -3.2	67 -1.7	67 -3.0	67 -1.8	67 -1	67 -0.3	67 +1.0	70 -1.2	70 -0.2	70 -3.7
c. Same as (b) with 75' extension	67 -3.6			67 -2.0			67 +1.0			70 -4.0

S.G.M. Sending. Measuring hydrophone receiving. Attenuation same as in measuring field.

Response full volume (Attenuation.....db)	-21	-20.5	-22.5	-22.5	-21	-21	-18	-17.5	-18	-17.5
Response 10 db in	-32	-31	-33.5	-32.5	-32.2	-30.5	-28.5	-26.5	-27	-27

* May be computed later

FIGURE 53. Data sheet for SGM calibration.

vice were built at HUSL. In addition, the laboratory was called upon for production tests of selected units supplied by outside manufacturers. An outline of the procedure followed in the calibration of these instruments is given here.

A B-19B hydrophone is used (1) to set up a sound field of known intensity at a specified distance in the water and (2) to receive the acoustic signal from sound gear under test.⁷⁴

The SGM comprises a transmitting oscillator to

cover the frequency range from 17 to 26 kc and a receiving amplifier with an attenuator meter and a meter graduated in decibels to indicate the pressure level of the received signal. These are carried in a metal box with externally mounted frequency dial and attenuator knobs. One of the two attenuators in the receiving circuit is a 30-db pad. The other is a 40-db potentiometer, variable in steps of 2 db.

The calibration of the SGM consisted of two steps: a calibration of its receiving system so that it could

CONFIDENTIAL

be used as a direct reading instrument for the measurement of sound-pressure level, and a measurement of the sound-pressure level developed by the transmitting section of the unit at a given distance from the B-19B hydrophone. The procedure followed is indicated in outline form in the headings on the data sheet shown in Figure 53.

For the check on receiving characteristics, a pure tone field was set up and measured by a standard hydrophone at a distance of 5 ft. The Ballantine VTVM (decibel scale) was used as the measuring instrument. The field was measured at 1,000-cycle intervals over the 17- to 26-ke range. The standard was then replaced by the B-19B hydrophone of the sound gear monitor. No special precautions were taken to orient this B-19B, since its horizontal pattern is flat in the frequency range used. The settings of the 40-db attenuator on the monitor with the 30-db pad out and the meter reading at each frequency were recorded. As a check on the 30-db pad, the readings were repeated with this attenuator inserted. A check on the 75-ft extension cable used with the transducer was made by connecting the cable and repeating the last set of measurements at four frequencies.

For the check on transmitting behavior, the SGM control switch was changed over to the "send" position in which the standard hydrophone is used as the receiver. It was aligned acoustically and set at exactly 5 ft from the monitor transducer. The output of the standard was fed into the same receiving channel used in measuring the field, with the same attenuation in the measuring amplifier to avoid the necessity of repeating the voltage calibration. As a check on the 10-db pad, the same set of readings was repeated with this attenuation added.

The pressure level corresponding to the lowest attenuator setting and to the zero meter reading could be computed for each frequency from the attenuator setting and meter reading when receiving and from the measured values of the field. These computed values constituted a calibration of the SGM as a sound level meter. Comparison of the response of the standard to the measured field with its response to the field generated by the monitor in the "send" position gave the value of the field set up by the monitor at 5 ft.

10.12 INCIDENTAL STUDIES

During the course of the work directed specifically to the study of transducer characteristics, some sig-

nificant data were obtained on water conditions as they affect acoustic measurements.

10.12.1 Measurement of Velocity of Sound

A fairly precise direct measurement of the velocity of sound in water was made using the phase-measuring apparatus previously described. The phase difference ϕ between the output signals of two similar hydrophones is given in degrees by the equation,

$$\phi = \frac{360r}{\lambda} = \frac{360rf}{c},$$

whence

$$c = 360r \frac{df}{d\phi},$$

where r is the difference in path length of the sound arriving at the two transducers. Thus, with two calibrated B-19B hydrophones mounted on a fixed support and so oriented that one was directly behind the other on the principal axis of the projector, the following measured values were obtained.

Water temperature = 0.5 C

Distance between hydrophones $r = 22.8$ in.

df = frequency difference = 24,000 cycles per sec.

$d\phi = 3464$ degrees

$$c = 360 \times 22.8 \times \frac{24,000}{3,464} = 56,580 \text{ in. per sec.} \\ = 1,444 \text{ meters per sec.}$$

The phase difference was determined by taking the cumulative value of the observed phase changes at 5-ke intervals from 16 to 40 ke.

10.12.2 Fluctuations in the Acoustic Field

Fluctuations in the sound field have already been mentioned as a source of measurement error. Reference is made here only to those random variations, sometimes as great as ± 2 db within a period of a few seconds, that were observed at various times at both the barge and Spy Pond. The magnitude of the fluctuations was seen to increase with increasing distance between projector and receiver and in general to be less with transducers having a large area of radiating surface than with small transducers. The spring and fall seasons were periods when bad days

were most frequent, but in midwinter and in summer smaller changes were common. They were of the order of ± 0.2 db and extended over a period of ten minutes or so.

For a time, the fluctuations were thought to be due to the presence of fish, lured into the sound field by the siren voice of the supersonic projector. This explanation was eliminated by illuminating the space between projector and receiver and noting the fluctuations when no fish were present. Careful checking of the electronic gear ruled out instability there as a possible explanation. Similar fluctuations were observed at the Sweetwater Station of the San Diego Laboratory.^{39, 57}

An unstable state of thermal equilibrium in the water at levels below the level of the projector and receiver has been confirmed as a cause of fluctuations by bathythermograph measurement at Spy Pond on

days of severe field fluctuations. Temperature variations as great as 8 F per foot change of depth have been noted. A partial remedy was the use of pressure-release screens. The screens first used at HUSL were of $\frac{1}{2}$ -in. Celotex encased in thin sheet metal. An improved screen was of solid sheet metal surfaced on both sides with $\frac{1}{4}$ -in. air-cell neoprene. Various arrangements of the screens were tried and found more or less effective, depending on the particular water conditions. The lowering of an inverted V-shaped screen proved effective in some instances. The screen consisted of two sections, each 2 ft by 4 ft, hinged along a long edge, and locked at an angle of 90 degrees. Another arrangement that could be used in certain types of measurements consisted of two flat screens placed one above the other in the sound field and separated from each other to form a horizontal collimating slit.

Chapter 11

HIGH POWER DRIVING OF MAGNETOSTRICTIVE TRANSDUCERS

11.1 INTRODUCTION

11.1.1 Statement and Discussion of Problem

In many applications of magnetostrictive transducers, the level of operation is low enough to make the performance of the transducer closely linear. Such an assumption underlies the greater part of this book. In particular, there are linear equations (17) of Chapter 2, and (10), (11), and (13) of Chapter 3 on which this analysis has heretofore been based. Such analysis of operation has been found to be useful even when the basic linear equations are known to be badly in error. This apparent validity of the linear theory stems from the fact that useful, efficient magnetostrictive transducers are operated at frequencies of mechanical resonance, and, therefore, the mechanical vibration will be largely that of the fundamental, even though the magnetostrictive forces contain appreciable second and higher harmonics. Similarly, the efficiency will remain nearly constant as the level is raised far beyond the point at which equations for the fundamental fail.

When a transducer is operated at a rather high power level in an effort to make use of its full acoustic capabilities, nonlinearity will become very evident and must be taken into account. There are two places where nonlinearities enter. The first is in magnetic behavior. Where previously proportionality was assured between increments in B and in H , with a constant proportionality factor μ , it will now be necessary to utilize the actual magnetization curve for this relation. The second departure from linearity concerns the magnetostrictive constant λ . At high levels the magnetostrictive stress that was previously written $-\lambda B$ is no longer proportional to B . In equation (9) of Chapter 3 this stress is given as $-\epsilon B^2$, which implies that the value of λ measured at low level is proportional to the polarizing induction. As shown in Chapter 4, this is true for nickel although apparently not for 2V-Permendur.

Any analysis taking into account this nonlinearity

is necessarily much more complex and involved than the linear theory. For example, since the magnetization curve is not approximated by any simple analytical function, most calculations must be developed graphically or numerically. In the nonlinear case, it is necessary to specialize to a definite magnetic cycle and magnetization curve, so that the results that can be obtained without very elaborate calculations are limited. Hence the experimental approach, using a certain amount of theoretical analysis as a guide, appears the best method of attacking the problem. The most important overall quantities to determine are the acoustic power output at the desired frequency and the electric power input. The idea of impedance loses much of its meaning when the transducer is operated at high power, since voltage and current are no longer proportional and do not have the same wave form. However, the ratio of the fundamental components of voltage and current may still be determined under specified conditions of operation. Such information may be used to determine the proper matching network for the efficient transfer of electric power to the transducer and to analyze the various loss components at the fundamental frequency.

The problem of dynamic magnetostriction is analogous to many other physical problems in which analytical theory has been usefully worked out only for small variations of the parameters. As these variations become large, the nonlinearities so complicate the analysis as to render quantitative development useless. In several such cases graphical presentation of experimental data has served to point the way toward the best operation of the device in regions where the nonlinearities make analysis impractical. The so-called contour charts of Chaffee¹⁴ have been useful in specifying optimum parameters for operation of triode power oscillators and amplifiers. H. Chang and E. L. Chaffee¹⁶ extended the method to the steady-state operation of a magnetron oscillating in its negative resistance mode. It is believed that conditions for optimum power conversion by magnetostrictive devices operating in the nonlinear region

may best be presented through similar graphical means. At present, low-level operation may be adequately predicted from vector or motional impedance loci. No extension of this method to prediction of operation at high levels is known to have been proposed. An exploratory investigation of the change with power level in the low-level vector impedance loci has been carried out. It will be presented even though it differs widely in character from other successful graphical analyses of nonlinear data.

The work reported in this chapter was initially directed to the determination of the power-handling capacity of a particular transducer, on which no data were available. Experiment revealed the wide variation in the characteristics of a magnetostrictive transducer with variation in the driving level. The initial attack led only to results applicable to the transducer under investigation. As the work progressed, the desirability of a more fundamental approach appeared. The following questions became important. What, for example, is the upper limit of the electric power that can be converted into acoustic power per unit weight or volume? What are the merits of magnetostrictive as compared with electrostrictive materials in this respect? What is the efficiency of conversion of electric to acoustic power as a function of the level at which the conversion takes place? The answers to these questions are obviously very useful when the size and weight of the transducer and the power available enter into the design problem.

The program of research was carried on with this broader purpose in mind. Definite and final answers have not been found to any of the foregoing questions. The data presented, it is hoped, will be valuable as the basis for a more conclusive investigation of a problem involving a considerable number of variables with complex interrelations.

11.2

CAVITATION

Cavitation is a phenomenon which imposes a unique upper limit to the acoustic intensity that can be established in a liquid medium. Although cavitation is not specifically related to the properties of the transducer, it is an important factor in determining the performance limits of high-powered transducers for sound generation in liquids. No systematic investigations of cavitation were carried out at the Harvard Underwater Sound Laboratory [HUSL].

Some work on the general problem was done at the San Diego Laboratory, but most of the information on this subject is based on a continuing investigation carried out by Bell Telephone Laboratories under a Navy development contract.

Definitive results on the occurrence of cavitation are difficult to obtain, since obscure small-scale phenomena seem capable of exerting considerable influence on the onset of cavitation. Tentative results based on the Bell Telephone Laboratories' work may be summarized as follows.

In general, steady-state cavitation occurs in sea water or light liquids containing dissolved air or gas when the negative phase of the sound-pressure wave reaches 1 atm. Increased hydrostatic pressure throughout the liquid produces a corresponding increase in the sound pressure at which cavitation first occurs. Removal of dissolved gases increases the sound pressure required to produce cavitation, indicating that different liquids display in varying degrees an ability to support tension under dynamic conditions. Heavy viscous liquids will usually support higher sound intensities without cavitation than light liquids, and degassed "bd" (bone-dry) castor oil permits higher steady-state sound intensity than other liquids so far investigated.

Experiments indicate that sound pressures higher than steady-state values may be established without cavitation for short-duration pulses, and that the allowable power level increases as the pulse duration decreases. Numerical values characterizing this phenomenon are influenced by experimental details involving degassing of the liquid, adsorption of gas on the transducer face, temperature, geometrical details of the transducer, and probably by other variables. The data presented in Figures 1A and B (from BTL) show spot values obtained with certain small transducer models. The validity of these tentative data in prediction of the performance of full-scale transducers under pulsing conditions has not been experimentally verified and the information should therefore be used with caution.

It appears safe to conclude, however, that short-pulse techniques offer the possibility of radiating much higher specific acoustic power into water or other liquids than had hitherto been thought possible. A considerable effort would seem to be justified in determining the influence of these considerations on the design of transducers for high-level operation and in further investigation of the basic physical factors that control the onset of cavitation.

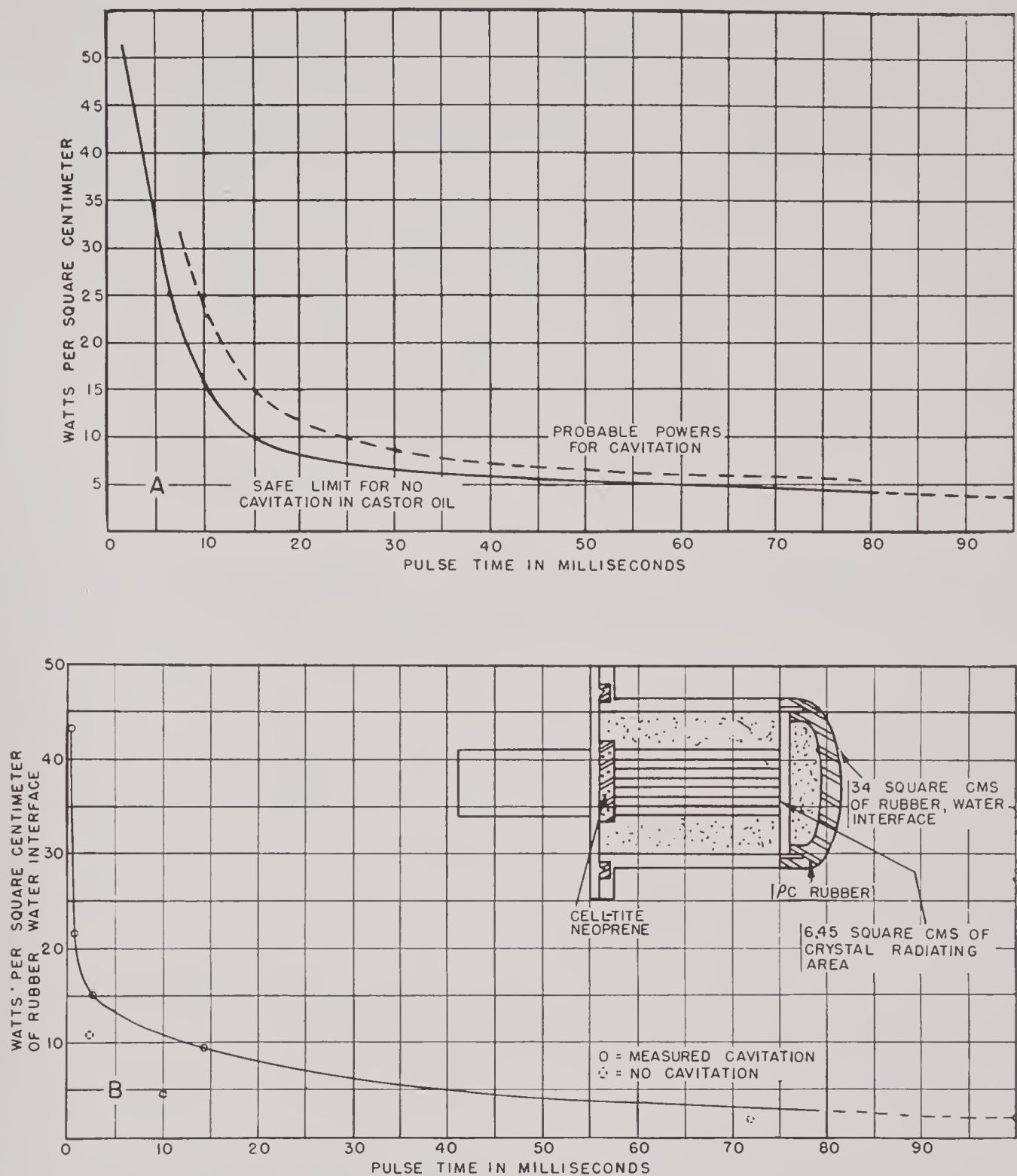


FIGURE 1. Power-producing cavitation vs pulse length (Bell Telephone Laboratories).

11.3 PREVIOUS WORK

A cursory search of the literature disclosed that very little work dealing with power or high-level operation of magnetostrictive devices has been done. In the early work of G. W. Pierce¹⁰ and K. C. Black,⁹ nearly all observations were carried out at very low

levels of alternating excitation and limited values of polarizing field. K. C. Black⁹ states, "... for nickel the [electrical] reaction increases to the highest [polarizing] field used in this experiment." Later work carried out in England and in the United States indicates definitely that for low-level operation an optimum value of magnetic polarization exists. On

the other hand, F. D. Smith¹² states, "In general, the larger the alternating field, the larger the polarizing field must be to obtain best working conditions." Here he has assumed best working conditions to mean greatest efficiency. He also presents evidence indicating that a large cross section of nickel of low energy density is also essential to high efficiency of operation. Certain modern transducer applications in which size and weight are important, coupled with the advantages of short-pulse operation, indicate that design for maximum acoustic output may be at least equal in importance to design for maximum efficiency.

Smith has also emphasized the complexity of the problem of high-level operation. He has given data for annealed nickel in the form of graphs giving eddy-current and hysteresis losses per unit volume as a function of polarizing field for constant a-c amplitude and as a function of a-c amplitude for constant polarizing field. In addition, an overall core-loss factor is presented as a function of the so-called eddy-current parameter

$$Z = \pi t \sqrt{\frac{2\mu_r f}{\rho}}$$

for constant a-c amplitude for various values of the polarizing field. Here t is lamination thickness, μ_r the reversible permeability, f frequency, and ρ resistivity. This approach and presentation of data is particularly adapted for delineating transducer design procedures but masks the practical problem of correct matching and tuning. Presenting the data in terms of the equivalent resistance and reactance of the device masks actual losses but assists the designer of the electric power source that supplies the transducer. Both methods of giving the experimental results are useful. The second method will be used here, since time necessitates presentation of data rather than of quantities derived from it.

Salisbury and Porter¹⁵ have described a magnetostrictive oscillator with a d-c power supply of 2 kw. With the various arrangements of oscillator coils which they described, a frequency range from 7,000 to 50,000 cycles per second could be covered. From the dimensions of their half-wave nickel tube and the construction of the apparatus, the potential power density in the active magnetostrictive material at the highest frequency was 180 watts per cubic centimeter if the full 2,000 watts were used. It is doubtful, however, if full power was utilized at the highest frequency. At the lowest frequency the maximum

potential power density was only 51 watts per cu cm. The transformation of electric energy into mechanical energy by the magnetostrictive process is only a little less efficient for a tube-type oscillator than for a toroid. It is therefore possible that Salisbury and Porter may have approached input power densities sufficient to give the idealized maximum acoustic output. (See Section 11.4). In view of the use of non-laminated nickel and the evident difficulties encountered in cooling, it is probable that the overall efficiency of the equipment was low and that the nickel was not used efficiently. No data were given concerning impedance measurements, efficiency, or estimates of the various power losses.

11.4 IDEALIZED POWER LIMITATIONS OF MAGNETOSTRICTIVE MATERIAL: FREQUENCY DOUBLING

In the operation of a magnetostrictive transducer at high power, it is important to have an estimate of the maximum acoustic power that the transducer can deliver. As has already been pointed out, it appears that, in the proper circumstances, it will be quite possible to utilize such high powers that the magnetostrictive material is the limiting factor. Under these conditions there will be an optimum wave form for the voltage or current in order that the limiting acoustic power be as large as possible.

The starting point here will be equations (9) in Chapter 3, viz.:

$$\begin{aligned} P &= -\epsilon B^2 + Es \\ H_e &= H - 8\pi\epsilon Bs, \end{aligned} \quad (1)$$

where P and s are respectively the longitudinal static stress and strain in the magnetostrictive material, B and H are the total induction and field, and H_e is the field applied by an external winding. The magnetostrictive coefficient ϵ is one-half the slope of the usual λ plotted against the polarizing induction B_0 (see equation (12) of Chapter 3). Now the mechanical portion of the system is linear. Thus, in order to deliver large power to the mechanical system without generation of harmonics, the magnetostrictive stress $-\epsilon B^2$ should vary sinusoidally with the time at a frequency near resonance. Let

$$\begin{aligned} B^2 &= \frac{1}{2}[(B^2)_{\max} + (B^2)_{\min}] \\ &\quad + \frac{1}{2}[(B^2)_{\max} - (B^2)_{\min}] \cos \omega t \\ &= (B^2)_{\min} + [(B^2)_{\max} - (B^2)_{\min}] \cos^2 \frac{\omega t}{2}, \end{aligned} \quad (2)$$

where $(B^2)_{\max}$ and $(B^2)_{\min}$ are the maximum and minimum values of B^2 and ω is the angular frequency at which the motion is to take place. In order that the coefficient $(B^2)_{\max} - (B^2)_{\min}$ be as large as possible, $(B^2)_{\max}$ should be increased to saturation, while $(B^2)_{\min}$ goes to zero. Then

$$B^2 = (B^2)_{\max} \cos^2 \frac{\omega t}{2}. \quad (3)$$

The simplest variation of the induction will be

$$B = B_{\max} \cos \frac{\omega t}{2}. \quad (4)$$

Thus, under the condition that no harmonics are to be impressed on the mechanical system, maximum power will be delivered at the fundamental when B varies at half frequency with average value zero and with amplitude limited by saturation.

The voltage across the transducer is closely related to equation (4), since if leakage inductance and copper resistance are neglected,

$$E = N \sigma \dot{B} = \frac{1}{2} N \sigma \omega B_{\max} \sin \frac{\omega t}{2}, \quad (5)$$

where N is the number of turns around the core, σ is the cross section and \dot{B} is the time derivative of the magnetic induction.

Consider a ring stack with radius a (cm), radial thickness b (cm), length l (cm). The angular frequency ω at resonance is $\sqrt{E/\rho a^2}$ where E is the Young's modulus and ρ the density of the core material. In accordance with the discussion above, the time-varying portion of the magnetostrictive stress is

$$P = -\frac{E}{Z} B_{\max}^2 \cos \omega t. \quad (6)$$

Since the system is at resonance, its mechanical impedance is a pure resistance and the time derivative of the strain s is in phase with the stress. It is found that

$$\dot{s} = \frac{QP a}{\sqrt{\rho E}} = \frac{QP \omega}{E}, \quad (7)$$

where Q is the ratio of the mass and/or stiffness reactance of the ring at resonance to the mechanical resistance. From equations (6) and (7), the mechanical power in watts per cubic centimeter of core is

$$\text{Power} = \overline{P \dot{s}} 10^{-7} = \frac{\overline{Q P^2 \omega} 10^{-7}}{E} = \frac{\epsilon^2 B_{\max}^4}{8E} \quad (\text{watts/cc}). \quad (8)$$

The following numerical values for nickel are assumed: $E = 2.1 \times 10^{12}$ dynes per sq cm. $\epsilon = -2.2$ dynes per sq cm per sq gauss, $B_{\max} = 6,000$ gauss. Then, from equation (8),

$$\text{Max power} \simeq \frac{Qf}{5} \text{ watts/cc}, \quad (9)$$

where f is the frequency in kilocycles per second. This is the theoretical maximum mechanical power, limited by magnetic saturation, that can be generated per cubic centimeter of nickel in the form of a

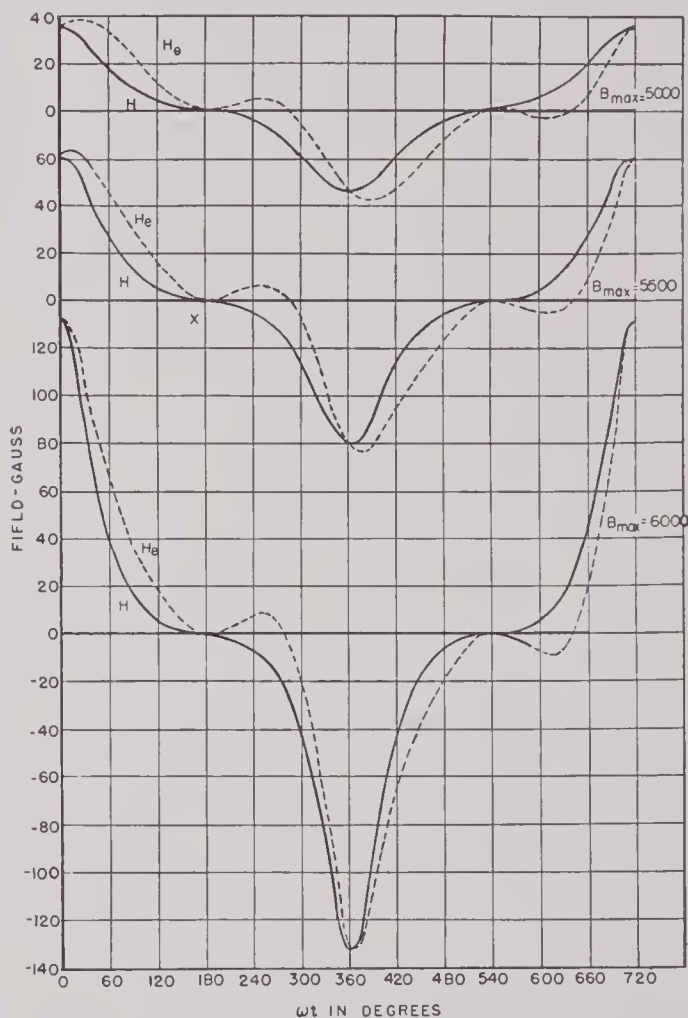


FIGURE 2. Calculated wave form of H and H_e for nickel ring stack with $Q = 5$.

ring. To obtain the useful radiated power, equation (9) must be multiplied by a "mechanical efficiency" that takes account of mechanical losses internal to the transducer. It is to be noticed that equations (8) and (9) are proportional to the fourth power of the maximum induction. Thus, for example, if the value assumed is reduced from 6,000 to 5,000 gauss, the maximum power is approximately halved.

Equation (9) was derived for a ring stack. Similar

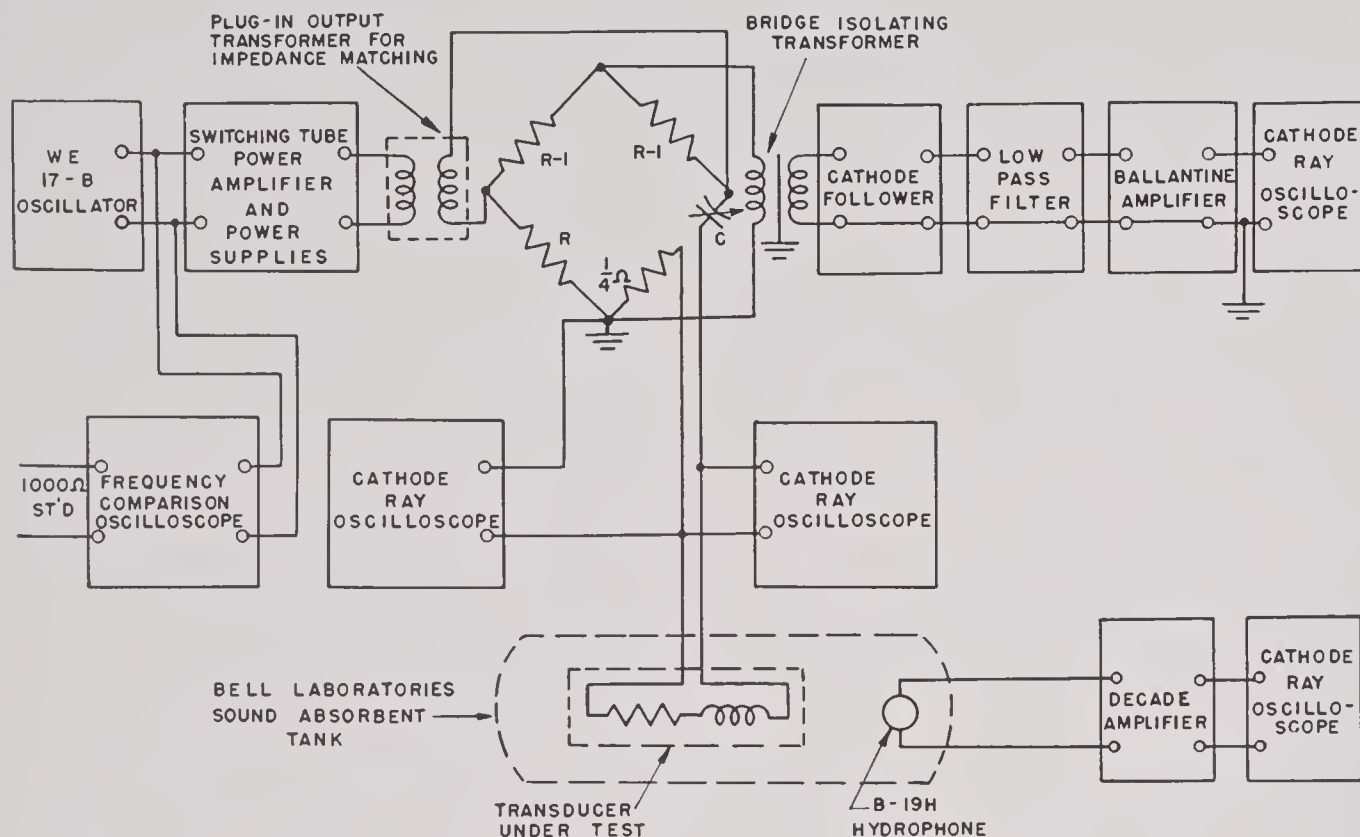


FIGURE 3. Schematic diagram of experimental setup. (Note: Ground point of bridge should be lettered *B*; opposite junction, *A*.)

formulas giving lower maximum power hold for other forms. Thus equation (8) holds for a half-wave rod if an additional factor $8/\pi^2$ is inserted on the right. In general, the multiplying factor is the ratio of the squared average stress throughout the core to the average squared stress.

The wave form of the voltage has already been given by equation (5). Being sinusoidal, it can be attained by operating the transducer from a generator with low impedance and good wave form. The wave form of the current that is proportional to H_e will then depart appreciably from sinusoidal. Calculated wave forms for H and H_e for a nickel ring stack, the Q of which is 5, are shown in Figure 2 for $B_{\max} = 5,000, 5,500, \text{ and } 6,000$.

The presence of harmonics in the current wave form suggests the possibility of applying a small percentage of harmonics to the exciting voltage. In the case of the triode vacuum-tube oscillator operating at high levels, it has been shown¹⁷ that the introduction of a small per cent of harmonic voltage in the system properly phased with respect to the fundamental increases the efficiency of the oscillator. Possibly a similar result would apply to a magnetostrictive device.

11.5 EXPERIMENTAL STUDY AND DESCRIPTION OF RESULTS

11.5.1 Method and Equipment

It would be desirable to approach the problem of high-level operation experimentally from the point of view of steady-state measurements, so that conventional methods might be used. However, if the object is to ascertain a useful upper limit of electric power to be delivered to the magnetostrictive material, heat is certain to be a limiting factor. As already pointed out, the theoretical upper limit of acoustic output power per unit volume of active magnetostrictive material leads, even on the basis of the most optimistic efficiencies, to values of electric input powers far greater than can be dissipated without elaborate cooling means. Hence some form of intermittent operation must be used. This leads to difficulties in determining the electric input powers. Under the circumstances, the use of a pulsed-power bridge seemed most feasible. This permits of direct measurement of effective resistance and reactance. With measurement of the voltage across the transducer, electric input powers can be determined from the resistive component. Effective values of the

permeability may be computed from the reactive component.

Figure 3 shows schematically the experimental arrangement which was used. Pulses of approximately 10-milliseconds duration were applied roughly twice a second to the suppressor grid of a switching tube on the control grid of which a steady voltage of the desired ultrasonic frequency was continuously impressed by the Western Electric 17B oscillator. Thus trains of several hundred cycles length were periodically impressed through an efficient impedance-matching transformer across the terminals of a resonance bridge. Balance was attained by proper adjustment of R and C , using a cathode-ray oscilloscope with synchronized sweep as the bridge detector. A step attenuator controlled the input of the power amplifier so that a wide range of voltage could be applied to the bridge. Measurements of effective resistance and reactance as a function of the alternating excitation level could then be made. This pulsed-bridge technique allowed investigation of fairly high levels of transducer excitation using ordinary standard measuring equipment without overheating any of the components.

During the course of the measurements, one disadvantage of the resonance bridge method was encountered. If the reactance of the transducer becomes capacitive during a run, either an appropriate capacitor must be added on the other side of the bridge, or a variable inductor must be introduced in series with the transducer under test. Either of these solutions is undesirable. In the first case the transducer will be untuned and the resultant power factor may reduce the level below that desired though, if a generous supply is being used, this may not be a serious handicap. In the second case the inductor introduces a troublesome resistance correction factor and the necessary means of blocking the d-c polarizing current from parallel paths is lost. In many cases, however, the resonance bridge is adequate and little inconvenience is experienced.

In order to correlate observed measurements with theory, a number of precautions must be observed. Ideally the wave form of the voltage across the transducer must be sinusoidal and uninfluenced by the source. A zero-resistance generator would be ideal. To achieve this effectively is difficult. Strictly, all bridge measurements would be ruled out under such conditions, since one arm of the bridge in series with the unknown would always vitiate these ideal assumptions. Factors influencing wave form can,

however, be minimized. An obvious precaution is to reduce the internal impedance of the source to as low a value as possible. This is done most simply by employing voltage feedback in a conventional manner. The amplifier employed in this work was originally designed for steady-state continuous measurements and voltage was fed back from a special winding on the output transformer to the cathodes of the exciting stage. A complete diagram of this unit, including power supplies, is shown in Figures 4, 5, and 6. The power supplies consist of four units.

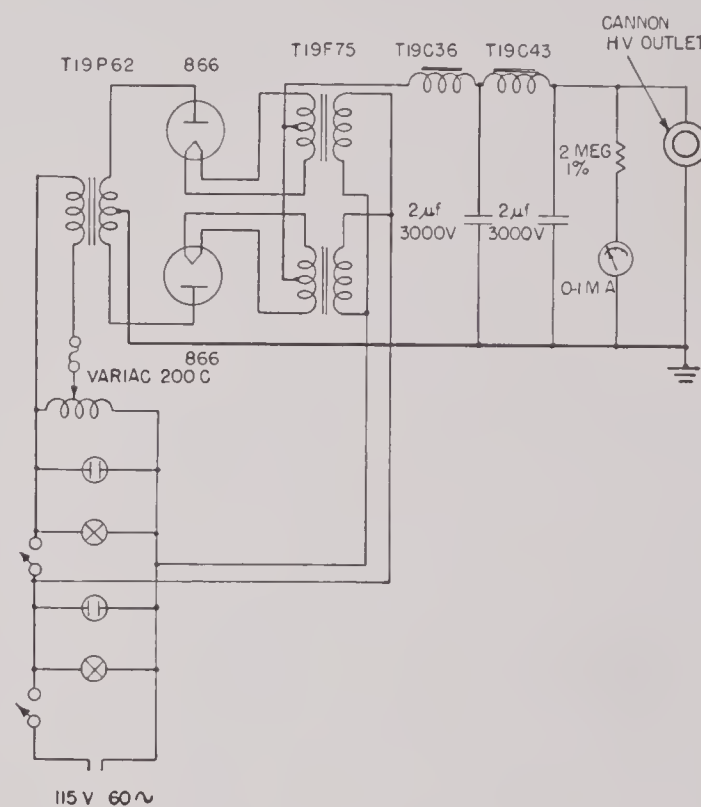


FIGURE 4. High-voltage supply.

A 2,000-volt unregulated unit (Figure 4) was provided for the plate supply of the final power amplifier pentode stage (Type 828 tubes). A stabilized screen supply (Figure 5) was provided for the 828 tubes. This unit, taking part of the control grid voltage for its amplifier stage from the input side of the series regulator tube, could be adjusted to have perfect voltage stabilization and essentially zero internal resistance for a given load. A bias supply and another stabilized supply for general utility purposes completed the four units. This arrangement provided flexibility of control for the experimental work that was carried out. Stabilization of the screen voltage assisted materially in maintaining constant amplitude wave train in any one pulse. The internal re-

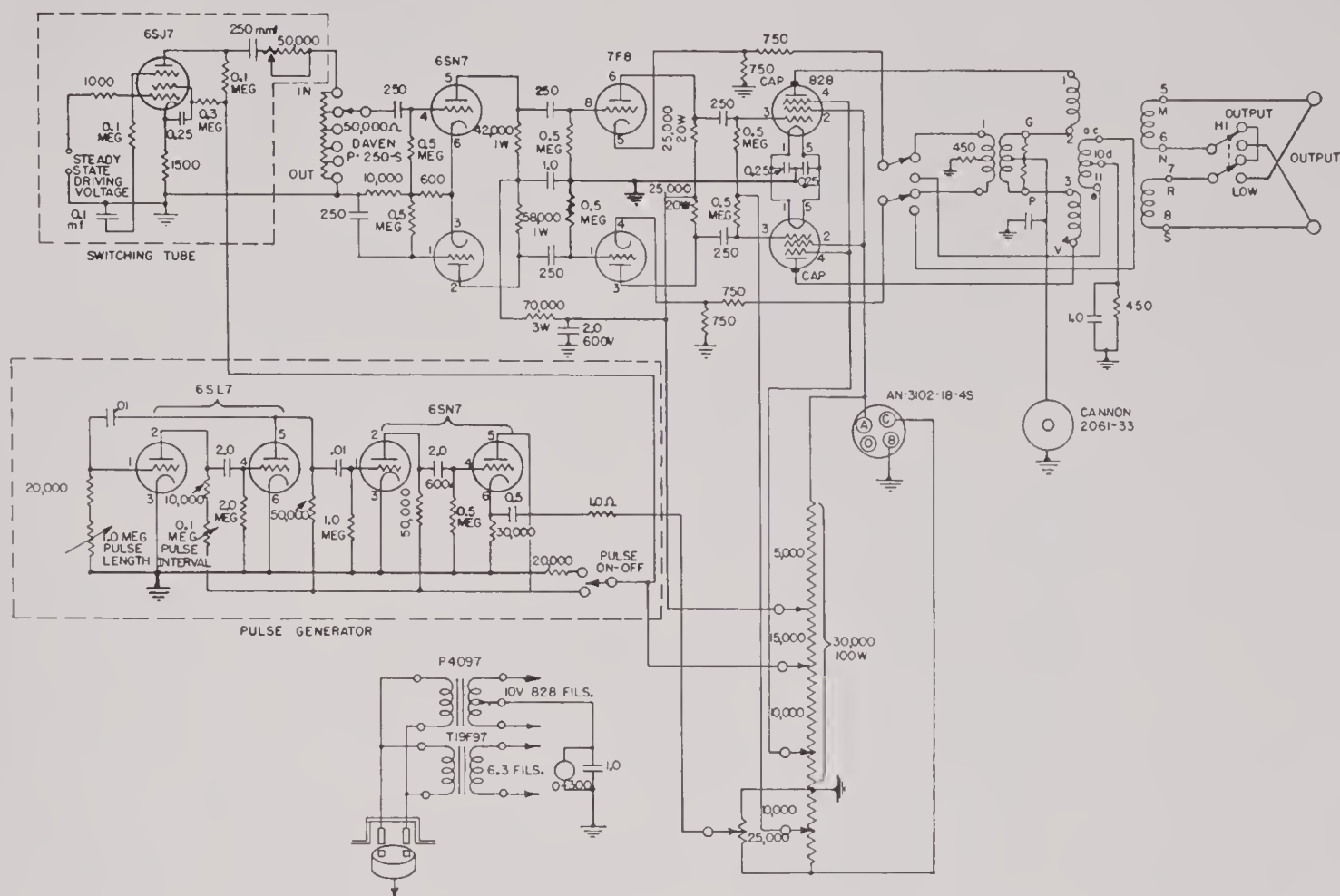


FIGURE 6. Power amplifier.

sistance of the power amplifier was found by varying the value of a resistive load and plotting the resistance R against the reciprocal of the load current. A typical example of the data resulting is shown in Figure 7. The intercept on the negative R axis gives the internal resistance. It can be seen that the internal resistance is approximately one-third the value of the design output resistance. This value might be reduced by proper adjustment of the voltage feedback. In future equipment, means should be provided for altering the feedback and thus determining the effect of this internal resistance in any particular case. Purity of wave form requires operation of the power amplifier well below its overload point. It is desirable to have excess power available.

The amount of power needed for an investigation of this sort can be estimated roughly from the theoretical upper limit of acoustic output. This is of the order of $Qf/5$ watts per cubic centimeter of actively working nickel for a toroid, as discussed earlier in the chapter, where f is in kilocycles and Q is the so-called Q in water. If a reasonable overall efficiency of 30 per cent is assumed, and if f may be

supposed to vary between 10 and 90 kc while Q lies between 1 and 10, then reasonable upper limits of electric input power per cubic centimeter of actively working nickel would range between 6.6 and 600 watts. The possible magnitude of the cooling problem if steady-state measurements were attempted is evident. Table 1 lists the active volume of nickel in several practical transducers and the upper limit of power which it would be desirable to have available (even with no margin for conservative operation) if high-level studies are to be made within the assumptions mentioned above.

The resistive components of the bridge must be able to dissipate the average power put into the transducer. For the pulse length and repetition frequency quoted, the average power is $1/50$ of the pulse power. More difficulty will probably be encountered at lower levels with the decade resistance than with the decade condenser. In the equipment under description a standard General Radio compensated decade resistor Type 670-F was used. The manufacturer states that $1/4$ watt per unit of resistance in each decade is allowable if the limit of tem-

perature rise is to be 40 C. Within this limit the resistance change is less than 0.1 per cent. For a decade of tenths, unit, and tens, allowable currents are 11.3, 3.5, and 1.1 amp, respectively. The lack of other compensated decade resistor ranges limits the impedance range of transducers that can be measured in a resonance bridge employing 1/1 ratio arms.

The decade tuning condenser employed in the bridge was specially constructed of GR Type 505 mica condensers, each unit of which, conservatively, will dissipate 1 watt. Peak voltages of 500 volts are permissible across any of the condenser units. With a dissipation factor of less than 0.1 per cent at all

Current wave form was observed by inserting a small 1/4-ohm resistor between the transducer *T* and the grounded junction of the bridge, amplifying the voltage across it, and by observing the resultant pattern on a synchronized cathode-ray oscilloscope. These oscilloscopes were calibrated by steady-state

TABLE 1

Transducer type	Nominal res. freq. ke	Q	Active volume of magnetostrictive material per cm stack height	Power required per cm of stack height
SPEP element	58	8	0.60 cm ³	192 watts
HP-3	24	9	2.33 cm ³	336 watts
Thick-walled 60-ke ring stack	60	10	3.49 cm ³	1,390 watts
Thin-walled ring stack	60	5	1.93 cm ³	386 watts

Computed on basis of $B_{max} = 6,000$. [See numerical values used in equation (8)].

voltages of the same frequency as used in the bridge measurements. A GR shielded transformer was used for isolating the chain of equipment between the detector junctions of the bridge *A* and *B* and the final cathode-ray oscilloscope detector. For sufficient sensitivity, considerable amplification was necessary in the detecting circuit. As balance at the fundamental frequency was approached, amplification was increased. Harmonic voltages then predominated and tended to mask the balance. It was found absolutely necessary to insert a high-discrimination low-pass filter between the bridge and the oscilloscope indicator. Three filters were built with the cutoff frequencies so disposed that it was always possible by proper filter selection to obtain high discrimination against harmonics of the measuring frequency. Cutoff frequencies were placed at 33, 67, and 100 ke. Each filter consisted of three *m*-derived sections, having *m* equal 0.7, 1, and 0.8, terminated in two *m*-derived half sections, *m* = 0.6. Each section or half section was placed in a separately shielded compartment, and for the 33-ke cutoff unit a full 80-db discrimination was realized. For the other two units the discrimination was slightly less. This amount of discrimination was needed and more would have been useful under some conditions of operation. The filters were designed to operate between 600-ohm terminating resistances. Complete design data are

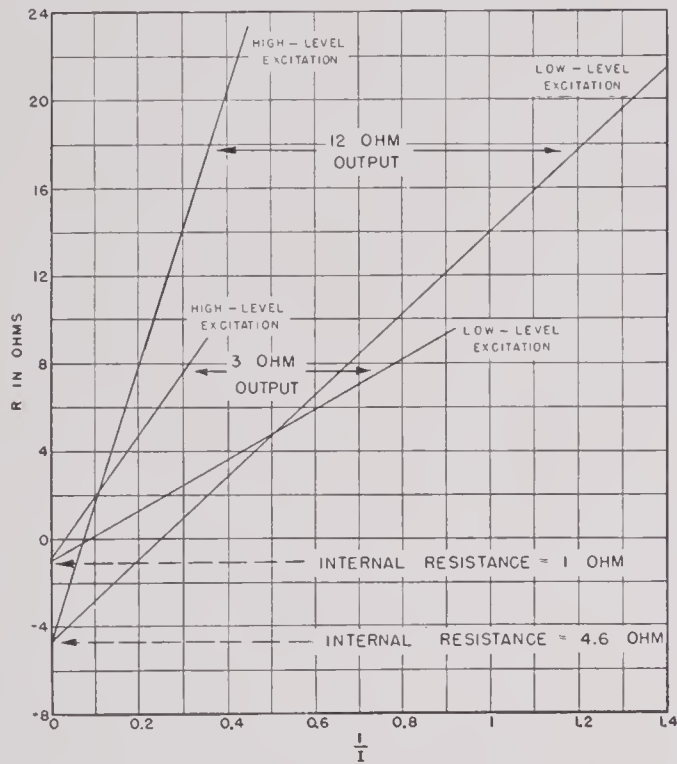


FIGURE 7. Determination of internal resistance of the power amplifier.

frequencies between 10 and 90 ke, it is not believed that any serious limitations will be imposed by the mica condenser as used in such a pulsed-bridge application. However, care should be taken with the contacts involved in the switching of the various units in a decade.

The bridge shown in Figure 3 was used with a 1/1 ratio to minimize errors in making all measurements. One terminal of the transducer was ordinarily effectively grounded at one of the detector junctions of the bridge. A cathode-ray oscilloscope with synchronized sweep was used to measure the voltage across the transducer and to observe its wave form.

given in Table 2. To insure proper termination under various bridge adjustments, a cathode follower adjusted to have the proper output resistance was used between the bridge isolating transformer and the filter input.

A B-19H hydrophone, described in Chapter 6, was used as the detector of sound emitted from the trans-

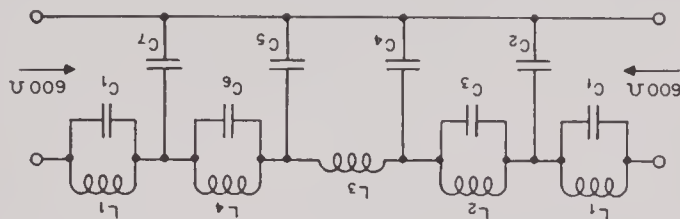


TABLE 2. Frequencies in kc, inductances in mH, capacities in μ f.

Filters		I	II	III
Cutoff freq. = f_c		33	67	100
Freq. of infinite attenuation = f_∞	$m = .6$	41.2	83.7	125
	$m = .7$	46.2	93.8	140
	$m = .8$	55.0	111.8	167
Values of inductance	L_1	1.736	0.8553	0.5727
	L_2	4.051	1.996	1.336
	L_3	5.787	2.851	1.909
	L_4	4.630	2.281	1.527
Values of capacitance	C_1	0.00857	0.004223	0.002829
	C_2	0.01045	0.005147	0.003449
	C_3	0.002929	0.001442	0.000966
	C_4	0.01367	0.006730	0.004510
	C_5	0.01447	0.007126	0.004775
	C_6	0.001809	0.000891	0.000597
	C_7	0.01125	0.005542	0.003714

ducer under test. Its response was amplified and calipers used to measure the amplitude of the synchronized pulse pattern on a calibrated cathode-ray oscilloscope.

Measurements were made on the following laminated stack elements.

1. SPEP stack, as described in Chapter 7.
2. Thin-walled 2V-Permendur ring stack.
3. *Specially annealed ring stacks* [SPARS] of nickel of various thicknesses.

11.5.2 Measurements on SPEP Elements

A single SPEP element with permanent-magnet polarization, described in considerable detail in Chapter 7, was first investigated. This element was

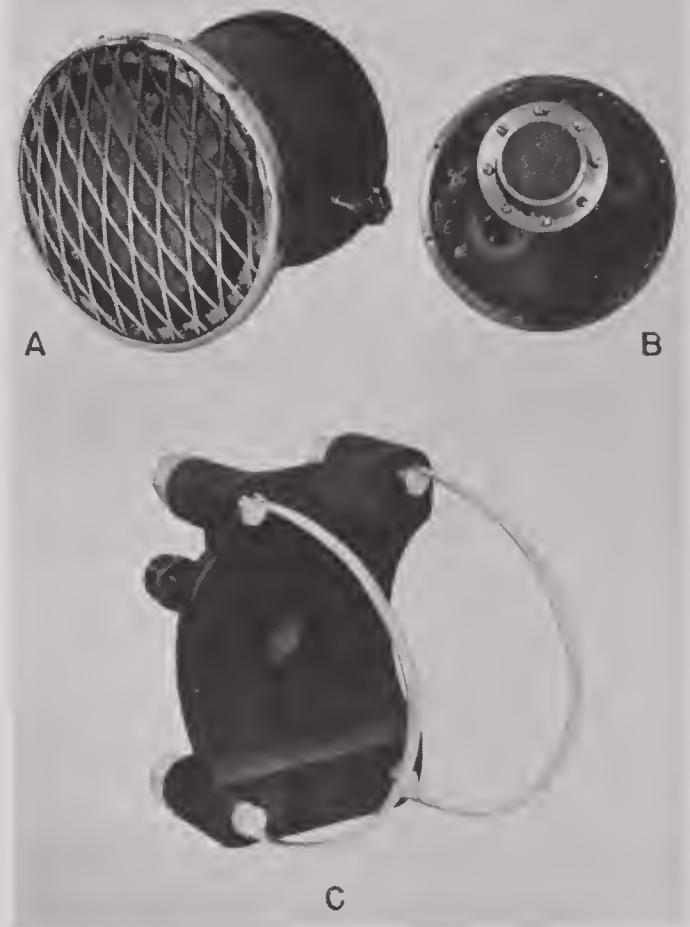


FIGURE 8. Pressure chamber.

mounted inside a chamber lined with butyl rubber to minimize reflections and filled with degassed castor oil under pressure to avoid cavitation difficulties. A flexible metal tubing led from this to the compression chamber of a small hydraulic automobile jack. One end of the chamber was enclosed by ρ c rubber with a supporting cover of $\frac{1}{16}$ -in. stainless-steel expanded metal with diamond-shaped mesh openings approximately $1\frac{3}{4} \times \frac{5}{8}$ in. in size. A small direct-reading pressure gauge was attached and pressures up to 5 atm were ordinarily used during power testing. Figure 8 shows A, a front view of the pressure chamber; B, a specially constructed transducer element mounted on the backplate of the pressure chamber; and C, the modified pipe-saddle mounting arrangement used for holding the chamber in the sound absorbent tank. Figure 9 shows the assembled pressure chamber, hydrostatic press, and B-19H hydrophone mounted for use in the absorbent tank. Two different means of mounting the SPEP stack in the chamber were utilized. The first is shown schematically in Figure 10.

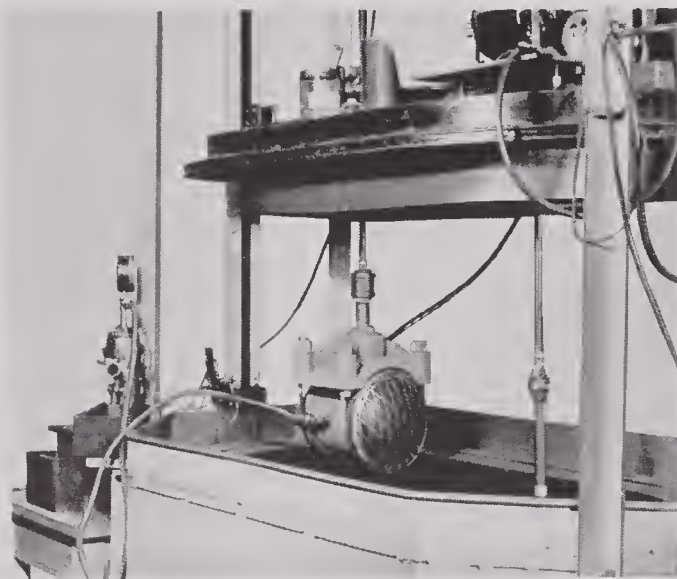


FIGURE 9. Pressure chamber in tank.

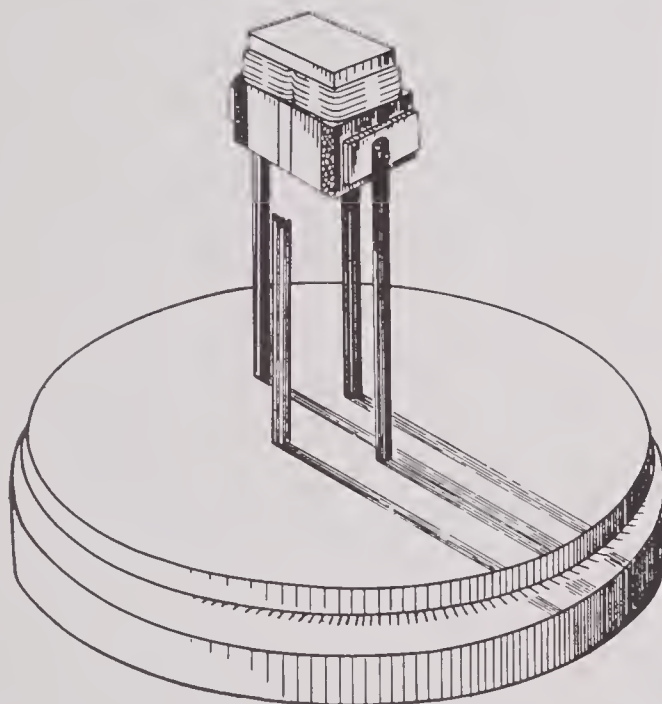


FIGURE 10. Original SPEP mounting in castor oil.

The SPEP stack was immersed directly in castor oil. A slight lowering of the Q of the device was observed and was thought to be caused by additional damping added by the oil. A different mounting was then arranged, as shown in Figure 11. Here the stack was Cycle-Welded to a truncated conical rubber diaphragm, which in turn was Cycle-Welded to a steel supporting plate. This supporting plate closed one end of a steel housing so that air and sponge rubber rather than oil now surrounded the stack itself. This

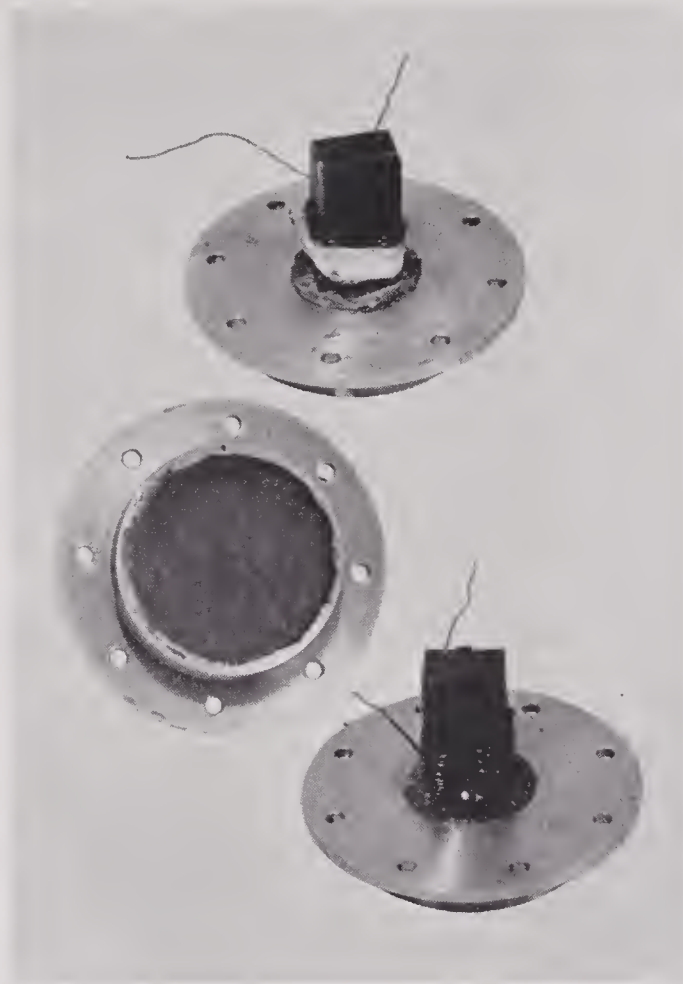


FIGURE 11. Mounting of element with rubber face.

closely simulated the mechanical arrangement of one element of a full 32-element SPEP transducer.

This type of mounting, in which the rubber diaphragm was an appreciable fraction of a wave length in thickness, gave rise to the air vector impedance locus shown in Figure 12A. However, when the same characteristic was measured in water, the locus changed to that shown at B. For both A and B, plots of R and X against frequency were made and the purely motional components were separated out as previously described in Chapter 2. A plot was then made of the square of the motional impedance against frequency, as shown in Figure 12C for both the air and water cases. Since the motional impedance is nearly proportional to the amplitude of vibration, this plot shows roughly the frequency distribution of mechanical energy. It is interesting to point out that this system, having more than one simple mode of vibration, exhibits characteristics typical of two coupled electric circuits when the coupling is altered by changing the loading.

Figures 13 and 14 show typical curves of resistance

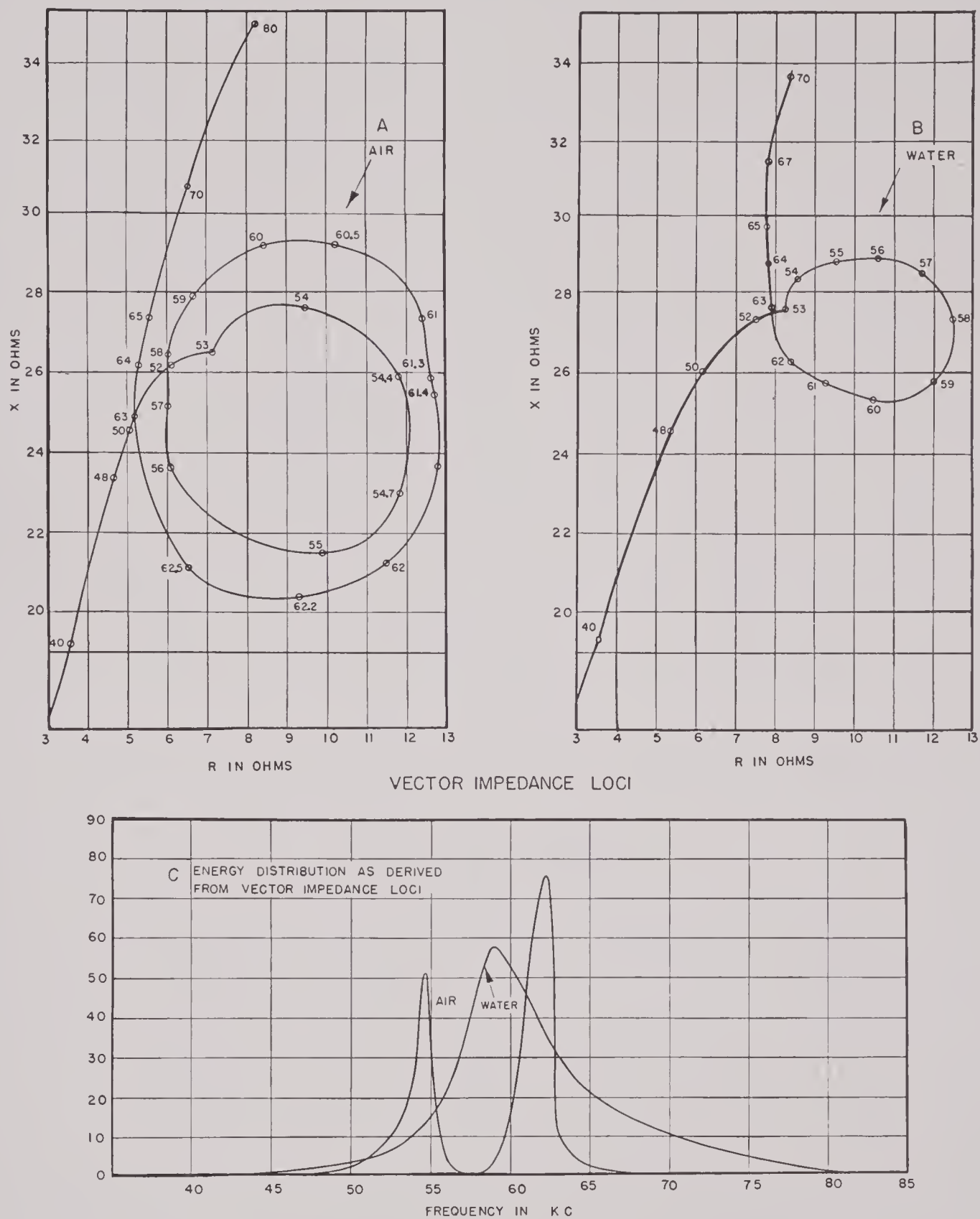


FIGURE 12. Impedance curves of element mounted as in Figure 11. A. In air. B. In water. C. Energy distribution in air and in water.

CONFIDENTIAL

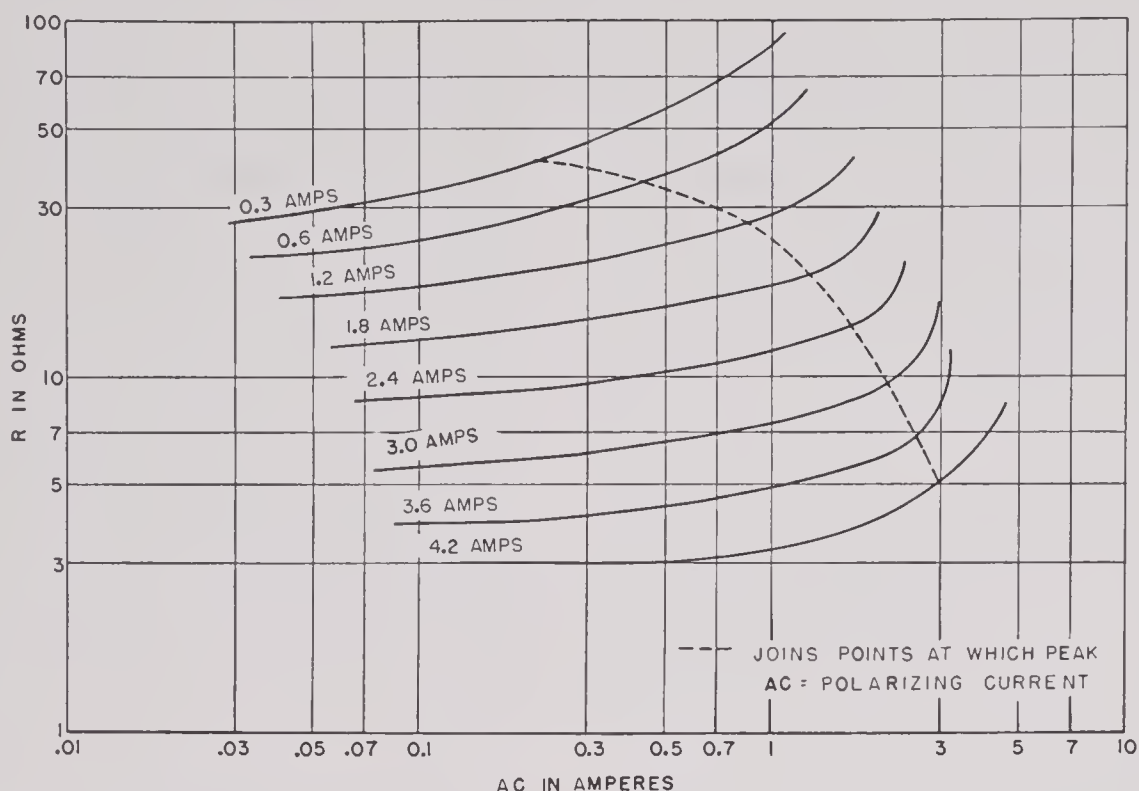


FIGURE 13. Resistance of element as a function of level and polarizing current.

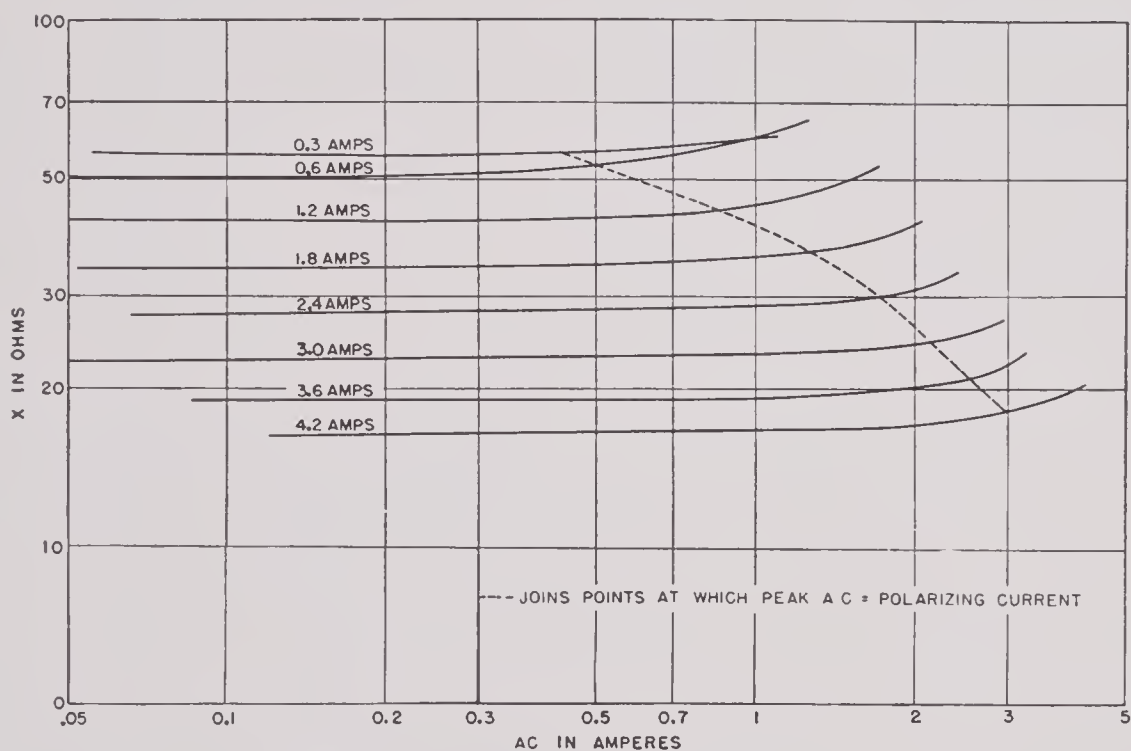


FIGURE 14. Reactance of element as a function of level and polarizing current.

and reactance of a SPEP unit with d-c polarization as a function of excitation level for various values of polarizing current. In general it should be noted that both resistance and reactance increase much more rapidly when the peak value of the alternating field exceeds the fixed polarizing field. All these measure-

ments were made at or near the resonant frequency. Figure 15 presents the same data in a different way. It shows sections of the curves of Figure 13, illustrating the changes that occur at constant a-c level when the polarizing current is varied.

The first high-level driving experiments were made

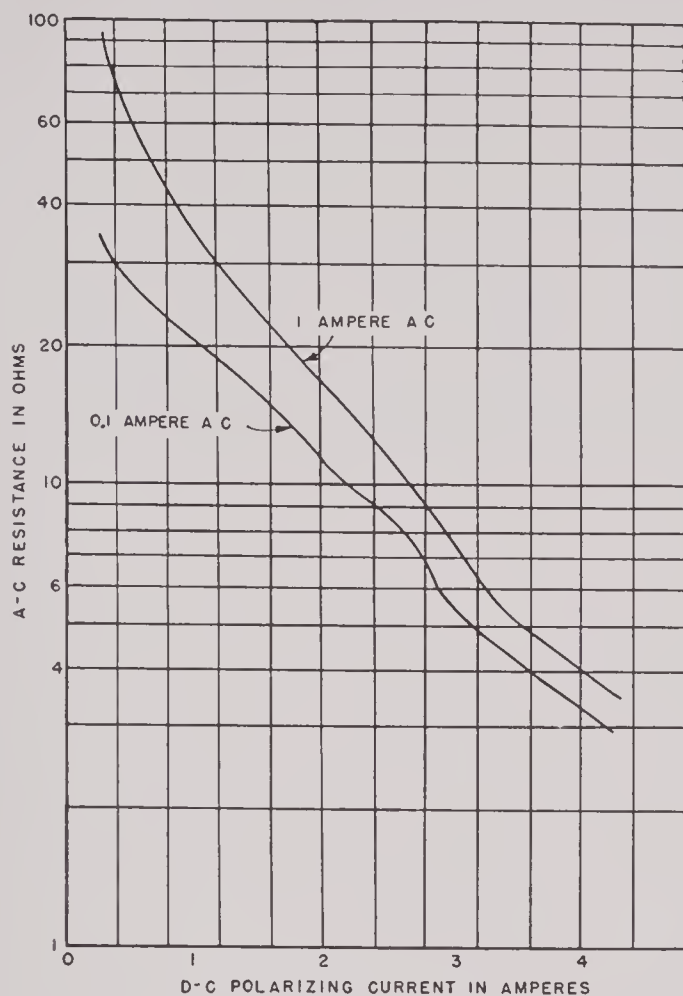


FIGURE 15. Resistance of constant-current driving as a function of polarizing current.

resistive component of the device was not determined. Impedance data at low signal levels were taken so that a rough estimate of the resistance could be determined by interpolation from the data of Figure 13. Input powers were computed and averaged values of data derived from several runs are shown in Figure 16. The data are shown only because higher levels were reached in these particular runs than later, when the available power was divided by the bridge. It is to be noted that although a linear relationship exists between input and output for input power as great as 30 watts, the slope of the line deviates considerably from unity. It is quite probable that the values of resistance used are in error as experimental evidence was found showing considerable variation in flux density in the legs of the PM unit. Later data taken using the bridge technique and a d-c polarized SPEP unit gave plots in which the slope was nearly unity over a wider range. A typical curve is shown in Figure 17A. These later data, though considerably more reliable, are much more limited in range.

Data such as Figure 17A shows were used in calculating the total acoustic output to be expected from one of the 32-element SPEP transducers. The elements of this unit were not all wound with the same number of turns. There were four 50-turn, eight 31-

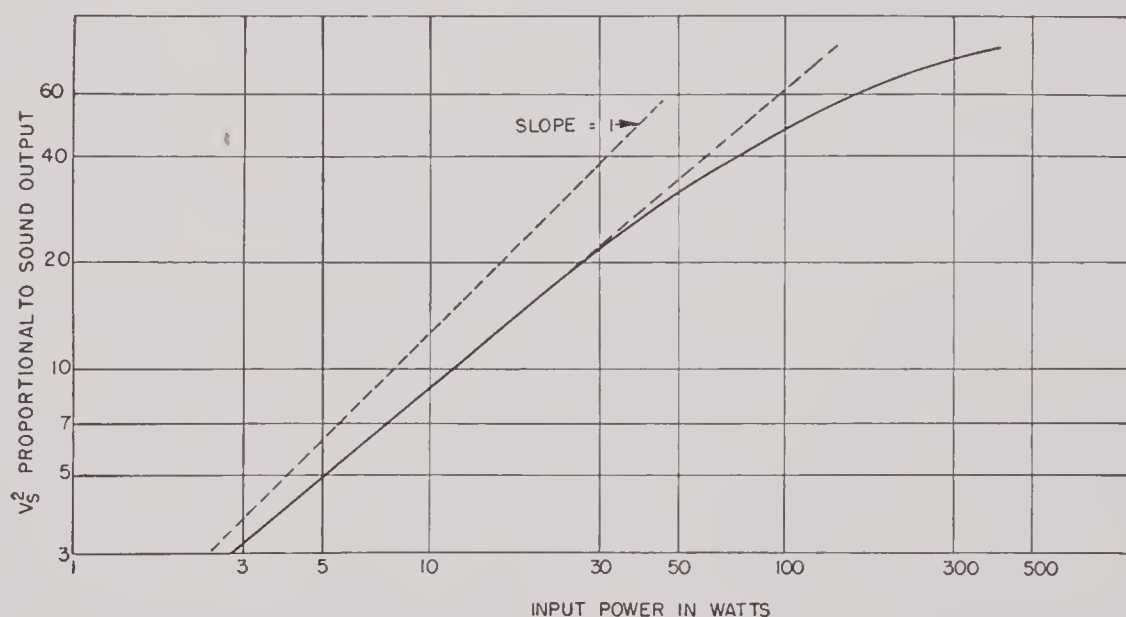


FIGURE 16. Output vs input of PM polarized SPEP.

on a *permanent magnet* [PM] SPEP stack before the pulsed-bridge technique had been adopted. The current through the transducer was measured but the

turn, four 20-turn, eight 15-turn, and eight 9-turn elements arranged to produce the desired pattern of acoustic output. In order to estimate the power

CONFIDENTIAL

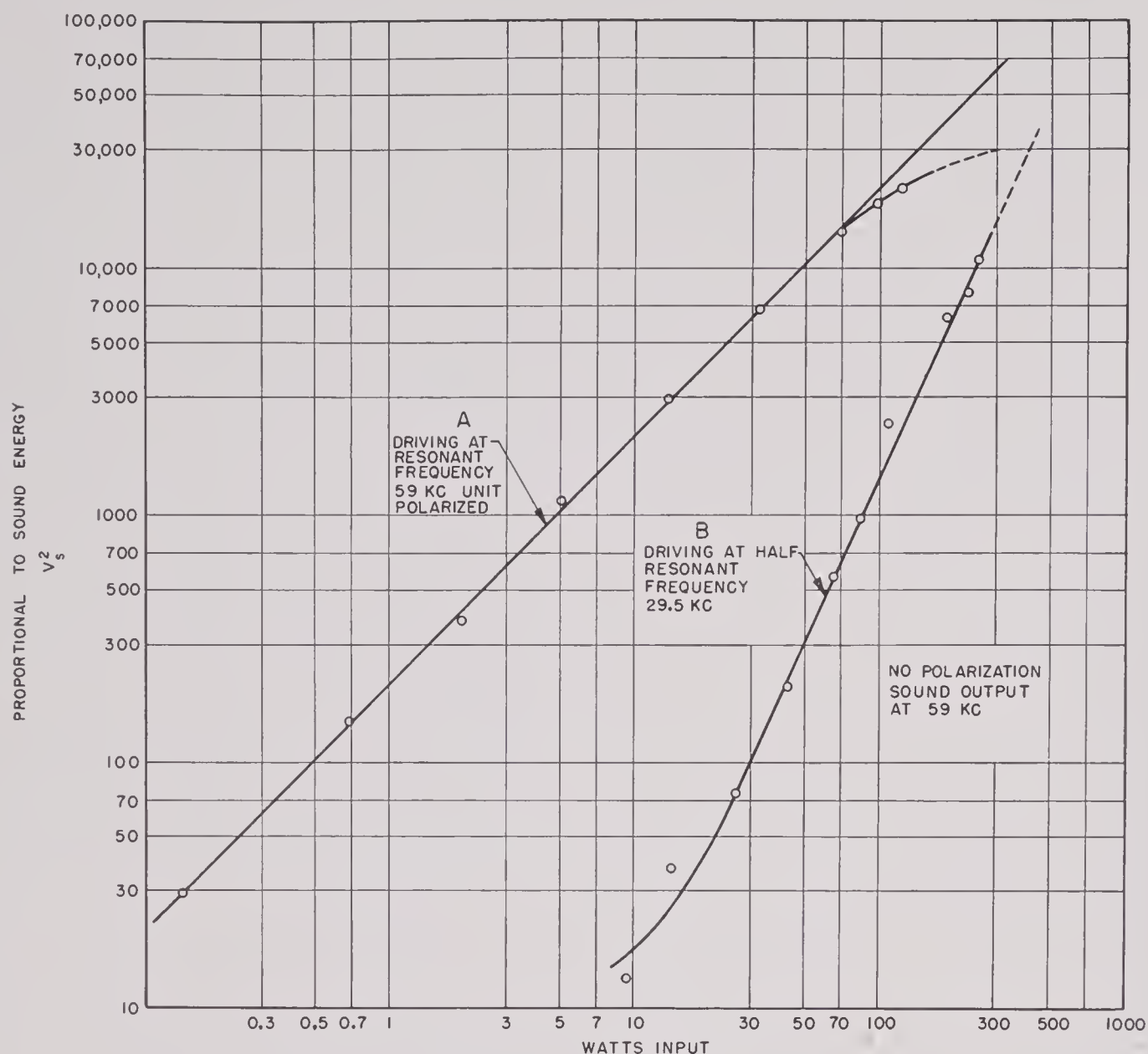


FIGURE 17. Output vs input of a d-c polarized SPEP.

handling capabilities of this unit, it is necessary to find the number of normal 50-turn elements to which the complete shaded unit is equivalent. By assuming that the power absorbed in any element is proportional to the square of the number of turns in the windings, it is found that 8.7 50-turn elements would be equivalent to the 32-element shaded units in power-handling capacity. This factor is used to multiply all powers measured on a single element. Figure 18 shows the acoustic output of the 32-element unit predicted from the data of Figure 17A and the shading factor 8.7, assuming an efficiency of 30 per cent. This extrapolation from the single element to the complete 32-element shaded unit involves a number of assumptions, and the result given agrees only

roughly with the best experimental work that has been done on the 32-element assembled unit. In order to test the effect on the pattern of a high level of operation, input powers as high as 1,300 watts were used and at this level the measured acoustic output was 400 watts. This is to be compared with the value of 275 as read from the curve of Figure 18. The patterns at the 1,300-watt and 150-watt levels were essentially the same.

Since the theory worked out under Section 11.4 implies operation with no polarization, it was of interest to compare the acoustic outputs of the polarized and nonpolarized cases. Nonpolarized operation offers attractive possibilities for certain applications, since it involves applying a driving voltage of half

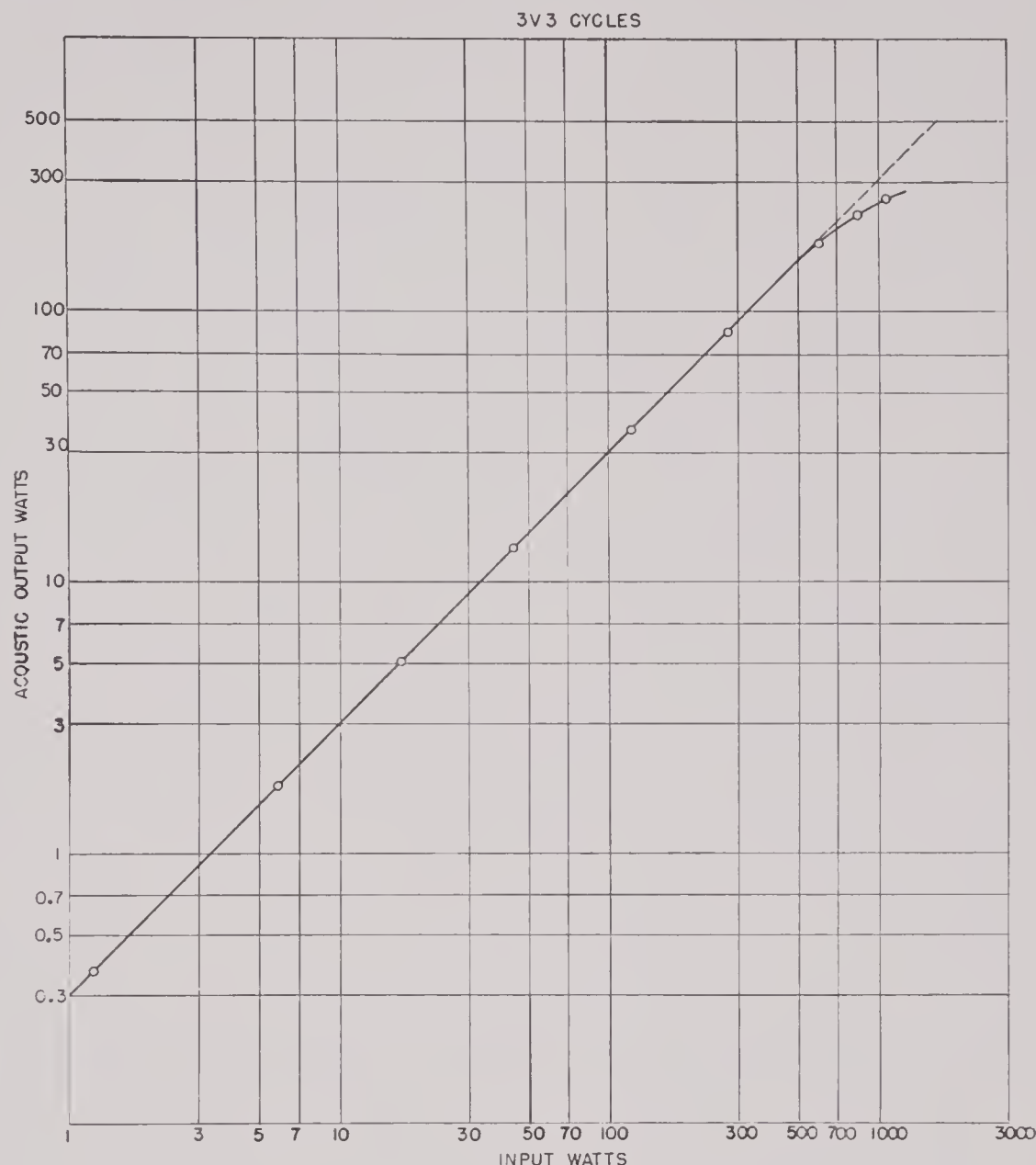


FIGURE 18. Output vs input of 32-element SPEP transducer.

the frequency of mechanical resonance. This lowering of the frequency increases the range within which it might be possible to employ highly efficient gas tube oscillators. In Figure 17B is shown a plot of acoustic output vs electric input for half-frequency driving. It is interesting to note that for the half-frequency use the efficiency is increasing continuously with level. The dotted extrapolation suggests the possibility that at very high input levels nonpolarized operation might equal or exceed the efficiency of that with polarization. Regardless of efficiency, nonpolarized operation might in some cases be definitely advantageous. Figure 19 shows the typical change of R and X with level for the nonpolarized case. These data were taken on the same d-c SPEP unit used in the

half-frequency driving tests. Comparison with Figures 13 and 14 shows the essential difference in character of these changes with level. A maximum in the resistance curve at fairly low values of peak H is the most distinguishing feature. This will be referred to later in connection with the work on laminated ring stacks, where there is greater possibility of correlating the results with theory.

It is of interest to investigate what changes take place in the impedance curves as a function of power level. Since this is unimportant for receiving hydrophones where the power levels are usually very low, the practice of making impedance measurements at some low but unspecified level became established at HUSL. At power levels usually encountered in pro-

CONFIDENTIAL

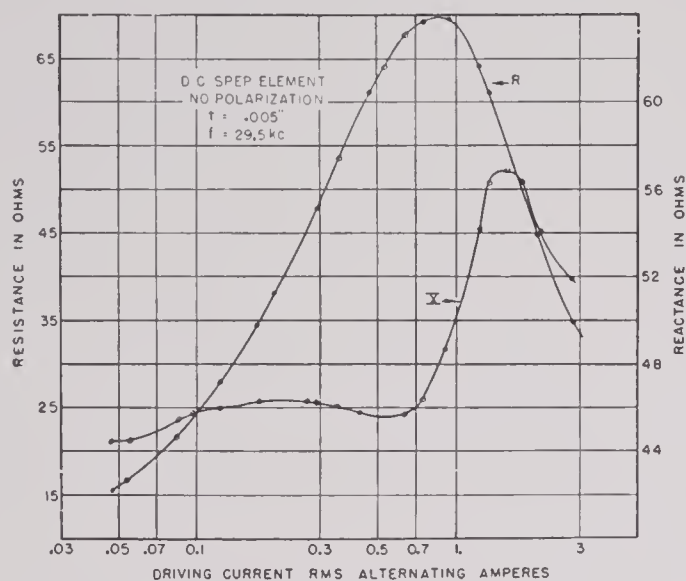


FIGURE 19. Resistance and reactance of a nonpolarized SPEP as a function of driving current.

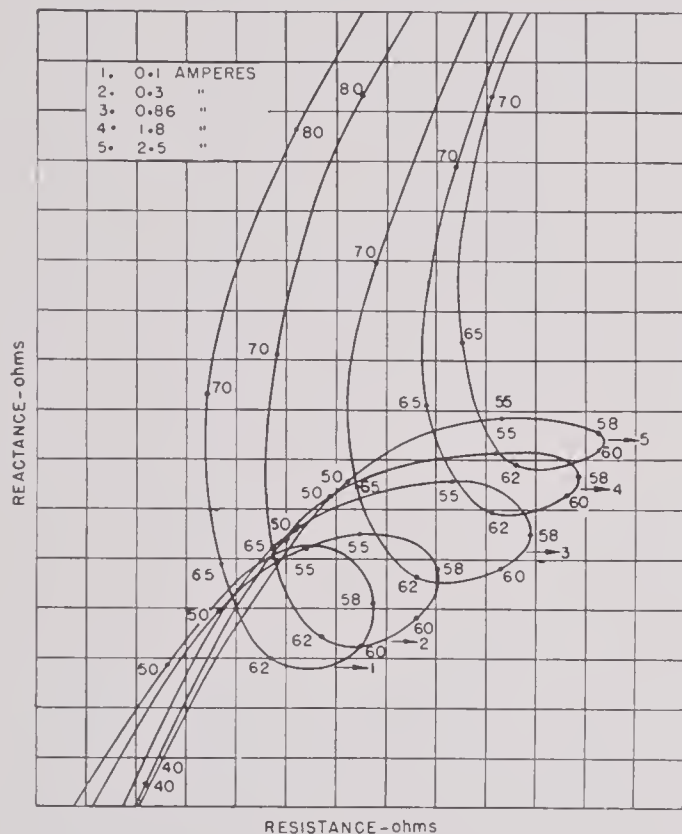


FIGURE 20. Variation of impedance loci with driving current.

jector operation, the changes in R and X with level cannot be neglected.

A series of runs was made on a single SPEP element in the pressure chamber, keeping the frequency in each run constant and varying power level. Plots of R and X against driving current were then made. For each of several constant values of current, R and X were determined by sectioning the above-

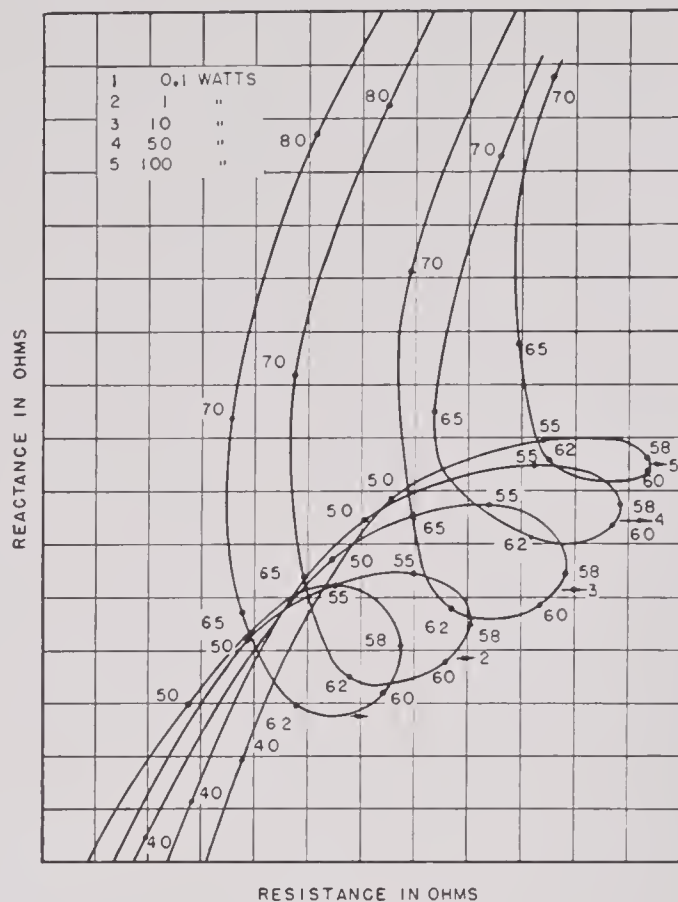


FIGURE 21. Variation in impedance loci with input power.

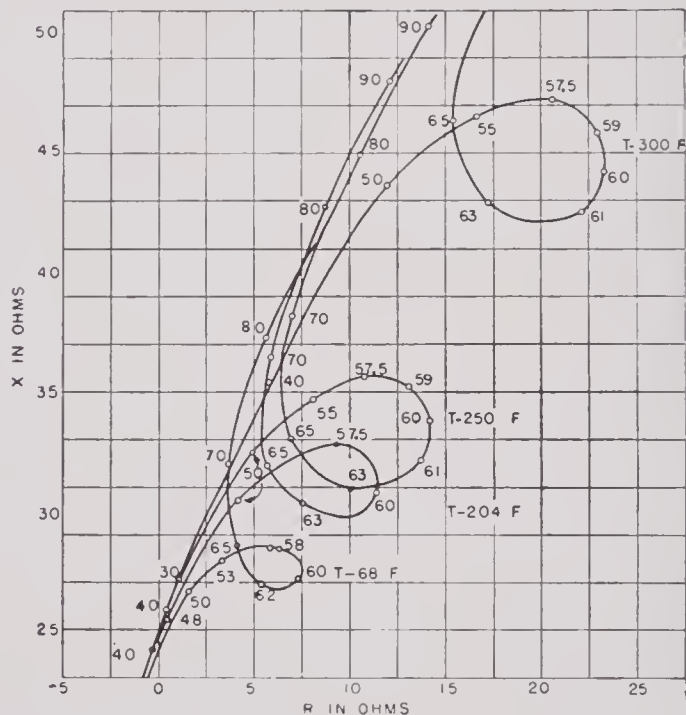


FIGURE 22. Observed changes in impedance loci due to heating and subsequent cooling.

mentioned curves and the resulting vector impedance loci plotted as in Figure 20. Similarly, the original values of R and X were plotted against power

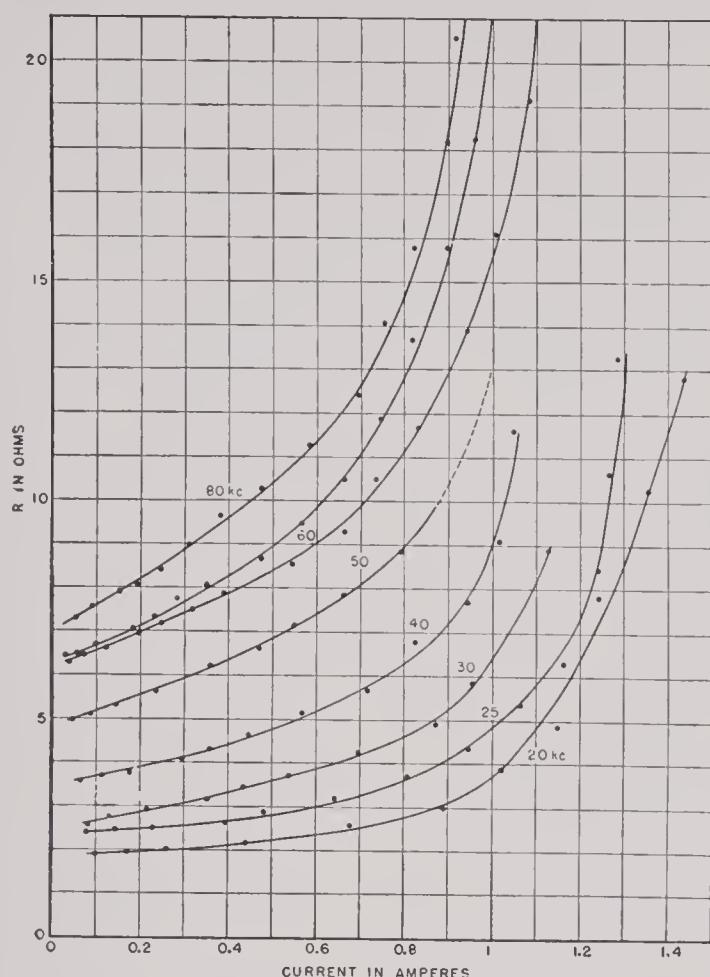


FIGURE 23. Resistance of 2V-Permendur ring stack as a function of driving level.

and the resulting vector impedance loci for various values of constant power are plotted in Figure 21. Because of the difficulty of computing the core impedance for the geometry of the SPEP element, no attempt was made to derive the strictly motional impedance diagram. The change with level from a fairly circular locus to an elongated egg-shaped one is common to both Figures 20 and 21. It is believed the power level was sufficiently high to extend well into the region of magnetic nonlinearity. At this point it is not known what significance can be attached to these families of curves. They are shown primarily to indicate typical changes in the loci that occur as a result of changes in driving level.

Figure 22 exhibits another type of change that may take place in the vector impedance loci of units polarized by sintered-oxide magnets if the unit is subjected to an appreciable temperature change. Here the SPEP element was heated by the application of alternating current of resonant frequency. Its temperature was determined by a thermocouple placed between the two windings and just below the arch of

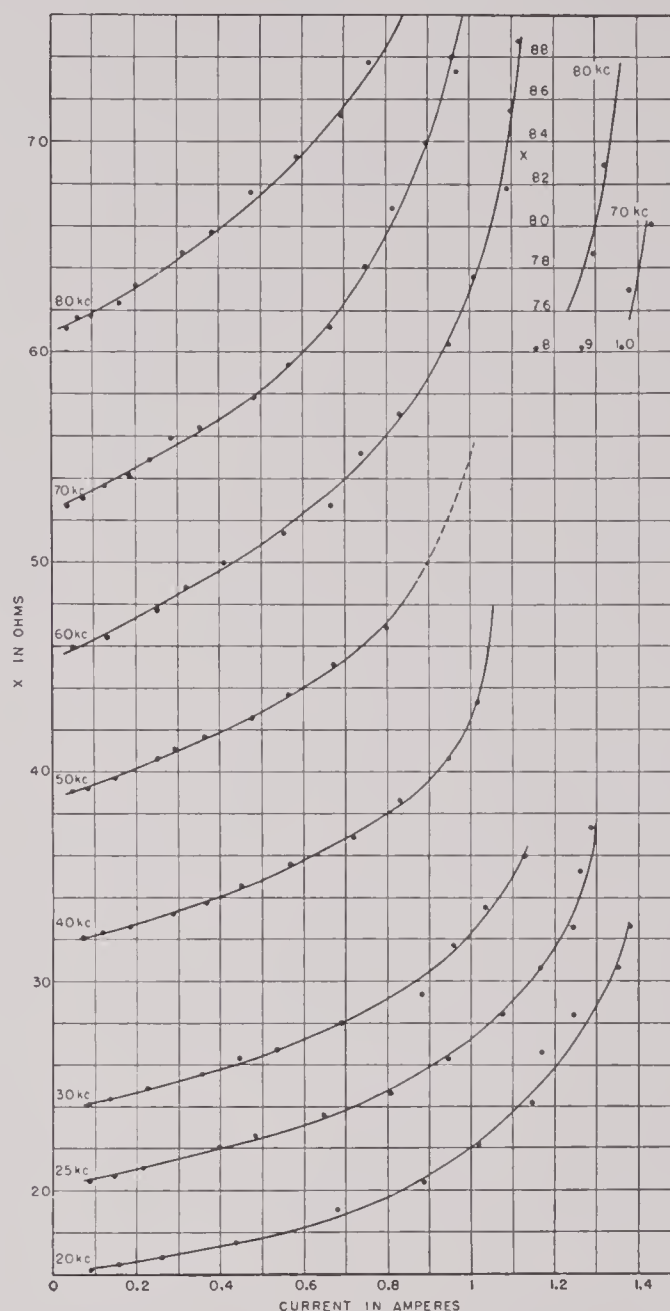


FIGURE 24. Reactance of 2V-Permendur ring stack as a function of driving level.

the core. After reaching the temperature indicated, the unit was allowed to cool to room temperature. Low-level impedance measurements were then made. The permanent changes in impedance are typical of a decreased polarization and are probably completely accounted for on this basis. This particular experiment does not of itself provide sufficient evidence to decide the role played by each of several possible factors. The decrease in strength of the sintered-oxide magnet may be ascribed to the effect of temperature, to prolonged application of a strong a-c, to a single pulse of high intensity, or to a combination of two or more of these causes. A great amount

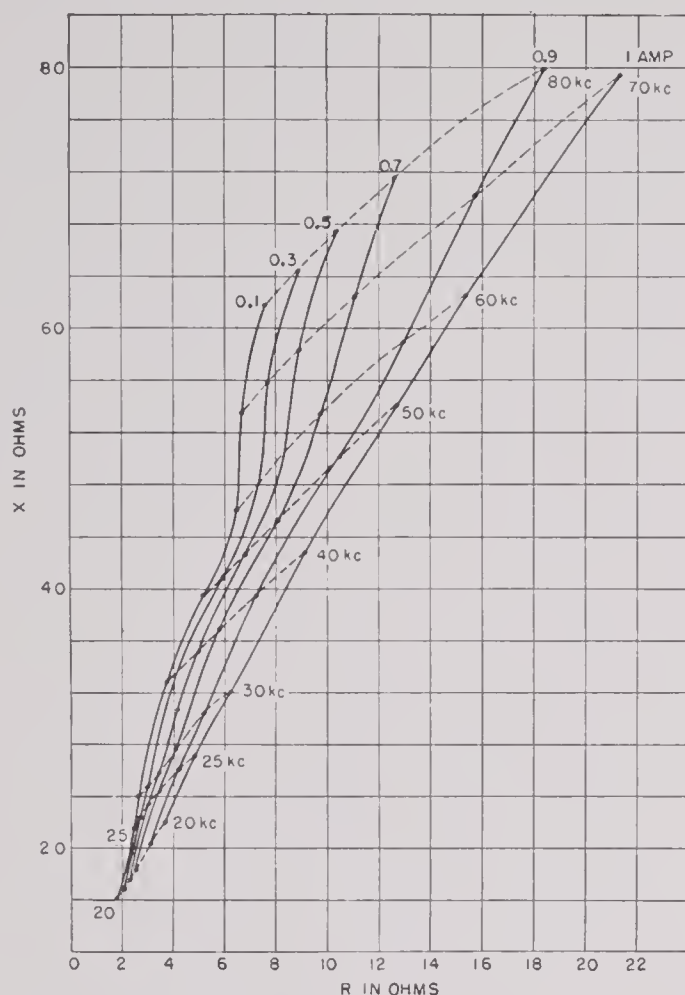


FIGURE 25. Impedance curves of 2V-Permendur for various constant values of driving current.

of experimental evidence exists to indicate that high-level pulsing, with low average power and hence very little production of heat, produces no permanent changes in impedance in units polarized by permanent magnets.

11.5.3 Measurements on the 2V-Permendur Stack

Figures 23 and 24 show the resistance and reactance change as a function of level for a thin-walled 2V-Permendur ring stack. Here the total percentage change in R and X is considerably greater than for the SPEP element of annealed nickel. Figure 25 shows a family of vector impedance loci plotted from data obtained by sectioning the curves of Figures 23 and 24 for various constant values of current. The Q of the device is so low that the vector impedance locus does not even open at resonance and at this frequency only an indentation appears in the curve. As the level increases, this bump becomes less pronounced until

MEAN DIAMETER = 1.06 INCHES
RADIAL WALL THICKNESS = .090 INCHES

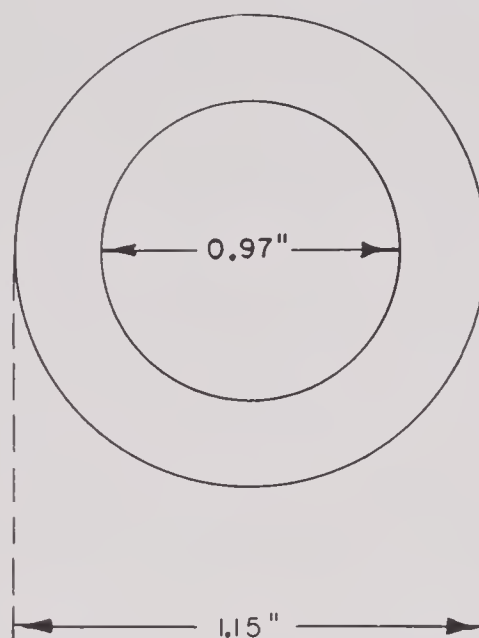


FIGURE 26. Drawing of SPARS lamination with dimensions.

at a level of 1 amp the locus has become essentially a smooth curve giving no indication of resonance.

11.5.1 Measurements on Annealed-Nickel Ring Stacks

A series of thin-walled SPARS (Figure 26) were constructed with the expectation that the data from this geometrically simple transducer would be helpful in formulating a theory of high-level losses. The nominal resonant frequency was 60 kc. Lamination thicknesses of 1, 3, 5, 10, and 25 mils were chosen. All laminations were given the same heat treatment, but apparently differences in magnetic properties arise during the rolling process which are not removed by subsequent heat treatment. Tests made by the routine methods described in Chapter 4 showed considerable variation in magnetization curves, permeability, and hysteresis loops among the different samples. Magnetization curves are shown in Figure 27 and major hysteresis loops in Figure 28.

In order to study effectively the operation of a magnetostrictive transducer under high-level operation, it is first necessary to understand core effects at high level without the complication of the magnetostriction. Consequently, the laminated stacks were first wound tightly with 70 turns of wire over a thin insulating layer of silk tape and measurements

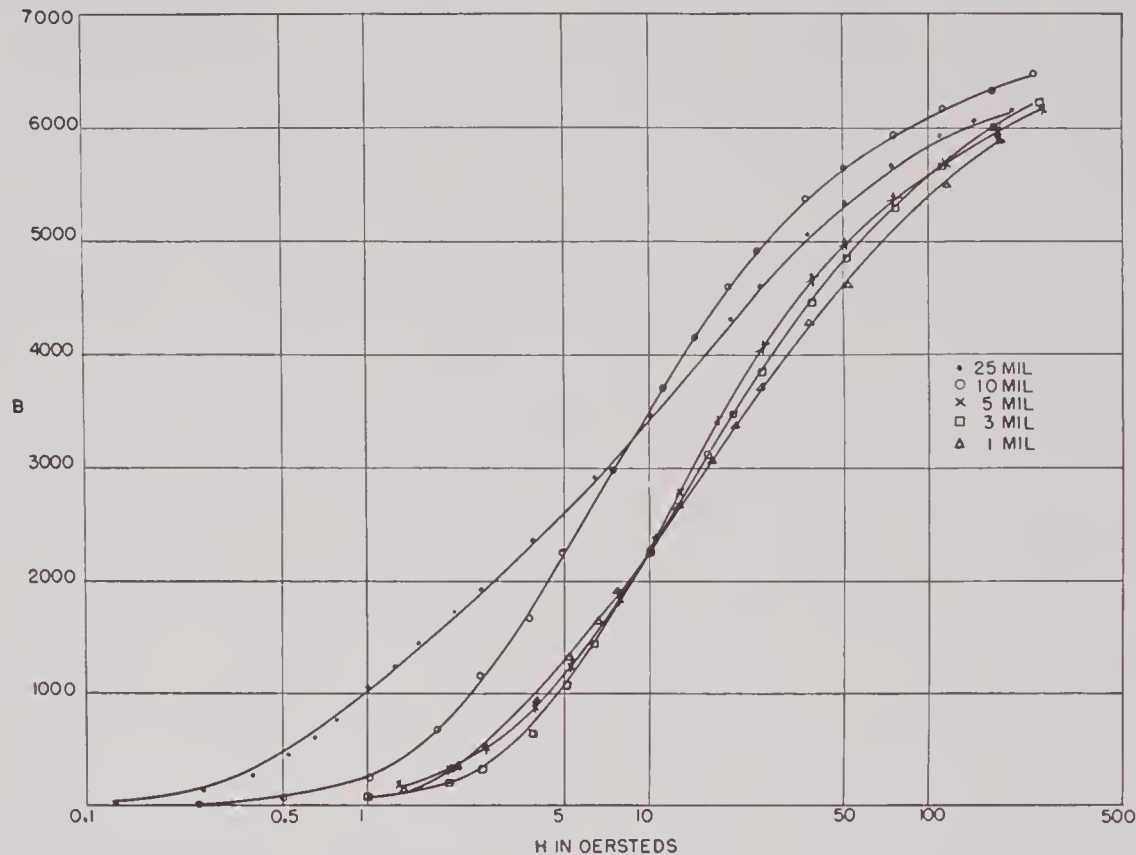


FIGURE 27. Magnetization curves of SPARS stacks.

were made to determine the low-level value of reactance and a-c resistance. In order to obtain the true value of the inductance, it was necessary to carry out the measurements at such a low frequency that the effect of eddy currents would be negligible. Experimentally this is determined when the curve of measured inductance plotted against frequency approaches a constant as frequency is reduced. In terms of the eddy-current theory developed in Chapter 3 this means that the ratio f/f_c is much less than unity. The stack of laminations of 0.025-in. thickness showed variations in inductance at frequencies well below 1,000 cycles, so that it was necessary to extend the measurements to frequencies as low as the available apparatus would permit. To judge from the value of f_c computed for the 25-mil lamination and the slope of the experimental inductance curve, it is doubtful if measurements were carried to as low a frequency as was desirable. Measurements of resistance were originally made between 10 and 90 kc. In this frequency range the core of thickest lamination proved to have less resistance than some of the thinner samples. This rather unexpected result stimulated the taking of data over as wide a frequency range as easily available equipment permitted. Figures 29 and 30 show families of R and L

respectively as a function of frequency for the samples of different thickness.

In making measurements over the frequency range shown, it was necessary to use three different bridges. Below 2,000 cycles a Heaviside bridge using a Campbell mutual inductometer was used. By reversing the 1/1 ratio arms and by using a substitution method, it was possible to measure consistently resistances of less than 0.1 ohm. At these low frequencies it was impossible to use an oscilloscope detector without high-discrimination low-pass filters to eliminate harmonics; a GR wave analyzer was finally used for this purpose. Between 2,000 and 10,000 cycles a direct-comparison four-arm inductance bridge was used. Above 10 kc the standard resonance impedance bridge described in Chapter 9 proved entirely adequate. During the course of these measurements, variations in R and L were observed at very low levels. Figure 31 shows an example of this, again emphasizing the importance of specifying power level when electrical measurements are made on coils having ferromagnetic cores.

In Figure 29 the distinct crossing-over of the curves of resistance vs frequency on going from the thick to thin laminations can be easily explained in terms of the classical theory of eddy currents in

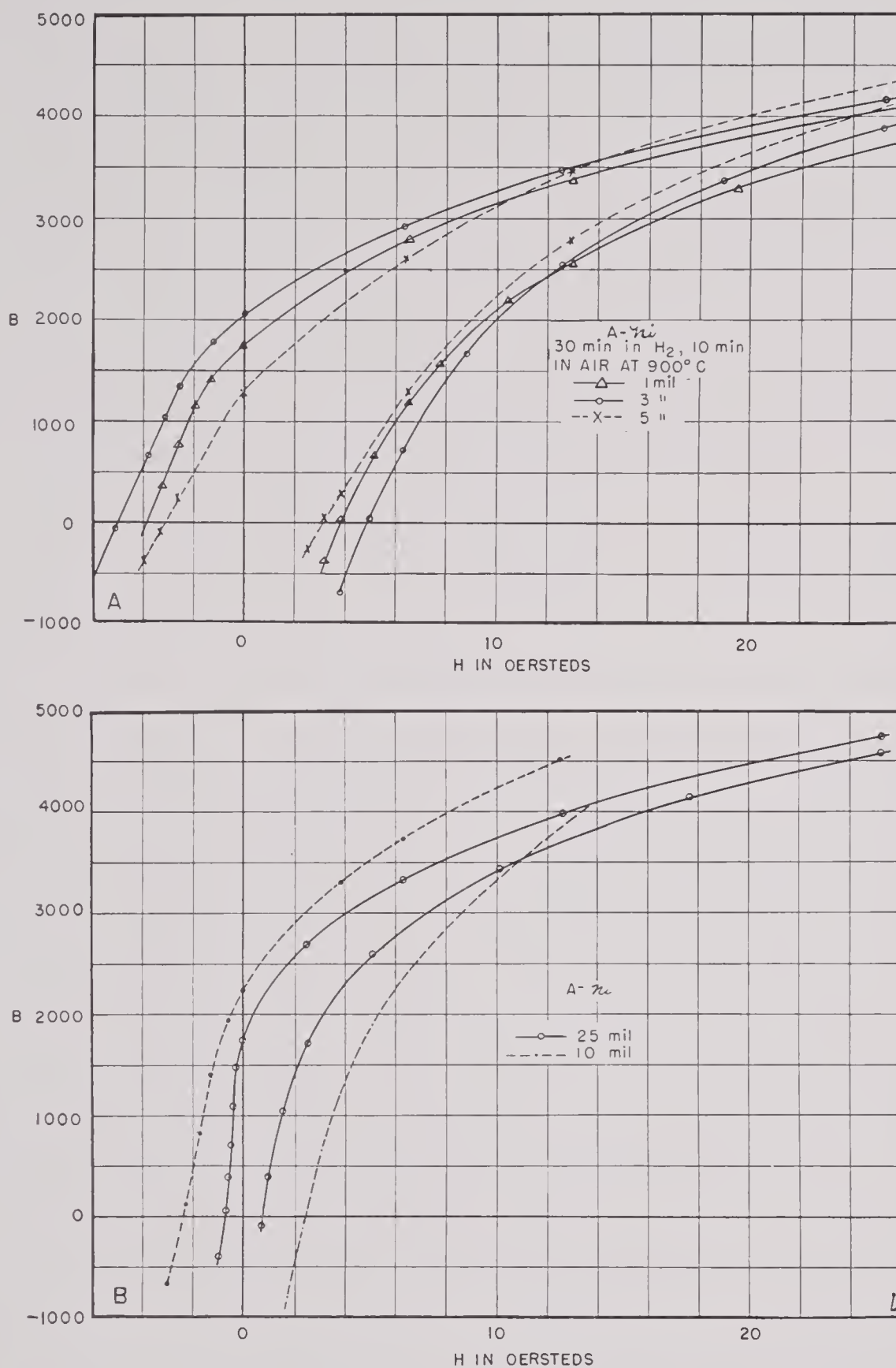


FIGURE 28. Hysteresis loops of SPARS stacks.

CONFIDENTIAL

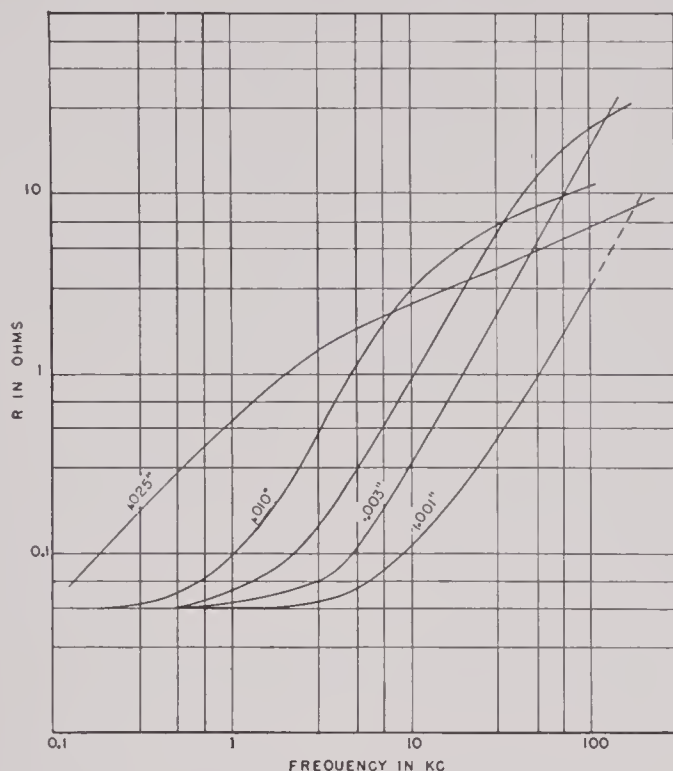


FIGURE 29. Resistance of SPARS stacks as a function of frequency at low levels.

flat laminae. The core impedance for the toroidal-shaped cores used in these experiments is given in equation (6) of Chapter 3 as

$$Z_c = j\omega L_0 \chi = j\omega L_0 (\chi_R - j\chi_i) = \omega L_0 \chi_i + j\omega L_0 \chi_R.$$

Figure 1 of Chapter 3 shows that χ_i passes through a maximum at approximately $f/f_c = 2.5$, that for small values of the variable f/f_c it approaches the limiting value $\frac{1}{3}f/f_c$, and that for high values the limit becomes $\sqrt{f_c/2f}$. For two geometrically similar samples differing widely in values of f_c , there will be a frequency somewhere between the two values of f_c at which they will have the same value of χ_i . It should thus be possible to predict the crossover frequency with an accuracy dependent on the degree to which the assumptions are satisfied, namely $f_{c1} \gg f \gg f_{c2}$.

At the crossover point,

$$R_1 = \omega L_{01} \chi_{i1} \quad (\text{for the sample with high } f_c)$$

$$R_2 = \omega L_{02} \chi_{i2} \quad (\text{for the sample with low } f_c).$$

It is assumed that the total resistance arises only from the effect of eddy currents, copper and hysteresis losses being neglected.

In all cases then,

$$L_{01} \chi_{i1} = L_{02} \chi_{i2}$$

and if $f_{c1} \gg f \gg f_{c2}$ then

$$\frac{1}{3} \left(\frac{L_{01} f}{f_{c1}} \right) = \sqrt{\frac{f_{c2}}{2f}} \cdot L_{02}.$$

For the toroids under discussion, L_{01} and L_{02} differed only because of slightly different cross-sectional (A_1 and A_2) areas and different permeabilities. By taking this into account,

$$\frac{1}{3} \left(\frac{f}{f_{c1}} \right) \mu_1 A_1 = \mu_2 A_2 \sqrt{\frac{f_{c2}}{2f}},$$

which with rearrangement yields the expression

$$f = \sqrt[3]{\frac{9}{2} f_{c2} f_{c1}^2 \left(\frac{\mu_1 A_1}{\mu_2 A_2} \right)^2}. \quad (10)$$

The following are the values of the constants necessary to apply the above equation to the data of Figure 29.

Lamination thickness (in inches)	0.001	0.003	0.005	0.010	0.025
μ_0 from measured L_0 (Figure 31)	87	86	115	124	226
A , cross-sectional area in sq cm	0.151	0.138	0.149	0.139	0.146
f_c in cycles per sec.	7.2×10^5	8.06×10^4	2.18×10^4	5.06×10^3	4.45×10^2
using tabulated μ_0					

Here f_c was calculated from equation (2) of Chapter 3. By using the above values, the frequencies were calculated at which the curve for the 25-mil lamination crosses successively the curves for the 10-, 5-, 3-, and 1-mil samples. The values are as follows.

Crossover	Calculated	Observed	Examination of Assumption $f_{c1} \gg f \gg f_{c2}$	
0.025-0.010	5.7×10^3	7.0×10^3	5.06×10^3	$5.7 \times 10^3 \gg 4.45 \times 10^2$
0.025-0.005	1.5×10^4	2.1×10^4	2.1×10^4	$2.1 \times 10^4 \gg 4.45 \times 10^2$
0.025-0.003	4.6×10^4	4.6×10^4	8.06×10^4	$\gg 4.6 \times 10^4 \gg 4.45 \times 10^2$
0.025-0.001	1.9×10^5	1.8×10^5	7.2×10^5	$\gg 1.8 \times 10^5 \gg 4.45 \times 10^2$

The last column shows that only in the last two cases could even a qualitative agreement be expected between the calculated and observed values.

Exploratory measurements of resistance and reactance as functions of the applied field were carried out for three of the five samples, namely the 1-, 5-, and 25-mil cases. Because of lack of time it appeared that this selection would give the best survey of representative phenomena, since it included the

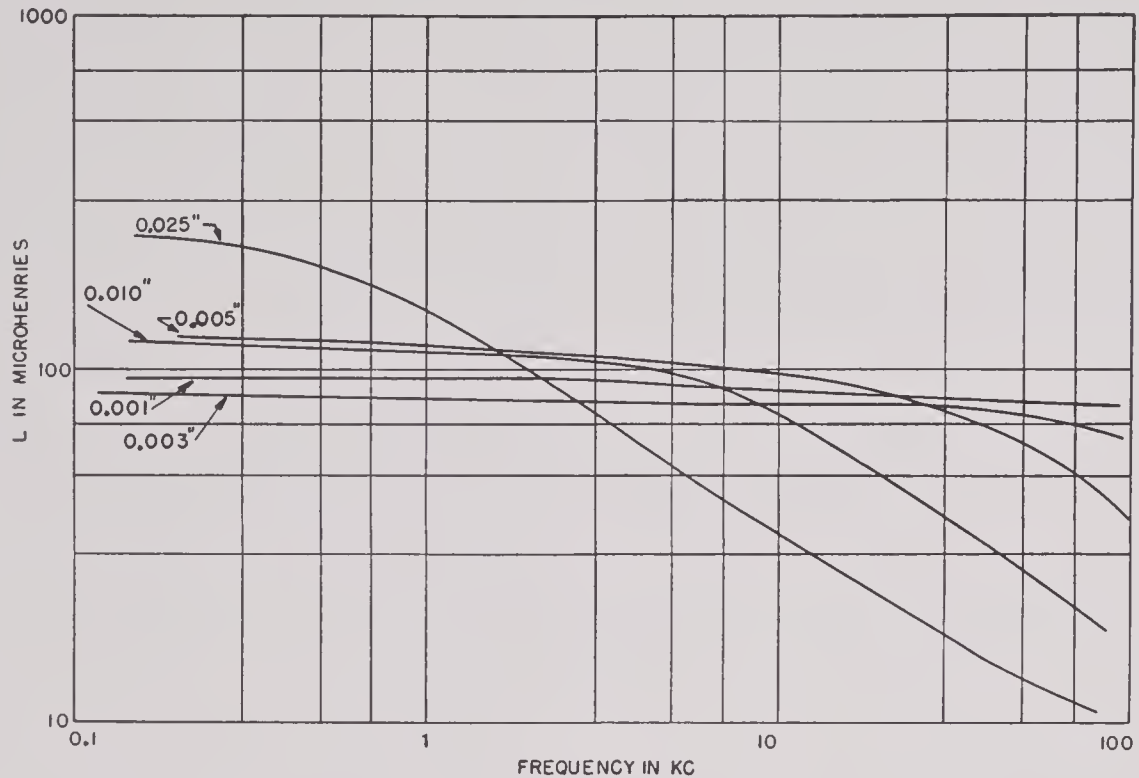


FIGURE 30. Inductance of SPARS stacks as a function of frequency at low levels.

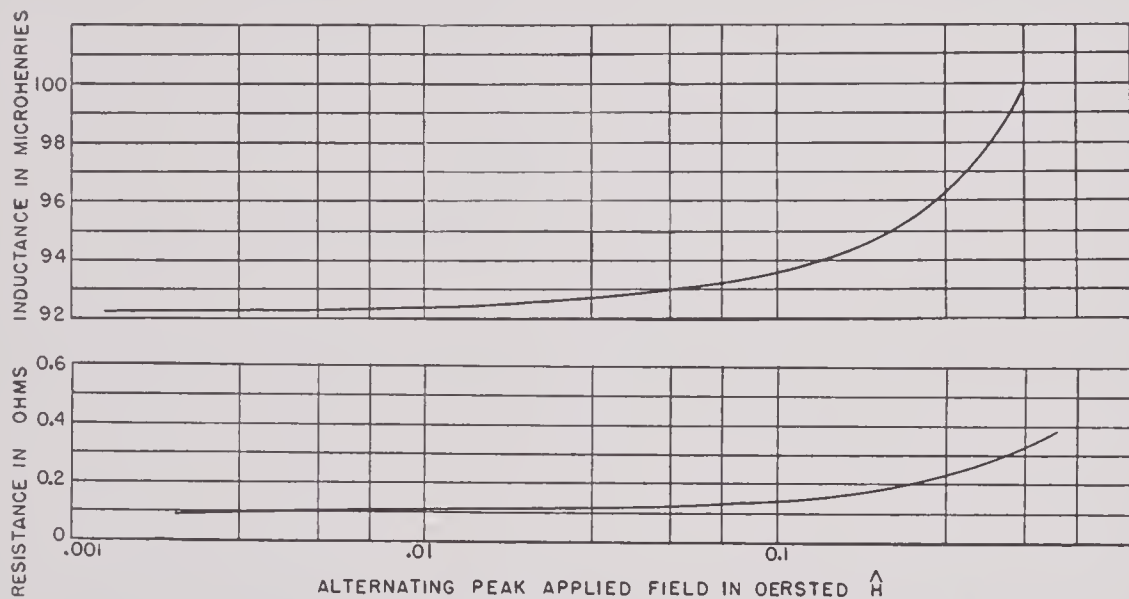


FIGURE 31. Variation in resistance and inductance for very small applied fields.

two extremes of lamination thickness as well as that of which most of HUSL's practical transducers were constructed.

Figures 32, 33, and 34 present most of this observational data in approximately 90 curves. In all cases these figures show plots of resistance and reactance as a function of the peak applied alternating field \hat{H} , measured by the pulsed-bridge technique. As noted earlier, the changes in resistance

and reactance appeared to differ in character, depending on whether the sample under test was or was not subjected to a steady d-c polarizing field. Accordingly, three types of data are presented, namely nonpolarized (Figure 32), polarized (Figure 34), and what has here been called transition data (Figure 33). This latter shows the gradual shift from the nonpolarized to polarized type when measurements are made for successively increasing values of steady

CONFIDENTIAL

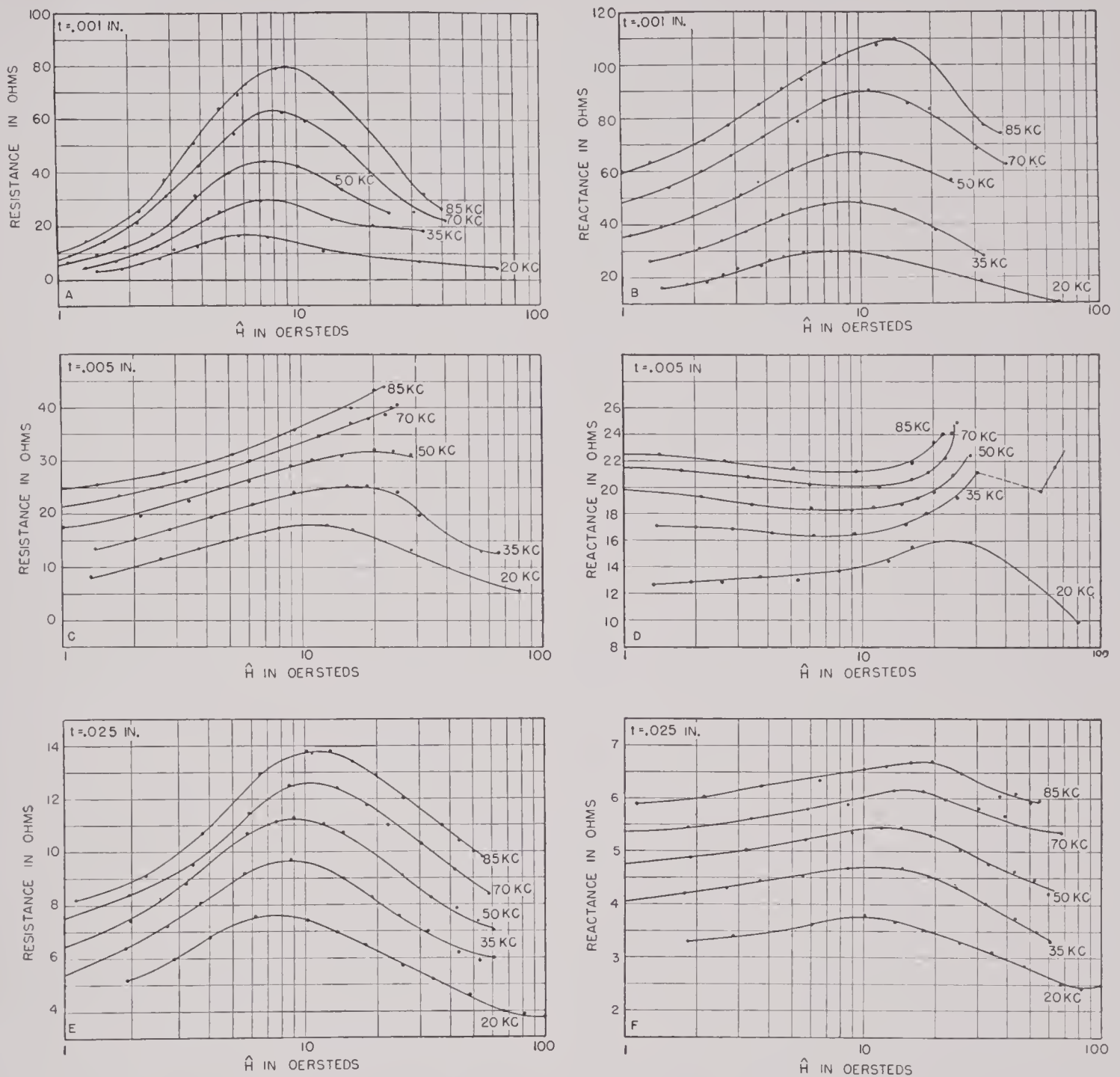


FIGURE 32. Resistance and reactance of unpolarized SPARS as a function of peak alternating field at different frequencies.

polarization H_0 . The range of H_0 extends from values that are small compared with the peak alternating field \hat{H} for most of a test to values large enough to exhibit the characteristics of a typical polarized case.

Figure 32 shows the nonpolarized case, with frequency the parameter in each family of curves. The range of this parameter was determined roughly by the required magnitude of the bridge components and their believed frequency characteristics. Fre-

quencies in the neighborhood of the mechanical resonance of the stacks were avoided in order to minimize motional magnetostrictive effects. Values of 20, 35, 50, 70, and 85 kc were chosen. The outstanding characteristic of these families is that there is a maximum in the majority of the curves for relatively low values of \hat{H} . In a rough way this maximum may be accounted for in terms of the variation of permeability with peak driving field \hat{H} .

CONFIDENTIAL

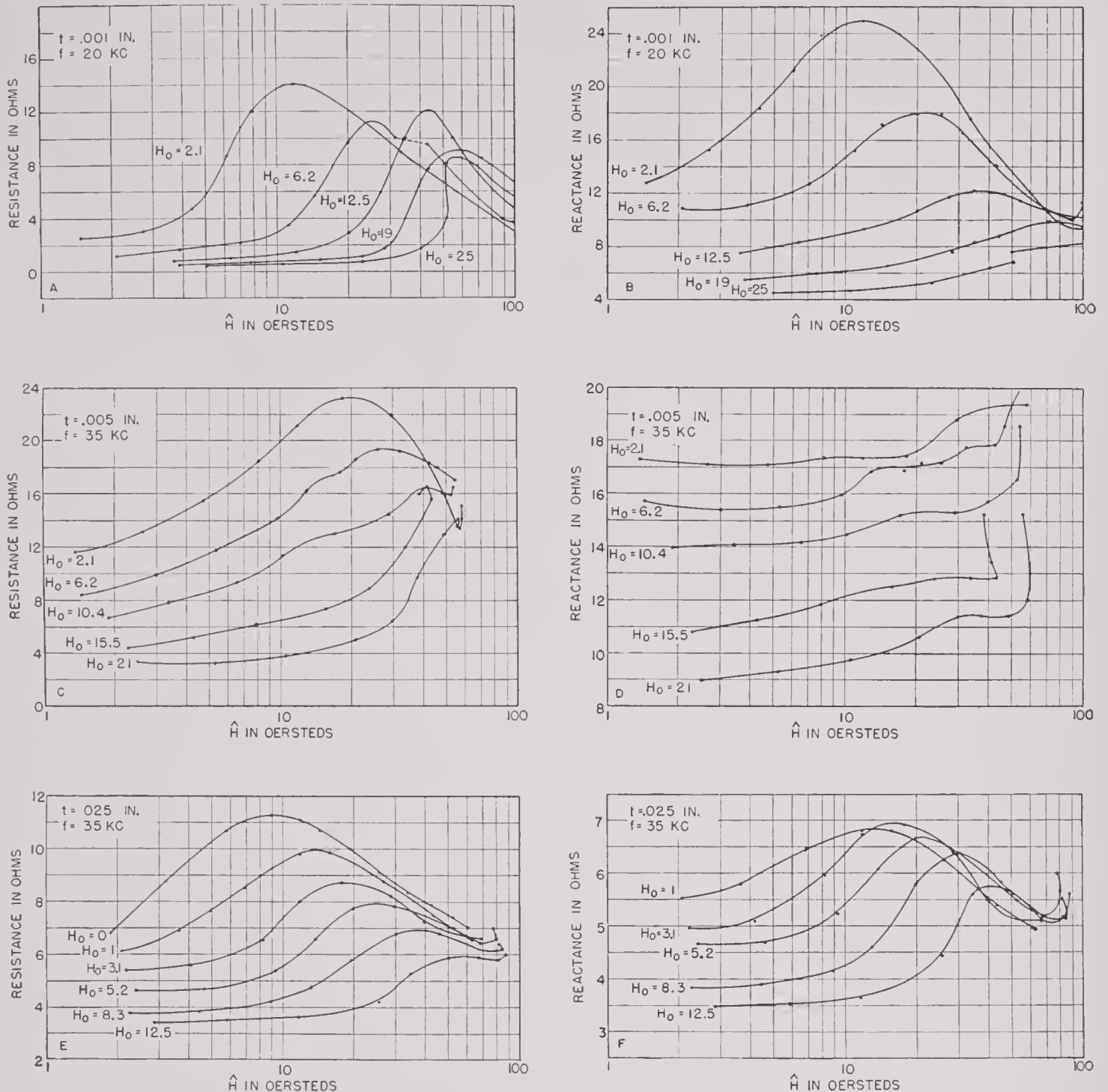


FIGURE 33. Resistance and reactance of SPARS as a function of peak alternating field for different values of polarizing field.

Figure 35 shows a plot of $\mu = B/H$ for the 0.001-in. lamination. This curve has a maximum at 6 oersteds. It was then assumed that H varied sinusoidally with time, and for each of several peak values of H average values of permeability $\bar{\mu}$ were computed. These are shown plotted on the same area as a function of \hat{H} . The net result is to lower the effective permeability for any given \hat{H} below approximately 9.8 oersteds and to increase it for \hat{H} above that value.

At the same time the maximum is shifted to about 8.5 oersteds. The curve of reactance for 20 kc in Figure 32B has its maximum at slightly over 8 oersteds.

On the other hand, the variational permeability measured near a steady $B_0 = 3,800$ gaussses increases smoothly as the variational amplitude is increased.⁷ This accounts in general for the two main types of data observed. For both the 1-mil and 25-mil cases

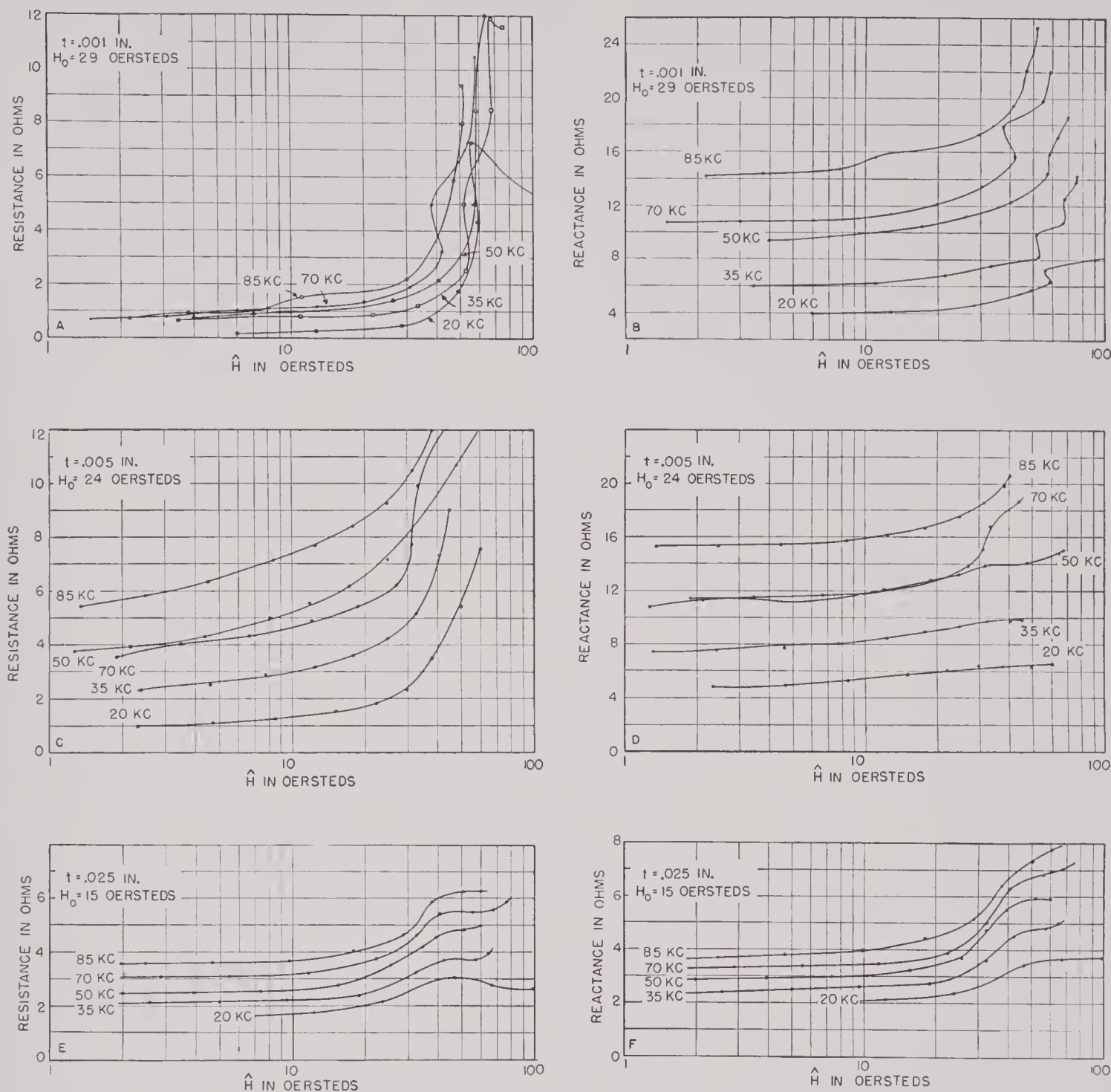


FIGURE 34. Resistance and reactance of polarized SPARS as a function of peak alternating field at different frequencies and constant value of polarizing field.

the maximum is without exception common to all resistance and reactance curves. Similarly, in all cases the maximum in the resistance appears at lower values of \hat{H} than the maximum in the corresponding reactance curves. For both resistance and reactance this maximum moves toward higher values of \hat{H} as frequency increases.

The families for the 5-mil stack exhibit characteristics slightly different from those common to

both a thinner and a thicker lamination. Here the maximum in the resistance curve is less pronounced. At the lowest frequency it occurs at a value of \hat{H} equal to or higher than that at even the highest frequency in the other two cases. The shift of this maximum toward higher \hat{H} is more pronounced as frequency increases. In fact there is doubt whether the maximum exists at frequencies of 70 and 85 kc.

Data taken on a second sample indicate a sharp

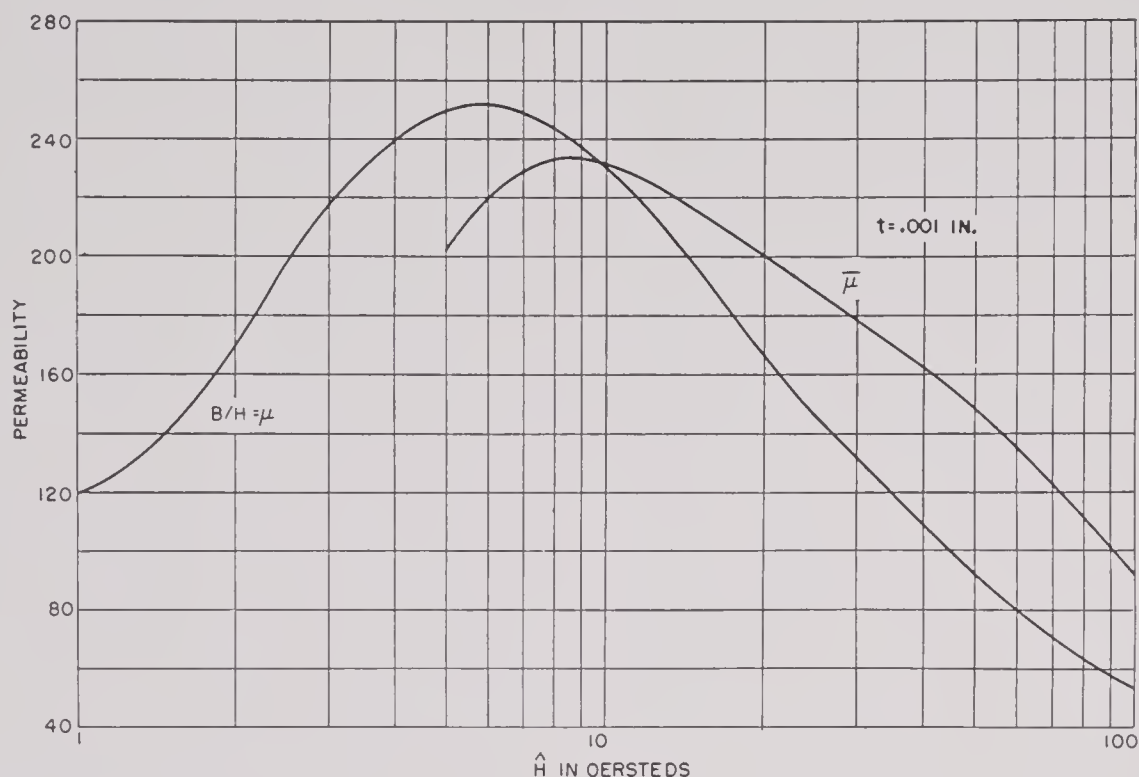


FIGURE 35. Variation in μ and $\bar{\mu}$ of 0.001-in. SPARS lamination with peak alternating field.

upward trend of these two curves in the neighborhood of \hat{H} equal to 30 oersteds. The curves of reactance exhibit even greater differences. At 20 kc the reactance *increases* with \hat{H} and passes through a maximum. For 85 kc it first *decreases* and then increases, with \hat{H} exhibiting a peculiar discontinuity between 30 and 60 oersteds. The second sample showed only an increase in reactance with \hat{H} at 35 kc and confirmed the maximum occurring for the 20-kc case. The discontinuity shown was definitely observed but it may have resulted from a few pulses of current at higher levels, since unit jumps in the decade of 10-ohm steps were undoubtedly made during the balancing of the bridge. This might have altered, through some rectification process, the magnetic state at which measurements were being made. In fact, it seems more surprising that other discontinuities were not observed than that only a single one should occur in the 30 curves of Figure 32.

On the basis of the eddy-current theory presented in Chapter 3 and by *neglecting hysteresis entirely*, it seems reasonable to expect the data for the 5-mil case to cover a wider range of phenomena. It is the only lamination thickness on which measurements were made whose critical frequency f_c was of such a magnitude that χ_i passed through a maximum and χ_R through a point of inflection within the range of measuring frequencies. This, of course, is based on

an f_c using the initial permeability. For the 1-mil case f/f_c , on the assumption just noted, *did not exceed* 1.2 and for the 25-mil case it was *never less* than approximately 45. By reference to Figure 1 of Chapter 3, it is observed that both χ_i and χ_R are smooth functions approaching limiting values as f/f_c approaches zero and as f/f_c becomes large compared to 2.5.

Confirmation of the expectance of more complex phenomena for the 5-mil case is found in the work of Cauer.⁸ He extended the solution of the classical eddy-current problem in which the permeability is regarded as a constant to a specialized case in which μ is a variable and B is given by Rayleigh's equation, namely

$$B = (\mu_0 + \hat{H})H \pm \frac{\alpha}{2}(\hat{H}^2 - H^2).$$

Here μ_0 is the initial permeability; \hat{H} refers to the maximum value of H , and α is a constant given by the expression¹³

$$\alpha = \hat{\mu} \frac{(\hat{\mu} - \mu_0)}{\hat{B}}.$$

The diacritical mark \wedge refers to the maximum value of the quantity.

Complete solution under the above assumptions would involve production of harmonics, but Cauer has carried out the solution for the fundamental

only. For a-c bridge measurements as made here, this is the solution that applies, since filters of high discrimination eliminated all harmonics. Legg¹³ has summarized Cauer's results and it is of interest to show that the results presented here for the 5-mil case are in qualitative agreement, at least with Cauer's⁸ complicated analysis. He found, for example, that the apparent permeability μ as calculated from inductance measurements is given theoretically by the expression

$$\mu = \frac{\mu_0 \sinh \theta + \sin \theta}{\theta \cosh \theta + \cos \theta} + \alpha \hat{H} \left(1 - \frac{4\theta^2}{9\pi} - \frac{7\theta^4}{60} + \frac{2\theta^6}{45\pi} + \dots \right),$$

where $\theta = 2\pi t \sqrt{\mu_0 f / \rho}$ with ρ in emu. This analysis predicts that the apparent permeability will decrease with increasing H for frequencies higher than that necessary to make $\theta > 1.6$ approximately. By assuming $\theta = 1.6$, $\rho = 8 \times 10^{-6}$ ohm cm for nickel, it can be found that for any frequency above the one given by

$$f = \frac{8.06}{\mu_0 t^2} \times 10^7 \quad (11)$$

the apparent permeability, or in this case the measured reactance, will decrease with increasing H . For the 5-mil example, from the equation above, $f = 2.8 \times 10^4$ was obtained. Reference to Figure 32D shows that at 20 kc the reactance is increasing with \hat{H} up to the maximum, while at 35 kc and higher the reactance is decreasing up to peak fields of approximately 10 oersteds. For the 1-mil example, equation (11) yields a value of 920 kilocycles as the critical frequency for the change of sign in the slope of the reactance vs applied field curve.

On the other hand, for the 25-mil example the frequency given by (11) is 571 c. This would indicate that all the reactance curves of Figure 32F should start with a negative rather than a positive slope. The thickness of this lamination is roughly a third of its breadth, so that the usual assumption that the thickness is small compared with the breadth is probably not justified. This would undoubtedly modify the ordinary linear theory of eddy currents and probably also Cauer's extended treatment.

Figure 33 shows the six families of so-called transition curves. The family for the resistance of the 25-mil laminations shows the smoothest transition between the types represented by Figures 32 and 34. Hysteresis losses are believed to be much more in

evidence in this type of family than in that of Figure 32. The areas of the hysteresis loops of Figure 28 have been found to have the following relative values.

$$\frac{\text{Area 1 mil}}{\text{Area 25 mil}} \approx 2, \quad \frac{\text{Area 5 mil}}{\text{Area 25 mil}} \approx 1.9.$$

The importance of eddy-current losses relative to hysteresis losses decreases on proceeding from 25 to 1 mil. Hence the diminution of eddy-current losses and the largest hysteresis losses combine in the 1-mil sample to produce the sharpest rise of resistance as a function of \hat{H} . For 25 mils the eddy-current shielding has certainly greatly reduced the effective volume of the nickel, and again hysteresis losses are minimized in this sample and no very marked resistance increases are noted. It is also of interest to note that the relative change in apparent permeability in B is much less than the relative increase in resistance, again an indication that hysteresis losses are most important in the 1-mil case. Family D, the 5-mil example, again exhibits the most peculiar characteristics. The apparent permeability as reflected in the reactance curves first decreases and then increases in only two of the five cases, even though the frequency is above 28 kc. It would be a difficult matter in these hybrid families to know how to calculate the frequency marking the change in initial slope of the reactance versus \hat{H} curve.

It is believed that this data is of little value beyond satisfaction of curiosity as to how one type of family merges into the other. If one were interested in the detail of electric wave forms, these findings would probably be of more value.

Figure 34 shows the six families of curves taken in each case for a steady polarization H_0 to produce a magnetic induction B_0 of 3,900 gauss. The different values of H_0 to be used for the various lamination thicknesses were determined from the magnetization curves of Figure 27. The families for the 25-mil example display the smallest increments in either R or X with frequency. As noted earlier, eddy-current shielding reducing the active volume of nickel, the inherently small hysteresis loss per cycle in this sample, and the very large value of f/f_c for all measured points combine to bring about the small changes noted. The 5-mil sample shows no marked change in sign of the slope of reactance curve. Using a value of 4.8 ohms as the smallest measured reactance at 20 kc yields an effective permeability of 35. Applying this value to equation (11) yields a value for f of 92

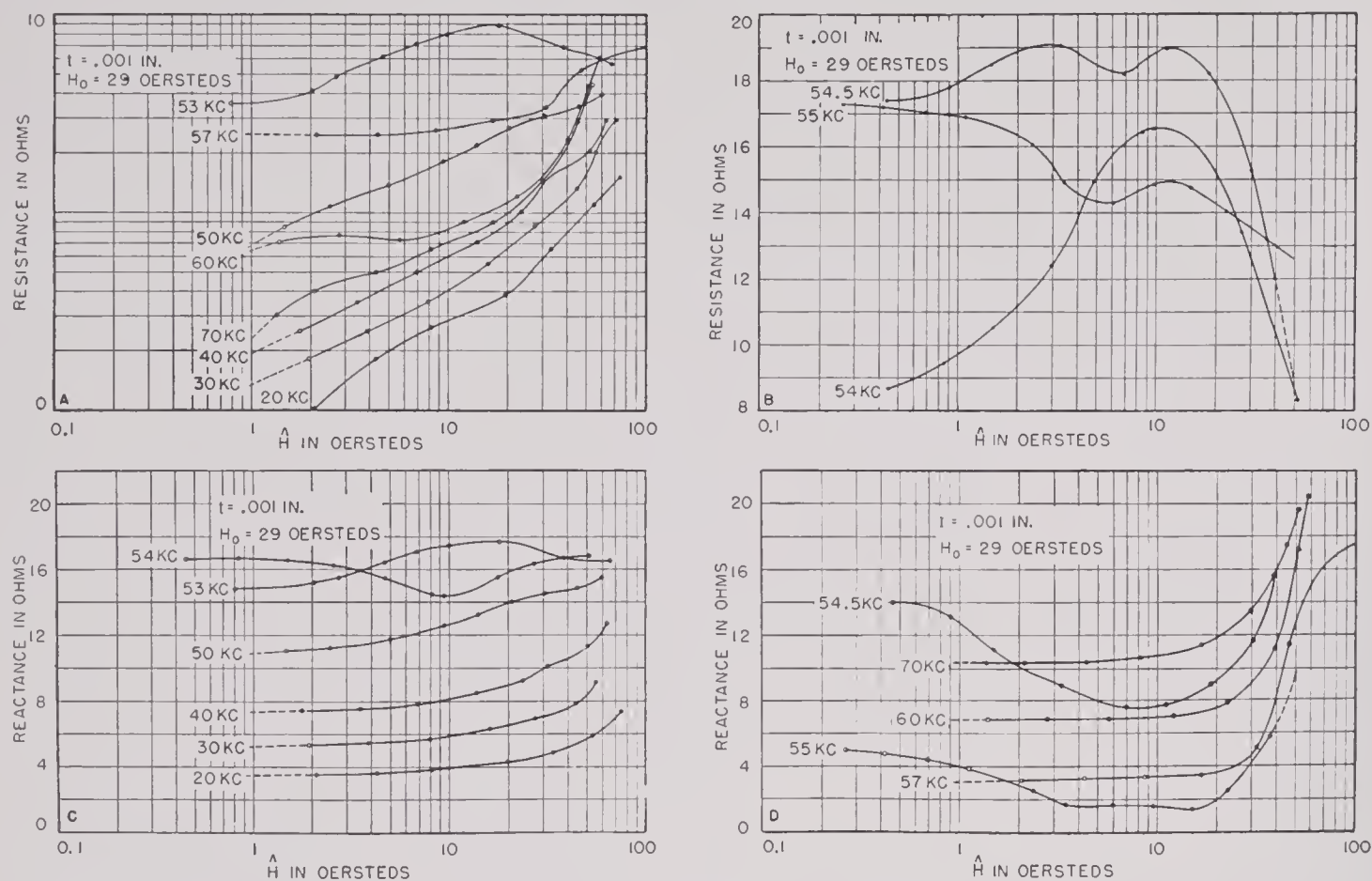


FIGURE 36. Resistance and reactance at various frequencies of SPARS transducer in air as a function of peak alternating field.

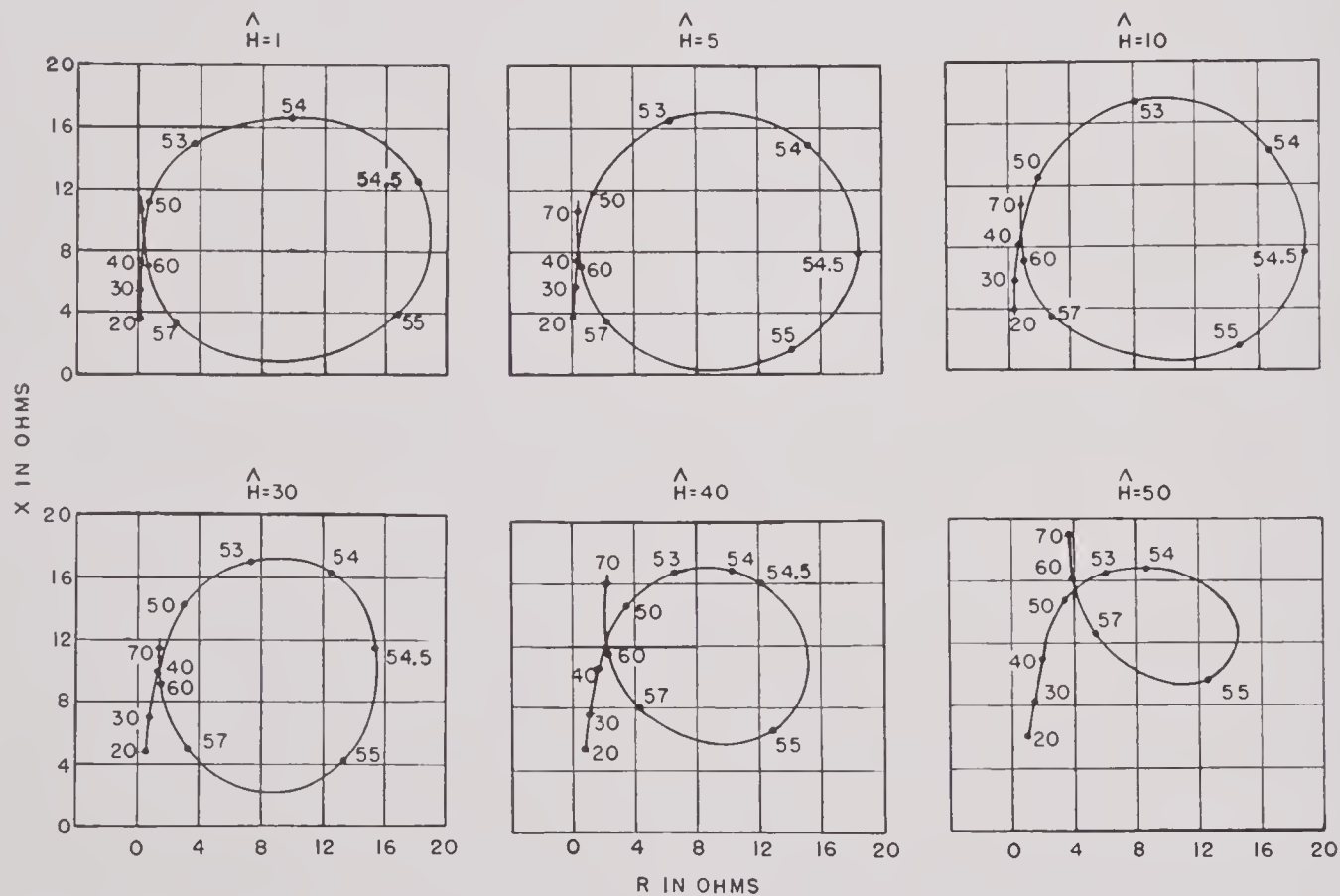


FIGURE 37. Impedance circles of SPARS transducer in air for different constant values of peak alternating field. $H_0 = 29$ oersteds, $t = 0.001$ in.

CONFIDENTIAL

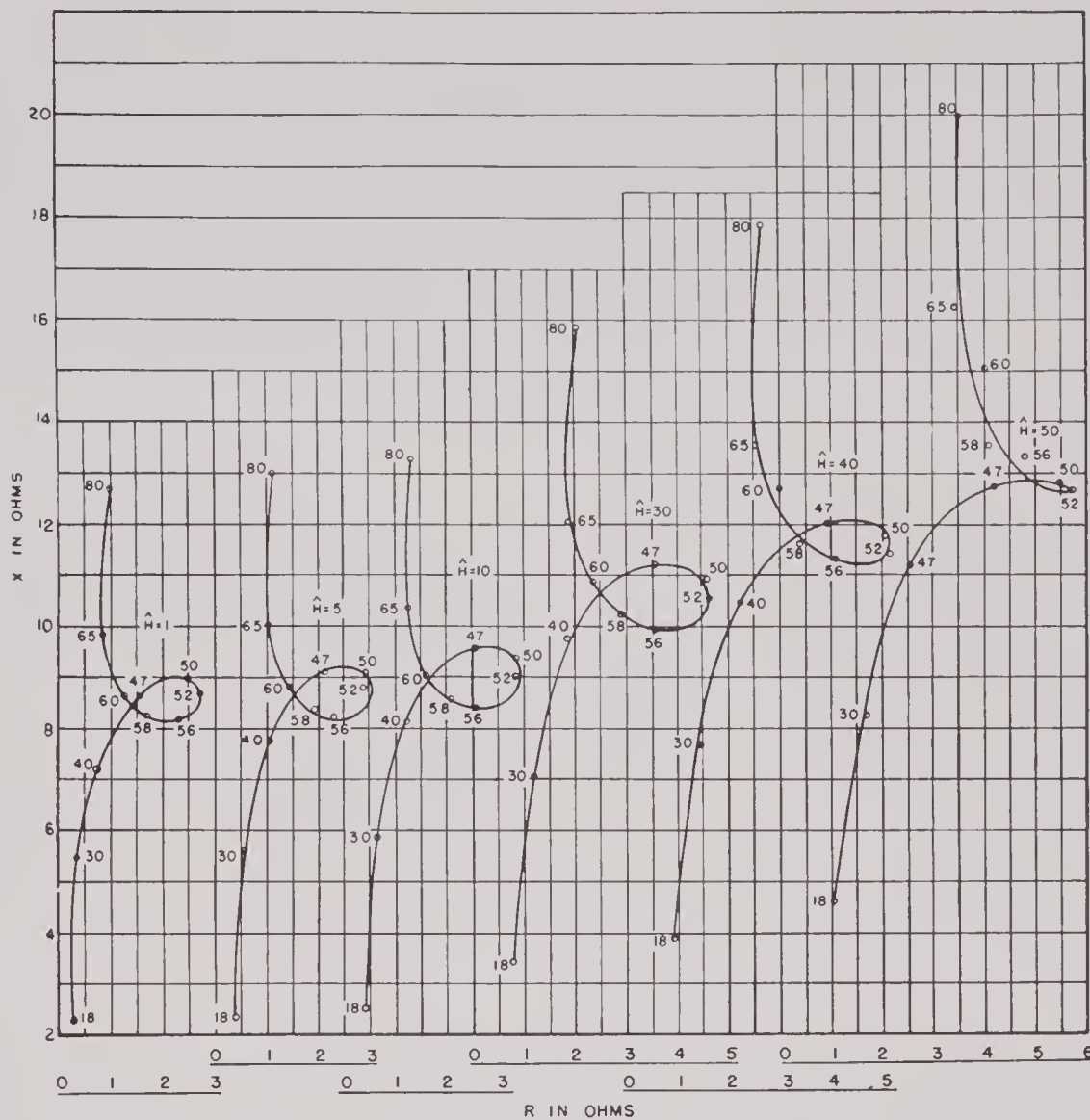


FIGURE 38. Data corresponding to Figure 37 but with transducer in water.

ke, which on Cauer's theory is the critical frequency for change in sign of the slope of the apparent permeability curve. All measurements, however, were below this frequency. Again, the 1-mil family displays very sharp increases in resistance at values of \hat{H} a little in excess of H_0 . This is believed to result largely from hysteresis loss. Evidence of hysteresis effects are rather obvious in the stepwise jumps in the reactance curves at high values of H and probably result from the process of balancing the bridge.

It is also illuminating to make a study of the total angle of lag arising from eddy currents and hysteresis. S. Butterworth and F. D. Smith¹¹ have shown that

$$\frac{R_{\text{core}}}{\omega L_{\text{core}}} = \tan(\zeta + \eta),$$

where ζ and η are the angles of lag arising from these

two effects. The total angle ($\zeta + \eta$) may be derived from the data shown in Figures 32, 33, and 34. Only a few computations of this angle were made and they were in general agreement with what was to be expected. For the 25-mil sample the angle was always greater than 45 degrees, indicating the asymptotic value of the eddy-current lag angle in agreement with the high value of f/f_c . For the 1-mil sample at the other extreme, the total angle at low levels was only a few degrees but rose rapidly in the region where \hat{H} exceeded H_0 in the polarized case.

Much more may be done toward interpretation of the data by Cauer's theory and the aim here has been to present the data in sufficient detail so that anyone interested may carry out additional computations. There has been no opportunity to attempt to separate the losses by standard methods such as

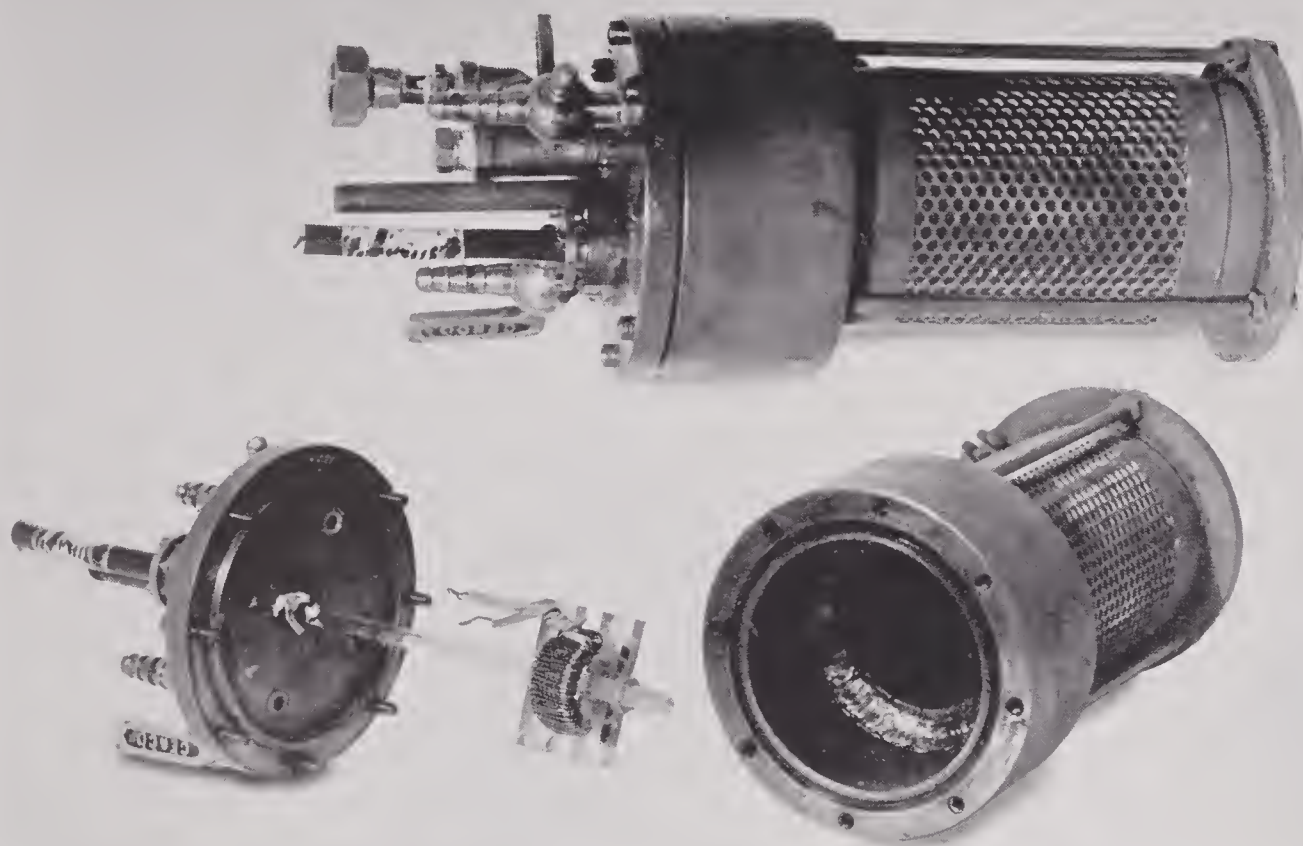


FIGURE 39. Modified pressure chamber.

outlined by Legg. It is believed at least that at the lower levels his methods should apply. Then perhaps Cauer's work will be useful at slightly higher fields, though it is probable that as yet no adequate theory has been developed for the highest levels.

After the data were taken with the three test cores wound tightly with 70 turns of wire, they were each unwound and reassembled with pressure-release material isolating the nickel stacks between fiber rings. Windings of 60 turns were then put on to make a typical ring stack transducer as described in Chapter 6. The 60-turn winding was tried out on the 1-mil stack and sufficient data taken to obtain vector impedance loci by sectioning runs made at constant frequency.

This procedure was exactly similar to that used earlier in connection with the SPEP element. Curves of resistance and reactance as a function of peak-applied alternating field (\hat{H}) are shown in Figure 36 for each of eleven different frequencies. These data were taken with the stack in air. For six constant values of \hat{H} , resistance and reactance values were read from the curves; the six vector impedance loci

are shown in Figure 37. This example reflects the maximum motional effects. Figure 38 is similar to Figure 37 except that the stack was submerged in water and the overall effects here include that of loading. Data for Figure 38 were, of course, taken from a series of curves analogous to those shown in Figure 36. By use of the data from Figure 34 in conjunction with that of Figure 36 and by the best possible estimation of the leakage inductance, it is probable that a reasonable separation of purely motional resistance and reactance could be made. If this were done, deviations from the predictions of small signal impedance data would be obtained. Unfortunately, lack of time prevented this analysis.

Finally it may be of interest to note that the pressure container shown in Figures 8 and 9 was not suitable for acoustical measurements on ring stacks. The vessel and stack mounting shown in Figure 39 was devised, having symmetry about its vertical axis. Here perforated metal was used to prevent the bulging of the rubber side walls under pressure. Practically no acoustical measurements were made with this device and the question of polarized driving ver-

CONFIDENTIAL

sus half-frequency driving with no polarization had to be deferred for the case of ring stacks. The type of mounting, however, illustrates a useful construction for further work.

11.6 CONCLUDING COMMENT

It should again be emphasized that the material presented here represents a general survey of the phenomena to be encountered and of the problems arising in the field of high-level operation. It is not a precision study. In extending the matter further it is suggested that a rather critical appraisal of the data presented should be undertaken first. Accompanying this should be a thorough study of the theoretical work that has been published to date in this general field. It is believed that the partial quantitative agreement with certain of Cauer's results justifies this point of view. Specific power losses in nickel may be calculated approximately from the data presented in Figures 32 and 34. The data of Figures 37 and 38, coupled with that of Figure 34, should allow the separation of the purely motional part of the vector impedance loci. A comparison of the air and water circles at the various constant levels should then indi-

cate the trend with level of all properties derivable from motional impedance data. This study should provide evidence concerning the utility or lack of utility of impedance data at high levels.

The phenomena of nonpolarized half-frequency driving certainly merits more exhaustive study, both theoretical and experimental. The rapid decrease of the resistance in the high-field region where acoustic output and efficiency are both increasing should be investigated further. Experimental investigation should be made of the possibilities of nonsinusoidal driving currents, since the idealized theory points definitely in this direction. References have been cited to other nonlinear problems which also support this view. In fact, it is suggested that a careful study of the complex wave forms encountered in high-level driving should be carried out to ascertain definitely the part played by source impedance. For this purpose the development of a power amplifier with adjustable internal impedance and higher output power should be carried out. Similarly a reliable recording-pulse voltmeter with logarithmic scales would greatly facilitate the experimental work. Such an instrument should if possible have the reliability of the well-known Ballantine electronic voltmeter.

Chapter 12

FUTURE DEVELOPMENTS

12.1 MAGNETOSTRICTIVE MATERIALS

12.1.1 New Materials

The ideal material for magnetostrictive transducers would have high coercive force, high reversible permeability, high remanence flux density, high constant of magnetostriction, high electric resistivity, and relatively low cost. It should be capable of being rolled, punched, or formed into accurate shapes. It should have uniform mechanical and chemical properties. A material having the characteristics shown in the second column of Table 1 could be used to make a transducer which would be nearly ideal.

TABLE 1. Characteristic values for ideal and various currently used magnetostrictive materials.

Property	Ideal material (approximate values)	Annealed nickel	Semi-annealed nickel	Annealed 45-Permalloy	Semi-annealed 2V-Permendur
H_c (oersteds)	100	4	25	0.32	25
B_r (lines/cm ²)	5,000	1,400	3,000	10,000	17,000
μ_r (at B_r)	100	80	18	800	50
λ (at B_r)*	2×10^4	0.7×10^4	1.1×10^4	0.22×10^4	1.1×10^4
ρ_r (ohm/cm)	10^{-3}	10×10^{-6}	10×10^{-6}	54×10^{-6}	39×10^{-6}
ρ (g/cm ³)†	3	8.9	8.9	8.3	8.2
E (dynes/cm ²)	5×10^{11}	2.10×10^{12}	2.2×10^{12}	1.4×10^{12}	2.15×10^{12}
η^\ddagger	0.005	0.013	0.030

*Magnetostriction constant.

†Density.

‡Coefficient of magnet hysteresis loss (as in energy loss per cycle = $\eta B^{1.6}$).

A transducer made of a material like this, which could be made to have a Q of 2 and a maximum efficiency of about 80 per cent, would need no polarization other than the magnetic remanence. Unfortunately, some of the values given above are naturally incompatible. For instance, high coercive force and high reversible permeability are natural opposites.

The same is generally true of coercive force and the coefficient of magnetic hysteresis. Consequently, the development of new magnetostrictive materials must be in the direction of finding favorable compromises among the various sets of characteristic values.

The values for several currently used magnetostrictive materials are given in Table 1. At present, 2V-Permendur is the best magnetostrictive material for use at magnetic remanence at reasonably high power levels. In the most efficient geometrical form, i.e., in laminated ring stack, 2V-Permendur can be made to give efficiencies up to 50 per cent and rms pressures of about 10^6 dynes per sq cm at a mechanical Q of about 6 when operating at magnetic remanence. Due to the trends toward high power transmitting it is desirable to have a magnetostrictive material capable of giving acoustic pressures of the order of 2×10^6 to 5×10^6 dynes per sq cm when operating at magnetic remanence and at mechanical Q 's of the order of 6 to 12. The material should not be prohibitively expensive, as 2V-Permendur is at \$8.30 per lb.

If a material could be found that has all the ideal properties suggested except the high coercive force, it could still be used very satisfactorily in many designs by polarizing it with permanent magnets or with direct current in the windings.

12.1.2 New Techniques in Making and Treating Materials

ROLLING, SINTERING POWDERS, ELECTROPLATING

The magnetic and magnetostrictive properties of some metals and alloys can be influenced to a considerable extent by the degree of cold-working to which they are subjected before heat treatment. Sometimes the direction of rolling produces definite orientation effects which are quite desirable for use in certain types of elements. Consequently in the development of new materials not only new alloys but different methods of mechanical preparation and heat treatment should be tried.

The idea of making magnetostrictive transducer

elements by consolidating powdered magnetostrictive metals in accurately formed molds (in about the same manner as consolidated powder transformer cores are made) is very attractive because of its inherent simplicity. Some experiments of this type, in which powdered nickel and powdered 45-Permalloy were used, have been tried¹³ without success. In a material thus formed, the electric contact between particles must be small, the Young's modulus large and uniform, and the internal friction nearly as small as that in a solid metal. The samples made up to the date of this writing have shown only very small magnetostriction and rather high internal friction. It is possible that proper methods of powdering, consolidation, and heat treatment could result in a satisfactory material. The advantages of such a material, compared with the conventional stacks of laminations, would justify the expenditure of a considerable amount of time and effort to develop it.

Forming magnetostrictive elements by electroplating has some attractive advantages over other methods, especially if the material could be deposited in layers, with considerable resistivity between the successive layers. Some experiments have been performed along this line without very much success. It was found that semiconducting layers of oxides or sulfides covering the previously deposited layer of nickel did not have enough conductivity and did not provide a proper base for the deposition of the next layer. The magnetostrictive quality of the nickel so deposited was found inferior to that of rolled nickel sheet that has been properly heat treated. However, the possibility of forming laminated tubes or plates by electroplating magnetostrictive material is interesting and the advantages it offers make further consideration and experimentation worth while.

HEAT TREATMENTS

Much work has been done in the past in determining the effects of various heat treatments on the magnetic and magnetostrictive properties of metals. This is particularly true of nickel, 45-Permalloy, and 2V-Permendur. The results of this work show that the initial structure of the metal, the temperature, the time, and the atmosphere in which the annealing is done all affect the result. It is also known in a general way that heat treating in a magnetic field can influence the magnetic and magnetostrictive properties of the material. On the basis of the magnetic domain theory of magnetism, it can be shown that the magnetostriction of a sample with all its domains

oriented transverse to the final field direction by heat treatment in a magnetic field should be $3/2$ times that of a sample of the same material whose magnetic domains are oriented at random. Very little experimental work has been done along this line. The possible gain in magnetostrictive properties indicates that further work would be worth while.

12.2 PERMANENT MAGNET MATERIALS

It has been shown in previous chapters that when the return paths of the polarizing flux and the high-frequency flux are separate, magnets made of some of the Alnico alloys can be used to provide the polarizing flux. This is especially true of those transducers in which there is adequate space between the vibrating elements for the relatively bulky magnets. In such cases it is good practice to shield out the high-frequency flux from the Alnico magnets to prevent losses due to eddy currents. The Alnico alloys, naturally very brittle materials, must be cast in relatively thick sections and consequently cannot be laminated to minimize eddy-current losses. Nevertheless it is economical and practical to use the commercial varieties of Alnico magnets in certain types of magnetostrictive transducers.

There are many cases in which the space available for the transducer elements is so limited that there is not sufficient room for polarizing magnets outside the element itself. In these cases it is convenient and practical to include the polarizing magnet in the high-frequency flux path. Polarizing magnets so used should occupy the smallest possible fraction of the length of the high-frequency flux path so as not to increase the reluctance of the high-frequency magnetic circuit more than is absolutely necessary. The polarizing magnet material should, therefore, have a very high coercive force, even at the expense of flux density. To minimize losses due to eddy currents and eddy-current shielding, the permanent magnets used as part of the high-frequency magnetic circuit should have a very high resistivity or be laminated or both. Such magnets should also have as high a reversible permeability as is consistent with the required large coercive force. The material of this type which has proved best up to the time of this writing is sintered iron oxide (Vectolite), a permanent magnet material made by the General Electric Company. Although sintered iron oxide is satisfactory in most respects, it would be better if it could be made to have a higher coercive force, a greater remanence

flux density, and a greater permeability for high-frequency flux. The ideal permanent magnet material for use in polarizing transducer elements by inserting the magnet in the high-frequency magnetic path should have the following approximate characteristics:

1. $H_c \geq 1,000$ oersteds.
2. $B_r \geq 2,000$ lines per sq cm.
3. $\rho_c \geq 10^{-2}$ ohm-cm.
4. $\mu_r \geq 5$.
5. Negligible magnetic hysteresis loss.
6. Should be capable of being formed or molded to accurate mechanical dimensions.
7. Should maintain nearly its full coercive force up to temperatures as great as 250 F.

It is possible that some material similar to sintered oxide could be developed that would have the properties listed above. It is also possible that some metallic alloy with the desired properties might be developed. It would be practical to compromise on a lower value of resistivity if the material had, in addition to all the other properties listed, the property of malleability, so that it could be rolled into sheets thin enough to make the eddy-current losses very small.

12.3 RADIALLY VIBRATING RINGS

12.3.1 Conventional Ring Stacks

CONSTRUCTION OF STACKS

Satisfactory methods of punching and heat-treating ring-shaped laminations have already been discussed in Chapter 6. The new types of design and construction suggested below may be of interest in special applications.

The method usually employed to reduce the mechanical Q of a ring stack is to decrease the ratio of wall thickness to mean radius. This automatically decreases the crushing strength of the ring stack. A method of reducing the Q without decreasing the strength of the walls is to intersperse rings of aluminum, magnesium, or their alloys between rings of magnetostrictive material. In rings made of the light alloy the velocity of sound should be very nearly the same as that in the magnetostrictive rings but their mass is much less. Mixing the two types of laminations causes an increase in radiation resistance, without a proportionate increase in the mass of the vibrating parts, and a consequent lowering of the Q . The electromechanical efficiency would be decreased

by about the same amount as that of a stack composed entirely of magnetostrictive material but having a wall thickness with the same mechanical Q as the composite stack.

The problem, never so far satisfactorily solved, of polarizing ring stacks made of magnetically soft magnetostrictive materials could be resolved by using the permanent magnet material proposed in Section 12.2 as a magnet extending across the diameter of the stack. This magnet would be surrounded by a winding and would furnish a return path for the high-frequency flux as well as provide the polarizing flux.

When the laminations of a ring stack are firmly bonded together, mechanical coupling between the longitudinal and radial modes of vibration sometimes causes trouble. This trouble generally occurs when the natural frequency of one of the longitudinal modes of vibration is nearly equal to that of the radial mode of vibration. Troubles of this kind might be eliminated by breaking the stack into longitudinal segments, with laminations of corprene or air-cell neoprene cemented between the segments. The height of the segments would be determined by the size of the rings and the frequency at which they are to be operated.

METHODS OF MOUNTING AND HOUSING

Many methods of mounting and housing ring-stack transducers have been developed to fit the specific requirements of different jobs. One of the most common uses of ring stacks is in echo repeaters, where the electrical, mechanical, and acoustical coupling between the transmitting and receiving transducers must be kept at a minimum. Nearly all the designs for echo repeaters have used ring stacks in isolated mounts, housed in rubber tubes and filled with castor oil. This type of construction is inherently complicated and expensive. Some further development work in the direction of simplifying ring-stack housings and water seals for echo repeaters and similar devices is indicated.

The design and construction of conventional singly mounted ring stacks used as monitors or as noise sources have been described in detail in Chapter 6. These mountings and housings are quite simple and rugged and improvements will be mainly in minor details.

An unusual method of winding and housing a ring stack, illustrated in Figure 1, was suggested but never tried. In this design the copper case also serves as the single-turn toroidal winding of the ring stack and the

enclosed transformer. The cable leads are attached to the terminals of the enclosed transformer's secondary winding, which has the proper number of turns to give the desired impedance for the device. Acoustic contact between the outside wall of the housing and the ring stack can be made by using

vious way of making any marked improvements over the present forms until new magnetostrictive materials are developed that have sufficient coercive force and remanence to make possible the construction of toroidally wound tubular units that can be operated at reasonably high power levels at magnetic remanence without danger of demagnetization. A material that nearly meets the magnetic and magnetostriction requirements is 2V-Permendur but whether or not it can be drawn into tubular form is questionable. Also, it is almost prohibitively expensive.

12.3.3 Flat-Wound Scrolls and Layer-Built Tubes

CONSOLIDATION

Flat-wound scrolls and layer-built tubes or rings (layer-built tubes are made of discrete layers of laminations, like an onion) are superior to solid-walled tubes or rings in that the eddy-current losses are less because of the lamination effect. However, when these are used as radial vibrators, pressure must be transmitted from layer to layer uniformly and without loss. It is, therefore, necessary that all the voids between successive layers be completely filled with solid bonding material. A great amount of development work has been done at the Bell Telephone Laboratories and at Harvard on methods of producing satisfactory impregnation and bonding of transducer cores of this type. Only moderate success has been attained. The economical use of magnetostrictive material and the flexibility of design which are characteristic of this method of making rings and tubes make it worth while to continue research on methods of consolidating the layers perfectly. In addition to giving good adhesion and mechanical contact between successive layers of laminations, the method should also leave the lamination layers properly heat-treated and free of mechanical strains which detract from the optimum magnetic and magnetostrictive performance.

POLARIZATION

The lamination effect of ring-shaped scrolls or layer-built rings can be utilized only if the magnetic circuit is purely circumferential. This means that the polarizing flux must be maintained by the use of a component of direct current in a toroidal winding or that the material must be operated at its magnetic remanence. Polarizing current is undesirable because of all the auxiliary equipment it entails. The best

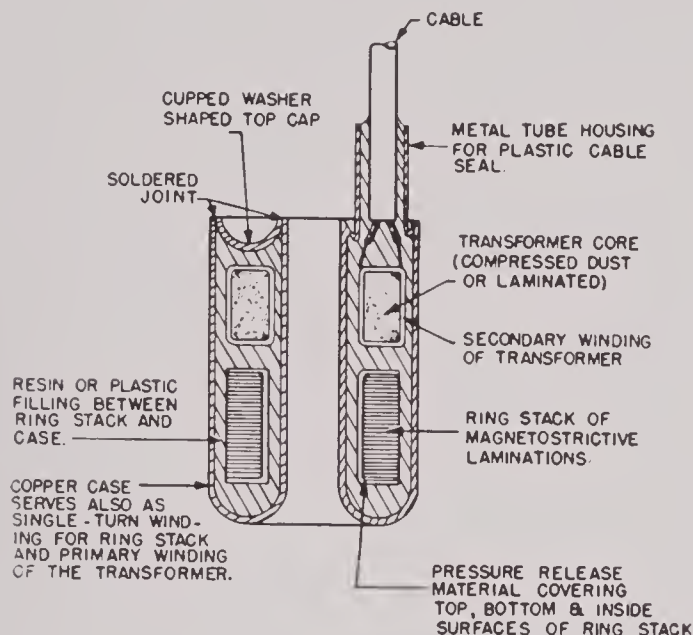


FIGURE 1. A design for a ring-stack transducer in which the case serves as a single-turn toroidal winding. Any desired output impedance is obtained by use of the self-enclosed transformer.

some type of plastic or liquid filling free from any gas bubbles or voids. These units are rugged, simple, and easy to manufacture. They could be readily adapted for use with radio sono buoys, echo repeaters, noise sources, etc. They should be able to withstand submersion to great depths without danger of crushing or leaking.

12.3.2 Solid-Walled Tubes

Solid-walled tubes can be wound toroidally so that the magnetic flux is circumferential, or a core piece or polarizing magnet can be inserted across the diameter with a coil surrounding it so that the flux path extends across the tube parallel to the diameter and returns circumferentially through the two halves of the magnetostrictive tube (B-19 type). The toroidally wound type is inherently more efficient because the high-frequency flux remains within the tube wall, whereas in the second type the flux must enter and leave the tube walls at the opposite ends of the diameter. Both these types have been developed to a considerable degree of perfection. There is no ob-

solution to the problem is the development of a magnetostrictive material that can be operated with high efficiency at high power levels at magnetic remanence without danger of depolarization.

12.3.1 Edgewise-Wound Tape to Form Tubes

Stacks of ring-shaped laminations make the most nearly ideal radial magnetostrictive vibrators. However, the production of such ring laminations wastes magnetostrictive material, since the rings must be punched from flat sheets. This waste may be eliminated by making the tubes or rings by edgewise winding of narrow tape made of magnetostrictive metal. The width of the tape should be very nearly equal to the desired wall thickness of the final tube or ring. After the tape is wound it should be consolidated with a resin to form a firm solid-walled structure. It appears that this method could be applied particularly well to the construction of relatively thin-walled tubes. Some experimental work on this method has been pursued at HUSL but without much success. The samples made showed lower permeability and higher internal mechanical damping than equivalent ring stacks of standard construction. There is no reason to believe, however, that the difficulties cannot be overcome by development of the proper techniques.

The problem of polarizing rings or tubes of this type is the same as for standard laminated ring stacks.

12.4 LONGITUDINALLY VIBRATING LAMINATED STACKS

12.4.1 Conventional Forms — HP and SP Types

Most of the problems involved in making conventional punchings have been solved in one way or another. Very good dies are required to punch laminations from thin, tough nickel sheet without the formation of bad burrs at the edges. Some improvements could be made in methods of collecting laminations from the punch press, cleaning them, and annealing them. Several reasonably successful methods of consolidating laminations into stacks have been developed and described. However, problems keep arising in the production of laminated stack transducers which indicate that considerable improvement could be made in the methods.

The design of laminations of the HP and SP types proved to be quite satisfactory. It has been suggested that laminations might be modified in shape and size so that two frequencies of resonance fall close enough together with the proper degree of mechanical coupling to obtain a flat frequency response over a short frequency interval. This result was obtained accidentally in the laminations of the HP-1 transducer. Also, experiments have been made by building stacks made up of short stack segments of slightly different lengths. Broadened frequency responses have been obtained by these methods but always at the expense of maximum efficiency. Further systematic investigation of this effect would be of theoretical interest and possibly of some practical importance.

Methods of supporting and mounting laminated stacks in a more rugged and efficient manner should be developed. This is particularly true of those transducers that must be subjected to great mechanical shocks and stresses. Many new methods have already been proposed in the preceding chapters.

12.4.2 Bookphone Type

The original *bookphone* described in Chapter 7 did not prove to be of practical importance because of difficulties involved in attaching the ends of the booklike laminated stacks to the diaphragm plates and because of the imperfect high-frequency magnetic circuits. Experience gained in design and techniques since the bookphone type of transducer was first investigated indicates that a practical and efficient transducer of this type could now be made. However, about the only advantage of the bookphone type over the HP or SP types is that the laminations can be made without any waste of material.

12.5 TUBE-AND-PLATE TRANSDUCERS

Tube-and-plate type transducers are perhaps the oldest and the best developed type of magnetostrictive transducers. The QC series of sharp-beam echoranging transducers used by the Navy for years have demonstrated their ruggedness, stability, and practicability. The QC series of transducers have moderate efficiencies because of their relatively high mechanical Q 's. Some of the later models are polarized with permanent magnets so that no auxiliary equipment is needed for polarizing current.

Improvements most needed in transducers of this type are lower mechanical Q 's and higher efficiencies.

Much experimental work has been done in this line by Peek² of the Bell Telephone Laboratories. By use of thin-walled annealed nickel tubes and a diaphragm of magnesium alloy, Peek was able to make a transducer which is about 10 per cent efficient at a mechanical Q of 10. This is about as high an efficiency as can be obtained with a tube-and-plate type of transducer at this Q . There is some question, therefore, as to whether much time should be spent in developing further details of the tube-and-plate type of transducer when transducers of lower Q , greater efficiency, and equal ruggedness can be made with laminated-stack elements. The chief practical argument in favor of the use of tube-and-plate transducers is that they use much less magnetostrictive material than do the laminated stack types.

If tube-and-plate type elements of relatively high Q are to be developed for use in multielement transducers, where the elements must match each other closely in phase, methods must be found for matching the frequencies of the individual elements within very close tolerance.

12.6 MULTIELEMENT CYLINDRICAL TRANSDUCERS

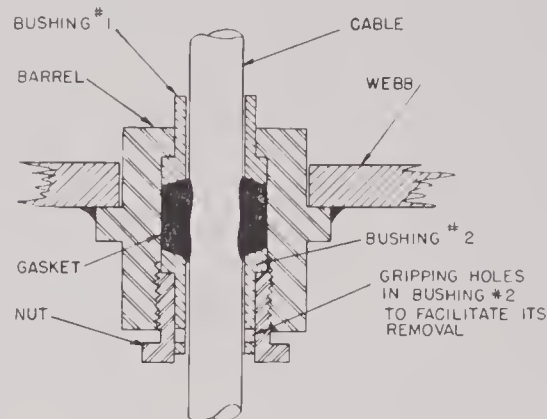
12.6.1 General Strength and Ruggedness

Most of the multielement cylindrical transducers designed and constructed have been reasonably strong, rugged, and satisfactory for operation down to depths of the order of 400 to 500 ft of water. It is desirable, however, to make transducers that will withstand at least twice these external pressures in order to withstand depth charges and deep submersions without breaking down. Improved methods of making cast or forged frames for these large transducers should be developed because much trouble has been experienced with porous places in the metal castings. Attention should also be paid to chemical corrosion resistance of exposed parts of the transducers.

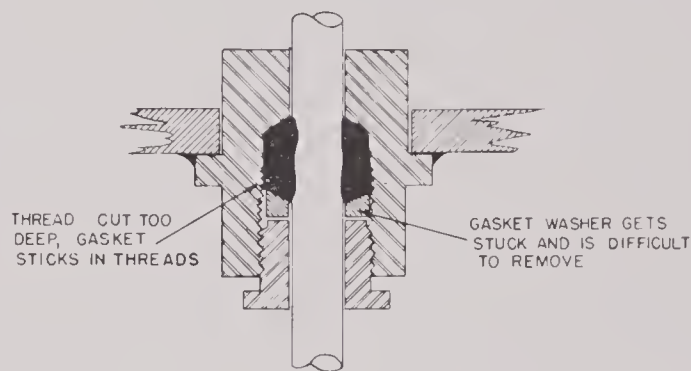
There are some advantages in housing the elements of a cylindrical transducer separately in watertight containers easily removable from the main frame of the transducer. All developments in this direction have so far been unsuccessful. If the advantages of removable separate elements are deemed great enough, more development work along this line should be done.

It is difficult to make satisfactory cable seals for

the large cables needed for multielement transducers on submarines. The seals should be designed to hold satisfactorily at water pressures as great as 500 or more lb per sq in. At pressures as high as these, the cables tend to extrude through the water seal. In the design of new water seals, attention should also be paid to the ease with which the seal can be taken



A TYPE THAT IS EASILY TAKEN APART



B TYPE THAT IS VERY DIFFICULT TO TAKE APART

FIGURE 2. Two cable seals which have equally good sealing qualities but widely different disassembly characteristics.

apart after it has been assembled for a long time. To illustrate this Figure 2 shows two large cable seals with equal sealing powers. The one shown in A, however, can be taken apart much more easily than the one shown in B.

Most of the water seals between flanges and plates of large transducers make use of rubber gaskets in a tongue-and-groove assembly. In this type of seal it is common practice to leave 0.015 in. or more clearance between the tongue and the groove wall on the water side of the gasket in order that the excess rubber of the gasket can extrude between the tongue and the groove when the two flanges are bolted down tight, metal to metal. This method has been quite

successful. Another successful type of seal uses a rather close-fitting tongue-and-groove with a corprene gasket. The corprene gasket is made with dimensions giving it a volume about 10 per cent greater than the closed volume of the tongue-and-groove gasket chamber. The compressibility of the cork particles in the corprene gives the gasket resilience so that the seal remains tight regardless of temperature changes and aging.

Most sonar transducers have rubber parts which are exposed to the sea water, mineral oil, grease, etc. When on topside-mounted transducers on submarines, the rubber is also subjected to the action of sunlight and air. The rubber used for such parts should be as highly resistant as possible to the agents just listed and should be, in addition, acoustically transparent and mechanically strong and tough. The ρ c rubber developed for the Navy by the Goodrich Rubber Company has most of the characteristics mentioned except high mechanical strength and resistance to decomposition by the action of sunlight. Further development work should be done toward making a rubber or rubber-like material which has all the desirable characteristics listed above.

Transducers must often be mounted in places where surfaces in the vicinity of the transducer give troublesome reflections of sound. These reflection troubles could be greatly reduced if the reflecting surfaces could be covered with some rubber-like material which has a ρ c nearly equal to that of water and a very high coefficient of absorption. Butyl rubber more nearly fills these requirements than any other generally known type, but it is not good enough at the usual sonar frequencies. The development of a better material of this type would be very worth while.

12.6.2 Cost of Production

The cost of producing magnetostrictive multi-element transducers of the laminated stack type which had been completed before the time of this writing range upward from about \$8,000 each. Of this amount, about \$1,200 is required to purchase the nickel strip material from which the laminations are punched. This amount cannot be reduced unless the price of nickel is reduced. It is believed that in routine production, by use of good manufacturing economy, the cost of transducers of this type could be brought down to about \$5,000 or \$6,000.

The cost of the nickel used in a tube-and-plate type

of multielement transducer would be almost insignificant, but the labor cost of the manufacture of the multiplicity of small accurate parts would still be quite high, so that the total cost would be about \$5,000.

12.6.3 Noncircular Transducers for Eliminating Domes

When the conventional cylindrical-shaped multi-element transducer is mounted on a ship that can travel at speeds greater than 10 or 12 knots, the transducer must be surrounded by a streamlined dome which is acoustically transparent in the regions where the main acoustic beam of the transducer strikes it. The streamlined dome is necessary to prevent turbulence and cavitation of the water around the transducer. It has been suggested independently by various persons that the necessity for a dome might be eliminated if the shape of the transducer itself be an approximately streamlined form. If the active faces of the elements should be made to fall on such a streamlined contour, each element would have to be equipped with an electric delay section so that the electric signals would be phased as if they had come directly from elements mounted on a cylinder.

Another way of accomplishing the same result would be to mount the elements so that their active faces fall on a cylinder and to make the transducer case in a streamlined form. This would be equivalent to building the dome on the transducer rather than on the ship.

12.6.1 Submarine Types

Transducers used on submarines must be capable of withstanding greater external hydraulic pressures and greater shock wave pressures than those used on surface craft. If submarines are intended to go to depths of 1,000 ft, the transducer must be capable of withstanding static hydraulic pressures of 450 lb per sq in. and should be able to withstand twice that amount in order to have a reasonable factor of safety. The transducer must also be capable of withstanding impulsive pressures as great as the submarine itself will withstand. These requirements make it necessary to design all parts of the transducer frame stronger than those for use on surface craft. These requirements also make it necessary to design and construct the vibrating elements of the transducer so that they

will not collapse or become inoperative when subjected to large hydraulic pressures.

It has been found that laminated stacks of the HP type have strength enough to withstand compressive loads of 2,000 or more lb per sq in. pressing on the active faces. However, in this type of construction there are two weak places. The first is the small gap between the active faces of neighboring stacks where the rubber boot is not supported. High external hydraulic pressures cause the rubber boot material to extrude into the gaps between the elements. Under extreme conditions this would cut the boot and cause trouble. The second weak point is at the back faces of the laminated stacks where the stacks rest against the cushioning material on the spool core. If the laminated stacks contain magnet slots, the bearing area at the back end of the stack is only about 0.4 that of the front face. Consequently, the bearing pressure of the back faces of the stacks against the cushioning material is about 2.5 times the pressure on the active face. Thus, for pressures of the order of 500 lb per sq in. on the active face, the pressures exerted by the back faces against the cushioning material are of the order of 1,250 lb per sq in. Such pressures are sufficient to crush or deform most cushioning materials, especially if the layer is very thick. Consequently, the cushioning material will be forced into the magnet slot and the gaps between neighboring stacks. This trouble can be decreased to some extent by placing a strip of bakelite, laminated glass fiber, or aluminum between the back faces of the stacks and the layer of cushioning material, so that there is a greater bearing area and no open gaps into which the cushioning material can extrude. However, when material of appreciable mass is added to back faces of the stacks, undesirable frequency changes may result. Consequently, the material should be small in mass, stiff, and uniform. A considerable amount of research work should be done toward finding or developing better cushioning (i.e., pressure-release) materials which will withstand great static pressures without permanent deformation and without losing their pressure release or cushioning properties. Also, some methods should be worked out for properly supporting the rubber boot over its entire inner surface. The most obvious method would be to extend the faces of the laminated stacks so that the gap between the edges of the faces would be too small to allow extrusion of the rubber boot material. This would entail some other difficulties, however.

The problem of making trustworthy cable seals for transducers used on submarines is somewhat complicated. This problem should be given further experimental study and improved forms of seals should be developed.

12.7 HIGH-POWER TRANSDUCERS

When underwater-sound echo-ranging systems are used on high-speed vessels, the noise level produced in the water by the ship is so high that the intensity of the echoes must be relatively high to be detected above the noise. In this case the best method for increasing the signal-to-noise ratio is to increase the signal strength. This can be accomplished by increasing the strength of the initial ping. The only limitations to the ultimate power levels that can be reached are the ability of the water to transmit the power without cavitating and the ability of the transducer to convert electrical power to mechanical power without breakdown or saturation.

It has been found that the acoustic pressure may be increased to several times the local hydrostatic pressure in water if the periods of transmission are of quite short duration. For example, if the transmission periods are made as short as one millisecond, the acoustic pressure may be made many times as high as atmospheric pressure without trouble from cavitation.

The upper power limit on magnetostrictive transducers is set by magnetic saturation of the magnetostrictive material and by the efficiency of the transducer elements. It has been shown (Chapter 11) that the upper limit to the mechanical power which can be produced by annealed nickel is about Q_{mf} 5 watts per cu cm of *active* nickel. In radially vibrating ring stacks the entire volume of nickel is fully active, whereas in the tubes of a tube-and-plate transducer or the legs of the HP type of laminated stacks only about one-half of the actual volume of nickel approximates full activity. The amount of this available mechanical power which is converted into acoustical power in the water is determined by the mechanical efficiency of the unit.

It is estimated from actual measurements at lower power levels that the maximum acoustic pressure that can be produced in water at the active face of the 26-ke HP-3 type cylindrical transducer is about 3 or 4×10^6 dynes per sq cm (20 to 30 watts per sq in.). This is at a Q_m of approximately 10. If the laminations should be redesigned to give twice this Q , then the maximum acoustic power output could be

doubled, provided the mechanical efficiency remained constant.

Unfortunately, transducers with very high mechanical Q 's cannot respond fully to very short pulses. Consequently, the requirement that the transmitting pulses must be short in order that the water can absorb the power without cavitating and that the mechanical Q of a magnetostrictive transducer must be high to make it capable of producing high acoustic power levels are inconsistent. It appears, therefore, that transducers intended for use at extremely high power levels for very short pulses should be made of

piezoelectric crystals which have higher electro-mechanical coupling coefficients than magnetostrictive materials and which can be operated at lower Q 's. This does not mean that magnetostrictive transducers cannot be used for moderately high power applications. For example, the Sangamo 26-ke QH cylindrical transducer, which has an active face approximately 18 in. in diameter and 16 in. high and a mechanical Q of 12, should be capable of giving, during short pulses, as much as 15 kw of acoustic power in the water from about 60 to 80 kw of electric input power.

Chapter 13

THEORY AND DESIGN OF MAGNETOSTRICTION SCANNING SONAR TRANSDUCERS

13.1 FUNDAMENTAL REQUIREMENTS

13.1.1 Principle of Operation of Beam Scanning Systems

In a typical horizontal scanning sonar system the transducer is used as a transmitter and as a receiver. First, it is used to transmit a strong pulse of high-frequency sound into the water uniformly in all directions in the horizontal plane. Second, it is used to receive the echoes of the original pulse which are reflected from various objects in the surrounding water in such a manner that the electric receiving network connected to the transducer can indicate the direction from which the echoes come. The distance to the reflecting object is determined from the velocity of sound in water and the time interval between the initial pulse and the reception of the echo.

Accurate determination of the direction from which the echo comes requires that the electric receiving network, with the aid of the transducer, form a sharp directional acoustic receiving beam of sensitivity in the horizontal plane, and this beam of sensitivity must be rotated in the horizontal plane at such a rate that the revolution of scanning requires less time than the length of the initial pulse of sound. The general scheme is illustrated in Figure 1.

The beam of receiving sensitivity may be fixed with respect to the transducer and the transducer rotated, or the transducer may be fixed and the beam of receiving sensitivity rotated electrically with respect to the transducer. This latter system has proved to be the more practical because higher scanning speeds can be attained and fewer mechanical complications are involved. In general, two types of electric rotation of the beam of receiving sensitivity have been developed. One of these types involves the use of a mechanically rotated commutator which links the transducer elements to the beam-forming network by electric or magnetic coupling. In the other general type the coupling between the trans-

ducer elements and the electric receiving network is made through electronic vacuum tubes or their equivalent. The electronically rotated systems can use much shorter pulse lengths than those that are mechanically rotated. This gives some advantage in signal-to-reverberation ratio, especially if the reflecting object is small.⁹⁰

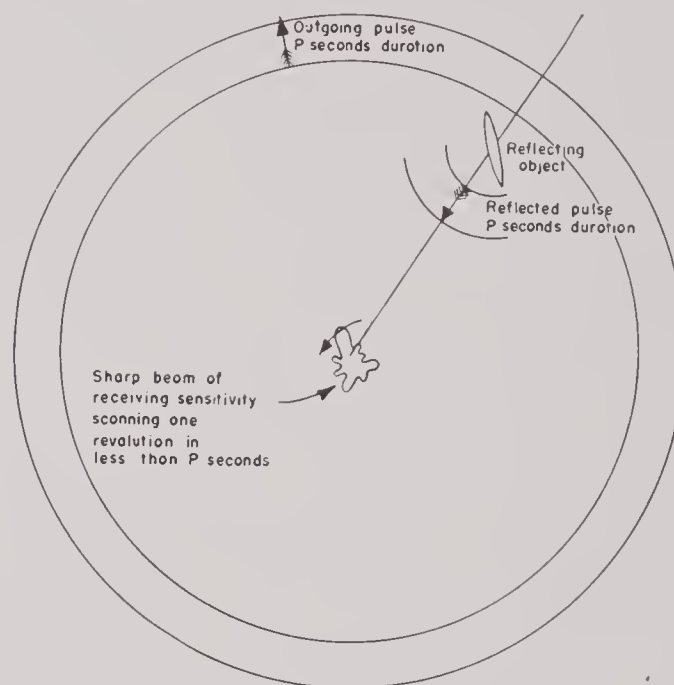


FIGURE 1. Diagram illustrating the basic principles of operation of a scanning sonar system.

13.1.2 Acoustic Patterns

RECEIVING PATTERNS

The function of the typical horizontal scanning sonar transducer requires that it must be made up of quite uniform elements arranged symmetrically about a vertical axis. There is evidence to indicate that satisfactory receiving patterns can be produced only if the distance between centers of the elements, measured around the circumference, does not exceed one-half wave length by more than a few per cent. If the spacing is greater than this, it appears that the

height of the minor lobes, 90 degrees or more around from the major lobe of the receiving beam, will be too great for satisfactory operation.

A diagram of a simplified rotatable beam-forming system for a cylindrical transducer is shown in Figure 2. A front of a sound wave which advances in the direction of the acoustic axis is represented by ww . The transducer elements are represented by the coils arranged around the periphery of the circle. These

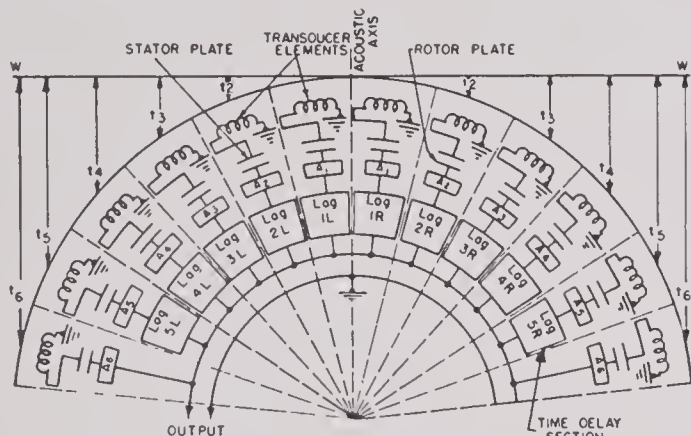


FIGURE 2. Diagram of a simplified rotatable beam-forming system for a cylindrical transducer.

coils are placed in the geometrical positions occupied by the active faces of the transducer elements on the actual transducer in the water. Two wires come from each transducer element to the commutator device. One wire from each transducer element is attached to its respective condenser plate on the stator of the condenser-coupled commutator and the other wire is connected to the system ground. Corresponding to each stator plate is a rotor plate which is connected through an attenuator resistor and a time-delay section to the common output line.

If the center of the beam-forming network is turned in the direction of the acoustic axis, the signal output should be maximum. This condition will be realized if the time-delay sections introduce as much time delay in the signals from the elements as is necessary to compensate for the time delay of the acoustic signal in the water. For example, to make the signal from element 1R come into the output line in phase with that from element 6R, the lag section in series with element 1R should delay the signal by the same amount as the water delays the acoustic signal to element 6R, viz., t_6 sec.

If the rotor of the commutator is turned so that the center of the beam-forming network is not on the acoustic axis, the signals from the various elements are not delayed by the proper amounts to come into

the output line in phase, and hence the total output signal is weak. If the output signal is recorded as the rotor of the commutator is turned, a pattern is obtained which is similar to that obtained by rotating a flat-faced transducer.

The heights of the side lobes of the pattern may be reduced considerably by tapering the amplitude of the signals from the various elements. This is accomplished by use of the attenuator pads marked A_n in Figure 2. The amplitude of the centermost element is not diminished, while that of the outermost element is diminished to about one-fourth of its normal value. A typical receiving pattern taken with a beam-forming system of this general type is shown in Figure 3. The system shown in Figure 2 is diagrammatic only. In the design of the system, arrangements must be made for transmitting as well as for receiving. To make the system efficient, care must be taken to match impedances properly.

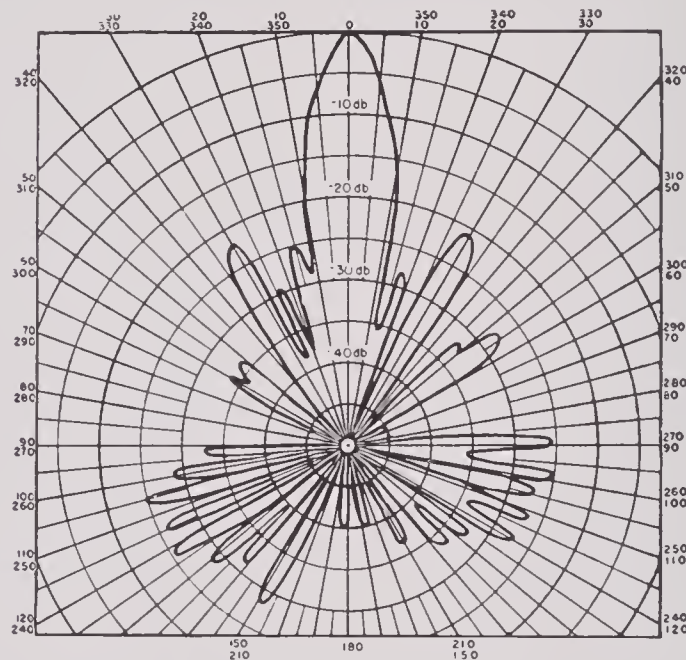


FIGURE 3. A typical receiving pattern taken with a beam-forming system and a 48-element cylindrical transducer.

In the beam-forming network the signal amplitudes and phase shifts must be held to close tolerances if sharp symmetrical acoustic patterns are to be obtained. There are several ways in which unwanted phase shifts can arise in the signals from the elements, some of them in the transducer itself, others in the beam-forming network. The former are of importance in transducer design and construction and will be considered here.

First, the active faces of the transducer elements

must be accurately aligned around a true circular cylindrical surface. Otherwise the times at which the signals in the water arrive at the transducer faces will differ from those for which the beam-forming network is designed.

Second, if the elements are rather sharply resonant and their frequencies of resonance vary, there will be a varying phase difference between the sound pressure on the active face and the velocity of vibration of the stack. The phase of the signal voltage generated in the windings of a magnetostrictive transducer element depends on the phase of the velocity of the element, and consequently any variation of phase between the driving sound pressure and the velocity of vibration of the element will also result in a variation in the phase of the generated signal in the winding. This mechanical phase variation in radians is related to the sharpness of mechanical resonance Q and the fractional deviation of the frequency from the frequency of resonance $\delta f/f_r$ by the relation

$$\phi = \tan^{-1} \left(2Q \frac{\delta f}{f_r} \right), \quad (1)$$

where $Q = f_r / (f_2 - f_1)$, and $f_2 - f_1$ is the difference in the frequencies of the half-power points. In degrees,

$$\phi \approx 114Q \frac{\delta f}{f}. \quad (1a)$$

It is desirable to keep the phase variation due to the variation in the frequencies of resonance of the elements to within ± 6 degrees. This means that the fractional variations of the frequencies of resonance of the elements used in making a transducer should satisfy the relation

$$\frac{\delta f}{f_r} < \frac{0.05}{Q}. \quad (2)$$

A third source of phase variation is that of electric impedance of the elements. Usually the windings of the transducer element are electrically terminated in approximately their complex conjugate impedance at the frequency of resonance. Under these circumstances the current that flows in the circuit is very nearly in phase with the generated voltage in the transducer windings. However, assuming that all termination impedances are identical, the terminal voltages vary with the magnitudes and phase angles of the impedances of the transducer elements. For this reason it is important that magnitudes and phase angles of the impedances of all the elements in a transducer be kept within rather close tolerances.

Experience has indicated that a scanning sonar transducer gives satisfactory uniformity of patterns for all azimuthal directions if the magnitude of the impedance of each element is within ± 5 per cent of the average of all of them and the impedance phase angles are within $\pm 2\frac{1}{2}$ degrees of the average.

Figure 4 shows the distribution of the impedances of the elements at two different frequencies, one at resonance and the other off resonance, for a satisfactory 48-element scanning transducer measured in water.

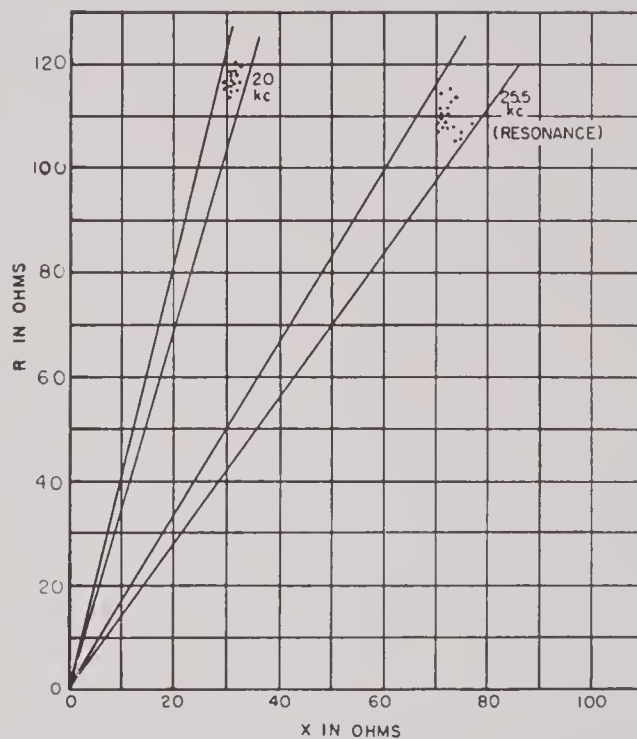


FIGURE 4. Graph showing the distribution of impedances at two different frequencies of a satisfactory 48-element scanning sonar transducer, measured in water.

If high-quality receiving patterns are to be obtained, all elements must make uniform acoustic contact with the water and be of uniform sensitivity. Experience with scanning sonar systems has shown that uniform patterns of good quality are obtained if the sensitivities of the elements are uniform within ± 1 db at any given frequency.

TRANSMITTING PATTERNS

The transmitting pattern in the horizontal plane should be uniform within ± 1 db. Average performance may be obtained even if the variation is ± 2 db. If the elements are sufficiently uniform and well matched to meet the receiving pattern requirements stated above, they will automatically satisfy the re-

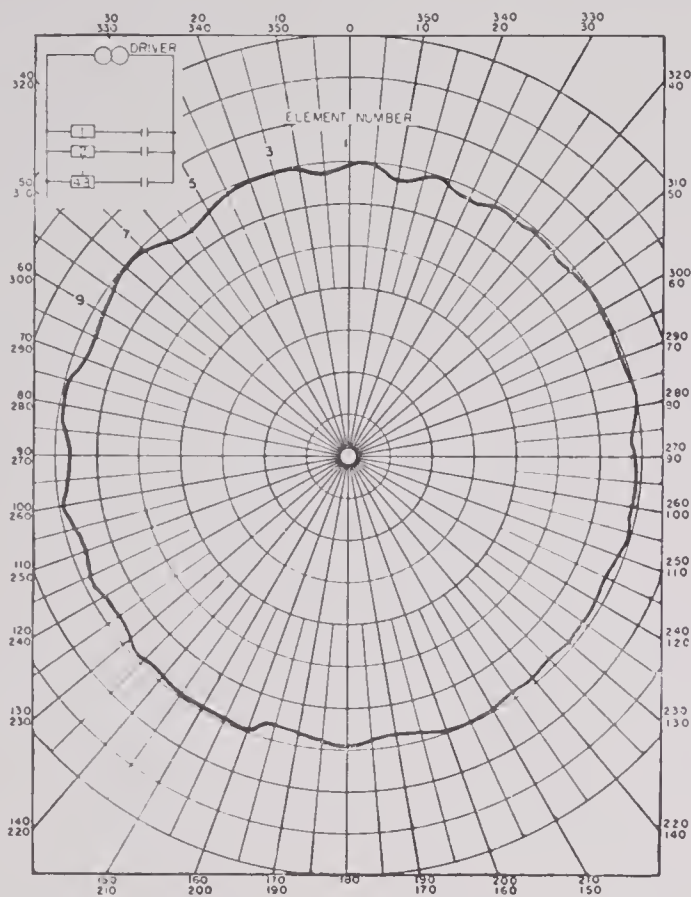


FIGURE 5. A typical transmitting pattern in the horizontal plane using a 48-element cylindrical transducer, circuit as shown.

quirements for good transmitting patterns. A typical transmitting pattern is shown in Figure 5.

The transmitting pattern in the vertical plane should be such as to throw as much of the acoustic power as possible into the main lobe in the region of the horizontal plane. Side lobes should be kept at a minimum but are not critical. The usual patterns produced by a uniform-line source, in which the side lobes are about 13 db lower than the main lobe, are generally satisfactory. If the elements are made up of sections spaced vertically, with inactive gaps between the active sections, the height of the side lobes will be greater than -13 db relative to the main lobe. An example of this type of vertical pattern is shown in Figure 6. If it is desired to reduce materially the heights of the side lobes, it is necessary to divide the elements into vertical sections approximately 1 wave length long, with very short gaps between sections, and taper the amplitude from the center in a parabolic or gaussian manner. It is debatable whether the slight improvement in performance that would result from this adjustment of the vertical pattern is worth the extra trouble and expense involved in effecting it.

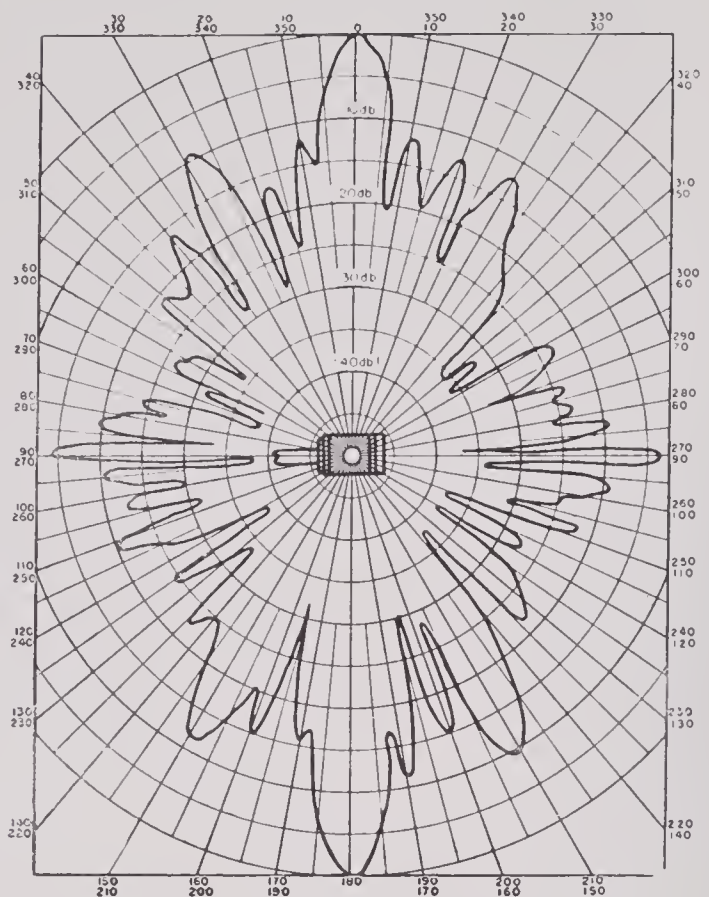


FIGURE 6. A typical vertical transmitting pattern of a 48-element cylindrical transducer in which the elements are made up of four vertical sections separated by short inactive spaces.

One disadvantage of a sharp vertical pattern is that the sound beam overshoots the target submarine if the depth angle of the submarine as seen from the attacking ship exceeds a few degrees. If it is desirable to maintain contact with a deep target at closer ranges with the horizontal scanning system, it is necessary either to widen the beam or tilt it downward. However, any broadening of the beam results in a lower signal-to-noise ratio. In actual practice a compromise must be made between these factors.

One proposed solution is to run three wires to each of the transducer elements so that the full length of the elements can be energized to give a sharp vertical pattern for general long-range searching, or a fraction of the total length of each element can be energized to give a broader vertical beam for maintaining contact with the target at shorter ranges.

Another way of maintaining contact at short ranges would be to tilt the sound beam slightly downward by mechanically tilting the elements or by phasing the vertical sections of the elements. Both these methods, however, are too complicated to be practical.

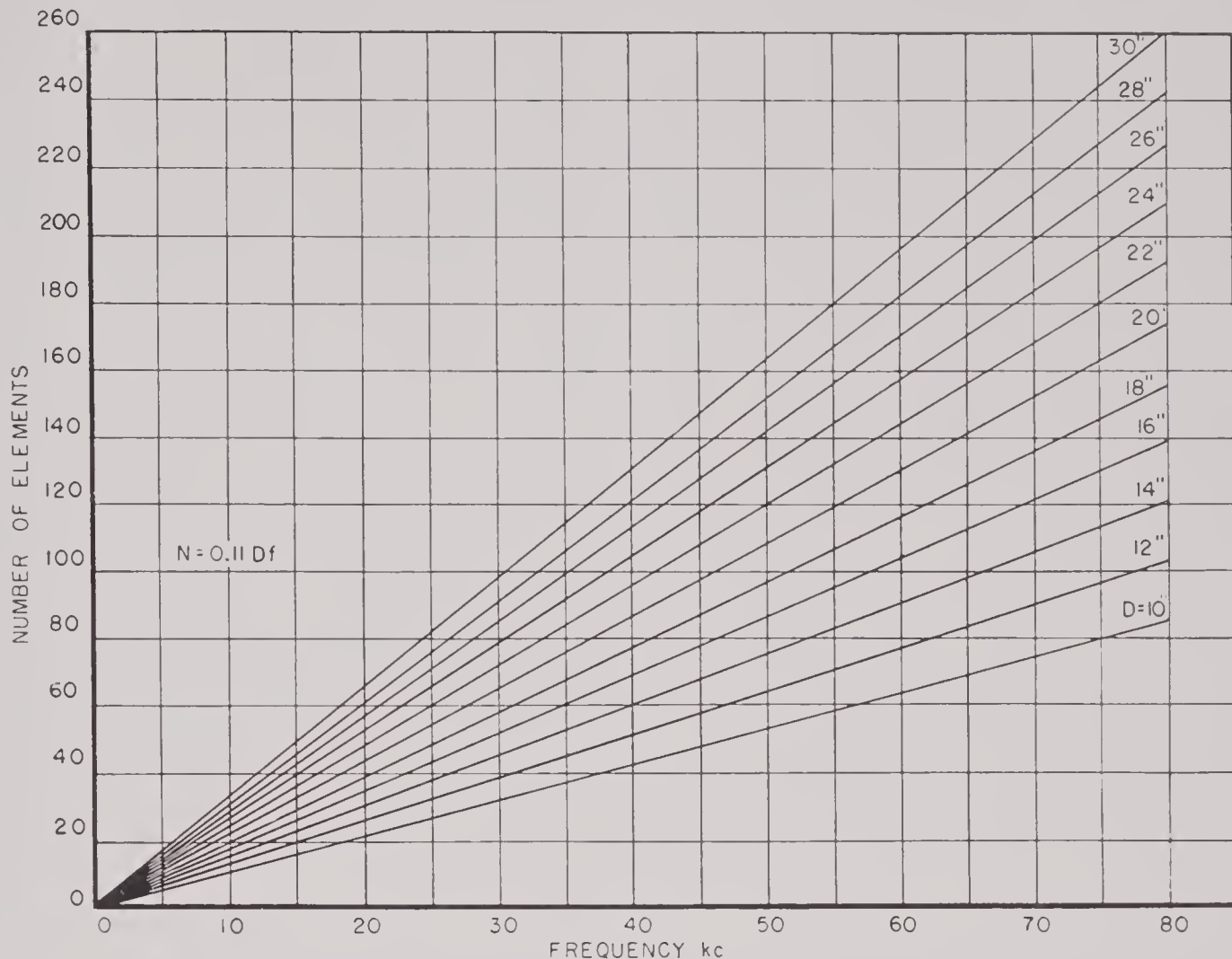


FIGURE 7. Relations among active face diameter D , frequency f , and number of elements N for cylindrical scanning sonar transducers. (The distance between the centers of the active faces of the elements is taken as one-half wave length.)

A more feasible method is to supplement the horizontal scanning system with a separate trainable depth scanning system or a sharp-beam echo-ranging system trainable in three dimensions. In such "integrated" systems the horizontal scanning system is used for general long-range continuous search around the horizon, whereas the other system would be used to maintain accurate contact with the target at close ranges and large depth angles.

The foregoing comments concerning the vertical transmitting patterns apply equally well to the vertical receiving patterns.

13.1.3 Selection of Frequency

ATTENUATION IN MEDIUM AND TRANSDUCER SIZE

After the pattern requirements are agreed upon, the size of the transducer and the frequency of operation must be adjusted to give those patterns. Usually the size of the transducer is limited by the size of

standard sea chests, domes, and mounting equipment on existing ships. The outside diameter of the transducer is usually kept less than 19 in. and the height less than 22 or 23 in. These dimensions automatically set a lower limit on the frequencies that can be used to obtain the desired patterns. The upper limit is set by the attenuation of the sound in the water. It is well known that the attenuation of sound waves in water increases rapidly with increasing frequency. It is difficult in practice to get desirable ranges with frequencies greater than 60 or 70 kc. With transducers of the maximum size mentioned above, it is possible to get patterns of satisfactory sharpness at 26 to 28 kc. If the transducer is made smaller than this, higher frequencies must be used. Figure 7 gives the frequencies that should be used for cylindrical transducers having different numbers of elements and different active face diameters, where the centers of the active faces of the elements are separated by one-half wave length.

RESPONSE CHARACTERISTICS AND TOLERANCES

The type of frequency response desired is determined by two factors. First, it is usually desirable to have a transducer which is capable of operating efficiently over a band of frequencies so that (1) the tuning of the associated electronic circuits is not critical; (2) two ships having the same equipment and operating as a team can each have their frequencies changed so as not to interfere with one another; and (3) any echoes that have considerable change in frequency due to Doppler shift can be received with little loss. Second, the sharpness of mechanical resonance of the transducer elements must be consistent with practical manufacturing tolerances of spread in resonant frequencies of individual elements in order that the requirements on the uniformity of the phases of the received signals are met. This requirement has already been stated in equation (1a).

In general, it is difficult to make magnetostrictive transducers with low Q 's (i.e., broad mechanical resonance) and high efficiencies. This is due to the low electromechanical coupling coefficients of magnetostrictive materials and the inherent eddy-current and magnetic hysteresis losses in them. The electromechanical coupling coefficient can be increased to a limited extent by proper selection and heat treatment of the magnetic materials and by proper design. However, up to the present time the upper limit on the electromechanical coupling coefficient of magnetostrictive materials is about 0.30. Some gain in the frequency band width of efficient operation can be made by reducing the eddy-current losses to very low values by constructing the transducer elements of very thin laminations which are carefully insulated from one another. In most magnetostrictive materials the magnetic hysteresis losses are negligible except at very high power levels, where the magnetic cycle begins to approach the proportions of the major magnetic hysteresis loop.

In the practical design of a scanning sonar transducer of the magnetostrictive type the Q is usually kept as low as possible consistent with the requirements on efficiency.

13.1.1 Efficiency and Power Requirements

Any echo-ranging system will perform as long as the signal-to-noise ratio is great enough. If the ship on which the echo-ranging system is mounted is per-

fectly quiet, the noise against which the signal competes is due to acoustic reverberation and electric noise in the system. Unless the efficiency of the transducer is very low (a fraction of 1 per cent), or the design of the electric receiving gear is poor, the noise level is due almost entirely to reverberation. Thus, under these conditions, the signal-to-noise ratio is determined almost entirely by the acoustic pattern, and the efficiency of the transducer is of little consequence.

However, if the ship must operate at high speed, so that the noise level due to its motion is high, the noise level against which the echoes must be distinguished is no longer set by reverberation, but by ship's noise. In this case greater ranges may be obtained by use of greater signal intensities up to the levels at which the reverberation becomes of the order of magnitude of the ship's noise. Under these conditions a transducer of high efficiency is desirable. This is even more true for scanning systems than for sharp beam systems of the QC type, because far more acoustic power is required to produce the same sound pressure over the full horizon than is required for the sharp beam. The transmitting system should be capable of putting at least 1 kw of acoustic power into the water. To produce such a great amount of sound power, a powerful driving circuit must be used and the transducer must be capable of transforming it without much departure from linearity due to magnetic saturation of the magnetostrictive material and without large losses due to magnetic hysteresis and eddy currents. Higher efficiency of the transducer as a transmitter also gives it greater sensitivity as a receiver.

13.1.5 Mechanical Requirements

RUGGEDNESS AGAINST MECHANICAL DAMAGE

A complete scanning sonar transducer should be as rugged as possible mechanically, consistent with the requirements on its acoustical performance. When mounted on the bottom of a surface ship or the topside of a submarine, the transducer is vulnerable to severe impacts due to dragging bottom or striking wreckage, floating objects, ropes, cables. Such transducers are also subject to damage by underwater explosions. The accepted practice is to design the transducers to withstand maximum impulsive pressures of 500 to 1,000 lb per sq in. for submarine use and 300 to 500 lb per sq in. for surface ship use.

CORROSION RESISTANCE

All the externally exposed parts of the transducers should be made of corrosion-resistant materials. The metals used should not only be corrosion resistant themselves but should not give undesirable galvanic battery action when in electric contact with other metals exposed to the same sea water. Exposed soldered joints, for example, are never trustworthy.

Stainless-steel castings have been found to be quite satisfactory in most respects. Navy bronze castings have sufficient strength and corrosion resistance, but it is difficult to get them sufficiently free from porosity to be watertight.

The exposed rubber parts, which are usually used as acoustically transparent faces, should withstand the corrosive action of grease, oil, and sea water. For transducers mounted on the topsides of submarines, where they are exposed to sunlight and air, the rubber parts should be highly resistant to decomposition and oxidation by light, heat, air, and salt water.

WATER TIGHTNESS

It is obvious that a transducer should be watertight. However, it is not easy to make transducers that are watertight and that remain so under service conditions. Great care must be taken to see that there are no porous spots in the metal parts and that the gaskets and packing glands are properly designed, constructed, and assembled. The number of watertight joints should be kept to an absolute minimum. Design details will be considered in a later section.

13.2 GENERAL DESIGN

13.2.1 Transducer Supports

TYPES OF MOUNTING

QC Flange. The standard QC flange is the most commonly used transducer mounting and has proved to be quite satisfactory in actual service in hundreds of installations. Changes to scanning sonar gear from standard QC gear can be made more quickly and economically if the scanning sonar transducer is made to fit the existing mountings. Figure 8 gives the essential details of a standard QC flange. The gasket groove is in the flange and the tongue that engages it is on the transducer. The inside surfaces of the tongue and groove are made to fit within a few thousandths of an inch, whereas the outside surfaces do not meet by several hundredths of an inch (as shown in the A detail in Figure 8) to permit the excess rub-

ber of the gasket to flow out of the groove when the transducer flange and the QC flange are pulled up to face-to-face contact by the 12 $\frac{3}{4}$ -in. bolts. The face-to-face contact of the flanges is necessary to give the full mechanical strength and rigidity of the joint. Otherwise any bending moment on the joint would compress the gasket on one side and relieve it on the other, perhaps enough to allow leakage of water.

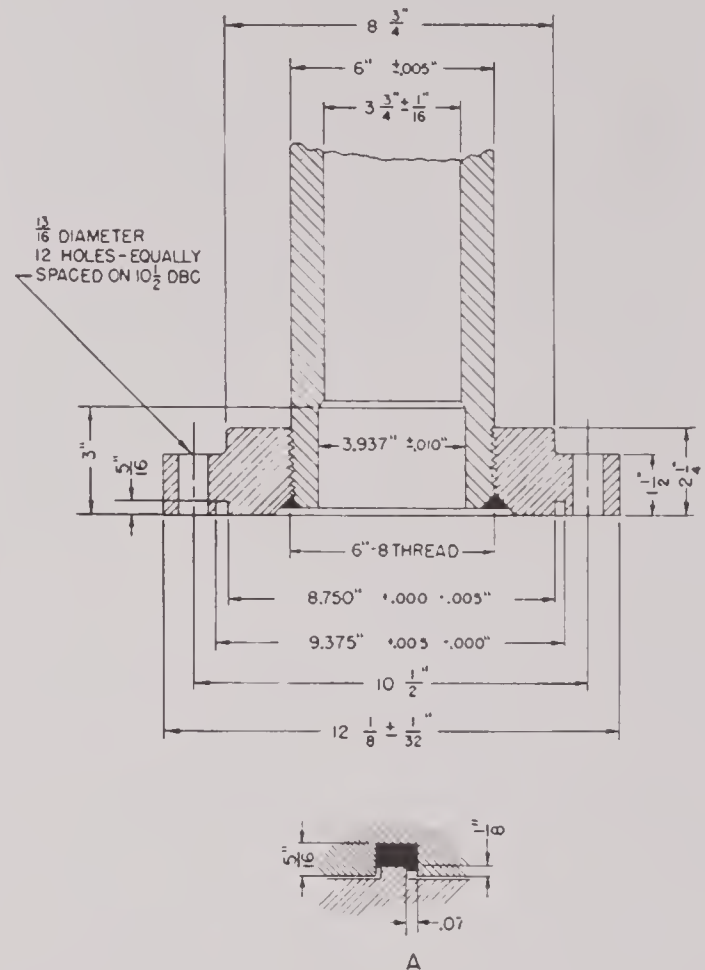


FIGURE 8. Essential details of a QC flange.

Deck Mounting. For mounting scanning sonar transducers on the topside of submarines, the transducers are usually equipped with a large flange extending beyond the periphery of the main body of the transducer at the base. This flange is bolted to the deck. An example of this type of mounting flange is shown in Figure 9, an illustration of the HP-3S transducer arranged for topside deck mounting on a submarine.

Horizontal Mounts. In depth scanning sonar systems, which scan in the vertical plane, the axis of symmetry of the transducer must lie in the horizontal plane, and the transducer assembly must be trainable about the vertical axis. In such transducers

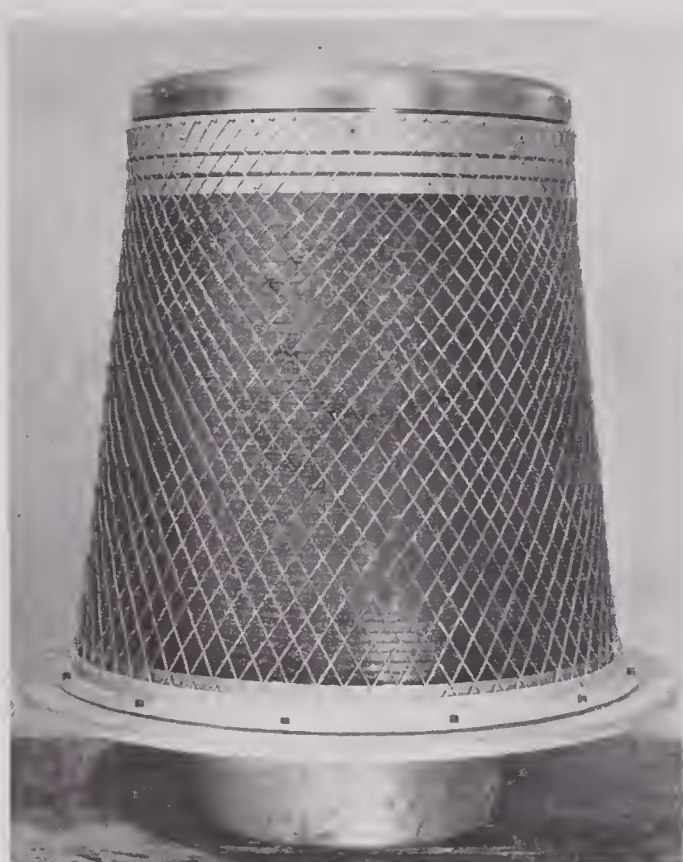


FIGURE 9. A 26-ke HP-3S transducer for topside mounting on a submarine.

the active elements are placed only on the two front quadrants and the lower back quadrant. This leaves the upper back quadrant free for mounting purposes if desired. Figure 10 shows a transducer that is supported by means of a gooseneck extending from the upper back quadrant of the transducer to a standard QC flange mounting. This type of mounting is difficult to manufacture unless special machining tools are set up. Also, it is difficult to make a satisfactory water seal between the case of the transducer and the ends of the rubber "blanket" in the vicinity of the gooseneck. (The rubber blanket extends around the cylindrical face of the transducer, covering the active faces of the elements and making acoustic contact between the elements and the water.)

Another method for mounting depth scanning transducers is illustrated in Figure 11. Here the entire cylindrical surface is covered with a stretched rubber boot and the transducer is supported by two hollow struts, one from each end bell. Each strut is also used as a watertight cableway. The flanges on the tops of the struts make watertight junctions with the flanges on the supporting casting. This transducer was originally designed to be mounted on the bottom of a standard horizontal scanning trans-

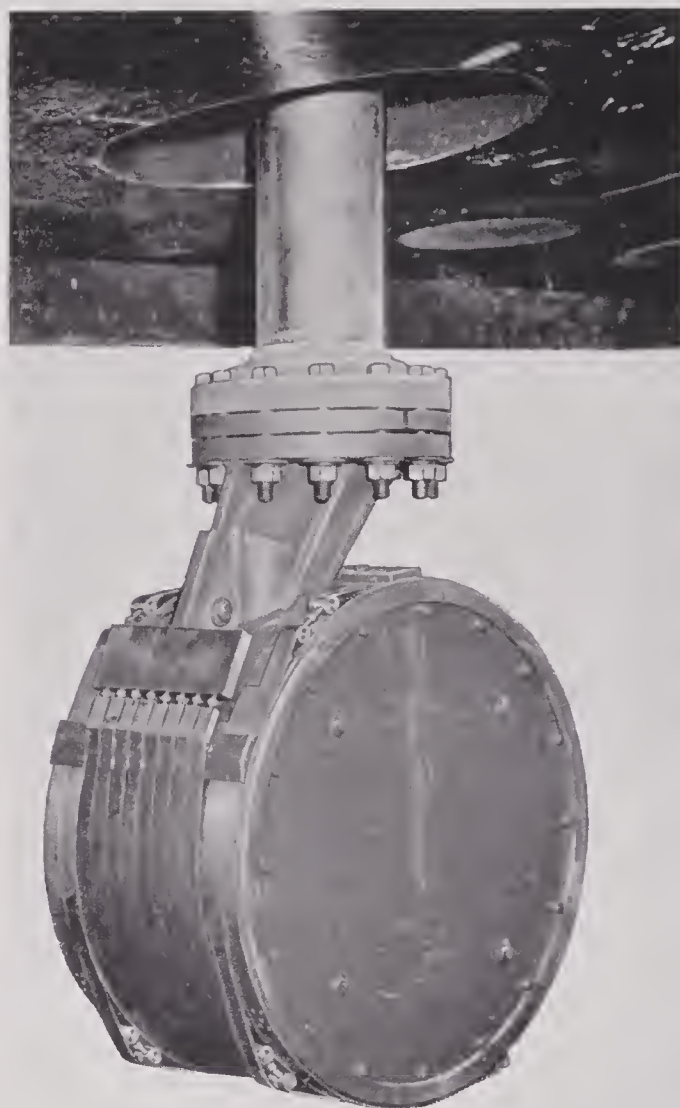


FIGURE 10. A 26-ke HP-3DS transducer for depth scanning sonar. Gooseneck support attached to a standard QC flange.

ducer. By use of a special adapter it could also be mounted directly on a standard QC flange.

MAIN TRANSDUCER FRAME

General Shape and Strength. The conventional scanning sonar transducer is cylindrical in shape, with the active faces of the elements on the face of the cylinder. The main frames of such transducers are generally spool-shaped. The side section of a typical unit is shown in Figure 12. There are so many ways in which elements of various kinds can be mounted on the spool that a comprehensive discussion of the subject cannot be given here. In some instances the elements are free-flooded with water. This necessitates covering the windings and lead wires with good watertight insulation and providing water seals where the lead wires enter the terminal box through the flange of the spool.

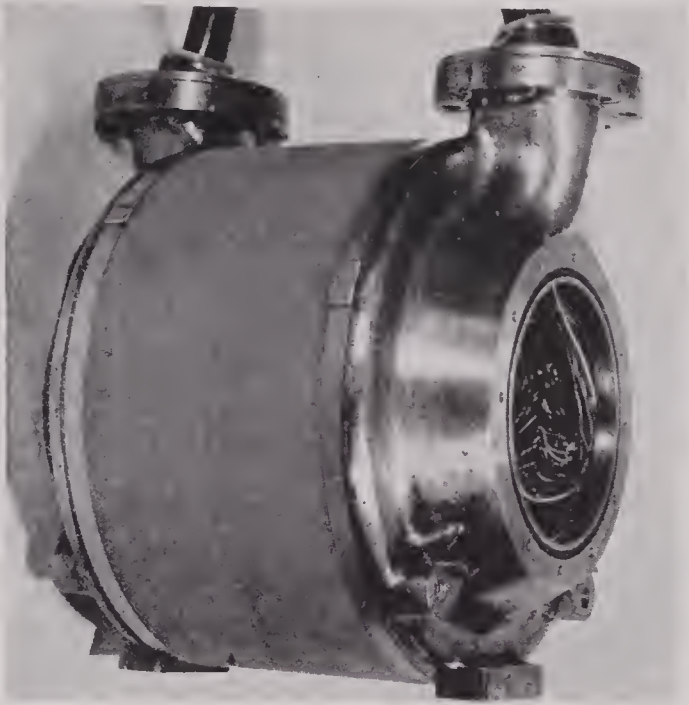


FIGURE 11. A 3S-kc HP-S transducer for depth scanning sonar with two-strut support.

In other cases the space around the elements is vacuum-filled with castor oil or its equivalent. When this method is used, the space for the elements, and therefore the rubber-boot joints and the seals where the lead wires enter the terminal box, must be vacuum-tight. The portion of the lead wires that passes through the seals must be made of solid wire, since stranded wire will not form a vacuum-tight seal.

In those cases where the transducer elements are surrounded by air, no vacuum seals are required for the lead wires. This is the simplest, and preferred, construction.

Except where the elements are free-flooded with water, the pressure of the water outside the transducer produces a crushing effect on the transducer frame. In designs similar to that shown in Figure 12, the total hydrostatic force exerted on the bottom plate is brought to bear on the outside edge of the bottom flange. The shear strength of the bottom flange must be made great enough to withstand this force ($\pi R^2 p$). The force on the top flange is nearly as great but is more evenly distributed. The core of the spool must bear the longitudinal compression resulting from the force on the two ends of the transducer and the circumferential compression due to the inward radial force transmitted by the transducer elements from the water. If the outside radius of the

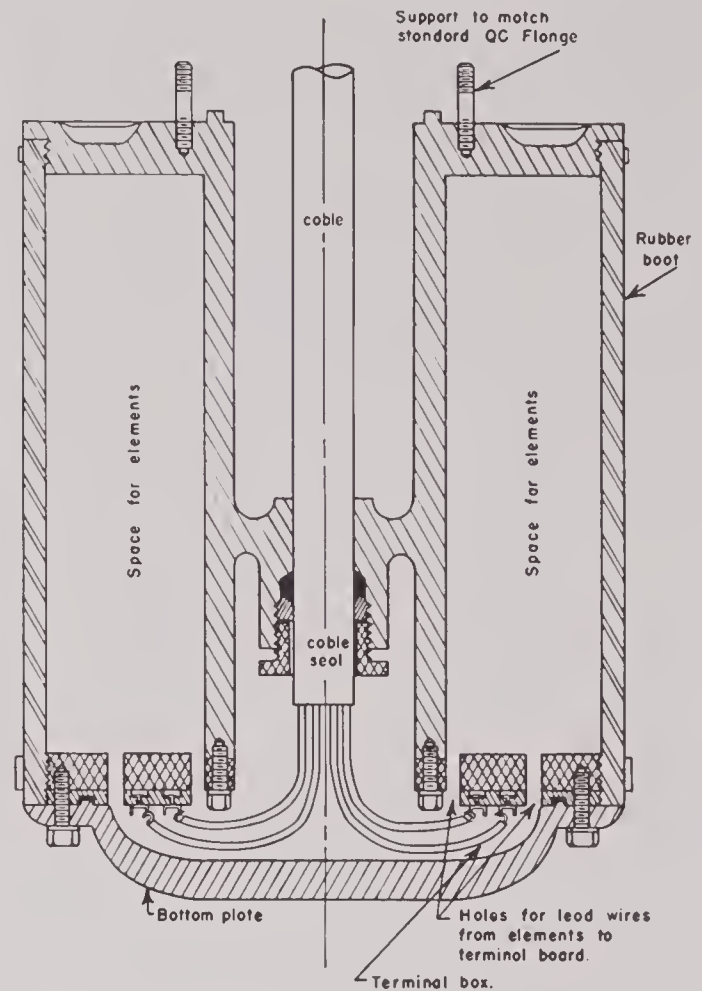


FIGURE 12. Side section of spool frame for transducer for horizontal scanning.

transducer is R_2 , the mean radius of the spool core R_1 , the wall thickness of the spool core t , and the outside water pressure p , then the longitudinal compressive stress in the spool core is

$$s_l = \frac{R_2^2}{2R_1 t} \quad (3)$$

and the circumferential compressive stress is

$$s_c = \frac{R_2}{t} p \quad (4)$$

If the allowable compressive strength of the metal from which the spool core is made is of the order of 35,000 lb per sq in., the wall thickness should be about 0.30 in. to withstand a maximum water pressure of 1,000 lb per sq in.

Materials. The spoollike frame of the transducer must be watertight, strong, and corrosion-resistant. Ordinary boilerplate steel is nonporous and strong, but will corrode severely in sea water. However, experimental scanning sonar transducer frames have been made of pieces cut from boilerplate sheets

welded together. The finished assembly was usually cadmium-plated or painted with red navy paint. Such construction practice is not recommended for permanent installations because corrosion would eventually cause trouble.

Navy bronze (Navy M-46-B-8) castings are mechanically strong and highly resistant to corrosion, but unless the casting is done under ideal conditions considerable trouble is caused by water leakage due to porosity in the metal. For experimental purposes, porous castings can be made watertight by carefully tinning them with solder or by vacuum-impregnating them with special thermosetting resins, but the practice is not recommended for permanent installations because corrosion may open up new leaks at any time. It is possible that centrifugal casting would eliminate porosity in navy bronze castings.

Stainless-steel castings, made by the Allegheny Ludlum Steel Corporation, have proved the most satisfactory for transducer frames up to the present time. This material is strong, corrosion-resistant, and comparatively free from porosity. It is somewhat difficult to machine with ordinary tools because of its tendency to harden by the action of the heat generated by the cutting tool. However, if hard sharp cutting tools are used, the machining presents no great difficulties.

13.2.2 Design of Active Face Area

FACE AREA REQUIRED

It has been pointed out in Section 13.1.4 that a horizontal scanning sonar transducer should be capable of putting roughly 1 kw of sound power into the water. When the peak sound pressure in water reaches atmospheric pressure (about 10^6 dynes per sq cm), the acoustic power per sq in. is about 2.2 watts. If it is assumed that the maximum possible sound pressure is limited to this value by cavitation, the active face area of the transducer would have to be about 450 sq in. to give a total sound power of 1 kw. On this same basis, a transducer having an active face $17\frac{1}{2}$ in. in diameter and 14 in. high should be capable of emitting 1.7 kw of sound power from its 770 sq in. of active face area without danger of cavitation. If the same transducer were 10 ft below the surface of the water, the additional pressure would permit it to radiate 3 kw of sound power without danger of cavitation.

It has been shown by Mason and others at the Bell Telephone Laboratories that, for short pulses, radi-

ation intensities considerably greater than 2 watts per sq in. can be produced in water at atmospheric pressure, and that the maximum sound pressure attainable without cavitation occurring increases with decreasing pulse length. Although it has not as yet been fully demonstrated, it is possible that a $17\frac{1}{2} \times 14$ -in. scanning sonar transducer in 10 ft of water could radiate as much as 5 kw of sound power into the water during 0.035-sec pulses without trouble from cavitation. If this is the case, then it should be possible to radiate 1 kw of sound power into the water with a transducer having about 200 sq in. of actual face area. This would accordingly be the probable lower limit of the active surface area which a conventional scanning sonar transducer should have.

LENGTH AND WIDTH OF ELEMENTS

The length of the active faces of the elements of a scanning sonar transducer is determined by the desired vertical pattern. To give a pattern of the type shown in Figure 6, in which the main lobe is about 12 degrees wide at -10 db, the length of the elements should be about 7 wave lengths. The effect on the pattern of altering the velocity amplitude of vibration along the length of the elements has been discussed in Section 13.1.2. There it is shown that inactive spaces between segments along the length of an element should be kept to a minimum in order to keep down the heights of the minor lobes.

Figure 13 illustrates several possible designs of the active face area of the elements of scanning sonar transducers. Table 1 gives the corresponding total active face areas for a transducer measuring $17\frac{1}{2} \times 16$ in. and the ratios of the active areas to the total available area for the seven different designs shown in Figure 13. The element marked 1 is made up of a series of active circular areas such as would be produced by constructing the element of a series of tube-and-plate oscillator units in which the plates would be in the shape of circular buttons. Such a design would provide sufficient active face area and could be readily adapted to give side-lobe reduction by amplitude shading. The element marked 5 is essentially the same as 1.

The element marked 2 in Figure 13 is made up of four segments separated by inactive gaps which are about $\frac{1}{4}$ wave length long. This design was used in the Harvard HP-3 and the Sangamo HP-5 transducers in which each element is made up of four laminated stacks. The inactive space between segments is required for the windings, and caps, and

supporting structure. The design provides sufficient active face area and gives vertical patterns of the form shown in Figure 6. A rough form of amplitude shading can be attained with this type of element by adjusting the amplitude of each stack.

TABLE 1. Total Active Face Areas and Area Ratios for Different Designs of Active Faces, as Shown in Figure 13.

Element	Ratio of active area to available area	Area for $17\frac{1}{2} \times 16$ in. transducer (sq in.)	Radiation eff	Quality of vertical pattern
1	0.81	710	Good	Good
2	0.88	770	Good	Good
3	0.50—0.80	440—700	Poor to fair	Poor to fair
4	1.00	880	Good	Good
5	0.80—0.90	700—790	Good	Good
6	0.30—0.50	260—440	Poor	Good
7	0.30—0.50	260—440	Poor	Good

The element marked 3 is an extreme example of the 2 type and is not recommended because of poor radiation efficiency and unsatisfactory vertical pattern.

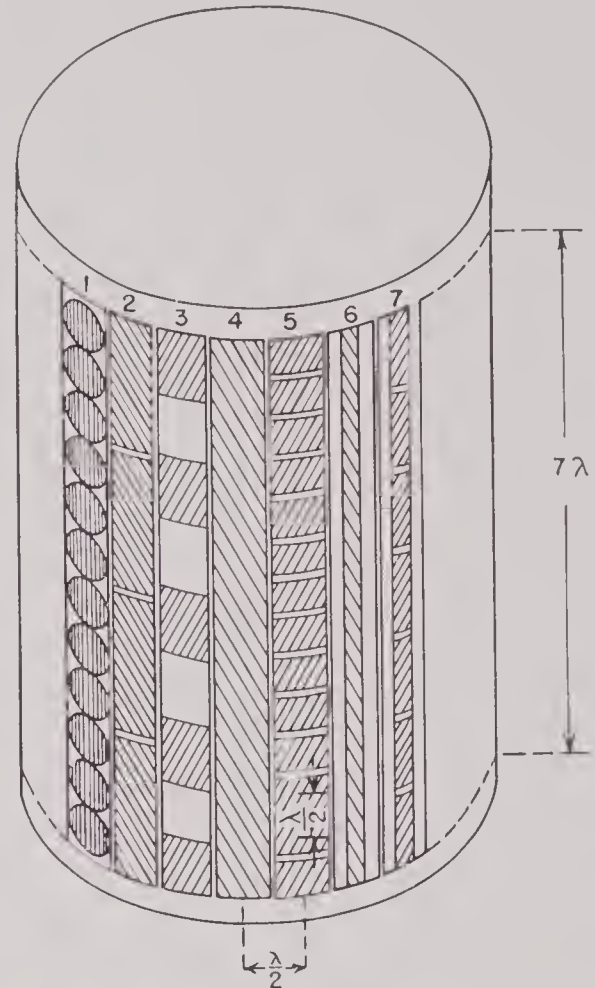
The element marked 4 makes use of all the available face area and is probably superior to the other designs shown. The design can be realized by use of a single long laminated stack for each element, or by a long stavelike metal diaphragm with magnetostrictive tubes or stacks to drive it. The Harvard HP-1 and HP-2 scanning sonar transducers have this type of active face area.

The design for elements 6 and 7 calls for quite narrow active face areas, which would be obtained if the elements were radially placed laminated stacks with the planes of the laminations parallel to the axis of the transducer. Such types have been proposed and have been experimented with in the form of small models. Active face areas of this design should give satisfactory vertical and horizontal patterns in transmitting and receiving. The chief fault of the design is that it does not make efficient use of the available radiating area. Moreover, the radiation efficiency is low because each active face area is bounded by wide pressure-release areas, causing the sharpness of mechanical resonance to increase (higher Q) and reducing the maximum amount of acoustic power which can be radiated.

ACCURACY OF LOCATION OF ELEMENTS

The importance of placing the active faces of the elements accurately on a circularly cylindrical sur-

face has been pointed out in Section 13.1.2. It is equally important to have the center lines of the active face areas spaced at equal angles around the circumference of the cylinder. This prevents the unequal time lags that would otherwise occur in the arrival of the sound waves at the centers of the elements for different azimuthal positions of the acous-



SHADED AREAS REPRESENT ACTIVE FACE AREAS

FIGURE 13. Diagram illustrating several possible designs of active face area.

face axis relative to the transducer (see Figure 2). At 26 kc, for example, each 0.1-in. error in position of the center of the element causes a phase error of about 16 degrees.

The supports of the elements should be designed so that the elements are held accurately in position in spite of the normal impacts and jostling that a transducer receives in ordinary service. The effects of pressure waves due to near underwater explosions should also be taken into account in the design of the supports of the elements.

13.2.3 Overall Shape and Mounting of Elements

SPACE AVAILABLE FOR ELEMENTS

The space available for each element of a scanning sonar transducer is somewhat limited. It has already been pointed out that the distance between the centers of the active faces of the elements should not exceed one-half wave length (in water) by more than a few per cent. Measured in inches, this distance is about $28.5f$, where f is in kc. If the elements are of the longitudinal vibrator type, the length of the elementary oscillators in their direction of vibration

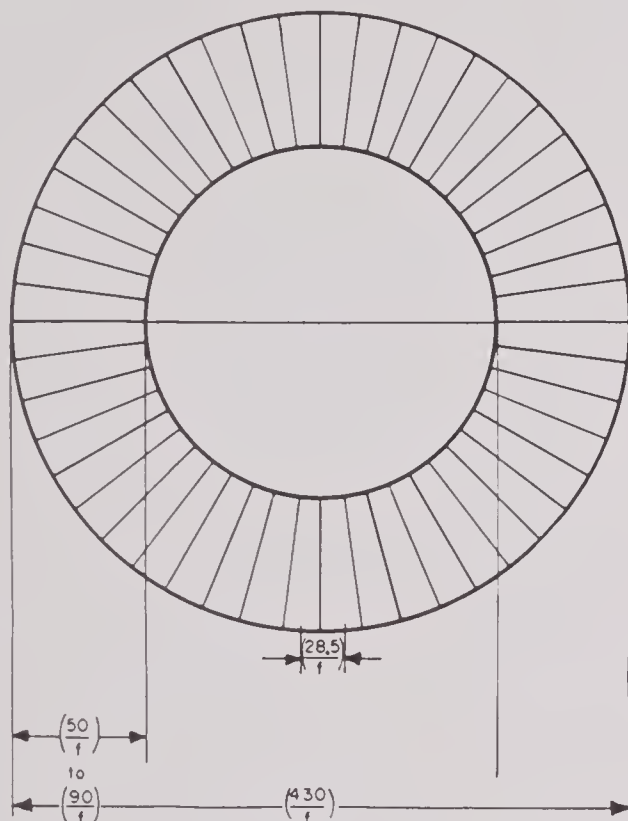


FIGURE 14. General shape and size in inches of space available for elements in a typical 48-element transducer designed to operate at f kilocycles.

will be between one-fourth and one-half of a wave length in the magnetostrictive material used. If nickel or some similar material is used for making the oscillators, the distance in inches the elements extend radially inward from the active face is between $47.5f$ and $95f$, where f is in kc.

The general shape and dimensions (in inches) of the space available for single elements in typical 48-element transducers are shown in Figure 14. The entire element, complete with its supporting and housing structures, must lie within this space. The

limited space for each element and the desirability of having as large an active face area as possible make it difficult to design element structures that are supported and watersealed independently of each other. Many attempts have been made in this direction without any notable success. However, several of the general designs of element supports and housings that have been used or proposed are shown in following illustrations.

HP-2B TYPE

Figure 15 shows a design in which the elements consisted of single long stacks of nickel laminations consolidated with resin and equipped with end caps

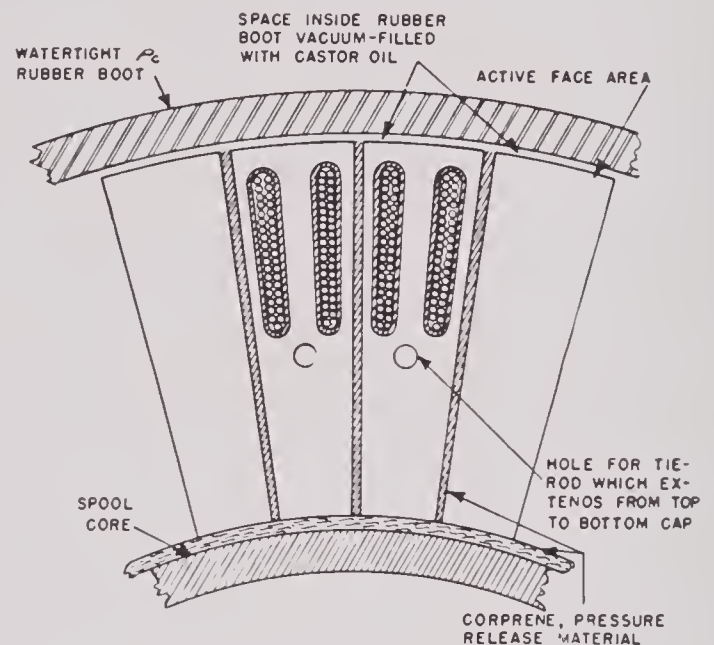


FIGURE 15. General design of element support and housing used on Harvard HP-1B and HP-2B scanning sonar transducers.

held to the ends of the stacks by cement and by a tie rod extending through the stack from one end to the other. The elements were held to the flanges of the supporting spool by screws which engaged the end caps. In one version of this design the elements were exposed directly to the water, so that the windings had to be of the watertight insulated type. In an improved form of design, the whole assembly of elements was surrounded by a watertight ρ c rubber boot and the space between the boot and the elements filled with castor oil or its equivalent to give acoustic contact between the elements and the water. The spaces between and in back of the elements and between the windings and the laminated stacks were filled with a good pressure-release material, such as corprene or air-cell neoprene, to prevent excessive

CONFIDENTIAL

mechanical damping and undesirable acoustic coupling of the vibrating elements.

HP-3 TYPE

Figure 16 shows a general design in which the entire transducer is housed in a watertight, sound-transparent rubber boot with air-filled space around

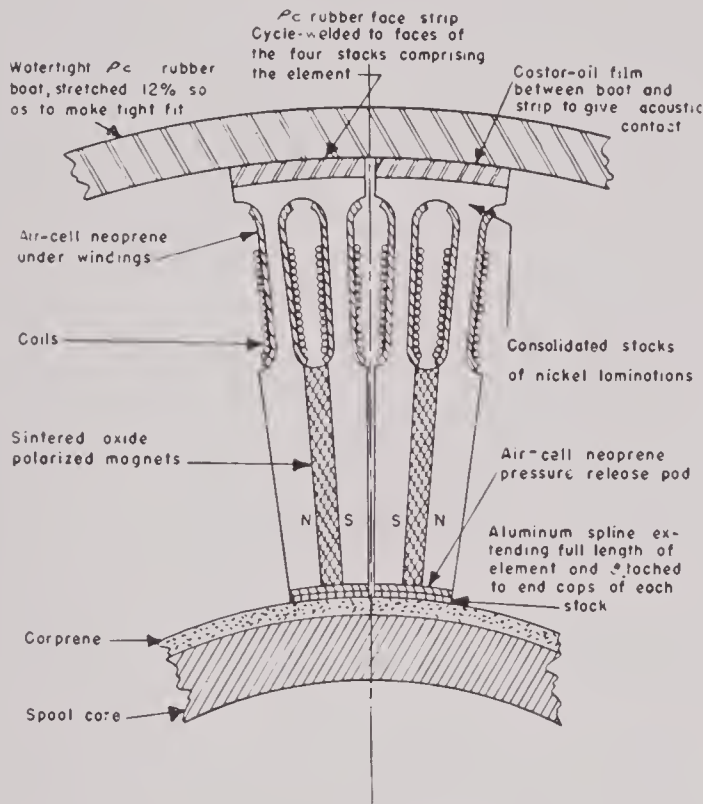


FIGURE 16. General design of element support and housing used on the Harvard HP-3 scanning sonar transducer.

the elements. The elements do not have separate housings. In this case acoustic contact is made between the active faces of the laminated stacks and the water through a thin rubber face strip, which is Cycle-Welded to the face of the laminated stack, through a thin film of castor oil, and then through the rubber boot. The boot was made approximately 12 per cent under size so that it had to be stretched to fit over the transducer. The tension developed in the stretched boot produced intimate acoustic contact with the castor-oil film on the smooth rubber face strips on the elements. These face strips were of rubber, molded to the proper radius of curvature on the exposed face. The inward radial pressure exerted by the stretched rubber boot is given by the expression

$$p_r = \frac{tE}{R} \cdot \frac{\Delta R}{R_0}, \quad (5)$$

where t is the wall thickness of the boot, E the Young's modulus of the rubber, R the mean radius of the boot when stretched, and $\Delta R/R_0$ is the fractional increase in radius of the boot due to the stretching. A boot $\frac{1}{2}$ in. thick, with a mean final diameter of 18 in. and a Young's modulus of 300 lb per sq in., will give an inward radial pressure of about 2 lb per sq in. when stretched 12 per cent.

The stretching of the circumference of the rubber boot causes the boot to shorten in the axial direction, because of the Poisson ratio effect. This must be allowed for in specifying the length of the unstretched

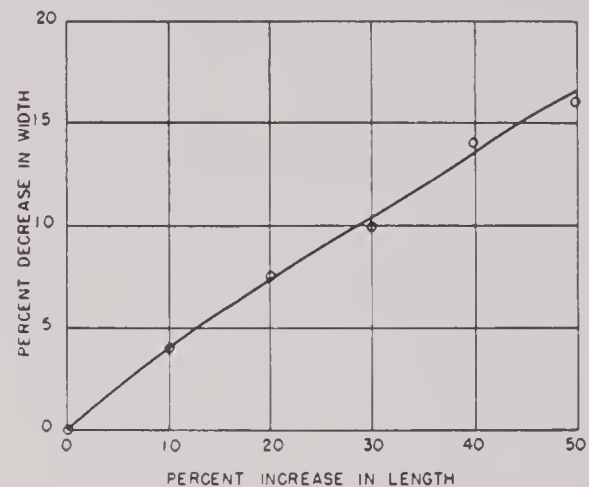


FIGURE 17. Graph showing fractional change in width of a pc rubber strip which is due to stretching it longitudinally by various fractional amounts.

boot. Figure 17 shows the relationship between the fractional change in width of pc rubber as a function of the fraction change in length due to stretching.

There are many ways of supporting the individual laminated stacks in this type of general design. In the Harvard HP-3 transducer, four laminated stacks are fastened together end to end by a common rubber strip on the face and an aluminum spline on the back to form the long stavelike elements that are fastened to the flanges of the supporting spool at each end. In the Sangamo HP-5 transducer, each of the 48 elements is composed of four laminated stacks, mounted one above the other. Each stack is supported at both ends by means of flat, ring-shaped support disks which lie between the end caps of the four circular layers of stacks. Each layer comprises 48 stacks, one for each element. The molded bakelite end caps of the stacks have two protruding bosses, which engage holes in the support disks and hold the stacks accurately in position. In this type of construction the wires connecting the four stacks of an element cannot be permanently connected until all the stacks in

the transducer are in place. Conversely, it would be very difficult to replace an element without disassembly of the entire transducer. But in spite of the difficulty in repairing or servicing it, this type of mounting is still among the best available because of its mechanical accuracy, strength, and reliability.

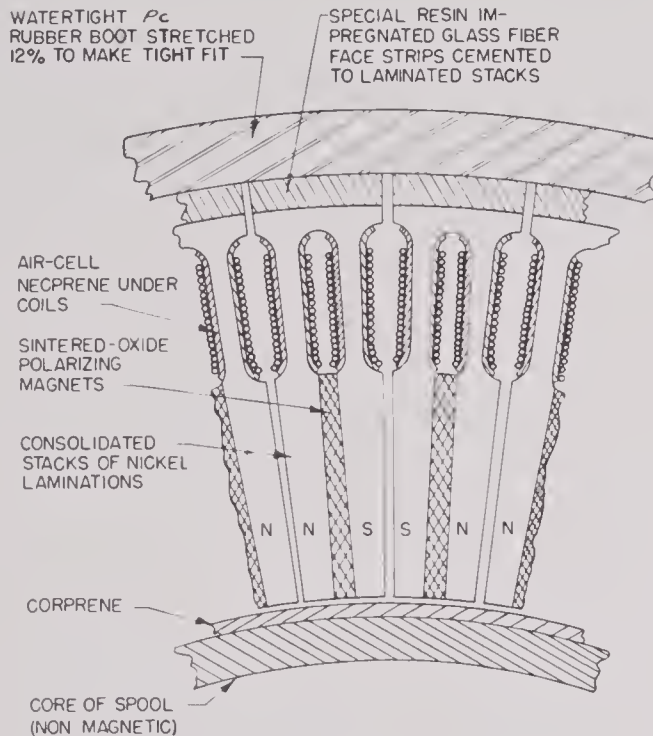


FIGURE 18. General design of element support and housing using stacks of HP-3-like laminations cemented to resin-impregnated glass fiber face strips.

HP-3 WITH PLASTIC FACE STRIP

Figure 18 shows a similar design, in which the mechanical support of the laminated stack elements is provided by the strong, relatively thick face strips, which extend along the full length of the element and fasten to the flanges of the supporting spool at each end. These face strips can be made of any material that has the requisite strength, low density, and small acoustic damping and can be bonded securely to the faces of the laminated stacks. All the metals, with the possible exception of magnesium, are so dense as to increase the mass reactance of the vibrating system, and thereby the mechanical Q , by an undesirable amount. No complete transducer of this type has ever been constructed, but preliminary experiments indicate that the best materials for the face strips are certain of the resin-impregnated glass fiber laminates. These materials have all the desirable mechanical characteristics listed above.

The shape of the laminated stacks used with this

type of construction is not limited to the form shown in Figure 18. In fact, it would be entirely possible to replace the laminated stacks with tube-and-plate type units, for example, square magnesium blocks bearing nickel tubes and coils.

If the type of construction illustrated in Figure 18 were to be used, the simplest element would be made by a uniform stack extending the full length of the element without gaps or amplitude shading. If desired, amplitude shading could be secured by inserting narrow inactive gaps in the stack at selected intervals, in accordance with some amplitude shading curve. It is also possible to make the element in many segments, each with a separate winding of the proper number of turns to give the desired amplitude shading. In this case no special end caps would be required for the segments so that the inactive spaces between them would need to be only wide enough to accommodate the windings at the ends of segments.

One important advantage of this type of construction is that the elements are strong separate mechanical units which can be put in or taken out of the transducer with very little trouble.

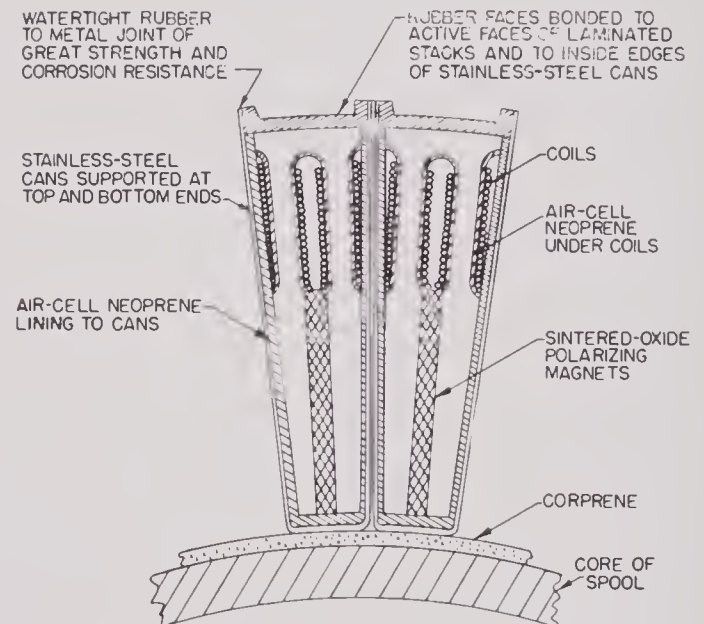


FIGURE 19. General design of element support and housing in the Harvard HP-2 scanning sonar transducer.

HP-2 TYPE TRANSDUCER MOUNTED IN CONTAINERS

Figure 19 shows the general design of the element support and housing used in the Harvard HP-2 scanning sonar transducer. This was the first major attempt at housing the elements in separate watertight containers. These were made of approximately

0.032 in. thick stainless-steel sheet formed into tapered cans and were lined with air-cell neoprene to provide pressure-release support for the laminated stacks on all sides except the active face. The molded rubber faces were Cycle-Welded to the active face of the stack and to the inside surface of the containers in a single operation.

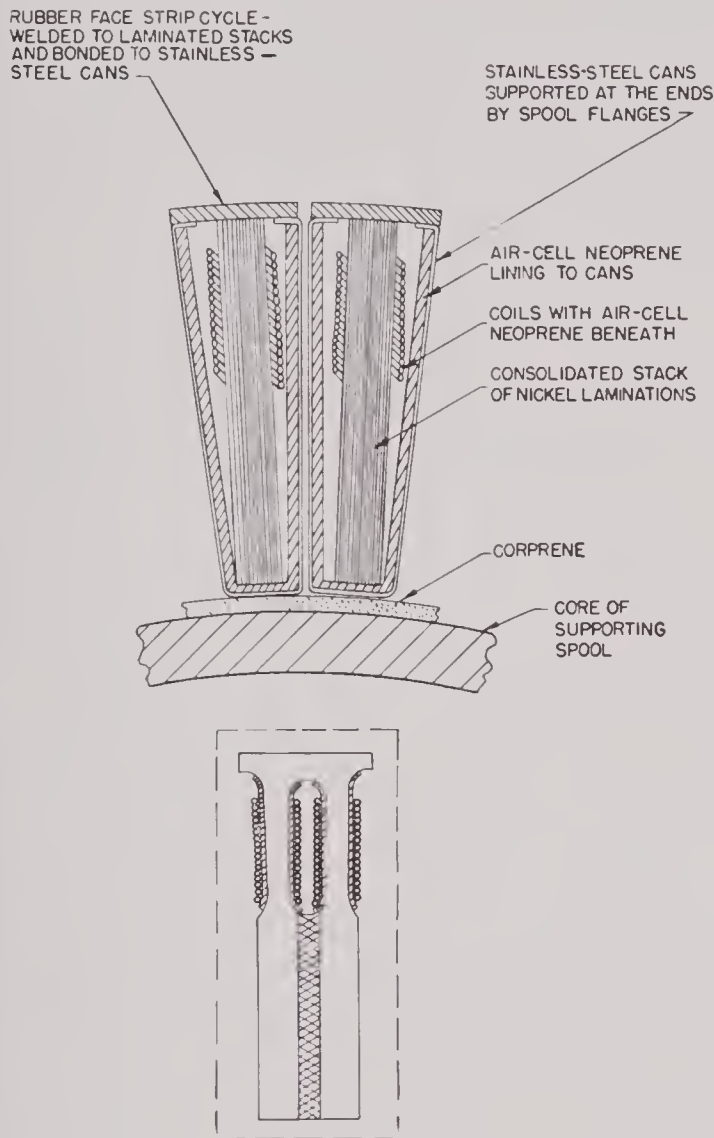


FIGURE 20. General design of element support and housing as proposed in the Harvard SP-1 scanning sonar transducer.

The two lead wires from the windings on the laminated stack were brought through a small stainless-steel tube at one end of the container. A watertight seal was made between the solid lead wires and the stainless-steel tube by filling it with Rubberseal compound. When the complete elements were mounted in the supporting spool the little tubes through which the lead wires passed projected through holes with

water seals into the terminal box. A detailed description of this transducer will be found in Chapter 14.

The chief advantage of this type of construction is that the elements are mechanically, electrically, and acoustically independent of each other. Removal and replacement of elements are relatively easy. Furthermore, the elements have considerable mechanical strength except at the edges of the containers. There are disadvantages, however. These include the large number of water seals that must remain perfectly tight under all service conditions, the vulnerability of the edges of the containers to damage by impacts from external objects, and the difficulty of getting the active faces of the elements arranged accurately at equal angles and on a true circle. In the one HP-2 transducer that was constructed, small leaks developed in the Cycle-Welded joints between the rubber faces and the stainless-steel cans. After much experimentation, this transducer was modified to the form shown in Figure 15.

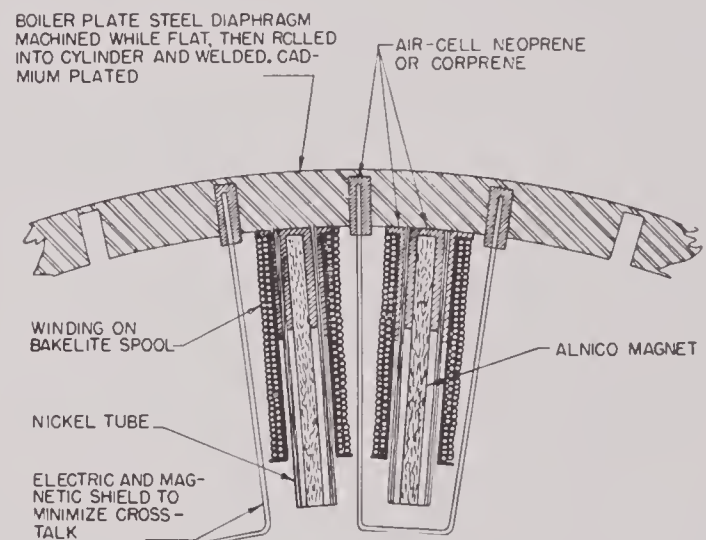


FIGURE 21. General design of element support and housing used on the Harvard "millerphone" scanning sonar transducer.

SP-1 TYPE TRANSDUCER MOUNTED IN CONTAINERS

Figure 20 shows another form of self-contained water-tight element construction, designated as the Harvard SP-1 type. Construction of this type was abandoned, however, because of the difficulties experienced with the leakage of the Cycle-Weld joints in the Harvard HP-2 transducer and because experiments on a small model showed that the narrow width of the active face did not have enough radiation resistance to give a sufficiently low Q . There were two definite advantages to this type of con-

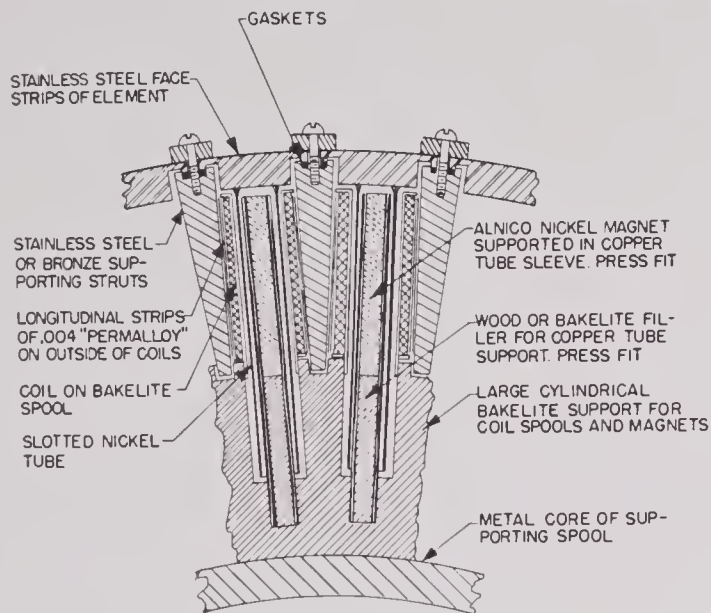


FIGURE 22. General design and element support and housing for a tube-and-plate type of scanning sonar transducer.

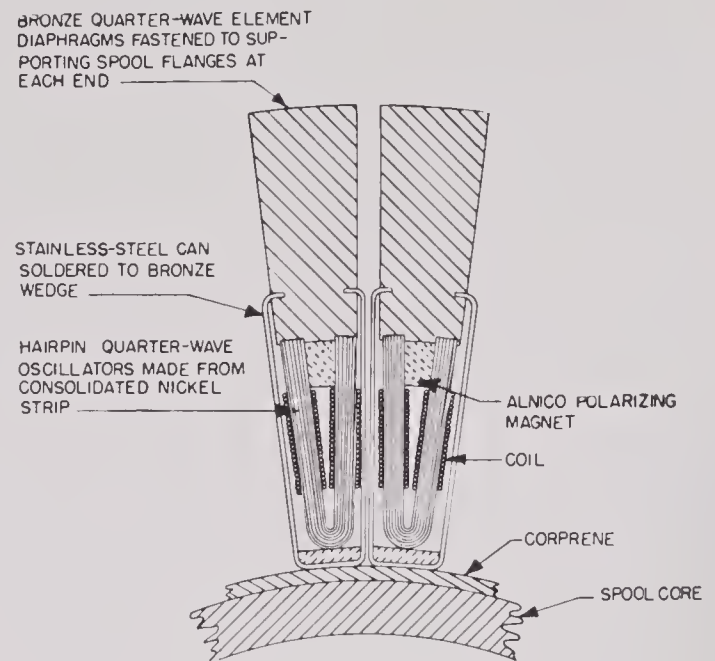


FIGURE 24. General design of element support and housing for a permanent-magnet, polarized nickel scroll type of scanning sonar transducer.

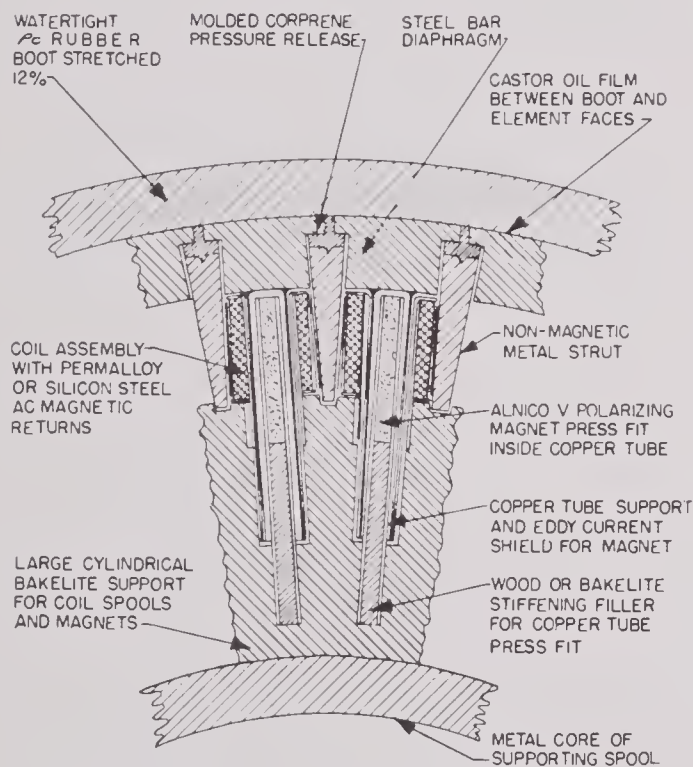


FIGURE 23. General design of element support and housing for a tube-and-plate type of scanning sonar transducer with rubber boot.

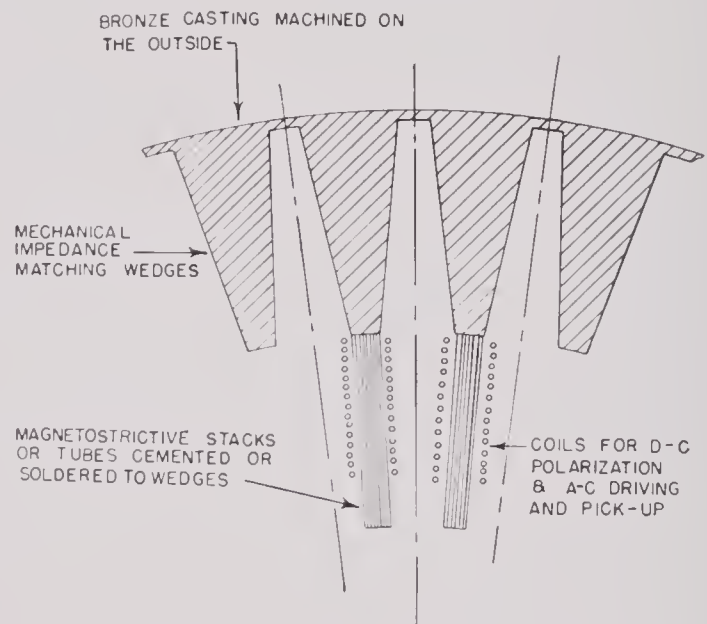


FIGURE 25. General design of elements and housing for a scanning sonar transducer with special impedance matching wedges integral with the diaphragm.

struction, however: (1) the independent housing of the elements and (2) the natural adaptability to vertical amplitude shading for the reduction of minor lobe heights in the vertical acoustic pattern.

"MILLERPHONE" TUBE-AND-PLATE TYPE

Figure 21 shows a design of the tube-and-plate type of transducer adapted to the general form required for scanning sonar use. In this type the diaphragms of all the elements were an integral part of a cylindrical steel shell which had deep longitudinal notches on the inside or outside surface to reduce the mechanical coupling from one element to the next.

The cylindrical steel shell served as the watertight housing for the transducer, the diaphragm for the elements, and the mechanical support for the interior structure. The top and bottom caps of the transducer made a tongue-and-groove water seal with the top and bottom edges of the cylindrical shell. This transducer was much lighter than the laminated stack type.

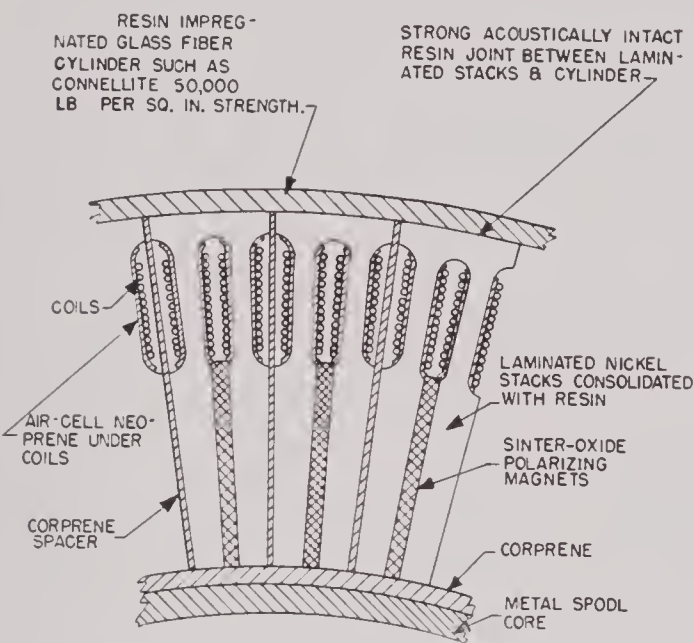


FIGURE 26. General design of the elements and housing of a scanning sonar transducer using a laminated resin-impregnated fiber-glass cylinder for the outside water-proof housing and element support.

One transducer of this sort was constructed at HUSL. Tests showed its efficiency to be low but satisfactory. However, the frequency-matching of the elements was so unsatisfactory that the transducer was given up as a failure on this score as well as on account of its inherent mechanical weakness.

TUBE-AND-PLATE WITH INDIVIDUAL SEALED DIA-PHRAGMS

The various designs described in the foregoing paragraphs have all been executed as experimental models for the scanning sonar program at HUSL. In the search for magnetostrictive transducers that would meet the requirements, a number of ideas were proposed, some of which were discarded without experimental study. Figures 22 to 26 are presented partly to trace the course of the laboratory's efforts and partly with the thought that they may be of assistance in future development. Prominent in these suggestions are (1) the desirability of a design that will allow the removal of single elements and (2) an

attempt to adapt to scanning sonar use the transducers already successful in other applications. The structural features of the various designs are indicated in the figures. The merits and defects of the various designs are briefly summarized as follows.

Fig.	Type	Merits	Objections
22	Tube-and-plate	(a) Permits vertical shading (b) Separate elements removable	(a) Large number of water seals (b) Structurally weak
23	Tube-and-plate	(a) Permits vertical shading (b) Separate elements removable (c) Mechanically strong (d) Small number of water seals	(a) Too sharply resonant (b) Possible inter-element mechanical coupling
24	Quarter-wave bronze wedge driven by hairpin laminations	Separate elements removable	(a) Too sharply resonant (b) Poor a-c magnetic flux circuit (c) Structurally weak
25	Bronze wedges cast integrally with shell, driven by book-type laminations	No supporting spool needed	(a) Too sharply resonant (b) Structurally weak (c) Requires d-c polarization
26	Plastic cylindrical shell, driving elements cemented to inner surfaces	Plastic shell provides water seal, support for elements, and acoustic window	(a) Elements not removable (b) Can be assembled only as a complete unit (c) Structurally weak

LADDERPHONE

Figure 27 shows the design of a transducer known as the Harvard *ring ladderphone*, [H-RLP]. This transducer will be considered here only for the design of its housing and support. The elements consist of adjacent pairs of legs, effectively fastened together at inside and outside ends by continuous face arches. This arrangement introduces mechanical and magnetic coupling between neighboring elements, which affects the phases and amplitudes of the signals generated in the windings of the elements when the transducer is excited by plane waves. Thus the receiving beam-forming network which must be used with this type of transducer may be slightly different from those used with transducers which have mechanically separated elements.

The laminated ring-shaped stack is supported on corprene pads between the top and bottom flanges of the spool. The laminated stack alone has sufficient mechanical strength to withstand most of the abuses anticipated by the regular specifications. The water-tight housing is provided by a ρc rubber boot which is Cycle-Welded to the outside surface of the laminated ring stack and clamped at its ends against the edges of the flanges of the supporting spool.

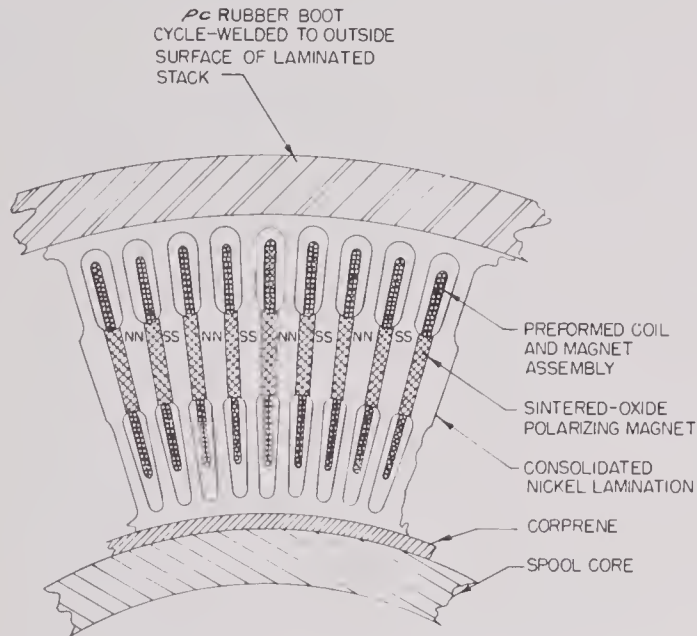


FIGURE 27. General design of the elements and housing for the Harvard 36-ke "ring ladderphone" scanning sonar transducer.

TUBULAR-TYPE ELEMENTS

There are many possible ways in which tubular-type transducer elements can be used to make up scanning sonar transducers. Figure 28 shows a design in which an array of tubular elements of the B-19H monitor type is mounted around the periphery of a supporting spool. One of several possible ways in which tubular transducers may be mounted on a supporting spool and the lead wires brought into the terminal box is suggested in the partial side-section drawing shown in Figure 28. It will be seen that the lead wires are brought out through a metal tube in the top cap of the transducer element tube and the small metal tube is passed through a water seal into the terminal box. In this type of construction, however, the entire transducer would become flooded if one element leaked. Some method of water-sealing the lead wires in the stem tube would eliminate this effect.

It would also be possible in construction of this type to use laminated ring-stack elements or tubular

units made up as laminated scrolls. At the time of writing it is unfortunately not possible to make radially vibrating thin-walled tubular transducer units which give efficiencies greater than a few per cent. Thicker-walled stacks of rings can be made to have high efficiencies in the frequency region of their mechanical resonance, but because of the ratio of the velocity of sound in magnetostrictive materials compared to that in water the wave length of the sound in water at the frequency of resonance is nearly equal

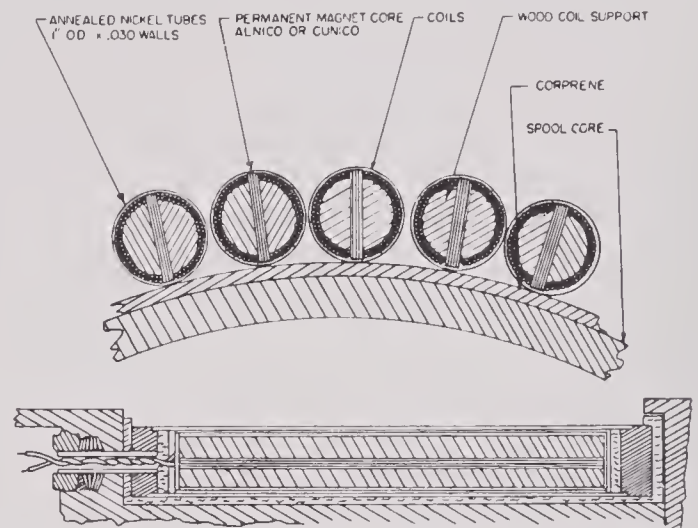


FIGURE 28. General design and mounting of the element type of scanning sonar transducer.

to the diameter of the ring stack. Thus, to maintain the required one-half wave-length spacing between elements, the ring stacks would have to be operated at one-half their frequency of resonance where their efficiency is not much greater than that of thin-walled tubes or scrolls. The resonant frequency of ring stacks may be reduced by increasing the mass loading and decreasing the stiffness by such methods as cutting notches in the periphery of the rings and bonding heavy copper windings to the stack. Such methods result in the transducer having a higher mechanical Q at a lower frequency, but the higher Q makes it necessary to operate close to the frequency of resonance and makes it more difficult to keep the elements within the necessary close phase tolerances.

Figure 29 shows the design of an early tubular-type scanning sonar transducer in which the elements consisted of arches of magnetostrictive material placed around the periphery of the supporting spool. The considerable extent of soldered joints made it fairly susceptible to corrosion and leakage. This fact, together with the requirement of d-c polarizing current and very low efficiency, led to its abandonment.

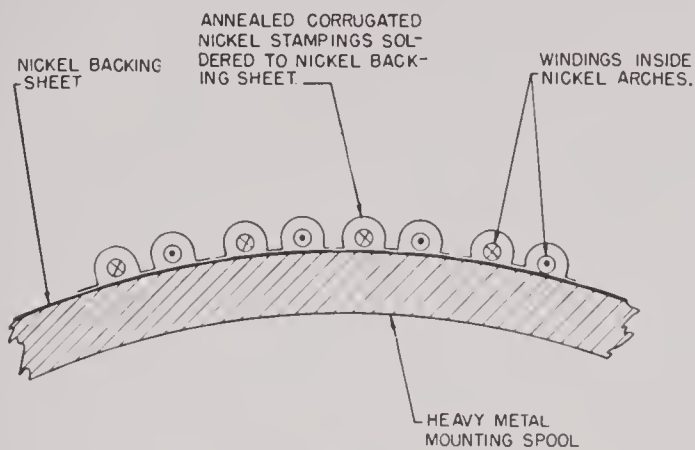


FIGURE 29. General design of elements using the multiple arch system.

rounded by a large rubber boot, with the space between the boot and tubes filled with castor oil or its equivalent, the elements would still be liable to damage by impact.

The inherently low efficiency of tubular transducers makes it impractical to use them for transmitting the powerful sound pulse required in normal scanning sonar operation. This would necessitate the use of some more efficient transducer as a sound source, with the tubular scanning sonar transducer used as a receiver only.

GENERAL

In the preceding sections a number of general de-

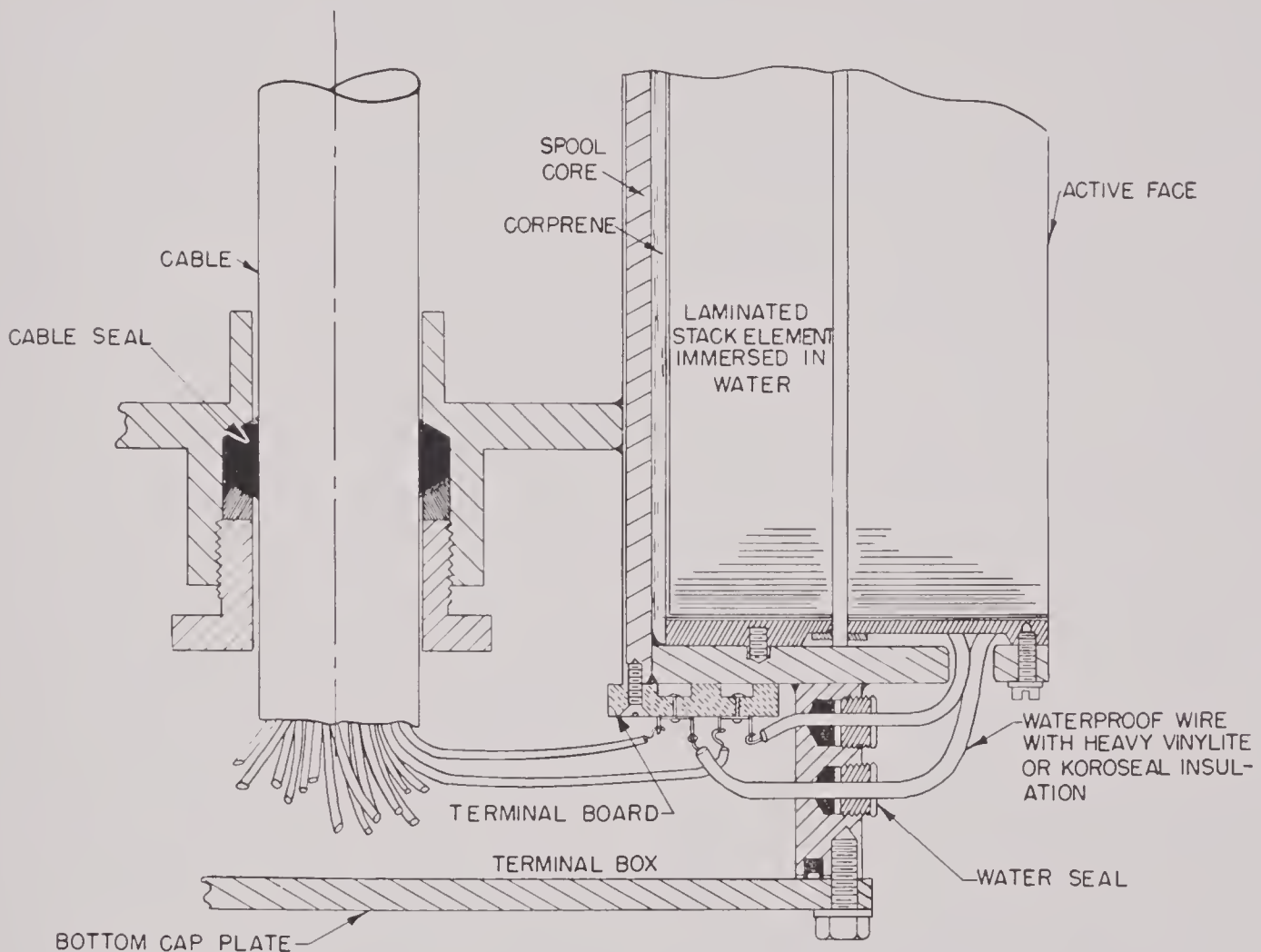


FIGURE 30. Typical design of the terminal box on a scanning sonar transducer with free-flooding elements and windings.

An outstanding weakness of all scanning sonar transducers made of tubular elements is their liability to mechanical damage from impacts of sharp objects against the sides of the transducer. Tubes of the type required will readily withstand 500 lb per sq in. hydrostatic pressure but are easily crushed by heavy, sharp objects. Even if the array of tubes were sur-

rounded by a large rubber boot, with the space between the boot and tubes filled with castor oil or its equivalent, the elements would still be liable to damage by impact.

The inherently low efficiency of tubular transducers makes it impractical to use them for transmitting the powerful sound pulse required in normal scanning sonar operation. This would necessitate the use of some more efficient transducer as a sound source, with the tubular scanning sonar transducer used as a receiver only.

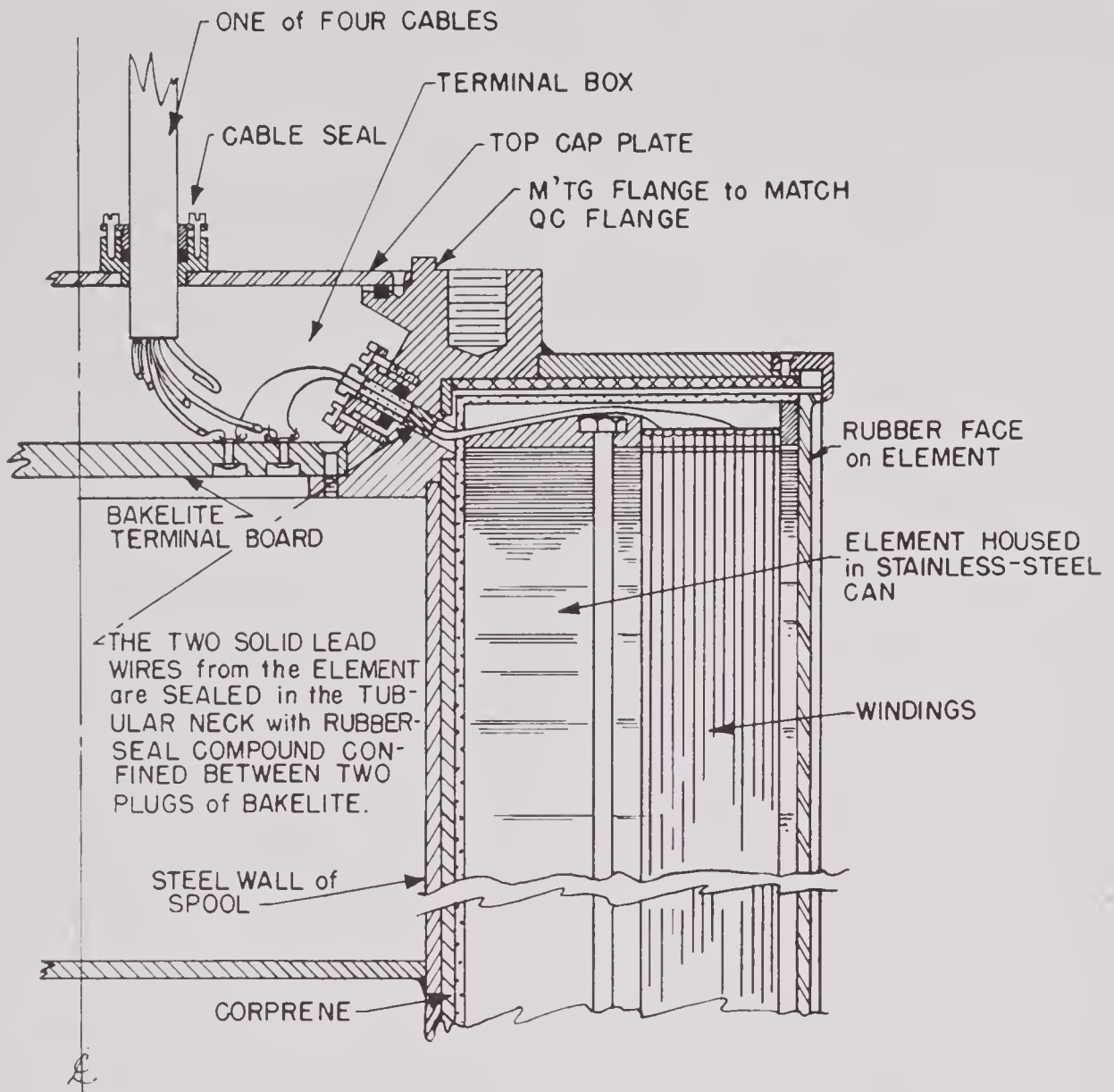


FIGURE 31. A terminal box design for a scanning sonar transducer with separately housed watertight elements.

13.2.4 Terminal Box and Cable Seals

1. Most scanning sonar transducers are equipped with cables before installation on ships. These cables are shipped separately, however, and must occasionally be changed because of damage or wear. Therefore, it is not feasible to attach the cable wires directly to the lead wires from the transducer elements. Instead the lead wires from the elements and the conductor wires of the cable are terminated on lugs on a terminal board in the transducer.

The terminal board is located in that part of the transducer commonly called the terminal box or terminal chamber, which is usually located at one end of the supporting spool to make it as accessible as possible. Present practice is to place the terminal

box on the end of the transducer which is opposite the end attached to the support. This permits access to the terminal box by merely removing the cover plate and eliminates the need to disconnect the transducer from its support. A typical arrangement is shown in Figure 12.

The terminal box should be both watertight and vaportight. This latter requirement means that the cable must enter the terminal box through a seal or packing gland. If this precaution is not taken, water vapor diffuses down the hollow center of the training shaft and condenses on the cold walls of the submerged transducer. In addition to sealing against water and vapor, it is good practice to install a packet of dehydrated silica gel to absorb any small amounts of water or water vapor present in the terminal box at the time it is closed.

CONFIDENTIAL

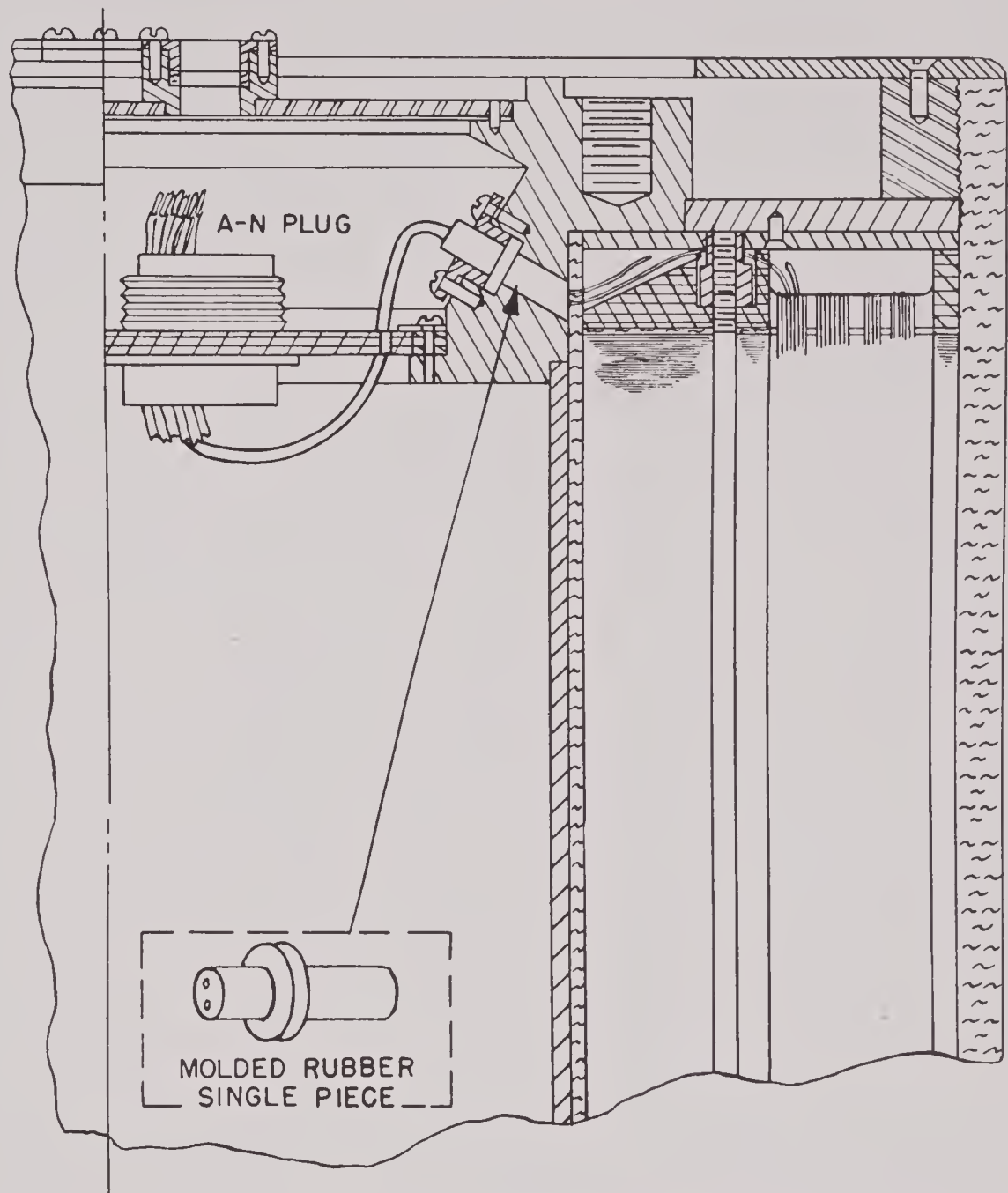


FIGURE 32. A terminal box design for a scanning sonar transducer in which the terminal board lugs are replaced by 4 A-N plugs. The elements are housed in a common castor-oil-filled chamber surrounded by a rubber boot.

A second reason for sealing the cable entry to the terminal box is to prevent water from flowing up the training shaft into the ship in case of damage to the watertight covering of the transducer.

2. If the transducer elements are free-flooding, or if the elements are in separate watertight housings, the element lead wires must enter the terminal box through water seals. Solid (not stranded) lead wires and solid watertight insulation must be used if leakage from the insulation or the housing of any one element is not to interfere with the operation of the other elements. Stranded wire conductors or unim-

pregnated textile insulation under the insulation sheath will permit seepage of water through the water seal if the water enters the wire at any place along its length.

Figures 30 and 31 show two typical designs of terminal boxes for transducers with free-flooding or separately housed elements. In Figure 30 the elements consisting of laminated stacks of nickel wound with waterproof insulated wire are immersed directly in the sea water. The lead wires from the elements are passed through water seals into the terminal box and soldered to the lugs on the terminal board. The

cable is brought through a large seal in the top of the terminal box and the wires from it are connected to the proper lugs on the terminal board. The terminal box is finally sealed by the bottom cap plate.

Figure 31 shows a terminal box design for a scanning sonar transducer with separately housed watertight elements. Here the terminal box is at the top end of the transducer for convenience in mounting the elements on the spool. Each element is housed in a stainless-steel can, from which a stainless-steel tube projects. This tube passes through a water seal into the terminal box. The solid wires from the windings pass through the tube into the terminal box. These are water-sealed in the tube with Rubberseal compound confined between two plugs of bakelite as shown in the diagram. These seals are to prevent flooding of the terminal box and of the remaining elements in case one element should leak. This type of seal is very effective and reliable, although it is difficult to service. In this particular model the total cable was made up of four separate watertight cables, each of which passed through a water seal in the top cap plate. The individual wires of the cable were soldered, as usual, to the proper lugs on the terminal board.

A modification of this terminal board design which makes it possible to remove the cable and top cap plate from the transducer with comparatively little trouble is shown in Figure 32. In this modified design the lugs on the terminal board are replaced by four A-N plugs. The female parts of the plugs are fastened to the bakelite terminal board and the male parts to the cable wires. The cable can be removed from the transducer by loosening the water seals in the top cap plate of the terminal box, unfastening the top cap plate and sliding it up along the cables, then disengaging the A-N plugs. The cable is reconnected to the transducer by following the reverse procedure. It is often very convenient to have the cable easily removable from the transducer and it is especially so when a transducer must be installed through a hole in the side of a sea chest which is too small for the transducer with its cable attached.

3. The design of the terminal boxes for scanning sonar transducers in which the elements are enclosed in a single castor-oil-filled chamber surrounded by a rubber boot is not very different from the design for those with free-flooding elements. For the oil-filled transducer, the seals must be vacuum-tight as well as watertight, whereas lead wires and windings do not require heavy watertight insulation because castor oil (or its equivalent) is a good insulating material.

A design with the terminal box at the top end of the transducer is shown in Figure 32. The seals where the lead wires pass from the oil-filled chamber to the terminal box are made by passing the two solid, enamel-covered lead wires through holes in specially molded rubber gasket pieces. The pressure exerted by the plunger of the seal squeezes the rubber against the outside wall of the seal and against the solid wires, making a complete vacuum-tight seal.

The terminal board and cable seal arrangements for this design have already been discussed in Section 13.2.4.

Figure 33 shows a design with the terminal box at the bottom of a transducer in which the elements are immersed in castor oil. In this case the individual wires are brought through separate seals consisting of solid rods threaded at each end, insulated from the metal frame by bakelite bushings, and sealed by rubber gaskets which are squeezed between the bushings.

The cable seal shown for this case is the pothead type in which the wires of the cable pass through holes in a bakelite disk at the base of the pothead and the wires are sealed by pouring in Rubberseal compound, a thermosetting resin, or similar material. The cable above the pothead is sealed against water or vapor by a sheath made of firehose or its equivalent. The pothead itself is sealed to the baffle plate in the transducer spool.

4. When the elements are mounted in an air-filled space, no seals are needed where the lead wires from the elements enter the terminal box. In a transducer of this type, a water leak in the element chamber would flood all the elements, making the entire transducer inoperative, so that there would be little purpose in having the terminal box remain dry. An example of this type is shown in Figure 12. Here, the wires pass through holes in the flange of the spool to the lugs on the terminal board.

5. The location of the cable seal in the transducer is determined chiefly by its accessibility. It should be placed at some point between the terminal box and the flange which supports the transducer so that, if there should be any leakage in any part of the supporting shaft or its flange, the water cannot enter the terminal box. In conventional horizontal scanning transducers it has been the practice to locate the cable seal within the spool core near the top or the bottom end. Typical cases are illustrated in Figures 12, 30, 31, 32, and 33.

In transducers designed for scanning in the vertical

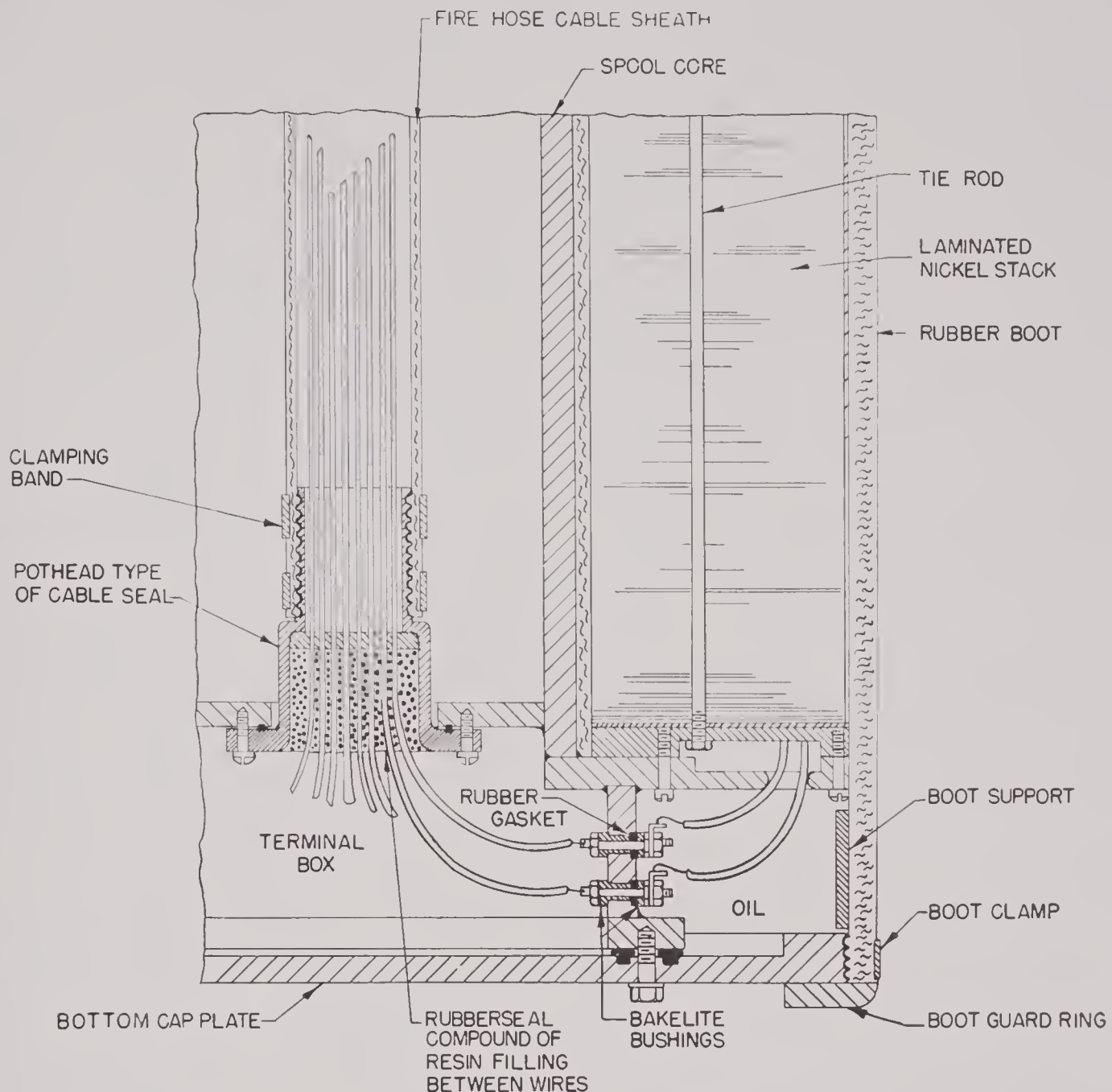


FIGURE 33. A design for a terminal box located in the bottom of a scanning sonar transducer in which the elements are immersed in castor oil.

plane, the elements are usually divided into left and right halves to give *bearing deviation indication* [BDI].⁸⁹ Each half has its own terminal board. In some designs the double cable required was brought through a single cable seal, as in the first form of the Harvard HP-3DS transducer (see Figure 10). A cable seal of the type shown in Figure 33 was used at the position of the flange on the transducer, as indicated in Figure 34. This cable and water seal were later replaced by two 50-twisted-pair telephone cables and two packing-gland seals located at the same position as the pothead seal. The packing-gland

type of cable seal is preferred, provided satisfactory watertight sheathed cable is available.

Another arrangement for the cable seals and terminal box for depth scanning sonar transducers is shown in Figure 35. Here a cable passes through each of the two supporting flanges and the cable seal is located in a "dutchman," which is inserted between the transducer flanges and the supporting flanges.

6. It is desirable to have the cable or cables sealed on the outside of the sheath and between the individual conductor wires at the place where they leave the terminal box. Such double sealing not only pre-

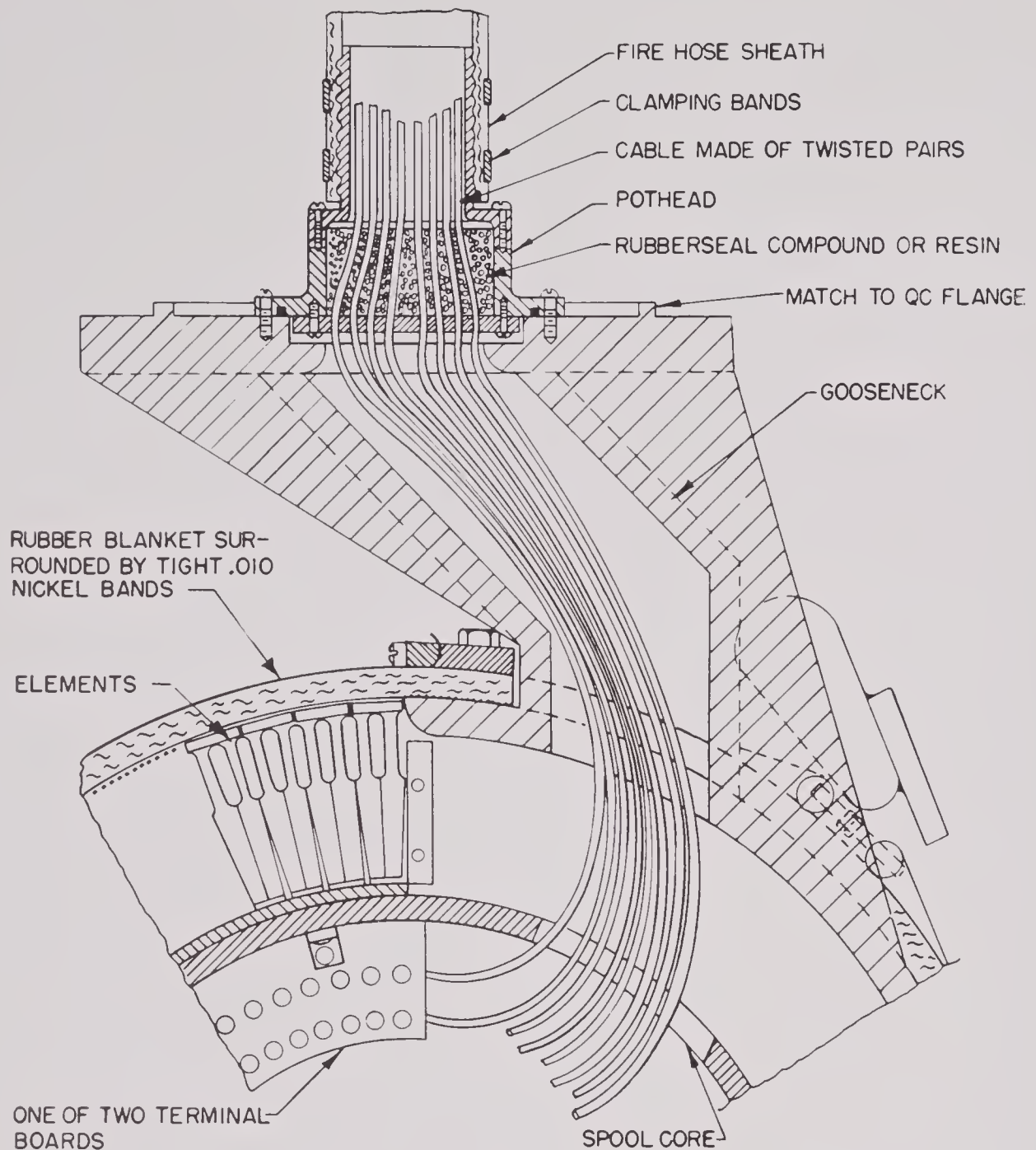


FIGURE 34. Terminal box and cable seal design used in the HP-3DS depth scanning sonar transducer.

vents the entrance of water or water vapor into the terminal box through the inside of the supporting shaft, but also prevents the leakage of vapor or water between the individual wires of the cable. The sealing of the individual wires is desirable but not essential because the rate of flow of water or vapor between the wires of a compact multiconductor cable 40 or 50 ft in length is very small.

The terminal box cable seals illustrated in Figures 12, 30, 31, 32, and 35 are of the conventional packing-gland type in which a rubber gasket is

squeezed tightly against the outside of the cable sheath and the inside packing-gland wall. In seals of this type, the gasket should grip a length of the cable at least as great as half the diameter of the cable and preferably as great as the diameter. Likewise, the bushings, or parts of the seal on each side of the gasket, should extend a distance approximately equal to the diameter of the cable.

If the length of cable against which the gasket squeezes is too small, the seal may gradually loosen because of the cold-flow of the sheath material, with

CONFIDENTIAL

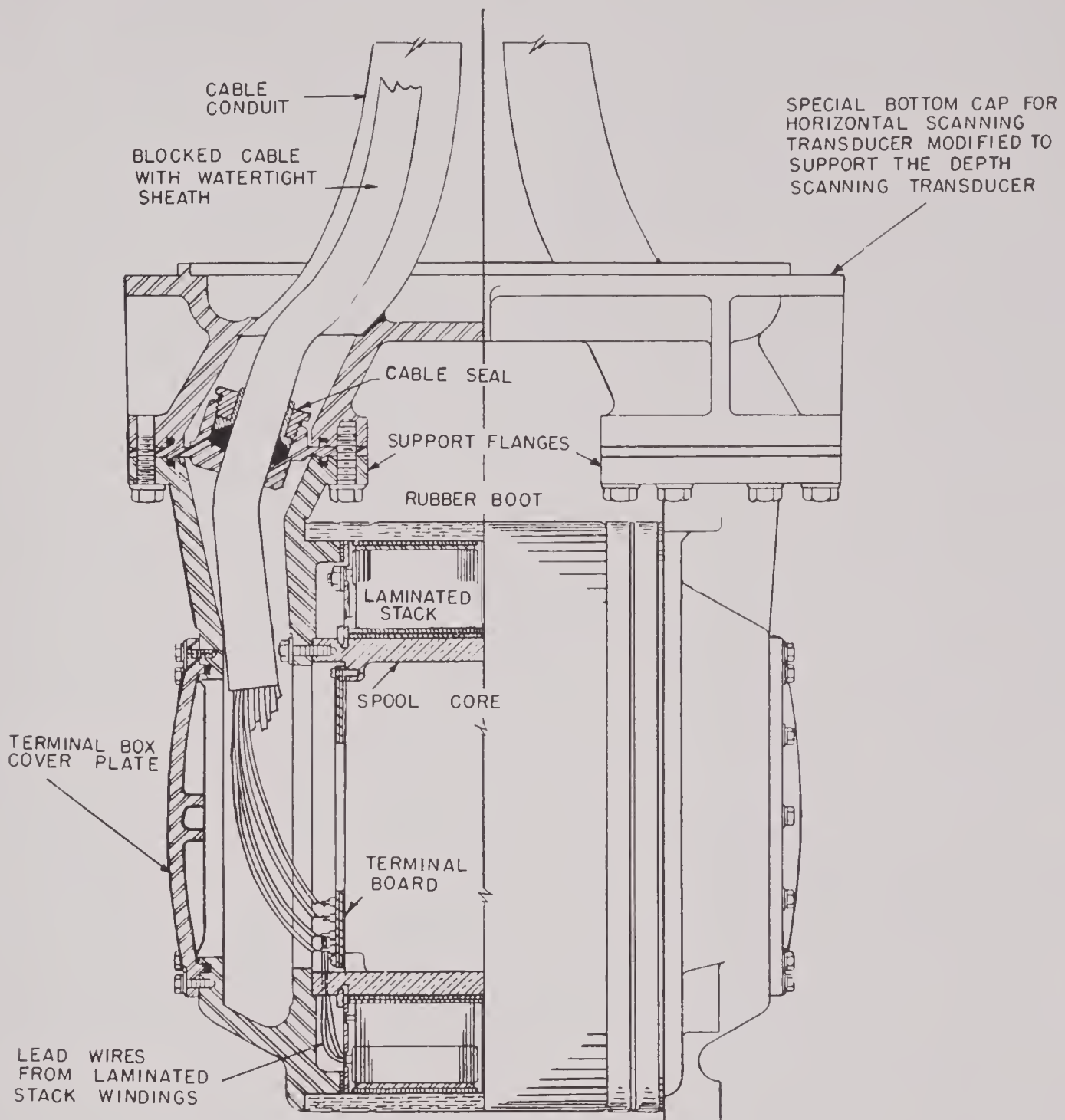


FIGURE 35. Design details of a depth scanning transducer with a two-flange support and two cable seals.

a consequent "hourglass" deformation. This effect can be minimized by use of close-fitting bushings, which give the cable sheath good support on each side of the pressure gasket.

Some of the characteristics of cable seal designs of the packing-gland type are shown in Figure 36. Part A shows a seal that is poor because the gasket is too thin and because the cable sheath is not given proper support on each side of the gasket. The pressure of the thin gasket causes cold-flow of the sheath

material away from the gasket region and a bulge out beyond each narrow gasket washer. The seal shown in part B has adequate width and thickness but the washers or bushings are not long enough to give the cable sheath sufficient support to minimize cold-flow. The seal shown in part C is very good, provided the bushings fit the cable sheath close enough to minimize cold-flow of the sheath material. The diameter clearance of the bushings from the cable should be approximately 2 per cent of the diameter

CONFIDENTIAL

of the cable. Part D shows a seal that may be tightened from each end. Part E shows a seal that is designed to seal and hold a cable against the very high water pressures encountered by submarines which go deep and are subjected to pressure waves set up by depth charges. Under very high pressures a cable is likely to slide through a packing gland, much like a piston rod. In such cases it is good practice to mold

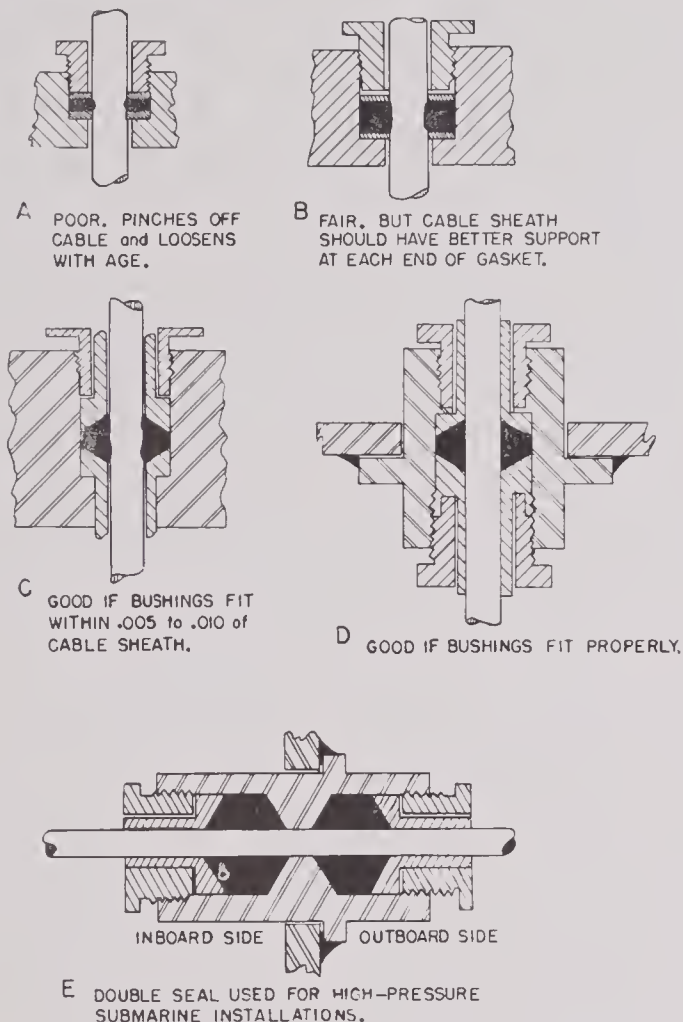


FIGURE 36. Some designs of cable seals of the packing-gland type.

one of the gaskets directly to the sheath of the cable. There are many possible variations in the design of packing-gland seals, but whatever they are they should use gaskets of adequate radial and longitudinal thickness and should give the cable sheath side support for a sufficient distance on each side of the gasket.

To prevent leakage of water through the spaces between the many conductors of a sheathed cable which is sealed on the outside by a conventional packing-gland type of seal, it is necessary to fill all the spaces between the conductors with a blocking material such as tar or resin. One popular method is

to introduce a monomer liquid into the interstices of the cable conductors in the region of the seal and cause this liquid to polymerize to form a gummy-to-hard resin. When the cable must be flexible on each side of the seal, care should be taken that the resin-forming liquid is not allowed to penetrate too far on either side of the seal.

The pothead type of cable seal illustrated in Figures 33 and 34 is most often used with homemade cables made up of twisted pairs of single wires. These pothead seals are made by threading each wire through its proper hole in the base plate of the pot. Then the space between wires in the pot is filled with material such as Rubberseal compound (or some thermosetting resin), which adheres closely to the wires and to the sides of the pot. Seals of this type have proved satisfactorily watertight. Their mechanical strength to withstand hydrostatic pressure is determined by the strength of the pot and its bottom plate. The examples shown in Figures 33 and 34 were not designed for high mechanical strength.

13.2.5 Cables for Scanning Sonar Transducers

1. In most scanning sonar systems the scanning commutator is located inside the ship. It is necessary, therefore, to run wires from each element of the transducer to the commutator chassis, usually 40 to 50 ft away. To minimize electromagnetic and electric pickup and cross talk in these long wires, it is good practice to use a twisted pair of conductors from each element. Because of pickup and cross-talk troubles it is not good practice to connect one terminal of each element to a common ground in the transducer or to a common shield of the cable. It has been found preferable to bring out both wires from each element to the commutator chassis. When three or more leads are brought from each transducer element, these should be run in the cable as a twisted multiplet. When the lead wires are run in the cable as twisted pairs or multiplets, there is no need for a common electric shield around the whole cable. The conductors forming the cable should be color-coded to eliminate the necessity of "ringing through" and marking each wire with a label.

The bundle of wires forming the cable should be surrounded by a watertight sheath. The complete cable should be as flexible as possible, especially when the transducer must be trained to point in different directions with respect to the ship by rotation of the

transducer shaft. In such cases a stiff cable would be worn out in a few weeks of steady operation, due to internal straining and rubbing of the conductors in the cable. In this respect, solid wire conductors are particularly unsatisfactory because they "work-harden" and break when subjected to continuous flexing and twisting. The insulation on the individual conductors should be capable of withstanding abrasion against neighboring conductors. Abrasion can be minimized by use of certain waxy lubricants. If the cable is to be properly flexible it should have a core of some pliable material, such as hemp or jute, and the sheath should not bind the conductors together too compactly.

For those installations in which the transducer must be rotated, the cable should be able to withstand, during continuous duty, torsional rotation of 360 degrees or more in both directions in about 10 ft of length. A number of specifications may be laid down for construction of a satisfactory cable. (1) The resistance of the individual conductors should not be greater than 10 ohms per 1,000 ft. (2) The insulation resistance between any pair of wires should be at least 10 megohms for 1,000 ft of cable. (3) The electric capacity between the wires of any twisted pair should not exceed approximately 50 mmf per ft and the capacity between any two wires not in the same twisted multiplet should not exceed about 30 mmf per ft. (4) The cross talk between any two twisted pairs should be less than -50 db. (5) The strength of insulation between any two wires in the cable should be at least 1,000 volts. (6) The insulating material should have reasonably low dielectric hysteresis loss in the frequency region of 10 to 60 kc.

The outside diameter of the cable should not exceed 1½ in.; its sheath should be watertight, tough, and flexible and resistant to abrasion and to deterioration by action of grease, oil, salt water, air or sunlight. It should have as little tendency as possible to cold-flow when under pressure from the gasket of a cable seal. Several of the synthetic and natural rubber compounds meet most of these requirements. In some scanning sonar transducer cables, rubber-lined fire hose has been used satisfactorily as the cable sheath.

The cable should be able to withstand and operate at temperatures up to about 170 F and down to about 20 F. Cables with Vinylite insulation on the conductors or Vinylite sheaths become soft and weak at the higher temperatures and stiff at the lower, possibly causing some impairment in performance.

Neoprene or rubber insulations, on the other hand, seem to be satisfactory in this respect. Cables intended for use on submarine installations should be able to withstand external pressures of at least 1,000 lb per sq in. without damage to the internal insulations or the sheath.

2. The cables used on the earliest scanning sonar transducers were constructed at HUSL because commercial cables with the proper characteristics were not immediately available.

Details of construction of the one that proved reasonably satisfactory for a 48-element scanning sonar transducer are given in Chapter 14. This had the general appearance and flexibility of a manila rope. Provided with a loose-fitting fire hose and sealed into the terminal box with a pothead seal of the type shown in Figures 33 and 34, this cable met the requirements outlined above in an experimental installation on board ship.

A Navy-approved armored telephone cable, TTHFA-50, meets most of the specifications, but it is too stiff for installations in which the transducer has to be rotated. At present there is no commercial cable that is satisfactory for scanning sonar in all regards, and a development program looking to the production of such a cable is highly desirable.

13.2.6 Acoustic Contact Between Elements and the Water

The problem of getting good acoustic contact between the vibrating elements and the water is an important one, especially so when the elements are housed in watertight casings. Included in this problem is the nature of the surface that makes contact with the water. Some surfaces have a greater tendency than others to collect or generate gas bubbles. Even a small collection of these bubbles on the active face of a transducer can cause poor acoustic contact with the water. A smooth surface exposed to the water gives much less trouble than a rough one, and for this reason metal surfaces frequently prove troublesome unless they are smoothly coated with certain paints or enamels. Smooth rubber surfaces, free from oil or grease, are usually satisfactory. Bubbles are most likely to collect when the transducer is put into water that is colder than itself. The warm transducer increases the temperature of the water in contact with it, causing some of the dissolved gas to come out of solution and accumulate on its surface.

Transducers with free-flooding elements usually

present few problems in maintenance of acoustic contact when precautions are taken against the condition just described. With metal-faced transducers, smooth, nonporous material that is resistant to corrosion and electrolysis should be used. Uncoated steel is notably poor in these respects. Stainless steel and Navy M bronze are usually quite satisfactory. Experiment has shown that uniform and reproducible acoustic contact between most metals and water can be obtained if the metal is coated over with some nonporous, water-resistant, firmly adhering paint. Vinylite, rubber, neoprene, or polystyrene base paints have been found to be well adapted to this purpose. The active faces of laminated stacks are not perfectly smooth even when the stacks are constructed with the greatest care and are, therefore, apt to collect bubbles on their surfaces when in direct contact with the water. One of the best means of obtaining good contact between the stack face and water is to cement rubber, or its equivalent, securely to the face of the stack.

The most satisfactory bond between the laminated stacks and rubber faces so far found at HUSL is made with Cycle-Weld 55-6 resin. An example of a design making use of this type of acoustic contact with water is shown in Figure 19. If the laminated stack elements of a complete transducer are housed by a single rubber boot, acoustic contact may be made between the rough active faces of the stacks and the inside of the rubber boot by vacuum-filling the space between the elements and the boot with a liquid like castor oil or its equivalent. An example of this type of construction is illustrated in Figure 15.

Another method is illustrated in Figures 16 and 18. Here molded face strips of rubber or other suitable material are bonded securely to the active faces of the laminated stacks. The rubber boot is made 12 to 15 per cent undersize so that when it is stretched on the transducer it makes tight contact with the face strips of the elements. A film of castor oil is painted on the faces of the elements and on the inside surface of the rubber boot before they are put together. The film of castor oil aids the acoustic contact between the face strips and the rubber boot by filling in small irregularities in both surfaces. The external water pressure helps to make this acoustic contact more nearly perfect.

In special cases in which the rubber envelope cannot be made in the form of a complete cylindrical boot, the necessary pressure on the rubber may be secured by surrounding the outside of it with narrow

thin bands of stainless steel and drawing these tight by means of turnbuckles (see Figure 10). The thickness of the bands should not exceed 0.015 in. and the width should not be greater than 1 in. The turnbuckle assembly required to tighten the bands is somewhat clumsy, difficult to streamline, and vulnerable to damage by catching on external objects.

13.2.7 Streamlining of Scanning Sonar Transducers

In any echo-ranging system on shipboard, the transducer must be mounted so that no part of the ship's hull interferes with the reception or transmission of sound through the water. In surface ships the transducer should be placed well below keel level, and for topside submarine mounting the transducer should be placed in a position where none of the superstructure interferes seriously with the sound beam. These requirements make it necessary to place the transducer in the fastest part of the water stream around the ship, and streamlining in some form becomes essential.

The solution may be to streamline the transducer itself as much as possible without interfering with its acoustic behavior, but, if it is intended that the sound gear operate satisfactorily when the ship's speed exceeds 10 or 12 knots, it is necessary to surround the transducer with a streamlined dome having a length-to-width ratio of the order of 3 or 4. At water speeds greater than 10 or 12 knots, turbulence occurs around the surface of the large cylindrical transducer, producing a great amount of acoustic noise, which masks the relatively weak echo signals.

Acoustic considerations limit the amount of streamlining that can be applied directly to the main body of a scanning sonar transducer. Hence the streamlining must be limited to rounding all sharp corners and irregularities on the ends and edges of the transducer body. This is usually accomplished by the use of spun sheet-metal fairings or specially shaped blocks of waterproof wood.

If a transducer is to be used without the protection of a dome, some consideration should also be given to the mechanical effects of the water stream on the active face. The mechanical abuse, by the water, of the active face of a transducer mounted on the topside of a submarine is quite severe when the submarine is cruising on the surface at such a level that the waves break over the bow and crash into the transducer. The impacts of the waves might cause

some flapping of the rubber boot against the element faces and perhaps some distortion of the elements. Figure 9 illustrates one way of holding the rubber boot firmly against the element faces and at the same time giving mechanical strength and protection to the face of the transducer without acoustic interference.

13.3 DESIGN OF VIBRATING ELEMENTS

13.3.1 General Considerations

Requirements for the generation of acoustic power by a scanning sonar transducer and the limitation on the mechanical and electrical phase variation have been set forth in sections 13.1.3 and 13.1.4. The tolerance on the mechanical phase variations among the elements automatically sets the tolerance on the product of the Q_m and the $\delta f/f_{avg}$. Consequently, if Q_m is large, then $\delta f/f_{avg}$ must be small, and vice versa. Since Q_m , the maximum efficiency, the coupling coefficient, etc. are all related and are all involved in the design of transducer elements, the relationship will be discussed at this point.

Equation (81) of Chapter 3 gives the relation

$$\text{Eff}_{\max} = \left(\frac{1}{1 + \frac{1}{k_{\text{eff}}^2 Q_{YW} Q_c}} \right) \left(1 - \frac{Q_{YW}}{Q_{YA}} \right),$$

in which k_{eff} is the effective electromechanical coupling coefficient; Q_{YW} is the Q shown by the motional admittance circle when the measurement is made with the transducer loaded by water radiation resistance; Q_c (the electrical Q) is the ratio of the reactive and conductive components of the clamped-core admittance; and Q_{YA} is the Q shown by the motional admittance circle when the transducer is subjected to no radiation loading. The first factor of the right-hand side of equation (81) of Chapter 3 may be thought of as the electromechanical efficiency, that is, the fraction of the electric input power that is converted into mechanical power. The second term may be thought of as the purely mechanical efficiency which is the fraction of the total mechanical power radiated as acoustical power. If R_L is the radiation resistance and R_m'' is the equivalent internal frictional resistance, then the mechanical efficiency is

$$\frac{R_L}{R_L + R_m''} = \frac{Q_{YA} - Q_{YW}}{Q_{YA}}, \quad (6)$$

$$Q_{YA} = \frac{2\pi f_0 M^*}{R_m''} \quad \text{and} \quad Q_{YW} = \frac{2\pi f_0 M^*}{R_L + R_m''}, \quad (6a)$$

where f_0 is the frequency of resonance and M^* is the equivalent mass of the vibrating parts, i.e., the mass which, when vibrating with the same frequency and amplitude as the active face, has the same kinetic energy as the actual vibrating system.

Let us now suppose that a magnetostrictive transducer element is made which has a given geometry, magnetic circuit, windings, etc., but that the area of the radiating face can be changed without altering any of the other characteristics, so that R_L can be varied while k_{eff} , Q_c , and Q_{YA} (or R_m'') remain constant. It will be of interest to study briefly the effect on the efficiency due to varying R_L . This is important in design because the ratio of the radiation resistance to the internal frictional resistance should be adjusted roughly to give maximum efficiency.

Let $R_L = x R_m''$. Then, the mechanical efficiency

$$\text{Eff}_m = \frac{R_L}{R_L + R_m''} = \frac{x}{x + 1}, \quad (7)$$

and the electromechanical efficiency (equations (81) of Chapter 3 and (1) and (1a) of this chapter),

$$\text{Eff}_{em} = \frac{k_{\text{eff}}^2 Q_c Q_{YA}}{k_{\text{eff}}^2 Q_c Q_{YA} + 1 + x}. \quad (8)$$

Two cases will be considered. First, a typical tube-and-plate type of transducer will be used to illustrate the effect of a low k_{eff} and, second, a typical laminated stack made of thin ring laminations will be used to show the effect of a high k_{eff} .

1. Typical values for a tube-and-plate transducer are: $k_{\text{eff}}^2 = 0.0011$, $Q_c = 5.0$, $Q_{YA} = 180$. These values give

$$\text{Eff}_{em} = \frac{0.99}{1.99 + x},$$

$$\text{Eff}_m = \frac{x}{1 + x},$$

$$\text{Eff}_{\text{total}} = (\text{Eff}_{em})(\text{Eff}_m).$$

The values of these three efficiencies and Q_{YW} are plotted against x in Figure 37. The electromechanical efficiency drops steadily and the mechanical efficiency increases as the radiation load increases. The total efficiency reaches a broad maximum of 16 per cent in the region of $R_L = 1.4 R_m''$, at which the Q_{YW} is about 75. For practical purposes it would be better to design for $R_L = 4 R_m''$, which would give an efficiency of about 12 per cent and a Q_{YW} of 35. The adjustment of R_L in a design of this type can be accomplished by changing the area of the face associated with each

tube and changing the thickness of the plate accordingly to provide the same mass load for each tube.

2. Typical values for a stack of thin annealed nickel rings are: $k_{eff}^2 = 0.057$, $Q_c = 7.0$, $Q_{YA} = 45$. These values give

$$\text{Eff}_{em} = \frac{18}{19 + x}$$

$$\text{Eff}_{total} = \left(\frac{18}{19 + x} \right) \left(\frac{x}{1 + x} \right).$$

The values of the three efficiencies and the values of Q_{YW} are plotted against x in Figure 38. The relatively large values k_{eff} and Q_c keep the electrome-

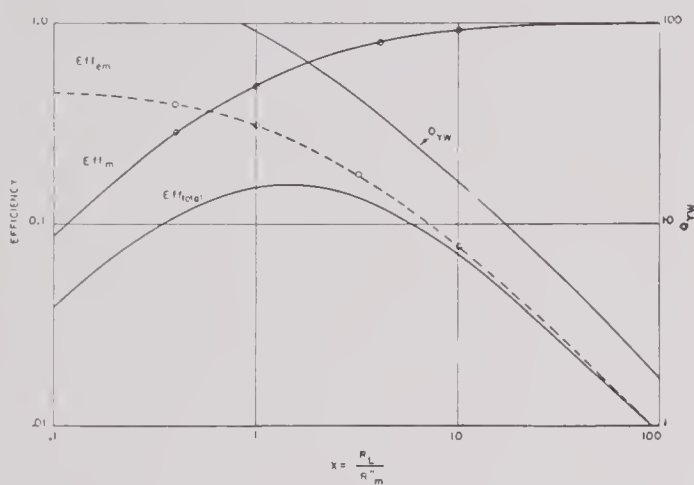


FIGURE 37. Relation between the efficiency and R_L / R_m'' for a typical plate-and-tube type (WEA-1), on the assumption that $2\pi f M^* R_m'' = Q_A$ is constant and R_L is varied.

chanical efficiency at a high level even though the load resistance is increased to large values. In this case the total efficiency reaches a broad maximum of 65 per cent at $x = 4$, where the $Q_{YW} = 9$. Even at a $Q_{YW} = 2$, the total efficiency is of the order of 40 per cent. This performance is about the best that can be obtained from magnetostrictive ring stacks made for practical use. In practice the ratio of R_L / R_m'' for ring stacks can be most easily controlled by adjusting the ratio of the wall thickness to radius.

The last example shows the importance of large values of k_{eff} and Q_c in keeping the electromechanical efficiency at relatively high values. The k_{eff} is determined by the geometry of the magnetostrictive vibrator, by the perfection of the magnetic circuits for the polarizing flux and high-frequency flux, and by the kind of magnetostrictive material which is used, its heat treatment and degree of polarization. The highest possible value of k_{eff} is obtained from a magnetostrictive vibrator in which all the parts of

the magnetic path in the magnetostrictive material are subjected to a uniform alternating mechanical strain and uniform optimum polarization. This set of conditions is realized in a stack of rings or a tube in which the direction of the flux and the mechanical strain is circumferential and uniform. In this case

$$k_{eff} = \left(\frac{4\pi\lambda^2\mu_r'}{E} \right)^{\frac{1}{2}}.$$

The k_{eff} is less than this for all the various kinds of longitudinal vibrators because the mechanical strain is not uniformly distributed along the magnetostrictive parts of the magnetic circuit. In such cases it is

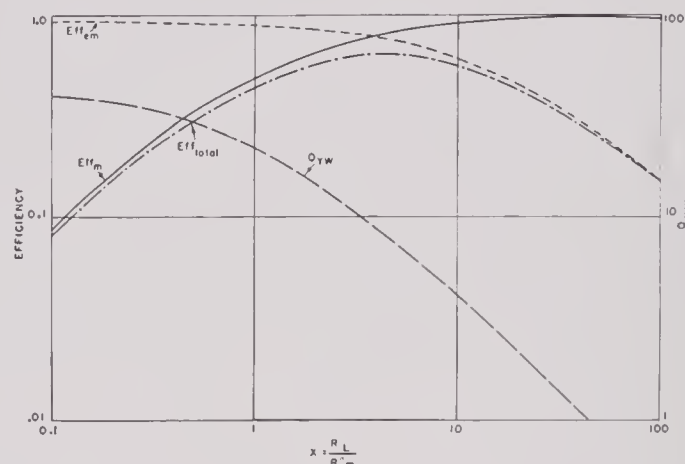


FIGURE 38. Relation between the efficiency and R_L / R_m'' for a stack of thin annealed nickel laminations. It is assumed that $Q_{YA} = 2\pi f M^* R_m''$ is constant and that R_L is varied.

all the more important to do everything possible to keep the $\lambda^2\mu_r'$ factor as large as possible. μ_r' is the effective reversible permeability of the *complete* magnetic circuit.

Occasionally requests are made for magnetostriction transducer elements which are 75 per cent efficient at a Q_m of about 4. To show how difficult it would be to make a transducer element of the longitudinal vibrator type having these characteristics, the case will be analyzed. By using great care in the construction of the unit, it might be possible to make the mechanical efficiency as great as 90 per cent. Consequently the electromechanical efficiency would have to be about 85 per cent. This requires that the value of $k_{eff}^2 Q_{YW} Q_c$ be about 5.5. The maximum attainable value of k_{eff}^2 for this type of oscillator is about 0.035. As Q_{YW} is required to be 4, it follows that Q_c would have to be about 40. This high electrical Q_c for the clamped-core impedance could be obtained only by the use of very thin laminations, so that the eddy-current losses would be very small.

Even the use of thin laminations would not be effective in maintaining the high Q_c at high power levels on account of magnetic hysteresis losses. Very thin laminations are difficult to punch and handle. A very large number of them are required to give the requisite stack height. Consequently, in practical design and construction work it is generally better to use thicker laminations and higher Q_m 's to get high efficiencies.

13.3.2 Tubular Transducer Elements

Transducers made of relatively thin-walled magnetostrictive tubes (i.e., with wall thickness to diameter ratios of the order of 0.025) which oscillate in the radial direction are noted for their flatness of frequency response, uniform horizontal patterns, and moderately low efficiency. Transducers of this type would, therefore, make good elements for a scanning sonar transducer intended primarily for listening over a wide frequency range.

A design of this type is illustrated in Figure 28. In this design each element would consist of a complete tubular transducer of the B-19H type described in Chapter 5. The length of the tubes should be about 4 to 7 wave lengths of the sound in water at the frequency used. The outside diameter of the tubes should not exceed 0.6 the wave length of sound in water at the highest frequency to be used. The frequency of resonance in kilocycles of tubes of this type is about $60/D$, where D is the mean diameter in inches but the Q is so low that the resonance is not very pronounced. The efficiency also has a small maximum at the frequency of resonance.

The natural frequency of radial resonance of a tubular type transducer can be lowered by effectively decreasing the circumferential stiffness without reducing its mass. It is possible that this result could be obtained by corrugating the tube lengthwise so that the circumference of the tube is a wavy circle. By adjusting the width and depth of the corrugations, almost any mass-to-stiffness ratio within reasonable limits can be produced, and consequently the frequency of resonance can be controlled toward lower values, although the mechanical Q would increase. By this method it should be possible to make tubular transducers with frequencies of resonance low enough so that the outside diameters of the tubes are less than the corresponding wave lengths of sound in water. Tubular transducers of this kind could be used as elements in a scanning sonar transducer of the

type illustrated in Figure 28 and could be operated at frequencies up to their resonance without difficulty from poor patterns. It is questionable whether any gain in efficiency could be made in this way, as compared to the uniform circular tube, because some of the circumferential stiffness of the tube is due to bending stiffness, and deformations caused by bending give no net magnetostrictive action. This would effectively reduce the electromechanical coupling coefficient.

Another variation of the tubular type of scanning sonar element is illustrated in Figure 29. This has been called the "tubular-arch" type. In this design one element consists of an adjacent pair of tubular arches which are welded or soldered down to the solid backing plate. It can be shown that the frequency of resonance in the extensional mode of vibration of such an arch, which is rigidly hinged at each end, is the same as that of a complete tube having the same radius. Thus if the tubular arches are semicircular and have a span of $\frac{3}{8}$ in., the frequency of resonance (without load) would be about 160 kc. The spacing between elements is about $1\frac{1}{4}$ in., and if this spacing is held below one-half wave length the highest frequency at which the transducer should be operated is about 28 kc. Thus the tubular-arch transducer elements would have to be operated at frequencies far below their resonance, with consequent loss in efficiency. The efficiency of this type of element is not very high at best, because of too great water radiation loading, eddy-current losses, and an inherent shorted turn. Furthermore, it is almost impossible actually to construct the units so that the arches are uniformly and firmly attached to the backing plate at each edge. Direct-current polarizing is required to produce the polarizing flux.

Another type of radially vibrating tube is the laminated stack of rings, wound toroidally. The natural frequency of vibration of such ring stacks is the same as for tubes, i.e., about $60/D$ kc where D is the mean diameter of the rings in inches. Consequently the wave length of the sound in water at the frequency of resonance is about equal to the diameter of the tube, which is inconsistent with the requirement for scanning sonar transducers that the elements be spaced one-half wave length apart. To satisfy the last requirement, the ring stacks would have to be operated at approximately one-half their natural frequency, with consequent loss in efficiency. However, if the ring laminations are made thin enough to make the eddy-current losses very small, and if the

wall thickness of the ring stack is made sufficiently thin to lower the Q to the order of 3 to 5, the stacks can still be made to operate at half-resonance frequency with an efficiency of the order of 10 to 15 per cent. If the resistive loading of a ring stack or tube is due entirely to water radiation resistance, its mechanical Q should be $30.5 t/R$, where t is the wall thickness and R the mean radius. Thus to get a Q of 5 the t/R ratio should be about $1/6$.

If the stacks are wound toroidally, the polarizing flux has to be circumferential. The polarizing flux provided by the remanence flux is sufficient if the

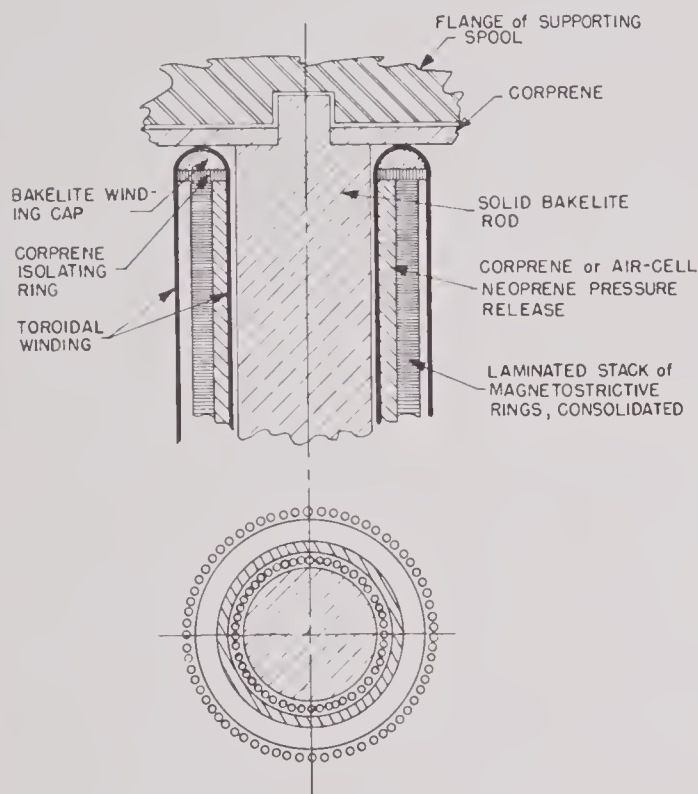


FIGURE 39. Suggested details of construction of a ring stack element for a scanning sonar transducer.

rings are made of semiannealed nickel or 2V-Permendur and if the ring stack elements are not driven magnetically beyond 10 or 12 oersteds (peak) during transmission of pings. If higher transmitting powers are required, the remanence polarization of ring stacks must be aided by some d-c polarizing current flowing in the windings in the proper direction.

A suggestion for making the long slender ring stacks into strong self-supporting units that could be mounted between the two flanges of a supporting spool is shown in Figure 39. The bakelite core is suggested because a shorted turn around the ring stack would be produced if the core were made of metal that would make electric contact with the metal sup-

porting spool at each end. A metal core would be satisfactory if its ends were insulated from the spool flanges. The complete array of ring stack elements would be housed within a rubber boot, and the space around the elements would be vacuum-filled with castor oil or its equivalent.

The rings used in making the laminated ring stack elements are punched from flat sheet stock of magnetostrictive material, a wasteful procedure since the rings are quite narrow. Sheet stock could be used without waste if it could be cut up into strips as wide as the desired wall thickness and these strips wound edgewise to form a ring stack. Some experiments have been performed on the edgewise winding of such narrow thin strips but with not too successful results. The success of this method depends mostly on the development of a good edgewise-winding machine.

13.3.3 Laminated Stack Transducer Elements of the Longitudinal Oscillator Type

WEDGE-SHAPED TYPE

The space available for all the parts of a single element in a scanning sonar transducer has the shape of a trapezoidal prism. To fill this space efficiently, the active parts of the element should have the same trapezoidal section. Elements having this shape are shown in Figures 15, 16, 18, and 19. In elements of this type the node is approximately at the center, and the outer faces are the loops. The outside face works against the acoustic resistance of the water while the inside face works against the pressure-release backing material which, ideally, should present no mechanical load at all. Consequently, except for internal energy losses in the laminated stack itself, the mechanical energy of the vibrating stack is directed into the water as sound radiation. This type of element makes use of nearly all the active area of the transducer face and consequently is capable of radiating the maximum amount of power into the water during transmission.

Lamination Design. The points that must be taken into consideration in the detailed design of a lamination are:

1. Diameter of the cylinder formed by the active faces of the elements;
2. Available active face width for each element;
3. Angle of taper, or number of elements;
4. Ratio of active face width to total leg width;

5. Depth of active face;
6. Position of node;
7. Magnet slot, if the laminated stacks are to have permanent-magnet polarization.

The *approximate* dimensions for laminations of this type are shown for active face diameters of 12 and 17½ in. in Figures 40 and 41, respectively. It is assumed that the face width of the laminations is

of elements, the beam width is independent of the diameter.

To derive the exact dimensions of the lamination it is suggested that the following procedure be used. First decide on the width of the receiving beam pattern desired and the active face diameter to be used (see Figures 40 and 41). These factors determine the frequency and the number of elements which must

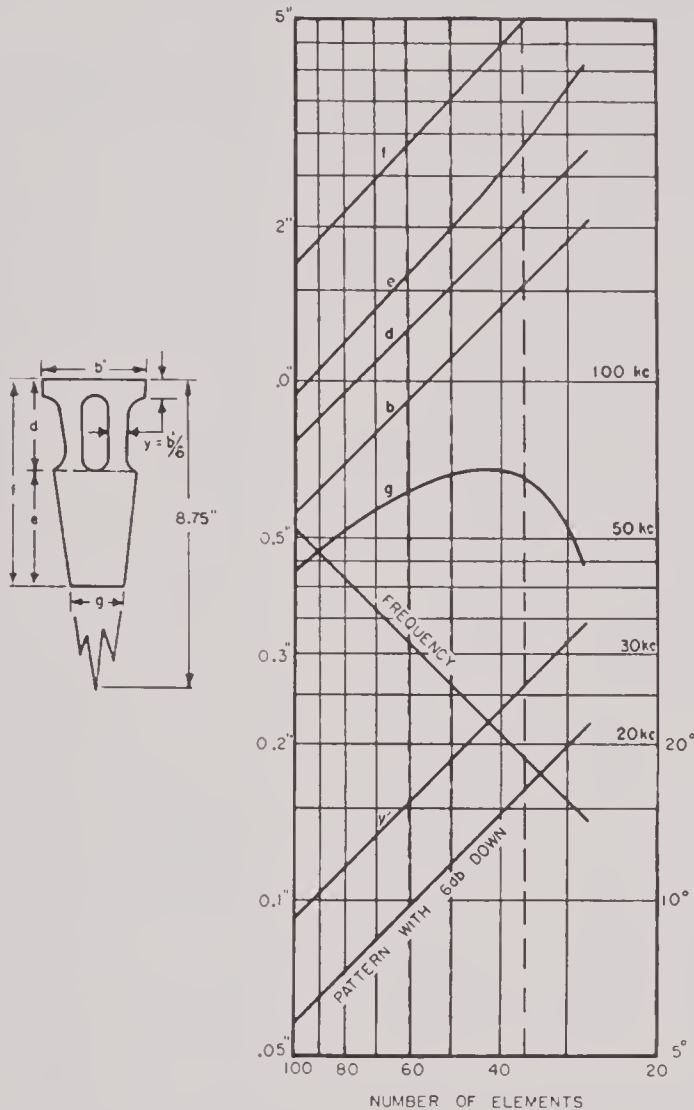


FIGURE 40. Approximate dimensions of wedge-shaped scanning sonar transducer laminations for 12-in. active face diameter.

one-half wave length in water, and the leg width is one-sixth of this. No allowance is made for space between adjacent elements or for a magnet slot. The beam width listed is ± 3 that for the pattern of minimum directivity ratio, as this has been found to be a value within practical attainment. It is to be noted that for a given number of elements the dimensions vary directly and the frequency inversely as the diameter of the transducer. Also, for a given number

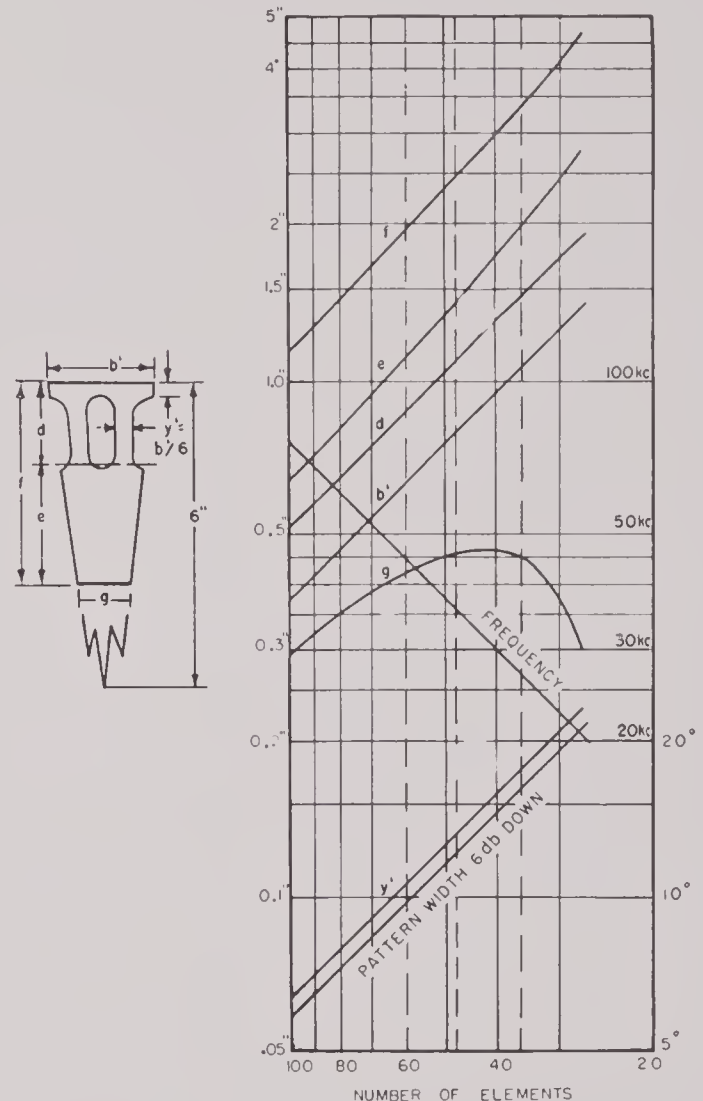


FIGURE 41. Approximate dimensions of wedge-shaped scanning sonar transducer laminations for 17½-in. active face diameter.

be used. About 0.030 in. to 0.050 in. space should be allowed between adjacent elements. This determines the face width, b . To get a mechanical Q of about 12, the width of the legs and the minimum depth of the face section should be about one-sixth the face width. The Q can be adjusted by varying the mass of the face and the stiffness (width) of the legs. This will be discussed in some detail later. The length of the legs should then be calculated by one of the methods out-

lined below. The sum of the face depth and the leg length subtracted from the radius of the active face circle gives the radius of the nodal line (see Figure 42). The length of the tapered tail section must be effectively one-fourth wave length in the lamination. However, due to the fact that the tail section is tapered, the distance from the node to the loop is greater than one-fourth wave length as measured in

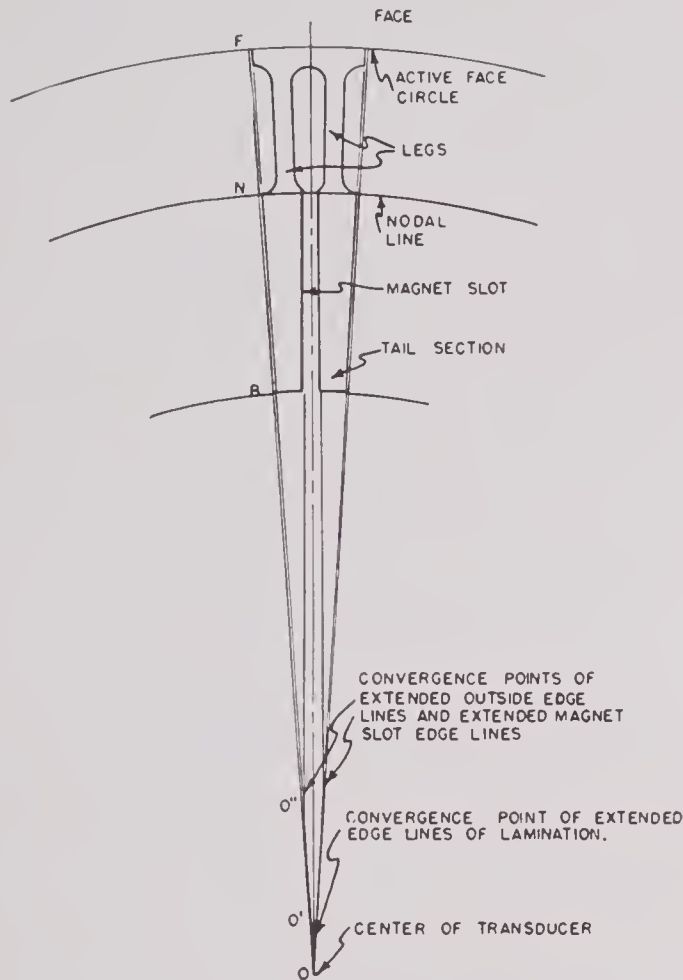


FIGURE 42. Some geometrical relationships to be considered in the design of tapered laminations for scanning sonar transducers.

a bar of uniform cross section. The calculation of this distance will be considered in detail later.

The distance from the front face of the lamination to the node may be calculated by the mechanical impedance method or by the "spring-and-mass" method. In either case, the front half of the lamination is considered to have the equivalent simplified form shown in Figure 43. The mass of the face portion includes some of the arch portion, so that the effective mass is about 20 per cent greater than that included in the thickness y . Allowance should also be made for the taper of the face portion. If δ is the

amount of taper on one edge of the face, as shown in Figure 43, the average span of the face section is $(b - \delta)$. The total effective mass of the face portion then becomes

$$M = \rho t(b - \delta) 1.2y, \quad (9)$$

where ρ is the density and t is the thickness of the lamination. The effective length of the leg portion is as shown in Figure 43, i.e.,

$$L = d - 1.2y. \quad (10)$$

In the mechanical impedance method, the leg portion is treated as a mechanical transmission line

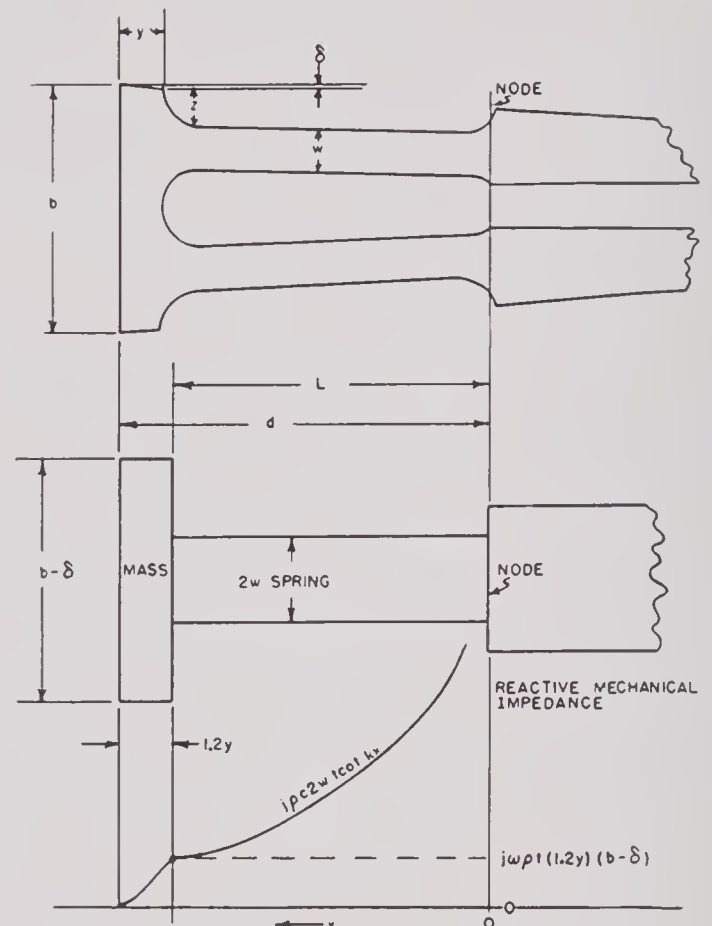


FIGURE 43. Equivalent simplified form of the front half of a tapered scanning sonar transducer lamination.

which is terminated by an infinite mass on one end and the face mass at the other. If this mechanical transmission line is to resonate in its first mode of vibration, the frequency must be such that the mechanical impedance at the one end is infinite and at the other end is $-j2\pi f M$ (i.e., mechanical stiffness reactance). If the distance x is measured along the length of the legs from the node, the mechanical impedance is given by the expression

$$X_m = -j\rho c 2wt \cot \frac{2\pi f}{c} x, \quad (11)$$

where c is the velocity of sound in the lamination material. The first value of x that makes X_m equal to $2\pi f M$ at the desired frequency is the proper length of the legs, L . This can be simplified to the expression,

$$L = \frac{c}{2\pi f} \tan^{-1} \left[\frac{cw}{1.2\pi f y (b - \delta)} \right]. \quad (12)$$

The total distance from the lamination face to the node is, then,

$$d = L + 1.2y, \quad (13)$$

and this determines the position of the nodal line relative to the center of the transducer.

The velocity of sound, c , in magnetostrictive materials depends upon the state of anneal and the degree of magnetic polarization. Consequently, to determine the lamination dimensions that are required to give some nominal *frequency of mechanical resonance*, it is necessary to know the velocity of sound in the material under its specific conditions of anneal and polarization. For nickel which has been oxide-annealed at 900 C and which is polarized to approximately 4,000 gauss, the velocity of sound is about 4.75×10^5 cm per sec and the Young's modulus is about 2.00×10^{12} dynes per sq cm. However, it can be shown theoretically that the frequency of maximum efficiency (which is always a little higher than the frequency of mechanical resonance) remains the same regardless of the degree of magnetic polarization. This frequency is related to the Young's modulus of the unmagnetized lamination material. In many respects it is more logical to design laminations for a nominal frequency of maximum efficiency because this frequency is independent of the degree of polarization, because the maximum efficiency of transmission is obtained at this frequency, and because the maximum receiving response is obtained at this frequency when the transducer element is terminated in its conjugate impedance. The Young's modulus of unpolarized, oxide-annealed nickel is about 2.10×10^{12} dynes per sq cm, and the corresponding velocity of sound is 4.85×10^5 cm per sec. If these values and the nominal frequency of maximum efficiency are used in equations (9), (12), (14), and (15), the proper dimensions will be obtained for laminations having the desired frequency of maximum efficiency. However, since the shape of laminations of this type is so complicated that the actual frequency of a given lamination may differ from the

calculated value by as much as 5 per cent, the above distinction may be of little importance from a practical standpoint.

In the spring-and-mass method, the frequency of the front half of the lamination is taken to be

$$f = \frac{1}{2\pi} \sqrt{\frac{K}{(M + \frac{1}{3}m)}}. \quad (14)$$

where K is the static spring constant of the equivalent single leg, M is the mass of the face section, and m is the mass of the equivalent leg section. The spring constant is given by

$$K = \frac{E2wt}{L}, \quad (15)$$

where E is the Young's modulus for the lamination material and the other quantities are as shown in Figure 43. If this value for K is used, together with the other values as given in Figure 43, the frequency becomes

$$f = \frac{1}{2\pi} \left[\frac{Ew}{\rho L [0.60y(b - \delta) + \frac{1}{3}wL]} \right]^{\frac{1}{2}} \quad (16)$$

and the length, from this, is

$$L = \left[\left(\frac{0.90y(b - \delta)}{w} \right)^2 + \frac{0.75E}{\rho\pi^2 f^2} \right]^{\frac{1}{2}} - \frac{0.90y(b - \delta)}{w}. \quad (17)$$

The distance between the node and the loop at the end of the tapered tailpiece may be calculated from the radius of the nodal line and the velocity of sound in the lamination by the following relation between the Bessel and Neumann functions of the zero and first orders,

$$\frac{J_0(kr)}{N_0(kr)} = \frac{J_1(kr')}{N_1(kr')}, \quad (18)$$

where r and r' are the radii of the node and loop, respectively. Figure 44 gives a curve showing the relationship between kr and $k(r - r')$, where k is the wave number, $2\pi/\lambda = 2\pi f/c$. The two radii, r and r' , are measured outward from the point of convergence of the edge lines of the tapered lamination. Because of the spaces between neighboring laminated stacks, the point of convergence of the extended outside edge lines of the laminations does not coincide with the center of the transducer, O , but falls a little distance out from it, as shown in the point O' in Figure 42. In this case, in which the lamination has no magnet slot, the distances r and r' would be taken

as $O'N$ and $O'B$ respectively. If the lamination does have a magnet slot, the extended edge lines of each half of the tail section have separate convergence points near O'' , as shown in Figure 42. In this case r and r' are taken as $O''N$ and $O''B$ respectively.

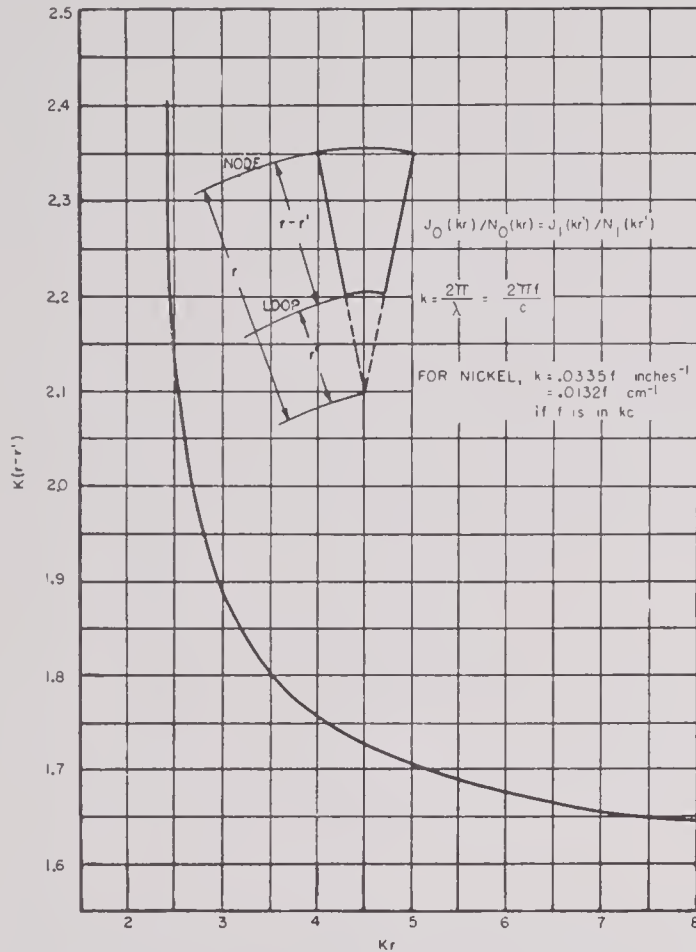


FIGURE 44. Distance between node and loop in tapered lamina.

In the design of the face section of the lamination it is important to make it stiff enough so that all parts of the face move as a single piston when it is working against the stiff water load. The parts of the face section that extend beyond the region of direct support by the legs should be designed so that their frequency of vibration as a cantilever beam in the plane of the lamination is at least four times the frequency at which the lamination is to operate. Consider, for example, the "ears" on the lamination shown in Figure 43. The natural frequency of vibration of this as a cantilever beam is approximately

$$f = \frac{6y}{2\pi z^2} \left(\frac{E}{12\rho} \right)^{\frac{1}{2}}. \quad (19)$$

If b is about 1 in., and y and z each about $\frac{1}{6}$ in., this frequency is of the order of 200 kc, which is sufficiently high for a 26 kc lamination.

The stiffness of the ears on the face section must be great enough to provide the necessary force against the radiation resistance of the water with a deflection which is small in comparison with the amplitude of the face. If the ear is considered as a cantilever beam, as shown in Figure 43, the maximum deflection due to the radiation load is

$$d_{\max} = \frac{\rho c v_0 z^4}{\left(\frac{8E y^3}{12} \right)} = \frac{3\pi \rho c z^4}{E y^3} f A_0, \quad (20)$$

where v_0 is the maximum velocity amplitude of the face, A_0 is the maximum amplitude, and ρc is the specific acoustic resistance of water. The ratio of d_{\max} to A_0 should be of the order of 0.1 or less. As an example of this, the ears on the lamination of the HP-3 type shown in Figure 16 have a d_{\max}/A_0 ratio of 0.018 at 26 kc. In this case, at atmospheric cavitation pressure in water (i.e., 10^6 dynes per sq cm) the rms displacement amplitude of the face is 4×10^{-5} cm, so the deflection of the ear is about 7×10^{-7} cm.

For some applications it may be desirable to design laminations which have higher or lower Q 's than those which are suggested in Figures 40 and 41. To change the Q without altering the frequency it is necessary to change the width and length of the legs and the depth of the face section. Since

$$Q = \frac{\sqrt{K \left(M + \frac{m}{3} \right)}}{b \rho c} \quad (21)$$

and

$$2\pi f = \sqrt{\frac{K}{\left(M + \frac{m}{3} \right)}} \quad (22)$$

(where K , M , and m refer to a unit height of stack), it is necessary to decrease both K and M if the Q is to be decreased without change of frequency, and vice versa. The relations between the Q , the face dimensions, and the leg dimensions are shown graphically in Figure 45. These Q 's are based on the assumption that all the damping of the laminated stack is due to acoustic radiation resistance on the active face. Actually, in any practical laminated stack, there is some internal mechanical damping in the stack. The amount of this internal mechanical damping can be determined by measuring the Q of the laminated stack when the active face of the stack has no mechanical load on it. This is usually done

by measuring the Q when the stack is in air, and the Q under these circumstances is usually referred to as Q_A . The corresponding Q when the laminated stack is loaded with water is usually referred to as Q_W . The relationship between these Q 's and the theoretical one is

$$Q_W = \frac{QQ_A}{Q + Q_A} \quad (23)$$

If the tail portion of the lamination is not so massive as that shown in Figure 45, as is the case for tapered laminations with magnet slots, the Q 's are higher

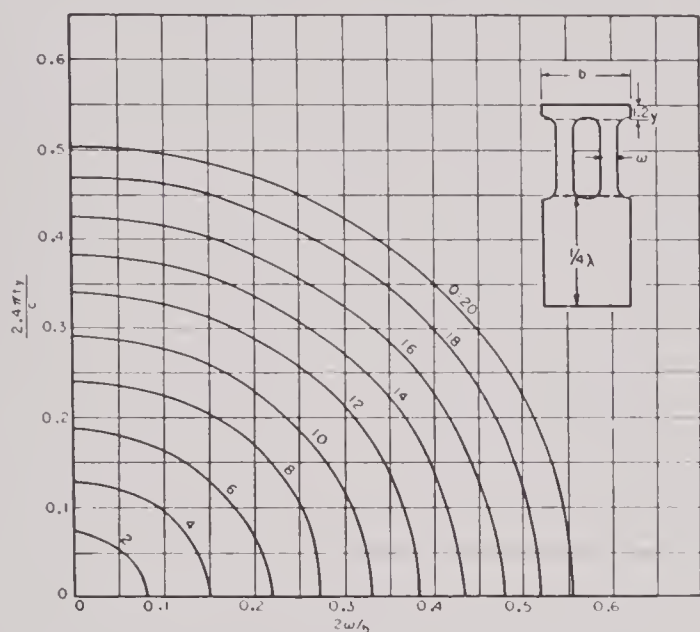


FIGURE 45. Relations among Q , face dimensions, and leg dimensions of laminations of the type shown. (Curves are a plot of $2.4\pi f y / c$ versus $2\omega / b$.)

than those indicated in the graph but less than twice as great. For laminations of the type illustrated in Figure 19, the ideal Q 's should be about 1.4 or 1.5 times those shown in Figure 45.

Polarization. It will be instructive to consider at this point some of the detailed characteristics of the polarization of tapered laminated stack elements for use in scanning sonar transducers.

Some typical tapered laminations are shown in Figure 46. The HP-1 and HP-2 types were designed to be polarized by a component of direct current in the windings, while the HP-3 and HP-8 types were designed to be polarized by permanent magnets. The most active portion of these laminations is in the legs, especially at the base of the legs near the nodal point where the mechanical strain is the greatest. It is therefore important to have the necessary amount

of polarizing flux running parallel to the axis of strain in the legs.

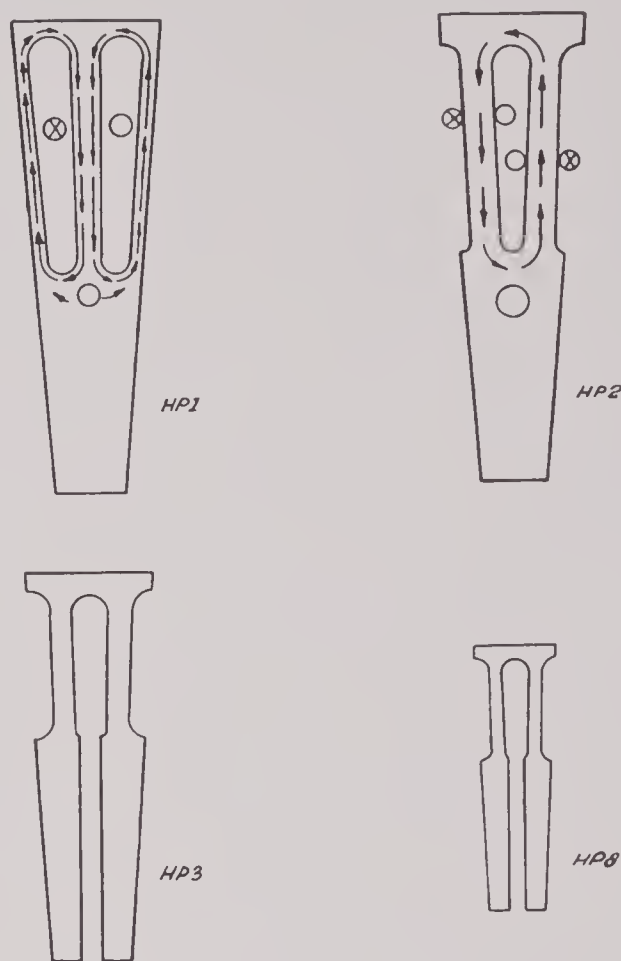


FIGURE 46. Typical tapered lamination forms for use in scanning sonar transducers.

The production of the desired flux density of 3,800 to 4,000 lines per sq cm in the d-c polarized units requires about 40 oersteds of magnetizing field (i.e., about 80 amp turns per inch of magnetic path length) if the laminations are made of oxide-annealed nickel. The length of the magnetic path for laminations of this type is very nearly 2.5 times the leg length. Thus the total number of ampere turns needed is $200L$, where L is the leg length in inches. The determination of the number of turns and size of wire to use in winding a stack of laminations of this type should be based upon the source of polarizing current, the desired a-c impedance, and the available space for windings in the laminated stacks. In the polarizing current circuit, isolating choke coils must be used for each element of the transducer to prevent the alternating-current path through the transducer elements from being shunted by the source of the direct current.

A typical polarizing circuit for use with a 36-element d-c polarized scanning sonar transducer is shown in Figure 47. In this case the polarizing current was passed through the group of 18 even elements in parallel and then through the group of 18 odd elements in parallel. The polarizing current was provided by a large commercial copper-oxide rectifier with filters to smooth out any a-c ripple. The total

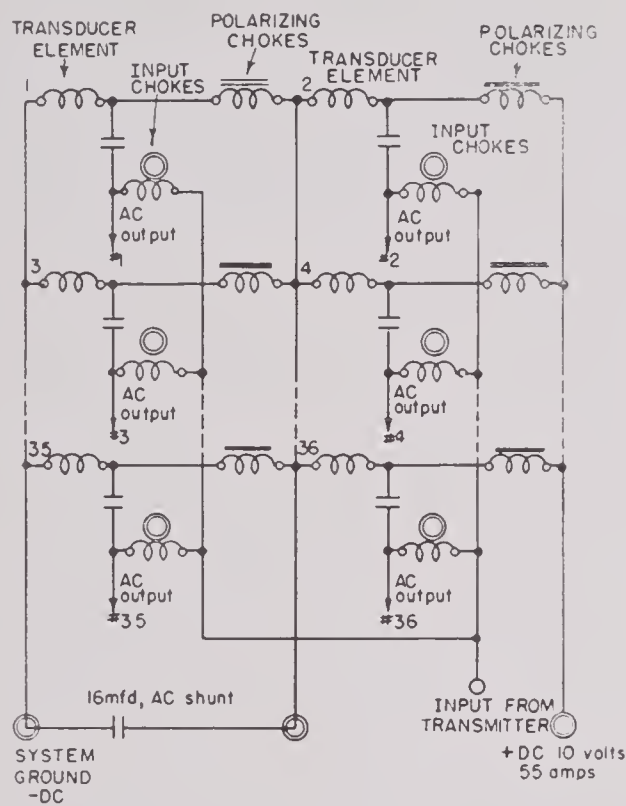


FIGURE 47. Typical polarizing-current circuit for a scanning sonar transducer (36 elements).

power loss in the d-c polarizing current circuit was about 550 watts. This loss was divided about equally between the 36 chokes and the 36 transducer elements. Also, during the pinging interval approximately half of the a-c input power was dissipated in the input chokes and polarizing chokes together. Both these d-c and a-c power losses could be eliminated by making the transducer elements polarized by permanent magnets. In addition, the electric network associated with the transducer is simplified very considerably. For this reason scanning sonar transducers with elements that are polarized with permanent magnets are preferred. For comparison with Figure 47, the electric network associated with a transducer polarized with permanent magnets is shown in Figure 48.

There are several ways in which laminated stacks made of tapered laminations can be polarized by use

of permanent magnets. However, only about four of these ways are practical in terms of the available space, available magnetic materials, and performance. Of these four methods, the one that makes use of sintered-oxide magnets has proved to be the most practical.

One method of polarizing laminations of the HP-2 type shown in Figure 46 is to make the laminations from a bimetal sheet in which the upper half of the strip is of nickel and the lower half of Cunico. Cunico

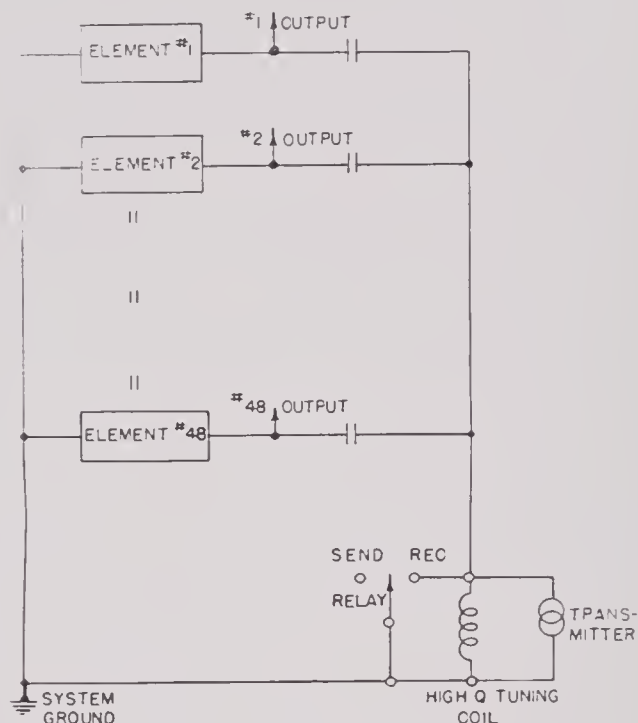


FIGURE 48. Typical electric network associated with a scanning sonar transducer with elements polarized by permanent magnets.

is a copper-nickel-cobalt alloy made by the General Electric Company which can be heat-treated to be malleable enough to roll into thin sheets and later heat-treated to develop magnetic hardness. It is possible to butt-weld a block of nickel and a block of Cunico, edge to edge, in a huge spot-welding machine. These blocks can then be rolled to the desired thickness so that half the width of the strip is of nickel and the other half is of Cunico, with a sharp, straight line of demarcation between the two metals. The laminations are then punched from this bimetal strip so that the face and leg sections are of nickel and the base portion of Cunico, with the line of demarcation at the base of the legs. After the laminations are punched, they are heat-treated to harden the Cunico. Fortunately, the hardening treatment for the Cunico simultaneously anneals the nickel

part. The laminations are then assembled into stacks and magnetized in such a manner that a North pole is located in the Cunico at the base of one leg, and a South pole at the base of the other leg. This can be accomplished best by passing a heavy copper bus bar through the center slot and passing a pulse of direct current through it large enough to produce a magnetizing field strength of 2,500 to 3,000 oersteds in the Cunico in the region of the base of the legs.

The electric and magnetic characteristics of Cunico after it has been heat treated for magnetic hardness are about as follows:

$$H_{\max} = 3,200 \text{ oersteds,}$$

$$B_{\max} = 8,000 \text{ gaussses,}$$

$$B_r = 3,400 \text{ gaussses,}$$

$$H_c = 710 \text{ oersteds,}$$

$$\mu_r \approx 2.5,$$

$$(B_d H_d)_{\max} = 0.85 \times 10^6 \text{ ergs per cubic cm at}$$

$$H_d \approx 420,$$

$$\text{Density} = 0.30 \text{ lb per cubic in. or } 8.3 \text{ g per cubic cm, and}$$

$$\text{Resistivity} = 32 \times 10^{-6} \text{ ohm-cm.}$$

A magnetomotive force of about 350 gilberts is required to produce a flux density of 4,000 gaussses in the magnetic circuit consisting of the two legs and face arch of the oxide-annealed nickel HP-2 laminations, as shown in Figure 46. The average length of the flux path in the Cunico section below the legs is about 1.5 cm, so that the average demagnetizing force in the Cunico due to the opposing magnetomotive force in the nickel is about 165 oersteds. This demagnetizing force reduces the flux density in the Cunico to about 3,000 gaussses. However, because of the flaring of the legs at their bases the pole face area of the Cunico is about 1.3 times the cross section of the nickel legs, and consequently the flux density in the nickel should be nearly 4,000 gaussses.

The a-c flux path in the Cunico is estimated to have about one half as much magnetic reluctance as the flux path in the nickel. The eddy-current shielding and a-c power loss in the Cunico portion of the magnetic path is quite small because of the thin laminations, relatively high resistivity, and low a-c permeability.

A small sample stack of this type was constructed and subjected to electrical measurements. No acoustic tests were made because the stack face was too small to give the acoustic loading necessary for such tests to have any meaning. The electric tests showed that the Cunico magnet gave an equivalent magnetiz-

ing field of about 15 oersteds in the nickel legs. This corresponds to a total magnetomotive force of about 150 gilberts, which is less than half what it should be. The electromechanical coupling coefficient was about 0.10, whereas it should have been at least 0.15. This low coefficient was due to insufficient polarization and to the relatively high reluctance of the magnetic path in the Cunico section of the stack. These facts, together with the difficulty and expense of producing the bimetal strip from which the laminations must be punched, make this type of polarization less desirable and less efficient than some others.

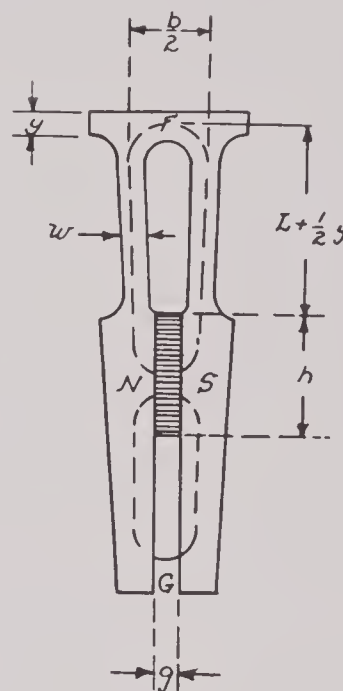


FIGURE 49. Tapered, laminated transducer stack polarized by a laminated Cunico magnet in a tail slot.

The second method of polarization by permanent magnets also makes use of laminated Cunico. This method is illustrated in Figure 49. The magnet is made up of a consolidated stack of Cunico laminations of a proper thickness to keep the eddy-current losses to a low value. The thickness of the laminations should be such that their characteristic eddy-current frequency is higher than the operating frequency. A graph showing the characteristic frequency of Cunico as a function of the lamination thickness is given in Figure 50. For example, if the operating frequency is 20 kc, the thickness of the Cunico magnet laminations should be less than 0.050 in.

The proper dimensions of the magnet slot and magnet must be determined by consideration of the magnetic circuit and the characteristics of the mag-

net material. First, the d-c magnetic path may be considered as being made up of two parallel paths *NFS* and *NGS* (see Figure 49). The average length of the path *NFS* is about $2(L + y) + b/2$. To maintain a flux density of 4,000 gauss in this path requires a magnetizing field strength of 40 oersteds, which when

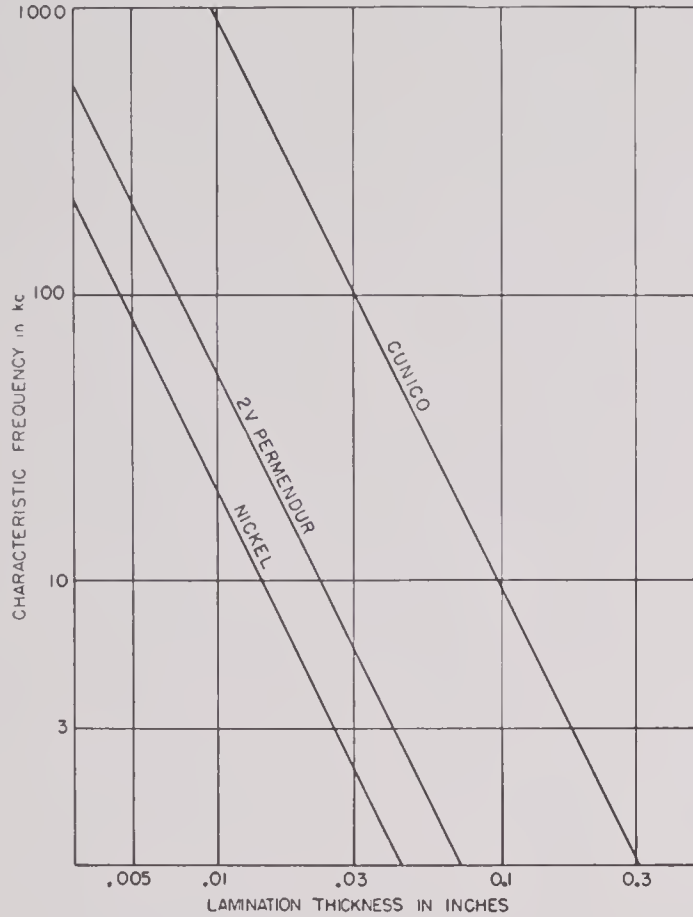


FIGURE 50. Eddy-current parameter diagram for Cunico permanent-magnet alloy, 2V-Permendur and oxide-annealed nickel.

summed along the path adds up to a total magnetomotive force of $40[2(L + y) + b/2]$ gilberts. This causes a demagnetizing field in the magnet which has the value

$$H_d = \frac{mmf}{g} = \frac{40 \left[2(L + y) + \frac{b}{2} \right]}{g} \text{ oersteds.} \quad (24)$$

The magnetic reluctance of the circuit *NGS* is difficult to estimate, but it is found to be roughly twice that of *NFS*. Hence, since the same magnetomotive force is applied to both circuits, twice as much flux will pass through the *NFS* circuit as through the *NGS* circuit. The total flux through the *NFS* circuit is $4,000wt$, and hence the total flux which must be provided by the magnet is about $6,000wt$. The cross-

sectional area of the magnet which must provide this flux is ht . If the flux density in the magnet is B_m , the total flux of the magnet is $B_m ht$, and this must be equal to $6,000wt$. Therefore,

$$h = \frac{6,000w}{B_m}. \quad (25)$$

The value of B_m for the magnet is determined from the demagnetizing force on the magnet and the magnet characteristics. The demagnetization curve for

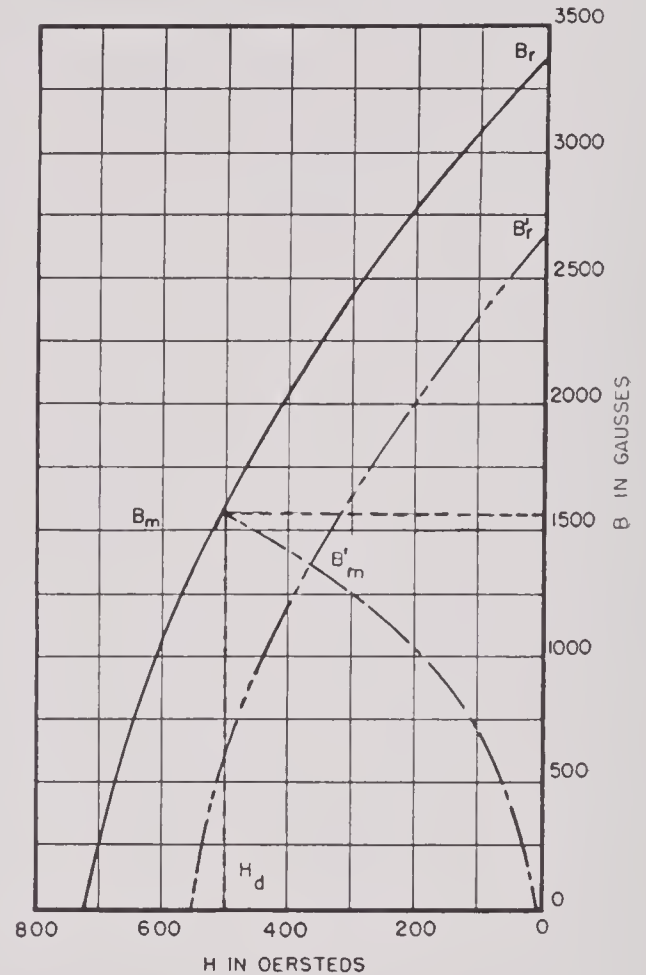


FIGURE 51. Nominal demagnetization curve for Cunico. $H_{\max} = 3,200$, $B_{\max} = 8,000$.

Cunico is shown in Figure 51. The magnet gap width g should be made as small as possible, but not so small as to make H_d exceed about 500 oersteds. Actually, in laminations of the type shown in Figure 49, the narrow space available for a magnet slot makes it necessary to use an H_d of fully 500 oersteds. Referring to Figure 51 again, it is found that the magnetic flux density corresponding to H_d equal to 500 is about 1,600 gauss. Thus the height of the magnet should be about 4 to 5 times the leg width w . The line $B_m O$ indicates the line of magnetic equi-

librium of the Cunico magnet while in the nickel stack. That is, if the magnet is magnetized fully while in the stack and then gradually demagnetized, its magnetic state will follow the line $B_m O$. Likewise, if the Cunico is not magnetized fully in the beginning, its magnetic state will follow a line similar to $B_r' B_m'$ as the external magnetizing field is removed and finally settle at the value B_m' .

The a-c magnetic reluctance of the magnetic circuit is the sum of that of the nickel path and of the magnet and air-gap path. To give an idea of the relative magnitudes of these reluctances, those for the design shown in Figure 49 are 1.06 for the nickel path and 0.075 cgs units for the gap path. This shows that only about 7 per cent of the total a-c reluctance is contributed by the gap path. This means that the insertion of the gap and the magnet does not greatly alter the a-c magnetic characteristics from those of a solid, d-c polarized type of lamination.

Two sample stacks of this type were constructed, using modified laminations of the HP-2 form shown in Figure 46. The laminated Cunico magnets were cemented solidly in place in the slots. The electrical measurements showed that the stacks were somewhat underpolarized for maximum efficiency and that the presence of the magnets and magnet slots disturbed the frequency of resonance and tended to cause multiple resonances. It was learned later that if the magnets are not cemented to the stacks most of the variations in the frequency of resonance can be eliminated. The polarization can be increased by increasing the height of the magnet. Acoustic tests showed the same characteristics of the stacks as did the electric tests. The efficiencies of these experimental stacks were of the order of 20 per cent.

A third method of polarization, which does not require the use of polarizing current, provided the stacks are not driven harder than 15 oersteds of peak magnetizing force, is to make the entire laminations of 2V-Permendur and operate them at magnetic remanence. The chief objection to this method is the present high cost of 2V-Permendur.

If 2V-Permendur is used, the thickness of the laminations should be selected on the basis of the curve shown in Figure 50. For example, for 26-ke operation the laminations should not be thicker than 0.020 in., and the strip from which they are punched should be hard-rolled. The laminations should have the general shape of the HP-2 type shown in Figure 46. After they are punched, they should be annealed at 500 to 525 C in a hydrogen atmosphere

to give the following approximate magnetic characteristics:

$$\begin{aligned} \text{At } H_{\max} &\approx 100 \text{ oersteds,} \\ B_{\max} &\approx 20,500 \text{ gauss,} \\ B_r &\approx 17,000 \text{ gauss,} \\ H_c &\approx 27 \text{ oersteds,} \\ \mu_r &\approx 55. \end{aligned}$$

Stacks made of laminations of this kind should be capable of producing sound pressures at the active face of considerably more than 10^6 dynes per sq cm without danger of magnetic depolarization. However, care would have to be taken that the *peak* values of any currents (transients included) in the windings should not exceed the value which would produce a magnetizing field of 15 oersteds in the legs.

The fourth and most successful method of polarization by permanent magnets makes use of sintered-oxide magnets. These are used in the same way as the Cunico, as shown in Figure 49. Sintered oxide is an oriented magnetic material supplied by the General Electric Company. The desired direction of magnetic polarization must be specified to the manufacturer so that the material can be heat-treated in a magnetic field in the proper direction. The characteristics of sintered oxide are about as follows (the magnetic characteristics refer to the principal axis of orientation):

$$\begin{aligned} \text{At } H_{\max} &\approx 4,000 \text{ oersteds,} \\ B_{\max} &\approx 6,400 \text{ gauss,} \\ B_r &\approx 1,800 \text{ gauss,} \\ H_c &\approx 1,000 \text{ oersteds,} \\ \mu_r &\approx 1.15, \end{aligned}$$

$$(B_d H_d)_{\max} 0.7 \times 10^6 \text{ at } H_d = 700,$$

$$\text{Resistivity} \approx 10^6 \text{ ohm-cm, and}$$

$$\text{Density} \approx 0.13 \text{ lb per cubic in. or } 3.6 \text{ g per cubic cm.}$$

The high resistivity of this material makes it unnecessary to laminate it to reduce eddy-current losses at high frequencies. In fact, it is such a good insulator that these losses in it are entirely insignificant. Because of its high coercive force, the dimensions of the magnets in the direction of magnetization can be made quite small, a great advantage in this application since it is desirable to keep the magnet slot as narrow as possible.

The design procedure for magnets of this type is the same as that described above for Cunico magnets. The demagnetization diagram for sintered oxide is shown in Figure 52. The magnet slot in this

case should be kept wide enough to make the demagnetizing force on the magnet less than 700 oersteds.

If design calculations of this type are made for a lamination of the size and shape shown in Figure 49, with a magnet slot width of $\frac{3}{16}$ in. and a flux density of 4,000 gauss in the legs, the demagnetizing field on the magnet itself is about 700 oersteds, and the height h of the magnet is about 2.5 cm. This indicates that the magnet should fill about half the slot.

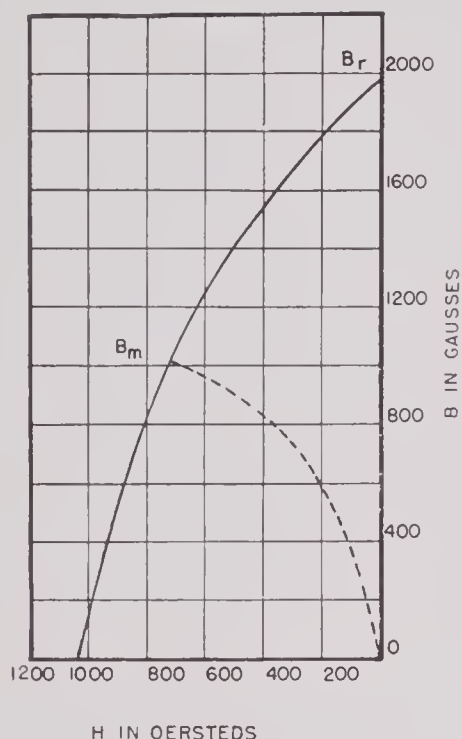


FIGURE 52. Nominal demagnetization curve for sintered oxide. $H_{\max} = 4,000$, $B_{\max} = 6,400$.

Actually it was found by experiment that the flux leakage is greater than that estimated and that the flux density at the bases of the nickel legs should be made a little higher than 4,000 gauss. These effects make it necessary to fill the entire slot with magnet. To eliminate any effects on the vibration characteristics of the stack, it was found necessary to grind the magnets to a thickness that allowed them to slide freely in the slot. The magnets should never be cemented or bonded directly to the stack in any way. The most important results of measurement on this type of stack will be presented here to illustrate their various properties.

The stacks used in the tests were made of oxide annealed 0.01-in. nickel laminations (unless otherwise specified) cemented together with C-3 Cycle-Weld resin. The stacks were 3.75 in. high and were

wound with the standard $37\frac{1}{2}$ -turn winding (19 turns on one leg and $18\frac{1}{2}$ turns on the other). In addition to the regular windings, search coils were wound on the legs at the places indicated in Figure 53. A search coil was also wound around the periphery of the sintered-oxide magnet to measure flux changes in the magnet itself. The magnets were magnetized while in

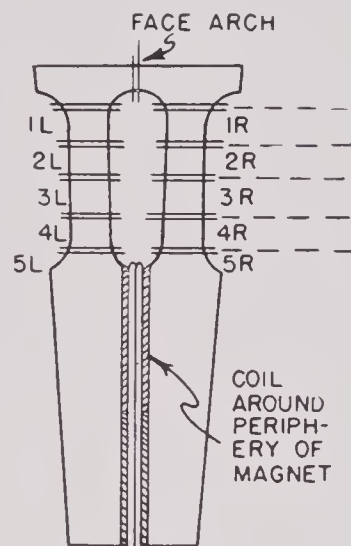


FIGURE 53. Diagram showing various positions of search coils used in making flux tests on HIP-3 stacks.

place in the nickel stacks by placing the entire stack assembly in a specially shaped jig between the pole pieces of a large electromagnet. The magnetizing field in the gap was about 3,000 oersteds.

The flux densities in different parts of the legs were determined by measuring the flux change in the various search coils when the sintered-oxide magnet was suddenly withdrawn, and adding to this value that of the remanence flux which was determined by suddenly removing the search coil from the stack after the magnet had been withdrawn. Two sets of values of flux are specified, viz., those determined during the first withdrawal of the magnet and those determined after the magnet has been inserted and withdrawn from the slot several times. The magnet is slightly depolarized by pulling it out of the slot into the air where the demagnetizing effect of its own external magnetic field is greater than it is in the nickel yoke. Thus, when the magnet is inserted in the slot again the flux produced in the nickel legs is slightly less than the initial value. These two values are referred to as initial and steady-state values.

Figure 54 shows the measured flux densities plotted against the position in the legs. The laminations annealed in hydrogen show the highest flux

densities because of their greater d-c permeability. The curves shown in dotted lines refer to a special stack made in short sections but having the same height as the standard ones. The lower solid curves refer to a standard stack. Magnets of different thickness were used in this latter stack to determine the effect of making the magnet thinner than necessary. The nominal width of the magnet slot was 0.188 in., but because of irregularities in it the thickest magnet that could be used was 0.180 in. The thinnest magnet used was 0.150 in. The flux density produced in the legs by the 0.150-in. magnet was about 12 per cent less than that produced by the 0.180-in. magnet. This

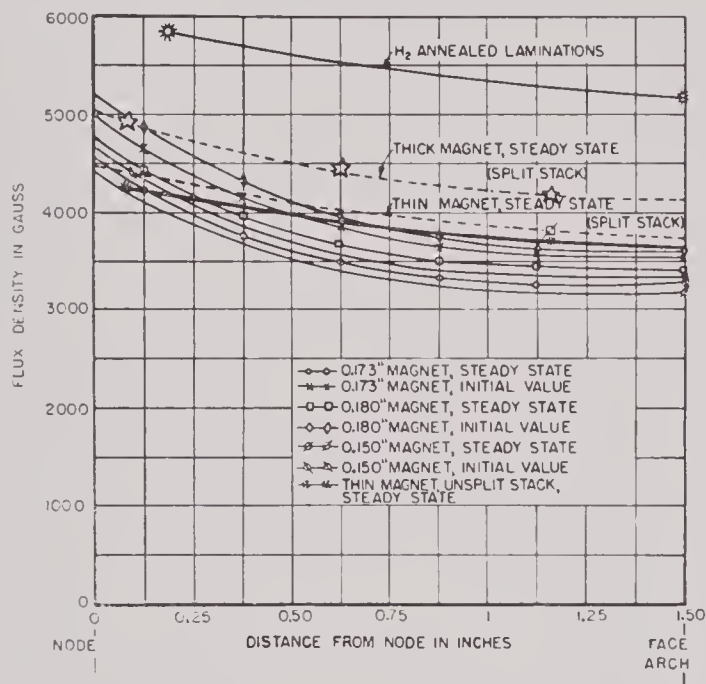


FIGURE 54. Flux density in the legs of HP-3 stack.

degree of variation in the polarization would produce an unsatisfactory amount of variation in the impedance of the elements; the thickness of the magnets should therefore be held to much closer tolerances. All the flux-density curves show that a considerable fraction of the flux leaks across from one leg to the other before the face arch is reached. This has very little detrimental effect as far as the magnetostrictive action is concerned because the most important region is that near the node where the flux density is maximum. This does indicate, however, that the coils should be kept as near the node as possible so as to link the maximum of a-c flux during receiving or transmitting.

The magnetization curve for a sample of General Electric No. 50 sintered oxide is shown in Figure 55, in which $4\pi I = B/H$ is plotted against H . After the

material is magnetized the removal of the magnetizing field causes very little decrease in the degree of magnetization. This effect is shown in Figure 56 for a sample of GE No. 132 sintered oxide. This means that after the material is magnetized the major part of the change in flux density in the magnet is the magnetizing field itself and not the change in $4\pi I$. This effect is illustrated in Figure 57, which shows a family of demagnetization curves (B vs H) and some minor hysteresis loops.

The magnetic state R shown in Figure 57 is reached by removing the magnetizing force after the magnet has been magnetized in a close-fitting iron yoke. The

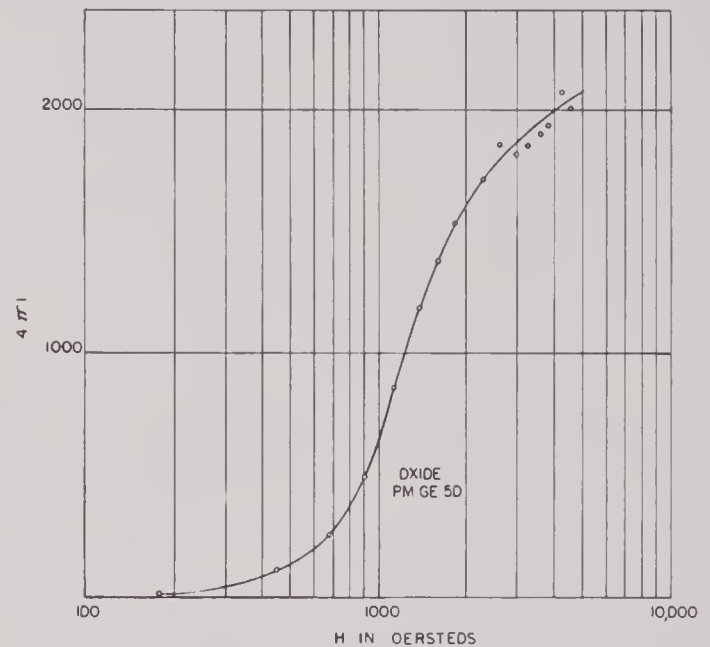


FIGURE 55. Magnetization curve for sintered oxide.

magnetic state A is reached from the state R by pulling the magnet out of the iron yoke into the air. The state R' is reached from the state A by inserting the magnet into the iron yoke again. The magnetic cycle $AR'A$ can be repeated any number of times without change. If the same magnet is magnetized while in place in a nickel stack it comes to equilibrium in the magnetic state S . If then the magnet is removed from the nickel stack, it drops to the magnetic state A . When it is reinserted in the nickel stack it goes up to the state S' . The cycle $AS'A$ can be repeated any number of times. The slopes of the minor hysteresis loops show the reversible permeability of sintered oxide to be about 1.15. The line $SS'O$ is the locus of the state of magnetic equilibrium of sintered oxide magnets in HP-3 nickel stacks. The line AO is the corresponding equilibrium line for the same magnets in air.

If the magnet has been newly magnetized in the nickel stack and is initially in state S and an alternating magnetizing field applied to it (as would be the case if alternating current were passed through the windings of the stack), then on the first quarter-cycle in the demagnetizing direction the state of the magnet would move to D and from then on it would follow the stable minor hysteresis loop $DS''E$. The slight demagnetization caused by such treatment is beneficial because it puts the magnet in a stable state

passing a 15-amp (peak) current through the windings. After the equilibrium state S_2 had been reached, the flux changes produced by positive and negative currents of 3, 6, 9, and 12 amp were measured. In Figure 58 it will be noticed that the depolarizing currents produce much greater flux changes in the magnet than do the magnetizing currents. This is attributable to the fact that flux density in the nickel is so great in the first place that a large magnetizing force is required to increase it, whereas if the current

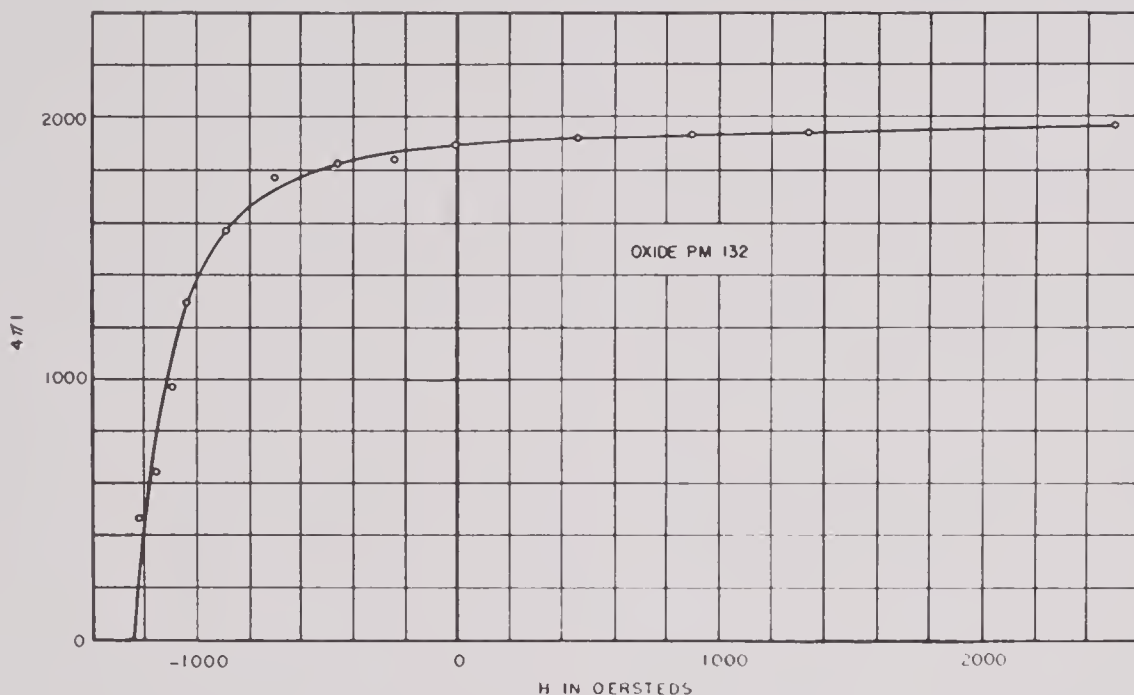


FIGURE 56. Demagnetization curve for sintered oxide.

of equilibrium from which it cannot be disturbed by the alternating current during pinging, unless this driving current should exceed the current used in the initial stabilization. It is interesting to note that because the left portion of the equilibrium curve $SS'O$ is quite flat, the magnet can be depolarized a considerable amount without any significant decrease in the flux density of the magnet or of the nickel legs.

The depolarizing effects of very large currents in the windings of the nickel stacks were investigated quantitatively by observing the changes in flux through the magnet when the direct current in the windings of the stack was changed by known amounts. These results are shown in Figure 58. The states S , A , and S_1 were obtained in the same manner as before, i.e., by removing the magnet from the slot and replacing it. The state S_2 was then reached after the application of a depolarizing current of 13 amp through the windings. The state S_3 was reached after

is in the direction to demagnetize, the permeability of the nickel is increased and a larger part of the demagnetizing force is effective on the magnet. For example, an analysis shows that 30 per cent of the total magnetomotive force produced by the opposing current of 12 amp is applied across the magnet, whereas it is only 5 per cent for an aiding current of 12 amp. (In the HP-3 laminated stacks with $37\frac{1}{2}$ turns, the average magnetizing field in oersteds is about 5.4 times the current in amperes.)

The total flux in the magnet, in the base of the nickel legs, and in the face arch of a standard HP-3 stack is plotted in Figure 59 as a function of the direct current in the windings. From this graph the amounts of flux leakage can readily be seen. Approximately one-fourth of the flux of the magnet does not enter the base of the legs, and of the amount that does about one-fifth leaks across before reaching the face arch. These ratios break down rapidly when the

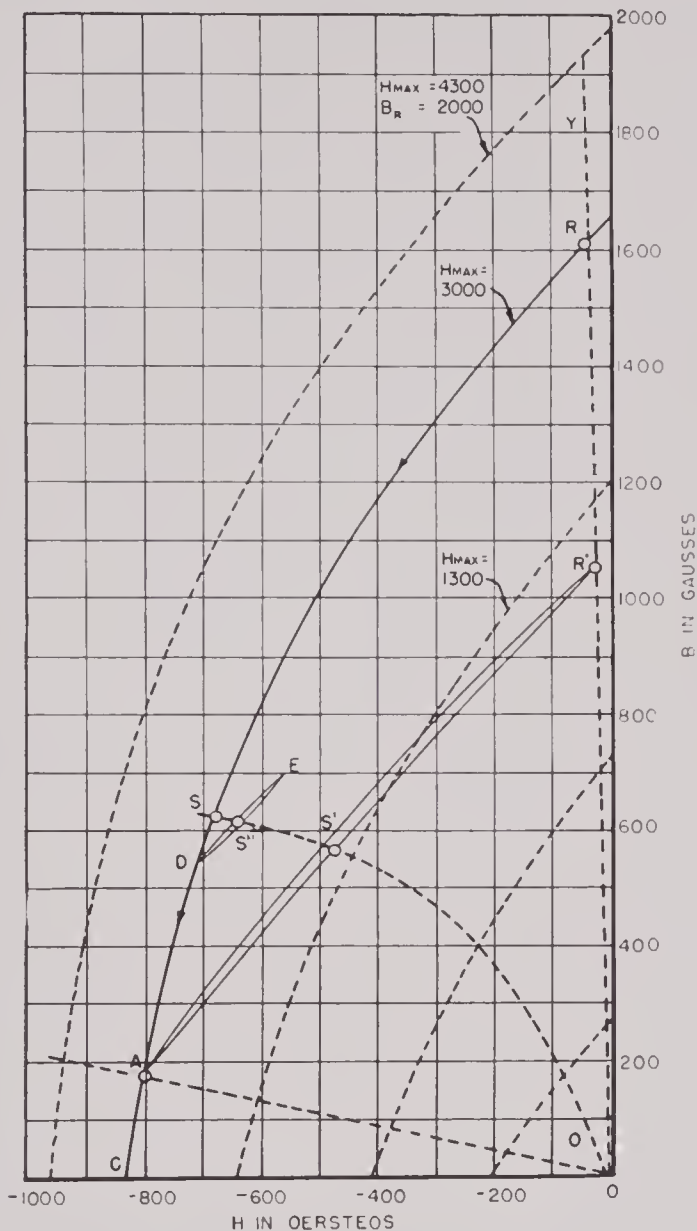


FIGURE 57. Demagnetization curve and minor hysteresis loops for sintered-oxide magnets determined from steel yoke and nickel stack measurements.

average depolarizing field in the legs exceeds 20 oersteds. This graph also shows that the flux-current ratio is reasonably linear only over the range of $H = \pm 16$ oersteds. This is not such a great limitation, however, when it is recalled that at the frequency of resonance a peak current of ± 2 amperes is sufficient to cause cavitation of the water at the active faces of the elements (at atmospheric pressure). The intercept of the curve on the H axis shows that the magnet provides polarization equivalent to an average polarizing field in the legs of 45 oersteds.

The demagnetizing effects on the magnet due to vigorous 60-cycle a-c pulsing of an HP-3 stack at room temperature (75 F) are shown in Figure 60.

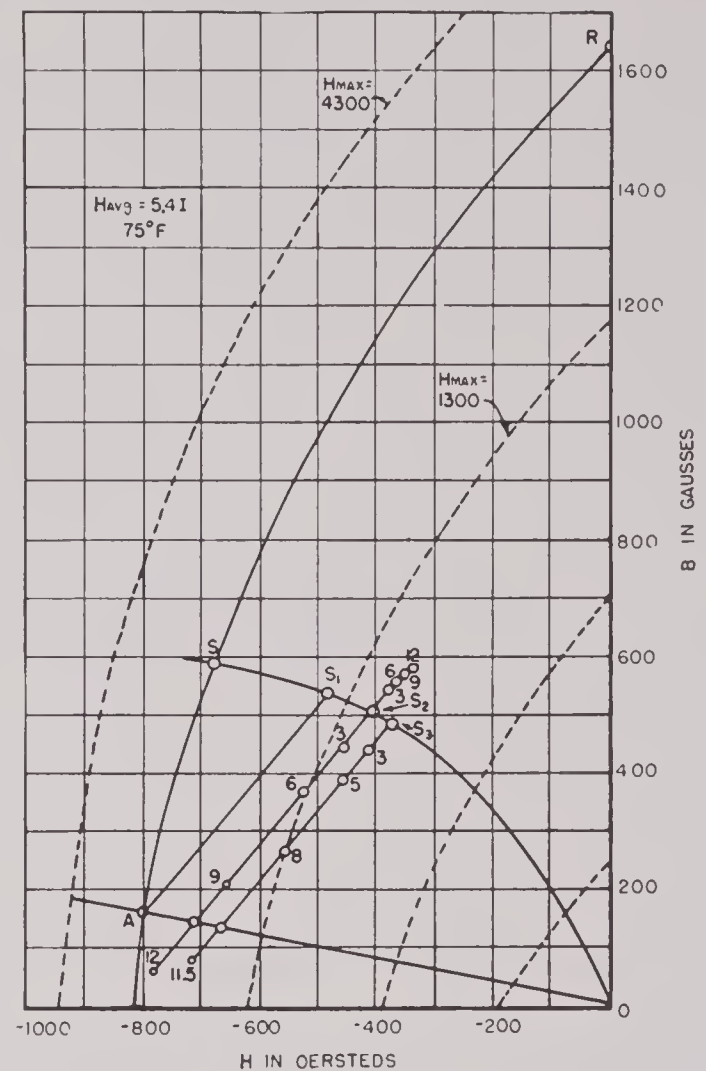


FIGURE 58. Minor hysteresis loops for sintered-oxide magnets in HP-3 stacks produced by changes in direct current in the windings of the stacks.

The duration of each pulse was about one second. The loci of the lower left ends of all the minor hysteresis loops nearly coincide with the primary demagnetization curve corresponding to the initial magnetization. Repeated pulses at 11.3 amp (peak) produced no more demagnetization than the first pulse. However, at 14 amp (peak) additional pulses produced additional demagnetization until a final stable value was reached. The measured values of the impedance of the stack at 20 kc Z_{20} under the various states of magnetization are shown by the scale at the left.

It was found that subjecting the magnets to a-c magnetic pulsing while they are hot produces more demagnetization than when they are cool. Figure 61 shows the results for one pulse and 10 pulses at temperatures of 200 F and 300 F. At temperatures above 300 F, considerable demagnetization is produced by

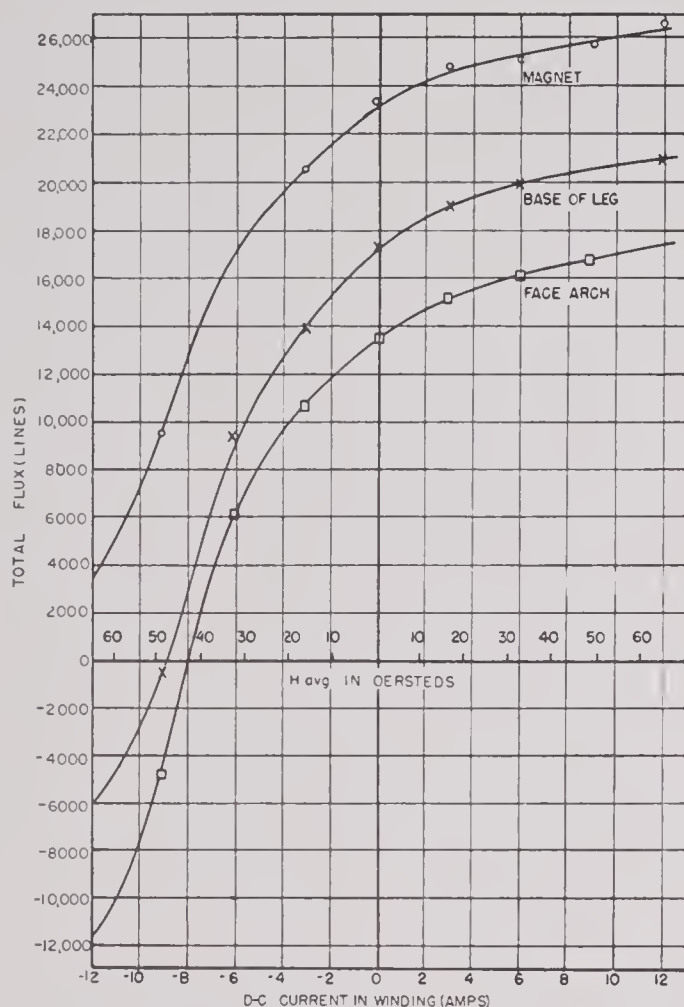


FIGURE 59. Total flux in magnet, legs, and face arch of an HP-3 stack as a function of direct current in the windings.

relatively small currents. The reduction of the coercive force due to increase in temperature makes it necessary to limit the amplitude of magnetic pulsing of the stacks at temperatures above 200 F. The most adverse conditions of operation for the magnets would be to drive the stacks continuously at such a high level that the heat produced by copper losses and core losses would raise the stack temperature to 200–300 F. There is practically no danger of this happening in a full-sized transducer driven by a generator that derives its energy in pulses from an energy storage system working on the duty-cycle principle.

No observable effects on the magnetic properties of the sintered-oxide magnets have been found as a result of soaking them in water, Ucon oil, or castor oil. Heating them after they are soaked and vacuum-impregnating them with resins have also been found to produce negligible effects. The impregnation of the magnets with such resins as GE Permafil or some of the bakelite resins increases their mechanical strength

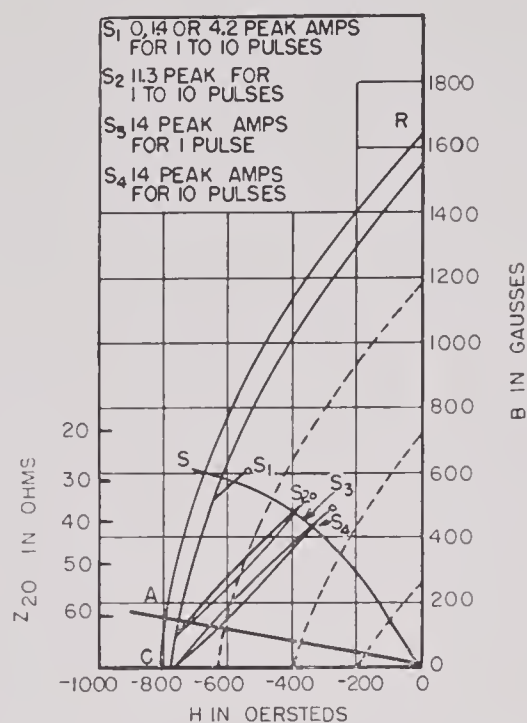


FIGURE 60. Demagnetizing effect due to 60-cycle a-c pulsing at room temperature (75 F.).

and reduces their porosity. There is nothing about the mechanical, magnetic, or chemical properties of the magnets that should prevent their use in oil-filled or water-filled transducers.

The scanning sonar transducer elements that are polarized by permanent magnets inserted in the tail section must be placed in the supporting spool so that like magnetic poles are adjacent, otherwise the full circle of tail sections would form a magnetic short circuit around the spool. The flux measurements which have been presented in the foregoing material were made on single isolated stacks. To find the effect on the flux densities of bringing several stacks close to each other, three stacks were measured alone and then together (1 $\frac{1}{16}$ -in. spacing). The flux density of the magnet in the center stack of the group decreased about 12 per cent, while the flux density in the nickel face arch increased about 2 per cent. The fraction of the flux of the magnet which passed through the face arch increased from 58 to 67 per cent.

In some scanning sonar transducers the back ends of the laminated stacks are separated from the steel core of the spool by only a $\frac{1}{2}$ -in. layer of corprene or other nonmagnetic material. The magnetic short-circuiting effect of this steel on the magnets in the stacks was measured and found to be negligible. However, the distance of separation should not be made much less than $\frac{1}{4}$ in.

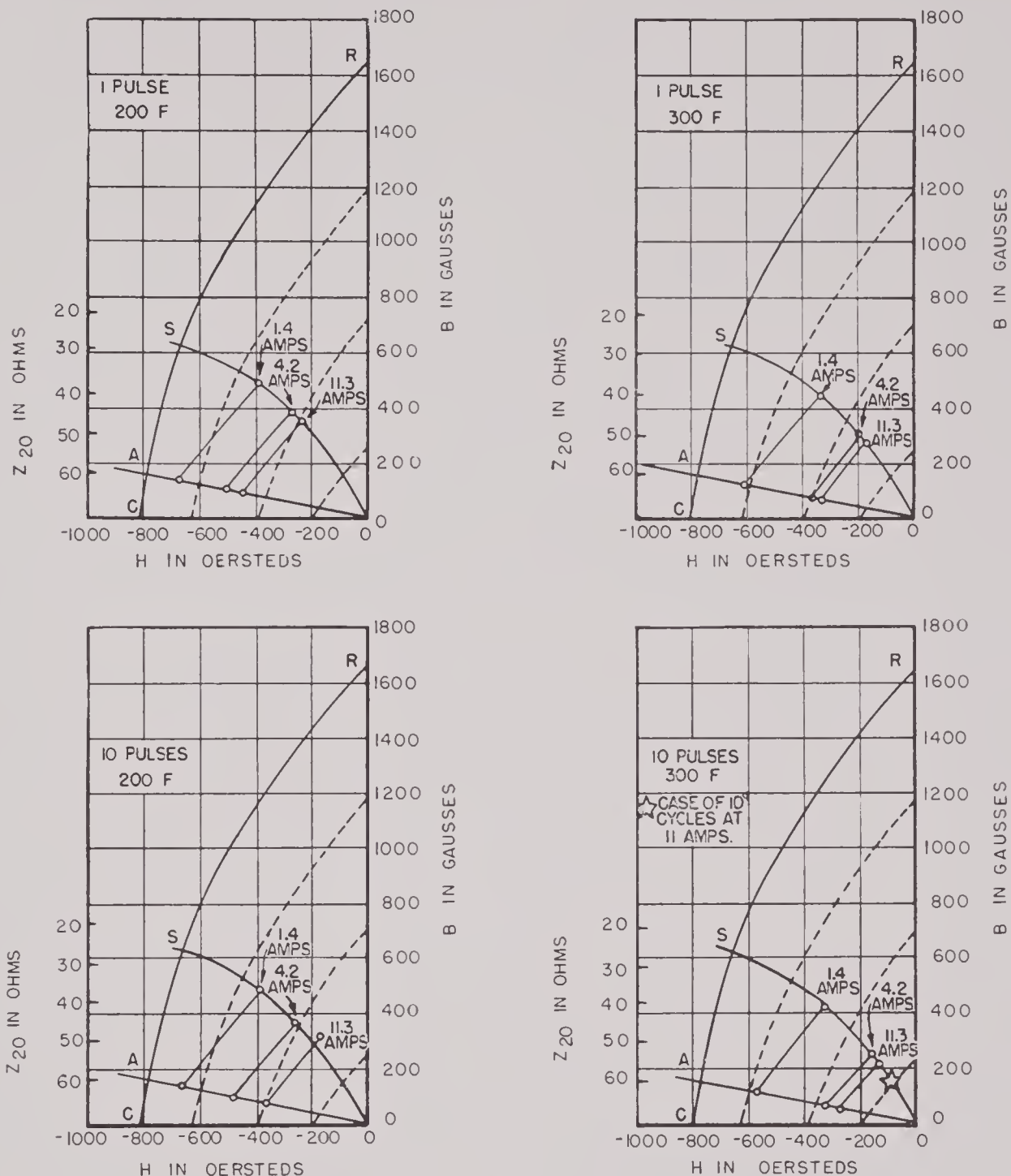


FIGURE 61. Demagnetizing effect due to simultaneous heating and a-c magnetic pulsing.

SP TYPE OF LAMINATED STACKS

The general design of an element made from stacks of laminations of the SP type is shown in Figure 20. Some of the advantages of this type of construction are: preformed coils can be used on the stacks; the elements are made of relatively short sections which can be readily adapted to amplitude shading to produce minor lobe reduction in the vertical pattern; and the individual stacks are so short that no trouble should be caused by multiple resonances of the type

that are produced in thicker stacks by too-strong consolidation. However, the fact that the active face area of the elements made up of SP stacks is less than half the available face area causes the mechanical Q to be higher than it should be and limits the total radiation area. Greater care must be used in aligning the large number of small stacks, and the unsupported spaces of the transducer face between elements are vulnerable to damage from pressure or impact.

CONFIDENTIAL

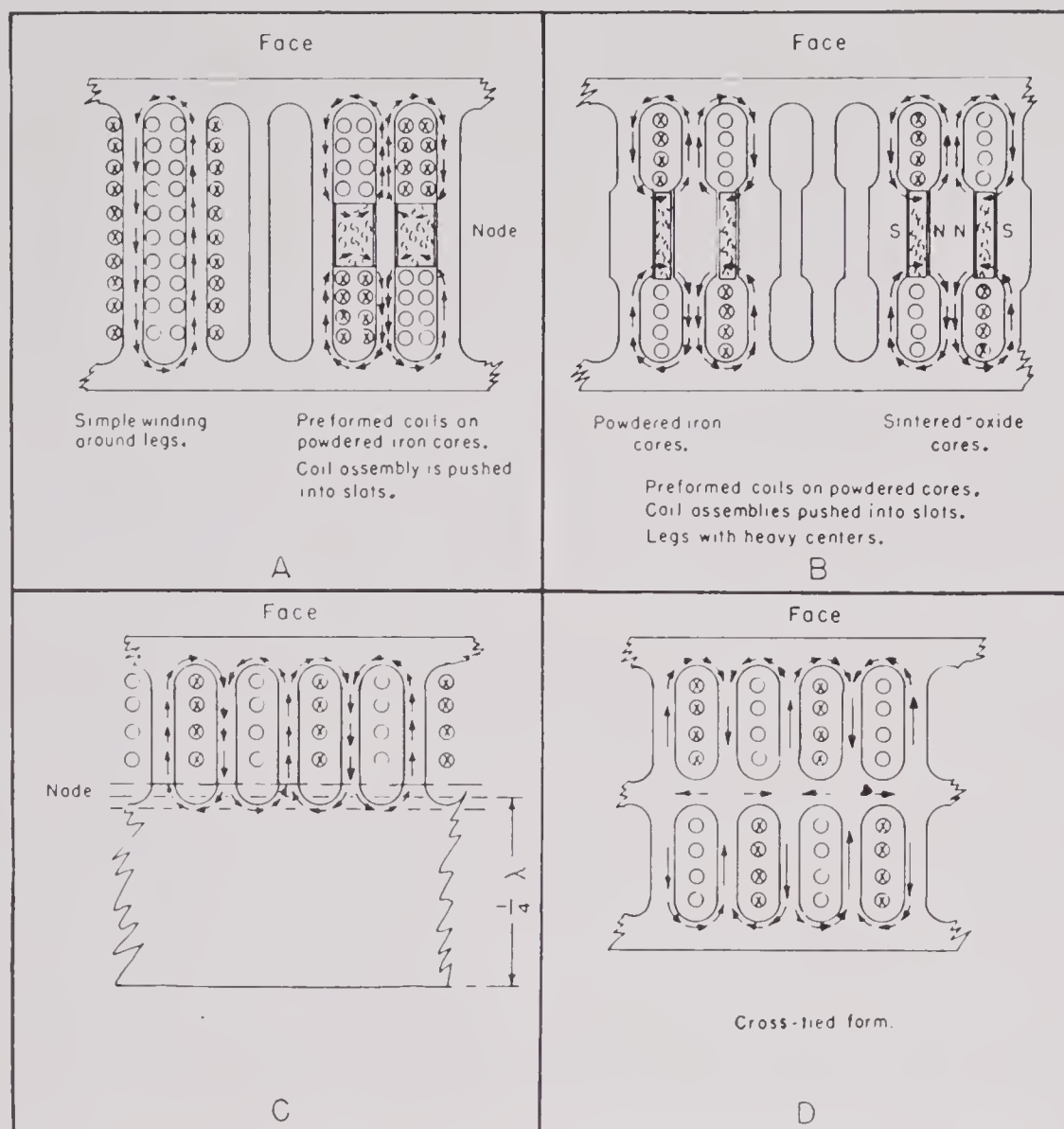


FIGURE 62. Some general forms of ladder-shaped laminations.

Lamination Design. The detailed design of laminations of the SP type is very similar to that for the wedge-shaped laminations as discussed in Section 13.3.3. The only difference is that the length of the heavy tail section of the SP laminations is made exactly equal to one-fourth wave length because of its uniform cross section. Thus the length of the tail section is $c/4f$, where c is the velocity of sound in nickel.

The mechanical Q of laminations of this type is determined as indicated in Figure 45 and as described in Section 13.3.3. All other design considerations are essentially the same as those discussed in Section 13.3.3.

Stack Mounting and Acoustical Contact. Some methods of mounting stacks of the SP type and of providing for acoustic contact between the active

faces of the stacks and the water have been discussed in Section 13.2.3. With the aid of some imagination, a designer can make up variations of the design shown in Figure 20. For example, the stacks might be cemented to impregnated glass fiber face strips of the type indicated in Figure 18 and the entire array of elements enclosed in a watertight rubber boot. If the face strips are sufficiently light and strong, they will not influence the frequency very much and yet will increase the area of the radiating active face by a considerable amount.

LADDER-TYPE ELEMENTS

General Form. The general types of elements which can be made up of SP-type laminations can also be made from laminations having the form of a ladder. Some general forms of this type are shown in

Figure 62. These can be punched in continuous strip form by using a die with an accurately indexed feed mechanism. A transducer element would be made by cutting the continuous strip material into lengths corresponding to the length of the element and consolidating them to form the complete ladder-shaped stack.

The form shown in Figure 62A is symmetrical, with legs of uniform width. Two ways of winding are shown. The one on the left is made by threading the wire around the legs. This is tedious and time-consuming. The one on the right is made by winding the coils around powdered iron cores. The windings and cores are made solid by impregnating them with some type of resin or cement. Then the preformed coil and powdered core assemblies are slipped into the slots of the laminated stack. Powdered iron is used to reduce eddy-current losses. The first method of winding gives the best magnetic circuit and the greatest electromechanical coefficient, whereas the second method is poorer in these respects because the magnetic flux is not parallel to the mechanical strain in the region of the node where the greatest magnetostrictive driving force is needed.

Figure 62B shows a type of lamination which can use the preformed coil type of winding without much reduction in the electromechanical coupling coefficient and efficiency. This improvement over the form shown in Figure 62A results from making the center portion of the legs wider in section so that the region of maximum strain is shifted from the nodal point to the points where the narrow part of the legs joins the wide part. At this latter point the direction of the magnetic flux is parallel to the direction of mechanical strain. Theoretical calculations show that the effective electromechanical coupling coefficients for the left- and right-hand cases of Figure 62A and case B of Figure 62 are 0.20, 0.08, and 0.16 respectively.

The form shown in Figure 62B can be readily polarized by use of sintered-oxide magnet material. Since the magnetic paths are symmetrical there is not so much flux leakage as there is in the case of the open-ended wedge-shaped laminations.

Figure 62C shows an asymmetrical form of the ladder type of laminations, which has the lowest mechanical Q of any of the forms shown. This type must be wound by threading the wires through the winding slots. It must be polarized by use of direct current in the windings or by using the magnetostrictive lamination material at its magnetic remanence.

The lamination form shown in Figure 62D is a hybrid which is stronger and easier to handle than the form shown in A. However, it must be wound by threading the wire through the slots and must be polarized by direct current or magnetic remanence flux.

Design Details. The dimensions required to give a desired frequency in laminations of the form shown in Figure 62A are determined in the same way as for the front half of a wedge-shaped lamination de-

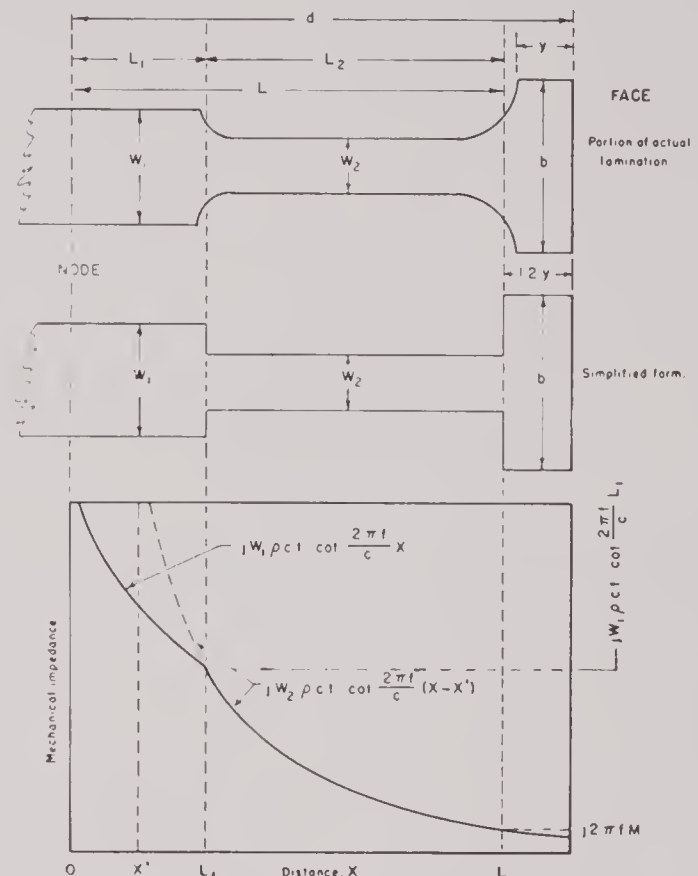


FIGURE 63. Mechanical impedance along the legs of the type of lamination shown.

scribed in Section 13.3.3. The node is taken to be at the center of the length of the legs and the dimensions are symmetrical on each side of the node. The mechanical Q 's for laminations of this type are approximately 1.5 times those indicated in Figure 45.

The dimensions that will give a specified frequency for laminations of the form shown in Figure 62B are somewhat difficult to derive because of the change in the width of the legs. The most direct method is to use the mechanical impedance concept. Figure 63 shows a section of a leg with the amount of the face section which is associated with it. A simplified, equivalent block section is also shown to aid in the calculation. The distance x along the legs is measured

from the node toward the face. In a typical design the width w_2 of the narrow portion of the leg is about one-third the width of the associated face section b . The width w_1 of the wide part of the leg is about twice that of the narrow part. The equivalent depth of the face section is about 1.2 times the depth y of the face arch. If sintered-oxide magnets are to be used, the width of the magnet slot must be about one-fourth the length of the narrow part of the leg, and the total length of the magnet slot $2L_1$ must be about five or six times the width of the narrow part of the leg, w_2 .

The lower part of Figure 63 shows a plot of the mechanical impedance along the length of the legs. The mechanical impedance (i.e., force \div velocity) in the wide part of the leg is given by the expression

$$jw_1\rho ct \cot \frac{2\pi f}{c}x, \quad (26)$$

where ρ is the density, c the velocity of sound, t the thickness of the laminations, and f the frequency. The length of the wide portion of the leg is set by the magnetic requirement described above, viz., $L_1 \simeq 3w_2$. Hence the mechanical impedance at the junction of the wide and narrow parts of the leg is $jw_1\rho ct \cot \frac{2\pi f}{c}L_1$. From this position on out to the face block, the mechanical impedance is given by the expression

$$jw_2\rho ct \cot \frac{2\pi f}{c}(x - x'), \quad (27)$$

where x' is determined by the condition that the impedance given by equations (26) and (27) is the same at the position L_1 , that is,

$$w_1 \cot \frac{2\pi f}{c}L_1 = w_2 \cot \frac{2\pi f}{c}(L_1 - x'). \quad (28)$$

The end of the effective part of the leg would come at the position $x = L$ where the mechanical impedance of the leg is equal to that of the face block, which is considered to act as a rigid mass $M = 1.2ybt\rho$. Thus L is given by the relation

$$jw_2\rho ct \cot \frac{2\pi f}{c}(L - x') = j2\pi fM. \quad (29)$$

The dimensions required to give a desired frequency for laminations of the type shown in Figure 62C are determined in the same way as for laminations of the SP type as described in Section 13.3.3. The Q 's for laminations of this type are given by the graph shown in Figure 45. This type of lamination has the disadvantage that there is a large amount of

mechanical coupling along the length because of the transverse stiffness of the deep tail section. Stacks of such laminations do not operate well when amplitude shading or phasing of the different leg sections is applied.

The calculation of the dimensions of laminations of the form shown in Figure 62D is about the same as for the type shown in Figure 62B. The width of the wide section of the leg in this case is approximately three times that of the narrow part of the leg. The "spring-and-mass" method (see Section 13.3.3) of calculation can also be readily applied to this case. In such a calculation, the "spring" portion would be considered as extending from the bottom of the winding slots nearest the node to within $1.2y$ of the face.

RING-SHAPED LADDER TYPE

General Form. The general form of a ring-shaped ladder type of lamination designed for polarization by sintered-oxide permanent magnets is shown in Figure 27. The "element" consists of a pair of adjacent legs in the ring. The node is located approximately at the middle of the magnet slot and extends parallel to the outside and inside faces of the ring. The outside and inside faces have the maximum amplitude of motion. The legs joining the outside and inside faces are made wide in the center to improve the magnetic circuit and increase the electromechanical coupling as described above in Section 13.3.3. The elements are mechanically coupled at the outside and inside ends but experiments show that the coupling is not enough to cause trouble in phasing and amplitude shading.³⁷

Lamination Design. The detailed design of laminations of this kind is somewhat complicated. The face width of an element should be made about equal to one-half wave length just as in other scanning sonar transducers, and consequently the usual relationship between the number of elements, active face diameter, and frequency is applicable. The frequency and active face diameter are chosen on the basis of the width of the receiving pattern desired. After the active face diameter, frequency, and number of elements have been decided upon, the details of the design of the remainder of the laminations can be completed. The portion of the active face that is devoted to one element can be supported by one or two legs. The two-legged support fits the requirements on the magnetic circuit and magnets somewhat better than the one-legged support. The design procedure which will be presented here will apply to

the case of two legs per element. If a design using one leg per element is desired the same general method can be followed.

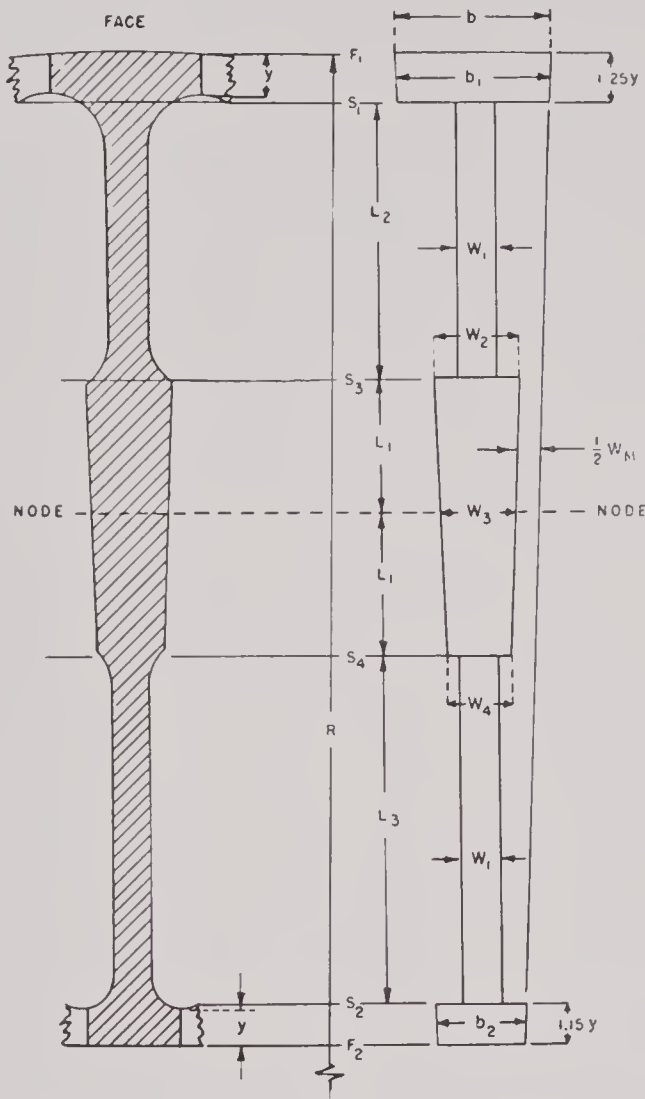


FIGURE 64. One leg of a ring-shaped, ladder-type lamination and its simplified equivalent form for use in design.

The RLP-type laminations are perfectly uniform around the ring and the detailed design calculations can therefore be concentrated upon one leg and the outer and inner face masses which are associated with it. It is true that the outer and inner face rings contribute some stiffness against which the face masses must work (as in a pure annular lamination), but this stiffness is small in comparison with the stiffness of the legs. For example, in a lamination which is 12 in. in outside diameter, 7 in. in inside diameter, and designed to operate at 36 kc, the stiffness reactance due to compression and expansion of the outer face ring is about 2 per cent of that due to the legs, and the stiffness reactance of the inner ring face is about 6 per cent of that due to the legs. Con-

sequently the frequency of resonance should be slightly higher than that calculated on the basis of neglecting the stiffness of the inner and outer face rings.

Figure 64 shows a small section of a lamination which consists of one leg and the associated face masses. At the right hand of the same figure a simplified form of the lamination is shown which is convenient to use in the design calculations. It is suggested that the following steps be followed in determining the exact dimensions of the lamination.

1. To get a mechanical Q of about 10, the face depth and the leg width should be made approximately one-fourth the width of the outer face per leg.

2. If the face depth y is about one-fourth the face width b , then, because of the mass of the face arches in the actual lamination, the effective mass of the outer face section is

$$M_1 \simeq 1.25yb_1t\rho. \quad (30)$$

3. Write the general expression for the mechanical impedance of the outer leg section as a function of the distance x_2 measured from S_1 toward S_3 :

$$X_{x_2} = j\rho ctw_1 \tan \frac{2\pi f}{c}(x'_2 + x'_2), \quad (31)$$

where x'_2 is given by the condition that the magnitude of the reactive impedance of the leg section is equal to that of the face block at S_1 ,

$$\text{viz., } j\rho ctw_1 \tan \frac{2\pi f}{c}x'_2 = j2\pi f(1.25yb_1t\rho),$$

$$\text{or, } x'_2 = \frac{c}{2\pi f} \tan^{-1} \frac{2\pi f(1.25yb_1)}{cw_1}. \quad (32)$$

4. The width and length of the magnet slot is determined by the type of permanent magnet to be used and by the length and width of the legs of the lamination. For sintered-oxide permanent-magnet material, the total width of the magnet slot w_m should be approximately $\frac{1}{5}L_2$, and the total length of magnet slot $2L_1$ should be about eight times the width of the legs w_1 . This means that $L_1 \simeq b$ because $w_1 \simeq b/4$.

5. After w_m and L_1 are determined, then w_3 can be expressed in terms of b , y , L_1 , and L_2 , because the leg section has a definite taper determined by the central angle $360^\circ/2N$, where N is the number of elements or pairs of legs. Thus

$$w_3 = b - w_m - 2\left(1.25y + L_1 + L_2\right) \tan \frac{360^\circ}{4N}. \quad (33)$$

As b , w_m , L_1 , and N have already been determined, w_3 is a function of the variable L_2 alone.

6. The length L_2 can now be found by calculating the mechanical impedance at S_3 by starting at the node and equating this to X_{x_2} . The value of x_2 that satisfies the equation is the proper value for L_2 . If the common factor $j\rho c t$ is omitted, this equation is

$$\left(w_3 + 2L_1 \tan \frac{360^\circ}{4N} \right) \cot \frac{2\pi f}{c} L_1 = w_1 \tan \frac{2\pi f}{c} (L_2 + x'_2). \quad (34)$$

(Strictly speaking, the mechanical impedance in the wedge-shaped center portion of the leg should be represented by a combination of Bessel and Neumann functions, but the cotangent representation is reasonably accurate and more readily solved.) This equation can be solved most readily by plotting the functions on each side against L_2 and noting the value of L_2 at which the two curves intersect.

7. After L_2 is found, the numerical value of w_3 can be calculated and the approximate mechanical impedance at S_4 can be determined from the expression,

$$j\rho c t \left(w_3 - 2L_1 \tan \frac{360^\circ}{4N} \right) \cot \frac{2\pi f}{c} L_1. \quad (35)$$

8. The mechanical impedance along the inner leg can now be written as a function of x_3 , the distance along the inner leg measured from S_4 toward S_2 . This is

$$j\rho c t w_1 \cot \frac{2\pi f}{c} (x_3 + x'_3), \quad (35a)$$

where x'_3 is given by the condition that the mechanical impedances at S_4 are the same for both the thick and thin sections. Thus

$$x'_3 = \frac{c}{2\pi f} \cot^{-1} \left[\frac{\left(w_3 - 2L_1 \tan \frac{360^\circ}{4N} \right) \cot \frac{2\pi f}{c} L_1}{w_1} \right]. \quad (36)$$

9. The length of the inner leg can now be determined by the matching of the mechanical impedance of the leg at its innermost end with that of the inner face mass. However, the magnitude of the inner face mass also depends upon the length of the leg. The easiest method of solution is to plot the mechanical impedances of the inner face mass and of the leg as functions of L_3 and find the value of L_3 at which the two curves intersect. This is the proper value for L_3 obtained from the equality:

$$j2\pi f(1.15yb_2t\rho) = j\rho c t w_1 \cot \frac{2\pi f}{c} (L_3 + x'_3),$$

$$\text{or} \quad 2\pi f(1.15yb_2) = cw_1 \cot \frac{2\pi f}{c} (L_3 + x'_3), \quad (37)$$

where $b_2 = w_3 + w_m$

$$- 2(L_1 + 0.575y + L_3) \tan \frac{360^\circ}{4N}. \quad (38)$$

This completes the determination of all the essential dimensions.

In all the equations above in which dimensions are determined it will be noticed that the thickness and density of the laminations cancel out. Consequently, the dimensions of the laminations depend only on the geometry of the lamination and the velocity of sound in the lamination material.

13.3.4 Tube-and-Plate Transducer Elements

DESIGN OF THE MECHANICAL PARTS OF THE ELEMENT

Conventional QC-Like Type. The conventional QC-like transducer consists of a heavy steel diaphragm plate which is backed by a large number of thin-walled magnetostrictive tubes. The distance between centers of the tubes should not be greater than one-eighth of a flexural wave length in the diaphragm plate at the frequency of operation. If the distance between centers is much greater than this, the diaphragm will not act as a unit piston but like an array

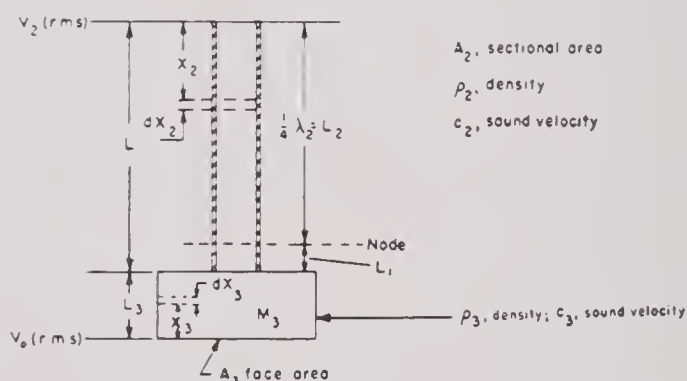


FIGURE 65. Simplified element of a tube-and-plate type of transducer.

of more or less independent small sources which can easily get out of phase with each other and cause pattern trouble. If the thickness of the diaphragm plate is less than one-eighth of a compressional wave length in the steel, it acts as an almost pure mass attached to the magnetostrictive tubes. The node is located in the tubes a short distance from the plane of attachment to the plate. Figure 65 shows a simplified form of such a vibrating element. The distance

from the free end of the tube to the node is just one-fourth wave length in the metal tube. In conventional designs, the mass of the short length of tube L_1 between the node and the diaphragm mass is usually negligible in comparison to the diaphragm mass, and consequently it can be considered as a massless spring having a spring constant,

$$K = \frac{A_2 E_2}{L_1}, \quad (39)$$

where A_2 is the cross-sectional area of the tube in a plane parallel to the diaphragm, and E is Young's modulus. The lowest frequency of resonance of such a system is therefore,

$$f_0 = \frac{1}{2\pi} \sqrt{\frac{K}{M_3}} = \frac{1}{2\pi} \sqrt{\frac{A_2 E_2}{M_3 L_1}}. \quad (40)$$

From this,

$$L_1 = \frac{A_2 E_2}{4\pi^2 f_0^2 M_3} \quad (41)$$

Also,

$$L_2 = \frac{\lambda_2}{4} = \frac{c_2}{4f_0}$$

Thus the total length of the tube is

$$L = L_1 + L_2 = \frac{A_2 E_2}{4\pi^2 f_0^2 M_3} + \frac{c_2}{4f_0}. \quad (42)$$

The mechanical Q of a transducer of this type, based on the ratio of the mechanical reactance to the water radiation resistance (i.e., not considering any internal mechanical damping), can be found by determining the effective mass of the vibrating parts, multiplying this by the angular frequency and comparing the product with the radiation resistance. That is,

$$Q_m = \frac{2\pi f_0 M^*}{A_3 (\rho c)_{\text{water}}}. \quad (43)$$

The effective mass M^* is defined in equation (6a). The effective mass may be found by determining the peak kinetic energy of the actual system and dividing it by the square of the rms velocity of the radiating face.

If the rms velocity of the radiating face is denoted by v_0 , and if the plate portion of the elementary vibrator as shown in Figure 65 is considered to act as a lumped mass, the peak kinetic energy of the lumped mass is $M_3 v_0^2$. It can be readily shown that the peak kinetic energy of the quarter-wave portion of the tube is equal to the mass of one-eighth of a wave

length of the tube times the square of the rms velocity of the free end of the tube. The velocity of the free end of the tube can be derived from the condition that total momentum of the vibrating element must be zero. This velocity turns out to be

$$v_2 = v_0 \left[\left(\frac{M_3}{m_0} \right)^2 + 1 \right]^{\frac{1}{2}}, \quad (44)$$

where

$$m_0 = \frac{\rho_2 A_2 c_2}{2\pi f_0} \quad (45)$$

is the mass of a length of the tube corresponding to $1/2\pi$ times the wave length. Consequently the kinetic energy of the quarter-wave portion of the tube is

$$\frac{\pi}{4} m_0 v_0^2 \left[\left(\frac{M_3}{m_0} \right)^2 + 1 \right]. \quad (46)$$

In practical cases the mass and velocity of the L_1 portion of the tube are so small that the resulting

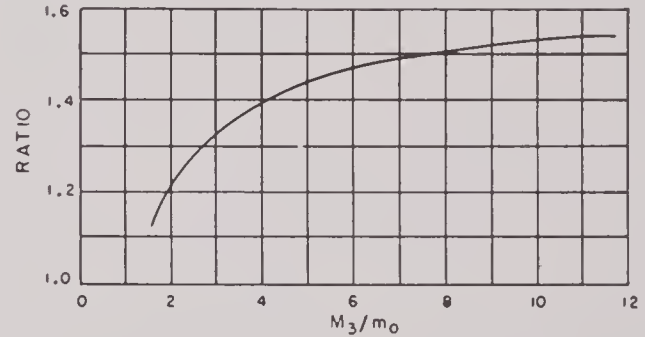


FIGURE 66. Ratio of M^* as calculated by $M^* = M_3(1 + 4M_3/\pi m_0)$ compared to the correct value for various values of M_3/m_0 .

contribution to the total kinetic energy is negligible in comparison to that of the other parts. Therefore the total kinetic energy of the element is very nearly

$$v_0^2 \left\{ M_3 + \frac{\pi}{4} m_0 \left[\left(\frac{M_3}{m_0} \right)^2 + 1 \right] \right\}, \quad (47)$$

and consequently the effective mass is

$$M^* = M_3 + \frac{\pi}{4} m_0 \left[\left(\frac{M_3}{m_0} \right)^2 + 1 \right]. \quad (48)$$

In engineering practice hitherto, the effective mass has been calculated on the assumption that the kinetic energy of the quarter-wave portion of the tube is equivalent to one-half of its mass vibrating with an amplitude which is,

$$v_2 = v_0 \frac{M_3}{\frac{\pi}{4} m_0} = v_0 \frac{4M_3}{\pi m_0}. \quad (49)$$

This value of v_2 is derived from the balance of momentum when the vibrator is assumed to consist of two lumped masses, one of mass M_3 and velocity v_0 and the other of mass $(\pi/4)m_0$ and velocity v_2 . Actually this gives too high a value for v_2 and consequently gives values of

$$M^* = M_3 \left(1 + \frac{4M_3}{\pi m_0} \right), \quad (50)$$

which are too high by about 40 to 50 per cent. Figure 66 shows the ratio of the M^* given by this method to the correct value, plotted against M_3/m_0 . This ratio is

$$\frac{\left(\frac{16 - \pi^2}{4\pi} \right) \left(\frac{M_3}{m_0} \right)^2 - \frac{\pi}{4}}{\frac{\pi}{4} \left[\left(\frac{M_3}{m_0} \right)^2 + 1 \right] + \frac{M_3}{m_0}} + 1. \quad (51)$$

It has also been considered that the contribution of the tube to the effective mass is $2M_3^2/m$, where m is the mass of the entire tube. This makes the total effective mass

$$M^* = M_3 \left(1 + \frac{2M_3}{m} \right). \quad (52)$$

This is a better approximation than that given in equation (50), but for practical values of M_3/m_0 it is still 35 to 45 per cent higher than the correct value.

A general discussion of the theory of a magnetostrictive tube free at one end and terminated by a lumped mass at the other end is given in Chapter 3. Equivalent circuit diagrams are shown in Figures 25 and 27 of Chapter 3. The ratio of the mechanical Q to its value Q_0 when $M_3/m_0 = 0$ is plotted against M_3/m_0 in Figure 26 of Chapter 3.

$$Q_0 = \frac{\pi}{2} \cdot \frac{(\rho c) A_{\text{tube}}}{(\rho c)_w A_{\text{face}}} \quad (53)$$

For nickel tubes

$$Q_0 = 46 \frac{A_{\text{tube}}}{A_{\text{face}}}.$$

Sometimes it is desired to design a tube-and-plate transducer in which the plate thickness is greater than $\lambda/8$. Such a thick plate does not act as a lumped mass. The general theory of design of such elements in which the thickness of the plate is equal to or less than $\lambda/4$ will now be given. The symbols are as given in Figure 65. Also, f_0 = frequency of mechanical resonance.

$$\begin{aligned} (m_0)_2 &= \frac{\rho_2 A_2 c_2}{2\pi f_0} = \frac{\rho_2 A_2}{(k_0)_2} \\ (m_0)_3 &= \frac{\rho_3 A_3 c_3}{2\pi f_0} = \frac{\rho_3 A_3}{(k_0)_3} \end{aligned} \quad (54)$$

$$\begin{aligned} (k_0)_2 &= \frac{2\pi f_0}{c_2} \\ (k_0)_3 &= \frac{2\pi f_0}{c_3}. \end{aligned}$$

Now consider the portion of the tube L_2 :

$$L_2 = \frac{c_2}{4f_0}, \quad \text{Peak momentum} = -(m_0)_2 v_2, \quad (55)$$

$$\text{Peak kinetic energy} = \frac{\pi}{4} (m_0)_2 v_2^2.$$

In the L_1 portion of the tube:

$$L_1 = \frac{1}{(k_0)_2} \cot^{-1} \left[\frac{\rho_3 A_3}{\rho_2 A_2} \tan (k_0)_3 L_3 \right],$$

$$\text{Peak momentum} = + (m_0)_2 v_2 [1 - \cos (k_0)_2 L_1], \quad (56)$$

$$\begin{aligned} \text{Peak kinetic energy} &= \frac{(m_0)_2 v_2^2}{2} \left[(k_0)_2 L_1 \right. \\ &\quad \left. - (\sin (k_0)_2 L_1) (\cos (k_0)_2 L_1) \right]. \end{aligned}$$

In the L_3 (plate) section:

$$\text{Peak momentum} = + (m_0)_3 v_0 \sin (k_0)_3 L_3,$$

$$\begin{aligned} \text{Peak kinetic energy} &= \frac{(m_0)_3 v_0^2}{2} \left[(k_0)_3 L_3 \right. \\ &\quad \left. + (\sin (k_0)_3 L_3) (\cos (k_0)_3 L_3) \right]. \end{aligned} \quad (57)$$

The condition that the total momentum be zero gives the relation between v_2 and v_0 :

$$\frac{v_2}{v_0} = \frac{(m_0)_3 \sin (k_0)_3 L_3}{(m_0)_2 \cos (k_0)_2 L_1}. \quad (58)$$

The effective mass of the entire system is the total kinetic energy divided by v_0^2 . This is,

$$\begin{aligned} M^* &= \frac{1}{2} \left\{ (m_0)_2 \cdot \frac{(m_0)_3^2 \sin^2 (k_0)_3 L_3}{(m_0)_2^2 \cos^2 (k_0)_2 L_1} \right. \\ &\quad \left[(k_0)_2 (L_1 + L_2) - (\sin (k_0)_2 L_1) (\cos (k_0)_2 L_1) \right] \\ &\quad \left. + (m_0)_3 [(k_0)_3 L_3 + (\sin (k_0)_3 L_3) (\cos (k_0)_3 L_3)] \right\}. \end{aligned} \quad (59)$$

It is evident from either equation (48) or equation (59) that the effective mass of the system reduces

rapidly as the ratio of M_3/m_0 is decreased. If M_3/m_0 can be decreased without decreasing the effective radiating area A_3 , then the mechanical Q can be decreased. However, this decrease in Q automatically decreases the efficiency, as may be seen by inspection of Figure 27 in Chapter 3. There it is to be noted that if the magnetic flux density (both a-c and d-c) is uniform along the entire length of the tube and if all of this flux is linked by every turn of the winding, then the mechanical impedance seen from the electric side of the hypothetical transformer is

$$\frac{1}{(\Phi\Phi')^2} \simeq \frac{4\pi^2 f^2 N^2}{\lambda^2 \left[\frac{M_3}{m_0} + \frac{m_0}{2M_3} + 1 \right]^2} \quad (60)$$

times the actual mechanical impedance. (Here λ is the magnetostriction constant.) At mechanical resonance the mechanical branch of the circuit is resistive and this resistance appears as

$$R_L(\text{elec}) = \frac{4\pi^2 f^2 N^2 R_L(\text{mechanical})}{\lambda^2 \left[\frac{M_3}{m_0} + 1 + \frac{m_0}{2M_3} \right]^2} \quad (61)$$

on the electric side. This resistance is in parallel with the core resistance R_c and hence competes with it for current. As the power dissipated in each of these parallel branches is inversely proportional to the resistances, it is desirable that R_L (electrical) be as small as possible in comparison with R_c in order to get high electromechanical efficiency. From equation (61) it is obvious that the value of R_L (elec) is made smaller by increasing the (M_3/m_0) ratio. Consequently the efficiency at resonance increases with the (M_3/m_0) ratio until the load resistance R_L (elec) becomes smaller than the copper winding resistance. The values of M_3/m_0 used in conventional tube-and-plate transducer elements range from about 4 to 10.

Magnesium or Plastic Faces. The close tolerances on the phases of the elements of a given scanning sonar transducer make it desirable to keep the mechanical Q of the elements comparatively low so as to allow reasonable tolerances on the frequencies of resonance of the elements. It has been pointed out above that the mechanical Q of the tube-and-plate type of elements can be lowered by making the mass of the plate portion less without changing the ratio of the radiating face area to the cross-sectional area of the tube. It has also been pointed out that lowering the Q decreases the efficiency at resonance unless something is done to increase the effective core re-

sistance (R_c as indicated in the equivalent circuit shown in Figure 27 of Chapter 3).

One way of decreasing the mass of the plate portion of the element is to make it thinner. There is a limit to this, however, because if the plate is made too thin it becomes too flexible and does not act as a rigid piston. The plate mass may be reduced without excessive flexibility if the plate is made of a material with low density and reasonably high modulus of elasticity.

Aluminum and its alloys or magnesium and its alloys are materials of this type in which the velocities of sound are nearly as great as those in steel or nickel but the densities only about one-fourth to one-third as great. By the use of such materials it is possible to make a diaphragm plate which has a mechanical strength as great as steel but with a mass about one-third as great. Some successful model transducers of this type have been designed and constructed by Peek of the Bell Telephone Laboratories (see Tables 3 and 4 of Chapter 8) which have efficiencies of the order of 10 per cent and Q 's of about 10. One of the difficult technical problems encountered in the construction of transducer elements of this type is the attachment of the tubes to the plate in a uniform and satisfactory manner.

Certain of the plastic materials, or laminated materials impregnated with plastics, can also be used as diaphragm plates of low mass. Most of the pure plastics have moduli which are too low to be satisfactory unless the face is made more than a quarter wave length thick. Most of the pure plastics are too compliant to distribute the force from the end of the magnetostrictive tube to the broad area of the plate, and consequently the plate acts neither as a lumped mass nor as a stiff piston. Troubles due to odd modes of vibration in the plates usually result. Plates made of laminated glass fiber impregnated with bakelite-type resins have mechanical characteristics that are practical for transducer diaphragm plates. Such laminated materials are not mechanically isotropic. The modulus is greatest in the directions parallel to the glass fibers. The technical problem of satisfactorily attaching tubes to plates of this kind has not yet been solved. One of the best ways is to terminate the tube on a small metal button with a good soldered joint and then cement the button to the plastic with some suitable cement such as Cycle-Weld.

Half-Wave Plates with Tubes. A section of a half-wave plate backed by a half-wave magnetostrictive tube is shown in Figure 67. In this case the particle

velocity is the same for all three of the antinodal positions. The effective mass of the system is very nearly the mass of half the plate portion and the mechanical Q 's are approximately 46, 43, 15, and 10 for plates of nickel, steel, aluminum, and magnesium respectively. This particular design gives a very low efficiency because the electromechanical coupling is so small. The coupling can be improved by increasing the length of the plate to slightly over a half wave length and decreasing the length of the magnetostrictive tube until it approaches a length somewhat greater than a quarter wave length. This brings the

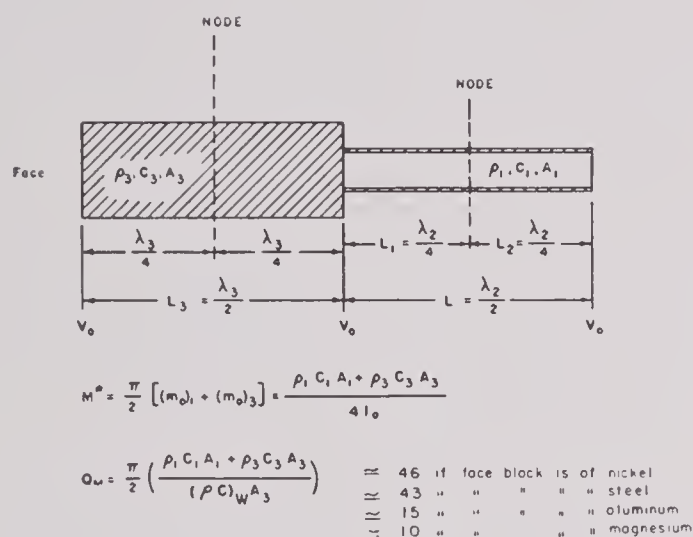


FIGURE 67. Half-wave, tube-and-plate oscillator.

node near the point of attachment of the tube to the plate, allows the velocity of the free end of the tube to increase to a value much greater than v_0 , and consequently increases the strain in the nickel for a given v_0 of the front face. However, this increases the mechanical Q of the system considerably. For the same mechanical Q , this type of element is less efficient than the conventional QC type.

In a half-wave plate type of transducer, which consists of a large number of tubes mounted on the same plate, trouble is usually caused by mechanical coupling due to the Poisson effect in the region of the node. This effect can be minimized by cutting notches between the portions of the plate that belong to the individual tubes. If a metallic bridge connecting the various blocks is desired, it should be located near the top or bottom surfaces away from the nodal region to prevent the type of coupling just mentioned. In any type of tube-and-plate construction it is good practice to have only one node in the vibrating system, and this node should be located a short distance

up the tubes from the plate so that a minimum amount of mechanical coupling is produced.

Wedge-Type Plate. An example of the wedge-type plate is shown in Figure 25. There are few advantages in this type of element. However, sufficient information will be given to aid in the design of such an element and to help understand its mechanical characteristics.

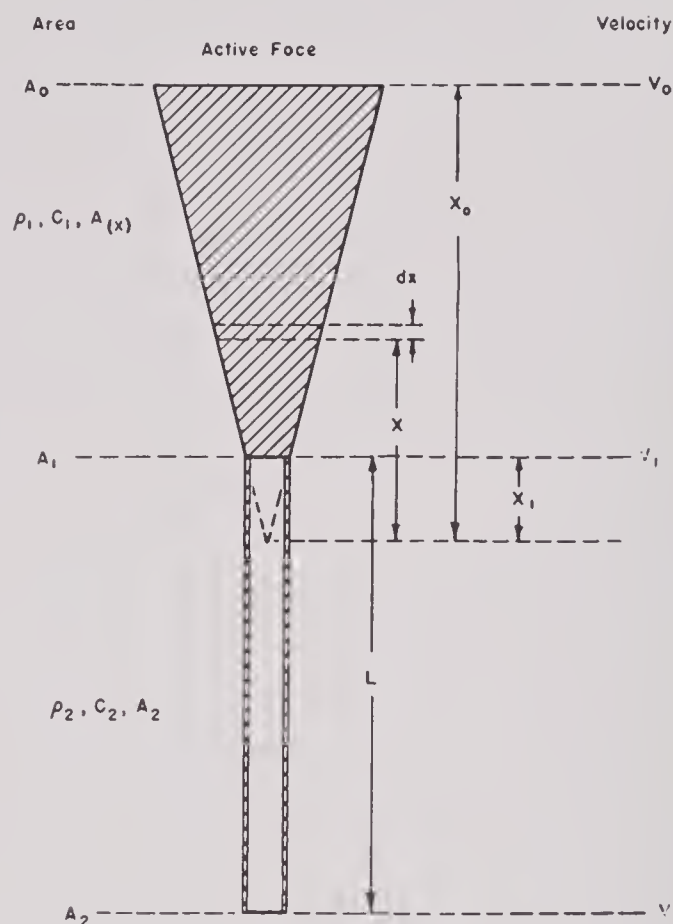


FIGURE 68. Fundamental section of a tube-and-plate type element in which the plate portion is wedge shaped.

A section of an element of this type is shown in Figure 68. The plate portion may be considered as a long, narrow prism, the active face of which is about one-half wave length wide and 5 to 7 wave lengths long (these wave lengths are for water at the frequency of resonance), and the tubes or their equivalent extend out from the narrow face of the prism. The areas indicated refer to the cross-sectional areas corresponding to a unit height of the prism and these areas lie in planes perpendicular to the direction of the strain or particle velocity.

The ratio of the particle velocities at A_1 and A_0 is

$$\frac{v_1}{v_0} = \frac{N_1(kx_0) \cdot J_0(kx_1) - J_1(kx_0) \cdot N_0(kx_1)}{N_1(kx_0) \cdot J_0(kx_0) - J_1(kx_0) \cdot N_0(kx_0)} \quad (62)$$

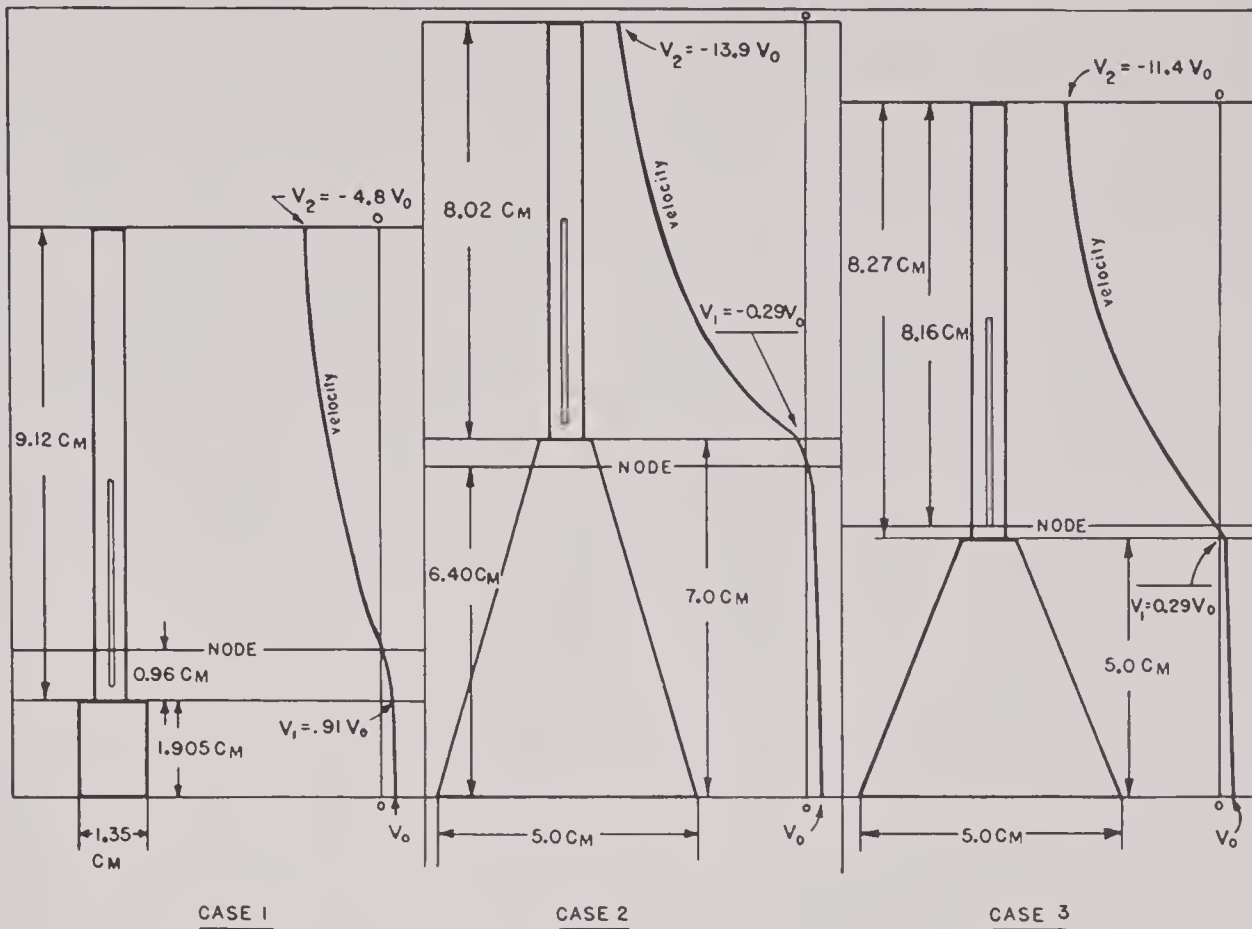


FIGURE 69. Comparison of a standard tube-and-plate element with two kinds of wedge-and-tube elements. In each case $A_{\text{tube}} = 0.114 \text{ cm}^2$, $A_{\text{face}} = 1.82 \text{ cm}^2$, frequency = 14.87 kc.

where the J 's and N 's are the Bessel and Neumann functions of the orders indicated by the subscripts.

The condition for resonance in the first mode of vibration is

$$\frac{J_1(kx_1)N_1(kx_0) - N_1(kx_1)J_1(kx_0)}{J_0(kx_1)N_1(kx_0) - N_0(kx_1)J_1(kx_0)} = \frac{\rho_2 c_2 A_2}{\rho_1 c_1 A_1} \tan k'L, \quad (63)$$

where $k = 2\pi f/c_1$ and $k' = 2\pi f'/c_2$. The frequency of resonance will be designated by f_0 and the corresponding k 's by k_0 's.

The ratio of the particle velocity at the free end of the tube to that at the active face is

$$\frac{v_2}{v_0} = \frac{v_1}{v_0} \sec k_0' L. \quad (64)$$

The kinetic energy of the tube part of the system is

$$\frac{\rho_2 A_2 v_2^2}{2} \left[L + \frac{1}{2k_0'} \sin 2k_0' L \right] \quad (65)$$

and that of the wedge part is

$$\frac{\rho_1 A_0 v_0^2}{x_0} \int_{x_1}^{x_0} \left[\frac{N_1(k_0 x_0) J_0(k_0 x) - J_1(k_0 x_0) N_0(k_0 x)}{N_1(k_0 x_0) J_0(k_0 x_0) - J_1(k_0 x_0) N_0(k_0 x_0)} \right]^2 x dx, \quad (66)$$

where x is the distance measured outward from the virtual vertex of the wedge. Consequently the effective mass of the system is

$$M^* = \frac{\rho_2 A_2}{2} \left(L + \frac{1}{2k_0'} \sin 2k_0' L \right) \left(\frac{v_1}{v_0} \right)^2 \sec^2 k_0' L + \frac{\rho_1 A_0}{x_0} \int_{x_1}^{x_0} \left[\frac{N_1(k_0 x_0) J_0(k_0 x) - J_1(k_0 x_0) N_0(k_0 x)}{N_1(k_0 x_0) J_0(k_0 x_0) - J_1(k_0 x_0) N_0(k_0 x_0)} \right]^2 x dx. \quad (67)$$

Just as for all the other types, the mechanical Q is given by

$$\frac{2\pi f_0 M^*}{A_0 (\rho c)_w}.$$

The equivalent circuit shown in Figure 27 of Chapter 3 may be applied to this type of transducer ele-

ment by taking $R_L = A_0(\rho c)_w(v_0/v_1)^2$, M_L equal to the second term of equation (67), multiplied by $(v_0/v_1)^2$, L_1 (mechanical inductance) equal to the first term of equation (67), and making the transformation ratio

$$\frac{1}{(\Phi\Phi')^2} = \frac{4\pi^2 f_0^2 N^2}{\lambda^2(1 - \sec k'L)^2}. \quad (68)$$

To give the reader a concrete idea of the velocity distributions, equivalent masses, mechanical Q 's, etc., of the wedge-and-tube type element as compared to the conventional tube-and-plate type, three

TABLE 2.

	Tube and plate	Tube and long wedge	Tube and short wedge
Actual mass of plate or wedge (gms)	27.0	59.7	42.5
m_0 (grams/radian)	5.20	5.20	5.20
M/m_0	5.20
M^* (effective mass, gms)	137	837	567
Q_M	49	298	198
R_L/R_c	0.76	0.16	0.22
Maximum efficiency	0.57	0.85	0.82

specific cases have been analyzed quantitatively: (1) the standard QGA Type 941, 14.87 ke; (2) a long wedge having the same face area, nickel tube area, and frequency as the QGA; (3) a short wedge having the same face area, nickel tube area, and frequency as the QGA.

In Figure 69, a comparison is made between the standard tube and plate of the QGA Type 941 projector, with resonant frequency of 14.9 ke and two tube-driven wedges. The elements are drawn to scale, and it is assumed in each case that the slotted tubes are made of annealed nickel, with a 0.025-in. wall. The plate and wedges are of steel. The windings are assumed to extend along 4 cm of the tube nearest the node, so that this length of tube contributes to the core impedance. Computed values of significant characteristics of the three elements are given in Table 2. These computations are based on the following values:

$$f_0 = 14.9 \text{ ke},$$

$$k'_{Ni} = 0.193,$$

$$k'_{steel} = 0.187,$$

$$R_c = 1.9 \times 10^{-7} N^2 \text{ ohms } (N = \text{turns of windings}),$$

$$X_c = 1.85 \times 10^{-4} N^2 \text{ ohms},$$

$$\mu_r = 30, \text{ and}$$

$$\text{Resistivity} = 8 \times 10^{-6} \text{ ohm cm.}$$

Eddy currents are assumed the same as for flat lamina and resistance of windings is negligible.

It is to be noted that the high efficiencies for the wedges as computed for the ideal conditions assumed are obtained at the price of values of Q which are prohibitively high for scanning sonar use. Moreover, efficiencies that could be obtained in any actual case would be much lower than those shown because of the copper losses in the windings and internal mechanical resistance, both of which were neglected in the computation for Table 2.

Chapter 14

CONSTRUCTION AND TESTING OF SCANNING TRANSDUCERS

14.1 INTRODUCTION

The preceding chapter presented designs for several fundamentally different types of transducers that might be successfully used in scanning a sound field. Each type possesses its own peculiar set of problems and advantages. This discussion will be limited to an assembly of laminated stacks arranged so that the active faces form a cylinder. Practical methods of construction and precautions for maintaining tolerances will be described. The testing program, both before and after assembly, will be given in detail. A brief outline of the experience gained in building and testing several models is also included.

14.2 MANUFACTURE OF LAMINATED STACKS

There was considerable variety in the types of laminated stacks built by Harvard Underwater Sound Laboratory [HUSL]. They ranged in size from the large $8\frac{3}{4} \times 8\frac{3}{4} \times 3\frac{1}{2}$ -in. block of laminations down to the $1\frac{1}{4} \times \frac{3}{4} \times \frac{9}{16}$ -in. stack used as one element in an array. This chapter, however, will be limited largely to those used in the scanning sonar and related projects. In general, they are illustrated by the two stacks shown in Figure 1. One of these has a slot completely across the magnetic circuit into which a permanent magnet is inserted for polarization. The other must be polarized by sending direct current through its windings. In every case they have been built up of thin nickel laminations with a bonding cement to assure permanent form and rigidity. They are provided with windings, end caps for mounting, and some means of polarization. This section will deal with the details of this process and the means of determining how successfully it has been done.

14.2.1 Problems Involved in Construction

There are a number of problems involved in the manufacture of laminated stacks. The bond between

laminations must give the stack strength to withstand the handling of winding and mounting. In its mounted position the stack will not ordinarily be subjected to tension or compression, but it will have to stand the shear and bending stress of accidental blows. Since the binding material may strongly influence the characteristics of the stack, choice of binding material is also limited by factors other than strength.

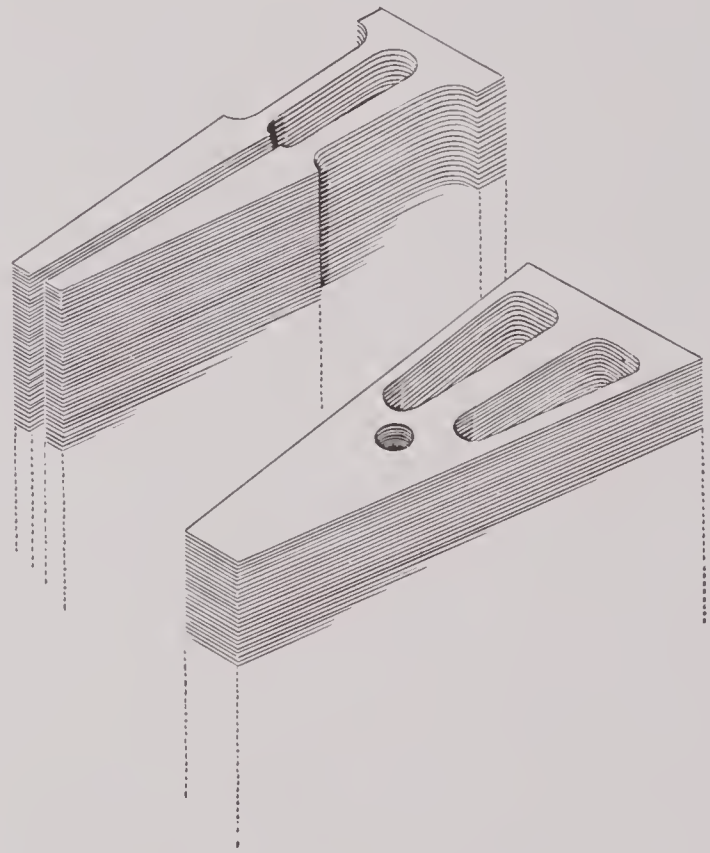


FIGURE 1. Scanning sonar stacks.

Where a number of stacks are assembled into one unit to give a composite pattern, these stacks must be quite uniform in frequency and amplitude. The methods of stack manufacture used must result in stacks that are close duplicates of one another. Rapid and accurate methods of testing frequency and amplitude should be available. To avoid the introduction of phase differences, careful alignment of the lamina-

tions in the stack and installation of the stack in the mounting are also necessary.

In a complete scanning sonar transducer there may be from 40,000–80,000 laminations. The handling of such a quantity of fragile parts presents a difficult problem to the manufacturer. After being punched, the laminations must be carefully cleaned, annealed, and given a coat of consolidating cement. If the necessary tolerances are to be maintained in matching stacks, the laminations must be handled in such a way as to avoid deformation of any kind. These laminations may be made into as many as 192 stacks, each of which must be equipped with winding caps, end plates, a rubber diaphragm, and a coil on each of the two winding cores. To turn this amount of detailed work into an acceptable manufacturing process is a problem rivaling that of the original design.

11.2.2 Preparation of Laminations

Before going into a detailed description of the manufacturing methods in use at present, it would be well to point out a few precautions. However rugged a laminated stack may be in appearance, it is really a delicate temperamental instrument in behavior, prone to spurious modes of vibration and high internal mechanical losses when poorly constructed. A good design can easily be lost through poor execution. Methods of handling laminations have developed gradually under stress of growing demand. Investigation of problems has gone along with production, and usually the aim of an investigation has been to find something that would *do* rather than to discover the best possible method. Therefore, the following description presents a technique that has been found to work in practice but does not represent the best development possible.

A good die for cutting the laminations is essential. The laminations should be consolidated into stacks under pressure. Stacks more than 4 in. high should be consolidated in sections. If stacks are higher than this, it is difficult to hold the laminations in proper alignment and to develop a pressure evenly distributed through the stack. The bonding cement should be thermosetting rather than thermoplastic.

Laminations that have been battered and bent by careless handling cannot be consolidated into stacks that meet the required dimensional tolerances; they are likely to stack higher on one end or on one side than on the other. Crimps and kinks may permit strains to be relieved in undesired directions. A cer-

tain amount of cold-working results from mistreatment after annealing. To avoid deformation, laminations should be racked up as they come from the punch press. Figure 2 shows a satisfactory rack and tray for this purpose that also permits the storage of large quantities in a small space.

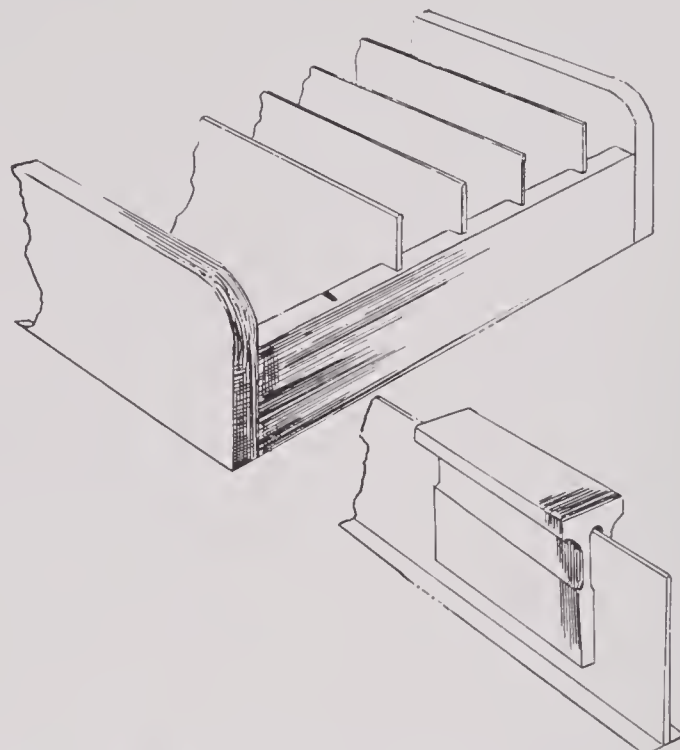


FIGURE 2. Rack for laminations as they come from the punch press.

The metal strip from which the laminations are punched comes coated with an oil film which, along with other dirt, must be removed before annealing. Nickel laminations which show the slightest oil stain beforehand will show, after annealing in air, a gray-green scale quite loosely attached to the metal surface. The appearance of scale has at times been ascribed to other causes, but it seems reasonably certain that a clean lamination will never show the effect.

For cleaning, the racks of closely packed laminations are placed in a tray containing enough ethylene trichloride to cover them. The solvent penetrates rapidly into the capillary spaces between laminations and in a short while the oil has diffused throughout the solvent. The rack of laminations is then placed in a tray of clean solvent, where the oil again becomes diluted. Four such treatments, with a 4-hr soaking for each, produce clean laminations. This method requires a little time, but it involves no handling of the lamination and practically no labor.

Nickel is usually annealed at 930 to 1000 C in air. The thin oxide coating so produced has excellent insulating properties, and no other insulation is needed if during the annealing the laminations are so spaced that oxygen is available to give a uniform coat over the entire surface. An annealing rack of stainless steel is shown in Figure 3. Clean laminations may be loaded rapidly onto these racks with minimum handling. One method uses a $\frac{1}{8}$ -in. brass tube

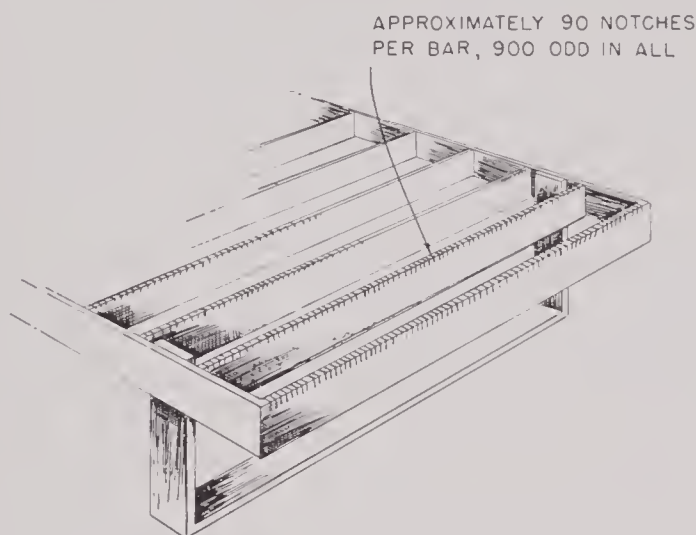


FIGURE 3. Annealing rack.

that has one end fashioned to slide along the top of the rack. This tube carries the laminations to be racked, and they are fed off into the slots as the rod slides along the top of the rack. This scheme, of course, can be used only with the slotted type of lamination, but some similar scheme will serve for other types. The laminations may also be speedily removed by reversing the loading process.

11.2.3

Consolidation

The choice of a bonding material for consolidation, the method of applying it, and the pressure used during curing depend upon the amount of mechanical strength that can be sacrificed for uniformity and efficiency. It has been repeatedly demonstrated that too strong a bond between laminations is a source of trouble. Stacks so built show unwanted resonances near the main resonance frequency, a wide variation in resonance frequency, and a low potential efficiency. The minor resonances of a 25-ke stack will disappear if the stack height is cut down to 1 in. or less for stacks of higher frequency. Increasing the thickness of the bonding layer will yield a stronger stack but may result in lower efficiency.⁵⁹

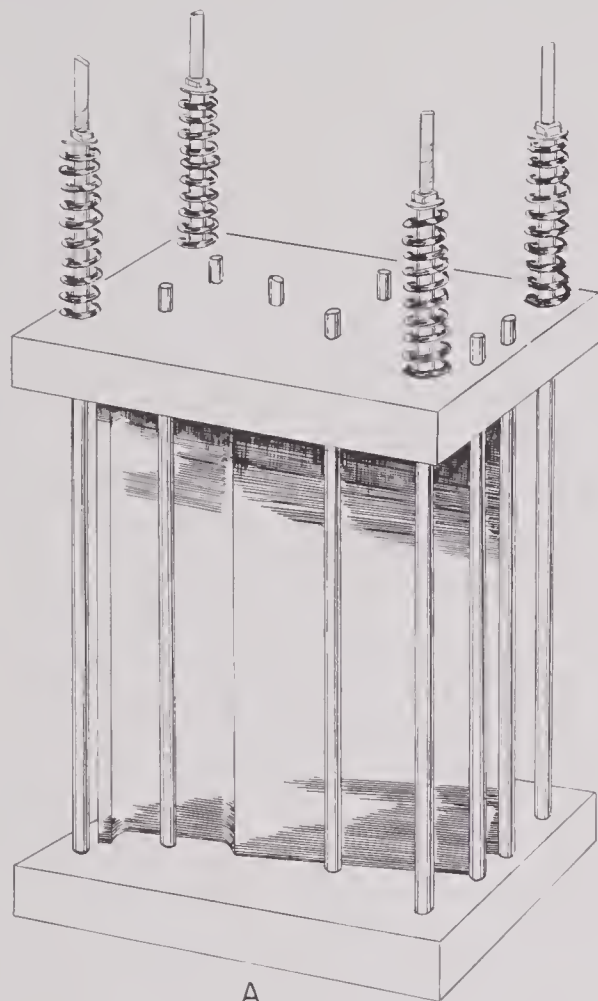
METHODS OF APPLYING CEMENT

Three different methods of applying the bonding cement and consolidating the stack have been successfully used in the laboratory. One method takes advantage of capillarity in the thin spaces between laminations. The correct number of laminations are placed in the stacking jig and put under slight pressure. The outside aligning pins are withdrawn from the jig and a medium coat of Cycle-Weld P-55-6 cement is brushed on the outside surface of the stack. The cement is rapidly absorbed into the spaces between laminations. The stack should be given a 30-min. air dry, and a 30-min. oven dry at 180 F. The aligning pins are then replaced and the laminations put under a pressure of 50 to 100 lb per sq in., depending on the amount of burr and lamination thickness. The cement cures in about 15 min. after the stack has reached a temperature of 300 F. This procedure results in stacks that are uniform in frequency behavior and of high potential efficiency but moderate strength. If stacks of greater strength are desired, this method may be modified. The cement is brushed on in considerable quantities and given an 8- or 10-hr cure at 260 F. The longer curing period allows the solvent to escape before the bond is completely established.

In a second method of consolidation, the laminations are placed flat on wire mesh and sprayed with Cycle-Weld C-3 cement. After a 5-min. air dry, they are turned over and sprayed on the reverse side. An air dry of 20 min. is followed by an oven dry at 180 F of about 20 min. The laminations are put in a jig under a pressure of about 200 to 300 lb per sq in. and given a 20-min. cure at 320 F. It is important that the actual temperature of the stack be 320 F. The coat of cement may be built up to any desired thickness by repeated spraying; great strength can be attained in this way. Coats of 0.0015-0.002 in. are sufficient for maximum strength, but, for stacks used in scanning sonar transducers, coats thicker than 0.0005 in. are not desirable.

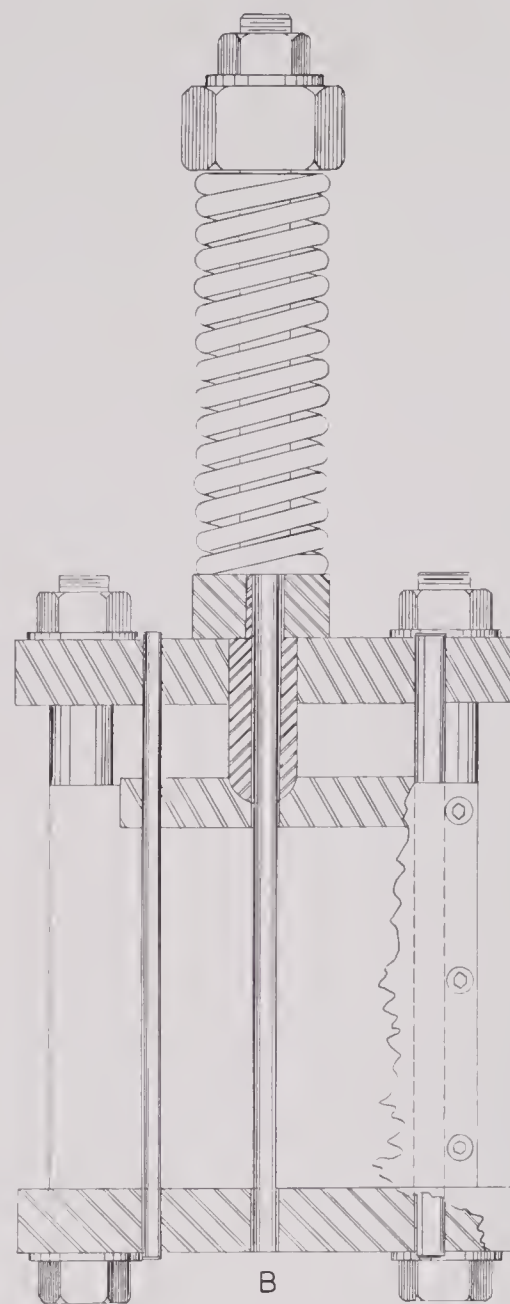
Cements like Cycle-Weld P-55-6 that flow when heated are likely to bond over the whole surface. Such bonds are usually strong enough to introduce parasitic resonances. Cycle-Weld C-3 is a nonflowing cement and, when applied in thin coats, bonds the lamination only by a narrow strip around its edge. Stacks thus consolidated very seldom show undesired resonances.

The bakelite resins are excellent if strength of bond is the prime requisite. It is also likely that proper



A

USE OF TOP PLATE TO EXERT PRESSURE



B

USE OF PLUNGER TO EXERT PRESSURE

FIGURE 4. A. Stacking jig, original model. B. Stacking jig, improved model.

solvents could be found to permit their application by any of the methods recommended here.

The cement may also be applied by dipping. Close control of the time of withdrawal of the lamination from the cement must be maintained to avoid the formation of a bead on the end. Dipping has two advantages: a more uniform coat is possible and less handling is necessary than with spraying. The laminations are hung on hooks and lowered into a vat of the cement. A mechanical device for withdrawing them at a uniform rate of speed is easily arranged. The speed of withdrawal depends upon the viscosity

of the cement used. With Cycle-Weld C-3, of specific gravity 0.92, this speed is about 9 in. per minute. Rapid evaporation of solvent from the dipping vat requires frequent checks on the density of the cement and the addition of solvent. The same drying and curing procedure is used as with spraying. The success of this process depends upon having laminations free of burrs, excellent consolidating jigs, and close control on the cement. It has been used to produce uniform stacks of good strength with Cycle-Weld spray-type C-3 as the cement. Cycle-Weld P-55-6 may also be used, but it must be thinned to a specific

CONFIDENTIAL

gravity of about 0.86 and the laminations consolidated with pressures of 30 to 50 lb per sq in.

CONSOLIDATING JIGS

A good jig is an essential feature of a successful consolidating technique. A shrinkage in height usually occurs during the curing process, necessitating the use of calibrated springs to insure a constant pressure as the stack shrinks. Aligning pins must be carefully spaced to maintain close tolerances on stack dimensions. As the pressure is applied, the laminations should slide freely along the pins to produce uniform pressure throughout the length of the stack. This applies also to top and bottom plates of the jig of Figure 4A. The slightest misalignment of the plate at either end of the stack would make it lodge on one or more of the pins, thus reducing the pressure on the stack. The improved jig shown in 4B prevents this. A piston slightly smaller than the laminations, fitting loosely between the pins, applies the pressure through a ball-and-socket joint.

HEAT TREATMENT AND RECOVERY OF POOR STACKS

Experiment has shown that the characteristics of a stack will be slightly changed if it is heated to a temperature higher than that at which it was consolidated. If it is not raised above this temperature, further heating for short periods does not seem to affect it. If a rubber diaphragm is to be attached by heating, the consolidated stack should be raised to the temperature required for attaching the rubber before measurements are made on it. In general, one may safely assume that a poor stack is the result of too strong a bond between laminations. This bond may be weakened by raising the temperature of the stack to the point of decomposition of the cement. The resulting stack will have little mechanical strength, but, if it is a split stack and was produced by brushing cement onto the outside surface, it may be strengthened by brushing cement onto the inside surface and curing a second time.

11.2.1 Testing Equipment and Preliminary Testing

Stacks used as elements in an assembly must meet certain requirements with regard to potential efficiency and resonance frequency. A standard procedure for determining these characteristics has been to make impedance measurements at a sufficiently large number of frequencies, in both air and water, to determine the motional impedance circles. This

was so long a task in the case of a 192-stack assembly that it was necessary to devise quick and easy substitutes for these measurements. The impedometer, the conductometer, and the vector impedance locus plotter were developed for this purpose. Descriptions of these devices are given in Chapter 9.

To use the impedometer, the stack to be measured is connected in the circuit of Figure 5A as element T .

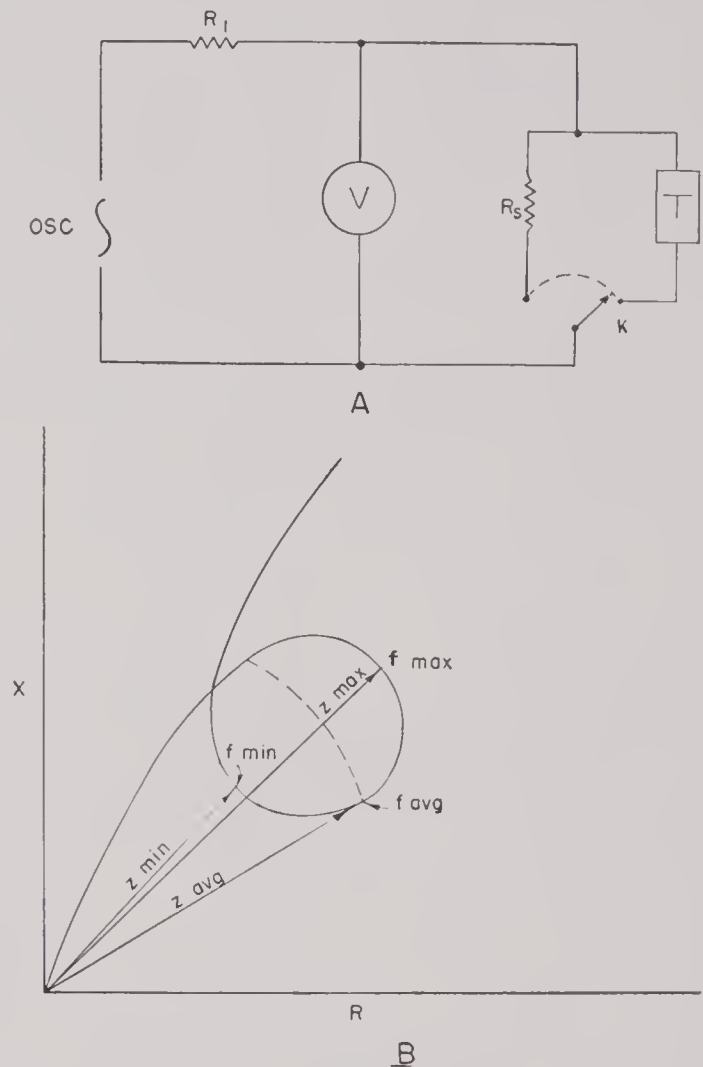


FIGURE 5. A. Circuit of impedometer. B. Impedance diagram.

The switch K is thrown to R_s and the output of the oscillator is regulated until the voltmeter reads $R_s/10^n$, where n is a small integer. The switch K is thrown to T , making the voltmeter read $|Z_T|/10^n$. The oscillator frequency is then varied through the range of the impedance circle. Figure 5B shows the position of the vectors for which magnitudes are read from the voltmeter. The maximum impedance on the circle Z_{max} may be averaged with the minimum impedance on the circle Z_{min} to give the average impedance Z_{avg} . The average frequency f_{avg} is obtained

by varying the oscillator frequency between f_{\max} and f_{\min} until the voltmeter indicates the value of the average impedance. An impedance measurement taken several kilocycles away from the resonance frequency is quite useful for comparing the extent of magnetic polarization and the core impedance with those of other stacks.

While the impedometer measures magnitudes of the impedance vectors only, experience has shown that stacks uniform with respect to these quantities and without any minor resonances within the main impedance circle will work together satisfactorily. The presence of minor resonances is indicated by irregular variations in the impedance readings taken through the frequency range. The ratio of Z_{\max} to Z_{\min} gives an approximate value of the diameter of the impedance circle and, therefore, of the potential efficiency. The mean frequency, f_r , is ordinarily quite close to the resonance frequency and can be used in frequency-matching of the stacks. The method is fast; scarcely more than 1 min. per stack is necessary to obtain and record all the data.

A preliminary test with the impedometer may be made before winding to avoid the expense of winding a stack that may later be discarded. A coil of the kind to be used in the transducer may be preformed slightly oversize so that it will slip down into place around the winding core. A magnet, used at the strength that it maintains in air, is put into the magnet slot. Thus equipped, the stack can be tested for the presence of minor resonances, and a good value of the ratio of Z_{\max} to Z_{\min} can thus be obtained. Accurate frequency measurements cannot be made under these conditions since the stack will be under-polarized and there will be considerable flux leakage due to the loose windings.

11.2.5

Winding

Before the final tests can be made for the selection of stacks to go into an assembly, the stacks must be wound, and this winding must thereafter remain permanently fixed in position. To prepare a stack for winding, a collar of insulating material is put around each leg. It has been found convenient to use a band of $\frac{1}{16}$ -in. air-cell neoprene which is slightly wider than the length of the coil and fits snugly on the core. This band should be cemented to the core in two places to prevent slipping. The air-cell neoprene affords excellent mechanical insulation and will furnish the pressure release necessary if the stack is to be mounted in oil.

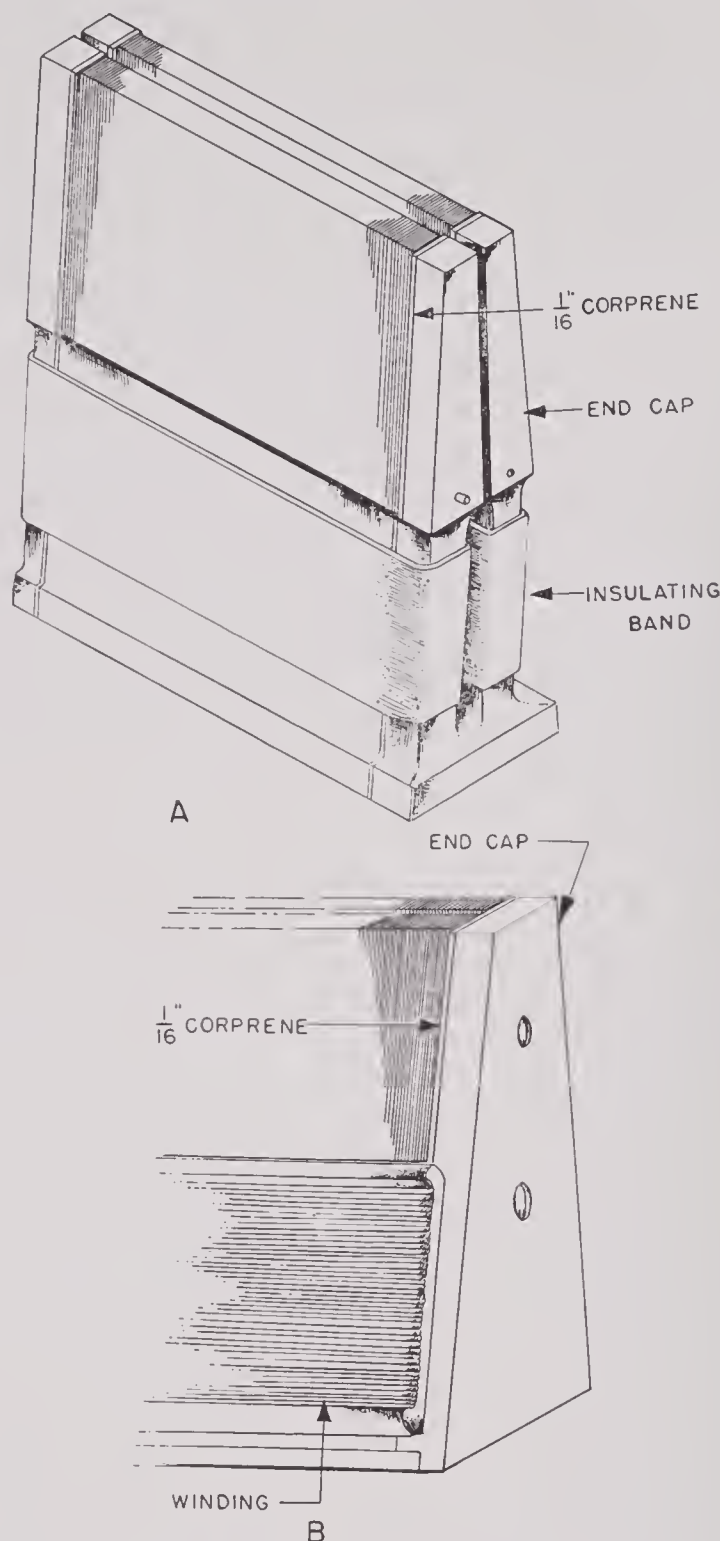


FIGURE 6. A. Aluminum end cap; end cap under winding. B. Bakelite end cap; end cap over winding.

Two types of end caps, shown in Figure 6, have been used for stack mounting in scanning sonar transducers. Figure 6A shows an aluminum-cast end cap which is attached before winding. A $\frac{1}{16}$ -in. thickness of corprene or air-cell neoprene isolates the end cap from the stack. Since the end caps hold the stacks in operating positions that are quite critical with

respect to spacing, close tolerances must be maintained in placing the end cap on the stack. Vulcalock cement serves very well to attach these parts, but care must be taken to avoid an excess that will run over into the magnet slot. If the end cap of Figure 6A is used, it is attached first and the insulating band and windings are put on over it. The bakelite molded end cap of Figure 6B is attached after the winding is done.

The presence of the magnet slot and the fact that few turns of wire are used make it practicable to wind these stacks by hand. A winding jig of the type

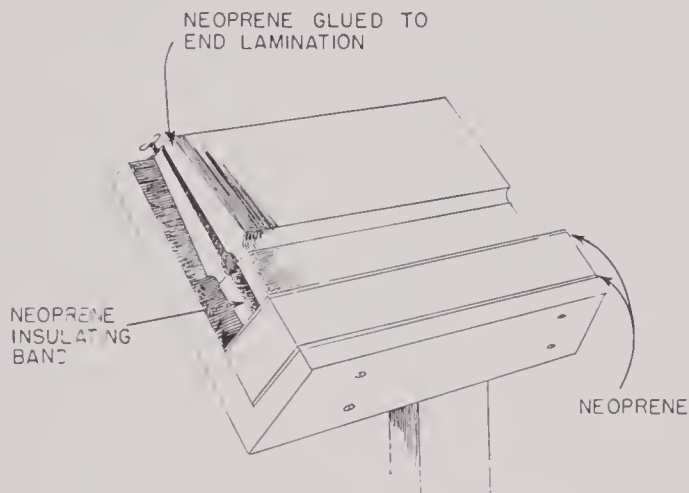


FIGURE 7. Winding jig.

shown in Figure 7 is convenient for this purpose. It should be remembered that these stacks are made of soft annealed nickel and that dropping them, letting them fall over, or clamping them in a vise is to be carefully avoided. To minimize mechanical losses, the windings must fit loosely. The use of 0.010-in. removable spacers at each end of the stack during winding makes it possible to put on a neat, well-placed winding that will not bind the stack after the spacers are withdrawn. Because of the flux leakage across the winding slot, the placing of the winding is critical. The position of the winding relative to the motion made by the stack affects the potential efficiency and the resonance frequency. Therefore, the winding must be firmly attached to prevent slipping. This can be effectively done after winding by brushing on a heavy coat of thermosetting cement to hold the winding to the rubber band beneath it.

14.2.6 Selection of Stacks

At the time of this writing no satisfactory method for testing stacks after attaching the rubber dia-

phragm had been developed. Impedance measurements in air with the diaphragm attached do not show the behavior of an unloaded stack and are not indicative of the stack's behavior in water. Impedance measurements in water are not a sufficiently sensitive means of detecting frequency variations between stacks. It was necessary therefore to use, as a basis of selection, the data taken on the stacks before the rubber diaphragm was attached, on the assumption that the process of cementing rubber to the stack never results in a radical change in its behavior. Since there is considerable evidence that this assumption is unsafe, it should be investigated further.

The best procedure developed at HUSL is the basing of stack selection on conductometer measurements made after the stack has had its final winding and is polarized as it will be in the final assembly. A description of this step is given in the next section. The conductometer measures the maximum conductance and, as shown by the admittance circle, the frequency of maximum conductance, which is quite close to the frequency of maximum efficiency.

14.2.7 Polarization of Stacks

The last step in the assembly of a stack is to provide it with a permanent magnet. A description of the magnet to be used and its characteristics have been given in Section 13.3.3. The magnet may be a single block or several blocks cemented together and shaped to fit the slot precisely. This must present a clean smooth surface free of any material that might cement the magnet to the stack. The magnet is kept in place, without binding, by the coil and the end caps. In some cases the open end of the magnet slot has been closed by nonmagnetic metal strips, isolated from the stack with air-cell neoprene and attached by screws to the end caps. In others the slot was closed temporarily by paper tape and permanently by the final mounting base. Early experiments showed that cementing the magnets into the slots seriously affects the behavior of the stack.

With the magnet in position, the stack is placed in a magnetic field of sufficient strength to saturate it. The stacks are to be mounted with like poles adjacent; therefore, the direction of magnetization and the polarity of the winding terminals must be recorded. Experience has shown that after magnetization there may be considerable variation from stack to stack in the core impedance and the impedance

at resonance. This is partially due to lack of uniformity in the magnets and to variation in the incremental permeability of the stacks. This situation may be improved by a slight demagnetization.

The practice was to bring the impedance of all stacks that go into the same assembly to the same magnitude at a frequency about 10 ke away from resonance. The reason for this operation may be readily understood by referring to the two impedance circles of Figure 8. The two curves show the relative

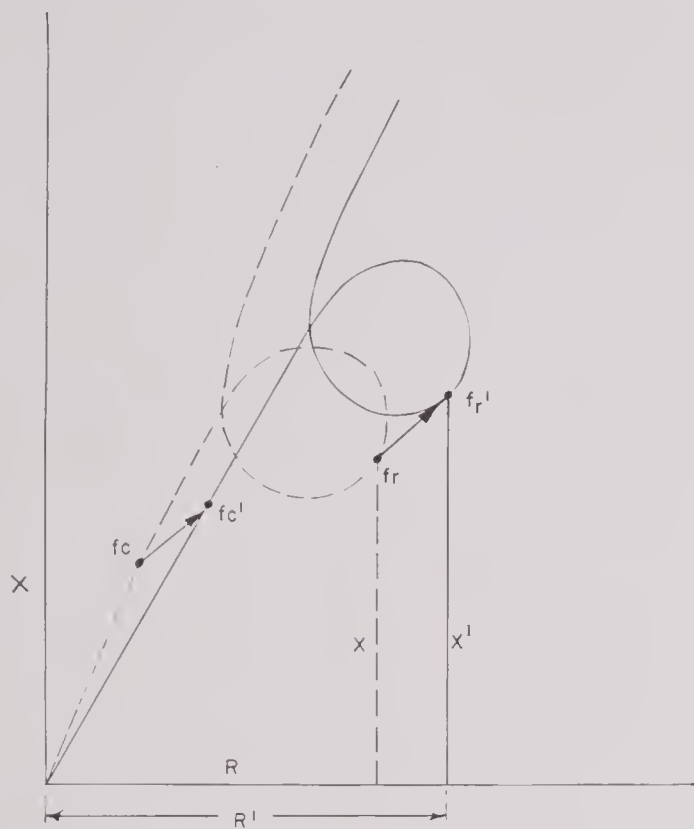


FIGURE 8. Dependence of impedance curve on magnetization.

values of impedance of two stacks polarized to different degrees. The frequency f_c on the dotted curve is the same as the frequency f_c' of the solid line, and if the impedance of the two stacks can be made to match at this frequency, the two impedance curves will practically coincide — an essential requirement if the two stacks are to vibrate in phase when driven from a common source. If the stack represented by the dashed line is depolarized slightly, its impedance at f_c will move up the arrow to the impedance at f_c' . The frequency f_c is chosen some distance from resonance, since at such a point frequency settings are not so critical and the impedance becomes truly representative of the core impedance.

Demagnetization is easily effected by sending 60-cycle current through the windings of the stack. The

circuit of Figure 9 provides a quick and easy scheme. On the right of the diagram is the impedometer and on the left is a Variac transformer; T is the stack, A an a-c ammeter, R_2 a resistor to protect the am-

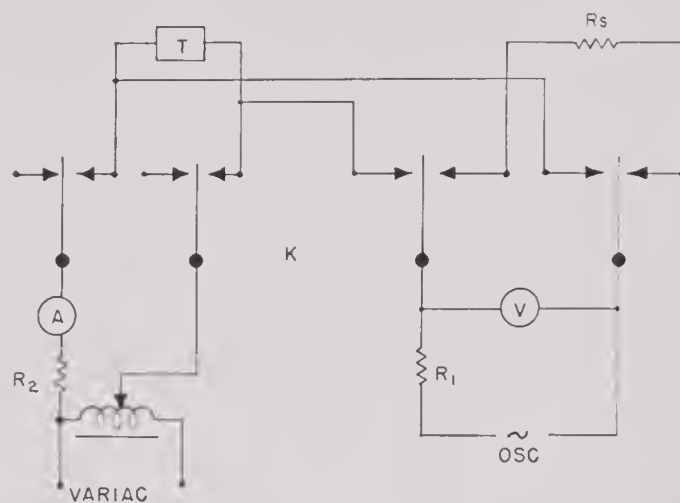


FIGURE 9. Circuit for adjusting magnetization.

meter, and K a multiple switch. When K is thrown to the right, the Variac is connected to the stack, and the oscillator and voltmeter are across the standard resistor R_s . In this position, the oscillator is set at the frequency at which the impedance of the stack is to be stabilized, and the output of the oscillator is set to make the voltmeter read impedance directly. From the Variac, a surge of a-c current is sent through the windings of the stack. Then switch K is thrown to the left, taking the Variac out of the circuit and putting the voltmeter and oscillator across the stack. The resulting impedance of the stack can be read directly from the voltmeter. Getting the desired impedance is necessarily a trial-and-error process, but it is greatly facilitated by this easy switching circuit. If one overshoots the mark, the stack must be repolarized and the demagnetization repeated. It is to be noted that stacks whose impedances are higher when saturated than the impedance chosen for polarization cannot be used in the assembly.

14.3 PREPARATION OF THE TRANSDUCER ELEMENT

14.3.1

General Design

One element of a scanning transducer may consist of a single stack or of two or more stacks operating in series, parallel, or in series-parallel combination. Where a thin rubber diaphragm is cemented to the

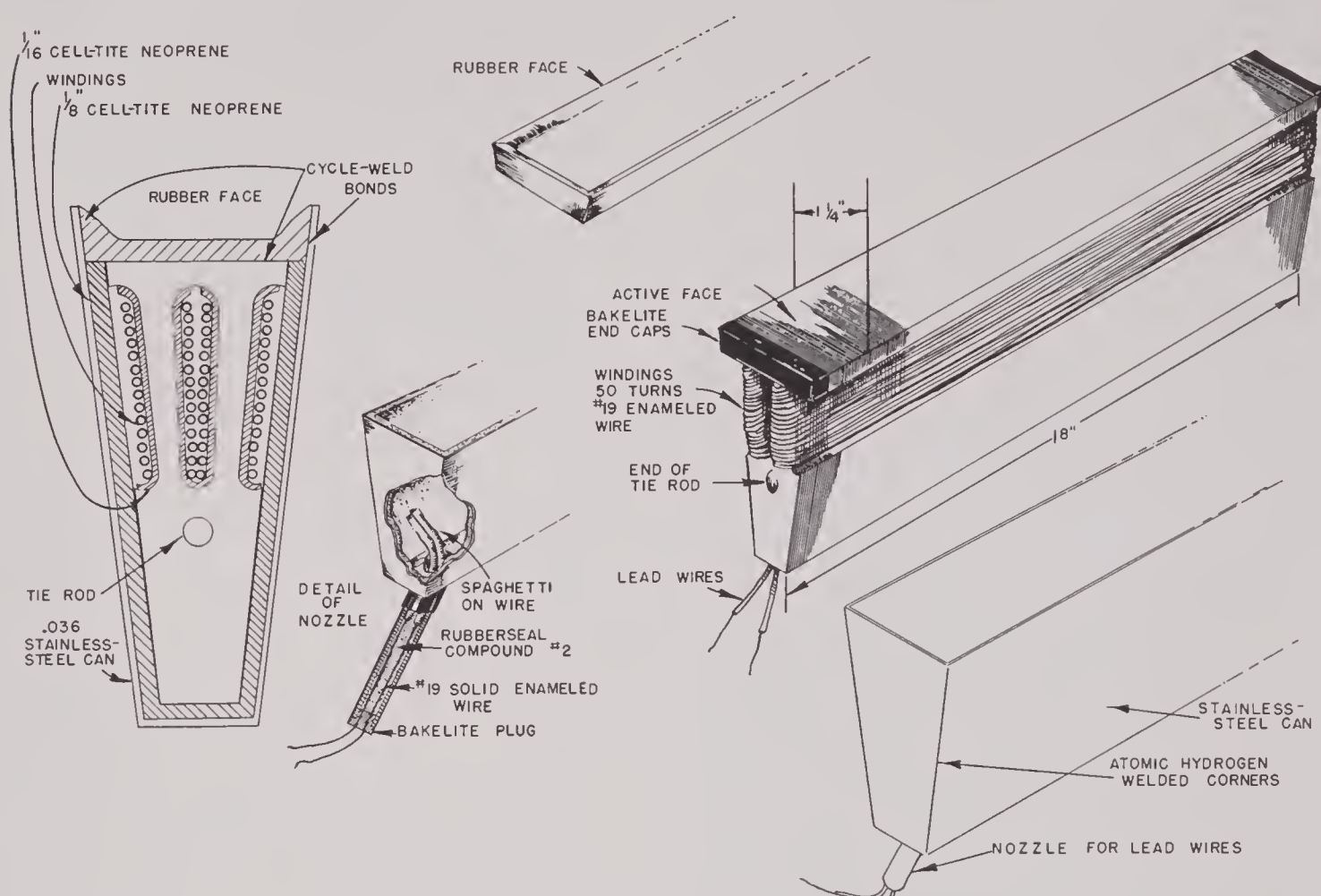


FIGURE 10. Component parts of HP-2 element.

radiating faces of the stacks, this diaphragm may be continuous for the full length of the element. This assembly is further strengthened by a thin aluminum spline fastened to the back of each stack. A preferred way of building up the element is to provide each stack with a separate diaphragm and mounting. A brief description of the various methods used at HUSL follows.

The first of the HP series of scanning transducers was like that shown in Figure 15 of Chapter 13, except that it was not enclosed in a rubber boot. The windings, winding slots, and stack face were in direct contact with water. Each element consisted of one 12-in. stack wound with a wire whose insulation was supposedly water-resistant. Two defects in the operation of the transducer called for a change in element design. The bare metal face of the laminated stack was quite erratic in its contact with the water and the wire insulation would not stand up under operating conditions. These difficulties were solved by the rubber jacket shown in Figure 15 of Chapter 13.

11.3.2 Elements Housed as Individual Units

The second transducer of the HP series, the HP-2 (Figure 19 of Chapter 13), was so designed that each element, consisting of a single 18-in. stack, was housed in a stainless-steel container made watertight by a seal for the conductors and a rubber strip cemented to the container and to the active face of the stack. The component parts of such an element are shown in Figure 10 and the assembled transducer in Figure 11.

In this design, the fatal defect, the inherent weakness of the bond between the rubber diaphragm and the stainless-steel container, has already been indicated in Chapter 13. The difficulty is twofold. The first is the fact that a bond between stainless steel and rubber using the usual techniques has proved inherently weak. The second is the difficulty of applying and maintaining the necessary pressures simultaneously to the face of the stack and to the edge of

the stainless-steel housing. After several months of experimentation, a 36-element unit was produced which was sufficiently watertight for a trial at New London but which developed leaks after a very short period of use.

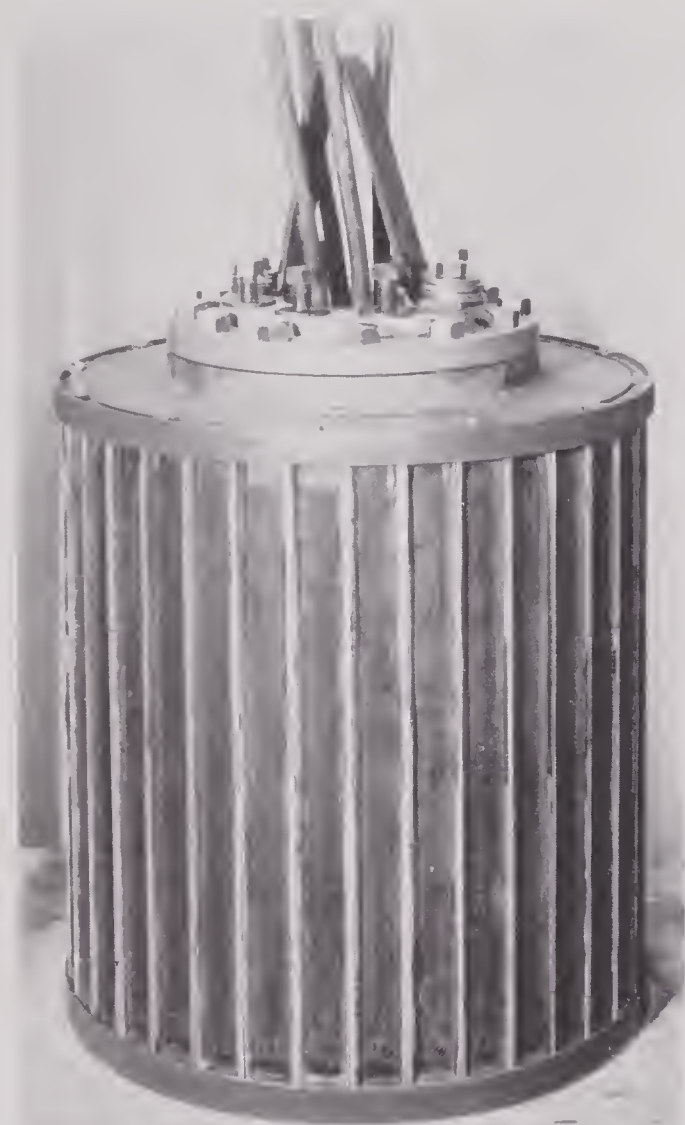


FIGURE 11. HP-2 transducer.

The most effective means found of securing a bond between the rubber diaphragm and the stainless steel was to etch the steel with concentrated hydrochloric acid. The outside lips of the container were coated with petroleum jelly, and the container was immersed to a depth of $\frac{1}{2}$ in. for 5 min. in the acid bath, giving an etched inner surface to which the rubber would adhere. Various other methods of mechanically roughening the surface of the stainless steel, such as sanding or filing, were tried but acid-etching proved the simplest and most effective.

Various methods of producing the requisite pres-

ures between diaphragm and stack and diaphragm and housing are shown in Figure 12. Of these methods, that shown in Figure 12D proved the simplest for securing a reliable bond between the molded rubber face and the stainless steel. The following detailed description of the procedure is given to illustrate the general method of Cycle-Welding rubber to metal, a process that was used in all subsequent scanning sonar transducers built at HUSL.

The rubber face is first "cyclized." Those portions of the rubber that are not to be treated are coated with petroleum jelly, and the face is immersed for 5 min. in concentrated sulphuric acid. This produces a hard surface layer, which then is thoroughly broken up by bending and stretching the rubber. Cycle-Weld 55-6 is then brushed onto the cyclized surface and allowed to dry for at least 12 hr. To speed up the operation, the brushed surface may be allowed to air dry for 30 min. and then placed in an oven for an equal time at a temperature of 180 F.

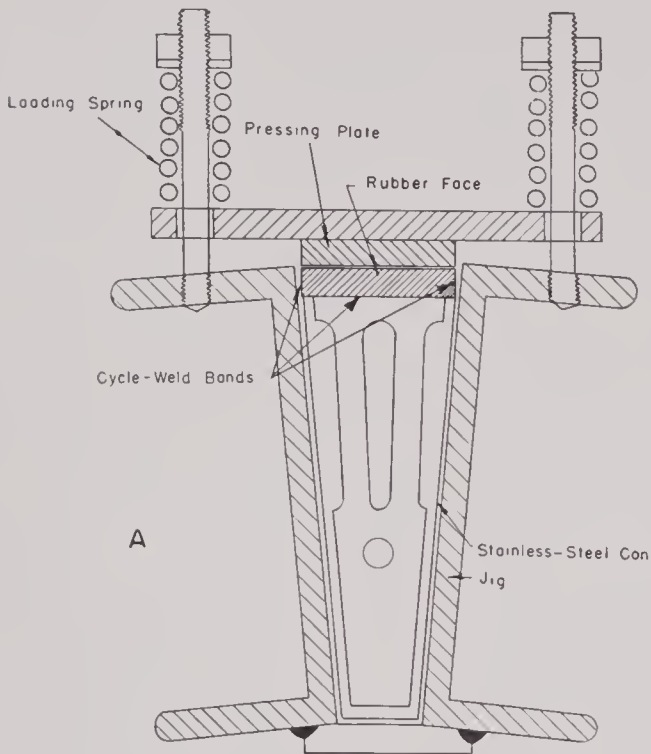
A heavy metal jig is used for cementing the rubber to the stack face. The particular form of jig used depends upon the contours to which the rubber is to be cemented. That for the HP-2 elements is shown in Figure 12. The assembled unit is placed in the jig and the rubber face fitted into position, with the exposed rubber surface dusted with talcum and covered with thin paper to prevent the rubber from sticking to the pressure plate of the jig. The closely fitting wood strip (12D) is laid on the rubber face and the cover plate is screwed into position. A thermocouple is placed between the rubber face and the wood strip so that the face temperature can be measured.

Six or eight of the assembled jigs, each with an air pressure line attached, are placed in a thermostatically controlled oven. An air pressure of 45 lb per sq in. is applied to give the needed pressure between the rubber and the sides of the container, and the oven is heated to a temperature (usually 350 F) that will yield a stack temperature of 300 F. This condition of temperature and pressure is maintained for a period of 20 min.

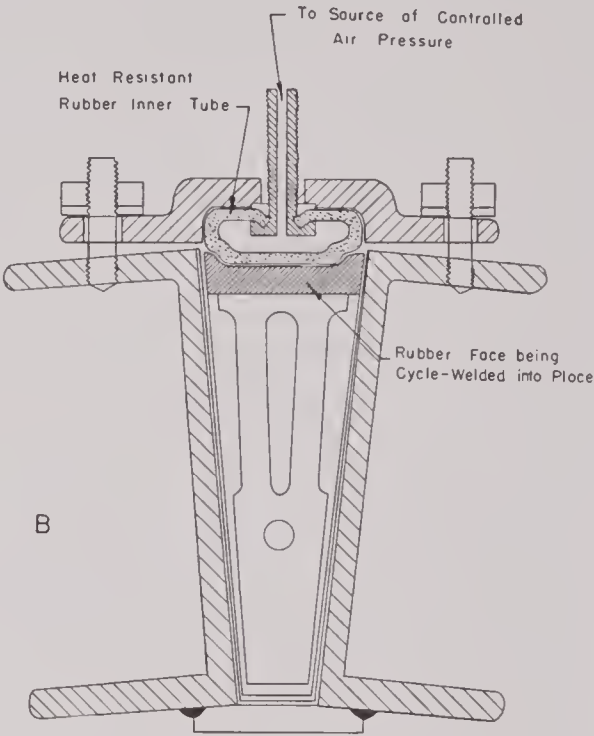
The procedure just described was the most involved of any of the Cycle-Welding processes used in the production of scanning sonar transducers. It was complicated by the necessity of applying vertical and lateral pressures simultaneously during the curing of the Cycle-Weld.

The other methods that were tried are indicated in Figure 12. That indicated in 12C was fairly successful. The inner tubes of 12B were apt to blow out.

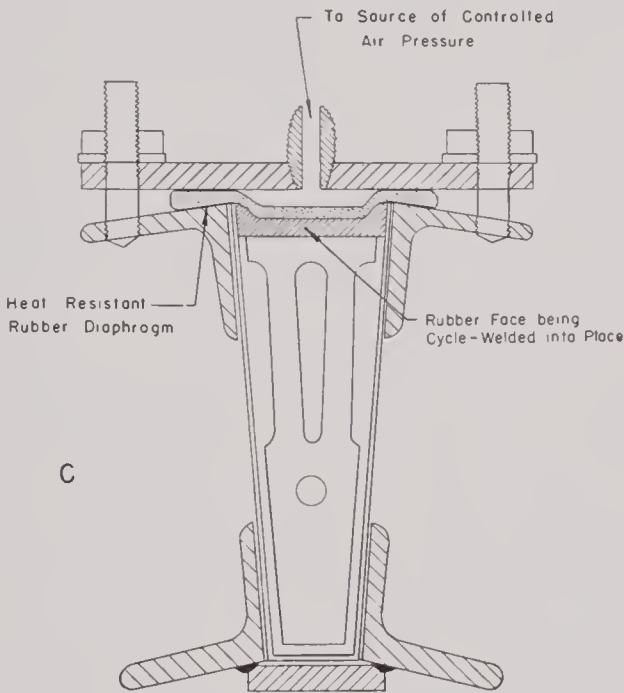
CONFIDENTIAL



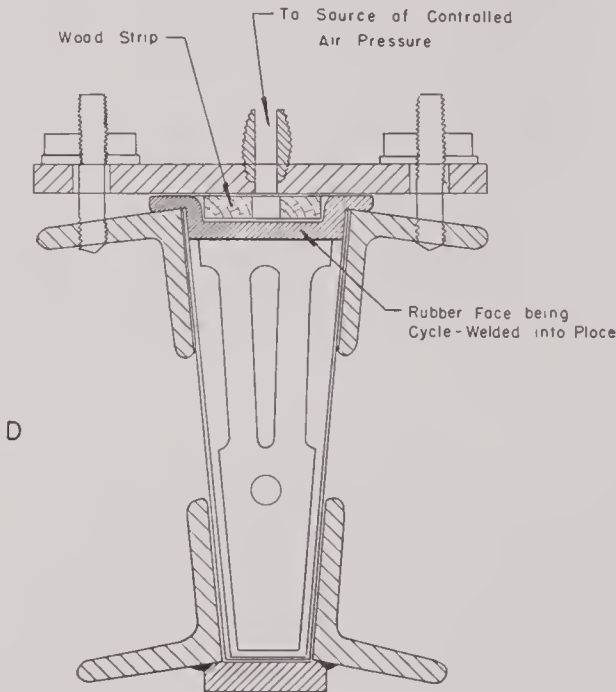
CYCLE-WELDING of FACES in CANS,
MECHANICAL PRESS METHOD



CYCLE-WELDING of FACES in CANS,
RUBBER INNER TUBE METHOD



CYCLE-WELDING of RUBBER FACES,
RUBBER PRESSURE DIAPHRAGM METHOD



CYCLE-WELDING of RUBBER FACES,
DIRECT AIR PRESSURE ON SPECIAL FACES

FIGURE 12. Jigs for Cycle-Welding HP-2 element.

Many elements were "canned" by one or other of the methods described. Some of them showed apparently perfect adhesion of the rubber to the stainless steel after a period of more than 18 months. Nevertheless, the uncertainty of a permanent bond with Cycle-Weld thermosetting resin makes this method one that cannot be recommended, much as separately housed elements are to be desired.

11.3.3 Elements Housed in a Rubber Boot

The magnetostrictive elements of HP-2 were salvaged and incorporated in the form shown in Figure 15 of Chapter 13, designated as HP-2B. They were mounted on a cylindrical spool and the whole assembly enclosed in a molded rubber boot $\frac{1}{2}$ in. thick. To secure acoustic contact between the elements and the water, the entire transducer was evacuated and filled with outgassed castor oil, using the method and apparatus shown later in Figure 20. This transducer proved seaworthy and was installed on the USS *Cythera*, where it served a useful purpose in the scanning sonar experimental program. All subsequent models were housed in the same general fashion, differing only in details of the means of securing acoustic contact with the water.

11.3.4 Transducers with PM Polarization

The elements of the transducers described in the preceding sections each comprised a single continuous stack of laminations held in place by tie rods passing through the entire length of the stacks and attached to the flanges of the supporting spool by screws engaging the end caps. All were polarized by a d-c component of the current through the windings.

This construction was not possible with elements polarized by sintered-oxide magnets. The sintered oxide itself is fragile, and since it is carried loosely in slots in the laminations, the use of elements consisting of two or more short stacks is definitely indicated. The HP-3 transducer is typical and its assembly will be given in detail. Each element contains four wound stacks, each with a sintered-oxide magnet and end caps. The steps in the assembly of the four stacks into an element are clearly indicated in Figure 13.

The rubber face strip is cyclized and coated with 55-6 Cycle-Weld. The fronts of the stacks are also

given a coat of the same material and both are allowed to dry.

The sintered-oxide magnet plates are removed from the stacks, each one marked with the serial number of the stack from which it was taken. The four stacks are fitted together as shown at *B* of Figure 13, a tie frame made of two plates and two tie rods being used to hold them in place while the rubber face is fitted into position. The element is then placed face down in the curing jig as shown at *C*. The assembly frame is removed and replaced by another adjusted to hold the element to its proper length. The top plate of the jig is screwed down, compressing the springs to give the desired pressure of 45 lb per sq in. A thermocouple is placed at the center of the element near the face. The curing process is the same as that described in the case of the HP-2B.

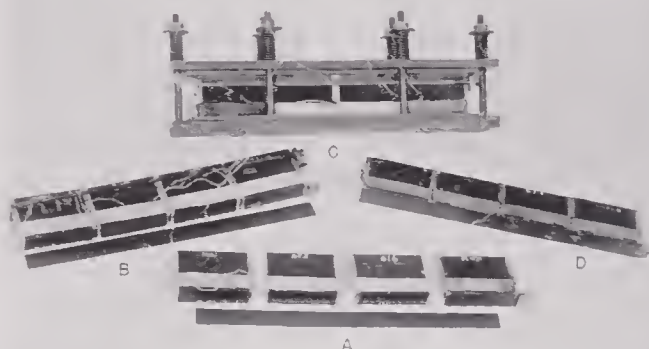


FIGURE 13. Illustration of HP-3 element assembly.

After the element has cooled, the magnets are replaced, each in its proper stack. The element is strengthened by a thin strip of aluminum faced with $\frac{1}{16}$ -in. air-cell neoprene fastened to the back by screws which pass into the end caps. The magnets are repolarized in place in the stacks, by placing the element in the field of a powerful electromagnet.

This procedure completes the assembly of the element except for electric connection of the elements and adjustment of the magnetization.

11.4 ASSEMBLY OF A TRANSDUCER

11.4.1 Selection of Elements

Individual elements in the cylindrical array are selected and arranged with a view to obtaining the minimum difference in resonant frequency between adjacent elements. The procedure followed in the case of the HP-3 is illustrative of the method fol-

lowed generally in building scanning sonar transducers.

The frequencies of maximum conductance of the individual stacks of each element were averaged. The elements were then chosen in the order of these averages. They were arranged in the transducer so that the elements with the lowest and highest averaged frequencies were diametrically opposite, with the intervening elements placed in the order of their averaged frequencies, as shown in Figure 14. The outer number identifies the selected stack and the inner one gives the deviation in its measured frequency from 27,000 c.

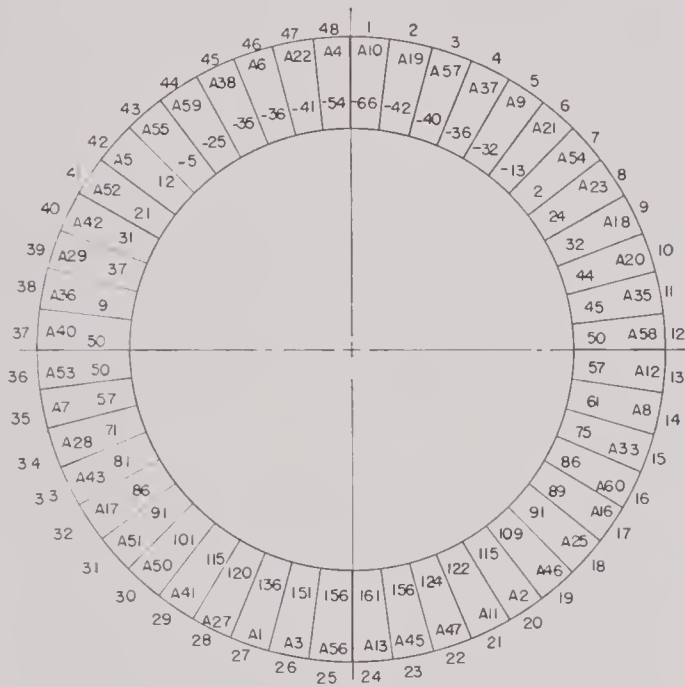


FIGURE 14. Stack arrangement of 48-element transducer.

This method of arranging the elements leaves something to be desired, since it is quite probable that handling of the individual stacks in assembling them into elements may materially change their resonant frequencies. Precise determination of the frequency of maximum conductance of the assembled elements would furnish a better criterion for arranging them in the assembled transducer. This would, however, involve another set of measurements and it is doubtful whether the possible improvement in receiving pattern that might result would warrant the expenditure of time required to make them.

Elements were so oriented that the magnetic polarities of the sintered-oxide plates were opposed in adjacent elements, a North pole being placed next to another North, and so on.

TABLE 1. Data of Figure 14*.

Position	Stack no.	Segment no. 1 freq.	Segment no. 2 freq.	Segment no. 3 freq.	Segment no. 4 freq.	Average freq.
1	A10	741 -55	456 -95	458 -45	731 -70	-66
2	A19	767 -60	492 -60	522 -35	751 -15	-42
3	A57	773 -40	332 -20	534 -50	771 -30	-40
4	A37	807 -55	552 -20	528 -25	799 -45	-36
5	A9	763 -35	470 -30	472 -40	689 -25	-32
6	A21	727 -10	518 0	504 0	769 -40	-13
7	A54	855 -15	538 5	546 20	841 -20	2
8	A23	725 20	524 25	410 25	779 25	24
9	A18	663 35	494 30	498 40	655 25	32
10	A20	703 60	516 35	490 30	693 50	44
39	A29	709 35	512 15	484 65	787 35	37
40	A42	305 10	582 50	126 40	299 25	31
41	A52	671 15	530 10	536 25	509 35	21
42	A5	587 0	462 25	468 25	591 0	12
43	A55	717 -10	228 -15	324 0	765 5	-5
44	A59	691 -30	482 -35	526 -5	729 -30	-25
45	A38	825 -50	564 -45	94 -15	859 -30	-35
46	A6	291 -55	230 -30	354 -30	297 -30	-36
47	A22	707 -30	486 -35	488 -65	747 -35	-41
48	A4	555 -40	406 -80	464 -55	753 -40	-54

*If complete data are desired see reference 56.

11.1.2 Assembly on the Spool

The spool for the HP-3 is shown in Figure 15. An annular disk is welded inside the spool 4 in. from the bottom end. The disk is used for the cable water seal into the junction box at the lower end of the transducer. The bottom end of the spool contains the water seals for the sets of three wires which lead to each of the elements. The top end is machined to take a standard QC flange for support of the transducer.

The cylindrical portion of the spool is covered with

a piece of $\frac{1}{8}$ -in. corprene and a piece of $\frac{1}{8}$ -in. Cell-Tite neoprene cemented into place with Vulcalock. The corprene provides a firm backing for the elements and the neoprene is sufficiently soft so that the elements can be fitted accurately into place. Rings of $\frac{1}{8}$ -in. corprene were cemented to the inner faces of the spool ends.

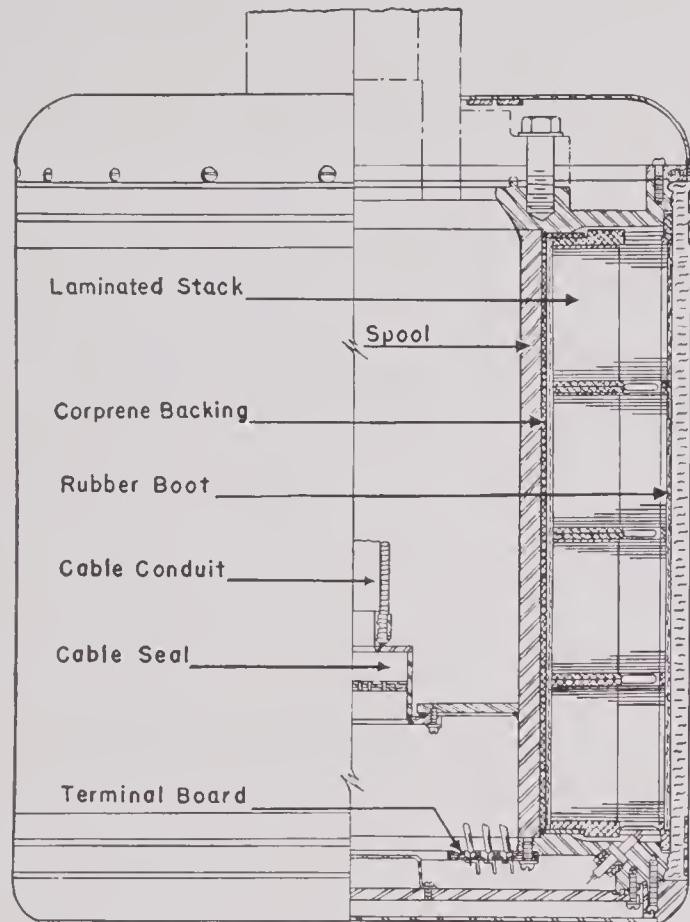


FIGURE 15. Spool of HP-3 transducer.

Holes for the element-retaining screws were drilled into the top and bottom ends of the spool while they were being machined. A piece of steel strap was cut so that it fitted into the spool in place of an element. This strap was drilled carefully to match the holes in the ends of the spool so that the strap could be used as a templet in drilling the holes in the ends of the element supports. After being drilled and counter-sunk, the elements were pressed into place and the leads drawn through the holes in the bottom plate. The retaining screws were then put in and the element fastened. Pieces of $\frac{1}{16}$ -in. corprene were placed between the elements to cushion them and provide pressure-release material should it become necessary to fill the transducers with castor oil.

The three leads for each element were brought into the junction box space at the bottom of the trans-

ducer through molded rubber pieces. Sealing was accomplished by screwing a hollow plug down on top of the rubber pieces. This expanded the rubber and sealed the hole from the element chamber to the junction box. This method of sealing was not very satisfactory. There was a strong tendency for the rubber pieces to twist as the seals were screwed into place, causing a short circuit in the element chamber. In the HP-2, the water seals were forced into place by machine screws and there was no tendency for the lead wires to twist. The use of this type of press-in seal, when possible, is recommended instead of the screw-in seals.



FIGURE 16. HP-3 transducer before application of rubber boot.

The diameter of the rubber boot for the HP-3 was 12 per cent smaller than the outside diameter of the element circle. Both the faces of the elements and the inside of the boot were given repeated coats of castor

oil beginning several days before the boot was to be applied. Finally one end of the boot was clamped to a circular piece of iron strap and stretched to a diameter greater than that of the element circle. After a rush coat of castor oil, the boot was pulled down over the transducer. Figure 16 shows the assembled transducer ready for the application of the boot.

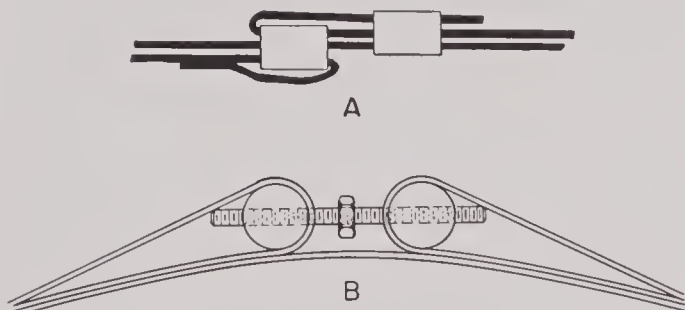


FIGURE 17. Clamping devices for rubber boot.

preferable to any of the commercial devices tried, particularly those in which the fastening was accomplished by making a punch mark in the buckle to hold the strap. Punch locking failed repeatedly and was definitely unsatisfactory.

Another type of clamping band illustrated in Figure 17B offers the advantage that it can be tightened from time to time. It is not entirely evident that this is necessary, however. Its greatest disadvantage is that the buckles are large and project so far beyond the body of the transducer that there is danger of displacing the straps in handling.

11.1.3 Cable Connections

The cable for the HP-3 required 147 conductors. Commercial cable was not immediately available and resort to a homemade cable was necessary. Forty-nine triplets were twisted first, from which seven

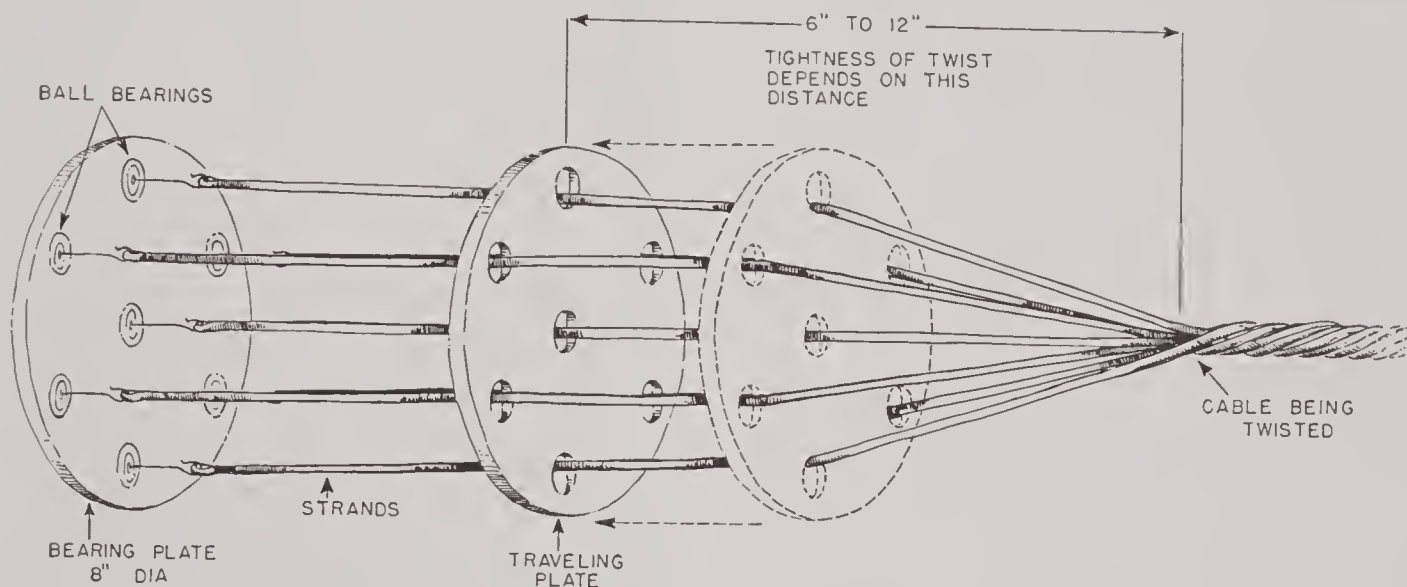


FIGURE 18. Device for twisting cable.

The methods of clamping the rubber to the end plates are shown in Figure 17. In the first method, shown in A, a stainless-steel strap wrapped twice around the transducer was threaded through two buckles, one of which was free to slide along the strap. A number of methods were tried for tightening the strap. A simple screw clamp was finally devised with which the strap could be pulled against the end buckle. When adequate tension was secured, the clamp was folded away from the transducer and the strap snubbed over the buckle. The free end was then tucked through the sliding buckle, which was tapped into place next to the end buckle. The excess strap was then removed. This method of fastening proved

strands containing seven triplets each were made. The seven strands were then twisted into a single cable.

The making of multistrand cables in lengths of 50 ft or less for experimental and emergency use proved quite feasible. When two or more wires are twisted together, each wire must be free to twist on its own axis. The simple device for permitting this is shown in Figure 18. The ball bearings permit the wire to twist freely even when under considerable tension. The procedure for making the 147-conductor cable was as follows.

Three wires of equal lengths were fastened in the hooks projecting from the bearing plate, passed

through holes in the following plate, and the free ends fastened to a hook in an ordinary hand drill. As the hand drill was operated, the following plate was carried back toward the bearing plate. The tightness of twist was controlled by adjusting the rate of movement of the bearing plate to the rate of twisting. Care was taken to see that the untwisted wires between the two plates were free to turn each about its own axis during the twisting. After seven triplets had been twisted, they were attached to the bearing plate and twisted in the opposite direction to the twist given the triplets. The cable was completed by twist-

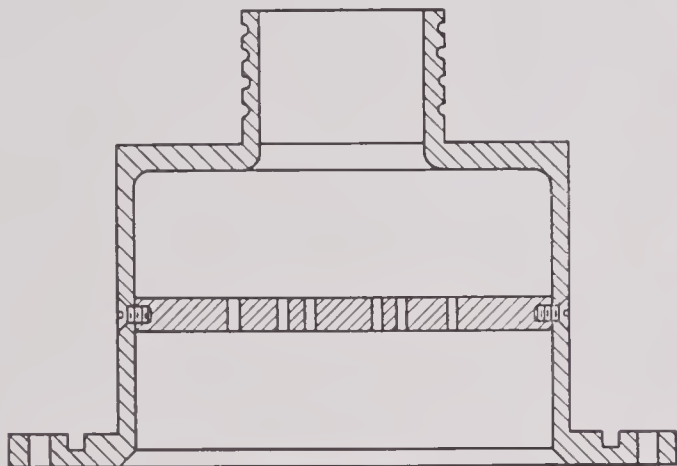


FIGURE 19. Water seal of cable to junction box.

ing the seven strands together, again reversing the direction of twist so that the final direction was the same as the original twist given the triplets. The assembled cable was so heavy that several people were required to support it to maintain a reasonably uniform tension in the seven strands during the final twisting, which had to be done by hand by the person working next to the follower plate. When completed, it was bound with adhesive tape at intervals of 3 ft and encased in fabric-coated fire hose.

All the triplets in any one strand were color-coded so that any triplet could be selected and any wire of that triplet identified. All seven strands were identical in color codes but a string tracer was twisted in one of the strands. In the completed cable this strand was one of the outside six. It was thus possible to select any strand, any triplet, and any wire at any point in the cable.

The water seal admitting the cable to the transducer junction box is shown in Figure 19. Each conductor was passed through a hole in a bakelite plate. This plate was held by screws in a potlike container which was heated and filled with Rubberseal compound No. 2. This container was then screwed into

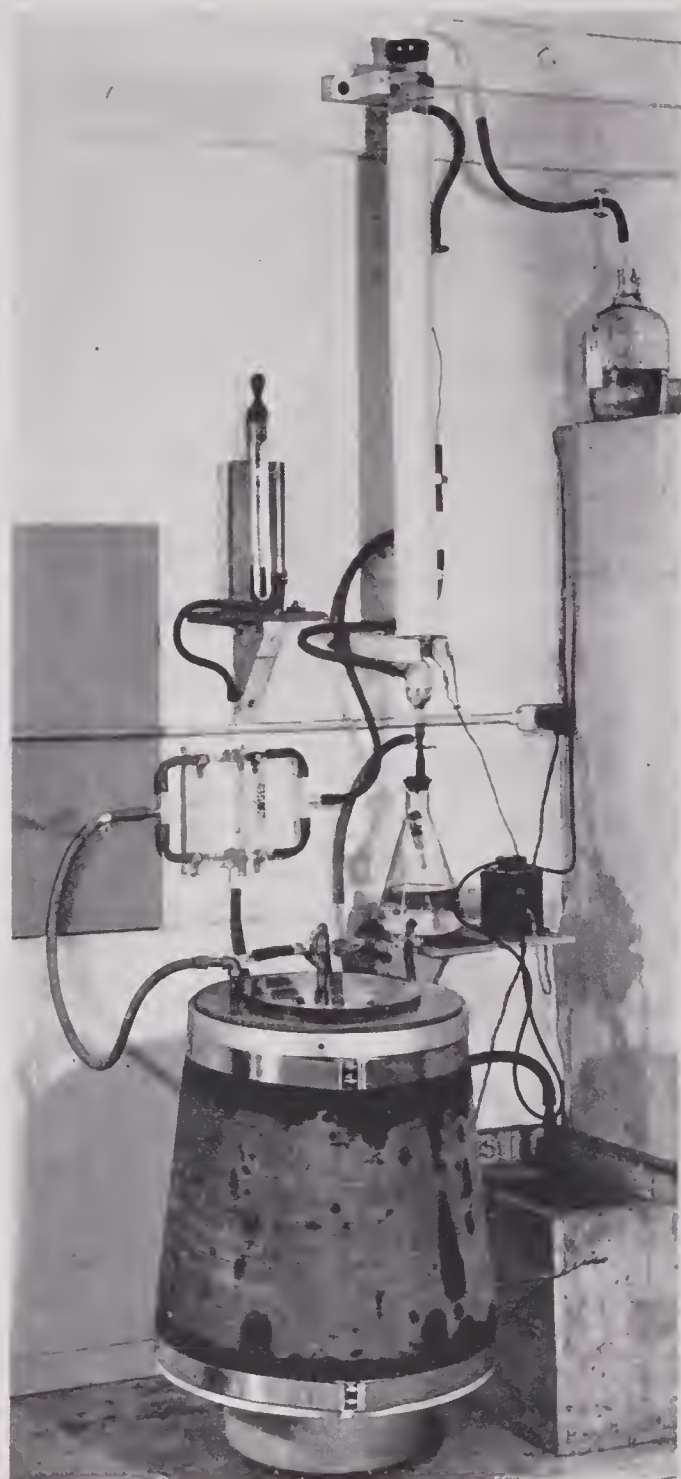


FIGURE 20. Apparatus for castor-oil filling.

place on the annular plate inside the spool cylinder. A rubber ring gasket between the container and the ring completed the water sealing of the transducer junction box.

11.1.1 Filling with Castor Oil

The technique of filling a transducer with castor oil is well illustrated in the assembly of the HP-3S transducer.

At first it was believed necessary to fill this transducer with castor oil, since its conical shape might cause poor acoustic contact between the rubber boot and the faces of the elements. The procedure followed will serve to demonstrate the precautions that

making the connection to the oil lead. The transducer was tipped slightly so that this seal was lower than the others to prevent entrapment of air released in the last stages of the process. Procedure was as follows.

1. The entire apparatus, including the transducer, was evacuated to a pressure of 1 mm of mercury or less.

2. Heating current was applied to the coil of resistance wire on the column. The temperature of the column was raised to approximately 50 C.

3. The oil lead to the transducer was closed and the hose to the oil reservoir was opened slightly so that oil entered the top of the column slowly. A great amount of gas dissolved in the oil came out as it entered the top of the column. The rate of admission of oil was determined mostly by the amount of foaming. The oil descended the column over a loose packing of stirrup-shaped pieces cut from rubber tubing.

4. When the pressure flask below the column was filled, the pinchcock between it and the column was closed. The vacuum lead to the flask was then closed and the oil lead to the transducer opened. Air was then admitted to the top of the flask and the oil entered the transducer partly by gravity but mostly by atmospheric pressure.

5. When the flask was nearly empty, the oil lead to the transducer was closed and the flask was evacuated and reopened to the column. A large transducer such as this requires several gallons of oil and about 3 hours to fill.

6. When oil appeared in all water-seal holes, the process was stopped and air admitted to the transducer. This had to be done slowly with an extra supply of outgassed oil on hand, since as the air entered the boot expanded, calling for an additional quantity of oil. It was necessary during this last stage to be able to see what was going on inside the transducer, hence the glass plate.

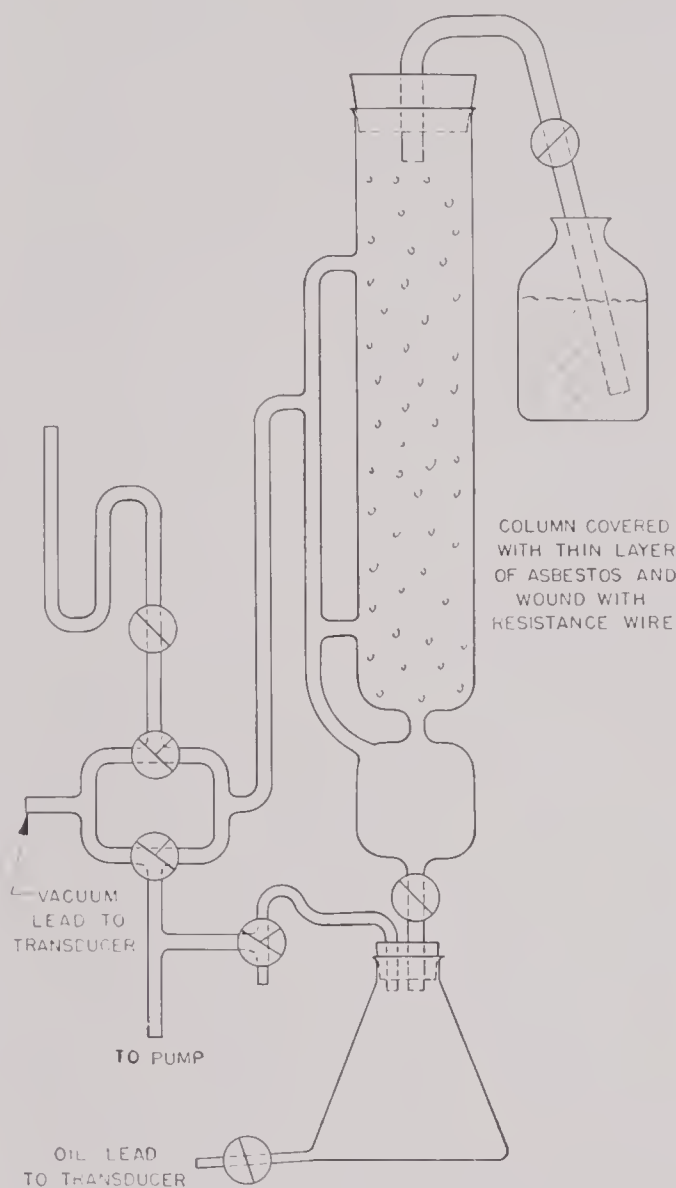


FIGURE 21. Schematic of oil-filling apparatus.

should be taken in cases where oil filling is necessary.

The apparatus is shown in Figure 20 and illustrated schematically in Figure 21. An annular plate of metal rested on the gaskets at the top of the transducer. In the top of the plate was a groove for another gasket, on which rested a thick disk of plate glass. Two pieces of pipe were screwed in the ring. One of these was used for exhausting the entire transducer by means of a Megavac pump. The other was used for admitting castor oil. During the filling process all water seals were left open except one, which was used for

14.5

TESTING SCANNING TRANSDUCERS

14.5.1

Purpose

The complete study of the behavior of a multielement transducer calls for a large number of acoustical measurements on the completed instrument. Such a study is desirable on transducers of this type during the experimental stage. Although a small number of

response and pattern measurements will serve to show whether the overall performance is as expected, an extensive program of tests covering the full range of operational requirements is needed to detect and diagnose minor failures and to supply information for possible improvement.

11.5.2 Tests of HP-3 No. 1

As an illustration of these tests, measurements made on the HP-3 No. 1 will be presented with an analysis of their significance. The HP-3 No. 1 is a 48-element transducer resonating at 26.2 kc. Each element is composed of four stacks so connected that the two center stacks may be used alone for a broad vertical beam (called the 0:1:1:0 connection) or the two center stacks may be used in series with the outside stacks in parallel (called the 1:2:2:1 connection) to give amplitude shading.

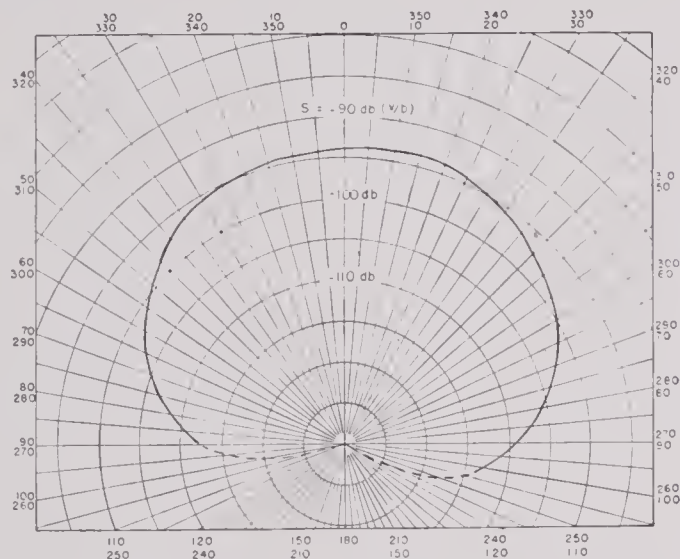


FIGURE 22. Receiving pattern of single element of HP-3 in horizontal plane.

TESTS WITH TRANSDUCER MOUNTED VERTICALLY, MEASUREMENTS WITH 0:1:1:0

The receiving responses of all 48 elements were taken. The frequencies of maximum response ranged from 25.8 to 26.2. The width of the response peak 3 db below the maximum was (with a single exception) between 2.9 and 3.4 kc. The Q 's lay between 7.4 and 9.0, with an average of 8. (One element showed a Q of 12.4, indicating poor acoustic contact with the rubber boot.) The open circuit sensitivities ranged from -91.1 to -89.1 db, with an average of about -90.1 db vs 1 volt per dyne per sq cm.

A sample receiving pattern of a single element in

TABLE 2. HP-3 No. 1 Transducer with a 0:1:1:0* Connection.

Element	Res. frequency	Width 3-db down	Q .	Sensitivity
1	26 kc	3.2 kc	8.1	-89.6
2	25.8	3.3	7.8	-89.5
3	26	3.2	8.1	-90.4
4	26.1	3.4	7.65	-90.7
5	26	3	8.7	-89.6
6	26	3.3	7.9	-89.4
7	26	2.9	9	-90.4
8	26	2.9	9	-90.1
9	26	3.4	7.65	-90.7
10	26	3.3	7.9	-89.6
39	26	3.4	7.65	-89.8
40	26	3.2	8.1	-90.6
41	26	3.3	7.9	-90.7
42	26	3.4	7.65	-89.8
43	26	3.2	8.1	-90.6
44	26	3.3	7.9	-90
45	26	3.5	7.4	-89.8
46	26	3	8.7	-90
47	26	3.2	8.1	-89.3
48	26	2.9	9	-89.2

*If complete data are desired, see reference 56.

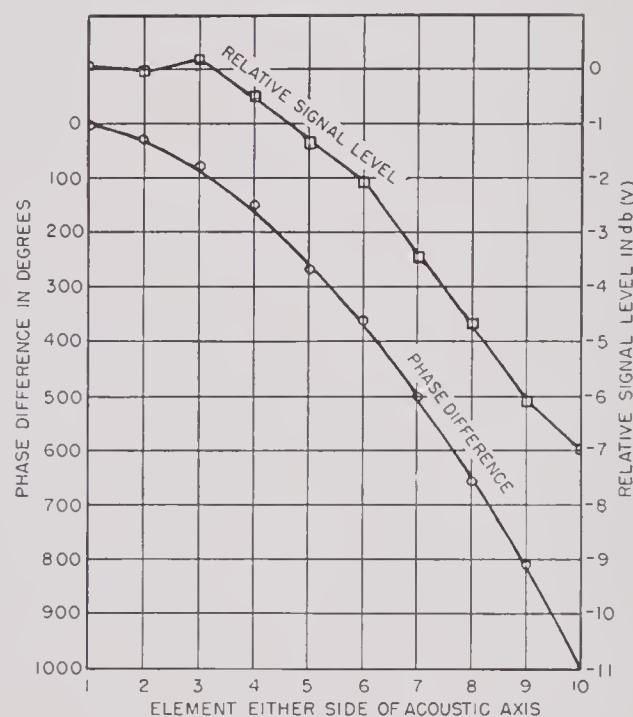


FIGURE 23. Pressure and phase differences at different elements of HP-3 transducer, referred to values at element on which incidence of plane wave was normal to the surface.

the horizontal plane is shown in Figure 22. All the patterns taken were nearly identical with this one.

The results of the phase-pattern measurements and pressure-pattern measurements are given in Figure 23. The agreement between the pressure pattern of a single element of Figure 22 and the pressures

shown in Figure 23 is within the experimental error of the measurements. The phase pattern is about normal. The observed phase differences between elements are about 1 to 2 per cent higher than those predicted by assuming that the path differences are proportional to 1 minus the cosine of the angle of incidence and that the velocity of sound is 57,000 in. per sec.

The pattern at 26 kc shows a variation of ± 1 db, that at 24 kc ± 2 db, and that at 28 kc ± 2 db. The pattern at 26 kc is quite satisfactory, while those at 24 kc and 28 kc are only fair.

Admittance measurements were made with the transducer in water at the Charles River barge. The values of the admittance components for single elements at 20 kc and 26 kc are shown in Figures 26

TABLE 3. Pressure pattern measurements on HP-3 No. 1 Transducer measured at 26 kc, sound source 16.3 ft distant. (The 0:1:1:0 connection.)

Acoustic axis centered on elements	Branch	Relative Element Number									
		1	2	3	4	5	6	7	8	9	10
48-1	<i>R</i>	0	0.1	-0.6	-1.0	-0.6	-2.5	-4.3	-4.3	-7.0	-7.2
	<i>L</i>	0	0.1	-0.5	-0.9	-1.9	-3.3	-4.0	-6.3	-7.4	-7.8
18-19	<i>R</i>	0	-0.3	1.1	0.5	-1	-0.8	-2.8	-3.5	-4.9	-5.9
	<i>L</i>	0.0	0.1	-2	0	-1	-1.2	-3.3	-3.8	-5.4	-6.8
32-33	<i>R</i>	0.2	0.5	0	-0.7	-2.3	-2.3	-3.2	-5.1	-6.4	-6.7
	<i>L</i>	0	-0.5	1	-0.5	-1	-2.2	-3	-5	-5.2	-7
Sum		0.2	0	+1.2	-2.6	-7.8	-12.3	-20.6	-28.0	-36.3	-41.4
Average		+0.06	0	+0.2	-0.43	-1.3	-2.05	-3.4	-4.65	-6.05	-6.9

TABLE 4. Phase pattern measurements on HP-3 No. 1 Transducer measured at 26 kc, sound source 16.3 ft distant. All readings corrected for sphericity of wave front. (The 0:1:1:0 connection.)

Acoustic axis centered on elements	Branch	Relative Element Number									
		1	2	3	4	5	6	7	8	9	10
48-1	<i>R</i>	2	21	66	150	220	342	487	623	791	956
	<i>L</i>	0	29	87	173	259	379	525	673	841	1012
18-19	<i>R</i>	0	17	72	148	216.5	342.5	482	620	790	966
	<i>L</i>	0	27	93	181	279	398	548	678	869	1044
32-33	<i>R</i>	0	28	86	172	258	383.5	528	679	844	1021
	<i>L</i>	0	19.5	72	146	226	354	496	638	817	981
Sum		2	141.5	476	970	1458.5	2199	3066	3911	4952	5980
Average		0.3	24.5	88	158	265	366	510	653	826	996
Theor. value ($1 - \cos \theta$)		3	27.8	77	149	244	360	494	644	809	984

$$\frac{360 R}{\lambda}(1 - \cos \theta); R = 8.75 \text{ in.}; \lambda \text{ at } 26.2 \text{ kc} = \frac{57,000}{26,220} = 2.17 \text{ in.}$$

The open-circuit frequency response of all the elements in parallel is shown in Figure 24. During this measurement there was an unusually high noise level due to electric pickup. However, the portions of the response near the frequencies of resonance rose well above the noise background. The sensitivity at 26 kc is about -112 db and that at 52.5 kc is about -123 db referred to 1 volt per dyne per sq cm. The *Q*'s for the 26-kc and the 52.5-kc resonances are 9.3 and 33 respectively.

The patterns at 24, 26, and 28 kc with all the elements connected in parallel are shown in Figure 25.

and 27. The conductances and susceptances are plotted against the element numbers in Figure 26 and the same values are shown in Figure 27 with the *B*'s (susceptances) plotted against the *G*'s (conductances). The latter diagram shows that at 26 kc the admittance angles varied over a range of 6.5 degrees and the admittances had a variation of ± 5 per cent. These variations are somewhat greater than desired, but satisfactory performance of the transducer in a trial installation has shown that tolerances as great as these are allowable.

The transmitting response at 16.3 ft with all the

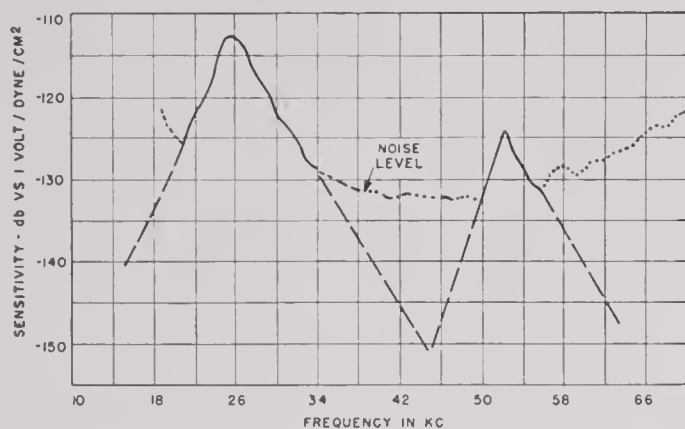


FIGURE 24. Receiving response of HP-3 No. 1, all elements in parallel.

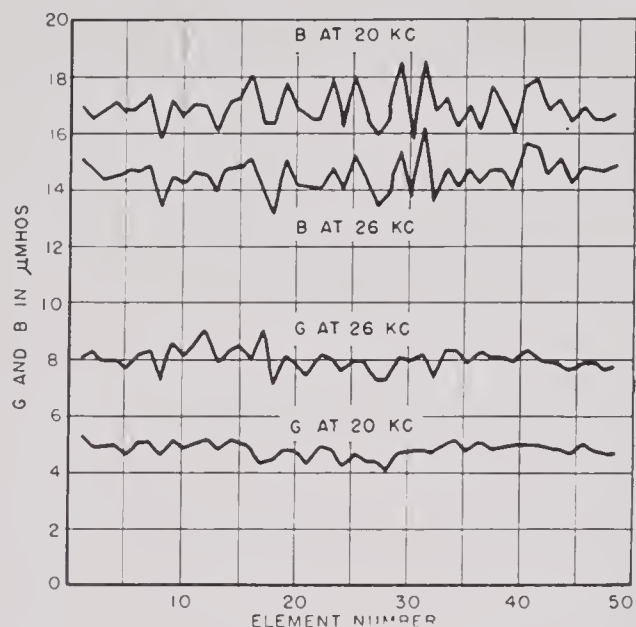


FIGURE 26. Admittance of single elements of HP-3 No. 1 at 20 kc and 26 kc, plotted against element numbers.

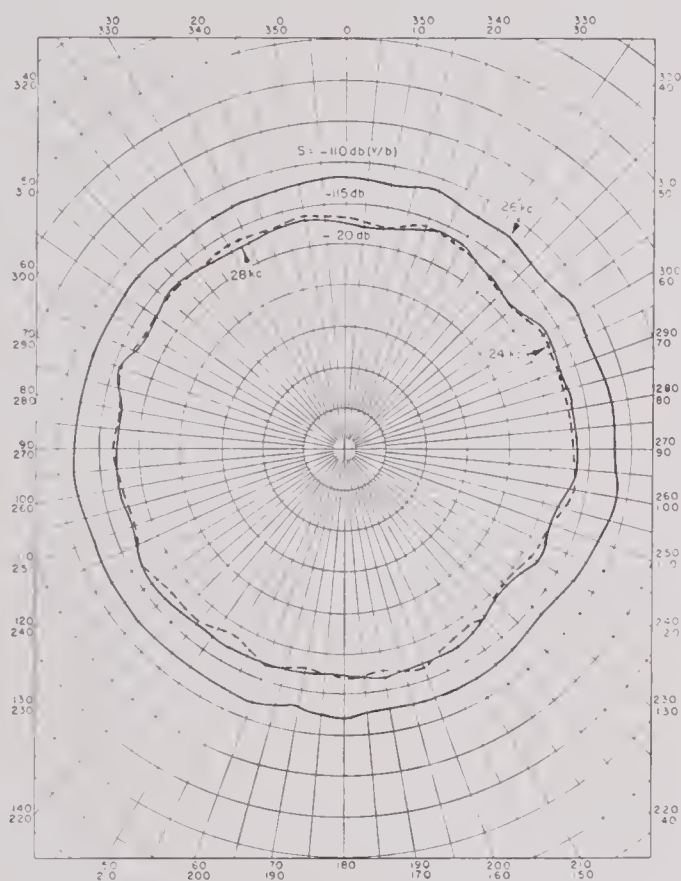


FIGURE 25. Horizontal patterns of HP-3 No. 1, all elements in parallel.

elements connected in parallel and driven at a constant voltage of 1 volt is shown in Figure 28. The peak responses under these conditions are 52 db at 26.4 kc and 44.5 db vs 1 dyne per sq cm at 52.3 kc. The Q 's for these resonances are approximately 10 and 22.7 respectively.

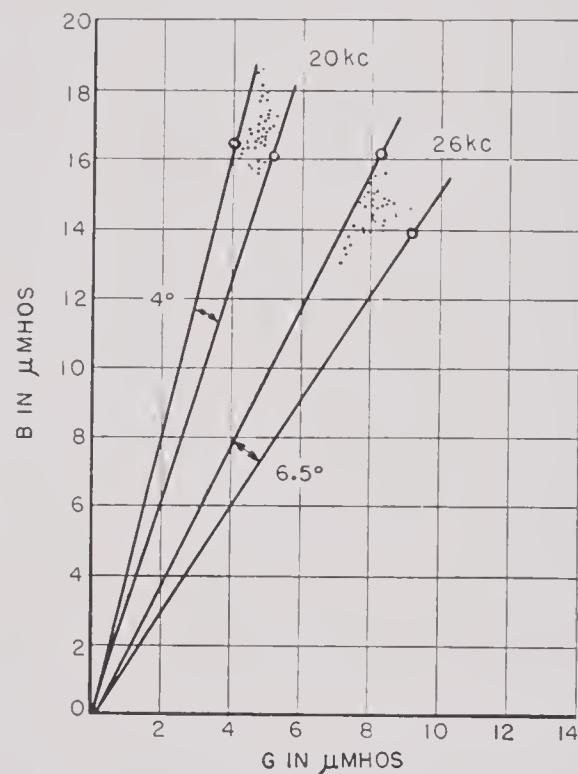


FIGURE 27. Spread in admittances of single elements of HP-3 No. 1 at 20 kc and 26 kc.

TESTS WITH THE TRANSDUCER MOUNTED HORIZONTALLY, WITH 0:1:1:0 CONNECTION

Vertical receiving patterns for single elements at 26 kc, 24 kc, and 28 kc are shown in Figures 29A, B, and C respectively. These patterns are about as they should be according to theory.

The patterns at 26 kc, with all elements connected in parallel, are shown in Figure 30. The side lobes on these patterns are higher than predicted by the theory for a line source. This shows clearly that the side lobes are higher for a large cylindrical source than they are for a line source of the same length.

DIRECTIVITY INDEX AND EFFICIENCY

From receiving and transmitting response data, the measured impedance, and a knowledge of the directivity index, estimates of the efficiency of the transducer may be made. A single element may be regarded as a rectangular source whose length is large compared with the wave length of the radiated sound. The directivity index D may be determined by the method given in Chapter 5 (see Figure 29 of Chap-

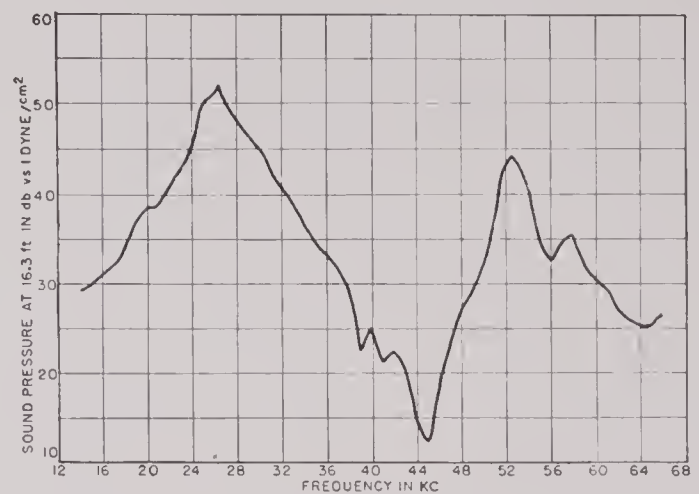


FIGURE 28. Transmitting response of HP-2 No. 1, all elements in parallel.

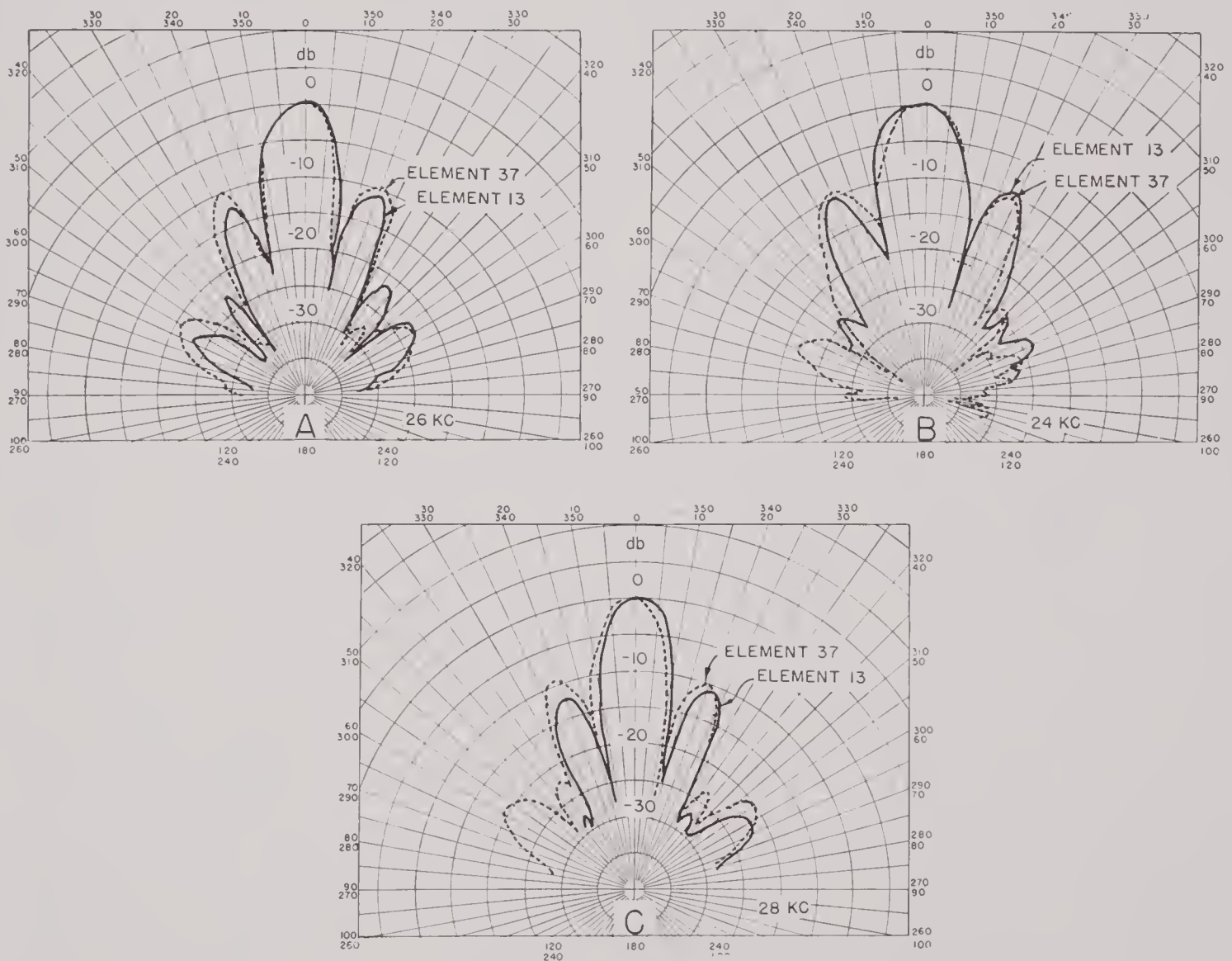


FIGURE 29. Vertical patterns of two single elements at 24, 26, and 28 kc.

CONFIDENTIAL

ter 5). At 26 kc, the effective radiating width w of a single element as indicated by the horizontal pattern (Figure 22) is 3.8 cm, and the effective length as given by the main lobe width of the vertical pattern is 22 cm. The wave length at 26 kc is 5.5 cm. From this, $2\pi w/\lambda = 4.3$ and $l/\lambda = 4.1$. From the graph of Figure 29 of Chapter 5, $l/\lambda D = 0.092$, $D = 0.023$, and $10 \log D = -16.4$.

To calculate the efficiency from equation (25a) of Chapter 1, the following values are used.

$$\text{Sensitivity} = -90 \text{ db ref. 1 volt/dyne/cm}^2$$

$$Z_i = 29 + j53, |Z| = 60.4 \text{ ohms.}$$

$$\begin{aligned} \text{Eff (decibels)} &= -90 - 20 \log 5.5 - 16.4 - \\ &\quad 10 \log 29 + 127 \\ &= -8.8 \text{ db} = 0.13. \end{aligned}$$

The efficiency from the transmitting response is computed from equation (20) of Chapter 1, using the following values for the measured quantities:

$$r = 4.96 \text{ meters;}$$

$$20 \log p' = 41.5;$$

$$E = 1 \text{ volt;}$$

$$20 \log |Z_i| = 35.6;$$

$$10 \log D = -16.4;$$

$$10 \log R_i = 14.6$$

$$\begin{aligned} \text{Eff (decibels)} &= 14 + 41.5 + 35.2 - 16.4 - \\ &\quad 14.6 - 70.9 \\ &= -10.8 \text{ db} = 0.084 \end{aligned}$$

From similar data for the transducer with all 48 elements connected in parallel, an efficiency of 0.18 was computed from the sensitivity and 0.11 from the transmitting response.

In addition to these tests, receiving patterns were taken through the lag line and commutator of the CR scanning sonar to show how the transducer would actually operate in scanning sonar use. Such a pattern is shown in Figure 31.

14.6 SCANNING TRANSDUCERS BUILT AT HUSL

14.6.1 Early Models

While the techniques just described were being developed, the HP series of scanning transducers was being built. The HP-1 and HP-2 are described in *Scanning Sonar*.⁵⁸ The HP-3 has just been described in illustrating the testing and assembly procedures.⁵⁸ There remain for brief treatment the HP-3 and HP-3DS modifications.^{53a}

14.6.2

HP-3S

The HP-3S was built for use with a pro-submarine system. It differs from the HP-3 primarily in that the elements are mounted on a portion of a cone having a vertex angle of 12 degrees. This feature was designed to compensate in part at least for the refractive effect of temperature gradient, which on the average tends to bend the sound pattern downward.

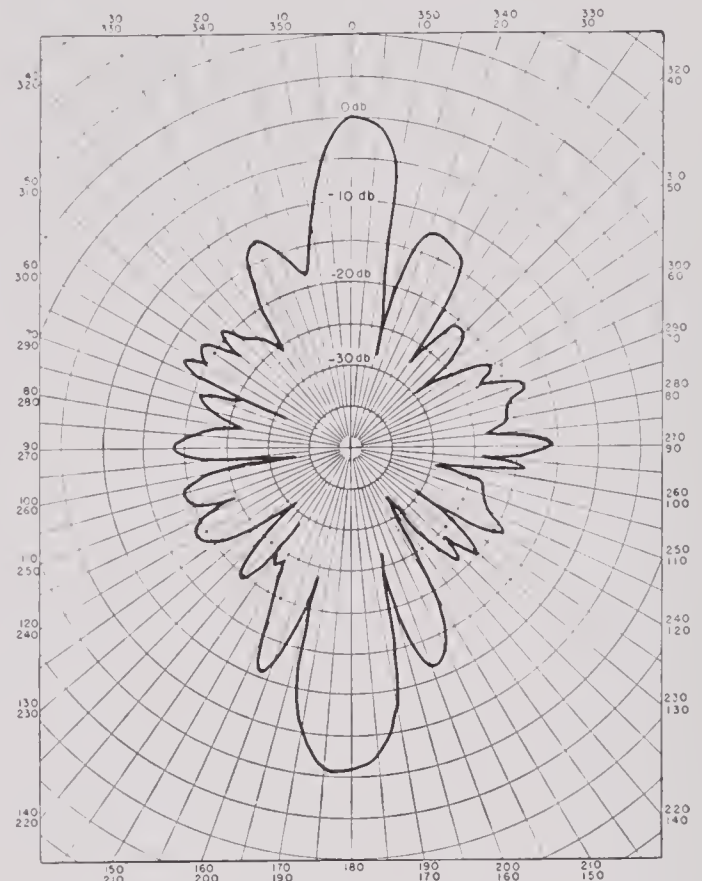


FIGURE 30. Vertical receiving pattern, all elements in parallel at 26 kc with 0:1:1:0 connection of stacks in elements.

The general plan of the HP-3S is shown in Figure 32. The spool was made in three pieces: the base, the cone, and the top. The base and the cone were welded together. The top was screwed to the upper end of the cone with a copper gasket well cemented with gasket-cementing compound between the two parts. After the top had been attached, it was not again removed.

As in the HP-3, the top and bottom flanges were slotted to provide attachment for the elements. Each element consisted of four stacks identical with those used in the HP-3 except that, being connected in series, only two leads were necessary for each element. These leads were brought out through rubber-stem water seals similar to those previously used.

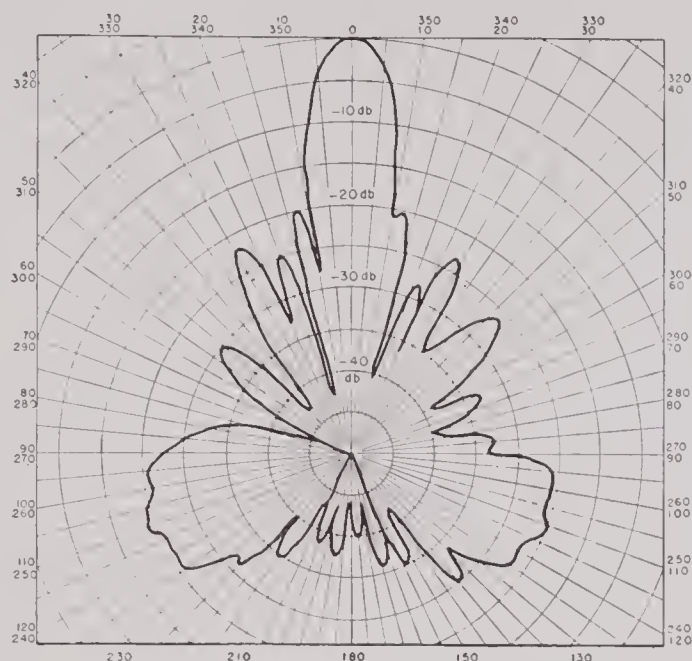


FIGURE 31. Receiving pattern of 48-element scanning sonar transducer at 25.6 kc through commutator lag lines.

The HP-3S was designed to be mounted on the forward deck of a submarine. When so mounted, the cable would be brought in from the bottom. For testing purposes, a 50-pair telephone cable in a rubber sheath armored with woven wire was used.

The rubber boot to cover the transducer was molded on a specially constructed mandrel. The inside surface of the boot was repeatedly painted with castor oil over a period of several days. The faces of the elements were coated in the same way. The boot was then lowered into place and fastened with the same type of bands as were on the HP-3.

The completed transducer was shown in Figure 9 of Chapter 13 with the basket or "Turk's-head" woven from stainless steel wire covering the exposed surface of the rubber boot. This was held at top and bottom by two rings, each with 71 projecting pins over which the meshes of the basket were hooked. The lower ring was drawn down by means of screws into the lower flange, thus causing the basket to grip the rubber over the entire surface and insuring intimate contact between the rubber and the element faces. The device serves the further purpose of preventing flapping and loosening of the boot under the impact of the waves when the submarine is operating on the surface. The research program at HUSL was terminated before full-scale tests were made on this transducer.

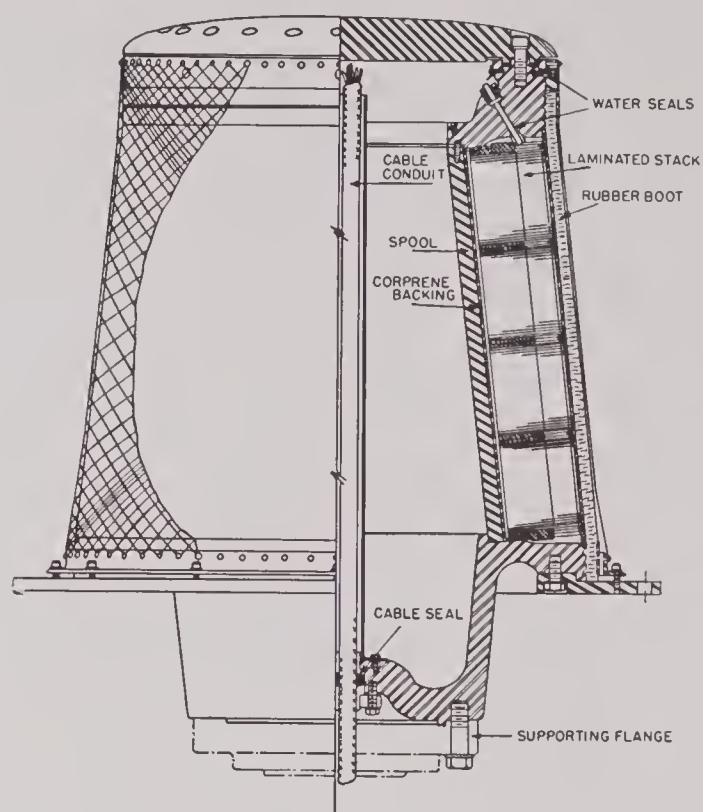


FIGURE 32. Section of the HP-3S transducer.

11.6.3

HP-3DS

After it had been demonstrated that horizontal CR scanning sonar was a feasible underwater detection system, the idea of applying the same sort of system to the vertical plane was considered for use in detecting deep targets. In this system a sound pulse was to be sent out mainly in the vertical plane in the front two quadrants and the lower back quadrant, followed by reception with a sharp receiving beam of sensitivity (10 degrees wide at -6 db), scanning in the vertical plane at approximately 30 rps. The beam was split for BDI to aid in training the main beam in the horizontal plane.

It was planned to mount the transducer on a standard vertical training shaft for azimuth training. The active elements extending over three quadrants were to be arranged in two circular arrays side by side on a spool with its axis of symmetry lying in the horizontal plane. BDI indications in the plane defined by the instantaneous main axis of the scanning beam and the axis of symmetry of the spool were to be given by comparing the signals from the left and right circular arrays. The design called for a beam width in the BDI plane of 20 degrees at -6 db.

The "junction-box" rack was planned to contain the mica tuning condensers for the individual trans-

CONFIDENTIAL

ducer elements, a "sum" scanning CR rotor, a "sum" listening CR rotor, a "difference" scanning CR rotor to give the signal for BDI between the left and right banks of transducer elements, and arrangements for lifting the grounding bus bars of the condenser banks and the transformer banks during the pinging interval.



FIGURE 33. Spool of the HP-3DS transducer.

The steel supporting spool is shown in Figure 33. The outside diameter of the flange rings is $23\frac{5}{8}$ in. and the distance between the inside faces of these flanges is 9 in. The special "gooseneck" support was welded to a curved boiler plate which bolted on to the spool flanges over the upper back quadrant and matched a standard QC flange at the top. The mounting flange was designed to hold the spool in the position in which the extended axis of the training shaft would pass through the axis of the spool. The mounting slots for the elements are shown on the inside surfaces of the spool flanges.

Figure 34A shows the spool with the transducer elements in place. The lead wires from the left bank of transducer stacks and the terminal board to which they are to be attached are shown, as are the 48 elements that extend over 270 degrees of the circumference of the spool. The transducer cable was brought

through a Rubberseal watertight plug at the top of the gooseneck, through the gooseneck, into the center of the spool where the individual wires were splayed out, and soldered to the proper clips on the terminal board. Details of a single stack are shown in Figure 35.

The construction, testing, and assembly of the stacks to form the two stack elements were essentially the same as those described in the case of the HP-3.

Figures 34B and 34C show a later stage of construction and the transducer in its finished condition except for the side cover plate. The pair of large bands near each edge in Figure 34C were of stainless steel and were used to seal the edges of the rubber blanket to the flanges of the spool. The eight narrow bands in the center portion were of 0.010-in. hard nickel. These bands were used to hold the $\frac{1}{2}$ -in. rubber blanket in firm acoustic contact with the active faces of the staves underneath. A film of castor oil was applied between the rubber faces of the elements and the inner surface of the rubber blanket and another layer was applied between the nickel bands and the outer surface of the blanket to assure acoustic contact. The nickel bands were drawn tight by the stainless-steel turnbuckles shown in the photograph. Tests made at Spy Pond showed this somewhat complicated face assembly to be quite satisfactory.

A full series of tests was carried out on the completed transducer. The results of only a part of them need be presented here. In judging the patterns, it is well to note that the gooseneck causes considerable distortion of the sound field.

The patterns received through the sum listening rotor by rotating with the transducer at rest are shown in the series of Figure 36 for transducer orientations, from the vertical, of 45, 90, 135, and 225 degrees. The angular widths of these patterns are about $\frac{4}{3}$ as wide as would be expected from the angular span of each element. This resulted from the fact that the turntable of the pattern tracer was synchronized with the listening rotor in which the angular span of each condenser element was $\frac{4}{3}$ times the angular span of each transducer element. In fact, these patterns correspond exactly to the brightening presentation on the *plan position indicator* [PPI] screen, with all the azimuthal angle distortion resulting from the fact that the transducer elements cover only $\frac{3}{4}$ of the circumference.

The receiving pattern of all the elements in parallel

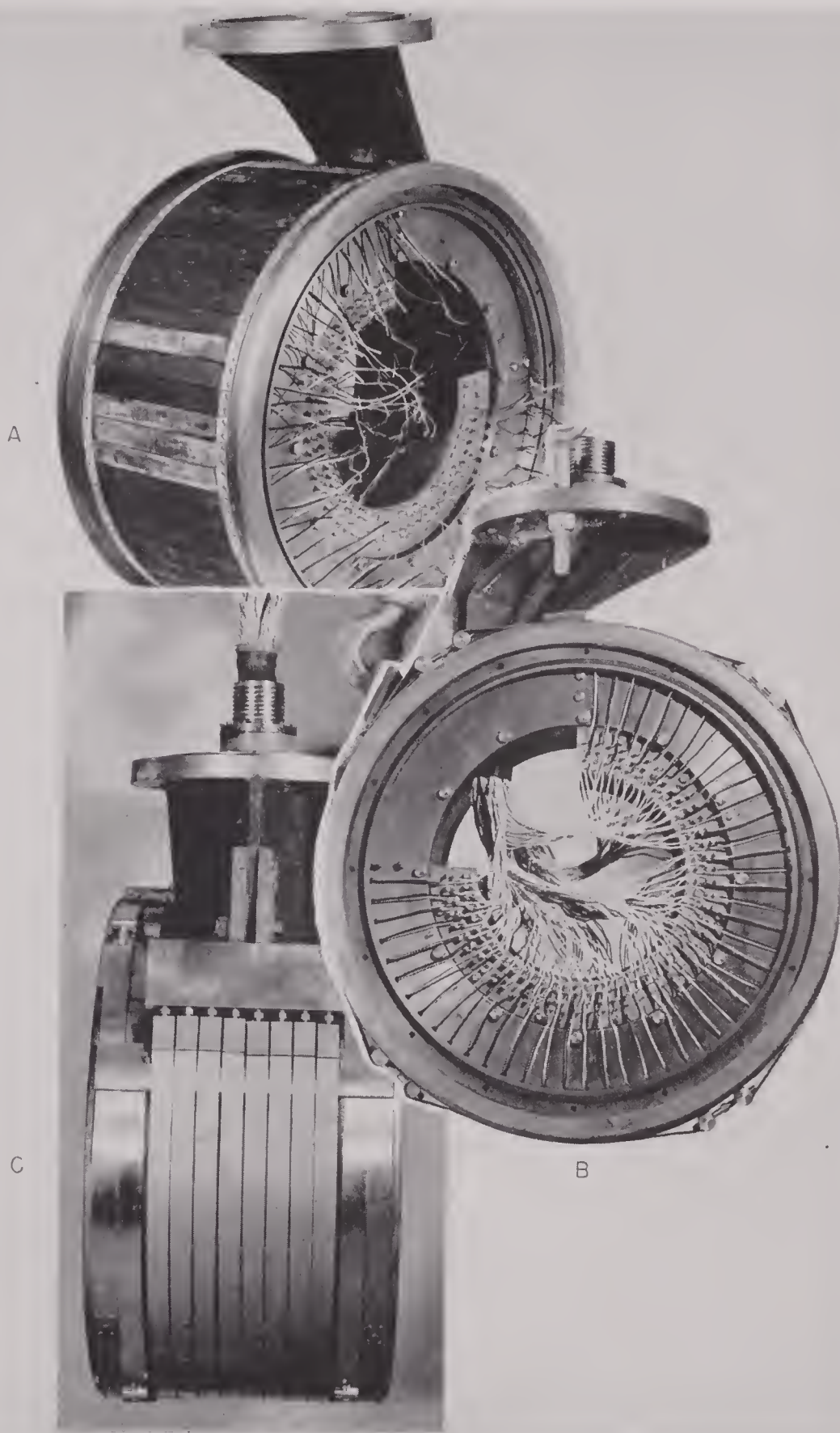


FIGURE 34. A. HP-3DS transducer with elements in place. B. End view showing element lead connections. C. Completed transducer without end caps.

CONFIDENTIAL

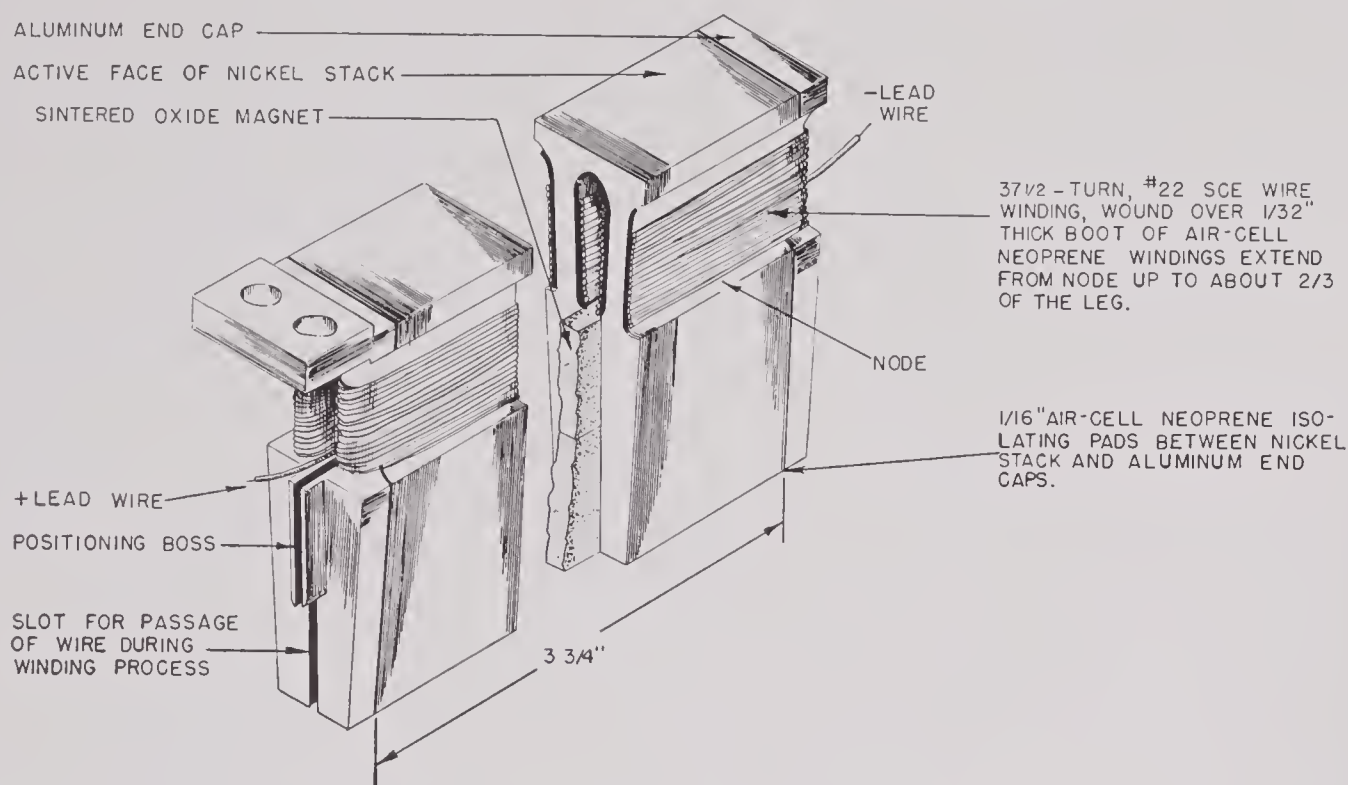


FIGURE 35. Detail of HP-3DS stack.

is shown in Figure 37. The approximately sinusoidal fluctuations in the pattern should be noted. These have an amplitude of about ± 2 db near the 0 and 270 degree positions and about ± 1 db in the center region (135 degrees). The average is very nearly uniform over the 270 degrees of active surface. The period of the fluctuation is about 12 degrees of arc on the average. This corresponds closely to the angle of 11.3 degrees covered by two elements. The same period (i.e., the angular span of two elements) fluctuation of intensity with azimuth angle has been observed in the HP-1 and the HP-2 transducers. A theoretical study of the phenomenon was made in the case of the HP-2, from which it appeared that the fluctuations in the horizontal pattern could be accounted for by variation in impedance among the elements. Phase variation between elements would tend to increase the intensity fluctuation. Although the elements in the HP-3DS transducer were rather carefully adjusted for impedance and were placed around the spool in the order of their frequencies, the observed fluctuation of response or level with azimuth angle may be due to the variations in phase and impedance which remain. Calculations from the theory of the form of the patterns from a 270 degree sector for both pressure release and for stiff baffles show close agreement between the calculated patterns and the ones observed.

By using the method described for the HP-3 transducer, the directivity index for a single HP-3DS element was found to be about 0.078. The measured receiving sensitivity was -95 db vs 1 volt per dyne per sq cm, and the resistive component of impedance was 19.5 ohms. The efficiency of a single stack computed from these data is about 0.30.

With all 96 stacks connected in parallel with their condensers, as in transmitting, the directivity index was estimated to be 0.10, the resistive component of the impedance 0.27 ohm, and the receiving sensitivity was observed to be -111 db vs 1 volt per dyne per sq cm. These values give a computed efficiency of 0.42. During transmission with the same circuit connections, a voltage of 0.094 volt produced a field of 29 db vs 1 dyne per sq cm at 24 ft. If the impedance is taken as $0.27 - j0.96$ ohms and the directivity index as 0.10, the efficiency is 0.16. This latter value should not be considered as firm, however, because there was some question as to the exact value of the sound field produced.

The HP-3DS was built as an experimental unit in an integrated sonar system and installed as part of such a system.³ The design has, however, certain inherent defects. The gooseneck connection with the training shaft is mechanically weak. The use of only three quadrants of the cylinder makes the problem of mounting and water-sealing the rubber blanket

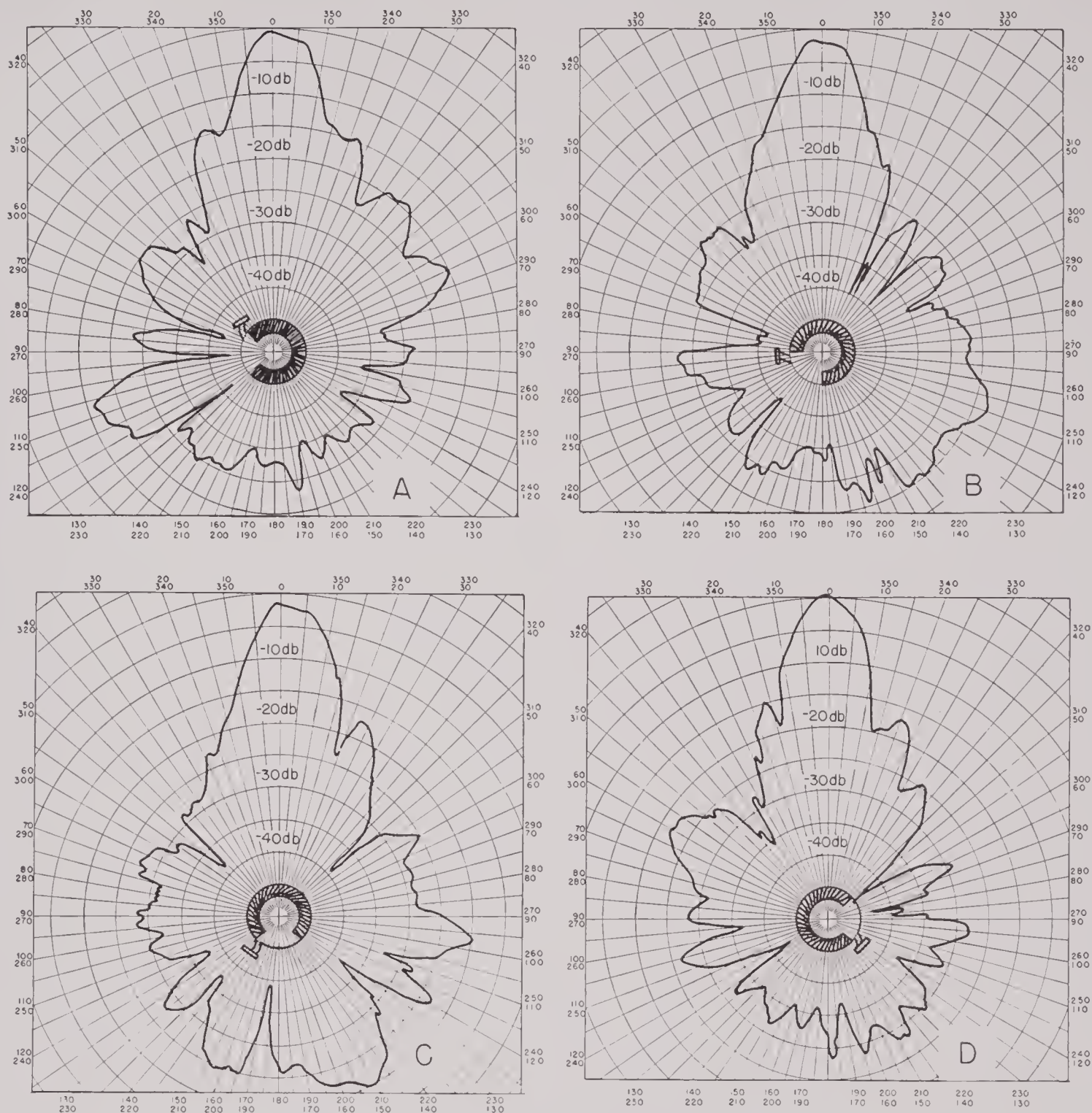


FIGURE 36. Receiving patterns of HP-3DS transducer for orientations of A, 45 degrees; B, 90 degrees; C, 135 degrees; D, 225 degrees, taken through sum listening rotor with transducer stationary.

face unduly complicated. However, the tests showed that, in point of water tightness and acoustic transmission, the construction employed was satisfactory. The measured phase difference between the generated signal voltage in the various stacks and that in the stack on the acoustic axis was about 15 per cent greater than would be expected from simple wave

theory, an effect that can probably be assigned to acoustic baffling produced by the size and shape of the transducer itself. The receiving patterns through the lag line and CR rotor were satisfactory, though not ideal. The side lobes were down by at least 12 db, and the back response was 25 db below that of the main lobe. The overall efficiency was about 0.30.

CONFIDENTIAL

The size of the HP-3DS was dictated by the pattern requirements for operation at the resonant frequency of 26 kc. Reduction in size is possible only by going to a higher frequency. This was done³ in the

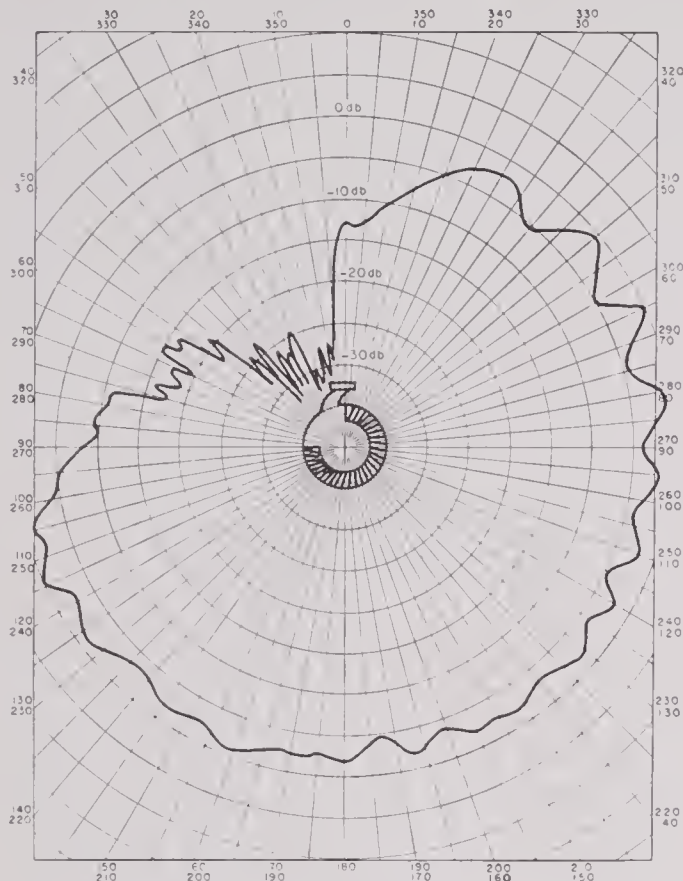


FIGURE 37. Receiving pattern of HP-3DS transducer, all elements in parallel.

case of the HP-8D shown in Figures 11 and 35 of Chapter 13. In the HP-8D the resonant frequency was 38 kc, and the diameter of the active face was 15 in., as compared with the 17½ in. of the HP-3DS. The lamination used is shown in Figure 46 of Chapter 13. Each stack in the two-stack element was

3½ in. long and the overall height of the elements was 7⁹/₁₆ in. Forty-eight elements were mounted in three quadrants of the cylinder, the full surface of which was covered with a stretched rubber boot. In all respects, the design of the HP-8D is better than that of the HP-3DS. The construction and testing were essentially the same as those described in the case of the HP-3. Acoustic tests on the completed transducer showed an overall efficiency of approximately 0.30. The vertical listening beam with the CR rotor and lag line was about 10 degrees wide, 6 db down from the maximum, with the first minor lobes down 15 db and back radiation 22 db down from the major lobe maximum.

14.7

SUMMARY

During the later stages of the development of scanning sonar transducers at HUSL, collaboration was maintained with the Sangamo Electric Company of Springfield, Illinois, in the building of three production models of the HP-5 transducer. This differed only in minor details from the HP-3. Sangamo's experience would seem to bear out the statement that the various laboratory techniques described in the preceding section are applicable to mass production without demanding special skills on the part of manufacturing personnel. It is reasonably certain that with well-regulated and carefully supervised manufacturing procedure, uniform products can be turned out without the multiplicity of detailed tests outlined in the foregoing. In fact, it appears that the preassembly testing might, under good manufacturing conditions, be waived entirely, since it is probable that changes taking place in the process of assembly are greater than the differences between well-built individual stacks before mounting.

GLOSSARY

CHAPTERS 2 AND 3

a	Radius.	p	$(f/f_0 - f_0/f)/2$.
B	Magnetic induction (B_e due to external field; B_o , polarizing).	Q	Electrical or mechanical sharpness of resonance (subscripts A , air, W , water; Z , impedance data; Y , admittance data; c , core; e , blocked electrical, etc.).
B'	B - H (equation [4.2]).	R	Electrical or mechanical resistance; R_{\max} , R_{\min} , maximum and minimum resistances on impedance loop (see Z).
B	Electrical or mechanical susceptance (negative imaginary part of admittance, see Y).	R	Resonance.
b	Radial thickness.	r	Distance between transducer and point of observation or distance between two transducers.
C	Capacity.	S_V, S_I	Open-circuit voltage and short-circuit current sensitivities.
c	Speed of sound (usually c in water, c_m in magnetostrictive core).	s	Longitudinal strain.
D	Directivity ratio.	t	Thickness of lamina.
D	Diameter of motional circle (subscripts A , air; W , water; Z , impedance circle; Y , admittance circle).	t	Time.
d	Length characteristic of penetration of eddy currents.	T_V, T_I	Voltage and current transmitting responses.
E	Potential, voltage.	v	Velocity of radiating surface of transducer.
E	Young's modulus (E' , modulus with magnetostrictive coupling).	W	Potential energy per unit volume.
E	Point of maximum efficiency in impedance or admittance diagram.	X	Electrical or mechanical reactance.
E'	Point of maximum conductance in admittance diagram.	x	Distance.
Eff	Efficiency of transducer in converting electrical to mechanical power.	$Y = G - jB$	Electrical or mechanical admittance; $Y_e = 1/Z_e$, blocked electrical admittance; $Y_i = 1/Z_i$, loaded electrical admittance; $Y_{\text{mot}} = Y_i - Y_e$, motional admittance; $Y_c = 1/Z_c$, core admittance.
e	Voltage representing force in equivalent circuit.	$Z = R + jX$	Electrical or mechanical impedance; Z_e , blocked electrical impedance; Z_i , loaded electric impedance; $Z_{\text{mot}} = Z_i - Z_e$, motional impedance; $Z_m = Z'_m + Z''_m$, open-circuit mechanical impedance; Z''_m , mechanical impedance without magnetostrictive coupling; Z'_m , additional mechanical impedance produced by coupling; Z_L , mechanical load impedance, radiation impedance; Z_c , core impedance; Z_l , leakage impedance.
F	Force.	ϵ	Magnetostrictive coefficient, equation (3) ff.
f	Frequency (subscripts 0, center; 1, 2, "3 db"; E , maximum efficiency; R , resonance).	ξ	Negative phase of eddy-current factor (see x).
f_1, f_4	Frequencies at which rod is $1/2, 1/4$ wave length.	ξ_e, ξ_{cm}	Phase angles related to Z_e, Z_{cm} , [see equation (59)].
f_c	Characteristic frequency for eddy-current effects.	η	Phase lag due to hysteresis.
G	Electromechanical mutual impedance for rod.	Λ	$(\partial B'/\partial p)$ at constant H .
G	Conductance, G_{\max}, G_{\min} , maximum and minimum conductances on admittance loop (see Y).	λ	Wave length in water, equation (88)ff.; magnetostrictive constant, equation (10)ff.
H	Magnetic field, H_e : field applied externally.	μ	Permeability (clamped core).
I	Intensity of magnetization, $(B - H)/4\pi$.	μ'	Permeability at constant stress.
I	Current.	ξ	Displacement.
i	Current representing velocity in equivalent circuit.	ρ	Density (usually ρ for water, ρ_m for magnetostrictive core).
J	Reciprocity parameter (J_1 , at one meter).	ρ_c	Specific acoustic resistance.
K	Stiffness, K_0 : stiffness without magnetostrictive coupling.	ρ_e	Electric resistivity.
K	Image impedance of constant- K filter at mid-band.	σ	Area (usually σ for radiating face, σ_m for core section).
k	Coefficient of electromechanical coupling; k_{eff} : effective coefficient of electromechanical coupling.	σ'	Effective area, equation (92).
k	Wave number = $2\pi/(\text{wave length})$.	Φ	Magnetic flux.
L	Inductance, L_0 : inductance of core at low frequencies.	Φ	Turns ratio of ideal transformer.
l	Length.	$X = X_R - j^2 I = X_0 e^{-j^2}$	Eddy-current factors, Section 3.1.
M	Mass, M_L , mass of plate per tube, Section 3.44; m_0 , mass of tube $1/2\pi$ of wave length, Section 3.44.	$\omega = 2\pi f$	Angular frequency.
N	Number of turns around core.		
P	Longitudinal stress.		
Pot eff	Potential efficiency.		
p	Pressure.		

GENERAL

- ACOUSTIC AXIS.** Reference line adopted in transducer calibration, usually the direction of maximum response.
- BAFFLE.** A shield used to modify an acoustic path.
- BAFFLE, RELEASE.** A baffle satisfying the boundary condition of zero variational pressure.
- BAFFLE, STIFF.** An ideally rigid baffle.
- BDI.** Bearing deviation indicator.
- BEARING DEVIATION INDICATOR.** A system which utilizes the outputs of the halves of a split transducer to provide accurate bearing indication.
- BTL.** Bell Telephone Laboratories.
- CAVITATION.** The formation of vapor or gas cavities in water, caused by sharp reductions in local pressure.
- CR SYSTEM.** Commutated-rotation scanning sonar.
- CRYSTAL TRANSDUCER.** A transducer which utilizes piezoelectric crystals, usually Rochelle Salt, ADP, quartz, or tourmaline.
- CURIE POINT.** The temperature above which a ferromagnetic substance becomes paramagnetic. The Curie point for iron is 769 C, for nickel 356 C.
- CYCLICLY MAGNETIZED.** A magnetic material is in a cyclicly magnetized condition when it has been under the influence of a magnetizing force varying between two specific limits until, for each increasing or decreasing value of the magnetizing force, the magnetic induction has the same value in successive cycles.
- DCDI.** Depth charge direction indicator.
- DIRECTIVITY INDEX.** A measure of the directional properties of a transducer. It is the ratio in decibels of the average intensity or response over the whole sphere surrounding the projector or hydrophone to the intensity or response on the acoustic axis.
- DIRECTIVITY RATIO.** A measure of the directional properties of a transducer. It is the numerical ratio of the intensity or response on the acoustic axis to the average intensity or response over the whole sphere surrounding the projector or hydrophone.
- DOME.** A transducer enclosure, usually streamlined, used with echo-ranging or listening devices to minimize turbulence and cavitation noises arising from the transducer's passage through the water.
- DRSB.** Directional radio sono buoy.
- ECHO REPEATER.** Artificial target, used in sonar calibration and training, which returns a synthetic echo by receiving, amplifying, and retransmitting an incident ping.
- ERSB.** Expendable radio sono buoy.
- HP-TYPE TRANSDUCER.** Hebb phone, a longitudinally vibrating laminated stack transducer of type used in final QH design.
- H-RLP.** Harvard ring ladderphone.
- HUSL.** Harvard Underwater Sound Laboratory.
- HYDROPHONE.** Underwater microphone.
- JP.** A submarine listening system employing magnetostriction line hydrophone.
- MAGNETOCALORIC EFFECT.** Changes in magnetism with temperature changes.
- MAGNETOMOTIVE FORCE.** Magnetic analogue of electromotive force.
- MAGNETOSTRICTION EFFECT.** Phenomenon exhibited by certain metals, particularly nickel and its alloys, which change in length when magnetized, or, (Villari Effect) when magnetized and then mechanically distorted, and undergo a corresponding change in magnetization.
- NEOPRENE.** Generic name for synthetic rubber made by polymerization of 2-chloro-1, 3-butadiene. Vulcanizates are markedly resistant to oils, greases, chemicals, sunlight, ozone, and heat.
- OAX MONITOR.** A portable sound gear monitor, with range from 15 kc to 26 kc.
- OCP MONITOR.** A portable sound gear monitor, with range from 10 kc to 70 kc.
- PERMENDUR.** Alloy of iron, cobalt, and not more than 2% vanadium which maintains uniformly high permeability to alternating flux in the presence of a superposed polarizing flux.
- PIEZOELECTRIC EFFECT.** Phenomenon exhibited by certain crystals in which mechanical compression produces a potential difference between opposite crystal faces or an applied electric field produces corresponding changes in dimensions.
- PING.** Acoustic pulse signal projected from echo-ranging transducer.
- PPCR.** Portable polar chart recorder.
- PPI.** Plan position indicator.
- PRESSURE RELEASE.** Material, such as air-cell rubber, incapable of supporting variational acoustic pressure.
- PROJECTOR.** An underwater acoustic transmitter.
- QH.** Navy designation for scanning sonar of CR type using magnetostriction transducer.
- ρc RUBBER.** A rubber compound with the same ρc (density x velocity of sound) product as water.
- RING STACK.** A magnetostrictive transducer composed of ring laminations which vibrate radially.
- SCANNING SONAR.** Echo-ranging system in which the ping is transmitted simultaneously throughout the entire angle to be searched and a rapidly-rotating narrow beam scans for the returning echoes.
- SEARCHLIGHT-TYPE SONAR.** Echo-ranging system in which the same narrow beam pattern is used for transmission and reception.
- SGM.** Sound gear monitor.
- SONAR.** Generic term applied to methods or apparatus that use Sound for Navigation and Ranging.
- SONIC FREQUENCIES.** Range of audible frequencies, sometimes taken as from .02 kc to 15 kc.
- SONO BUOY.** A buoy listening device that contains a hydrophone for receiving target signals and a radio transmitter for relaying the signals to patrolling air or surface craft.
- SPEP OR SP-TYPE TRANSDUCER.** A small longitudinally-vibrating laminated stack transducer element, having permanent magnet polarization.
- SSI.** Sector scan indicator.
- STACKS, LAMINATED.** Pile of consolidated laminations.
- STAVE.** Individual longitudinal transducer element, a number of which make up a sonar transducer.

SUPERSONIC FREQUENCIES. Range of frequencies higher than sonic. Sometimes referred to as ultrasonic to avoid confusion with growing use of the term supersonic in connection with higher-than-sound velocities.

TRANSDUCER. Any device for converting energy from one form to another (electrical, mechanical, or acoustical). In sonar, it usually combines the functions of a hydrophone and a projector.

TUBE-AND-CONE. A transducer element using a magnetostriction tube to drive a radiating cone.

TUBE-AND-PLATE. A transducer using one or more magneto-

strictive tubes to drive a flat diaphragm, as in the QC transducer.

TUBULAR-TYPE TRANSDUCER. Thin-walled magnetostrictive tube which vibrates radially.

"TURK'S HEAD." A stainless-steel woven wire covering used to hold the protective rubber boot in place over the transducer.

VALP. Vector admittance locus plotter.

VILLARI EFFECT. The inverse magnetostriction effect.

VILP. Vector impedance locus plotter.

VTVM. Vacuum tube voltmeter.

BIBLIOGRAPHY

Numbers such as Div. 6-551-M3 indicate that the document listed has been microfilmed and that its title appears in the microfilm index printed in a separate volume. For access to the index volume and to the microfilm, consult the Army or Navy agency listed on the reverse of the half-title page.

Chapter 1

1. *Absolute Efficiency of Projectors and Hydrophones*, Eginhard Dietze, NDRC C4-sr20-150, USRL, Aug. 3, 1942.
Div. 6-551-M3
2. *The Absolute Efficiency of a Device Used as a Projector and as a Hydrophone*, Eginhard Dietze, NDRC C4-sr20-197, USRL, Aug. 18, 1942.
Div. 6-551-M4
3. *The Relation between the Absolute Efficiency of a Hydrophone and Its Thermal Noise Level*, Eginhard Dietze, OSRD 1086, NDRC C4-sr20-593, USRL, Dec. 11, 1942.
Div. 6-552-M5
4. *Magnetostrictive Transducers*, Malcolm H. Hebb, Harvey A. Brooks, NDRC 6.1-sr287-898, HUSL, June 22, 1943.
Div. 6-612.1-M2
5. *Open-Circuit Frequency Response of Parallel Tuned Transducer* (Memorandum), Malcolm H. Hebb, HUSL, Nov. 16, 1943.
Div. 6-612.23-M2
6. *Measurement of Projector and Hydrophone Performance, Definition and Terms*, Eginhard Dietze, NDRC 6.1-sr1130-[1833], NS-182, USRL, Sept. 19, 1944.
Div. 6-551-M12
7. *Q and the BTL*, Malcolm H. Hebb, M 01.10-172, HUSL, Mar. 12, 1945.
Div. 6-612.34-M7
8. *Scanning Sonar*, Summary Technical Report, NDRC Division 6, Vol. 16, Chap. 5.
9. *Computation of Absolute Efficiency of a Hydrophone from Its Sensitivity*, Eginhard Dietze, Report 2420-ED-F, BTL, Aug. 29, 1941.
Div. 6-612.22-M2
10. *Relation between Power Delivered by a Hydrophone and Its Absolute Efficiency*, Eginhard Dietze, Report 2420-ED-LA, BTL, Aug. 29, 1941.
Div. 6-612.22-M1
11. *Absolute Efficiency of Hydrophones*, Eginhard Dietze, Report 2420-ED-EN, BTL, Oct. 18, 1941.
Div. 6-612.22-M3
12. *Hydrodynamic Listening Devices*, Eginhard Dietze, Walter D. Goodale, Jr., Report 2420-ED-WDG-KM, BTL, Dec. 3, 1941.
Div. 6-612.1-M1
13. *Hydrodynamic Instruments*, A. H. Inglis, Report 2240-AHI-VD, BTL, Dec. 13, 1941.
Div. 6-612.54-M1
14. "On the Effects of Magnetism upon the Dimensions of Iron and Steel Bars," J. P. Joule, Esq., *The London, Edinburgh and Dublin Philosophical Magazine and Journal of Science*, Ser. 3, Vol. 30, January to June 1847, pp. 225-241.
15. "Ueber die Aenderungen des Magnetischen Moments, Welche der Zug und das Hindurchleiten Eines Galvanischer Stroms in Einem Stabe von Stahl oder Eisen Hervorbringen," E. Villari, *Annalen der Physik und Chemie*, J. G. Poggendorff, Vol. 126, 1865, pp. 87-142.
16. *Magnetic Induction in Iron and Other Metals*, Sir James Alfred Ewing, D. Van Nostrand Co., Inc., New York, N. Y., 1891.
17. British Patent 145,691, P. Langevin, 1920.
18. *Unterwasser Schalltechnik*, Franz Aigner, M. Krayn, Berlin, Germany, 1922.
19. *Transmission Circuits for Telephone Communications*, K. S. Johnson, D. Van Nostrand Co., Inc., New York, N. Y., 1925, pp. 32, 33.
20. *Theory of Vibrating Systems and Sound*, I. B. Crandall, D. Van Nostrand Co., Inc., New York, N. Y., 1927, p. 118.
21. U. S. Patent 1,750,124, G. W. Pierce, 1927.
22. "A Dynamic Study of Magnetostriction," K. C. Black, *Proceedings of the American Academy of Arts and Sciences*, Ser. 2, Vol. 53, 1928.
23. "Magnetostriction," A. Schulze, *Zeitschrift für Physik*, Vol. 50, 1928, pp. 448-505.
24. "Magnetostriction Oscillator," G. W. Pierce, *Proceedings of the American Academy of Arts and Sciences*, Vol. 63, 1928, p. 1.
25. *Magnetic Properties of Matter*, Kotaro Honda, Syokwabo and Co., Tokyo, Japan, 1928.
26. "Reciprocity in Electromagnetic, Mechanical, Acoustical and Interconnected Systems," Stuart Ballantine, *Proceedings of the Institute of Radio Engineers*, Vol. 17, June 1929, pp. 929-951.
27. *Magnetic Phenomena*, Samuel R. Williams, McGraw-Hill Book Co., Inc., New York, N. Y., 1930.
28. *Fairlie Magnetostriction Reports*, F. D. Smith, HUSL File B[ritish 10], 1931.
29. U. S. Patent 2,005,741, H. C. Hayes, June 25, 1935.
30. U. S. Patent 2,063,951, R. L. Steinberger, Dec. 15, 1936.
31. *Alloys of Iron and Nickel* (Monograph Series), J. S. March, McGraw-Hill Book Co., Inc., New York, N. Y., 1938.
32. "Impedance of Telephone Receivers as Affected by the Motion of Their Diaphragms," A. E. Kennelly, G. W. Pierce, *Electrical World*, Sept. 14, 1942.

Chapter 2

1. *Equivalent Circuits for Electromechanical Transducers*, Edwin M. McMillan, HUSL File SD 29, UCDWR, Jan. 10, 1942.
Div. 6-612.31-M1
2. *Optimum Coupling between Microphones and Amplifiers*, William B. Snow, Report G12/2805, CUDWR-NLL, May 15, 1942.
Div. 6-612.33-M1
3. *Relation between Sensitivity and Efficiency of a Hydrophone*, Harvey A. Brooks, M 01.213-10, HUSL, Dec. 4, 1942.
Div. 6-612.22-M6
4. *Motional Impedance Analysis of Underwater Sound Devices*, Frank H. Graham, Eginhard Dietze, NDRC C4-sr20-591, USRL, Dec. 5, 1942.
Div. 6-551-M7

5. *Shock Excitation of Resonant Transducers*, Harvey A. Brooks, M 01.213-12, HUSL, Dec. 17, 1942.
Div. 6-612.22-M7
6. *Efficiency of Magnetostrictive Transducers*, Harvey A. Brooks, M 01.213-25, HUSL, Jan. 19, 1943.
Div. 6-612.22-M9
7. *Theory of Passive Linear Electromechanical Transducers*, Leslie L. Foldy, NDRC 6.1-sr20-878, Navy Project NS-139, USRL, June 9, 1943.
Div. 6-551-M10
8. *Magnetostrictive Transducers*, Malcolm H. Hebb, Harvey A. Brooks, NDRC 6.1-sr287-898, HUSL, June 22, 1943.
Div. 6-612.1-M2
9. *Figure of Merit for Magnetostrictive Transducers*, Harvey A. Brooks, Malcolm H. Hebb, M 01.213-50, HUSL, June 29, 1943.
Div. 6-612.22-M10
10. *A Simplified Method of Computing Potential Efficiencies* (Memorandum), Harvey A. Brooks, HUSL, Sept. 30, 1943.
Div. 6-612.22-M11
11. *Further Generalization of the Concept of Potential Efficiency Applicable to Any Resonant Transducer* (Memorandum), Harvey A. Brooks, HUSL, Oct. 1, 1943.
Div. 6-612.22-M12
12. *Motional Admittance* (Memorandum), Malcolm H. Hebb, HUSL, Nov. 20, 1943.
Div. 6-612.3-M2
13. *Reciprocity of Linear Electromechanical Systems* (Memorandum), Malcolm H. Hebb, HUSL, Dec. 8, 1943.
Div. 6-612.512-M5
14. *The Geometrical Inversion Transformation and Its Application in the Admittance-Impedance Relations, Analytical Admittance-Impedance Relations* (Memorandum), Robert E. Payne, Malcolm H. Hebb, HUSL, Jan. 26, 1944.
Div. 6-612.32-M1
15. *Electrodynamic Transducers for Supersonic Underwater Sound*, Malcolm H. Hebb, M 01.214-10, HUSL, Sept. 13, 1944.
Div. 6-612.1-M7

Chapter 3

1. *Equivalent Circuits for Electromechanical Transducers* (Preliminary Draft), Edwin M. McMillan, UCDWR, Jan. 10, 1942.
Div. 6-612.31-M1
2. *Equivalent Circuit of Magnetostriction Oscillators*, Harvey A. Brooks, M 01.10-12, HUSL, June 5, 1942.
Div. 6-612.31-M2
3. *Efficiency of Magnetostriction Transducers*, Malcolm H. Hebb, M 01.213-3, HUSL, Aug. 14, 1942.
Div. 6-612.22-M5
4. *Series and Parallel Tuning of Transducers*, Malcolm H. Hebb, M 01.213-7, HUSL, Oct. 13, 1942.
Div. 6-612.31-M3
5. *Laminated Magnetostriction Tubes*, Malcolm H. Hebb, M 01.213-7.1, HUSL, Nov. 7, 1942.
Div. 6-612.63-M1
6. *The Alleged Failure of Reciprocity in Electroacoustical Systems*, Frederick V. Hunt, M 01.213-8, HUSL, Nov. 30, 1942.
Div. 6-612.512-M1
7. *Elementary Results Regarding Tuning of Magnetostriction Microphones*, Harvey A. Brooks, M 01.213-9, HUSL, Dec. 1, 1942.
Div. 6-612.31-M4
8. *Relation between Sensitivity and Efficiency of a Hydrophone*, Harvey A. Brooks, M 01.213-10, HUSL, Dec. 4, 1942.
Div. 6-612.22-M6
9. *Motional Impedance Analysis of Underwater Sound Devices*, Frank H. Graham, Eginhard Dietze, NDRC, C4-sr20-591, USRL, Dec. 5, 1942.
Div. 6-551-M7
10. *Shock Excitation of Resonant Transducers*, Harvey A. Brooks, M 01.213-12, HUSL, Dec. 17, 1942.
Div. 6-612.22-M7
11. *Efficiency and Sensitivity of Cone-Type Magnetostriction Transducers*, Harvey A. Brooks, M 01.213-18, HUSL, Jan. 4, 1943.
Div. 6-612.22-M8
12. *Frequency Response Curves*, Malcolm H. Hebb, M 01.213-20, HUSL, Jan. 7, 1943.
Div. 6-612.51-M1
13. *Efficiency of Magnetostrictive Transducers*, Harvey A. Brooks, M 01.213-25, HUSL, Jan. 19, 1943.
Div. 6-612.22-M9
14. *Capacity of Ground in Calibration of Transducers*, Harvey A. Brooks, Malcolm H. Hebb, M 01.10-27, HUSL, Feb. 1, 1943.
Div. 6-612.51-M2
15. *Theory of Passive Linear Electromechanical Transducers*, Leslie L. Foldy, NDRC, 6.1-sr20-878, Navy Project NS-139, USRL, June 9, 1943.
Div. 6-551-M10
16. *Magnetostrictive Transducers*, Malcolm H. Hebb, Harvey A. Brooks, NDRC, 6.1-sr287-898, HUSL, June 22, 1943.
Div. 6-612.1-M2
17. *Figure of Merit for Magnetostrictive Transducers*, Harvey A. Brooks, Malcolm H. Hebb, M 01.213-50, HUSL, June 29, 1943.
Div. 6-612.22-M10
18. *Equivalent Circuit for Magnetostrictive Transducers* (Memorandum), Malcolm H. Hebb, HUSL, July 12, 1943.
Div. 6-612.31-M5
19. *Reduction of Eddy Currents in Magnetostrictive Tubes*, Malcolm H. Hebb, M 01.213-62, HUSL, July 24, 1943.
Div. 6-612.8-M4
20. *A Simplified Method of Computing Potential Efficiencies*, Harvey A. Brooks, M 01.213-86, HUSL, Sept. 30, 1943.
Div. 6-612.22-M11
21. *Further Generalization of the Concept of Potential Efficiency Applicable to Any Resonant Transducer*, Harvey A. Brooks, M 01.213-88, HUSL, Oct. 1, 1943.
Div. 6-612.22-M12
22. *Some Geometrical Relations in the Impedance Diagram*, James W. Follin, Jr., M 01.213-92, HUSL, Oct. 11, 1943.
Div. 6-612.511-M6
23. *Magnetostrictive Transducers, Representation of Solid Horn by Four-Terminal Network*, Malcolm H. Hebb, M 01.213-107, HUSL, Nov. 3, 1943.
Div. 6-612.3-M1
24. *Motional Admittance*, Malcolm H. Hebb, M 01.213-113, HUSL, Nov. 20, 1943.
Div. 6-612.3-M2
25. *Measurements on $\frac{1}{4}$ -in. 20-kc Ring Stack*, James W. Follin, Jr., M 01.213-115, HUSL, Nov. 20, 1943.
Div. 6-612.61-M4

26. *Reciprocity of Linear Electromechanical Systems*, Malcolm H. Hebb, M 01.213-125, HUSL, Dec. 8, 1943.
Div. 6-612.512-M5
27. *Determination of E , λ , and Electromechanical Coupling Coefficient from Impedance Data*, S. T. Pan, M 01.213-130, HUSL, Dec. 22, 1943.
Div. 6-612.51-M5
28. *The Geometrical Inversion Transformation and Its Application in the Admittance-Impedance Relations, Analytical Admittance-Impedance Relations*, Robert E. Payne, Malcolm H. Hebb, M 01.213-141, HUSL, Jan. 26, 1944.
Div. 6-612.32-M1
29. *Band-Pass Characteristics of Magnetostrictive Transducers*, Malcolm H. Hebb, Nelson M. Blachman, M 01.213-142, HUSL, Jan. 28, 1944.
Div. 6-612.34-M1
30. *Relation between Electromechanical Coupling and DQ/Z_c* , Malcolm H. Hebb, M 01.213-153, HUSL, Feb. 16, 1944.
Div. 6-612.31-M6
31. *Methods of Obtaining Band-Pass Characteristics with Magnetostriction Transducers*, James W. Follin, Jr., M 01.213-155, HUSL, Feb. 17, 1944.
Div. 6-612.34-M2
32. *Band-Pass Transducers*, Frederick V. Hunt, M 01.213-158, HUSL, Feb. 19, 1944.
Div. 6-612.34-M3
33. *Elimination of Eddy Currents in Magnetostriction Hydrophones*, James W. Follin, Jr., Report G12 742, NS-139, CUDWR-NLL, Feb. 24, 1944.
Div. 6-612.31-M7
34. *Some Qualitative Notes on Band-Pass Transducers*, Benjamin B. Drisko, M 01.213-169, HUSL, Mar. 8, 1944.
Div. 6-612.34-M4
35. *Coupling Tests on Segmented and Unsegmented Ladderphone Stacks, LDPI No. 1 and No. 2*, William T. Bartholomew, Francis P. Bundy, M 01.213-173, HUSL, Mar. 16, 1944.
Div. 6-612.31-M8
36. *Band-Pass Transducers*, Malcolm H. Hebb, Nelson M. Blachman, M 01.213-176, HUSL, Mar. 23, 1944.
Div. 6-612.34-M5
37. *Transducers Separated from the Water by Rubber or Oil*, Nelson M. Blachman, M 01.21-72, HUSL, May 12, 1944.
Div. 6-612.43-M6
38. *Lamination Design to Minimize the Q* , Nelson M. Blachman, M 01.213-200, HUSL, June 17, 1944.
Div. 6-612.34-M6
39. *Impedance Diagram for Parallel Tuned MS Transducer*, Malcolm H. Hebb, M 01.213-205, HUSL, June 28, 1944.
Div. 6-612.32-M3
40. *Compressed Metallic Dust as a Magnetostrictive Material*, William T. Bartholomew, Francis P. Bundy, M 113.5-147, HUSL, July 7, 1944.
Div. 6-612.42-M8
41. *Equivalent Circuit for Magnetostrictive Transducers*, Robert E. Payne, M 01.213-213, HUSL, Aug. 3, 1944.
Div. 6-612.31-M9
42. *Tests and Analysis of British Scanning Sonar Transducer Element*, Francis P. Bundy, M 02.45.7-120, HUSL, Oct. 25, 1944.
Div. 6-612.55-M16
43. *Equalization of Hydrophones*, Nelson M. Blachman, M 01.21-101, HUSL, Oct. 31, 1944.
Div. 6-612.31-M10
44. *Q and the BTL*, Malcolm H. Hebb, M 01.10-172, HUSL, Mar. 12, 1945.
Div. 6-612.34-M7
45. *Transducer Research and Production at the New London Laboratory*, William B. Snow, James W. Follin, Jr., Wilbur T. Harris, NDRC 6.1-sr1128-2212, Report G12/1418, NS-113, CUDWR-NLL, May 25, 1945.
Div. 6-612.1-M8
46. *Electromechanical Transducers and Wave Filters*, W. P. Mason, D. Van Nostrand Co., Inc., New York, N. Y., 1942, Section 6.5.

Chapter 4

1. *Measurements of the Permeability of Magnetostrictive Materials*, Howard C. Hardy, M 01.213-23, HUSL, Jan. 14, 1943.
Div. 6-612.4-M2
2. *Properties and Uses of Alnico Magnets*, Kenneth N. Fromm, Francis P. Bundy, M 01.213-35, HUSL, Apr. 23, 1943.
Div. 6-612.42-M1
3. *Magnetostrictive Transducers*, Malcolm H. Hebb, Harvey A. Brooks, NDRC 6.1-sr287-898, HUSL, June 22, 1943.
Div. 6-612.1-M2
4. *Acoustic Properties of Hydrogen Annealed Nickel*, Nelson K. Moody, Jr., Harvey A. Brooks, M 113.5-28, HUSL, July 5, 1943.
Div. 6-612.41-M2
5. *Visit to Laboratory of E. M. Wise of the International Nickel Company, Inc., on July 13, 1943*, Malcolm H. Hebb, Francis P. Bundy, M 113.50-37, HUSL, July 27, 1943.
Div. 6-612.41-M3
6. *Nickel Alloys for Transducers*, Frederick V. Hunt, M 113.50-39, HUSL, July 30, 1943.
Div. 6-612.41-M4
7. *Tests on Hydrophones with Shells Specially Heat Treated by C. G. Conn, Ltd.*, Robert R. MacLaughlin, Report D16/473, NS-102, CUDWR-NLL, Aug. 11, 1943.
Div. 6-612.41-M5
8. *Nickel Strip Material*, Alan H. Selker, M 113.50-46, HUSL, Aug. 24, 1943.
Div. 6-612.41-M6
9. *Heat Treatment of Nickel*, Robert R. MacLaughlin, Report G12/530, CUDWR-NLL, Sept. 14, 1943.
Div. 6-612.41-M7
10. *Visit to West Lynn Laboratory of General Electric regarding Materials for Permanent Magnets*, Francis P. Bundy, M 113.50-59, HUSL, Sept. 25, 1943.
Div. 6-612.42-M2
11. *Measurements of 5-in. Toroidally Wound Magnetostriction Hydrophones, Evaluation of Annealing of Nickel*, Edward Gerjuoy, Wilbur T. Harris, Report D16/555, CUDWR-NLL, Oct. 19, 1943.
Div. 6-612.41-M8
12. *Magnetic Properties and Electrical Resistivities of Oxide Annealed and Cold-Worked Nickel [Grade] A*, S. T. Pan, M 113.50-73, HUSL, Nov. 8, 1943.
Div. 6-612.41-M9
13. *Visit to Bell Telephone Laboratories, November 18 and 19 [1943]*, Francis P. Bundy, M 113.50-79, HUSL, Nov. 27, 1943.
Div. 6-612.4-M3
14. *Visit to Bell Telephone Laboratories, November 18 and 19 [1943]*, James W. Follin, Jr., M 113.50-82, HUSL, Dec. 3, 1943.
Div. 6-612.4-M4
15. *Determination of E , λ , and Electromechanical Coupling Coefficient from Impedance Data*, S. T. Pan, M 01.213-130, HUSL, Dec. 22, 1943.
Div. 6-612.51-M5

CONFIDENTIAL

16. *General Magnetic Properties and Magnetostrictive Properties of Hydrogen-Annealed 0.005" 45-Permalloy Sheets*, S. T. Pan, M 113.50-93, HUSL, Jan. 15, 1944.
Div. 6-612.42-M3
17. *Magnetic Properties of [Grade] A Nickel for Use in Laminated Stack Transducers*, James W. Follin, Jr., S. T. Pan, NDRC, 6.1-sr287-1352, H-234, HUSL, Jan. 25, 1944.
Div. 6-612.41-M13
18. *The 8 Va Vicalloy*, S. T. Pan, M 113.50-98, HUSL, Feb. 15, 1944.
Div. 6-612.42-M4
19. *Annealing of JP-1 Straight Wood Core Hydrophone*, Hector F. Bernier, Report G12/753, NS-139 and NS-113, CUDWR-NLL, Feb. 26, 1944.
Div. 6-612.41-M16
20. *The 2 V Permendur*, S. T. Pan, M 113.50-104, HUSL, Mar. 14, 1944.
Div. 6-612.42-M5
21. *Grade A Nickel Annealed in Hydrogen*, S. T. Pan, M 113.50-112, HUSL, Apr. 13, 1944.
Div. 6-612.41-M17
22. *Bieber's Alloy*, S. T. Pan, M 113.50-119, HUSL, Apr. 26, 1944.
Div. 6-612.42-M6
23. *Magnetic Properties of 45 Permalloy*, S. T. Pan, B. A. Wooten, NDRC 6.1-sr287-1542, H-264, HUSL, Apr. 30, 1944.
Div. 6-612.42-M7
24. *Self-Polarized Ring Stacks*, Francis P. Bundy, G. W. Renner, M 01.213-194, HUSL, May 9, 1944.
Div. 6-612.61-M9
25. *Effect of Annealing on the Magnetic Properties of Nickel Tubing* (Memorandum for File), Arthur L. Thuras, James W. Follin, Jr., Report G12/928, CUDWR-NLL, May 16, 1944.
Div. 6-612.41-M19
26. *Half-Hard Grade A Nickel*, S. T. Pan, M 113.5-145, HUSL, July 6, 1944.
Div. 6-612.41-M20
27. *The 6.5 V Vicalloy*, S. T. Pan, M 113.5-150, HUSL, July 12, 1944.
Div. 6-612.42-M9
28. *Weston Permalloy Powder Cores*, S. T. Pan, M 110.5-102, HUSL, July 19, 1944.
Div. 6-612.42-M10
29. *The 2-V Permendur Hydrophones*, Wilbur T. Harris, David W. Van Lennep, Phillip B. Edwards, Report G12/1168, NS-102, CUDWR-NLL, Oct. 6, 1944.
Div. 6-612.8-M16
30. *Test Equipment and Methods for Relative Permeability Measurements on Nickel Tubing* (Memorandum for File), Robert R. MacLaughlin, Report G12/1230, NS-102, CUDWR-NLL, Nov. 10, 1944.
Div. 6-612.8-M18
31. *Variation of Magnetization in Legs of PM Polarized SPEP Element with Driving Field*, S. T. Pan, M 01.213-291, HUSL, Dec. 6, 1944.
Div. 6-612.41-M21
32. *Reversible Permeability and Hysteresis Loss in Oxide-Annealed [Grade] A Nickel Polarized at $B_0 = 4100$* , S. T. Pan, M 113.5-180, HUSL, Dec. 12, 1944.
Div. 6-612.41-M22
33. *A Detailed Study of Sintered-Oxide Magnets in HP-3 Stacks*, S. T. Pan, Milton R. Carlson, Francis P. Bundy, M 01.213-285, HUSL, Dec. 15, 1944.
Div. 6-612.42-M11
34. *Transducer Research and Production at the New London Laboratory*, William B. Snow, James W. Follin, Jr., Wilbur T. Harris, NDRC 6.1-sr1128-2212, Report G12/1418, NS-113, CUDWR-NLL, May 25, 1945.
Div. 6-612.1-M8
35. *Magnetic Materials for Magnetostriction Microphones* (Bell Laboratories Technical Memorandum), H. J. Williams, R. M. Bozorth, Report 37063, BTL, July 7, 1942.
Div. 6-612.4 M1
36. *Magnetic Materials for Magnetostriction Microphones and Projectors*, H. J. Williams, E. A. Nesbitt, M. Goertz, Reports 27063-4 and 24714-1, BTL, Mar. 22, 1944.
Div. 6-612.4-M6
37. *The Magnetostriction, Young's Modulus and Damping of 68 Permalloy as Dependent on Magnetization and Heat Treatment*, H. J. Williams, R. M. Bozorth, H. Christensen, Monograph B-1303, BTL.
Div. 6-612.42-M12
38. Case Report 4399.1, Research Laboratory, International Nickel Co.
39. "Ferromagnetismus und Phasengestaltung im Zweistoffsystem Nickel Mangan," Seiji Kaya, A. Kussman, *Zeitschrift für Physik*, Vol. 72, 1931, pp. 293-309.
40. *Fairlie Magnetostriction Report*, F. D. Smith, HUSL File B[ritish 10], 1931.
41. "Notes on Electricity and Magnetism," Lord Rayleigh, Sec. R. S., *The London, Edinburgh and Dublin Philosophical Magazine and Journal of Science*, Ser. 5, Vol. 23, March 1887, pp. 225-245.
42. "Magnetic Measurements at Low Flux Densities Using the Alternating Current Bridge," Victor E. Legg, *Bell System Technical Journal*, Vol. XV, 1936, pp. 39-62.
43. *Magnetische und Electriche Eigenschaften des Eisens und Seiner Legierungen*, O. V. Auer, 1938.
44. "Die Kobaltecke des Systems Eisens-Kobalt-Vanadin," Werner Koester, Karl Lang, *Zeitschrift für Metallkunde*, Vol. 30, 1938, pp. 350-352.
45. *Metals Handbook*, American Institute of Mining Engineers, 1939, p. 1664.
46. *Die Magnetisierung bei Schwachen Feldern, a die Rayleigh Schleife, Wechselstromuntersuchungen im Rayleigh Gebiet*, R. Becker, W. Doering, Julius Springer, Berlin, Germany, 1939 (Edwards Bros. Inc., Ann Arbor, Mich., 1943) pp. 218-228.
47. "Demagnetizing Factor of Rods," R. M. Bozorth, D. M. Chapin, *Journal of Applied Physics*, Vol. 13, 1942, pp. 320-326.
48. "On the Magnetostriction of Iron-Cobalt Alloys," Yosio Masiyama, *The Science Reports of the Tohoku Imperial University*, Tohoku Imperial University, Sendai, Japan, Ser. 1, Vol 21, 1932, pp. 394-410.

Chapter 5

1. *Directivity of Radiation*, O. Hugo Schueck and Others (October 1941 to March 1942), M 01.21-1, HUSL, March 1942.
Div. 6-612.21-M1
2. *Directivity Patterns of Sound Sources*, W. O. Pennell, Malcolm H. Hebb, Harvey A. Brooks and Others, NDRC C4-sr287-089, HUSL, Apr. 29, 1942.
Div. 6-551-M2

CONFIDENTIAL

3. *Absolute Efficiency of Projectors and Hydrophones*, Eginhard Dietze, NDRC C4-sr20-150, USRL, Aug. 3, 1942.
Div. 6-551-M3
4. *The Absolute Efficiency of a Device Used as a Projector and as a Hydrophone*, Eginhard Dietze, NDRC C4-sr20-197, USRL, Aug. 18, 1942.
Div. 6-551-M4
5. *Program for Studies of Delay Method of Making Toroidal Hydrophone Uni-Directive*, J. Warren Horton, Report G12/3769, CUDWR-NLL, Aug. 21, 1942.
Div. 6-612.21-M4
6. *Angular Characteristics of the WEA-1 Used as a Hydrophone* (Memorandum for File), Edward Gerjuoy, Report G13/176, CUDWR-NLL, Mar. 2, 1943.
Div. 6-556.1-M9
7. *Directivity Considerations for Echo Ranging Projectors*, Eginhard Dietze, Leslie L. Foldy, NDRC 6.1-sr20-617, Navy Project NS-139, USRL, Apr. 30, 1943.
Div. 6-551-M9
8. *Magnetostrictive Transducers*, Malcolm H. Hebb, Harvey A. Brooks, NDRC 6.1-sr287-898, HUSL, June 22, 1943.
Div. 6-612.1-M2
9. *Theoretical Directivity Characteristics for Line Hydrophones*, Wilbur T. Harris, Report G12/450, CUDWR-NLL, Aug. 26, 1943.
Div. 6-612.21-M6
10. *Bearing Accuracy of 3-ft, 2-ft, and 1-ft Straight Magnetostriction Hydrophones* (Memorandum for File), Ralph C. Maninger, Report D17/543, CUDWR-NLL, Oct. 9, 1943.
Div. 6-612.62-M17
11. *Pattern Requirements for Sonar Transducer*, Malcolm H. Hebb, M 02.45.70-38, HUSL, Oct. 15, 1943.
Div. 6-612.21-M7
12. *Shifted Lobe and SLC Patterns of a Phase and Shaded-Square Transducer*, Gerald I. Harrison, M 01.21-41, HUSL, Nov. 19, 1943.
Div. 6-612.21-M8
13. *Advantages of Increased Hydrophone Length to Sonic Listening*, Arthur L. Thuras, Report G12/631, CUDWR-NLL, Dec. 6, 1943.
Div. 6-612.21-M9
14. *Performance of the JP Baffle at Supersonic Frequencies*, Edward Gerjuoy, Report G12/643, CUDWR-NLL, Dec. 11, 1943.
Div. 6-612.62-M19
15. *Theoretical Patterns for Circular Radiators*, Nelson M. Blachman, M 01.21-44, HUSL, Dec. 30, 1943.
Div. 6-612.21-M10
16. *Acoustic Radiation from Sources at the Top of a Semi-Infinite Cylinder*, J. K. L. MacDonald, AMP, NDRC, M 01.21-45, HUSL, Jan. 5, 1944.
17. *Directivity Ratios for Circular Pistons*, Nelson M. Blachman, M 01.21-50, HUSL, Feb. 3, 1944.
Div. 6-612.21-M11
18. *Delay Network to Obtain Front-to-Back Discrimination*, James W. Follin, Jr., Report G12/743, NS-129, CUDWR-NLL, Feb. 11, 1944.
Div. 6-612.21-M12
19. *The Vertical Pattern of a Split Sonar Element*, Malcolm H. Hebb, Nelson M. Blachman, M 01.21-56, HUSL, Mar. 1, 1944.
Div. 6-612.21-M13
20. *Circular Transducer Patterns*, Gerald I. Harrison, M 01.21-62, HUSL, Apr. 7, 1944.
Div. 6-612.21-M14
21. *Patterns of Radiators in Pressure-Release Baffles*, Gerald I. Harrison, M 01.21-65, HUSL, Apr. 12, 1944.
Div. 6-612.21-M15
22. *Single Element Pattern of Cylindrical Transducer*, Gerald I. Harrison, M 01.21-68, HUSL, Apr. 28, 1944.
Div. 6-612.21-M16
23. *Appearance of 90° Minor Lobes in Scanning Sonar Transducer Patterns*, Thomas P. Merritt, Francis P. Bundy, M 02.45.7-90, HUSL, May 13, 1944.
Div. 6-632.61-M2
24. *Elimination of Side-Lobe Interference in the RLI, Part I Theoretic* (Memorandum for File), James W. Follin, Jr., Report G12/947, CUDWR-NLL, June 8, 1944.
Div. 6-612.21-M17
25. *Comparative Tests on 3-ft, 4-ft, and 5-ft Hydrophones*, Ralph C. Maninger, Report P33/949, CUDWR-NLL, June 12, 1944.
Div. 6-612.62-M27
26. *Radiation Impedance and Equivalent Circuits*, Malcolm H. Hebb, Gerald I. Harrison, Nelson M. Blachman, M 01.21-84, HUSL, June 17, 1944.
Div. 6-612.32-M2
27. *Directivity Ratio of Transducers*, Gerald I. Harrison, M 01.21-88, HUSL, Aug. 21, 1944.
Div. 6-612.21-M18
28. *Shaded Line Sources*, Gerald I. Harrison, M 01.21-91, HUSL, Sept. 7, 1944.
Div. 6-612.21-M19
29. *Directivity Ratio of Long Sources*, Gerald I. Harrison, M 01.21-96, HUSL, Oct. 9, 1944.
Div. 6-632.0-M19
30. *Sound Beam Patterns in Sea Water*, NDRC 6.1-sr31-1730, WHOI, Oct. 10, 1944.
Div. 6-510.11-M9
31. *Directivity Ratios*, Malcolm H. Hebb, M 01.21-103, HUSL, Nov. 2, 1944.
Div. 6-612.21-M20
32. *Directivity at Low Sonic Frequencies* (Memorandum for File), Walter F. Graham, Ralph C. Maninger, Report P33/1067, CUDWR-NLL, Nov. 8, 1944.
Div. 6-612.21-M21
33. *Pattern of a Sector of a Cylinder*, Gerald I. Harrison, M 01.21-107, HUSL, Nov. 14, 1944.
Div. 6-612.21-M22
34. *Improvement in Submarine Sonic Listening and Bearing Accuracy*, Arthur L. Thuras, Report G12/1251, NS-102, CUDWR-NLL, Nov. 21, 1944.
Div. 6-612.21-M23
35. *Single Element Scanning Sonar Patterns*, Gerald I. Harrison, M 02.45.7-143, HUSL, Nov. 24, 1944.
Div. 6-632.61-M3
36. *Directivity Patterns of a Delobed Hydrophone for Various Octave Bands* (Memorandum for File), Jordan J. Markham, Report G12/1254, NS-102, CUDWR-NLL, Nov. 27, 1944.
Div. 6-612.21-M24
37. *A Statistical Theory of Errors in Pattern Formation*, Gerald I. Harrison, M 02.45.1-21, HUSL, Dec. 28, 1944.
Div. 6-612.21-M25
38. *Theoretical Formulae of Hydrophone Patterns Integrated over a Band of Frequencies*, LeRoy A. Woodward, Report G12/1301, NS-102, CUDWR-NLL, Jan. 8, 1945.
Div. 6-612.21-M27
39. *Theoretical Scanning Sonar Patterns*, Gerald I. Harrison, M 02.45.1-22, HUSL, Jan. 19, 1945.
Div. 6-632.61-M4
40. *Pattern of a 270° Sector (Corrected)*, Gerald I. Harrison, M 01.21-113, HUSL, Jan. 26, 1945.
Div. 6-612.21-M28
41. *Scattering and Radiation from Circular Cylinders and Spheres, Tables of Amplitudes and Phase Angles*, Arnold N. Lowan, Phillip M. Morse, H. Feshbach, Marvin Lax, NDRC 6.1-sr1046-2032, AMP Report 62.1 R, MIT and AMP, February 1945.
Div. 6-612.21-M29

42. *Pattern of 270° and 90° Sectors (Really Correct)*, Gerald I. Harrison, M 01.21-115, HUSL, Feb. 26, 1945.
Div. 6-612.21-M30
43. *Total Attenuation Patterns*, Gerald I. Harrison, M 01.21-119, HUSL, Mar. 24, 1945. Div. 6-612.21-M32
44. *Transmission Pattern for Constant Echo Strength*, Gerald I. Harrison, M 01.75-15, HUSL, Mar. 26, 1945.
Div. 6-612.21-M33
45. *Recommendations on Attenuation and Lag Lines for the Sangamo XQHA System*, Gerald I. Harrison, M 01.21-126, HUSL, Apr. 2, 1945. Div. 6-632.221-M4
46. *Design B for Scanning Sonar XQHA*, Gerald I. Harrison, M 02.45.1-26, HUSL, Apr. 14, 1945. Div. 6-632.221-M6
47. *Scanning Sonar Pattern Formation*, Gerald I. Harrison, M 02.45.1-27, HUSL, Apr. 14, 1945. Div. 6-632.61-M6
48. *Theoretical Scanning Sonar Patterns*, Gerald I. Harrison, M 02.45.1-29, HUSL, Apr. 16, 1945. Div. 6-632.61-M7
49. *Further Subdivision of Scanning Rotor to Achieve More Uniform Rotation of Beam*, Malcolm H. Hebb, M 02.45.1-31, HUSL, Apr. 19, 1945. Div. 6-632.61-M8
50. *Transducer Research and Production at the New London Laboratory*, William B. Snow, James W. Follin, Jr., Wilbur T. Harris, NDRC 6.1-sr1128-2212, Report G12 1418, CUDWR-NLL, May 25, 1945.
Div. 6-612.1-M8
51. *Advance Notice of Report on Directivity Patterns*, HUSL.
Div. 6-612.21-M34
52. *Submarine Detection, Directivity Indications*, Harry Nyquist, BTL, Oct. 11, 1941. Div. 6-560.2-M1
53. *On the theory of the directionality patterns of continuous source distributions on a plane surface*, R. Clark Jones, Report MM-42-110-5, BTL, Mar. 10, 1942.
Div. 6-612.21-M2
54. *Subaqueous Listening, Directivity of a Pair of Rings*, Harry Nyquist, C4-NDRC-064, BTL, Apr. 2, 1942.
Div. 6-560.2-M2
55. *Directivity with Two Microphones*, Harry Nyquist, C4-NDRC-071, BTL, June 12, 1942. Div. 6-560.2-M4
56. *Directivity of Sound in Water, Elementary Arrays (Memorandum)*, Harry Nyquist, C4-NDRC-072, BTL, June 24, 1942. Div. 6-612.21-M3
57. *Directivity with Two Microphones, Addition vs Multiplication of Outputs*, Harry Nyquist, C4-NDRC-073, BTL, July 1, 1942. Div. 6-560.2-M5
58. *Diffraction around a Cylinder*, W. H. Wise, C4-NDRC-117, BTL, July 15, 1942. Div. 6-530.1-M2
59. "Über die Richtwirkung von Schallstrahlern," H. Stenzel, *Elektrische Nachrichten-Technik*, Vol. 4, 1927, p. 239.
60. "Reciprocity in Electromagnetic, Mechanical, Acoustical, and Interconnected Systems," Stuart Ballantine, *Proceedings of the Institute of Radio Engineers*, Vol. 17, June 1929, pp. 929-951.
61. *A Short Table of Integrals*, B. O. Pierce, Ginn and Co., Boston, Mass., 1929, pp. 116-119.
62. *Vibration and Sound*, P. M. Morse, McGraw-Hill Book Co., Inc., New York, N. Y., 1936, p. 246.
63. *Tables of Functions*, Eugen Jahnke, Fritz Emde, B. G. Teubner, Leipzig and Berlin, Germany, 1938 (Dover Publications, New York, N. Y., 1943), p. 24.
63a. *Ibid.*, p. 29.
63b. *Ibid.*, p. 219.
64. *Theory of Bessel Functions*, G. N. Watson, Macmillan Co., New York, N. Y., 1944, p. 328.

Chapter 6

1. *The Tubular Magnetostriction Microphone*, Arthur L. Thuras, Report G4 1937, CUDWR-NLL, Mar. 17, 1942. Div. 6-554.2-M1
2. *Listening Tests on Thuras Doughnut Hydrophone*, Donald P. Loye, Report G12 2679, CUDWR-NLL, Apr. 30, 1942. Div. 6-612.62-M1
3. *Disclosure of Invention, Magnetostriction Microphone*, Arthur L. Thuras, Report G5 2625, CUDWR-NLL, May 2, 1942. Div. 6-612.62-M2
4. *Present Status of the Development of Line Microphones*, J. Warren Horton, Report G12 3129, CUDWR-NLL, June 13, 1942. Div. 6-612.62-M3
5. *Development of the Directional Voice-Frequency Toroidal Magnetostriction Hydrophone (Progress Report)*, Arthur L. Thuras, NDRC C4-sr20-214, OSRD 775, Report G5s, 3413, CUDWR-NLL, July 1, 1942.
Div. 6-554.2-M3
6. *Laminated Magnetostriction Tubes*, Malcolm H. Hebb, M 01.213-7.1, HUSL, Nov. 7, 1942. Div. 6-612.63-M1
7. *Thuras Type Microphones at 100 kc and 1 mc*, Malcolm H. Hebb, M 01.213-9.1, HUSL, Dec. 1, 1942.
Div. 6-612.62-M4
8. *Tubular Magnetostriction Hydrophone with Cylindrical Internal Coil*, Heeter F. Bernier, Report G27 131, CUDWR-NLL, Dec. 18, 1942. Div. 6-612.62-M5
9. *Residual Magnetism in an Unannealed Nickel B-Type Hydrophone*, Paul E. Sabine, M 01.213-28, HUSL, Jan. 28, 1943. Div. 6-612.41-M1
10. *Comparison of Piezoelectric and Magnetostriction Hydrophones for Sonic Listening (Memorandum)*, James W. Follin, Jr., NDRC 6.1-sr20-653, Report G27 130, CUDWR-NLL, Mar. 21, 1943. Div. 6-554-M19
11. *Development of Magnetostriction Hydrophones, July 1, 1942-Apr. 1, 1943 (Progress Report)*, Arthur L. Thuras, NDRC 6.1-sr20-639, Report G12/158, CUDWR-NLL [1943]. Div. 6-612.62-M6
12. *Notes and Observations from Lecture by Arthur L. Thuras at New London, March 24, 1943*, Francis P. Bundy, M 01.213-34, HUSL, Apr. 3, 1943. Div. 6-612.62-M7
13. *Information on B-27A Nos. 1 and 2, 39-kc Ni[ckel] Ring Stack Transducer*, Francis P. Bundy, M 01.223-24, HUSL, May 12, 1943. Div. 6-612.61-M1

CONFIDENTIAL

14. *Tests on Small Straight Magnetostriction Hydrophones Constructed with Electroformed Shells* (Memorandum for File), Robert R. MacLaughlin, Report D16/315, CUDWR-NLL, May 18, 1943. Div. 6-612.62-M8
15. *Type Tests on AN/CRT-1 Units, Second Group* (Memorandum for File), Henry M. Jasper, Jr., Report D16/376, NS-106, CUDWR-NLL, May 19, 1943. Div. 6-612.62-M9
16. *Characteristics of B-19B SGM Transducer*, Francis P. Bundy, M 02.331.7-24, HUSL, June 7, 1943. Div. 6-612.611-M1
17. *Straight Toroidally Wound Magnetostriction Hydrophone, TMS-53*, James W. Follin, Jr., Report G12/394, CUDWR-NLL, June 8, 1943. Div. 6-612.62-M10
18. *Portable SGM Transducers*, Francis P. Bundy, M 02.331.7-26, HUSL, June 10, 1943. Div. 6-612.611-M2
19. *Sensitivity of B-19B SGM Transducer*, Francis P. Bundy, M 02.331.7-28, HUSL, June 15, 1943. Div. 6-612.611-M3
20. *Orlando Calibration of Proposed Mark 24 Mine Microphone*, Lyman N. Miller, M 61.2165-319, HUSL, June 17, 1943. Div. 6-612.55-M3
21. *Tests on Small Hydrophones, for ERSB, Submitted by Aircraft Radio Laboratory* (Memorandum for File), Robert R. MacLaughlin, Report D16/433, NS-106, CUDWR-NLL, July 16, 1943. Div. 6-612.62-M11
22. *Reduction of Eddy Currents in Magnetostrictive Tubes*, Malcolm H. Hebb, M 01.213-62, HUSL, July 24, 1943. Div. 6-612.8-M4
23. *Suggestions on Procedures for Testing SGM Transducers as They Proceed through the Production Line*, Francis P. Bundy, M 02.331.37-9, HUSL, July 29, 1943. Div. 6-612.611-M4
24. *Proposed Changes in D16 Mark IV-E Hydrophones* (Memorandum for File), Robert R. MacLaughlin, Report D16/467, CUDWR-NLL, Aug. 3, 1943. Div. 6-612.62-M13
25. *Tests on Hydrophones with Shells Specially Heat Treated by C. G. Conn, Ltd.*, Robert R. MacLaughlin, Report D16/473, NS-102, CUDWR-NLL, Aug. 11, 1943. Div. 6-612.41-M5
26. *Criticism of MOX and MKX Magnetostrictive Hydrophones*, Lyman N. Miller, M 61.036-372, HUSL, Aug. 19, 1943. Div. 6-612.63-M3
27. *Theoretical Directivity Characteristics for Line Hydrophones*, Wilbur T. Harris, Report G12/450, CUDWR-NLL, Aug. 26, 1943. Div. 6-612.21-M6
28. *Bell Telephone Laboratories' Magnetostrictive Brainstorm, Type MKX*, Frederick V. Hunt, M 01.223-42, HUSL, Aug. 30, 1943. Div. 6-612.63-M4
29. *Tests on Twenty ERSB Hydrophones* (Memorandum for File), Edward Gerjuoy, Robert R. MacLaughlin, Report D16/496, CUDWR-NLL, Sept. 3, 1943. Div. 6-612.62-M14
30. *Heat Treatment of Nickel*, Robert R. MacLaughlin, Report G12/530, CUDWR-NLL, Sept. 14, 1943. Div. 6-612.41-M7
31. *Tests of the First of Harvey Radio Laboratories' B-19B Transducer*, Francis P. Bundy, M 02.331.37-27, HUSL, Sept. 28, 1943. Div. 6-612.611-M5
32. *Methods of Constructing Layer-Built Magnetostrictive Tubes to Be Used as Radial Oscillators*, Francis P. Bundy, M 01.213-85, HUSL, Sept. 30, 1943. Div. 6-612.62-M15
33. *Tests on Ten Series C ERSB Hydrophones* (Memorandum), Edward Gerjuoy, Robert R. MacLaughlin, Report D16/536, CUDWR-NLL, Oct. 1, 1943. Div. 6-612.62-M16
34. *Notes on Painting JP-1 Hydrophones*, Frank M. Goyan, Report D24/539, CUDWR-NLL, Oct. 6, 1943. Div. 6-612.44-M4
35. *Performance Tests on SGM Monitor Model 50, Serial No. 2, with B-19B No. 26 Hydrophone*, Paul E. Sabine, M 02.331.7-35, HUSL, Oct. 7, 1943. Div. 6-612.611-M6
36. *Results of Tests on Cyclewelded 20 ke Ring Stack*, Francis P. Bundy, M 01.213-96, HUSL, Oct. 14, 1943. Div. 6-612.61-M2
37. *Measurements of Three-Foot Straight Wood Core Hydrophone, D546-6 and D546-7*, Edward Gerjuoy, Frank M. Goyan, Report G12/547, CUDWR-NLL, Oct. 15, 1943. Div. 6-612.62-M18
38. *Measurements of 5-In[eh] Toroidally Wound Magnetostriction Hydrophones, Evaluation of Annealing of Nickel*, Edward Gerjuoy, Wilbur T. Harris, Report D16/555, CUDWR-NLL, Oct. 19, 1943. Div. 6-612.41-M8
39. *Measurements of 5-Inch Toroidally Wound Magnetostriction Hydrophones*, Edward Gerjuoy, Report D16/557, CUDWR-NLL, Oct. 20, 1943. Div. 6-612.55-M5
40. *Tests of the Large 4-Segment 20-ke Ring Stack*, Francis P. Bundy, M 01.213-98, HUSL, Oct. 21, 1943. Div. 6-612.61-M3
41. *VIR Teardrop Transducer for Installed Sound Gear Monitor*, Francis P. Bundy, M 02.331-83, HUSL, Oct. 22, 1943. Div. 6-612.611-M7
42. *Permanent Magnet Polarization of Laminated Ring Stacks*, Francis P. Bundy, M 01.213-100, HUSL, Oct. 25, 1943. Div. 6-612.1-M6
43. *Sea Tests of JP-1 Hydrophone*, A. L. Thuras, Ralph C. Maninger, Hector F. Bernier, Report G12/581, CUDWR-NLL, Nov. 1, 1943. Div. 6-612.55-M6
44. *Measurements of JP Hydrophones*, Edward Gerjuoy, Report G12/597, CUDWR-NLL, Nov. 8, 1943. Div. 6-612.55-M7
45. *Performance of the 5", 20-ke, Oxide Annealed Ring-Stacks, 20 ARS-2*, Francis P. Bundy, M 01.213-110, HUSL, Nov. 8, 1943. Div. 6-612.41-M10
46. *Performance of the 5" 20-ke Hardened Nickel Ring Stack, 20 HRS-1*, Jack C. Cotton, Francis P. Bundy, M 01.-213-112, HUSL, Nov. 17, 1943. Div. 6-612.41-M11
47. *Measurements on 1/4" 20-ke Ring Stack*, James W. Follin, Jr., M 01.213-115, HUSL, Nov. 20, 1943. Div. 6-612.61-M4
48. *Performance of the 60 ke Ring Stacks H-9 and H-10, Individually and in Combination*, Jack C. Cotton, Francis P. Bundy, M 01.213-114, HUSL, Nov. 23, 1943. Div. 6-612.61-M5
49. *JP-1 Hydrophone Vibration Measurement*, Arthur L. Thuras, Hector F. Bernier, Report G12/620, NS-113, CUDWR-NLL, Nov. 23, 1943. Div. 6-612.55-M8
50. *Ring Stacks, Response of Arrays of*, Frederick V. Hunt, M 01.213-119, HUSL, Nov. 29, 1943. Div. 6-612.61-M6

51. *Performance of the 60-ARS-1 and -2 Ring Stacks*, Jack C. Cotton, Francis P. Bundy, M 01.213-121, HUSL, Dec. 1, 1943. Div. 6-612.61-M7
52. *Hard Nickel Laminated Transducers as Powerful Underwater Sound Projectors*, Francis P. Bundy, Roland E. Mueser, M 01.213-123, HUSL, Dec. 3, 1943. Div. 6-612.41-M12
53. *Advantages of Increased Hydrophone Length to Sonic Listening*, Arthur L. Thuras, Report G12/631, NS-113, CUDWR-NLL, Dec. 6, 1943. Div. 6-612.21-M9
54. *Performance of the JP Baffle at Supersonic Frequencies*, Edward Gerjuoy, Report G12/643, CUDWR-NLL, Dec. 11, 1943. Div. 6-612.62-M19
55. *Measurements of Two JP-1 Hydrophones with NL-105 No. 4 Amplifier*, Edward Gerjuoy, Report G12/664, CUDWR-NLL, Dec. 27, 1943. Div. 6-612.55-M9
56. *Improved Preamplifier Mounting for OAY S. L. Meter Hydrophone* (Memorandum for File), Garland W. Areher, Report P35/679, NO-163, CUDWR-NLL, Jan. 11, 1944. Div. 6-612.62-M20
57. *Measurements of Two-Section Three-Foot Hydrophones*, Edward Gerjuoy, Report G12/683, CUDWR-NLL, Jan. 11, 1944. Div. 6-612.55-M10
58. *Data on B-19B Hydrophones*, Paul E. Sabine, M 01.213-136, HUSL, Jan. 14, 1944. Div. 6-612.611-M8
59. *The Complete Magnetizing of a 3-Foot Toroidally Wound Magnetostriction Hydrophone*, Wilbur T. Harris, Edward Gerjuoy, Report G12/691, NS-139, CUDWR-NLL, Jan. 14, 1944. Div. 6-612.62-M21
60. *Performance Characteristics of a Plastic-Covered Toroidally Wound Hydrophone and Baffle Assembly*, Wilbur T. Harris, Report G12/708, NS-139, CUDWR-NLL, Jan. 19, 1944. Div. 6-612.44-M6
61. *The B-19G, No. 1 Transducer*, G. W. Renner, M 01.213-139, HUSL, Jan. 24, 1944. Div. 6-612.612-M1
62. *Installed SGM Transducer, B-19D, No. 4 in VIR Tear-drop Shell*, Francis P. Bundy, Jack C. Cotton, M 02.331-105, HUSL, Jan. 28, 1944. Div. 6-612.612-M2
63. *Tests on 22 B-19B Hydrophones Made by Harvey Radio Laboratories*, Paul E. Sabine, M 02.331.37-44, HUSL, Jan. 29, 1944. Div. 6-612.611-M9
64. *The Complete Magnetization of the JP-1 Hydrophone* (Memorandum for File), Edward Gerjuoy, Report D24 G12/727, NS-113 and NS-139, CUDWR-NLL, Jan. 31, 1944. Div. 6-612.55-M11
65. *Effect of Depth and Depth Charges on a B-19B Hydrophone*, Paul E. Sabine, M 01.213-151, HUSL, Feb. 15, 1944. Div. 6-612.611-M10
66. *Monitor Transducer Failures*, Fred H. Smith, M 02.331-116, HUSL, Feb. 15, 1944. Div. 6-612.611-M11
67. *Special Hydrophones for Range and Bearing Studies*, Wilbur T. Harris, Report G12/746, NS-139, CUDWR-NLL, Feb. 15, 1944. Div. 6-612.55-M12
68. *Construction and Performance of Echo-Repeater Pair, 1" Hard Nickel and 2" Annealed Nickel Ring Stacks*, Jack C. Cotton, Francis P. Bundy, M 01.236-81, HUSL, Feb. 17, 1944. Div. 6-612.41-M14
69. *Methods of Obtaining Band-Pass Characteristics with Magnetostriction Transducers*, James W. Follin, Jr., M 01.213-155, HUSL, Feb. 17, 1944. Div. 6-612.34-M2
70. *The B-19H Transducers*, J. R. Reitz, M 01.223-74, HUSL, Feb. 21, 1944. Div. 6-612.613-M1
71. *Retest of 6 B-19B Hydrophones from Harvey Radio after Recannealing the Shells*, Paul E. Sabine, M 02.331.37-55, HUSL, Feb. 24, 1944. Div. 6-612.41-M15
72. *Annealing of JP-1 Straight Wood Core Hydrophone*, Heeter F. Bernier, Report G12/753, NS-139 and NS-113, CUDWR-NLL, Feb. 26, 1944. Div. 6-612.41-M16
73. *Field and Frequency Response Sheet for B-19B, No. 18 Standard, Simplified Conversion Procedure*, Jack C. Cotton, M 01.213-165, HUSL, Feb. 29, 1944. Div. 6-612.611-M12
74. *Plastic Molding Materials for Transducers as Developed at New London Laboratory*, Francis P. Bundy, M 01.-223-81, HUSL, Mar. 6, 1944. Div. 6-612.44-M7
75. *Temperature Variation in Sensitivity of B-19B Hydrophones*, Paul E. Sabine, M 02-331.37-58, HUSL, Mar. 6, 1944. Div. 6-612.611-M13
76. *Two Thimble Hydrophones*, Wilbur T. Harris, Report G12/779, NS-102, CUDWR-NLL, Mar. 6, 1944. Div. 6-612.6-M1
77. *Tests on Lucite-Impregnated 60-Kc Ring Stacks*, Jack C. Cotton, Francis P. Bundy, M 01.213-174, HUSL, Mar. 11, 1944. Div. 6-612.61-M8
78. *Depth Charge Tests on Hydrophones, Effect of Annealing on Performance* (Memorandum for File), Wilbur T. Harris, Phillip B. Edwards, Robert R. MacLaughlin, Report G12/754, NS-139, CUDWR-NLL, Mar. 14, 1944. Div. 6-612.55-M13
79. *A Comparison of Some Possible Materials for Use in JP-1 Baffles*, Wilbur T. Harris, David W. Van Lennep, Robert R. MacLaughlin, Report G12/805, NS-113, CUDWR-NLL, Mar. 15, 1944. Div. 6-612.55-M13
80. *Installed SGM Transducer B-19H in VIR Pit Log Strut Extension*, J. R. Reitz, M 02.331-138, HUSL, Mar. 16, 1944. Div. 6-612.613-M2
81. *Effect of Tape Ties upon the Acoustic Functioning of the M7 CRT-1A Hydrophone* (Memorandum for File), Robert R. MacLaughlin, David W. Van Lennep, Henry Suter, Report D16/798, NS-106, CUDWR-NLL, Mar. 20, 1944. Div. 6-612.62-M22
82. *Effect of Shell Painting upon the Acoustic Functioning of the M7 CRT-1A Hydrophone* (Memorandum for File), Robert R. MacLaughlin, David W. Van Lennep, Report D16/799, NS-106, CUDWR-NLL, Mar. 20, 1944. Div. 6-612.51-M8
83. *Permanent Magnet Core Blastphone*, Arthur L. Thuras, Report G12/853, CUDWR-NLL, Apr. 6, 1944. Div. 6-612.62-M23
84. *General Purpose Nondirectional Sonic Magnetostriction Hydrophones*, Wilbur T. Harris, David W. Van Lennep, Phillip B. Edwards, Report G12/852, CUDWR-NLL, Apr. 10, 1944. Div. 6-612.62-M24
85. *A Permanent Magnet Magnetostriction Hydrophone Construction*, Wilbur T. Harris, David W. Van Lennep, Report G12/858, CUDWR-NLL, Apr. 12, 1944. Div. 6-612.62-M25
86. *The B-19H Transducers* [Memorandum] II, J. R. Reitz, M 01.223-186, HUSL, Apr. 13, 1944. Div. 6-612.613-M3

87. *Effect of Hanging Weights from the Bottom of Monitor Transducers*, J. R. Reitz, M 02.331.7-73, HUSL, Apr. 17, 1944. Div. 6-612.613-M4
88. *Scroll Stack Transducer, April 18, 1944*, John D. Lane, M 01.213-189, HUSL, Apr. 19, 1944. Div. 6-612.63-M5
89. *Magnetostriction Buzzer Listening Hydrophone*, R. W. Marsh, M 60.064-677, HUSL, Apr. 19, 1944. Div. 6-612.611-M14
90. *Visit to New London, April 19 [1944], Plastic Potting*, Alan H. Selker, M 110.10-128, HUSL, Apr. 20, 1944. Div. 6-612.44-M8
91. *Self-Polarized Ring Stacks*, Francis P. Bundy, G. W. Renner, M 01.213-194, HUSL, May 9, 1944. Div. 6-612.61-M9
92. *Measurements on Two B-19B Hydrophones to Be Used as Secondary Standard for Production Tests on OAX-1 Monitors by Harvey Radio Corporation*, Paul E. Sabine, M 02.331.37-65, HUSL, May 11, 1944. Div. 6-612.611-M15
93. *The B-19H Expanded Range Monitor*, J. R. Reitz, M 02.331-168, HUSL, May 12, 1944. Div. 6-612.613-M5
94. *Tests on Two Plastic-Covered, Three-Foot Straight Toroidally Wound Hydrophones*, David W. Van Lennep, Report G12/915, NS-139, CUDWR-NLL, May 12, 1944. Div. 6-612.44-M9
95. *Effect of Annealing on the Magnetic Properties of Nickel Tubing* (Memorandum for File), Arthur L. Thuras, James W. Follin, Jr., Report G12/928, CUDWR-NLL, May 16, 1944. Div. 6-612.41-M19
96. *The Hydrophone II-115*, Wilbur T. Harris, David W. Van Lennep, Report G12/929, CUDWR-NLL, May 19, 1944. Div. 6-612.62-M26
97. *Midget Element Magnetostriction Hydrophones*, Wilbur T. Harris, Phillip B. Edwards, David W. Van Lennep, Report G12/889, CUDWR-NLL, May 23, 1944. Div. 6-612.6-M2
98. *Construction and Performance of 60-kc Echo Repeater Transducer, Pair No. 3*, Francis P. Bundy, Milton R. Carlson, M 91.236-106, HUSL, May 24, 1944. Div. 6-612.61-M10
99. *Sensitivity and Pattern Measurements on Five Monitor Hydrophones Submitted by Presto Recording Corporation*, Paul E. Sabine, M 02.331.37-73, HUSL, June 8, 1944. Div. 6-612.611-M16
100. *Elimination of Side-Lobe Interference in the RLI, Part I Theoretic* (Memorandum for File), James W. Follin, Jr., Report G12/947, CUDWR-NLL, June 8, 1944. Div. 6-612.21-M17
101. *Comparative Tests on 3-ft, 4-ft, and 5-ft Hydrophones*, Ralph C. Maninger, Report P33/949, CUDWR-NLL, June 12, 1944. Div. 6-612.62-M27
102. *Procedure for Assembly of B-19H Expanded Range Monitor Hydrophones*, J. R. Reitz, M 02.331.2-59, HUSL, June 13, 1944. Div. 6-612.613-M6
103. *The Straight Toroidally Wound Plastic Covered Magnetostriction Hydrophone* (Interim Report), Wilbur T. Harris, NDRC 6.1-sr1128-1573, Report G12/804, CUDWR-NLL, June 15, 1944. Div. 6-612.62-M28
104. *Scroll Transducer Project*, John D. Lane, M 01.223-102, HUSL, June 17, 1944. Div. 6-612.63-M6
105. *Testing of B-19B Transducers at Presto Recording Corporation*, Francis P. Bundy, M 02.331.37-79, HUSL, June 28, 1944. Div. 6-612.611-M17
106. *Tubular MS Transducer Consisting of Helix of Fine Nickel Tubing*, Nelson M. Blahelman, Malcolm H. Hebb, M 01.223-104, HUSL, July 1, 1944. Div. 6-612.62-M29
107. *Elimination of Longitudinal Resonance in the Straight Magnetostriction Hydrophone* (Memorandum for File), Heeter F. Bernier, Report G12/1014, CUDWR-NLL, July 7, 1944. Div. 6-612.62-M30
108. *Preliminary Specification for the NL-124 Hydrophone of the D55 Sonar System*, Report D55/966, CUDWR-NLL, July 21, 1944. Div. 6-612.62-M31
109. *Comparison of HUSL and Presto Pattern and Sensitivity Measurements on Presto Hydrophones*, Paul E. Sabine, M 02.331.37-90, HUSL, July 24, 1944. Div. 6-612.611-M18
110. *Construction of B-19H Transducers in the Transducer Shop*, J. R. Reitz, M 02.331.2-63, HUSL, Aug. 1, 1944. Div. 6-612.613-M7
111. *Use of B-19H Hydrophones as Projectors*, Frederiek V. Hunt, M 02.331.7-89, HUSL, Aug. 9, 1944. Div. 6-612.613-M10
112. *Recalibration of B-19F Hydrophone*, Paul E. Sabine, M 01.213-219, HUSL, Aug. 11, 1944. Div. 6-612.612-M3
113. *The Modified Baffle for Topside Straight Hydrophones* (Memorandum for File), James W. Follin, Jr., Report G12/1010, CUDWR-NLL, Aug. 12, 1944. Div. 6-612.62-M32
114. *Plastic Casting of Ring-Stack Transducers*, G. W. Renner, Alan H. Selker, M 113.5-162, HUSL, Aug. 29, 1944. Div. 6-612.61-M11
115. *Tests on Six NL-130 Hydrophones*, David W. Van Lennep, Report D50/1110, NS-238, CUDWR-NLL, Sept. 4, 1944. Div. 6-612.62-M33
116. *Measurements on New London Permanent Magnet Hydrophone, II-192*, Paul E. Sabine, Lou Fein, M 01.213-223, HUSL, Sept. 7, 1944. Div. 6-612.62-M34
117. *A 12"×12" Square Magnetostriction Transducer*, Wilbur T. Harris, Phillip B. Edwards, David W. Van Lennep, Report G12/1171, CUDWR-NLL, Sept. 7, 1944. Div. 6-612.8-M15
118. *Five-Foot Split JP-1 Type Permanent Magnet Hydrophone, TMS-97*, Arthur L. Thuras, Report G12/1125, CUDWR-NLL, Sept. 14, 1944. Div. 6-612.62-M35
119. *Operation of Topside Sonic Gear on USS Blueback*, Arthur L. Thuras, Report G12/1127, CUDWR-NLL, Sept. 18, 1944. Div. 6-612.62-M36
120. *Magnetostriction Hydrophone Design*, Arthur L. Thuras, Report G12/1137, CUDWR-NLL, Sept. 21, 1944. Div. 6-612.62-M37
121. *[The] 24.5-kc Spherical Source No. 3, Delivered September 22, 1944*, G. W. Renner, M 01.213-234, HUSL, Sept. 22, 1944. Div. 6-612.61-M13
122. *Control of Pattern of a Radially Vibrating Transducer*, Paul E. Sabine, M 01.213-235, HUSL, Sept. 22, 1944. Div. 6-612.61-M12
123. *Graphical Evaluation of the Effect on RLI Accuracy of an Interfering Signal and a Study of the Relative Merits of the Two-Section, 5-Foot Hydrophone vs the Ten-Section, P.M., 5-Foot Lobe Reduction Hydrophone from an Interference*

- View Point, Frontal Lobe Section Only*, Frederick C. Reed, Jr., Report D55 1144, NS-113, CUDWR-NLL, Sept. 22, 1944. Div. 6-612.5-M1
124. *High-Pressure Water Test on Plastic Cast Transducer*, G. W. Renner, Alan H. Selker, M 113.5-166, HUSL, Oct. 2, 1944. Div. 6-612.44-M12
125. *Tests of an Improved JP-1 Type Hydrophone on the USS Blueback* (Memorandum for File), Arthur L. Thuras, Report P33/1161, NS-113, CUDWR-NLL, Oct. 3, 1944. Div. 6-612.62-M38
126. *The 2 V Permendur Hydrophones*, Wilbur T. Harris, David W. Van Lennep, Paul B. Edwards, Report G12-1168, NS-102, CUDWR-NLL, Oct. 6, 1944. Div. 6-612.8-M16
127. *Funnel Transducers*, Wilbur T. Harris, David W. Van Lennep, Report G27 1166, CUDWR-NLL, Oct. 6, 1944. Div. 6-612.8-M17
128. [The] *24.5-kc Spherical Source No. 4, Delivered October 6, 1944*, G. W. Renner, M 01.213-246, HUSL, Oct. 9, 1944. Div. 6-612.61-M14
129. [The] *60-kc 2 VP-1, [No.] 1 [Ring Stack]*, G. W. Renner, M 01.213-263, HUSL, Oct. 24, 1944. Div. 6-612.61-M15
130. [The] *24.5-kc Spherical Source Transducers, Nos. 5 and 6*, G. W. Renner, M 01.213-270, HUSL, Oct. 27, 1944. Div. 6-612.61-M16
131. *The B-19H Standard Transducers, Production Tests*, J. R. Reitz, M 01.213-274, HUSL, Oct. 31, 1944. Div. 6-612.613-M11
132. *Acoustical Measurements on B-19B, No. 123*, Paul E. Sabine, M 01.213-275, HUSL, Oct. 31, 1944. Div. 6-612.611-M21
133. *Tests on Thin-Walled 2 V Permendur 60-kc Ring Stack*, Francis P. Bundy, M 01.213-278, HUSL, Nov. 2, 1944. Div. 6-612.61-M18
134. [The] *26-kc Projectors for Aide de Camp*, G. W. Renner, M 02.45-228, HUSL, Nov. 2, 1944. Div. 6-612.61-M17
135. *Directivity at Low Sonic Frequencies* (Memorandum for File), Walter F. Graham, Ralph C. Maninger, Report P33 1067, CUDWR-NLL, Nov. 8, 1944. Div. 6-612.21-M21
136. *Test Equipment and Methods for Relative Permeability Measurements on Nickel Tubing* (Memorandum for File), Robert R. MacLaughlin, Report G12/1230, NS-102, CUDWR-NLL, Nov. 10, 1944. Div. 6-612.8-M18
137. [The] *60-kc 2 VP-1, [No.] 2 [Ring Stack]*, G. W. Renner, M 01.213-281, HUSL, Nov. 16, 1944. Div. 6-612.61-M19
138. *Tests on Two COG 51053, JP-1, Hydrophones in NL-109 Baffles Removed from USS Sargo and USS Gabilan*, David W. Van Lennep, Wilbur T. Harris, Report D24 1243, CUDWR-NLL, Nov. 17, 1944. Div. 6-612.62-M39
139. [The] *60 ARS [No.] 10 [Ring Stack]*, G. W. Renner, M 01.213-284, HUSL, Nov. 20, 1944. Div. 6-612.61-M20
140. *Improvement in Submarine Sonic Listening and Bearing Accuracy*, Arthur L. Thuras, Report G12/1251, NS-102, CUDWR-NLL, Nov. 21, 1944. Div. 6-612.21-M23
141. *Directivity Patterns of a Delobed Hydrophone for Various Octave Bands* (Memorandum for File), Jordan J. Markham, Report G12 1254, NS-102, CUDWR-NLL, Nov. 27, 1944. Div. 6-612.21-M24
142. *The B-19J Hydrophones*, J. R. Reitz, M 01.223-120, HUSL, Nov. 29, 1944. Div. 6-612.614-M1
143. [The] *60-kc 2 VP Spherical Source [No.] 1 [Ring Stack]*, G. W. Renner, M 01.213-290, HUSL, Dec. 5, 1944. Div. 6-612.61-M21
144. *Sensitivity of B-19K, No. 1*, Lou Fein, M 01.213-293, HUSL, Dec. 8, 1944. Div. 6-612.615-M2
145. *Tests on NL-124 Hydrophones Manufactured by Astatic Corporation*, David W. Van Lennep, Wilbur T. Harris, Report G12/1284, NS-102, CUDWR-NLL, Dec. 15, 1944. Div. 6-612.62-M40
146. *Hydrophone Specification for X-OCP Monitors*, J. R. Reitz, M 02.331.7-118, HUSL, Dec. 18, 1944. Div. 6-612.613-M12
147. *Use of Filament Heater for Soldering and Design of New Soldering Jig for B-19H*, J. R. Reitz, Alan H. Selker, M 110.1-169, HUSL, Dec. 19, 1944. Div. 6-612.613-M13
148. *A Permanent Magnet Magnetostriction Hydrophone Construction* (Completion Report), Wilbur T. Harris, NDRC 6.1-sr1128-1921, Report G12 1248, NS-102, CUDWR-NLL, Dec. 20, 1944. Div. 6-612.62-M41
149. *Low Frequency Thin-Walled 2 VP Ring Stacks*, G. W. Renner, M 01.213-298, HUSL, Jan. 18, 1945. Div. 6-612.61-M22
150. *The B-19K Hydrophone for Low-Frequency Monitoring*, J. R. Reitz, M 01.223-127, HUSL, Jan. 26, 1945. Div. 6-612.615-M3
151. [The] *60-Kc 2 VP Spherical Source [No.] 3 [Ring Stack]*, G. W. Renner, M 01.213-300, HUSL, Feb. 2, 1945. Div. 6-612.61-M23
152. *The JP Overside and Through-the-Hull Directive Sonic Listening Equipment for Small Patrol Craft*, Russell O. Hanson, Edwin E. Teal, OSRD 4744, NDRC 6.1-sr1128-1928, Report D22 D38 1310, CUDWR-NLL, Feb. 7, 1945. Div. 6-622.2-M5
153. *An Experimental Streamlined Baffle for Two Hydrophones*, Wilbur T. Harris, David W. Van Lennep, Report G12/1327, NS-102, CUDWR-NLL, Feb. 9, 1945. Div. 6-612.62-M42
154. *Permanent Magnet Sonic Projectors*, Wilbur T. Harris, Phillip B. Edwards, David W. Van Lennep, Report G27/-1353, NS-102, CUDWR-NLL, Feb. 11, 1945. Div. 6-612.62-M43
155. *Pit-Log Strut Hydrophone, Conclusions and Recommendations*, J. R. Reitz, M 02.331-209, HUSL, Feb. 21, 1945. Div. 6-612.613-M14
156. *A New and Fitting Design for NL-124 and NL-130 Hydrophones*, Wilbur T. Harris, Phillip B. Edwards, Report G12/1373, NS-102, CUDWR-NLL, Feb. 24, 1945. Div. 6-612.62-M44
157. [The] *24.5-Kc No. 2 V Permendur Spherical Source Transducer [No.] 7 [Ring Stack]*, G. W. Renner, M 01.213-306, HUSL, Feb. 26, 1945. Div. 6-612.61-M24
158. [The] *24.5-kc 2 VP Spherical Source [No.] 8 [Ring Stack]*, G. W. Renner, M 01.213-310, HUSL, Feb. 28, 1945. Div. 6-612.61-M25
159. *Tests on Beeper Listening Hydrophones*, Paul E. Sabine, M 60.264-1160, HUSL, Feb. 28, 1945. Div. 6-612.611-M23

160. [The] 60 kc 2 VP Spherical Source [No.] 2 [Ring Stack], G. W. Renner, M 01.213-316, HUSL, Mar. 21, 1945.
Div. 6-612.61-M26
161. The B-19H Hydrophone Specifications, J. R. Reitz, M 02.331.3-117, HUSL, Apr. 5, 1945.
Div. 6-612.613-M15
162. High-Pressure Test of Three B-19H Hydrophones, J. R. Reitz, M 01.213-320, HUSL, Apr. 9, 1945.
Div. 6-612.613-M16
163. Sound Attenuation in Coating Materials, Alan H. Selker, G. W. Renner, M 01.21-128, HUSL, Apr. 9, 1945.
Div. 6-612.43-M16
164. Plastic Cast 2 VP Ring Stack, Projector for 25.5-Kc Use, G. W. Renner, M 01.213-323, HUSL, Apr. 10, 1945.
Div. 6-612.61-M27
165. Oil Filling of Transducers, Alan H. Selker, M 01.213-324, HUSL, Apr. 10, 1945.
Div. 6-612.44-M13
166. [The] 24.5 kc 2 VP Spherical Source, Nos. 9 and 10 [Ring Stacks], G. W. Renner, M 01.213-326, HUSL, Apr. 16, 1945.
Div. 6-612.61-M28
167. Test on Beeper Listening Hydrophones, Paul E. Sabine, M 60.264-1285, HUSL, Apr. 20, 1945.
Div. 6-612.611-M24
168. Underwater Sonic Loudspeaker, Arthur L. Thuras, NDRC 6.1-sr1128-1936, Report G13/1352, NS-182, CUDWR-NLL, Apr. 24, 1945.
Div. 6-612.62-M45
169. Experiment in Alteration of the Baffle of a B-19L Beeper Listening Hydrophone, Francis P. Bundy, M 60.264-1317, HUSL, May 4, 1945.
Div. 6-612.616-M1
170. Transducer Construction in the Low-Frequency Self-Contained Echo Repeater, Model II, Milton R. Carlson, M 91.236-238, HUSL, May 5, 1945.
Div. 6-612.61-M29
171. High-Pressure Tests on B-19H Hydrophones, Paul E. Sabine, M 01.213-330, HUSL, May 9, 1945.
Div. 6-612.613-M17
172. The Directional Radio Sona Buoy, NDRC 6.1-sr1128-2224, Report D34/1200, NS-106 and NS-198, OSRD 5279, CUDWR-NLL, May 20, 1945.
Div. 6-624.2-M7
173. Results of Tests on Eleven David Bogen OBY Hydrophones, J. R. Reitz, M 02.331.7-137, HUSL, May 25, 1945.
Div. 6-612.613-M18
174. Transducer Research and Production at the New London Laboratory, William B. Snow, James W. Follin, Jr., Wilbur T. Harris, NDRC 6.1-sr1128-2212, Report G12/-1418, NS-113, CUDWR-NLL, May 25, 1945.
Div. 6-612.1-M8
175. Transducer Research and Production at the New London Laboratory, William B. Snow, James W. Follin, Jr., Wilbur T. Harris, NDRC 6.1-sr1128-2212, Report G12/-1418, NS-113, CUDWR-NLL, May 25, 1945.
Div. 6-612.1-M8
176. Some Applications of Organic Plastics and Rubber in Underwater Sound Apparatus, Alan H. Selker, M 113.5-191, HUSL, May 26, 1945.
Div. 6-612.43-M17
177. Recent Tests on B-19J Hydrophones, J. R. Reitz, M 01.-223-133, HUSL, June 8, 1945.
Div. 6-612.614-M2
178. The 40PR No. 1, J. R. Reitz, Roland E. Mueser, M 69.-016-29, HUSL, Aug. 14, 1945.
Div. 6-612.6-M3
179. The 40PR No. 2, Esplanadephone, J. R. Reitz, Roland E. Mueser, M 69.016-33, HUSL, Aug. 20, 1945.
Div. 6-612.6-M5
180. Future Work in the PR Field, J. R. Reitz, Roland E. Mueser, M 69.016-34, HUSL, Aug. 20, 1945.
Div. 6-612.6-M4
181. Sound Gear Monitor, Underwater Sound Portable Test Equipment (Completion Report), NDRC 6.1-sr287-2086, HUSL, Nov. 1, 1945, pp. 106-107.
Div. 6-641.1-M9
182. Testing Specification for Toroidal Hydrophone, Report D22.6/3615, CUDWR-NLL.
Div. 6-612.62-M46
183. MOX and MKX Magnetostriction Hydrophones [R. L. Peek], Report 2210-RLP-MS, BTL, June 10, 1943.
Div. 6-612.63-M2
184. Non-Directional Magnetostriction Transducer, W. H. Martin, NDRC 6.1-sr1097-1328, BTL, Feb. 1, 1945.
Div. 6-554.2-M18
185. Task No. 4A, Broad Band Magnetostriction Projector (Final Report), U. S. Navy BuShips, Contract NX sr-26932, BTL, June 25, 1945.

Chapter 7

1. Laminated Stack Transducer, O. Hugo Schuck, M 01.-223-5, HUSL, Sept. 2, 1942.
Div. 6-612.71-M1
2. Tests Suggested for Midget Asymmetrical Stack, O. Hugo Schuck, M 01.213-5, HUSL, Sept. 19, 1942.
Div. 6-612.716-M1
3. Laminated Projectors, Frederick V. Hunt, M 01.223-7, HUSL, Nov. 10, 1942.
Div. 6-612.71-M2
4. Winding for 9×9 Asymmetrical Laminated Stack, O. Hugo Schuck, M 01.223-10, HUSL, Dec. 5, 1942.
Div. 6-612.71-M3
5. The 9"×9" Tests to Be Made at Barge: Patterns, Frequency Response [and] Absolute Calibration, Robert L. Cumberow, M 01.213-27, HUSL, Jan. 21, 1943.
Div. 6-612.71-M4
6. Completing of Mark II, 9"×9" Asymmetrical Stack of 0.005" Ni[ckel] Punchings, Francis P. Bundy, M 01.-223-13, HUSL, Jan. 26, 1943.
Div. 6-612.71-M5
7. Classification of Stereophones, Lyman N. Miller, M 01.-223-15, HUSL, Feb. 3, 1943.
Div. 6-612.716-M2
8. Efficiency Measurements of the Mark I Hugophone, Paul E. Sabine, M 01.213-30, HUSL, Feb. 4, 1943.
Div. 6-612.71-M6
9. Properties and Uses of Alnico Magnets, Kenneth N. Fromm, Francis P. Bundy, M 01.213-35, HUSL, Apr. 23, 1943.
Div. 6-612.42-M1
10. Information on the Mark I, 9"×9" Asymmetric Laminated Stack Hydrophone, Leon W. Camp, Francis P. Bundy, Paul E. Sabine, M 01.223-25, HUSL, May 29, 1943.
Div. 6-612.71-M8
11. The ρ c Rubber, Francis P. Bundy, M 113.50-25, HUSL, June 10, 1943.
Div. 6-612.43-M1
12. Winding and Circuit Diagram of the 9"×9" Asymmetric Stack, Mark II Hydrophone, Leon W. Camp, M 01.-223-29, HUSL, June 10, 1943.
Div. 6-612.71-M9

CONFIDENTIAL

13. *Harmonic Operation of Standard Projectors*, Frederick V. Hunt, M 01.12-30, HUSL, June 23, 1943.
Div. 6-612.23-M1
14. *Transducer Cable Shield with Conducting Rubber*, H. R. Stewart, M 113-52, HUSL, July 13, 1943.
Div. 6-612.43-M2
15. *Transducer Diaphragms*, Fred H. Smith, M 01.221-22, HUSL, July 14, 1943.
Div. 6-612.8-M3
16. *Criticism of MOX and MKX Magnetostrictive Hydrophones*, Lyman N. Miller, M 61.036-372, HUSL, Aug. 19, 1943.
Div. 6-612.63-M3
17. *Sonar, Test and Analysis of Laminated Transducer Element*, James W. Follin, Jr., Robert A. Payne, Malcolm H. Hebb, M 02.45-87, HUSL, Sept. 17, 1943.
Div. 6-612.71-M12
18. *Cycleweld*, Francis P. Bundy, M 110.10-37, HUSL, Sept. 18, 1943.
Div. 6-612.44-M2
19. *The 1"×1½" Nickel Laminated Stack*, Leon W. Camp, M 01.223-51, HUSL, Sept. 24, 1943. Div. 6-612.716-M3
20. *Visit to West Lynn Lab[oratory] of General Electric regarding Materials for Permanent Magnets*, Francis P. Bundy, M 113.50-59, HUSL, Sept. 25, 1943.
Div. 6-612.42-M2
21. *General Ideas on Permanent Magnet Polarization of Magnetostrictive Transducers*, Francis P. Bundy, M 01.-213-82, HUSL, Sept. 29, 1943.
Div. 6-612.1-M3
22. *Magnetic Polarization of the Drisko T*, Francis P. Bundy, M 01.213-84, HUSL, Sept. 30, 1943. Div. 6-612.71-M13
23. *Tests on Some New DuPont Adhesives*, G. W. Renner, M 113.50-62, HUSL, Oct. 4, 1943.
Div. 6-612.44-M3
24. *Transducers, Thoughts on Laminated*, Frederick V. Hunt, M 01.213-101, HUSL, Oct. 25, 1943. Div. 6-612.71-M15
25. *Transducers, Thoughts on Laminated*, Eric A. Walker, M 01.213-102, HUSL, Oct. 25, 1943. Div. 6-612.71-M14
26. *Laminated Transducers, Further Thoughts on*, Francis P. Bundy, M 01.213-104, HUSL, Nov. 2, 1943.
Div. 6-612.71-M16
27. *Blister Rubber Paint*, Francis P. Bundy, M 113.50-74, HUSL, Nov. 9, 1943.
Div. 6-612.44-M5
28. *Sword Arm Transducer for Depth Determining Gear*, Frederick V. Hunt, M 02.50-10, HUSL, Dec. 4, 1943.
Div. 6-612.717-M1
29. *Design, Construction, and Performance of SPEP-1 Transducer*, Leon W. Camp, Francis P. Bundy, M 66.036-98, HUSL, Dec. 8, 1943.
Div. 6-612.716-M4
30. *Sword Depth Finding Hydrophone*, Robert B. Watson, M 02.50-13, HUSL, Dec. 18, 1943.
Div. 6-612.717-M2
31. *A Study of the Behavior of Consolidated and Unconsolidated Stack Transducers in Castor Oil and in Water*, Leon W. Camp, Francis P. Bundy, M 01.213-134, HUSL, Jan. 13, 1944.
Div. 6-612.71-M21
32. *Calibrations and Patterns of SPEP Model No. 1 [and] No. 2 [with] Four Quadrants in Parallel*, Nelson K. Moody, Jr., M 66.016-146, HUSL, Jan. 24, 1944.
Div. 6-612.716-M5
33. *A Study of PM Polarized SPEP Elements*, Francis P. Bundy, M 66.036-148, HUSL, Jan. 26, 1944.
Div. 6-612.716-M6
34. *Concluding Report on Bookphones*, G. W. Renner, M 01.223-66, HUSL, Feb. 7, 1944.
Div. 6-612.71-M22
35. *Efficiencies of Consolidated and Unconsolidated Stack Transducers in Castor Oil and in Water* (External Memorandum), Francis P. Bundy, Leon W. Camp, NDRC 6.1-sr287-1356, HUSL, Feb. 10, 1944.
Div. 6-612.71-M23
36. *Results of Drop Tests of SPEP-2, Nos. 1 and 2*, Francis P. Bundy, Leon W. Camp, M 66.436-170, HUSL, Feb. 12, 1944.
Div. 6-612.716-M7
37. *Design, Construction, and Performance of the DT Transducer*, Benjamin B. Drisko, M 01.223-78, HUSL, Feb. 28, 1944.
Div. 6-612.71-M24
38. *Shading for 3"×6" SPEP Transducer for General Electric*, Nelson M. Blachman, M 66.036-192, HUSL, Mar. 9, 1944.
Div. 6-612.716-M8
39. *Coupling Tests on Segmented and Unsegmented Ladderphone Stacks, LDPI No. 1 and No. 2*, William T. Bartholomew, F. P. Bundy, M 01.213-173, HUSL, Mar. 16, 1944.
Div. 6-612.31-M8
40. *Rubber for Underwater Use*, Alan H. Selker, M 113.50-109, HUSL, Mar. 31, 1944.
Div. 6-612.43-M3
41. *Coupling Tests on Ladderphone Stacks*, Frederick V. Hunt, M 01.213-183, HUSL, Apr. 10, 1944.
Div. 6-612.71-M26
42. *Instructions for Construction, Testing, and Assembly of G.E. SPEP Transducers*, Francis P. Bundy, M 66.036-241, HUSL, Apr. 15, 1944.
Div. 6-612.716-M9
43. *Instructions for Construction, Testing, and Assembly of Harvard SPEP Transducers*, Francis P. Bundy, M 66.-036-247, HUSL, Apr. 19, 1944.
Div. 6-612.716-M10
44. *Handling Equipment for Cleaning, Annealing, and Coating Nickel Laminations*, Paul E. Sabine, M 110.10-127, HUSL, Apr. 20, 1944.
Div. 6-612.41-M18
45. *Suggested Tests of Acoustical Transparency and Damping of Rubber and Rubber Substitutes*, Francis P. Bundy, M 01.21-70, HUSL, May 2, 1944.
Div. 6-612.43-M4
46. *Stepped Frequency Transducers*, G. W. Renner, Francis P. Bundy, M 01.223-90, HUSL, May 4, 1944.
Div. 6-612.71-M27
47. *Acoustic Loading Tests on Transducers with Narrow Radiating Faces*, Francis P. Bundy, Milton R. Carlson, M 01.21-71, HUSL, May 11, 1944.
Div. 6-612.716-M11
48. *Transmission and Reflection Characteristics of Rubber Discs, Natural and GR-S (Artificial)*, Jack C. Cotton, M 113.5-122, HUSL, May 11, 1944.
Div. 6-612.43-M5
49. *Transducers Separated from the Water by Rubber or Oil*, Nelson M. Blachman, M 01.21-72, HUSL, May 12, 1944.
Div. 6-612.43-M6
50. *Rubber-Covered SPEP Element*, G. W. Renner, M 01.213-197, HUSL, May 15, 1944.
Div. 6-612.43-M7
51. *Miracle Adhesives*, Francis P. Bundy, Leon W. Camp, M 113.5-127, HUSL, May 18, 1944.
Div. 6-612.44-M10
52. *Transmission Loss in Natural and Synthetic Rubbers*, Paul E. Sabine, M 113.5-130, HUSL, May 24, 1944.
Div. 6-612.43-M8
53. *Transmission and Reflection Characteristics of Rubber Discs, Natural and Artificial [Part] II*, Jack C. Cotton, M 113.5-134, HUSL, June 3, 1944.
Div. 6-612.43-M9
54. *Transmission and Density Tests on Twenty-One Natural Rubber Discs*, Jack C. Cotton, M 113.5-136, HUSL, June 9, 1944.
Div. 6-612.43-M10

55. *SPEP Beam Patterns*, R. C. McLoughlin, M 66.036-391, HUSL, June 13, 1944. Div. 6-612.716-M12
56. *More Transmission Tests*, Tyler No. 212, Rubberized Canvas, Neoprene [and] *pe* Rubber, Jack C. Cotton, M 113.5-138, HUSL, June 14, 1944. Div. 6-612.43-M11
57. *Lamination Design to Minimize the Q*, Nelson M. Blachman, M 01.213-200, HUSL, June 17, 1944. Div. 6-612.34-M6
58. *Design, Construction and Performance of the 60 kc Sword Arm Depth Angle Transducer*, G. W. Renner, Francis P. Bundy, M 02.50-56, HUSL, July 1, 1944. Div. 6-612.717-M3
59. *SPEP Faces*, Francis P. Bundy, M 66.036-449, HUSL, July 10, 1944. Div. 6-612.716-M13
60. *Transmission Tests*, 15 Tyler Rubber No. 212 *SPEP Faces*, July 8, 1944, Jack C. Cotton, M 01.213-209, HUSL, July 10, 1944. Div. 6-612.43-M12
61. *The Construction and Performance of the Whale Transducer* (Preliminary Report), Milton R. Carlson, Francis P. Bundy, M 91.236-129, HUSL, July 16, 1944. Div. 6-612.71-M29
62. *Consolidation of Nickel Laminations*, Leon W. Camp, M 02.453.2-49, HUSL, July 26, 1944. Div. 6-612.44-M11
63. *Density and Transmission Tests on Nineteen SPEP Disks*, Jack C. Cotton, M 66.036-486, HUSL, July 28, 1944. Div. 6-612.716-M14
64. *Preliminary Results on High Level Pulsing of a Single SPEP Element*, Roger W. Hickman, M 01.213-239, HUSL, Sept. 25, 1944. Div. 6-612.716-M15
65. *Tests on a Production Unit of SPEP Transducer Made by the Gamewell Company*, Jack C. Cotton, Paul E. Sabine, M 01.213-242, HUSL, Sept. 28, 1944. Div. 6-612.716-M16
66. *Sound Transmission Loss of SPEP Face Made by Alfred Hale Rubber Company*, Paul E. Sabine, M 66.036-581, HUSL, Oct. 4, 1944. Div. 6-612.43-M13
67. *Tests on Gamewell Production SPEP Units No. 3 and No. 4*, Paul E. Sabine, Jack C. Cotton, M 01.213-249, HUSL, Oct. 10, 1944. Div. 6-612.716-M17
68. *Shading for Additional Minor Lobe Reduction in GE SPEP*, Nelson M. Blachman, M 01.213-266, HUSL, Oct. 25, 1944. Div. 6-612.716-M18
69. *Tests and Analysis of British Scanning Sonar Transducer Element*, Francis P. Bundy, M 02.45.7-120, HUSL, Oct. 25, 1944. Div. 6-612.55-M16
70. *Measurement on SPEP Stacks Cemented to Various Diaphragms, Rubber, Stainless Steel, [and] Plastic*, Jack C. Cotton, M 66.036-676, HUSL, Nov. 24, 1944. Div. 6-612.43-M14
71. *Some Observations on the Effect of Current Amplitude and Temperature on the Characteristics of a Single SPEP Element (MINI-SPEP)*, Roger W. Hickman, M 01.213-287, HUSL, Nov. 29, 1944. Div. 6-612.716-M19
72. *Lamination Cleaning*, Jack C. Cotton, M 110.1-158, HUSL, Dec. 1, 1944. Div. 6-612.71-M31
73. *Variation of Magnetization in Legs of PM Polarized SPEP Element with Driving Field*, S. T. Pan, M 01.213-291, HUSL, Dec. 6, 1944. Div. 6-612.41-M21
74. *Reversible Permeability and Hysteresis Loss in Oxide-Annealed [Grade] A Nickel Polarized at $B_0 = 4100$* , S. T. Pan, M 113.5-180, HUSL, Dec. 12, 1944. Div. 6-612.41-M22
75. *Test Results on SPEP's 6-22, -23, -24 (Gamewell-5, -6, -7)*, Jack C. Cotton, M 66.016-741, HUSL, Jan. 15, 1945. Div. 6-612.716-M20
76. *Rubber Faces for Leeds and Northrup SPEP Transducers*, Francis P. Bundy, M 66.636-774, HUSL, Feb. 23, 1945. Div. 6-612.43-M15
77. *Tests Results on Two GE Type SPEP Units Made by Leeds and Northrup*, Francis P. Bundy, Jack C. Cotton, M 66.016-784, HUSL, Mar. 15, 1945. Div. 6-612.716-M21
78. *Test Results on SPEP's 6-25, -26, -27 (Gamewell-8, -9, -10)*, Jack C. Cotton, M 66.016-816, HUSL, Apr. 9, 1945. Div. 6-612.716-M22
79. *Sound Attenuation in Coating Materials*, Alan H. Selker, G. W. Renner, M 01.21-128, HUSL, Apr. 9, 1945. Div. 6-612.43-M16
80. *Organic Cements in Underwater Sound Apparatus*, Alan H. Selker, M 113.5-185, HUSL, Apr. 18, 1945. Div. 6-612.44-M14
81. *Some Applications of Organic Plastics and Rubber in Underwater Sound Apparatus*, Alan H. Selker, M 113.5-191, HUSL, May 26, 1945. Div. 6-612.43-M17
82. *MOX and MKX Magnetostriction Hydrophones* [R. L. Peek], Case 23240, Report 2210-RLP-MS, BTL, June 10, 1943. Div. 6-612.63-M2
83. *Task No. 4B, Modification of QC-Type Projector* (Final Report), Section 6.67, U. S. Navy BuShips, Sonar Development Contract NX sr-46932 with Western Electric Co., Inc., BTL, Dec. 1, 1944.

Chapter 8

1. *Laminated Magnetostriction Tubes*, Malcolm H. Hebb, M 01.213-07.1, HUSL, Nov. 7, 1942. Div. 6-612.63-M1
2. *The Construction of the "Tomato-Can" MS Tube Tester and the Results Obtained with It*, Francis P. Bundy, M 01.10-20, HUSL, Nov. 11, 1942. Div. 6-612.8-M1
3. *Efficiency and Sensitivity of Cone-Type Magnetostriction Transducers*, Harvey A. Brooks, M 01.213-18, HUSL, Jan. 4, 1943. Div. 6-612.22-M8
4. *Angular Characteristics of the WEA-1 Used as a Hydrophone* (Memorandum for File), Edward Gerjuoy, Report G13/176, CUDWR-NLL, Mar. 2, 1943. Div. 6-556.1-M9
5. *Liquid within Dome, Addition of Acrosol*, H. W. Henderson, M 01.12-21, HUSL, Apr. 22, 1943. Div. 6-612.44-M1
6. *Spherical WEA-1 Projector*, Francis P. Bundy, M 02-21, HUSL, June 17, 1943. Div. 6-612.8-M2

CONFIDENTIAL

7. *Reduction of Eddy Currents in Magnetostrictive Tubes*, Malcolm H. Hebb, M 01.213-62, HUSL, July 24, 1943.
Div. 6-612.8-M4
8. *Line Source Transducer and Possible Sonar Application*, Roland E. Mueser, M 02.45-70, HUSL, July 30, 1943.
Div. 6-612.62-M12
9. *Spherical WEA-1 Projector for Aide de Camp*, Francis P. Bundy, M 02-23, HUSL, Aug. 14, 1943.
Div. 6-612.8-M5
10. *Optimum Coil Location for MS Transducers*, Frederick V. Hunt, M 01.213-77, HUSL, Sept. 2, 1943.
Div. 6-612.8-M6
11. *Preliminary Impedance Measurements Which Led to the Design of the Honeycomb (19 Element) Transducer*, P. M. Kendig, M 60.0360-254, HUSL, Sept. 20, 1943.
Div. 6-612.7-M1
12. *Results of Spy Pond Tests on Waffle Iron EP Transducer*, Nelson K. Moody, Jr., M 66.236-23, HUSL, Sept. 21, 1943.
Div. 6-612.55-M4
13. *Further Studies of Optimum Coil Location for Nickel Tube Transducers*, Nelson K. Moody, Jr., M 01.213-80, HUSL, Sept. 27, 1943.
Div. 6-612.8-M7
14. *The 4-Tube Hydrophone*, H. R. Stewart, M 60.0360-301, HUSL, Oct. 1, 1943.
Div. 6-612.8-M8
15. *Performance Variations in Tube Type MS Transducers*, Benjamin B. Drisko, M 60.0360-323, HUSL, Oct. 6, 1943.
Div. 6-612.8-M9
16. *Tube Driven Transducer Design Considerations*, Francis P. Bundy, Harold P. Knauss, John D. Lane, M 02.45-20-43, HUSL, Dec. 8, 1943.
Div. 6-612.8-M11
17. *Measurements on Galaxy QC Head and Associated Wiring*, J. F. Hersh, James J. Faran, Jr., M 02.07-46, HUSL, Apr. 24, 1944.
Div. 6-612.8-M14
18. *Patterns of 12-Tube Hydrophones*, Lyman N. Miller, M 60.036-1074, HUSL, Jan. 15, 1945.
Div. 6-612.8-M19
19. *Twelve-Tube Hydrophone*, R. W. Marsh, M 60.036-1094, HUSL, Jan. 24, 1945.
Div. 6-612.8-M20
20. *Calibration of Experimental QCU Projectors, Models No. 1 and No. 2*, Eginhard Dietze, NDRC 6.1-sr1130-2138, USRL, Feb. 24, 1945.
Div. 6-556.1-M34
21. *Some Applications of Organic Plastics and Rubber in Underwater Sound Apparatus*, Alan H. Selker, M 113.5-191, HUSL, May 26, 1945.
Div. 6-612.43-M17
22. *Analysis of QC and JK Type Projectors* [Summary of (1) Report 2420-WDG-ED-VP, Mar. 18, 1942; (2) Report 2420-WDG-ED-HI, Mar. 18, 1942; and (3) Report 2420-WDG-ED-MA, Mar. 27, 1942], Walter D. Goodale, Jr., Eginhard Dietze, NDRC C4-sr212-077, BTL, Apr. 10, 1942.
(1) Div. 6-554-M10
(2) Div. 6-556.1-M1
(3) Div. 6-554.1-M1
23. *Measuring Tank Suitable for Acoustic Measurements in Water*, R. L. Jones, 6.1-NDRC-S36, BTL, Mar. 31, 1943.
Div. 6-553.4-M2
24. *Task No. 4B, Modification of QC-Type Projector* (Final Report), Section 6.67, U. S. Navy BuShips, Sonar Development Contract NX sr-46932, Western Electric Co., Inc., BTL, Dec. 1, 1944.
25. U. S. Patent 2,063,951, R. L. Steinberger, Dec. 15, 1936.

Chapter 9

1. *Underwater Impedance Measurements*, R. L. Brown, John R. Pellam, NDRC C4-sr287-093, HUSL, May 8, 1942.
Div. 6-612.511-M1
2. *Underwater Impedance Measurements* (Condensed Report), Richard L. Brown, John R. Pellam, NDRC C4-sr287-094, HUSL, May 8, 1942.
Div. 6-612.511-M2
3. *Comments on Underwater Impedance Measurements*, R. L. Brown, John R. Pellam, H. T. O'Neill, NDRC C4-sr287-094, [Report] 264.1, UCDWR, Aug. 12, 1942.
Div. 6-612.511-M3
4. *Capacity of Ground in Calibration of Transducers*, Harvey A. Brooks, Malcolm H. Hebb, M 01.10-27, HUSL, Feb. 1, 1943.
Div. 6-612.51-M2
5. *Bell Laboratories' Absorbent-Lined Tank*, K. N. Fromm, Paul E. Sabine, M 01.11-18, HUSL, Mar. 9, 1943.
Div. 6-612.53-M2
6. *Direct Measurement of Complex Impedance*, O. Hugo Schuck, M 01.10-32, HUSL, Mar. 31, 1943.
Div. 6-612.511-M4
7. *Comparison of Data Taken at Barge and Fur-Lined Bath-tub*, Robert B. Watson, M 01.10-40, HUSL, June 14, 1943.
Div. 6-612.53-M5
8. *Fourth Floor Impedance Measurements*, P. M. Kendig, M 60.21-174, HUSL, Aug. 23, 1943.
Div. 6-612.511-M5
9. *Amplifier and Power Supply for Harvard Laboratory*, F. P. Herrnfeld, Sylvester J. Haefner, Report 630 569, NL 165, UCDWR-NLL, Oct. 25, 1943.
Div. 6-612.53-M6
10. *Sound Apparatus Recorders*, J. F. Hersh, M 110.50-83, HUSL, Dec. 10, 1943.
Div. 6-612.53-M7
11. *The Geometrical Inversion Transformation and Its Application in the Admittance-Impedance Relations, Analytical Admittance-Impedance Relations*, Robert E. Payne, Malcolm H. Hebb, M 01.213-141, HUSL, Jan. 26, 1944.
Div. 6-612.32-M1
12. *New London Measuring Amplifier*, H. Newburg, M 110-250, HUSL, Feb. 2, 1944.
Div. 6-612.53-M9
13. *New London Measuring Amplifier*, Fred H. Smith, M 110-251, HUSL, Feb. 3, 1944.
Div. 6-612.53-M10
14. *A Power Amplifier and Bridge for the Measurement of Impedance at High Power Level* (Memorandum for File), Sylvester J. Haefner, Report P35 653, UCDWR-NLL, Feb. 15, 1944.
Div. 6-612.53-M11
15. *Effect of Cable on the Measured Voltage Terminal of a Transducer*, Lou Fein, M 01.21-53, HUSL, Feb. 22, 1944.
Div. 6-612.51-M7
16. *Development of Bridge Circuits for the Measurement of the Transducer Characteristics*, Robert E. Payne, M 01.10-120, HUSL, Apr. 21, 1944.
Div. 6-612.53-M12

CONFIDENTIAL

17. *Transducers Separated from the Water by Rubber or Oil*, Nelson M. Blahman, HUSL, May 12, 1944.
Div. 6-612.43-M6
18. *Measurement of Reflection Coefficient*, M. H. Hebb, Nelson M. Blahman, M 01.21-74, HUSL, May 19, 1944.
Div. 6-612.51-M9
19. *Production Testing of Projectors*, Erwin F. Schroder, NDRC 6.1-sr1130-1622, NS-182, USRL, May 22, 1944, p. 9.
Div. 6-552-M11
20. *Fairprene for Absorbent Tank Linings*, Ref[erence] Dr. Hunt's Memo[andum] of July 24, 1944, Paul E. Sabine, M 113.5-154, HUSL, July 26, 1944. Div. 6-612.53-M15
21. *The Varistor Conductometer*, J. F. Hersh, James J. Faran, Jr., M 01.10-143, HUSL, Sept. 20, 1944.
Div. 6-612.53-M16
22. *Artificial Transducers for Seanning Sonar*, Robert E. Payne, M 91.20-242, HUSL, Oct. 30, 1944.
Div. 6-612.53-M17
23. *The Conductometer*, James J. Faran, Jr., M 01.10-164, HUSL, Nov. 17, 1944.
Div. 6-612.53-M18
24. *Networks with 90 Degrees Difference in Phase over Two Octaves*, C. W. Horton, M 110.3-165, HUSL, Dec. 11, 1944.
Div. 6-612.3-M3
25. *The Vector Impedance Locus Plotter*, J. F. Hersh, James J. Faran, Jr., M 01.10-170, HUSL, Mar. 2, 1945.
Div. 6-612.53-M20
26. *Design of Potentiometer Phase Shifter for Phase Measurements over a Broad Frequency Band*, Robert L. Cumberow, M 110-373, HUSL, Mar. 5, 1945.
Div. 6-612.53-M21
27. *Vector Impedance Locus Plotter*, J. F. Hersh, James J. Faran, Jr., M 01.10-170, NDRC 6.1-sr287-2175, HUSL, Mar. 15, 1945.
Div. 6-612.53-M22
28. *Transducer Research and Production at the New London Laboratory*, William B. Snow, James W. Follin, Jr., Wilbur T. Harris, NDRC 6.1-sr1128-2212, Report G12 - 1418, NS-113, CUDWR-NLL, May 25, 1945.
Div. 6-612.1-M8
29. *Mechanical and Acoustic Attachments for Piezoelectric Crystals Used in Transducers*, NDRC 6.1-sr346-628, Div. 6, Vol. 12, BTL, Dec. 15, 1942.
30. *Acoustic Tank*, Arthur C. Keller, Case 37866-1, Report 2210-ACK-MS, BT-63, BTL, Mar. 8, 1943.
Div. 6-553.4-M1
31. *Measuring Tank Suitable for Acoustic Measurements in Water*, 6.1-NDRC-836, BTL, Mar. 31, 1943.
Div. 6-553.4-M2
32. "High Frequency Resistance Standard," W. D. Voelker, *Bell Laboratories Record*, Vol. XIII, No. 5, January 1935.
33. "A 5-Megaohm Impedance Bridge," C. H. Young, *Bell Laboratories Record*, Vol. XV, No. 8, April 1937.
34. "An Electronic Null Detector for Impedance Bridges," Horatio W. Lamson, *The Review of Scientific Instruments*, Vol. 9, 1938, pp. 272-275.
35. "A New Type of Selective Circuit and Applications," H. H. Scott, *Proceedings of the Institute of Radio Engineers*, Vol. 26, No. 2, February 1938.
36. "An Inductance and Capacitance Bridge," S. J. Zammataro, *Bell Laboratories Record*, Vol. XVI, No. 10, June 1938.
37. "The 17B Oscillator," W. J. Means, *Bell Laboratories Record*, Vol. XVII, No. 9, May 1939.
38. "Applications of Copper Oxide Rectifiers," Leo L. Beranek, *Electronics*, Vol. 12, July 1939, p. 15.
39. "Applications of Negative Feedback with Particular Reference to Laboratory Equipment," F. E. Terman, R. R. Buss, W. R. Hewitt, F. C. Cahill, *Proceedings of the Institute of Radio Engineers*, Vol. 10, October 1939, p. 649.
40. "Bridged-T and Parallel-T Null Circuits for Measurements at Radio Frequencies," W. N. Tuttle, *Proceedings of the Institute of Radio Engineers*, Vol. 28, 1940, pp. 23-29.
41. "A Bridge for Measuring Core Loss," H. T. Wilhelm, *Bell Laboratories Record*, Vol. XIX, No. 3, November 1940, p. 94.
42. "Some Characteristics of a Stable Negative Resistance," Clelio Brunetti, Leighton Greenough, *Proceedings of the Institute of Radio Engineers*, Vol. 13, December 1942, pp. 542-546.
43. *Alternating Current Bridge Methods*, B. Hague, Sir Isaac Pitman and Sons, Ltd., London, Eng., 1943, pp. 566-571.
44. *Radio Engineers' Handbook*, F. E. Terman, McGraw-Hill Book Co., New York, N. Y., 1943, p. 943.
45. "High Selectivity at Audio and Intermediate Frequencies," E. Lloyd Thomas, *Wireless World*, Vol. 50, No. 6, June 1944, pp. 175-178.
46. "Electronics in the Study of Head Injuries," Charles Sheer, John G. Lynn, *Electronics*, Vol. 17, January 1944, p. 114.
47. "A Cathode-Ray Bridge Detector," E. H. Eveland, *Bell Laboratories Record*, Vol. XXIII, No. 3, March 1945.
48. "Impedance Bridge with a Billion-to-One Range," H. T. Wilhelm, *Bell Laboratories Record*, Vol. XXIII, No. 3, March 1945.

Chapter 10

1. *Interecomparison of Microphones between MIT Project DIC 5985 and Other Groups*, [Report from] January 1, 1941 to February 24, 1942, CUDWR-NLL, Feb. 24, 1942.
Div. 6-612.55-M1
2. *Listening Tests on Thuras Doughnut Hydrophone*, D. P. Loye, Report G12 2679, CUDWR-NLL, Apr. 30, 1942.
Div. 6-612.62-M1
3. *Noise Level in Small Magnetostriction Hydrophones*, William B. Snow, Report D16 2814, CUDWR-NLL, May 15, 1942.
Div. 6-612.22-M4
4. *Mechanical Driver for Testing 3"×5" Magnetostriction Hydrophone*, W. L. Widlar, Report D16.2/3716, CUDWR-NLL, Aug. 17, 1942.
Div. 6-612.53-M1

5. *Free Field Reciprocity Calibration of Underwater Sound Laboratories' Standards*, Leslie L. Foldy, NDRC C4-sr20-206, USRL, Sept. 11, 1942. Div. 6-552-M3
6. *The Relation Between the Absolute Efficiency of a Hydrophone and Its Thermal Noise Level*, Eginhard Dietze, NDRC C4-sr20-593, Dec. 11, 1942. Div. 6-552-M5
7. *Capacity of Ground in Calibration of Transducers*, Harvey A. Brooks, Malcolm H. Hebb, M 01.10-27, HUSL, Feb. 1, 1943. Div. 6-612.51-M2
8. *Status of Barge Plans*, Robert L. Cummerow, M 01.10-31, HUSL, Mar. 10, 1943. Div. 6-612.52-M1
9. *Markers for Frequency Scale in Measurement Set-Up*, O. Hugo Schuck, M 01.10-37, HUSL, Apr. 5, 1943. Div. 6-612.53-M3
10. *Characteristics of GB5-2 and C-26 Transducers*, Edward Gerjuoy, Report G12/298, CUDWR-NLL, Apr. 22, 1943. Div. 6-612.55-M2
11. *Results of Reciprocity Calibration as Applied to Hebbphone No. 4*, Robert L. Cummerow, M 01.213-40, HUSL, May 12, 1943. Div. 6-612.512-M2
12. *Comparison of Data Taken at Barge and Fur-Lined Bath-tub*, Robert B. Watson, M 01.10-40, HUSL, June 14, 1943. Div. 6-612.53-M5
13. *Temperature Dependence of Our 6"x6" X-Cut Crystal Projector, Precision of Barge Measurements*, Paul E. Sabine, M 01.212-10, HUSL, June 22, 1943. Div. 6-612.54-M3
14. *Direction of Rotation of Transducers in the Measurement of Directivity Patterns*, Robert L. Cummerow, M 01.10-45, HUSL, July 3, 1943. Div. 6-612.51-M3
15. *Spy Pond Equipment*, Paul Ebaugh, M 110.20-25, HUSL, July 8, 1943. Div. 6-612.52-M2
16. *Sign Convention in Pattern Measurements*, Frederick V. Hunt, M 01.10-53, HUSL, July 14, 1943. Div. 6-612.21-M5
17. "3A Standard Crystal Hydrophone," Oct. 1, 1942, *Card No. 50 Practical Dictionary of Underwater Acoustical Devices, and Supplementary Loose Leaf Sheets*, NDRC 6.1-sr20-889, OSRD 772, USRL, July 27, 1943. Div. 6-554-M28
18. "Asidie Echo Ranging Receiver," *Card No. 55 Practical Dictionary of Underwater Acoustical Devices, and Supplementary Loose Leaf Sheets*, NDRC 6.1-sr20-889, OSRD 772, USRL, July 27, 1943. Div. 6-554-M28
19. "IK Type Projector (superceding IJ Type)," *Card No. 57 Practical Dictionary of Underwater Acoustical Devices, and Supplementary Loose Leaf Sheets*, Vol. 1, OSRD 772, NDRC 6.1-sr20-889, USRL, July 27, 1943. Div. 6-554-M28
20. "IHK Series Crystal Hydrophones," Jan. 19, 1944, *Card No. 84 Practical Dictionary of Underwater Acoustical Devices, and Supplementary Loose Leaf Sheets*, Vol. 1, OSRD 772, NDRC 6.1-sr20-889, USRL, July 27, 1943. Div. 6-554-M28
21. "5E Crystal Hydrophone," Mar. 20, 1944, *Card No. 126 Practical Dictionary of Underwater Acoustical Devices, and Supplementary Loose Leaf Sheets*, OSRD 772, NDRC 6.1-sr20-889, USRL, July 27, 1943. Div. 6-554-M28
22. "2A Pressure Gradient Hydrophone," Oct. 5, 1944, *Card No. 128, Practical Dictionary of Underwater Acoustical Devices, and Supplementary Loose Leaf Sheets*, OSRD 772, NDRC 6.1-sr20-889, USRL, July 27, 1943. Div. 6-554-M28
23. "XPA Crystal Projector," Oct. 5, 1944, *Card No. 133, Practical Dictionary of Underwater Acoustical Devices, and Supplementary Loose Leaf Sheets*, Vol. 1, OSRD 772, NDRC 6.1-sr20-889, USRL, July 27, 1943. Div. 6-554-M28
24. *Absorbent Lined Tank for SGM Monitor Tests*, Paul E. Sabine, M 02.331.37-16, HUSL, Aug. 16, 1943. Div. 6-612.52-M3
25. *First Reciprocity Measurements at Spy Pond*, Robert E. Mueser, M 01.10-76 (1), HUSL, Sept. 21, 1943. Div. 6-612.512-M3
26. *Sensitivity of Standard Hydrophones*, Paul E. Sabine, M 01.10-79, HUSL, Sept. 23, 1943. Div. 6-612.54-M4
27. *Projector Test Gear for Field Testing of Echo Ranging Projectors*, NDRC 6.1-sr287-1160, HUSL, Oct. 15, 1943.
28. *The 4th and 5th Reciprocities at Spy Pond and Summary*, Robert E. Mueser, M 01.10-76 (4-5), HUSL, Nov. 15, 1943. Div. 6-612.512-M4
29. *Directivity Index Data Sheets*, Jack C. Cotton, M 01.-10-90, HUSL, Dec. 10, 1943. Div. 6-612.51-M4
30. *Sound Apparatus Recorders*, J. F. Hersh, M 110.60-83, HUSL, Dec. 10, 1943. Div. 6-612.53-M7
31. *Directional Pattern Tracer*, Robert B. Watson, M 02.-333-23, HUSL, Jan. 19, 1944. Div. 6-612.53-M8
32. *Field and Pattern of 3x12 X-Cut Crystal Transducer Made by M. I. T.*, Paul E. Sabine, M 01.212-50, HUSL, Jan. 20, 1944. Div. 6, Vol. 12
33. *A Power Amplifier and Bridge for the Measurement of Impedance at High Power Level* (Memorandum for File), Sylvester J. Haefner, Report P35.653, CUDWR-NLL, Feb. 15, 1944. Div. 6-612.53-M11
34. *Broad Frequency Reciprocity Calibration of Standards*, Robert E. Mueser, M 01.213-154, HUSL, Feb. 16, 1944. Div. 6-612.512-M6
35. *Simplified Conversion Procedure for Field and Frequency-Response Data*, Jack C. Cotton, M 01.10-97, HUSL, Feb. 18, 1944. Div. 6-612.51-M6
36. *Field and Frequency Response Sheet for B-19B No. 18 Standard, Simplified Conversion Procedure*, Jack C. Cotton, M 01.213-165, HUSL, Feb. 29, 1944. Div. 6-612.611-M12
37. *New Thermal Wattmeter, Mountain Lakes Design*, Jack C. Cotton, M 01.10-124, HUSL, May 3, 1944. Div. 6-612.53-M13
38. *Secondary Tuning Fork Frequency Standard and Harmonic Generator*, Paul Ebaugh, M 01.10-127, HUSL, May 15, 1944. Div. 6-612.53-M14
39. *Succetwater Lake Calibration Station*, N. J. Holter, HUSL File N52, UCDWR, July 20, 1944.
40. *Fairprene for Absorbent Tank Linings, Ref[erence] Dr. Hunt's Memo[randum] of July 24, 1944*, Paul E. Sabine, M 113.5-154, HUSL, July 26, 1944. Div. 6-612.53-M15
41. *Recent Measurements on Standard Hydrophone B-19B No. 18, B-19H No. 2, and B-19B No. 1*, Paul Ebaugh, M 01.213-215, HUSL, Aug. 4, 1944. Div. 6-612.611-M19

CONFIDENTIAL

42. *Overload Pressure on a B-19H Type Transducer*, Lou Fein, A. B. Powers, M 01.213-216, HUSL, Aug. 4, 1944.
Div. 6-612.613-M8
43. *Field Variations at the Barge*, Lou Fein, A. B. Powers, M 01.10-140, HUSL, Aug. 7, 1944.
Div. 6-612.51-M10
44. *Characteristics of B-19H Hydrophone Used as Projector*, Paul E. Sabine, Paul Ebaugh, M 02.331.7-85, HUSL, Aug. 7, 1944.
Div. 6-612.613-M9
45. *Calibration of HUSL HP-4 Laminated Stack Transducer, Sword and Depth Angle Transducer, and B-19H Hydrophone*, Eginhard Dietze, NDRC 6.1-sr1130-1826, USRL, Aug. 28, 1944.
Div. 6-556.1-M27
46. *Hydrophone Tests Adopted at the New London Laboratory of Columbia University, Division of War Research*, William B. Snow, NDRC 6.1-sr1121-1849, Report G12 1092, CUDWR-NLL, Sept. 1, 1944.
Div. 6-612.51-M11
47. *Sensitivities of B-19B No. 6 and B-19H No. 1 Standard Hydrophones Used at the Barge*, Lou Fein, A. B. Powers, M 01.213-232, HUSL, Sept. 20, 1944.
Div. 6-612.611-M20
48. *Sensitivity of B-19K No. 1 Standard Hydrophone Used at the Barge*, Lou Fein, L. C. Foster, M 01.213-254, HUSL, Oct. 17, 1944.
Div. 6-612.615-M1
49. *Measurements of High Impedance Transducers at the Barge, Even If One Side Is Grounded*, Lou Fein, M 01.10-160, HUSL, Nov. 15, 1944.
Div. 6-612.511-M7
50. *Portable Polar Chart Recorder (Status Report)*, NS-142, HUSL, Dec. 1, 1944.
Div. 6-612.53-M19
51. *Sensitivity of B-19K No. 1*, Lou Fein, M 01.213-293, HUSL, Dec. 8, 1944.
Div. 6-612.615-M2
52. *Suggested Simplifications in Testing at Spy Pond*, Robert E. Mueser, M 60.016-1085, HUSL, Jan. 21, 1945.
Div. 6-612.52-M4
53. *Tests Adopted by the Hydrophone Standards Committee, July 10, 1944*, William B. Snow, James W. Follin, Jr., G. O. Rockwell, C. R. Sawyer, David W. Van Lennep, T. E. Shea, Report G12 1342, NS-102 and NS-139, CUDWR-NLL, Jan. 27, 1945.
Div. 6-612.51-M12
54. *Suggestions for Layout and Handling Gear at the Penn State Measurement Station*, Paul Ebaugh, M 60.063-1119, HUSL, Feb. 7, 1945.
Div. 6-612.52-M5
55. *Sensitivities of B-19B No. 6 QP2*, Lou Fein, Nelson M. Blachman, M 01.213-304, HUSL, Feb. 7, 1945.
Div. 6-612.611-M22
56. *Comments on Suggestions for Layout and Handling Gear at the Penn State Measurement Station*, Francis P. Bundy, M 60.063-1147, HUSL, Feb. 20, 1945.
Div. 6-612.52-M6
57. *Field Variations at the Sweetwater Lake Calibration Station of the University of California, Division of War Research*, Paul Ebaugh, M 01.10-167, HUSL, Feb. 20, 1945.
Div. 6-612.51-M13
58. *The Nature of Field Intensity Variations at Spy Pond*, Robert E. Mueser, M 01.10-168, HUSL, Feb. 21, 1945.
Div. 6-612.51-M14
59. *Suggestions on Penn State Measurement Station*, Robert E. Mueser, M 60.063-1186, HUSL, Mar. 14, 1945.
Div. 6-612.52-M7
60. *Polar Pattern Plotting at Penn State*, Harvey A. Brooks, M 60.016-1203, HUSL, Mar. 23, 1945.
Div. 6-612.53-M23
61. *Magnetostriction Dual-Purpose Projectors for Moshannon Test Station*, Robert E. Mueser, J. R. Reitz, M 01.10-179, HUSL, Apr. 18, 1945.
Div. 6-612.54-M5
62. *Reply to Memo[andum] April 18, 1945 [from] Robert E. Mueser and J. R. Reitz, Magnetostriction Dual Purpose Projectors for Black Moshannon Test Station*, Paul Ebaugh, M 01.10-182, HUSL, Apr. 24, 1945.
Div. 6-612.54-M6
63. *Black Moshannon*, A. N. Butz, Jr., M 60.063-1331, HUSL, May 19, 1945.
Div. 6-612.52-M8
64. *Transducer Research and Production at the New London Laboratory*, William B. Snow, James W. Follin, Jr., Wilbur T. Harris, NDRC 6.1-sr1128-2212, Report G12/1418, CUDWR-NLL, May 25, 1945.
Div. 6-612.1-M8
65. *How Not to Explain Field Variations*, Lou Fein, Paul Ebaugh, Robert E. Mueser, M 01.10-198, HUSL, May 28, 1945.
Div. 6-612.51-M15
66. *Bubble Trouble Continued*, Robert E. Mueser, M 01.10-200, HUSL, May 29, 1945.
Div. 6-612.51-M16
67. *The Accuracy of an Acoustic Measurement [Memorandum] A*, Robert E. Mueser, M 01.1-203, HUSL, June 6, 1945.
Div. 6-612.51-M18
68. *Spy Pond Standards, [Memorandum] B*, Robert E. Mueser, M 01.1-204, HUSL, June 6, 1945.
Div. 6-612.52-M9
69. *A Calibrated Field for Hydrophone Testing [Memorandum] C*, Robert E. Mueser, M 01.1-205, HUSL, June 6, 1945.
Div. 6-612.51-M17
70. *Field of QP No. 2 in May and June 1945*, J. R. Reitz, M 01.213-334, HUSL, June 7, 1945.
Div. 6-612.55-M17
71. *Electronic Layout for Black Moshannon*, Paul Ebaugh, M 60.063.1391, HUSL, June 21, 1945.
Div. 6-612.52-M10
72. *Wetting Agents*, Paul Ebaugh, M 01.10-207, HUSL, June 29, 1945.
Div. 6-612.53-M24
73. *Portable Polar Chart Recorder and Servomechanism (Completion Report)*, NDRC 6.1-sr287-2069, HUSL, Sept. 15, 1945.
Div. 6-553.5-M2
74. *Sound Gear Monitor, Underwater Sound Portable Test Equipment (Completion Report)*, NDRC 6.1-sr287-2086, HUSL, Nov. 1, 1945, pp. 106-107.
Div. 6-641.1-M9
75. *A Primary Standard Pressure Gradient Hydrophone*, NDRC C4-sr212-058, BTL, Mar. 2, 1942.
Div. 6-553.1-M1
76. *A Subaqueous Projector for Hydrophone Calibration in the Audible Frequency Range*, Reginald L. Jones, NDRC C4-sr212-103, BTL, June 1, 1942.
Div. 6-553.2-M3
77. *A Standard Crystal Hydrophone*, NDRC C4-sr212-507, BTL, Oct. 1, 1942.
Div. 6-553.1-M2
78. *Operating Instructions for 2A and 3A Projectors*, BTL, Dec. 7, 1942.
Div. 6-612.54-M2
79. *Standard Pressure Gradient Hydrophone (Operating Notes)*, Eginhard Dietze, Reports D-173204 and D-173206, BTL, May 3, 1943.
Div. 6-612.53-M4
80. *Wide Range Hydrophones for Low Sound Fields*, OSRD Report, NDRC 6.1-sr346-1321, BTL, Mar. 20, 1944.
Div. 6-553.1-M7

Chapter 11

1. *Transducer Cable Shield with Conducting Rubber*, H. R. Stewart, M 113-52, HUSL, July 13, 1943. Div. 6-612.43-M2
2. *A Power Amplifier and Bridge for the Measurement of Impedance at High Power Level* (Memorandum for File), Sylvester J. Haefner, Report P35 653, CUDWR-NLL, Feb. 15, 1944. Div. 6-612.53-M11
3. *Magnetostriction Transducers and High Power Super Sonic Pulsing*, Frederick V. Hunt, Roger W. Hickman, Malcolm H. Hebb, Lyman N. Miller, Francis P. Bundy, M 01.213-171, HUSL, Mar. 4, 1944. Div. 6-632.01-M4
4. *Non-Linear Magnetostrictive Equations, Magnetostrictive Transducer at High Power*, Malcolm H. Hebb, M 01.213-175, HUSL, Mar. 23, 1944. Div. 6-612.22-M13
5. *Preliminary Results on High Level Pulsing of a Single SPEP Element*, Roger W. Hickman, M 01.213-239, HUSL, Sept. 25, 1944. Div. 6-612.716-M15
6. *Some Observations on the Effect of Current Amplitude and Temperature on the Characteristics of a Single SPEP Element (MINI-SPEP)*, Roger W. Hickman, M 01.213-287, HUSL, Nov. 29, 1944. Div. 6-612.716-M19
7. *Reversible Permeability and Hysteresis Loss in Oxide-Annealed [Grade] A Nickel Polarized at $B_0 = 4100$* , S. T. Pan, M 113.5-180, HUSL, Dec. 12, 1944. Div. 6-612.41-M22
8. "Wirksame Permeabilität und Eisenverlust in Blechen und Drahten bei Schwachen Magnetischen Feldern," W. Cauer, *Archive für Electrotechnik*, Vol. 15, 1925-6, p. 308.
9. "A Dynamic Study of Magnetostriction," K. C. Black, *Proceedings of the American Academy of Arts and Sciences*, Vol. 53, No. 2, 1928.
10. "Magnetostriction Oscillators," G. W. Pierce, *Proceedings of the American Academy of Arts and Sciences*, Vol. 63, 1928, p. 1.
11. "The Equivalent Circuit of the Magnetostriction Oscillator," S. Butterworth, F. D. Smith, *The Proceedings of the Physical Society*, London, Eng. Vol. 43, 1931, p. 166.
12. *Fairlie Magnetostriction Reports*, F. D. Smith, HUSL File B[ritish 10], 1931.
13. "Magnetic Measurements at Low Flux Densities Using the A-C Bridge," Victor E. Legg, *Bell System Technical Journal*, Vol. 15, 1936, p. 39.
14. "Operating Characteristics of Power Tubes," E. L. Chaffee, *Journal of Applied Physics*, Vol. 9, 1938, p. 471.
15. "An Improved Magnetostriction Oscillator," W. W. Salisbury, C. W. Porter, *The Review of Scientific Instruments*, Vol. 10, 1939, pp. 142-146.
16. "The Characteristics of the Negative Resistance Magnetron Oscillator," H. Chang, E. L. Chaffee, *Proceedings of the Institute of Radio Engineers*, Vol. 28, 1940, p. 519.
17. "Power Tube Performance in Class C Amplifiers and Frequency Multipliers as Influenced by Harmonic Voltage," R. Sarbacher, *Proceedings of the Institute of Radio Engineers*, Vol. 31, 1943, p. 607.

Chapter 12

1. *Harmonic Operation of Standard Projectors*, Frederick V. Hunt, M 01.12-30, HUSL, June 23, 1943. Div. 6-612.23-M1
2. *Nickel Alloys for Transducers*, Frederick V. Hunt, M 113.50-39, HUSL, July 30, 1943. Div. 6-612.41-M4
3. *Visit to West Lynn Laboratory of General Electric regarding Materials for Permanent Magnets*, Francis P. Bundy, M 113.50-59, HUSL, Sept. 25, 1943. Div. 6-612.42-M2
4. *General Ideas on Permanent Magnet Polarization of Magnetostrictive Transducers*, Francis P. Bundy, M 01.213-82, HUSL, Sept. 29, 1943. Div. 6-612.1-M3
5. *Permanent Magnet Polarization of Laminated MS Transducer Elements by Use of Bimetallic Sheets, Specific Application to No. 2 Sonar Elements*, Francis P. Bundy, M 01.213-94, HUSL, Oct. 14, 1943. Div. 6-612.1-M5
6. *Blister Rubber Paint*, Francis P. Bundy, M 113.50-74, HUSL, Nov. 9, 1943. Div. 6-612.44-M5
7. *Thoughts on Design of Transducers for an 80 ke Sonar System*, Francis P. Bundy, M 02.453-49, HUSL, Dec. 7, 1943. Div. 6-612.71-M18
8. *Rubber for Underwater Use*, Alan H. Selker, M 113.50-109, HUSL, Mar. 31, 1944. Div. 6-612.43-M3
9. *Sonar Transducer Proposals*, John D. Lane, M 02.45-165, HUSL, Apr. 4, 1944. Div. 6-612.71-M25
10. *Suggested Tests of Acoustical Transparency and Damping of Rubber and Rubber Substitutes*, Francis P. Bundy, M 01.21-70, HUSL, May 2, 1944. Div. 6-612.43-M4
11. *Stepped Frequency Transducers*, G. W. Renner, Francis P. Bundy, M 01.223-90, HUSL, May 4, 1944. Div. 6-612.71-M27
12. *Measurement of Reflection Coefficient*, Malcolm H. Hebb, Nelson M. Blachman, HUSL, May 19, 1944. Div. 6-612.51-M9
13. *Compressed Metallic Dust as a Magnetostrictive Material*, William T. Bartholomew, Francis P. Bundy, M 113.5-147, HUSL, July 7, 1944. Div. 6-612.42-M8
14. *Task No. 4B, Modification of QC-Type Projector* (Final Report), Section 6.67, U. S. Navy BuShips, Sonar Development Contract NX sr-46932 with Western Electric Co., Inc., BTL, Dec. 1, 1944.

Chapter 13

1. *Liquid within Dome, Addition of Aerosol*, Hayward W. Henderson, M 01.12-21, HUSL, Apr. 22, 1943. Div. 6-612.44-M1
2. *Properties and Uses of Alnico Magnets*, Kenneth N. Fromm, Francis P. Bundy, M 01.213-35, HUSL, Apr. 23, 1943. Div. 6-612.42-M1
3. *The pc Rubber*, Francis P. Bundy, M 113.50-25, HUSL, June 10, 1943. Div. 6-612.43-M1
4. *Harmonic Operation of Standard Projectors*, Frederick V. Hunt, M 01.12-30, HUSL, June 23, 1943. Div. 6-612.23-M1
5. *Transducer Cable Shield with Conducting Rubber*, H. R. Stewart, M 113-52, HUSL, July 13, 1943. Div. 6-612.43-M2
6. *Sonar MS Transducer*, Frederick V. Hunt, M 02.45-54, HUSL, July 14, 1943. Div. 6-612.711-M1
7. *Transducer Diaphragms*, Fred H. Smith, M 01.221-22, HUSL, July 14, 1943. Div. 6-612.8-M3
8. *Interlaced Transducer for Sonar*, J. Lewis Hathaway, M 02.452.20-30, HUSL, July 15, 1943. Div. 6-612.71-M10
9. *The Problem of Sonar Transducers*, Roderic M. Scott, M 02.45-56, HUSL, July 17, 1943. Div. 6-612.711-M2
10. *Interleaved Transducer for Sonar, San Diego Echo Repeaters*, Roderic M. Scott, M 02.45-57, HUSL, July 21, 1943. Div. 6-612.71-M11
11. *Reduction of Eddy Currents in Magnetostrictive Tubes*, Malcolm H. Hebb, M 01.213-62, HUSL, July 24, 1943. Div. 6-612.8-M4
12. *Lamination for Model 2 Sonar Transducer*, Malcolm H. Hebb, M 02.452.20-38, HUSL, July 30, 1943. Div. 6-612.712-M1
13. *Line Source Transducer and Possible Sonar Application*, Roland E. Mueser, M 02.45-70, HUSL, July 30, 1943. Div. 6-612.62-M12
14. *The No. 2 Sonar Transducer Element*, Francis P. Bundy, M 02.45-84, HUSL, Sept. 10, 1943. Div. 6-612.712-M2
15. *Sonar, Test and Analysis of Laminated Transducer Element*, James W. Follin, Jr., Robert A. Payne, Malcolm H. Hebb, M 02.45-87, HUSL, Sept. 17, 1943. Div. 6-612.71-M12
16. *Cycleweld*, Francis P. Bundy, M 110.10-37, HUSL, Sept. 18, 1943. Div. 6-612.44-M2
17. *Visit to West Lynn Laboratory of General Electric regarding Materials for Permanent Magnets*, Francis P. Bundy, M 113.50-59, HUSL, Sept. 25, 1943. Div. 6-612.42-M2
18. *General Ideas on Permanent Magnet Polarization of Magnetostrictive Transducers*, Francis P. Bundy, M 01.213-82, HUSL, Sept. 29, 1943. Div. 6-612.1-M3
19. *Permanent Magnet Polarization of Magnetostrictive Sonar Transducer*, Francis P. Bundy, M 02.45-90, HUSL, Oct. 4, 1943. Div. 6-612.1-M4
20. *Tests on Some New DuPont Adhesives*, G. W. Renner, M 113.50-62, HUSL, Oct. 4, 1943. Div. 6-612.44-M3
21. *Tests on Model No. 2 Sonar Transducer*, James W. Follin, Jr., Malcolm H. Hebb, M 02.45.70-35, HUSL, Oct. 7, 1943. Div. 6-612.712-M3
22. *Permanent Magnet Polarization of Laminated MS Transducer Elements by Use of Bimetallic Sheets, Specific Application to No. 2 Sonar Elements*, Francis P. Bundy, M 01.213-94, HUSL, Oct. 14, 1943. Div. 6-612.1-M5
23. *Pattern Requirements for Sonar Transducer*, Malcolm H. Hebb, M 02.45.70-38, HUSL, Oct. 15, 1943. Div. 6-612.21-M7
24. *Transducers, Thoughts on Laminated*, Frederick V. Hunt, M 01.213-101, HUSL, Oct. 25, 1943. Div. 6-612.71-M15
25. *Transducers, Thoughts on Laminated*, Eric A. Walker, M 01.213-102, HUSL, Oct. 25, 1943. Div. 6-612.71-M14
26. *Laminated Transducers, Further Thoughts on*, Francis P. Bundy, M 01.213-104, HUSL, Nov. 2, 1943. Div. 6-612.71-M16
27. *Millerphone*, John D. Lane, M 01.213-105, HUSL, Nov. 2, 1943. Div. 6-612.8-M10
28. *Blister Rubber Paint*, Francis P. Bundy, M 113.50-74, HUSL, Nov. 9, 1943. Div. 6-612.44-M5
29. *Sonar Transducer, Certain Measurements and Recommendations*, F. Burton Jones, M 02.45.70-48, HUSL, Nov. 16, 1943. Div. 6-612.71-M17
30. *Thoughts on Design of Transducers for an 80 kc Sonar System*, Francis P. Bundy, M 02.453-49, HUSL, Dec. 7, 1943. Div. 6-612.71-M18
31. *Millerphone, Casketphone*, John D. Lane, J. O. Natwick, M 01.213-127, HUSL, Dec. 10, 1943. Div. 6-612.8-M12
32. *Remarks on Suggested Design of Transducers for High-Frequency Sonar Systems*, Roderic M. Scott, M 02.453-52, HUSL, Dec. 11, 1943. Div. 6-612.71-M19
33. *Answers to Questions in Scott's Memorandum of Dec. 11 [1943] regarding High Frequency Sonar Transducers*, Francis P. Bundy, M 02.453-55, HUSL, Dec. 15, 1943. Div. 6-612.71-M20
34. *Results of Comparison Tests on Campbell and Murphy 10 mil 2" Stacks*, Thomas P. Merritt, M 01.213-145, HUSL, Feb. 1, 1944. Div. 6-612.712-M4
35. *Millerphone [No.] II Report*, John D. Lane, M 01.213-166, HUSL, Feb. 29, 1944. Div. 6-612.8-M13
36. *The Vertical Pattern of a Split Sonar Element*, Malcolm H. Hebb, Nelson M. Blachman, M 01.21-56, HUSL, Mar. 1, 1944. Div. 6-612.21-M13
37. *Coupling Tests on Segmented and Unsegmented Ladderphone Stacks, LDPI No. 1 and No. 2*, William T. Bartholomew, Francis P. Bundy, M 01.213-173, HUSL, Mar. 16, 1944. Div. 6-612.31-M8
38. *Rubber for Underwater Use*, A. H. Selker, M 113.50-109, HUSL, Mar. 31, 1944. Div. 6-612.43-M3
39. *Sonar Transducer Proposals*, John D. Lane, M 02.45-165, HUSL, Apr. 4, 1944. Div. 6-612.71-M25
40. *Preliminary Survey of the Analysis of the Impedance and Admittance Data on the HP-II Stacks*, Robert E. Payne, M 02.45.7-73, HUSL, Apr. 6, 1944. Div. 6-612.55-M14

41. *Results of the Analysis of the Admittance Data on the Individual HP-II Stacks, including the Selection and Arrangement of the Elements in HP-II No. 1B*, Robert E. Payne, M 02.45.7-78, HUSL, Apr. 13, 1944.
Div. 6-612.55-M15
42. *Single Element Pattern of Cylindrical Transducer*, Gerald I. Harrison, M 01.21-68, HUSL, Apr. 28, 1944.
Div. 6-612.21-M16
43. *Suggested Tests of Acoustical Transparency and Damping of Rubber and Rubber Substitutes*, Francis P. Bundy, M 01.21-70, HUSL, May 2, 1944. Div. 6-612.43-M4
44. *Tests on 2" HP-2 Stacks*, Thomas P. Merritt, Francis P. Bundy, M 02.45.7-87, HUSL, May 3, 1944.
Div. 6-612.712-M7
45. *Transducers Separated from the Water by Rubber or Oil*, Nelson M. Blachman, M 01.21-72, HUSL, May 12, 1944.
Div. 6-612.43-M6
46. *Appearance of 90° Minor Lobes in Scanning Sonar Transducer Patterns*, Thomas P. Merritt, Francis P. Bundy, M 02.45.7-90, HUSL, May 13, 1944.
Div. 6-632.61-M2
47. *Transmission Loss in Natural and Synthetic Rubbers*, Paul E. Sabine, M 113.5-130, HUSL, May 24, 1944.
Div. 6-612.43-M8
48. *Lamination Design to Minimize the Q*, Nelson M. Blachman, M 01.213-200, HUSL, June 17, 1944.
Div. 6-612.34-M6
49. *QH Sonar, Depression of Beam*, Malcolm H. Hebb, M 02.45-195, HUSL, June 19, 1944. Div. 6-612.714-M1
50. *Sonar-Lamination Dimensions as Functions of the Number of Sections*, Nelson M. Blachman, M 01.213-203, HUSL, June 26, 1944. Div. 6-612.71-M28
51. *Compressed Metallic Dust as a Magnetostrictive Material*, William T. Bartholomew, Francis P. Bundy, M 113.5-147, HUSL, July 7, 1944. Div. 6-612.42-M8
52. *Transducer Nomenclature [Part] No. 11*, C. E. Hesthal, M 01.20-50, HUSL, Aug. 24, 1944. Div. 6-612.71-M30
53. *Capacitive Commutators*, F. Burton Jones, Reubin H. Wallace, M 02.452-86, HUSL, Oct. 5, 1944.
Div. 6-612.713-M7
54. *Domc for Ultimate Sonar Transducer*, H. E. Harlow, M 02.302-32, HUSL, Nov. 3, 1944. Div. 6-612.714-M5
55. *Pattern of a Sector of a Cylinder*, Gerald I. Harrison, M 01.21-107, HUSL, Nov. 14, 1944. Div. 6-612.21-M22
56. *Single Element Scanning Sonar Patterns*, Gerald I. Harrison, M 02.45.7-143, HUSL, Nov. 24, 1944.
Div. 6-632.61-M3
57. *Water Seal for 100-Conductor Sonar Cable*, Alan H. Selker, M 110.1-163, HUSL, Dec. 6, 1944.
Div. 6-612.714-M6
58. *Construction and First Tests of the Magnetostrictive Scanning Sonar Transducer HP-3DS*, Robert B. Watson, Francis P. Bundy, M 02.502-6, HUSL, Dec. 13, 1944.
Div. 6-612.713-M9
59. *A Detailed Study of Sintered-Oxide Magnets in HP-3 Stacks*, Milton R. Carlson, S. T. Pan, Francis P. Bundy, M 01.213-285, HUSL, Dec. 15, 1944.
Div. 6-612.42-M11
60. *Submarine Bottom Side Transducer*, H. E. Harlow, M 02.453.2-116, HUSL, Jan. 4, 1945.
Div. 6-612.71-M32
61. *Pattern of a 270° Sector*, Gerald I. Harrison, M 01.21-109, HUSL, Jan. 5, 1945. Div. 6-612.21-M26
62. *Trip to Bell Telephone Laboratories on the Question of HP-8 Cable*, H. E. Harlow, M 02.502-10, HUSL, Jan. 15, 1945. Div. 6-612.715-M2
63. *Theoretical Scanning Sonar Patterns*, Gerald I. Harrison, M 02.45.1-22, HUSL, Jan. 19, 1945. Div. 6-632.61-M4
64. *Pattern of a 270° Sector (Corrected)*, Gerald I. Harrison, M 01.21-113, HUSL, Jan. 26, 1945. Div. 6-612.21-M28
65. *The BTL 50-Pair Cable*, H. E. Harlow, M 02.502.16, HUSL, Feb. 7, 1945. Div. 6-612.715-M4
66. *Present Bad Terminology relating to Diameter of Scanning Transducers*, Malcolm H. Hebb, M 02.45.2-194, HUSL, Feb. 8, 1945. Div. 6-612.71-M33
67. *Directional Transmission for Depth Scanning*, Frederick V. Hunt, M 02.502-20, HUSL, Feb. 15, 1945.
Div. 6-612.715-M7
68. *Pattern of 270° and 90° Sectors (Really Correct)*, Gerald I. Harrison, M 01.21-115, HUSL, Feb. 26, 1945.
Div. 6-612.21-M30
69. *Tests of the Partially Complete Sangamo XQHA System at the HUSL Barge*, Francis P. Bundy, M 02.45.7-158, HUSL, Mar. 1, 1945. Div. 6-632.222-M1
70. *Technical Literature for Indoctrination of Prospective Manufacturers of QH Sonar Transducers*, Francis P. Bundy, M 02.45.3-102, HUSL, Mar. 6, 1945.
Div. 6-612.71-M34
71. *Method for Sealing Collyer 50-Pair Flexible, Blocked Cable*, Alan H. Selker, M 02.502-36, HUSL, Mar. 9, 1945.
Div. 6-612.715-M9
72. *Scanning Sonar, Directional Transmitting Beam for*, Frederick V. Hunt, M 02.502-38, HUSL, Mar. 17, 1945.
Div. 6-612.21-M31
73. *Turkshead Covering for HP-3S*, C. E. Hesthal, M 02.-453.2-142, HUSL, Mar. 19, 1945. Div. 6-612.713-M13
74. *Study of Difference between Commutators 1 and 2 of the Depth Scanning System*, Robert H. Hughes, M 02.507-28, HUSL, Mar. 23, 1945. Div. 6-612.715-M10
75. *Total Attenuation Patterns*, Gerald I. Harrison, M 01.21-119, HUSL, Mar. 24, 1945. Div. 6-612.21-M32
76. *Transmission Pattern for Constant Echo Strength*, Gerald I. Harrison, M 01.75-15, HUSL, Mar. 26, 1945.
Div. 6-612.21-M33
77. *Recommendations on Attenuation and Lag Lines for the Sangamo XQHA System*, Gerald I. Harrison, M 01.21-126, HUSL, Apr. 2, 1945. Div. 6-632.221-M4
78. *Repair of HP-3DS No. 1 Transducer*, N. H. Godbold, M 02.502-41, HUSL, Apr. 5, 1945. Div. 6-612.713-M15
79. *Sound Attenuation in Coating Materials*, Alan H. Selker, G. W. Renner, M 01.21-128, HUSL, Apr. 9, 1945.
Div. 6-612.43-M16
80. *Oil Filling of Transducers*, Alan H. Selker, M 01.213-324, HUSL, Apr. 10, 1945. Div. 6-612.44-M13
81. *Cable for Ultimate Type B and Submarine Systems*, Robert B. Watson, M 02.502-43, HUSL, Apr. 12, 1945.
Div. 6-632.421-M17
82. *Design B for Scanning Sonar XQHA*, Gerald I. Harrison, M 02.45.1-26, HUSL, Apr. 14, 1945.
Div. 6-632.221-M6
83. *Theoretical Scanning Sonar Patterns*, Gerald I. Harrison, M 02.45.1-29, HUSL, Apr. 16, 1945. Div. 6-632.61-M7

84. *Organic Cements in Underwater Sound Apparatus*, Alan H. Selker, M 113.5-185, HUSL, Apr. 18, 1945. Div. 6-612.44-M14
85. *Further Subdivision of Scanning Rotor to Achieve More Uniform Rotation of Beam*, Malcolm H. Hebb, M 02.-45.1-31, HUSL, Apr. 19, 1945. Div. 6-632.61-M8
86. *Seanning Sonar Transducer Cable*, H. E. Harlow, M 02.45.2-204, HUSL, May 11, 1945. Div. 6-632.53-M6
87. *Some Applications of Organic Plastics and Rubber in Underwater Sound Apparatus*, Alan H. Selker, M 113.5-191, HUSL, May 26, 1945. Div. 6-612.43-M17
88. *Construction and First Tests of Magnetostrictive Seanning Sonar Transducer HP-SD No. 2*, Leon W. Camp, Robert B. Watson, M 02.502-50, HUSL, July 3, 1945. Div. 6-632.51-M9
89. *Bearing Deviation Indicator* (Completion Report), OSRD 6425, NDRC 6.1-sr287-2075, HUSL, Nov. 1, 1945. Div. 6-631.4-M1
90. *Scanning Sonar*, Summary Technical Report, NDRC Division 6, Volume 16.

Chapter 14

1. *Tests on the Hebbphone*, Roderic M. Scott, M 01.213-33, HUSL, Mar. 18, 1943. Div. 6-612.71-M7
2. *Change of Resistance to Ground of the 36-Element Transducer*, Roderic M. Scott, M 02.452.70-24, HUSL, July 23, 1943. Div. 6-612.711-M3
3. *Cycleweld*, Francis P. Bundy, M 110.10-37, HUSL, Sept. 18, 1943. Div. 6-612.44-M2
4. *Tests on Model No. 2 Sonar Transducer*, James W. Follin, Jr., Malcolm H. Hebb, M 02.45.70-35, HUSL, Oct. 7, 1943. Div. 6-612.712-M3
5. *Millerphone*, John D. Lane, M 01.213-105, HUSL, Nov. 2, 1943. Div. 6-612.8-M10
6. *Millerphone, Casketphone*, John D. Lane, J. O. Natwick, M 01.213-127, HUSL, Dec. 10, 1943. Div. 6-612.8-M12
7. *Tests on the 36-Element Hebbphone I Transducer*, Thomas P. Merritt, Harold P. Knauss, Arthur C. Clatfelter, M 02.45.70-56, HUSL, Dec. 30, 1943. Div. 6-612.711-M4
8. *Results of Comparison Tests on Campbell and Murphy 10 Mil 2" Stacks*, Thomas P. Merritt, M 01.213-145, HUSL, Feb. 1, 1944. Div. 6-612.712-M4
9. *Millerphone [No.] II Report*, John D. Lane, M 01.213-166, HUSL, Feb. 29, 1944. Div. 6-612.8-M13
10. *Performance of HP-2 [No.] 1 on USS Sardonyx*, C. E. Hesthal, M 02.45.4-50, HUSL, Mar. 4, 1944. Div. 6-612.712-M5
11. *Construction and First Tests of the HP-2 [No.] 1 Transducer*, Francis P. Bundy, C. E. Hesthal, Thomas P. Merritt, Arthur Clatfelter, M 02.45-161, HUSL, Mar. 21, 1944. Div. 6-612.712-M6
12. *Proposed Tests for HP-1 Transducer*, Francis P. Bundy, M 02.45.7-71, HUSL, Mar. 27, 1944. Div. 6-612.711-M5
13. *Preliminary Survey of the Analysis of the Impedance and Admittance Data on the HP-II Stacks*, Robert E. Payne, M 02.45.7-73, HUSL, Apr. 6, 1944. Div. 6-612.55-M14
14. *Results of the Analysis of the Admittance Data on the Individual HP-II Stacks, including the Selection and Arrangement of the Elements in IIP-II, No. 1B*, Robert E. Payne, M 02.45.7-78, HUSL, Apr. 13, 1944. Div. 6-612.55-M15
15. *Handling Equipment for Cleaning, Annealing, and Coating Nickel Laminations*, Paul E. Sabine, M 110.10-127, HUSL, Apr. 20, 1944. Div. 6-612.41-M18
16. *That Which Is Rotten with HP-1*, Stanley R. Rich, David C. Whitmarsh, M 02.45.7-82, HUSL, Apr. 21, 1944. Div. 6-612.711-M6
17. *Comparison Tests on Hebbphone 1 and Hebbphone 2*, Thomas P. Merritt, Francis P. Bundy, F. Burton Jones, Arthur C. Clatfelter, C. H. Hesthal, M 02.45.7-85, HUSL, May 2, 1944. Div. 6-612.711-M7
18. *Tests on 2" HP-2 Stacks*, Thomas P. Merritt, Francis P. Bundy, M 02.45.7-87, HUSL, May 3, 1944. Div. 6-612.712-M7
19. *Miracle Adhesives*, Francis P. Bundy, Leon W. Camp, M 113.5-127, HUSL, May 18, 1944. Div. 6-612.44-M10
20. *Assembly of HP-3 Stacks*, Leon W. Camp, M 02.453.2-45, HUSL, July 13, 1944. Div. 6-612.713-M1
21. *Consolidation of HP-3 Laminations*, Leon W. Camp, M 02.453.2-47, HUSL, July 15, 1944. Div. 6-612.713-M2
22. *Assembly of HP-3 Stacks, Supplementary Memo[andum] of July 13 [1944]*, Leon W. Camp, M 02.453.2-48, HUSL, July 24, 1944. Div. 6-612.713-M3
23. *Consolidation of Nickel Laminations*, Leon W. Camp, M 02.453.2-49, HUSL, July 26, 1944. Div. 6-612.44-M11
24. *Construction and Testing of HP-5 Transducer Stacks at the Sangamo Electric Company*, Francis P. Bundy, James J. Faran, Jr., M 02.45-208, HUSL, Aug. 21, 1944. Div. 6-612.714-M2
25. *Specifications for Consolidation and Winding of Laminations*, Leon W. Camp, M 02.453.2-52, HUSL, Aug. 24, 1944. Div. 6-612.713-M4
26. *Transducer Nomenclature [Part] No. II*, C. E. Hesthal, M 01.20-50, HUSL, Aug. 24, 1944. Div. 6-612.71-M30
27. *Harvey Radio [Laboratories'] First HP-3 Stack*, Francis P. Bundy, M 02.45.7-99, HUSL, Sept. 6, 1944. Div. 6-612.713-M5
28. *Tests on 5 Sangamo HP-5 Transducer Stacks*, Francis P. Bundy, M 02.45.7-101, HUSL, Sept. 8, 1944. Div. 6-612.714-M3
29. *Transmission Directivity Indices of Hebbphone 1, Hebbphone 2-B and Other Similar Hydrophones*, F. Burton Jones, M 02.45.7-109, HUSL, Sept. 21, 1944. Div. 6-612.711-M8
30. *Impedance of HP-3 Stacks*, Francis P. Bundy, M 02.50-116, HUSL, Oct. 5, 1944. Div. 6-612.713-M6

31. *Acoustic Patterns of the HP-2B Scanning Sonar Transducer on the USS Cythera*, Harold P. Knauss, A. B. Powers, Francis P. Bundy, M 02.45.7-114, HUSL, Oct. 10, 1944. Div. 6-612.712-M8
32. *Tests on 6 Sangamo HP-5 Transducer Stacks*, Francis P. Bundy, M 02.45.7-117, HUSL, Oct. 14, 1944. Div. 6-612.714-M4
33. *Cycle-Welding of HP-3 Stacks*, Paul E. Sabine, M 02.45.2-129, HUSL, Oct. 28, 1944. Div. 6-612.713-M8
34. *HP-8 Laminations in the Light of our HP-3 Experience*, Paul E. Sabine, M 02.45.2-113, HUSL, Nov. 1, 1944. Div. 6-612.715-M1
35. *Lamination Cleaning*, Jack C. Cotton, M 110.1-158, HUSL, Dec. 1, 1944. Div. 6-612.71-M31
36. *Water Seal for 100-Conductor Sonar Cable*, Alan H. Selker, M 110.1-163, HUSL, Dec. 6, 1944. Div. 6-612.714-M6
37. *Construction and First Tests of the Magnetostrictive Scanning Sonar Transducer HP-3DS*, Robert B. Watson, Francis P. Bundy, M 02.502-6, HUSL, Dec. 13, 1944. Div. 6-612.713-M9
38. *HP-3 Stacks Submitted by Harvey Radio Corporation*, Leon W. Camp, M 02.45.7-149, HUSL, Dec. 29, 1944. Div. 6-612.713-M10
39. *Plans for Testing HP-5 Sangamo Assembly at Barge*, Francis P. Bundy, M 02.45.4-132, HUSL, Jan. 17, 1945. Div. 6-612.714-M7
40. *HP-8 Laminated Stacks*, Leon W. Camp, M 01.213-302, HUSL, Feb. 5, 1945. Div. 6-612.715-M3
41. *Cleaning and Consolidation of HP-8 Laminations*, Leon W. Camp, M 02.45.2-193, HUSL, Feb. 8, 1945. Div. 6-612.715-M5
42. *Tentative Schedule of Measurements on 26 kc Depth Scanning System Aboard USS Cythera*, Robert B. Watson, M 02.507-10, HUSL, Feb. 14, 1945. Div. 6-612.715-M6
43. *Directional Transmission for Depth Scanning*, Frederick V. Hunt, M 02.502-20, HUSL, Feb. 15, 1945. Div. 6-612.715-M7
44. *Final Tests on Sangamo HP-5 No. 1 Transducer before Installation on the Galaxy*, Francis P. Bundy, M 02.45.4-135, HUSL, Feb. 27, 1945. Div. 6-612.714-M8
45. *Tests of the Partially Complete Sangamo XQHA System at the HUSL Barge*, Francis P. Bundy, M 02.45.7-158, HUSL, Mar. 1, 1945. Div. 6-632.222-M1
46. *Measurements on HP-3DS as Installed on USS Cythera*, Robert B. Watson, M 02.507-21, HUSL, Mar. 3, 1945. Div. 6-612.713-M11
47. *Measurements of Depth Scanning System on USS Cythera*, Robert B. Watson, M 02.507-22, HUSL, Mar. 8, 1945. Div. 6-612.715-M8
48. *Tests on Sangamo HP-5 No. 3 Transducer*, C. E. Hesthal, Francis P. Bundy, M 02.45.7-159, HUSL, Mar. 9, 1945. Div. 6-612.714-M9
49. *Measurements on HP-3DS as Installed on USS Cythera*, Robert B. Watson, M 02.507-23, HUSL, Mar. 10, 1945. Div. 6-612.713-M12
50. *Tests on Sangamo HP-5 No. 4 Transducer*, Ray Rast, Francis P. Bundy, M 02.45.7-161, HUSL, Mar. 22, 1945. Div. 6-612.714-M10
51. *Outline of Tests Suggested for HP-3*, Francis P. Bundy, M 02.45.7-162, HUSL, Mar. 24, 1945. Div. 6-612.713-M14
52. *Addendum to Memo[rum] of March 9, 1945, Entitled, "Tests of Sangamo HP-5 No. 3 Transducer,"* C. E. Hesthal, Francis P. Bundy, M 02.45.7-160, HUSL, Mar. 26, 1945. Div. 6-612.714-M11
53. *Recommendations on Attenuation and Lag Lines for the Sangamo XQHA System*, Gerald I. Harrison, M 01.21-126, HUSL, Apr. 2, 1945. Div. 6-632.221-M4
54. *Tests of Sangamo HP-5 No. 5 Transducer*, Jack C. Cotton, M 02.45.7-172, HUSL, May 7, 1945. Div. 6-612.714-M12
55. *Program of Tests for HP-8D No. 2 at Barge*, Leon W. Camp, Robert B. Watson, Francis P. Bundy, M 02.-507-32, HUSL, May 8, 1945. Div. 6-612.715-M11
56. *Tests of HP-3 No. 1 Transducer*, M. J. Foral, Francis P. Bundy, M 02.45.7-174, HUSL, May 23, 1945. Div. 6-612.713-M16
57. *Construction and First Tests of Magnetostrictive Scanning Sonar Transducer, HP-8D No. 2*, Leon W. Camp, Robert B. Watson, M 02.502-50, HUSL, July 3, 1945. Div. 6-632.51-M9
58. *Scanning Sonar*, Summary Technical Report, NDRC Division 6, Vol. 16, Chap. 5.
58a. *Ibid.*, Chap. 6.
59. *Task No. 4B Modification of QC-Type Projector* (Final Report), Section 6.67, U. S. Navy BuShips, Sonar Development Contract NX sr-46932 with Western Electric Co., Inc., BTL, Dec. 1, 1944.

CONTRACT NUMBERS, CONTRACTORS, AND SUBJECT OF CONTRACTS FOR DIVISION 6

<i>Contract Number</i>	<i>Name and Address of Contractor</i>	<i>Subject</i>
OEMsr-20	The Trustees of Columbia University in the City of New York, New York, N. Y.	Studies and experimental investigations in connection with and for the development of equipment and methods pertaining to submarine warfare
OEMsr-1128	The Trustees of Columbia University in the City of New York, New York, N. Y.	Conduct studies and experimental investigations in connection with and for the development of equipment and methods involved in submarine and subsurface warfare
OEMsr-287	President and Fellows of Harvard College, Cambridge, Massachusetts	Studies and experimental investigations in connection with (i) the development of equipment and devices relating to subsurface warfare.
OEMsr-346	Western Electric Company, Inc., New York, N. Y.	Studies and experimental investigations in connection with submarine and subsurface warfare
OEMsr-785	Western Electric Company, Inc., New York, N. Y.	Studies and experimental investigations in connection with Project 61

INDEX

The subject indexes of all STR volumes are combined in a master index printed in a separate volume. For access to the index volume consult the Army or Navy Agency listed on the reverse of the half-title page.

- A nickel, properties, 65-104
 - composition, 65
 - dependence of remanence on annealing temperature, 78
 - effect of annealing on magnetic properties, 72
 - effect of grain orientation on magnetic properties, 74
 - effect of temperature on magnetic properties, 101-104
 - magnetic strain curves, 83
 - magnetostrictive constant, 89
 - maximum coercive force, 75
 - normal magnetization curve, 67
 - resistivity, 93
 - reversible permeability, 88
 - uniformity of stock, 74
 - Young's modulus when magnetized, 93
- Absolute calibration of hydrophones, 311
- Absorbing screens, acoustic, 322
- Acoustic axis of transducer, definition, 14
- Acoustic contact between water and transducer, 279, 391
- Acoustic impedance
 - see* Radiation impedance
- Acoustic intensity, effect of cavitation, 324
- Acoustic loading
 - on inside of ring transducer, 172
 - radially vibrating transducer, 140
- Acoustic patterns of transducers
 - see* Directivity patterns, theoretical
- Acoustic pressure, maximum obtainable from magnetostriction, 9
- Acoustic resistance, definition, 13
- Active face of transducer, design, 374-375
- Adiabatic magnetostriction coefficients, 64
- Admittance bridge, portable, 280
- Admittance diagrams
 - see* Impedance and admittance diagrams
- Admittance locus plotter, 277
- Admittance measurement methods, transducer
 - see* Impedance measurement methods, transducer
- Admittometer, 269
- Air, radiation impedance, 28
- Alnico magnets, polarizing, 151
- Aluminum faces for transducer elements, 419
- Amercoat 33, water-resistant paint, 166
- Annealing magnetostrictive materials, 66, 73, 141
- Assembly and mounting of transducers
 - breakage precautions, 370
 - cable design, 390
 - consolidating jigs, 427
 - consolidation, 162, 173
 - corrosion resistance, 371
 - deck mounting, 371
 - facing material, 391
 - horizontal mounts, 371
 - IIP-2 type in containers, 378
 - HP-2B element assembly, 376
 - HP-3 assembly with plastic face strip, 378
 - IIP-3 element assembly, 377
 - ladderphone assembly, 381
 - materials of construction, 373
 - millerphone assembly, 380
 - mounting methods, 157, 291, 371
 - production testing, 427
 - QC flange, 371
 - SP-1 type in containers, 379
 - spool assembly, 435
 - streamlining, 392
 - support materials, 373
 - tolerance in location of elements, 375
 - tolerance on element uniformity, 367
 - tube and plate types with sealed diaphragms, 381
 - tubular arrays, 382
 - water seals, 361, 385, 436
 - winding, 428
- Asymmetrical stack transducer 9×9 in., 202-207
 - acoustic measurements, 205
 - directivity patterns, 205
 - laminations, 202
 - polarization, 204
 - sensitivity, 205
 - windings, 203
- Automatic plotting of transducer impedance, 273-277
- Axis of transducer, definition, 14
- B-6 hydrophone series, 148-150
- B-19 hydrophone, 150
- B-19A hydrophone, 150
- B-19B hydrophone, 148-151, 154
 - use as a standard, 310
- B-19H hydrophone, 154-156, 382
 - midget model, 156
 - use as a standard, 310
- B-19K hydrophone, 156
- B-19L hydrophone, 156
- Baffle types, theoretical, 120
- Baffles, effect on transducer directivity patterns, 120
- Balance indicators (tuned circuits) for impedance bridges, 261-264
- Bandwidth of transducer
 - see also* Q of transducer
 - definition, 20-21
 - effect on directivity, 130
 - effect of termination, 57
 - in scanning systems, 370
 - response curve measurement, 281-287, 295
- Bar and piston type laminated elements
 - see* Laminated bar stacks
- Beam patterns
 - see* Directivity patterns, theoretical
- Beam-forming network, 366
- Becker and Kersten's initial permeability formula, 73
- Bell Telephone Laboratories
 - broad band magnetostriction projector, 171
 - cavitation studies, 324
 - CI-100 transducer, 194
 - electrodynamic projector, Type 1K, 308
 - laminated block transducers, 200
 - MKN hydrophone, 161
 - MOX transducer, 193
 - non-directional ring stack transducer, 168
 - QC projector studies, 231
 - ring scroll hydrophone, 160
 - ring transducer, 171
 - survey of magnetostrictive material, 62
 - tube-and-plate transducers, 360
 - W-10125 impedance bridge, 255
- Bimetal laminations, 402
- Blocked impedance of transducer, 26
- Bookphone transducer, 187-197, 360
 - acoustic measurements, 190
 - multielement type, 190
 - performance characteristics of elements, 188
- Bostick T46M cement for laminated stacks, 189

- Breakage precautions for transducers, 371
- Bridge methods for transducer impedance measurement, 239-267
frequency-standard equipment, 257-261
general discussion, 239-246
HUSL admittance bridge, 252-255
HUSL impedance bridge, 246-252
reduction of bridge data, 264
special frequency doubler used, 256-257
special oscillators used, 255
tuned detectors used for bridge balancing, 261-264
W-10125 bridge of BTL, 255
- Broad band transducers, 171, 208-210, 225
- Brush Model C-13-2 crystal hydrophone, 308
- Bubbles on transducer face, avoidance, 206, 279, 391
- C-13-2 standard crystal hydrophone, 308
- Cable designing, transducer, 390, 437
- Cable seals, transducer, 384
- Calibration of transducers
measuring equipment, 297
reciprocity method, 17-18, 311-313
use of absorbent-lined tanks, 281-287
- Cashew-base varnish for coating transducers, 165
- Castor oil filling for transducers, 163, 438
- Cavitation limit on transducer, 324, 374
- Cementing laminated stacks to diaphragms, 189
- Centrifugal castings for transducer frames, 373
- Characteristic frequency for a magnetic sheet, 35, 37
- CI-50 transducer, 200
- CI-60 transducer, 200
- CI-61 transducer, 200
- CI-63 transducer, 200
- CI-64 transducer, 200
- CI-65 transducer, 200
- CI-100 transducer, 194
- Circular disk sources, directivity patterns, 128, 129
- Circular piston, radiation impedance, 137
- Coatings for transducer elements, 165
- Coercive force, definition, 3
- Coercive force, variation with temperature, 102
- Coercivity, definition, 3
- Conductometer, 271
- Cone hydrophones, 224
- Consolidation of laminated stacks, 162, 173, 425
- Core impedance, transducer, 35
- Corrosion resistance of scanning transducers, 371
- Corrugated tube transducer elements, 395
- Cost of scanning transducers, 362
- Coupling between transducer sections, 197-200
- Cunio, characteristics of, 402
- Current analogues of force, 57
- Current transmitting response, projector, 295
- Cycle-weld cement for laminated stacks, 66, 162, 189, 425
- Cylindrical dipole, radiation impedance, 136
- Cylindrical source, electrical impedance formulas, 39-42
- Cylindrical source, radiation impedance, 136
- D nickel, properties
composition, 65
effect of annealing on magnetic properties, 75
magnetostrictive constant, 91
resistivity, 93
reversible permeability, 75
Young's modulus when magnetized, 93
- Decibel levels, definition, 13
- Deck mounting of transducers, 371
- Demagnetization of magnets while hot, 409
- Demagnetizing factors of cylindrical rods, 67
- Demagnetizing strain, 98
- Depth angle transducers
HP-3DS scanning transducer, 445
HP-8D scanning transducer, 450
possible patterns, 368
sword-arm, 219
transducer mounting, 371
- Design factors for transducers
see Scanning transducer design; Transducer theory
- Diaphragm as lumped impedance, 180
- Diaphragms for transducers
magnesium, 419
plastics, 419
- Dipole source directivity patterns, 107
- Dipole sphere, radiation impedance, 136
- Direction pattern tracer, 317
- Directivity index
see also Directivity ratio
definition, 138
- Directivity pattern measurement methods
direction pattern tracer, 317
measurement in absorbent-lined tanks, 281
use of standard hydrophones, 297
- Directivity pattern requirements for a scanning transducer, 367-370
- Directivity patterns, theoretical, 105-138
see also Directivity ratio
array of point sources, 107, 108, 112
circular disk, 128
circular disk, clamped at edge, 129
circular disk, shaded, 128
designing transducers for desired pattern, 111-113
dipole source, 106
effect of baffles, 120
effect of frequency band-width, 131
Gaussian pattern, 111-113, 117, 123
line sources, 113-119
normalization, 105
plane radiator in stiff baffle, 121-125
point source, 106
product theorem for line source, 116
product theorem for surface source, 125
reciprocity theorem, 105-106
rectangular source, 125
relation to source strengths, 110-125
shaded line source, 115
split disk, phased, 129
split square, phased, 127
square source, 126
- Directivity ratio
calculation from pattern shape, 132
circular disk, 129
circular disk, shaded, 129
definition, 15, 138
dipole source, 106, 107
importance for listening devices, 141
line of point sources, 110
line source, 114
rectangular source, 128
shaded line source, 115
use in calculating transducer efficiency, 443
- Domains, magnetic, 1
- Domes, elimination of, 362
- Dynamic magnetostriction measurements, 69, 84
- Eddy current losses in transducers
complex eddy current factor, 35
curved sheets, 35
eddy current parameter, 326
laminated cores, 35-38, 350
polarizing magnets, 236
- Effective area of transducer, 60
- Efficiency of four terminal network, 22, 24
- Efficiency of transducers
see also Eddy current losses in transducers; Electromechanical cou-

- pling coefficient; Hysteresis losses in transducers at resonance, 30, 53, 55, 56
- calculation from motional impedance, 27
- definition, 14
- effect of electromechanical coupling, 58
- effect of termination, 57
- electromechanical, 393
- formula, general, 14-15, 17
- generalized transducer, 24
- high power level, 339
- IIP-3; 444
- mechanical, 393
- QC projector, 234
- radially vibrating, 139
- sample calculation, 20
- scanning system requirements, 370
- tube and plate, 223
- Efficiency of transducers, potential, 31
- admittance calculation, 53, 55
- impedance calculation, 55
- tube and plate element, 224
- variation with temperature, 103
- Elastic hysteresis, 65
- Electric analogues for transducers
 - see* Equivalent circuits for transducers; Network equivalents, transducers
- Electrolytically cut laminations, 207
- Electromagnetic units, table, 3
- Electromechanical coupling coefficient, 56, 58, 87, 393
- definition, 7
- for scanning transducers, 370
- variation with temperature, 101
- Electromechanical mutual impedance, transducer, 23
- Electromechanical networks, transducers, 23-24
- Electronic switch (100 kc frequency), 271
- Energy accompanying magnetostriction, 64
- Energy radiated by transducer, formula, 134-137
- Equivalent circuits for transducers, 57
 - see also* Network equivalent, transducer
- loudspeaker, 25
- magnetostrictive transducers, 22-34
- radially vibrating transducer, 39-43
- ring transducer, 42
- Equivalent mass, transducer element, 393
- bar and piston, 181
- longitudinally vibrating bar, 177
- symmetrically closed multiple laminated bars, 182
- symmetrically closed multiple laminated bars with diaphragm, 183
- unsymmetrical closed multiple bars, 185
- Facings, transducer
 - aluminum, 419
 - impregnated glass fiber, 412
 - rubber, 377, 391
 - synthetic coatings, 165
- Faraday's law for induced emf, 1
- Fathometer transducer, 20 ke, 196-198
- Flux, definition, 1
- Flux density, definition, 2
- Flux meter, elementary, 1
- Formulas
 - see also* Network equivalent, transducers
 - acoustic power of transducer, 15
 - admittance diagrams, 55
 - dependence of Young's modulus on magnetization, 7
 - directivity patterns and directivity ratios, 105-138
 - effective electromechanical coupling coefficient, 56, 57, 69
 - efficiency at resonance, 55, 69
 - Faraday's, for induced emf, 1, 2, 3
 - field within a solenoid, 1, 3
 - impedance diagrams, 55
 - magnetic susceptibility, definition, 2
 - potential efficiency, 55
 - Q of a mechanical system, 55
 - radiation impedance of various sources, 134-137
 - Rayleigh's, reversible permeability, 68
 - resonant frequencies for various shapes, 177, 180, 182, 183
 - sound intensity vs. pressure, 13
 - strain vs. flux density, 5, 6
 - threshold of a hydrophone, 14
 - transducer efficiency, 15, 17
 - velocity of sound wave, 13
- Four terminal network, transducer, 23-24
- Fourier integrals for directivity patterns, 117
- Fourier series for directivity patterns, 110
- Frequencies desirable for scanning systems, 369
- Frequency, resonant
 - laminated bar, 177
 - laminated bar and piston, 180
 - symmetrically closed multiple laminated bars, 182
 - symmetrically closed multiple bars with diaphragm, 183
- Frequency doubler for impedance measurements, parabolic type, 256-257
- Frequency doubling in high power transducers, 326
- Frequency response analyzer for transducers, 315
- Frequency response measurements, transducer, 281-287
- Frequency response of transducer
 - see* Bandwidth of transducer, Q of transducer
- Frequency standard equipment for impedance measurements, 259-261
- Frictional resistance, transducer, 393
- Gaussian directivity patterns, 111, 117
- Gibbs' thermodynamic potential, 63
- Hairpin shaped laminations, 221
- Half frequency driving current, 327
- Half hard annealing, 66
- Half-wave oscillators for testing magnetostrictive materials, 187
- Half-wave tube and plate transducers, 225-236, 360, 419
- Harmonic injection in transducer driving current, 328
- Harvard 6 X 6 projectors, 308
- Harvard Underwater Sound Laboratory
 - Ladderphone transducers, 197-199
 - magnetostrictive properties of ferromagnetic materials, 62
 - tubular transducers, 146
- Heat treatment for transducer elements
 - half-hard, 66
 - hydrogen annealing, 66
 - oxide annealing, 66
 - partial annealing of hard nickel, 141
 - ring stack laminations, 162
- High power driving of magnetostrictive transducers, 95, 217, 323-355, 363
- High power level transducer impedance, 339
- History of magnetostrictive transducer research, 3-6, 9-11
- HP-2 transducer, 378, 431
- HP-2B transducer, 375, 434
- HP-3 transducer, 332, 377, 434-444
- HP-3DS transducers, 445
- HP-3S transducer, 438, 444
- HP-5 transducer, 377, 450
- HP-8D scanning transducer, 450
- H-RLP (ring ladderphone), 381
- HUSL admittance bridge, 252-255
 - advantages and disadvantages, 249, 250
 - operation, 252-254
- HUSL impedance bridge, 246-252
 - description of operation, 246-250
 - evaluation, 249
- Hydrogen annealing of nickel, 66

- Hysteresis losses in transducers
 definition, 3
 effect of lamination thickness, 351
 effect on response, 5
 measurement, 67
 temperature dependence, 102
- IJ-10 transducer, 200
- IJ-20 transducer, 200
- Impedance and admittance diagrams
 calculation of Q , 26
 geometrical relations, 49-51
 loudspeaker, 25
 motional admittance circle, 393
 ring transducer, 52
 sensitivity calculation, 59
 summary of formulas, 55
- Impedance locus plotter
 description of circuit, 273-277
 possible improvement, 276-277
- Impedance measurement methods, transducer
see also Impedance measuring equipment
- accuracy required, 237-239
 avoidance of air bubbles, 278
 bridge methods, discussion, 239-267
 bridge methods, pulsed, 328-342
 deflection methods, 268-277
 high power level measurements, 339
 impedance vs. admittance calculations, 54
 network methods, discussion, 266-268
 production tests, 427
 range and accuracy requirements, 238-239
 reduction of bridge data, 264
 reflection errors, 279
- Impedance measuring equipment
 admittance bridge, portable, 280
 admittance locus plotter, 277
 admittometer, 269
 conductometer, 271
 frequency-standard equipment, 259-261
 HUSL admittance bridge, 252-255
 HUSL impedance bridge, 246-252
 impedance locus plotter, 273-278
 impedometer, 268
 oscilloscope plotting methods, 273-278
 special frequency doubler, 256-257
 special oscillators, 255
 tuned detectors for bridge balancing, 261-264
 vector resolver circuit, 269-273
 W-10125 impedance bridge, 255
- Impedance quantities characteristic of transducers
 blocked impedance, 26
 core impedance, 35
 electromechanical mutual impedance, 23
 frictional resistance, 393
 motional admittance, 51, 52
 motional impedance, 25, 29-30, 50
 motional reactance, 34
 mutual impedance, 60
 radiation impedance; *see* Radiation impedance
 total impedance, 27
 typical formulas and graphs, 31-33, 39-42
- Impedometer, 268
- Intensity of magnetization, 62
- Intensity of sound, definition, 13
- Inverse magnetostrictive effect, 40
- Iron-cobalt alloys, magnetostriction tests, 66, 77
- Jahnke and Emde tables, 111
- Joule's magnetostriction experiments, 4, 5
- Ladderphone transducer, 197, 381
- Laminated bar stacks
 hairpin-shaped, 221
 ladder type, 412
 multiple bars with diaphragm, 181-187, 194-221, 334-345
 ring-shaped ladder type, 414
 SP type, 411
 uniform bar with diaphragm, 176-181, 187-194, 361
 wedge-shaped type, 396
- Laminated ring stacks, 161-169, 342-358, 396
- Laminated scrolls, 382
- Laminated tube hydrophones, 159-160
- Laminations
 bimetal, 402
 consolidation, 425
 electrolytically cut, 207
 preparation, 424
- Latex rubber for coating transducers, 165
- Line source bookphone, 190
- Line source directivity patterns, 113-119
- Linearity of transducers, discussion, 323
- Loading of transducer
see Acoustic loading; Radiation impedance
- Longitudinally vibrating transducer theory, 44-49
- Longitudinally vibrating transducers
see Magnetostrictive elements, longitudinally vibrating
- Losses in transducers
see Eddy current losses in transducers, Hysteresis losses in transducers
- Loudspeaker, impedance diagram, 25
- Loudspeaker, network equivalent, 24, 28-29
- Loudspeaker, underwater, 145
- M-5 transducer, 173
- Magnesium faces for transducer elements, 419
- Magnetic circuits in tapered laminated stacks, 401-411
- Magnetic domains, description, 1
- Magnetic field, definition, 1
- Magnetic flux, definition, 1, 2
- Magnetic induction, definition, 1
- Magnetic measurements
see Magnetostrictive materials
- Magnetic moment per unit volume, formula, 2
- Magnetization curves at high temperatures, 79, 80
- Magnetocaloric effect, 64
- Magnetomechanical formulas, 62
- Magnetostriction
 description, 3
 force available, 8
 history of research, 3-6, 9-11
 hysteresis effect, 5
 inverse, 4
 measurements, 5, 79
- Magnetostriction constant, 6, 38, 44, 63
 measurement, 89
 variation with temperature, 104
- Magnetostrictive elements, longitudinally vibrating
see also name of design
 future developments, 360
 hairpin-shaped laminations, 221-222
 multiple bar and piston lamination types, 181-187, 194-221, 333-342, 411-414
 ring-shaped ladder, 414-416
 T-shaped laminations, 191-193
 tube and cone, 224
 tube and cylinder, 223
 tube and plate designs, 225-236, 360, 416-422
 uniform bar and piston laminations, 176-181, 187-194, 360
 wedge-shaped laminations, 396-411
- Magnetostrictive elements, radially vibrating
see also name of design
 corrugated tubes, 395
 cylindrical tubes, 140-151, 359, 395
 internally-radiating rings, 171-175
 laminated ring stacks, 161-169, 342-355, 358-360, 396

- laminated tubes, 159-160
 ring scrolls and spirally-wound tubes, 160-161, 173, 359-361
 toroidal tubes, 143
 tubular arches, 395
 tubular arrays, 146, 169-171
- Magnetostrictive materials**
 cold working effects, 356
 criteria for selection, 65, 95, 100
 dynamic measurements of properties, 69, 84
 electroplating, 357
 heat treatment, 66, 356
 ideal characteristics, 356
 iron cobalt alloys, 65, 77, 88, 89
 magnetostrictive formulas, 62
 nickel and nickel alloys, 65, 70, 71, 89
 sintered powders, 356
 static measurement of properties, 68, 79
 vicalloys, 79, 91
- Magnetostrictive stress, maximum usable, 9**
- Magnetostrictive transducers**
 as electrical networks, 22-34
 definitions of characteristic properties, 13-17
 history and survey, 1-21
 summary of types, 11-13
- Magnetostrictive transducers, general types**
see also under name of type
 asymmetrical stacks, 202-207
 bookphone, 187-191, 360
 depth-angle transducers, 219-221, 445
 high-power types, 323-355
 HP transducers, 376, 431-450
 ladderphone, 197, 381
 laminated tubes, 159-160
 longitudinally vibrating types, 176-236, 333-416
 multiple bar and piston laminations, 181-187, 194-221, 333-342
 nickel stacks, 166
 Permendur-2V stacks, 167
 QC projectors, 230-236
 radially vibrating types, 139-175
 ring scrolls, 160-161, 173
 ring stacks, 161-169, 342-358, 395
 ring-shaped ladder, 414-416
 seanning types, 366-422
 sonic listening hydrophones, 141
 SP type stacks, 411
 SPEP transducers, 210-219, 332
 stepped-frequency, 208-210
 tube and cone, 11, 224, 225
 tube and cylinder, 223
 tube and plate, 225-236, 360, 416-422
 tubular arch, 395
 tubular hydrophones, 140-151, 169-171
 wedge-shaped stacks, 396-411
 wide-band, 171, 208-210, 224
- Magnetostrictive transducers, specific models**
 B-6A hydrophone, 148
 B-6B hydrophone, 150
 B-6C hydrophone, 148
 B-19 hydrophone, 150
 B-19A hydrophone, 150
 B-19B hydrophone, 148-151, 154, 310
 B-19H hydrophone, 154-156, 310, 382
 B-19H midget hydrophone, 156
 B-19K hydrophone, 156
 B-19L hydrophone, 156
 CI-50; 200
 CI-60; 200
 CI-61; 200
 CI-63; 200
 CI-64; 200
 CI-65; 200
 CI-100; 194
 HP-2; 378, 431
 HP-2B; 376, 434
 HP-3; 332, 377, 434-444
 HP-3DS, 445
 HP-3S, 438, 444
 HP-5; 377, 450
 HP-8D, 450
 IJ-10; 200
 IJ-20; 200
 line source bookphone, 190
 M-5; 173
 MKX hydrophone (BTL), 161
 MOX, 193
 NL-124; 144
 NL-130; 144
 QCL projector, 230, 235
 QCU projector, 234, 235
 QGA projector, 235
 QP projector, 170
 ring ladderphone, 381
 SP-1; 379
 20-ke fathometer transducer (Sub. Sig. Co.), 196
 XI-10; 232
 XI-15; 232
 XI-20; 232
 XI-30; 232
 XI-40; 232
 XI-50; 232
 XI-60; 232
 XI-100; 234, 235
 XJ-20; 232
 XJ-30; 232
 XJ-40; 232
- Magnets, polarization and aging, 151**
- Materials for transducer mountings, 373**
- Materials survey, magnetostrictive, 62-104**
- Meehanomotive force, 59**
- Millerphone transducer assembly, 380**
- Minor hysteresis loop, 68, 97**
- MKX hydrophone, 161**
- Motional admittance, transducer, 51, 393**
- Motional impedance, loudspeaker, 25**
- Motional impedance, transducer, 29-30, 50**
- Motional reactance, transducer, 34**
- Mountings for transducers**
see Assembly and mounting of transducers
- MOX transducer, 193**
- Mutual impedance, transducer, 23, 59 60**
- Naval Research Laboratory, 12**
- Neoprene paint for coating transducers, 165**
- Network equivalent, loudspeaker**
 four terminal, 23-24, 28-29
 two terminal, 25
- Network equivalent, transducer, 22-34**
see also Equivalent circuits for transducers
 band-pass filter, 56
 electromechanical network, 23-24
 mass loaded rod, 47
 mechanical losses in a rod, 49
 reciprocity theorem, 22, 23
 rod with one free end, 46
 six terminal, 45
 T networks, 23, 191, 266-268
- New London Laboratory**
 thimble hydrophones, 169
 tubular hydrophones, 140, 143, 145
- Nickel, properties**
see A nickel, properties; D nickel, properties; Z nickel, properties
- 9 × 9 inch asymmetrical stack transducer, 202-207**
- Noise generators for transducer measurements, 315**
- Noise signals, effect on directivity patterns, 130**
- Non-linear operation of transducers, 323-355**
- Normal magnetization curve, 2, 62**
- Oil filling of transducers**
 HP-2B, 434
 ring stacks, 163
 seanning transducers, 438
- Open-circuit sensitivity, transducer, 296**
- Oscillators for impedance bridge measurements, 255**

- Oscilloscope plotting of transducer impedances, 273-277
- Oxide annealing of nickel, 66
- Permalloy-45
composition, 65
dependence of remanence on annealing temperature, 79
resistivity, 93
Young's modulus when magnetized, 93
- Permanent magnet materials, 357
- Permanent magnet polarization of wedge-shaped stacks, 402-406
- Permeability
at constant strain, 64
at constant stress, 64
calculated from impedance data, 84
curve for nickel, 6
incremental, 38
reversible, definition, 7
static, definition, 7
temperature variation, 102
- Permendur laminations, wedge shaped, 405
- Permendur stack, at high power level, 342
- Permendur-2V
composition, 66
dependence of remanence on annealing temperature, 79
magnetic characteristics, 405
normal magnetization curve, 79
resistivity, 93
Young's modulus when magnetized, 93
- Phase differences between transducer elements, 367
- Phase patterns of transducer, 105
- Phasing of point sources in transducer, 109, 112
- Phenol-formaldehyde compound for casting tubes and ring stacks, 144, 165
- Pitometer Log hydrophone, 157
- Plastic faces for transducer elements, 378, 419
- Plastics for consolidating transducers
cast-in-plastic ring stacks, 165
cast-in-plastic tubes, 144
- Point source arrays, directivity patterns, 106, 110, 112
- Polarization, transducer
by permanent magnet, 150
laminated bar, 177-179
laminated stacks, 429
tube and plate transducers, 236
wedge-shaped laminated stacks, 401-411
- Portable polar chart recorder (PPCR), 317
- Portable transducer measuring equipment, 280
- Potential efficiency of transducers
see Efficiency of transducers, potential
- Power output of transducer, ultimate limit, 326
- Power requirements for scanning transducers, 370
- Pressure, maximum obtainable from magnetostriction, 9, 374
- Pressure-release materials, 363
- Pressure-release screens, 322
- Product theorem for line sources, 115
- Product theorem for surface sources, 125
- Pulsed impedance bridge measurements, 328-342
- Q of a mechanical system, 29, 55
- Q of transducer
see also Bandwidth of transducer bar and piston, 181
determination from response curve, 21
effect on efficiency, 395
mechanical Q, 56
motional impedance calculation, 26
multiple bar types, 177, 182, 183, 185
QC projector, 236
radially vibrating transducer, 139
ring stack, 161
tube and plate, 417
- QC transducers
see Tube and plate transducers
- QCL projectors, 230, 235
- QCU projectors, 234, 235
- QGA projectors, 235
- QP projectors, 170, 310
- Radial transducer theory, 39-44
efficiency, 43
electrical impedance, 40
equivalent electrical circuits, 42
impedance diagrams, 49
maximum efficiency, 43
mechanical impedance, 39
motional admittance, 51
mutual impedance, 40
resonant frequency, 43
- Radially vibrating transducers, 140-175, 342-396
see also Magnetostrictive elements, radially vibrating
acoustic loading, 140
efficiency, 139
general characteristics, 139
- Radiation impedance
circular piston, 136
cylinder, 136
cylindrical dipole, 136
dipole sphere, 136
flat strip, 137
in terms of efficiency, 393
laminated bar, 177
laminated bar and piston, 181
of air, 28
of water, 30
specific radiation admittance, def., 136
specific radiation impedance, def., 135
sphere, 136
- Radiation patterns
see Directivity patterns, theoretical
- Radio sono buoy hydrophones, 142
- Rayleigh's reversible permeability formula, 68
- Receiving patterns
see Directivity patterns, theoretical
- Receiving response
see Sensitivity of transducers
- Reciprocity calibration of transducers, 17-18, 311-313
- Reciprocity parameter, 16, 312
- Reciprocity theorem, 15-16, 22-23, 59, 105-106
- Recommendations for future research
see also Chapter 12
high power driving methods, 355
investigation of short pulse techniques, 324
use of harmonics in driving high power transducers, 328
- Recorders for sound level, 307
- Rectangular source, directivity pattern, 125
- Reflection errors in transducer testing, 279
- Reflections due to improper transducer mounting, 362
- Release baffle, definition, 120
- Remanence, definition, 3
- Remanence-operated transducers, 75, 96, 141, 148
- Resinox for coating transducers, 144, 166
- Resistance, acoustic (def.), 13
- Resistivity of magnetic materials, variation with temperature, 102
- Resistivity measurements, 69
- Resolver circuits, 269-273
- Resonance of radially vibrating transducer, 139
- Resonant frequency of wedge-shaped laminations, 399
- Response curve determination, 295
- Retentivity, definition, 3
- Reversible permeability, definition, 6, 7, 64, 68
- Reversible permeability of sintered oxide magnets, 408

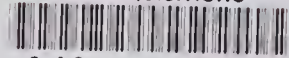
- Ring ladderphone, 381
- Ring scroll transducers, 160-161, 173
- Ring shaped ladder type laminations, 414-416
- Ring source (cylindrical shell)
electrical impedance formulas, 39-42
radiation impedance, 136
- Ring stack transducers, 161-169
bonding, 162
cast-in-plastic, 165
design, 161
edgewise wound, 396
half hard nickel, 167
heat treatment of laminations, 162
high power level, 342-355
internally radiating, 172-175
M-5; 173
maximum power output, 327
mountings, 164, 358
non-directional ring stacks, 168
oil filling, 163
one-turn winding, 358
Q, 161, 358
radiation patterns, 174
scanning, 393, 396
segmented, 358
thin walled stack, 166
2V Permendur stack, 166
windings, 162, 173
- Rod and plate transducer
see Tube and plate transducers
- Rod transducer, theory
see Tube transducer, theory
- Rubber "boots" for transducers, 392
- Rubber facings for transducers, 377, 431
- Sangamo HP5 transducers, 377, 450
- Saturation, magnetic, 3
- Scanning transducer design
see also Transducer theory
accuracy of element placement, 375
active face design, 374-375
assembly of elements, 430-439
beam rotation method, 366
cables, 390
cavitation, 374
construction, 423
cost, 362
design and assembly factors affecting
beam patterns, 365-370
efficiency and power requirements, 370
frequency selection, 369
future development, 359-362
lamination design, 396-401
maximum efficiency, 393
mechanical requirements, 370
mounting supports, 371
non-circular, 362
pattern requirements, 365-370
performance tests, 439
phase shifts, 367
plastic faced, 378
polarization, 401-411
rubber faced, 377
shape of elements, 376
size of transducer, 369
streamlined, 362, 392
submarine types, 362
terminal box and cable seals, 384-390
testing, 427, 439
types of elements, 375, 393-422
- Sensitivity of transducers
B-19B hydrophone, 153
impedance diagram calculation, 59
open-circuit (voltage) sensitivity, definition, 14, 292
receiving and transmitting responses, 14, 17
short-circuit (current) sensitivity, definition, 14
tube and cone, 224
- Shaded arrays
9 × 9 inch laminated stack, 203
SPEP transducers, 210-219
- Shaded transducer patterns, 108, 115
- Shock resistance, B-19B hydrophone, 153
- Sintered oxide magnets, characteristics, 405
- Six terminal networks, transducers, 45
- Sonic listening hydrophones
see also Tubular hydrophones
directivity index, 141
noise discrimination, 141
sensitivity, 141
- Sound field measurement, 293
- Sound gear monitor, calibration procedure, 319
- Sound gear monitor, hydrophone, 146-159
- Sound intensity, definition, 13
- Sound velocity
formula, 13
in nickel, 399
in water, 321
- SP type laminated stacks, 411
- SP-1 transducer, 379
- Specific radiation admittance, 136
- Specific radiation impedance, 135
- SPEP transducers, 210-219, 332
acoustic and electric performance, 212
direct current polarized models, 210-214
directivity patterns, 212
high power level performance, 217, 333
impedance measurements, 214-219
laminations, 211
permanent magnet polarized models, 214
shaded windings, 211
sword arm depth angle transducer, 219-221
- Spherical source
radiation impedance, 136
ring stack, 168
- Spiral-wound tube transducer elements, 160, 173, 358
- Spool assembly of transducers, 435
- Spy Pond transducer test station, 289
electronic equipment, 297-308
- Square radiator, directivity patterns, 127
- Standard frequency equipment, 259-261
- Standard hydrophones, 308
- Static magnetostriction
measurements on iron-cobalt rods, 79
measurements on nickel, 79
research history, 3
- Static permeability, definition, 3
- Stepped-frequency transducers, 208-210
- Strain, magnetostrictive, 83
- Strain demagnetization, 98
- Strain vs. flux density, formula, 5
- Streamlining scanning transducers, 362, 392
- Strength of a point source, definition, 105
- Stress formulas, magnetostrictive, 38
- Stress from magnetizing a clamped rod, 8
- Submarine scanning transducer types, 362
- Submarine Signal Company, 20-ke fathometer transducer, 196
- Support materials for transducers, 373
- Surface sources, radiating conditions, 119
- Susceptibility, definition, 2
- Sword arm depth angle transducer, 219-221
- T networks, transducer, 23, 191, 266-268
- Tanks for transducer testing, absorbent-lined, 281
- Temperature effects in magnetostriction, 101-104
- Terminal box seals, transducer, 384
- Termination of transducer, effect on efficiency, 57
- Test facilities at HUSL
Charles River barge, 288
Spy Pond station, 289
Tippecanoe, 288
USS Galaxy, 288

- Theory of magnetostrictive transducers
see Transducer theory
- "Thimble" hydrophones, 169
- Threshold of hydrophone, definition, 14
- "Tippecanoe", transducer test barge, 289
- Tolerances in transducer assembly, 367, 375
- Toroidal tube transducer elements, 143
- Transducer assembly and mounting
see Assembly and mounting of transducers
- Transducer coupling coefficients
see Electromechanical coupling coefficient
- Transducer design, scanning
see Scanning transducer design
- Transducer efficiency and losses
see Eddy current losses in transducers; Efficiency of transducers; Hysteresis losses in transducers
- Transducer elements and arrays, magnetostrictive
see Magnetostrictive elements, longitudinally vibrating; Magnetostrictive elements, radially vibrating
also see under name of type
- Transducer frequency response
see Bandwidth of transducer; Q of transducer
- Transducer impedances
see Impedance, Radiation impedance
- Transducer network equivalents
see Network equivalent, transducer
- Transducer termination, effect on efficiency, 57
- Transducer tests
see Impedance measurement
- Transducer theory
see also Scanning transducer design
 calibration theory, 311
 designing for desired pattern, 117
 directivity pattern prediction, 111
 effective area of, 60
 efficiency at resonance, 30
 equivalent electrical circuits, 22-34
 longitudinally vibrating transducers, 44-49
 loudspeaker as example, 24
 motional impedance, 31
 motional reactance, 34
 maximum power output, 100
 noise, 14
 optimum Q, 99
 potential efficiency, 31
 radially vibrating transducers, 39-44
 reciprocity, 15, 17-18
 sensitivity, 14
 shading methods, 115
 tubular transducer theory, 44-49
- Transducer types, magnetostrictive
see Magnetostrictive transducers, general types; Magnetostrictive transducers, specific models
see also under name of type
- Transmitting patterns
see Directivity patterns, theoretical
- Transmitting response
 definition, 292
 relation to receiving response, 17
- Transmitting response curve, 295
- T-shaped laminated elements, 191-193
- Tube and cone transducers, 11 224
- Tube and cylinder transducers, 223
- Tube and plate transducers, 223-236, 416-422
 comparison, 234
 early model, 223
 four-tube hydrophone, 225
 future development, 360
 magnesium plate, 234, 419
 magnetic circuit, 236
 millerphone, 380
 QC projector, 230-236
 scanning, 378, 393, 416-422
 tube and slotted-plate projector, 228
 wedge-shaped plate, 420
- Tube and plate transducer elements
 QC-like type, 416-419
- Tube transducer theory, 44-49
 equivalent circuit for a mass loaded rod, 47
 equivalent circuit for a rod with one free end, 46
 equivalent network, six terminal, 44, 45
 internal mechanical losses, 49
- Tubular arch transducer element, 395
- Tubular element transducer arrays
 B-19H, (QP), 170
 design considerations, 381, 395
 four tube, 146
 ten element, 170
 twenty-eight element, 169
- Tubular hydrophones
 B-6 hydrophones, 150
 B-19 hydrophones, 150
 B-19B, 150-154
 B-19H, 154-156
 B-19H midget, 156
 B-19K, 156
 B-19L, 156
 cast in plastic, 143
 early types, 146-151
 Harvard models, 146
 installed SGM, 157
 laminated tube, 159
 NL-124; 144
 NL-130; 144
 radio sono buoy, 142
 requirements, 141
 sonic listening, 141, 143-146
 "thimble" hydrophone, 169
 underwater loudspeaker, 145
- Tuning, electrical
 tube and plate hydrophone, 225
- Tuning, mechanical
 stagger-tuned laminated stacks, 209
 tube and plate element, 223
 tube and plate hydrophone, 225
- "Turk's-head", 445
- 20 ke fathometer transducer, 196-198
- Two terminal networks, transducer, 25
- Underwater loud speaker, 145
- Uniform bar transducer elements, 176-179, 187
- Uniform bars with pistons, 179-181, 187-194
- Units, electromagnetic, 3
- Vectolite (sintered powder magnet material), 358
- Vector admittance locus plotter, 277
- Vector impedance locus plotter
 description of circuit, 273-277
 possible improvement, 276-277
- Vector resolving circuits, 269-273
- Velocity of sound
 formula, 13
 in nickel, 399
 in water, 321
- Vicalloy-6.5V
 composition, 66
 resistivity, 93
 reversible permeability, 79
 Young's modulus when magnetized, 93
- Vinylseal cement for consolidating transducers, 66
- Voltage analogues of velocity, 57
- Voltage level recorders, 307
- Voltage transmitting response, projector, 296
- Water, radiation impedance, 30
- Water seals for transducers, 361, 384, 436
- Wave number (acoustic), 108
- Wedge-shaped laminated stacks, 396-411
- Wedge-type plate and tube transducer element, 420
- Wide band transducers, 171, 208-210, 225
- Winding methods for laminated stacks, 428
- XI-10 projector, 232
- XI-15 projector, 232
- XI-20 projector, 232
- XI-30 projector, 233

- XI-40 projector, 234
- XI-50 projector, 234
- XI-60 projector, 233
- XI-100 projector, 231, 234
- XJ-20 projector, 232
- XJ-30 projector, 233
- XJ-40 projector, 234
- Young's modulus, isothermal and adiabatic, 64
- Young's modulus for magnetized material
 - calculated from impedance data, 91
 - dependence on B, 7
 - nickel, 93
 - variation with temperature, 103
 - with polarizing flux, formula, 38
- Z nickel, properties
 - magnetostrictive constant, 90
 - maximum coercive force, 75
 - resistivity, 93
 - reversible permeability, 75
 - Young's modulus when magnetized, 93



LC ACQUISITIONS



0 043 384 018 5